UNIVERSAL
LIBRARY

ADDISON-WESLEY BOOKS IN NUCLEAR SCIENCE AND METALLURGY

Bishop—PROJECT SHERWOOD—THE U. S. PROGRAM IN CONTROLLED FUSION

Chastain—U. S. RESEARCH REACTOR OPERATION AND USE

Claus—RADIATION BIOLOGY AND MEDICINE

Clegg and Foley—URANIUM ORE PROCESSING

Cullity—ELEMENTS OF X-RAY DIFFRACTION

Cuthbert—THORIUM PRODUCTION TECHNOLOGY

Goldstein—FUNDAMENTAL ASPECTS OF REACTOR SHIELDING

Goodman—INTRODUCTION TO PILE THEORY
(The Science and Engineering of Nuclear Power, I)

Goodman—APPLICATIONS OF NUCLEAR ENERGY
(The Science and Engineering of Nuclear Power, II)

Guy—ELEMENTS OF PHYSICAL METALLURGY

Holden—PHYSICAL METALLURGY OF URANIUM

Hughes—PILE NEUTRON RESEARCH

Kaplan—NUCLEAR PHYSICS

Kramer—BOILING WATER REACTORS

Lane, MacPherson, and Maslan—FLUID FUEL REACTORS

Norton—ELEMENTS OF CERAMICS

Rough and Bauer—CONSTITUTIONAL DIAGRAMS OF URANIUM AND THORIUM

Sachs—NUCLEAR THEORY

Schuhmann—METALLURGICAL ENGINEERING
VOL. I: ENGINEERING PRINCIPLES

Seaborg—THE TRANSURANIUM ELEMENTS

Starr and Dickinson—SODIUM GRAPHITE REACTORS

USAEC—SHIPPINGPORT PRESSURIZED WATER REACTOR

Zinn and Dietrich—SOLID FUEL REACTORS

SOLID FUEL REACTORS

SOLID FUEL REACTORS

Compiled and Edited by

JOSEPH R DIETRICH

and

WALTER H ZINN

General Nuclear Engineering Corporation

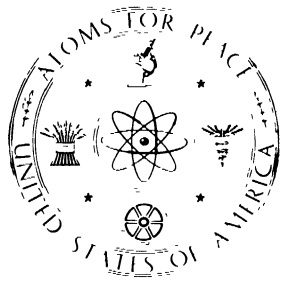

PREPARED UNDER CONTRACT WITH THE
UNITED STATES ATOMIC ENERGY COMMISSION

ADDISON-WESLEY PUBLISHING COMPANY, INC.

READING, MASSACHUSETTS, U.S.A.

Printed in the United States of America

Library of Congress Catalog Card No. 58–12601

First printing, September 1958

PREFACE

The United States program for the development of nuclear power is a very broad one. It is based on the conviction that the greatest advances in a complex technology are achieved when the broadest possible field of operation is provided for human ingenuity and inventiveness. The ultimate result of the program is expected to be the establishment of more or less standardized and generally applicable techniques for extracting useful power from nuclear fuels efficiently and economically. The immediate result is a steadily growing body of technical knowledge which is made available for general use through the publication of many reports and papers.

This volume attempts to consolidate the information that has been developed for several solid-fuel reactor types which have received serious attention in the United States but which are not yet represented by operating prototype plants.

Solid fuel reactors have been in operation on a sizable scale since 1944. Mechanical handling of the fuel has been carried out successfully for a variety of fuel types, and there is no question that solid fuel reactors can be operated in a routine manner with no more difficulty than is associated with non-nuclear equipment of similar complexity. The operation of solid fuel reactors at sufficiently high temperature to permit efficient conversion of heat energy to electrical energy is in a much earlier stage of development. Problems of corrosion, chemical compatibility, fuel performance, and control are seriously complicated by the need for higher temperature. The use of aqueous coolants, which is particularly attractive at low temperatures, is complicated by the effects of high vapor pressures. The reactors discussed in this book offer a variety of solutions to the problems created by high temperature in solid fuel reactors.

The present reports quite evidently must be of an interim nature, and their significance is not that they can point out proven ways of achieving economic nuclear power, but that they contain technical information representing the results of the work done and the experience obtained to this date. Very little emphasis has been given to cost estimates in this volume, since experience has indicated that such estimates are likely to be poor before a prototype reactor has been built and operated. The information presented is of three main types: (1) general research and development results, such as data of reactor physics experiments, fuel-element developments, and advances in various coolant technologies; (2) design data for specific reactors, which represent the integration of research and development results with design studies; and (3) analytical

studies whose purpose has been to direct developmental efforts and to define the design areas for various reactor types.

It is essential that a review of this kind be up to date. To achieve this objective the editors have had as many chapters as possible prepared by organizations carrying out the work described, and all of us have worked on a very rapid schedule. The various chapters reflect the approaches, judgments, and enthusiasms of their authors; it is not to be expected that they would be consistent in these respects. No relative evaluation of the merits of the various reactor concepts has been attempted; however, all the concepts discussed are receiving serious attention in the United States and all have promise for improving the production of nuclear power. In common with other concepts, they also have problems and limitations. As work proceeds, the degree to which the promises can be realized and the problems and limitations dealt with will become evident.

The reader can obtain additional information from the numerous references. The Atomic Energy Commission publications listed among them are available for inspection at the Commission's depository libraries in the United States and abroad and are sold by the Office of Technical Services, U. S. Department of Commerce, Washington 25, D. C.

Our sincere appreciation goes to the people and organizations who have contributed, particularly for their cooperation in meeting the schedule. We especially wish to thank Dr. Hoylande D. Young, of Argonne National Laboratory, who gave valuable assistance in collecting information, and the following representatives of the Atomic Energy Commission's Industrial Information Branch, Technical Information Service: Wilson R. Cooper, loaned from the Tennessee Valley Authority, who as book project officer worked painstakingly and continuously in gathering information, making arrangements, and editing; DeWitt O. Myatt, who guided the styling of the illustrations; and James R. Aswell and Jefferson D. Bates, who gave editorial assistance.

Dunedin, Florida
June, 1958

JOSEPH R. DIETRICH
WALTER H. ZINN

LIST OF AUTHORS AND CONTRIBUTORS

(Specific credits have been given in the text)

D. F. Babcock
W. R. Baldwin
D. W. Bareis
F. Bevilacqua
J. R. Dietrich
F. E. Driggers
R. H. J. Gercke
S. Goldsmith
M. Levenson
A. M. Perry
D. S. St. John
J. Schraidt
A. Shuck
A. R. Snider
E. Sowa
F. P. Storrer
C. A. Trilling
M. F. Valerino
J. L. Watkins
C. W. Wheelock
E. F. Weisner

TABLE OF CONTENTS

CHAPTER 1

INTRODUCTION*

There are now in the world two classes of nuclear power reactors that have been developed to the point of practical use for electric power production. These are the pressurized water moderated and cooled reactors (both boiling and nonboiling), and the graphite-moderated, gas-cooled reactor. Several other kinds of reactors are being developed; in the United States, for example, a small experimental sodium-graphite power reactor is now operating. The power reactor systems operating in this country are described in separate books in this series; another covers fluid-fuel reactor developments. This volume reviews the status of U. S work on a number of solid fuel reactors not yet represented by power-producing prototypes.

The concepts covered in this book are in various stages of development. The fast breeder reactor, for which there is a very large volume of developmental information, is represented by two rather large-scale reactor projects. At the opposite end of the scale are projects still partly in the planning stage, such as the program for developing plutonium recycling in thermal reactors, and the heavy-water moderated and cooled reactor. The information, then, ranges from well-established experimental, theoretical, and developmental results to analyses intended chiefly to provide direction for future work.

1–1. Objectives

The objective of a power reactor development program is always better reactors. Improvements can be of two kinds: those that improve immediate economic performance, and those that improve long-term utilization of nuclear fuels. Both objectives are economic in their ultimate goals, but the economic motivations of the former are short-term; those of the latter are long-term. A society foreseeing ultimate dependence on nuclear fuels cannot afford to ignore the problem of effectively utilizing its nuclear resources. On the other hand, very high levels of research and development can seldom be justified solely by very long-term goals. Consequently, the reactors that hold the highest promise for economic production of nuclear power in the near future will receive the most intensive research and development effort, while those whose main advantage is fuel conservation will follow on a schedule consistent with the need.

*By J. R. Dietrich, General Nuclear Engineering Corporation.

In their present forms, neither the pressurized-water nor the gas-cooled, graphite-moderated reactor utilizes nuclear fuels very effectively. Neither can utilize much more of the latent energy of natural uranium than is represented by its U^{235} content. These reactors fall short, too, of short-term economic goals. Different kinds of improvement are needed for these different reactors. The pressurized-water reactor is deficient primarily in the area of fuel cost; and the gas-cooled, natural uranium reactor is expensive primarily because of the high capital cost of the plant itself. These deficiencies may well be reduced or eliminated by further development, but it is possible that, ultimately, the cheapest nuclear power may be produced by a different kind of reactor or by a basic variation of one of the present kinds. Some factors that influence capital costs and fuel costs of reactors will be discussed.

1–1.1 Capital costs. Characteristics that affect capital costs interact with one another quite strongly, and it is not possible to assign a degree of importance to each of them. The only reasonable method for estimating the capital cost of a particular kind of reactor is to estimate the cost of a reactor and power plant of definite design; even then, there may be large errors if research and development is yet to be done. Nevertheless, it is possible to recognize characteristics that have important effects on capital costs and to understand the kinds of development needed to lower the costs of a given type of reactor.

The power density that can be attained in a reactor is important, since it determines how large a reactor must be for a given power output. Sizes of equipment outside the reactor, such as boilers and pumps, are also important. Thus power density limits dictated by nuclear performance bear differently on capital cost than do those imposed by the coolant. Basically, it is a power-density limitation that makes present graphite-moderated, gas-cooled reactors expensive. This limitation originates in both the nuclear and the coolant characteristics. An example of power-density limitation by neutron physics characteristics is in the D_2O-cooled, D_2O-moderated reactor. Here the thermal characteristics of the coolant are nearly the same as for ordinary water, but the power density is much lower because neutron physics requires that fuel be lumped and moderator-to-fuel ratio be high (see Chapter 5).

Increasing power density by high-performance design can, of course, be overdone. It can lead to increasing rather than decreasing capital cost if it requires very close tolerances or other expensive manufacturing procedures. The fast breeder reactor may perhaps be considered an example of this type. It has the highest power density of any present reactor, but hardly the lowest capital cost.

Related to the question of power density is the question of how much power a single reactor can deliver. Large units commonly cost less, per unit output, than do small ones. A power reactor type that is inherently limited to low total output is not likely to be competitive in the long-term future. Of course, there may be a limit to the amount of power that can be economically distributed from a single location. Such a limitation—and perhaps more important, the economical reserve capacity of a power network—may set limits on desirable output capability per reactor in the future Meeting this goal may prove difficult for some reactor types. At present, limitations on total power output usually arise from practical limitations on pressure vessel size.

Of itself, high thermal efficiency in the reactor plant favors low capital cost, but increasing reactor coolant temperature (usually necessary to substantially increase efficiency) may or may not reduce the capital cost of the reactor. In the steam system of the plant, higher temperatures usually lead to lower capital costs. It is in thermal efficiency that water-cooled (light and heavy) reactors are most seriously limited.

Obviously, any requirement of expensive materials or expensive construction techniques will increase the cost of a given plant. Pressurized-water reactors are handicapped because they use stainless steel extensively in their primary systems. Gas-cooled, graphite-moderated reactors do not suffer from this problem, but they do require expensive field fabrication and annealing of their large pressure vessels.

Related to the problem of special materials and special construction techniques are some unique problems of particular reactor types. It is always hard to assess the long-term effects of such problems on reactor costs, since it is always possible that inexpensive methods of coping with them will be developed. Yet certain problems, such as the problem of heat exchange between sodium and water, may prove to be important for a long time to come.

1-1.2 Fuel costs. Fuel cost factors are more clearly interrelated than those affecting capital cost. One need only list the various items of cost involved in producing, using, recycling, handling, and disposing of fuel elements, with reasonable estimates for their values, to demonstrate this interrelation. This will not be done here, since the several items of fuel cost vary radically between fuel elements. Rather, some major factors affecting fuel cost will be considered.

Three types of fuel cycles must be considered separately: the natural uranium cycles, enriched uranium cycles in which converted material is not recycled, and cycles in which converted material (plutonium or U^{233}) is recycled. From the standpoint of fuel cost alone, there is little doubt

that the natural uranium fuel cycle is now most attractive. Arguments against using natural uranium are usually based on the lower specific output of the plant and the consequent higher specific capital cost which may be necessary for using natural uranium. There is little doubt that developing a high-performance reactor fueled with natural uranium would be a worth-while step toward economic nuclear power. On the basis of present chemical processing cost estimates, the fuel cost with natural uranium does not appear to be very sensitive to the difference between recovering and not recovering plutonium from the spent fuel. The fuel cost considerations in the natural uranium fuel cycle then boil down to only two: keeping the fuel fabrication costs low and the life of the fuel elements long.

When partially enriched fuel is used in the reactor, there are two new considerations. First, the U^{235} burned in the reactor is more expensive than that in natural uranium, so other fuel costs must be reduced to remain competitive with natural uranium. Second, the U^{235} remaining in the fuel after it is discharged is usually too valuable to be discarded, and therefore must be chemically reprocessed to remove fission-product contamination. For these reasons it is usually necessary, with partially enriched fuel, to achieve very long fuel life (at least 10,000 Mwd/t) to bring chemical processing and fabrication costs low enough per unit of energy obtained from the fuel. Fortunately, such long fuel lifetimes appear possible with oxide fuels, and the potentialities of reactors using partially enriched fuel can thus be exploited.

Recycling converted material (plutonium or U^{233}) extends the utilization of the basic fuel material and reduces the importance of the cost of the fissionable isotope burned. In a self-sustaining breeder reactor the cost or value of the fissionable isotope does not directly affect fuel cost—except that investment charges against its value may be applicable as part of the power cost, and that there may be additional revenues from selling excess fuel produced in the reactor. Recycling either plutonium or U^{233} involves fabricating material that is alpha-active and probably gamma-active; these fuels would almost certainly be more expensive to fabricate than normal uranium. However, if by recycling plutonium, natural uranium could be used in reactors that otherwise would require partially enriched uranium, recycling might reduce fuel cost. For the future, recycling converted fuel is the only known method of greatly improving the utilization of nuclear fuel resources.

Although these three types of fuel cycles differ markedly, clearly there are only two straightforward avenues open to the designer for reducing fuel cost in a particular reactor. One is to extend fuel life; the other, to design fuel elements with low fabrication cost. These two principles apply whatever fuel cycle is considered, although their relative importance may vary.

1-1.3 Utilization of nuclear fuel resources. The only method by which a substantial fraction of the energy potentially available in natural uranium or thorium can be utilized is by recycling plutonium or U^{233}. Otherwise it is not likely that the energy output of natural uranium can be extended to more than about twice the energy content of the U^{235} in the uranium and it is questionable whether thorium will be utilized at all. Consequently, the development of recycling methods is of great significance for the future, whether or not it contributes immediately to lowering costs of nuclear fuel. There are quite basic differences between recycling fuels for fast reactors and for thermal reactors. These differences may well prove more important than the differences between plutonium and U^{233} recycling in the same kind of reactor (i.e., fast or thermal). The differences, of course, originate in the different tolerances of fast and thermal reactors for diluent materials and fission products.

1-2. Methods of Approaching the Objectives

The several reactor development projects discussed in this volume represent as many approaches toward reducing capital and nuclear fuel costs and improving utilization of nuclear fuels. The projects will be discussed briefly in relation to these objectives.

1-2.1 The fast neutron reactor. Of the reactor types discussed, the fast neutron reactor is by far the most highly developed. Its excellent potentialities were broadly recognized [1,2*] at an early date. By 1951 the Experimental Breeder Reactor I [3] was operating in the United States; it produced the first nuclear electric power in December of that year. Design and development were under way on three fast neutron reactors of substantial size by 1955 [2,4,5]. These reactors are now being built; two of them are described in Chapters 3 and 4 of this volume.

The performance potentialities of the fast neutron reactor are indeed outstanding. Its neutron economy is higher than that of any other reactor. Measurements made on the EBR-I reactor [3] and fast critical experiments [6,7] have proved that practical fast reactors can have substantial breeding gains. At the same time, with sodium as coolant, temperatures can be high enough for good thermal efficiency. From the standpoint of fuel utilization, the fast reactor is the only known method of extracting the energy from a large fraction of the available U^{238}. It can also utilize thorium.

Despite these advantages, the fast reactor is not yet the cheapest source of nuclear power. Experience has shown that capital costs of fast reactor systems are high. The high cost is associated partly with the circulation of sodium, partly with the use of an intermediate sodium system between

*References are listed at the end of each chapter.

the primary and steam systems, and partly with the high density of fissionable isotope in the core, which imposes the requirements of extremely high power density. To what extent these high costs are inherent in the system, and to what extent they can be eliminated by experience and development, remains to be demonstrated.

With respect to fuel cost, the fast reactor has no logical place in the field of nuclear power unless plutonium is recycled; otherwise the reactor is only a burner of expensive, highly enriched uranium. Although markets may now exist for the plutonium produced, the fast reactor in the long term must be considered a breeder utilizing its own bred plutonium as fuel. If present methods of fuel processing for thermal reactors are to be used also for extracting and processing the plutonium from fast reactors, then low fuel costs can be achieved only after the costs of these processes have been substantially reduced. It appears, however, that simpler and presumably cheaper processes should be adequate for processing fast reactor fuel, since fission-product removal is far less important than for thermal reactors.

To summarize, the fast reactor has been proven feasible and has great promise for the future, although in many areas cost improvements are needed and it must be developed to operate on a self-sufficient fuel cycle if it is to be economical. From this combination of potentialities and problems has evolved the two-pronged attack now under way in the United States. It is recognized, on the one hand, that large developmental steps are made by using experimental reactors with few operating restrictions imposed by considerations of economy, service continuity, or risk of equipment damage, and that, on the other hand, development of practical design and operating procedures is stimulated by practical operation of a large reactor to produce power for a utility system. Consequently, two fast reactor projects are under way. Both involve reactors large enough to obtain results that could be applied to large central station power plants.

The Experimental Breeder Reactor II will be built at the National Reactor Testing Station in Idaho. Although it will generate electricity, no obligation to produce power will interfere with experimental operation. The (remote) location of the reactor at the testing station will give it the greatest possible flexibility of operation and experimentation without undue hazards to people or property. Finally, the reactor complex will include a chemical processing and fuel refabricating plant, completing a self-sufficient nuclear power operation which, in equilibrium, will require only a small feed of U^{238}.

In contrast, the Enrico Fermi Atomic Power Plant will be a fast reactor fueled with U^{235} and tied into a normal power system. Here, developments and operating procedures for practical electrical power generation will be worked out. This dual approach to developing the fast reactor is

expected to be most effective in realizing the long-term potentialities of the fast reactor system on a practical time schedule.

1-2.2 The D_2O reactor. In the thermal neutron energy range, the D_2O-moderated reactor approaches most closely the high neutron economy of the fast reactor. Lewis has pointed out many advantages resulting from this characteristic [8–10], and the Canadian program on the D_2O-moderated concept has progressed through two research reactors to a project for constructing a D_2O-moderated, D_2O-cooled power reactor [11]. In the United States, the major use has been as production reactors at the Savannah River Site (see Chapter 5).

Much of the technology required for the D_2O power reactor has already been developed for pressurized, H_2O-moderated, H_2O-cooled reactors. The unique problems in using heavy water are those of an expensive material for the moderator, and of extracting large amounts of power from reactors that are inherently rather large yet must be highly pressurized. Reactor systems in which D_2O can serve as moderator are numerous. The coolant may be D_2O itself (either in a pressure vessel reactor or in a pressure tube reactor), or it may be a gas, a liquid metal [12], ordinary water, or an organic liquid. The high neutron economy achievable with D_2O-moderated reactors can be utilized in many ways: to permit operation with natural uranium fuel, to achieve efficient recycling of plutonium in thermal reactors, or to use the thorium-U^{233} cycle with a very high conversion ratio or with net breeding of U^{233}.

Most of these applications of D_2O-moderated reactors are being explored in the United States. A pressure-vessel type, D_2O-moderated, D_2O-cooled reactor is being developed to use natural uranium (Chapter 5). Another approach is by way of a gas-cooled, D_2O-moderated reactor (Chapter 6). The plutonium recycle application is to be investigated with a pressure-tube, D_2O-moderated, D_2O-cooled reactor (Chapter 8). The thorium-U^{233} cycle appears especially suited to the boiling D_2O approach, and development is proceeding in this direction.

1-2.3 The gas-cooled reactor. The reactor concepts described so far have emphasized characteristic neutron physics behavior. Another approach is to concentrate on the potentialities of a particular reactor coolant. One group of possibilities of this kind embraces the gaseous coolants. To a large degree the technology and engineering character of a reactor depends upon choice of coolant. This is true of water-cooled reactors, and a special branch of reactor technology has developed around the British [13–17] application of gas cooling also. Gases allow relatively high coolant temperatures, have relatively poor heat-transport characteristics unless used at high pressures, temperatures, and flow velocities, and (unlike

water) require a separate reactor moderator. Thus the neutron characteristics are determined by the moderator, and the thermal performance by the gaseous coolant. The combination of graphite moderation, carbon-dioxide cooling, and fueling with natural uranium metal in magnesium alloy jackets has led to a reactor that is particularly attractive for the nuclear power economy of Great Britain. These reactors have good neutron economy and give reasonably high steam temperatures, but their power densities are low.

The combination of graphite as moderator with a gaseous coolant has many attractive features. Fundamentally it is capable of high neutron economy and good thermal efficiency. Unfortunately, materials so far developed for jacketing nuclear fuels have either mediocre temperature capabilities and good nuclear properties, or fairly high thermal capabilities and rather poor nuclear properties. Potentially, gas-cooled systems have attractive possibilities, but at present they suffer from low power density and relatively modest temperatures. It is characteristic of the gas-cooled system that as the temperature capability is increased the power density will automatically increase also. Investigation of this system is just beginning in the United States, and design studies [18–22] have been made to predict the design areas most favorable for this reactor type (Chapter 6). Lacking a fuel element jacketing material with both high neutron economy and high thermal performance, the latter is being chosen at the expense of neutron economy. This is the approach selected in the graphite-moderated, gas-cooled reactor concept, using slightly enriched uranium oxide with stainless steel jackets.

Simultaneously, a gas-cooled reactor employing D_2O as moderator was proposed to the U. S. Atomic Energy Commission (Chapter 6). In this concept a pressure-tube reactor employs cool D_2O as moderator. Using D_2O minimizes the loss of neutrons to the moderator and offers reasonably good neutron economy even if rather absorbent materials are necessary for fuel-element jackets. At the same time, it avoids size limitations, because need for pressurizing the reactor in a single vessel is avoided.

1–2.4 Organic coolants and moderators. A second approach emphasizing the reactor coolant employs organic liquids as coolants, or as coolants and moderators. The use of organics in reactors has been under investigation in the United States for a number of years [23–32]. An experimental reactor moderated and cooled by an organic liquid has recently been built and operated (see Chapter 7) [30].

The promise of the organic system lies in the case of attaining fairly high coolant temperatures, and in its freedom from corrosion. Organic liquids at relatively high temperatures have quite low vapor pressures, and are compatible with most metals usable as fuel jackets. Furthermore,

they are not strongly activated by neutron irradiation Thus very substantial reductions in capital cost might be achieved by using them for reactor coolants or for coolants and moderators, and reasonably high steam temperatures might also be possible. The disadvantage of the organic liquids is their chemical dissociation by radiation and high temperature, which requires investment in cleanup systems and operating expenditures to continually replace the dissociated organic liquids.

Since the dissociation of organic liquids is their only feasibility problem, the obvious approach has been to build an experimental reactor using them. It happens that the reactor built (the Organic Moderated Reactor Experiment) employs organic liquid both as coolant and as moderator, but this does not necessarily mean that this will always be the most effective way of using organic liquids. Indeed organics can be used to very good advantage as coolants with any suitable moderator, with consequent reduction in the rate of dissociation. The question of how far this approach can go toward developing economic nuclear power can be determined only after the behavior of the organic liquid has been established. Thus the outcome of the current organic moderated reactor experiment is crucial for future reactor applications of organic liquids, but it does not necessarily establish the most attractive design for a reactor utilizing them.

1–2.5 Plutonium recycling in thermal reactors. The final phase of development discussed in this volume centers around neither a particular neutron spectrum nor a particular reactor coolant, but rather around a fuel cycle. The program for recycling plutonium in thermal reactors has its greatest significance in the area of nuclear fuel utilization. Recycling converted fissionable isotopes is probably essential to any really significant development of the nuclear power industry. It is perhaps not a matter of great urgency to recycle converted fuel so long as supplies of nuclear fuel are plentiful, but since economic recycling will not be accomplished easily, it appears prudent to attack the problems early enough to establish firm foundations and consistent directions for the development of the industry.

A number of analyses of the physics and economics of plutonium recycle have been made [33–36]. The work described in this volume represents an integrated program, now in the planning and analysis stage, concerned with all problems of recycling plutonium in thermal solid fuel reactors. The program includes the construction and operation of a test reactor, and for reasons of convenience and flexibility in experiments, a pressure-tube, D_2O-moderated, D_2O-cooled reactor has been selected. It seems probable that reactors of this type would also be well suited for power production with plutonium recycling. The test reactor will be used in conjunction with a laboratory for processing and fabricating recycled fuels.

1–3. Plan of Presentation

There is no obvious direct and single path leading to the development of economic nuclear power and optimum long-range utilization of nuclear resources. It has been the policy of the United States to seek possible paths that may lead to these goals and, where practical, to sponsor work along these paths by organizations that have demonstrated an enthusiasm for them. The same approach has been used in assembling this volume: where possible, the individual programs have been described by the groups carrying them out. This approach inevitably results in a certain degree of inconsistency of organization. It is hoped that such inconsistencies represent a tolerable price for the advantages gained in obtaining information from its source.

In the following chapters, the various systems are presented in the order in which they have been discussed above. The fast reactor system, farther advanced than the others, is described in three chapters, one dealing with general fast reactor technology and the others with the two current fast reactor projects.

References

1. W. H. Zinn, Review of Fast Power Reactors, in *Proceedings of the International Conference on the Peaceful Uses of Atomic Energy*, Vol. 3. New York: United Nations, 1956. (P/814, pp. 198–204)

2. J. W. Kendall and T. M. Fry, The Dounreay Fast Reactor Project, in *Proceedings of the International Conference on the Peaceful Uses of Atomic Energy*, Vol. 3. New York: United Nations, 1956. (P/405, pp 193–197)

3. H. V. Lichtenberger et al., Operating Experience Obtained from an NaK-Cooled Fast Reactor, in *Proceedings of the International Conference on the Peaceful Uses of Atomic Energy*, Vol. 3. New York: United Nations, 1956. (P/813/Rev. 1, pp. 345–360)

4. A. H. Barnes et al., The Engineering Design of EBR-II, A Prototype Fast Neutron Reactor Power Plant, in *Proceedings of the International Conference on the Peaceful Uses of Atomic Energy*, Vol. 3. New York: United Nations, 1956. (P/501, pp. 330–344)

5. A. Amorosi et al., A Developmental Fast Neutron Breeder Reactor, in *Proceedings of the International Conference on the Peaceful Uses of Atomic Energy*, Vol. 3. New York: United Nations, 1956. (P/491, pp. 134–142)

6. J. E. R. Holmes et al., Experimental Studies on Fast Neutron Reactors at A.E.R.E., in *Proceedings of the International Conference on the Peaceful Uses of Atomic Energy*, Vol. 5. New York: United Nations, 1956. (P/404, pp. 331–341)

7. J. K. Long et al., Fast Neutron Power Reactor Studies on ZPR-III, paper prepared for the Second International Conference on the Peaceful Uses of Atomic Energy, Geneva, 1958. (P/598)

8. W. B. Lewis, *The Heavy Water Reactor for Power* (paper presented to the European Atomic Energy Society at Monte Faito, Italy), Report DL-25, Atomic Energy of Canada, Ltd., May 14, 1956.

9. W. B. Lewis, *Low Cost Fueling without Recycling,* Report DR-39, Atomic Energy of Canada, Ltd., Dec. 10, 1956.

10. W. B Lewis, *High Burn-up from Fixed Fuel,* Report DM-47, Atomic Energy of Canada, Ltd., Nov. 27, 1957.

11. Atomic Energy of Canada, Ltd., *The Canadian Study for a Full-Scale Nuclear Power Plant,* Report AECL-557, January 1958

12. Kurt Goldmann and Charles K. Leeper, The Sodium-Cooled, D_2O Moderated Reactor (SDR), a status report presented at the Fourth Nuclear Engineering and Science Conference Held in Chicago, Ill., March 17–21, 1958.

13. Sir Christopher Hinton, The Graphite-Moderated, Gas-Cooled Pile and Its Place in Power Production, in *Proceedings of the International Conference on the Peaceful Uses of Atomic Energy,* Vol. 3. New York: United Nations, 1956. (P/406, pp. 322–329)

14. *J. Brit. Nuclear Energy Conf* **2**(2) (April 1957).

15. *J. Brit. Nuclear Energy Conf* **2**(3) (July 1957).

16. A B McIntosh and K. Q. Bagley, Selection of Canning Materials for Reactors Cooled by Sodium/Potassium and Carbon Dioxide, *J. Inst. Metals* **84,** 251 (1955–1956)

17 Sir John Cockcroft, Further Development of Nuclear Power, The James Forrest Lecture, 1958, *Engineer* **205,** 435–436 (Mar 21, 1958).

18 Oak Ridge National Laboratory, *The ORNL Gas-Cooled Reactor,* USAEC Report ORNL-2500(Pts. 1–4), April 1958

19 Kaiser Engineers, *Gas Cooled Power Reactor, Preliminary Design, 55,000 Kw Prototype, Natural Uranium Nuclear Power Plant,* USAEC Report IDO-2021(Rev. 1), April 1958

20. Kaiser Engineers, *Gas Cooled Power Reactor, Feasibility Study, Optimum Natural Uranium Nuclear Power Plant,* USAEC Report IDO-2022(Rev. 1), April 1958

21 Kaiser Engineers, *Gas Cooled Power Reactor, Feasibility Study, 44,000 Kw Prototype, Partially Enriched Uranium Nuclear Power Plant,* USAEC Report IDO-2023(Rev. 1), April 1958.

22. Kaiser Engineers, *Gas Cooled Power Reactor, Feasibility Study, Optimum Partially Enriched Uranium Nuclear Power Plant,* USAEC Report IDO-2024(Rev 1), April 1958

23. C D. Bopp and O Sisman, *Radiation Stability of Plastics and Elastomers* (supplement to ORNL-928), USAEC Report ORNL-1373, Oak Ridge National Laboratory, 1954; *Physical Properties of Irradiated Plastics,* USAEC Report ORNL-928, Oak Ridge National Laboratory, 1951

24. R. O. Bolt et al. Organics as Reactor Moderator-Coolants: Some Aspects of Their Thermal and Radiation Stabilities, in *Proceedings of the International Conference on the Peaceful Uses of Atomic Energy,* Vol. 7. New York: United Nations, 1956. (P/742, pp. 546–555)

25. E. F. Fricke, *A Preliminary Nuclear Design Study of Diphenyl Moderated*

and Cooled Reactors, USAEC Report ANL-5457, Argonne National Laboratory, November 1955.

26. SHERMAN GREENBERG, Stability of Diphenyl Under Fast Flux Irradiation in a Dynamic System, in *Compilation of Organic Moderator and Coolant Technology*, comp. by H. P. Smith, USAEC Report TID-7007[Pt. 2(Del.)], Argonne National Laboratory, Jan. 24, 1957.

27. L. W. FROMM and KERMIT ANDERSON, Engineering Data for Diphenyl Cooled Nuclear Reactors, *Nuclear Sci. and Eng.* **2**(2), 160–169 (April 1957).

28. G. A. FREUND, The Case for Organic Coolant-Moderators for Power Reactors, *Nucleonics* **14**(8), 62 (August 1956).

29. HARRY P. SMITH (Comp.), *Compilation of Organic Moderator and Coolant Technology*, USAEC Report TID-7007(Pt. 1), Division of Reactor Development, AEC, Jan. 24, 1957.

30. THE STAFF, NORTH AMERICAN AVIATION, INC., An Organic Moderated Reactor Experiment, in *Compilation of Organic Moderator and Coolant Technology*, comp. by H. P. Smith, USAEC Report TID-7007[Pt. 2(Del.)], Jan. 24, 1957.

31. K. SATO, *Determination of Burnout Limits of Polyphenyl Coolants*, USAEC Report AGC-AE-32, Aerojet-General Corporation, February 1957.

32. T. C. CORE and K. SATO, *Determination of Burnout Limits of Polyphenyl Coolants*, USAEC Report IDO-28007, Aerojet-General Corporation, February 1958.

33. J. V. DUNWORTH, Fuel Cycles and Types of Reactors, in *Proceedings of the International Conference on the Peaceful Uses of Atomic Energy*, Vol. 3. New York: United Nations, 1956. (P/403, pp. 14–18)

34. W. B. LEWIS, Some Economic Aspects of Nuclear Fuel Cycles, in *Proceedings of the International Conference on the Peaceful Uses of Atomic Energy*, Vol. 3. New York: United Nations, 1956. (P/4, pp. 3–13)

35. B. I. SPINRAD et al., Reactivity Changes and Reactivity Lifetimes of Fixed-Fuel Elements in Thermal Reactors, in *Proceedings of the International Conference on the Peaceful Uses of Atomic Energy*, Vol. 5. New York: United Nations, 1956. (P/835, pp. 125–140)

36. M. F. DURET, *Reactivity and Fuel Balance in Recycled Plutonium Reactors*, Report RPI-12 (AECL), Atomic Energy of Canada, Ltd., Oct. 24, 1955.

CHAPTER 2

THE FAST NEUTRON POWER REACTOR*

2–1. Introduction

The outstanding characteristic of the fast reactor is its high neutron economy, in which lies its promise to extend the nuclear fuel supply. The fast reactor is the only known means of extracting a large fraction of the energy potentially available in U^{238}. It is also a means, probably not the only one, of extracting energy from thorium. These possibilities result from the fast reactor's high breeding ratio. Reactors now being built will have breeding ratios substantially greater than unity. That is to say, they will produce from the fertile U^{238} more fissionable material than they consume. In future reactors operating with plutonium fuel, larger breeding gains can be expected.

The advantages and problems of a fast reactor are easily recognized. Its high breeding ratio [1] results from three characteristics: the value of η is high (neutrons liberated per neutron absorbed by the fissionable isotope), fissions in the fertile isotope U^{238} are a rather high fraction of the total, and parasitic neutron absorption by structural and coolant materials is low. High neutron energy accounts for the first two of these. If a moderator is used the fast neutron qualities are lost and the breeding ratio decreases; consequently, neutron moderation must be kept to a minimum. However, there is always some neutron moderation in the reactor from elastic and inelastic scattering by the fuel, structure, and coolant.

For many fast reactor designs, the median energy at which fissions occur is about 0.2 Mev. A fast reactor will typically include a fissionable material, a fertile material, a coolant, and whatever structural material is necessary.

It is useful to adopt the approach of Reference 2 to develop a rough picture of fast reactor composition and characteristics. For neutrons of energy about 0.2 Mev, the scattering mean free path in pure U^{235} is about 2.5 cm and the absorption mean free path about 12 cm. For this medium and this neutron energy an effective diffusion area L^2 is given by

$$L^2 \simeq \frac{\lambda_s \lambda_a}{3} \simeq \frac{(2.5)(12)}{3} \simeq 10 \text{ cm}^2.$$

*Compiled by J. R. Dietrich, W. R. Baldwin, and J. L. Watkins, GNEC.

The following authors furnished manuscripts and prepublication copies of papers which supplied an important part of the information in this chapter: A. Amorosi, W. J. McCarthy, Jr., and J. J. Morabito, of Atomic Power Development Associates; and R. O. Brittan, J. R. Humphreys, Jr., R. A. Jaross, L. J. Koch, W. B. Loewenstein, J. K. Long, D. Okrent, F. A. Smith, and F. W. Thalgott, of Argonne National Laboratory.

If the U^{235} is to be the starting point for a fast reactor, we might consider first diluting the material with a coolant, perhaps sodium in the volume ratio 1:1. Since sodium is practically transparent to neutrons in the relevant energy range, L^2 would be increased in the ratio 2^2, or to about 40 cm^2. If the reactor is to be large, the ratio of coolant to solid material might be maintained and the U^{235} diluted further with U^{238} and structural materials. The U^{238} (the major constituent) will have an absorption cross section about 1/10 that of U^{235}, and roughly the same scattering cross section as U^{235}. If the reactor is quite large, the dilution can be increased until absorption by the diluents is comparable to that in the U^{235}, but if diluents absorb more than about half the neutrons a chain reaction cannot be maintained. Thus the maximum dilution D (volume of total solid material/volume U^{235}) will be of the order 10. If the scattering cross section of the diluent is assumed equal to that of U^{235}, then L would increase to $40D$ if there were no absorptions in the diluent and to $40D/2$ if half the neutrons were absorbed by the diluent. Thus the diffusion area becomes rather large as the dilution is increased, and substantial leakage from the core can be expected even in relatively large fast reactors.

The reactor described has the following characteristics:

(1) The U^{235} density in the core is high; therefore high power density is necessary to keep the specific fuel investment charges low. In this example, with a dilution of 10 and a coolant fraction of 0.5, the U^{235} (or plutonium) content will be 50 cm^3/liter of core, or 900 g/liter. The plutonium in one liter of core then has a value of about \$15,000; at an annual rate of 4%, the use charge per liter would be \$600. If this charge is to be no more than 0.5 mill/kwh (electrical), the thermal power density must be about 0.5 Mw/liter. This estimate does not include the part of the fuel investment from processing, fabricating, and cooling spent fuel elements. Usually it is assumed that power density for fast reactors must approach 1 Mw/liter to make them economically attractive. Fortunately, power densities in this range can be reached with sodium as the coolant; they would be difficult to attain with other coolants.

(2) Since the power density is high, the reactor will be small for a given power output. Consequently, neutron leakage is high and much of the breeding must be in an external blanket. In a self-maintaining system, bred fuel is cycled from blanket to core.

(3) The neutrons make relatively few collisions before they are absorbed; consequently their lifetime is short (of the order 10^{-7} sec). The short lifetime suggests the possibility of rather large accidental nuclear power excursions and resulting safety problems.

(4) Because a large coolant fraction is necessary for heat removal, the typical fast reactor will contain enough fuel to make several critical masses if it were arranged compactly. It is difficult to prove that such a

compaction could not occur if an accident should melt the fuel. This, too, poses a safety question.

The two most important fast reactor characteristics affecting cost are the related high power density and sodium cooling. The high power density requires careful design and construction, particularly to ensure adequate coolant flow in all possible circumstances. It also complicates handling irradiated fuel, requires the fuel to be highly subdivided, and demands a high temperature rise in the coolant as it traverses the reactor core. These requisites are reflected in high capital and fuel costs and in thermal shock problems. On the other hand, high power density means small plant size, tending toward lower capital costs.

In using sodium, numerous problems influence costs. The chemical reactivity of sodium with water and air makes the use of an intermediate heat-exchange system, to isolate the radioactive primary sodium from the steam system, highly desirable if not essential. It leads to steam boiler construction problems and imposes rather severe requirements of secondary containment. Because the sodium is radioactive, the primary cooling system must be shielded and maintenance is complicated. The high melting point requires heating the sodium circulating system. Free surfaces must be blanketed with inert gases and cleanup systems must be provided to maintain high purity of the sodium. Problems of operating mechanisms in sodium are important today, but may be reduced by further research and development.

Counterbalancing these difficulties are the very considerable assets of excellent nuclear and thermal performance. The neutron economy of the fast reactor cannot be exceeded, and the thermal performance of the sodium coolant is outstanding. Indeed, if the use of sodium is justified anywhere in the reactor field, it is as coolant for the fast reactor.

In the long term, the fast reactor would have little attraction unless recycling bred fuel proves economical. Consequently, the fast reactor system cannot be considered fully developed until a practical and economical method for fuel recycling is also developed, and this may be true for most other reactors. However, some features of fuel recycling may prove easier with the fast reactor because fission products are less harmful to the neutron economy.

The fast reactor is not yet the cheapest means of generating nuclear power, but if nuclear fission is to be a lasting power source, future reactors must be able to utilize large fractions of the energy latent in U^{238} and thorium. The urgency of such development will depend on the supplies of nuclear fuel. Although there is no immediate prospect of a nuclear fuel shortage, it is prudent that early nuclear development take this possibility into account. In this context, it is significant that some problems of the fast reactor appear to be unique, and that large improvements will

probably come as a result of a direct attack on these specific problems, rather than from broad developments in reactor technology. It is significant also that the major disadvantages of the fast reactor do not inherently limit its performance, but are technological problems that at present are expensive. Thus there is good potentiality for improving the reactor through well-directed research and development. These considerations have led to a rather strong program of developing and constructing fast reactors in the United States.

Fast reactor development was begun early in the United States, at a time when known uranium reserves were much lower than at this writing. The Experimental Breeder Reactor I (EBR-I), completed in 1951 [3], was the first reactor to produce electric power, on December 21, 1951. It operated at a thermal power of 1.4 Mw, producing 250 kw of electricity. It is still in operation. Besides proving the technical feasibility of a fast reactor, the EBR-I was employed first to establish the feasibility of breeding, and later to provide information on the neutron spectra characteristics of fast reactors and capture-to-fission ratios in such spectra. More recently it has been used to study the stability and safety of fast reactors.

The EBR-I has been followed by two reactors in the United States and one in the United Kingdom [4,5]. The Experimental Breeder Reactor II (EBR-II), an experimental reactor of 20 Mw (electrical) output to be completed in 1960, will carry on investigations begun on EBR-I. It is to have a fuel reprocessing and refabrication plant for recycling the bred plutonium. The Enrico Fermi Atomic Power Plant (EFAPP) is scheduled to operate in 1960, with an electrical power output of 100 megawatts. It will demonstrate the application of a fast reactor in a commercial electrical network.

These reactors are to be fueled initially with mixtures of metallic U^{235} and U^{238}. The EBR-II and possibly the Enrico Fermi Reactor will operate later with a Pu-U^{238} mixture. There has also been some work on fueling fast breeder reactors with oxides of plutonium and uranium [6–11]. Design studies have been reported on a large oxide breeder (240 Mw, electrical) with a breeding ratio of 1.3 and a coolant outlet temperature of 1000°F [6].

The subject of fast reactors is treated here in three chapters. Chapter 3 describes the EBR-II design and Chapter 4 the Enrico Fermi Atomic Power Plant. This chapter (Chapter 2) covers in a general way three of the major technical areas of basic importance to the fast reactor concept: reactor physics, reactor safety, and sodium system technology.

2-2. Reactor Physics*

There are many good summaries of the neutron physics of fast reactors [12–15]. These papers treat both the theoretical methods and their applications to experimental data. Such data come from a number of sources: the Experimental Breeder Reactor I [3,16], the British low-power fast reactor, ZEPHYR [15], various critical assemblies at Los Alamos [17–21], and the Argonne Fast Exponential Experiment [22]. Recently an extensive body of data has become available from the ZPR-III critical assembly at the National Reactor Testing Station [23,24]. This facility was constructed specifically to obtain data on assemblies for fast neutron power reactors. From it has come the most extensive available collection of data for this application.

This section describes only the reactor physics features that define the fast neutron reactor and that have a significant bearing on reactor design. The methods of calculation are described only briefly, to define the framework within which the physics studies are made.

2-2.1 Aspects of the reactor physics problem. In fast reactors fission and capture occur over a wide range of energies, and it is not feasible to average the cross sections. Thus, a central problem in fast reactor physics is to determine the energy spectrum of the neutrons. The spectrum, of course, depends on the composition and "geometry" of the reactor. The practical method is to divide the energy range into a number of subranges, and to treat the neutrons in each subrange as a group of constant-energy neutrons for which average cross sections can be determined. By judicious choice of the number of groups and of the energy ranges of each group, this multigroup technique can be adapted to any available experimental data and to any known energy-dependent peculiarities of the reactor. The number of groups can vary rather widely, depending on the character of the problem. For some problems one group may be feasible, and as many as 20 groups have been used for others. Often about 10 groups are enough to apply the available data. Calculations with more than two or three groups require large digital computers, unless for a reactor with a single, uniformly composed region or one that can be approximated by an equivalent single-region assembly.

An 11-group breakdown used for many calculations at Argonne National Laboratory is summarized in Table 2–1, taken from Reference 14.

---

*Most of the material of this section has been extracted from Reference 14 by W. B. Loewenstein and D. Okrent, and Reference 24 by J. K. Long, W. B. Loewenstein, C. E. Branyan, G. S. Brunson, F. S. Kion, D. Okrent, R. E. Rice, and F. W. Thalgott.

TABLE 2–1

SYMBOLS AND GROUP INTERVALS FOR ELEVEN-GROUP BREAKDOWN [14]

j = Energy group

χ = Fission spectrum (fraction of fission neutrons born into each group)

E_L = Lower boundary of energy group, Mev

Δu = Group lethargy interval (approximate)

v = Average velocity of neutrons in energy group $\times 10^{-8}$

σ_{tr} = Transport cross section, barns

σ_f = Fission cross section, barns

σ_c = Parasitic neutron absorption cross section, barns

$\alpha \equiv \sigma_c/\sigma_f$ for Pu^{239}, U^{235}, and U^{233}

σ_{el} = Cross section for neutrons removed to the next lowest energy group by elastic scattering

σ_{in} = Cross section for neutrons removed from energy group by inelastic scattering

$\sigma_{in,j\to j+k}$ = Transfer cross section for inelastic scattering from group j to group $j+k$

$$\sum_{k\neq 0} \sigma_{in\,j\to j+k} = \sigma_{in}$$

j	χ	E_L	Δu	v
1	0 338	2 25	—	25 6
2	0 236	1 35	0 5	18 3
3	0.178	0 825	0.5	14.5
4	0.116	0 5	0 5	11.5
5	0 066	0.3	0 5	8 8
6	0 033	0 18	0.5	6.7
7	0.017	0 11	0.5	5 2
8	0 008	0.067	0.5	4.0
9	0.006	0.025	1.0	2.8
10	0 002	0 0091	1.0	1.7
11	0	0	—	0.8

Table 2–2, also from Reference 14, gives the group cross sections for a number of materials that might be used in fast reactors. In the case of Pu^{239}, three values are given for α (the ratio of capture cross section to fission cross section) in each energy range. These values cover the present range of experimental uncertainty of α. The calculated results mentioned later in this chapter are based on the constants of Table 2–2 (see pp. 98–108); the standard value of α is used for plutonium.

The second problem is to determine neutron transport from point to point in the reactor within each energy group. In the size range of central station power reactors, it has been found that the transport of neutrons is described well enough by the diffusion approximation. For smaller assemblies, or where local flux variations must be investigated in larger assemblies, other approximate solutions to the Boltzmann equation have been used. In the United States the S_n method of Carlson [25,26] has been applied most extensively. Various approximations to transport theory are discussed in References 12 and 15, and calculational results by the various methods are compared in Reference 12.

Although fast neutron power reactors will usually have rather fine-grained structures,* in order to achieve the very high power densities required, it is nevertheless necessary to consider the fine structure of the neutron flux distribution in the reactor. This is important when critical assemblies are designed to approximate the performance of a contemplated power reactor. A related problem is that of neutron streaming through materials, such as sodium, that have long neutron mean-free paths. Critical experiments have shown only small effects of streaming in configurations suitable for power reactors. Local variations in the neutron flux caused by structural inhomogeneities do exist however, and must be taken into account in the calculations.

Figure 2-1 plots relative fission rate distributions, as measured by U^{235} and U^{238} foils, through a series of plates of various materials which were used to build up the ZPR-III critical assembly. Two cases are illustrated. In one case slabs of enriched and depleted uranium were purposely made thick to accentuate the fine structure effect. Normally, the ZPR core was built up of the thinner plates illustrated in the lower section of Fig. 2-1, and the flux variations were therefore small. For both U^{235} and U^{238} the fission rate is seen to peak in the enriched uranium slab. This peaking results from the higher neutron energy spectrum in the enriched slab, where the proportion of uncollided neutrons is greater. The peaking is much more pronounced for the U^{238} foils, as would be expected, since only high-energy neutrons fission U^{238}. The procedure used to account for the local variations in neutron flux and spectrum is to apply corrections which are either measured (if the assembly is an experimental one) or calculated from one of the better approximations to transport theory. The corrections convert the assembly to an equivalent homogeneous assembly.

The final aspect of the neutron physics problem is to account for the effects of the gross geometry of the assembly. Two-dimensional calculations are possible with digital computing machines if the number of neutron energy groups is no greater than two. These calculations, of course, amount to three-dimensional calculations if there is an axis of symmetry,

*That is, fuel elements of small cross-sectional area, closely spaced.

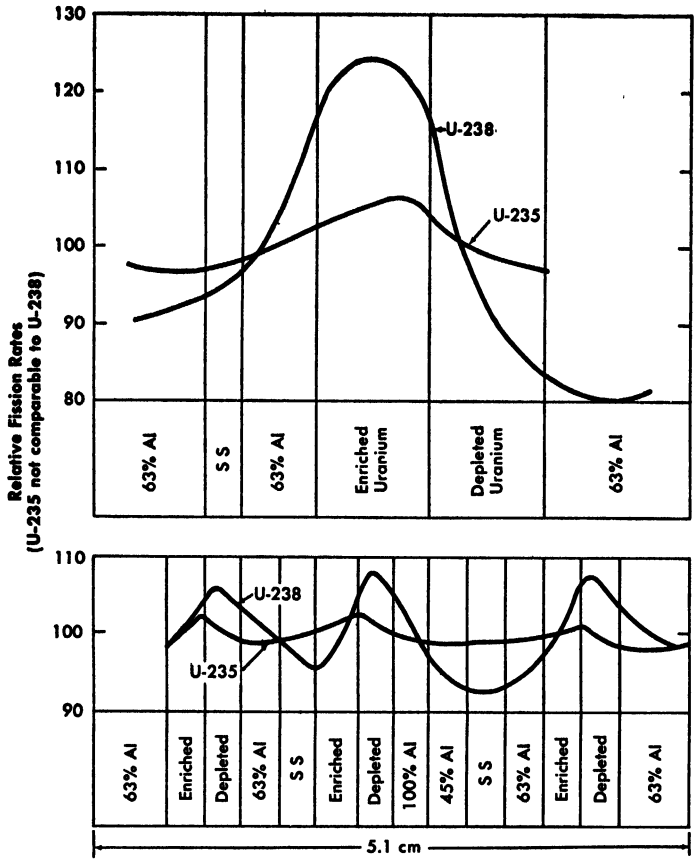

FIG. 2–1. Fission rate distribution across drawer of ZPR-III assembly with bunched materials (above) compared with separated materials. [24]

as for example in a right circular cylinder. Reasonably accurate computations can be made using only two groups of neutrons if the constants are adjusted so that the results agree with those of multigroup calculations on simpler assemblies (of the same composition). Two-group constants which have been used are given in Table 2–3. When great accuracy is not required, the usual method of one-dimensional calculation is applicable, using fundamental-mode bucklings for the dimensions not involved in the calculation. For assemblies with high volume-to-surface ratio, critical masses may be calculated by computing the critical mass of an equivalent sphere and applying an appropriate shape factor. Experimentally determined shape factors for various cases are given in Reference 14.

Although many aspects of neutron physics must be considered for the design of a reactor, much of the calculation and experimentation is di-

TABLE 2-3

TWO-GROUP CONSTANTS [16]

Material	Energy group, j*	σ_{tr}	ν	σ_f	σ_c	$\sigma_{in,\ 1\to2}$	α
Pu^{239}	1	5	2 9	1 85	0.1	0 9	0 054
	2	7	2.9	1 85	0 4	—	0.22
U^{235}	1	5	2 5	1 25	0.15	1 5	0 12
	2	7	2 5	1 5	0 4	—	0.27
U^{238}	1	5	2 5	0 522	0 05	2 1	
	2	7	—	0	0 22	—	
Fe	1	2	0	0	0 006	0.7	
	2	3	0	0	0 006	—	
Na	1	2	0	0	0 0005	0 1	
	2	3	0	0	0.001	—	
Al	1	1 7	0	0	0 0002	0 4	
	2	4 0	0	0	0 0004	—	

*Fission spectrum: $\chi_1 = 0.575$, $\chi_2 = 0.425$.
$j = 1$ corresponds to neutrons above U^{238} fission threshold (~1.4 Mev).
$j = 2$ corresponds to neutrons below U^{238} fission threshold.

rected to the critical mass of the reactor in some significant stage of operation. Critical masses of a number of fast-neutron assemblies have been determined experimentally in the ZPR-III facility. The results of these measurements are summarized in Table 2-4.

The column of Table 2-4 which shows the order of pieces in a typical core drawer can be interpreted to describe the assembly. The core structure consists of stacked 2-inch-square aluminum tubes into which fit aluminum drawers; the two halves of the core structure are loaded with these drawers from all four faces. The front drawers (2 internal faces) are 15 inches long, the back ones 17 inches long. The drawers have internal slots arranged so that plates of various materials (see Table 2-4) can be loaded into them; the plate size is 1/8 inch thick by 2 inches high and varies in length.

Assemblies 12, 14, 16, and 17 contain graphite as one of the constituents. These assemblies were made to obtain lower-energy neutron spectra, cov-

TABLE 2–4

CRITICAL MASSES DETERMINED IN ZPR-III [24]

Ass'y no.	Core description	Critical core dimensions, cm (length × diameter or length × depth × width or diameter)	Core composition, volume %					Blanket*	Order of pieces† in typical core drawer	Critical mass, kg U^{235} in core	
			U^{235}	U^{238}	Al	SS (304)	C			Expt.	CECM‡
6C		18 × 72.1	14.0	15.9	31.4	12.3		(a)	4142441424641424	221.0	
6B	1:1	20.55 × 65.6	14.0	15.9	31.4	12.3		(a)	Same as 6C	183.0	
1B	(U^{238}:U^{235})	30.7 × 46.6	14.1	16.0	31.5	12.4		(a)	Same as 6C	137.1	
2		40.8 × 40.1	14.0	15.7	31.5	12.3		(a)	Same as 6C	136.0	138.5
6D	Cylinders	56.1 × 35.7	14.0	15.7	31.4	12.3		(a)	Same as 6C	147.4	
6E		71.4 × 33.55	14.0	15.9	31.4	12.3		(a)	Same as 6C	164.2	
1A		30.7 × 38.73 × 45.4	14.1	16.0	31.5	12.4		(a)	Same as 6C	142.4	
1C	1:1	30.7 × 33.2 × 56.2	14.1	16.0	31.5	12.4		(a)	Same as 6C	151.0	
1D	Rectangle	30.7 × 27.65 × 82.5	14.0	15.9	31.5	12.4		(a)	Same as 6C	183.4	
6A		40.8 × 22.17 × 81.4	14.0	15.9	31.4	12.3		(a)	Same as 6C	194.5	
6F	1:1 Sphere	45.6	14.0	15.9	31.4	12.3		(a)	Same as 6C	131.1	133.3
3	1:1 Annular	40.8 × 17.1 (inside) × 48.6 (outside)	14.2	15.9	31.0	12.1		(b)	Same as 6C	176.9	
4	Cylinders	40.8 × 17.23 (inside) × 51.9 (outside)	14.0	15.9	31.5	12.2		(c)	4412441244644124	201.1	
5	Cylinder, Lt. Blkt.	40.8 × 43.6	14.0	15.9	31.5	12.2		(d)	Same as 4	159.5	162.8

2A	0:1 Cylinders	40.8 × 42.0	14.0	1.0	31.4	27.5		(a)	4146441464641464	147.7	150.3
9B		25.6 × 66.8	11.6	37.8	21.3	14.4		(e)	3212423(1/2)26232124	193.3	
9	3:1 Cylinders	40.8 × 46.5	11.7	38.0	21.6	15.0		(a)	421223(2/6)(1/4)26322124	151.9	156.5
15		51.0 × 57.4	9.4	31.5	19.4	11.7		(e)	55251252(5/6)2512525	220.4	226.5
9A	3:1 Sphere	50.4	11.7	38.0	21.5	14.22		(e)	Same as 9B	146.2	150.6
10	5:1 Cylinders	45.9 × 44.25	11.8	57.9	0	19.3		(e)	22216222(1/2)2622122	155.8	163.0
11	7:1 Cylinders	51.0 × 58.0	9.5	71.7	0	9.15		(e)	2221222222221222	240.6	267.0
16		51.0 × 55.9	9.4	49.6	0	9.15	20.8	(e)	2721272227221722	204.8	212.8
12	Cylinders with	45.9 × 52.75	9.4	35.4	0	9.15	36.8	(e)	2727127272712727	176.8	180.0
17	graphite	45.9 × 49.5	9.4	20.6	0	9.15	52.6	(e)	7277127772717277	156.5	158.9
14		45.9 × 46.3	9.4	0.7	0	9.15	73.6	(e)	7777177777717777	136.0	137.4

*Blanket compositions: (a) 0.19% U^{235}, 83.3% U^{238}, 2.27% Al, 7.31% stainless steel. (b) Central blanket region 17.1 cm diameter, 0.08% U^{235}, 39.7% U^{238}, 24.6% Al, 7.31% stainless steel. Outer blanket same as (a). (c) Central blanket region 17.1 cm diameter and inner annular blanket 18.1 cm thick, both of composition (b). Outer blanket 18.1 cm thick of composition (a). (d) No central blanket. Otherwise like (c). (e) 0.19% U^{235}, 83.3% U^{238}, 7.31% stainless steel.

Blanket thickness: In Assemblies 1A, 1B, 1C and 1D the full density blanket was at least 23 cm thick on all sides. In other assemblies with (a) or (e) blankets, the thickness was at least 30 cm.

Assumed specific gravities used in calculating the above volume percentages: U^{235}, 18.75; U^{238}, 19.0; Al, 2.70; stainless steel, 7.85; C, 1.45.

†Key to order of pieces:
1. 93% U^{235} (enriched)
2. 99.8% U^{238} (depleted)
3. 100% aluminum
4. 63% aluminum (perforated)
5. 45% aluminum (perforated)
6. Stainless steel 304
7. Graphite

‡CECM = corrected experimental critical mass; corrected for inhomogeneity and irregularity of edges.

ering in relatively small assemblies the range to be expected in very large fast breeder reactors.

Using these methods, the critical masses given in Table 2–4 have been predicted theoretically with reasonable success. Much better knowledge of cross sections (particularly inelastic scattering cross sections) is needed, however, before calculations from "first principles" can confidently be made. The agreement between reactor theory and experiment is discussed in some detail in Reference 14.

2–2.2 Breeding ratio. The breeding ratio is defined as the number of atoms of fissionable isotope formed in the reactor per fissionable atom destroyed. If the fissionable atom produced is of different chemical element than that destroyed (e.g., if U^{235} is consumed and Pu^{239} is produced), the ratio is often called the conversion ratio. In either case, if the ratio is exactly unity, the reactor produces as many fissionable atoms as it consumes, and the net consumption of fuel is zero. If the ratio is greater than one there is a net gain in fuel.

The breeding (or conversion) ratio R is given in terms of important reactor characteristics by the following equation:

$$R = \frac{\nu - 1 - \alpha - A - \Lambda + F(\nu' - 1)}{1 + \alpha},$$

where

A = number of neutrons captured by parasitic absorbers,
Λ = number of neutrons leaking from the reactor (core plus blanket),
F = number of U^{238} atoms fissioned,
} per fission of primary fissionable isotope

ν = number of neutrons produced per fission in fissionable isotope (U^{235} or Pu^{239}),
ν' = number of neutrons produced per fission in fertile isotope (U^{238}), and
α = ratio of capture cross section to fission cross section of the fissionable isotope.

The high breeding ratio in fast reactors results from the following: (1) the value of α is low for neutrons of very high energy. Note that α appears twice in the equation for breeding ratio, in such a way that it decreases breeding ratio in both cases. This is to be expected, since capturing a neutron in a fissionable atom wastes both the atom and the neutron. (2) The value of F, the fraction of fissions in fertile material, can be relatively large when U^{238} is the fertile material with fast neutrons. The benefits from fission of U^{238} are somewhat greater than suggested by the breeding ratio equation, for such fissions produce not only neutrons but also energy. (3) The value of A, the parasitic neutron loss, is usually

low in a fast neutron reactor. This is because the ratio of fissionable fuel to parasitic absorber is much higher than in other reactor types.

The value of α is perhaps the most important of the above characteristics. Since plutonium must ultimately be the fuel for the fast breeder reactor, the value of α for Pu^{239} has great significance. There is still some uncertainty as to the variation of α for plutonium with neutron energy, as suggested by the three sets of values included in Table 2–2. The "standard" values listed in the table are from Reference 18. Measurements of α for Pu^{239} and U^{235} in the EBR-I by radiochemical and mass spectrographic analyses have verified that the values are in the predicted range (Figs. 2–2 and 2–3).

The measured radial variations of α for Pu^{239} and U^{235} are shown in Fig. 2–3. Here, of course, α varies because the average neutron energy varies as the neutrons diffuse outward through the blanket. Since few fission neutrons are produced in the blanket except very near the core boundary, there is very little replacement of the fast neutrons as they are slowed down by scattering in the blanket. Near the outer edge of the blanket the energy spectrum is much lower because many neutrons are moderated in the surrounding graphite. The calculated curves in the figure [12] describe the neutron energy spectrum as a function of position. A region of the blanket is defined where the neutron spectrum is calculated to approach that of a large fast breeder reactor. The values of α measured in this region should therefore apply to the large reactor core. Note that the values are pleasingly low in this region. The abrupt increase in α of Pu^{239} in the low-energy spectrum near the outer edge of the blanket shows how important it is to keep the energy spectrum high when Pu^{239} is the fuel.

2–2.3 Effects of reactor size and dilution. In a small fast reactor, such as EBR-I or even EBR-II, a rather large fraction of the fission neutrons leaks out of the core. If the core is made larger, the fractional leakage becomes less and relatively more nonfissionable material can be used in the core. Obviously, as much of the diluting material as possible should be fertile, so that the neutrons can be absorbed productively. As the dilution is increased, the ratio of (macroscopic) scattering to fission cross sections will also increase, and the effective energy of the neutron spectrum will decrease. The effects of such changes can be examined by considering a series of multigroup calculations by Loewenstein and Okrent [14]. These apply to idealized fast neutron reactors of four different sizes: a small, highly concentrated reactor, a reactor of EBR-II size, a reactor of medium size (200 liters core volume), and a large fast breeder reactor (800 liters). These reactor sizes can be related to power output by assuming that the power density in the core will be one ther-

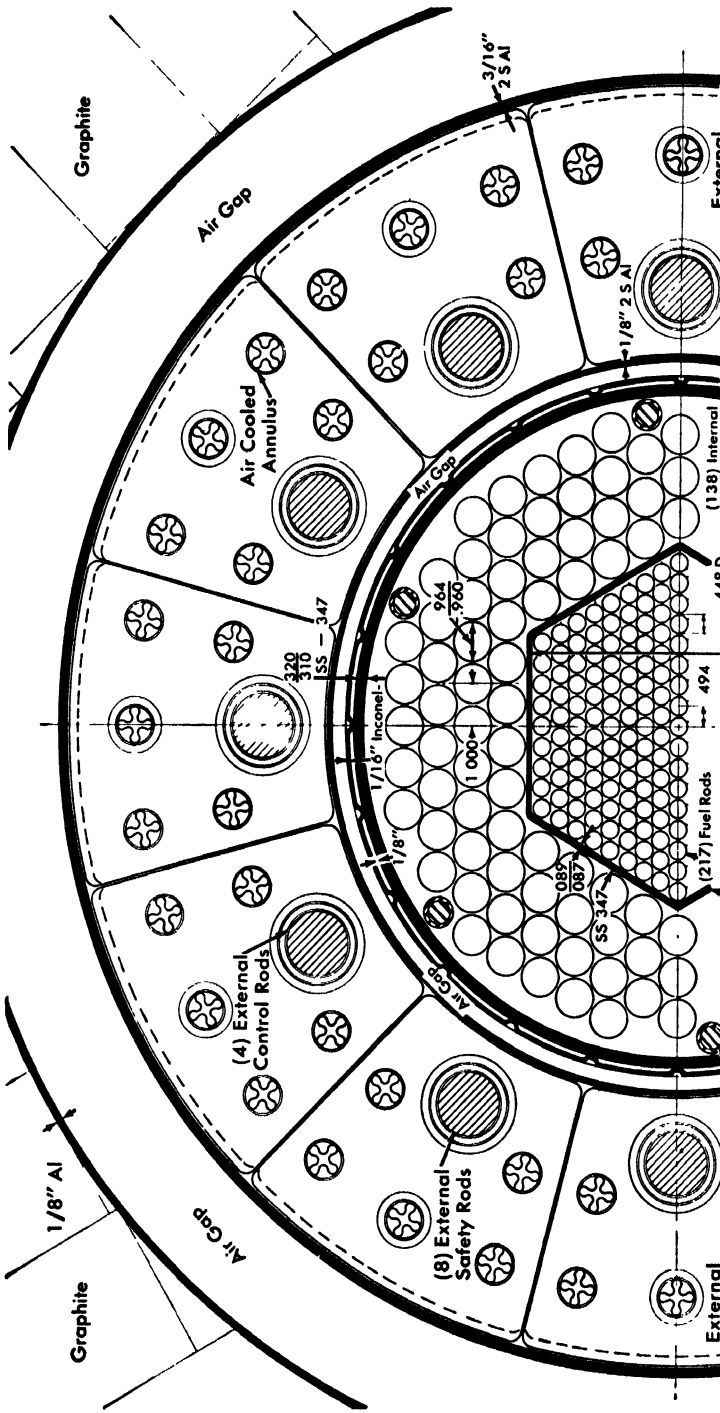

FIG. 2–2. Horizontal cross section at midplane of MARK II core (the EBR-I).

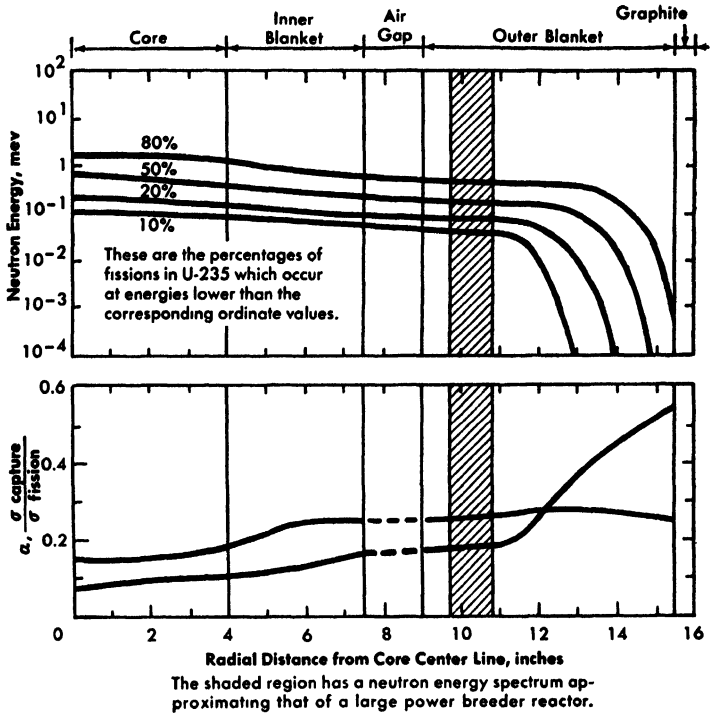

FIG. 2-3. Values of α for U^{235} and Pu^{239} in EBR-I [12,16]. (In the lower figure, Pu^{239} is the curve that rises sharply at the right.)

mal megawatt per liter. The reactors calculated are spherical, with completely surrounding blankets 45 cm thick. Both Pu^{239} and U^{235} are considered as the fissionable isotope. The results of the calculations are given in Table 2-5 (see pp. 110-113).

The effects of larger size and dilution can be observed by comparing, for example, the plutonium-fueled EBR-II reactor with the large plutonium breeder. The lower energy of the neutron spectrum in the large reactor is evident when the flux integrals for the various energy groups are compared. This lower energy means a higher average value for α in the large reactor and consequently a larger ratio of neutron captures in Pu^{239} to fissions (0.195 as compared with 0.146 for the EBR-II case). The average microscopic fission cross section of U^{238} relative to that of Pu^{239} is also lower, but this effect is counterbalanced by the larger quantity of U^{238} in the core. Thus the ratio of fissions in U^{238} to fissions in the Pu^{239} is actually much greater in the core of the larger reactor than in the smaller one (0.224 as compared with 0.119). On the other hand, with the smaller fractional leakage into the blanket of the larger reactor,

the fractional fissioning of U^{238} in the blanket is also smaller. The net result is that both reactors, as a whole, have very nearly the same ratio of U^{238} fission to Pu^{239} fission (0.28).

The proportion of structural material and coolant must, of course, be considerably greater in the large reactor; therefore the loss of neutrons to coolant and structure is also markedly larger, but it amounts to only 0.05 neutron per Pu^{239} fission. As a net result, the breeding ratio for the large reactor is somewhat, but not much, smaller than that for the reactor of EBR-II size (1.77 as compared with 1.84). Note that even in the large reactor, over half the breeding occurs in the blanket. This signifies that even in large plutonium breeder reactors, plutonium must be extracted chemically from the blanket and recycled to the core if the system is to be self-sustaining.

In a practical reactor design, conversion ratios will be lower, mostly because of difficulties in achieving an efficient blanket. For example, the breeding ratio for the actual EBR-II, when fueled with U^{235}, is estimated to be about 1.15, rather than 1.35 as indicated in Table 2–5. The discrepancy between the practical and the ideal will probably be smaller in the larger reactors, because more of the breeding is in the core.

2–2.4 Effects of other fuels. Using metallic plutonium and U^{238} for fissionable and fertile materials in the fast reactor yields the highest neutron performance. Other materials, however, have other advantages. Table 2–6 (see pp. 114–117) gives calculated characteristics for a number of spherical reactors using different materials.

The ratios of material quantities in Table 2–6 differ somewhat from those in Table 2–5. The core composition has been taken as 50% sodium, 25% steel, and 25% fissionable plus fertile material, with the blanket 20% sodium, 20% steel, and 60% fertile material. Here the proportion of structural materials and additives is higher than before, following present trends in designing fast reactors. The critical mass and breeding ratio of reactor No. 2 of this table are seen to be slightly lower than the corresponding reactor of Table 2–5. Reactor No. 3 is fueled with a mixture of 20% Pu^{240} and 80% Pu^{239}, as it might be if plutonium generated during long exposure in a thermal reactor were used as fuel for the fast reactor. The critical mass quoted is that of Pu^{239}, and the conversion ratio is based on the destruction of Pu^{239} only and production of Pu^{239} and Pu^{241}. The conversion ratio is seen to be slightly higher and the critical mass slightly lower than for reactor No. 2. This follows from the higher fission probability of Pu^{240}, compared with U^{238}.

Reactors 4 and 5 are fueled with mixtures of oxides of Pu^{239} and U^{238}. Since reactor No. 5 has the higher ratio of fuel to structure and coolant, its breeding ratio is likewise higher. In both, the neutron energy spec-

trum is considerably lower than in the metal-fueled reactors, and the loss of neutrons to structure and coolant is higher. The characteristics of reactors fueled with plutonium carbide (reactors 6 and 7) are much like those fueled with the oxide. Again higher-density fuel markedly improves the neutron performance, but, of course, at the expense of power capability.

The last two reactors of Table 2–6 utilize thorium metal as the fertile material. Reactor 8 is fueled with U^{233} while reactor 9 uses Pu^{239} as the fissionable isotope. Both reactors suffer in conversion ratio because the thorium is less fissile. Note that the neutron leakage from the blanket is high in both thorium reactors. If the thorium blankets of reactors 8 and 9 were thicker, the breeding ratio for reactor 8 might rise to approximately 1.27, while that for reactor 9 might rise to 1.40. It has been suggested in Reference 14 that the plutonium-thorium reactor might be employed in combination with a thermal reactor fueled with U^{233}, utilizing U^{238} as the fertile material. Thus the fast plutonium-thorium system would burn plutonium to make U^{233}, and this would be used in the thermal reactor to produce Pu^{239} for the fast reactor; the over-all neutron economy should be quite good.

2–2.5 Effects of absorbing materials. In most cases the neutron absorption by structural materials and coolant in the fast reactor does not represent a large neutron loss. The results of the calculations that have been discussed thus far bear this out. If materials more strongly absorbing than iron are used in the structure, however, the effect on neutron economy may be pronounced. Table 2–7 shows the effect of substituting tantalum or molybdenum for iron in various fast reactors. The reflector compositions are the same as for the reactors of Table 2–6. The effect of the tantalum is quite drastic and, as would be expected, both tantalum and molybdenum affect most the reactors of lowest energy spectrum (those fueled with oxides or carbides of uranium and plutonium). The cross sections of tantalum and molybdenum are given among the multigroup cross sections in Table 2–2.

The measured central reactivity coefficients of various materials in assembly 5 (Table 2–4) are given in Table 2–8. The central reactivity coefficient is defined as the change in reactivity caused by placing unit mass of the material at the center of the reactor core. The reactivity change is measured with respect to the reactivity of the assembly when the test space is empty. Moderating and fuel materials give strong positive reactivity increases. Most other materials decrease reactivity, although some (with small absorption cross sections in the fast neutron spectrum) show reactivity increases because of their scattering properties. Boron carbide gives a negative effect about as large as the positive

TABLE 2-7

EFFECT OF C, O, Ta, AND Mo ON CRITICAL MASS, BREEDING RATIO, AND α FOR VARIOUS REFLECTED SPHERICAL REACTORS [14]

Reactor	Volume, liters	Core volume fractions								Critical mass, kg	Total breeding ratio	Fuel captures / Fuel fissions
		Pu^{239}	U^{238}	Fe	Na	C	O	Ta	Mo			
32	800	0 046	0 204	0	0.50	0	0	0.25	0	700	1.02	0.163
33	400	0 053	0 197	0	0.50	0	0	0 25	0	404	1.13	0 158
34	800	0 033	0 217	0	0.50	0	0	0	0.25	497	1.46	0.194
35	400	0.039	0 211	0	0.50	0	0	0	0 25	300	1.57	0 183
36	800	0.0433	0 0397	0	0.50	0	0 083	0 25	0	660	0.81	0.175
37	800	0.028	0.055	0	0.50	0	0 083	0	0 25	427	1.20	0.227
38	800	0 C44	0 0585	0	0.50	0.088	0	0 25	0	671	0.82	0.177
39	800	0 0287	0.0738	0	0.50	0.088	0	0	0 25	437	1.22	0.231
2	800	0 0307	0 2193	0 25	0 50	0	0	0	0	468	1.61	0 207
4	800	0 0248	0 0582	0 25	0.50	0	0.083	0	0	378	1.37	0.257

TABLE 2-8

CENTRAL REACTIVITY COEFFICIENTS, ASSEMBLY 5 [24]

(5.1 × 5.1 × 5.1 cm samples)

Material	Reactivity relative to void, inhours/kg	Material	Reactivity relative to void, inhours/kg
C (graphite)	+85 6	Cb	−28.0
Cd	−30 4	Ti	+2 2
Fe	−8.0	I	−42.9
Sb	−36 6	Ru	−35 1
Co	+1 8	Pd	−57.8
Hg	−9 0	Te	−11 9
Ta	−38 0	Ce	−1 9
Hf	−34 3	Si	+8.2
Se	−3 7	As	−29 9
Cr	−6 4	S	−32.5
W	−17 9	CH_2 (polyethylene)	+3400
Mo	−17 0	Stainless steel*	−6 4
Li	−140	Depleted uranium*	+2 6
B_4C	−440	Enriched uranium*	+258
Mn	+3 9	Plutonium*	+498
V	+8 2		

*5.1 × 5.1 × 1.27 cm samples.

coefficient for the fertile isotopes, and so evidently can be considered as a material for control rods in fast reactors.

The reactivity coefficients, of course, are dependent upon the neutron energy spectrum. Coefficients are given in Table 2-9 for a number of different assemblies whose compositions are described in Table 2-4.

2-2.6 Kinetic characteristics. The prompt neutron lifetime in a fast neutron assembly, which is quite short, increases with higher dilution of the fuel, since the spectrum will then be less energetic. Measurements have been made of neutron lifetime in a number of ZPR-III assemblies by the Rossi α method [24], which requires measuring the time interval between consecutive pulses of a counter at the center of the reactor. The background of random time intervals is subtracted, leaving just those time intervals associated with the decay of prompt neutron chains. The slope of the logarithm of the distribution of these time intervals is the Rossi α. The prompt neutron lifetime is the ratio of β, the effective fraction of de-

TABLE 2–9

CENTRAL REACTIVITY COEFFICIENTS RELATIVE TO VOID [24]

(inhours/kg)

Material	Assembly				
	9A	11	16	12	14
131 *cm*^{3} *samples:*					
Fe	−12 7				
Al	−11 5				
Mo	−23.4	−24 3		−30 5	
Cu	−18 4				
Mn	−5 1				
Ag	−89 3				
B-10	−3560	−2761		−4258	
C		−34.6	+4.1	+34 6	+143 8
Ta		−49.4		−66 8	
Ru		−48 7		−66 7	
Nb		−35 7		−45 5	
32.7 *cm*^{3} *samples:*					
U^{233}		506		+548 3	
U^{235}		272		+287 5	
Pu		460		+479 6	

layed neutrons, to the Rossi α at delayed critical. The results of the measurements are tabulated in Table 2–10.

Determining the effective number of delayed neutrons per fission in a fast system is complicated because a fission in U^{238} yields about two and one-half times as many delayed neutrons as one in U^{235}, and because the importance of a neutron in maintaining the chain reaction depends upon its energy. The delayed neutrons, emerging with an average energy of about 400 Kev, are less effective than the prompt neutrons in promoting the chain reaction, since their energy is below the fission threshold of U^{238}. The relative worths of fissions in a number of the ZPR-III critical assemblies have been calculated by multigroup perturbation theory (Table 2–11). When the delayed neutrons from the appropriate fractions of U^{235} and U^{238} fissions in these assemblies are weighted with the relative importance of the delayed neutrons, the effective delayed neutron fractions tabulated in Table 2–12 are obtained. All these assemblies were fueled with U^{235}; in plutonium-fueled assemblies, the effective

TABLE 2-10

PROMPT-NEUTRON LIFETIME ESTIMATED FROM ROSSI-ALPHA MEASUREMENTS [24]

Assembly	Alpha ($\times 10^{-4}$ sec^{-1})	Estimated effective beta (± 0.0003)	Measured prompt-neutron lifetime ($\times 10^{8}$ sec)	Predicted prompt-neutron lifetime ($\times 10^{8}$ sec)
5	$-8\ 45 \pm 0\ 2$	0073	$8\ 6 \pm 0.4$	—
6F	$-9\ 85 \pm 0\ 2$	0073	$7\ 4 \pm 0.4$	7.0
9	-9.0 ± 0.2	0073	$8\ 1 \pm 0.4$	6.9
10	$-10\ 8 \pm 0\ 3$	0073	$6.75 \pm 0\ 4$	6.0
11	$-10\ 4 \pm 0\ 3$	.0074	$7.1 \pm 0\ 4$	6 2
12	$-6\ 85 \pm 0\ 3$	.0075	$10.9 \pm 0\ 4$	10.
17	-5.35 ± 0.15	0075	$14.0 \pm 0\ 5$	—
14	$-3\ 85 \pm 0\ 1$	0075	$19.5 \pm 0\ 8$	19.7
EBR-I mockup	$-17\ 4 \pm 0\ 4$	0068	$3.9 \pm 0\ 2$	—

delayed fraction will be considerably shorter because the delayed fraction from plutonium fission is smaller.

Delayed neutron fractions from fission in various isotopes are recorded in Table 2-13. These measurements were made [34] by irradiating appropriate fissionable samples, using sharp neutron bursts from the reactor "Godiva" and counting the delayed neutrons. The average delayed neutron yield per fission was the measured quantity. The delayed neutron fraction, β, is derived by dividing by $\bar{\nu}$, the average total number of neutrons per fission.

2-2.7 Temperature effects. Since the neutrons in a fast reactor never come into thermal equilibrium with the atoms of the reactor materials, the temperatures of these materials do not directly affect the neutron energy spectrum. The effects from thermal expansion of the reactor materials are relatively small unless displacements resulting from expansion are magnified. The calculated isothermal temperature coefficient of the EBR-II reactor is $-3.6 \times 10^{-5}(\Delta k/k)/°C$. If the core is arranged so that relative expansions of materials, or uneven expansions, can cause comparatively large mechanical motions, then reactivity may be strongly affected. An example of such an effect is fuel-element bowing, which is discussed at greater length in Section 2-3.

TABLE 2–11

RELATIVE WORTHS OF FISSION EVENTS IN TYPICAL ZPR-III ASSEMBLIES [24]

Assembly	7 (EBR-I)	2A	6F	5	9A	10	11	12	PBR*
Number of U^{238} fissions per U^{235} fission	0 18	0.18	0 24	0 23	0 27	0 30	0.36	0 32	0.28
Worth of prompt U^{238} fission neutron†	0 40	0.50	0 62	0 61	0.75	0.79	0 87	0 77	0 85
Worth of delayed U^{238} fission neutron†	0 36	0.46	0.56	0 56	0 66	0.68	0.73	0 68	0 73
Worth of delayed U^{235} fission neutron†	0.97	1 01	0.96	0.98	0.91	0 88	0 84	0 91	0 87

*800-liter dilute core with typical breeder blanket.

†Relative to a prompt U^{235} fission neutron.

TABLE 2–12

CALCULATED EFFECTIVE DELAYED NEUTRON FRACTIONS [24]

Assembly	Number of U^{238} fissions per U^{235} fission	β_{eff}	No. of inhours per dollar* of reactivity	No. of inhours per percent of reactivity
2A	0 19	0 0073	300	410
6F	0.24	0.0073	310	425
5	0 23	0.0074	307	415
9A	0 27	0.0073	318	436
10	0 32	0 0074	324	438
11	0.36	0.0074	331	447
12	0.30	0 0075	322	427
PBR (conceptual 800-liter core)	0 27	0 0072	322	447
EBR-I	0.18	0 0068	297	437

*A dollar of reactivity is defined to be the amount of reactivity required to bring the system from delayed to prompt critical (β_{eff} is one dollar of reactivity).

TABLE 2–13

TOTAL YIELDS OF DELAYED NEUTRONS FROM SEVERAL ISOTOPES [34]

Isotope	Average number delayed neutrons per fission	$\bar{\nu}$, average total number neutrons per fission	β, fraction of total neutrons which are delayed
Pu^{239} (fast fission)	0.0063 ± 0.0003	3.01 ± 0.09	0.00209 ± 0.00016
Pu^{239} (thermal fission)	0.0061 ± 0.0003	2.91 ± 0.06	0.00210 ± 0.00016
U^{233} (fast fission)	0.0070 ± 0.0004	2.63 ± 0.08	0.00266 ± 0.00017
U^{233} (thermal fission)	0.0066 ± 0.0003	2.55 ± 0.06	0.00259 ± 0.00018
Pu^{240} (fast fission)	0.0088 ± 0.0006	3.42 ± 0.20	0.00257 ± 0.00030
U^{235} (fast fission)	0.0165 ± 0.0005	2.56 ± 0.06	0.00645 ± 0.00033
U^{235} (thermal fission)	0.0158 ± 0.0005	2.47 ± 0.05	0.00640 ± 0.00032
U^{238} (fast fission)	0.0412 ± 0.0017	2.62 ± 0.13	0.0157 ± 0.0012
Th^{232} (fast fission)	0.0496 ± 0.0020	~2.3	~0.022

The Doppler broadening of resonances in the neutron cross sections of both U^{235} and U^{238} is a direct effect of temperature. Since the U^{235} has fission resonances, their broadening would tend to increase reactivity. This would be offset by decreases due to broadening of U^{238} resonances if the ratio of U^{238} to U^{235} in the reactor is large enough. Theoretical estimates of Doppler effects have predicted that the two effects will balance in the range of U^{238}:U^{235} ratios from 0.8 to 1.85 [28–31]. The estimates of Bethe [31] also indicate that the positive effect in the EBR-I reactor fueled with pure U^{235} should be approximately $dk/dt = +0.6 \times 10^{-6}/°C$. Experimental measurements have been made on mockups of EBR-II and EBR-I [32], and there have been attempts to measure the positive Doppler effects of U^{235} by oscillating the temperature of a sample of U^{235} in a critical assembly. These measurements have indicated that the effect is not large, and is probably no larger than the theoretical prediction [33].

2–3. Reactor Safety

Nuclear reactors are not considered unusually hazardous to operating personnel and others closely connected with their operation. In discussing reactor safety, attention is usually focused on the types of mishap that have an extremely low probability of occurrence, but might cause widespread damage if they should occur. Invariably, such accidents are conceived as releasing substantial fractions of the fission-product content of the reactor to the outside atmosphere. In most solid fuel reactors there are at least three barriers to such a fission product release: the fuel element jacket, the reactor vessel with its shielding and support structure, and the gastight containment building or vessel surrounding the reactor and its coolant system. The function of the containment building is simply to prevent the escape of airborne fission products which could be released by an accident. The building must be gastight and able to maintain its gastightness in the event of a reactor accident with the greatest possible energy release.

The fast reactor, while posing characteristic safety problems, has some unique advantages that can simplify containment problems. One very important characteristic is that no mechanical or chemical energy is stored in the reactor proper. With no pressurization required to achieve high coolant temperatures, the usual sources of stored mechanical energy (a high-pressure gas or a high vapor pressure liquid) are absent. The sodium coolant does not react chemically with any of the materials normally in the reactor. Sodium will, of course, burn in air, but in the reactor vessel little energy could be released rapidly by burning, even if the spaces normally filled with inert gas should somehow be filled with air. Consequently, only a nuclear power excursion could conceivably

release enough energy to breach the containment vessel. If a nuclear power excursion should rupture the vessel, then a large amount of chemical energy could be released from the burning of sodium. It is this hypothetical situation that determines the design of containment buildings for fast reactors. Of course, the oxygen available for such a reaction can be diminished by diluting the air in the building with inert gas, and this approach is followed in the Enrico Fermi Reactor. Thus it is evident that the fast reactor would be a very safe one, and design requirements for the containment building would not be stringent if it could be demonstrated that accidental nuclear energy releases could not build up high pressures in the reactor vessel.

The low excess reactivity requirement, which is characteristic of the fast reactor, decreases probability of reactivity accidents. The reasons for the small excess reactivity are:

(1) Reactivity changes due to neutron absorption by fission products are small because the fission-product content is always low relative to fissionable isotope content (for any reasonable exposure of the fuel), and because the neutron energy spectrum lies above the absorption resonances of xenon and samarium.

(2) Reactivity changes little with fuel exposure. In large fast breeder reactors the internal conversion ratio is fairly high and in all fast reactors only a small fraction of the fissionable isotope can be burned out of the fuel in any one exposure.

(3) The temperature coefficients of well-designed fast reactors are small because (a) there is no appreciable neutron temperature effect from varying reactor material temperature, and (b) the reactivity is not sensitive to the sodium density.

Because of these characteristics it is feasible to design a fast reactor to operate with a total excess reactivity less than the delayed neutron fraction. Such a reactor cannot be made prompt critical by any manipulation of the controls. This limitation, used in the Enrico Fermi Reactor, is important to the over-all safety of the reactor. However, it is also an important limitation on reactor performance, and consequently would probably be unacceptable in a reactor using plutonium as fuel, because of the smaller fraction of delayed neutrons produced in plutonium fission. The low total excess reactivity does, however, offer an advantage that is available to all fast reactors, i.e., the feasibility of inserting reactivity very slowly for normal operation and control. Avoiding all possibility of rapid reactivity insertion under normal operating conditions is a real and practical contribution to safety.

Certain peculiar characteristics of a fast reactor make it difficult to ensure that a nuclear power excursion cannot possibly release destructive mechanical energy:

(1) The short prompt neutron lifetime favors very rapid increases in power level, should the reactivity ever exceed prompt critical.

(2) Although the excess reactivity may be held quite small so long as the normal structure of the reactor is maintained, the potentially available excess becomes very large if the normal structure is disturbed, as in the case of an extensive core meltdown. It is because of this, and because power densities are so very high, that the fast reactor must be meticulously designed to ensure adequate cooling under all conceivable conditions of operation and shutdown.

(3) Because of the very short neutron lifetime, it is extremely important to eliminate effects that could conceivably give positive power coefficients of reactivity, and to avoid design features that could possibly lead to instabilities capable of causing increased reactivity. The problem of eliminating such possibilities is complicated, because small changes in relative positions of fuel elements can substantially change the reactivity of fast reactors.

In the following sections the above three nuclear characteristics are treated at greater length because they are uniquely involved in the analysis of the safety of a fast reactor, and not because they necessarily make fast reactors less safe than other types.

2–3.1 Neutron lifetime. The prompt neutron lifetime for fast power reactors is usually of the order of 10^{-7} sec. The calculated lifetime for the EBR-II reactor is 0.8×10^{-7} sec, and for the Enrico Fermi Reactor 2×10^{-7} sec. Lifetimes for very large reactors will be somewhat longer, but not longer by an order of magnitude.

If excess reactivity of some magnitude is inserted into a nuclear reactor the power level will increase in a characteristic manner. After a short time the increase becomes exponential, with a period determined by the amount of excess reactivity, the prompt neutron lifetime, and the characteristics of the delayed neutrons. Figure 2–4 shows how this period of exponential increase is related to the excess reactivity for three different prompt neutron lifetimes for reactors fueled with U^{235}. The curve for the lifetime of 6.17×10^{-9} sec was determined experimentally for the Godiva Reactor. The curve for lifetime 2×10^{-7} sec can be considered typical for fast power reactors, while that for 5×10^{-5} sec is in the range for water-moderated thermal neutron power reactors. In Fig. 2–4 the reactivity is expressed in dollars. The relationship of the dollar unit to the fractional reactivity varies from reactor to reactor, depending on the fraction of delayed neutrons. A reactivity change of \$1 is defined as the reactivity difference between delayed critical and prompt critical. Therefore, in Fig. 2–4, the excess reactivity of \$1 corresponds identically to prompt criticality. From the curve for neutron lifetime,

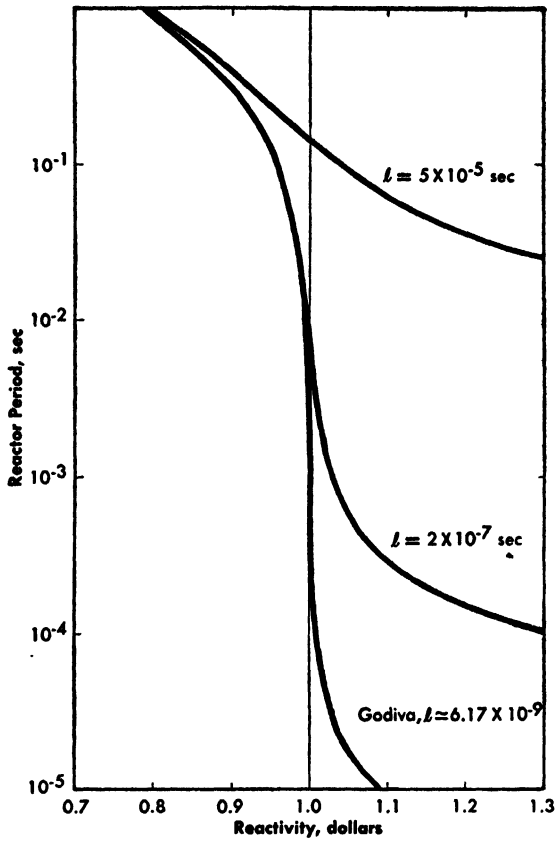

FIG. 2–4 Asymptotic period of exponential power rise due to excess reactivity in reactors having three different effective prompt neutron lifetimes. (General Nuclear Engineering Corporation)

2×10^{-7} sec, near the point of prompt criticality, it is evident that an increase of only 10ϕ would shorten the reactor period from 0.14 sec to 0.0006 sec. This amount of reactivity change corresponds to 0.07% k_{eff}, or 30 inhours. Clearly, if the reactivity in a fast reactor should ever become as high as prompt critical, a very small increment would increase the rate of power generation drastically. Any positive power coefficient of reactivity, however small, would therefore be dangerous in the vicinity of prompt criticality.

2–3.2 Reactivity increases due to structural failures. Most fast power reactors consist of several potential critical masses, which collectively are just critical in the reactor because they are diluted by the coolant. Furthermore, in such reactors the ratio of structure volume to fuel-element

volume is small. Should the fuel elements melt because of some accident (either a relatively mild nuclear power excursion or simply a failure of cooling), then the subsequent movement of the fuel would be little restrained and very difficult to predict. If the molten fuel can possibly rearrange itself into a more compact mass than the original, then the reactivity may increase by a large amount.

In analyzing a postulated meltdown accident, two primary problems are involved. One is the question of how much reactivity results from the meltdown or, more precisely, the rate of reactivity addition at the time when prompt criticality is reached, since shortly thereafter the reactor will be broken up by the energy generated in the nuclear excursion. The second question is how much nuclear energy is generated as a result of a given reassembly rate. Both problems involve unknown quantities, and the former must take into account a very wide range of possibilities. The estimation of both quantities is discussed in Reference 35.

Rates of reassembly of the core after meltdown may be determined by both the force due to gravity and forces due to the sodium coolant. The effects of gravity can presumably be predicted if they can be isolated, and in some reactor designs, notably the British Dounreay design, there are provisions to promote the fall of molten fuel to regions where criticality will not occur. Probably such an arrangement would be effective only when the fuel melts slowly, as for example when cooling fails. The sodium effects are more complex, including those of flow velocity and vaporization. In the one case where actual meltdown of a fast reactor core has occurred, the EBR-I case [35–37], subsequent examination of the core showed that the density of the fuel near the core center had been substantially reduced, presumably an effect of sodium vaporization [38]. Since the core regions that produce highest power density are usually also most important for reactivity, forces from sodium vapor should, on the whole, move fuel material away from regions of high importance and thereby decrease reactivity. Such a qualitative argument, however, cannot dispose of the problem, particularly with rapid fuel melting, when inertial forces might appreciably modify the dynamics. Attempts to set upper limits on possible reassembly rates caused by both gravity and coolant forces have led to the estimation of rates between $0.4(\Delta k/k)$/sec and $9(\Delta k/k)$/sec [33]. It is generally agreed that such estimates are pessimistic; much of the uncertainty stems from the difficulty of setting limits on the extremely complex problems by means of a relatively simple model.

Once a rate has been established (or assumed) for the reactivity insertion due to reassembly of the core there are still major uncertainties in evaluating the energy release of the nuclear excursion. The equation

of state of the reactor material at high temperatures is not known, and the very complexity of the problem inhibits accuracy. Energy release is estimated by a method originated by Bethe and Tait [39]. Later calculations [33] with rates of reactivity increase assumed in the range from \$10/sec to \$1000/sec have given total energy releases in EBR-II that vary from 0.65×16^{16} to 4×10^{16} ergs; for the larger Enrico Fermi Reactor approximately five times these values are estimated. An energy release of 10^{16} ergs (1000 Mw-sec) is about equal to that from 500 lb of TNT. The energy release in the one reactor that has been experimentally destroyed by its own power (the BORAX-I) was measured to be 135 Mw-sec. Thus quite substantial energy releases would be possible from fast reactors if rates of reactivity insertion were great enough, but the releases are comparable with those from reasonably small amounts of chemical explosives, and it should be possible to confine them in practical containment structures.

2–3.3 Reactivity coefficients and reactor stability. Whenever reactor power is changed, the over-all reactor temperature and the temperature distribution usually change as well. If reactivity changes follow, the reactor is said to have a power coefficient of reactivity that is due to the temperature changes. In certain reactors the power coefficient of reactivity may depend also on other kinds of changes (e.g., changes in xenon concentration). In the fast reactor, however, all known power coefficients of reactivity are related to either temperatures or temperature gradients. The components of the temperature effects may be varied and complex, as illustrated by the calculated components [33] of the isothermal* temperature coefficients of reactivity for the EBR-II and the Enrico Fermi reactors, given in Table 2–14. Note that all components of the coefficients in this table are negative in sign. This is important because of the special significance (mentioned earlier) of prompt coefficients in the vicinity of prompt criticality. The isothermal coefficients of Table 2–14, by definition, do not include effects of temperature gradients.

A reactor with a power coefficient of reactivity can be considered as part of a feedback loop. If increasing power causes reactivity to increase, the power coefficient of reactivity is positive and the loop has positive feedback; conversely, a reactivity decrease with increasing power means a negative coefficient or negative feedback. The power coefficient of reactivity is conveniently expressed as the ratio of the reactivity change

*In this context, *isothermal* means that the temperature of the reactor is assumed to change uniformly.

TABLE 2-14

CALCULATED ISOTHERMAL TEMPERATURE COEFFICIENTS OF REACTIVITY [33]

Mechanism	$(\Delta k/k)/°C \times 10^{-6}$	
	EBR-II	Fermi
Core:		
Axial fuel expansion	−3.9	−2.5
Radial fuel expansion (Na expulsion)	−0 9	−0.6
Density change of coolant and subassembly material	−9.1	−7.1
Structure expansion	−9.7	−6 0
Blanket:		
Density change of coolant and subassembly material	−9 5	−3.3
Growth of uranium	−1.0	−0.5
Structure expansion	−2 0	−0 6
Total	−36.1	−20 6

to the related power change (the latter expressed as a fraction of normal operation power, p_0):

$$\text{Power coefficient of reactivity} = \frac{\Delta k/k}{\Delta p/p_0}.$$

Unless there is some kind of reactivity feedback in the reactor system (either from a power coefficient of reactivity or from an artificial control system), the reactor system is not a closed servo loop, and it is meaningless to speak of the "stability" or "instability" of the system. Without feedback power would stay constant only if the reactor were exactly critical, a situation that cannot be attained in practice. With a power coefficient of reactivity, the system becomes a closed loop. If the reactor has a positive power coefficient of reactivity, it is unstable; if it has a negative coefficient the power tends to be self-regulating. Regulation may be good or poor, depending on the size of the coefficient, and the system may be stable or unstable, depending on the magnitude of the coefficient and its time lag. Obviously, more complex cases may exist in which the various components of the total power coefficient of reactivity

have different time lags. This will in fact be the case expected in a practical reactor such as that exemplified by Table 2–14.

By proper design the power coefficients for a fast reactor can be made negative, small, and rapid in response (because of the high heat-transfer ratio). All these factors tend to produce coefficients that lead to stability. However, most fast reactors, as previously explained, are particularly sensitive to reactivity changes caused by fuel position changes. This characteristic can be described very roughly in terms of a "coefficient of compaction." If, for example, a reactor core is made smaller by uniform compaction, its reactivity will increase. From this follow the large reactivity increases postulated in assumed meltdown accidents. For a bare spherical reactor, the coefficient of compaction can be expressed as the ratio of the fractional change in reactivity to the fractional change in radius of the sphere. It has been shown [2] that for the spherical bare reactor this coefficient is given approximately by

$$C = \frac{\Delta k/k}{\Delta R/R} \simeq 4\,\frac{k-1}{k},$$

where R is the reactor radius and k is the infinite multiplication constant. The effect of a reflector or blanket (assumed not to participate in the compaction) will be to reduce the coefficient by some factor, of the order 2, depending on the core and reflector size and composition. Even quite large fast reactors have values of k in the vicinity 1.4 to 1.5, and the EBR-II reactor has k near 2.0. Therefore these reactors will be sensitive to any motions of the fuel tending to move it into a more compact configuration.

Ordinary expansions of the fuel and structure will, of course, tend to decrease the average density of the core—the opposite of compaction. There are, however, possible ways in which a compacting effect can occur. For reactors with long thin continuous fuel elements the two possibilities are buckling and bowing of the elements. If its longitudinal expansion is restrained by the structure, the element may buckle, and the center portion of the element may move laterally toward the center of the core. Buckling can be avoided by avoiding restraints on expansion. Bowing is caused by greater expansion of one side of the fuel element than of the other. The parts of an individual fuel element closer to the center of the reactor will become slightly hotter and expand more than the parts away from the center, and the fuel element will bow with its convex side toward the center of the reactor. If the fuel element is restrained laterally at both ends the bowing will move the center of the fuel element toward the reactor center and increase reactivity (resulting in a positive power coefficient of reactivity). If points of restraint

are properly selected, the direction of motion from bowing can be controlled, and indeed the net motion can be made small. These effects can occur in fuel element assemblies as well as in individual elements. The fast reactors now being built have been designed with a great deal of attention to fuel-element bowing and buckling, and no undesirable power coefficients of reactivity are expected from these causes.

Much thought has been given to the problem of fuel-element bowing, following the experience with the EBR-I. Early in the operating history of this reactor a positive component of the temperature coefficient of reactivity was detected. It was demonstrated by an experiment in which the coolant circulation was stopped, a small excess reactivity was introduced, and the power was allowed to rise until it attained a value in the normal operating range of the reactor. As the power increased the exponential period of power increase became shorter, indicating that the reactivity was increasing. Later it was observed that when the reactor was operated under abnormal conditions of power and coolant flow, i.e., with less coolant flowing than normal for the particular power output, the power would oscillate with a period of about 30 sec. In some cases the amplitude of the oscillation was seen to increase with time, and it was presumed that the oscillation was unstable, but the reactor was shut down before the amplitude of the reactivity changes became dangerously large.

Later the power oscillations were studied by means of the reactor oscillator technique. This experimental method consists of imposing a sinusoidal oscillation on the reactivity and observing the reactor power response. By this means, analogous to the usual frequency response analysis of any dynamic system, resonant frequencies of the reactor can be detected at power levels that are too low to involve any danger of reactor instability. The results of the oscillation measurements were reported by Brittan [37]. By analyzing the shapes of the reactor resonance curves found by such methods, Bethe found that the combination of a positive power coefficient of reactivity of 0.8×10^{-3} with a time constant of approximately 1 sec, and a negative coefficient of -3.8×10^{-3}, with a time delay of 10 sec, would account for the shapes of the power response curves [40]. These power coefficients would correspond to temperature coefficients of 0.6×10^{-5}/°C and -3.0×10^{-5}/°C, respectively. Thus there is a positive component to the power coefficient, but it is considerably smaller than the negative component, and consequently the net coefficient of the reactor would be negative for slow power variations. However, since the positive coefficient has the shorter time delay, it is the one that would be operative in any fast reactor accident.

Neither the small positive coefficient of reactivity nor the potential instability of the reactor caused difficulties in the normal power operation of the EBR-I, which was carried on without mishap for several years.

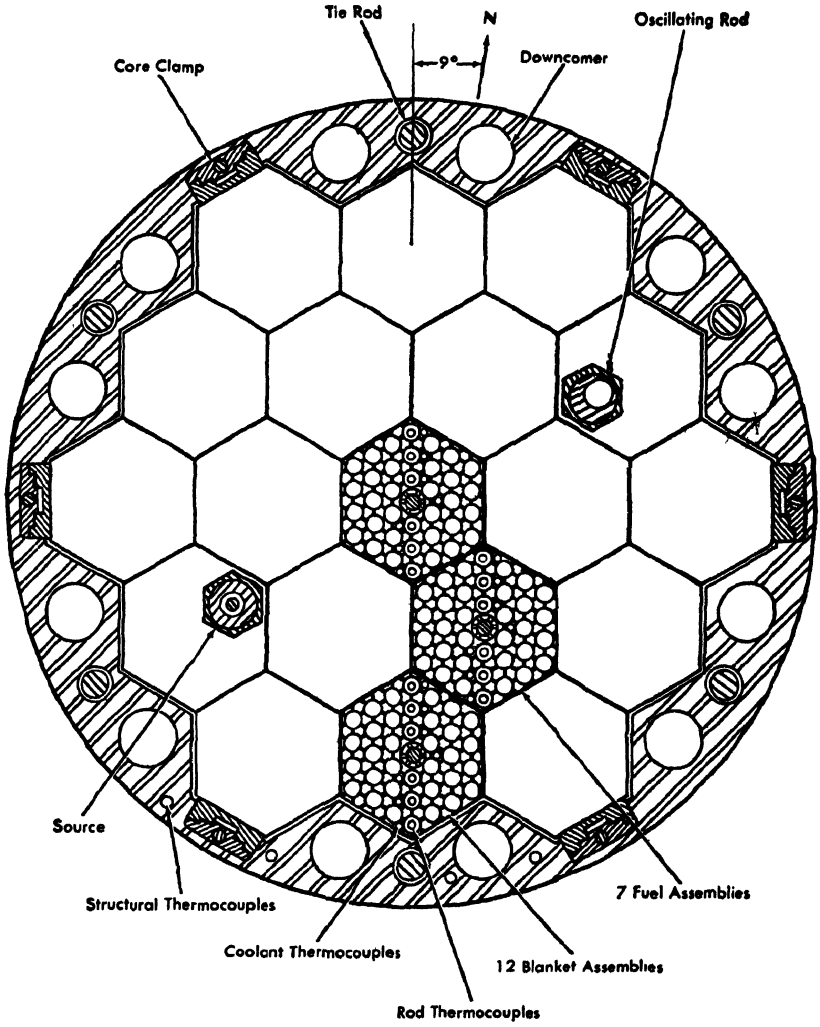

FIG. 2–5. Cross section view of MARK-III core. [42]

Then, during further experiments to determine more precisely the characteristics of the positive power coefficient, the reactor power was allowed to rise to an excessive value and the core melted [41]. However, even this did not result in hazard to personnel.

After many analyses of possible reactivity effects in the EBR-I reactor, it was concluded that only bowing of the fuel elements could reasonably have caused the observed characteristics. To test this hypothesis, a new core (the MARK-III core) was designed for the reactor,

in which the possibilities of bowing were reduced to a minimum. The new core design is described in Reference 42. In the two previous cores used in EBR-I (MARK-I and MARK-II), the fuel rods were restrained and held in place individually by upper and lower holding plates. In the MARK-III design, the fuel rods, of diameter 0.4 inch, are assembled into hexagonal subassemblies containing 36 rods each. On the ends of the fuel rods are triangular adapters that fit into locating holes in a rod sheet at the bottom of the subassembly structure. Longitudinal external ribs on the rods act as spacers, and a tightening mechanism at the center of the subassembly forces the rods against each other and against the hexagonal steel subassembly wall. The mechanism can be tightened after the subassemblies are installed in the reactor, and loosened for removal of individual rods. The subassemblies, in turn, are held in a firmly packed array by core clamps around the periphery of a form-fitting retainer ring. The core is thus restrained against bowing of either fuel rods or subassemblies.

The core is made even more rigid by using coextruded zirconium-clad uranium rods, rather than the steel-canned, sodium-bonded rods of the MARK-I and MARK-II cores. Two modes of coolant flow are provided: a series path, first through the blanket and then through the core (as in MARK-I and MARK-II), or parallel paths through the blanket and core. A diagram of the MARK-III core is given in Fig. 2–5. The previous cores are described in Reference 3. In the MARK-III arrangement the reactor can be operated with either flow path.

Oscillator experiments made with the new MARK-III core have led to the following conclusions [43]:

(1) The rigid arrangement of the fuel rods eliminates the positive temperature coefficient of reactivity observed in the MARK-I and II designs.

(2) A slight increase (about 8%) in the amplitude of the transfer function in the vicinity of 0.06 to 0.15 cps is a direct result of feedback from a strongly negative power coefficient of reactivity.

(3) The frequency-dependent feedback is in qualitative agreement with the model discussed by Kinchin [44] and Bethe [40].

(4) The reactor is stable to impressed reactivity oscillations for power levels below a hypothetical value of roughly 18 Mw. (The normal maximum operating power of the reactor is 1.4 Mw.)

(5) No significant changes in reactor behavior were seen to result from changing from series to parallel coolant flow.

Results of one of the oscillation tests [43] on the MARK-III core are given in Fig. 2–6. The transfer function, as determined from the oscillator test, is defined by curves of (1) the amplitude response of reactor power to the sinusoidal reactivity oscillation, and (2) the phase lag

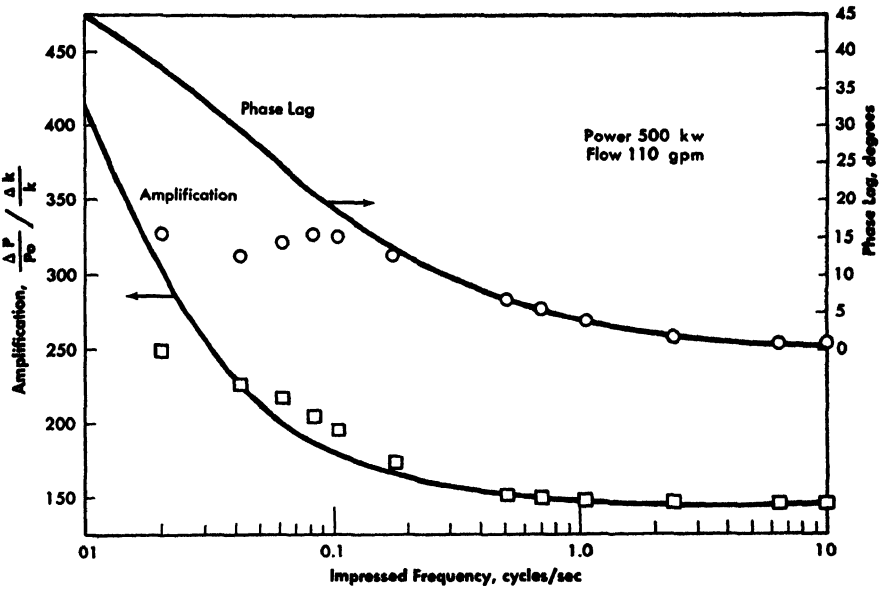

FIG. 2–6. Transfer function of EBR-I with MARK-III core (parallel flow). [43]

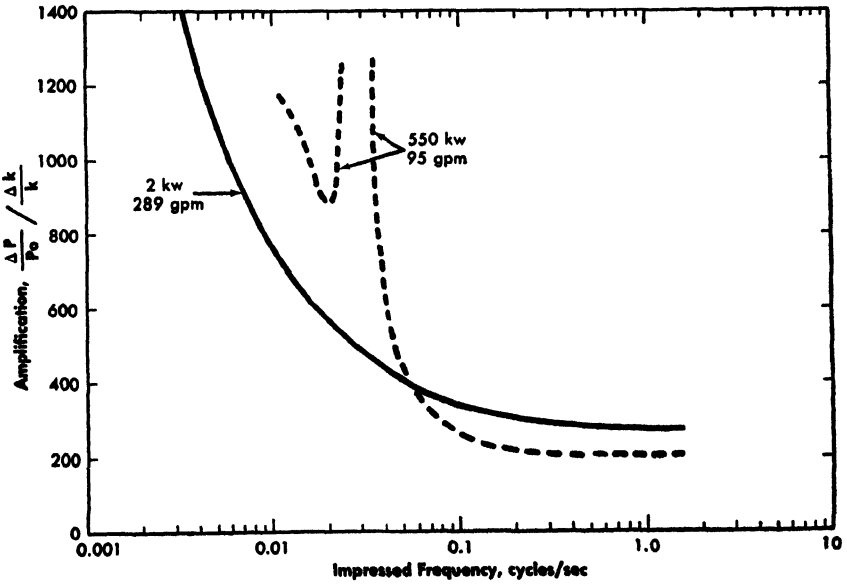

FIG. 2–7. Transfer function of EBR-I with MARK-II core. [37]

of the power response behind reactivity. The measurement was at a reactor power level of 500 kw with an abnormally low coolant flow rate of 110 gpm. The plotted points are the results of the experiment, and the solid curves show the results adjusted for essentially zero power (so that there is no appreciable effect of the power coefficient of reactivity). The deviations from the solid curves at low frequencies are caused by the negative power coefficient of reactivity. There is no indication of instability.

Figure 2–7 gives the amplitude response of the MARK-II reactor under similar operating conditions [37]. In this figure the solid curve is the zero power curve, and the dashed curve is the one taken with the reactor under power. The resonance in the reactor response is obvious.

2–3.4 Summary. Present fast reactor designs achieve safety by assuring coolant flow in all conceivable circumstances, by limiting available reactivity and reactivity insertion rates, by careful fuel element and fuel assembly design, and by providing adequate (and relatively expensive) containment structures. There remain areas of uncertainty in the analysis of reactor safety, primarily in the estimation of (1) possible reactivity increases due to core meltdown and (2) energy releases resulting from such reactivity increases. Fuel-element bowing, an important factor in the power coefficient of reactivity, is controllable by careful design of fuel elements and fuel assemblies. Much of the uncertainty once connected with the behavior of the EBR-I has been resolved [45] and the reactor oscillation technique has been established [40] as a practical method for safely determining reactor stability.

2–4. Sodium Plant Technology

2–4.1 Introduction. Thus far in the development of fast breeder power reactors no other coolant has been found competitive with liquid sodium. If, as seems probable, sodium continues to be the unique coolant for this application, improvements in fast reactors may often depend upon developments in liquid sodium technology. The present status of sodium and sodium-potassium coolant technology in the United States is summarized here. More detailed information is to be found in the references of this chapter and of Chapter 3, particularly in *The Liquid-Metals Handbook, Sodium-NaK Supplement* [46].

Briefly, the following sections will describe fundamental chemical and physical properties, advances in the use of full-scale pumps and other equipment, and advances in liquid metal transfer and handling systems. In general, "sodium" and "NaK" will be used interchangeably with reference to equipment.

TABLE 2–15

COMPARISON OF REACTOR COOLANTS

	Sodium	NaK eutectic	Ordinary Water	Carbon dioxide
*Assumed heat-transfer conditions**				
Pressure, psia	100	100	2000	300
Temperature, °C	300	300	300	300
Heat and mass transfer properties				
Boiling point, °C	880 (1 atm)	780 (1 atm)	336	—
Melting point, °C	98	−11	—	—
Heat capacity, cal/(g)(°C)	0.31	0.21	1.30	0.23
Thermal conductivity watt/(cm)(°C)	0.76	0.26	0.0007	0.004
Viscosity, centipoises	0.35	0.28	0.09	0.03
Nuclear properties				
Thermal microscopic absorption cross section, barns	0.5	1.7	0.7	0.003
Moderating ratio, $\sigma_s\xi/\sigma_a$	0.5	0.1	150	200
Induced activity	Na^{24} 15h; 1.38-, 2.75-Mev γ	Na^{24} 15h, 1.38-, 2.75-Mev γ; K^{42} 12.4h, 1.5-Mev γ	N^{16} 7.3s; 6-Mev γ	N^{16} 7.3s; 6-Mev γ

*Possible reactor operating conditions.

Compared with water or gas, sodium has the following advantages as a heat-transfer medium: high thermal conductivity, high transfer rates at moderate velocities, low film temperature drops, high boiling temperatures (good power plant efficiency), low operating pressure, no thermal or radiation decomposition, and chemical compatibility with uranium. In addition, the thermal neutron absorption cross section of sodium compares with that of ordinary water, but its moderating ability is weak (see Table 2–15), as is necessary for the coolant of a fast-neutron reactor. The corrosion properties of sodium are favorable; properly purified, sodium is practically noncorrosive to many high-temperature steels and is compatible with a number of other useful metals, such as zirconium and niobium.

The undesirable features of sodium as coolant are (1) it reacts violently with moist air and water, (2) high purity is required, (3) leakage must be kept small, (4) its melting temperature is relatively high (see Table 2–15), (5) large temperature rise is necessary for high densities of heat transport, and (6) radioactive isotopes with relatively long decay half-lives are formed by neutron capture. Despite these shortcomings, successful large-scale heat-transfer systems are operating with sodium. Thus operating feasibility has been established, but economy and ease of maintenance need to be improved.

2–4.2 Properties and characteristics of sodium and NaK. Sodium, produced commercially by electrolysis of molten sodium chloride, is available in various purities; the regular commercial grade is ~99.8% sodium and the high-purity grade (filtered) is ~99.9% sodium. Sodium-potassium alloys (NaK), produced commercially by distilling the reaction products of potassium chloride and sodium, are available with total impurity of approximately 100 ppm. In Table 2–16 some properties of sodium and NaK [47] are compared with those of water, lithium, and the lead-bismuth eutectic. Sodium, NaK, ordinary water, and carbon dioxide are compared in Table 2–15 for conditions of temperature and pressure commonly found in reactor designs. The sodium-potassium equilibrium phase diagram, Fig. 2–8 [48], shows the eutectic composition at 77.2% potassium, with a melting point of −12.3°C (9 9°F).

Thermal and fluid properties. One significant characteristic of liquid metals is their high thermal conductivity, which permits heat to be readily conducted through narrow channels independent of convection or eddy current diffusion. In fluid-flow heat transfer this effect is reflected in a low Prandtl modulus and in a low temperature drop across the laminar-flow boundary layer. A low Prandtl number means that wall temperatures of materials in contact with the sodium will follow closely the bulk stream temperature. The combination of high thermal conductivity, reasonably high specific heat, and density in a favorable range accounts for the high heat-transfer performance of sodium systems (Table 2–15).

Of the many factors involved in designing a heat-transfer system, two in particular are influenced by the differences between sodium (and NaK) and other coolants. These are system pressure and fluid velocity.

Sodium, with a melting point of 208°F and a boiling point of 1618°F at a pressure of one atmosphere, can accommodate a wide temperature range. Hence the system need not be pressurized to accommodate the high temperatures desired in a heat-transfer cycle. The system pressure is determined, instead, by the pressure drop required to circulate the sodium at the desired velocity.

TABLE 2-16

THERMAL AND FLUID PROPERTIES OF COOLANTS [49]

	Water		Sodium	56% Na 44% K	Lithium	Pb-Bi eutectic
Pressure, psia	14 7	1500	14 7	14.7	14.7	14.7
Boiling point, °F	212	596.23	1618	1518	2403	3038
Freezing point, °F	32	—	208	66.2	354	257
Density, lb/ft^3, at:						
100°F	62 0	—	—	51.6	—	—
500°F	—	48 6	53 3	52.9	31.3	646
1000°F	—	—	51.1	48 7	29.8	624
Specific heat, Btu/(lb)(°F), at:						
100°F	0.9976	—	—	0.2733	—	—
500°F	—	1 165	0.3150	0 2583	1.000	0.035
1000°F	—	—	0 3005	0.2486	1.000	0.035
Heat-transfer coefficients,* Btu/(ft^2)(hr)(°F), at:						
100°F	3970	—	—	7870	—	—
500°F	—	6030	15200	7630	14100	7150
1000°F	—	—	13200	7400	13900	8120
Pumping power for equivalent heat removal† for °F temperature rise at:						
100°F	1 000	—	—	57.8	—	—
500°F	—	0 674	26 5	48 7	3.16	134
1000°F	—	—	34 0	63 4	3.41	133
Pumping power for equivalent volumetric flow‡ at:						
100°F	1 00	—	—	0.758	—	—
500°F	—	0 544	0.717	0.662	0.457	7.39
1000°F	—	—	0.625	0.582	0.418	6.63
Pressure, psia	14 7	100	500	14 7	100	500

*Water and metal coolant coefficients determined for a velocity of 20 fps in a ½-inch ID tube.

†Normalized to a value for water at 100°F and 14.7 psia with a velocity of 20 fps in a ½-inch ID, 10-ft-long tube.

‡Water and metal coolants normalized to water at 100°F, 14.7 psia with a velocity of 20 fps in a ½-inch ID, 10-ft-long tube.

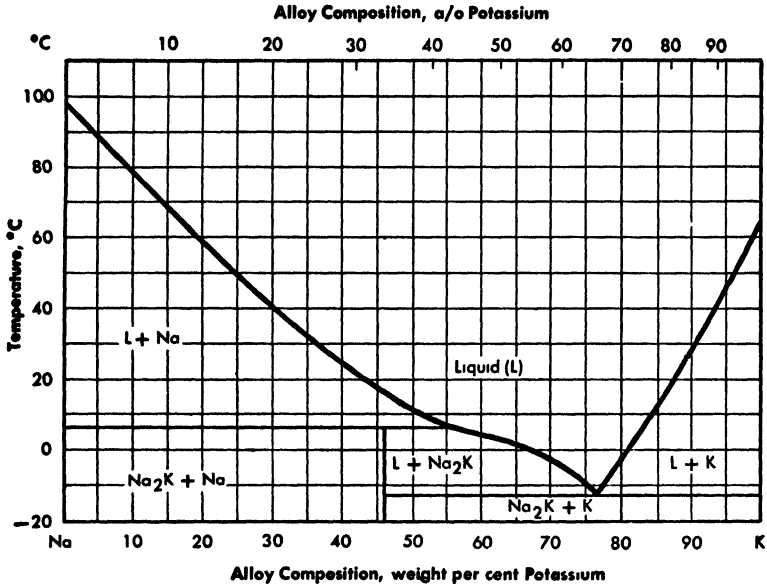

FIG. 2-8. Sodium-potassium phase diagram [48]

Fluid velocity in a coolant system is often limited by the cost of pumping power, although in some cases, heat-transfer requirements may take precedence and dictate higher velocities. No definite limit for fluid velocity in a sodium or NaK system has been established; design velocities of 30 fps, 40 fps, and even higher are being considered. Velocity has been found to have little, if any, effect on corrosion.

Another factor affecting both system pressure and velocity is the problem of cavitation, which can occur at points where the liquid pressure equals the vapor pressure at the existing temperature The vulnerable areas are the pump and other points where local increases in velocity can produce such pressure conditions.

One very important problem in liquid metal systems is that substantial temperature differences can develop in solid components in contact with the liquid metal. Such temperature differences can cause serious thermal stresses. Those that usually give trouble in sodium systems are the transient thermal shock stresses caused by sudden changes in surface temperature. Thermal shock can cause immediate failure of brittle materials, but thermal stress fatigue failures in more ductile materials, after a number of thermal shock cycles, are more common.

Thermal stresses can be important in liquid metal systems because the high heat-transfer rates permit large temperature differences to develop in metallic structures. Certain metals, notably the austenitic steels,

are more susceptible to thermal stress damage than other structural metals because of a unique combination of the important physical properties, particularly low thermal conductivity coupled with high thermal coefficients of expansion.

Corrosion. There are two fundamentally different corrosion processes operative in sodium. The first is a property peculiar to this class of coolant: alloying elements of structural material will go into solution in sodium, unoxidized. The second involves chemical reactions between metal surfaces and impurities in the sodium. Although equilibrium solubilities depend little on sodium purity, solution corrosion phenomena may be significantly affected by impurities.

Dissolution can lead to a major form of corrosive attack in sodium, i.e., the mass transport of alloying constituents from one surface to another The severity of mass transport depends on the temperature and the particular alloy system in use. The most detrimental type of mass transport occurs because solubility varies with temperature. In a monometallic, isothermal system, corrosion stops when the liquid metal becomes saturated with alloying constituents In a power system, power generation is accompanied by heat removal and a corresponding temperature drop Even where solubility is very low, excessive corrosion can occur in systems where there is lower solubility at lower temperatures, since then dissolved material precipitates, relieving a supersaturated condition.

Mass transport is increased by oxygen in sodium or NaK, although it occurs also in pure sodium or NaK. Therefore, in high-temperature operation, oxygen content must be low enough to both minimize oxidation reactions and avoid detrimental mass transport.

Preferential attack can occur on alloys containing soluble constituents. The general behavior of materials in sodium is summarized in Fig. 2-9 [47]. Because tin, zinc, and the noble metals are highly soluble in sodium, alloys containing these materials are extremely susceptible to attack. Thus silver solders and copper-tin bearing alloys are not to be used in alkali liquid systems. Most materials usable in sodium are ferrous-base. Almost all the sodium experience to date has been with the austenitic stainless steels of the basic 18% Cr-8% Ni composition. In early work, columbium-stabilized, type-347 stainless steel was used because carbide stabilization was thought necessary for corrosion resistance. The ferritic alloy steels are more susceptible to oxidation in sodium containing sodium oxide than are the austenitic stainless steels, but the differences become less with higher chromium content.

Corrosion from chemical reactions arises from the presence of impurities in the liquid metals. Although most contamination can be reduced to very low levels, it is extremely difficult to remove trace amounts of

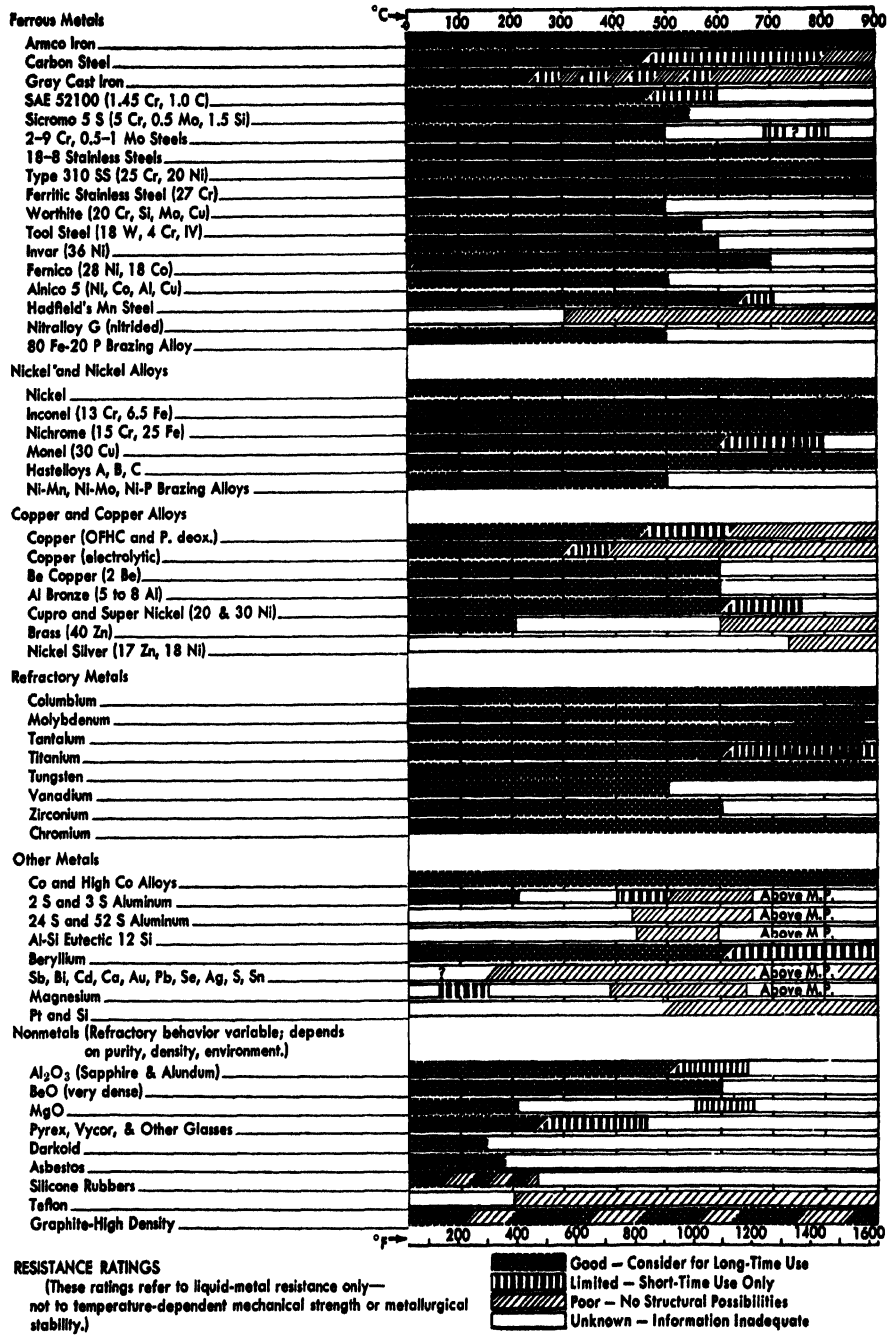

FIG. 2-9. Resistance of materials to liquid sodium and sodium-potassium alloys. [46]

oxygen and carbon, both of which have profound surface effects, especially at high temperatures.

Of special importance is the corrosion behavior of uranium in liquid sodium and NaK. The corrosion rate of uranium is much the same in both liquid metals, although data are somewhat limited. Up to 500 or 600°C in oxygen-free sodium, the rate is quite small, but as little as 1 or 2% oxygen can increase it by a factor of ten. Thus there is no problem with uranium in contact with sodium or NaK if the liquids are kept essentially free of oxide impurity.

The corrosion behavior of welds and brazes is also important. Among the brazing alloys that resist sodium are: 60% Mn-40% Ni, high chromium-nickel alloys, and chromium-nickel-silicon alloys. Welds of either austenitic or ferritic alloys resist sodium corrosion as well as the base metal. For system cleanliness and subsequent sodium purity, joints should be avoided where large quantities of welding slag can be trapped, since the slag may later be leached out.

Since sodium and NaK react with the oxygen and moisture in air, in many operations the metals must be protected from exposure by a relatively inert gas cover. Nitrogen is often used. Argon is useful where a heavy gas is desirable, particularly to protect open-lidded sodium vessels. Helium is especially suited for nuclear power systems because it does not activate, but nitrogen also may be considered for this application. Helium and argon are rare and relatively expensive but present no difficulties.

Impurities and their removal. Impurities in sodium accelerate corrosion, impair mechanical and thermal performance of equipment, and in nuclear reactor coolants add to induced radioactivity. Sodium impurities affecting system corrosion most are oxygen, hydrogen, carbon, and calcium. Of these, oxygen and carbon have been investigated most extensively.

Oxygen combines with sodium to give sodium oxide, an aggressive oxidant toward all metallic surfaces. The degree of damage depends on the alloy, the concentration, and the temperature. The behavior of the ferrous base alloys toward sodium oxide is significant, since these are most commonly used in heat-transfer systems. The austenitic stainless steels are not severely attacked by sodium oxide in less than saturation quantities up to 1000°F. But if the oxide contamination exceeds saturation solubility, there may be intergranular attack at temperatures as low as 700°F, resulting in an embrittled surface layer that cracks upon deformation. Oxide contamination can also form brittle surface layers through molecular absorption in materials like zirconium, which are active oxygen "getters" in high-temperature gaseous media.

Hydrocarbons in the inert gas are undesirable, since they will "crack" in the presence of high-temperature sodium, adding hydrogen to it. More important, steels can be carburized by the cracked oil-sodium mixture. However, at temperatures up to 1000°F, with only reasonable amounts of hydrocarbons added, such carburization is extremely small—of the order of a mil in depth. This would be of concern only in a system with exceptionally thin members subjected to cycled strains, e g., certain valve bellows.

With sodium containing calcium, nitrogen is a problem because it forms calcium nitride, an insoluble precipitate. Calcium in sodium attacks nickel, and in the presence of excess calcium metal it will reduce sodium oxide to form the even less-soluble calcium oxide. The possibility of hydrogen contamination (as, for example, dissolved sodium hydroxide) has caused some concern because of its moderating effect in fast reactors. In the absence of irradiation, no detrimental effects on the structural materials have been observed with either nitrogen or hydrogen below 1000°F. In any case, nitrogen contamination is not expected to be important except when this gas is used as a cover.

There are three principal methods of purifying sodium continuously: cold traps, hot traps, and solution gettering. The cold trap, standard for all stainless steel systems at temperatures below 1000°F, is used primarily to maintain low Na_2O concentrations by precipitating oxide in excess of the low-temperature saturation limit in a bypass digestion tank.

Improper or careless precleaning of the system can leave dirt, grease, oil, weld slag, surface oxides, moisture, etc., which can be major sources of contamination. These will add to the oxygen, hydrogen, carbon, and insolubles in the sodium. However, even with the best precleaning procedures, some impurities will be picked up from metal surface oxides and absorbed gases. Other sources of impurities during system operation are water, hydrocarbons, and other materials in the atmosphere that may leak in whenever the system is opened for any reason. The former can be minimized by good system design, fabrication, and maintenance; the latter by carefully excluding the atmosphere when the system is opened.

Cold trapping. One method of removing impurities, cold trapping, is based on the solubility-temperature relationship. The simplest cold trap is a surface cold enough to cause precipitation below the saturation temperature of the impurity (see Fig. 2–27). The basic function of the cold trap is to remove sodium monoxide, but other materials with a strong temperature-dependent solubility in sodium can also be removed, e.g., antimony and silver. There are two kinds of cold traps: natural circulation and forced circulation. A natural circulation trap can be merely a cold stub-end somewhere in the system. Delivery of impurities from the stream to the cold surface of the cold trap depends on

natural circulation engendered by turbulence at the entrance of the cold trap, and diffusion of the impurity into it. In the forced circulation cold trap, a portion of the main stream is bypassed and pumped over a cold surface, producing more intimate and more rapid mixing than is possible with natural circulation. Added surface is provided, in some instances, by inserting stainless steel mesh in the digestion tank (see Fig. 2–27 for an example). Hot traps are now being investigated for use in higher-temperature systems to reduce sodium oxide concentrations still further. This method also employs the bypass technique, using a reaction tank packed with zirconium or titanium to reduce the sodium oxide chemically.

Solution gettering. Chemical purification is used to reduce oxygen content, employing substances that can reduce sodium monoxide. The free energies of the oxides and the kinetics of the reaction must favor the reduction. "Gettering agents" are in two classes: the first group comprises materials, soluble in sodium, that form an oxide with limited solubility (e.g., calcium, lithium, magnesium, barium). The second class includes those that are essentially insoluble in sodium and reduce sodium monoxide to the "getter" oxide, also insoluble in sodium (e.g., uranium, titanium, zirconium). If a gettering agent is to be used in a reactor cooling system, its cross section should be low, for neutron economy. Also, the products of irradiation of the getter obviously should not be long-lived nor emit high-energy radiation.

Mechanical effects. Galling of threaded and sliding parts presents a mechanical difficulty. (Galling means increasing resistance to sliding of one solid surface over another, and eventual stoppage or surface damage.) Since sodium is a poor lubricant and most conventional lubricants react with it, galling can occur easily in a sodium system. Finally, sodium prevents an oxide film from forming on the surface to slow the galling action. Galling can be prevented by good design and by other methods, such as surface treatments. Design possibilities are (1) very loose, running fits, (2) tapered threads, and (3) exceptionally smooth surfaces. Of potential surface treatments, nitriding has probably been used most widely and successfully.

Another metallurgical problem that results from solution and diffusion effects is diffusion bonding or self-welding. Mating surfaces of similar alloys or of materials with high mutual solid solubility tend to weld together in sodium at temperatures much lower than those required for normal resistance or flash welding. The effectiveness of such a bond depends on time and temperature, rather than contact pressures. Using unlike materials, particularly combinations having little or no mutual solid solubility, is the best known way to minimize bonding. Mechanical effects related to experience with sodium systems and components are discussed later.

Radioactivity considerations. Radioactivities in sodium-cooled reactor systems come from (1) transferred system structural material, (2) sodium and its impurities, and (3) fission products released to the coolant.

Material transfer results from the solution, diffusion, and subsequent deposition of radioactive material through a sodium system. Deposition occurs in the normally nonradioactive portions of the system; it is accompanied by self-diffusion into the walls of the piping, heat-exchanger equipment, and other components. The resulting radioactivity is not easily removed; however, long-lived activity can be held down by using tantalum- and cobalt-free materials in the reactor core and in the primary coolant system. Chromium-51, manganese-56, and iron-59, which result from thermal neutron capture, are the principal radioisotopes producing short-lived, high-level activity. Another isotope of manganese, Mn^{54}, is formed from stable Fe^{54} through fast neutron capture and proton loss. Its formation depends upon the energy spectrum. When ferrous-base alloys must be used at temperatures above 1000°F, Mn^{54} appears to transport at rates higher than stoichiometric. Also, Mn^{54} has a relatively long half-life (310 days), and so could create an accessibility problem.

The radioactive isotope of sodium that presents a special problem is Na^{24}, created from Na^{23} by neutron capture. Sodium, with a macroscopic cross section for thermal neutrons of 0.012 cm^{-1}, activates to saturation rapidly. Sodium-24 has a 15-hr half-life, and emits hard gamma radiation (2.75 and 3.7 Mev), so that heat-transfer equipment outside the reactor must be shielded. Installing adequate shielding is not very difficult, and during power operation the gamma radiation presents no problem. However, when access is required to maintain system components (other than the reactor), the system must be drained and flushed with fresh nonactive sodium to reduce the radiation to tolerable levels, or the active coolant charge must be permitted to decay. For prompt accessibility, the major components can be isolated in shielded cells, or "plug-in" components can be hung from a shielded deck and disconnected or repaired without exposing personnel to the radioactive coolant.

Impurities can also be activated by the neutrons. They may be present in the original sodium, or may be picked up by corrosion or erosion in the reactor system. If the contaminants form radioactive isotopes with long half-lives, a significant activity level may remain, making the coolant unsafe to handle and presenting problems of disposal. Two grades of commercial sodium are compared in Table 2–17. Both of these are satisfactory and would undoubtedly be acceptable for reactor application. However, if the sodium should contain large quantities of cobalt or iron, the residual activity would not decay in a reasonable time. These elements could, of course, be picked up by corrosion in a reactor system.

TABLE 2–17

TYPICAL ANALYSIS OF "ETHYL"* SODIUM

	Weight percent	
	Commercial grade	High purity
Oxygen	0.005	0 005
Calcium	0.040	0 020
Nitride	0 001†	0.001†
Chloride	0 002	0.001
Sulfate	0 003‡	0 003‡
Carbon	0.008	—
Hydrogen	—	—
Potassium	0 100	0.100
Iron	0.004	0.004
Copper	0.002	0.001
Aluminum	0 002	0.001
Magnesium	0 001	0 001
Bismuth	0 003‡	0 003‡
Lithium	0 003‡	0.003‡
Silicon	0 003	0.003
Tin	0 002	0.002‡
Lead	0.001	0.001‡
Nickel	0 001	0 001
Manganese	0.001	0.001‡
Strontium	0 0004	0.0004
Barium	0 005‡	0.005‡
Sodium	99.8126	99 8436

*Manufactured by the Ethyl Corporation.
†May be present.
‡Probably not present.

Chemical reactions with water and air. Sodium and sodium-potassium alloys are extremely reactive substances that oxidize freely in air and combine explosively with water. If complete reaction at 25°C is assumed, the final condition of a sodium-water reaction can be expressed by either or both of the following equations:

$$2Na + H_2O \rightarrow Na_2O + 31.08 \text{ kcal},$$
$$Na + H_2O \rightarrow NaOH + \tfrac{1}{2}H_2 + 33.67 \text{ kcal}.$$

Calculations of the free energies show that the reaction of sodium and water below the melting point of sodium hydroxide will proceed to sodium

hydroxide and hydrogen, even with excess sodium. If the temperature is above the melting point of sodium hydroxide, then sodium hydroxide will react with additional sodium to produce sodium oxide and hydrogen. When NaK is used instead of sodium alone, the hydroxides formed on reaction with water may melt at as low a temperature as 329°F, the melting point of the eutectic mixture of 58 w/o potassium hydroxide. This lowering of the hydroxide melting point may lower the temperature at which the oxides are formed. The reaction of sodium and water, for all practical purposes, cannot be reversed by the pressure of the hydrogen. Equilibrium calculations show that hydrogen pressures of some 10^{50} atmospheres are required to reverse the reaction.

The rate of reaction of liquid metals with water is limited by the reaction contact area and by the formation of products which tend to separate the reactants. When the liquid metal and water make contact they react and are quickly separated by the liberated hydrogen. Shock effects due to these reactions have been investigated* and the energy of the shock wave found to be small.

Besides the primary hazards of the initial sodium-water reaction, there are secondary effects of the reaction products. Hydrogen, if allowed to mix with air, creates a serious explosion hazard. For high-temperature, sodium-cooled reactor systems, safety requires the reactor system to be enclosed in a shell or building that can retain scattered radioactive materials under the pressures and temperatures that might follow a nuclear accident or equipment failure. There are three types of accidents involving exposure of sodium to the building atmosphere: stagnant pool, pressurized spray, and explosive ejection.

The stagnant pool exposure, which could follow low-pressure equipment failure, spillage, or opening of sodium-containing tanks or lines, is least serious. Sodium released as a pressurized spray leads to much faster reaction rates and higher building pressures. An accidental discharge of this type might result from failure of equipment or pipes containing sodium under pressure. The third, and potentially most severe of the sodium exposure accidents, occurs when sodium is explosively ejected into the building atmosphere. The important difference between the second and third types of accident is in the mixing rates, since both reactions occur primarily while the sodium is in flight. At a given temperature, the rate of reaction depends on the mass rate of the sodium discharge, its distribution within the building, and the velocity and size of the sodium particles. Only when a very large mass of efficiently dispersed sodium is ejected with high energy is the most severe (maximum theoretical) reaction rate likely to be approached. When high-temperature molten sodium, finely divided,

*Page 126, *Liquid Metals Handbook*, Sodium-NaK Supplement, TID-5277.

is mixed with air, the predominant reaction is oxidation of the sodium to form sodium peroxide:

$$2Na + O_2 \rightarrow Na_2O_2; \qquad \Delta H = -124 \text{ kcal.}$$

2-4.3 Heat exchangers and steam generators.* The heat exchangers used for liquid metal service are not very different from those for normal fluid service. Some factors to be considered in their design are:

(1) Selection of materials.

(2) Welding for leaktightness.

(3) Effects of thermal transients, usually much larger than normal because temperature differences are large and thermal conductivity of the liquid metal is extremely high.

(4) Steady-state thermal stresses because of high temperature differences and high heat-transfer rates.

(5) Provisions for handling (or preventing) water-to-sodium leakage.

Selection of materials for construction. The materials that have been used in liquid metal heat exchangers are the 18-8 stainless steels and 2¼% Cr-1% Mo steels. The 18-8 stainless steels have been used in the primary system exchangers (intermediate heat-exchangers) principally because of their low mass-transfer rates. Both 18-8 material and chrome molybdenum alloy have been used in steam generator units. Below 900°F the 2¼% Cr-1% Mo composition is favored because it is not as susceptible to rapid chloride and caustic stress corrosion as the 18-8 material. Since the chrome alloys tend to decarbonize in sodium above 900°F, only the 18-8 material remains for use at the higher temperatures. Laboratory work has been performed to determine whether low concentrations of NaOH in sodium produce the same rapid stress corrosion as is evidenced on the water side. These experiments showed no rapid stress corrosion with concentration as low as 1% and as high as 8% in 18-8 material and in chrome molybdenum material. The steam generator can be designed so that if a leak occurs the water enters the sodium rather than the reverse.

Welded construction. All-welded construction should be used where possible to ensure leaktightness. Butt welds should be used where possible, as they can be radiographed. In welding tubes to tube sheets care must be taken not to produce crevices on the water side of the unit. If possible, crevices should be avoided on both sides.

Effects of thermal transients. To minimize pumping power, liquid metal systems are designed for fluid temperature rises as high as 450°F. This high temperature rise can cause rather severe thermal shocks when power

*Extracted from "Heat Exchangers and Steam Generators for Liquid Metal Systems," by J. J. Morabito, Atomic Power Development Associates, Inc., 1958 (unpublished). See also References 46 and 62.

or flow rates are varied. The excellent thermal conductivity of sodium aggravates the situation. Through care in design and arrangement of heat-transfer surface it is sometimes possible to avoid having thick members, such as tube sheets, in direct contact with sodium. In intermediate heat exchangers this is almost impossible; therefore a careful analysis of the need for thermal shielding on both tube sheets and tube-to-tube-sheet joints must be made. Nozzles usually require thermal shielding inserts. In many instances, where configurations are extremely complex, an analytical approach is difficult and prototype tests are called for.

Steady-state thermal stresses. Steady-state thermal stresses are usually produced by the high heat-transfer rates in liquid metal heat exchangers, often by the large temperature rise through the unit. To minimize gradients through thick members, it is sometimes necessary to transfer these gradients to walls that can be more readily shielded. In steam generators, the great temperature difference between the sodium and the boiling water, often as much as 200°F, produces high temperature gradients across the tube wall. The effects of these gradients can be lessened by choosing material with high thermal conductivity, low coefficient of thermal expansion, and high strength at the operating temperature. In these respects chrome-molybdenum ($2\frac{1}{4}$–1%) is better than 18-8 austenitic stainless steel.

Sodium-water reactions. In the United States two kinds of defense have been used against sodium-water reactions. One approach is to provide double tube walls and double tube sheets, with an intermediate fluid between water and sodium tubes. The principle here is to provide a system so reliable that contact between the two fluids is impossible. The other approach is to provide a single-wall tube steam generator with relief devices to handle the pressure effects from a major leak, and facilities to detect small leaks by plugging indicators on the sodium side and sampling devices on the water side. This latter approach is based on experience with small test units. In every instance the leaks that have occurred in such units have been small; often they have not been detected until oxide has built up in the sodium to plug such equipment as electromagnetic pumps.

To determine the effects of a complete tube failure, studies have been made at APDA of the reaction rates between water and sodium and the resulting pressures. These experiments indicate that it is extremely difficult to predict the reaction rate, since it is highly dependent on the rate of mixing. The mixing rate in turn is affected by the reaction products, which tend to separate the reactants. Tests in which 1200-psi water was injected through a $\frac{1}{2}$-inch diameter opening into a small vessel completely filled with NaK have shown an average rise above steam pressure of about 400 psi. Thus, for safe operation, the steam generator must be designed

for high pressures or else a relief device is needed to release the products of reaction (mainly H_2) so that pressure surges will not rupture the unit. A series of experiments is now in progress at APDA to simulate the effect of a tube failure in a steam generator with a gas blanket to minimize the surge of pressure, and a rupture diaphragm to relieve the products of reaction. It is anticipated that a system such as this will permit designing steam generators for pressures as low as 100 psi.

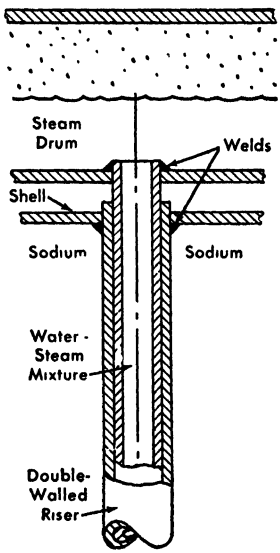

FIG. 2–10. Schematic drawing of steam generator tube configuration. (GNEC)

Heat-exchange equipment for EBR-II and the Enrico Fermi Reactor. Chapter 3 describes the EBR-II steam generator. The concentric tube configuration here employs no thermal bond (third fluid) annulus or leak detection equipment. A schematic drawing of such a configuration is shown in Fig. 2–10. The EBR-II primary to secondary sodium heat exchanger, shown in Fig. 3–22, is a shell-and-tube exchanger with secondary sodium in the tubes. The secondary circuit is at slightly higher pressure so that any leakage will be toward the radioactive primary circuit.

The intermediate heat exchanger in the Enrico Fermi Atomic Power Plant (see Fig. 4–67) is similar to that of EBR-II. The steam generator, however, illustrates another configuration, the bayonet type, where system leaktightness depends on the integrity of welds (Fig. 4–69).

2–4.4 Pumps. For liquid sodium pumps the principal design objectives are to eliminate leakage and minimize maintenance; these are im-

portant because of chemical activity and induced radioactivity of the sodium coolant. Pump development has been on two primary types, electromagnetic and mechanical. The electromagnetic pumps take advantage of the high electrical conductivity of sodium to effect pumping by electrical forces. Mechanical pumps have been redesigned and features added to meet the special requirements for liquid metals.

Electromagnetic pumps. The electromagnetic pump is very well suited for circulating radioactive sodium because it uses no moving parts, bearings, or seals. Electrical power is transformed directly into pumping power by the interaction of current and magnetic field in the liquid conductor, without the complexities of an intermediate mechanical stage. There is an obvious comparison with electric motors; electromagnetic pumps are either alternating current or direct current, and in the case of the former, current is fed to the moving sodium either by induction or conduction.

In a conduction (Faraday-type) pump, current passes to and from the liquid by means of electrodes connected along the edges of the coolant duct. Direct current pumps are, of course, conductive.

As illustrated in Fig. 2–11, liquid sodium flows in a narrow rectangular duct passing between the poles of an electromagnet while current passes through the liquid. The pumping rate depends on the current, magnetic field intensity, and duct size. Direct current electromagnetic pumps have the advantages of simple construction and freedom from insulation difficulties. They have operated reliably at high temperatures for long periods. Efficiencies vary from 15 to 20% for small pumps, to 40% for large systems where homopolar generators supply the current.

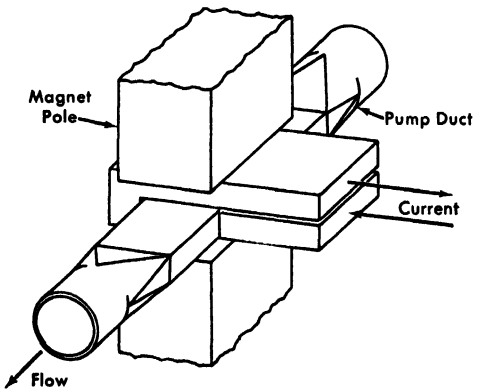

FIG. 2–11. Schematic diagram of DC pump showing arrangement of current flow for field compensation. [46]

An AC conduction pump operates on the same principle except that the magnetic field reverses in synchronism with the alternating current in the liquid sodium. The field winding is connected in series with the current path through the liquid, as with series-field motors. While no large AC conduction pumps have been constructed, small models have been used widely, since they can be operated directly from a single-phase power line. Pumping efficiencies range from 5 to 20%.

With alternating current induction pumps, large currents can be developed directly in the moving liquid by electromagnetic induction. Under the classification of induction or "traveling-field" pumps, development has been centered primarily on three versions: the flat linear induction pump (FLIP), the annular linear pump (ALIP), and the helical or spiral-channel induction pump (SIP). All of these utilize the same principle of inducing current in the moving liquid by means of polyphase AC, multipole windings mounted in slotted fixed "stators," adjacent to the pump duct. In the FLIP type (Fig. 2–12), the liquid duct is a flattened tube between two core sections that contain the polyphase winding. Here a linearly traveling or "sliding" flux wave is produced—as though the conventional stator of an induction motor were laid out flat.

To reduce field losses at the edges of the flat cores, an annular geometry was developed (ALIP) The liquid flows in an annular duct between inner and outer core sections. In the outer cylindrical core section, toroidal coils are connected so as to produce a polyphase traveling wave with resulting induced current paths that are annular. Although this was a decided improvement because of its better symmetry, its development has been inhibited by fabrication difficulties. The third arrangement (SIP) employs a helical duct in a conventional induction motor stator, with a

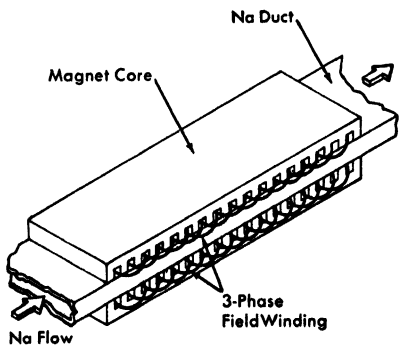

FIG. 2–12. Schematic drawing showing the principle of an alternating current flat linear induction pump. (GNEC)

TABLE 2–18

ELECTROMAGNETIC PUMP TYPES

Type	Application	Flow rate, gpm	Pumping head, psi	Over-all efficiency
Conduction (Faraday)				
DC	EBR-I primary system (NaK)	300	40	17
AC	Laboratory test systems (Na, NaK)	20	15	15
Induction (traveling-field)				
FLIP	EBR-II secondary system (Na)	5000	40	40
ALIP	Laboratory test systems (Na)	400	15	40
SIP	Laboratory test systems (Na)	300	40	20
DC *conduction pump with homopolar generator**	Alternate for EBR-II primary system (Na)	10,000	75	40

*The DC pump with homopolar generator is listed separately in the table because of the difference in power supply. This pump unit, and others that are operational, are discussed in the text.

laminated core inside the helix. This development also has been discouraged by fabrication problems and low efficiencies. The several electromagnetic types which have been studied, and working examples of each, are summarized in Table 2–18.

EBR-I primary pump. A fundamental problem in designing DC pumps is magnetic field distortion, which results from interaction of the field between the magnet poles (Fig. 2–11) and the field due to current across the duct. It can be seen that if the conductor did not pass back through the gap and provide a compensating field, the resultant field intensity within the duct would be higher at the pump exit than at the entrance (the field produced by the current would reinforce the pump field at the exit and partially cancel it at the entrance). Another method is used to eliminate distortion in the EBR-I pump design. Here, the poles are tapered so that the magnetic gap is wider toward the entrance end, and in addition the duct cross section is tapered so that a constant current density is maintained between the entrance and exit. Unfortunately, compensation is complete for only one condition of current and field intensity. For the EBR-I pump (500 gpm capacity at 25 psi), the pole pieces are 4 inches at the entrance to 1.50 inches at the exit. The tapered Nichrome duct has an average cross section of 1.5 by 3.25 inches, with a wall thickness of 0.025 inch [50,51].

The field winding employed depends on operating requirements of the pump. For high temperatures, a series-connected winding is preferred because it requires only a few turns of large cross-section copper and consequently has a small voltage drop. The low voltage drop means no auxiliary cooling and only minimum insulation problems. This is illustrated in the EBR-I pump, which has two turns of 6 by 6 inch cross section copper connected in series with the current path across the duct. The current requirement of 300 gpm and 4 psi head is 18,500 amp, and for the 12.5-kw power input the voltage drop is approximately 0.68 volt. Duct and magnet are in a welded stainless steel, boxlike enclosure to retain the liquid metal (NaK) in the event a duct fails. Mica insulation is used, and no external cooling is provided. The current leads are brought out through stainless steel bellows that provide an "insulating" seal, since the current leakage is negligible. The enclosure is pressurized with helium at 5 psi.

Clearly, the main virtues of large DC pumps are simple construction and reliable operation at high temperatures (over 1400°F) for long periods. Their operation in the presence of intense radiation has presented no difficulty. The main undesirable features are low efficiency and problems of supplying the low-voltage, high-amperage direct current. At the reference conditions of 300 gpm, 40 psi head, and NaK temperature of 480°F, EBR-I pump efficiency is 42%. Then, with a rectifier efficiency of 40%, the overall efficiency is 17%. Since the electrical resistivity of NaK eutectic is ap-

proximately twice that of sodium, efficiencies would be somewhat higher when pumping the latter. Also, with the homopolar generator, over-all efficiencies of nearly 45% may be reached.

DC *pump development at Argonne National Laboratory* [52,53]. Direct current electromagnetic pumps have been studied at Argonne National Laboratory since 1947. Some 30 different pump designs have been employed, ranging from 5 to 10,000 gpm capacity. During the first years, most investigations were concerned with electrical design. These design procedures are now well established. It was apparent early that the mechanical design of DC pumps would be more difficult than the electrical design, especially as pump size was increased. Thus construction techniques have been strongly emphasized.

As discussed previously, the principal advantage of the DC conduction pump is its ability to operate in highly radioactive regions at elevated temperatures. For high-temperature operation, all electrical connections in the pump must be made reliable. Conventional soldering and brazing methods are not adequate at high temperatures.

The pump duct material most often used in liquid sodium pumps at Argonne is 18% Cr-8% Ni stainless steel. It is chosen for the following reasons:

(1) Good corrosion characteristics in sodium.
(2) High electrical resistivity.
(3) Good weldability.
(4) Nonmagnetic property.
(5) High-temperature strength.

Other materials surpass 18-8 stainless steel in one or more of these characteristics but experience has justified its use. In selecting a current conducting material, the choice is much more limited. Low electrical resistivity is of paramount importance, and consideration must be given to the problem of joining the conductor to the pump duct. Choice is limited to copper, aluminum, silver, nickel, sodium, or NaK. Most pumps built at Argonne use either copper, sodium, NaK, or combinations of these. If space is unimportant sodium or NaK are attractive, because when they are molten no thermal stress problems are encountered in making electrical contact to the pump duct. This technique, modified, is used extensively in pumps built at Argonne. For example, the bus from the current source to one large pump consists of molten sodium in a long, irregularly shaped box of rectangular section. Where space limitations are important (as near the electromagnet of the pump) copper replaces most of the sodium. Where the actual electrical junction is made to the pump duct, sodium is again employed. Figure 2–14 illustrates a pump design with this sodium-to-copper-to-sodium electrical conductor. With this conductor welds of copper to stainless steel can be avoided completely. If welds of this type

are necessary, intermediate welds of nickel and nickel-copper alloy are placed between the stainless steel and copper. This expensive method should be avoided in large pumps.

The pump duct in small pumps is a rectangular section, formed from a round tube. This method is inexpensive but strength and reliability are sacrificed, since to attach the electrical conductor welding must now be done on the thin tube wall. It is much better to form the rectangular duct from four separate stainless steel sheets welded together. Two of these (parallel to the direction of current) must be thin, but the sheets composing the electrical junction can be quite heavy, thus adding strength and rigidity to the pump duct. Using heavy sheets, in some cases the copper conductor can be welded directly to the stainless steel sheets. Here the copper conductor is made up of many smaller bars, stacked together in parallel. Distortion of the heavy stainless steel sheet is a major difficulty.

As stated earlier, it has been found advisable to build DC pumps with series-excited electromagnets. This is especially true in large pumps. As the current requirements of the pump increase, the flux density does not alter greatly, hence the ampere-turns needed for the electromagnet depend on the air gap size and ultimately on the pump capacity. The pump in Fig. 2–14 has a one-turn, series-excited electromagnet. While this design is not good from the standpoint of flux leakage, it is simple and inexpensive.

When large currents and electromagnets with few turns are used some compensating device must overcome the cross-magnetizing magnetomotive force produced by current passing through the pump duct. Graded field poles and tapered pump ducts could be employed, but for simplicity a series compensating turn is almost always used. After the current passes through the pump duct, it immediately returns in an opposite direction through a path parallel to the pump duct current path. Since no magnetic material is linked by this turn, it cancels the cross-magnetizing effect of the pumping current. In Fig. 2–14 the compensating turn comprises two parallel conductors on each side of the pump duct.

As pump sizes increase, another serious problem confronts the designer. The head-capacity relationship of the pump depends on the amount of current that actually traverses the pump duct in the region of strong magnetic field. In practice it has been found that much current does bypass this region by traveling down the pump duct and crossing outside magnetic field boundaries. Of course, this current diversion reduces pump efficiency. To avoid such a loss, the pump duct is subdivided into several separate and electrically insulated channels, increasing the resistance of the diversion path.

The approaches described for pump design may be summarized as follows:

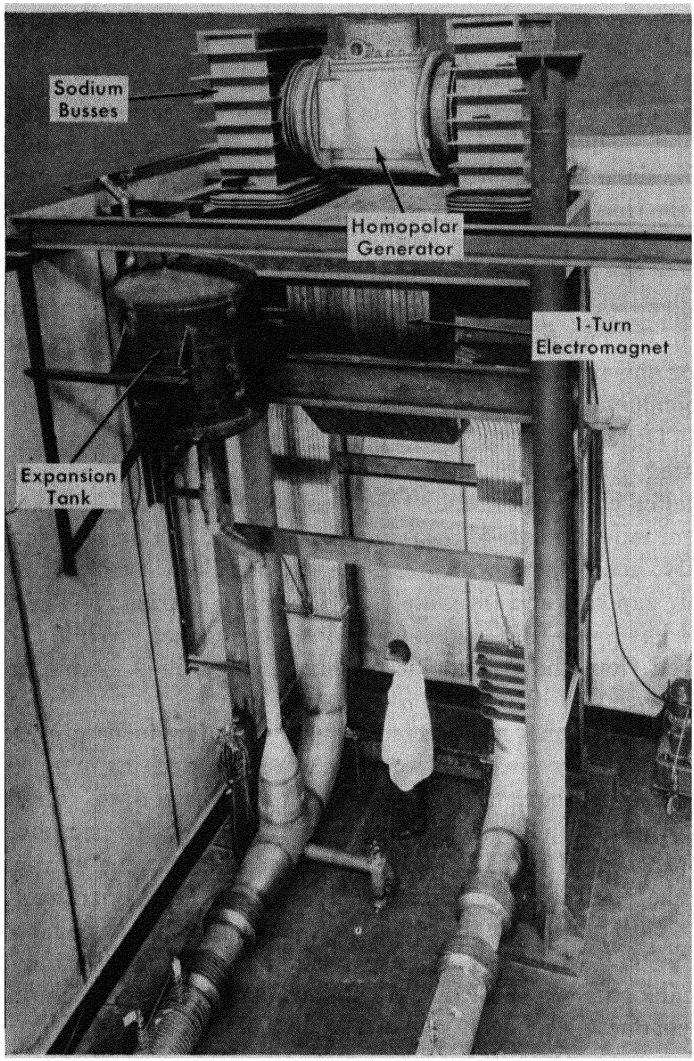

FIG. 2–13. View of 10,000-gpm DC electromagnetic pump in test facility, showing the large amount of welding necessary for such an installation.

(1) Sodium-to-copper-to-sodium electrical conductors.

(2) Welded fabrication of pump ducts from heavy and light gauge sheet.

(3) Series field excitation for pump winding.

(4) Series compensating turn of a conductor within the magnetic gap.

(5) Subdivided pump duct to reduce current bypassing.

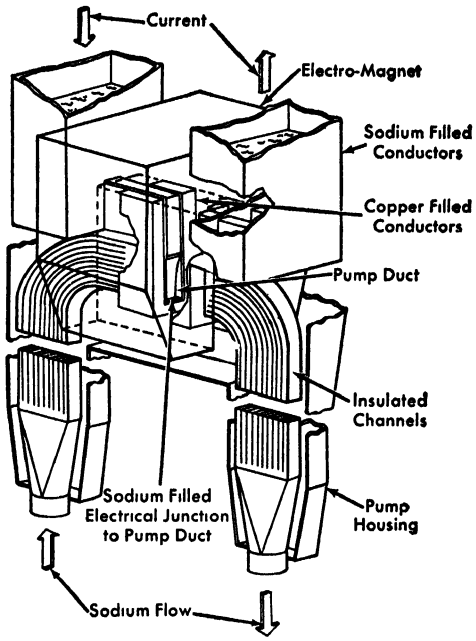

FIG. 2–14. Cutaway perspective of 10,000-gpm DC electromagnetic sodium pump.

All these concepts have been used recently in designing and constructing a high-temperature, large-capacity DC pump.

The 10,000-gpm direct current electromagnetic pump [54]. The Argonne National Laboratory has recently completed tests on a 10,000-gpm DC pump. Pumping high-temperature intensely radioactive molten sodium in a completely sealed duct, this pump utilizes a power supply with an efficiency greater than 80%; by contrast, metallic rectifiers have efficiencies of 20 to 40%.

The pump-power supply combination is a single compact unit, aligned vertically to reduce electrical conductor length between generator and pump. Pictorial and schematic representations of the unit are shown in Figs. 2–13 through 2–16. With reference to Fig. 2–13, the unit components and a functional description of each are listed in Table 2–19. It should be noted that many lineal feet of welding are necessary to install such a large DC pump (Fig. 2–13). Because of this and because testing of mechanical pumps has shown good results, the consensus now is that large "cast" mechanical pumps are preferable. Accordingly, in the EBR-II design electromagnetic pumps have been replaced by mechanical pumps of the same capacity.

TABLE 2–19

CHARACTERISTICS OF THE 10,000-GPM PUMP POWER SUPPLY UNIT [52,54]

Item	Functional description	Capacity
Structural characteristics		
Arrangement	Vertical alignment of components	—
Over-all height	30 ft	—
Over-all weight	35 tons	—
Drive motor		
Type	Induction, squirrel cage	1250 hp
Input voltage	3-phase, 60-cycle	2300 volts
Set connection	Direct	—
Homopolar generator		
Type	Liquid brush	250,000 amp, 2.5 volts
Brush conducting material	NaK eutectic, water-cooled, argon blanketed	—
Machine winding	Excitation coil, Cu strap, water-cooled	13 turns
Field excitation	Separate DC source, dry rectifier	2500 amp
Rotor	12-inch Fe rotor, Ag-soldered, Cu plugs	—
Stator-NaK insulation	Stainless steel, double-walled cylinder	—
Terminal ring	2 inches wide, Cu	—
Temperature	Maximum operating	150°C
Losses, full load	Excitation, bearings	60 kw
Test loading	Maximum generator load current	425,000 amp, 1.8 volts
Test loading	Maximum generator field current	2450 amp
Efficiency	Over-all full load	92%
Electromagnet		
Excitation	Homopolar generator output, one-turn coil, series excited	250,000 amp
Flux density	Na-filled duct	7000 gauss
Core composition and weight	Carbon-steel plates, 20, 2 inches thick, $\frac{1}{8}$-inch spacing	16 tons

TABLE 2-19 (*continued*)

Item	Functional description	Capacity
Gap dimensions	Between plates rectangular cross section	21 inches high, 6 inches wide, 42 inches long
Pump duct		
Material	18 Cr-8 Ni stainless steel sheet	—
Geometry, pumping region	Single duct at center of gap	21 inches high, 6 inches wide, 30 inches long
Geometry, flow regions	Multiple-channel duct on either side	12, $1\frac{5}{8}$ inches × 6 inches cross section
Insulation	Flat sheet, mica or ceramic	—
Temperature limit	Curie point of iron	763°C

EBR-II secondary pump [55]. Two types of 5000-gpm sodium pumps have been constructed for possible use in the secondary heat-transfer system at Argonne's Experimental Breeder Reactor II, and some tests have been completed. The type finally chosen will depend, in part, on operating performance data from these tests. One pump, an Allis-Chalmers single-stage centrifugal type, is described in subsequent paragraphs. The other, an AC linear induction pump (FLIP), was manufactured by the General Electric Company and is rated at 5000 gpm at 40 psi head. Design and performance characteristics are listed in Table 2-20.

A general view of the pump in its test facility is shown in Fig. 2-17. Preliminary operating tests have shown that this pump meets flow, pressure, and power input requirements. After it operated 10 hr, the instrumentation was adjusted in preparation for longer runs.

United Kingdom Dounreay pumps [56]. The primary and secondary coolant circuits of the Dounreay Fast Reactor (DFR) [57] are to be divided into twenty-four parallel paths with sodium circulated by twenty-four FLIP* type pumps. According to p. 275 of Reference 56:

". . . The design of the pumping unit was based on the following main assumptions:

"a. The pump channel could be made reliable and so would not require maintenance.

"b. The shape, construction, and wall thickness of the channel would be such that only small loads could be applied to it by the main piping.

*Flat linear induction pump.

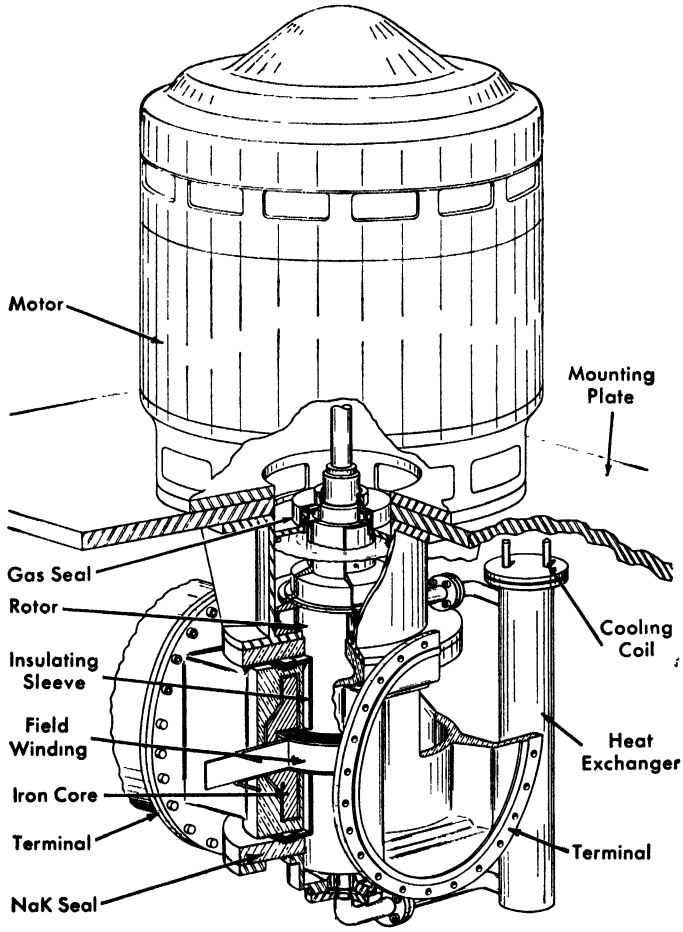

FIG. 2–15. Cutaway perspective of 250,000-ampere homopolar generator.

"c. The wound cores on either side of the channel might be a source of trouble and so should be designed so that they could be remotely removed for maintenance.

"d. The channel would not withstand a high internal pressure when the wound cores were removed.

"e. Containment of the pump in air inert-gas-filled enclosure would be necessary."

An early prototype of the DFR induction pump, supplied by The English Electric Company Limited [56], was rated [58] at 400 gpm at 30 psi head when pumping sodium at 250°C with an efficiency of 30%. When pumping sodium-potassium alloy with the same stator current, performance was 400 gpm, 15 psi, and 23% efficiency.

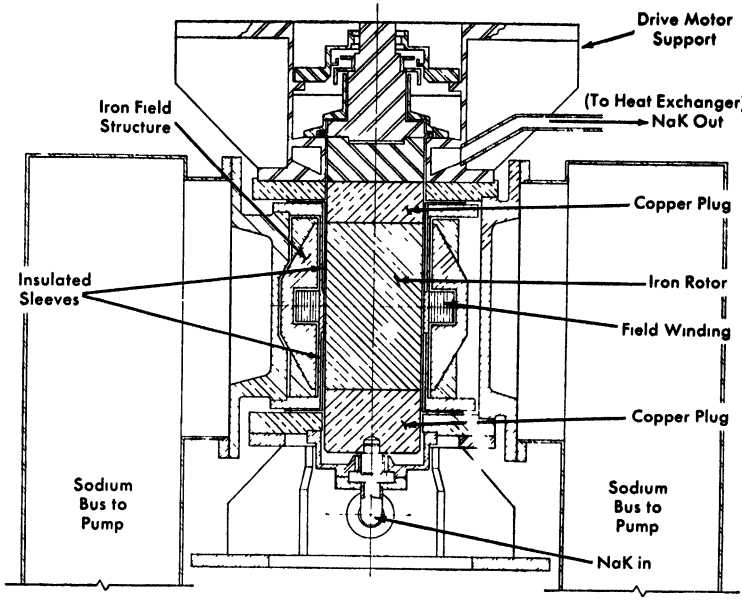

FIG. 2–16. Schematic diagram of 250,000-ampere homopolar generator.

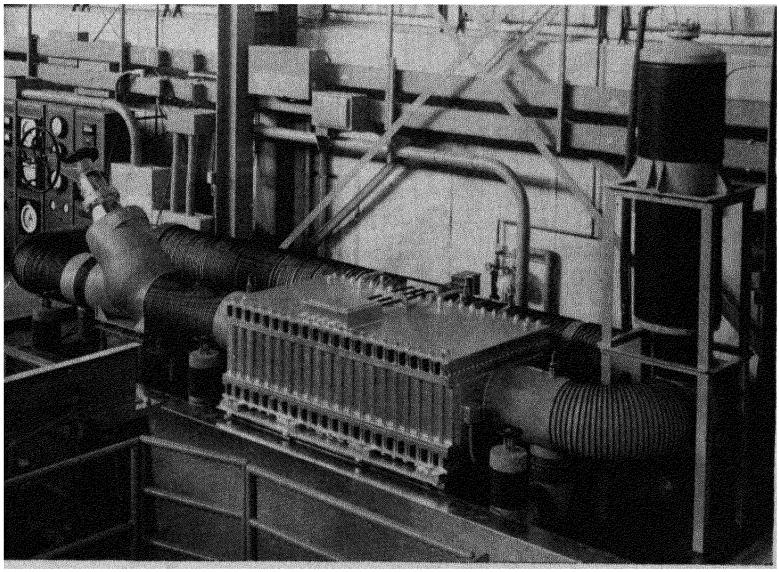

FIG. 2–17. General view of 5000-gpm AC linear induction sodium pump.

TABLE 2–20

CHARACTERISTICS OF THE EBR-II FLIP TYPE PUMP [55]

General data	
Manufacturer	General Electric Co.
Type	AC linear induction
Capacity, gpm	5000
Pumping head, psi	40 at flow capacity
Input power, kw	220 at 480 volts
Efficiency, %	43 at 5000 gpm
Operating temperature, rated, °F	700 (370°C)
Stator characteristics	
Stator dimensions, inches	27 × 41
Winding temperature, maximum, °F	390 (200°C)
Winding coolant, water, gpm	15
Winding arrangement	Six-pole field, linear synchronous speed of 58.5 fps to 60 cycles/sec
Pump duct characteristics	
Material	AISI type-347 stainless steel
Cross section, inches	$1\frac{3}{8} \times 27$
Length, inches	41
Wall thickness, inches	$\frac{1}{16}$
Pump enclosure	
Shape	Right-rectangular parallelopiped
Flow nozzles, welded, inches	12
Test facility	
Pipe and fittings material	Type-304 stainless steel
Pipe size, schedule-10, inches	12
Throttle valve	12-inch bellows-sealed wye type
Heat removal	Finned air cooler over 12-ft length of test loop
Preheating	From 70 to 250°F; resistance heating for pump, 60 cps induction heating for test loop
Test operating time	10 hr

Mechanical pumps. Even with the requirements of no leakage, minimum maintenance, and with the problems involved in rubbing and bearing surfaces, mechanical pumping of liquid sodium at high temperatures is desirable because of high pump efficiencies and absence of power-supply problems. Mechanical pump development has drawn upon existing technology in pumping molten metals and other fluids at high temperatures. Emphasis has been almost exclusively on single-stage centrifugal pumps because they are mechanically simple and have favorable hydraulic characteristics. Multistage units have not been employed because sodium loops do not usually require high delivery heads. Gas-sealed reciprocating pumps have been built for special process systems requiring high head and low capacity at low temperature.

Problems encountered in pump design, summarized in order of importance, are as follows:

(1) Adequate lubrication to bearings whether rotating in or out of the sodium.

(2) Abrasion of bearing materials in contact with the high-temperature liquid, since sodium has poor lubrication qualities.

(3) High mechanical strength required because of vibration and bearing load problems.

(4) Cooling and radiation shielding of parts.

Items 1 and 2 are the only really vexatious problems. Vibration and bearing load problems have been reduced by using pumps with double volute cases. It has not been difficult to develop high-strength parts, since heavy sections are employed for all pressure containers and stressed parts. Cooling and radiation shielding problems are relatively simple. Most adversely affected parts can be removed and shielded from the heat and radiation source without impairing pump efficiency.

Mechanical pump development may be classified according to the type of pump seals employed: (1) membrane, (2) frozen, (3) gas. These general types indicate both the approach and specific design conditions. Three seal types are listed below, along with industrial or national research organizations largely responsible for developing them:

Membrane seal	—Byron-Jackson Westinghouse Allis-Chalmers
Frozen seal	—ORNL North American Aviation
Gas seal	—ANL, ORNL, KAPL

The gas-seal pump can be employed only in systems where the seal can be installed above a free surface of the liquid metal. Here they operate well and reliably.

Argonne National Laboratory [53] is now testing a 5000-gpm, 40-psi head, sump-type centrifugal pump with continuous argon gas leakage past a labyrinth seal and a dynamic hydraulic sodium bearing. The pump has operated for 6700 hr without incident at 700°F, 40 psi head. It was arbitrarily disassembled for inspection at 6700 hr. Inspection showed no wear of the bearing surfaces, and the pump life test is continuing. The pump has a 78% over-all efficiency. The mechanical pump is the least costly of the three types tested. Simplicity of construction, freedom from maintenance, and over-all good performance of the new mechanical pumps have brought about redesign of the EBR-II primary system to use them. The "submerged" arrangement of the EBR-II, with all mechanisms operating from above through an inert-gas blanket is particularly favorable to the use of such pumps. On the other hand, in systems where a pump must be installed in all-welded piping where pump seals would be in contact with sodium, the electromagnetic pump may be better suited.

Another characteristic favoring mechanical pumps is over-all efficiency. This is illustrated by comparing the efficiency of Argonne's 10,000-gpm DC

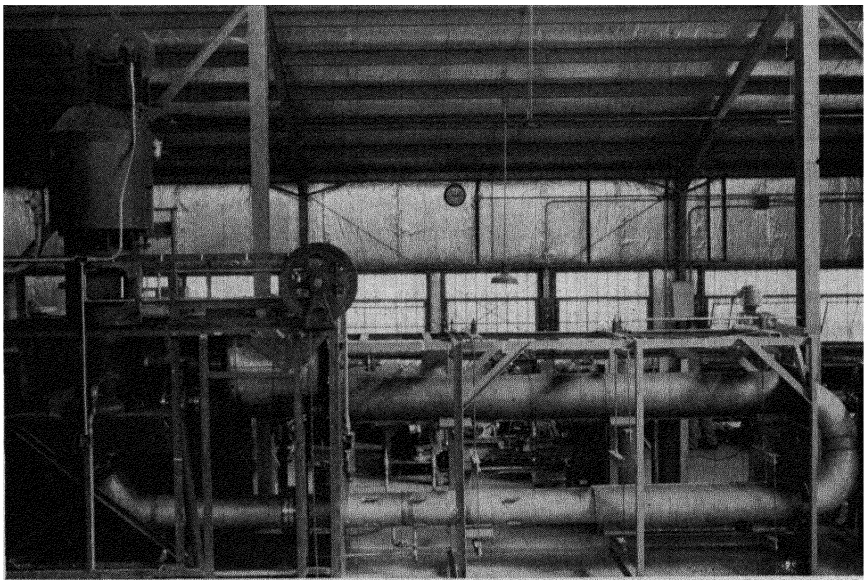

FIG. 2–18. General view of 5000-gpm mechanical pump test facility. This pump was operated for over 7000 hours at 700 to 900°F and 78% over-all efficiency without malfunction or maintenance.

electromagnetic pump with that of their 5000-gpm centrifugal pump [53], both of which recently completed preliminary testing. Even though the low-efficiency (~40%) rectifier was replaced by a more efficient (85 to 90%) homopolar generator, the over-all efficiency of the 10,000-gpm pump is still in the range of 40 to 45%, as compared with 78% for the centrifugal sump pump (Fig. 2–18).

As described in Chapter 4 and illustrated by Figs. 4–65 and 4–66, sodium is circulated in the Enrico Fermi Reactor by three 11,800-gpm centrifugal pumps in parallel loops. They are electric motor-driven, vertical-shaft, sump-type pumps, with inert gas seals, operating at 110 psi head at 550°F. Their over-all efficiency is 77%.

2–4.5 Transfer and handling systems [46,53]. Important aspects of sodium piping system design, construction, and operation are integrity, leaktightness, welding, and precleaning of austenitic stainless steel systems; methods of pre-heating systems; and instrumentation for flow control and for measuring flow rate, temperature, pressure, and liquid level.

Austenitic stainless steels are commonly used for sodium at least up to 900°F. A test loop of 2-inch (schedule-5) pipe—with sections of stainless steel types 304, 304L, 316, 321, and 347 welded together in various combinations—has operated at Argonne National Laboratory at about this temperature for two years without a weld or pipe failure. Two sodium pump test loops, constructed of 12-inch (schedule-10) pipe of stainless steel, type 304, have operated at 700 to 900°F for approximately 6000 hr each without difficulty. One loop employing ring joint flanges with stainless steel oval rings, studs, and nuts has not leaked. At Argonne National Laboratory, argon gas-blanketed, heliarc, first-pass welds are used without backup rings. Pipe and fittings are not cleaned in the completed system before filling with sodium, but dirt and grease are removed with solvents before welding in each section or component. Large systems, such as the pump test loops, are flushed with hot sodium and drained several times before final filling and startup. The following paragraphs discuss component types and design, and service techniques now in use.

*Piping.** Liquid metal piping is designed according to the same general rules that apply for more familiar fluids. The problem is more severe because of higher operating temperatures and the greater possibility of thermal shock and fatigue.

Thermal expansion is more severe than in most industrial piping because operating temperatures are higher (up to 1700°F) and because piping materials for sodium have high coefficients of thermal expansion. For temperatures above 800°F, one of the austenitic stainless steels (such as

*Condensed from Reference 59.

types 304, 316, 321, 347, and 310) is generally used. Their mean expansion coefficients are about 40% higher than those of carbon or intermediate alloy steels. There are indications that intermediate alloy and the ferritic stainless steels can be used with NaK or sodium up to 1100 or 1200°F. Should these materials prove feasible, pipe expansion will be decreased and cost should be less.

The low system design pressures for sodium-cooled reactors do not require heavy-walled piping.

Current liquid metal technology has need of a reliable high-temperature, breakable pipe joint. Threaded joints are often employed in small lines that must be disassembled frequently and are also used when some leakage can be tolerated. However, threaded joints are definitely not recommended for applications requiring long, reliable service at temperatures exceeding 500°F. Ground joint unions (metal-to-metal seat) have been successful in both carbon steel and stainless steel pipelines, but they are best employed only where they can be checked often or where some liquid metal leakage is tolerable. Most operating experience with ground joint unions has been with smaller sizes (1 inch or less) at temperatures under 500°F. A few have been utilized in 800 to 1000°F NaK lines.

The use of flanged joints in liquid metal service has been limited chiefly to components that must be removed from the system frequently and for joining dissimilar materials. Flange bolting and gaskets often relax at elevated temperatures, and leakage occurs. It has been recommended that socket welds be used with piping one inch or less in size, rather than conventional backing rings. In small piping, where the backing ring occupies too much of the flow area, it may increase pressure drop and interfere with drainage. Whenever possible, joints of a liquid metal piping system should be butt-welded. Butt welds have the advantages that they can be x-rayed, there is no appreciable reduction in pipe flexibility, less welding is required, and the piping system is stronger because there is little stress concentration.

Copper tubing with flared brass fittings is most commonly used for transferring small quantities of NaK at temperatures below 250°F. It is not suitable for high-temperature service or where thermal shock may be encountered.

Steel tubing with compression fittings can be employed over a wider range than can copper tubing. Satisfactory service up to 1400°F has been reported for "Swagelok" stainless steel fittings. However, there is comparatively little data on the use of tube and tube fittings at high temperatures. The system designer should utilize tube fittings with caution until their limitations are more clearly established. One thing is definite: only seamless pressure tubing should be used.

Supports for liquid metal piping are not much different from those used on conventional power piping, but because temperatures are likely to be higher, larger movement may have to be accommodated. For this reason, counterbalanced and constant support hangers may be called for.

Valves. Valves common in test facilities at Argonne National Laboratory are of stainless steel, with cast bodies, bellows seal, and backup packing. Drain and fill valves are usually 1 and 2-inch Crane gate valves. They have proved adequate and reliable. In each of the 12-inch pump test loops, a 12-inch Crane angle valve throttles pump flow. This stop valve will throttle about 50% flow. The valves have not leaked. In 1-inch, 2-inch, and 4-inch sizes, a reliable valve for 100% flow control is the Hammel-Dahl all-stainless steel bellows seal type with a remotely controlled air-diaphragm operator (Fig. 2–19). The valve has a cast body with a stellite seat; the stainless steel casting permits induction heating of contained sodium. Performance is without "chatter" at high or low flow, and without failures.

Another example of present application is the sodium throttle valve for the Enrico Fermi Atomic Power Plant (Chapter 4). As shown in Fig. 4–68, this is an angle type, double-bellows seal valve. The entire assembly is within a pipe riser that can be sealed above the hand wheel of the valve. The valve inner section is removable when the reactor is shut

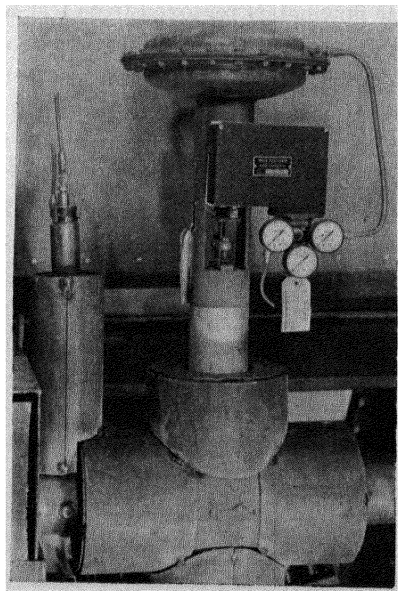

FIG. 2–19. General view of Hammel-Dahl control valve used in liquid sodium systems. All stainless steel construction permits induction heating.

down, without draining the primary system. The valve opening cannot be completely closed and flow inadvertently shut off.

Instruments. The range of operating temperatures encountered in sodium heat-transfer systems, from near the freezing point (208°F) to 1100°F, is a major factor in designing instruments. Operating pressure does not seriously affect instrument design but does influence the choice of instrument types for specific uses.

The magnetic flowmeter, entirely outside the sodium system, is a safe and reliable instrument with no moving parts. In addition, it will withstand the high temperature of the liquid sodium system. It consists of a permanent magnet fastened mechanically to the outside of a stainless steel pipe passing through the center of the air gap. Two wire output leads are welded to the pipe diametrically opposite each other at the center of the magnet air gap, in a plane 90° from that of the magnetic field.

Electromagnetic flowmeters calibrated with an orifice meter are in each major test facility at Argonne National Laboratory. For the 12-inch, schedule-10 piping system a small, inexpensive permanent magnet gives a flux of 200 gauss and an emf output of 12 mv at 5000-gpm flow. Experience with 30 electromagnetic flowmeters indicates that calibration against an orifice or weigh tank gives the most accurate flow measurements. This is especially desirable in the large pipe magnets where generated voltage is not quite proportional to flow. In EBR-I experience, laboratory calibrated electromagnetic flowmeters removed from test loops in Chicago and shipped as far as Idaho retained their calibration to within 2%.

Pressure transmitters with all-welded stainless steel bellows sensing elements have been used almost exclusively during the past three years in a variety of test facilities. Experience shows several things: the original factory "Zero" should not be tampered with, the air piping at the transmitter should be stainless steel if temperatures are over 800°F because, with copper, oxidation plugs the instrument, and the air supply should be free of moisture and dirt.

The simplest sodium level indicator is a probe: a metal rod, insulated from the tank or container, which can be lowered through an insulating packing gland into contact with the liquid sodium to complete an electrical circuit. This probe can also be mounted vertically on the tank bottom. A resistance level detector has been developed that offers maximum safety and reliability, requires no maintenance, operates in radioactive areas indefinitely, withstands shock and vibration, functions over a wide temperature range, and employs fairly simple, rugged auxiliary amplifier and measuring components.

Cleaning [60]. If the system is improperly or carelessly precleaned, the residual dirt, grease or oil, weld slag, surface oxides, moisture, etc.,

can be major sources of contamination. These will add oxygen, hydrogen, carbon, and insolubles to the sodium. However, even when precleaning is thorough, some pickup of impurities from metal surface oxides and absorbed gases is certain. Insoluble material can be removed by filtering. For startup, where cleanliness is important, the system should be conditioned by a series of high-temperature flushes, drainings, and refiltrations at low temperature.

All components should be installed free of grease, dirt, oil, and other foreign materials that could later react chemically with liquid metal or plug the piping or valves. During fabrication, metals are usually coated with oil or grease (which can carburize when exposed to high-temperature NaK or sodium) and they must be degreased. Pickling solutions, degreasing solutions, and detergent compounds can remove these organics. In the case of pickling, care must be taken to choose a solution suitable for all materials in both the system and components. While most systems are basically unimetallic, instruments and special equipment may contain other materials. After use, all traces of the pickling solution must be removed to prevent contamination of the liquid metal.

Degreasing solutions are satisfactory, but here again care must be taken to remove all traces of the solution to guard against halogenated hydrocarbons that could react chemically with the sodium or NaK, and hydrocarbons that could carburize the materials of construction.

An effective method is to flush the component with a nonsudsing detergent in hot water. After the system has been thoroughly flushed, it is

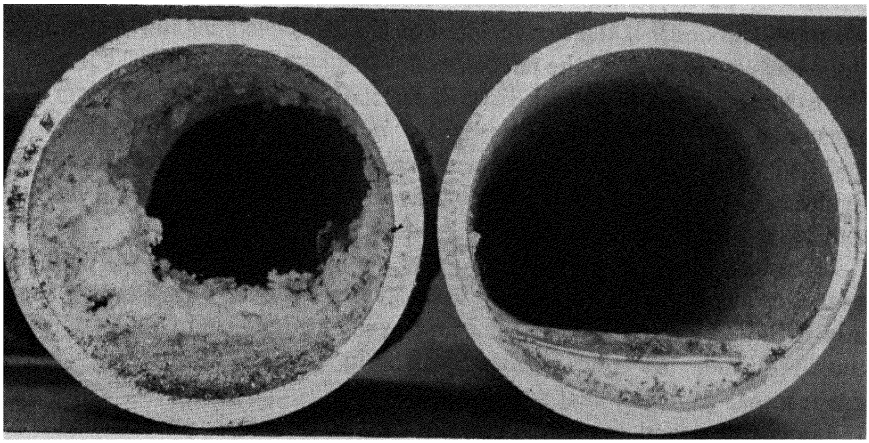

FIG. 2-20. View of sectional cut through two-inch pipe, showing partial plug of sodium oxide.

rinsed with hot water and dried completely under a vacuum or a flowing inert gas. Drying is very important in alkali metal systems, because of the chemical reactivity of these metals with water. Usually the system is heated to some definite temperature and evacuated to below the vapor pressure of water at that temperature.

Impurities are removed from the liquid metal system by cold trapping or by filtering. Two types of cold traps have been successful. The diffusion cold trap which operates continuously can remove slowly forming oxides if rapid decontamination is not required. However, if impurities enter the system in large quantities or if fast purification is necessary, a circulating cold trap is commonly used. It bears repeating that these systems must be operated within the maximum allowable cooling rate to prevent equipment plugging from precipitation in connecting piping. An example of partial plugging is shown in Fig. 2–20.

Heating. Large piping systems at Argonne National Laboratory have been preheated by electrical resistance, eddy currents, and by hot air forced over external piping surfaces. Sixty-cycle eddy-current heating appears to be most satisfactory, particularly for large systems (see Fig. 2–21). The larger the installation, the more the advantage of the few induction heating coils as compared with the increasing number of resistive heating circuits required. Also, the induction coils are outside the thermal insulating jacket, and their electrical insulation is protected from the high temperatures of the piping.

Maintenance and replacement of components. Auxiliaries such as vent, drain and instrument lines should be monitored frequently to ensure that their temperature is higher than the saturation temperature of the impurities of the system. These blind ends act as diffusion cold traps, and plugging will occur if the temperature of the lines becomes low enough for the oxides to deposit on the surfaces.

Instrument and cover gas lines connected to the gas space over the expansion tank often become plugged in high-temperature systems as distilled vapors cool and solidify. Proper design can minimize these difficulties, but temperature control of the lines near the nozzles to the system is required.

Liquid metal can be removed from or added to the system during operation, as necessary. In very large systems, liquid metal is occasionally withdrawn during normal heating to reduce the size of the expansion tank required. At times, leaking valves in the charge line may slowly drain metal from the heat-transfer system.

Maintaining and repairing sodium systems demands precautions that must be strictly observed. These are necessary to prevent excessive sodium oxidation when the system is exposed to the atmosphere.

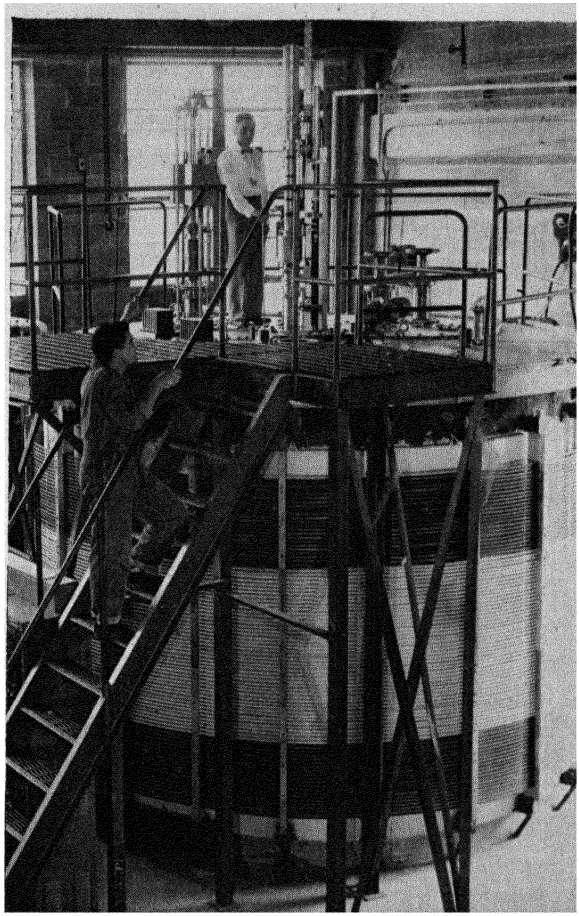

FIG. 2–21. General view of EBR-II model tank (5000-gallon Na capacity), showing induction heating coils and fuel-handling mechanism.

Three techniques are suited to sodium piping systems. If repair or modifications are extensive and involve many openings, it is advisable to clear all sodium from the system. After the piping is drained, the residual sodium film is chemically removed. This is laborious and complex, but once the sodium is removed from the system, repairs can take place in a conventional manner, i.e., no inert blanket gas is required. Removing sodium film is described later.

The other two repair methods are known as the "balloon" and "freeze" techniques. They are considered suitable for all but the most involved

and extensive maintenance and repair. The balloon technique, for piping 4 inches in diameter and larger, requires draining the sodium. A 2-inch hole is drilled on the side away from the pipe section to be removed, and an empty balloon is inserted in the hole and inflated. A balloon pressure 1 to 3 psi above the system pressure will effectively hold the inert gas in the system, to prevent oxidation. After the repair weld is made, the balloon is removed and a plug is welded into the hole. The balloon technique is particularly useful where excessive oxidation of the sodium is undesirable.

For smaller piping, or where oxygen contamination is less critical, the system can be drained, allowed to cool, and cut open. Rubber stoppers or caps made of masking tape prevent gross contamination by the atmosphere.

In the freezing technique, the sodium is not drained from the piping. The pipe is sealed by allowing the liquid metal to solidify in it. When the pipe is cut frozen sodium is exposed, and although the surface will oxidize, the solid sodium plug protects the rest of the system from contamination.

If it is not necessary to remove a component, welding can usually be done in place. The sodium is drained and the system filled with inert gas at about atmospheric pressure. Although the sodium film should be removed, this is not absolutely necessary. Standard welding procedures can be utilized on the outer system surfaces.

2–4.6 EBR-II working model.* To demonstrate the feasibility of the submerged primary system design concept, a fairly large working model of the EBR-II was built (Figs. 2–21, 2–22, and 2–23). The model duplicates major components of the parent design,* appropriately scaled. It comprises:

(1) The primary tank (approximately 11 ft in diameter by 8 ft deep), which contains approximately 5000 gal of sodium; the sodium is heated electrically and is maintained at approximately 750°F, approximating the ambient sodium temperature in the EBR-II system.

(2) A reactor mockup of 61 "dummy fuel subassemblies."

(3) A prototype DC electromagnetic pump with a capacity of 1000 gpm at 40 psi head;† the pump, piping, reactor, and instrumentation are interconnected as in the EBR-II primary system. Since this is an isothermal experiment, the heat exchanger is omitted and a throttle valve

*Taken from Reference 61.

†Because of a design change, the EBR-II will employ two 5000-gpm mechanical pumps (described in Chapter 3).

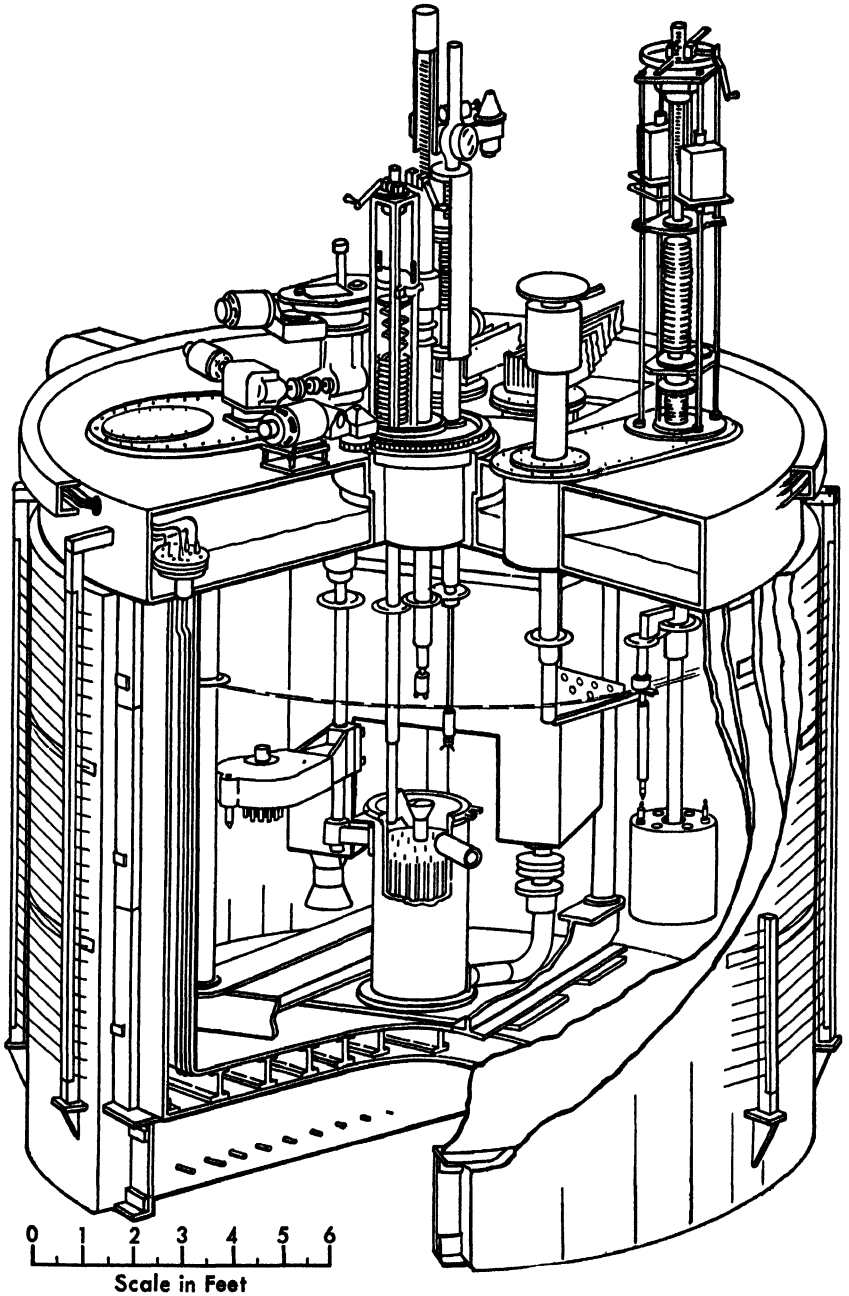

FIG. 2-22. Cutaway perspective of EBR-II model tank, showing internal arrangement of core assembly, inner tank support, pump enclosures, and subassembly storage, as well as external top-mounted access and handling equipment.

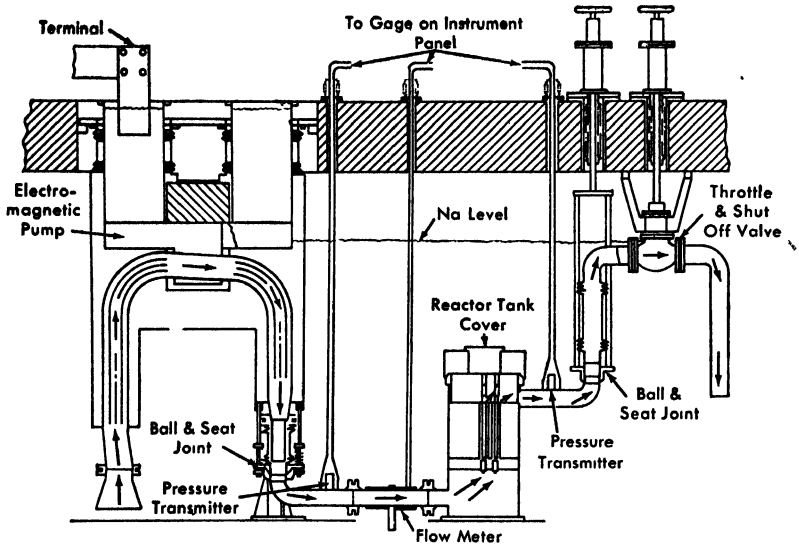

FIG. 2–23. Schematic drawing of EBR-II model tank internals, showing coolant flow path and important instrumentation.

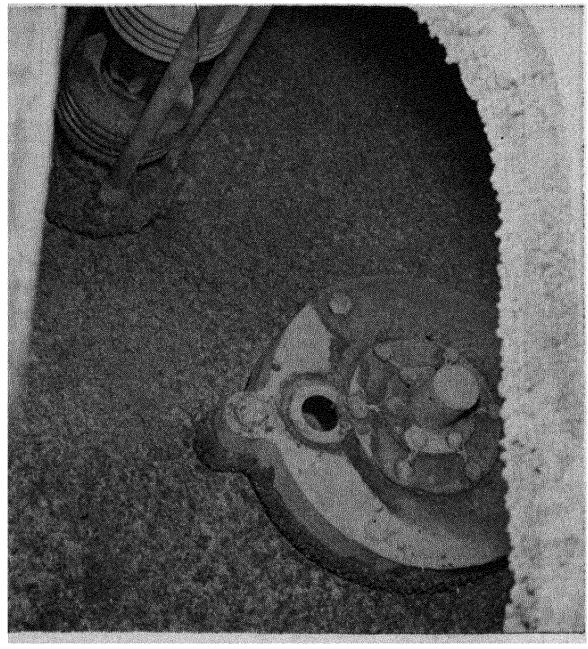

FIG. 2–24. View into sodium tank following equipment removal. Sodium in tank is frozen and covered with oxide; subsequently, this oxide was removed within three days by cold trapping.

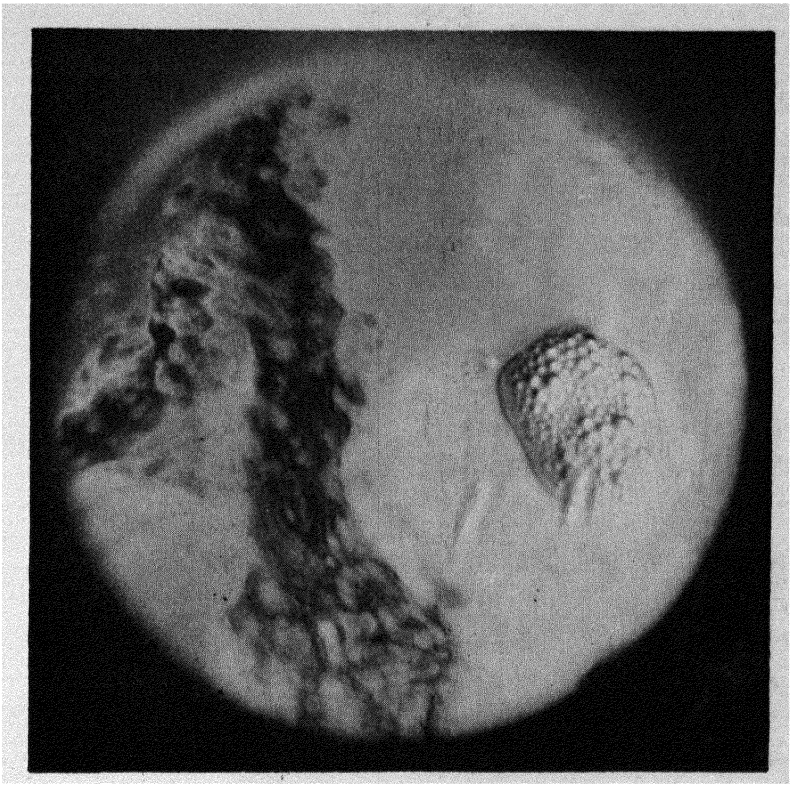

FIG. 2–25. Free sodium surface through viewport during operation, showing bubbles and ripples caused by free-falling sodium from cold trap return line.

substituted. The arrangement of the flow system is shown schematically in Fig. 2–23.

(4) A bypass circulation sodium purification system which includes a pump, regenerative heat exchanger, and cold trap for the continuous circulation of sodium and continuous removal of sodium oxide.

(5) A prototype shutdown cooler.

Operation of the system components has shown that the physical arrangement and the operational procedures are entirely feasible. There has been periodic fuel handling with approximately 80 loading and unloading operations to date. The pump has operated 4500 hr without difficulty. The continuous bypass sodium purification system has shown that it is feasible to maintain sodium purity below 0.002 w/o O_2. This was accomplished in a system in which the inert gas blanket leakage is higher than is expected in the EBR-II system. The shutdown cooler has functioned satisfactorily, and the heat-removal capability has met expectations.

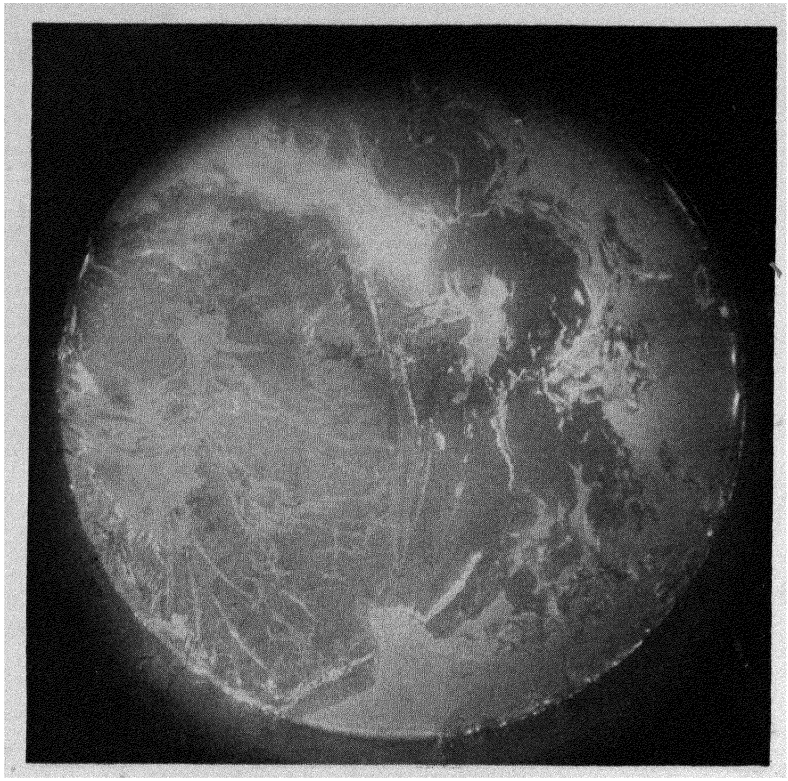

FIG. 2–26. Free sodium surface during operation, shown for comparison with oxide coated surface of Fig. 2–24.

Particularly significant has been the comparative ease with which the system has been modified. Of course, there is no radioactivity, but these modifications have been made in the face of all the "chemical problems" associated with sodium. This has shown that maintenance problems expected in the EBR-II can be solved if added precautions are taken for radioactive sodium.

Valuable experience was obtained from the system after the sodium was contaminated with oxygen during maintenance. Comparable system contamination in small experimental loops and apparatus has caused much difficulty in the past. In the working model, the system was quickly and easily purified, and normal operation resumed. Large amounts of sodium oxide formed after major component removal can simply and economically be removed by cold trapping. A view through an open equipment hatch in the sodium tank is shown in Fig. 2–24. Sodium in the tank is frozen and covered with oxide. Three days after

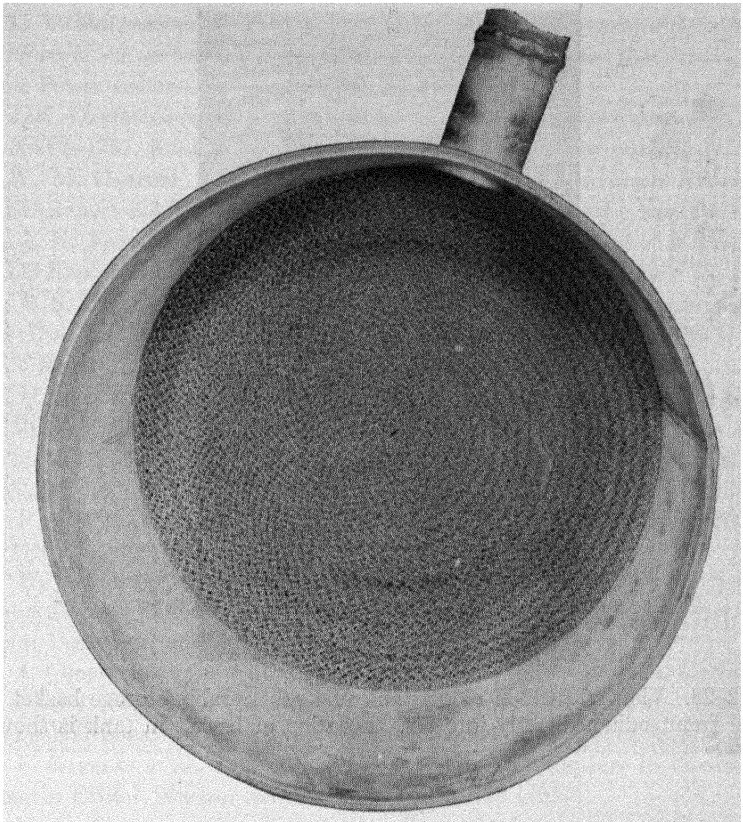

FIG. 2-27. View of stainless steel mesh packing in cold trap.

operation was resumed, this oxide was removed by the cold trap. Figures 2–25 and 2–26 show the free sodium surface during operation. In Fig. 2–25, the bubbles and ripples are caused by free-falling sodium from the cold trap return line. Figure 2–26 should be compared with the oxide coated surface in Fig. 2–24. A view of the stainless steel mesh packing in the cold trap is shown in Fig. 2–27. A view of the EBR-II model tank fuel subassembly storage basket is shown in Fig. 2–28; the particles adhering to the basket outer surface are sodium oxide formed upon removal of the basket directly into air. Location of the subassembly basket in the tank is shown in Fig. 2–22. This experience has lessened concern over inadvertent oxygen contamination of the sodium system. It also suggests that larger sodium systems are much more reliable than the small experimental systems from which most previous experience has been drawn.

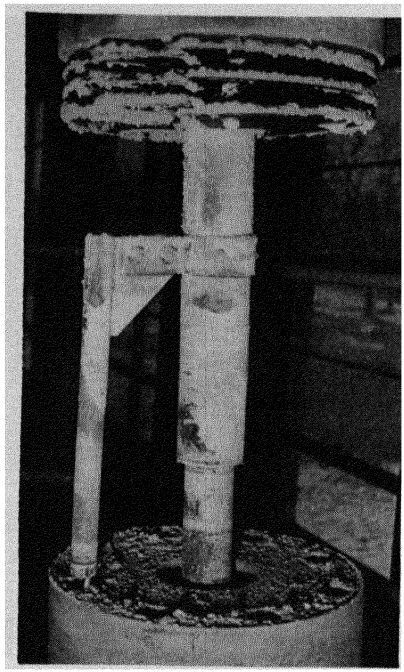

FIG. 2–28. View of EBR-II model tank fuel subassembly storage basket after removal from sodium directly into air. Location of basket in tank is shown in Fig. 2–22.

REFERENCES

1. W. H. ZINN, Review of Fast Power Reactors, in *Proceedings of the International Conference on the Peaceful Uses of Atomic Energy*, Vol. 3. New York: United Nations, 1956. (P/814, p. 198)

2. J. R. DIETRICH, The Physics of Nuclear Reactors: The Physics of Advanced Reactors, *Brit. J. Appl. Phys. Suppl. No. 5*, S9–S26 (1956).

3. H. V. LICHTENBERGER et al., Operating Experience Obtained from an NaK-Cooled Fast Reactor, in *Proceedings of the International Conference on the Peaceful Uses of Atomic Energy*, Vol. 3. New York: United Nations, 1956. (P/813, p. 345)

4. J. W. KENDALL and T. M. FRY, The Dounreay Fast Reactor Project, in *Proceedings of the International Conference on the Peaceful Uses of Atomic Energy*, Vol. 3. New York: United Nations, 1956. (P/405, p. 193)

5. Dounreay Fast Reactor, *Nuclear Power* **2**(14), 221 (June 1957).

6. J. K. DAVIDSON, *The Fast Oxide Breeder—A Summary*, USAEC Report KAPL-1701, Knolls Atomic Power Laboratory, July 1, 1957.

7. D. F. MOLINO and J. K. DAVIDSON, *The Fast Oxide Breeder—Reactor Analysis. Part II. Reactor Calculations*, USAEC Report KAPL-1756(Pt. II), Knolls Atomic Power Laboratory, June 30, 1957.

8. J. K. DAVIDSON et al., *The Fast Oxide Breeder, The Fuel Cycle*, USAEC Report KAPL-1757, Knolls Atomic Power Laboratory. (To be published)

9. W. M. CASHIN, *The Fast Oxide Breeder—Fuel Irradiation Experiments*, USAEC Report KAPL-1784, Knolls Atomic Power Laboratory, Aug. 26, 1957.

10. J. N. FRANK, *The Fast Oxide Breeder—Sintering Studies of PuO_2-UO_2*, USAEC Report KAPL-1837, Knolls Atomic Power Laboratory, July 15, 1957.

11. R. S. MILLER, *Estimated Internal Pressure in Fast Oxide Breeder Fuel Elements Due to Fission Gas Release*, USAEC Report KAPL-M-RSM-3, Knolls Atomic Power Laboratory, Dec. 5, 1956.

12. D. OKRENT et al., A Survey of the Theoretical and Experimental Aspects of Fast Reactor Physics, in *Proceedings of the International Conference on the Peaceful Uses of Atomic Energy*, Vol. 5. New York: United Nations, 1956. (P/609, p. 345)

13. R. AVERY, *Fast Reactor Physics Calculations*, USAEC Report ANL-5492(Del.), Argonne National Laboratory, January 1956.

14. W. B. LOEWENSTEIN and D. OKRENT, The Physics of Fast Power Reactors: A Status Report, paper prepared for the Second International Conference on the Peaceful Uses of Atomic Energy, Geneva, 1958. (P/637)

15. J. CODD et al., The Physics of Fast Reactors, in *Progress in Nuclear Energy, Series I, Physics and Mathematics*, ed. by R. A. Charpie et al. New York: McGraw-Hill Book Company, Inc., 1956. (Chap. 9)

16. P. KAFALAS et al., Determination of the Ratio of Capture to Fission Cross Sections in EBR-I, *Nuclear Sci. and Eng.* **2**, 657–663 (1957).

17. H. C. PAXTON et al., Los Alamos Scientific Laboratory, 1956. Unpublished.

18. J. J NEUER et al., Los Alamos Scientific Laboratory, 1956. Unpublished.

19. G. A. JARVIS et al., Los Alamos Scientific Laboratory, 1956. Unpublished.

20. V. R. JOSEPHSON et al., *Oralloy Shape Factor Measurements*, USAEC Report LA-1155(Del.), Los Alamos Scientific Laboratory, Aug. 8, 1950.

21. H. C. PAXTON and G. A. GRAVES, *Critical Masses of Fissionable Metals as Basic Nuclear Safety Data*, USAEC Report LA-1958, Los Alamos Scientific Laboratory, 1956.

22. F. C. BEYER et al., The Fast Exponential Experiment, in *Proceedings of the International Conference on the Peaceful Uses of Atomic Energy*, Vol. 5. New York: United Nations, 1956. (P/598, p. 342)

23. B. C. CERUTTI et al., ZPR-III, Argonne's Fast Critical Facility, *Nuclear Sci. and Eng.* **1**, 126–134 (1956).

24. J. K. LONG et al., Fast Neutron Power Reactor Studies on ZPR-III, paper prepared for the Second International Conference on the Peaceful Uses of Atomic Energy, Geneva, 1958. (P/598)

25. B. G. CARLSON, *Solution of the Transport Equation by S_n Approximations*, USAEC Report LA-1891, Los Alamos Scientific Laboratory, February 1955.

26. B. CARLSON et al., The S_n Method for Solution of the Transport Equation, paper prepared for the Second International Conference on the Peaceful Uses of Atomic Energy, Geneva, 1958. (P/626)

27. J. B. SAMPSON and D. F. MOLINO, *An α_{49} (E) Curve Consistent with EBR-I Measurements and Also with Most Former Measurements*, USAEC Report KAPL-1793, Knolls Atomic Power Laboratory, May 16, 1957.

28. G. GOERTZEL, An Estimation of Doppler Effect in Intermediate and Fast Neutron Reactors, in *Proceedings of the International Conference on the Peaceful Uses of Atomic Energy*, Vol. 5. New York: United Nations, 1956. (P/613, p. 472)

29. H. YAMAUCHI and J. DEFELICE, Nuclear Development Associates, Inc., 1955. Unpublished

30. A. M. LANE, *An Estimation of the Doppler Effect in Fast Neutron Reactors*, Report AERE-T/M-137, Great Britain, Atomic Energy Research Establishment, July, 1956.

31. H. A. BETHE, *On the Doppler Effect in Fast Reactors*, Report APDA-119, Atomic Power Development Associates, Inc., 1957.

32. L J KOCH et al., *Experimental Breeder Reactor II (EBR-II), Hazard Summary Report*, USAEC Report ANL-5719, Argonne National Laboratory, May 1957.

33. W. J. MCCARTHY, JR., et al., Studies of Nuclear Accidents in Fast Power Reactors, paper prepared for the Second International Conference on the Peaceful Uses of Atomic Energy, Geneva, 1958. (P/2165)

34 G. R. KEEPIN et al., *Delayed Neutrons from Fissionable Isotopes of Uranium, Plutonium, and Thorium*, USAEC Report LA-2118, Los Alamos Scientific Laboratory, February 1957; *Phys. Rev* **107**, 1044–1049 (1957).

35. R. O. BRITTAN and F. W. THALGOTT, The EBR-I Meltdown—Course of the Experiment, paper presented at the American Nuclear Society Third Annual Meeting, June 1957. (Paper 25-1)

36. R. O. BRITTAN, The EBR-I Meltdown—Analysis of the Incident, paper presented at the Third American Nuclear Society Annual Meeting, June 1957. (Paper 25-2)

37. R. O. BRITTAN, *Some Problems in the Safety of Fast Reactors*, USAEC Report ANL-5577, Argonne National Laboratory, May 1956.

38. J. H. KITTEL et al., *The EBR-I Meltdown—Physical and Metallurgical Changes in the Core*, USAEC Report ANL-5731, Argonne National Laboratory, November 1957.

39. H. A. BETHE and J. H TAIT, Great Britain, Atomic Energy Research Establishment; 1956. Unpublished.

40. H. A. BETHE, *Reactor Safety and Oscillator Tests*, Report APDA-117, Atomic Power Development Associates, Inc., Oct. 15, 1956.

41. R. O. BRITTAN, Analysis of the EBR-I Core Meltdown, paper prepared for the Second International Conference on the Peaceful Uses of Atomic Energy, Geneva, 1958. (P/2156)

42. R. E. RICE et al., *EBR-I, MARK-III—Design Report*, USAEC Report ANL-5836, Argonne National Laboratory, March 1958.

43. Staff of Argonne National Laboratory, Idaho Division, 1957. Personal communication.

44. G. H. Kinchin, *The Stability of Fast Reactors*, Report AERE-RP/M-83, Great Britain, Atomic Energy Research Establishment, June 1956.

45. J. F. Boland, Stability Studies on EBR-I, paper prepared for the Second International Conference on Peaceful Uses of Atomic Energy, Geneva, 1958. (P/1845)

46. C. B. Jackson et al. (Eds.), *Liquid Metals Handbook, Sodium-NaK Supplement,* USAEC Report TID-5277, U. S. Atomic Energy Commission and Bureau of Ships, July 1, 1955.

47. W. L. Fleischmann and R. F. Koenig, Materials and Fabrication, in *Liquid Metals Handbook, Sodium-NaK Supplement*, ed. by C. B. Jackson, USAEC Report TID-5277, U. S. Atomic Energy Commission and Bureau of Ships, July 1, 1955. (Chap. 3, p. 178)

48. R. R. Miller and L. F. Epstein, Physical Properties, in *Liquid Metals Handbook, Sodium-NaK Supplement*, ed by C. B. Jackson, USAEC Report TID-5277, U. S. Atomic Energy Commission and Bureau of Ships, July 1, 1955. (Chap. 1, p. 33)

49. O. J. Woodruff et al., Coolant, *Nucleonics* **11**(6), 27 (1953).

50. A. H. Barnes and J. F Cage, Jr., Pumps—Electromagnetic, in *Liquid Metals Handbook, Sodium-NaK Supplement*, ed. by C B. Jackson, USAEC Report TID-5277, U S Atomic Energy Commission and Bureau of Ships, July 1, 1955. (Chap. 4, p. 288)

51. A. H. Barnes, Pumping of Liquid Metals, Progress in Nuclear Energy, Series IV, *Technology and Engineering*, ed. by R Hurst and S. McLain. New York: McGraw-Hill Book Company, Inc., 1956. (Chap. 5, Sec 5.1, p. 165)

52. R. A. Jaross, Argonne National Laboratory, 1958 Unpublished.

53. F. A. Smith, Argonne National Laboratory, March 1958. Unpublished.

54. A H. Barnes and R A. Jaross, Design and Operation of a 10,000 GPM D-C Electromagnetic Sodium Pump and Its Associated 250,000 Ampere Homopolar Generator, paper prepared for the Second International Conference on the Peaceful Uses of Atomic Energy, Geneva, 1958. (P/2157)

55. O. S. Seim and R A. Jaross, 5,000 GPM Electromagnetic and Mechanical Pumps for the EBR-II Sodium System, *Second Nuclear Engineering and Science Conference*, Held at Philadelphia, Pa., Mar. 11–14, 1957. (Paper 57-NESC-94)

56. W. B. Woolen, Electromagnetic Pumps for Reactors, *Nuclear Power* **2**(15), 267 (July 1957).

57. W. J. Kendall and T. M. Fry, Dounreay Fast Reactor Project, in *Proceedings of the International Conference on the Peaceful Uses of Atomic Energy*, Vol. 3. New York: United Nations, 1956. (P/405, p. 193)

58. D. A. Watt, Design of Traveling Field Electromagnetic Pumps for Liquid Metals, *Engineering* **181**, 264 (Apr. 27, 1956).

59. S. N. Tower and J. E. Bowker, Piping Considerations, in *Liquid Metals Handbook, Sodium-NaK Supplement*, ed. by C. B. Jackson, USAEC Report TID-5277, U. S. Atomic Energy Commission and Bureau of Ships, July 1, 1955. (Chap. 3, p. 236)

60. C. B. JACKSON (Ed.), *Liquid Metals Handbook, Sodium-NaK Supplement*, USAEC Report TID–5277, U. S. Atomic Energy Commission and Bureau of Ships, July 1, 1955.

61. L. J. KOCH et al., *Hazard Summary Report, Experimental Breeder Reactor II (EBR-II)*; USAEC Report ANL-5719, Argonne National Laboratory, May 1957. (p. 44)

62. FRANK BONI, On the Design of a Liquid-Metal-Heated Bayonet-Tube Steam Generator, paper presented at the American Society of Mechanical Engineers Semi-Annual Meeting, San Francisco, Calif., June 9–13, 1957. (Paper 57-SA-24)

TABLE 2-2

TABLE 2–2

ELEVEN-GROUP CROSS SECTIONS FOR VARIOUS MATERIALS [14]

(Refer to Table 2–1 for definition of symbols.)

Pu^{239} ($N = 0.048 \times 10^{24}$)																
											$\sigma_{in,\ j\to j+k}$					
j	σ_{tr}	ν	σ_f	α (std)	α (high)	α (low)	σ_{el} α (std)	σ_{el} α (high)	σ_{el} α (low)	σ_{in}	$k = 1$	2	3	4	5	6
1	4.6	3.18	2.0	0.02	0.02	0.02	0.0142	0.0142	0.0142	1.35	0.513	0.382	0.221	0.120	0.0648	0.0486
2	4.6	3.09	1.95	0.04	0.04	0.02	0.0238	0.0238	0.0244	1.0	0.457	0.264	0.143	0.0780	0.0385	0.0195
3	5.26	3.02	1.86	0.05	0.05	0.03	0.0438	0.0438	0.0444	0.7	0.331	0.179	0.0980	0.0490	0.0245	0.0182
4	5.9	2.97	1.75	0.07	0.08	0.04	0.0559	0.0554	0.0568	0.7	0.336	0.183	0.0917	0.0446	0.0340	0.0084
5	7.1	2.95	1.70	0.10	0.12	0.05	0.0811	0.0806	0.0826	0.4	0.200	0.100	0.0512	0.0371	0.00884	0.00248
6	8.5	2.93	1.68	0.16	0.20	0.07	0.106	0.105	0.109	0.23	0.115	0.0591	0.0428	0.0101	0.00276	—
7	9.5	2.92	1.73	0.23	0.30	0.12	0.124	0.122	0.127	0						
8	10.8	2.91	1.80	0.30	0.37	0.20	0.142	0.140	0.145	0						
9	12.3	2.91	2.0	0.37	0.42	0.30	0.0803	0.0795	0.0815	0						
10	16.4	2.91	2.25	0.47	0.50	0.40	0.110	0.109	0.115	0						
11	16.8	2.91	3.5	0.60	0.60	0.50	0	0	0	0						

TABLE 2-2 (*continued*)

	U^{233} ($N = 0.048 \times 10^{24}$)											
							$\sigma_{in,\ j \to j+k}$					
j	σ_{tr}	ν	σ_f	α	σ_{el}	σ_{in}	$k = 1$	2	3	4	5	6
1	4 3	2 8	1.80	0 028	0 0141	1 25	0 479	0 359	0.208	0.112	0.0625	0 030
2	4.5	2.65	1 85	0 043	0 0237	1 00	0 457	0 264	0 143	0 078	0.039	0.019
3	4.8	2 59	1.94	0 057	0 0336	0 75	0 355	0 192	0 105	0 0525	0 0262	0.0195
4	5.5	2 55	2.04	0 074	0.0497	0 35	0 168	0 0917	0 0458	0 0234	0.0168	0.0042
5	5.7	2 53	2.21	0 090	0 0536	0.10	0 0501	0 0250	0 0128	0.00927	0 00221	0 00062
6	7.0	2.52	2 27	0 10	0 0756	0						
7	9.0	2 52	2.43	0 10	0 106	0						
8	11.0	2.51	2 57	0 10	0.137	0						
9	15 0	2 51	3 0	0 10	0 0983	0						
10	20 0	2 51	4.2	0 10	0 129	0						
11	25 0	2.51	7 0	0 10	0	0						

(*continued*)

TABLE 2-2 (*continued*)

	U^{235} ($N = 0.048 \times 10^{24}$)											
							$\sigma_{in,\ j \to j+k}$					
j	σ_{tr}	ν	σ_f	α	σ_{el}	σ_{in}	$k = 1$	2	3	4	5	6
1	4 5	2.77	1.3	0 077	0.00941	2.3	0 881	0.660	0.382	0 207	0.115	0.0552
2	4.5	2 65	1 28	0.078	0 0192	1 85	0.845	0.488	0 265	0.144	0.0712	0.0361
3	4.8	2.58	1.25	0.08	0.0386	1.15	0.544	0.294	0.161	0.0805	0.0402	0.0299
4	5.1	2.53	1.20	0.12	0.0429	1 2	0.576	0.341	0.157	0.0798	0.0582	0.0144
5	6.3	2.51	1.28	0.15	0.0694	0 7	0.351	0 175	0.0896	0.0649	0.0155	0 00434
6	7.9	2.49	1.42	0.18	0.0978	0.4	0.200	0.103	0.0744	0.0176	0.0048	0
7	9.65	2 48	1 6	0.20	0.130							
8	10 9	2.47	1.9	0.25	0.143							
9	12.25	2.47	2 3	0.30	0 0778							
10	13 5	2.47	3.4	0 35	0 0748							
11	14.3	2.47	6 0	0.42	0							

TABLE 2–2 (*continued*)

	U^{238} ($N = 0.048 \times 10^{24}$)											
							$\sigma_{in,\ j \to j+k}$					
j	σ_{tr}	ν	σ_f	σ_c	σ_{el}	σ_{in}	$k = 1$	2	3	4	5	6
1	4.7	2.65	0.59	0.015	0 0144	2.87	1.06	0.46	0.66	0.39	0.12	0 18
2	4.5	2.55	0.45	0.062	0.0234	2 44	0.62	0.89	0.52	0.16	0.10	0.15
3	5.0	2.47	0 003	0.13	0 0616	1.20	0 52	0 35	0 22	0 11	0	0
4	5.5	0	0	0.143	0 0826	0 44	0 44	0				
5	6.7	0	0	0.13	0 102	0 47	0.47	0				
6	8.25	0	0	0 15	0 127	0 55	0.50	0.05				
7	9.65	0	0	0 20	0.150	0.55	0.55	0				
8	10.9	0	0	0.30	0 171	0 40	0.38	0.02				
9	12.25	0	0	0.40	0.0991	0 05	0 03	0.02				
10	13.5	0	0	0.61	0.108	0						
11	14.3	0	0	0 80	0	0						

(*continued*)

TABLE 2-2 (*continued*)

	Th^{232} ($N = 0.03 \times 10^{24}$)											
							$\sigma_{in,j\to j+k}$					
j	σ_{tr}	ν	σ_f	σ_c	σ_{el}	σ_{in}	$k = 1$	2	3	4	5	6
1	4.3	2 4	0 135	0 03	0 0102	3.3	1 22	0 53	0.76	0 45	0.14	0 20
2	4.5	2 3	0 10	0 04	0 0244	2 8	0 71	1 02	0 60	0 18	0 12	0 17
3	4 6	0	0	0 08	0 0569	1 25	0 54	0.37	0.23	0.11	0	0
4	5 1	0	0	0 15	0 0786	0 43	0.43	0	0	0	0	0
5	6 6	0	0	0 20	0 104	0 40	0 40	0	0	0	0	0
6	8.0	0	0	0 25	0 127	0 45	0 40	0 05				
7	9 2	0	0	0 32	0 147	0 43	0 43					
8	10 5	0	0	0 38	0 171	0 32	0 32					
9	11 6	0	0	0 50	0 0966	0						
10	13 5	0	0	0 60	0.112	0						
11	14 0	0	0	0 80	0	0						

TABLE 2–2 (*continued*)

Pu^{240} ($N = 0.048 \times 10^{24}$)												
							$\sigma_{in,\ j\to j+k}$					
j	σ_{tr}	ν	σ_f	σ_c	σ_{el}	σ_{in}	$k = 1$	2	3	4	5	6
1	4 6	2 65	1.6	0 02	0 0127	1 9	0 701	0 304	0 437	0.258	0.0798	0 120
2	4 6	2.55	1 5	0 08	0 0237	1 45	0 368	0 529	0 309	0 0957	0 0594	0 0885
3	5 3	2 47	1 35	0 18	0 0516	0 70	0 303	0 204	0 128	0 0644	0	0
4	5.9	2 47	0 7	0 20	0 0764	0 45	0 45	0	0	0	0	0
5	7 1	2.47	0.18	0.20	0 105	0 45	0 45	0	0	0	0	0
6	8 5	2.47	0.03	0 20	0 131	0 45	0 410	0 040	0	0	0	0
7	9 5	0	0	0 30	0 147	0 45	0 45	0	0	0	0	0
8	10 8	0	0	0 45	0 170	0 25	0 238	0 012	0	0	0	0
9	12 3	0	0	0.70	0 0974	0						
10	16.4	0	0	1 0	0 129	0						
11	16 8	0	0	1 5	0	0						

(*continued*)

TABLE 2-2 (*continued*)

	O ($N = 0.096 \times 10^{24}$)		Na ($N = 0.022 \times 10^{24}$)				$\sigma_{in,\ j \to j+k}$					
j	σ_{tr}	σ_{el}	σ_{tr}	σ_c	σ_{el}	σ_{in}	$k = 1$	2	3	4	5	6
1	1 05	0 178	1 9	0 0003	0.167	0 50	0.32	0 065	0 04	0 03	0 015	0.03
2	1.6	0.348	2 5	0 0003	0.337	0 30	0.30	0	0	0	0	0
3	3.6	0.871	3.3	0 0005	0.494	0.40	0 284	0 116	0	0	0	0
4	3.0	0.726	3 2	0 0006	0 477	0 40	0 08	0 128	0 076	0 044	0.044	0 028
5	5.7	1.379	3 3	0 0008	0.562	0						
6	3 35	0.811	3.6	0 001	0.613	0						
7	3.26	0.789	3 5	0 001	0.596	0						
8	3.26	0.789	3 3	0 001	0 562	0						
9	3.26	0.394	4 9	0 003	0 417	0						
10	3.26	0.394	4 9	0 001	0 417	0						
11	3 26	0	10.0	0 005	0	0						

TABLE 2–2 (*continued*)

j	C ($N = 0.0838 \times 10^{24}$)		Mo ($N = 0.0640 \times 10^{24}$)				$\sigma_{in,\ j \to j+k}$					
	σ_{tr}	σ_{el}	σ_{tr}	σ_c	σ_{el}	σ_{in}	$k = 1$	2	3	4	5	6
1	1.4	0.311	2.5	0 010	0 0320	1.40	0 35	0.40	0 30	0.15	0.10	0 10
2	1.8	0.515	3.2	0.017	0 0886	0.84	0.411	0.33	0.099	0	0	0
3	2.17	0.690	4.0	0.024	0.150	0.40	0	0 108	0.117	0.068	0.042	0.065
4	2.97	0.944	5.3	0.034	0.221							
5	3.24	1.030	6.4	0.040	0.267							
6	3.79	1.204	7.2	0 046	0.300							
7	3.98	1.265	7.8	0.057	0 325							
8	4.16	1.322	7.9	0.066	0.329							
9	4.25	0.675	7 4	0.090	0 154							
10	4.36	0.693	7.1	0.120	0.147							
11	4.33	0	7.2	0.200	0							

(*continued*)

TABLE 2–2 (*continued*)

	Fe ($N = 0.0847 \times 10^{24}$)										
					$\sigma_{in,\ j \to j+k}$						
j	σ_{tr}	σ_c	σ_{el}	σ_{in}	$k = 1$	2	3	4	5	6	7
1	2.05	0.005	0.0432	1.18	0.450	0.206	0 196	0.122	0.0802	0 0448	0.0814
2	2.0	0.005	0 0864	0 65	0	0 39	0 26	0	0	0	0
3	1.9	0.005	0.107	0 4	0 170	0 104	0 0592	0 0332	0.0332	0	0
4	2.2	0.005	0 157	0							
5	3.0	0.006	0 214	0							
6	3.5	0 007	0.249	0							
7	4.3	0.008	0.306	0							
8	5.3	0.008	0.378	0							
9	6.8	0 025	0.242	0							
10	4 0	0.012	0.142	0							
11	8.0	0 014	0	0							

TABLE 2-2 (*continued*)

Al ($N = 0.0603 \times 10^{24}$)

j	σ_{tr}	σ_c	σ_{el}	σ_{in}	$\sigma_{in,\, j \to j+k}$						
					$k = 1$	2	3	4	5	6	7
1	1 45	0 0003	0 0930	0.54	0.211	0 108	0 081	0.0648	0.0270	0.0324	0.0162
2	1.8	0 0004	0.197	0.30	0.147	0 123	0 030	0	0	0	0
3	2 0	0 0005	0 279	0 09	0 018	0 0279	0 0189	0 0135	0.0117	0	0
4	2.85	0 0007	0 416	0							
5	3.1	0 0015	0.452	0							
6	4.1	0.0018	0.598	0							
7	5.6	0 0040	0 817	0							
8	4 0	0.0035	0 583	0							
9	5 5	0 0090	0.401	0							
10	1 8	0 0080	0.131	0							
11	1 6	0.0120	0	0							

(*continued*)

TABLE 2–2 (*continued*)

	Ta (N = 0.0553 × 10)									
					$\sigma_{in,\ j\to j+k}$					
j	σ_{tr}	σ_c	σ_{el}	σ_{in}	k = 1	2	3	4	5	6
1	3.7	0.07	0.0174	2 5	0 95	0 708	0 410	0 222	0 120	0.09
2	4.5	0.09	0 0438	2 2	1 005	0 581	0 315	0.172	0 0847	0 0429
3	5.0	0.10	0.0748	1 5	0.710	0.384	0 21	0.105	0 0525	0 039
4	5 2	0.14	0 0937	0 8	0 384	0.210	0 105	0 0532	0 0388	0.0096
5	5.6	0.20	0.119	0						
6	6.3	0.25	0.133	0						
7	7.5	0.30	0.158	0						
8	8.1	0 35	0.170	0						
9	9.9	0 40	0.104	0						
10	10.0	0 70	0.102	0						
11	17.0	1 50	0	0						

(*concluded*)

TABLES 2-5 AND 2-6

TABLE 2–5

SURVEY OF STEADY-STATE PROPERTIES OF REFLECTED SPHERICAL REACTORS WITH VARIOUS ENRICHMENTS [14]

	Concentrated Pu^{239} fuel		EBR-II Pu^{239} fuel		EBR-II U^{235} fuel	
Core volume,* liters	12.5		50		50	
Core radius,† cm	14.4		22 85		22 85	
Ratio fuel atoms to U^{238} atoms	1.23		0.38		0.86	
Critical mass of fuel, kg	42.0		84.4		138.5	
Flux integral for:	Core	Blanket	Core	Blanket	Core	Blanket
Group *Energy interval, Mev*						
1 2 25 $-\infty$	2.24	1 78	2.98	1.19	2.71	1.19
2 1 35 –2 25	2.29	2.43	3 32	1.71	3.26	1.70
3 0.825 –1.35	2.68	4 55	4 27	3 41	4 24	3 42
4 0 500 –0.825	3 46	19 53	6 41	9 62	5 02	9.19
5 0 300 –0.500	3.31	15 40	6.62	12 82	5 99	12.18
6 0 183 –0 300	2.45	13.71	5 20	11.72	4.76	11 12
7 0.110 –0.183	1.83	11.43	4 05	9 96	3 73	9.45
8 0.067 –0.110	1 24	10 33	2 97	9 19	2.53	8 60
9 0.025 –0.067	0 91	10 73	2 37	9 81	1 79	8 96
10 0.00911–0 025	0.29	3 46	0 85	3 27	0.51	2 87
11 0 –0 00911	0.059	1 07	0 22	1.04	0 084	0 87

Pu^{239} fissions	0 320	0	0 304	0	0	0
Pu^{239} captures	0 0394	0	0 0444	0	0	0
U^{235} fissions	0	0	0	0	0 367	0
U^{235} captures	0	0	0	0	0 0617	0
U^{238} fissions	0 0163	0.0726	0 0363	0 0499	0 0265	0.0497
U^{238} captures	0 0217	0.681	0 0746	0 567	0 0473	0 526
Na + Fe captures	0 00188	0 00748	0 00385	0 00624	0.00336	0.00581
Internal breeding ratio	0 0604		0 214		0 110	
Total breeding ratio	1 96		1 84		1.34	
Ratio fuel captures to fuel fissions	0 123		0 146		0 168	
Escape from blanket	0 0657		0 0439		0 0422	
Median fission energy for all core fissions, Mev	0 61		0 51		0 40	

*Volume fractions for the above assemblies are:

	Pu^{239}	U^{235}	U^{238}	Fe	Na
Core	←	0 32	→	0 14	0 54
Blanket	0	0	0 70	0.10	0 20

†Blanket thickness = 45 cm.

(*continued*)

TABLE 2-5

TABLE 2–5 (*continued*)

	Intermediate Pu^{239} fuel		PBR Pu^{239} fuel		PBR U^{235} fuel	
Core volume,* liters	200		800		800	
Core radius,† cm	36.28		57.59		57.59	
Ratio fuel atoms to U^{238} atoms	0.19		0.113		0.175	
Critical mass of fuel, kg	190.1		496.8		714.0	
Flux integral for:	Core	Blanket	Core	Blanket	Core	Blanket
Group *Energy interval, Mev*						
1 2.25 –∞	3 58	0 71	3 98	0.38	3 94	0.39
2 1 35 –2 25	4 26	1.06	4.94	0.58	4.90	0.59
3 0 825 –1.35	5 93	2 22	7 28	1 27	7.27	1.29
4 0.500 –0 825	8.88	6 76	13 56	4 08	13 03	4.05
5 0 300 –0.500	11.24	9 39	16.08	5 88	15 41	5.81
6 0 183 –0.300	9 40	8 88	14.16	5.73	13.62	5.64
7 0.110 –0 183	7.66	7 74	12 02	5 12	11 59	5.04
8 0.067 –0.110	6 06	7 33	10 08	4 98	9 38	4 85
9 0.025 –0.067	5 36	8 16	9.74	5.78	8 37	5.50
10 0.00911–0.025	2.18	2.86	4.39	2 14	3.23	1.94
11 0 –0.00911	0 74	0 96	1 82	0.77	0.94	0 64

Pu^{239} fissions	0 286	0	0.283	0	0	0
Pu^{239} captures	0 0496	0	0.0553	0	0	0
U^{235} fissions	0	0	0	0	0.337	0
U^{235} captures	0	0	0	0	0.0687	0
U^{238} fissions	0 0525	0.0304	0.0634	0.0165	0 0596	0.0168
U^{238} captures	0.164	0 450	0 289	0 308	0 241	0 294
Na + Fe captures	0 00702	0 00492	0 0113	0 00333	0 0102	0.00320
Internal breeding ratio	0 489		0.854		0 594	
Total breeding ratio	1 83		1 77		1.32	
Ratio fuel captures to fuel fissions	0.174		0.196		0 204	
Escape from blanket	0 0260		0 0136		0.0135	
Median fission energy for all core fissions, Mev	0 43		0 39		0 27	

TABLE 2-5

*Volume fractions for the above assemblies are:

	Pu^{239}	U^{235}	U^{238}	Fe	Na
Core	←	0 32	→	0 14	0 54
Blanket	0	0	0 70	0.10	0.20

†Blanket thickness = 45 cm.

TABLE 2–6

STATIC PARAMETER STUDY OF 400- AND 800-LITER SPHERICAL REACTORS FUELED WITH Pu^{239} AND U^{233} [14]

Reactor No.	1*		2*		3*†		4		5	
Fuel	Pu^{239}		Pu^{239}		Pu^{239} and Pu^{240}		Pu^{239}-oxide core		Pu^{239}-oxide core	
Core volume, liters	400		800		800		800		800	
Ratio fuel atoms to diluent atoms	0.178		0.140		0.136		0.426		0.199	
Critical mass of fuel, kg	288		468		456		378		419	
Flux integral for:	Core	Blanket‡	Core	Blanket	Core	Blanket	Core	Blanket	Core	Blanket
Group energy interval. Mev:										
1 2.25 –∞	3.84	0.55	4.02	0.40	4.02	0.39	5.76	0.64	5.54	0.59
2 1.35 –2.25	4.93	0.88	5.27	0.64	5.27	0.64	7.80	1.05	6.80	0.90
3 0.825 –1.35	7.11	1.91	7.81	1.42	7.75	1.41	9.71	2.01	8.00	1.63
4 0.500 –0.825	12.89	6.07	14.80	4.68	14.61	4.62	16.31	6.15	14.09	5.10
5 0.300 –0.500	14.27	8.36	16.87	6.52	16.70	6.46	14.94	7.69	12.01	6.18
6 0.183 –0.300	12.39	8.09	15.02	6.41	14.91	6.35	17.00	7.93	15.15	6.32
7 0.110 –0.183	10.40	7.18	12.85	5.76	12.76	5.71	15.41	7.39	13.69	6.10
8 0.067 –0.110	8.40	6.80	10.66	5.52	10.60	5.47	13.04	7.14	11.82	5.99
9 0.025 –0.067	8.20	8.00	10.84	6.62	10.76	6.57	15.38	8.94	14.38	7.66
10 0.00911–0.025	4.20	3.58	5.87	3.06	5.81	3.03	10.85	4.65	8.77	3.83
11 0.0 –0.00911	1.90	1.46	2.95	1.30	2.91	1.28	10.67	2.67	7.21	2.04

Fuel fissions	0.297	0.0	0.294	0.0	0.284	0.0	0.321	0.0	0.302	0.0
Fuel captures	0.0576	0.0	0.0609	0.0	0.0588	0.0	0.0825	0.0	0.0742	0.0
Diluent fissions	0.0459	0.0208	0.0502	0.0152	0.0625	0.0151	0.0194	0.0246	0.0422	0.02185
Diluent captures	0.192	0.389	0.253	0.319	0.256	0.316	0.103	0.448	0.2031	0.3689
Coolant (Na) captures	0.00104	0.000303	0.00133	0.000247	0.00132	0.000245	0.00205	0.00036	0.00119	0.000285
Structural captures	0.0159	0.00897	0.0198	0.00729	0.0197	0.00723	0.0275	0.00989	0.01424	0.00822
Internal breeding ratio	0.540		0.713		0.748		0.256		0.540	
Total breeding ratio	1.64		1.61		1.63		1.37		1.52	
Ratio fuel captures to fuel fissions	0.194		0.207		0.207		0.257		0.246	
Escape from blanket	0.0254		0.0183		0.0181		0.0239		0.0199	
Median fission energy, Mev, for all core fissions	0.367		0.334		0.365		0.181		0.234	

*Volume fractions for reactors 1, 2, 3 are:

	Pu^{239}	Pu^{240}	U^{238}	Fe	Na
Core	←———	0.25	———→	0.25	0.50
Blanket	0	0	0.60	0.20	0.20

20% of the fuel in Reactor 3 is Pu^{240}.

†A reactor identical to 3 except that 50% of the fuel is Pu^{240} yielded the following results:
Critical mass (kg) = 421. Total breeding ratio = 1.70.
Ratio of fuel captures to fuel fissions = 0.207.

‡All blankets have a thickness of 45 cm.

(*continued*)

TABLE 2–6 (*continued*)

Reactor No.	6		7		8		9	
Fuel	Pu^{239}-carbide core		Pu^{239}-carbide core		U^{233}-Th core		Pu^{239}-Th core	
Core volume, liters	800		800		800		800	
Ratio fuel atoms to diluent atoms	0.334		0.165		0.236		0.256	
Critical mass of fuel, kg	390		444		475		524	
Flux integral for:	Core	Blanket	Core	Blanket	Core	Blanket	Core	Blanket
Group energy interval, Mev:								
1 2.25 –∞	5.49	0.58	4.92	0.49	4.73	0.61	4.70	0.60
2 1.35 –2.25	7.28	0.95	6.05	0.77	6.40	1.10	6.37	1.07
3 0.825 –1.35	9.77	1.98	8.18	1.58	9.04	2.44	9.05	2.40
4 0.500 –0.825	15.02	5.69	12.30	4.45	16.16	7.58	15.96	7.42
5 0.300 –0.500	16.49	7.70	13.95	6.09	17.31	9.93	17.45	9.80
6 0.183 –0.300	15.03	7.51	12.46	5.90	14.56	9.09	15.05	9.08
7 0.110 –0.183	13.67	6.82	11.28	5.35	11.67	7.51	12.47	7.62
8 0.067 –0.110	11.73	6.58	9.89	5.18	8.88	6.45	9.68	6.61
9 0.025 –0.067	14.45	8.27	12.83	6.64	8.28	6.94	9.29	7.24
10 0.00911–0.025	10.25	4.29	8.11	3.34	4.34	3.37	5.22	3.64
11 0.0 –0.00911	11.05	2.58	7.94	1.93	1.98	1.52	2.74	1.74

Fuel fissions	0.310	0	0.296	0.0	0.386	0	0.331	0
Fuel captures	0.0822	0	0.0744	0.0	0.0326	0	0.0641	0
Diluent fissions	0.0242	0.0224	0.0477	0.0184	0.00836	0.00346	0.00823	0.00338
Diluent captures	0.131	0.420	0.2416	0.329	0.171	0.310	0.184	0.319
Coolant (Na) captures	0.00198	0.0261	0.00112	0.000256	0.00116	0.000304	0.00127	0.00031
Structural captures	0.000326	0.00926	0.01305	0.00731	0.0178	0.00896	0.191	0.0092
Internal breeding ratio	0.328		0.652		0.408		0.465	
Total breeding ratio	1.38		1.54		1.15		1.27	
Ratio fuel captures to fuel fissions	0.259		0.251		0.0845		0.194	
Escape from blanket	0.0225		0.0180		0.069§		0.068§	
Median fission energy, Mev, for all core fissions	0.197		0.260		0.251			

TABLE 2-6

§It is apparent that a 45-cm reflector is not adequate for these two systems.

CHAPTER 3

THE EXPERIMENTAL BREEDER REACTOR II*

3–1. Introduction

The Experimental Breeder Reactor II (EBR-II) is one of the reactors being built under the Civilian Power Reactor Development Program initiated in 1955. It is a sodium-cooled, fast-neutron power reactor with a gross electrical output of 20 Mw, to be fueled initially with U^{235} and later with plutonium. The plant includes an integral fuel-processing facility where the irradiated fuel is processed, fabricated, and assembled for return to the reactor.

EBR-II will extend research and development begun by the Experimental Breeder Reactor No. I [1], which first produced power in 1951; it is to be large enough to give results that can be extrapolated confidently to practical central station reactors. The program objective is to develop and demonstrate principles of design and operation that can be used to achieve economic power production by full-scale fast-breeder reactors. These principles lie in three major areas: (1) establishing an economic fuel cycle; (2) ensuring safety of the reactor without sacrificing its economic potentialities; and (3) improving and simplifying liquid sodium technology.

To establish an economic fuel cycle for a fast breeder reactor it must be shown that the breeding of plutonium is feasible, that plutonium can be recycled economically, and that specific power can be high enough to avoid excessive fuel investment charges. The EBR-II facility is pertinent to all of these aspects of the fuel cycle. The reactor will indeed be a breeder, designed for self-sustaining operation once the initial U^{235} fuel has been replaced by plutonium. An integral fuel-processing and refabrication plant will make it a self-sustaining nuclear system that will re-

*Compiled by J. R. Dietrich, W. R. Baldwin, and J. L. Watkins, GNEC. Much of the material of this chapter was taken from references [2] and [3]. Reference [2] was written by L. J. Koch, H. O. Monson, D. Okrent, M. Levenson, W. R. Simmons, J. R. Humphreys, J. Haugsnes, V. C. Jankus, and W. B. Loewenstein; reference [3] by L. J. Koch, H. O. Monson, W. R. Simmons, M. Levenson, F. Verber, E. Hutter, R. A. Jaross, T. R. Spalding, J. R. Simanton, and A. Lovoff (all of Argonne National Laboratory). Important contributions to this chapter in the form of manuscripts and prepublication copies of papers were made by J. H. Kittel and M. V. Levitt of ANL.

All figures for this chapter, except as noted, were furnished by Argonne National Laboratory.

quire a feed of only small quantities of U^{238}. Large reactors of this type would have quite acceptable fuel inventory charges (a fraction of a mill per kilowatt hour) should they attain specific powers comparable to that of EBR-II.

It is necessary to demonstrate that the reactor can be operated safely and reliably without unduly large expenditures for safety devices, and without uneconomic restrictions on operating characteristics such as excess reactivity allowance and thermal performance. Safety questions include (1) those that have to do with controlling reactor power and providing against any possible uncontrolled power increases, and (2) those that have to do with maintaining adequate cooling for the fuel elements under all possible conditions of operation and shutdown. In these areas the reactor will represent an integral experiment and demonstration, embodying design principles that have been developed to provide high inherent safety, multiple barriers against the release of radioactive material, and maximum integrity of the cooling system, without sacrifice of reactor performance. Dynamic experiments with the reactor by the oscillator technique will help to demonstrate the effectiveness of these design principles.

The goal of sodium technology development is to improve and simplify the technology so that sodium can be used as a power reactor coolant without unduly increasing capital and operating expenses. The problems include those of maintaining a circuit of flowing hot liquid sodium, operating and maintaining the highly radioactive sodium circuit, keeping the sodium molten, and developing and proving components for use in sodium systems. In these areas the reactor again has its major significance as an integrated facility whose design principles are expected to lead to economy and reliability. This integral test of design principles is more significant because the reactor system will employ large components whose

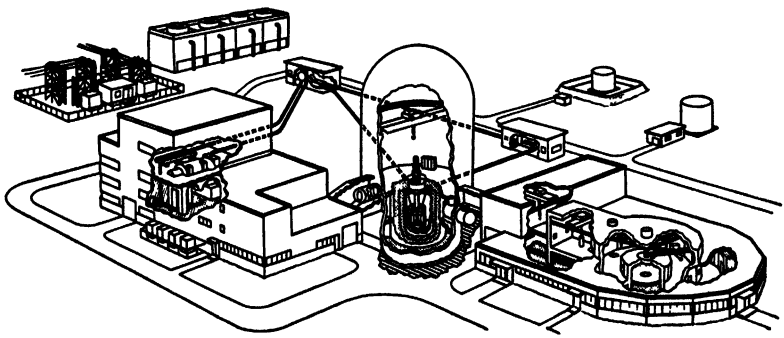

FIG. 3–1. Artist's sketch of EBR-II plant with associated power and fuel processing plants.

performance characteristics can be applied with confidence to full-scale power reactor systems.

The EBR-II facility, shown in Fig. 3–1, comprises four major functional systems:

(1) The primary system: the reactor, its associated equipment, and the primary sodium cooling system.

(2) The secondary system: the intermediate sodium heat-transfer system.

(3) The steam-electric system.

(4) The fuel process system: the system for decontaminating, fabricating, and assembling fuel elements.

Heat produced in the reactor is removed by the primary sodium system and transferred to the secondary sodium system by the heat exchanger. From the secondary system, the heat is transferred in the steam generator to produce superheated steam which is then delivered to a conventional condensing turbine at 850°F and 1250 psig. A simplified flow diagram of the power system is shown in Fig. 3–3.

To remove the greater portion of the fission products the irradiated fuel is subjected to a high-temperature oxidative slagging process. It is then fabricated and assembled into new fuel elements, for recycling through the reactor. These operations are carried out remotely in a large, high-radiation level, inert atmosphere, hot laboratory facility.

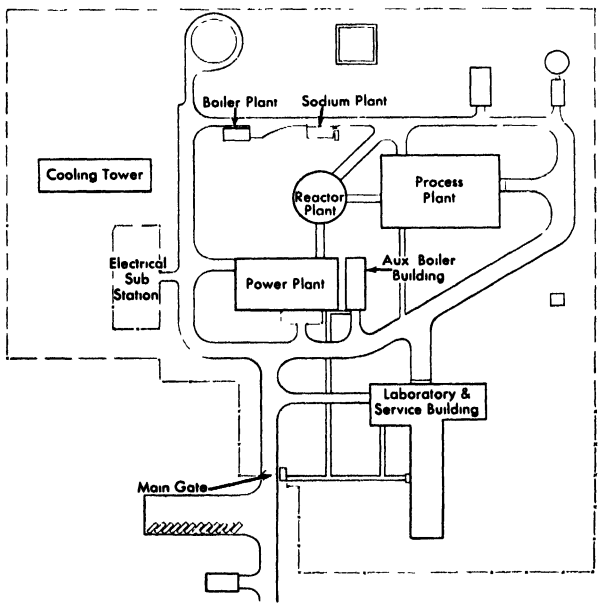

FIG. 3–2. Plot plan showing plant arrangement.

The EBR-II facility consists of five plants with the following supporting facilities and structures (Fig. 3–2):

(1) *The reactor plant* includes the reactor system, the reactor primary sodium cooling system, and services to these facilities. The reactor building is a cylindrical gastight steel shell, of steel plate 1 inch thick, designed for an internal pressure of 24 psi.

(2) *The power plant* includes the turbogenerator and associated equipment, the control room for the reactor and power plants, and the major personnel facilities for the entire facility.

(3) *The sodium plant* includes pumping, purification, and storage facilities for the secondary sodium system, and a receiving station for the sodium. It is of simple construction, containing only the minimum facilities required for operation. The building normally will not be occupied by operating personnel.

(4) *The boiler plant,* housing the steam generator, is somewhat isolated, with sodium lines linking it to the sodium plant, and steam and condensate lines linking it with the power plant. Like the sodium plant, it is simply constructed and contains only the minimum facilities required for operation.

(5) *The process plant* includes the fuel process cell and supporting facilities, inert gas storage facilities, the sodium equipment cleanup cell,

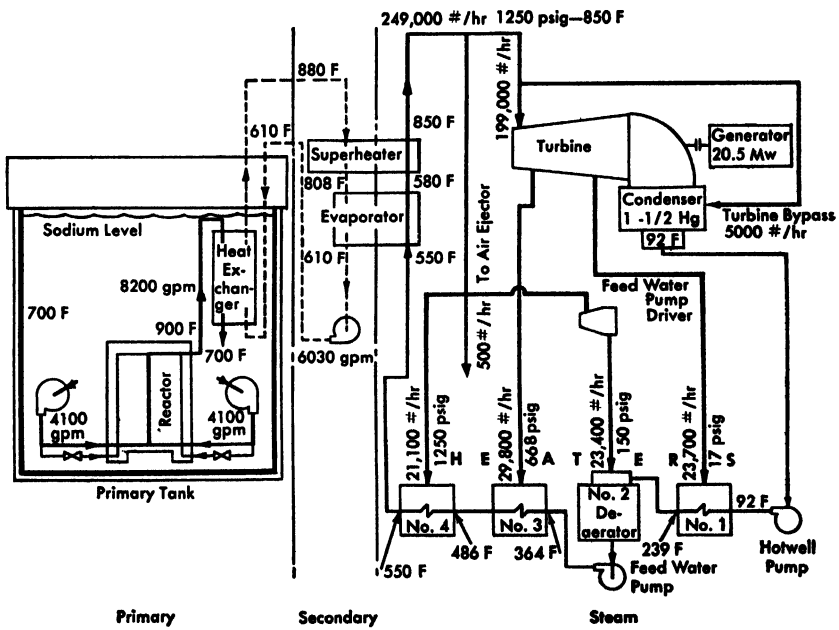

FIG. 3–3. Simplified flow diagram of EBR-II power cycle. (GNEC)

and exhaust ventilation equipment for the process plant and reactor plant.

An additional building (laboratory and service building) located adjacent to the above plants houses analytical facilities and personnel for control of the fuel process cycle.

The EBR-II facility will be constructed on a new site at the National Reactor Testing Station in Idaho at an estimated cost of $29,100,000. The estimate includes all general site development and supporting facilities as well as the reactor and equipment for the complete power cycle and fuel cycle. Construction began near the end of 1957 and is to be completed in 1960.

The description that follows is organized around the four major functional systems enumerated above, rather than around the system of buildings that make up the facility. Most attention is given to the systems that seem most important in developing safe, economical fast reactors: the primary system and the fuel process system.

3–2. General Plant Description

The EBR-II reactor proper consists of an enriched uranium core surrounded on all sides by a fertile blanket of depleted uranium. Maximum power density in the core is about 1370 kw/liter. The sodium coolant flows at a maximum of 26 fps with temperatures of 700°F at the reactor inlet and 900°F at the outlet. The fuel elements making up the core section consist of core-length, small diameter (0.144-inch) cylindrical pin units; they are designed for high thermal performance, high burnup capability, and simple construction. The fuel pin fits loosely in its jacket, a thin-walled steel tube; the space between the pin and the tube wall is filled with sodium to provide a heat-transfer bond. Heat is removed by primary sodium flowing along the outside of the fuel tube. Individual fuel elements are assembled into fuel subassemblies of hexagonal cross section; these are held in a close-packed array by a bottom support grid to form the reactor core. The reactor is controlled by moving some of the fuel into and out of the core. This is accomplished by 12 vertically movable fuel subassemblies, located at the outer edge of the core. Two additional movable subassemblies, which serve as "safety rods," are moved only during loading or unloading of the reactor.

Construction of the blanket is similar to that of the core except that larger diameter elements are used. The blanket reduces neutron leakage from the core, thus reducing the critical mass, and captures a large fraction of the neutrons which do leak from the core in U^{238} to produce plutonium. In EBR-II most of the plutonium is produced in the blanket, and a significant fraction of the reactor power is generated there. To simplify the problem of matching the coolant flow to the power produc-

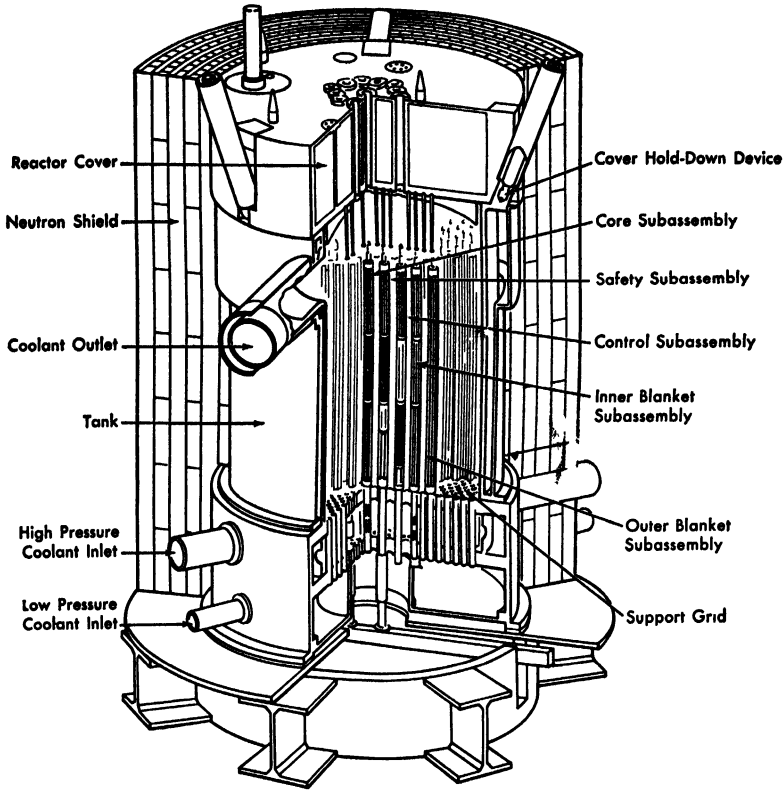

FIG. 3–4. Schematic diagram of the EBR-II.

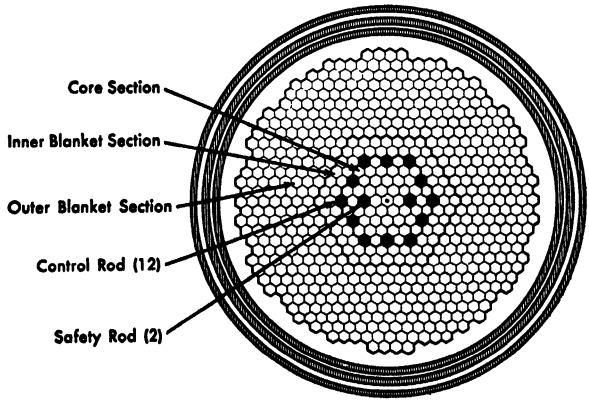

FIG. 3–5. Schematic cross section of EBR-II, showing the arrangement of subassemblies in the reactor tank. The core can be enlarged or reshaped by substituting core-type subassemblies in the inner blanket.

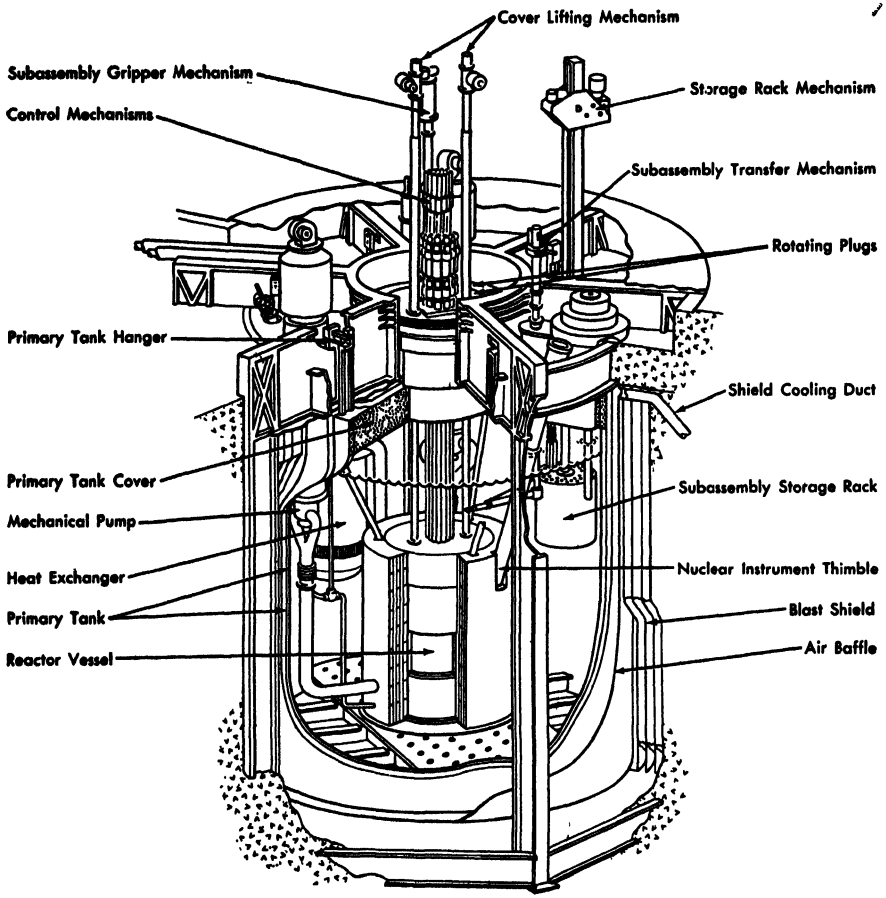

FIG. 3–6. Cutaway drawing of the EBR-II primary system.

tion for each subassembly, the radial blanket is divided into inner and outer sections. The inner section, like the core, is supplied with the full circulating pressure of the primary pumps, while the circulating pressure for the outer blanket is reduced by an orifice in the inlet line.

The vertical section of the reactor (Fig. 3–4) shows the arrangement of core and blanket subassemblies in the reactor tank, while a horizontal section (Fig. 3–5) shows the relative size of the core and blanket sections.

The reactor, the primary sodium pumps and piping, the primary-secondary heat exchanger, and the fuel-handling system are all contained in the "primary tank," submerged in a pool of sodium (Fig. 3–6). Two primary mechanical pumps force sodium from the pool through the reactor, then through the heat exchanger, and back to the pool. This "sub-

merged concept," as an approach to the problems of fast reactors and liquid sodium systems, is expected to have a number of practical advantages. Among these are:

(1) The arrangement contributes significantly to the reliability of the primary coolant system. The primary tank can be built to have a very high degree of integrity, since it is of relatively simple design (essentially, an unmodified right circular cylinder). The tank is built with double walls, and with no external connections below the liquid sodium level. Because the entire coolant system is flooded with sodium (to a level about 10 ft above the top of the reactor), loss of reactor coolant is virtually impossible. (Even if both primary tank walls were to fail, the free volume between the inner tank and the liner of the biological shield is small enough to keep the sodium level above the top of the reactor.) In addition, the arrangement is ideally suited to natural convection cooling, providing extremely reliable shutdown cooling should forced convection be lost.

(2) In a practical power reactor, fuel must be replaced quickly to minimize outage time. So that unloading operations can begin immediately after shutdown, while heat generation is still high, fuel elements are unloaded and transferred while they are submerged in sodium, cooled by natural convection. The fuel elements are transferred to a fuel storage rack in the primary tank, where they are further cooled by the sodium until they are removed for processing.

(3) The primary coolant system piping need not be leaktight, since the leakage is internal. Such leakage occurs at the connections between the pumps and the reactor, between the reactor tank and cover, and around subassembly nozzles.

(4) The heat capacity of the very large mass of bulk sodium (approximately 620,000 lb) provides considerable "thermal inertia" to the primary system. It prevents rapid changes in the primary coolant inlet temperature, and makes the shutdown cooling system more reliable.

(5) Maximum integrity is provided for containing radioactive sodium. The entire radioactive coolant system, except for the single, small, sodium cleanup circulation circuit, is confined within the primary tank.

(6) Essentially all the radioactivity in the plant is confined to the primary tank; hence only this tank and the single circuit referred to under item (5) require shielding. Equipment cells and pipe galleries need not be shielded.

(7) Auxiliary heating of the primary system sodium (to prevent freezing) is simplified, since the entire system is heated as a unit. The individual components and pipes are in an environment of sodium, and the entire system is at one temperature.

Heat removed from the reactor by the primary coolant system is transferred to the secondary sodium system in a shell-and-tube heat exchanger (Fig. 3–6). The secondary system, a nonradioactive sodium heat-transfer loop between the radioactive primary system and the steam system, prevents any possibility of contact between water and radioactive sodium and avoids the need for shielding around the steam boiler. Sodium flows through the secondary system at 6050 gpm and its temperature increases from 610 to 880°F in the heat exchanger. Included in the secondary system are the AC linear-induction sodium circulating pump, the heat exchanger, the steam superheater, and the steam evaporator, in that sequence.

In the steam system, including the evaporator, superheater, turbogenerator, condenser, and associated equipment, steam is generated at 1310 psig, superheated to 850°F, and delivered to the turbine. At 62.5-Mw reactor output, 249,000 lb of steam per hour will be supplied to the 20-Mw turbogenerator. An induced draft cooling tower dissipates the low-temperature heat rejected in the condenser.

Shutdown cooling in the event of pump failure is provided by natural convection of the primary sodium through the reactor. If the secondary sodium system is inoperative, the heat is delivered to the bulk volume of sodium in the primary tank; shutdown coolers in the primary sodium, operating by natural convection, transfer the heat to the atmosphere. The bulk volume of sodium in the primary tank also cools the fuel during reactor unloading.

The reactor and primary coolant system equipment are contained in a gastight cylindrical steel shell designed to withstand a static internal pressure of 24 psig (with a normal safety factor of approximately four). The reactor plant is shown in Figs. 3–7, 3–8, and 3–9. Even though the reactor is located at the National Reactor Testing Station, a containment structure is provided so as to duplicate the conditions for which a practical central-station reactor would be designed, and to minimize any restrictions on experimental operation which might otherwise be imposed by hazard considerations.

The fuel process plant adjoins the reactor building. It is a pilot-scale plant of sufficient capacity for reprocessing, reconstituting, and refabricating the EBR-II fuel, utilizing pyrometallurgical reprocessing methods and remote fabrication techniques. The reactor and the process plant will operate together on a closed fuel cycle, under conditions characteristic of a large fast-breeder reactor complex. The equipment of the process plant will be designed specifically for the processes and techniques to be evaluated first (oxide slagging as the primary reprocessing procedure and pre-

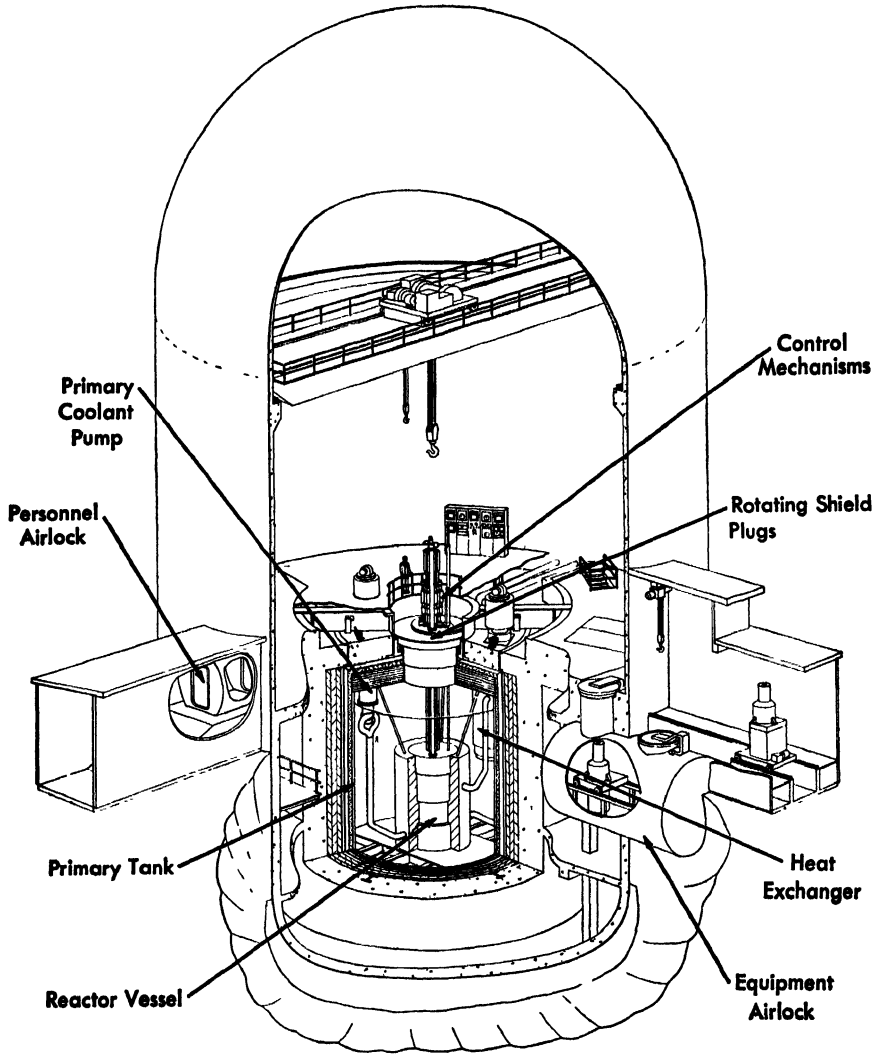

FIG. 3-7. Cutaway drawing of the EBR-II plant, showing the arrangement of major heat-transfer and service equipment.

cision casting as the basic fabrication technique), but the basic facilities of the plant are versatile enough for later modification to other processes.

Performance characteristics and design data for the EBR-II are given in Table 3-1 (see pp. 234-238), generally in the same order as the descriptions which follow in Sections 3-3, 3-4, and 3-5.

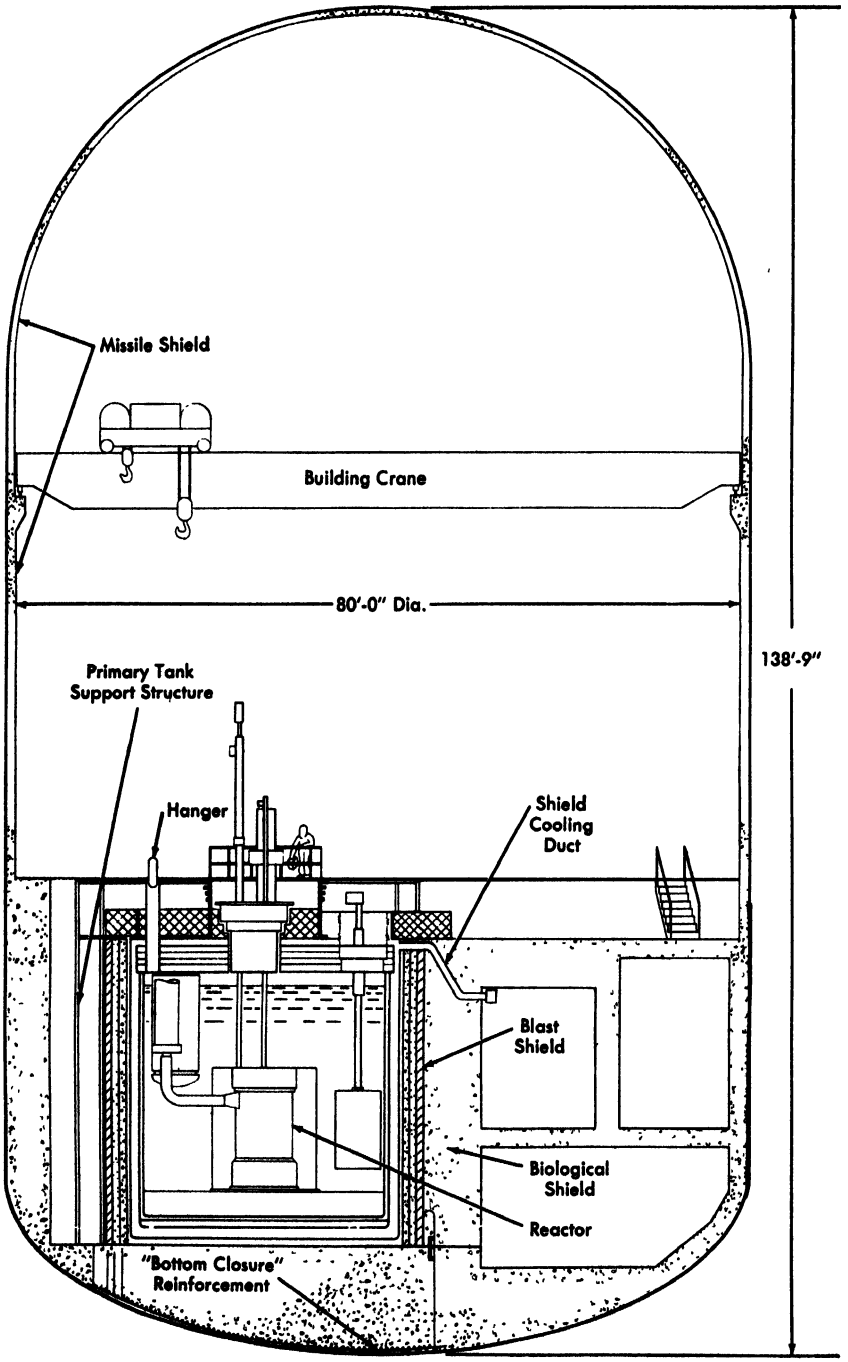

FIG. 3–8. Vertical section of the EBR-II plant.

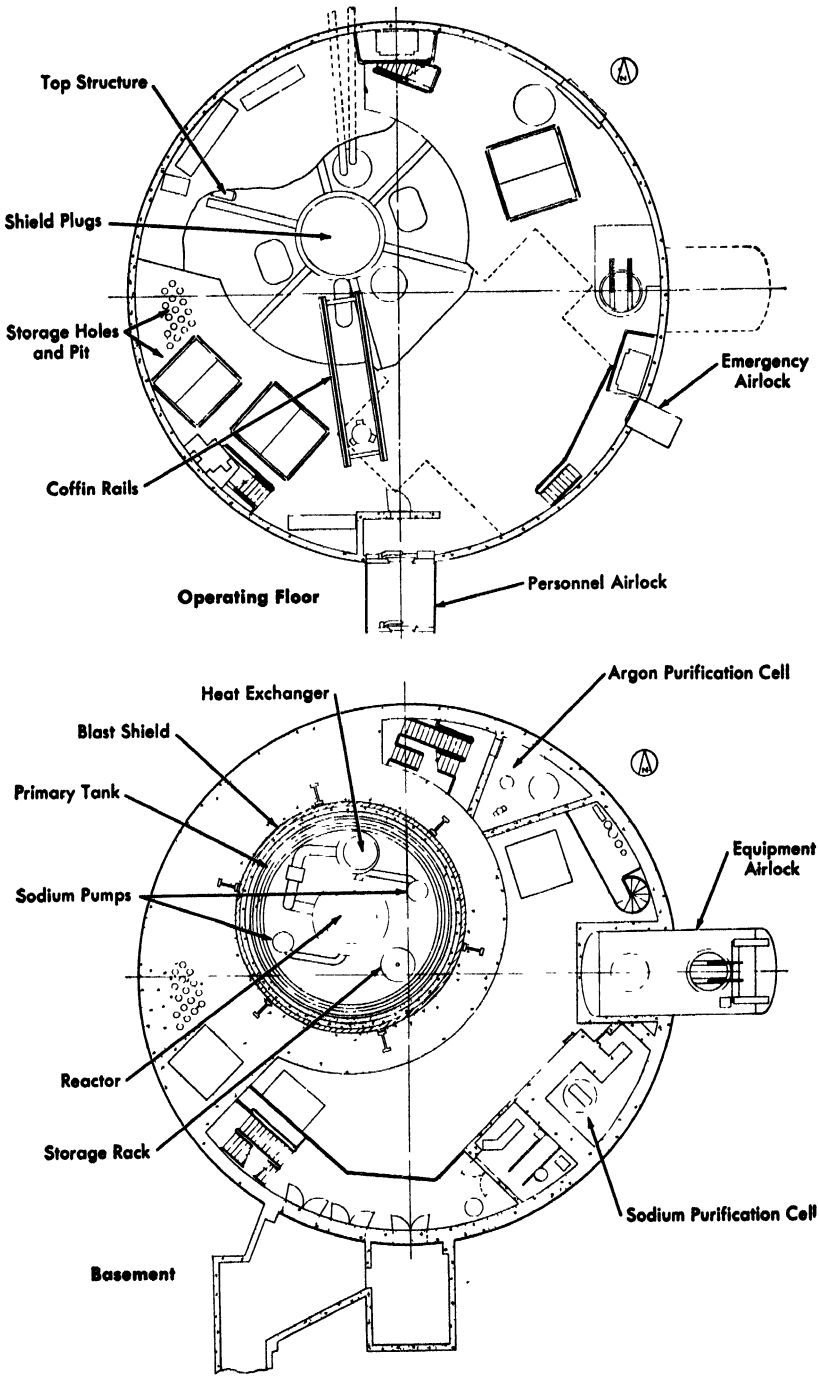

FIG. 3–9. Horizontal sections of the EBR-II plant.

3–3. Reactor and Primary System

3–3.1 Reactor. The reactor vessel is located centrally at the bottom of the primary tank (Fig. 3–6). Coolant is supplied by two "main" primary sodium mechanical pumps operating in parallel. The reactor is divided into three main zones: core, inner blanket, and outer blanket (Fig. 3–5). The reason for dividing the annular blanket (surrounding the core) into two separate zones is that power generation and hence coolant flow requirements vary widely across this region. Both the core and the blanket are composed of hexagonal subassemblies containing fuel elements, blanket elements, or both. All subassembies are the same size regardless of function; their numerical distribution is given in Table 3–2.

Core assembly. The core, including the control and safety rods, has the shape of a right equilateral hexagonal prism with an equivalent radius of 9.52 inches (24.17 cm), a height of 14.22 inches (36.12 cm), and a total volume of 2.34 ft^3 (66.3 liters). The core assembly comprises 61 vertically positioned, right hexagonal subassemblies of identical size: 2.29 inches across the flats of the hexagon (Fig. 3–5). Twelve of these subassemblies, at the outer edge of the core, function as control "rods," while two subassemblies, located more centrally, serve as safety "rods." The rods, which are modified movable fuel subassemblies within stationary thimbles, effect control by vertical movement into or out of the core. Slow movement is provided for operating control, and high speed is provided for rapid reactor shutdown (scram). The safety rods are operative only during normal reactor shutdown when fuel-loading operations are performed and the control rods are disconnected from their drives.

Table 3–2

Numerical Distribution of Reactor Subassemblies [2]

Type	Number
Core fuel subassemblies (containing three sections: upper blanket, core, lower blanket)	47
Control subassemblies (located in core fuel region)	12
Safety subassemblies (located in core fuel region)	2
Inner radial blanket subassemblies	66
Outer radial blanket subassemblies	510
Total reactor subassemblies	637

Each subassembly is positioned and supported at the bottom by a combination support grid and inlet coolant plenum. In addition, each subassembly makes contact with adjacent subassemblies by means of "buttons" formed by "dimpling" the walls of the hexagonal subassembly tubing. When the subassemblies are in place, there is a 0.030-inch nominal clearance between them. This arrangement permits a tight fit between subassemblies when buttons are aligned, but allows easy removal of units from the reactor when alignment is broken. The subassemblies are spaced on a triangular pitch of 2.320 inches, center to center. The tubes are 2.290 inches across the external flats, with walls 0.040 inch thick.

The upper ends of all subassemblies are identical, and all are accommodated by the same handling and transfer devices. The lower adapters are of different sizes to differentiate the three types of subassemblies (core, inner radial blanket, and outer radial blanket).

Heat is removed by sodium flowing up through the subassemblies and around the fuel and blanket elements. To accommodate the very large range of flow rates, two parallel flow systems are employed. Both systems are served by the same pumps, but in one the circulating pressure is reduced by orifices in the inlet lines. The high-pressure system supplies the core and the inner blanket; the low-pressure system supplies the outer blanket. The two systems have separate inlet plenum chambers and a common outlet plenum chamber, as shown in Fig. 3–4.

Because the inner blanket is included in the core-cooling system, experimental enlarging or reshaping of the core by substituting core-type subassemblies within the inner blanket is possible. The largest experimental core contemplated includes the inner row of subassembly positions of the normal inner blanket. It will be possible to operate the reactor with this row either partly or completely filled with core subassemblies. Such a configuration will be employed to adjust criticality of the reactor if the enrichment is not accurately established by critical experiments. The ability to vary the size of the reactor core also permits some variation in enrichment of the fuel alloy, making it possible to investigate such variables as Doppler coefficient as a function of enrichment over a limited range.

Fuel and blanket elements vary in size and shape according to the particular type of subassembly. The element types for a core subassembly are shown in Fig. 3–10, and the approximate composition of each type of subassembly is shown in Table 3–3. The composition is based on a unit volume of the lattice, and the sodium volume includes the static sodium in the reactor.

Core subassembly. Each core subassembly (Fig. 3–11) comprises three "active" sections: upper blanket, core, and lower blanket, end-to-end in a hexagonal tube. The core section consists of 91 cylindrical fuel ele-

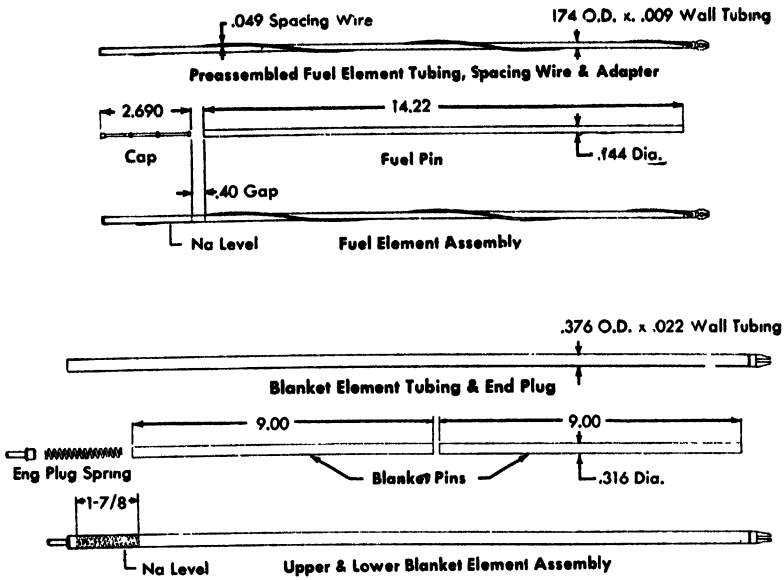

FIG. 3–10 EBR-II core subassembly elements.

TABLE 3–3

SUBASSEMBLY COMPOSITION [2]

Subassembly type	Volume, %			
	Fuel alloy	Uranium	Steel	Sodium
Core, fuel section	31.8	0	19.5	48.7
Core, blanket section	0	32.0	20.4	47.6
Control and safety, fuel section	21.3	0	20.8	57.9
Inner and outer blanket	0	60.0	17.6	22.4

ments spaced on a triangular lattice; a single, helical rib on the outside of each element provides the spacing. The elements in the subassembly are fastened at their lower ends to a support grid. Each fuel element (Fig. 3–10) is a slender cylinder or "pin" of fuel alloy (0.144 inch diameter by 14.22 inches long) fitted into a thin-walled, stainless steel tube. The coolant flows along the outside of the element tube.

Each fuel pin is precision cast to size. Pins consist of "equilibrium fissium alloy," an alloy approximating the chemical composition of equi-

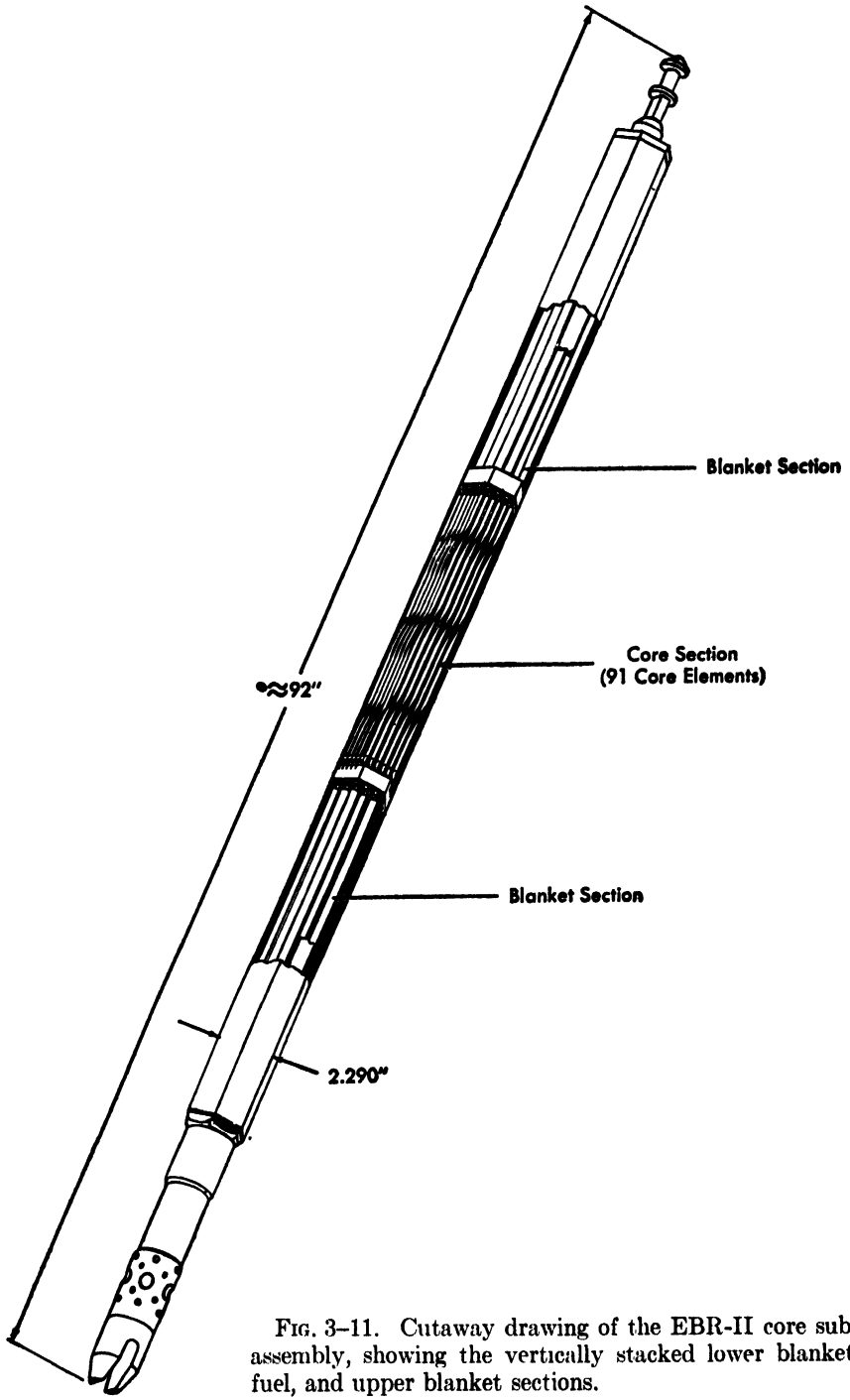

FIG. 3–11. Cutaway drawing of the EBR-II core subassembly, showing the vertically stacked lower blanket, fuel, and upper blanket sections.

librium recycled fuel. Initially, the fissionable constituent will be U^{235}; later Pu^{239} will be employed. The composition of the fissium alloy varies with the fissionable isotope employed because of the difference in fission product yields. Compositions of the alloys are given in Table 3–1, and discussed in Section 3–6. The stainless steel tube containing the pin has a wall thickness of 0.009 inch and an outside diameter of 0.174 inch. The resulting 0.006-inch annulus between the pin and the inside of the tube is filled with static sodium to provide a thermal bond, which extends 0.6 inch above the top of the fuel pin. A 2.35-inch inert gas space above the sodium accommodates its expansion. The fuel element tube is welded closed at each end.

The individual fuel elements are fastened in the hexagonal subassembly tube at their lower ends by hooking to a parallel strip grid (Fig. 3–12). The upper ends of the elements are unrestrained, to permit free axial expansion. This method of attachment is designed to facilitate remote assembly and disassembly.

The upper and lower blanket sections are similarly constructed; each blanket section consists of 19 pin-type elements on a triangular lattice. These pins are of unalloyed depleted uranium, 0.3165 inch in diameter and 18 inches long. Each pin fits loosely in a blanket element tube which is 0.376 inch OD and has a wall thickness of 0.022 inch (Fig. 3–10). The 0.008-inch clearance annulus is filled with sodium to provide a thermal bond. The blanket elements are positioned in the subassembly by a parallel strip grid similar to that for the fuel elements, and the upper ends are also positioned by grid strips which permit axial expansion but no other movement. Since the blanket elements are positioned at each end, no spacers are provided along their length. The lower adapter of the sub-

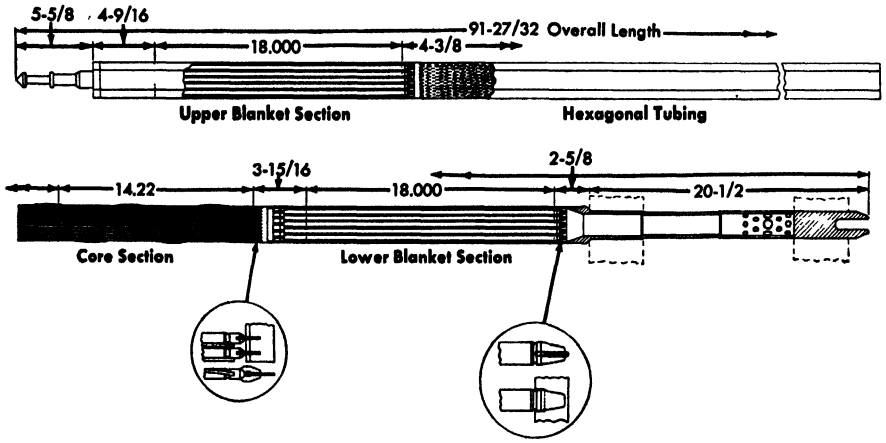

FIG. 3–12. EBR-II core subassembly.

assembly, which engages the reactor grid, contains holes for the coolant to enter from the high-pressure inlet coolant plenum chamber. The reactor grid and its relationship with the subassembly adapter are described in Article 3-3.2.

Blanket subassemblies. An inner blanket subassembly (Fig. 3-13) is composed of 19 cylindrical blanket elements spaced on a triangular pitch and contained in a hexagonal shell. The active material of an element consists of depleted uranium cylinders (0.433-inch diameter) totaling 55 inches in length. They are contained in stainless steel tubes 0.493-inch OD and of 0.018-inch wall thickness. The resulting 0.012-inch annulus is filled with sodium to provide a thermal bond. The sodium extends 2 inches above the top of the uranium, with a 4-inch argon gas expansion region above the sodium. End closures are sealed by welding. Each subassembly has a lower adapter similar to those in the core, but of smaller diameter. The inner blanket subassemblies engage the high-pressure inlet coolant plenum chamber in the reactor grid.

The outer blanket subassembly differs from that of the inner blanket in the design of the lower adapter, which is arranged to engage the reactor grid in the low-pressure inlet plenum chamber. The two different lower adapters are shown in Fig. 3-13; their functions are described in Article 3-3.2.

Control subassembly. Each control subassembly (Fig. 3-14) consists of a control rod and a guide thimble. The guide thimble is hexagonal in cross section and has the same dimensions as the stationary subassembly tubes. Each thimble thus occupies a unit lattice position identical to those occupied by stationary subassemblies.

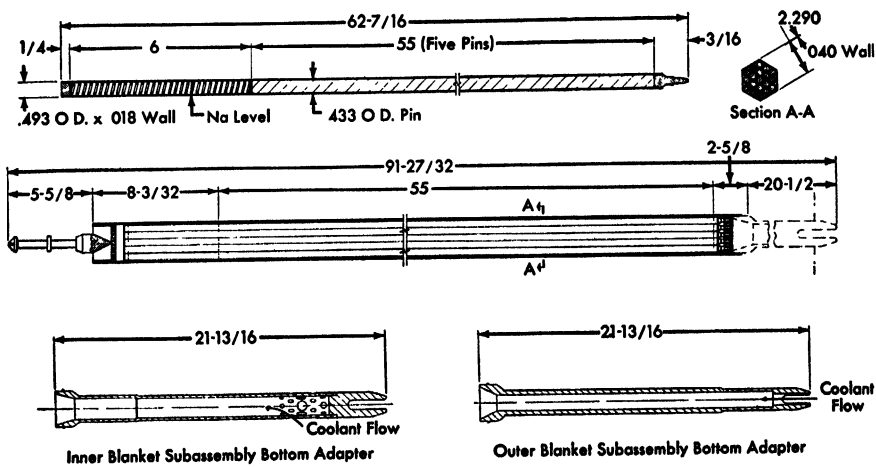

FIG. 3-13. EBR-II inner and outer blanket subassemblies.

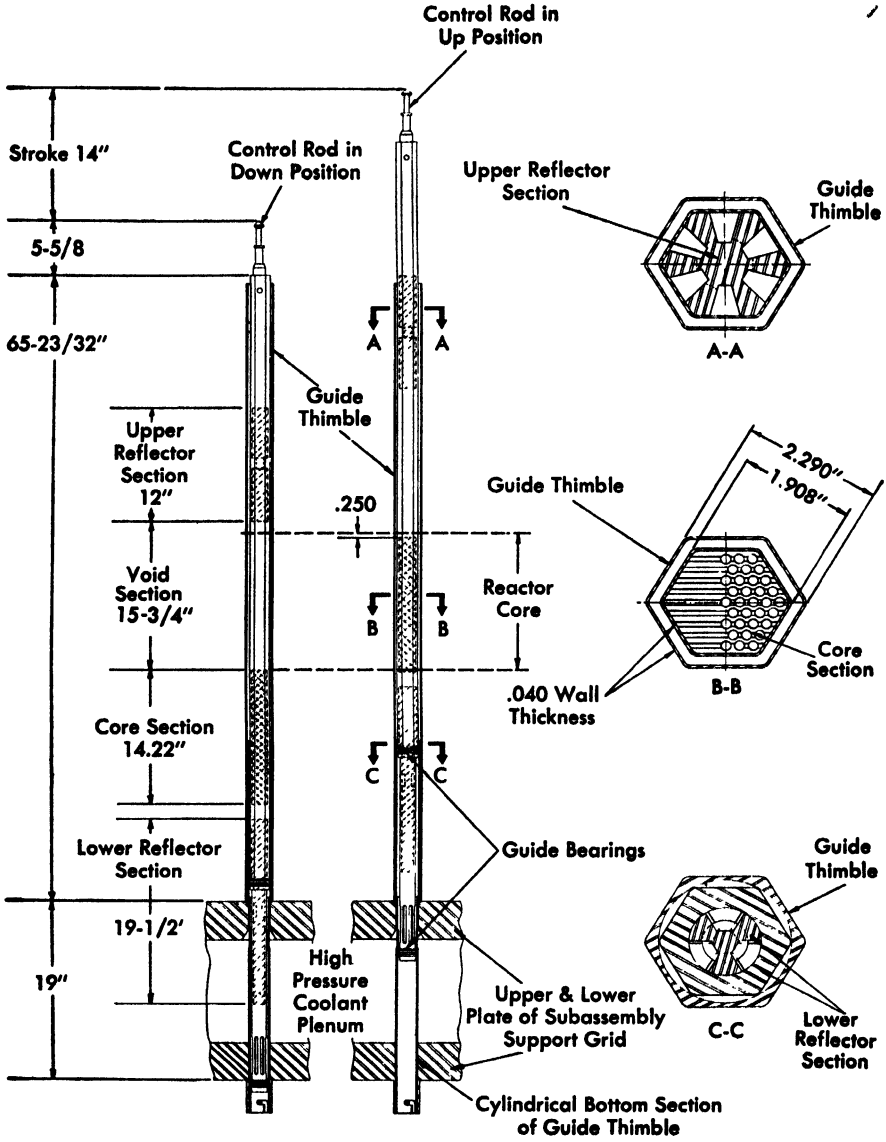

FIG. 3–14. Control subassembly.

Twelve identical control rods provide operational control for the reactor. The control rod is a modified core subassembly with 61 cylindrical fuel elements identical to those employed in a stationary core subassembly. It does not contain an axial blanket. The control rod is encased in a hexagonal tube 1.908 inches across flats, which is smaller than the hexagonal thimble tube by the equivalent of one row of fuel elements. A void section equal in height to the reactor core is provided above the core section. During operation this void section is filled with sodium. The reactor is controlled by vertical movement of the control rod, to adjust the proportion of fuel or void (sodium) in the core region. A reflector section of steel (solid, except for coolant flow passages) is immediately above the void section. At the upper end of the control rod is an adapter section, identical to those of the stationary subassemblies, which attaches to the control drive unit for operation of the rod, or to the fuel gripper unit for unloading. The lower end of the control rod below the fuel section is a cylindrical tube also containing a steel reflector section. It has guide bearings which act against the guide thimble.

The control rod, like the core subassemblies, is cooled by the high-pressure sodium coolant system. Sodium enters through slots in the lower end of the thimble and in the lower end of the control rod. The slots in the thimble section are above the lower bearing of the control rod throughout the control rod travel. The lower end of the thimble is open, and the lower control rod bearing serves as a flow restriction to prevent sodium leakage from the bottom of the thimble. The primary system sodium pressure, acting across the lower end of the control rod, exerts a downward force to oppose the lifting force of the coolant flowing through the rod.

When replacement is necessary, the control rod is removed from the reactor by the fuel-handling system in the normal manner. Considerations of radiation damage and fuel lifetime apply to the control rod. The guide thimble can be removed and replaced in the event of damage; it is locked in the lower reactor grid by a latch which is engaged by rotating the thimble. The six surrounding subassemblies must be removed for this operation.

Since the vertical position of a control rod in the reactor is variable, the heat generation within the control rod is also variable. The coolant flow must be established for the maximum heat generation, i.e., for the case of the control rod fully inserted in the reactor. With constant coolant flow, the temperature rise in the coolant decreases as the control rod is lowered out of the reactor, and the average sodium outlet temperature is degraded. Coolant flow can be made to vary according to the position of the control rod if the relative sizes and locations of the coolant slots in the guide thimble and in the control rod are properly chosen. The re-

quirements for this system will be established experimentally, to provide nearly constant sodium outlet temperature from the control rods in all operating positions.

Safety subassembly. Each safety subassembly (Fig. 3–15) consists of a safety rod and a guide thimble which are like those of the control subassembly except at the lower ends. The two safety rods are actuated as shown in Fig. 3–16. The safety rods are not used for normal operational control; they are always fully inserted in the reactor (in their most reactive position) during operation and normal shutdown. The purpose of the safety rods is to provide available negative reactivity when the reactor is shut down and the control rods are disconnected from their drives, as during reactor loading and unloading operations.

The safety rods are attached to a common drive unit extending below the reactor structure. The unit is driven by two shaft extensions outside the fuel transfer system and therefore is unaffected by fuel transfer operations. The guide thimble is locked to the lower reactor grid structure in the manner described for the control rod guide thimble. The safety rod is engaged to the driving mechanism by a rotational locking mechanism. Inadvertent disengagement of the safety rod is prevented by a hexagonal collar on the upper end of the safety rod, which normally engages the inside of the thimble, preventing rotation of the safety rod. To connect or disconnect the safety rod (as for replacement), it must be raised one inch above its normal up position by the safety rod drive mechanism.

The safety rod upper adapter is identical to those of the control rod and the stationary subassemblies, and is handled in the normal manner by the fuel transfer system. The guide thimble is removable in the manner previously described. Cooling of the safety rod is similar to that of the control rod, but no provisions are needed for variable flow. The safety rods must be in an up position before the reactor can be made critical.

3–3.2 Reactor vessel assembly. The reactor vessel assembly, as shown in Figs. 3–4 and 3–17, consists of the reactor vessel, the grid assembly, and the top cover. It contains the reactor core and blanket subassemblies, and control and safety rods, and keeps them properly oriented. The assembly is centered at the bottom of the primary tank, supported by the structural members, which reinforce the bottom of the primary tank inner shell. The vessel assembly, surrounded on all sides by the neutron shield, is submerged beneath 10 ft of sodium.

To ensure accurate alignment, the reactor vessel is fastened to the grid assembly by bolts, which are tack-welded to ensure a permanent connection. The vessel cover, serving as a neutron shield as well as a closure, is clamped to the vessel flange. Closing the cover completes the plenum

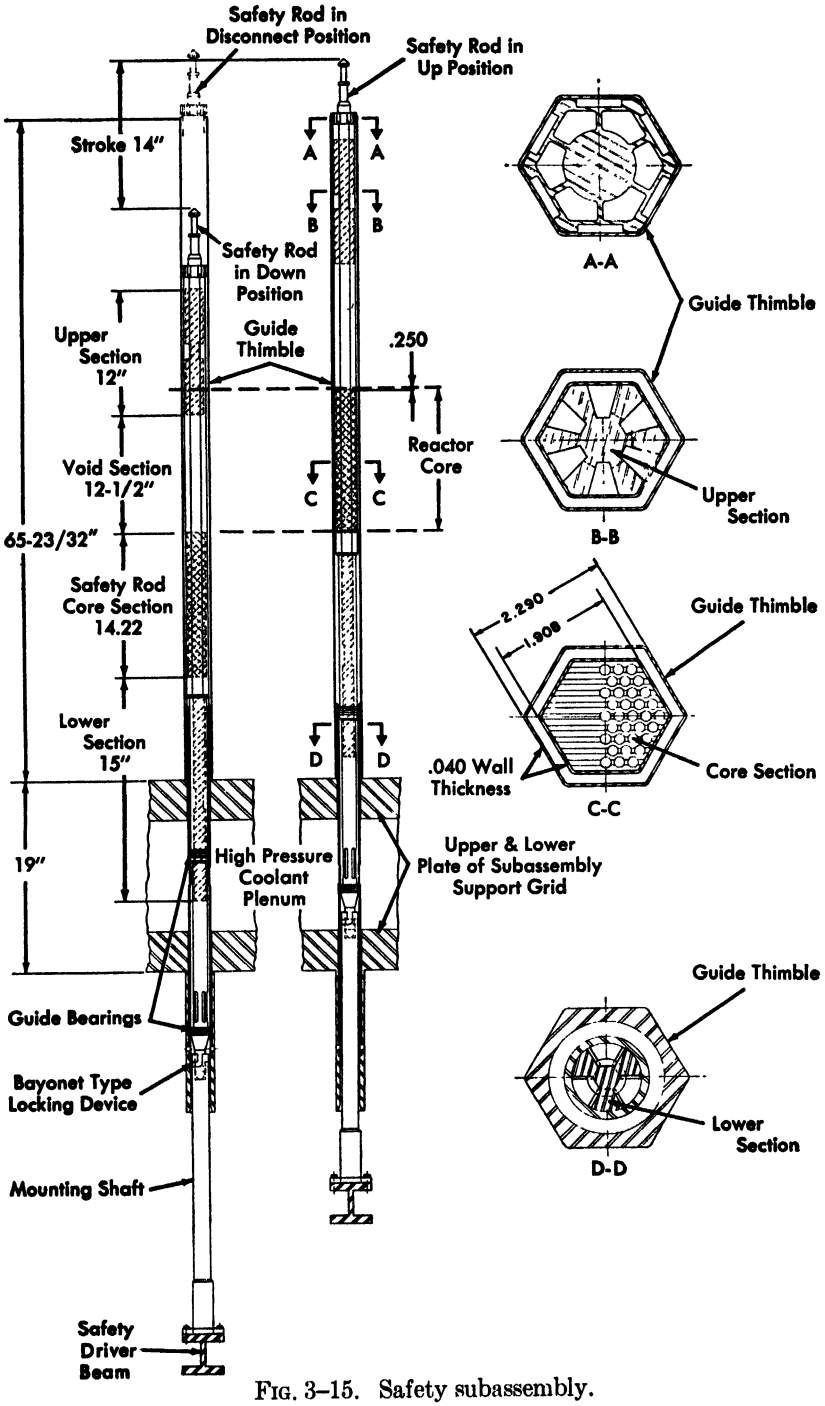

FIG. 3–15. Safety subassembly.

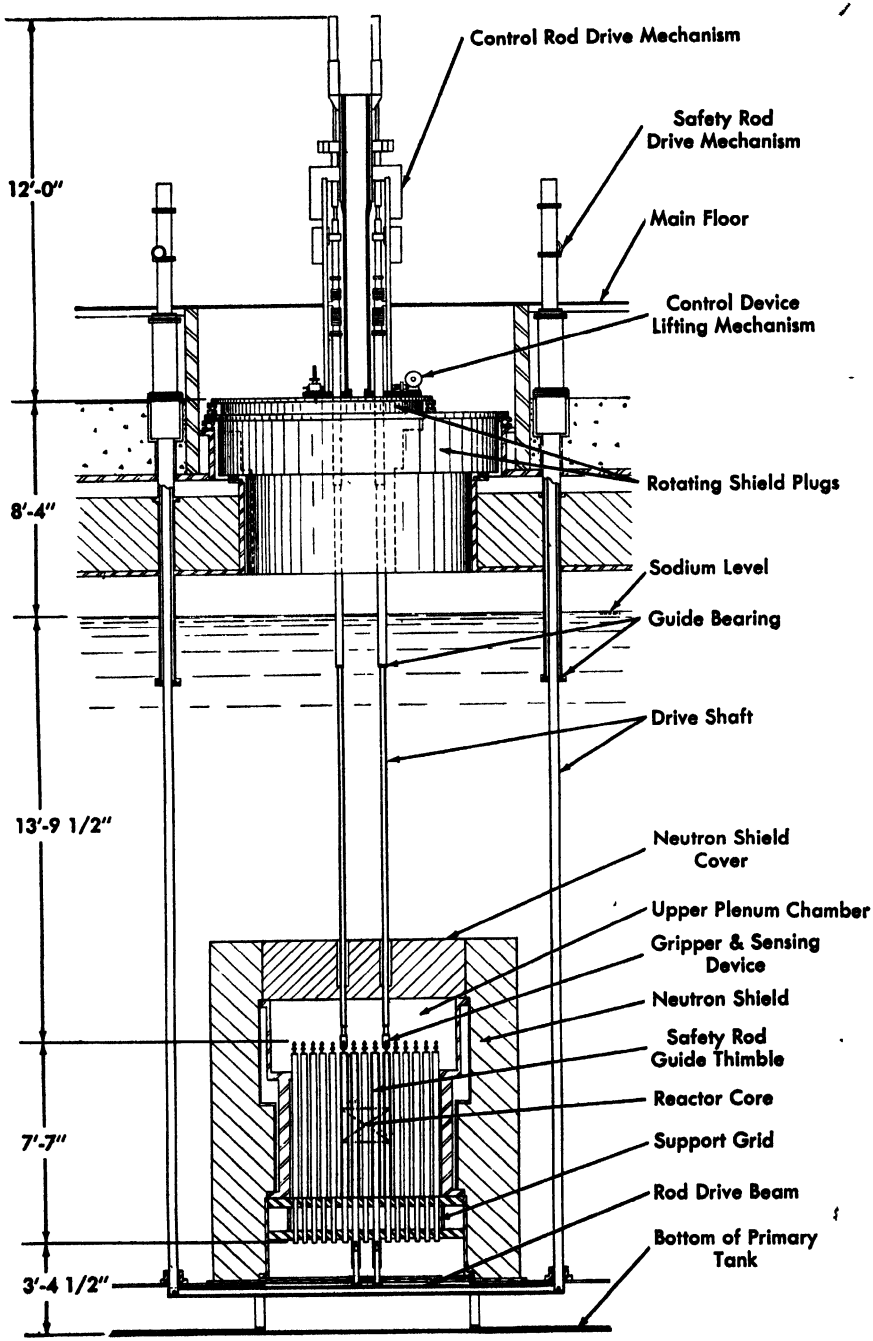

FIG. 3–16. Schematic diagram of the EBR-II control rod and safety rod drive system.

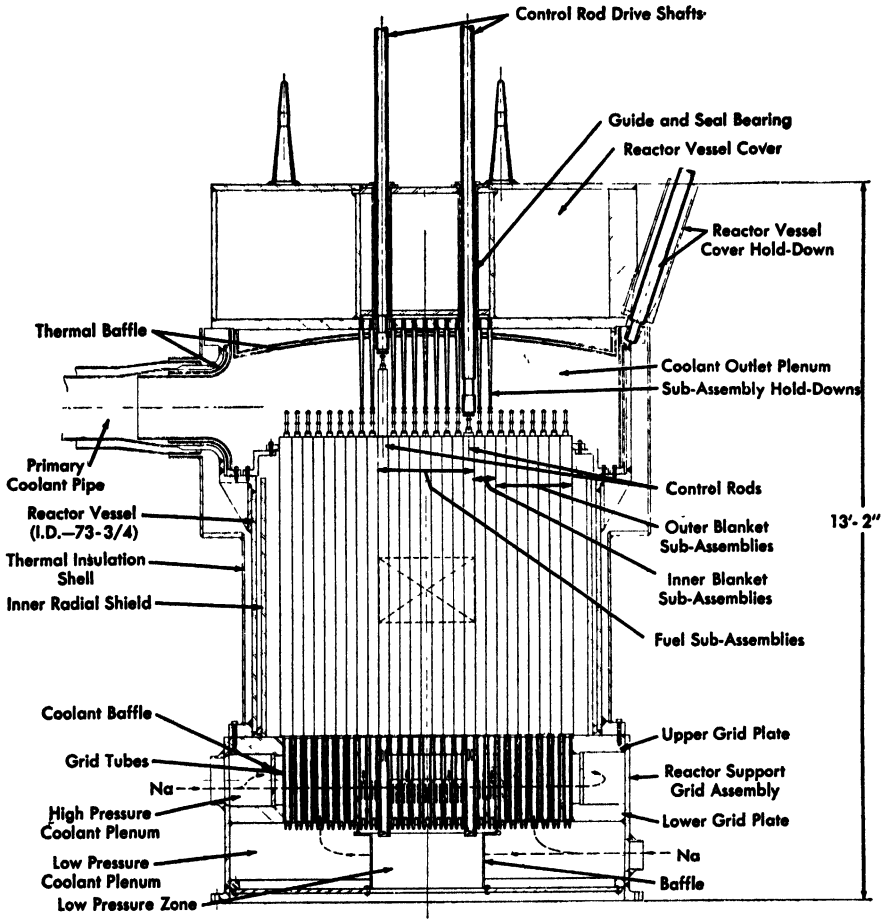

FIG. 3–17. Reactor vessel assembly.

from which coolant flows to the heat exchanger; within this plenum chamber, the coolant is at an average temperature of 900°F and a pressure of 18 psig. A sodium seal is formed between the vessel flange and the cover. For fuel unloading, the hold-down clamps are released and the cover is raised to the top of the primary tank. The clamps and cover elevating mechanism are shown in Fig. 3–23.

Reactor vessel. The reactor vessel is a cylindrical tank with flanged ends. A thermal baffle lines the upper plenum and the coolant outlet nozzle (Fig. 3–17), so as to lower the temperature difference across the vessel wall and across the nozzle wall. Below the plenum region is a laminated steel thermal shield. The vessel wall is "insulated" from the bulk sodium in which it is submerged by a vented outer steel shell which con-

tains static sodium. This shell-and-static-sodium combination provides sufficient thermal insulation to avoid unacceptable thermal stresses in the vessel wall.

Grid-plenum assembly. The grid-plenum assembly (Fig. 3–17) is a combination grid structure which supports and locates the subassemblies and forms the coolant inlet plenum chambers. Details of this assembly are shown in Fig. 3–18. It consists of two 4-inch-thick stainless steel plates containing the locating holes for the lower adapters of the subassemblies. The subassemblies are supported by the upper plate and extend through the lower plate. Each subassembly is supported by a spherical shoulder which engages a conical seat in the upper grid plate to provide a seal, minimizing the leakage flow of coolant along the outside surfaces of the subassemblies.

The high-pressure coolant plenum chamber, which provides the supply for the core and inner blanket, is formed between the two grid plates. The low-pressure coolant plenum chamber, which provides the supply for the outer blanket, consists of an annular chamber immediately below the lower grid plate. The grid-plenum chamber arrangement and coolant flow arrangement are shown in Figs. 3–17, 3–18, and 3–19. The upper and lower grid plates are interconnected by tubes welded to each plate in the outer blanket zone. This prevents short-circuiting of the high-pressure coolant through the outer blanket and provides the structural system required to support the entire reactor load on the upper plate. The high-pressure coolant flows between these tubes into the core and inner blanket region, where it enters the subassemblies. The lower nozzles of the core and inner blanket subassemblies contain holes located between the upper and lower grid plates. The coolant enters the subassembly through these holes and flows upward through the subassembly. The lower end of the subassembly nozzle is closed, forming a hydraulic piston.

The sodium in the high-pressure coolant plenum chamber is at a pressure of 68 psig, of which 8 psig is static head. The remainder gives a pressure difference of 60 psi acting across the piston. This provides a resultant total downward force of 120 lb on each of the core subassemblies and about 100 lb on the inner blanket subassemblies. The upper surface of the lower grid plate is stepped so as to vary the cross-sectional area of the holes in the subassemblies. This provides orificing of the flow through the subassemblies to match the heat generation rate.

The low-pressure coolant enters the low-pressure plenum chamber at 23 psig, and enters the lower nozzles of the outer blanket subassemblies through openings at the bottom. Because the pressure drop through the outer blanket subassemblies is much smaller and the weight of these units is larger, it is unnecessary to provide hydraulic hold-down.

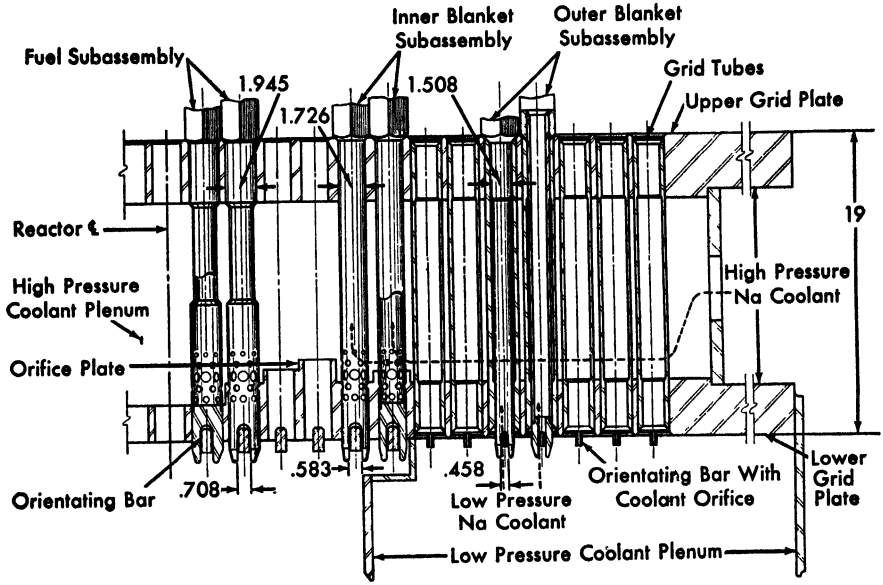

FIG. 3–18 Details of the EBR-II subassembly support grid.

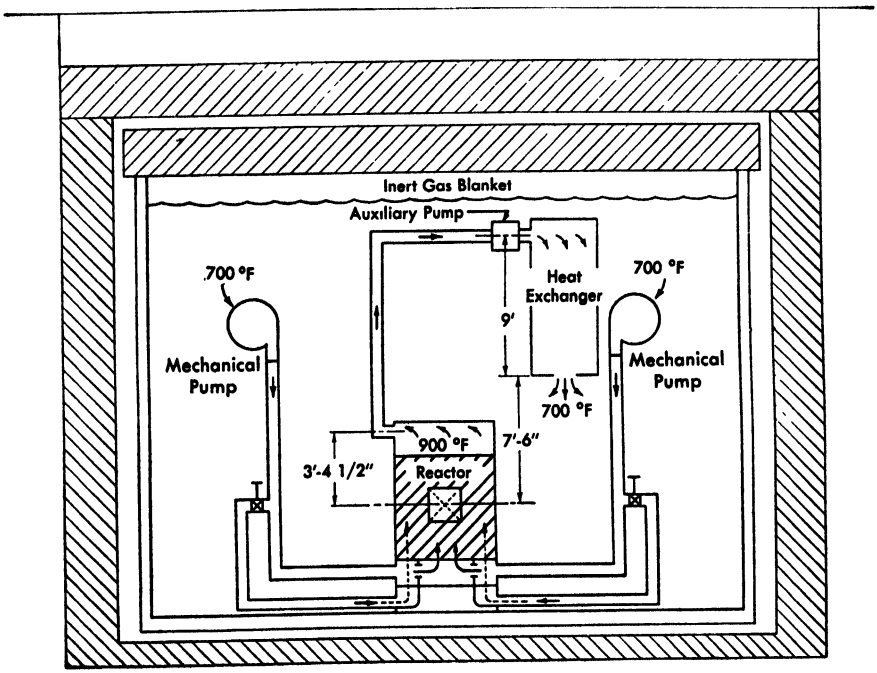

FIG. 3–19. Schematic diagram of the primary coolant system.

Holes of different sizes in the grid plate and orientation bars of different thicknesses below the plate prevent fuel and blanket subassemblies from being placed in wrong positions; such misplacement would introduce reactivity and cooling problems.

Top cover. The top cover (Figs. 3–4, 3–17) closes the reactor vessel, forms the upper surface of the outlet plenum chamber, and provides the upper portion of the neutron shield. Guide bearings are provided in the cover for the 12 control rod drive shafts which operate through it. During unloading, the fuel gripper mechanism also operates through an opening in the cover. The small leakage flow through the various openings during reactor operation is employed as a part of the neutron shield cooling system in this region.

The top cover is raised and lowered by two shafts penetrating the small rotating plug in the primary tank lid. The mechanism is designed to permit free expansion of the lifting shafts. From the underside of the top cover, pins project directly above each subassembly adapter, to within 1/4 inch of the adapter. The pins prevent any appreciable lifting of the subassemblies should the hydraulic hold-down system fail. Thermocouple wells adjacent to some of these pins measure the outlet sodium temperature in all regions of the reactor. The thermocouple leads pass through tubes brought out through the hollow cover-lifting drive shafts. Inside the cover, the tubes are manifolded to the various locations. The tubes are permanently installed in the assembly, but the thermocouple junctions and leads can be withdrawn.

3–3.3 Primary cooling system. The primary system component arrangement is shown schematically in Fig. 3–19. The pumps, heat exchangers, and connecting piping are disposed radially around the reactor vessel and elevated somewhat above it.

The coolant flow path in the primary cooling system is as follows:

(1) The mechanical coolant pumps take in bulk sodium about 19 ft above the bottom of the primary tank. Coolant flows from the pumps downward to the connecting piping.

(2) The flow from each pump separates into two streams, entering the high-pressure and low-pressure reactor inlet plenum chambers. The pump outlet line is connected to the high-pressure inlet plenum chamber. A smaller line connected to the outlet line supplies the low-pressure plenum chamber through an orifice and valve.

(3) In all regions of the reactor, coolant flows upward through the fuel and blanket subassemblies and into a common upper plenum chamber which has a single 14-inch outlet.

(4) The 14-inch upper plenum outlet nozzle is located on the opposite side of the reactor vessel from the heat exchanger. The connecting pipe

between these two components is designed to accommodate thermal expansion. The auxiliary pump is located in this line.

(5) The primary coolant flows downward through the shell side of the heat exchanger and discharges into the bulk sodium in the primary tank. The heat exchanger outlet is approximately 7½ ft above the centerline of the reactor. This arrangement assures a reliable natural convection cooling system for shutdown cooling.

Ball-seat pipe disconnects are used in the lines between the main sodium pumps and the lower plenums of the reactor vessel, so the pumps can be removed from the primary tank for maintenance. The sodium line between the upper plenum of the reactor vessel and the heat exchanger shell is permanently attached to the cover of the primary tank; however, the tube bundle, upper and lower plenums, secondary sodium inlet and outlet nozzles, and shield plug can be lifted out as a unit.

When the reactor is in operation, coolant is supplied by the two main primary sodium centrifugal pumps. At 100% power operation, each pump supplies approximately 4250 gpm of coolant at 62-psi head. Unequal flow through the two main pumps does not cause serious maldistribution of flow through the reactor because the pressure differential (42 psi) between the upper and lower plenums is much greater than the pressure differences (0.5 psi) within the lower plenum chambers. The vertically mounted, single stage, centrifugal pumps utilize hydraulic liquid sodium bearings located at the pump impellers. They are driven by totally enclosed, leakproof, 480-volt, AC motors. Labyrinth shaft seals minimize diffusion of sodium vapor toward the motor enclosure. The motors are frequency-controlled over about a 10 to 1 speed range, providing smooth continuous control over the entire range. There are no flow control valves in the primary coolant system.

A 5000-gpm, 40-psi head, centrifugal pump of similar design has been operated for more than 7500 hr at speeds of 1750, 890, and 175 rpm and at temperatures up to 900°F (Fig. 3–20). This pump has been subjected to 126 starts, 26 of them during low-speed operation. After 6500 hr of operation, the pump was disassembled and inspected, and found to be in excellent condition. The hydraulic bearing showed no significant wear.

During shutdown conditions, when the reactor power is 1% or less of the design value, sufficient coolant flow is established by thermal convection to remove fission-product decay energy without exceeding the established fuel alloy temperature limitations. For more drastic emergency shutdown conditions, including the case of complete failure of all pumps accompanied by reactor scram, analysis indicates that the fuel will overheat, but not dangerously. The relative elevations of the heat exchanger and reactor were established to ensure thermal convection of the primary sodium.

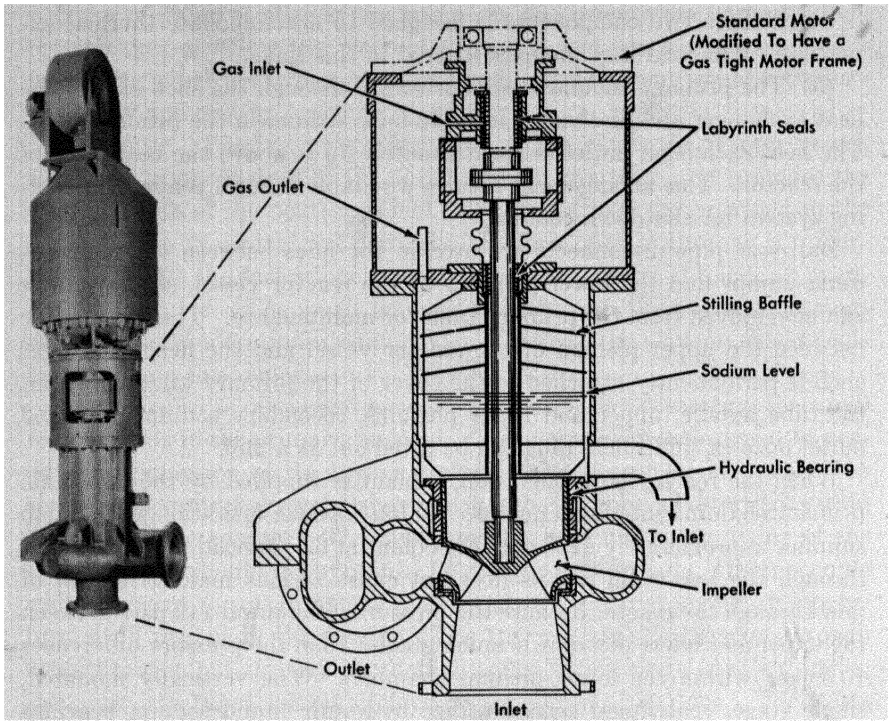

FIG. 3–20. General view and sectional diagram of an EBR-II type 5000-gpm mechanical pump.

The primary purpose of the auxiliary pump (Fig. 3–21) is to augment thermal convection under certain conditions of reactor shutdown. These conditions can result from any system malfunctions which destroy the normal temperature distributions that promote thermal convection. An example would be the case of a rapid reactor shutdown followed, not immediately, but after several seconds, by failure of the pumps. During the interim, the pumps would overcool the reactor and eliminate most of the temperature differential (and the thermal-convection head) which would normally exist across the reactor. The auxiliary pump ensures continuity of flow under these conditions. It is a DC electromagnetic pump in the reactor outlet line, in series with the main pumps. Its design capacity is approximately 500 gpm at 0.23 psi and 900°F sodium temperature. The pumping section is incorporated in the 14-inch outlet pipe with no change in pipe cross section. This is done to maintain the integrity of the piping system (at the expense of pumping efficiency, which is unimportant). Auxiliary pump power is supplied from metallic rectifier units backed up by storage batteries. During normal operation, these batteries float on the line and remain fully charged. In the event of a sustained power

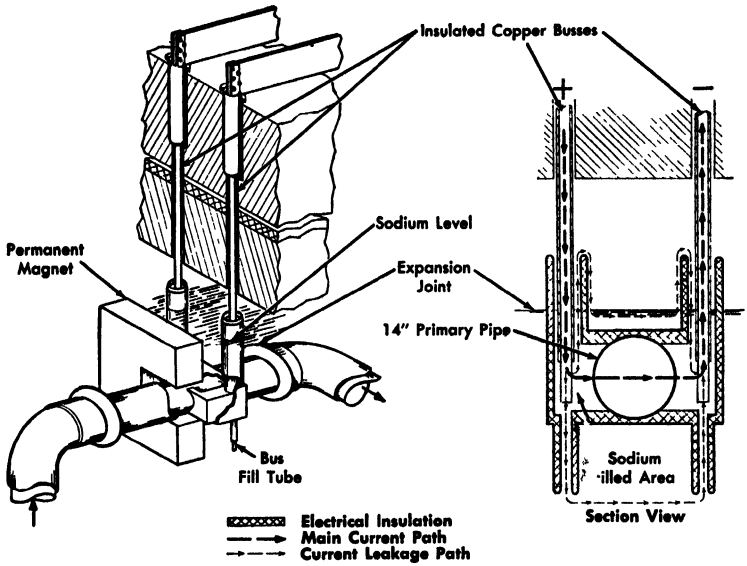

FIG. 3-21. Cutaway drawing and sectional view of auxiliary pump for the EBR-II primary system.

failure, the pump operates until the battery is discharged; the discharge results in a gradual decay of the flow rate and an ideal transition to thermal convection. Interlocks between the auxiliary pump and reactor controls prevent reactor startup unless the pump is connected and operating with the batteries fully charged.

The primary cooling system is instrumented to measure temperature, flow, pressure, and liquid level, and to initiate safety controls. The signals from these instruments are either recorded, indicated, or scanned.

The primary system is filled from the sodium receiving facility in the sodium plant (Figs. 3-1, 3-2) through a primary tank fill line and a primary sodium cleanup facility. To avoid thermal shock or local freezing of the sodium, the entire primary system is held at the temperature of the incoming sodium. Upon completion of the filling operation, the fill line is disconnected and capped. Draining will require considerable time (days), which is consistent with the requirements for fission-product decay cooling of the fuel, and considerations of radioactive decay of the sodium. Reactor operation is restricted to a minimum primary sodium temperature of 580°F. The bulk sodium is heated to this temperature electrically by immersion heaters. Expansion of the bulk sodium between 580°F and the 700°F normal operating temperature raises the sodium level approximately 4 inches. An 18-inch argon gas blanket is maintained between the sodium surface and the primary tank cover at 700°F.

3–3.4 Shutdown cooling. Fission-product decay heat is removed from the fuel after shutdown by maintaining sodium flow through the reactor and removing heat from the sodium. After shutdown, coolant flow through the reactor can be maintained by operating one or both of the main pumps, by operating the auxiliary pump, or by natural convection flow. Heat can be removed from the sodium by transferring it to the secondary system, or by transferring it to the bulk sodium in the primary tank, and then removing it by the shutdown coolers.

NaK enters the inner pipe of the bayonet cooler at the top and flows to the bottom, where it reverses direction and enters the annulus. Flow is then upward through the annulus, where heat is transferred to the NaK, then to the top of the bayonet cooler. Leaving the bayonet cooler, the NaK flows upward into a finned-tube air heat exchanger in a dampered air stack outside the reactor containment building. Here the heat is removed by natural convection of air. The cooled NaK then flows downward into the inlet of the bayonet cooler.

The system is designed for reliability and simplicity. The design of the bayonet coolers provides for minimum internal stresses over large temperature ranges and minimum obstructions in the flow circuit. All-welded construction is used and there are no valves in the system. After the system is filled with NaK, the filling line (which contains a valve) is capped. The system can be drained (except the bayonet cooler) by connecting a storage tank to the fill line. This is done only if the reactor is to be shut down for an extended period.

3–3.5 Neutron shield. The primary function of the neutron shield is to reduce the neutron flux at the primary heat exchanger below the level which would produce appreciable activation of the sodium of the secondary system. The shield surrounds the outside of the reactor vessel on all sides and is submerged in the bulk sodium of the primary tank (Figs. 3–4 and 3–6). The shielding material is graphite and graphite impregnated with 3 w/o natural boron. To prevent graphite from reacting with the sodium and contaminating it, the graphite is canned in stainless steel. For purposes of description, the shield can be separated into three sections: radial, top, and bottom. To facilitate fabrication, handling, and installation, the graphite and the borated graphite are canned in conveniently sized pieces which can be readily stacked and placed in position around the reactor vessel. The cans are leak-tested, loaded with graphite, and closed by welding. They are filled with helium to an absolute pressure of 10 inches of mercury (at room temperature) to minimize the internal pressure at operating temperature (12 psia at 700°F). The helium helps to conduct the heat generated in the graphite to the can wall. Additional helium generated by the (n, α) reaction with

boron will increase the pressure by approximately 19 psi (at operating temperature) during the life of the reactor, if all the helium generated is released to the helium atmosphere. The cans, which are designed for a positive net internal pressure of 50 psi, are cooled externally by natural convection flow of sodium.

The radial shield is assembled from graphite blocks ($4\frac{1}{8} \times 4\frac{1}{8} \times 18$ inches long) in stainless steel cans ($4\frac{7}{16} \times 4\frac{7}{16} \times 3/32$-inch wall thickness, and approximately 13 ft long). The cans are placed in rows around the periphery of the reactor vessel, and each row is held in place by stainless steel bands. Clearance between the cans permits natural convection flow of sodium. Rows are staggered to minimize neutron streaming. Specially shaped shielding cans are used around the inlet and outlet sodium pipes of the reactor vessel. The three inside rows of cans contain plain graphite, the fourth contains borated graphite, the fifth plain graphite, and the sixth borated graphite. The total graphite thickness of the radial neutron shield is $24\frac{3}{4}$ inches, of which $8\frac{1}{4}$ inches is borated and $16\frac{1}{2}$ inches is plain graphite.

The bottom shield is assembled from rectangular cans of composition and size similar to those used in the radial shield, except that the lengths are adjusted to fit the space. The staggering and spacing patterns of the cans are also similar. The first two layers of cans, adjacent to the bottom of the reactor vessel, contain plain graphite; the third contains borated graphite; the fourth contains plain graphite; and the fifth contains borated graphite. The total graphite thickness of the bottom shield is $20\frac{5}{8}$ inches, of which $12\frac{3}{8}$ inches is plain and $8\frac{1}{4}$ inches is borated graphite.

Because of the intricate structure of the reactor vessel cover, the top shield cans are of complex shape. They are stacked to prevent neutron streaming and to permit cooling. The cans in the center portion of the cover are cooled by the sodium that leaks from the upper plenum chamber, between the control rod drive shafts and guide bushings. The other cans are cooled by natural convection of the bulk sodium through openings in the periphery of the cover. There are six layers of cans filled with either 3% borated graphite or boron carbide, with a total thickness of $24\frac{3}{4}$ inches.

3–3.6 Control rod and safety rod drive systems. Operation of the reactor is controlled by 12 control rods (described in Article 3–3.1). Each rod is independently driven by an electrical-mechanical drive mechanism (Fig. 3–16). The drives are identical and are arranged so that only one drive can be operated at a time (with the exception of scram, when all twelve operate simultaneously). Operating control is achieved by 14-inch vertical motion of the control rods provided by a rack-and-

pinion drive with constant-speed electric motors; therefore only one speed of movement is possible. During fuel loading operations, the control rods are disconnected from their drives while in their down (least reactive) position. They remain in this position during the unloading procedure.

The control rod drive mechanism connects the drive to the control rod, and provides (1) slow-speed vertical motion (in both directions) for reactor control, and (2) high-speed downward motion for reactor scram. These operating functions, combined in a single unit, are appropriately interlocked to ensure the proper sequence of operation. The control rod drive mechanism is attached to the control rod by a double-jawed, cam and sleeve operated gripper. The gripper device is attached to the main drive shaft which extends upward through the biological shield into the operating area above the primary system. The shaft is driven by a rack and pinion at 5 in/min by a constant-speed, rapidly reversible polyphase motor. The drive shaft is connected to the rack by means of a fast-acting magnetic latch actuated by a magnetic clutch. Scram insertion of the rods is provided by pneumatic action.

The two safety rods (Article 3–3.1) provide additional reactivity shutdown capacity when the reactor is shut down and the control rods are disconnected. They provide a safety factor during reactor loading operations. The safety rod drive mechanisms are completely independent of the control drive systems and the fuel-handling systems. They are actuated by low-level detectors separate from the normal operational control system.

The rods are connected beneath the reactor to a horizontal bar which is moved by two vertical shafts extending upward through the biological shield (Fig. 3–16). Each shaft is coupled to a rack tube by a magnetic clutch latch arrangement similar in design to the one described above for the control rod drive. The rods are driven by synchronous motor drives and simply raise the system to the cocked position. When the latch is released, the drive mechanism and the safety rods fall 14 inches under the force of gravity. A pneumatic shock absorber decelerates the mechanism during the last 5 inches of movement. All reactor operations, including actuation of the control system or actuation of the fuel-handling system, require the safety rods to be in the up position.

3–3.7 Nuclear instrumentation. *Neutron equipment channels.* There are 11 nuclear equipment channels, divided into five groups:

(1) Startup counting channels (1, 2, and 3). Each startup counting channel provides period and neutron flux level signals during reactor startup or fuel handling. Instruments indicate reactor period, record log count rate, and count neutron pulse signals.

(2) Log power channels (4, 5, and 6). Each of the three log power channels provides a period and log flux level signal from 300% full power to six decades below full power. There are adjustable period trip signals and a log flux level signal for bypassing the startup channel trips during fuel-handling operation.

Each channel comprises a compensated ionization chamber with its power supply, a log N preamplifier, a log N amplifier, and a period amplifier. The three channels have one common log N flux recorder with a selector switch for recording any one of the channels. Period signals from one channel, selected by a switch, are displayed on an indicating meter.

A neutron detector (gamma-compensated ionization chamber) produces a current signal proportional to the neutron flux level. A regulated power supply furnishes the required high voltages.

(3) Linear level channel (7). The linear level channel gives a linear flux level signal from 300% full power to six decades below full power. There is an adjustable linear flux level trip relay for future use.

This channel comprises a compensated ionization chamber, a high-voltage supply, a DC micromicroammeter with remote range switching, an indicator, and a linear flux level recorder.

The neutron detector will be a compensated ionization chamber like that for the log power channels. The micromicroammeter amplifies the output of the ionization chamber and produces a voltage to drive the linear level recorder.

(4) Auto flux regulation channel (8). This channel automatically regulates the neutron flux level from 10% to 100% reactor power.

(5) Safety trip channels (9, 10, and 11). The three safety trip channels each provide an adjustable linear level relay trip signal over a range from four decades below to one decade above reactor full power.

Thimbles. Eight instrument thimbles are available for housing the eleven counters and ion chambers. These thimbles extend downward through the primary tank cover into the sodium. Four are distributed along an arc just outside the reactor neutron shield and four along an arc inside the neutron shield. Each thimble is designed to reduce the high ambient temperature to a level tolerable for the type and function of the detector housed.

Instrument channels. The power ranges covered by the ten channels are:

(1) Startup range: covered by two identical fission counter channels arranged so that either may cause scram; they are disconnected as power level exceeds the upper limit of the range.

(2) Logarithmic range: covered by two wide-range, linear DC amplifier channels which measure current from ionization chambers; they are

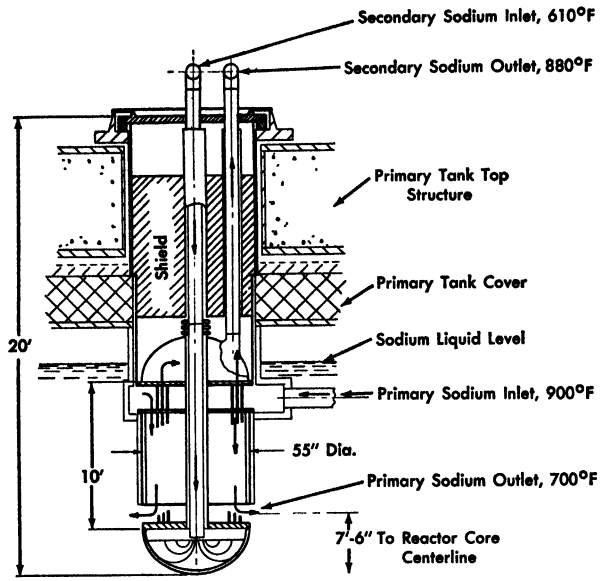

FIG. 3–22. Schematic representation of EBR-II primary to secondary heat exchanger.

used for accurate indication of power level up to the 50% level and for control of the regulating rod; either may cause scram.

(3) High-flux region: covered by four DC amplifier channels which measure current from ionization chambers; they are used for the high-power range and for high flux level trip only; two trips are required to cause scram.

Neutron source. The neutron source is contained in a specially designed subassembly which is positioned within the inner row of the inner blanket. This subassembly can be loaded into the reactor in the same manner as an inner blanket subassembly and can be periodically replaced. The source is approximately equal in length to the reactor core and at the same elevation. The source material is a solid cylinder of activated antimony in a cylindrical sleeve of beryllium metal.

The antimony-beryllium neutron source is designed so that the detector is exposed to a flux of at least 100 n/(cm^2)(sec) during reactor shutdown. Calculations indicate that, after irradiation in the MTR, the source will produce the required flux at the detector for a period of 60 days of zero-power EBR-II operation. Any extended period of high-power operation would tend to lengthen the cycle. Continuous operation of the reactor at full power (62.5 Mw) would keep the source strength essentially constant.

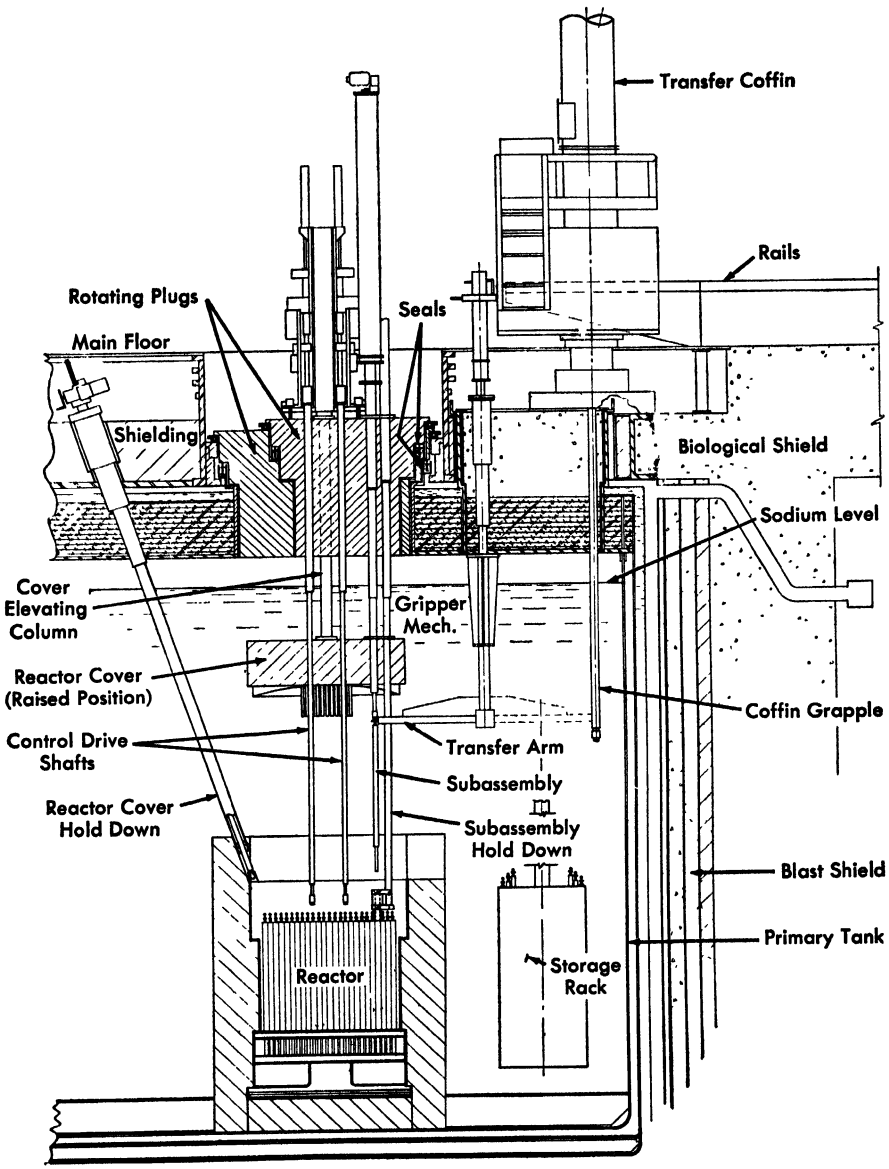

FIG. 3–23. Schematic diagram of the EBR-II fuel-handling system.

3–3.8 Primary tank and biological shield. The primary tank, primary structure, and shield cooling system constitute an integrated system which is designed to meet static load requirements, maintain accuracy of alignment, and withstand the effects of internal energy releases that might result from a nuclear accident. As shown in Fig. 3–6, the tank is surrounded and supported by the primary structure, which includes the biological shield. The primary tank and the primary structure are completely independent of each other on all sides except at the top, where the primary tank is supported. All units entering the primary tank pass through the top. Much of the primary system equipment is large and heavy and must be adequately supported, as must also the total weight of the primary tank. The top structure is designed to support these loads. The primary structure is also designed to contain the energy release associated with a nuclear accident. For design purposes, an energy release equivalent to 300 lb of TNT at the center of the reactor was assumed.

Primary tank. The primary tank is of double-wall construction (a tank within a tank) to provide maximum reliability of sodium containment. The tank is constructed of type-304 stainless steel. The inner tank is 26 ft ID and the outer tank is 26 ft 11 inches ID. The side walls are constructed of plates 1/2 inch thick; 1-inch plates are used for the tank bottoms. The space between the two tanks is filled with an inert gas, monitored to detect leakage through either tank wall (sodium or air). The outside of the tank is insulated to minimize heat loss from the primary system.

The bottom of each of the tanks is stiffened with radial beams. A similar structure is used for the primary tank cover, which is 39 inches deep. (This depth is used for shielding material and thermal insulation.) The inner tank bottom plate structure is designed to support the reactor tank, the subassemblies, neutron shield, and the entire sodium load. This load is transferred by the tank wall to the top cover, where the tank is supported.

The outer tank structure is designed to carry only the sodium load should a leak develop in the inner tank. The primary tank and its contents, and the components connected to the primary tank top cover, are supported by six hangers welded to the top cover beams, which in turn transfer these loads to the top structure beams. Each hanger is pin-connected so that differential radial expansion between the top structure and the primary tank cover will not impose additional stresses in the system.

The primary tank and the method of support are designed to permit radial expansion about the vertical centerline of the system. The most critical units—the reactor and the rotating plugs which locate the con-

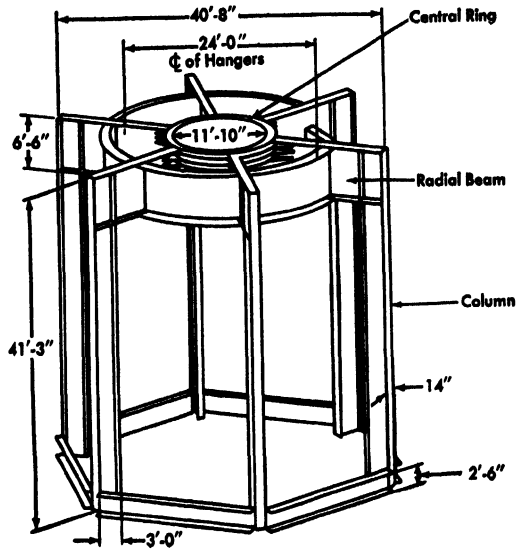

FIG. 3-24. Schematic drawing of the EBR-II primary tank support structure.

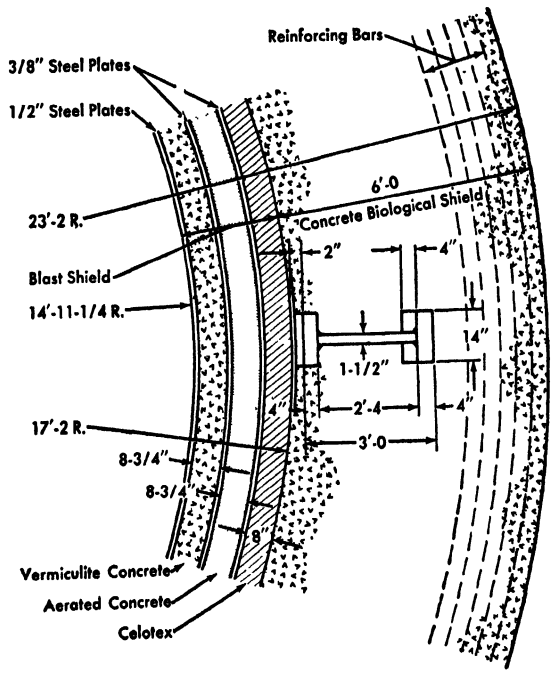

FIG. 3-25. Schematic representation of typical column detail for EBR-II primary system support structure.

trol drives and fuel unloading mechanisms—are located on this centerline. Differential vertical expansion is avoided by using identical material for all equipment in the system, and maintaining it at the same temperature.

Primary structure. The primary structure is a system of columns and beams which transmits the loads to the main internal building foundation. In combination with the biological shield, it forms a retainment vessel surrounding the primary tank (Figs. 3–24, 3–25). The bottom structure consists of six radial beams embedded in the heavily reinforced concrete with six columns connected to the beams. These columns are connected at the top to six radial beams which frame into a circular ring 6 inches thick located on the centerline of the system. This top structure, with additional stiffening members, provides the supporting structure for the primary tank and for the major primary system components supported external to the primary tank. The material proposed for this structure is USS Carilloy T-1 plate steel, which has a yield point of 90,000 psi and a tensile strength of 105,000 psi at room temperature. Using American Welding Society E-12015 electrodes, welded joint efficiencies of 100% are anticipated. A ring of ordinary concrete (6 ft thick) provides the radial biological shield, whose inside surface nearly coincides with the inside circle of the six vertical columns. The shield alone provides sufficient strength to carry the static loads imposed on the top structure; the steel columns provide the tensile strength to resist internal pressure against the top structure in the event of an internal energy release. Certain precautions must be taken to protect these columns from blast damage, as discussed immediately below.

Blast shield. To protect the primary structure (in particular, the columns) and the radial biological shield in the event of an explosion-type accident in the reactor, a laminated continuous blast shield about 2 ft thick is placed between the primary tank and the biological shield (Fig. 3–6). The three layers of absorbing materials, separated by steel cylinders, of which the blast shield is comprised are 8¾ inches of vermiculite concrete (22 lb/ft³); 8¾ inches of aerated concrete (16.5 lb/ft³); and 8 inches of Celotex. The steel cylinder walls are 1/2 inch or 3/8 inch thick. The blast shield serves as a cushion to absorb most of the released energy, and to reduce the pressure acting on the structure to allowable limits. Energy is attenuated and absorbed by crushing of the low-density concrete and Celotex, and stretching of the steel shells.

Biological shield. The radial biological shield (Fig. 3–3) is of ordinary concrete 6 ft thick, reinforced with continuous hoops of rods so that the shield will safely resist an internal pressure of 75 psig. (The estimated resultant pressure beyond the blast shield is only a few psig.) Structural columns have been set back 2 inches from the inner face of the biological shield to avoid lateral loading of the columns should the concrete tend

to move outward. The radial biological shield and structure is continuous except near the top of the primary tank, where it is penetrated by several horizontal offset holes (approximately 8 inches in diameter) for ventilation ducts required for shield cooling. Cooling is necessary to remove the heat absorbed from the primary system, and from neutrons and gamma rays, to avoid overheating the steel plates and the concrete.

The top biological shield is penetrated by a large rotating plug directly above the reactor vessel (Fig. 3–7). The large plug is in turn penetrated by a smaller, off-center plug. The gripper mechanism for fuel handling penetrates the smaller plug eccentrically and extends downward through a hole near the edge of the reactor cover. The cover is supported from the small rotating plug by shafts which penetrate the plug and may be retracted to lift the reactor cover for fuel-changing operations (Article 3–3.9). The shield plugs are supported by roller bearings and are rotated by electric motors. Each plug is sealed around its periphery by a freeze seal employing a bismuth-tin alloy in a trough around the plug, while a baffle fastened to the plug dips into it. During reactor operation the alloy is frozen (melting point 280°F), forming a gastight, pressure-proof seal. During fuel-handling operations, the alloy is melted so that the plugs can be rotated.

Shield cooling. The shield cooling system is part of the building ventilation system; the air is exhausted from the building through the shield cooling system. The system operates at a pressure slightly below that of the building atmosphere, and provides in-leakage and also simplifies certain areas in the shield which cannot be connected to a closed circulation system. The top structure and shield plugs are cooled by air drawn from the building atmosphere. The radial shield and the structure below the primary tank are cooled primarily by recirculated air. Air from the building is drawn into the primary system through ducts in the rotating plugs and primary top structure, and is then circulated around the top cover of the primary tank and through ducts in the biological shield into exhaust blowers. It joins air which has circulated through the radial shield and bottom shield air space. The air flow then is split into two paths, one to the exhaust stack in the process plant, and the other through coolers.

The heat to be removed by the shield cooling system consists almost entirely of the heat lost from the primary system; the heating in the shield due to neutron and gamma-ray attenuation is only a small fraction of the total heat load (15,000 Btu/hr out of a total of 430,000 Btu/hr). An air-cooling system of 15,000-cfm capacity with a maximum air velocity of approximately 30 fps is required. For reliability, there are auxiliary power supplies to the exhaust blowers and coolers. Because of the large heat capacity of the system, interruption of the cooling system is not critical.

3–3.9 Fuel-handling system. Fuel handling includes removing the subassembly from the reactor, transferring it to the storage rack, and after a 15-day cooling period (for fission product decay), moving it to the process building. The fuel-handling system (Fig. 3–23) consists of the reactor gripper mechanism, the transfer arm, the storage rack, and the transfer coffin. The reactor gripper mechanism and the hold-down mechanism are located in the small rotating plug which is located off-center in the large rotating plug. The two plugs are rotated to locate the gripper over the desired spot in the reactor and to put the gripper in the transfer position.

Entrance to the reactor. After the reactor is shut down, the 12 control rods are released from their individual control rod drive mechanisms, and the hold-down clamps which fasten the cover to the reactor tank are released. These three clamps are equally spaced about the circumference of the cover, and clamping of each is accomplished by a tube which slides over a fixed rod. Sliding the clamping tubes upward provides clearance between the flange and the tubes, permitting the cover to be raised by the two elevating columns. The columns are raised by two synchronized electric motor-driven lifting mechanisms located on the small rotating plug. In the raised position, the reactor cover engages pins extending from the underside of the rotating plug, to prevent swinging of the relatively heavy mass (approximately 17 tons) during plug rotation. The cover is raised 9 ft 8 inches to provide enough clearance below for removing subassemblies from the reactor. The control drive mechanisms are then raised 3 inches to clear the subassembly adapters.

Angular orientation controls. All operations involved in the fuel-handling cycle include provisions for maintaining a "known" angular orientation control: (1) the cone-shaped adapter is slotted and engages a blade in the gripper mechanisms, (2) the section below the collar is rectangular and engages the slotted arm of the transfer arm, and (3) the lower nozzles of the subassemblies are slotted and engage orientation bars in the reactor grid and the storage rack. All these orientation controls on the subassemblies are in the same plane. Angular orientation is controlled and supervised at all times during the fuel-handling cycle.

Removal of the subassembly. The rotating plugs and gripper head are rotated to the proper position for the particular subassembly to be removed (there is a specified angular position for each of these three units for each lattice position in the reactor). The hold-down mechanism, a funnel-shaped sleeve, is lowered by an electrically driven screw over the subassembly. It contacts the six adjacent subassemblies, spreads them slightly, and keeps them in place as the subassembly is removed. This arrangement is shown in Fig. 3–23. The hold-down sleeve also acts as a guide for the gripper mechanism.

The gripper head is lowered (through the hold-down sleeve) and makes contact with the adapter on the subassembly. The gripper device on the lower end of the mechanism grips the subassembly adapter in the same fashion as the control drive gripper. The orientating blade between the gripper jaws engages the slot in the conical shaped head. A sensing device controls these movements in the same manner as with the control drive mechanism. The gripping mechanism is moved vertically by an electrically driven screw drive and the gripper jaws are motor-operated. Interlocks prevent the opening of the jaws except when the gripper head is in the upper plenum chamber of the reactor, or at the transfer point between the gripper and transfer arm.

Transfer of the subassembly. After the subassembly has been lifted out of the reactor, the hold-down tube is raised around the suspended subassembly and supports it while the two plugs are rotated to the transfer point and the gripper head is rotated to the transfer angle. When lowered by the gripper, the collar on the subassembly adapter fits into a recess in the U-shaped transfer arm holding device, as shown in Fig. 3–23. The rectangular section below the collar assures proper orientation. The locking bar on the transfer arm holding device locks the subassembly positively to the transfer arm. The subassembly is released by the gripper and the hold-down is lowered.

The transfer arm is rotated through a horizontal arc of about 80 degrees to position the subassembly above any one of three concentric rows of storage locations in the storage rack. The transfer arm is operated manually and, by "feel" provides several checkpoints for the operator; for example: the physical contact between the transfer arm and subassembly at the transfer position is felt, and the transfer arm cannot be moved while the subassembly is held by the gripper and hold-down sleeve; this provides a check that the transfer has been made correctly. Similar checks can be made between the transfer arm and the storage rack.

The storage rack. This structure, which is tank-shaped, provides 70 storage locations in three concentric rows. The storage rack is suspended by a shelf extending through the primary tank cover which can raise, lower, and rotate the rack. Rotating the storage rack positions an empty storage location underneath the suspended subassembly. The storage rack is raised to insert the subassembly into a storage location and, at the end of the upward movement, to lift it from the holding device when the transfer arm locking bar is released. A transfer-indicating device assures proper vertical movement of the storage rack. This is a sensing rod extending vertically from the disassembly cell ceiling to the transfer position. It is actuated by the upper adapter of the subassembly, which is raised when, by improper rotation of the storage rack, an already-

occupied storage location is placed below the subassembly, or when the storage rack lifting mechanism accidentally overtravels its correct transfer level. In either case, the transfer-indicating device acts as an electrical safety stop. There is a further checkpoint here: so long as the subassembly is held by both the storage rack and the transfer arm, the transfer arm cannot be moved. After subassembly transfer, the transfer arm is rotated to a neutral position, and the storage rack is lowered.

Transfer to the disassembly cell. After cooling for 15 days to permit fission-product decay, the subassembly is removed from the storage rack and moved by the transfer coffin (Fig. 3–23) to the disassembly cell in the process building (see Section 3–6). The heat generated from fission-product decay is significantly less after the cooling period than before, but cooling (by forced circulation of an inert gas) is still required when the subassembly is removed from the sodium. The subassembly is cooled through all subsequent steps in transporting and handling it until it has been disassembled and the fuel elements have been separated from the close-packed cluster.

A new fuel or blanket subassembly is introduced into the reactor by the steps described above, but in the reverse order.

3–3.10 Sodium cleanup system. A recirculating cold-trap system is used to continuously purify the primary sodium. This system holds impurity concentrations at or near their greatly reduced solubility limits for temperatures just above the melting point of sodium. Cold-trap precipitation is effective in maintaining low concentration of such impurities as sodium hydride, most fission products, and particularly sodium monoxide.

The cold trap consists of a 500-gal tank filled with type-304 stainless steel wire mesh, giving extra surface area to enhance sodium crystallization and deposition. A regenerative heat exchanger in the main sodium stream reduces over-all heat losses in the cold-trap system. The cold-trap operational temperature of 350°F is maintained by a secondary sodium cold-trap coolant loop. Two types of analytical devices are used to determine sodium quality: a plugging indicator mounted on the cold-trap inlet line monitors the oxygen concentration in the primary tank sodium, and two vacuum cup samplers remove sodium samples, for chemical or radiological analysis, from either the cold-trap inlet or discharge line.

Parts of the cold-trap circuit lie below the level of sodium in the primary tank. Since radioactive primary sodium is circulated in the cold-trap system, it is essential to eliminate the possibility that an accident or equipment failure might result in siphoning of primary tank sodium. To avoid this possibility, a surge tank is included in the cold-trap inlet

line at its highest point of elevation. An argon gas blanket pressure is maintained such that, under static conditions, the sodium level is just below the surge tank discharge opening. With the pump operating, the level rises sufficiently to establish flow. The power supply to the pump is interlocked to a sodium vapor monitor at the cold-trap floor level to stop the pump when a sodium leak is detected, thereby stopping sodium discharge from the tank. Further, an argon gas line is provided for positive gas addition to ensure breaking the sodium column in an emergency.

The cold-trap discharge line empties into a splash sleeve in the gas phase of the primary tank, precluding any possibility of siphoning through the discharge line. Five remotely controlled valves in the cold-trap circuit serve to isolate various sections of the system during emergencies and repairs. The horizontal sections of both the cold-trap inlet and discharge lines are pitched to drain back into the primary tank. These provisions ensure a minimum of sodium spillage in the event of system failure. Except for failure of the cold-trap tank proper, a rupture in the system can involve no more than the sodium in the cold-trap discharge line and in the vertical section of the inlet line.

3–3.11 Inert gas system. It is necessary to provide an inert gas blanket over the primary system sodium and an inert gas atmosphere within the disassembly cell. Of the noble gases, argon was chosen for this system because of its qualities with respect to pumping, heat transfer, and sealing. During normal operation, the pressure in the primary tank is approximately atmospheric.

Argon vented to the stack is continuously monitored for activity. If the activity exceeds the tolerable level, the gas is pumped into a retention tank and held until it decays sufficiently for safe disposal.

3–4. Secondary Cooling System

3–4.1 Introduction. This sodium system is the nonradioactive intermediary between the primary and steam systems; it includes a sodium-to-sodium heat exchanger located in the reactor plant, a sodium to water and steam heat exchanger (steam generator) located in the boiler plant, an AC electromagnetic linear-induction pump located in the sodium plant, a surge tank located in the sodium plant, and associated interconnecting piping (Figs. 3–1 and 3–3). At full power the pump gives a flow rate of 6050 gpm at a head of about 45 psi. Sodium coolant enters the primary to secondary exchanger at 610°F and leaves at 880°F. Since heat loss in the interconnecting piping is small, sodium enters the superheater section of the steam generator at approximately the same temperature, 880°F. Coolant leaves the steam generator at 610°F (Fig. 3–3).

3–4.2 System heat exchangers. The primary to secondary heat exchanger, shown in Fig. 3–22, is suspended from the primary tank cover (Fig. 3–7) and is almost totally submerged in primary sodium; it is a shell-and-tube heat exchanger with secondary sodium on the tube side. Inlet and outlet temperatures are 610 and 800°F, respectively, on the secondary side, and 700 and 900°F on the primary (shell) side.

The steam generator, of a natural recirculating type, consists of evaporator and superheater sections with a single steam drum. Each section is composed of a number of vertical units, with each evaporator unit connected to the steam drum by a single downcomer and riser; dry saturated steam passes from the drum downward through the superheater units. Both evaporator and superheater units use single-length, double-walled tubes with the outer walls welded to a shell tube sheet and the inner walls welded to an external tube sheet. The tube sheets are positioned a few inches apart and are connected only by the tubes. There are no welds serving as barriers between sodium and water or steam. A third fluid annulus or monitoring system is not employed.

3–4.3 Pumping requirements. The circulating pump is an AC linear-induction type (FLIP) with a capacity of 6500 gpm at about 53 psi. By varying the voltage of the alternating current, the flow rate is controlled down to less than 5% of nominal rating. The variable voltage is obtained by controlling the output voltage of a motor generator set. As shown in the discussion of the basic control scheme (Section 3–7), this pump is a critical link in the heat balance between the major thermal systems. Because rates of heat removal from both the primary system and secondary system are nearly proportional to the secondary system flow rate, the heat-removal balance between the reactor and the secondary system is maintained through control of the secondary pump.

3–4.4 System layout. The single-story sodium plant building, of fireproof construction, is located about 70 ft from the reactor plant building. It contains, in addition to the pump, the secondary sodium purification system, sodium receiving facilities, and the sodium storage tank. The sodium storage tank is below floor level in this building, and the entire secondary system sodium, except that in the heat exchanger, can drain into this tank. A surge tank connected into the piping at the circulating pump inlet maintains a constant head to the pump. The sodium purification system circulates a minimum of 20 gpm from the storage tank and discharges into the surge tank, ensuring constant level; the overflow returns to the storage tank through an internal overflow pipe in the surge tank. Argon at approximately 10 psi provides an inert gas atmosphere over the sodium in the surge and storage tanks.

The boiler plant building is almost 100 ft from the reactor plant building. The steam generation equipment is so located as to ensure drainage to the storage tank in the sodium plant. The secondary sodium passes through the superheater section and the evaporator section in series. Piping in the secondary system is capable of absorbing thermal expansions due to temperature changes from ambient to 1000°F. The sodium yard piping, heated, insulated, and weatherproofed, is carried on concrete piers fitted with pipe guide or anchor frames as required. Induction heating with 60-cycle current keeps the sodium temperature above its freezing point (208°F).

System operation is monitored by:

(1) An electromagnetic flowmeter in the pump discharge line backed up by an orifice-type meter.

(2) Nine pressure-sensing devices with provisions for recording or signaling, or both.

(3) Seven temperature-sensing thermocouple wells with provisions for recording or signaling, or both.

(4) Two sodium level detectors connected to continuous recording and alarm systems.

At full power, system pressure drops are 5 psi through the heat exchanger, 14 psi through the superheater and evaporator combined, and 26 psi through all connecting piping and fittings. The total pressure drop is about 45 psi. Since the inlet side of the pump is kept at a pressure of 10 psig by the argon gas blanket in the secondary system expansion tank, the maximum pressure in the secondary system is 55 psig.

3–5. Steam-Electrical System

3–5.1 Introduction. During full-power operation, the steam system (Fig. 3–3) will furnish 249,000 lb/hr of superheated steam at 1250 psig and 850°F to drive a 20,000-kw turbogenerator. In parallel with existing electricity sources, the electrical system will deliver an estimated 8500 kw of power to other NRTS* areas after feeding back 3500 kw to EBR-II auxiliaries; plant net electric output will be 16,500 kw.

Certain features have been included in the steam system to improve reliability and to isolate the reactor from load fluctuations on the turbine. A bypass system operates in conjunction with the turbine to permit absorption of all energy produced in the reactor, irrespective of elec-

*National Reactor Testing Station, Arco, Idaho. The anticipated load distribution is: 8500 kw to other experimental facilities; 8000 kw to the existing 138-kv NRTS supply system; 16,500 kw total.

trical output. Normal plant operation consists of a continuous bypass of steam to absorb load variations in the steam system without affecting the reactor. Steam conditions were selected to provide maximum stability of the heat-transfer loops with respect to system temperatures. The saturation temperature of 1250 psig steam (572°F) approximates the minimum temperature of the secondary system (610°F). Thus heat is removed from the reactor at a constant high temperature provided the steam pressure is maintained at a constant value, as it should be. The temperature of the secondary sodium, as sensed by the primary sodium coolant system, is essentially constant under all conditions of operation.

Recent experience has shown that high reliability of steam generator units (Section 3–4) is not easily attained. High thermal stresses are known to have contributed to failures. In an effort to minimize thermal stresses in the EBR-II steam generator, special feedwater temperature requirements have been included. After the feedwater has been heated by extraction from the turbine, its temperature is raised further by an additional heater supplied with steam directly from the 1250-psig system. In this manner, the feed water is heated to 550°F over the entire load range, and only a small temperature difference exists between the feedwater and the evaporator water (580°F). The steam generator is located in a separate building adequately removed from the reactor, with blowout panels designed to fail in a direction away from the reactor.

The electrical system is designed for simplicity of operation, ease of maintenance, and safety. The control circuits are interlocked, insofar as possible, to prevent improper sequence of operation due to human error.

3–5.2 Steam system. Feedwater at 550°F is supplied to the steam drum of the steam generator (249,000 lb/hr at full power), and saturated steam at 580°F is generated in the evaporator. After passing through moisture separators in the drum, the steam is heated to 850°F in the superheater. Steam conditions at the turbine throttle are 1250 psig and 850°F with a flow rate of about 199,000 lb/hr. The remaining steam (50,000 lb/hr) is employed for direct feedwater heating, for driving the feedwater pump turbine, and for maintaining bypass flow around the turbine to the condenser. The turbine exhausts 145,500 lb/hr of steam (14% moisture content) to the condenser at 1½ inches mercury pressure. The condenser, a deaerating type, employs a circulating flow rate of 21,500 gpm at 70°F inlet and 83°F outlet temperatures.

The feedwater heating system consists of a blowdown cooler, two feedwater heaters using steam extracted from the turbine, one deaerating heater which utilizes steam from the exhaust of the feedwater pump tur-

bine, and a high-pressure heater using steam from the main steam line (1250 psig, 850°F). This system is designed to supply feedwater to the steam generator at a constant temperature regardless of load conditions or mode of plant operation. Indication and recording are provided for turbine throttle pressure, feedwater and condensate pump outlet pressures, feedwater temperature and flow rate, and water levels in the deaerator feedwater heater and the evaporator. High- and low-limit relays are provided for alarm indication. Various other temperatures and pressures are measured, following conventional steam system practice.

The steam system flow diagram (Fig. 3–3) includes 5000 lb/hr of steam bypassed to the condenser at full load (62.5 Mw of heat). Under these conditions of operation, the generator produces 20,000 kw gross output.

3–5.3 Electrical system. There are four sources of power supply for the EBR-II facility: two from existing utility connections, an emergency automatic-starting diesel generator set for operating critical auxiliary loads, and the EBR-II generating system itself. The 20,000-kw gross output is delivered to the station bus through metal-clad switchgear. The 13.8-kv generator operates at 3600 rpm, with 0.85 power factor; auxiliaries are supplied from various 2400- and 480-volt circuits.

There are two independent transformer ties to a closed power loop (138 kv) served by two separate utility companies. Both transformers are connected to a sectionalized main bus (13.8 kv), the tie breakers being closed during normal operation. The EBR-II generator is connected to one of the two main bus sections. Thus there are three main sources of electrical power. For further reliability, there are duplicate circuits to each of the lower voltage systems (2400 and 480 volts) from auxiliary transformers fed by both of the main bus sections. A selective relaying scheme provides automatic protective isolation of a faulted portion of the system with no interruption of power.

The fourth power source is an automatically starting, 400-kw diesel generator set for operation of necessary or desirable auxiliaries in the remote event of a main power outage. This source is backed up by an additional 75-kw diesel generator set connected only to the two critical auxiliaries: the nuclear instrument thimble cooling system and the biological shield cooling system. This latter set also starts automatically upon loss of main power, but only if the large set fails to start within a predetermined period of time.

3–6. Fuel Cycle and Reprocessing*

3–6.1 Significance. The EBR-II is being built as a completely integrated nuclear power plant and so includes not only the facilities required for the power cycle (reactor, steam generator, turbine, etc.) but complete fuel cycle facilities as well. Since this is a closed cycle, the fuel alloy will be recycled through the reactor many times. One anticipated result of continued recycling is a substantial change in the isotopic character of the fuel. Less common isotopes of fissile and fertile materials (U^{236}, U^{237}, Pu^{240}, Pu^{238}, etc.) will build up so that even the presently used long cooling times and efficient chemical separation plants for the removal of fission-product elements will not reduce the radioactivity enough to permit contact refabrication.

Since continuous recycling appears to demand remote refabrication, it seemed reasonable to consider processes which provide only sufficient fission-product removal to satisfy reactor and metallurgical requirements. Pyrometallurgical processes (nonaqueous processes based on high-temperature reactions of a metallurgical nature) now under development satisfy these requirements and appear to offer certain economic advantages [4]. The encouraging results of development work in pyrometallurgy, as well as the potential advantages indicated by more fundamental research, led to the decision to build a pilot-scale plant to study further these nonaqueous methods for purifying spent reactor fuel. The operation of such a plant will provide data to permit evaluating the economic and technical feasibility of these procedures. If the potential advantages can indeed be realized, the part of the cost of nuclear power attributable to the fuel cycle will be substantially reduced.

Since the technical and economic advantages or disadvantages of a single step in the fuel cycle are seldom controlling, the feasibility and cost of the complete fuel cycle are of primary importance. Thus it was decided that a pilot-scale plant should operate in conjunction with a reactor as a closed fuel cycle. The reactor selected was the EBR-II. It will probably be the first in the U. S. power demonstration program to operate on a closed fuel cycle. This operation will provide an experience basis for evaluating pyrometallurgy and remote fabrication as applied to a fast reactor.

3–6.2 Pyrometallurgical purification. The fuel cycle plant will contain equipment for remote refabrication of fuel elements as well as for the pyrometallurgical purification operation. Provision is also being made for installing equipment to demonstrate pyrometallurgical processes

*By M. Levenson, J. Schraidt, A. Shuck, and E. Sowa, ANL.

for recovering reactor-grade plutonium from the blanket material and for recovering fissionable materials from process wastes.

Melt refining. The fuel purification technique first to be evaluated in the EBR-II fuel cycle is melt refining (oxide slagging or drossing). The general process has been described previously [4,5,6,7] and recent process developments are covered in a paper [8] of the Second International Conference on Peaceful Uses of Atomic Energy. Therefore only the actual flowsheet conditions selected for initial operation are described: 10 kg of fuel pins are considered a furnace charge; only three such melts per week are required when the reactor operates at 62.5 Mw and attains a fuel burnup of 2 a/o; the crucible material selected is dry pressed zirconium oxide, although many other materials were investigated. Refining is carried out under an inert atmosphere at 1300°C in 3 to 4 hr. Under these conditions the volatile fission products distill out of the metal. Elements forming oxides more stable than those of uranium oxidize and separate into a slag layer. The zirconium oxide crucible supplies the oxygen for these reactions and in turn is reduced to a suboxide. Practically no zirconium oxide is reduced to metal, so this operation does not add zirconium metal to the fuel alloy. The less reactive elements, niobium, molybdenum, technetium, ruthenium, rhodium, and palladium, are not removed by the melt refining process. Since adding these elements* has been shown [9,10] to improve the radiation stability and metallurgical properties of the fuel, their retention is desired. On continued recycling their concentrations will build up to equilibrium values controlled by the amount of new fuel material added per cycle.

Estimated equilibrium fission-product element concentrations, when 5 w/o fresh fuel is added each cycle, are shown in Table 3–4. These alloys, U-fission products or U-Pu fission products, are called "fissium" alloys.

The value 0.1% for zirconium is based on the assumption that it is largely removed in processing. This has been accomplished by reacting the zirconium in the melt with carbon to form the carbide which separates into the slag. Recent experiments indicate that adding carbon to the process increases fuel losses to the slag. As a result, work has been started to evaluate fissium containing higher zirconium concentrations, to determine its suitability from a metallurgical and radiation damage standpoint. If such an alloy is suitable, the zirconium removal step will be dropped.

Plutonium in the fuel remains largely with the metal phase, and its recovery is only slightly poorer than that of uranium. Therefore data obtained on the original reactor loading with U^{235} as the fissionable material

*As applied to technetium, this statement is an assumption.

TABLE 3–4

ESTIMATED EQUILIBRIUM FISSION-PRODUCT CONCENTRATION IN EBR-II FUEL

(Based on uranium metal with 60 w/o U^{235}; 5 w/o new metal per cycle)

Element	w/o
Zirconium	0.1
Niobium	0.01
Molybdenum	3.4
Technetium	1.0
Ruthenium	2.6
Rhodium	0.5
Palladium	0.3

should apply to later plutonium loadings. In addition, actual plutonium data will be obtained on the first loading because plutonium will be produced by internal breeding in the U^{238}, which makes up one-third of the fuel alloy.

The volatile fission products are noncondensable gases such as krypton and xenon, and the condensables such as cesium, strontium, barium, and cadmium. Because the process equipment is small, the rare gases are confined to a small volume. It is therefore feasible to hold these gases long enough for the active isotopes to decay sufficiently to permit their discharge to the environment. Condensable fission products are collected on surface-active media directly above the crucible. The surface-active agent selected is Molecular Sieves,* a dehydrated zeolite composed largely of calcium silicates.

Plutonium recovery. The blanket process (recovery of plutonium from irradiated depleted uranium) that will be evaluated first in this plant is a nonaqueous solvent extraction process. The solvent will be molten magnesium metal, and the feed molten uranium. The solute will be recovered from the solvent by distillation [11]. Although considerable laboratory and semi-works experience has accumulated on this process [5,12], it has not yet been adapted to plant-scale remote operations.

Pyrozinc process. The first process to be evaluated for the recovery of fissionable materials from melt-refining and metallurgical wastes will

*Product of Linde Air Products Corporation.

be the pyrozinc process [13,14,15]. It is based on the fact that the solubilities of uranium and fission-product elements in liquid zinc are different and change substantially with temperature. At 800°C zinc dissolves about 6 w/o uranium. The uranium can be almost completely precipitated from this solution as U_2Zn_{17} by cooling to 500°C. The U_2Zn_{17} crystals are separated from the liquid zinc and soluble fission products by filtration, and the uranium is recovered by heating the U_2Zn_{17} to 950°C. At this temperature the compound dissociates and the zinc is distilled off. If magnesium is dissolved in the zinc, it is possible to reduce uranium compounds, including the oxides, to produce a uranium-zinc-magnesium solution and thus recover uranium from oxide slags. The pyrozinc process shows much promise on the laboratory scale but it has not yet been adapted to plant-scale remote operation.

3–6.3 Equipment and facility design. Because the fuel cycle is experimental, equipment and facilities designs have been treated differently. The facilities are being designed to be flexible, while the equipment is to be specific and as simple as possible. Wherever practical, motive power will be supplied by operating manipulators. This is desirable so that changes in the fuel element or in the various processes can be accommodated by replacement rather than extensive modification of equipment items. Keeping items of equipment simple improves reliability, which is important for successful remote operation.

Many problems encountered in the design of the argon cell arose from the unique combination of heavy shielding and inert atmosphere. Remote-handling techniques ordinarily suitable for air-atmosphere caves could not be employed because of sealing problems. Techniques suitable for controlled atmosphere enclosures could not be used because of the high gamma radiation. In many instances the solutions proposed require modifications of existing designs. Others are new and cannot be fully evaluated until the cell has been placed in operation.

Since this is a closed cycle, the raw material is a spent fuel subassembly and the product is a refabricated subassembly (Fig. 3–12). The bare fuel material is designated fuel *pin;* the stainless steel canned, sodium-bonded fuel pin is designated fuel *element;* the assembly of 91 fuel elements (including necessary shrouds and end pieces) which is actually charged to the reactor is designated fuel *subassembly.*

Both the new and used fuel subassemblies are intensely radioactive, and therefore must be introduced into the processing facility, disassembled, purified, refabricated, and reassembled by remote operations. All steps must be done behind massive shielding, and many of them will be performed in an inert atmosphere. The building floor plan [16] evolved to meet these requirements is shown in Fig. 3–26, and a photo-

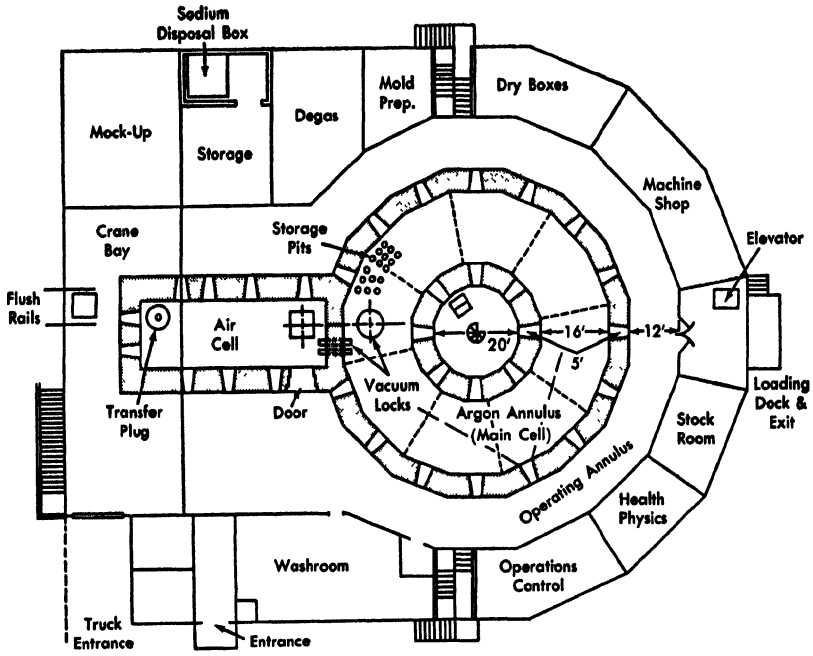

FIG. 3–26. Process building main floor plan.

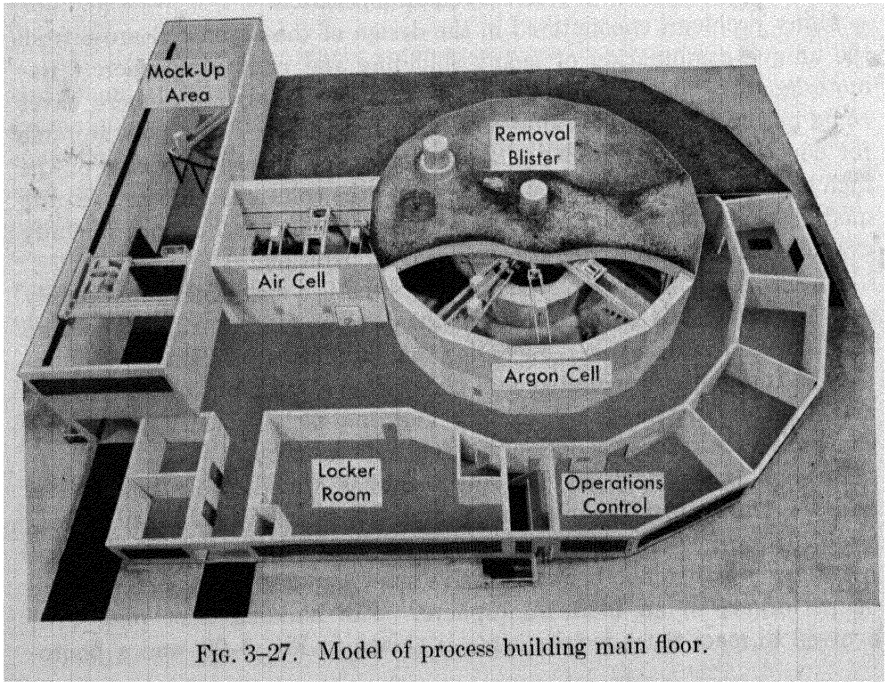

FIG. 3–27. Model of process building main floor.

graph of a scale model of the plant is in Fig. 3–27. The over-all building dimensions are 130 by 170 ft.

Disassembly cell. This rectangular cell is a rather conventional cave. It has an air atmosphere with filtered exhaust and the usual manipulators, cranes, windows, and miscellaneous services. In this cell the spent fuel subassembies are separated into individual fuel and blanket elements. Reassembly of new subassemblies as well as the routine operations of canning scrap and waste and maintaining equipment are also carried out in this area.

Process operations which release fission products are not carried out in the disassembly cell. Here, fuel elements are separated from the core subassembly, but the fuel-element containers are not removed from the irradiated fuel. The principal contaminant in this cell is activated sodium; gross fission-product contamination is confined to the process cell.

Reprocessing cell. The second cell, which is circular (actually a 16-sided polygon), contains a high-purity argon atmosphere. In this environment pyrophoric materials such as plutonium, uranium, and sodium can be handled safely at high temperatures. The cell is divided into two regions: the argon-blanketed annular structure (72 ft across flats on the outside) and the shielded central control room. The argon annulus is equivalent to a cell 150 ft long. Here all the spent fuel is mechanically decanned and purified, and the refined metal is fabricated into new pins and assembled into fuel elements. Here also such auxiliary steps as slag recovery and isolation of fuel-grade plutonium from blanket material will be demonstrated.

A section view of the argon cell is shown in Fig. 3–28. This cell adjoins the rectangular cell and is connected to it by one large and several small vacuum locks (Fig. 3–28). All materials are transferred into or out of the inert atmosphere circular cell through the air cell. Thus, if pyrophoric material is improperly contained or if such containers are contaminated on the outside, any resulting fire will be in the shielded rectangular cell where it will not endanger personnel or contaminate the working area. The entire inner surface of the cell is lined with steel, so that air from the cell exterior or moisture from the concrete cannot contaminate the argon atmosphere. The steel liner is surrounded by a biological shield of concrete.

Several cell configurations were studied before the circular cell was selected. The key consideration was that cranes and manipulators could be employed with greater flexibility than could be achieved in a rectangular cell. The power feed system which connects to the bridges near their pivots eliminates the complicated cable take-up systems required in rectangular cells. With one track for cranes and another for manipu-

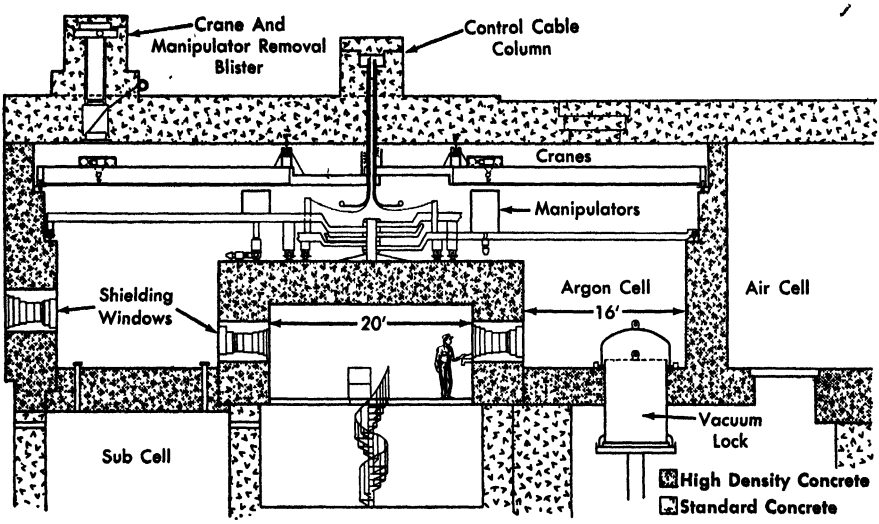

FIG. 3–28. Argon cell elevation.

lators, any crane or manipulator can serve any working area of the annulus. In a rectangular cell, a much larger number of tracks would be required, and the cell height would be so increased that the reach required of the upper manipulators would be too great to be practical. The central control room provides a good location for observing the entire cell area.

Service cell. Beneath the circular cell is a subcell area for housing various auxiliary equipment needed close to the argon cell equipment or likely to become contaminated. Included are such items as vacuum pumps, cell gas cleanup equipment, and capacitor sets for induction-heating equipment. The basement of the plant model including this subcell area is shown in Fig. 3–29 Also within the subcell area are the lines for carrying the various services into the process cell. These are generally inert gas, vacuum, and electrical; they enter the argon cell through a number of sealed service slots. Outside the subcell shield wall are "suspect equipment" cubicles (Fig. 3–29) containing process auxiliaries that might possibly become contaminated. If such equipment does become contaminated the cubicle can be enclosed with shielding. The floor of the process cell is 4 ft thick and is expected to reduce the radiation level in the subcell to approximately 100 mr/hr, permitting limited access to this area. A personnel access corridor leading to a spiral stairway provides access to the central control room.

Cell windows. Operations inside the cells are observed from shielding windows (Fig. 3–30). With windows in alternate faces of the circular

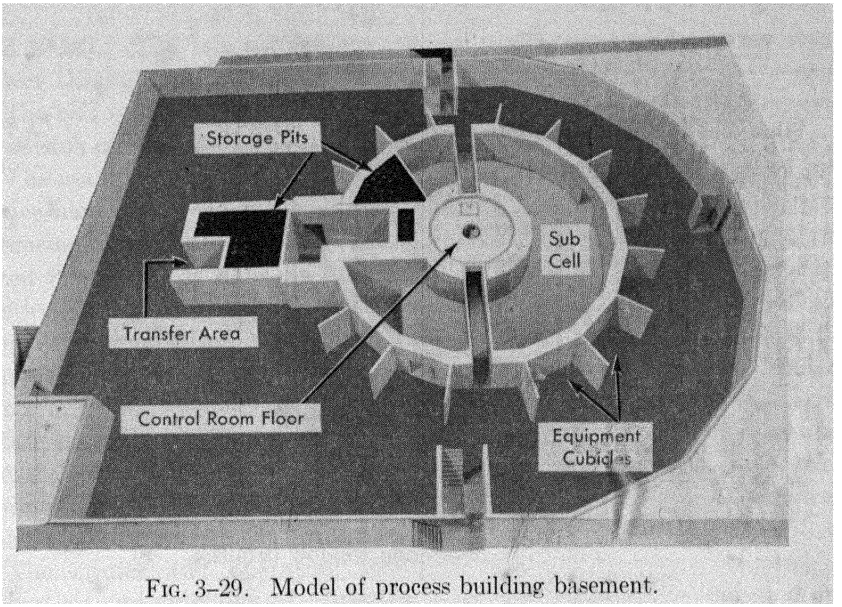

FIG. 3–29. Model of process building basement.

cell, any part of the shielded work area can be observed from at least one window. The windows are fabricated from thick slabs (6 to 10 inches) of nonbrowning, medium density (3.2 g/cm^3) glass. They must be gastight and have long lifetimes under high radiation levels. Processing of fuels irradiated in 135 days to 20,000 Mwd/t and cooled only 15 days results in a cell background approaching 10^6 r/hr, with some areas subject to much higher levels.

The gastight seal is made with double O-rings near the center of the window. In this way the "active side" of the window shields the gaskets. In addition, active-side window components can be replaced without disturbing the gastight seal. The slabs of glass on this side, even though fabricated of nonbrowning glass, are expected to have only a moderate life. Therefore the first 10-inch thickness is hinge-mounted so that it can be swung into the cell for easy replacement. One problem not completely resolved is gamma heating and resulting stresses in the glass.

A design feature presently under test is a polished, mirrored edge for the central window slabs. This will increase the observer's angle of view and convert the window into a reflector periscope with a viewing angle of approximately 160 degrees. A section of the argon cell with the shielding windows located in the inner and outer walls is shown in Fig. 3–31. The solid lines indicate the direct viewing angles; the dotted lines indicate the larger viewing angle obtained with the mirrored section. The vertical configuration of the windows is varied so that the windows in the outer shield have their widest vertical viewing angle downward,

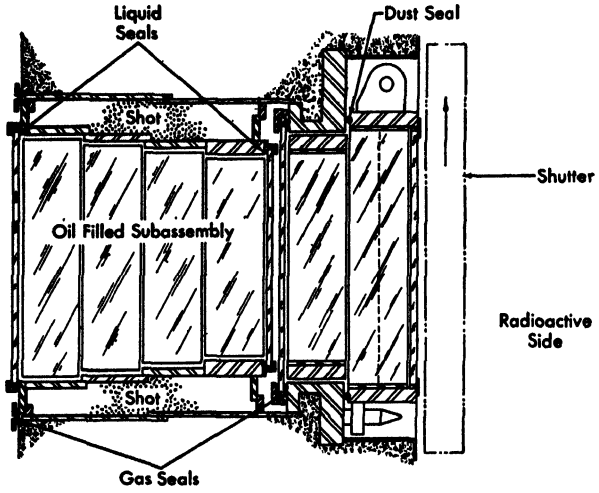

FIG. 3–30. Shielding window details.

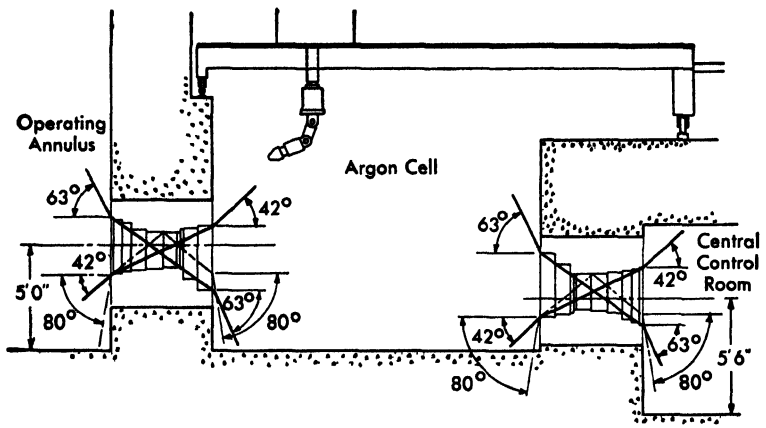

FIG. 3–31. Shielding window viewing angles.

while the control room windows have their widest vertical viewing angle upward. This combination provides excellent visual coverage of the working area.

Material handling. The nature of the operations to be conducted makes material handling an important function, but the high radiation background precludes use of conventional equipment. The principal motive service in the circular cell is provided by two 5-ton cranes and six manipulators, which revolve about the cell on two track levels (Figs. 3–27

and 3–28). The two cranes run on the upper level and receive their power through slip rings attached to a post suspended from the center of the cell roof. The cranes can pass over the manipulators but cannot pass each other.

The manipulators are interchangeable and of two types: operating and articulated. The operating manipulators provide radial and circumferential travel with gripping, rotating, and lifting motions. The articulated manipulators have, in addition to the above, elbow and shoulder motions. The manipulators revolve about a bearing post mounted on the central control room roof, and receive power through fixed multiconductor cables suspended from a central overhead supply duct. While the cranes can revolve continuously around the center post, the manipulators normally are limited to a 270-degree movement in either direction from a reference position. The crane and manipulator carriages take power from the bridges through slide contacts so arranged that electrical contact is made when the trolley or carriage is placed on the bridge.

The cranes and operating manipulators are designed for plug-in mounting and shielding of radiation sensitive components. Small portable control boxes are located near the observation windows of the cells. A centralized switchboard connects any control station to any manipulator or crane. An indicating board in the operations control room shows the position of the units and serves to reduce interference of one bridge with another and to permit the best distribution of these units around the cell. A safety interlock system cuts off power to manipulators when the bridges come into contact with each other.

It is not possible to maintain or repair the crane or manipulator carriages in place. A special blister (Fig. 3–28) located on the process cell roof contains a retracting mechanism which can lift any crane or manipulator carriage from its bridge and lower it to the cell floor, where simple repairs and routine maintenance can be done by other manipulators. If more extensive service is required, one of the cranes moves the piece to the material transfer lock for removal to the air cell. Here decontamination and contact maintenance can be employed. Either crane can push a disabled crane or manipulator bridge into position under the retracting mechanism. Periscopes will be placed in the cell wall and roof for viewing the operation of these devices.

The air cell is provided with a 5-ton crane and two manipulators (Fig. 3–27) similar to those in the argon cell. In addition there will be several mechanical master slave manipulators for such precision work as assembling fuel elements into subassemblies. A heavy shielding door at one side gives equipment or personnel access when the activity level in the cell is low. Normally, material is transferred through a floor hatch opening into the basement (Figs. 3–28 and 3–29).

Argon gas system. Because the fuel material is reactive and self-heating, the inert cell gas must be maintained at a high level of purity. The water content of the argon atmosphere has been limited to 5 ppm. Oxygen contamination is limited to 100 ppm and nitrogen is arbitrarily limited to less than 5 vol. %.

The cell gas is continuously treated to maintain the low oxygen and water levels. Treatment involves hydrogen addition and catalytic conversion of the oxygen to water with a palladium catalyst. The drying agent, Molecular Sieves, removes the water from the gas stream. This material can absorb up to 10% by weight of water under these conditions, and it is so efficient that for a linear flow of 2 fps and a bed length of 3 ft the water concentration in the effluent gas is less than 1 ppm.

The principal features of the purification system are a palladium catalyst chamber, a drying unit, and monitoring equipment for nitrogen, oxygen, and water. The palladium catalyst is 0.5 w/o of palladium-on-aluminum oxide. It has the very desirable characteristic of being able to absorb hydrogen up to 0.47 ml/ml of catalyst. This hydrogen is available to react with oxygen in the gas stream and thus serves as a reservoir to compensate for fluctuations in the hydrogen addition rate or variations in the oxygen content of the cell atmosphere.

3–6.4 Reprocessing operation. The part of the fuel cycle that is external to the reactor begins when the spent and cooled subassembly is removed from the storage rack. The subassembly is transferred in a shielded coffin from the reactor building to the process building. Before it goes into the air cell, the adhering sodium is removed by passing dry steam through the coffin. The subassembly enters the air cell through the transfer plug (Fig. 3–26).

Fuel disassembly. Fuel elements are removed from a subassembly by cutting the hexagonal tube close to the lower structural weld The lower plug and lower blanket section, with attached fuel elements, are slid free of the shroud tube. The fuel elements are removed from the cluster by sliding them off the grid rails, and are then stacked into suitable containers and transferred into the argon cell for the tube stripping operation. Because of the high fission-product decay heating (0.2 watts/g) resulting from the high burnup (2 a/o) and short cooling (2 wk) the subassembly must be cooled by forced gas circulation. Even after disassembly, fuel elements and pins must be properly arranged for convection cooling.

Melt refining. This operation begins with mechanical removal of the stainless steel tube from the fuel pin One method, already demonstrated, involves forcing the element through three fixed knives, located radially 120 degrees apart, which slit the can axially. The strips then are peeled

away by forcing the pin through a set of rollers. Other mechanical methods are being explored to improve reliability and simplify the machinery.

The actual purification process begins after the fuel has been separated from its stainless steel can and chopped into pieces less than 1½ inches long. Pieces of this length can be readily poured. Approximately a 0.003-inch-thick coating of the bonding sodium remains on the fuel pieces. The first step in the purification operation is to transfer the fuel pins from the decanning machine to the crucible in the melt refining furnace [17]. The important consideration in this operation is to remove heat from the fuel. The transfer container is a flat enclosed tray with a trap door opening at one end. Due to continuous self-heating, the bare fuel will react with the oxygen and nitrogen impurities in the cell atmosphere if cooling is inadequate. To prevent this, the tray has heat-dissipating fins. As an additional safety factor, handling and storage are done in closed containers, so that the fuel material is exposed to only a limited volume of potential reactants. The fuel-pin transfer container is used for temporary storage and for charging the melt-refining furnace.

A prototype of this furnace is shown in Fig. 3–32. The crucible, the susceptor, an insulating refractory sleeve, and the induction coil (in the order given from inside to outside) are positioned in a metal framework supported on two trunnions. The tilting mechanism consists of a pinion gear integral with the framework and operated by a drive rack which extends through the base and is activated by a manipulator. A fume trap filled with the solid sorbent is mounted directly over the crucible for trapping condensable materials. A linkage mechanism rotates the trap away from the crucible during pouring. The crucible, susceptor, supporting framework, and basket of sorbent can be individually replaced. The entire furnace can be replaced if necessary.

In operation this furnace is enclosed in a bell jar, sealed by a fusible metal seal. The fuel alloy is melted and after a liquation period of several hours the purified metal is poured into a massive metal mold (cast iron or copper). The slag forms a tightly adhering skin on the crucible and the metal is separated cleanly by simple pouring. Two small protrusions, that serve as samples, are cast on the bottom of the ingot. The fission-product gases released in the melt-refining operation and contained in the bell jar are transferred to a holding tank, and after the required decay, they are diluted and released to the atmosphere.

After the furnace and ingot have cooled, the bell jar is removed and the mold is transferred to the demolding and sampling machine, which separates the ingot from the mold. The two small protrusions are sheared off and used as samples. This sampling method was selected because it requires only simple equipment and avoids generation of chips and dust

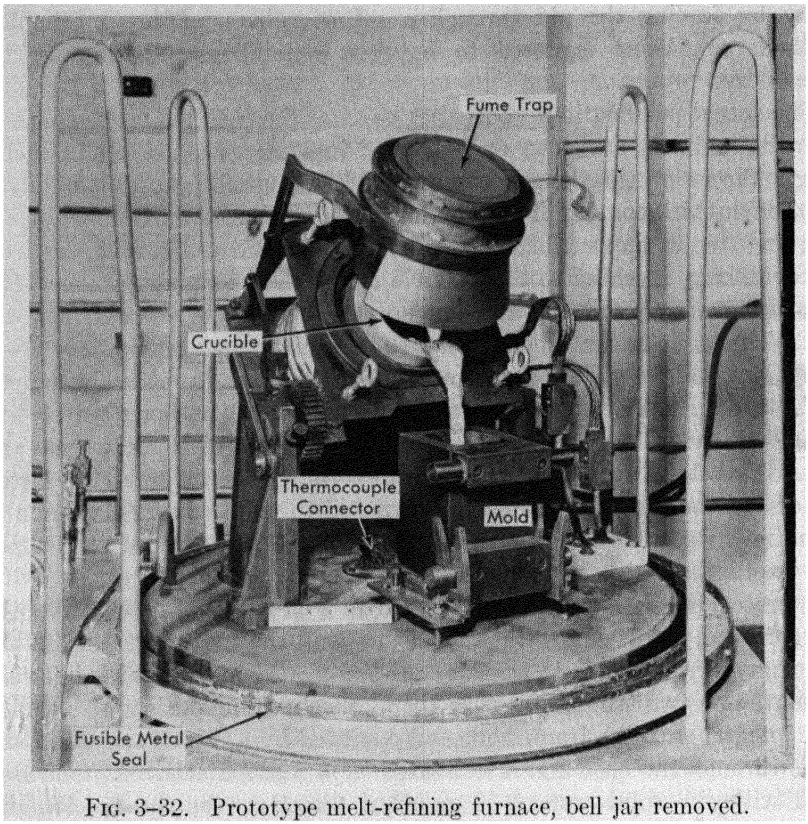

FIG. 3–32. Prototype melt-refining furnace, bell jar removed.

from drilling and cutting operations. The sampled ingot is placed in a storage container. As with unprocessed fuel, the container also serves as a transfer vessel, with heat dissipation a prime factor in its design. The ingot is transferred to the fuel fabrication area of the argon cell.

3–6.5 Refabrication operation. *Fuel pins.* The first step in fabricating new fuel subassemblies is to convert the 10-kg ingot of processed metal into fuel pins (0.144 ± 0.001 inch diameter $\times$ 14.22 ± 0.032 inches long). The pin surfaces must be suitable for sodium bonding. Since they must be internally sound, they are inspected for internal porosity or inclusions. Also, they should be in a single integral length, to take advantage of the positive coefficient of thermal expansion as an aid to reactor control.

The method selected for refabrication must produce fuel dimensionally stable to the burnup level selected. The fuel should not undergo phase transformations that cause nonlinear expansion or contraction upon heating or cooling in the reactor. The composition should be controllable

both as to alloy and fissile material content. Fortunately, alloys that produce a desirable combination of properties in the as-cast condition also appear in the equilibrium fissium compositions. The equilibrium composition, fissium, resulting from the pyrometallurgical process is about as stable in the as-cast condition as the desirable artificially produced alloys containing stabilizers of molybdenum and ruthenium. This makes it unnecessary to introduce additional alloy into the composition.

Several methods for fabrication of the fuel pins were considered. Conventional wire fabrication methods involving ingot casting, rolling, annealing, swaging, and drawing through dies were ruled out because of the comparative lack of ductility of the fuel alloys, the large number of process steps required, and the complexity and difficulty of adapting conventional equipment to remote operation. Powder metallurgy was considered because it is a traditional method of handling hard and brittle compositions, but investigation was not vigorously pursued because of the problems associated with producing and handling many kilograms of finely divided metal powders that would be thermally hot, explosively pyrophoric, and intensively radioactive. Extrusion did not appear well adapted to the production of the extremely small-diameter pins, nor did conventional hydraulic press equipment appear suitable for operation in the intensively radioactive environment. Because all the processes which produce pins by metal working cause some orientation of the structures, heat treatment would be required if metalworking methods were used for refabrication.

Because conventional equipment could not be adapted, a new fabrication method was required for the EBR-II fuel pins. Several preliminary requirements were set down. The process should have a minimum number of operations. The equipment should be designed with subassemblies that could be replaced as units. These units should need only minimum adjustment and assembly work by manipulators within the process cell. Routine operation of the equipment should be simple, and the manipulators should be used both to service the equipment and to perform nonroutine operations. Equipment operation, total replacement, and maintenance should be within the limited capabilities of the manipulators and cranes in the process cell. Construction materials should be chosen to withstand the radiation levels encountered. Radiation-sensitive auxiliary equipment should be shielded from direct exposure to the highly radioactive fuel.

Precision casting. Precision casting was the method selected as showing greatest promise for development because it produced the required nonorientated structure and would involve a simple sequence of manufacturing operations. Casting would consist of a simplified nonmechanical injection process using gas pressure to fill evacuated molds. A sche-

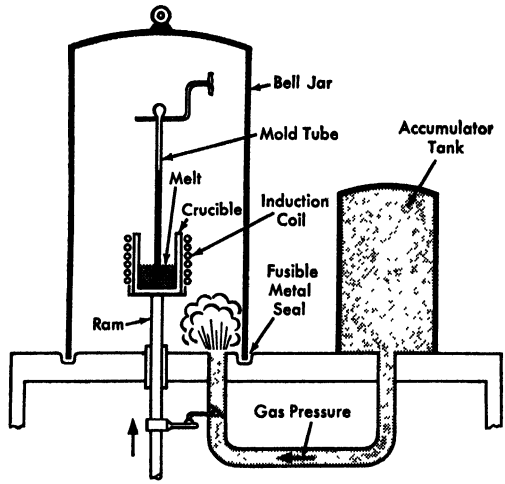

FIG. 3–33. Schematic representation of injection casting process.

matic diagram of this process and a drawing of the prototype casting machine constructed to test it are shown in Figs. 3–33 and 3–34.

The fissium alloy is induction-melted under vacuum to a temperature of 1375 to 1425°C in a graphite crucible which is flame-spray coated with ThO_2-ZrO_2. The molds are precision-bore, high-silica glass tubes, coated on the inside with a thin thoria wash and closed at the upper ends. They are suspended, open end down, above the crucible. The assembly of mold tubes is heated by resistance windings within the vacuum chamber. When the molten alloy has reached the selected casting temperature, the vacuum pumping system is isolated and the ram upon which the crucible is mounted is actuated, causing the crucible to rise and thus submerging the open tube ends. After a 2-sec time delay to allow quieting of the metal surface, the furnace is opened to an accumulator tank and pressurized with an inert gas, causing a rapid increase in the furnace pressure, The pressure difference across the walls of the submerged tubes raises the alloy into the tubes, where it freezes. The crucible containing the remainder of the molten charge is lowered while the metal in the crucible is still molten but after the castings have solidified. Because of self-heating from fission-product decay, the casting array will cool to an equilibrium temperature determined by the arrangement and number of castings made. This necessarily limits the number of pins that can be cast at one time without forced cooling.

An experimental mold-stripping and casting-cropping machine, shown in Fig. 3–35, has been built in which the glass molds are pulverized away from the castings by feeding the charged molds between roughened con-

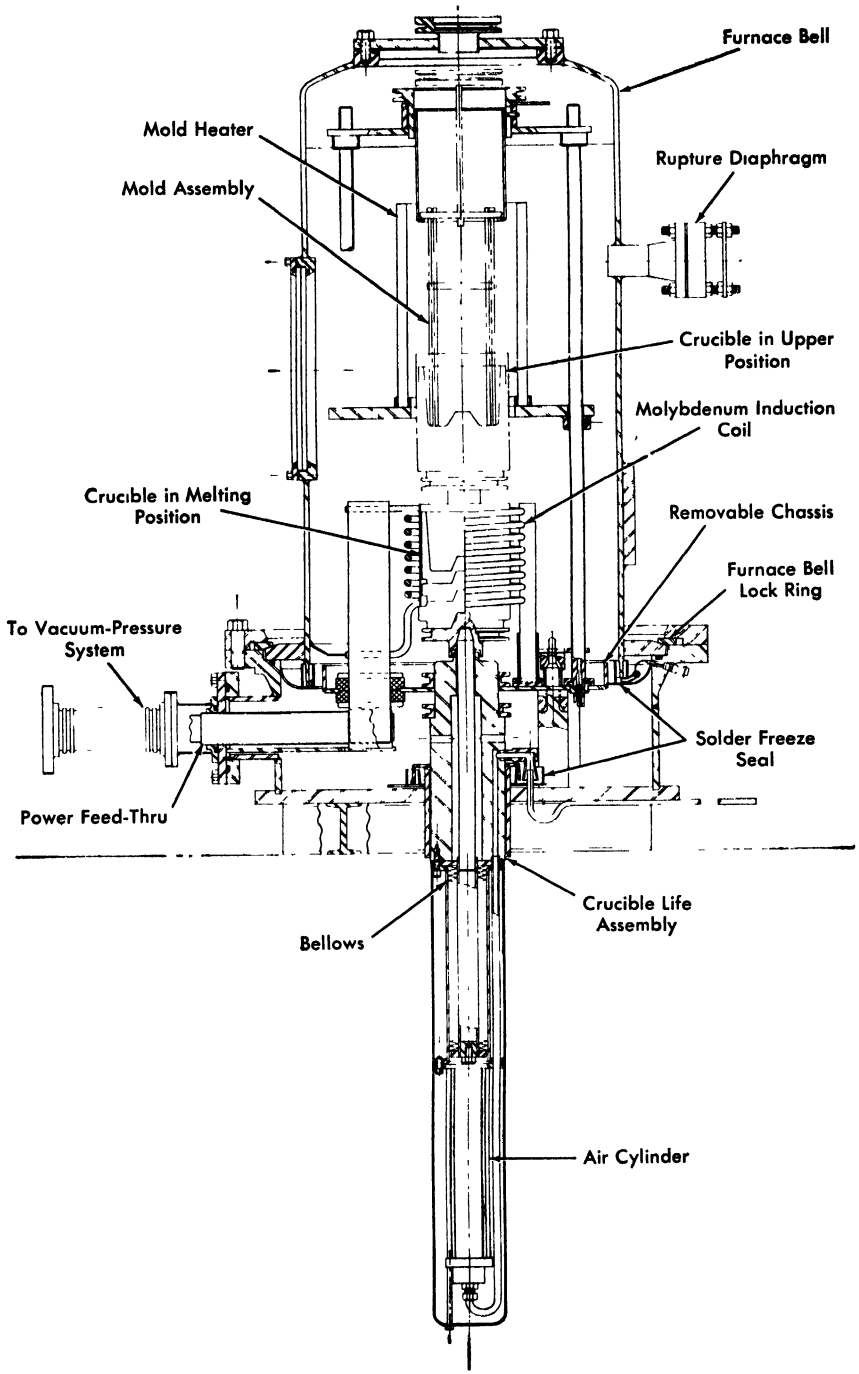

FIG. 3–34. Details of injection casting furnace.

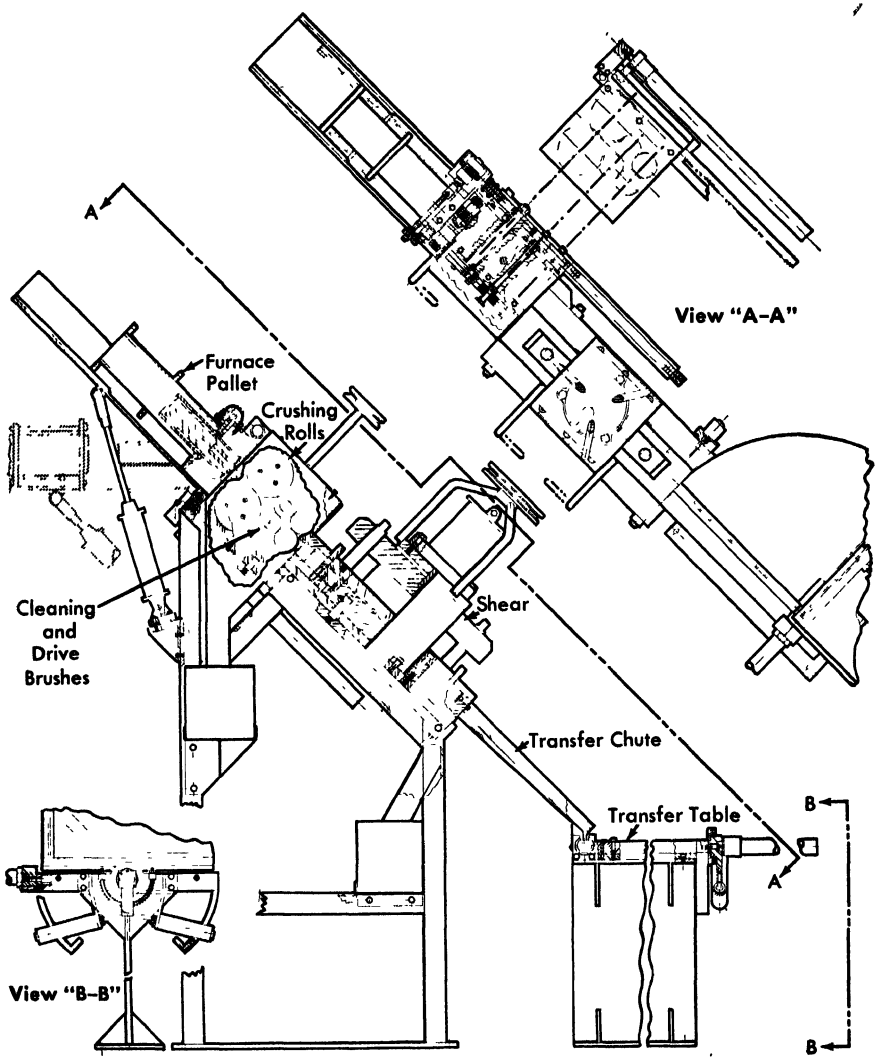

FIG. 3-35. Demolding and shearing machine.

cave rolls. The casting is first passed between two pairs of contrarotating wire brushes to clean the surface, then into a double shear that simultaneously crops both ends, leaving a pin 14.22 inches in length. The pins then move onto a slide transfer inspection table, where they are visually inspected by means of a magnifying periscope sealed through the wall of the cave and designed so that only reflecting optics are used within the cell. Provision is made for viewing at 1× and at 12× magnification.

An inspection machine next measures diameters as the pin is fed through argon jet gauges. Internal flaws and surface irregularities are sensed by an induction coil-eddy current inspection device. The pins are then weighed and their length measured. After inspection, they are pushed out of the inspection machine onto a transfer table. Rejected pins are moved to a chopper, where they are broken up for remelting. Satisfactory pins are transferred to a pin storage and fuel tube loading magazine. In-process storage is provided at the furnace and in storage magazines which can be placed between the shear and inspection stations or between inspection and reassembly. This allows continuous, semicontinuous, or batch operation.

The casting variables include heating rate and degree of superheat of the alloy, vacuum for melting and mold outgassing, mold temperature, rate of pressurization, and final furnace pressure. Optimum values were determined by experiment. To conserve material in the experiment and reduce the numbers of pins handled, a 1/4 size laboratory furnace for 2500 to 3000-g melts of simulated alloy was used. This information was then applied to the full-scale furnace. Flowsheet conditions are as shown in Table 3–5.

Protection of the high-silica glass molds against erosion by the molten alloy required the most experimental work. Various washes applied and tested included suspensions of magnesia, magnesium-zirconate, colloidal graphite, zirconia, urania and thoria, and mixtures of them. The smoothest surfaces were obtained with colloidal graphite applied as a thin coating from an ethyl alcohol suspension. The graphite coating, however, was difficult to outgas and did not provide sufficient protection against mold reaction. Of the oxide materials, minus-6 micron thoria particles, applied from an alcohol suspension, were found most satisfactory. The

TABLE 3–5

MELTING AND CASTING CONDITIONS FOR GAS PRESSURE INJECTION CASTING OF EBR-II FUEL PINS

	Range explored	Satisfactory range
Heating rate, °C/min	5.5 to 26.6	10 to 26.6
Casting temperature, °C	1275 to 1425	1325 to 1350
Vacuum, μHg	40 to 0.2	Less than 4
Mold temperature, °C	70 to 600	250 to 600
Pressurizing rate, psi/sec	4 to 30	18 to 22
Final pressure, psia	15 to 60	15 to 30

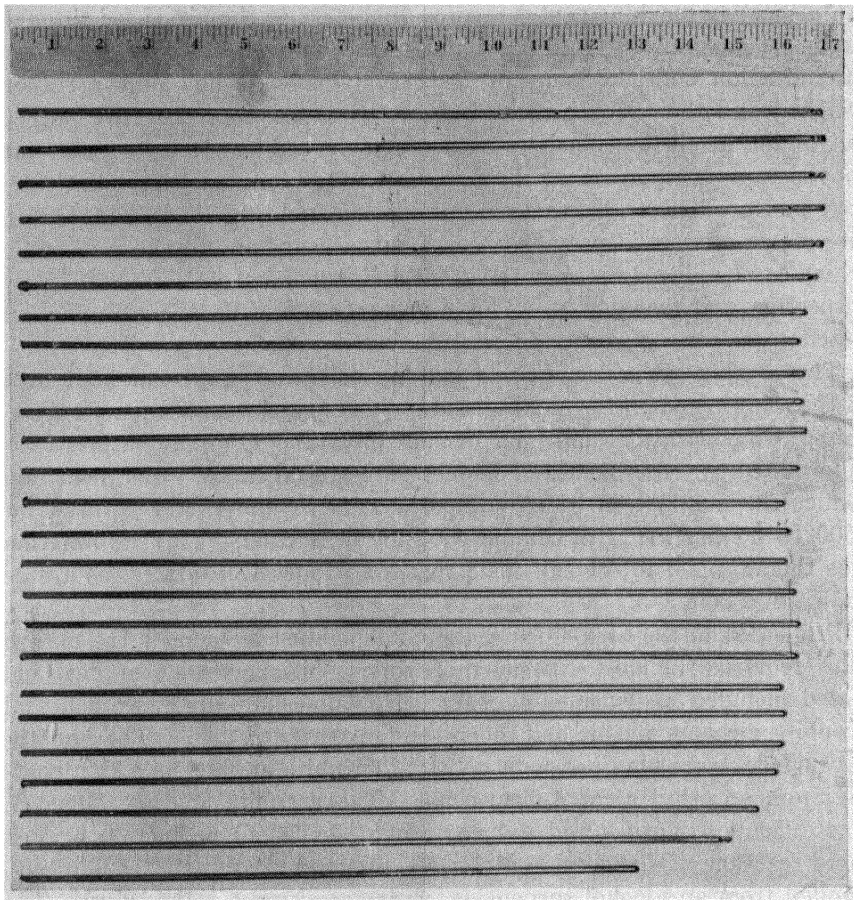

FIG. 3–36. Fissium alloy castings produced by injection casting.

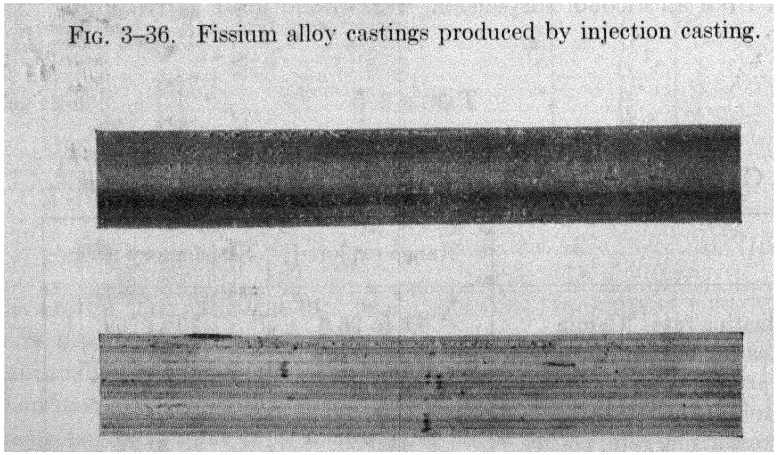

FIG. 3–37. Surfaces of pins produced by injection casting into thoria-coated molds. The pin at the bottom is before brush cleaning; at the top, after brush cleaning.

TABLE 3-6

DIAMETER, WEIGHT, DENSITY AND HARDNESS OF 5 W/O FISSIUM ALLOY INJECTION CAST PINS

	Number of observations	Average value	Standard deviation
Diameter, in.	659	0.1446	0.0006
Weight, g	93	67.929	0.507
Density	109	17.939	0.016
Rockwell A hardness	1414	69	—

disadvantage of thoria is that a fine chalky coating is left on the casting surface (Fig. 3-37) and must be removed.

Square-cut mold tubes were used in early experiments, resulting in a bulbous lower casting end that interfered with subsequent operations. This was eliminated by cutting the open ends of the tubes at an angle and by programming the period of immersion after pressurization.

The characteristics of pins produced within the range of conditions in Table 3-5 are given in Table 3-6.

A typical set of injection castings is shown in Fig. 3-36. Surfaces of two average pins produced in graphite-thoria coated molds are shown in Fig. 3-37, with and without cleaning.

3-6.6 Assembly operation. *Pins and elements.* The completed fuel pins are canned in a 0.009-inch wall stainless steel tube, and carefully bonded to the tube by sodium. Although fuel elements must be assembled in the argon cell, preliminary work on nonradioactive components is done outside the shielded areas. The fuel element tubes, with a lower plug welded in place and an attached spacer wire (helically wound along the length), are examined, cleaned, and placed in an argon-filled dry box. The required quantity of sodium is extruded in cylindrical form and placed in each tube. The tubes are then placed in a small vacuum furnace and heated above the melting point of sodium. Argon is admitted into the furnace and the temperature is held at 550°C for 10 min to ensure wetting of the wall by the sodium. The tubes are cooled to room temperature and transferred from the dry box to the shielded argon cell.

At the fuel element assembly station, the sodium-loaded tubes are placed into a 10-tube fuel element magazine, shown in Fig. 3-38. The loaded magazine is placed on a pedestal and the fuel pins are inserted

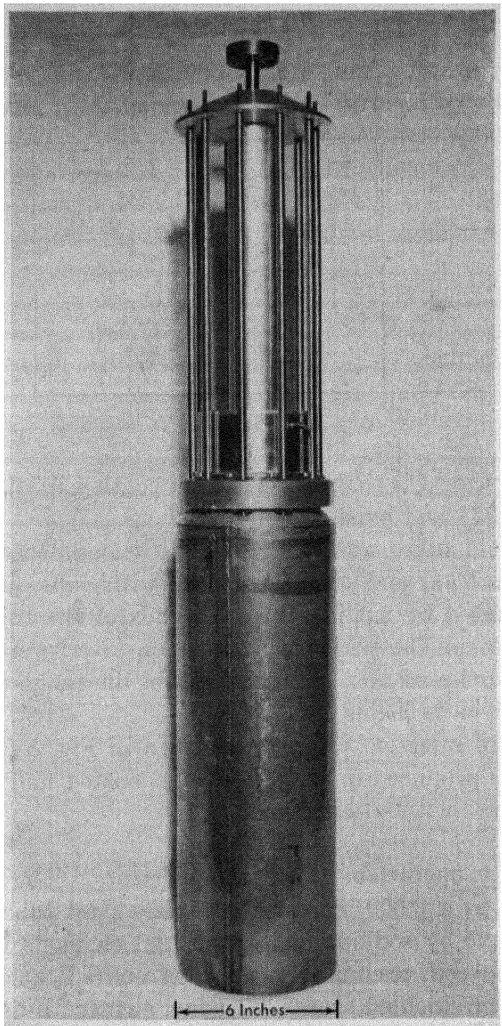

FIG. 3–38. Fuel-element magazine.

into the tubes. This is done by lowering the loaded fuel pin magazine into position above the sodium-filled tubes. When it is in position, a release trip mechanism is actuated and the fuel pins drop into the tubes. The loaded fuel element magazine is then placed on a heated platform connected to a mechanical vibrator. This melts the sodium, causing the uranium pins to settle to the bottom of the tubes.

After the uranium pins have settled, restrainers attached to the top plugs are inserted into the tubes in a manner similar to that used to in-

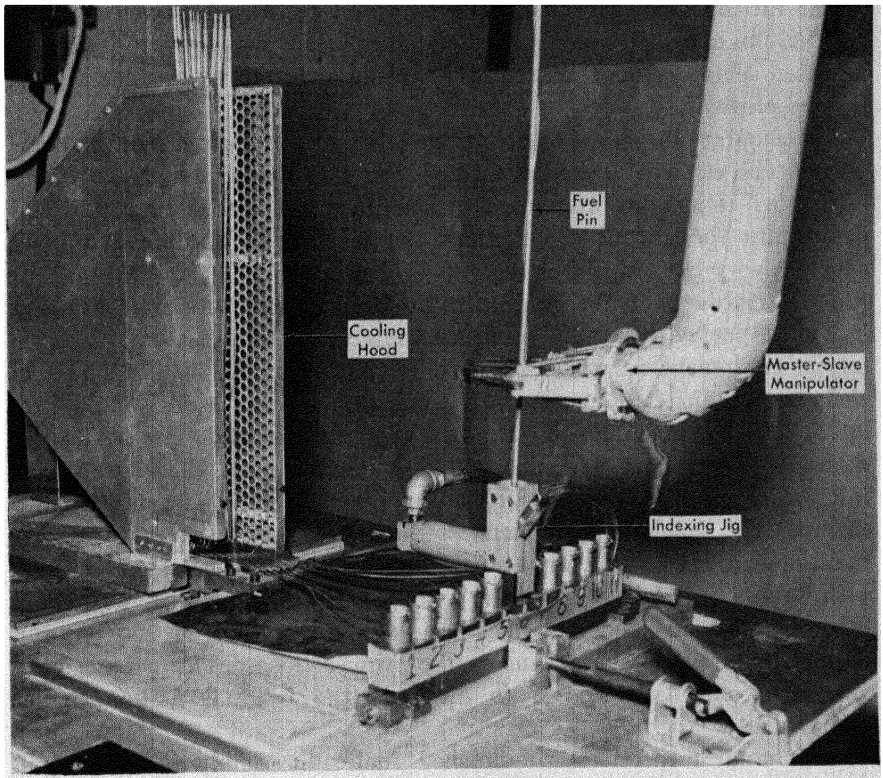

FIG. 3–39. Prototype remote fuel assembly apparatus.

sert the fuel pin, the magazine is transferred to the welding station, and the fuel elements are sealed.

When the fuel elements have been welded, the magazine is moved to the air cell by gravity through a vacuum lock. The magazine is inserted into the lock and rides (suspended by the upper carrier head) down inclined rails. Small ball bearings attached to the carrier head act as wheels, and gravity serves to carry the magazine through the lock.

In the air cell, the welded fuel elements are inspected with a magnifying (11×) periscope for gross welding defects. After passing the visual inspection test, a group of completed elements is placed in a chamber of the leak detector. The chamber is pressurized to 50 psig with helium, then the elements are quickly transferred to a helium-free chamber. The chamber is then evacuated through a helium leak detector. Any small weld defects present are detected here. Faulty elements are located by a partitioning process and rejected.

The fuel elements must be processed to ensure a sound bond between the fuel pin and the stainless steel cladding. The elements are placed in a heated centrifuge and rotated at 1000 rpm at 550°C to produce a well-bonded element.

Elements are inspected to determine whether the sodium bond is complete. The element is carried through the grid coil of a high-frequency oscillator. Magnetic interaction between the fuel element and the coil determines the output signal from the oscillator. A defective bond causes a very large signal change.

Subassemblies. In the final operation, 91 fuel elements are assembled in a close-packed hexagonal array on the grid of the subassembly. Prototype equipment for this operation is shown in Fig. 3–39. The fuel elements are inserted in sequence (with an Argonne Model 8 manipulator) in receiving funnels. The receiving funnels close circuits to activate a programmer and also act as guides to place the elements on rails which thread the element onto the receiving grid. The programmer ensures that the loading sequence required to orient spacer wires and fuel elements is followed. The cluster is cooled by exhausting air through a shrouding manifold. When the assembly is completed, the hexagonal tube and attached upper blanket are slipped over the fuel section, and a lower structural weld connects the two sections. The subassembly must be continually cooled to dissipate the residual fission-product decay heat.

After final inspection, the finished fuel subassembly is transferred from the process cell back to the reactor to complete the fuel cycle.

3–7. Operation and Control

3–7.1 General control method. Control of the power system is centralized in a control room in the power plant building. Control, in general, is manual. Only the simplest control functions, or those that might adversely affect facility safety if handled manually, are automatic. As examples, control of primary and secondary system coolant flow rates is manual; control of reactor power level is manual during raising or lowering of power, but is automatic at steady state; control of feedwater flow rate and steam pressure is automatic. A simplified block diagram of the control system is shown in Fig. 3–40.

In essence, basic control for the EBR-II power system includes (1) control of reactor power level, (2) maintaining balance between the rates of heat removal by each of the major thermal systems, from the cooling tower to the reactor, and (3) maintaining virtually complete isolation of the reactor from the effects of turbogenerator load variation. As with most thermal systems, there are additional control requirements

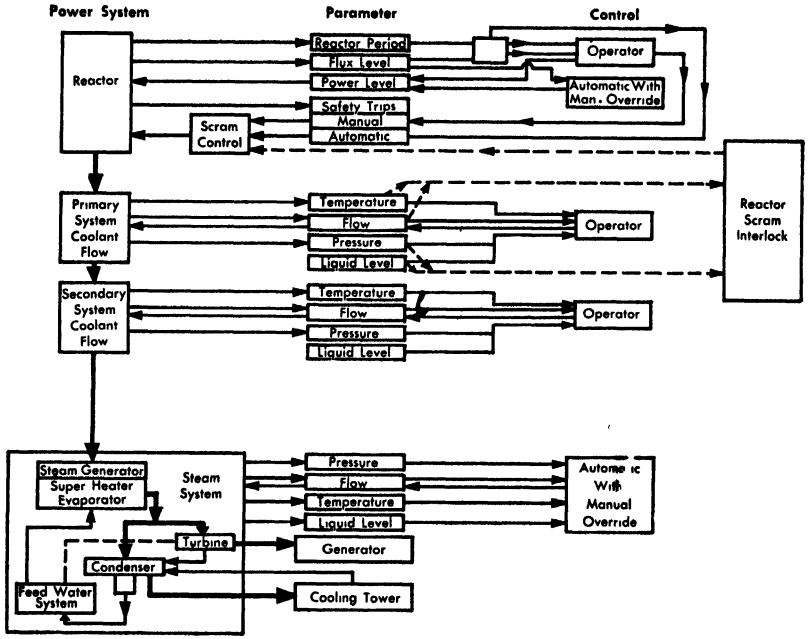

FIG. 3-40. Simplified block diagram of control system.

of maintaining desired system temperature and pressure levels and precluding excessively high rates of temperature change; e.g., as described earlier, throttle steam temperature and pressure are held constant at 850°F and 1250 psi, respectively, at all reactor or turbogenerator loads.

Reactor power. Operational control of reactor power is afforded by vertical movement of the twelve control rods, as described in Articles 3-3.1 and 3-3.6. Changes in reactor power level are made by manual adjustment of rod positions. Once operation has been stabilized at a given power level, the power level is maintained at steady state by automatic control of regulating rod motion (the control based on sensing of neutron flux level). If any abnormality initiates a reactor scram signal, all twelve rods automatically are ejected from the core at high speed.

A total of ten fission counters and ionization chambers enables sensing of reactor period, as well as of neutron flux level, throughout the range from source power to several times full power. These detectors provide the signals for measuring and controlling reactor power and for initiating reactor scram in the event of excessively short period or excessively high power. The detectors are in vertical thimbles at various positions outside the reactor tank. Instrumentation details are given in Article 3-3.7.

Thermal balance. As mentioned earlier, the major thermal systems of the facility are the primary, secondary, and steam systems (plus circulating water system). Heat generated within the reactor is removed by the primary system and delivered to the heat exchanger. From the exchanger heat is transferred by the secondary system to the steam generator (superheater and evaporator), then transported by the steam system to the turbine and condenser. The heat absorbed by the turbine is converted to electrical power, and that released in the condenser is absorbed by the circulating water system, which dissipates it to the atmosphere via the cooling tower.

Heat removal by the cooling tower is maintained at a rate equal to that from the condenser by conventional controls, similar to those for coal-fired or gas-fired plants. Similarly, conventional control keeps the heat-removal rate from the condenser and turbine equal to that from the secondary system (by the steam generator). Rates of heat removal from the secondary and primary systems are balanced by making the evaporator large enough to accommodate the maximum anticipated heat-transfer load, while the evaporator water temperature is kept constant by automatic regulation of the main steam system pressure.

The balance between rates of heat removal from the primary system and from the reactor requires a special control technique. Any imbalance of these two rates produces a continuous change in the primary tank bulk sodium temperature. To bring about the proper balance, the following control method is utilized.

(1) The primary system flow rate is regulated at any given power level to provide a predetermined reactor coolant outlet temperature varying from 900°F at full power to 850°F at very low power. The 50°F variation in reactor coolant outlet temperature is used to maintain a constant steam temperature of 850°F at all power levels.

(2) Irrespective of reactor power level, the temperature of the cold leg of the secondary system automatically remains between 580 and 610°F. This is because evaporator water temperature is kept constant and the evaporator is designed for a very small approach temperature at the sodium outlet end. Also, the temperature of the hot leg of the secondary system remains relatively constant; it varies from about 880°F at full power to 850°F at very low power (reflecting control of the reactor outlet coolant temperature). Consequently, the rates of heat removal from both the primary system and the secondary system are approximately proportional to the secondary system flow rate.

(3) Since the rate of heat removal from the primary system is a function of the secondary system flow rate, this flow rate is controlled to keep the rate of heat removal from the primary system equal to that from the reactor.

Reactor isolation. To keep the reactor stable, its operation must not be responsive to power system conditions external to the reactor. This is accomplished by (1) controlling the reactor power level so that changes in electrical load demand or in power system operating conditions will not cause changes in reactor power demand, and (2) designing the system so that a change in any system condition (or existence of any system abnormality) will have little effect upon coolant inlet temperature. The operator alone controls the reactor power level. There is no automatic adjustment of reactor power (other than scram) upon occurrence of change in electrical load demand or any power system operating condition.

The steam system is designed to bypass some steam around the turbogenerator at all times. This bypass steam flows directly from the steam generator to the condenser; the amount bypassed is automatically regulated to keep the main steam line pressure constant under all conditions. The operating procedure requires that the reactor power level must always exceed the maximum possible turbogenerator demand. The operator adjusts the turbine-admission valve stop to limit maximum steam flow (and, therefore, turbogenerator load) to a value which depends upon the desired reactor power operating level. With this method of operation, excess steam is always being bypassed to the condenser. As the turbogenerator load increases or decreases, the amount of excess steam being bypassed is automatically changed so that the steam generation rate and temperature in the steam generator will remain constant. Since the turbogenerator and the primary system are connected only through the steam generator (via the secondary system), this arrangement also prevents turbogenerator electrical load changes from affecting reactor inlet coolant temperature.

With the submerged primary system, the reactor inlet coolant temperature is identical with the bulk sodium temperature in the primary tank. The heat capacity of the bulk sodium plus that of the submerged components is large (the bulk sodium volume is about 88,000 gal). Accordingly, the average bulk sodium temperature changes very little, even though heat is added or removed rapidly. Heat is added to or removed from the sodium only when and to the extent that reactor power level is different from the rate of heat removal from the primary system. Therefore, even though the secondary system flow rate control should fail to function correctly, the resultant imbalance between heat generation and removal should affect the reactor coolant inlet temperature very little, unless the abnormality exists for a very long time. Under any condition, the rate of change of reactor coolant inlet temperature or bulk sodium temperature is very small and is readily correctable either through manual control or through automatic operation initiated by bulk sodium

temperature or reactor coolant temperature detectors. For example, if the reactor were operating at full power (62.5 Mw) with no heat being removed from the primary tank, the bulk sodium temperature would rise only about 14°F/min.

Alarm and scram provisions. Besides providing information necessary to control the power system, and indicating and recording sensings, the system instrumentation: (1) gives an alarm signal (annunciation and indication) in the control room when there is an abnormal condition in the system, (2) indicates in the control room which condition is abnormal, and (3) brings about automatic scram of the system when the abnormal condition justifies this action. Scram always includes switching off main pump power in the secondary system as well as fast shutdown of the reactor. For certain types of abnormality, the magnitude of the abnormality may determine whether an immediate scram is required. In these cases, a pre-scram warning alarm (annunciation and indication) is provided before the abnormality builds to dangerous magnitude. This warning gives the operator opportunity to apply manual corrective action. Only if such action proves inadequate does automatic scram result. Scram is always accompanied simultaneously by annunciation and indication.

3–7.2 Power cycle startup. Normal startup includes bringing the reactor and power systems to operating conditions from the shutdown condition. The process involves the reactor, the primary system, the secondary system, the steam system (including cooling water), and the turbogenerator and electrical system.

Conditions prior to startup. The system shutdown conditions prior to startup vary, depending upon the duration and purpose of the shutdown. The reactor is subcritical, and the primary system is at a temperature between 580 and 700°F. The secondary sodium cold leg is at a temperature of approximately 580°F, and the hot leg is between 580 and 700°F. The steam system is at 1250 psig pressure and essentially at saturation temperature (574°F). Temperature differences in the respective heat-transfer systems and the amount of steam being produced depend on the amount of heat being generated in the reactor (fission-product decay heat).

During a routine shutdown for fuel unloading, etc., the system temperatures will be held as closely as possible to normal operating temperatures. The primary system will be maintained at a temperature approaching 700°F. The rate of heat removal from the primary system will be kept approximately equal to the fission-product decay heat generation rate, to avoid lowering system temperatures. Heat will be removed by the secondary system and dissipated in the steam generator

by evaporating water. Heat will also be removed from the primary system by the auxiliaries, including the shield air-cooling system, the thimble cooling system, the sodium cleanup system, and the two shutdown coolers. The shutdown coolers are not employed during a short routine shutdown when the normal heat-transfer systems are operative. They are normally used when the secondary system is unable to remove the fission-product decay heat from the primary system, or for long-term shutdown.

Startup procedure. The following procedure is contemplated. Before startup of the reactor and power system components, system interlocks are checked and annunciation points are reset. Flow rates of the primary pumps are set for the power level at which the reactor will be operated. Since the shutdown power level is quite small (2% or less), there is little temperature rise in the entire primary system, which is at virtually isothermal conditions

After the reactor is critical, the power level is slowly raised. The secondary flow rate is adjusted to correspond approximately to the reactor power level If the primary sodium temperature is below 700°F, the secondary system flow rate is set somewhat below the corresponding reactor power level. This imbalance is continued until the primary system temperature reaches 700°F. The rate at which the power level is increased and the rate at which the secondary system flow rate is varied are limited by the maximum temperature change rate desired in the sodium systems (probably about 1°F/min).

During this entire period, steam is being generated at constant pressure and condensed. In the process, the steam system is gradually heated to operating temperatures. The steam is bypassed until the reactor and power system are at power and stabilized, then slowly diverted through the turbine in accordance with standard power plant operating procedures, and the turbine is brought up to speed. The generator, which operates in parallel with the NRTS 138-kv system, is then connected. The load applied to the generator is established at a level below the steam generation rate to permit bypassing steam.

3–7.3 Power cycle shutdown. Normal shutdown is a programmed shutdown of the reactor and power equipment during which reactor power is gradually reduced and the heat-transfer systems are simultaneously adjusted for the decreasing power level. Fast shutdown is brought about by certain primary system abnormalities, such as:

(1) Reactor period too short.
(2) Reactor power level, based on neutron flux level, too high.
(3) Loss of power to either primary pump.
(4) Core inlet coolant flow rate too low.

(5) Total reactor outlet flow rate too low.

(6) Coolant mean temperature in reactor upper plenum too high.

(7) Coolant pressure in upper plenum too high or too low.

(8) Temperature differential between heat exchanger outlet sodium and primary tank bulk sodium too high.

(9) Primary tank sodium temperature or level too high or too low.

After normal shutdown, coolant flow through the reactor is maintained either by operating the auxiliary pump alone or by operating one or both of the main pumps. Any of these flow sources is sufficient to cool the reactor. In the case of reactor scram, flow normally is maintained by operating the auxiliary pump or by operating both main pumps at high power (until manually reduced or cut out). In the remote event that a reactor scram occurs concurrently with failure of all primary system pumps, natural convection maintains enough flow to cool the reactor.

Normal shutdown. The first step in the normal shutdown procedure consists of dropping the load on the alternator, disconnecting it from the NRTS 138-kv system, and closing the turbine stop valve. The excess steam not required for turbine operation is delivered to the condenser via the steam bypass system. The turbogenerator is shut down in accordance with normal power plant practice. The steam system continues to operate in the normal manner for bypass operation. The reactor power level is slowly decreased and the secondary sodium flow rate is continually adjusted to maintain a primary bulk sodium temperature of 700°F and a steam pressure of 1250 psig at the turbine throttle. The rate at which the reactor power level and the secondary system flow rate are reduced is limited by the maximum allowed temperature changes in the sodium systems. The reactor power level is decreased until the reactor is subcritical and in the shutdown condition. The primary coolant flow rate is then gradually reduced until the pumping power is provided by the auxiliary pump (approximately 500 gpm). The secondary system flow rate is adjusted to maintain the desired 700°F bulk sodium temperature by keeping the evaporation rate of water in the steam generator at the controlled 1250-psig pressure.

Fast shutdown. In scram the reactor is shut down fast (by ejection of the control rods) and power to the secondary system pump is cut off. Two general scram conditions may be considered. The first represents the usual type of scram: both primary main pumps remain in operation. An initial condition of full reactor power is assumed, since at this level temperature transients are most severe. A total control rod worth of $0.05\Delta k/k$ and an initial rod insertion of 90% are assumed. The coolant temperature at outlet from the upper plenum is the most critical, in that it is indicative of the thermal shock potential at the upper plenum outlet nozzle and in the pipe leading to the heat exchanger. The tempera-

ture falls 150°F in 10 sec at a maximum rate of about 38°F/sec. Ample thermal barrier protection is provided in the upper plenum nozzle and in the outlet piping to preclude significant shock even under these conditions. The second case represents a scram caused by loss of primary system pumping due to pump failure or to loss of electric power. The primary auxiliary pump continues to operate even with loss of electric power, since its power supply is supplemented by a floating battery.

3–7.4 Fuel loading and unloading. Before unloading operations, the control rods are driven out of the reactor and disconnected from their drives. At the time these rods are disconnected, the automatic scram interlocks are shifted from operation of the control rods to operation of the safety rods. With the twelve control rods out of the reactor, it is subcritical by approximately $0.05\Delta k/k$ at operating temperature (approximately $0.04\Delta k/k$ at 208°F, the melting temperature of sodium). The two safety rods represent an additional 0.015 to $0.020\Delta k/k$ available negative reactivity.

Normal operation of the unloading system consists of removing a subassembly, moving it to the storage rack, selecting its replacement from the storage rack, and transferring it to the reactor. One subassembly is handled at a time, and the maximum expected change in reactivity is the difference between an irradiated and an unirradiated fuel subassembly. At 2% burnup of the fuel alloy, approximately 4% of the U^{235} is consumed. For a central fuel subassembly, this should produce a $\Delta k/k$ of less than 0.001; for the other locations the change is smaller.

3–8. Performance

3–8.1 Neutron physics. The neutron physics performance of the EBR-II has been investigated quite extensively, both by calculation and by critical experiments. The behavior of the reactor can best be illustrated by the results of a critical experiment in an idealized geometry, plus the results of multigroup calculations.

Static characteristics. The critical experiment described here was made on an assembly whose composition approximated that of the EBR-II reactor, and whose geometry was spherically symmetrical, with dimensions adjusted to give approximately equivalent neutron leakage characteristics. The dimensions of the assembly are given in Fig. 3–41, and the composition is given in Table 3–7. The fission rate was measured in this assembly as a function of position along the line indicated in Fig. 3–41, by fission counters containing, respectively, U^{235} and U^{238}. From these traverses and a knowledge of the composition of the regions of the assembly, it was possible to specify the relative rates of U^{235} and

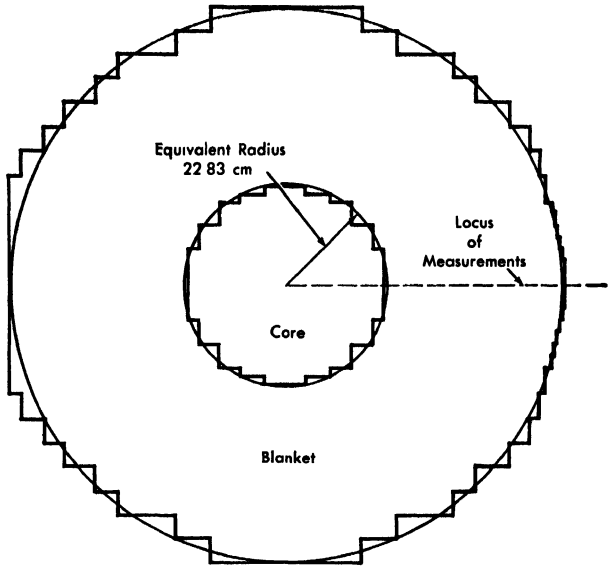

FIG. 3–41. Cross-sectional diagram of approximately spherical critical assembly Critical mass is 131.13 kg of U^{235}.

U^{238} fission in the assembly itself as functions of position. By the irradiation of U^{238} foils at various radial positions in the assembly and subsequent radiochemical determinations of the plutonium formed, it was possible to make a similar determination of the distribution of neutron capture by U^{238} throughout the assembly. This combination of measurements allows determination of both the distribution of power production through the assembly and the conversion ratio.

Results of the measurements are plotted in Fig. 3–42 as functions of distance from the center of the assembly. The solid curve, which is arbitrarily normalized to unity at the center of the assembly, gives the variation of total fission rate with position; it is very nearly identical with the variation of power production in the reactor. The upper dashed curve gives the distribution of the rate of destruction of U^{235} in the reactor core, properly normalized with respect to the fission rates. This curve is not identical with the total fission rate because some of the fissions are in U^{238}, and because the rate of destruction of U^{235} is higher than the rate of fissioning of U^{235} by the factor $1 + \alpha$ where α is the capture-to-fission ratio for U^{235}. In determining the curve, a constant value of 0.2 was assumed for α. This value is probably somewhat too high. The curve of U^{235} destruction is not continued into the blanket because the rate was quite low in the depleted uranium of the blanket.

TABLE 3–7

COMPOSITION OF SPHERICAL CRITICAL ASSEMBLY

	Volume, %*	
	Core	Blanket
U^{235}	14.00	0.14
U^{238}	15.86	83.26
Aluminum	31.44	2.27
Stainless steel 304	12.31	7.31

*Remainder of volume is occupied by air.

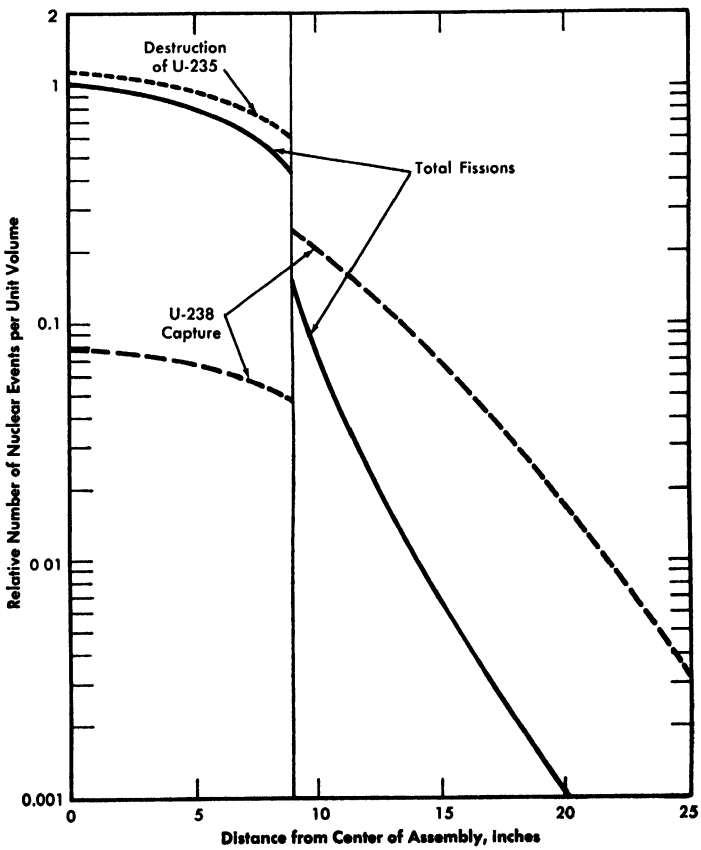

FIG. 3–42. Distribution of fission, U^{235} destruction, and capture by U^{238} in spherical critical assembly.

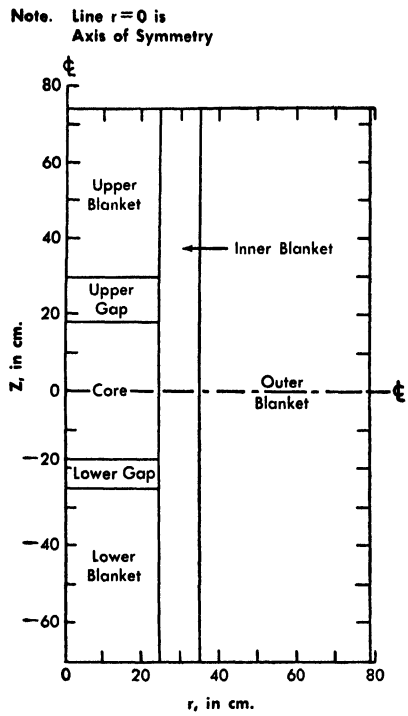

FIG 3–43. Reactor model for one-dimensional, ten-group analysis.

The lower dashed curve gives the rate of neutron capture in U^{238} (the rate of plutonium formation), also properly normalized with respect to the fission rate curve.

The conversion ratio of the assembly (the ratio of the rate of production of plutonium to the rate of destruction of U^{235}) can be determined by integrating the upper and lower dashed curves (Fig. 3–42) over the volume of the assembly and taking the ratio of the integrals. The conversion ratio has been so determined to be 1.29 for the assembly. The conversion ratio for EBR-II will be somewhat lower than this value because a higher neutron leakage results from the more practical shape of the reactor. By further experiments on assemblies which approximate more closely the geometry of EBR-II, and by theoretical corrections, the conversion ratio for EBR-II, when fueled with fresh U^{235}, is estimated to lie between 1.10 and 1.15. Of this, approximately 0.1 results from U^{238} capture in the reactor core, and the very much larger remainder results from U^{238} capture in the blanket.

Although the above measurements describe the most important physics features of the reactor—distribution of power and distribution of plu-

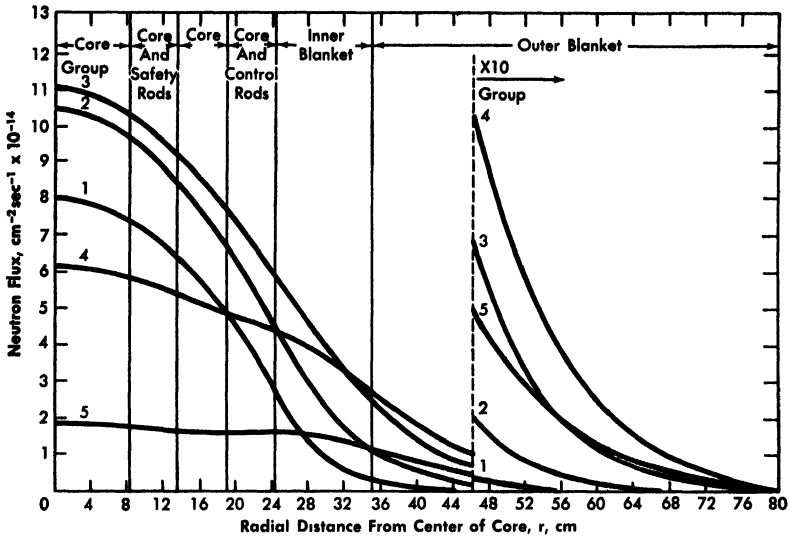

FIG. 3–44. Radial neutron flux distribution in $Z = 0$ plane, one-dimensional analysis.

tonium production—a better understanding of the physics performance is given by considering the neutron energy distribution within the reactor. This distribution has been calculated by a ten energy group diffusion theory analysis in one dimension. The reactor model used for the calculation is shown in Fig. 3–43. Separate calculations were made in the axial and radial directions to find the spatial distribution of the neutron flux in each of the ten energy groups. As the calculation was made in a given direction, leakage of neutrons in other directions was accounted for approximately by the usual equivalent bare reactor approximation. To simplify the graphical presentation of the results, the ten energy groups have been combined into a total of five groups. These groups cover the following energy ranges:

Group	*Energy interval, Mev*
1	Above 1.35
2	0.50 to 1.35
3	0.18 to 0.5
4	0.07 to 0.18
5	Zero to 0.07

The radial distributions of the neutron fluxes of the five energy groups in the $z = 0$ plane are shown in Fig. 3–44. The axial distributions are shown in Fig. 3–45. It is to be noted that the neutron energy spectrum

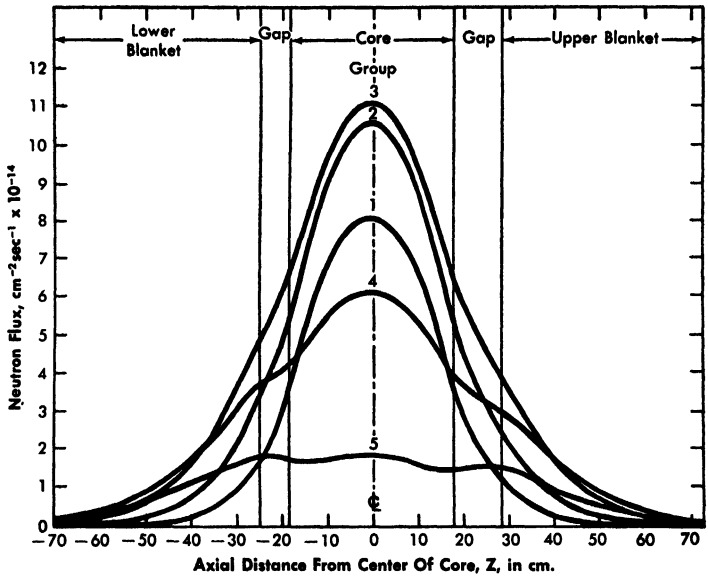

FIG. 3–45. Axial neutron flux distributions at $r = 0$, one-dimensional analysis.

becomes progressively less energetic along any traverse outward from the center of the core.

The calculated fission and flux densities at the center of the core, at the reactor design power, are as follows:

Power density	PD = 1.37 Mw/liter of core volume
Fission density	$\int_E \Sigma_f \phi dE = 4.4 \times 10^{13}$ fissions/(cm³)(sec)
Neutron flux (above 1.35 Mev)	$\phi_1 = 8.0 \times 10^{14}$ n/(cm²)(sec)
Neutron flux (0.5 to 1.35 Mev)	$\phi_2 = 10.5 \times 10^{14}$ n/(cm²)(sec)
Neutron flux (0.18 to 0.5 Mev)	$\phi_3 = 11.1 \times 10^{14}$ n/(cm²)(sec)
Neutron flux (0.07 to 0.18 Mev)	$\phi_4 = 6.2 \times 10^{14}$ n/(cm²)(sec)
Neutron flux (0 to 0.07 Mev)	$\phi_5 = 1.9 \times 10^{14}$ n/(cm²)(sec)
Total neutron flux	$\phi = 3.77 \times 10^{15}$ n/(cm²)(sec)

To investigate further the spatial distribution of power generation, a two-dimensional calculation (radial and axial) was carried out in two energy groups. The core geometry was idealized to a small extent: the axial asymmetries, and the radial asymmetries due to the presence of control rods, were neglected. The division between energy groups was taken as the U^{238} fission threshold at 1.35 Mev. Group I neutrons have energies above this threshold, while group II neutrons have energies below the threshold. The averaged cross sections used for the calculations were selected on the basis of agreement with multigroup calculations in

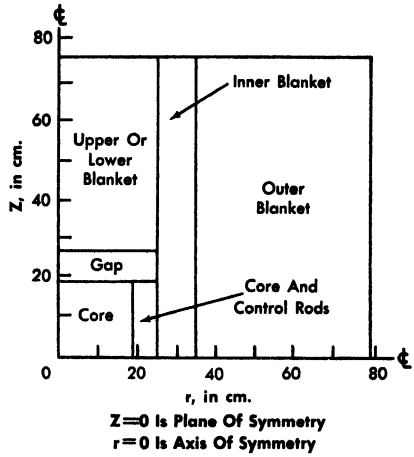

FIG. 3–46 Reactor model for two-dimensional, two-group analysis.

simpler geometry. Figure 3–46 is a diagram of the reactor model used for the two-dimensional calculation. Figures 3–47, 3–48, 3–49, and 3–50 show the radial distributions of neutron fluxes in the two energy groups at a number of axial locations. From these analyses the power distribution over the volume of the reactor can be computed after the contribution of gamma heating has been added. The detailed distribution of power generation is discussed in Article 3–8.2.

The isothermal temperature coefficient (that corresponding to a uniform heating of the entire reactor, including the structure) is calculated to be $-3.6 \times 10^{-5}(\Delta k/k)/°C$. The contributions of the various components to the total coefficient are given in Table 3–8.

The reactivity changes resulting from an average burnup of 2% of the U^{235} in the reactor core are the following:

Burnup of U^{235} in core	$-0.02\Delta k/k$
Buildup of Pu in core	$+0.002\Delta k/k$
Buildup of Pu in blanket	$+0.0072\Delta k/k$
Buildup of fission products	$-0.002\Delta k/k$
Irradiation growth of fuel (4% growth)	$-0.011\Delta k/k$
Total reactivity change	$-0.024\Delta k/k$

It is not necessary, of course, that the entire core be run to 2% burnup before any fuel elements are changed.

The combined worth of the twelve control rods is approximately 5% k_{eff}. The two safety rods are worth approximately 1.5% k_{eff}.

Dynamic characteristics. The effective neutron lifetime in the EBR-II reactor is calculated to be 8×10^{-8} sec.

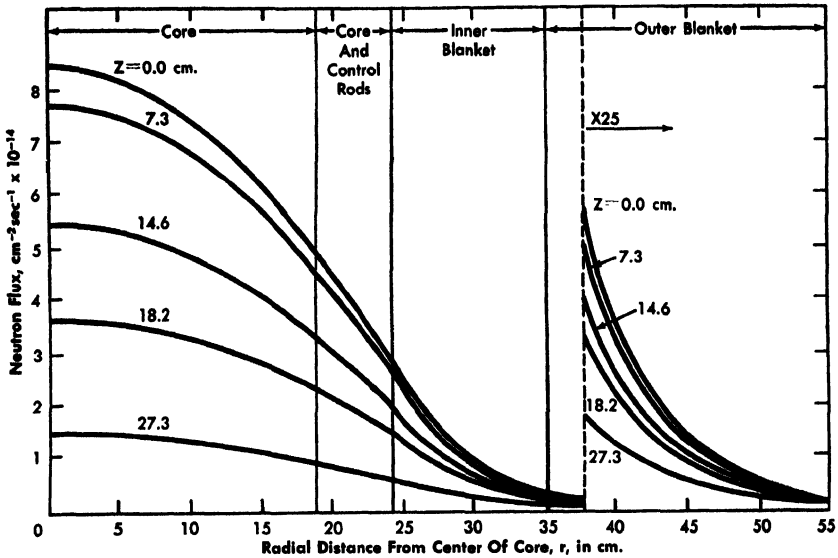

FIG. 3–47. Radial group I neutron flux distribution, two-dimensional analysis.

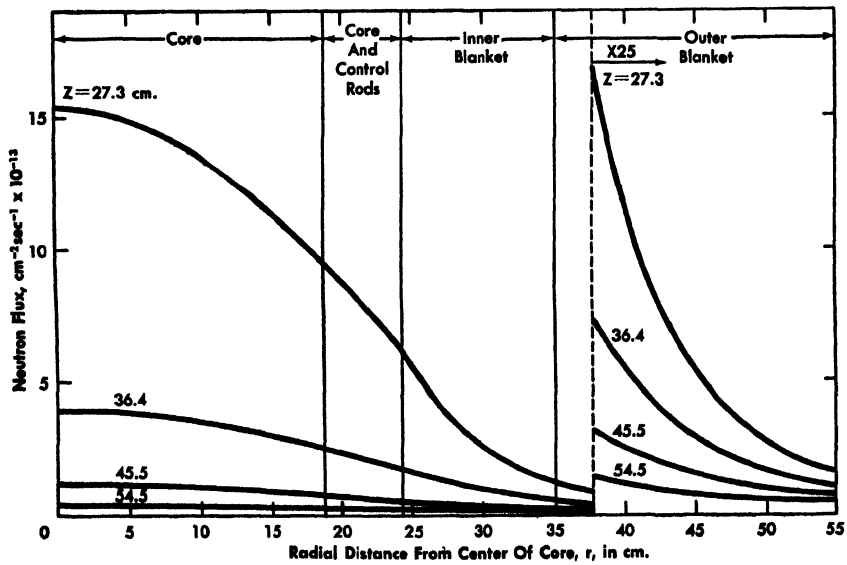

FIG. 3–48. Radial group I neutron flux distribution, two-dimensional analysis.

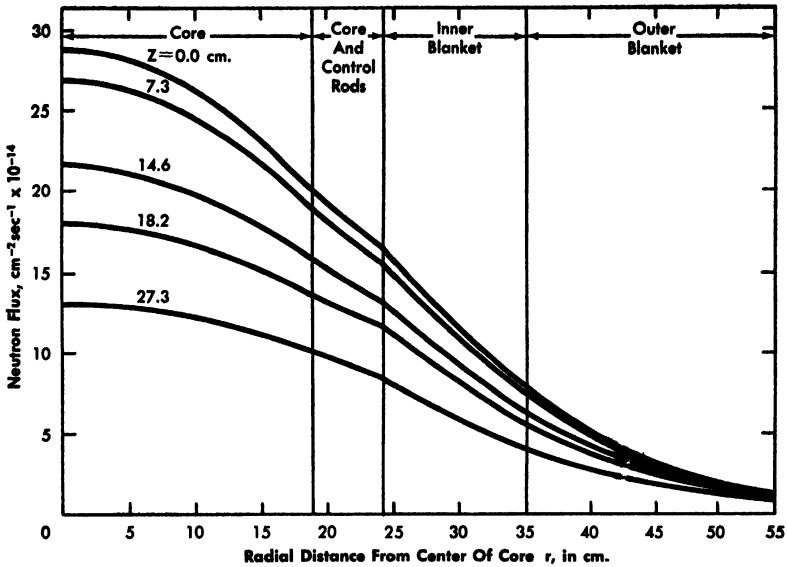

FIG. 3–49. Radial group II neutron flux distribution, two-dimensional analysis

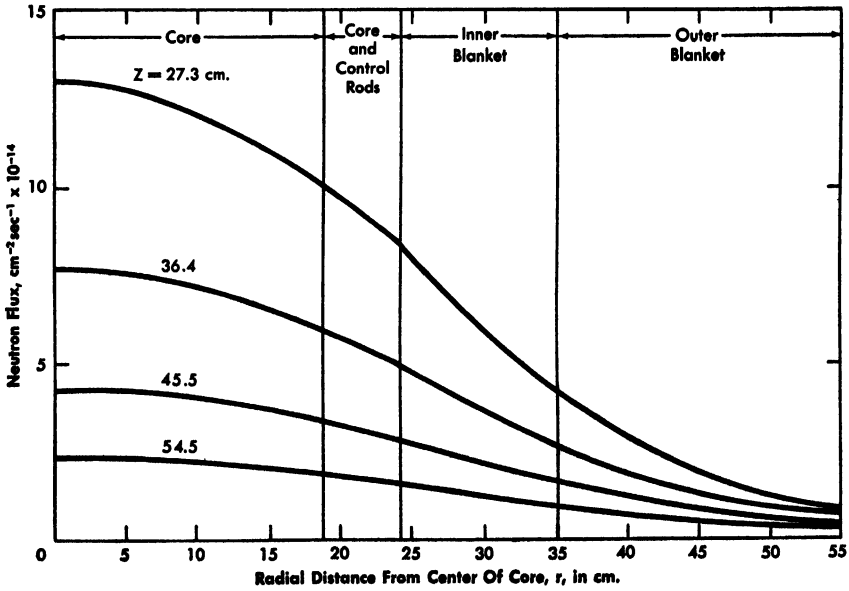

FIG. 3–50 Radial group II neutron flux distribution, two-dimensional analysis

TABLE 3–8

COMPONENTS OF THE ISOTHERMAL TEMPERATURE COEFFICIENT

	Coefficient, $[(\Delta k/k)/°C] \times 10^5$
Core	
Axial growth of fuel	−0.39
Radial growth of fuel (displacement of Na)	−0.09
Axial growth of structure (density change)	−0.039
Density change of coolant	−0.87
Radial growth of supporting structure	−0.97
Doppler effect, average	+0.04
Bowing	Zero
Gaps	
Density change of coolant	−0.38
Density change of structure	−0.036
Upper and lower blanket	
Density change of coolant	−0.21
Radial growth of uranium and jacket	−0.016
Axial growth of blanket uranium	−0.024
Axial growth of jacket	−0.021
Inner blanket	
Density change of coolant	−0.2
Axial growth of blanket uranium	−0.066
Axial growth of jacket	−0.022
Radial growth of uranium and jacket	−0.04
Radial growth of supporting structure	−0.17
Bowing	Zero
Outer blanket	
Density change of coolant	−0.017
Axial growth of blanket uranium	−0.014
Axial growth of jacket	−0.003
Radial growth of supporting structure	−0.034

TABLE 3-9

TEMPERATURE CHANGES FOR REACTOR REGIONS AS POWER LEVEL IS RAISED FROM ZERO LOAD TO FULL LOAD

Region	Average temperature,* °F	Temperature increase,† °C
Core coolant	810	61
Core uranium	975	153
Core cladding	862	90
Upper gap	919	122
Lower gap	702	1
Upper blanket	924	124
Lower blanket	705	3
Inner blanket	780	44
Outer blanket	745	25
Supporting structure	700	Zero

*At full power.
†With reference to coolant inlet temperature (700°F).

A power coefficient of reactivity can be calculated from the isothermal temperature coefficient components of Table 3-8, if the temperature change of each region of the reactor with power is taken into account. These temperature changes, as the reactor power is raised from zero to the full operating power of 62.5 Mw, are given in Table 3-9. The temperature increases correspond to a net reactivity change of $-0.0020\Delta k/k$. The effective power coefficient resulting from the temperature changes is therefore

$$\frac{-0.0020}{62.5} = -3.2 \times 10^{-5}(\Delta k/k)/\text{Mw}.$$

To this coefficient must be added any power coefficient resulting from bowing of the fuel elements.

Since the fuel elements are restrained by the walls of the subassemblies, bowing cannot occur individually in the fuel elements. However, the walls of the subassembly nearer the center of the reactor will become hotter than those farther from the center because of the greater temperature rise of the coolant as it passes over the more centrally located fuel elements. There is therefore a bowing of the subassembly itself caused by the differential expansion of opposite walls. The arc of the bow is

always convex toward the center of the reactor. The support points of the subassembly are such that for small temperature differentials the bowing causes a small net motion of the subassembly toward the center of the core and therefore a small reactivity increase [2]. Under normal conditions of coolant flow, this inward motion of the subassembly is calculated to occur for reactor powers between zero and 27 Mw. The positive contribution of the bowing to the power coefficient of reactivity is calculated to be $+1.1 \times 10^{-5}(\Delta k/k)$/Mw In combination with the negative components computed above, this gives a net negative power coefficient of $-2.1 \times 10^{-5}(\Delta k/k)$/Mw. For power levels above 27 Mw, the analysis indicates that the restraints on the subassembly are such as to cause the bowing to result in a net motion away from the center of the core, and therefore in a reactivity decrease The magnitude of this negative component at power levels between 27 and 62.5 Mw is calculated to be $-1.0 \times 10^{-5}(\Delta k/k)$/Mw.

In analyzing motions of the fuel subassemblies under bowing conditions, many assumptions about the mechanical interactions of neighboring elements are possible. It is possible to make assumptions which give higher positive components for the bowing coefficient at low reactor power, but it appears that in all conceivable cases the coefficient is substantially negative when the power level is higher than about 70% of the design power.

3–8.2 Thermal performance. *Reactor heat generation.* An approximate breakdown of power generation in the various zones of the "clean" reactor is given below:

Zone	*Power, Mw*	*% of total*
Core	53.3	85.4
Upper plus lower blanket	1.2	1.9
Inner blanket	5.2	8.3
Outer blanket	2.6	4.1
Neutron shield	0.2	0.3
Total	62.5	100.0

Analysis indicates that only small changes in heat generation distribution are caused by core burnup and plutonium formation, and these changes have been allowed for in calculation of maximum fuel and blanket temperatures.

The maximum power density in the core is 1.37 Mw/liter of core volume and the average core power density is 0.89 Mw/liter. The radial power density distribution at the center plane of the reactor is shown ir Fig. 3–51. This distribution is based on 82% insertion of each of the

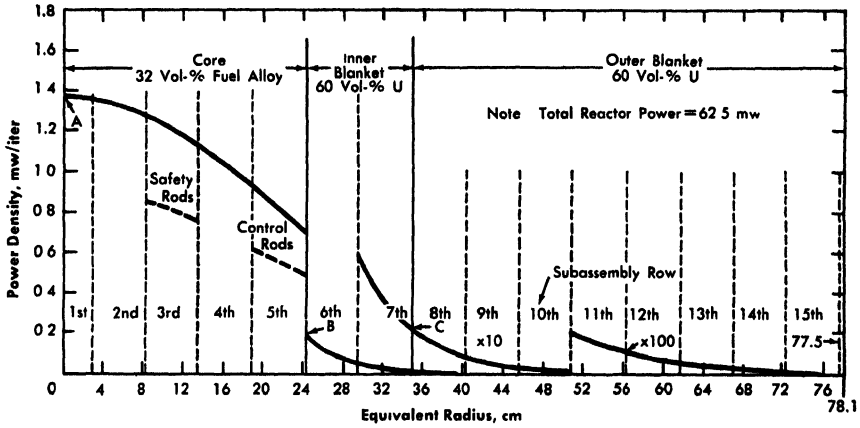

FIG. 3–51. Radial power density distribution at center plane of clean reactor.

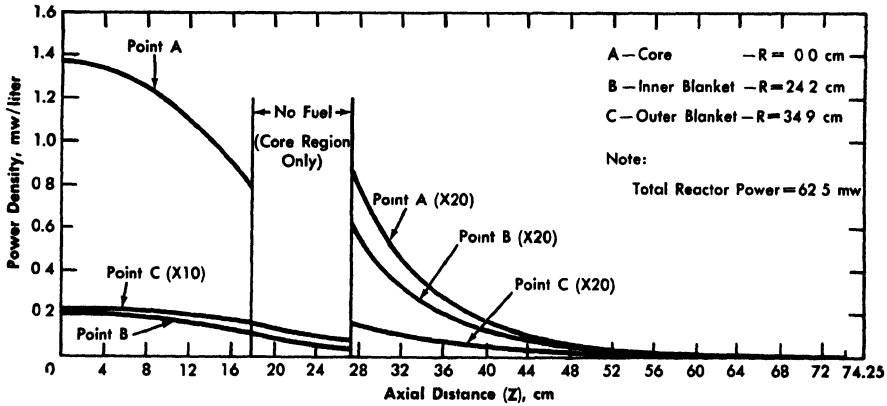

FIG. 3–52. Axial power density distributions of clean reactor.

twelve control rods and 100% insertion of the two safety rods. In the control rod and safety rod regions of Fig. 3–51, two power density distribution curves are presented. The dashed line shows anticipated power densities in control or safety subassemblies; the solid line indicates the power densities expected in the core subassemblies within these regions. The radial maximum-to-average power density ratio of the core at the reactor center plane is 1.33; the effective radial maximum-to-average ratio over the entire height of the core is 1.32.

The axial power density distributions at the centerline of the core, inner edge of the inner blanket, and inner edge of the outer blanket are shown in Fig. 3–52. The axial maximum-to-average power density ratio

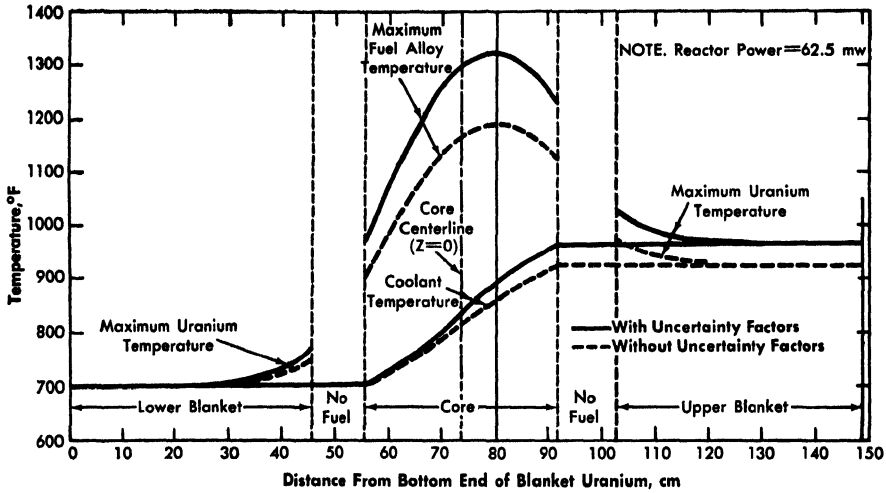

FIG. 3–53. Axial temperature distributions of fuel alloy and coolant.

at the inner edge of the inner blanket is 3.45; at the inner edge of the outer blanket, 2.84. The axial maximum-to-average ratio at the centerline of the core for the core section only is 1 17; over the entire radius of the core for the core section only, it is 1.16.

Reactor temperature distribution. The maximum mean reactor outlet coolant temperature achievable in a given reactor for specific maximum permissible fuel and blanket alloy temperatures (Figs. 3–53 and 3–54) are functions of various parameters; for example, reactor inlet coolant temperature, reactor power level, and the coolant distribution. In general, to attain high mean coolant outlet temperature at a practical coolant inlet temperature and high reactor power, it is necessary to orifice the coolant flow to certain of the subassemblies; that is, it is necessary to establish the proper coolant mass flow distribution. To achieve this distribution in the EBR-II, all subassembly rows are orificed except rows 1, 2, and 3 (numbered radially outward from the center of the core). In most cases, the various rows require orificing of different degrees, since different amounts of power per subassembly are generated in the various rows. The degree of orificing employed in each row is based on one or more of these limitations (depending upon the row): maximum permissible fuel alloy or blanket uranium temperature; maximum permissible coolant temperature at subassembly outlet; minimum acceptable orifice size.

In addition to flow distribution, another consideration affecting calculated temperature distributions within the reactor is the degree of uncertainty associated with each of the quantities (such as thermal conduc

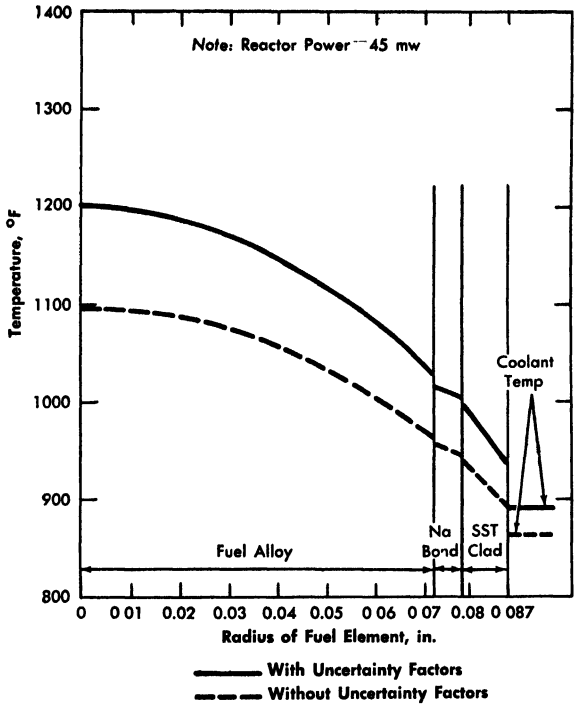

FIG. 3-54. Radial temperature distribution through a fuel element at point of maximum fuel temperature.

tivity value, heat-transfer coefficient, power-density level, etc.) entering into the temperature calculations. If each quantity is analyzed separately, a degree of uncertainty can be estimated and a factor assigned.* The magnitude of this uncertainty factor expresses the degree of uncertainty associated with the magnitude of the quantity. The various calculated temperature differences are increased by multiplication by the appropriate uncertainty factors. For example, if the uncertainty factor associated with the heat-transfer coefficient is 1.20 (i.e., the heat-transfer coefficient cannot be predicted to better than ±20%), the nominal film temperature drop, θ, is increased by 20% to 1.20 θ. Thus, in many of the figures referred to in this section, two temperature curves for the same conditions are shown: one which includes the use of uncertainty factors in the calculations, and one which does not. The temperature distributions which involve the use of these factors are considered very conservative. The temperature distributions based on nominal calcula-

*Reference 2, p. 80, Table VIII.

tions (without uncertainty factors) are those more representative of the average conditions expected to exist within the reactor. Table 3–10 gives pertinent temperatures, heat fluxes, and coolant flow rates in subassemblies of rows 1, 6, and 8. Uncertainty factors are not included. Table 3–11 gives the same information with uncertainty factors included.

3–8.3 Fuel performance.* The development of a fuel element for the EBR-II has been a major effort at Argonne National Laboratory. Fuel specifications for this reactor are (1) the fuel must be dimensionally stable to a burnup of at least 2 a/o or 20,000 Mwd/t at an operating temperature of approximately 600 to 700°C, and (2) the fuel should contain at least 20% plutonium for optimum breeding gain [18]. In addition, since the first loading of the EBR-II will be with U^{235}, development of a suitable uranium metal fuel element was also required.

Because dimensional instability has been experienced with uranium metal and its alloys at high temperatures and high burnups,† a very great effort was placed on the irradiation testing of suitable fuel alloys.

Irradiation effects. (1) Uranium-zirconium alloy. As part of the EBR-I and EBR-II test programs, experiments were made to investigate irradiation effects on uranium-zirconium (U-2 w/o Zr) fuel alloys [19,20]. Results indicated that U-2 w/o Zr fuel pins, as-cast, are stable to at least 0.6 a/o fuel alloy burnup, provided the alpha-beta transition temperature (665°C) is not exceeded. Even occasional cycling above this temperature causes instability, resulting in pronounced bumping of the fuel and container. Pertinent data for some of these irradiation experiments are shown in Table 3–12. Appearance of U-2 w/o Zr specimens, irradiated to total atom burnups greater than 1% at temperatures over 600°C, is shown in Fig. 3–55(a) [20]. Damage to specimens irradiated above 600°C is shown in Fig. 3–55(b) [20]. The severe swelling of the latter specimens is probably caused by creep of the high-temperature uranium under stress due to the accumulation of fission gases.

(2) Uranium-plutonium alloy. Because EBR-II will eventually be fueled with plutonium, a series of irradiation experiments were carried out on uranium-plutonium specimens of various compositions (5, 10, 15, 20% by weight Pu). Figure 3–56 shows the effect of irradiation on castings of uranium containing up to 15 w/o Pu and indicates that these alloys are unsuitable as a fuel material [22]. Extrusions of these same type alloys were also fabricated and tested. The results of the tests

---

*Compiled by F. Bevilacqua, GNEC, from the references and material supplied by F. G. Foote, J. H. Kittel, R. J. Dunworth, L. R. Kelman, and M. V. Nevitt, ANL.

†See Section 6–4.

TABLE 3–10

SUMMARY OF THERMAL ANALYSIS RESULTS FOR MAXIMUM TEMPERATURE REGION OF CORE AND BLANKETS

(No uncertainty factors included; reactor power = 62.5 Mw)

	Region			
	Core	Upper blanket	Inner blanket	Outer blanket
Coolant flow in maximum power subassembly				
Flow velocity, fps	25.8	25.2	10.4	2.6
Flow rate, gpm	152.1	152.1	19.6	4.9
Estimated pressure drop, psi	23.0	9.0	24.2	1.7
Maximum heat flux, Btu/(ft²)(hr)	1,034,000	78,800	285,900	30,200
Temperatures, °F				
Uranium, maximum	1189	974	1024	829
Coolant, at outlet	923	925	884	829
Coolant, at inlet	702	923	700	700
Coolant temperature rise, inlet to outlet	221	2	184	129
Coolant, at point of maximum uranium temperatures	863	923	824	829
Mixed mean coolant outlet temperature from entire region	918	921	845	790
Temperature difference at point of maximum uranium temperature, °F				
Through uranium	183	31	142	Zero
Through uranium-sodium interface	13	1	3	Zero
Through sodium "bond" layer	14	1	7	Zero
Through sodium-clad interface	11	1	3	Zero
Through clad layer	63	12	35	Zero
Through coolant film	42	5	10	Zero
Total element temperature difference	326	51	200	Zero

TABLE 3-11

SUMMARY OF THERMAL ANALYSIS RESULTS FOR MAXIMUM TEMPERATURE REGIONS OF CORE AND BLANKET

(Uncertainty factors included; reactor power = 62.5 Mw)

	Region			
	Core	Upper blanket	Inner blanket	Outer blanket
*Coolant flow in maximum power subassembly**				
Flow velocity, fps	25.8	25.2	10.4	2.6
Flow rate, gpm	152.1	152.1	19.6	4.9
Estimated pressure drop, psi	23.0	9.0	24.2	1.7
*Maximum heat flux, Btu/(ft²)(hr)**	1,034,000	78,800	285,900	30,200
Temperatures, °F				
Uranium, maximum	1320	1030	1100	852
Coolant, at outlet	963	965	917	852
Coolant, at inlet	702	963	700	700
Coolant temperature rise, inlet to outlet	261	2	217	152
Coolant, at point of maximum uranium temperature	892	963	842	852
Mixed mean coolant outlet temperature from entire region*	918	921	845	790
Temperature differences at point of maximum uranium temperature, °F				
Through uranium	243	40	186	Zero
Through uranium-sodium interface	13	1	3	Zero
Through sodium "bond" layer	18	2	9	Zero
Through sodium-clad interface	11	1	3	Zero
Through clad layer	84	16	45	Zero
Through coolant film	59	7	12	Zero
Total element temperature difference	428	67	258	Zero

*No uncertainty factors included.

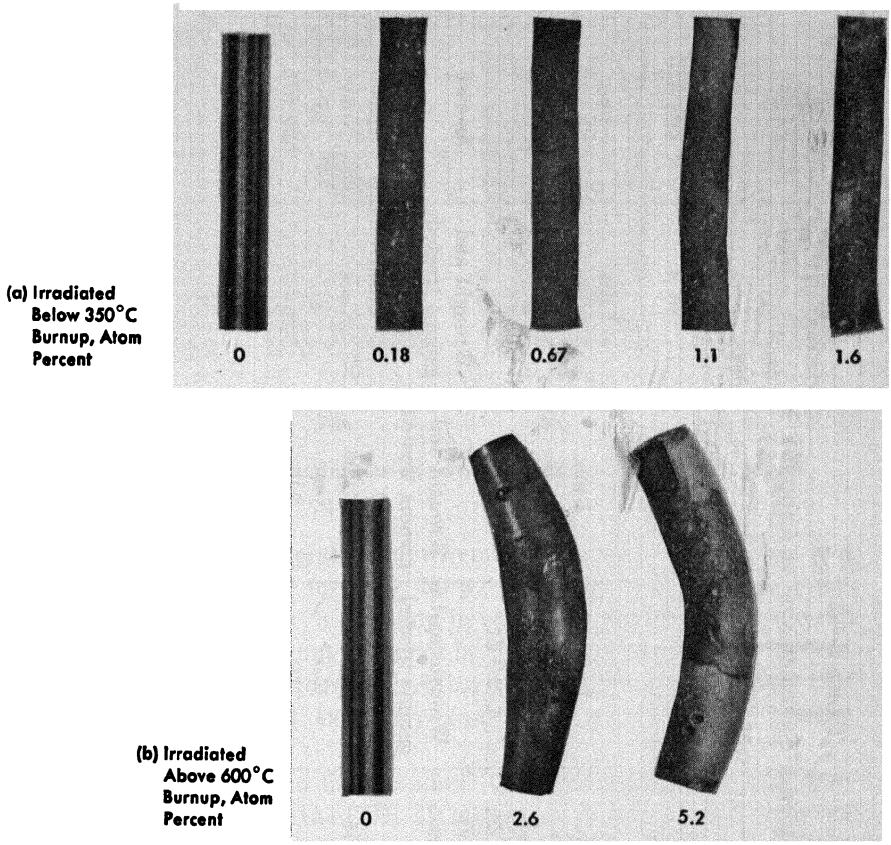

Fig. 3–55. Irradiated specimens, showing "ballooning" due to temperature effects.

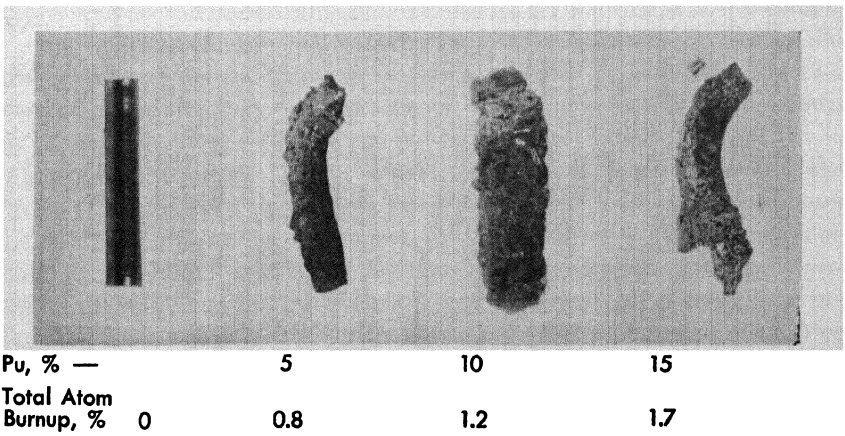

Fig. 3–56. Effect of irradiation on cast uranium-plutonium alloys.

TABLE 3–12

EBR-II FUEL ELEMENT IRRADIATION EXPERIMENTS AT ARGONNE NATIONAL LABORATORY

Fuel description and test conditions	Experimental test numbers				
	No. 1	No. 2	No. 3	No. 4	No. 5
Fuel geometry*	7 slugs	1 pin	1 pin	1 pin	6 slugs
Fuel length, in.	13.40	14.22	14.22	14.22	14.22
Fuel diameter, in.	0.164	0.144	0.144	0.144	0.144
Fuel alloy composition, w/o	U-2.0 Zr, U-1.3 Zr	U-2.0 Zr	U-2.0 Zr	U-2.0 Zr	U-2.0 Zr
Fabrication†	As-cast	Wrought and gamma treated	Wrought and gamma treated	Wrought and gamma treated	As-cast
Enrichment, w/o U^{235}	15	17	20	17	20
Bond thickness, in.	0.004	0.004	0.006	0.006	0.006
Gas reservoir,‡ in.	2.5	2.5	None	None	None
Growth gap, % of total length	3.2	2.0	2.0	2.0	2.0
Operating fuel temperature, °F	1000–1050	775–825	725–775	825–875	625–675
Number of thermal cycles	140	210	260	290	220
Estimated burnup, a/o	0.4	0.45	0.75	0.7	0.6

*Slugs indicate more than one piece used to obtain fuel length.

†Tests 1 and 5: statically cast, centerless ground to size (5% reduction). Tests 2, 3, and 4: rolled, swaged to size, heated to 800°C, furnace-cooled.

‡Tests 1 and 2: expansion space is provided within element. Tests 3, 4 and 5: element open at top, filled with sodium, expansion is into the finned capsule.

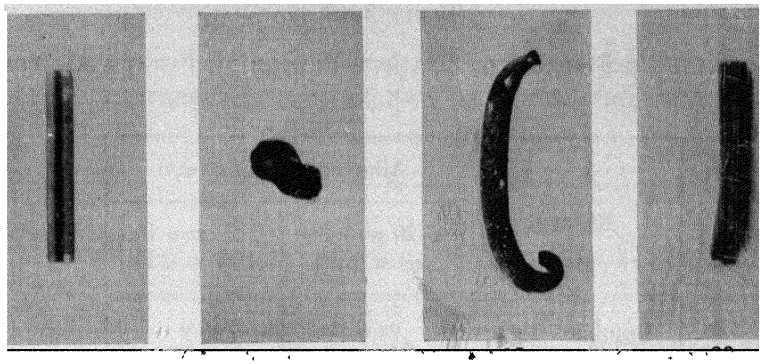

FIG. 3–57. Effect of irradiation on extruded uranium-plutonium alloys.

(Fig. 3–57) show considerable improvement in surface smoothness and fair dimensional stability for the U-20 w/o Pu alloy [18]. Further studies indicated that U-20 w/o Pu alloy in cast form contains micro-cracks which make it so brittle that it cannot be removed from the mold without cracking; also it falls apart under thermal cycling. In addition, this alloy is pyrophoric and extremely susceptible to irradiation damage [21,22].

(3) Uranium-plutonium-fissium alloy. In pyrometallurgical reprocessing of fuel elements from the EBR-II, a group of fission-product elements will remain in the melt as impurities and will tend to reach equilibrium amounts after several successive fuel recycles. The elements retained are molybdenum, ruthenium, rhodium, palladium, and technetium. To improve upon the undesirable characteristics of the binary U-Pu alloys, the above group of elements, called fissium (Fs) have been added in the proper ratio as natural alloying elements to the U-20 w/o Pu alloy fuel element. The nominal compositions of these U-Pu-Fs alloys are shown in Table 3–13.

Irradiation tests on these U-Pu-Fs alloys have been made and the effects of irradiation tabulated in Table 3–14 [21]. This table also shows the effects of irradiation on some U-20 w/o Pu-5 w/o Mo alloys. The molybdenum alloys were tested because of the beneficial effect of molybdenum in stabilizing the gamma phase and suppressing the zeta phase introduced when the solid solubility of plutonium in alpha uranium (10 or 11 w/o Pu in U at 25°C) is exceeded. Specimens (3/4 inch long × 0.125 inch diameter) were irradiated without physical restraint in NaK-filled capsules in the MTR.

TABLE 3–13

NOMINAL COMPOSITION OF URANIUM-PLUTONIUM-FISSIUM ALLOYS IRRADIATED BY ARGONNE NATIONAL LABORATORY

Element	Alloy composition, w/o	
	U-20 w/o Pu-5.4 w/o Fs	U-20 w/o Pu-10.8 w/o Fs
Uranium	74.6	69.2
Plutonium	20	20
Molybdenum	1.40	2.80
Zirconium	0.25	0.50
Ruthenium	2.15	4.30
Rhodium	0.35	0.70
Palladium	1.25	2.50

All the specimens appear highly stable under irradiation with the U-20 w/o Pu-5.4 w/o Fs alloy elongating at an average rate of 1.7% per a/o burnup and the U-20 w/o Pu-10.8 w/o Fs alloy elongating at a rate of 1.8% per a/o burnup. Excellent surface smoothness was retained during irradiation, as shown as Fig. 3–58.

Recent data on the behavior of a group of cast U-20 w/o Pu-10 w/o Fs alloys, irradiated to burnups up to 3.5 a/o and irradiation temperatures calculated to have ranged up to 840°C, showed large volume increases (~40% density decrease) from swelling of the specimens [23]. These specimens in the swelled condition were pyrophoric. The irradiation temperature of 840°C is far above what is to be used in the EBR-II, and good dimensional stability is expected with fissium alloys for 2 a/o burnups at approximately 600°C.

(4) Uranium-fissium alloy. Irradiation tests have also been made on U-Fs alloys for possible use as the first loading of the EBR-II [24]. The nominal compositions of the test specimens are shown in Table 3–15. The effect of molybdenum, one of the major constituents of the fissium composition, was examined by including in the tests specimens of U-2.5 w/o Mo containing no fissium. Results of the irradiation tests are shown in Table 3–16 and are presented pictorially in Figs. 3–58 through 3–63. The general conclusions based on the results of these tests are as follows [24]:

(a) Based on results of tests to 0.76% burnup of all atoms and temperatures in the 400 to 600°C range, both 2.5 w/o molybdenum and 5 w/o

TABLE 3–14

SPECIMEN DATA ON URANIUM-PLUTONIUM BASE ALLOYS*

Specimen No.	Composition, w/o	Approx. calc. max. temp., °C	Calc. burnup of all atoms, %	Length increase %	Diameter increase %	Calc. volume increase %	Hardness change, R_A	Weight change, mg	Density decrease, %
CF-1	U-20 Pu-5 Mo	340	0.27	0.74	0	0.74	−8.3	−4	0.74
CF-2	U-20 Pu-5 Mo	280	0.43	0.67	0.56	1.80	−8.3	−16	1.45
CF-3	U-20 Pu-5 Mo	270	0.20	0.79	0.48	1.76	−8.3	2	0.68
CF-4	U-20 Pu-5 Mo	260	0.38	1.26	0.40	2.07	—	1	0.62
CF-5	U-20 Pu-5 Mo	190	0.28	0.83	0.48	1.80	−23.9	1	1.08
CF-6	U-20 Pu-5 Mo	120	0.07	—	0	—	−17.2	—	—
CF-7	U-20 Pu-5 Mo	270	0.40	1.05	0.96	3.00	−7.0	0	1.59
CF-8	U-20 Pu-5 Mo	220	0.15	0.77	0.16	0.40	−7.7	0	0.23
CF-10	U-20 Pu-10.8 Fs	310	0.92	2.30	0.16	2.63	—	−1	1.29
CF-12	U-20 Pu-10.8 Fs	280	0.81	0.88	0.40	1.60	—	−1	0.18
CF-14	U-20 Pu-5.4 Fs	560	0.42	—	1.80	—	—	—	0.46
CF-15	U-20 Pu-5.4 Fs	520	0.40	0.57	0.89	2.37	—	−1	0.91
CF-16	U-20 Pu-5.4 Fs	450	0.33	0.62	0.08	0.78	—	−3	0.28

*Reference 21.

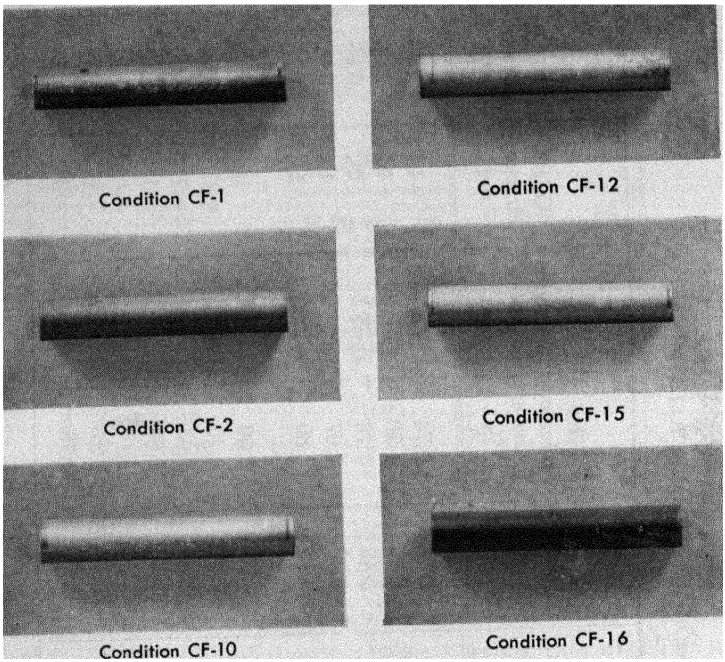

FIG 3–58. Effect of irradiation on uranium-plutonium base alloys.

TABLE 3–15

NOMINAL COMPOSITION OF URANIUM-FISSIUM ALLOYS IRRADIATED BY ARGONNE NATIONAL LABORATORY*

Element	Alloy Composition, w/o				
	U-2.5 w/o Mo	U-3.2 w/o Fs	U-5.0 w/o Fs	U-5 w/o Fs-2.5 w/o Mo	U-5 w/o Fs-7.5 w/o Mo
Uranium (5 wt. % U^{235})	97.5	96.83	95.00	92.55	87.69
Molybdenum	2.5	1.58	2.50	5.00	10.00
Zirconium	—	0.10	0.20	0.20	0.19
Ruthenium	—	1.18	1.50	1.46	1.38
Rhodium	—	0.20	0.30	0.29	0.27
Palladium	—	0.10	0.50	0.49	0.46
Niobium	—	0.01	—	0.01	0.01

*Reference 24.

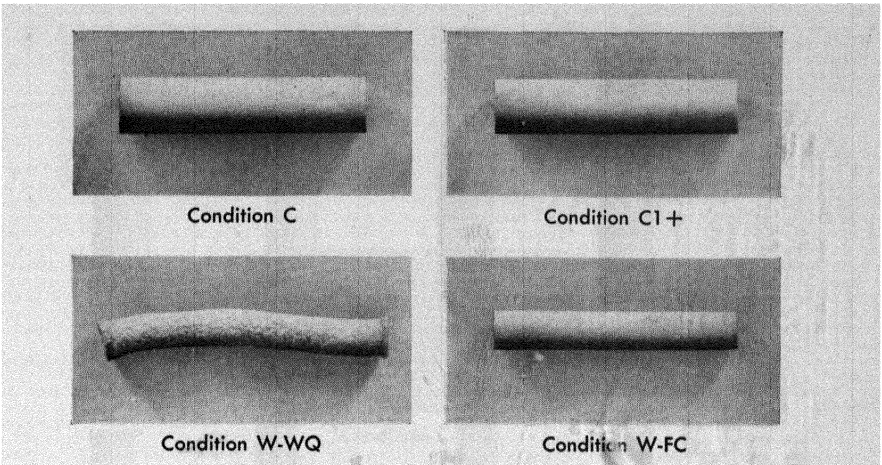

FIG. 3–59. Effect of irradiation on U-2.5 w/o Mo alloy prepared by different fabrication processes.

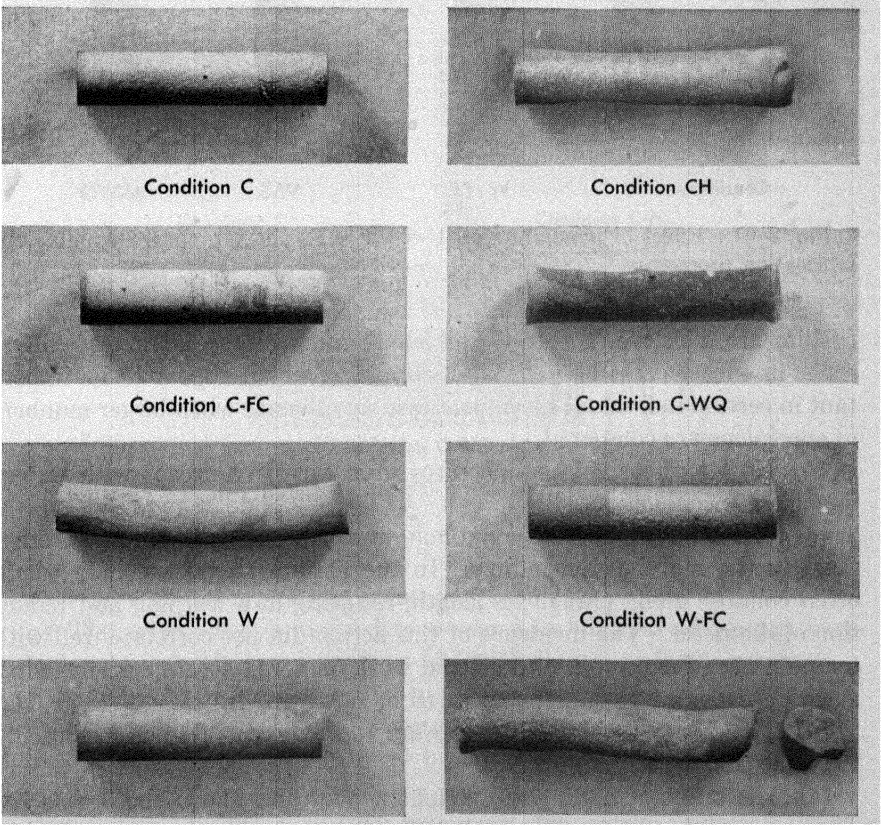

FIG. 3–60. Effect of irradiation on U-3.17 w/o Fs alloy, prepared by different fabrication processes.

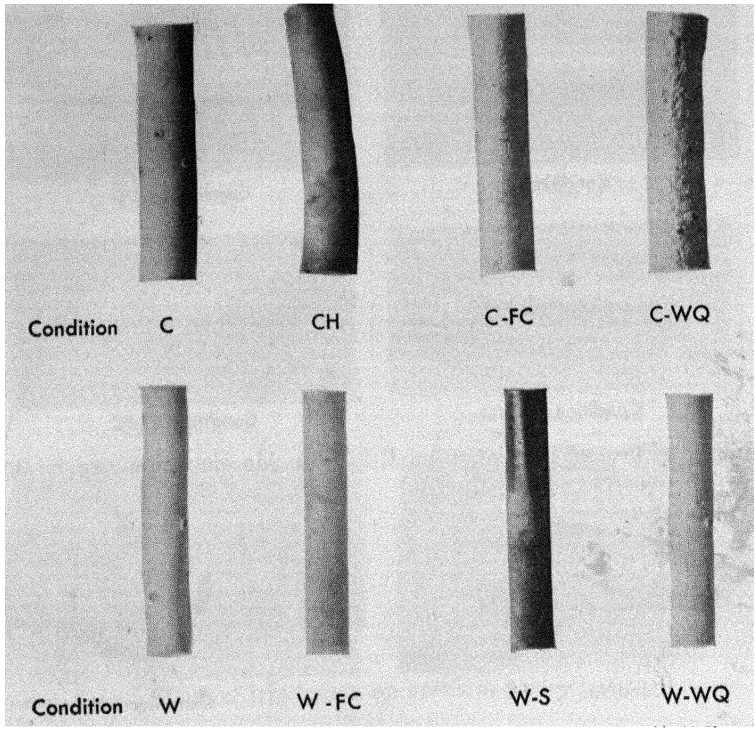

FIG. 3–61. Effect of irradiation on U-5.0 w/o Fs alloy, prepared by different fabrication processes.

fissium are effective in restraining length and volume increases; differences in effectiveness between the two alloys, which appear to be important in certain individual specimens, lose significance when larger numbers of specimens are compared.

(b) No length or volume increases were excessive except with water-quenched specimens.

(c) The effect of a 30-mil axial hole was erratic, appearing to be beneficial in the molybdenum alloys. In the fissium alloys the hole would often collapse along part of its length, resulting in a warping and reduction of diameter. The incidence of this action did not correlate well with temperature of exposure. Additional work on cored specimens is needed, since unsuspected variables appear to be operating in these tests.

(d) The 5 w/o fissium alloy appears to be more stable dimensionally than the 3.17 w/o fissium alloy.

(e) The effect of adding molybdenum over and above the 5 w/o fissium composition appears to be beneficial, but the low burnup values in these specimens make this conclusion subject to further confirmation.

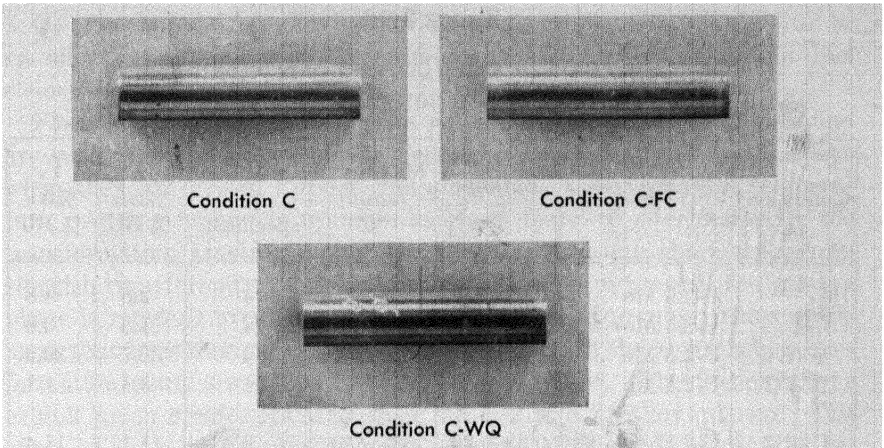

FIG. 3–62. Effect of irradiation on U-5.0 w/o Fs-2.5 w/o Mo alloy, prepared by different fabrication processes.

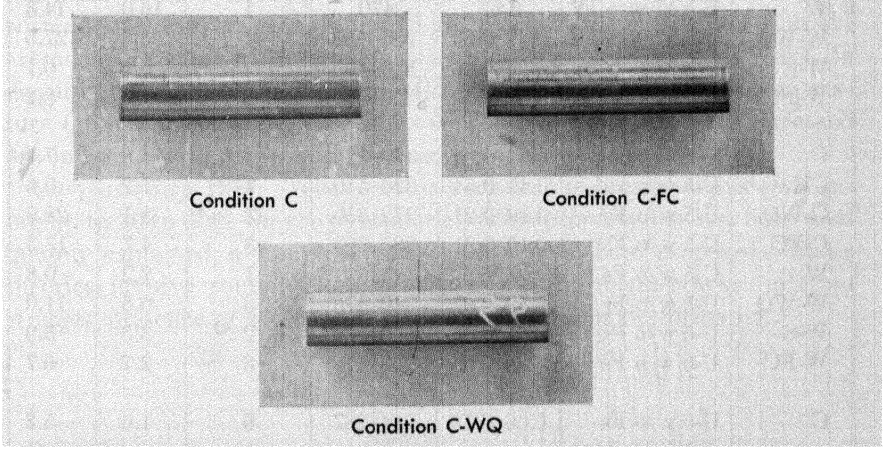

FIG. 3–63. Effect of irradiation on U-5.0 w/o Fs-7.5 w/o Mo alloy, prepared by different fabrication processes.

(f) Water-quenching is detrimental to both cast and wrought shapes.

(g) The extra 7.5 w/o molybdenum seems to have no advantage over the extra 2.5 w/o Mo as an additive to 5 w/o fissium at 0.1% burnup.

(h) Surface roughness appears to be slightly greater for uranium-fissium alloys than for uranium-plutonium-fissium alloys [21], but the former have an advantage of lower brittleness.

(i) Weight and hardness changes are within normal ranges for the postirradiation condition of the specimen; the softer materials show greater hardness increases.

TABLE 3–16

AVERAGE GROWTH AND VOLUME COEFFICIENTS FOR DIFFERENT COMPOSITIONS AND TREATMENTS*

Condition†	Type‡	Burnup, %	Maximum temp., °C	Number of specimens	G, $\%\Delta L$ % BU	V, $\%\Delta V$ % BU
C	U-2.5 Mo	0.42–0.53	568–786	4	2.8	4.8
CH	U-2.5 Mo	0.40–0.53	564–781	4	1.3	3.0
W-WQ	U-2.5 Mo	0.42–0.54	550–761	4	32.7	39.5
W-FC	U-2.5 Mo	0.42–0.56	554–767	4	3.4	4.1
C	U-3.17 w/o Fs	0.33–0.39	535–550	3	11.1	11.4
CH	U-3.17 w/o Fs	0.21–0.72	180–560	5	10.1	8.9
C-WQ	U-3.17 w/o Fs	0.19–0.21	270–374	3	24.4	18.4
C-FC	U-3.17 w/o Fs	0.19–0.20	280–388	3	3.1	17.8
W	U-3.17 w/o Fs	0.67	470	1	16.0	14.3
W-WQ	U-3.17 w/o Fs	0.32–0.69	235–480	4	53.8	27.5
W-S	U-3.17 w/o Fs	0.45–0.66	310–405	2	−0.1	6.1
W-FC	U-3.17 w/o Fs	0.33–0.56	320–480	3	1.2	8.2
C	U-5 w/o Fs	0.32–0.64	450–525	4	1.8	7.7
CH	U-5 w/o Fs	0.41–0.64	310–550	4	7.2	6.6
C-WQ	U-5 w/o Fs	0.19–0.21	272–550	3	8.1	28.9
C-FC	U-5 w/o Fs	0.19–0.21	283–393	3	4.7	13.3
W	U-5 w/o Fs	0.76	535	1	2.2	−0.8
W-WQ	U-5 w/o Fs	0.50–0.67	340–470	3	0.6	11.0
W-S	U-5 w/o Fs	0.41–0.66	460–550	2	3.5	5.9
W-FC	U-5 w/o Fs	0.25–0.56	200–470	3	2.7	6.7
C	U-5 w/o Fs-2.5 w/o Mo§	0.06–0.15	214–287	6	1.6	−5.2
C-WQ	U-5 w/o Fs-2.5 w/o Mo	0.06–0.15	223–296	6	2.4	−2.9
C-FC	U-5 w/o Fs-2.5 w/o Mo	0.06–0.15	225–301	6	2.3	3.7
C	U-5 w/o Fs-7.5 w/o Mo	0.03–0.12	193–256	5	2.8	5.6
C-WQ	U-5 w/o Fs-7.5 w/o Mo	0.03–0.12	224–300	5	0.8	−7.6
C-FC	U-5 w/o Fs-7.5 w/o Mo	0.03–0.12	216–288	5	2.2	3.3

See footnotes on opposing page

(j) The method of alloying for gamma stabilization appears to be an effective way of building considerable stability into uranium fuel elements.

Thermal cycling stability. The transformation kinetics of uranium are such that gross dimensional changes occur in many uranium alloys when they are cycled through the alpha-beta transformation temperature. Adding fissium to uranium has been found to alter markedly the transformation kinetics [25]. The fissium alloys are characterized by sluggish transformations, so that if enough fissium is present, the gamma phase is retained even with slow cooling. Several uranium alloy specimens that were thermal cycled many times through the alpha-beta transformation point are shown in Figs. 3–64 and 3–65. The fissium alloys exhibit much greater stability than the U-2 w/o Zr alloys shown. The effect of restraint by canning on the fissium alloy elements can also be noted by comparing Figs. 3–64 and 3–65.

Full-size EBR-II fuel elements containing cast uranium-5 w/o fissium alloy pins have been thermally cycled 200 times between 50 and 500°C with about 0.25% increase in length and about 0.3% decrease in density; extruded alloy pins increased 0.35% in length and decreased 1.0% in density. When cycled 200 times through the transformation temperature (150 to 700° C), the specimens of U-Pu-Fs cast alloy pins increased 3% in length with a hardness increase from 74 R_A to 81 R_A [26].

Compatibility [27]. When exposed to air, the binary alloys containing up to 20 to 30% Pu are pyrophoric. This property has not been adequately explained, although several theories have been proposed. These theories involve combinations of the effects of micro-cracks, internal stresses, presence of zeta phase, and hydride and oxide formation.

Footnotes for Table 3–16

*Reference 24.

†Conditions: C: as-cast. CH: as-cast, with 0.030″ axial hole. C-WQ: cast, water-quenched from 850°C. C-FC: cast, furnace-cooled from 850°C. W: rolled and swaged to 92% reduction. W-WQ: wrought as above, water-quenched from 850°C. W-S: wrought as above, furnace-cooled 850° to 650°C, held 24 hr and furnace-cooled. W-FC: wrought as above, furnace-cooled from 850°C.

‡See Table 3-15.

§Allowance should be made for low burnups in these series.

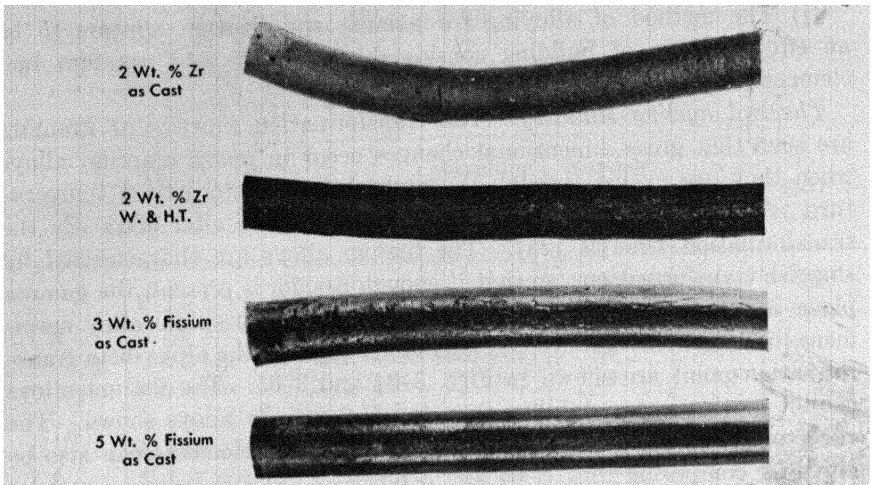

FIG. 3–64. Effect of 200 thermal cycles (100 to 715°C) on U-2 w/o Zr and U-3.5 w/o Fs alloys.

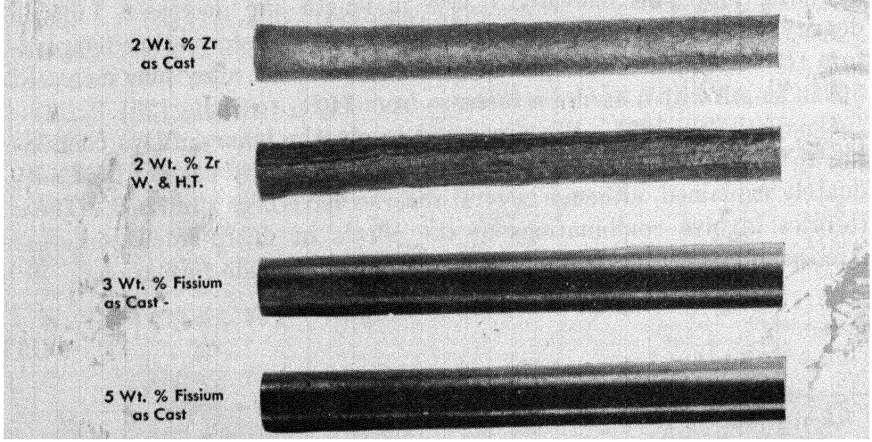

Adding the fissium elements to the U-Pu alloy appears to subdue this pyrophoric property, and fissium alloys have been stored for long periods in glove boxes with a helium atmosphere without any tendency to disintegrate. In this same atmosphere, binary alloys of U-Pu containing over 15 w/o plutonium tend to disintegrate to a powder [28]. Recently, it has been found that U-Pu-Fs alloy specimens are also pyrophoric, after having swelled severely under long-term irradiation [23].

TABLE 3-17

THERMAL EXPANSION COEFFICIENTS AND DENSITIES OF CASTINGS*

Alloy, w/o	Thermal expansion		Densities (R.T.), g/cm³
	Temp. range, °C	Coeff. × 10⁶, °C	
U-20 Pu-5.4 Fs	25–438	17.5	17.6
U-20 Pu-10.8 Fs	20–100	12.4	16.6
	20–500	15.2	
U-20 Pu-5 Mo	25–530	20	17.7
U-15 Pu	25–300	13	18.8
U-5 Fs†	20–100	13.7	17.95
	20–500	16	
Uranium‡	20–100	14.5	19.1
	20–500	18.5	

*Reference 27. †Reference 30. ‡Reference 31.

As in the case of unalloyed uranium, the U-Pu-Fs alloys show negligible tendency to dissolve in, or alloy with, clean sodium or NaK. Numerous tests by Argonne National Laboratory on specimens thermally bonded to their container with NaK and irradiated to various burnups at high temperatures, bear this out.

Studies of the interdiffusion of uranium and stainless steel have shown that diffusion zones are formed at temperatures as low as 500°C [29]. In addition, uranium forms low-melting eutectics with the three main elements in stainless steel: iron, nickel, and chromium. These eutectics melt at temperatures approximately 270 to 400°C lower than the melting point of unalloyed uranium.

Other properties [26]. Addition of plutonium and fissium decreases the density of the cast U-Pu-Fs alloys (Table 3-17 and Fig. 3-66) but does not appreciably affect the hardness, which averages about 70 R_A. The expansion coefficients are shown in Table 3-17 and Fig. 3-67 as a function of temperature. The coefficient increases rapidly up to about 250°C, more slowly between 250 and 500°C, reaching a value of about 19×10^{-6}/°C at 500°C. Above 600°C the expansion coefficient is about 22×10^{-6}/°C.

The expansion curve of an injection-cast U-20 w/o Pu-10 w/o Fs specimen is shown in Fig. 3-67. The transformations are very sluggish, taking 1½ hr to complete the contraction at 500°C and 40 hr to complete the

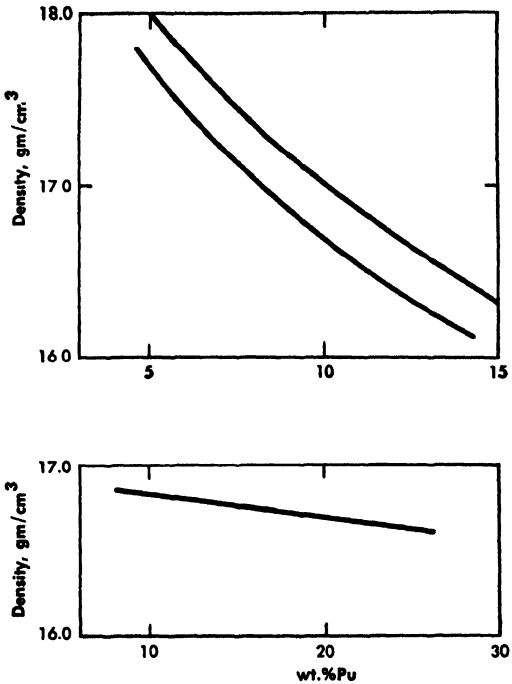

FIG. 3–66. Top: density of U-20 w/o Pu-X alloys with varying Fs content (lower curve) and varying Fs + Mo content (upper curve). Bottom: density of U-Pu-10 w/o Fs alloy with varying Pu content.

contraction at 700°C. After the cast alloy has been homogenized, the only discontinuities in the expansion curve are at 520 and 600°C.

Because of the high thermal performance required of the fast-breeder reactor, thermal conductivity of the fuel is very important. Adding the 10 w/o plutonium and fissium to uranium lowers the thermal conductivity of the element. Saller et al. [30] have shown that the thermal conductivity of U-5 w/o Fs at room temperature is about one-half that of unalloyed uranium. A comparison of thermal conductivity for unalloyed uranium and uranium-5 w/o fissium alloy is given in Table 3–18, and curves of thermal conductivity as a function of temperature for uranium, U-5 w/o Fs and U-20 w/o Pu-10 w/o Fs are shown in Fig. 3–68.

Melting, casting, and fabrication [26]. Most of the alloys have been successfully cast either by top pouring at 1500°C into cold graphite molds or by injection casting at 1150°C into hot Vycor tube molds (Article 3–6.5). The high pouring temperature probably causes contamination of the top-poured alloys, since they are harder than the injection-cast alloys. Thoria crucibles were used at 1500°C, and graphite crucibles, coated with a magnesium zirconate and thoria wash, were used at 1150°C.

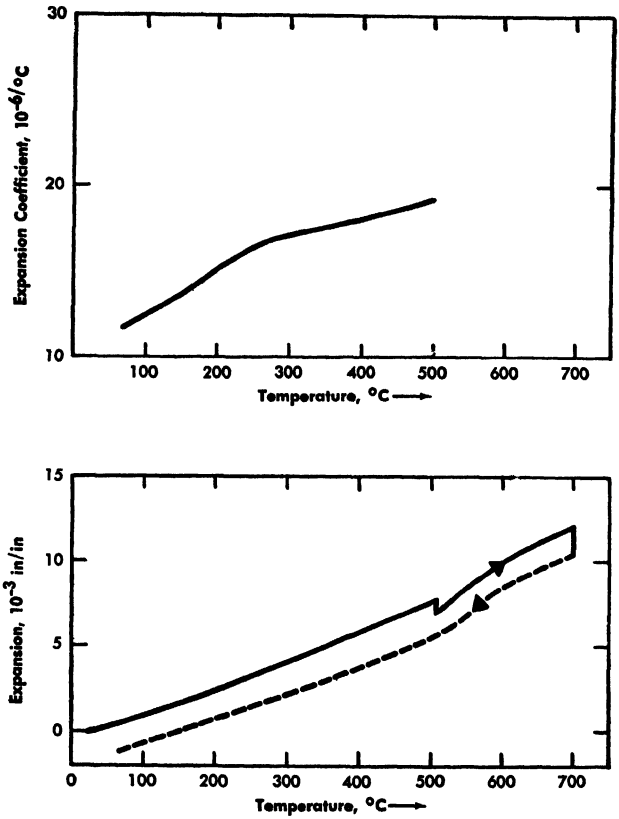

FIG. 3–67. Expansion coefficient and thermal expansion of U-20 w/o Pu-10 w/o Fs as a function of temperature.

Pins of these alloys have also been made by an inverse extrusion method at 500°C (7:1 reduction at 55,000 psi) with a ram speed of 1/4 in/min. This pressure is about four times the pressure required for unalloyed uranium extruded in the same apparatus. The ductility of the U-Pu-Fs alloy is less than that of unalloyed uranium but is sufficient to permit machining and handling; however, ductility is seriously impaired by a 3 w/o Zr addition. Such pins are not machinable and break easily with normal handling.

Structure [26]. The microstructure of an injection-cast, U-20 w/o Pu-10 w/o Fs pin is shown in Fig. 3–69. The principal phases are a primary dendrite phase (white), a partially transformed gamma phase (gray), and a stable gamma phase (white). The resistivity change of the cast pins between 20 and −196°C is characteristic of a largely gamma-phase alloy. An increase in plutonium or fissium increases the

TABLE 3–18

COMPARISON OF THE THERMAL CONDUCTIVITY OF URANIUM-5 W/O FISSIUM WITH UNALLOYED URANIUM*

(cal/(cm²)(sec)°C)

Temp., °C	BMI†	ANL‡	Uranium
20	0.026		0.066
100	0.034		0.068
200	0.044	0.040	0.069
300	0.053	0.048	0.074
400	0.062	0.056	0.081
500	0.071	0.063	0.088
600	0.080	0.071	0.096
700	0.088		0.105
800	0.097		0.115
900	0.125		0.127

*Reference 27.
†Data from Battelle Memorial Institute.
‡Data from Argonne National Laboratory.

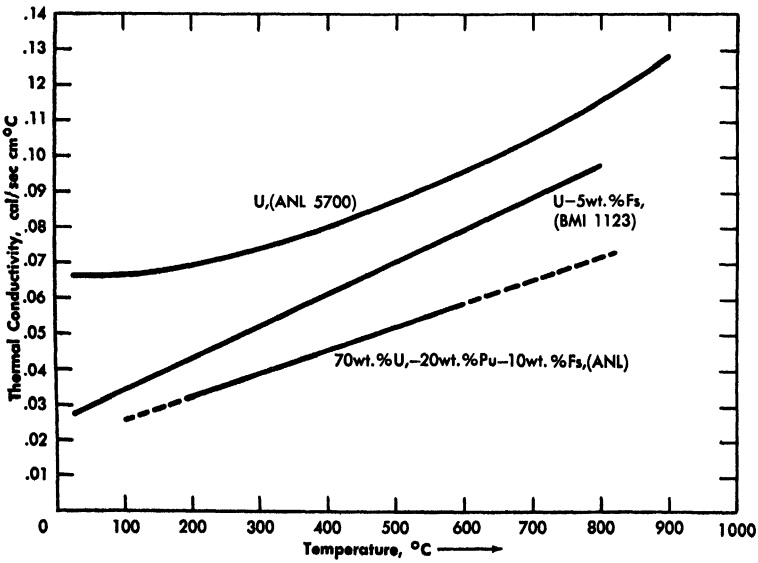

FIG. 3–68. Thermal conductivity of unalloyed uranium, U-5 w/o Fs, [30] and U-20 w/o Pu-10 w/o Fs as a function of temperature. (ANL)

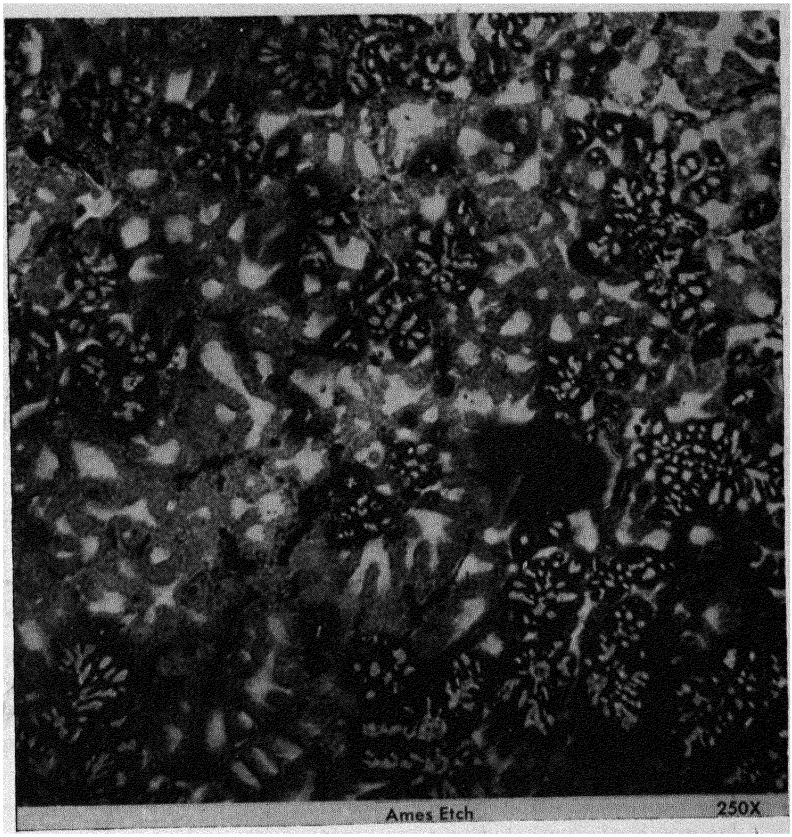

FIG. 3–69. Photomicrograph of cast U-20 w/o Pu-10 w/o Fs alloy pin. The large black area is microporosity.

amount of gamma phase in the cast alloys. After heating the specimen at 700°C for 48 hr, the matrix is homogenized into a single gamma phase, but the primary phase is not dissolved. Transformation of the quenched phase at 500°C is indicated by resistivity measurements and by the slight discontinuity of the thermal expansion curve (Fig. 3–67).

Summary. The uranium-plutonium-fissium, uranium-fissium, and uranium-molybdenum alloys, when stabilized in the gamma phase of uranium, have excellent irradiation and thermal-cycling stability, and reasonably good thermal-expansion characteristics. They can be remotely injection-cast into long, small-diameter pins which resist attack by the liquid sodium bond. A limitation is their poor thermal conductivity (but it is much higher than that of uranium oxide, for example).

3–8.4 Safety. A detailed analysis of the safety of the EBR-II reactor is contained in reference [2]. It is the purpose here to discuss only the

basic approaches which have been taken to the safety problem in the EBR-II design, and to point out the inherent safety characteristics which have resulted.

A safe reactor results not so much from the use of safety devices and special components as from basic safe design principles. In the case of EBR-II, the chief of these principles is that of submerged operation of the primary system, with all components of the primary system and all the primary sodium in a single large tank. This design approach is not the only possible safe one, but it is believed to be one of the better ones. The most important ways in which it promotes reactor safety in design are the following:

(1) All radioactive sodium and sodium that could become grossly contaminated by fission products is contained in a single large tank, which has no penetrations except through the top. The tank is constructed as a double-walled container, and the surrounding shield liner constitutes an effective third container wall. The possibility of leakage of radioactive or contaminated sodium is therefore virtually eliminated in all cases except those postulated to release enough nuclear energy inside the primary tank to breach the primary structure. As a further result of the high degree of integrity of the primary container, loss of coolant is a very remote possibility.

(2) The large heat capacity of the sodium represents a heat sink which greatly diminishes the probability of failure to cool the reactor. It also minimizes the probability of coolant failure by freezing of the sodium in a cool part of the circulating system.

(3) A simple containment structure can be built as part of the shield that completely surrounds the primary system. In EBR-II this primary containment structure is calculated to be capable of withstanding an explosive energy release inside the primary tank equivalent to at least 300 lb of TNT. A nuclear accident would therefore not result in sodium dispersion to the atmosphere of the reactor building unless the nuclear energy release exceeded the 300 lb TNT equivalent. Such an accident is believed highly improbable.

(4) The large mass of sodium surrounding the reactor vessel would provide an important degree of energy absorption in the event of a nuclear accident. Furthermore, the large free surface of sodium in the primary tank reduces greatly the magnitude of destructive pressure which could be propagated upward in the event of such an accident.

In addition to the primary containment structure, the reactor building shell constitutes a secondary gastight containment system, designed for an internal static pressure of 24 psig. Such a pressure could conceivably arise only from an accident which would breach the primary containment system and disperse sodium into the building atmosphere, where it would

burn. On the basis of sodium-air reaction experiments [32], it is estimated that ejection of some 3000 lb of sodium from the primary system, with highly efficient dispersion, would be required to produce an internal pressure of 24 psig. A considerably larger amount of sodium would be required if a more realistic degree of dispersion were assumed.

The advantages of the submerged design in maintaining cooling are supplemented in the EBR-II by thorough attention to providing coolant circulation in all conceivable situations. The primary circuit employs two main circulating pumps, operating in parallel, to reduce the effects of an individual failure. If both primary circulating pumps completely fail, more than adequate shutdown cooling is provided by the auxiliary electromagnetic pump which is in series with the main circulating pumps and which has an independent power source consisting of storage batteries. For all except the most unusual cases, adequate shutdown cooling would be provided by natural circulation of the primary coolant even if all pumps failed. Should the secondary heat-removal system fail, the natural convection coolers are adequate to cool the primary sodium under all conceivable shutdown conditions.

Finally, in the design of the reactor proper, all the usual good safety design practices are followed. In addition, careful attention is paid to avoiding undesirable power coefficients of reactivity that might result from the thermal distortion of fuel elements or fuel assemblies. Such distortion, or bowing, is uniquely troublesome in the fast reactor system. This sensitivity results from the characteristic high compression coefficient of reactivity of fast reactors, and from the circumstance that no massive structural parts can be used in the core. In the EBR-II this problem is attacked by a design that provides a rather high degree of restraint for the fuel subassemblies, restrains the individual fuel elements within the subassemblies, and supports the subassemblies in such a way that the residual bowing that does occur leads to a reactivity decrease (instead of a reactivity increase) with increasing power, over the important part of the power range of the reactor.

References

1. H. V. Lichtenberger et al., Operating Experience and Experimental Results Obtained from an NaK-Cooled Fast Reactor, in *Proceedings of the International Conference on the Peaceful Uses of Atomic Energy*, Vol. 3. New York: United Nations, 1956. (P/813, p. 345)

2. L. J. Koch, et al., *Experimental Breeder Reactor II (EBR-II); Hazard Summary Report*, USAEC Report ANL-5719, Argonne National Laboratory, May 1957.

3. L. J. Koch et al., Construction Design of EBR-II: An Integrated Unmoderated Nuclear Power Plant, paper prepared for the Second International Conference on the Peaceful Uses of Atomic Energy, Geneva, 1958. (P/1782)

4. J. H. Schraidt et al., Pyrometallurgical Processing: Economics and Proposed Engineering Applications, in *Symposium on Reprocessing of Irradiated Fuels Held at Brussels, Belgium, May 20–25, 1957*, USAEC Report TID-7534, Argonne National Laboratory, 1957. (Book 2, pp. 748–804)

5. H. M. Feder, The Chemistry of Pyrometallurgical Processes: A Review, in *Symposium on Reprocessing of Irradiated Fuels Held at Brussels, Belgium, May 20–25, 1957*, USAEC Report TID-7534, Argonne National Laboratory, 1957. (Book 2, pp 667–718)

6. H. M. Feder, Pyrometallurgical Processing of Nuclear Materials, in *Proceedings of the International Conference on the Peaceful Uses of Atomic Energy*, Vol. 9. New York: United Nations, 1956. (P/544, p 586)

7. E. E. Motta, High Temperature Fuel Processing Methods, in *Proceedings of the International Conference on the Peaceful Uses of Atomic Energy*, Vol 9 New York: United Nations, 1956. (P/542, p. 596)

8. L. Burris et al., Developments in Melt Refining of Reactor Fuels, paper prepared for the Second International Conference on the Peaceful Uses of Atomic Energy, Geneva, 1958. (P/538)

9. K. F. Smith and L. R. Kelman, *Irradiation of Cast Uranium-Plutonium Base Alloys*, USAEC Report ANL-5677, Argonne National Laboratory, May 1957.

10. K. F. Smith, *Irradiation of Uranium-Fissium Alloys and Related Compositions*, USAEC Report ANL-5736, Argonne National Laboratory, September 1957.

11. I. O. Winsch and L. Burris, Magnesium Extraction Process for Plutonium Separation from Uranium, in *Proceedings of the Second Nuclear Engineering and Science Conference, Vol. 1, Advances in Nuclear Engineering* New York: McGraw-Hill Book Company, Inc., 1957. (pp. 168–175)

12. E. Motta et al., Pyrometallurgical Processes: Process and Equipment Development, in *Symposium on Reprocessing of Irradiated Fuels Held at Brussels, Belgium, May 20–25, 1957*, USAEC Report TID–7534, Atomics International, North American Aviation, Inc., 1957. (Book 2, pp. 719–747)

13. J. Knighton et al., Argonne National Laboratory, 1957. Unpublished.

14. J. Knighton et al., The Use of Zinc in Pyrometallurgical Reprocessing of Reactor Fuels, paper presented at the Third Annual Meeting of the American Nuclear Society, Pittsburgh, Pa., June 1957.

15. H. M. Feder and R. J. Teitel, Purification of Reactor Fuels and Blankets by Crystallization from Liquid Metal Solvents, paper prepared for the Second International Conference on the Peaceful Uses of Atomic Energy, Geneva, 1958. (P/540)

16. G. J. Bernstein et al, Design for a Remotely Operated Facility for High Temperature Processing of Spent Reactor Fuels, paper presented at the Fourth Nuclear Engineering and Science Conference Held in Chicago, Ill., March 17–21, 1958. (To be published by American Institute of Chemical Engineers)

17. D. C. HAMPSON et al., Equipment for Purification of Spent Reactor Fuel by Melt Refining, paper presented at the Fourth Nuclear Engineering and Science Conference Held in Chicago, Ill., March 17–21, 1958. (To be published by American Institute of Chemical Engineers)

18. J. H. KITTEL and S H. PAINE, Argonne National Laboratory, 1956. Unpublished.

19. J. E. KEMME, Argonne National Laboratory, 1956. Unpublished.

20. J. H. KITTEL and S. H. PAINE, Effects of High Burnup on Some Cast Uranium-Zirconium Alloys, paper presented at the Second Winter Meeting of the American Nuclear Society, New York, 1957.

21. K F SMITH and L. R. KELMAN, *Irradiation of Cast Uranium-Plutonium Base Alloys*, USAEC Report ANL-5677, Argonne National Laboratory, May 1957.

22 J. H KITTEL and L. R. KELMAN, *Effect of Irradiation on Some Uranium-Plutonium Alloys*, USAEC Report ANL-5706, Argonne National Laboratory, 1958.

23. J. H. KITTEL, Argonne National Laboratory. Unpublished.

24 K. F. SMITH, *Irradiation of Uranium-Fissium Alloys and Related Compositions*, USAEC Report ANL-5736, Argonne National Laboratory, September 1957.

25. H. H. CHISWIK et al., Advances in Uranium and Uranium Alloys, paper prepared for the Second International Conference on the Peaceful Uses of Atomic Energy, Geneva, 1958

26. R J. DUNWORTH and L. R KELMAN, Argonne National Laboratory, personal communication, 1958.

27. L R. KELMAN, Argonne National Laboratory, 1957. Unpublished.

28. L. R. KELMAN et al, *The Safe Handling of Radioactive-Pyrophoric Materials*, USAEC Report ANL-5509, Argonne National Laboratory, December 1955.

29. J. H. KITTEL and S. H. PAINE, *Effects of High Burnup on Natural Uranium*, USAEC Report ANL-5539, Argonne National Laboratory, May 1957.

30. H. A SALLER et al., *Properties of a Fissium-Type Alloy*, USAEC Report BMI-1123, Battelle Memorial Institute, Aug. 3, 1956.

31. L. J KOCH et al., Engineering Report on EBR-II, USAEC Report ANL-5788, Argonne National Laboratory, 1958. (To be published)

32. J. R HUMPHREYS, Jr, Sodium-Air Reactions as They Pertain to Reactor Safety and Containment, paper prepared for the Second International Conference on the Peaceful Uses of Atomic Energy, Geneva, 1958. (P/1893)

TABLE 3–1

PERFORMANCE AND DESIGN DATA FOR THE EXPERIMENTAL BREEDER REACTOR II

General description

Reactor type: fast neutron, unmoderated, heterogeneous
Fuel type: enriched uranium or plutonium
Fuel composition: fissium alloy
Blanket composition: depleted uranium
Heat-transfer systems: primary, sodium; secondary, sodium; tertiary, steam

General plant performance

Net electric power, Mw	16.5
EBR–II internal power needs, Mw	3.5
Gross electric power, Mw	20.0
Net plant efficiency, %	26.4
Net cycle heat rate, Btu/kwh	12,900
Reactor thermal power, Mw	62.5
Initial conversion ratio, Pu atoms produced per U^{235} atom destroyed	1.10–1.15

General reactor core characteristics

Total loading (enriched U-fissium), kg	363
U^{235} enrichment, w/o	49
Critical mass (U^{235}), kg	170
Maximum heat flux, Btu/(ft^2)(hr)	1.03×10^6
Average heat flux, Btu/(ft^2)(hr)	0.68×10^6
Average power density, Mw/liter	0.89
Average specific power (total uranium), Mw/metric ton	154
Total neutron flux (core center), n/(cm^2)(sec)	3.7×10^{15}

Fuel composition

Composition of reference fissium alloy *A*	Weight percent
Uranium	95.0
Plutonium	—
Zirconium	0.2
Molybdenum	2.5
Ruthenium	1.5
Rhodium	0.3
Palladium	0.5

(*continued*)

Composition of reference fissium alloy *B*	
Uranium	69.2
Plutonium	20.0
Zirconium	0.5
Molybdenum	2.8
Ruthenium	4.3
Rhodium	0.7
Palladium	2.5

Fertile blanket material	
Total blanket loading kilograms (depleted uranium), kg	28,100

Reactor data	
Core dimensions:	
Equivalent diameter, in.	19.04
Height, in.	14.22
Total volume, liters	66.3
Upper and lower blanket dimensions:	
Equivalent diameter, in.	19.04
Length (each end), in.	18.00
Inner blanket dimensions:	
Equivalent OD, in.	27.46
Length, in.	55.0
Radial thickness, in.	4.21
Outer blanket dimensions:	
Equivalent OD, in.	61.5
Length, in.	55.0
Radial thickness, in.	17.02
Core composition:	
Fuel alloy, vol. %	31.8
Stainless steel (type-304), vol. %	19.5
Sodium, vol. %	48.7
Control and safety rod composition (fuel sections):	
Fuel alloy, vol. %	21.3
Stainless steel (type-304), vol. %	20.8
Sodium, vol. %	57.9

(*continued*)

Upper and lower blanket composition:	
Uranium (depleted), vol. %	32
Stainless steel (type-304), vol. %	20.4
Sodium, vol. %	47.6
Inner and outer blanket composition:	
Uranium, vol. %	60
Stainless steel (type-304), vol. %	17.6
Sodium, vol. %	22.4

Subassemblies	
Core	47
Control (rod and thimble)	12
Safety (rod and thimble)	2
Inner blanket	66
Outer blanket	510
Total subassemblies	637
Configuration	Hexagonal
Dimension across flats, in.	2.290
Hexagonal tube thickness, in.	0.040
Structural material, stainless steel	Type 304
Lattice spacing (pitch), in.	2.320
Clearance between subassemblies, in.	0.030
Subassembly elements (pin-type, sodium bonded)	
Fuel elements:	
Fuel pin diameter, in.	0.144
Fuel pin length, in.	14.22
Fuel tube OD, in.	0.174
Fuel tube wall thickness, in.	0.009
Thickness Na bond annulus, in.	0.006
Elements per subassembly	91
Upper and lower blanket elements:	
Blanket pin diameter, in.	0.3165
Blanket pin length (total), in.	18
Blanket tube OD, in.	0.376
Blanket tube wall thickness, in.	0.022
Thickness Na bond annulus, in.	0.008
Blanket elements per subassembly (each end)	19
Control and safety elements:	
Fuel-element geometry	same as core assembly
Elements per subassembly	61

(*continued*)

Inner and outer blanket elements:	
Blanket pin diameter, in.	0.433
Blanket pin length (total), in.	55
Blanket tube OD, in.	0.493
Blanket tube wall thickness, in.	0.018
Thickness Na bond annulus, in.	0.012
Blanket elements per subassembly	19

Physics data

Total fission/(cm^3)(sec) at center of core	4.4×10^{13}
Neutron energy distribution at center of core:	
Flux above 1.35 Mev, n/(cm^2)(sec)	0.8×10^{15}
Flux below 1.35 Mev, n/(cm^2)(sec)	2.9×10^{15}
Prompt neutron lifetime, sec	8×10^{-8}
Power coefficients:	
0 to 27 Mw, $(\Delta k/k)$/Mw	-2.1×10^{-5}
27 to 62.5 Mw, $(\Delta k/k)$/Mw	-4.2×10^{-5}
Doppler effect (average), $(\Delta k/k)$/°C	$+0.04 \times 10^{-5}$
Isothermal temperature coefficient, $(\Delta k/k)$/°C	-3.6×10^{-5}
Long-term reactivity effects (from clean to 2% burnup):	
Burnup of U^{235} in core, $\Delta k/k$	−0.02
Buildup of Pu in core, $\Delta k/k$	+0.002
Buildup of Pu in blanket, $\Delta k/k$	+0.0072
Buildup of fission products, $\Delta k/k$	−0.002
Irradiation growth of fuel (4% growth), $\Delta k/k$	−0.011

Reactor control data

Total reactivity worth:	
12 Control rods, $\Delta k/k$	0.05
2 Safety rods, $\Delta k/k$	0.015
Control rod:	
Total	12
Operating drive (each rod)	Rack and pinion
Velocity, in./min	5
Total movement, in.	14
Scram drive	Pneumatic

(*continued*)

Safety rod:	
Total	2
Operating drive	Rack and pinion
Velocity, in./min	2
Total movement, in.	14
Scram drive	Gravity

Heat-transfer data

Heat generation in reactor:	
Core, control and safety subassemblies, Mw	53.3
Upper and lower blanket, Mw	1.2
Inner blanket, Mw	5.2
Outer blanket, Mw	2.6
Neutron shield, Mw	0.2
Heat generation in core:	
Radial maximum to average power density at reactor center plane, ratio	1.33
Axial maximum to average power density at reactor centerline, ratio	1.17
Power density, average, Mw/liter	0.89
Power density, maximum, Mw/liter	1.37
Power density, maximum to average, ratio	1.53
Fuel elements, surface area, ft^2	231
Control elements, surface area (in active zone), ft^2	32.4
Safety elements, surface area, ft^2	6.6
Total surface area, ft^2	270
Maximum heat flux, Btu/(ft^2)(hr)	1,030,000
Average heat flux, Btu/(ft^2)(hr)	680,000
Primary sodium temperature, to reactor, °F	700
Primary sodium temperature, from reactor, °F	900
Primary sodium flow rate through reactor, gpm	8,200
Primary sodium maximum velocity in core, fps	26
Primary system sodium capacity, gal	88,000
Secondary sodium temperature to heat exchanger, °F	610
Secondary sodium temperature from heat exchanger, °F	880
Secondary sodium flow rate, gpm	6,050
Steam generator:	
Output, lb/hr	249,000
Steam temperature, °F	850
Steam pressure, psig	1,310
Feedwater temperature, °F	550
Turbine throttle conditions:	
Steam flow, lb/hr	199,000
Steam temperature, °F	850
Steam pressure, psig	1,250

CHAPTER 4

THE ENRICO FERMI ATOMIC POWER PLANT*

4–1. Introduction

The Enrico Fermi Atomic Power Plant, now under construction near Monroe, Michigan, is a privately financed fast-breeder reactor plant capable of generating 100 Mw net electrical power. At the same time, it can produce more fuel than it consumes. A general view of the plant site is shown in Fig. 4–1.

Three separate organizations, along with the U. S. Atomic Energy Commission, are participating in the Enrico Fermi project. Atomic Power Development Associates (APDA) is responsible for research, development, and design of the nuclear portion of the atomic plant. Power Reactor Development Company (PRDC) is financing and building the reactor facility which it will own and operate. The third organization, the Detroit Edison Company, is building the conventional turbogenerator section of the plant, and will operate it with steam purchased from PRDC. The electrical power generated will be fed into the Detroit Edison system, which serves southeastern Michigan.

An early APDA study showed the liquid-metal cooled, fast power breeder reactor most promising for industrial application. The choice was based on these precepts:

(1) The plant should provide a high cycle efficiency, a requirement met by using a liquid-metal coolant operating at high temperatures.

(2) The coolant should operate at low pressure, to avoid the heavy construction costs of high-pressure systems. It was also met by the use of the liquid-metal coolant.

(3) The plant must breed fuel so that available nuclear fuel supplies can be utilized most effectively. This requirement was met by choosing a fast breeder reactor to convert U^{238} to fuel-grade plutonium. Plutonium can be used more effectively as a fuel in a fast reactor than in a thermal reactor.

(4) The plant must be constructed from inexpensive materials. The choice of a fast reactor favored this objective, since the neutron absorption of most structural materials is insignificant in a fast reactor, but may be prohibitive in a thermal reactor.

---

*Compiled and edited by F. P. Storrer, assigned to Atomic Power Development Associates, Detroit, Mich., under contract with S.E.E.N., Belgium. Except as noted, all figures in this chapter were furnished by APDA.

FIG. 4–1. General view of site for Enrico Fermi Atomic Power Plant.

At the time the reactor type was chosen, it was recognized that the features desired for such a plant would require extensive research and development.

In the construction of the first large-scale plant utilizing new concepts, it is seldom, if ever, possible to achieve all the ultimate objectives. Thus several design compromises were accepted for the Fermi plant. A plot plan of the plant is given in Fig. 4–2. Location of major equipment in the reactor building and in the steam-electric building is shown in Fig. 4–3.

Aqueous reprocessing of fuel was accepted for the first plant, with the realization that fuel cycle economics would be poor, even though cheaper pyrometallurgical methods are basically applicable. Although plutonium is intended for the ultimate fuel, the first plant will use U^{235} because of its more advanced metallurgical development and its greater availability. Only limited reliable information exists on the operation of mechanisms in sodium liquid and sodium vapor; therefore the first plant minimizes the use of mechanisms operating in sodium.

For one year, beginning in February 1959, APDA will operate the primary system of the reactor plant without fuel to confirm its mechanical and hydraulic performance with high-temperature sodium coolant. During this period, full-scale reactor components will be tested under

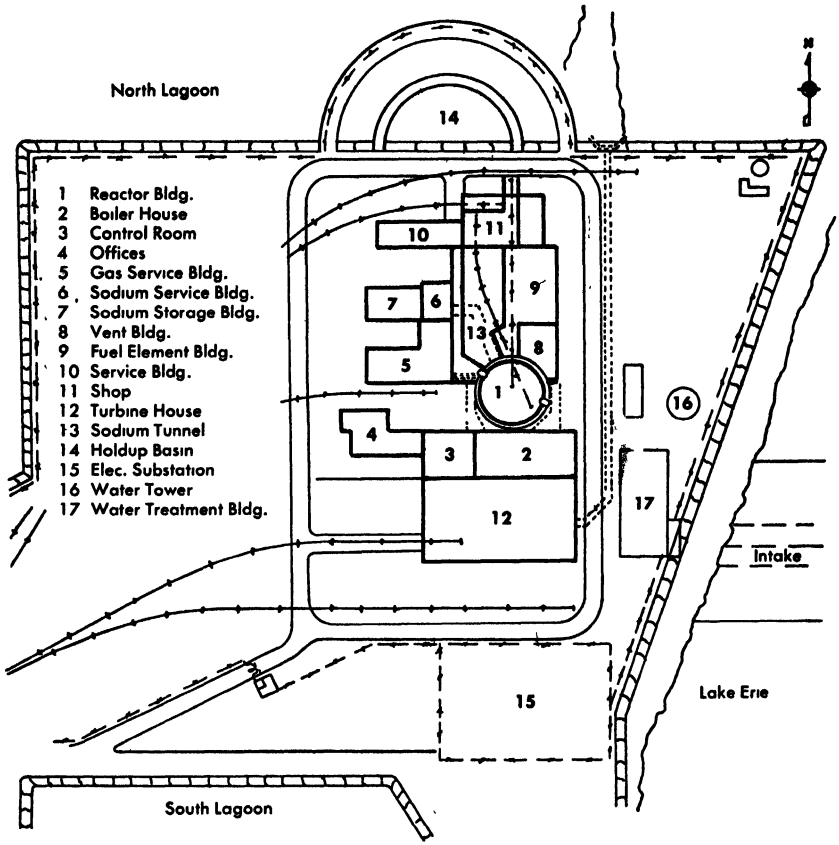

FIG. 4–2. Plot plan of EFAPP arrangement.

operating but non-nuclear conditions. The Enrico Fermi plant is expected to be ready for initial nuclear operation in 1960, at which time PRDC will have complete responsibility for operation of the reactor plant. After several months of nuclear operation at low power, operation at full power will begin. The steam produced will be used by the Detroit Edison Company to generate 100 Mw of electricity. At some later date the power output of the reactor will be raised to produce 150 Mw of electricity, enough electric power to meet the needs of a city with a population of 135,000.

The sponsoring companies making up the membership of APDA and PRDC are financing about $67 million of the total project cost, including all construction and most research and development. The AEC is contributing research and development valued at $4.5 million. Much of the pioneer research and development on sodium-cooled fast reactors in the United States was done by Argonne National Laboratory in the design

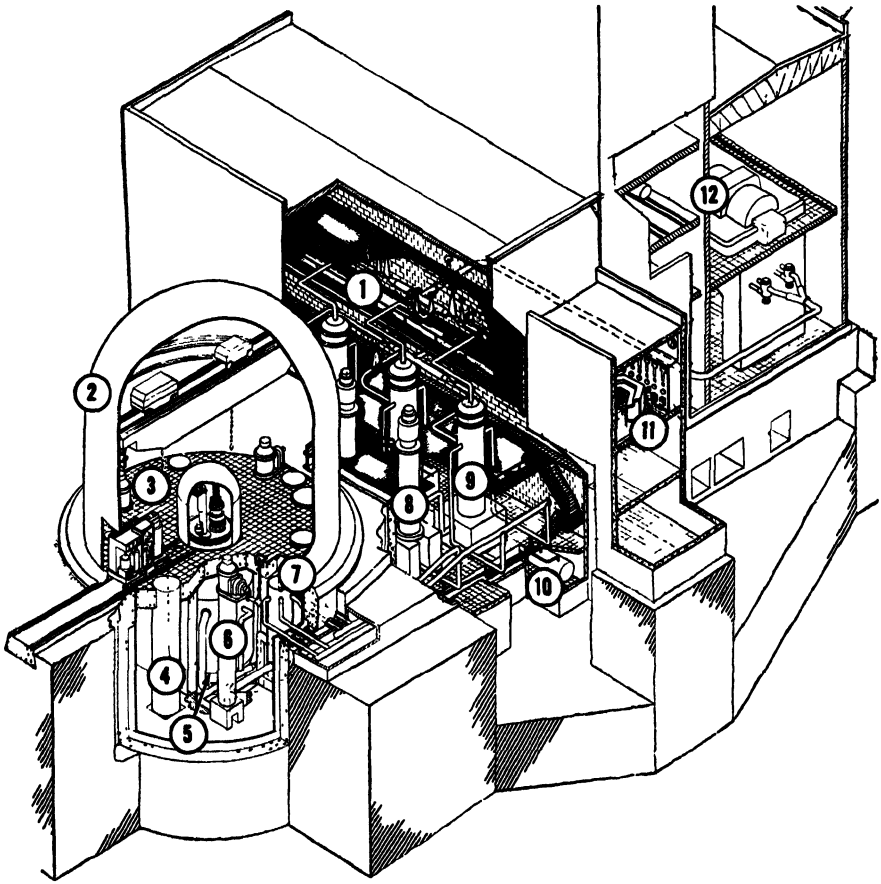

FIG. 4–3. Cutaway drawing of reactor and steam-electric buildings, showing location of major equipment. 1. Steam generator house; 2. Gastight building; 3. Transfer cask car; 4. Primary sodium overflow tank; 5. Reactor; 6. Primary sodium pump; 7. Intermediate heat exchanger; 8. Secondary sodium pump; 9. Steam generator; 10. Secondary sodium dump tank; 11. Control room; 12. Turbogenerator.

of the Experimental Breeder Reactors I and II. The resulting information on sodium technology was heavily drawn upon for the basic design features of the Fermi plant.

The name of the Enrico Fermi Atomic Power Plant was chosen not only because of the outstanding work done by Dr. Fermi in the field of physics, but also because he was among the first to recognize the importance of high utilization of nuclear fuel resources. When the term Fermi Reactor is used in the text, it refers to the reactor portion of Enrico Fermi Atomic Power Plant (EFAPP).

4–2. General Description of the Plant

4–2.1 Core and blanket. A perspective view of the reactor is shown in Fig. 4–4. The core and blanket consist of an assembly of square core and blanket subassemblies arranged to approximate a right circular cylinder about 80 inches in diameter and 70 inches high over-all. The core, containing the enriched fuel alloy, approximates a right circular cylinder 30.5 inches in diameter and 31.2 inches high; it is completely surrounded by the breeder blanket.

The reactor core, shown diagrammatically in Fig. 4–5, is made up of the central portions of 101 subassemblies, 91 of which contain fuel, the remaining 10 being control elements. Fuel is subdivided into a large number of partially enriched uranium alloy pins. The end portions of these 91 subassemblies (the axial blanket), and all the 572 radial blanket subassemblies, consist of uranium alloy that has been depleted in U^{235} and fabricated into cylindrical rods. Plutonium is produced both in the core and in the blanket.

Insertion of boron-containing poison rods in the core provides regulating and safety control. Regulating control is by two boron-containing rods located near the center of the reactor. Eight safety (shutdown) boron rods are situated at about the half-radius of the core. Both core and blanket are cooled by sodium that is pumped into the bottom of the reactor vessel, goes upward through these sections into a large sodium pool, and flows out near the top of the pool.

4–2.2 Fuel-handling mechanisms. Core and blanket subassemblies are loaded and unloaded by an offset handling mechanism mounted in a rotating shield plug, both shown in Fig. 4–4. A hold-down plate below the plug holds the core subassemblies against the pressure drop forces caused by coolant flow through the subassemblies. This plate and the hold-down drive shaft also guide the control element drives. The offset handling mechanism transfers the spent subassemblies to sodium-filled pots in the transfer rotor container, where they decay during the next cycle of operation at power. During the next plant shutdown the spent subassemblies, with their pots, are lifted through the exit pipe into a cask car. The car then carries the spent subassemblies from the reactor building to a decay storage building. In the car, decay heat from the subassemblies and pots is transferred to an inert gas atmosphere which will be circulated through an external heat exchanger that is integral with the cask car. New subassemblies are inserted by the reverse procedure.

4–2.3 Heat transport system. The heat transport system is shown schematically in Fig. 4–6. Heat, removed from the reactor core and

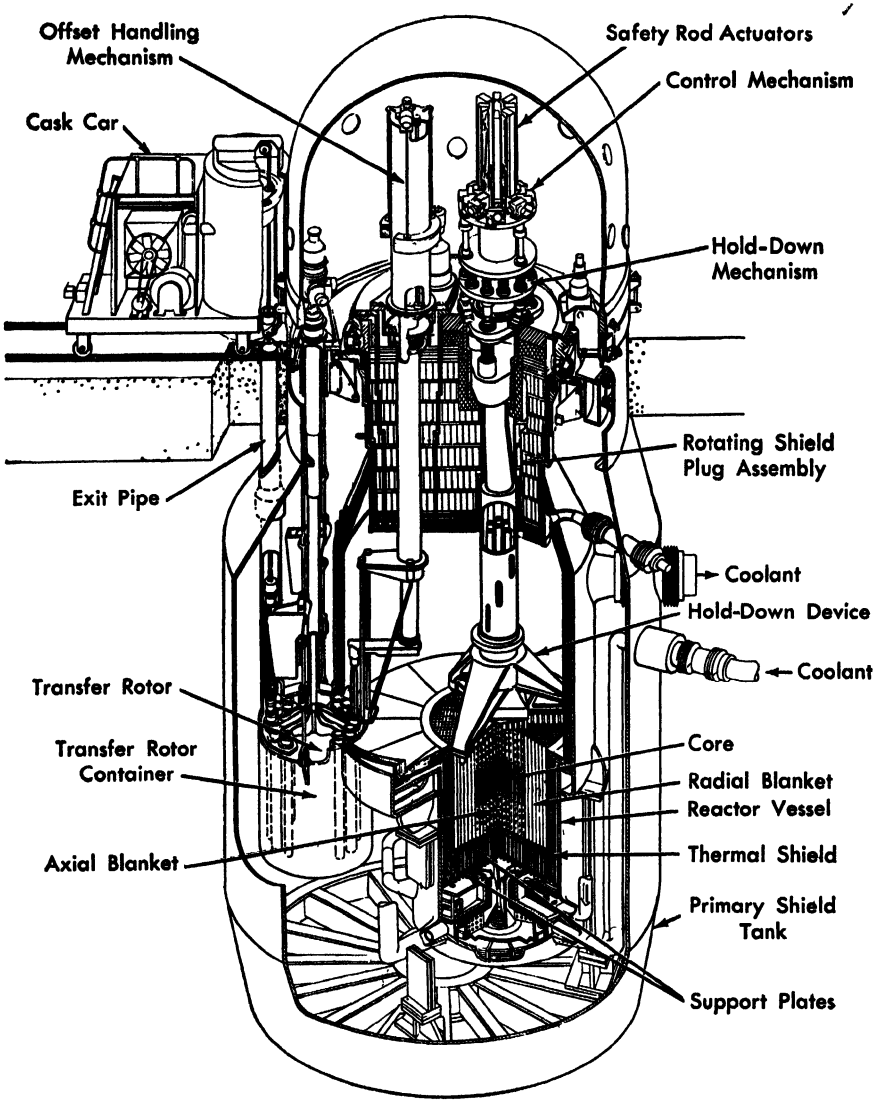

FIG. 4–4. Perspective view of the Enrico Fermi Reactor.

blanket by the primary system sodium coolant, is passed on to the secondary sodium coolant in three parallel intermediate heat exchangers, and finally is transferred to water and steam in three once-through type steam generators. There are three primary coolant loops and three secondary coolant loops.

In both primary and secondary systems, the sodium coolant flow rate is 13,200,000 lb/hr, resulting in an average coolant temperature rise

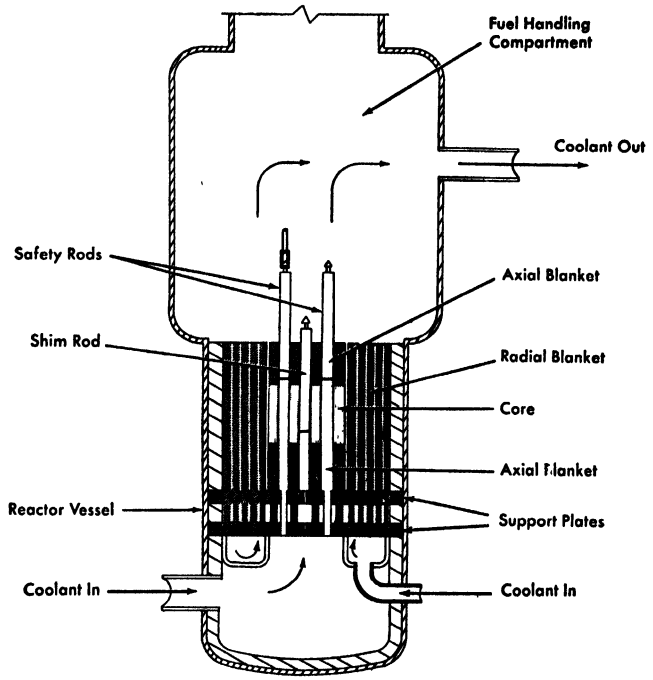

Fig. 4–5. Schematic drawing of the Enrico Fermi Reactor, showing core arrangement and coolant flow paths.

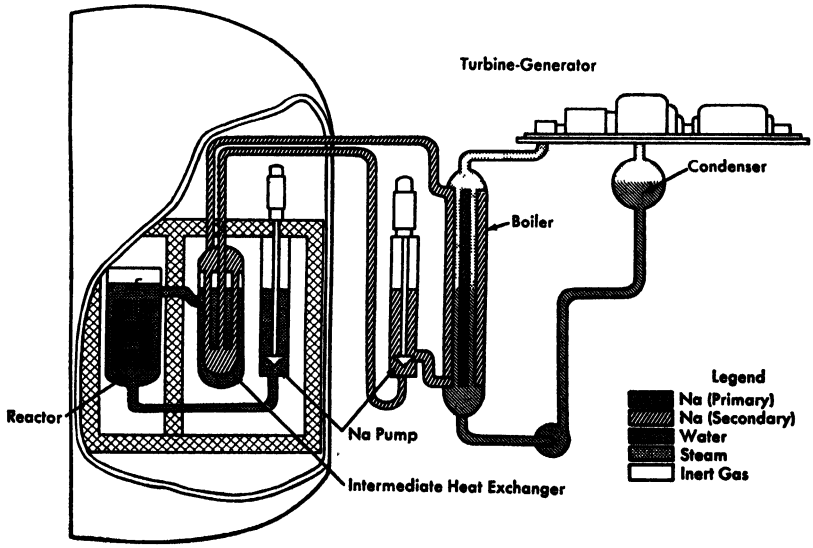

Fig. 4–6. Schematic diagram of the EFAPP heat-transport system, showing primary, secondary, and steam loops.

across the reactor or intermediate heat exchanger of 250°F and a thermal power level of 300 Mw. The primary sodium enters the reactor at 550°F and leaves at 800°F. Table 4–1 (see pages 392–397) summarizes plant performance at the 300-Mw power level.

4–2.4 Shielding and containment. The reactor vessel is completely surrounded by a primary shield tank, as shown in Figs. 4–7 and 4–8. This tank constitutes a fission-product secondary containment vessel. The primary shield consists of a 12-inch stainless steel thermal shield inside the reactor vessel and a 30-inch partially borated graphite shield between the reactor vessel and the primary shield tank. The thermal shield, positioned against the inner wall of the reactor vessel, protects it from radiation damage due to fast neutrons and also absorbs gamma rays, thus reducing heat generation within the vessel walls and the borated graphite.

The partially borated graphite shield is designed to moderate and absorb enough neutrons to avoid serious heating within the steel-lined concrete shield wall (2.6 ft thick) that completely surrounds the primary shield tank. This shield wall divides the lower part of the reactor build-

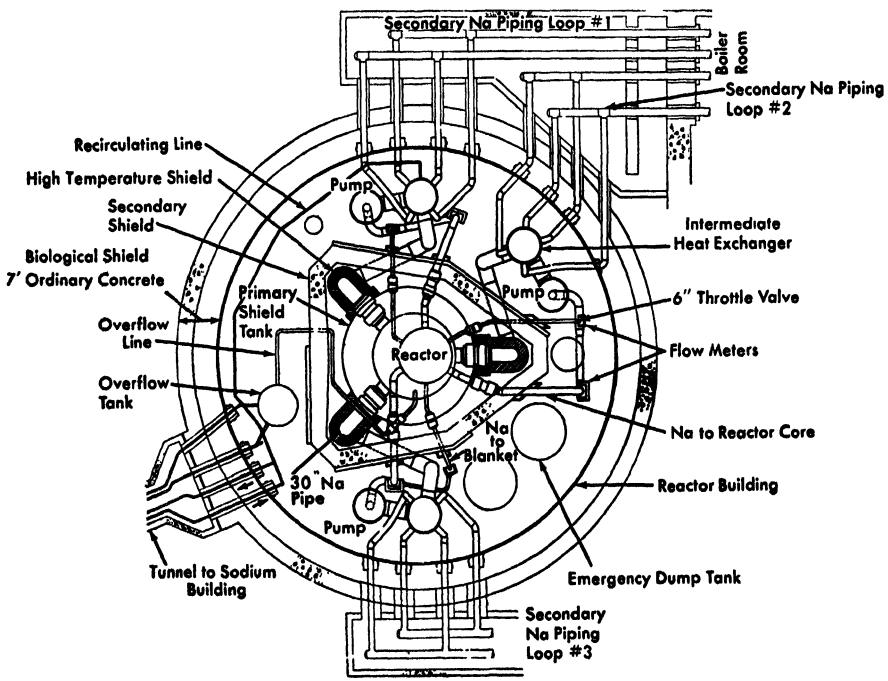

FIG. 4–7. Plan view of the Enrico Fermi Reactor building, below the operating floor.

ing into an inner reactor compartment and an outer equipment compartment. The latter contains all primary coolant system pumps and heat exchangers, as well as decay tanks and other equipment, as shown in Figs. 4–7 and 4–8. The shield is designed to reduce the neutron flux in the equipment compartment to less than $10^4 n/(cm^2)(sec)$ to prevent significant activation of the secondary coolant and the equipment in the outer compartment. The steel lining on both faces of the concrete prevents heating within the concrete due to intense Na^{24} gamma rays from the primary coolant, whose activity level is about 0.05 curie/cm^3.

Neutrons are kept from steaming down the large sodium pipes and into the equipment compartment by installing the greater part of the pipe length within the reactor compartment (i.e., inside the secondary shield), and by enclosing the pipes in a neutron shield. A concrete biological shield wall 7 ft thick is outside the reactor containment building, and a steel and concrete operating floor shield 5 ft thick is above the reactor and equipment compartment to reduce radiation levels to one-third AEC tolerance.

An airtight steel cylindrical reactor building (shown in Fig. 4–7) encloses the reactor, the fuel-handling mechanism, the intermediate heat

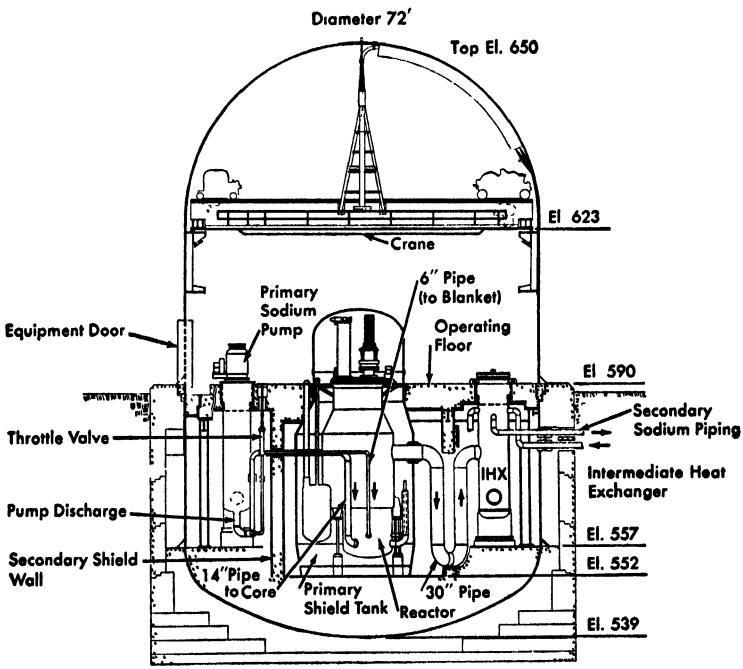

FIG. 4–8. Elevation of the Enrico Fermi Reactor building.

exchangers, and the sodium pumps, piping, and storage tanks. It is 72 ft in diameter and has a wall thickness of 1.125 inches. The purpose of this building is to contain radioactivity from any reactor accident that might release fission products and radioactive sodium. Air in the reactor and equipment compartments below the operating floor is depleted of oxygen to prevent fires in these compartments in case of a sodium leak.

4–2.5 General design considerations. Flexibility has been designed into the system. All mechanisms, including the rotating plug, the subassembly handling mechanism, and the hold-down mechanism, can be removed, as can the control drive, rods, guide tubes, and core subassembly support plates. The core subassemblies and the first row of blanket subassemblies are the same size and, with minor modifications, are interchangeable. Consequently, core size can be adjusted if necessary during initial startup to achieve criticality. Furthermore, after some years of successful operation at design power, the core size can be increased to augment the power output.

The conceptual design of the reactor has been established, and detailed design and fabrication of many of the components have been completed or are well advanced. As noted earlier, the primary system of the reactor plant will be operated without fuel, to check mechanical and hydraulic behavior, starting in February 1959. The nuclear reactor plant is expected to go into operation in 1960.

4–3. Core and Blanket

4–3.1 General considerations. *Physics.* Since the neutron energy spectrum of a fast reactor peaks at a few hundred Kev, and the fission cross section of U^{235} is only a few times greater than the absorption cross section of U^{238} at this energy level, enriched fuel must be used, regardless of the reactor size. This characteristic is illustrated by Fig. 4–9, which shows the regeneration factor,* η, for a mixture of U^{238} and U^{235} as a function of the enrichment, for a range of values of neutron energy and also for the average core spectrum of the Fermi reactor. For a reactor to be critical, the leakage of neutrons must be limited. In a reactor of reasonable size leakage is small only if the macroscopic neutron cross sections are reasonably large. The fact that the microscopic cross sections are small at high neutron energies must be compensated by high volumetric concentration of fuel.

*η is the number of neutrons produced per absorption in fissionable isotope.

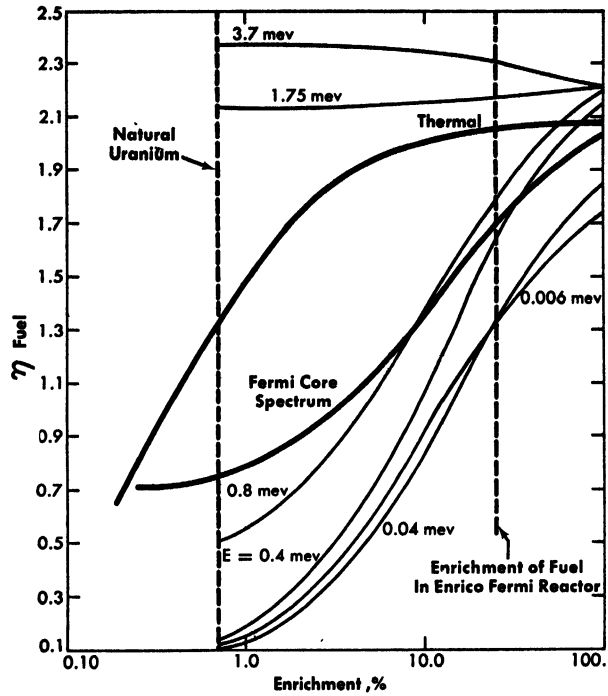

FIG. 4–9. Fuel regeneration factor, η, as a function of enrichment for various energies

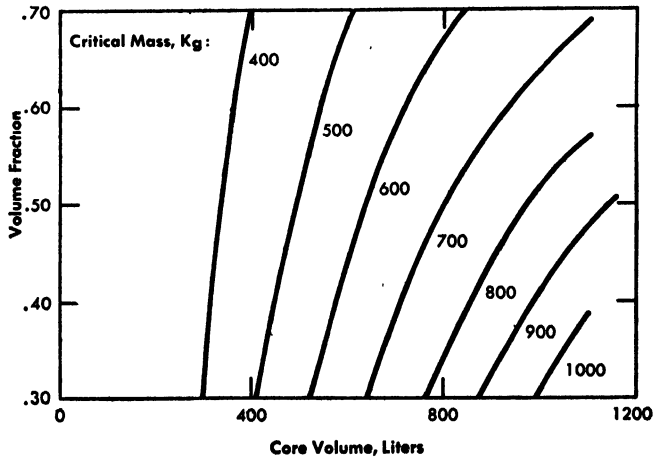

FIG. 4–10. The variation of U^{235} critical mass with core volume and coolant volume fraction.

The combination of high enrichment and high volumetric concentration of fuel means that for a given core volume the critical mass of a fast reactor will be considerably greater than that of a thermal reactor. In the range of practical reactor sizes, critical mass is lowest for the least core volume. High power can be attained from relatively small core volumes in fast reactors because there is no moderator and because the liquid metals used as coolants have excellent heat-removal properties. The variation of critical mass with core volume and coolant volume fraction is illustrated by Fig. 4–10.* Figures 4–11 and 4–12 show corresponding variations of enrichment and conversion ratios.

Core configuration. Determining exact core and fuel element configuration is a complex matter, best accomplished by trial and error, since it involves such widely different but economically and technologically important factors as maximum fuel temperature, steam temperature, coolant velocity, fuel-element fabrication cost, fuel inventory, fuel residence time, reactivity coefficients, and behavior during power transients.

It is useful to outline roughly the logical steps for determining the performance characteristics and the configuration of a fast reactor:

(1) Fuel-element geometry. Various fuel-element geometries are possible. A pin-type fuel element was selected for the Fermi reactor because of the advanced development in fabrication techniques for this shape.

(2) Total coolant cross-sectional area in the core. Coolant temperature rise and coolant velocity should both be large for high power density, but they are limited by other factors, such as thermal shock during power transients and the desire to keep coolant pumping power small. The average coolant temperature rise and velocity were chosen to be 250°F and 30 fps. These values, together with the total core power (roughly 90% of the reactor power, regardless of core size), determine the total cross-sectional area of the coolant passages in the core.

(3) Number and size of fuel elements. Basically, the number and size of fuel elements are determined by the degree of fuel subdivision necessary to achieve the required power density in the core and the required coolant outlet temperature, without exceeding the temperature limitations of the fuel material. Since the hottest point in the fuel is the determining one, it is necessary to take into account the nonuniform spatial distribution of power in the reactor core. In the following discussion it will be assumed that the power density along a fuel element has the shape of a chopped cosine curve. This distribution places the fuel hot spot adjacent to a point of the hottest coolant channel, where

*Based on a spherical model with a constant fraction of extraneous materials and with a standard blanket.

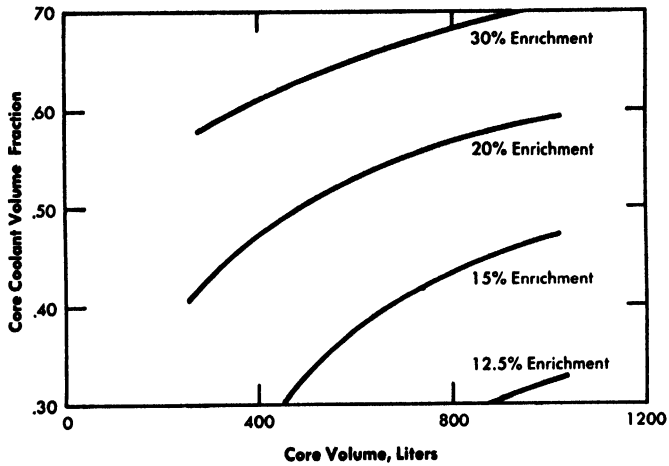

FIG. 4–11. The variation of uranium enrichment with core volume and coolant volume fraction.

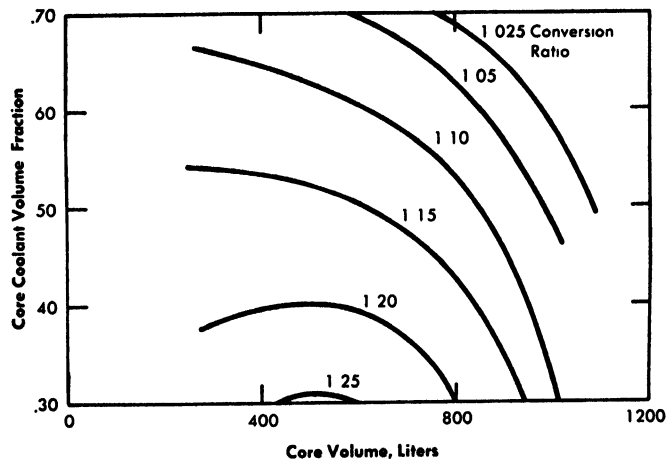

FIG. 4–12. The variation of conversion ratio with core volume and coolant volume fraction.

the temperature rise of the coolant is a fraction α of the total rise in the channel. The coolant temperature rise in the hottest channel is given by $\beta \times 250$, where β is the ratio of maximum to average radial power density in the core and 250°F is the previously selected average coolant temperature rise.

With these assumptions, the maximum fuel temperature T_f in the hottest channel is given by

$$T_f = T_{in} + \alpha\beta 250 + \Delta T_f,$$

where T_{in} is the coolant inlet temperature and ΔT_f is the temperature drop between fuel element hot spot and the adjacent bulk coolant.

Eliminating T_{in} between this expression and the expression for the average outlet coolant temperature:

$$\bar{T}_c = T_{in} + 250,$$

we find

$$\bar{T}_c = T_f - \Delta T_f + 250(1 - \alpha\beta).$$

It is interesting to note that the product $\alpha\beta$ is about unity; the expression for the average coolant outlet temperature therefore becomes, approximately,

$$\bar{T}_c \approx T_f - \Delta T_f.$$

The average outlet temperature of the coolant ($\bar{T}_c$), which essentially determines the steam temperature, should be as high as possible to give high steam cycle efficiency.

Maximum allowable fuel alloy temperature (T_f) is determined by considerations of fuel pin swelling. Because swelling is a function of both temperature and burnup, the fuel alloy temperature is limited to a value compatible with the burnup expected during reactor operation. At present, this temperature is thought to be in the region 1100 to 1300°F for the selected 10 w/o molybdenum fuel alloy.

The need for a high average coolant outlet temperature with a given maximum fuel temperature can best be met by keeping a minimum temperature drop of ΔT_f at the fuel element hot spot. The temperature drop in the fuel alloy, the major part of ΔT_f, is proportional to the power generated per unit length of the fuel element. Hence ΔT_f is nearly proportional to P/nL, where P is the total core power, n is the number of fuel elements, and L is the length of a fuel element. Thus, for high performance, nL, the total length of all fuel elements, should be as large as possible, with due regard for pressure drop and pumping power. On the other hand, fuel-element fabrication cost is probably proportional to nL. A value of nL is chosen as a compromise between these two contradictory requirements. In the Fermi reactor core, nL amounts to almost 33,000 ft. The average coolant outlet temperature is then 800°F, resulting in a steam temperature of 740°F.

The core volume is given approximately by $(A + n\pi r^2)L$, where A is the cross-sectional flow area for coolant and r is the fuel element radius. To minimize the critical mass, the fuel volume should be as small as possible. However, the following restrictions apply:

(1) Radiation damage limits burnup to about 1% of the total number of atoms in the alloy. Hence residence time of the fuel in the reactor is

proportional to the total fuel volume which, therefore, should not be reduced excessively.

(2) Since the coolant cross-sectional area A is fixed, it does not pay to reduce the core volume by reducing the fuel volume excessively. The critical mass can be lessened by reducing the fuel volume, but the breeding ratio decreases and the enrichment increases considerably, as can be seen from Figs. 4–11 and 4–12. Furthermore, to guarantee a negative Doppler coefficient of reactivity, the enrichment should not exceed about 50%. In practice, a coolant volume of about 50% usually proves to be optimum.

(3) If the heat flux, which for constant nL is inversely proportional to r, becomes too large, the temperature drop through the fuel cladding and the film drop are no longer a small fraction of T_f.

(4) Length-to-diameter ratio of core. In the preceding discussion, the length L of the fuel elements (and of the core) appeared only in the combination nL except in the expression for the total coolant volume, AL. Obviously, if one reduces L while keeping nL and A constant, the volume of the core will decrease and, for reasonable values of L, the critical mass will also decrease. Moreover, even for a given core volume and composition, the critical mass is minimum when the length-to-diameter ratio is about 0.9. These considerations favor the choice of a value of L/D somewhat smaller than 0.9. Of course, the diameter of the reactor vessel and the number of fuel elements will increase as L is decreased.

The design data of the Enrico Fermi reactor core are listed in Table 4–1. It can be seen that the number of fuel elements is high indeed ($91 \times 144 = 13{,}104$), and that their radius is quite small; L/D is about 1. However, at a later date the reactor will operate at 430 Mw with 139 subassemblies and the L/D will then be close to 0.8.

Blanket configuration. About 71% of the total plutonium production takes place in the blanket. The production rate decreases rapidly with increasing distance from the core. Beyond a certain radius, the revenue obtainable from plutonium formed in the blanket elements is offset by the costs of adding more elements. This balance sets the economic limit of blanket thickness. In the present design, the radial blanket is about 2 ft thick, and the calculated neutron leakage out of the blanket is about 0.4%. This blanket thickness is somewhat greater than the economic optimum, a deviation in the direction of high technical performance, appropriate in a rapidly developing technology.

The diameter and spacing of the blanket rods were determined by heat removal considerations, with the maximum temperature of the 2.75 w/o molybdenum alloy limited to 1000 to 1150°F. The first row of subassemblies connected with the low pressure (blanket) plenum is the most critical. These subassemblies will be immediately adjacent to the core

when the whole area connected with the high pressure (core) coolant plenum is filled with 139 core subassemblies to give an operating power of 430 Mw. The other blanket subassemblies will be orificed to approach a uniform coolant temperature rise of 250°F. The optimum uranium volume fraction again was found to be approximately 50%.

The upper and lower axial blankets are about 20 inches thick. Their cross-sectional geometry is essentially the same as that of the radial blanket, except that the nine central rods of each subassembly have been left out. This was done to reduce the pressure drop through those subassemblies, to balance axial blanket cost with plutonium revenue, and to prevent the core fuel from freezing in this area in the event of a meltdown.

Size of subassemblies. The outside dimensions of core and blanket subassemblies were chosen equal because they all go through the same handling and transfer processes, and because of geometrical considerations of matching blanket pattern to core pattern.

The outside dimensions of the square stainless steel cans are 2.646 inches on a side by 73½ inches long. They contain either 25 blanket rods or 144 fuel pins (16 blanket rods in the axial blanket). These dimensions were dictated primarily by the following considerations:

(1) The reactivity value of an outer edge core subassembly should not exceed that of a blanket subassembly by more than 30 cents.* This limitation will make possible close adjustment of reactivity during loading, as is required to meet the rigorous limitation on permissible excess reactivity. It is planned that the excess reactivity will not be allowed to exceed 92 cents. Within this limitation, sufficient reactivity must be provided to compensate for the reactivity losses due to burnup, fuel growth, and temperature.

(2) A larger subassembly size would make it much more difficult to dissipate the decay heat in handling or moving a spent core subassembly.

4–3.2 Description of core and blanket. The reactor is an assembly of square-shaped core and blanket subassemblies arranged to approximate a right circular cylinder about 80 inches in diameter and 70 inches high. The core, containing the fuel alloy, is approximately a right circular cylinder 30.5 inches in diameter and 31.2 inches high, and is completely surrounded by a breeder blanket. There are four types of reactor subassemblies, each having external dimensions of 2.646 × 2.646 × 98.625 inches, but containing different nuclear materials. There are 91 core subassemblies that contain U^{235} and U^{238}, 548 radial blanket subassemblies contain-

*One cent = 0.01 dollar of reactivity. A dollar is the reactivity change between delayed critical and prompt critical; in this reactor it is equal to approximately 0.7% k_{eff}.

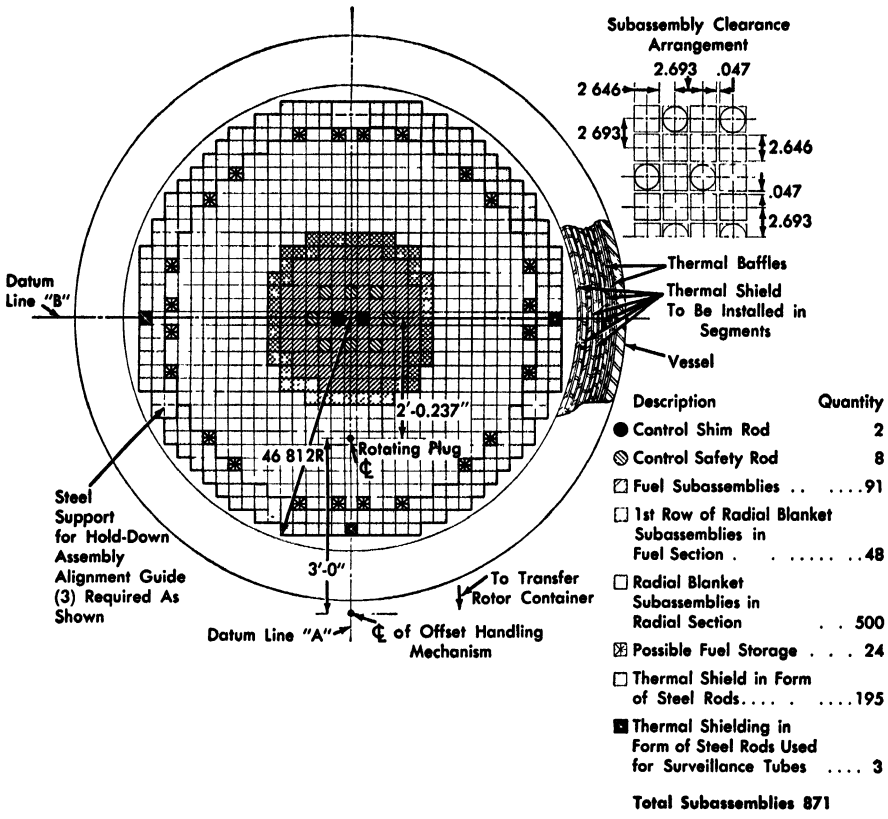

FIG. 4–13. Cross section of the Enrico Fermi Reactor, showing arrangement of subassemblies.

ing depleted uranium, 198 thermal shield subassemblies containing steel, and 10 control subassemblies that house the boron-containing control and safety rods. The arrangement of these subassemblies in the reactor is shown in Fig. 4–13.

Surrounding the 101 core and control subassemblies are 48 inner row blanket subassemblies with identical heads and support sections, which include a preset spring to allow for thermal expansion. Core subassemblies may be substituted for these blanket subassemblies, since they are under the hold-down plate and are cooled by sodium from the high-pressure plenum. Thus, for future operation at higher power levels, there can be as many as 139 core subassemblies. The two central control rods, each with a poison section about 10.25 inches long, are for operating control and will be in the core during operation. The other eight rods are safety rods, positioned above the reactor blanket during normal operation, leaving these positions in the core filled with sodium.

The material in the core and radial blanket subassemblies is subdivided into elements of sizes appropriate for heat-removal requirements. The fuel alloy and the uranium blanket elements are encased to prevent radioactive fission product particles from contaminating the coolant. The sodium coolant is pumped upward through the subassemblies, with 90% of the total flow directed through the core subassemblies.

Description of core subassemblies. A core subassembly consists of an upper and a lower axial blanket section between which the fuel is located. The fuel section contains 144 metallurgically bonded zirconium-clad pins arranged on a square pitch of 0.200 inch. A drawing of the core subassembly is shown in Fig. 4–14, which illustrates, in addition to the fuel and blanket sections, the handling head, self-orienting device, and method of support. The 0.158-inch-diameter fuel pins are clad with 0.005-inch-thick reactor-grade zirconium metallurgically bonded to U-10 w/o Mo fuel alloy. The pins are spaced by stainless steel wires at 2-inch intervals along the length of the fuel section. The lower end of each fuel pin is fixed and the upper end is free to accommodate changes in length resulting from temperature changes or irradiation growth.

Less heat is generated at the periphery of the core than at the center, because of the decreasing neutron flux. In any subassembly, therefore, the wall farthest from the center of the core will be cooler than the wall nearest the center. Because of this temperature difference, the subassembly tends to bow toward the center of the core and thus to reduce the core diameter. Since the subassembly is restrained at the top by the hold-down plate and at the bottom by the support plates, this action would result in compacting the core during a power increase and lead to a positive power coefficient of reactivity. A decrease in diameter is prevented by welding pads to the corners of the square tube at the axial location of maximum free deflection of the subassembly. These pads butt against one another and restrain the subassemblies from bowing inward.

The axial blanket elements are 0.415-inch-diameter, U-2¾ w/o Mo alloy rods in stainless steel tubes, 0.443-inch OD with a 0.010-inch wall. The radial clearance of 0.004 inch between the uranium and the tube is filled with sodium to provide a low-resistance thermal bond. Rods are held in the subassembly and spaced by lugged grids at the bottom and top of each axial blanket section. The center portion of the axial blanket section contains no blanket rods. This will minimize the pressure drop and optimize the plutonium revenue vs. blanket cycle cost. It also assures that melt-down products do not remain in the lower core and blanket section in the improbable event of a reactor melt-down. The seal cladding tube allows for increase in length of the uranium alloy due to thermal expansion and irradiation growth.

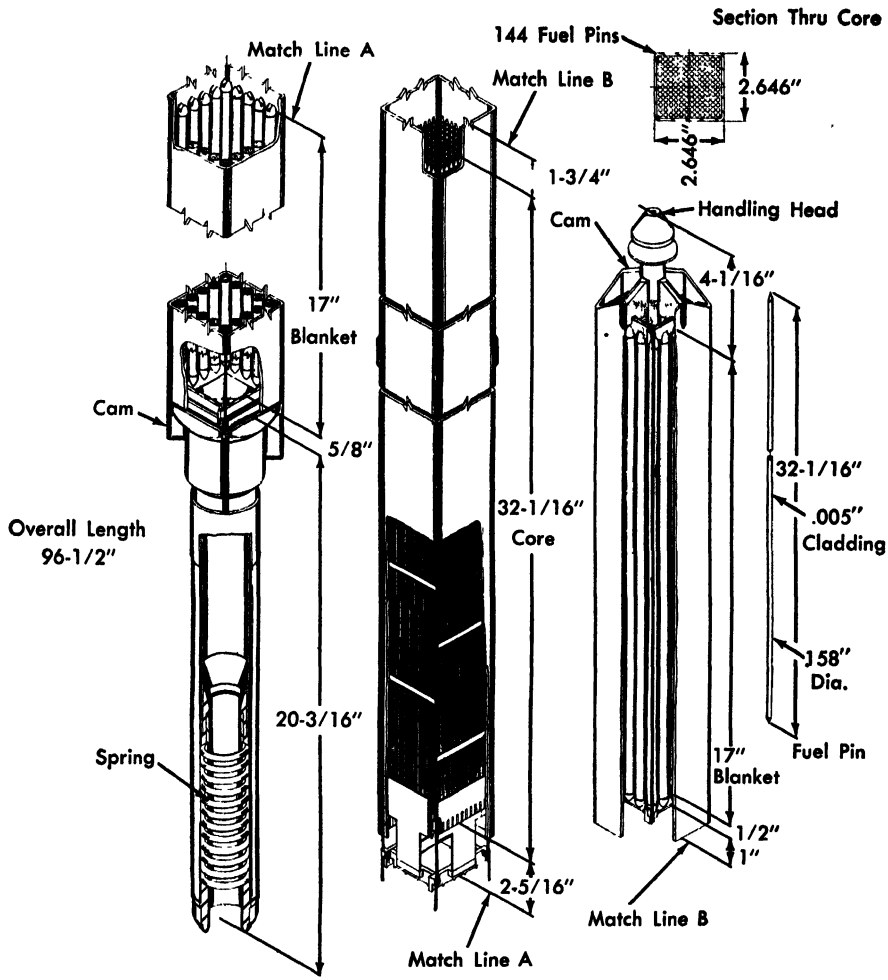

FIG. 4–14. Cutaway drawing of the Enrico Fermi Reactor core assembly.

Description of radial blanket subassemblies. The radial blanket subassemblies have essentially the same external dimensions and features as core subassemblies. Except for length, radial blanket elements have the same dimensions and composition as the axial blanket elements described above. The stainless steel tubes containing the radial blanket elements are 71.5 inches long, and the depleted uranium alloy in each element is 65 inches long. A gas and sodium space, totaling 6.1 inches in length, is provided at the top of each tube to permit growth of the uranium due to thermal expansion and radiation damage. The blanket elements are held in the subassembly much as are the axial blanket sections of the core sub-

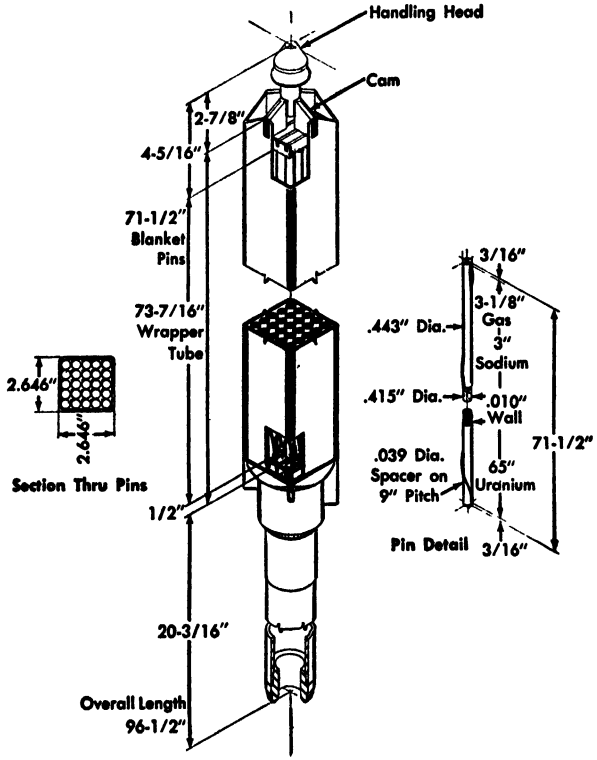

FIG. 4–15. Cutaway drawing of the Enrico Fermi Reactor radial blanket subassembly.

assembly. A removable orifice will be inserted into the lower support plate for each radial blanket subassembly position. An additional orifice will go in the entrance nozzle of the 48 inner row blanket subassemblies to obtain sufficient pressure drop to match the core subassemblies. Individual radial blanket elements are spaced by stainless steel wire wrapped spirally around the cladding tubes. A drawing of the radial blanket subassembly is shown in Fig. 4–15.

Fabrication of fuel and blanket subassemblies. The fuel pin is fabricated by coextrusion of fuel alloy slugs in zirconium tubing. During the coextrusion process, a metallurgical bond is formed between the cladding and the fuel alloy. Final dimensions are obtained with cold-working by rotary swaging. These operations result in 0.158-inch-diameter pins, 12 ft or more in length. These are sheared into 30.5-inch sections, and the ends of each section are pointed by cold swaging. Preformed stainless steel or zirconium caps are slipped over the pointed ends and locked onto the pin by cold-swaging. The stainless steel cap, attached to the bottom end of each pin, is slotted for anchoring. A zirconium cap is attached to the top

end of each pin. Each completed fuel element will receive a stress-relief heat treatment.

The axial and radial blanket elements are alloyed depleted uranium rods canned in stainless steel. The uranium rods are cast or swaged to size, cut to proper lengths, and heat-treated for stress relief. Sodium bonding is accomplished in an inert gas atmosphere by inserting first a slug of solid sodium and then the uranium rods into a stainless steel tube capped at one end. The temperature of the assembled element is then raised and held above the melting point of the sodium. Subsequently, the sodium-bonded blanket element is sealed by welding on the upper end cap. In the case of radial blanket elements, a spiral-wound spacer wire is attached to the stainless steel tube by welding the ends of the wire to the end caps.

Square bundles of 16 axial blanket elements, arranged around the periphery, are placed in cages as the first step in the assembly of a core subassembly. One cage, attached to the bottom of the handling head, forms the upper axial blanket section. A second cage is attached to the top of the support section, to form the lower axial blanket. A cartridge with 144 fuel pins inserted is attached to the top of the lower axial blanket cage. The lower end of the fuel pins is anchored to the cartridge by threading anchor bars through the slotted end caps. Cross wire grids in the cartridge maintain the pins on a square pitch within the cartridge. The upper axial blanket section is inserted into one end of the subassembly wrapper, and the loaded core cartridge with the lower axial blanket section is inserted into the other end of the wrapper. The wrapper is then welded at its ends to the handling head and to the lower support structure to complete the assembly.

The radial blanket subassembly is assembled by inserting a square bundle of 25 radial blanket elements into the square subassembly wrapper. The wrapper is then welded to its handling head and to its lower support structure.

4–3.3 Performance. The reactor is designed for an initial heat output of 300 Mw. With no blanket burnup, 281 Mw are released in the core and 19 Mw in the blanket. With 0.2% average burnup in the blanket (0.5% locally), 265 Mw are released in the core and 35 in the blanket. The total coolant flow rate for no blanket burnup is 12,455,000 lb/hr, resulting in an average coolant temperature rise of 250°F.

Performance characteristics summarized in Table 4–2 are based on no orificing of the core and complete orificing of the radial blanket. The resulting coolant temperature rise in a central core subassembly is about 360°F, while at the outer edge of the core it is about 170°F. Because a high amount of heat is generated in the innermost blanket rods, the blan-

TABLE 4–2

PERFORMANCE DATA FOR CORE AND BLANKET

	Fuel section	Axial blanket section	Radial blanket section
Subassembly dimensions, in.			
Shape	Square	Square	Square
Outside dimension	2.646	2.646	2.646
Inside dimension	2.454	2.454	2.454
Wall thickness	0.096	0.096	0.096
Space between subassemblies	0.047	0.047	0.047
Over-all length	98.625	98.625	98.625
Number of subassemblies	91	182*	548
Element dimensions, in.			
Shape	Round rod	Round rod	Round rod
Clad outside diameter	0.158	0.443	0.443
Clad inside diameter	0.148	0.423	0.423
Uranium diameter	0.148	0.415	0.415
Uranium length	30.5	14	65
Pitch (square)	0.200	—	0.483
Elements per subassembly	144	16	25
Composition, vol. %			
Uranium	27.9	28.3	44.6
Molybdenum	5.8	1.5	2.1
Zirconium	4.9	—	—
Stainless steel	14.2	16.7	18.6
Sodium	47.2	53.5	34.7

*There is an upper and lower section in each fuel subassembly.

ket coolant flow is set to limit coolant temperature rise in the innermost radial blanket subassemblies to about 200°F at 0.5% burnup. A greater temperature rise will be allowed in the outer radial blanket subassemblies to give an average temperature rise across the entire blanket of 250°F. During normal operation, the coolant temperature rise will vary from 160 to 200°F as the plutonium concentration builds up in the innermost blanket subassemblies. In all calculations, allowance was made for gamma-ray heating of the coolant; this effect reduces the temperature drop in the uranium alloy about 1.5%.

Thermal calculations. (1) Heat generation. Power distribution in the core was obtained from two-dimensional computation of the neutron flux

TABLE 4–2 (*Continued*)

	Fuel section		Axial blanket section	Radial blanket section
Thermal performance				
Average blanket burnup, %	0.0%	0.2%	0.2%	0.2%
Total volume, ft^3	11.65	11.65	13	161
Total power, Mw	281	265	5	30
Heat-transfer surface, ft^2	1378	1378	444	9250
Average heat flux, Btu/(ft^2)(hr)	696,000	656,000	35,700	11,100
Maximum heat flux, Btu/(ft^2)(hr)	1,200,000	1,135,000	—	447,000
Maximum/average heat flux, ratio	1.73	1.73	—	40
Coolant flow rate, lb/hr	12,455,000	11,750,000	11,750,000	31,600‡
Coolant velocity, fps	32.1	30.3	27.4	10.7‡
Entrance nozzle pressure loss, psi	9	8	—	61‡
Fuel section pressure loss, psi	58	52	—	—
Blanket section pressure loss, psi	11	10	—	9‡
Subassembly pressure loss, psi	78	70	—	70‡
Coolant inlet temperature, °F	550	550	550 (lower) 800 (upper)	550
Average coolant temperature rise, °F	250	250		250
Average coolant outlet temperature, °F	800	800	550 (lower) 800 (upper)	800
Maximum coolant temperature, °F†	1010	—	1038	860
Maximum clad temperature, °F†	1055	—	1040	860
Maximum uranium temperature, °F†	1316	—	1131	1119

†These temperatures include hot-channel factors.

‡These conditions are for an inner blanket subassembly and include an orifice in the entrance nozzle section.

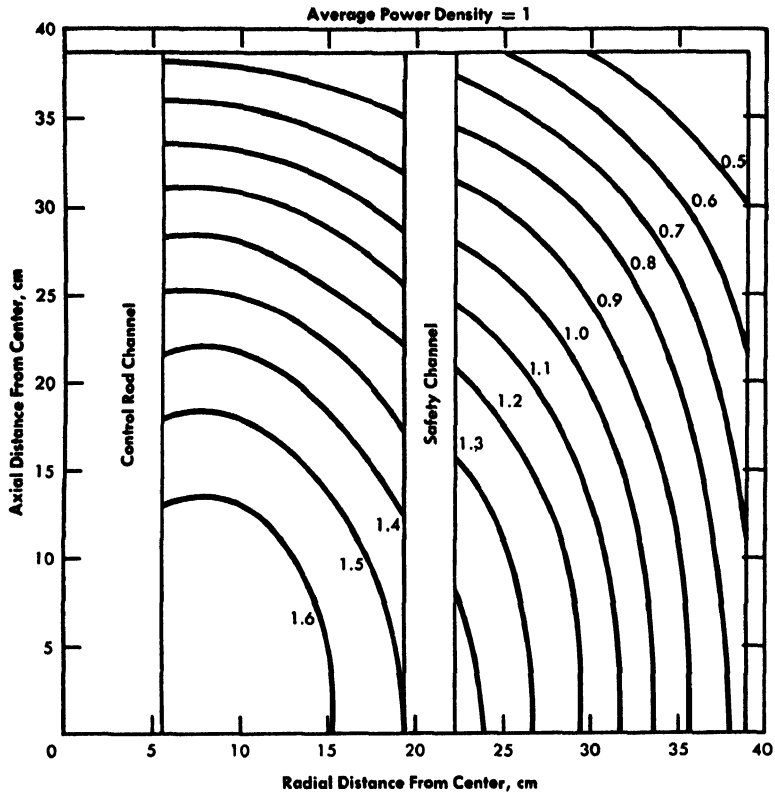

FIG. 4–16. Axial and radial power distributions in core.

distribution in a cylindrical reactor. In the cylindrical model, unlike the actual core, one operating control rod was simulated at the core center, instead of two offset control rods. The eight safety rods were simulated by a thin annulus of equivalent volume. Power distribution in the core, both axial and radial, is shown in Fig. 4–16. Heat generation in the hottest fuel element is shown in Fig. 4–17. Heat generation in the radial blanket was obtained from a two-dimensional computation of the neutron flux in the blanket. The heat generation and the integral of distribution for the hottest radial blanket element are shown in Fig. 4–18.

(2) "Hot-channel" factors. Factors to account for deviations from nominal dimensions, uncertainties in physical constants, and empirical correlations are included in the calculation of maximum fuel-element temperatures. The hot-channel factors are functions of the particular fuel-element design. The factors applied to the reference pin-type fuel element and reference blanket element are summarized in Tables 4–3 and 4–4. The expected temperatures in the hottest fuel element and radial

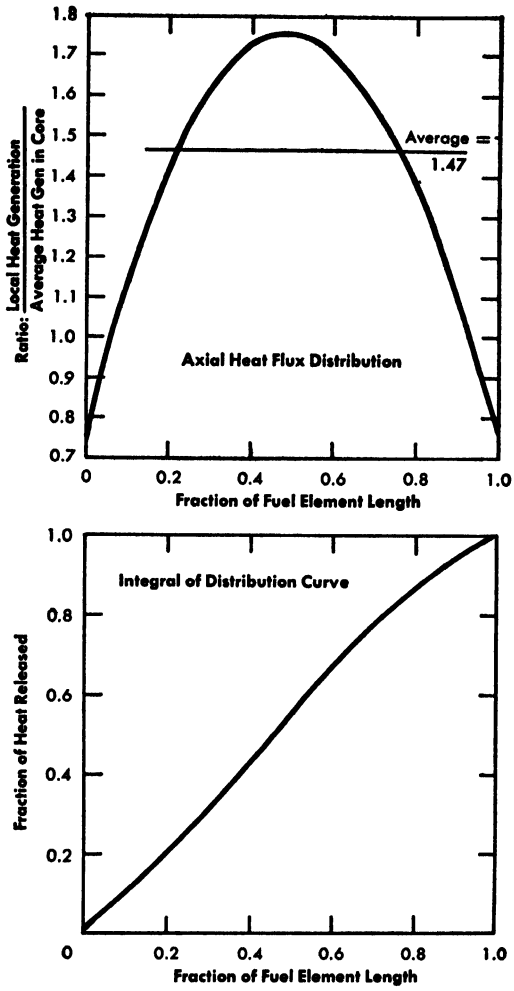

FIG. 4–17. Top: axial heat flux distribution (relative) for hottest fuel element. Bottom: axial heat generation (integrated) in hottest fuel element.

blanket element, calculated without hot-channel factors, are shown in Figs. 4–19 and 4–20.

Since it is extremely unlikely that all the factors will occur simultaneously, an over-all factor, based on a deviation of each individual factor by three standard deviations, was calculated by statistical methods. Calculation of the standard deviation is described by the upper part of Table 4–3, and application of the three standard deviations to the estimation of the maximum uranium temperature is shown in the bottom part of the table. The column $\Sigma\sigma$ in Tables 4–3 and 4–4 gives the temperature rise due to a factor equal to one standard deviation of the uncertainty in ques-

TABLE 4–3

HOT-CHANNEL FACTORS FOR FUEL ELEMENTS*

Uncertainty	Factor for coolant temp. rise, $\Delta t_C = 302°$		Factor for temp. drop thru film, $\Delta t_F = 43°$		Factor for temp. drop thru oxide layer, $\Delta t_O = 16°$		Factor for temp. drop thru clad, $\Delta t_{Zr} = 42°$		Factor for temp. drop thru fuel, $\Delta t_U = 205°$		Summation	
											$\Sigma\sigma$	$(\Sigma\sigma)^2$
	F	σ	F	σ	F	σ	F	σ	F	σ		
Maldistribution of coolant	1.15	15.0									15.0	225.0
To subassemblies												
Within subassemblies												
Pressure drop												
Fuel pin bowing												
Deviation from nominal dimensions	1.03	3.0									3.0	9.0
			1.04	0.6							0.6	0.4
					2.00	5.3					5.3	28.1
							1.02	0.3	1.02	1.4	1.7	2.9
Maldistribution of U^{235}	1.02	2.0	1.02	0.3	1.02	0.1	1.02	0.3	1.02	1.4	4.1	16.8
Maldistribution of flux	1.20	21.1	1.20	3.0	1.20	1.1	1.20	2.9	1.20	14.4	42.5	1806.0
Burnup and swelling in core fuel pin	1.10	10.0	1.10	1.4	1.10	0.5	1.10	1.4	1.10	6.8	20.1	404.0
Power measurement and control			1.15	2.2	1.15	0.8	1.15	2.1	1.15	10.3	15.4	237.0
Film heat-transfer coefficient			1.30	4.3							4.3	18.5

Thermal conductivity of zirconium oxide					1.20	1.10					1.1	1.2
Thermal conductivity of zirconium							1.10	1.4			1.4	2.0
Thermal conductivity of fuel alloy									1.10	6.8	6.8	46.2
Total $(\Sigma\sigma)^2$												2791.0
Square root of total (total temperature rise, °F)												52.8

*Hot spot located at $x/L = 0.75$. Uranium temperature (no hot-channel factors) = 1158°F.
Uranium temperature (with hot-channel factors): $T_U = 1158° + 53° = 1211°F$ (1σ), $T_U = 1158° + 106° = 1264°F$ (2σ), $T_U = 1158° + 158° = 1316°F$ (3σ).

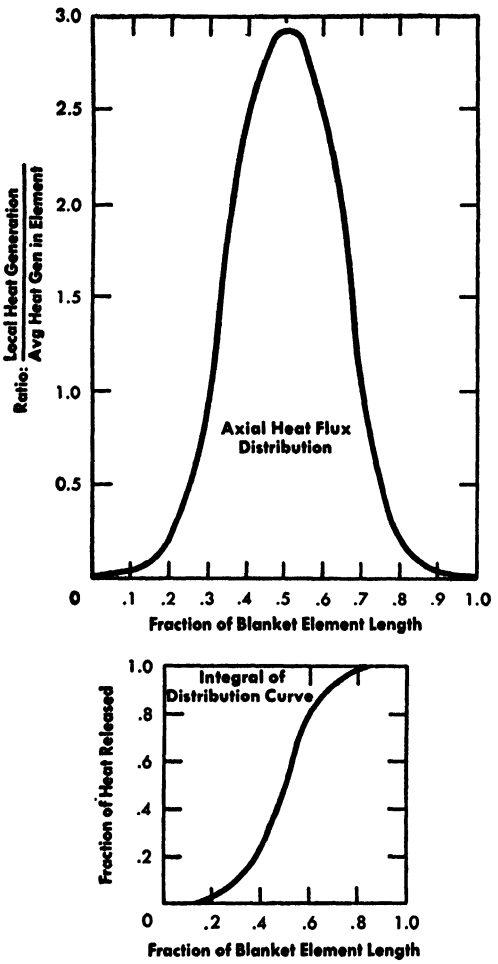

FIG. 4–18. Top: axial heat flux distribution (relative) for hottest radial blanket element. Bottom: axial heat generation (integrated) in hottest radial blanket element.

tion. The total temperature rise from one standard deviation is obtained from the square root of the sum of the squares of $\Sigma\sigma$. The application of three standard deviations to the over-all temperature factor represents a probability of 1.5 in 1000 that any fuel element in the highest flux region will have a maximum temperature equal to or higher than that specified.

(3) Thermal properties of reactor materials. The thermal properties of materials used in the calculations and the sources of the data are given in Table 4–5. The variation of thermal properties with temperature along the length of the fuel element was taken into account in all calculations.

(4) Film heat-transfer coefficient. The film heat-transfer coefficient

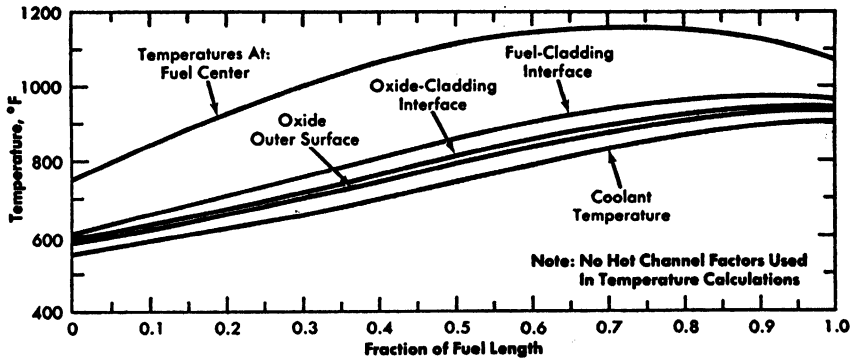

FIG. 4–19. Expected temperature distributions in hottest fuel element. Reactor power = 300 Mw; Blanket burnup = 0.0 a/o; Core power = 281 Mw; Fuel element OD = 0.158 in; Clad thickness = 0.005 in; Fuel element = 30.5 in.

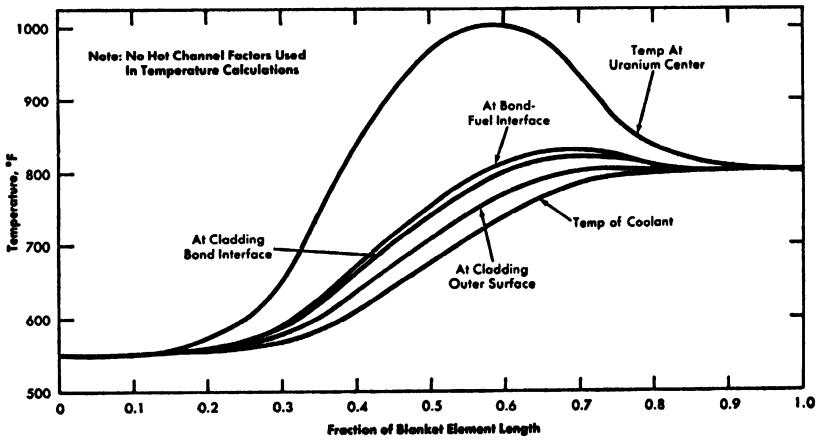

FIG. 4–20. Expected temperature distributions in hottest radial blanket element.

Reactor power = 300 Mw
Blanket power = 35 Mw
Blanket burnup (max) = 0.5 a/o
Blanket burnup (avg) = 0.2 a/o
Blanket element OD = 0.443 in
Clad thickness = 0.010 in
Na bond thickness = 0.004 in
Fuel element length = 65.0 in

was calculated from an empirical equation developed by Lubarsky and Kaufman [1]:

$$N_{Nu} = 0.625\ (N_{Re}N_{Pr})^{0.4}.$$

The variation of the heat-transfer coefficient with temperature along the length of the element was taken into account.

TABLE 4–4

HOT-CHANNEL FACTORS FOR BLANKET ELEMENTS*

Uncertainty	Factor for coolant temp. rise, $\Delta t_C = 190°$		Factor for temp. drop thru film, $\Delta t_F = 29°$		Factor for temp. drop thru clad, $\Delta t_{SS} = 30°$		Factor for temp. drop thru bond, $\Delta t_B = 11°$		Factor for temp. drop thru fuel, $\Delta t_F = 190°$		Summation	
											$\Sigma\sigma$	$(\Sigma\sigma)^2$
	F	σ	F	σ	F	σ	F	σ	F	σ		
Maldistribution of coolant												
To subassemblies												
Within subassemblies	1.00	0.0									0.0	0.0
Pressure drop												
Orifices												
Mixing factor												
Deviation from nominal dimensions	1.01	0.6	1.01	0.1	1.01	0.1	1.01		1.01	0.6	1.4	2.0
Uranium tolerance					1.10	1.0					1.0	1.0
Clad tolerance												
Inhomogeneity of fuel alloy												
Molybdenum	1.005	0.3	1.005		1.005		1.005		1.005	0.3	0.7	0.5
U^{235}	1.01	0.6	1.01	0.1	1.01	0.1	1.01		1.01	0.6	1.4	2.0
Maldistribution of flux	1.20	12.7	1.20	2.0	1.20	2.0	1.20	0.7	1.20	12.7	30.1	905.0
Influence of Pu buildup	1.12	7.6	1.12	1.2	1.12	1.2	1.12	0.4	1.12	7.6	18.0	324.0
Power measurement and control			1.15	1.5	1.15	1.5	1.15	0.5	1.15	9.5	13.0	169.0

Film heat-transfer coefficient			1.30	3.0							3.0	9.0
Thermal conductivity of stainless steel					1.05	0.5					0.5	0.3
Film conductance at bond interfaces							1.25	0.9			0.9	0.8
Thermal conductivity of fuel alloy									1.20	12.7	12.7	162.0
Total $(\Sigma\sigma)^2$												1576.0
Square root of total (total temperature rise, °F)												39.7

*Hot spot located at $x/L = 0.6$. Uranium temperature (no hot-channel factors) = 1000°F.
Uranium temperature (with hot-channel factors): $T_U = 1000° + 40° = 1040°F$ (1σ), $T_U = 1000° + 80° = 1079°F$ (2σ), $T_U = 1000° + 119° = 1119°F$ (3σ).

TABLE 4–5

THERMAL PROPERTIES OF REACTOR MATERIALS

	Temperature, °F	Density, lb/ft³	Thermal conductivity, Btu/(hr)(ft²)(°F/ft)	Specific heat Btu/(lb)(°F)
Sodium	550	55.2	44.3	0.313
	675	54.1	42.3	0.308
	800	53.1	40.4	0.304
Zirconium	800		11.3	0.082
	1000	406 (70°F)	10.0	0.084
Stainless steel (type-347)	800	493 (70°F)	11.5	0.135
	1000		12.4	0.140
10 w/o molybdenum-uranium alloy	1000	1082 (70°F)	16.1	0.046
	1200		18.6	0.051
U^{238} (depleted)	1000	1192 (70°F)	21.2	0.043
	1200		23.5	0.048
Zirconium oxide	800		0.7–1.2	

Considerations on the mixing properties of the flow. Hydraulic tests in which dye was dispersed in flowing water have been run on a full-scale model of a blanket subassembly to determine the mixing properties of the flow. The measurements indicated a gross eddy diffusion coefficient of about 0.002 ft²/sec, which is about three times the molecular diffusivity of sodium. This was taken into account when the hot-channel factor used in the blanket calculation was evaluated. In the case of the core, a rough test indicated a gross eddy diffusivity of about 0.001 ft²/sec. At the high coolant velocity in core subassemblies, mixing will not have time to occur appreciably; it was not considered in the hot-channel factor calculation.

Friction pressure loss in core and radial blanket. The results of experiments run in a water loop, converted to sodium flow at 765°F, are shown in Fig. 4–21. The upper curve was obtained for a full-scale core subassembly with 16 axial blanket rods arranged in a square pitch of 0.587 inch. The core pins were anchored at the bottom by diagonal bars having an open area of 1.95 in² and the pin spacer wires were perpendicular to flow

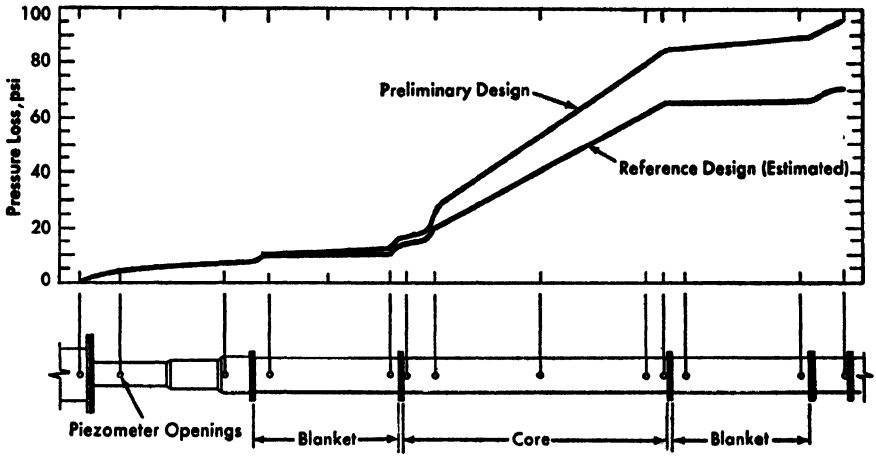

FIG. 4–21. Pressure drop through core subassembly.

direction. The lower curve, valid for the present reference design, results from theoretical corrections to experimental results obtained on an earlier subassembly design. By these changes in the design, the total pressure drop has been reduced by about 22 psi. It is planned to test hydraulically one complete reference design element in a water loop.

A full-size blanket subassembly, with and without orifices, was tested in a water loop and pressure loss was measured over a wide range of flow rates. Very roughly, pressure loss in the blanket subassembly is 30% larger than that calculated for a smooth round tube of the same area and equivalent diameter.

4–4. PHYSICS

4–4.1 Reactor statics. The nuclear characteristics of the reactor have been estimated by means of multigroup diffusion theory. For a reactor of this size, diffusion theory has been shown to give essentially the same results as more refined methods, such as the S_n methods of Carlson. Since the nuclear reactions are caused by neutrons with a large energy spread (from about 1 kev to 10 Mev) and since the cross sections vary strongly with energy in this range, a large number of neutron energy groups are required.

In calculating the critical mass, breeding ratio, and neutron balances, and in estimating how they are affected by geometry or composition changes, the neutron energy range is broken down into ten energy groups A one-dimensional spherical model is used. A correction factor is applied where necessary to take account of the actual geometry. This factor is

derived from theory and from critical experiments. Radial power distributions can be estimated by a one-dimensional cylindrical model with an assumed value of the axial buckling.

Two-dimensional cylindrical models are used for problems where it is necessary to consider more than one dimension, such as for power patterns and the variation of control rod reactivity with position. Two-dimensional calculations are run with only two energy groups, since they would be very complex if more groups were used. Furthermore, the average spectrum in each region is fairly well known from the ten-group one-dimensional calculations, and the two-group microscopic cross sections can be chosen accordingly in each region. Some of the general nuclear characteristics are summarized in Table 4–1. The estimated critical mass is 485 kg of U^{235}. This includes an allowance of a few percent for effects of neutron streaming through the coolant passages, for reactivity loss accompanying burnout, and for shim control. Enrichment of the core fuel alloy is approximately 28%. The reactor has an over-all breeding ratio of 1.12. Of this, about 29%, or 0.32, is accounted for by plutonium formed in the core. The remaining 71%, or 0.80, takes place in the radial and axial blanket sections. Approximately 17% of the blanket plutonium production is in the axial blanket section.

Table 4–6 shows the neutron balance of the reactor. It can be seen that 16% of the reactor fissions occur in either U^{238} or in the U^{235} of the de-

TABLE 4–6

NEUTRON ABSORPTION BREAKDOWN

	Neutron production			Neutron absorption		
	Core	Blanket	Total	Core	Blanket	Total
U^{235} fission	0.843	0.022	0.865	0.340	0.009	0.349
U^{238} fission	0.088	0.047	0.135	0.036	0.019	0.055
U^{238} capture				0.133	0.332	0.465
U^{235} capture				0.075	0.002	0.077
Zr capture				0.002	—	0.002
SS capture				0.004	0.003	0.007
Na capture				0.001	0.001	0.001
Mo capture				0.021	0.010	0.031
B_4C capture				0.009	—	0.009
Total	0.931	0.069	1.000	0.620	0.375	0.996

Neutron leakage: Core to blanket 0.311. Blanket to shield 0.004.

pleted blanket uranium. Approximately 10% of the core fission is by U^{238}.

Table 4–6 illustrates that a breeding ratio larger than one is made possible in a fast reactor by the favorable effect of the large fraction of fissions in U^{238}, and by the small parasitic absorption in materials other than U^{235} and U^{238}. The latter characteristic is due mainly to the high fuel concentration in the fast reactor. It can also be seen that the average value of α (the ratio of capture cross section to fission cross section) of U^{235} in the fast reactor spectrum is no smaller than in a thermal reactor. However, if Pu^{239} were the fuel, α would be much smaller than for Pu^{239} in a thermal reactor.

Even with 46% sodium coolant volume, neutron absorption in the sodium in the core is less than 0.1%. Although the reactor contains approximately 20% structural iron and zirconium, their neutron absorption is only about 1%. However, large amounts of these materials have the undesirable effect of lowering the effective neutron energy level in the reactor. It is desirable to keep this energy level high to take advantage of the fast fission effect in U^{238} and to minimize nonfission absorption in U^{235}.

The majority of the parasitic neutron losses in the reactor, aside from captures in U^{235}, are absorptions in molybdenum, the uranium alloying material. This material captures approximately 3% of all neutrons. Its use in the reactor is justified because it has beneficial properties as an alloying material to achieve high burnup.

The average core and blanket spectra are shown in Fig. 4–22 in relative flux per unit lethargy, and in Fig. 4–23 in relative flux per unit energy. As can be seen from Fig. 4–22, the flux in the lowest energy group is a small fraction of the total flux in both core and blanket. Thus, the energy range

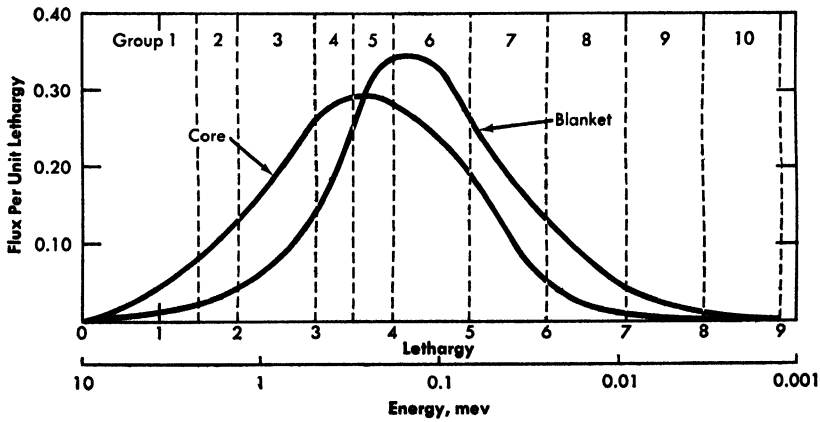

FIG. 4–22. Neutron flux spectra in core and blanket (per unit lethargy). Integral under curves equals 1.0.

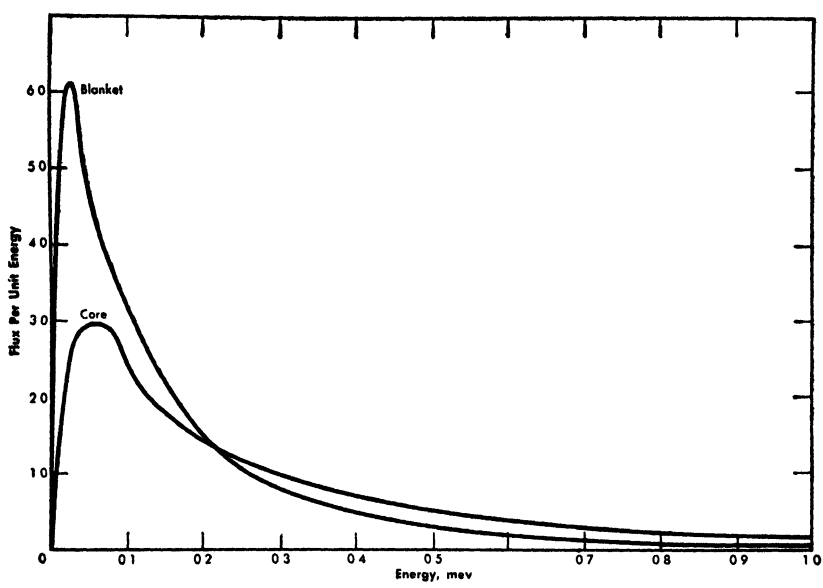

FIG. 4–23. Neutron flux spectra in core and blanket (per unit energy).

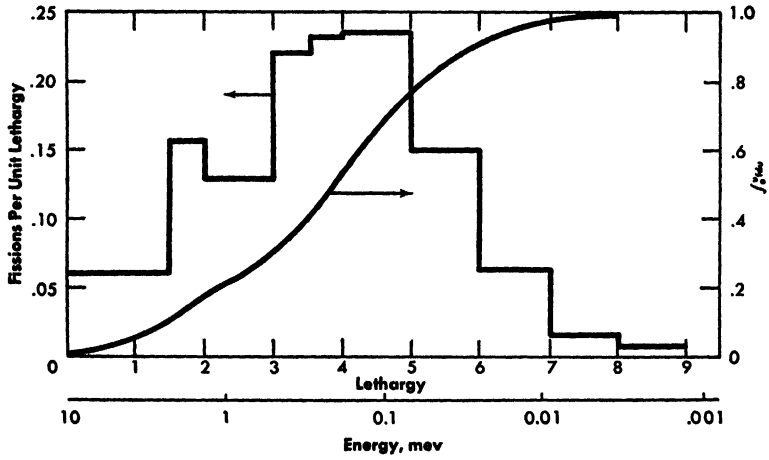

FIG. 4–24. Distribution of core fissions according to energy of neutrons producing the fissions.

covered by the ten groups is adequate for estimating the integral properties of the core and blanket. Figure 4–24 shows the distribution of fissions according to the energy of the neutrons by which they are induced. Peaking in the second group is caused by U^{238} fissions.

The power distribution in the core is shown in Figs. 4–25 and 4–26 for two extreme control rod positions. The eight safety rod channels are rep-

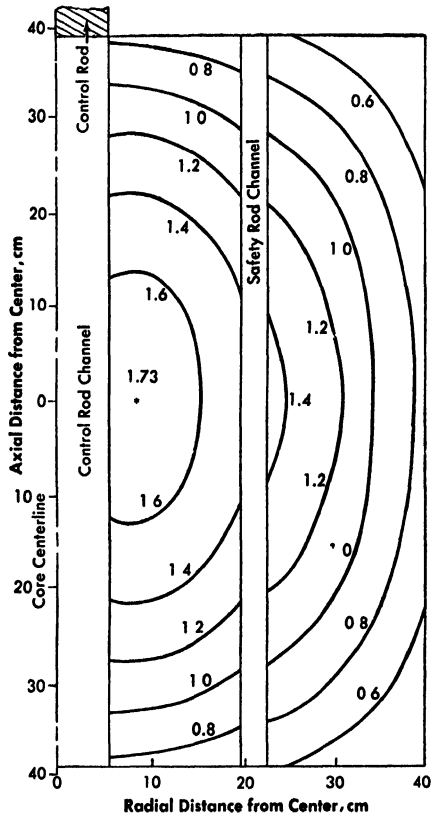

FIG. 4–25. Core power distribution with control rods in outer position, normalized to average power density.

resented by an annulus containing no poison, since the reactor will operate with the safety rods completely withdrawn. The two control rod channels are represented by a central cylinder. Similar two-dimensional calculations were carried out with the control rods in intermediate positions. The variation of control rod reactivity with position was thus determined. It is shown in Fig. 4–27, together with its derivative. The power distribution was also plotted for each control rod position. The maximum-to-average power ratio is greatest when the rods are in their extreme withdrawn position, i.e., with the bottom edge of the poison section at the upper edge of the core. A comparison of Figs. 4–25 and 4–26 shows that the power distribution over the major portion of the core is only slightly affected by a change in control rod position.

The power distribution in the blanket is much affected by the plutonium buildup. It is shown in Figs. 4–28 through 4–31 for extremes of burnup. At each position in the blanket the plutonium buildup is related to burnup.

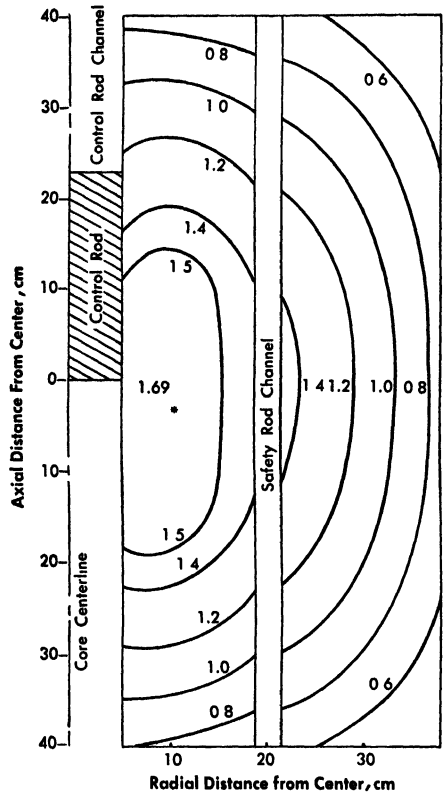

FIG. 4–26. Core power distribution with control rods in inner position, normalized to average power density.

However, this relationship depends on position and, indeed, close to the core the harder spectrum will cause more fissions in U^{238}, and hence less plutonium buildup for a given burnup.

The effect of neutron energy spectrum on the Pu^{240} content of the bred plutonium is illustrated by Fig. 4–32, which shows the ratio of the microscopic capture cross sections of Pu^{239} and U^{238} as a function of neutron energy. The fractional amount of the relatively useless Pu^{240} in the product plutonium is given in first approximation by

$$\frac{N^{40}}{N^{49}} \approx \frac{1}{2} \frac{\sigma_c^{49}}{\sigma_c^{28}} \frac{N^{49}}{N^{28}},$$

where N refers to the atomic concentrations of the isotopes. Clearly, a softer spectrum will result in a higher Pu^{240} content. It is also apparent that the Pu^{240} content of plutonium bred in a fast reactor is much lower than that of plutonium produced in a thermal converter.

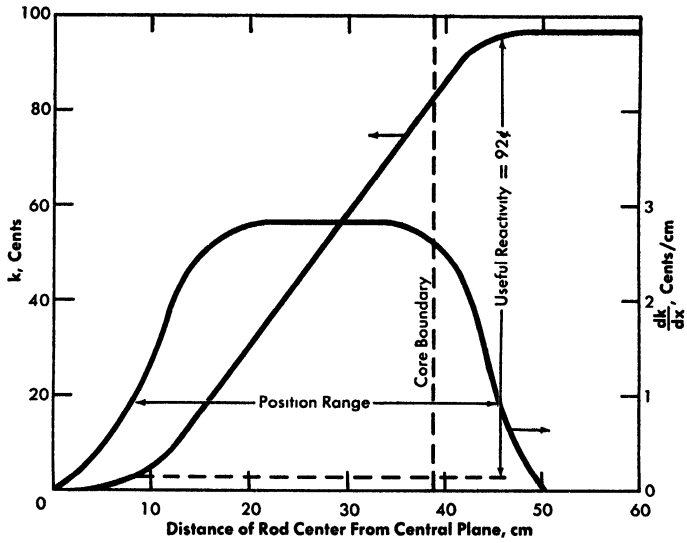

FIG. 4–27. Control rod reactivity and its derivative as functions of rod positions.

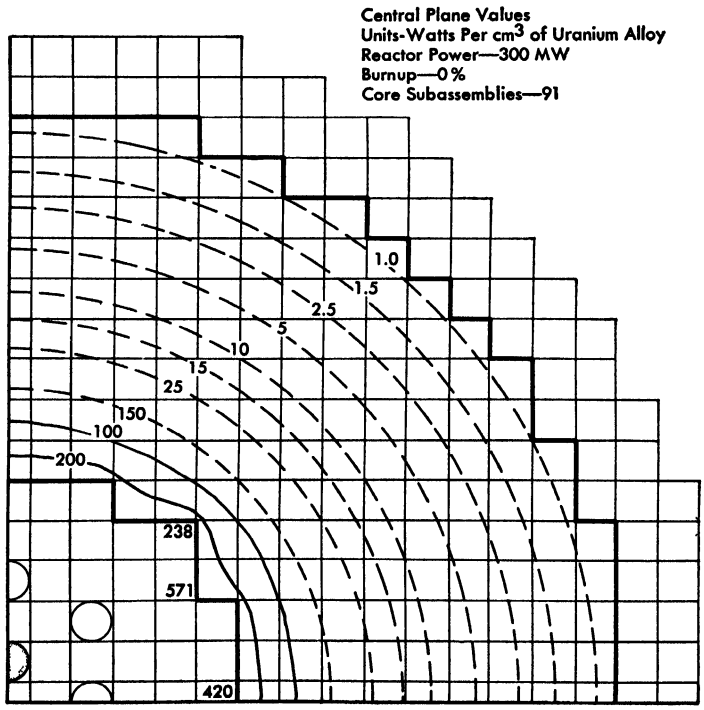

FIG. 4–28. Radial blanket heat generation rates at 0% burnup, central plane value.

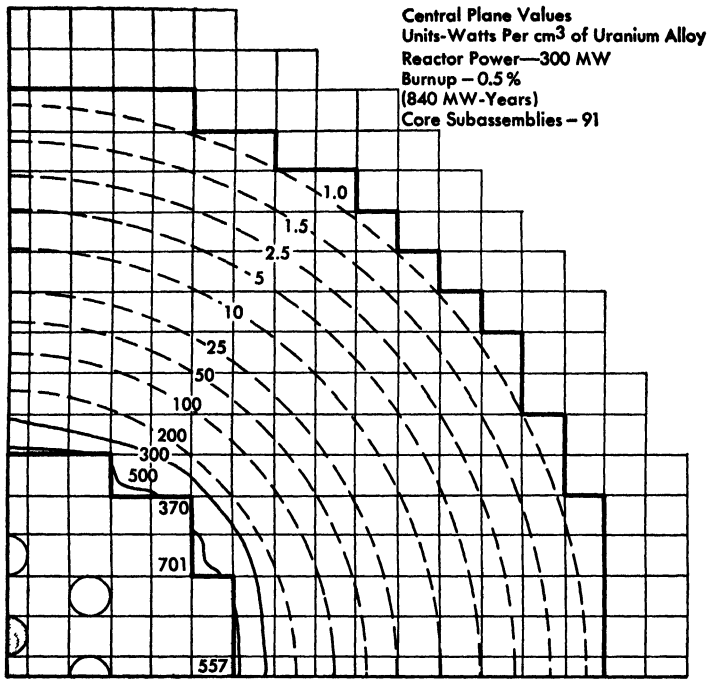

FIG. 4–29. Radial blanket heat generation rates at 0.5% burnup, central plane values.

Ten-group adjoint fluxes have also been calculated. The relative value of the adjoint flux depends on position in the reactor and on energy. The value at a given position and energy is a measure of the importance of a neutron of that energy and in that position for maintaining the chain reaction. The spatial average of the adjoint flux over the core (the important spectrum in the core) is shown in Fig. 4–33. The importance is a decreasing function of the energy below the U^{238} fission threshold because a higher energy results in a greater leakage probability which is not completely offset by the greater average neutron yield per absorption. Above the fission threshold of U^{238} there is a regain of importance with increasing energy.

When the multigroup fluxes, adjoint fluxes, and material cross sections are known, the danger coefficients of various materials can readily be determined by perturbation theory. The danger coefficient of a material, at a given position, is defined as the fractional change in reactivity resulting from the addition of a small unit quantity of the material at that position. Perturbation theory is valid only for small material additions. Danger coefficients are used mainly to determine the effect of small material addi-

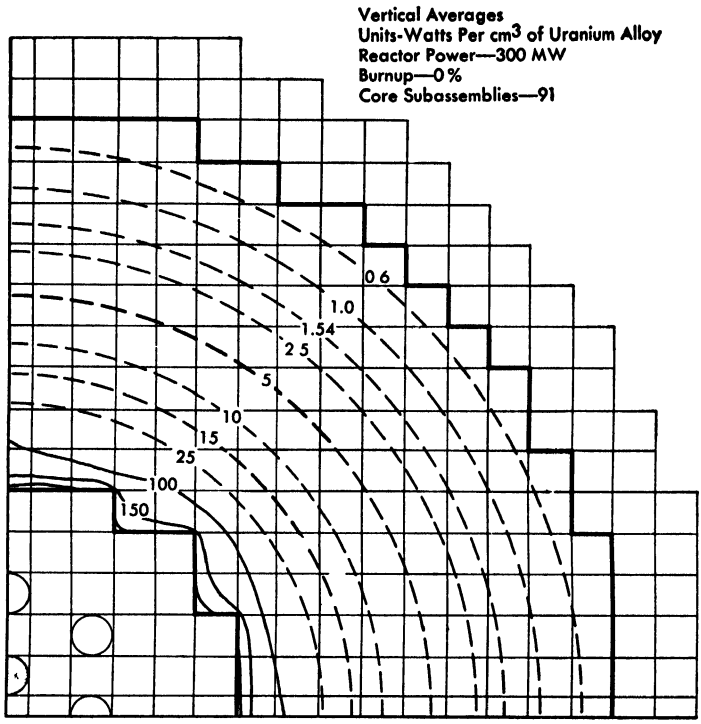

FIG. 4–30. Radial blanket heat generation rates at 0% burnup, vertical averages.

tions on critical mass, and to calculate temperature coefficients of reactivity.

The calculated danger coefficients of several materials of interest are shown in Figs. 4–34 and 4–35. The interpretation of the curves in Fig. 4–34 is as follows. When the material is essentially a neutron absorber or producer, the danger coefficient is roughly proportional to the product of flux and adjoint flux, since the flux determines the number of events, and the adjoint flux* is a measure of their importance. This relationship is illustrated by the behavior of the danger coefficients of U^{235}, Pu^{239}, and B^{10}. The dip toward the center of the reactor is caused by the presence of the control rods which depress both flux and adjoint flux.

When the material is essentially a neutron scatterer, the danger coefficient is roughly proportional to the product of the gradients of flux and adjoint flux, since the gradient of the flux determines the net change in neutron current, and the gradient of the adjoint flux is a measure of the

*The spatial dependence of adjoint flux is very similar to the spatial dependence of the real flux.

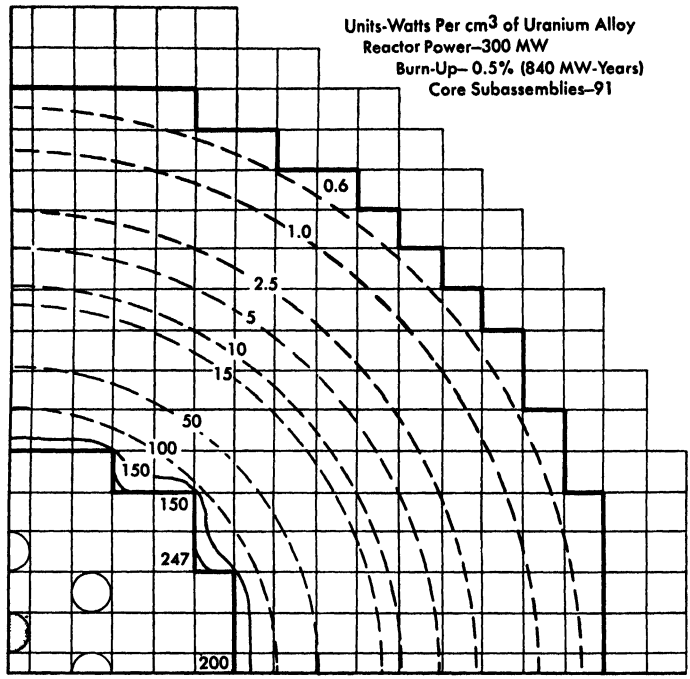

FIG. 4–31. Radial blanket heat generation rates at 0.5% burnup, vertical averages.

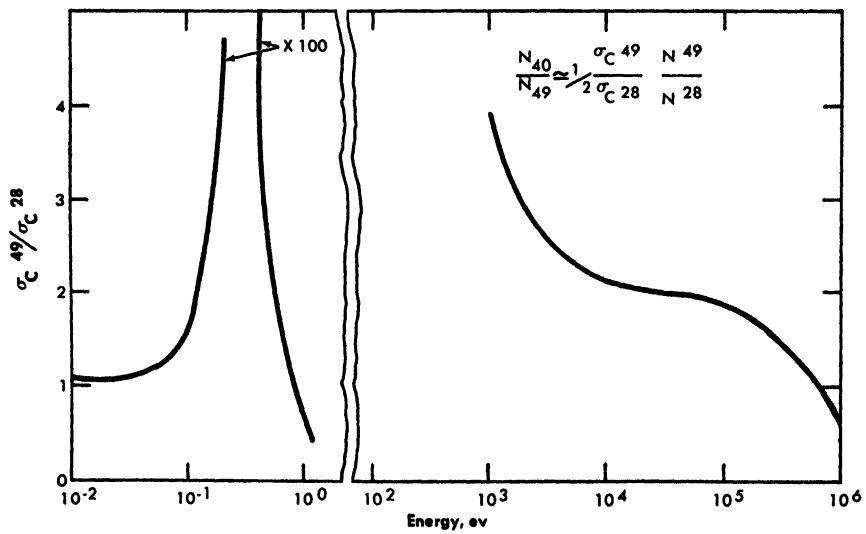

FIG. 4–32. Variation of capture cross sections of Pu^{239} and U^{238} with neutron energy.

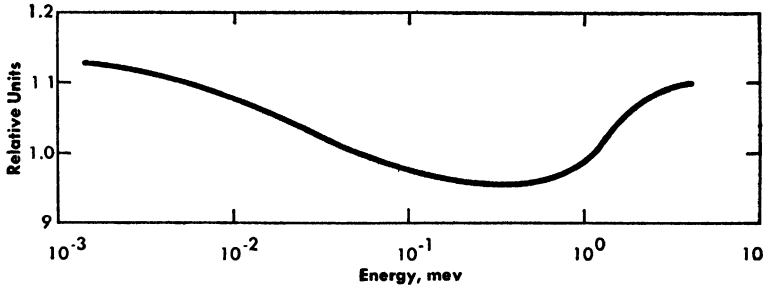

FIG. 4–33. Relative importance of core neutrons as a function of energy.

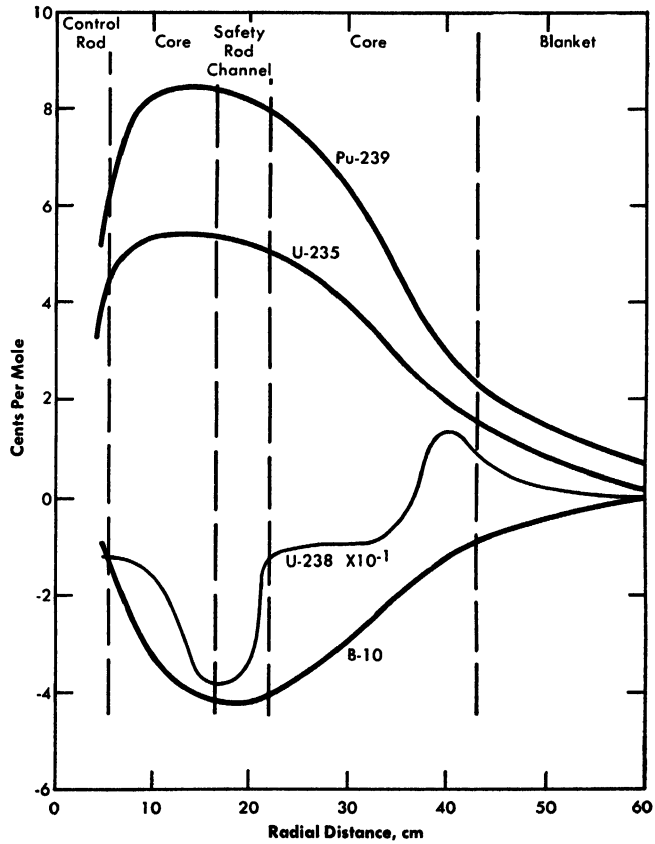

FIG. 4–34. Danger coefficients of U^{235}, U^{238}, Pu^{239}, and B^{10}.

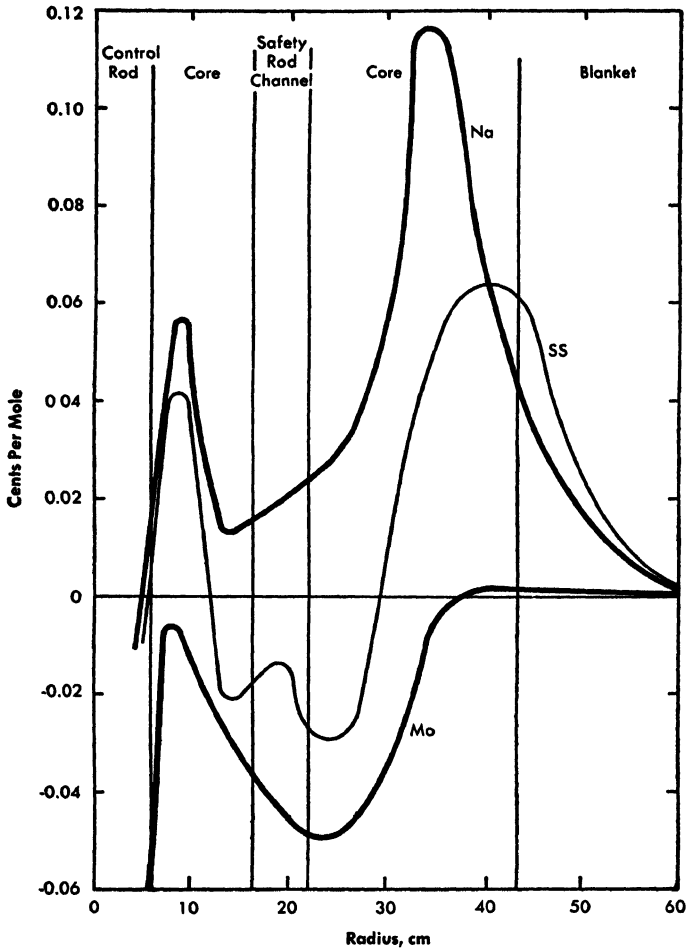

FIG. 4–35. Danger coefficients of sodium, stainless steel, and molybdenum.

importance of such a change. This behavior is illustrated by the danger coefficient of sodium. The mixed behavior of the danger coefficient of U^{238} can also be seen. In the core, U^{238} acts mostly as a neutron absorber (capturing more neutrons than it produces by fast fission), and in the blanket it acts more as a scatterer. On a volume basis, the danger coefficient of U^{238} in the blanket is larger than that of sodium. Hence displacing a certain quantity of sodium by adding a blanket subassembly increases the reactivity.

Besides reducing leakage, elastic scattering also tends to increase reactivity by slowing the neutrons down toward energies of higher importance (see Fig. 4–33). On the contrary, inelastic scattering, since it involves

mostly very fast neutrons, usually decreases the reactivity by slowing neutrons down across the U^{238} fission threshold. Of course any slowing down reduces the breeding ratio. Thus, for example, if an oxide fuel were used instead of the metallic fuel, the critical mass and the breeding ratio would both be smaller, both because of the elastic scattering properties of oxygen, and because of the reduction of U^{238} concentration in the core.

4–4.2 Reactor kinetic relationships. The relationships involved in the kinetic behavior of the reactor can be illustrated by the block diagram shown in Fig. 4–36. Three inputs are considered: the control rod reactivity, the coolant flow, and the inlet coolant temperature. The effects of burnup and associated fuel growth on the reactivity are not represented in the block diagram, since these processes are too slow to have a bearing on the kinetic behavior of the reactor. Other processes, such as sodium boiling, complete loss of coolant, and radical change in composition or geometry of the reactor, are not covered here, since they would conceivably occur only in extreme accidents.

The various relations represented on the block diagram are discussed in succession. Both the analytical solutions and the representation by a simulator are treated.

Reactivity-power relationship. This relationship is expressed by the well-known inhour equation. The important parameters in this equation are the mean neutron lifetime and the delayed neutron fractions. The calculated value of the lifetime is about 2×10^{-7} sec, much smaller than the values which characterize thermal reactors.

The delayed neutron fractions from fast fission of U^{235} and U^{238} are, respectively, 0.0064 and 0.0157. Because of the relatively large fraction of U^{238} fissions in the Fermi Reactor, for an average fission the delayed fraction is about 0.0077. However, the average importance of a delayed neutron is 10% less than that of a prompt neutron, as can be seen from Fig. 4–37, which shows their spectra, and Fig. 4–33, which shows the importance of a neutron as a function of energy. Thus the effective delayed neutron fraction is 0.0069.

When the excess reactivity is smaller than about 92 cents or 0.0064 k_{eff}, the delayed neutrons essentially control the kinetic behavior and the effective generation time is about 0.08 sec, compared with 0.09 sec for a thermal reactor fueled with U^{235}. For higher excess reactivities, the generation time approaches the neutron lifetime. The importance of neutron lifetime in determining the kinetic behavior for large values of excess reactivity is illustrated by Fig. 4–38, which shows the asymptotic period as a function of excess reactivity for widely different values of the lifetime.*

*This figure assumes a delay fraction of 0.0075.

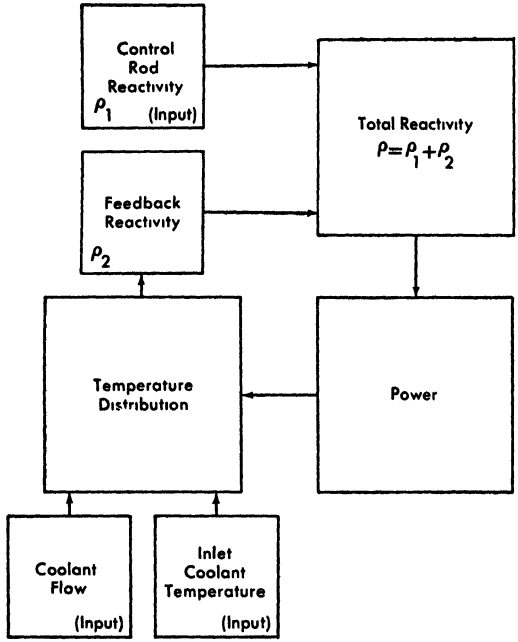

FIG. 4–36. Block diagram of reactor kinetics relations.

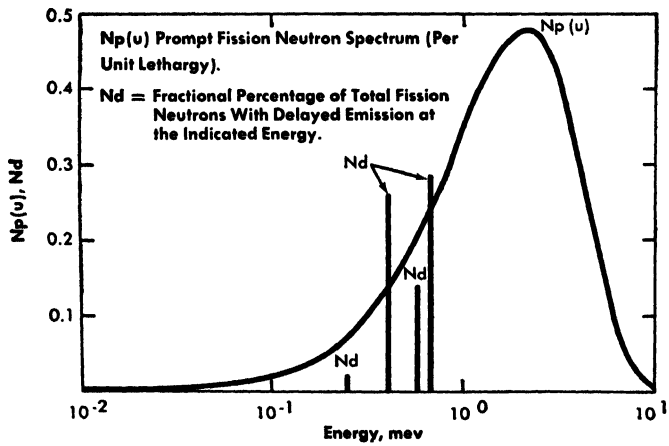

FIG. 4–37. Comparison of prompt and delayed neutron spectra.

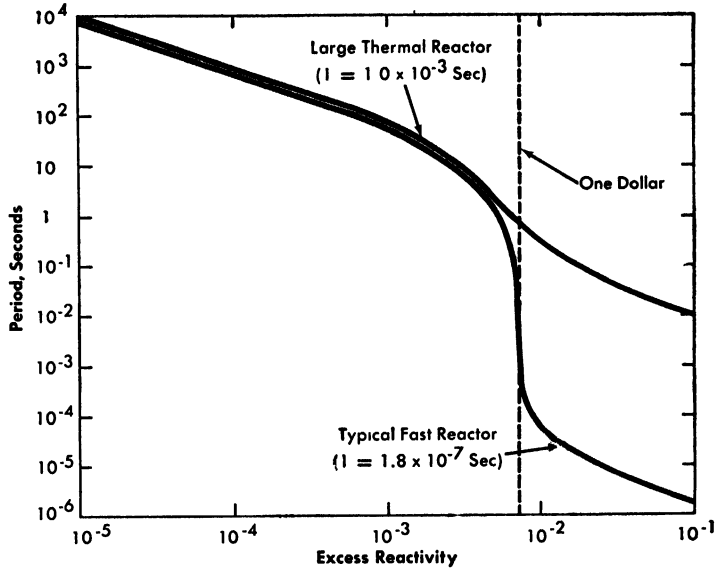

FIG. 4–38 Asymptotic period as a function of excess reactivity.

Numerical integration of the inhour equation can be carried out for any time variation of the excess reactivity and simple cases can be solved analytically. This equation also can be simulated by relatively simple electric circuits

For small-amplitude sinusoidal reactivity oscillations, a transfer function can be determined giving the amplitude and phase leg of the resulting power oscillation. The transfer function is plotted in Fig. 4–39. At low frequencies, the amplitude of the power oscillation, expressed as the fractional oscillation of power level for a given fractional oscillation of reactivity, is very large, and the phase lag is close to 90 degrees. At higher frequencies the amplitude decreases. The phase lag also decreases so long as the period of the oscillation is large compared with the prompt-neutron lifetime.

Power-temperature relationship. This relationship is described by coupled partial linear* differential equations with constant coefficients. Such equations lend themselves to analytic solution by Laplace transform techniques, and transfer functions can be determined.

For slow power variations the temperature distribution will not depart much from the equilibrium distribution. For faster power variations time

*The equations are linear only if it is assumed that material properties and heat-transfer coefficients are independent of temperature.

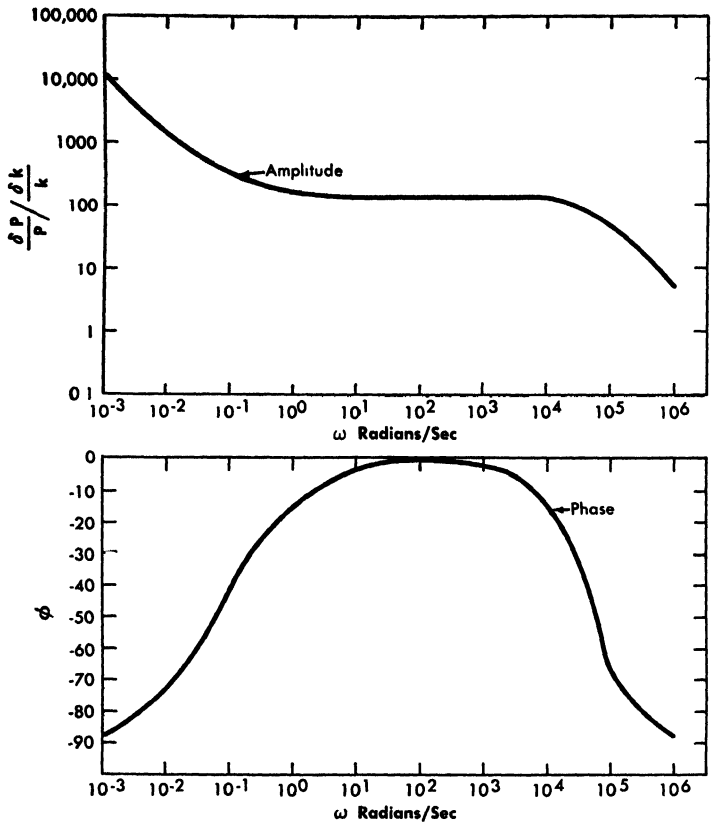

FIG. 4–39. Reactivity power transfer function without feedback.

lags of mixed conductive and convective types appear which also attenuate the temperature variations. Here conductive lags refer to those caused by the thermal resistance of materials through which heat is passing, whereas convective lags are caused by the time required by coolant flow to transport the heat between points of interest. The time lag is usually larger for coolant temperature than for fuel temperature, but in parts of the blanket where heat generation is low the situation may be reversed. The temperature of any structure always lags the temperature of the coolant with which it is in contact.

For complicated power transients, the analytical solution is difficult to carry out and one must resort to a simulation, usually by an electrical analog. The simulators, of course, also have practical limitations. An important feature of fast reactors designed for power production is that the time lags between power and temperatures are very small, because of high

heat-transfer coefficients, small fuel-element size, and small heat capacity of the coolant.

Inlet coolant temperature-temperature distribution relationship. This relationship is described by the same system of equations as has just been discussed, and the solution can be carried out in much the same way. Complicated variations can be analyzed by simulation. The time lag of the coolant, which in this case is essentially of the convective type throughout the reactor, increases with distance from the inlet, while the amplitude decreases; the fuel temperature always lags that of the local coolant.

Rate of flow-temperature distribution relationship. This is described by the same equations as before, but the coefficients are no longer constant when the rate of flow is a function of time. An analytic solution can therefore be obtained only in very special cases. However, a simulator can be adapted to handle variable flow.

Temperature distribution-feedback reactivity relationship. Fuel, coolant, and structure temperature changes cause small variations of the reactivity. The time or phase lags between temperature and reactivity are related to the velocity of pressure wave propagation through the different media, and are usually negligible compared with the lags between power and temperatures. Indeed, for other than extremely fast transients, which are not in the scope of this discussion on normal kinetics, inertial and damping forces can be neglected, since they are too small to effectively separate in time the various reactivity contributions and to alter their magnitude. Hence only the steady-state temperature-reactivity relationship will be considered here.

Temperatures affect reactivity in the following ways:

(1) Axial core fuel expansion reduces fuel density, but this effect is partially compensated by increase of core length. The negative temperature coefficient of reactivity thus introduced depends on position and is proportional to the difference of the fuel danger coefficient at the position under consideration and at the core edge.

(2) Radial expansion of fuel pins displaces sodium. This temperature coefficient is proportional to the local danger coefficient of sodium, but of opposite sign. It is also negative because presence of sodium reduces neutron leakage from the reactor.

(3) Heating of the sodium coolant causes it to expand, and thus also introduces a negative temperature coefficient which is proportional to the danger coefficient of sodium.

(4) Radial expansion of the core will result from the design features incorporated to eliminate subassembly bowing. The core subassemblies are in contact with each other near the central plane. On a temperature increase the core will expand radially according to the thermal expansion properties of stainless steel. The effect is analogous to that of axial fuel

expansion. It is believed that with the present design, top structure expansion will have a negligible reactivity effect. If anything, this effect would be negative.

(5) Doppler broadening of the resonances with increased temperature results in more captures in U^{238} (negative effect) and more fissions in U^{235} (positive effect). Recent experimental and theoretical work indicates that the net reactivity effect is approximately zero for an atomic U^{238}/U^{235} ratio of 1. In the Fermi Reactor the ratio is about 2.6, consequently the net Doppler effect is negative. The latest estimate for the Doppler coefficient in this reactor is -1.6×10^{-6}/°C at operating temperatures.

(6) The subassemblies are held in position both at the top and at the bottom. The power distribution is such that the inner walls of the subassemblies are hotter than the outer walls. This tends to cause the subassemblies to bow with the convex side toward the center of the reactor. Since both ends of the subassemblies are fixed, the bowing could cause a compacting of the reactor, resulting in a positive coefficient of reactivity comparable in magnitude to the coolant expansion coefficient.

Various designs have been considered to eliminate this effect. In the present reference design, pads are attached to the core subassemblies slightly above the midplane of the reactor core. These pads will be machined so that in the reactor there is no clearance between subassemblies. The subassembly bow will then be S-shaped. The vertical location of the pads is so chosen as to have a zero reactivity coefficient from subassembly bowing.

It is believed that none of the reactivity coefficients of the Fermi Reactor will be positive. All temperature coefficients of reactivity have been calculated as functions of position. As an illustration, isothermal coefficients are listed in Table 4–1. They correspond to the case in which all parts of the reactor are at the same temperature. Combination of the power-temperature, and temperature-reactivity relationship, yields the power-reactivity relationship* or power coefficient of reactivity. This relationship, of course, is dependent on the nature of the transient.

An important feature of fast reactors is the extremely rapid reactivity response to power changes. This rapid response is due to the circumstances that a large portion of the negative power coefficient is from thermal expansion of fuel and coolant and that in fast power reactors the temperatures of both fuel and coolant follow power changes very closely.

The equilibrium power coefficient of reactivity of the Fermi Reactor was calculated to be 0.076¢/Mw, resulting in a 23¢ reactivity change as power is changed from zero to 300 Mw. This change in reactivity (temperature override) is reduced to 15¢ if the shutdown temperature is chosen to be 600°F instead of 550°F.

*Constant inlet coolant temperature and full flow are assumed.

4–4.3 Dynamic response of the reactor. The entire block diagram of Fig. 4–36, with the three inputs, has been represented on a simulator, which is schematically shown in Fig. 4–40 for a "lumped" model. The responses of the reactor at the three possible inputs, as determined by the simulator, are considered separately.

Control rod reactivity. (1) Regulating control rods. Since the available excess reactivity is limited to 92¢, even an instantaneous withdrawal of the control rods from the cold reactor could not make it prompt-critical. Furthermore, as soon as the reactor heats up, the negative reactivity feedback reduces the excess reactivity, the period increases progressively, and the power levels off at a steady value. Of course, such a fast insertion of reactivity would cause a temporary overshooting of the steady power level, which could ruin the core of the reactor. The control rod reactivity insertion rate is therefore limited to 1¢/sec. When reactivity is inserted at this low rate, and when the power is at least 1% of full power, the reactivity feedback follows closely the inserted reactivity, so that the resulting total excess reactivity never becomes excessive. For these conditions the power level is closely coupled to the control rod position.

The worst situation is created by the classic startup accident which also has been analyzed on the simulator. In this case the full excess reactivity is inserted at 1¢/sec with the reactor initially at source power, about eight decades below the level at which temperature effects become important. Even in this drastic situation the minimum reactor period is of the order of 1 sec;* this period occurs when about 5% of full power is reached, and the power levels off with no overshoot.

When the full excess reactivity of 92¢ is inserted the power levels off at about four times normal power. Figures 4–41 and 4–42 show the results obtained from the simulator for a full insertion of the available excess reactivity at the rate of 1¢/sec with full coolant flow, starting from 1% power and from source power.

At this point, it is useful to discuss the reasons for limiting the available excess reactivity to 92¢.

The first concern in many minds during the early design of the Fermi Reactor was that of absolutely restricting operation to values of excess reactivity within the delayed critical region. The most certain way of allaying fears regarding prompt criticality was simply to restrict the available reactivity to less than 92¢, above which the period becomes very short. However, it has just been pointed out that when reactivity is inserted at 1¢/sec, even from source level, a maximum total excess reactivity of 71¢ is reached. The fact that a maximum is reached means that at this moment the negative reactivity feedback rate is exactly 1¢/sec. After this

*The excess reactivity is then about 71¢ and the reactivity feedback is only about 3¢.

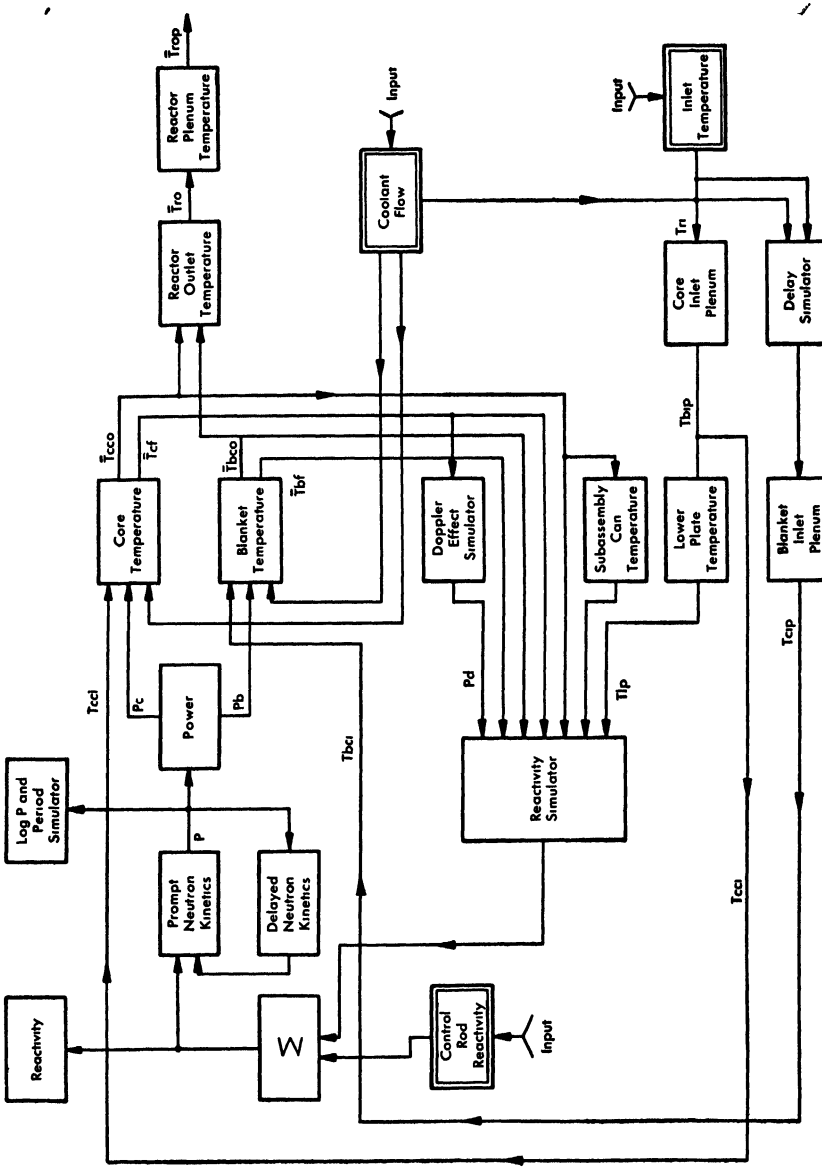

FIG. 4-40. Block diagram of analog computer circuit.

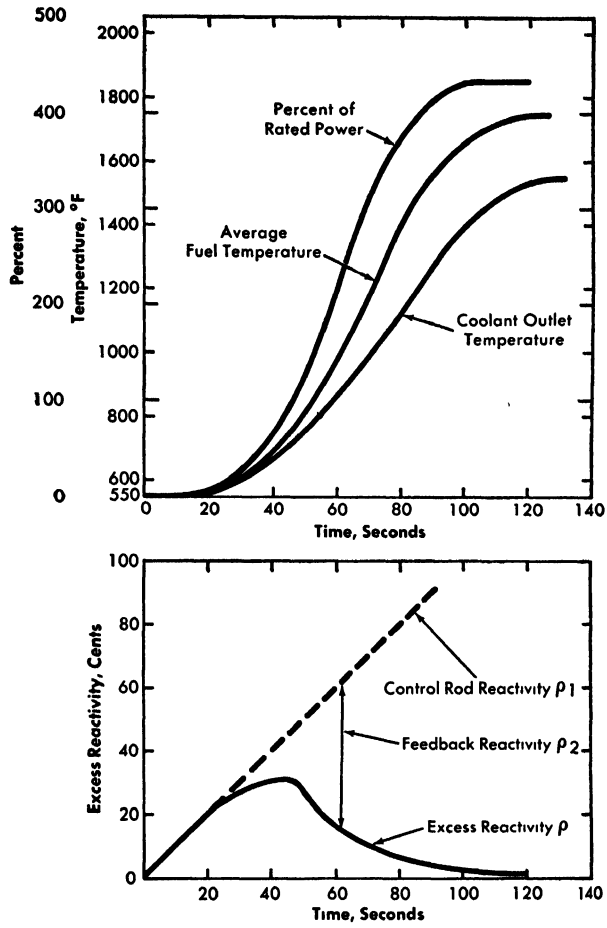

FIG. 4–41. Startup at one cent per second from one percent power.

moment the negative reactivity feedback is being inserted at an increasing rate since the power level is higher. Hence, the total excess reactivity can never increase after this maximum of 71¢ has been reached, even if many dollars of control setting excess reactivity were inserted at 1¢/sec.

One can therefore conclude that in order to prevent the total excess reactivity from ever exceeding 92¢, it is not necessary to limit the available excess reactivity to 92¢ but that the same goal can be achieved by simply limiting the *insertion rate* of excess reactivity. This conclusion does not hold for all power reactors, since in some reactors the reactivity response to power changes is much slower than in a fast sodium-cooled power reactor.

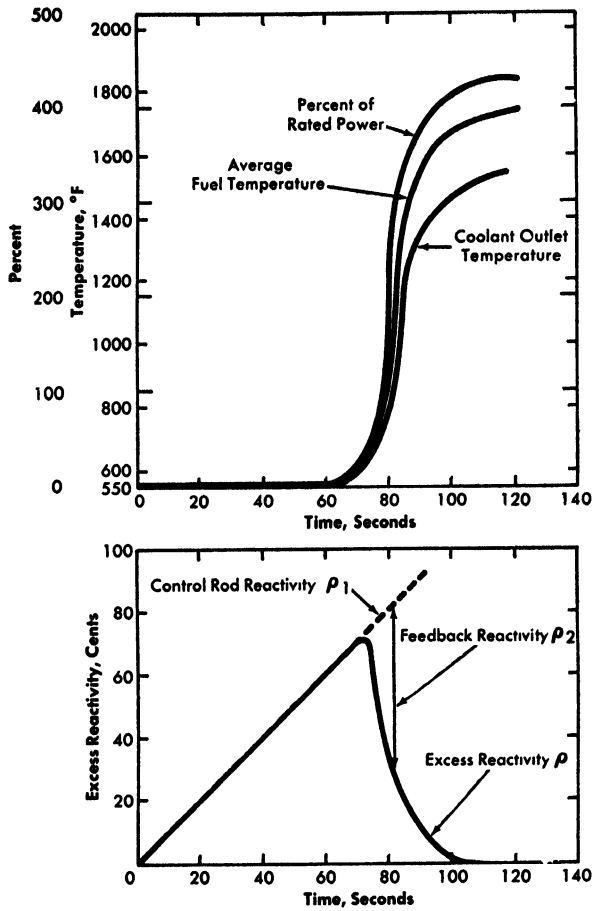

FIG. 4.42. Startup at one cent per second from source level.

There is nevertheless good reason for imposing an upper limit to the available excess reactivity. In all power reactor designs there is the problem of preventing insertion of so much reactivity that the power rises above the removal capacity of the cooling system. In any reactor, and particularly in some thermal reactors, where the available excess reactivity may be as high as \$20, a complete insertion of the available excess reactivity when the reactor is clean* would overheat the reactor and cause considerable damage. Such a situation, of course, can be prevented by a

*When the operating conditions and operating history are such that a large fraction of the initial excess reactivity has not been used up by fuel burnup, fission-product poisons, etc.

well-designed automatic control and safety system. However, for added safety, it was decided to limit the available excess reactivity in the Fermi Reactor to 92¢. This limitation prevents meltdown of the core, even in the incredible event that all control and safety systems failed. If the full 92¢ were inserted, the power would reach about four times its normal value. This high power would cause considerable damage to the reactor but would not result in a meltdown. It seems probable that after a period of full-power operation a reconsideration of the necessity for this restriction would be appropriate.

If the Fermi Reactor were later fueled with plutonium, and if the temperature coefficients of reactivity and the temperature limitations were the same, available excess reactivity could still be about 0.0064. This would be equivalent to about $1.50 because of the low delayed-neutron fraction in plutonium fission. The limits on insertion rate of reactivity would still be held at about 1¢/sec. Of course, 1¢ is in this case a smaller number expressed in fraction of k_{eff}. No change in the over-all temperature coefficients is expected. Therefore, the temperature reached in the startup accident, and in other accidents, would be similar to that reached for U^{235} fuel.

(2) Safety rods. The reactor is designed never to go critical before the safety rods are completely withdrawn. The rate at which safety rods insert positive reactivity was nevertheless also limited to 1¢/sec. However, when all eight safety rods are scrammed, the reactivity is decreased by $8, at the rate of $25/sec. Feedback effects are negligible in this case. The power drops almost instantaneously to a very low value and a rapid temperature change takes place. The vessel wall and internals are protected against such a rapid temperature change by thermal baffling. In addition, the thermal shock at the outlet nozzle, a critical area, is considerably dampened by coolant mixing in the upper sodium pool.

To minimize the frequency of these rapid temperature changes, the safety system is designed to initiate a fast rundown of the safety rods instead of a scram whenever a scram is not required.

Inlet coolant temperature. When the inlet coolant temperature changes suddenly, the effect on reactivity will appear without much delay. However, since the temperature coefficients are small, the reactivity variations will also be small. Entrance of a cold slug of coolant into the reactor is of consequence, not as an important reactivity change, but as a mild thermal shock problem that was taken into account in the design. The cold slug cannot be at a lower temperature than the feedwater (340°F) and cannot appear suddenly because of the long transport lags and the mixing in the secondary and primary loops. Figure 4–43 shows the result obtained from the simulator when the inlet coolant temperature drops from 550 to 300°F in 20 sec with the reactor operating at full flow and full

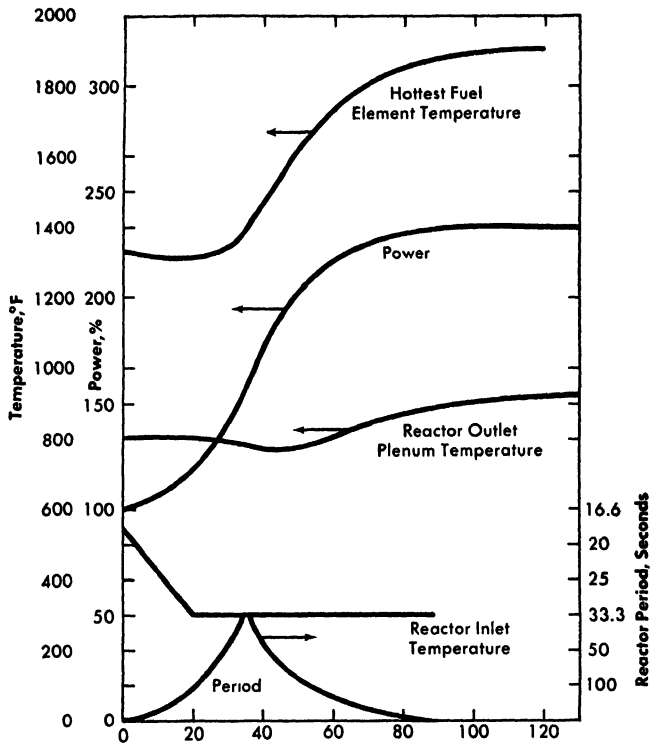

FIG. 4–43. Effect of a cold slug of coolant while operating at full power. The abscissa is time, in seconds

power and with the control system assumed to be inoperative. The initial reactivity insertion is much smaller than prompt-critical, and the power increases until the average temperature approaches its initial value.

In general, the reactor will respond very gently to small variations in inlet coolant temperature.

Coolant flow. Variations in coolant flow rate also cause relatively mild power and reactivity responses. Initially the temperatures change, causing a small change in reactivity which tends to restore the initial temperature distribution. The power-to-coolant flow ratio will then be unchanged.

A severe condition is created if all three primary pumps fail when the reactor is operating at full power and the safety rods fail to scram. The rate of flow decay is primarily dictated by the inertia of the pumps until natural circulation sets in. This situation is illustrated in Fig. 4–44. As soon as the flow starts to decrease, the resulting temperature increase begins to shut the reactor down. After some time, the fission power drops to zero and the decay of fission products is the principal remaining source of heat.

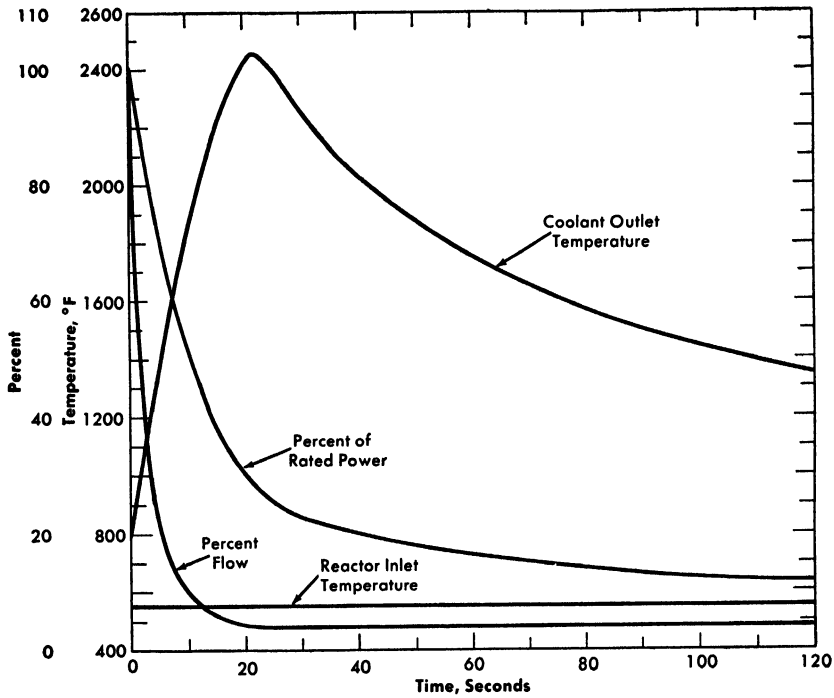

FIG. 4–44. Results of pump failure at full power.

Since there is still some uncertainty as to decay heat and degree of natural circulation, no final decision has yet been reached as to what should be done in the event of pump failure. A complete scram of the reactor would reduce the power so sharply as to produce some thermal shock. A sequential scram is being considered, consisting of consecutive insertion of all safety rods.

From the preceding discussion one can conclude that the kinetic response of the reactor to any of the three possible inputs is reasonably well-behaved even when all control systems fail, and that all situations can be taken care of by a well-designed automatic control and safety system. Those systems are discussed in a later section.

4–4.4 Reactor stability. Two possible modes of instability will be discussed, the autocatalytic or excursion instability, and the oscillating instability. Both have been observed in the Experimental Breeder Reactor I (see Chapter 2).

Autocatalytic instability. If the temperature coefficient of reactivity is positive the operation of the reactor is unstable. Any departure from

steady state is amplified at an increasing rate, since the period becomes shorter the more the power and temperatures depart from their steady-state values. Such an instability is even possible when the over-all temperature coefficient of reactivity is negative, if this coefficient contains a positive component which has less delay than the others. Indeed, if the reactor is put by external action on a sufficiently short period, the prompt positive coefficient becomes decisive, while the relative amplitudes of the other components are considerably reduced by their time lags.

This situation was apparently realized in the earlier version of the EBR-I. The bowing of the individual fuel elements is believed to have provided the prompt positive coefficient of reactivity. It is felt to be fairly certain that the Fermi Reactor will have no positive temperature coefficient, since the subassemblies will be so designed that bowing will produce no reactivity effect. Even if the bowing coefficient were slightly positive, its time delay would be relatively long and it would not produce instability. Any bowing that could occur would be from differential heating of the square subassembly wrapper tube, and hence would lag fuel and coolant expansions.

Oscillating instability. Small amplitude oscillations of the total reactivity ρ will cause oscillations of power, temperatures, and feedback reactivity ρ_2 (see Fig. 4–36). The amplitude and phase lag of ρ_2 can be estimated for any frequency and average power level. This situation may be visualized if one assumes that the control rod reactivity ρ_1 is made to oscillate. The reactivity balance is then $\rho_1 = \rho - \rho_2$. If at some frequency and power level, the phase of ρ and ρ_2 become identical, and the amplitude of ρ_2 is equal to or larger than that of ρ, the reactor power will oscillate without any external action.

This situation was realized in the earlier version of EBR-I, and has been analyzed by H. A. Bethe.* It was shown that such an instability can be caused by a negative temperature coefficient† with a large delay and small amplitude attenuation, and that its occurrence is favored by a prompt positive temperature coefficient. Calculations indicate that such an instability will not take place in the Fermi Reactor.

Prior to full-power operation, the stability of the reactor will be verified by oscillator tests. An external reactivity ρ_1 will be oscillated purposely at progressively increasing power levels. Observation of the reactor response at a given power permits prediction of the response at somewhat greater power.

---

*H. A. Bethe, Reactor Safety and Oscillator Tests, APDA-117, Atomic Power Development Associates, Inc., 1956.

†A negative temperature coefficient automatically introduces a 180° phase lag.

Oscillation of the reactivity will be accomplished by two steel rods containing eccentrically located boron poison, which will be rotated in two of the safety rod channels.

4–4.5 Critical experiment. As a part of the contract between the U. S. Atomic Energy Commission and Power Reactor Development Company, a critical experiment for the Fermi Reactor is to be run by Argonne National Laboratory. The experiment will be set up at the ZPR-III facility* at the National Reactor Testing Station, Arco, Idaho. Necessary materials have been ordered and the first mockup should be assembled in July 1958. To make the required detailed measurements, it is estimated that approximately one year of ZPR-III operating time will be needed.

Among the items to be established or checked by the experiments are: fuel enrichment; flux, power, and danger coefficient distributions; boron content of control rods; Doppler coefficient; and the reactivity of fuel configurations which could conceivably result from melting of the core.

4–4.6 Fuel reloading cycle. The control and fuel cycle for the Fermi Reactor are designed to keep the available excess reactivity small. Because of characteristics inherent in fast reactors, the excess reactivity needed in the clean cold condition to attain full power and override poison and burnout effects can be rather small. Four of these inherent characteristics are:

(1) Reactivity requirements for temperature override are smaller because the temperature coefficients in a fast reactor are less by a factor of ten than those in most thermal reactors.

(2) Poisoning by fission products, including xenon and samarium, is negligible.

(3) The relatively high enrichment characteristic of fast reactors results in a small reactivity loss due to fuel burnout, since the burnout will be limited to a small percentage of the total fuel (fissionable and fertile isotopes) by radiation damage.

(4) Because of the large conversion ratio, plutonium buildup compensates partially for the uranium burnout. A gram of plutonium in a given position adds about 1.5 times as much reactivity as a gram of U^{235}. Because a large fraction of the plutonium is bred in the blanket, however, the net reactivity effect of uranium burnout and plutonium buildup is negative.

With the temperature coefficients as presently calculated, 20¢ is more than adequate to override temperature effects in attaining full power from a proposed uniform startup temperature of 600°F.

*For a description of this facility, see *Nuclear Science and Engineering*, Vol. 1, No. 2, May 1956, p. 126.

It is estimated that 0.01 cents of reactivity/Mwd will be required to compensate for reactivity losses due to fuel element burnup and growth. This corresponds to 3¢/day for 300 Mw power at 100% load factor. Experimental data show that the 10 w/o molybdenum fuel alloy suffers a density reduction of approximately 3% for each percent burnup. A change in fuel pin length and radius of 1% per percent burnup was assumed in calculating the reactivity requirement of 0.01¢/Mwd.

It was decided early in the design to limit the available excess reactivity to less than one dollar of reactivity and about 92¢ has been chosen as the design figure. This constitutes a built-in safety feature, since to a large extent it prevents major accidents without relying on the automatic control and safety systems. Of the 92¢, 20¢ is set aside for temperature override, and an allowance of 30¢ is considered as the necessary control margin. Thus, during initial full power operation, only 42¢ is available to compensate for net fuel burnup and growth. This burnup allowance is a full order of magnitude less than that provided in many thermal reactors. Even with a reactivity loss as low as 3¢/day, the reactivity lifetime of the core is only two weeks at 300 Mw and 100% load factor.

The allowable residence time of the individual subassemblies is determined by the fission damage which the selected fuel alloy can withstand. One of the main research efforts has been to obtain a fuel alloy capable of withstanding considerably more burnup without excessive damage than has been attained. Temperature-controlled experiments irradiated in MTR have given assurance of at least 1% average burnup, and hope for larger burnup. One percent burnup in this context means that 1% of all the atoms present in the fuel alloy have been fissioned. This corresponds to about 5% depletion of U^{235}.

One percent has therefore been chosen as the reference average burnup that should be attained during early operation of the plant. The allowable residence time of the subassemblies is then 12 weeks on the average and 8 weeks for subassemblies in the highest flux region. This allowable residence time is much larger than the reactivity lifetime corresponding to 92¢ allowable excess reactivity. Therefore, partial reloading of the core will be used at each shutdown. Shutdowns will be scheduled for weekends, since the electric system power demand is then low. The fuel-handling mechanisms were designed for easy removal of the subassemblies so that the shutdown time can be kept as low as 10 hr.

The partial fuel replacements during a reloading period must be carefully programmed from three standpoints:

(1) To obtain a maximum useful life from each subassembly, only those which will have reached their maximum allowable burnup before the next scheduled reloading will be removed.

(2) To minimize control margin requirements, reactivity added by substituting fresh fuel for spent fuel must correspond closely to that lost since the last reloading.

(3) It is desirable to remove a uniform number of subassemblies per shutdown, particularly if the number involved is close to the maximum capacity (11 subassemblies) of the transfer rotor.

Because growth and short-time reactivity loss are assumed to be proportional to fuel burnup, and excess reactivity is limited to 92¢, reloading is required every 2 weeks at 300 Mw, even though a burnup much higher than 1% might be attained in individual fuel subassemblies. The number of subassemblies which are exchanged at each reloading depends on the burnup. With 6% burnup, only 1/6 as many subassemblies must be replaced every 2 weeks as with 1% burnup.

When an equilibrium operating schedule has been reached, some of the subassemblies in the core will be fresh and some will be almost spent. The average core subassembly will be one which is one-half spent or which has reached one-half of permissible burnup. For 1% average burnup, based on present conversion ratios and critical mass data, fresh subassemblies must therefore be loaded so that the core contains 1.6% more fuel than would be required if all subassemblies were clean. For 2% and 4% burnup, 3.3 and 6.6% more U^{235}, respectively, are needed. The initial reactor loading will therefore consist of fewer subassemblies than the loading during equilibrium operation. During the first 50 Mw-years of operation, until the first group of subassemblies has reached 1% allowable burnup, required reactivity additions are made by adding subassemblies at the core edge, replacing depleted uranium subassemblies.

The following tables and charts illustrate a possible reloading scheme. Table 4–7 shows residence times to 1% burnup of nine groups of subassemblies and their accompanying changes in reactivity. The nine groups of subassemblies are identified in Fig. 4–45. Two of the groups are first-row radial blanket subassemblies; the effects of other blanket subassemblies are small and have been neglected. The number of groups and the assignment of individual subassemblies to a given group have been somewhat arbitrary and will be optimized as further calculations are made and operating experience is obtained. In particular, data shown for subassembly groups 1, 2, and 3 are uncertain because of the varying influence of control rod position throughout the cycle.

A proposed operating schedule at 300 Mw is full power operation for 13 days with a shutdown for reloading on the 14th day. Table 4–8 gives pertinent data for an assumed burnup of 1.5%. Subassemblies capable of residence times between 14 and 16 weeks are unloaded at 14 weeks, since shutdown is not scheduled during odd weeks. A reloading schedule meeting these conditions and the three requirements outlined above is shown

TABLE 4–7

SUBASSEMBLY LIFETIMES AND REACTIVITY CHANGES FROM 0 TO 1% BURNUP*

Subassembly group	Number in group	τ, Mw-yr	Reactivity change, cents
1	10	50	−3.00
2	22	54	−3.00
3	19	58	−2.85
4	8	66	−2.65
5	8	77	−2.30
6	12	80	−1.75
7	12	88	−1.20
8	20	60	+0.5 (to 0.2% burnup)
9	28	100	+0.5 (to 0.2% burnup)

*Multiply τ and reactivity change by 2, 3, and 4 for 2, 3, and 4% burnup, respectively, for core subassemblies.

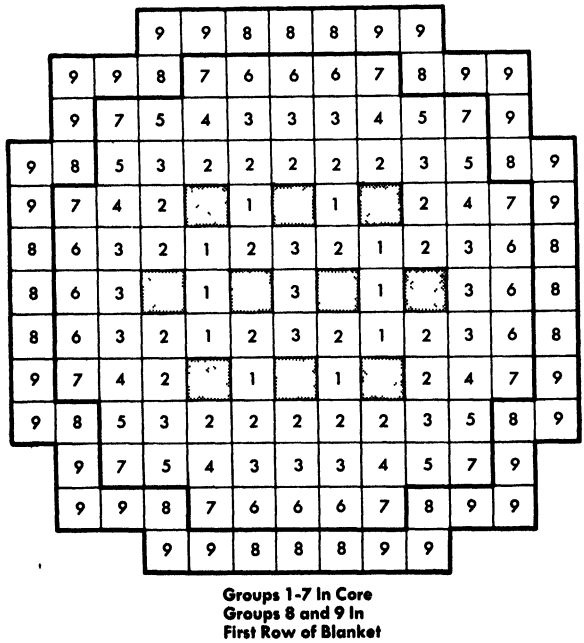

FIG. 4–45. Subassembly groups for core cycling.

in Table 4–9. There are thirteen shutdowns in 26 weeks. For group 1, a new subassembly installed at the first shutdown is replaced at the 8th shutdown, 14 weeks later, and the entire group is replaced in seven shutdowns. Similarly for the other groups, subassemblies loaded at a given schedule shutdown are removed 14 to 24 weeks later as bracketed in Table 4–9, and the entire group is replaced in the several intervening shutdowns. At the bottom of the table is shown the reactivity change for each biweekly subassembly substitution. With such a uniform schedule, very little if any control margin will be needed above the available 42¢ allowed for burnup. Unscheduled shutdowns will, of course, complicate the procedure. Note also in Table 4–9 that the total number of core subassemblies removed per cycle is quite uniform, remaining within the capacity of the transfer rotor. At the initially expected burnup of 1%, biweekly reloading requires changing approximately 16 subassemblies per shutdown. The transfer rotor capacity of 11 subassemblies is inadequate and some of the available 24 "possible fuel storage" positions shown in Fig. 4–13 will have to be used in a manner similar to the transfer rotor. A weekly cycle does not require the use of these positions. As increased burnups are attained, revised schedules will need only to show fewer subassembly removals per shutdown and the same frequency of shutdowns.

4–4.7 Choice of control elements. There are ten control channels, eight for safety rods and two for regulating rods. Boron-10 carbide will be used for both control and safety rods. The principal reason for selecting poison instead of fuel or reflector control is that mechanical design is much simpler. Less mass must be moved, and in shutdown material moves into the core from above rather than downward out of the core, thus reducing the size and complexity of the reactor vessel. A further advantage of poison over fuel control is that much less heat is generated in the control element for equal reactivity contribution.

There are two main disadvantages to using poison control, one involving the control rods and one the safety rods. Poison in control rods captures neutrons that could have been used to produce plutonium. In the Fermi Reactor, an initial poison shim control of 92¢ will reduce the conversion ratio by approximately 0.005, causing a plutonium revenue loss of about $15,000 per year under the initial operating conditions. Without partial reloading of the core, much more than 92¢ excess reactivity would be needed, and the plutonium revenue loss with poison control might then be prohibitive.

Poison in safety rods will have little or no effect on conversion, since the active section of each rod is poised above the axial blanket during operation. However, this poised position results in a delay between a scram signal and the negative reactivity insertion which would not be present

TABLE 4–8

SUBASSEMBLY LIFETIMES AND REACTIVITY CHANGES FOR 1.5% BURNUP AND A 13/14 LOAD FACTOR

Group	Number in group	τ, Mw-yr	Reactivity change, cents at 1.5% burnup	Maximum subassembly lifetime, weeks	Actual subassembly lifetime, weeks	Reactivity change at burnup
1	10	75	−4.50	14.0	14	−4.50
2	22	81	−4.50	15.1	14	−4.20
3	19	87	−4.35	16.25	16	−4.30
4	8	99	−4.00	18.5	18	−3.95
5	8	116	−3.45	21.7	20	−3.20
6	12	120	−2.65	22.4	22	−2.60
7	12	132	−1.80	24.7	24	−1.75
8	20	60	+ .5 (to 0.2%)	11.2	10	+ .5
9	28	100	+ .5 (to 0.2%)	18.7	18	+ .5

TABLE 4–9

BIWEEKLY UNLOADING SCHEDULE, 300 MW, 13/14 LOAD FACTOR, 1.5% BURNUP

Shutdown number	Subassemblies removed per cycle												
	1	2	3	4	5	6	7	8	9	10	11	12	13
Group 1	(2)	1	1	2	1	1	2	(2)	1	1	2	1	1
2	(3)	3	3	3	4	3	3	(3)	3	3	3	4	3
3	(3)	2	3	2	2	2	3	2	(3)	2	3	2	2
4	(1)	1	1	1	0	1	1	1	1	(1)	1	1	1
5	0	(1)	1	1	1	1	0	1	1	1	0	(1)	1
6	(1)	1	1	1	2	1	1	1	1	1	1	(1)	1
7	(1)	1	1	1	1	1	1	1	1	1	1	1	(1)
8	0	(20)	0	0	0	0	(20)	0	0	0	0	20	0
9	0	0	(28)	0	0	0	0	0	0	0	(28)	0	0
Total core subassemblies per cycle	11	10	11	11	11	10	11	11	11	10	11	11	10
Reactivity change per cycle, cents	42.8	27.2	27.5	41.7	40.5	37.2	32.8	41.7	41.5	37.2	28.8	31.4	41.5

Total reactivity change in 26 weeks: 4.70 dollars.

if fuel or reflector control were used. It is felt that the safety and reliability afforded by a simplified design more than compensates for the above as well as several less important disadvantages not discussed here.

4–5. Control Rods and Safety Rods

4–5.1 General description. The neutron-absorbing material in the safety and control rods is boron carbide enriched with B^{10}. Boron-10 has a significant absorption cross section for fast neutrons due to the $B^{10}(n,\alpha)Li^7$ reaction. The eight safety rods are uniformly spaced in a ring 7 inches from the core centerline; the two operating control rods are 2.5 inches on either side of the core axis. During reactor operation, the safety rods are held by a latch in the upper section of the axial blanket.

Each of the ten poison control elements is housed in a cylindrical guide tube, which in turn is inserted in a square can of the same size as a core subassembly. This arrangement is shown in Fig. 4–46. Heat generated by a poison control element is removed by sodium flowing from the core inlet plenum through pressure breakdown orifices in the bottom of the guide tube and thence through both the element and the annulus between the element and the guide tube.

4–5.2 Safety rods. The safety rods, each worth $1.00 of reactivity, are used for scramming the reactor in the event of unusual operating conditions. They are also inserted after normal shutdown. When a safety rod is put into use, sodium from the lower guide tube is forced through slots to the area between the guide tube and the can and then into the pool above. Tests in water indicate that 0.6 sec is required for full insertion of a rod. Of this, 0.2 sec is required for the rod to pass through the upper blanket region and into the core.

A safety rod has four sections: the poison section, the dashpot ram, the extension rod, and the pickup head, as shown in Fig. 4–47. The poison section, roughly the length of the core, is composed of a series of sealed stainless steel tubes each containing hollow cylinders of boron carbide, enriched with B^{10} isotope and hot-pressed to approximate theoretical density. The stainless steel tubes are designed as pressure vessels to contain the 2 liters of helium gas which will be generated by the $B^{10}(n,\alpha)Li^7$ reaction in 10 years of full power operation (at 75% plant factor). In the center of the hollow boron-carbide cylinders, a thin-walled, punched stainless steel tube serves as a well for the helium. Heat generated in the boron carbide is removed by sodium flowing around the outer stainless steel tubes.

The dashpot ram, a double-tapered piston with a 6-inch effective length, is the part of the hydraulic shock absorber which absorbs the ki-

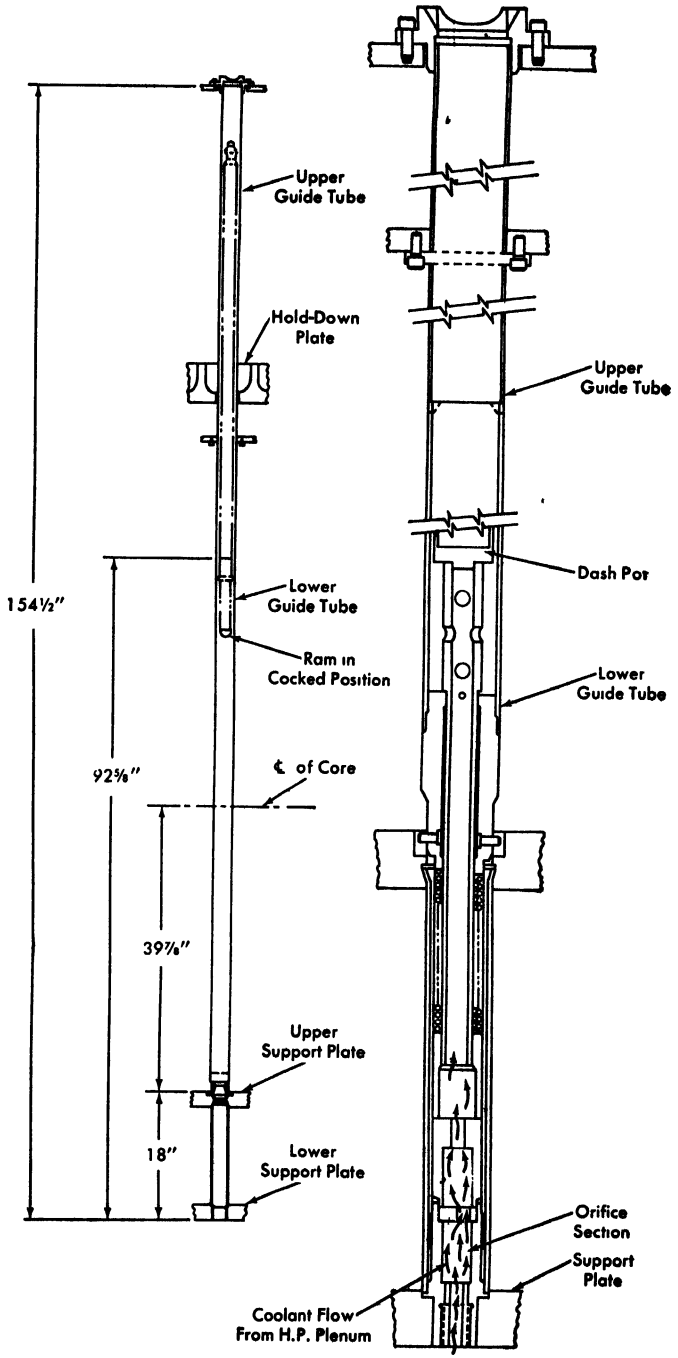

FIG. 4–46. Control rod channel.

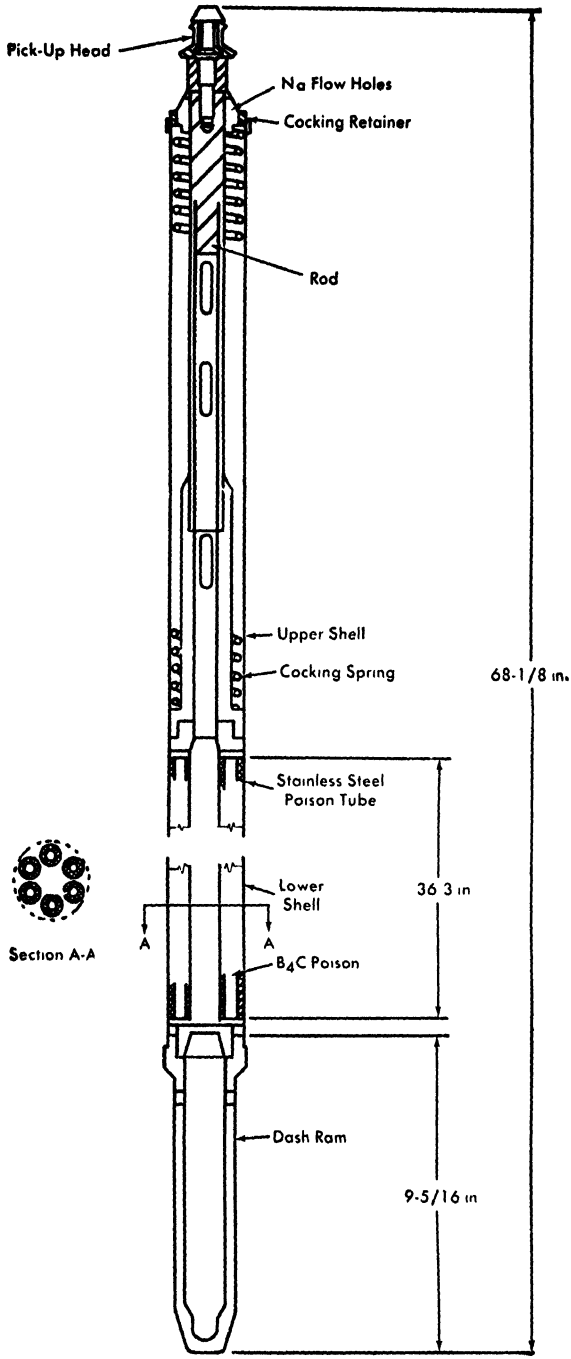

FIG. 4–47. Safety rod assembly.

netic energy of the safety rod after its free fall. Its entry into the dashpot slows the rod at a constant 3 g deceleration.

The extension rod is a transition piece between the poison section and the pickup head. It is long enough for the offset handling mechanism to handle it when the poison section of the control rod is fully inserted in the core. Adjacent core subassemblies must be removed before the safety rod can be removed. The extension rod section contains a spring that is compressed by the action of the drive mechanism and latched in a cocked position. When the latch is released, the spring gives the rod an average 2 g acceleration through its initial 10 inches of travel. The safety rod attains a maximum velocity of 9 fps.

The pickup head, located at the top of a subassembly, has a small diameter at the upper section to enable the control drive mechanism to lift the rod during reactor operation. The larger diameter at the lower section of the pickup head enables the offset handling mechanism to remove the safety rod for either repair or replacement.

4–5.3 Operating control rods. An operating control rod has three sections: the poison section, the extension rod, and the pickup head, as shown in Fig. 4–48. The poison section, approximately 10 inches in length, consists of solid boron carbide cylinders, hot-pressed to approximate theoretical density. The boron carbide is contained in sealed stainless steel tubes which, as with the safety rods, contain the generated helium gas. However, due to the continued high flux exposure, operating control rod containment tubes are designed for helium generation of 6 liters in 10 months, as compared with 2 liters over 10 years for the safety rods. Void space lies above the poison section in a 14-inch length of the containment tubes. The position of the B_4C in the tubes is maintained through the use of a sintered micrometallic (steel) plug installed above the B_4C and held in place by a welded collar.

The pickup head and the extension rod have functions similar to comparable parts of the safety rods, except that a small spring is at the top of the extension rod for positive latching of the control drive pickup mechanism. Control rods are not dropped during a reactor scram. The operating control rods are moved by a motor drive through a rack and pinion at a maximum linear rate of 6 in/min. The speed of insertion corresponds to a change in reactivity of less than 1¢/sec for both rods moving simultaneously.

4–5.4 Safety rod actuators. The safety rod drives, of electromechanical design, are on top of the shielding plug of the reactor (Fig. 4–4). Details of the safety rod actuator are shown in Fig. 4–49. The rods are grasped by a mechanical latch at the end of a long extension drive shaft,

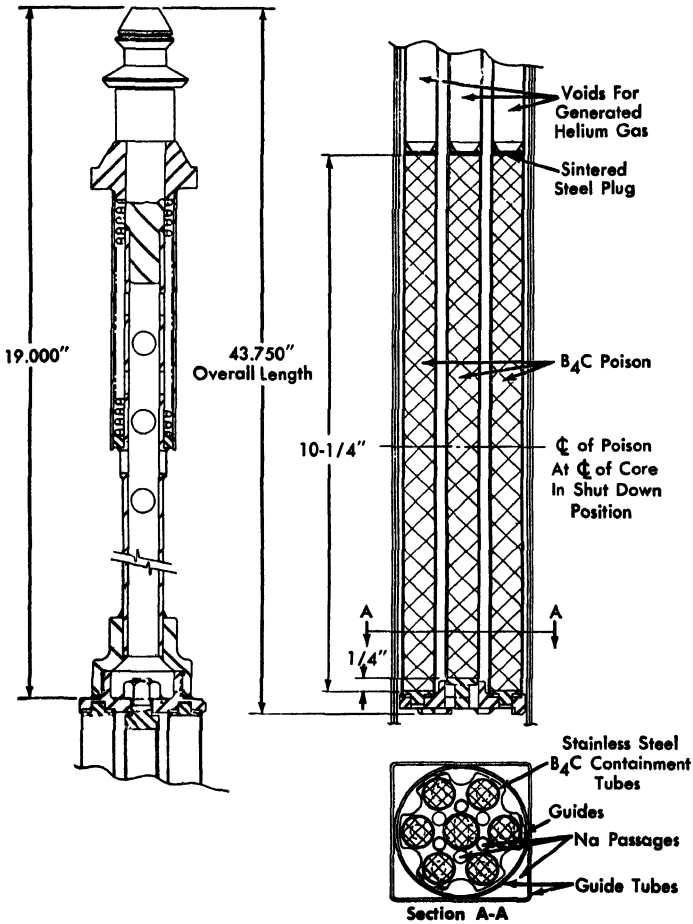

FIG. 4–48. Operating control rod.

raised and lowered by means of a rack and pinion. Where the extension drive shaft penetrates the rotating shield plug, a bellows seal with a packing seal backup prevents radioactive sodium vapor from entering the machinery space (section B of Fig. 4–49). The pickup fingers of the latch are cammed shut by action of the drive element and safety rod pickup head (section D). They are held in the latched position by the armature of an electromagnet, located above the rotating shield plug (section A). A long extension tube passing through the drive shaft extension tube connects the camming parts of the latch to the armature of the holding electromagnet. When the electromagnet is de-energized, the combined weight of the armature, extension tube, and camming parts together with the stored energy of

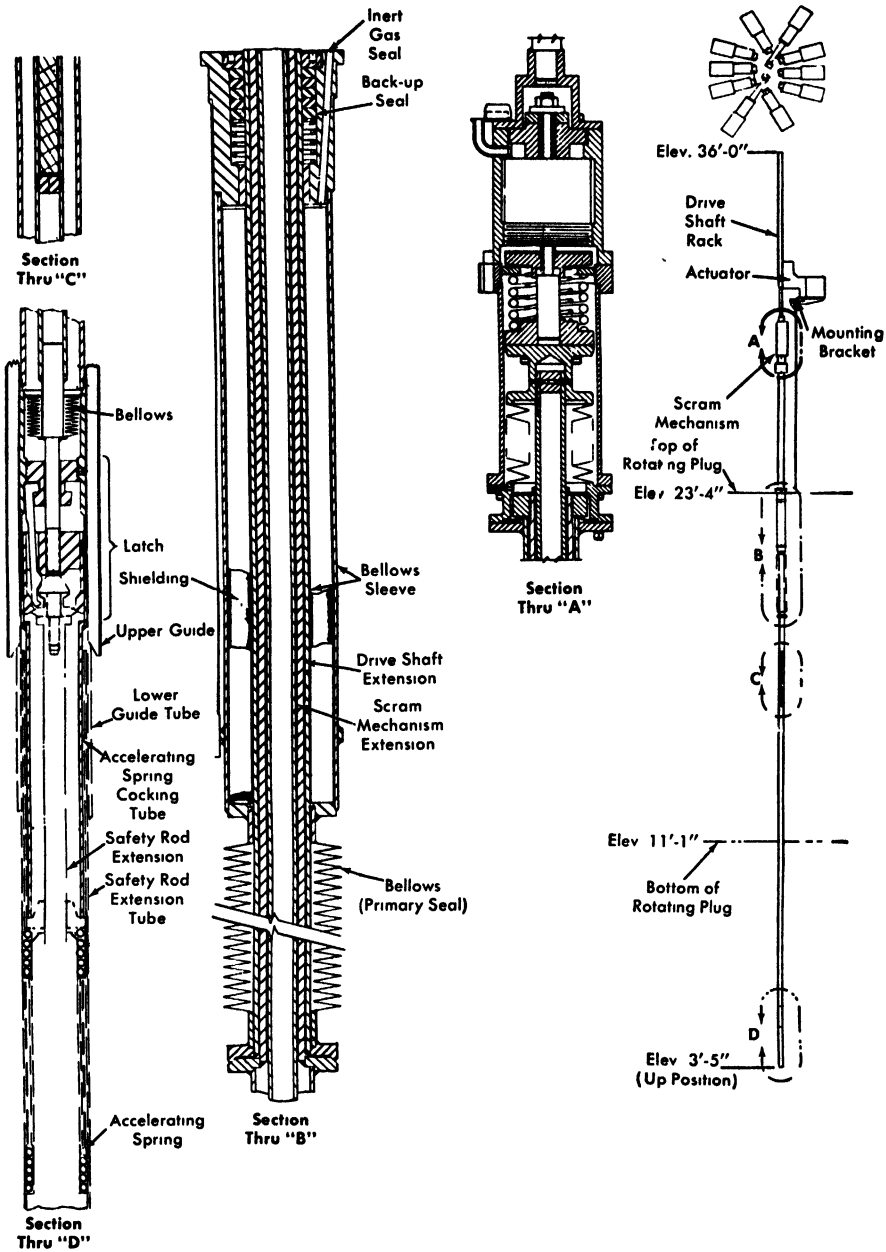

FIG. 4–49. Safety rod actuator mechanism.

a compression spring positively can open the latch fingers and release the rod. Loss of power to the holding electromagnet will scram the reactor.

The accelerating spring of the safety rod is compressed by a tube connected to and extending down from the latch body. Thus, the rod-accelerating spring is compressed by the downward motion of the drive shaft, and in the same motion the latch fingers are cammed into their pickup position over the safety rod pickup head. By energizing the holding electromagnet, the safety rod can be picked up and elevated with the accelerating spring in its cocked position. The safety rod can be released and accelerated from any position throughout its stroke by de-energizing the electromagnet.

The time for complete release of the safety rods is 0.05 sec after initiation of a scram signal. For fully withdrawn safety rods, the travel time through the upper blanket region is roughly 0.2 sec, making a total of approximately 0.3 sec before actual shutdown is begun.

The total time necessary to insert the $8 of negative reactivity in the 8 safety rods is about 0.75 sec from the time of initiation of a scram signal.

The safety rods can be moved vertically in three ways:

(1) Motor drive into or out of the core: The rods are driven through a rack and pinion by a reversible 3-phase induction motor at 2 in/min. This rate is equivalent to 1¢ of reactivity per second for 8 rods moving simultaneously.

(2) Controlled rundown of the drive shaft and rod into the core: The rod drive motor is disconnected from its gearing through a magnetic clutch so that the drive shafts and rods run down 2.5 in/sec, equivalent to a negative reactivity insertion of 75¢/sec for 8 rods moving simultaneously. The rundown speed of the drive shaft and rod is controlled by a centrifugal brake that is geared to the rack.

(3) Fast scram into core: Upon reception of a scram signal, the holding electromagnet is de-energized, releasing the mechanical latch. The spring-loaded rod is then accelerated into the core at an average velocity of about 100 in/sec, equivalent to a negative reactivity insertion of $25/sec for 8 rods dropping simultaneously.

4–5.5 Control rod physics. The two operating control rods are located in a higher flux than the safety rods. Together the two rods are worth 92¢ of reactivity. They are used to control the reactor operating power level, to override the negative temperature reactivity coefficient, and to compensate for fuel burnup and element growth. The reactor will not become critical until safety rods have been fully withdrawn and operating control rods have been partially withdrawn.

Although the use of poison control rods affects neutron economy adversely, the loss of neutrons is of minor importance, since only a small

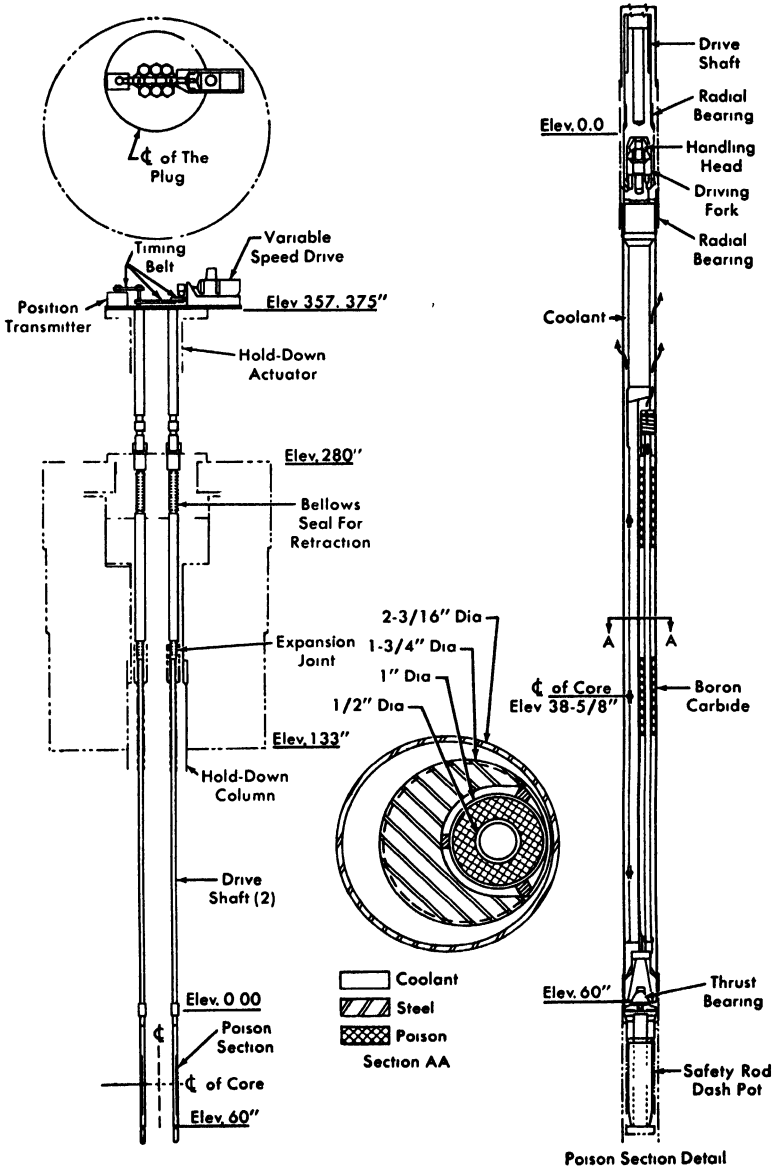

FIG. 4–50. Oscillator rod.

amount of reactivity control is needed to operate the reactor. Because of present uncertainties in the nuclear calculations, a safety factor of about two is being utilized in specifying the amount of poison material to be inserted into the control and safety rods. After the critical experiment has been run and the control rods have been calibrated, the amount of poison material will be specified to provide $1.00 per safety rod and 92¢ in the stroke of both control rods operating together.

4–5.6 Oscillator rod. The oscillator rods make possible a small-amplitude sinusoidal variation of reactivity, of adjustable frequency, for experimental studies of the dynamics of the reactor during the preoperational test period. Each oscillator rod is a rotating control rod having an eccentric boron carbide poison cartridge, as shown in Fig. 4–50. Such a rod can be placed in any safety channel. To achieve the necessary changes in reactivity, a pair of oscillator rods will be used, each rod contributing about 3¢ peak-to-peak reactivity change. The oscillator rods are rotated by drive shafts, terminating at the top of the hold-down actuator.

The drive shaft can be disconnected manually from the poison section to permit fuel handling. The poison section and its bearing carrier can be removed from the reactor and replaced by the fuel-handling system. Hydrodynamic radial and thrust bearings, made from specially hardened materials, are designed to operate dry or in sodium. They are mounted in a bearing carrier which is part of the driving mechanism and can be removed from the reactor. It is expected that about 100 kw of heat will be generated in the boron carbide at 300-Mw reactor output. This heat and that generated in the structural steel will be removed by sodium flowing through the guide tube, through and around the rod, and around the shaft.

With speed remotely adjustable between 0.06 and 600 rpm, the rods are rotated by a mechanical variable-speed drive with an integral $1\frac{1}{2}$-hp motor. Phase relationship between the two rods will be optimized experimentally by changing a mechanical adjustment on the drive pulleys while rotating the assembly. Positional information will be transmitted by a pair of sine potentiometers, one connected directly to the oscillator rod drive shafts, and the other connected through a mechanical differential. Thus, the phase relationship of the two potentiometers can be changed by energizing a servo motor to which the reactor flux signal is fed. When outputs of the two potentiometers are nulled by operating the servo motor, the phase displacement of the differential is equal to the phase angle between input Δk and reactor power.

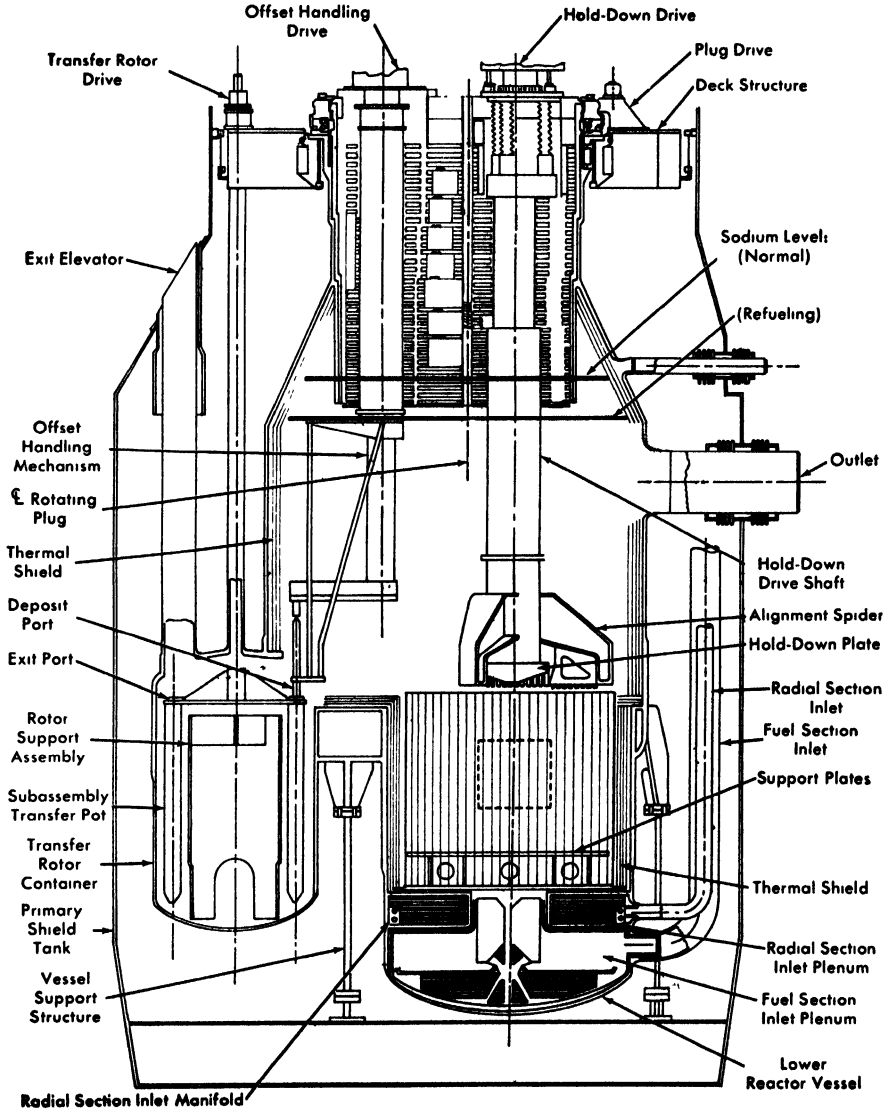

FIG. 4–51. Elevation of reactor vessel.

4–6 Reactor Compartment

4–6.1 General description. The reactor vessel and rotating plug are shown in Figs 4–51, 4–52, 4–53 Core and blanket subassemblies are housed within the lower reactor vessel, they are cooled by sodium that flows from the bottom of the lower vessel, through the subassemblies, and up into the upper reactor vessel which serves as a mixing pool The upper reactor vessel also houses the hold-down device and the offset fuel-handling mechanism The hold-down device, consisting of a plate, alignment spider, drive shaft and drive mechanism, holds the upper ends of the core subassemblies in radial alignment, holds the subassemblies down against pressure caused by the upflow through the subassemblies, and acts as a

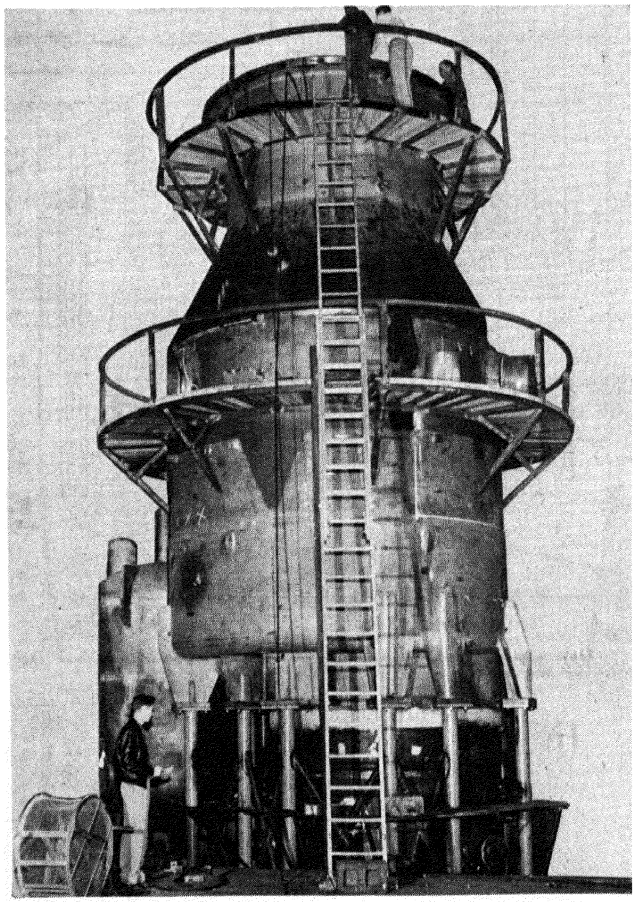

Fig. 4–52. The Enrico Fermi Reactor vessel.

guide for the control rod drives. The offset handling mechanism, in conjunction with the rotating shield plug, will be used to remove spent fuel and blanket subassemblies from the reactor and deposit them in finned pots in the transfer rotor. Each subassembly in its finned pot can then be placed by the transfer rotor under the exit port of the reactor and can be raised vertically upward into a self-propelled transfer cask car that is equipped with a vertically actuated gripper mechanism Subassemblies are installed in the reactor by reversing this process.

The rotating plug on top of the reactor vessel has both the hold-down device and the offset handling mechanism mounted eccentrically on it. When the plug is rotated, the hold-down device is swung away from the core as the handling mechanism is swung over the core.

The upper reactor vessel will be at approximately atmospheric pressure, with an inert gas atmosphere above the sodium. The entire reactor vessel will be enclosed in the primary shield tank, whose void space will be filled with an inert gas to prevent a reaction in case sodium leaks into it.

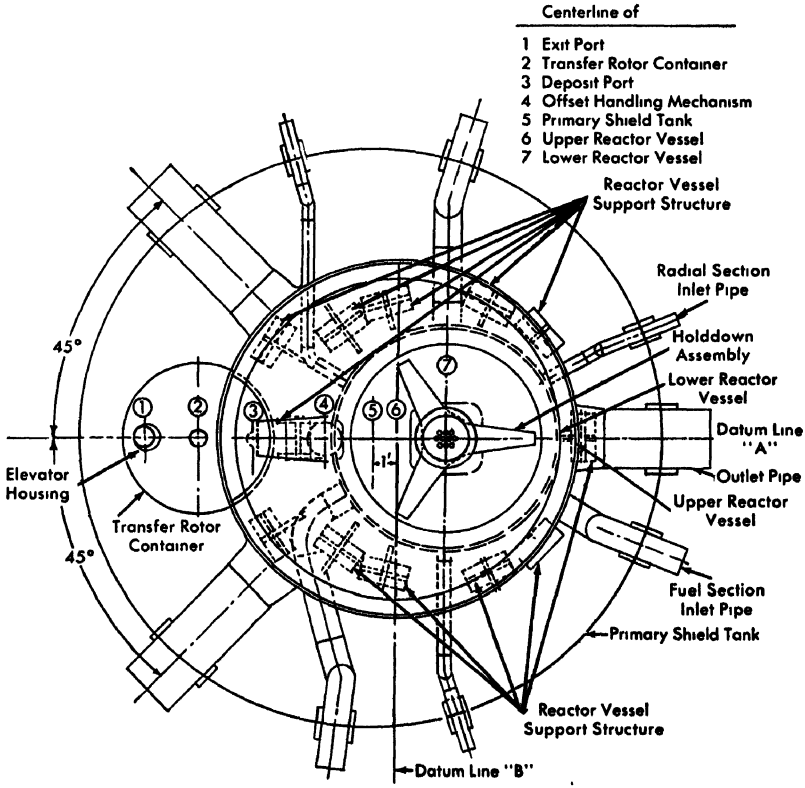

Fig. 4–53. Plan view of reactor vessel at sodium level (refueling).

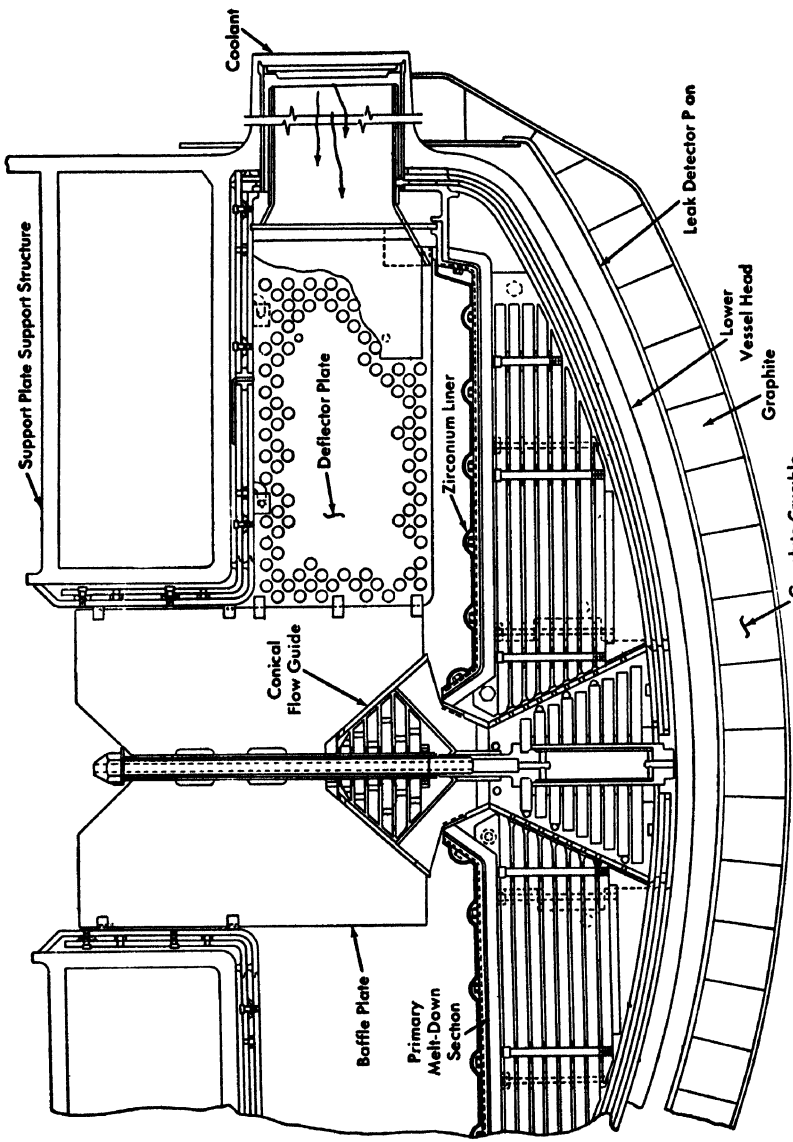

FIG. 4-54 Meltdown section in lower reactor vessel.

4–6.2 Lower reactor vessel. The lower reactor vessel is 9 ft, 6 inches in diameter. The cross-sectional view in Fig. 4–13 shows the arrangement of core and blanket subassemblies, control rod guide tubes, and thermal shielding rods. Each subassembly has an 18-inch-long nozzle at the bottom end for insertion into the two support plates. The two support plates, 2 inches thick, are spaced 14 inches apart by ribs welded to the plates (Fig. 4–4) The center section of the plates supporting the core subassemblies is separate and can be removed. This provides flexibility in the design of the core and its supports. Clearances between nozzles and plates, including tolerances, will be about 5 mils, limiting the misalignment to about 50 mils at the handling lug at the top of the subassemblies. The support plates rest on the bearing bars and seal rail (Figs. 4–4 and 4–51).

The transition section, connecting the lower reactor vessel, the upper reactor, and the transfer rotor container, consists of a flat head with vertical ribs and deck plate, Figs. 4–4 and 4–51. Brackets are welded under the transition section in line with the ribs to support the reactor vessel. Flexible support columns, plates 2 inches thick and 7 ft high, allow for thermal expansion of the reactor vessel and are oriented to hold the centerline of the upper reactor vessel fixed (Fig 4–51).

4–6.3 Meltdown section. Special design features incorporated in the lower reactor vessel provide for safe containment of the molten fuel, should the core melt down completely.

The primary meltdown section (Fig. 4–54) is in the lower sodium plenum. The dimensions are such that a meltdown section in the shape of a flat circular slab of zirconium 7 ft in diameter can be accommodated. With complete meltdown of the core, the thickness of the molten material in this region would be about 1.25 inches. This large surface area would satisfy the requirements of subcriticality and heat removal. The section is a pot made of a 1/8-inch-thick zirconium liner bolted to the top 1/2-inch-thick plate of the large assembly of stainless steel baffle and shield plates in the lower head.

Another feature shown in Fig. 4–54 is the conical flow guide. This will direct coolant flow during normal operation, and in case of a meltdown, it will have a dispersing effect on molten fuel as it enters the plenum, tending to prevent a pile-up of fuel in the center of the meltdown section.

The secondary meltdown section is immediately below the bottom head of the lower reactor vessel and follows the contour of the head. This section consists of a layer of 6-inch cubes of 5% borated graphite bonded together with boron-containing cement to form a crucible capable of containing molten uranium. The graphite crucible is supported by a 1/4-inch-thick steel head hung from the reactor vessel support brackets.

4–6.4 Coolant flow. Coolant is supplied to the high-pressure plenum through three 14-inch nozzles at 110 psi. It flows up through the square opening in the support structure to the subassemblies in the core and first row of the radial blanket (Fig. 4–5).

Coolant supplied at low pressure through three 6-inch nozzles to the manifold in the support structure flows back and forth up through the shielding plates in the structure to the radial blanket subassemblies, as shown in Fig. 4–51. Pressure in the manifold will be kept below 20 psi by restrictions in the system to prevent the blanket subassemblies from being lifted out of the support plate.

4–6.5 Hold-down device. Each subassembly that receives coolant from the high-pressure plenum must be prevented from rising due to coolant flow. The handling lug of each subassembly is held down with a female knob attached to the hold-down plate; this compresses a spring in the inlet nozzle of the subassembly, shown in Fig. 4–14, which holds the subassembly firmly against the knob and allows expansion.

The hold-down device is aligned by a three-arm spider, shown in Fig. 4–51. When the hold-down device is lowered into place, sockets attach to the hemispherical tops of the hold-down support columns. These support columns are supported and aligned at the bottom by the reactor support plates and are keyed at the top to the lower reactor vessel wall.

Each guide tube for the control rods has an upper matching section in the lower housing of the hold-down assembly which, when in place, forms the complete channel for the control rod and control rod actuator.

4–6.6 Rotating shield plug. The rotating shield plug is an integral part of the biological shield which serves as part of the subassembly handling equipment (Fig. 4–55). It is made up of a $1\frac{1}{32}$-inch-thick stainless steel shell containing layers of various shielding materials and insulation. The shielding materials are 18 inches of stainless steel, 7 ft of borated graphite, and 2 ft of carbon steel. The top of the plug is capped with a 12-inch-thick carbon steel cover plate which carries the hold-down assembly and the offset handling equipment. The plug load is transmitted to the reactor vessel plug container flange through the larger load carrying ring and the ball-bearing assembly. The plug gear is integral with the load carrying ring. Sealing between the rotating plug and the plug container is achieved with a liquid (NaK) dip seal, backed up with a mechanical seal. Provisions will be made for cold-trapping and determining liquid level and oxide concentration to minimize maintenance of the dip seal. All bolted covers and flanges are sealed with rubber O-rings and gaskets.

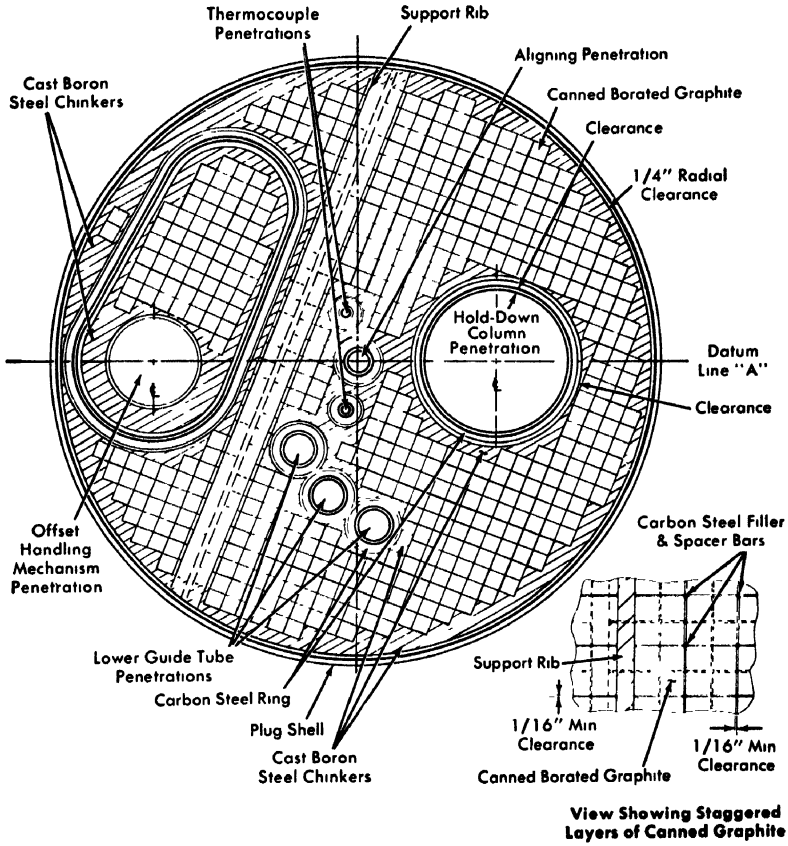

FIG. 4–55 Horizontal section of rotating shield plug

The stainless steel shielding consists of thin plates located at the bottom of the plug to a thickness of 18 inches; above this are seven layers of 5% borated graphite blocks, 3 inches by 3 inches by 4⅜ inches, sealed in stainless steel cans. Each layer of borated graphite cans is supported by a 1¼-inch-thick carbon steel plate. Spaces between the square graphite cans and the circular wall and penetrations of the plug are filled with layers of 1¾-inch-thick cast boron (1 to 1½%) steel plates. The remaining plug shielding consists of six 2-inch-thick carbon steel plates located above the graphite cans. A 12-inch-thick layer of canned stainless steel wool insulation is placed between the top carbon steel plate and the plug cover plate. Two steps are used in the plug skirt and in all plug penetrations to prevent neutron streaming.

A 3-inch hole through the center of the plug permits alignment, and three 5-inch holes are provided for removing the lower guide tubes.

4–6.7 Reactor vessel shielding. The interior of the lower reactor vessel contains a 12-inch stainless steel thermal shield to attenuate high-energy neutrons and thus minimize radiation damage to the vessel. It also attenuates the gamma flux emerging from the blanket, reducing heat generation within the vessel walls and in the borated graphite layer. The shield further serves to reflect some neutrons back into the blanket. As shown in Fig. 4–13, part of this shield will be in the form of stainless steel subassemblies that fit into the same grid structure as the blanket subassemblies. Two rows of these subassemblies will completely surround the blanket, forming a layer about 5 inches thick. The remaining part of the thermal shield will be attached to the inner wall of the vessel itself and will consist of several layers of cylindrical plate sections mounted concentrically with the vessel. With the vessel wall, the thickness of this part of the shield will add up to a total of 8 inches. Sodium coolant flows between these layers, removing the heat generated in them due to radiation absorption.

Outside the vessel, a borated graphite shield will reduce the intensity of neutrons escaping from the primary shield tank enough to prevent significant neutron heating of the secondary concrete shield wall and other concrete areas. This borated graphite shield is designed so that most of the heat generated in it flows back into the reactor vessel and is carried away by the sodium. This is accomplished by placing the first 6 inches of borated graphite next to the vessel, then an insulating layer The smaller fraction of the heat generated in the remaining graphite shielding is removed from the primary shield tank by the reactor compartment cooling system.

The stainless steel thermal shield and the borated graphite layers, together with the blanket, form the primary shield system and attenuate the core neutrons by a factor of approximately 10. This system is totally contained within the primary shield tank. For the upper reactor vessel, the primary shield system consists of a similar arrangement of stainless steel thermal shielding 6 inches thick within the vessel and layers of borated graphite and carbon outside the vessel.

4–6.8 Mechanical integrity and thermal stresses. Integrity of the reactor vessel is assured by careful design with low stress limits, proper welding procedures, and extensive tests. To avoid loss of strength from radiation damage, shielding is used between the reactor and the vessel wall. In areas subject to radiation damage, surveillance tubes containing specimens will be used to keep a continual check on the properties of the material. All plates have been ultrasonically tested, welds have been liquid penetrant-tested and radiographed, and the completed vessel has been subjected to vacuum leak tests and hydrostatic tests. The reactor

vessel is built in accordance with Section VIII of the ASME Boiler and Pressure Vessel Code.

Steady-state thermal stress will be minimized by the use of thin sections and shielding to reduce internal heat generation in structural material To minimize transient thermal stresses, thermal baffles are used next to all structural surfaces in the lower reactor vessel. These baffles consist of thin plates adjacent to the vessel surfaces with stagnant coolant between them, as shown in Fig. 4–13. Mixing in the plenums and in the upper reactor vessel, and the heat capacity of the large amount of steel in the radial section inlet plenum, will further reduce thermal shock. In the upper reactor vessel, the thermal baffles will be inside the shielding instead of being next to the vessel wall.

4–7. Mechanical Handling

4–7.1 General description. The subassembly handling equipment is used to remove radioactive core and blanket subassemblies from the reactor after irradiation to a prescribed burnup After being removed from the reactor, these subassemblies are transferred by cask car to a storage area, where U^{237} and the general level of fission-product radioactivity are allowed to decay to a suitable level for subsequent reprocessing. They are then transferred to the disassembly and shipping facility to be shipped to a fuel or a blanket reprocessing plant. Fresh subassemblies are transferred by the cask car from plant storage to the reactor The over-all arrangement of the handling equipment is shown in Fig 4–4.

Components of the primary handling system are located above and immediately adjacent to the reactor. The equipment consists of the offset handling mechanism, the rotating shield plug, and the transfer rotor. Motions of the plug and offset handling mechanism enable subassemblies to be withdrawn from any position in the reactor lattice and placed into the transfer rotor for storage under sodium during the period immediately after removal from the reactor when heat release is at its highest. Subassemblies will remain in the rotor between fuel transfer periods and will be transferred from the sodium to the cask while the reactor is being recharged with fresh fuel. This arrangement minimizes the reactor shutdown time required to transfer fuel. Provision is also being made to store 24 core subassemblies in the outer edge of the radial blanket, as shown in Fig. 4–13, should it be desirable to unload more than 11 core subassemblies at any one time.

It takes about 6 months for the internal heat generated in irradiated fuel subassemblies to decay enough so they can be removed from liquid or forced gas cooling. All subassemblies are, therefore, transferred to and from the reactor in sodium-filled pots that are essentially finned-tube heat

exchangers. The pots, which have a greater heat-transfer efficiency than the bare subassemblies, enable the decay heat to be dissipated to the inert gas atmosphere of the transfer chamber. Even with this greater heat-transfer efficiency, a waiting period of several hours after reactor shutdown is required before the subassembly in the pot can be removed from the reactor sodium pool. The storage capacity provided in the transfer rotor permits the necessary decay of radioactivity to take place while the reactor is running. Therefore, subassemblies can be removed immediately after the reactor is shut down, because in every case they were removed from the reactor core during the prior shutdown and stored in the rotor. The finned pots and the transfer rotor, providing adequate heat-transfer and storage space requirements, greatly simplify heat-transfer problems in unloading.

Between 10 and 20 hr of plant shutdown time per outage is chargeable to fuel loading operations. The required period will depend on the method of programming subassembly removals and fuel burnup, as well as relative frequency of recharging and, hence, the number of subassemblies to be handled. The reactor will be charged with fuel at either weekly, fortnightly, or monthly intervals, depending on the amount of control available and required. Some blanket subassemblies will be discharged along with fuel elements; others will be charged at less frequent intervals, possibly every 2 to 6 months, in groups of 20 or more. On the average, about 150 blanket subassemblies will be removed in a year. Table 4–10 shows the number of core subassemblies to be removed each time the reactor is refueled, for various burnups and power levels.

TABLE 4–10

NUMBER OF CORE SUBASSEMBLIES REMOVED EACH UNLOADING*

Burnup	300 Mw			430 Mw		
	One week between unloadings	One month between unloadings	Two months between unloadings	One week between unloadings	One month between unloadings	Two months between unloadings
1%	8	32		12		
2%		16	32	6	24	
3%		11	22		16	32
4%					12	24

*Based on plant factor of 100%.

4–7.2 Offset handling mechanism. The offset handling mechanism is shown in Figs. 4–56 and 4–57. This mechanism is designed so that no hazard will result due to equipment malfunction. The design requirements are outlined below.

Control and position indication. The offset handling mechanism is controlled by a semiautomatic system that provides positional accuracy of ±0.1 degree azimuth and constant-position indication of angular orientation and elevation. The latch lock and unlock motions are known positively through operation of limit switches. All motions are interlocked; no motion can be started until the preceding one has been completed. The interlock feature avoids equipment damage.

Mechanical design. A locking worm in the vertical drive stops the crane and keeps it in position if the power fails. The gripper mechanism is a positive acting device; loading and unloading actions are accomplished by direct action of a probe-actuated cam member in contact with the subassembly handling lug. As the handling mechanism moves downward over the subassembly to be gripped, the latch cam probe touches the top of the subassembly handling lug, and its downward movement is stopped. The handling mechanism continues downward, changing the relative position of the fingers and cams, until the fingers have been forced to the closed position. Sensing this action, the probe extension trips a switch to stop the downward travel of the handling mechanism. A spring-loaded tab plate locks the probe rod in the "up" position, fixing the relationship of the gripper fingers and cam. Actuation of the various members is indicated at the control panel. Each motion must be completed before the handling mechanism can proceed with the withdrawal.

The gripper fingers cannot be released in the "carry" position; it is necessary to seat the subassembly at the proper elevation to actuate the solenoid-operated tabplate. The action of lifting the handling mechanism then causes the gripper fingers to be cammed to the open position; as the handling mechanism rises, the element is released and remains in its proper position in the reactor.

The offset handling mechanism is designed for dual speed operation when lowering subassemblies into position in the reactor. If through some incredible combination of manufacturing and inspection errors, a sufficient number of greatly over-enriched core subassemblies should be loaded into the reactor to override the $8 of negative reactivity in the safety rods, then the reactor could become critical during loading. To avoid reaching criticality under these circumstances, the offset handling mechanism is automatically slowed down from 20 ft/min to 1 ft/min as the fuel portion of the subassembly enters the core. One foot per minute means addition of less than 1¢ reactivity per second for a normal subassembly in the center of the core, or about 1/4¢/sec at the outer edge of the core.

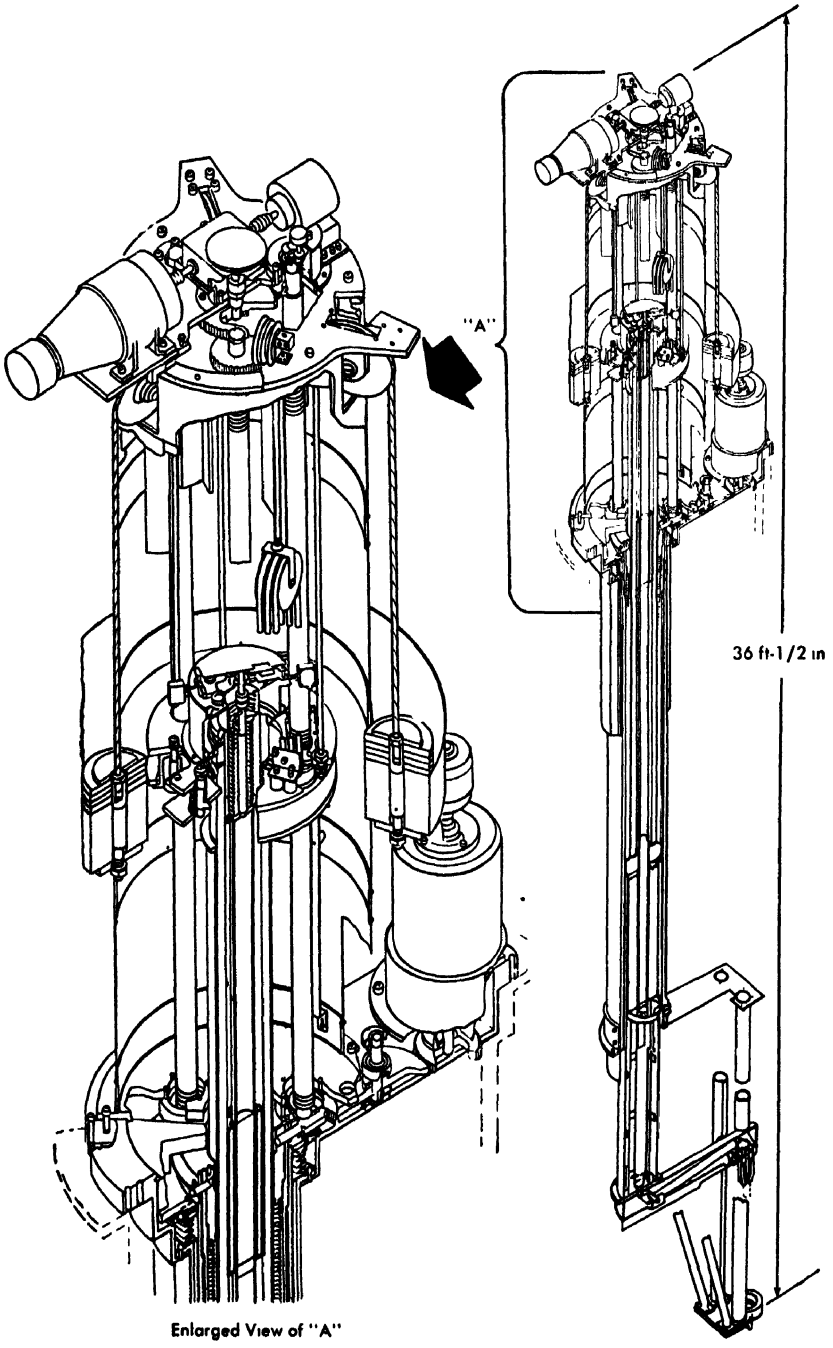

FIG 4–56. Cutaway drawing of offset handling mechanism.

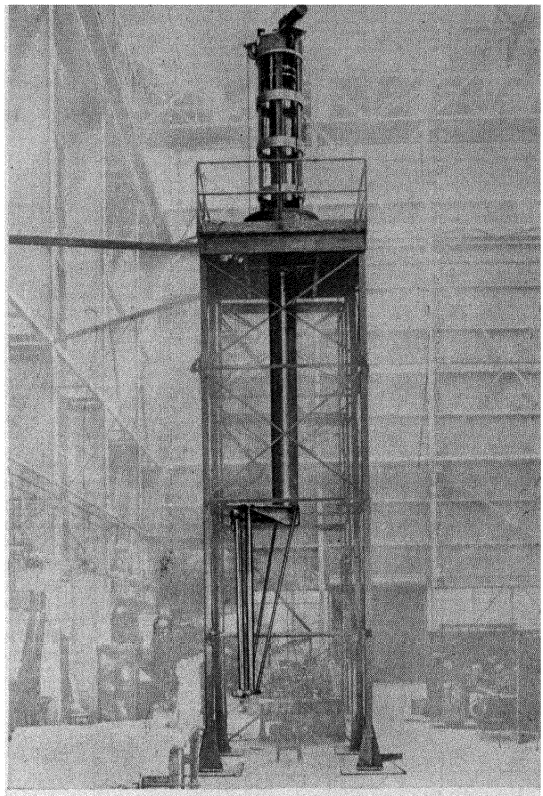

FIG. 4–57. General view of offset handling mechanism.

If the reactor should approach criticality as the core subassembly is lowered, the offset handling mechanism will automatically reverse and withdraw the fuel subassembly at a rate of 20 ft/min.

4–7.3 Transfer rotor assembly. The transfer rotor assembly is shown in Fig. 4–58. It consists of a rotary drive unit with indexing equipment, a vertical drive shaft to provide the rotary motion, and a rotor plate at the bottom of the shaft in which the subassemblies and finned pots will be stored. This device will serve a twofold purpose: Its primary function is to divert subassemblies horizontally from beneath the rotating plug and offset handling mechanism so that they can be raised into a cask car. It will also provide temporary storage for up to 11 irradiated core subassemblies while their residual heat generation is high.

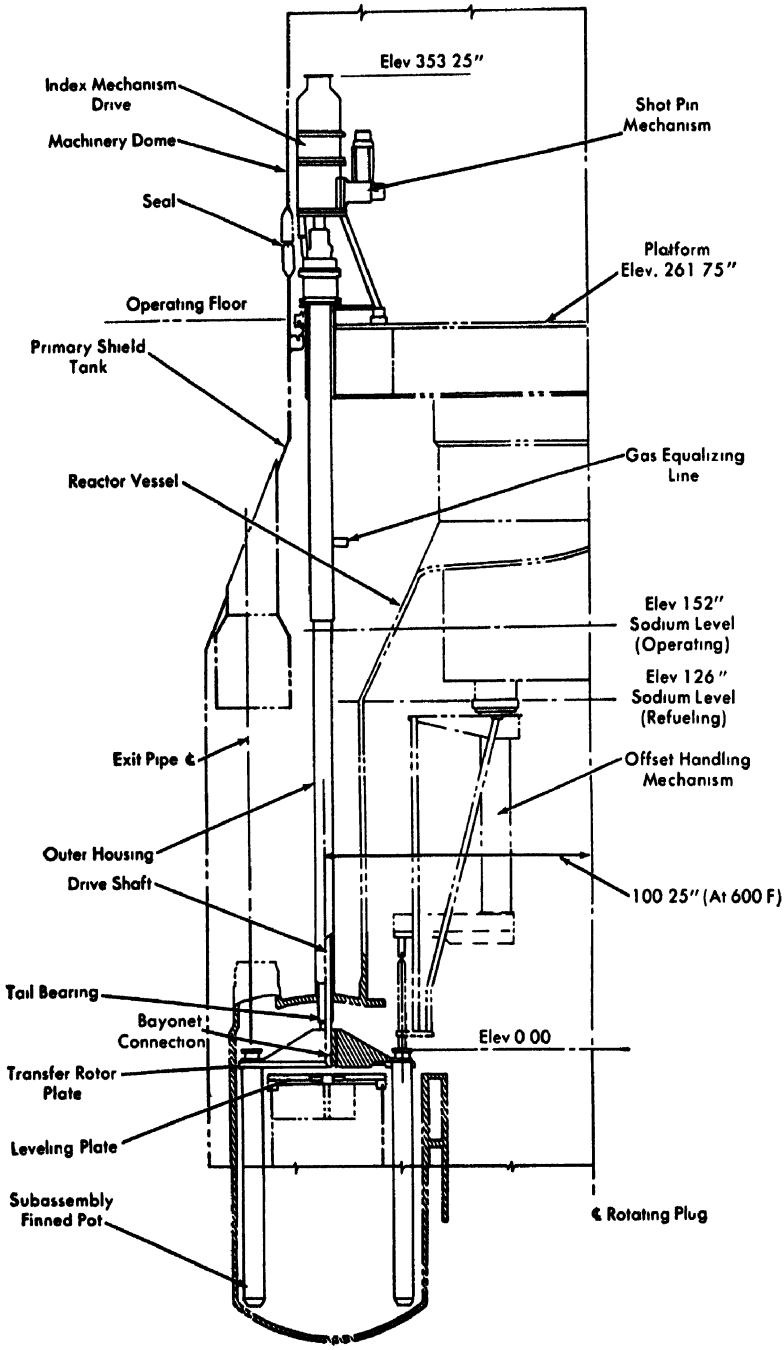

FIG 4–58. Schematic diagram of transfer rotor assembly.

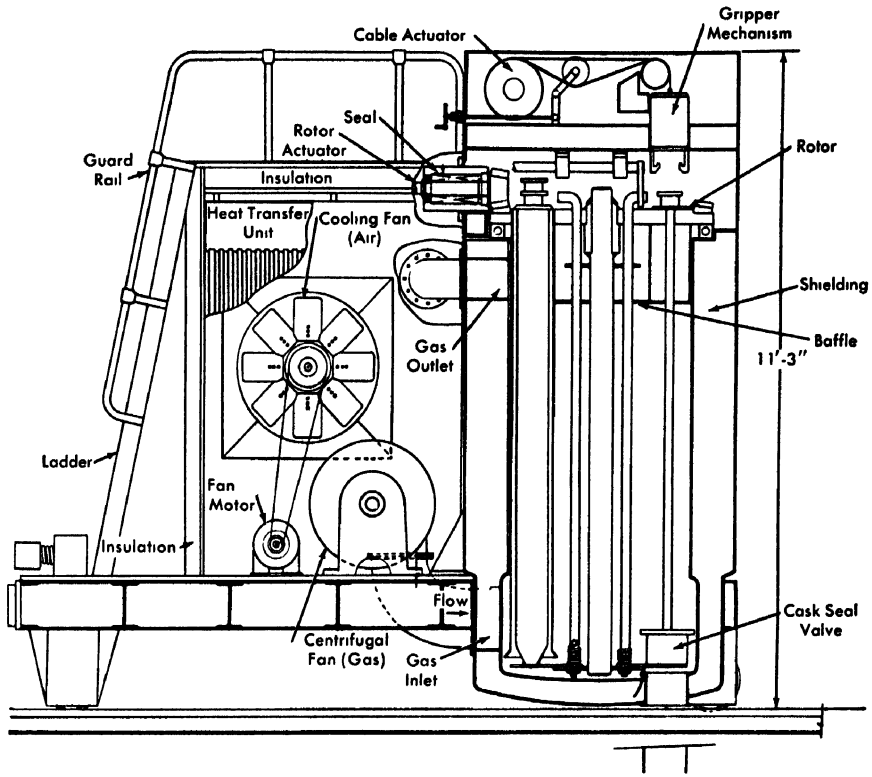

FIG 4–59 Sectional elevation of cask car, showing fuel element storage rack.

4–7.4 Cask car. The concept of the transfer cask car is illustrated in Fig 4–59, and its relationship with the reactor building in Fig. 4–60. This car is equipped with a cable-actuated gripper mechanism and rotor disk to remove and transport several subassemblies at a time. The car will be positioned next to the reactor, with the gripper mechanism over the discharge pipe of the reactor vessel, aligned with the center of the outside hole of the transfer rotor plate. Finned pots containing subassemblies will be withdrawn from the transfer rotor plate in the vessel and placed in the cask car rotor. The cask car will then move through the reactor building equipment door to a decay storage building located near the reactor building. The equipment door will be interlocked with the reactor control system so that the door cannot be opened during reactor operation.

In the cask car, heat from the subassemblies and pots will be transferred to an inert gas atmosphere, circulated through an external heat exchanger integral with the cask car, and dissipated to the surrounding atmosphere.

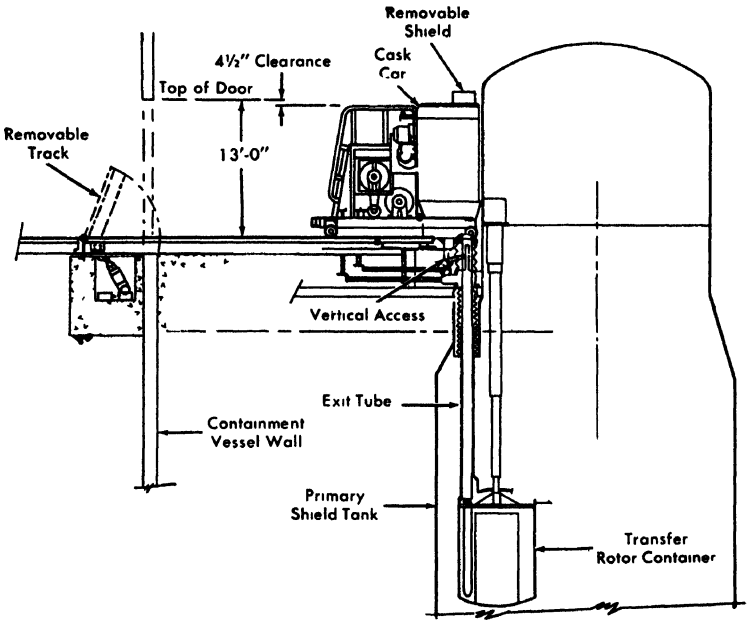

FIG. 4–60. Cask car arrangement in reactor building.

4–7.5 Hold-down actuator. The hold-down actuator, illustrated in Fig. 4–61, delivers a force of 110,000 lb to the hold-down plate, to resist the lifting force from the coolant pressure drop in the core subassemblies.

The power train runs from the motor, through a double-worm-gear reducer, idler, and pinion, to the ring gear which drives three ball-nut screws. The force is then transmitted downward through the spring plate assembly to three actuator shafts and through them to the triangular drum, below which is fastened the actuator column. The hold-down plate, to which the force is finally transmitted, is mounted on the bottom of the column. The plate must be raised 9 inches after reactor shutdown before the shield plug can be rotated for fuel handling.

The actuator column contains two shielding areas: 42 inches of stainless steel, and 83 inches of powdered iron-carbon-boron carbide mixture. The control rod drive mechanisms are mounted on a flange at the top of the structural housing, and the drive extensions pass through penetrations in the actuator column. Thermocouple leads from the core outlet area also pass up through the column.

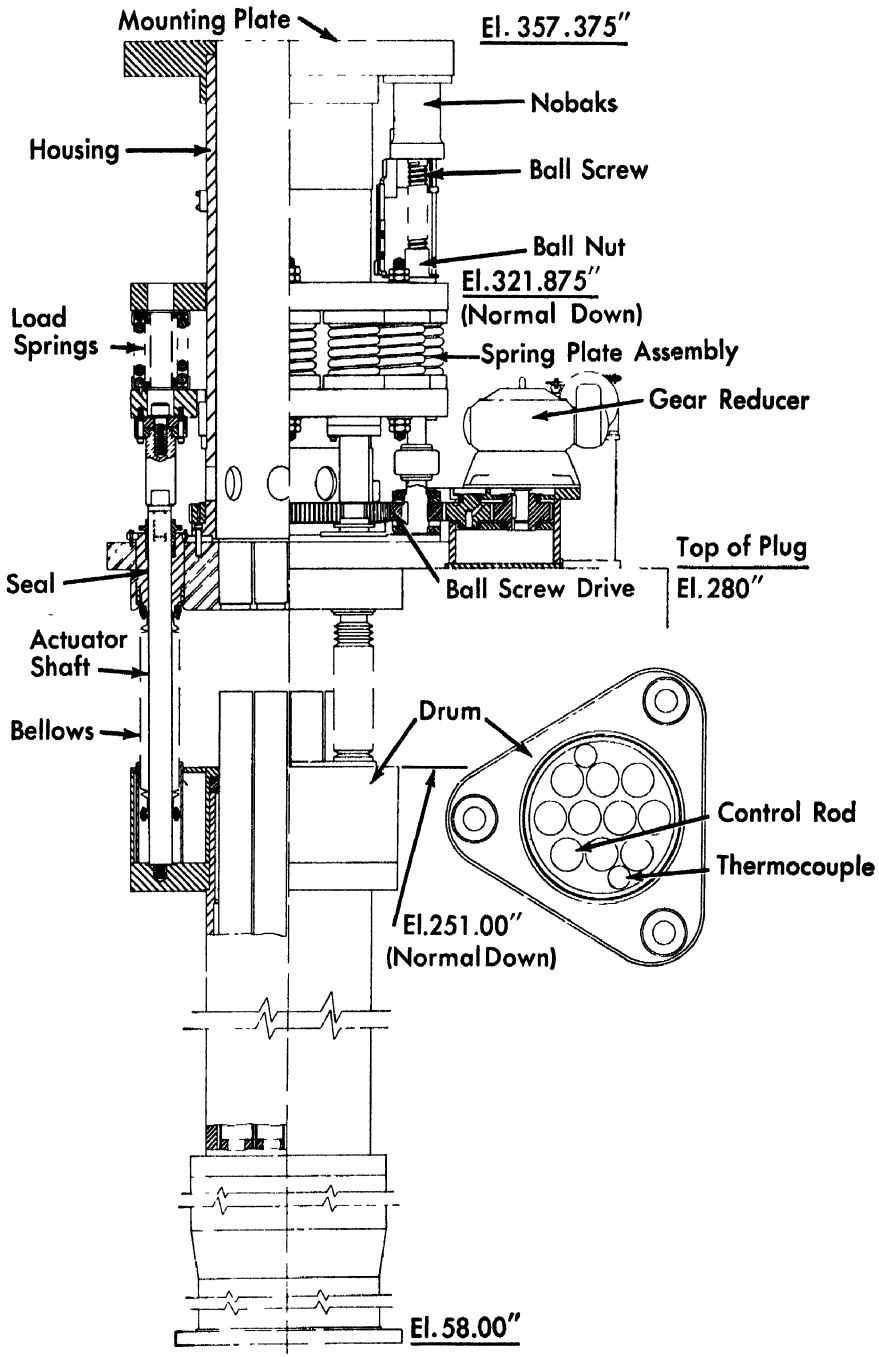

FIG. 4–61. Hold-down actuator.

4–7.6 Loading and unloading procedure. The various steps required during one complete cycle of core or blanket loading and unloading are as follows:

(1) Reduce reactor power to zero by lowering the shim and safety rods to shutdown position.

(2) Reduce sodium flow through reactor to a point where hydraulic forces on fuel subassemblies and control rod guide tubes will be well below that required to unseat them.

(3) Unlatch operating and safety control rods from actuators.

(4) Raise hold-down plate to a point where all structures under the hold-down plate are clear of the top of subassemblies.

(5) Raise all control rod actuators until they are clear of the fuel subassemblies.

(6) Rotate the transfer rotor to position subassemblies in their pots, one at a time, under the cable-actuated gripper mechanism of the cask car. Withdraw all pots from the rotor up into the cask car.

(7) Return a pot with a fresh subassembly in it to the rotor each time a pot is removed from it. The cable-actuated gripper lowers pots with new subassemblies into all but one of the positions in the rotor.

(8) Rotate the plug and offset handling mechanism to position the gripper over the core or radial blanket subassembly to be removed.

(9) Lower the gripper, grasp the subassembly, and withdraw it from the reactor lattice.

(10) Rotate plug and offset handling mechanism to position the subassembly over the empty pot in the transfer rotor.

(11) Lower the subassembly into the empty pot.

(12) Raise the gripper of the offset handling mechanism and rotate the transfer rotor to put the next pot with a fresh subassembly under the gripper.

(13) Lower the gripper of the offset handling mechanism into the pot, and pick up the fresh subassembly.

(14) Lift the subassembly to the carry position and rotate the plug and handling mechanism to place the subassembly over the empty hole in the reactor lattice.

(15) Lower the subassembly into the reactor. The offset handling mechanism will automatically reduce the speed of core subassembly insertion to 1 ft/min as the subassembly moves into its final position. Detach the gripper fingers and leave the subassembly in place as the offset handling mechanism is raised.

(16) Repeat the procedure until all fresh subassemblies have been moved into the reactor and all spent subassemblies being replaced are in the transfer rotor for decay. During the next shutdown they will be removed and transported to the decay storage area.

After all the subassemblies have been transferred, the procedure for returning the reactor to operation is as follows:

(1) Retract the offset handling mechanism and rotate it to storage position.

(2) Lower the hold-down about 5 inches until the straight section of each of the 3 lower alignment pins is just beginning to engage.

(3) Lower all control rod actuators until they engage the control rods and align the lower control rod guide tubes.

(4) Lower the hold-down device to the reactor operating position.

(5) Actuate the latches of the control rod actuators to couple all control rods.

(6) Start the sodium pump or pumps.

(7) Carry out the nuclear startup procedure.

4–7.7 Maintenance of radioactive equipment. The fuel-handling machines, the control rod actuators and lower guide tubes, the primary sodium pumps, and the intermediate heat exchangers have been designed so that each component can be remotely removed for inspection, disassembly, and replacement of certain parts. Personnel control measures become very important when access to radioactive areas is required. Three categories of maintenance are therefore distinguished, based primarily on the degree of potential hazard to personnel, and also reflecting the degree to which the primary system is interrupted during maintenance operations. These categories are routine maintenance, special maintenance, and major equipment removal.

Routine maintenance occurs as a regularly scheduled program of inspecting, adjusting, and replacing electrical and mechanical equipment located above the shield and sealed from the primary system. Drive units, limit switches, gearing, and electrical leads to moving machine components are examples of equipment in this category. During routine maintenance operations, the reactor will be shut down.

Special maintenance operations involve interrupting the shield or seals of the primary system. Some scheduled equipment removal falls in this category, if physical size does not make it a "major removal"—for example, the removal for inspection of the operating control rod drives, the safety rod drives, and the control rod lower guide tubes. A shielded coffin is used to transport the radioactive equipment.

Examples of nonscheduled removal operations utilizing the same protective equipment are the long reciprocating bellows and the tail bearing tubes of the offset handling mechanism, the transfer rotor drive shaft, and the transfer rotor shield-seal sleeves. Figure 4–62 shows one such special operation: removal of a safety rod drive unit. The upper drive structures are removed, bolt flanges are loosened, and lifting devices are

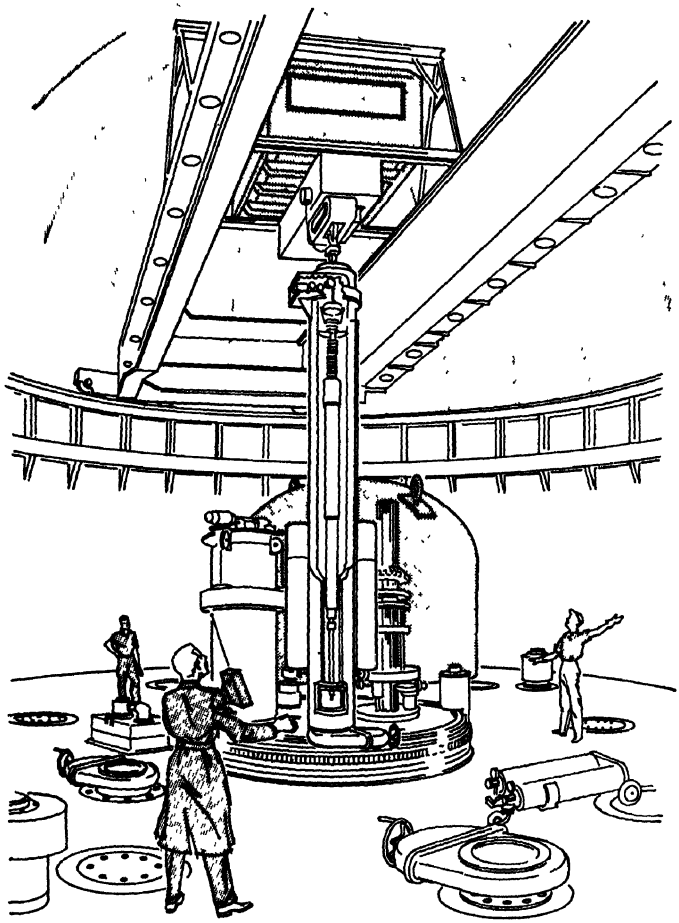

FIG. 4–62 Perspective view of operating floor, showing removal of a safety rod drive unit.

attached to the machine without special protection against radioactivity. A valve is mounted on the floor above the component, and the valve sealing faces are clamped together. Both valves are opened, a grapple is lowered and attached to the machine, which is then raised into the coffin, and both valves are closed. The area between the valves is purged with clean argon gas, the valve sealing faces are unclamped, and the coffin is lifted away to a previously prepared opening into an equipment storage pit beneath the reactor operating floor, or it is transported out of the reactor building into a shielded inspection area in an adjacent facility. Since the equipment for special operations gives complete personnel protection, remotely operated equipment is not required.

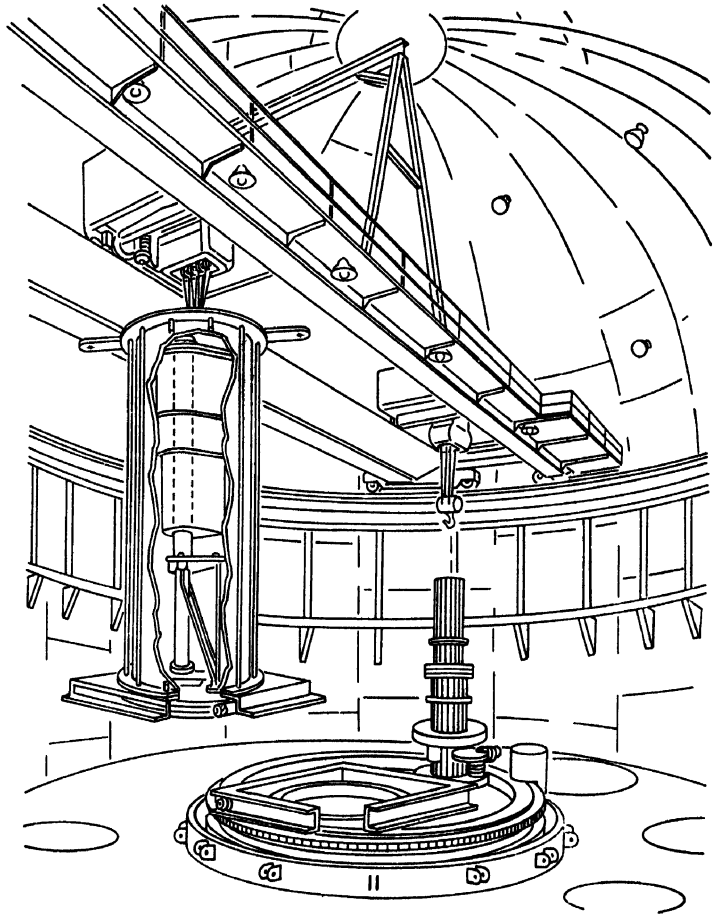

FIG 4-63 Perspective view of operating floor, showing removal of offset-handling mechanism from reactor

Equipment removal operations involve handling major system components such as the offset handling mechanism, the primary sodium pumps, and the tube bundle of the intermediate heat exchangers These components are very large and their removal requires interrupting the seals and shield of the primary system It is hoped that such removals will occur only once or twice during the life of the plant. For this reason, large investments in special equipment to implement removal operations are not justified. The approach has been to develop equipment that will prevent cross-contamination of reactor and external building environments. No shielding is placed around the radioactive component.

Because of the large amount of induced radioactivity in some of the ma-

jor components that will be exposed during removal operations, it is necessary to shield the control room for these operations. The design criteria for the control room shielding are: (1) a waiting period of 8 days, to let the short-lived activity in the components die away; and (2) total dose to the operator is to be held to 300 mr or less during the operation. In cases where the total dose may exceed 300 mr, a second operator will relieve the first.

Removal operations are remotely controlled from the central control room. Radioactive equipment is withdrawn into a positively sealed flexible container to prevent contaminating areas that will later be accessible to personnel. The container and seal arrangement also prevents oxidation of the sodium in the primary system.

Figure 4–63 shows the method used to remove and transport the offset handling mechanism in the reactor building. The machinery dome and drive unit superstructure have been removed. A grappling adapter has been attached and a seal unit has been put in place. Using the procedure previously outlined, the machine has been withdrawn into the container, the seals have been closed and unclamped, and the offset handling mechanism is being transported to its storage tank.

One method of making fine alignments is shown in this drawing. A cross bar is fixed to the rigid lifting plate at the top of the container. Targets on the under side at either end of this bar are located above points on the floor. Alignment of the targets with the locating points through a system of television cameras and mirrors will permit the crane operator to bring the component into alignment by remote control for insertion or withdrawal from close clearance openings.

The offset handling mechanism is inserted into a storage pit containing a bag and structural members in which the machine will subsequently be transported to the repair facility, right next to the reactor building. All these operations are remotely controlled. Again, positive containment is provided, but no shielding. Once the component has reached the repair facility, it will be placed in a pit and operating personnel can work on it from a shielded operating gallery.

4–8. Liquid Metal and Steam Systems

4–8.1 General description. Heat removed from the reactor core and blanket by the primary sodium coolant is transferred first to the secondary sodium coolant in the intermediate heat exchangers, and then to water and steam in once-through steam generators. The over-all system, shown diagrammatically in Fig. 4–64, is composed of the reactor with three pri-

mary coolant loops having a common point in the reactor vessel, and three independent secondary coolant loops having no common hydraulic point.

The choice of coolant fluids for a fast reactor is limited to those not containing hydrogen or other moderating elements. Sodium was chosen as both the primary and secondary coolant because it has a low vapor pressure at operating temperatures, a high thermal conductivity, and an acceptable specific heat. Further, it is inexpensive and, if the oxygen concentration is kept below 50 ppm, it is reasonably noncorrosive to zirconium and stainless steel, the primary system materials. Sodium also has some undesirable properties; it burns spontaneously in moist air, it reacts rapidly when in contact with water, and it freezes at 208°F. Because of the latter property, an external heating system is required to keep the piping and equipment temperatures above 208°F during filling, startup, and prolonged shutdown periods.

The reasons for using two liquid metal systems, including an intermediate heat exchanger, are (1) to avoid the hazard of chemical reaction between water and radioactive sodium in the event of an internal boiler leak, (2) to eliminate the production of free oxygen in the steam generator water by gamma rays from primary sodium, (3) to assure containment of all radioactivity in the reactor building, and (4) to prevent hydrogenous material from entering the reactor. A sodium-water reaction in the secondary system will not rupture the primary coolant system or destroy the integrity of the building.

The activation level of the Na^{24} in the primary coolant is expected to be about 0.05 curie/cm^3 at full power; the level of the Na^{24} in the secondary coolant is estimated to be less than 2×10^{-4} microcurie/cm^3. There will be a small amount of Na^{22} produced from high-energy neutrons in the reactor by the reaction $Na^{23}(n,2n)Na^{22}$. Sodium-22 emits a 1.28-Mev gamma ray that presents no problem during reactor operation. The expected equilibrium activity of the Na^{22} at full power is estimated to be in the order of 2 microcuries/cm^3.

The operating conditions of the sodium and steam systems is tabulated in Table 4–11. All piping and equipment is being designed and fabricated in accordance with Section VIII of the ASME Boiler and Pressure Vessel Code and Sections I and VI of the Code for Pressure Piping.

4–8.2 Primary coolant system. The primary system sodium flows by gravity from the free surface pool of the upper reactor vessel to the shell side of the intermediate heat exchanger and then to the pump tank. The space above the sodium in each piece of equipment is filled with inert gas and these gas spaces are interconnected by means of gas equalizing lines. The sodium is pumped from the pump tank back to the reactor, delivering approximately 90% of the flow to the plenum serving the reactor core and

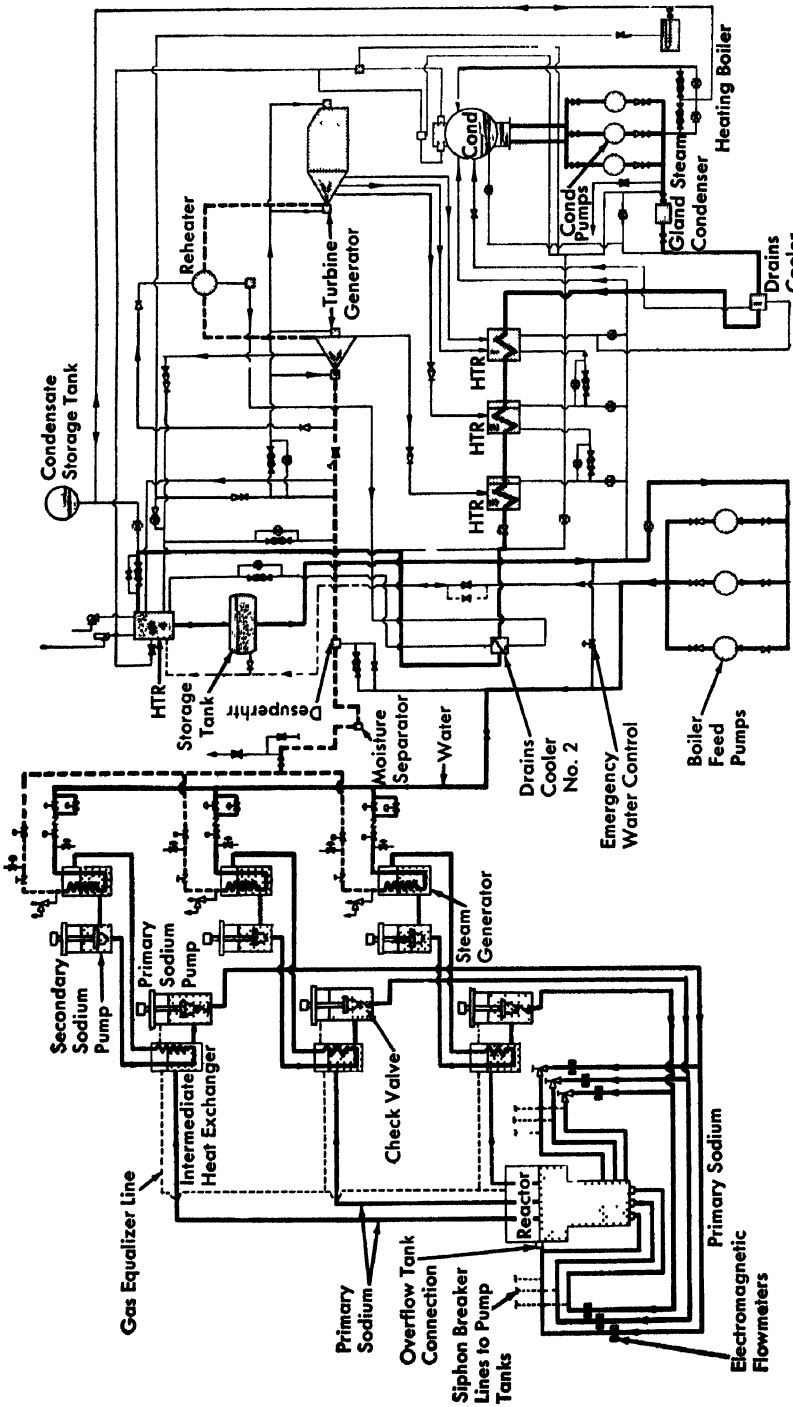

FIG 4-64 Flow diagram of the nuclear power plant.

TABLE 4–11

PERFORMANCE OF LIQUID METAL AND STEAM SYSTEMS AT 300-MW OPERATION; PRIMARY COOLANT SYSTEM

Coolant data	
Primary coolant material	Sodium
Flow rate per loop, lb/hr	4.4×10^6
Flow rate per loop, gpm at pump temp.	10,000
Total flow rate, lb/hr	13.2×10^6
Total flow rate, gpm at pump temp.	30,000
Temperature:	
Heat exchanger inlet, °F	800
Heat exchanger outlet, °F	550
Total sodium volume, ft^3	5,300
Total sodium weight at 350°F, lb	302,000
Piping layout	
Piping system, reactor to pump:	
Average fluid velocity in pipe, fps	4.9
Design pressure, psig	125
Design temperature, °F	1,000
Pipe size	30 in., $^3/_8$ in.-wall
Pipe material, stainless steel	Type 304
Piping system, pump to reactor:	
Pipe size and velocity:	
100% flow, 16 in., 0.375 in.-wall, fps	17.5
90% flow, 14 in., 0.375 in.-wall, fps	21.0
10% flow, 6 in., 0.280 in.-wall, fps	11 0
Pipe material, stainless steel	Type 304
Design pressure, psig	125
Design temperature, °F	1,000
Pressure drop, external system, psi	7.5
Intermediate heat exchangers	
Number of units	3
Material, tubes and shell, stainless steel	Type 304
Tubes, number	1860
Tube size	$^7/_8$ in. OD, 0.049 in.-wall
Fluid in tubes:	Sodium
Pressure loss, ft of sodium	4.9
Shellside fluid:	Sodium
Pressure loss, ft of sodium	1.3
Heat-transfer surface, ft^2	6200
Over-all heat-transfer coefficient, Btu/(ft^2)(hr)(°F)	1059
Heat transferred, Btu/hr	341.3×10^6

(*continued*)

TABLE 4-11 (*Continued*)

Pumping equipment

Number of pumps	3
Design data (each pump):	
Capacity, gpm	11,800
Temperature, °F	550
Total dynamic head, ft	310
Efficiency, %	77
Brake horsepower, hp	1060

approximately 10% to a plenum serving the radial blanket The flow of coolant to the blanket plenum is adjusted by a partially closed throttle valve. Flowmeters are located on both the core and blanket return lines

The primary coolant system had been designed to ensure that the reactor will be adequately cooled during all conceivable emergency conditions. The design provisions are briefly discussed here, and the equipment required is described under separate headings later

Safety design provisions If power to the primary coolant pumps is lost, natural circulation will remove the decay heat of the reactor. This degree of natural convection is made possible by the elevation and arrangement of the heat exchangers The sodium level in the reactor must remain above the 30-inch reactor nozzles to maintain this natural circulation during a leak in the piping or tanks of the primary system. Three measures were taken to protect against this situation. secondary containment, siphon breakers, and the elimination of a drain system.

Secondary containment is a welded leaktight system enclosing all the primary piping and tanks up to the level of the reactor sodium The siphon breakers prevent a siphoning action that would drain the sodium out of the reactor in the event of a leak in the pump discharge piping. These lines are tied into the gas space in the pump tanks, and a small flow of sodium is continually orificed through them to make sure they will be open when needed. To assure that the sodium will not be drained from the reactor or the piping, there are no drains in the primary system.

Primary piping The 30-inch, 16-inch, and 14-inch fusion-welded, stainless steel 304 piping is in accordance with ASTM A 358, and the 6-inch pipe is Schedule 40 seamless, in accordance with A 376. All the piping will be cold sprung 100% for 900°F preceding the intermediate heat exchanger and 600°F on the pump discharge piping. A thermal shock study and a vibrational analysis have been made on the system. Pressure and temperature instruments are housed in a standpipe, downstream of the throttle valve, and a resistance thermometer is welded into the 30-inch elbow at the reactor discharge.

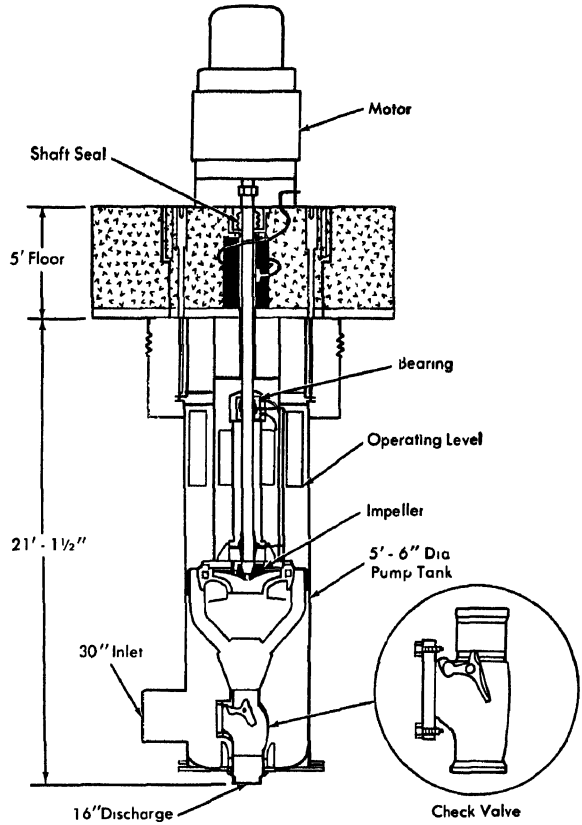

FIG. 4–65. Schematic diagram of sodium pump, including details of check valve

Pumps. The sodium pumps, shown in Figs 4–65 and 4–66, are electric motor driven, centrifugal, vertical shaft, sump-type pumps having an inert gas shaft seal. The pump shield plug, shaft, impeller, and casing are designed for removal as a unit. This assembly can be disconnected from the pump tank without draining the primary system. The pump is designed for 11,800 gpm at 110 psi. The pump motor has a wound rotor with liquid rheostat control A fluorocarbon oil seal (containing no hydrogen) will keep the inert atmosphere above the sodium level from escaping into the building. Pump characteristics are shown in Fig. 4–67.

Check valves. Check valves in each of the primary loops prevent backflow of sodium in case of a pump failure. Each valve is of the balanced disk type shown in Fig. 4–65. The valve body is welded to the pump casing discharge nozzle and is removed from the pump tank with the pump.

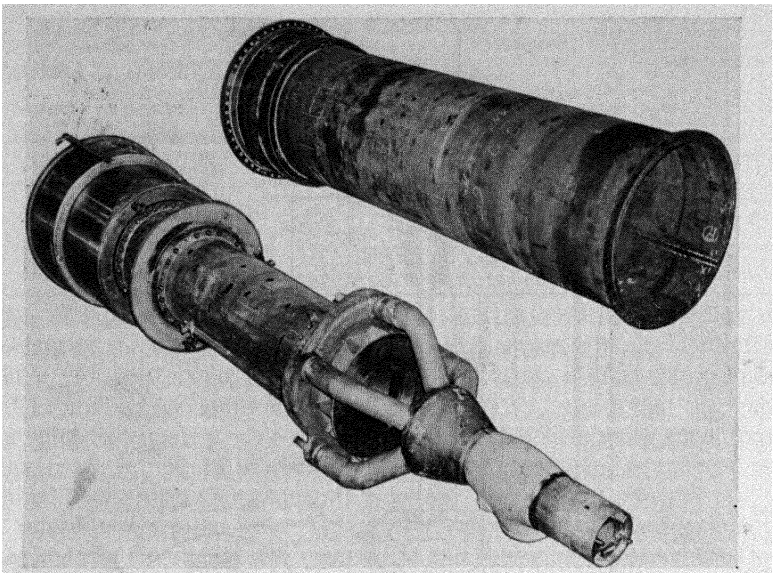

FIG. 4–66. General view of sodium pump assembly.

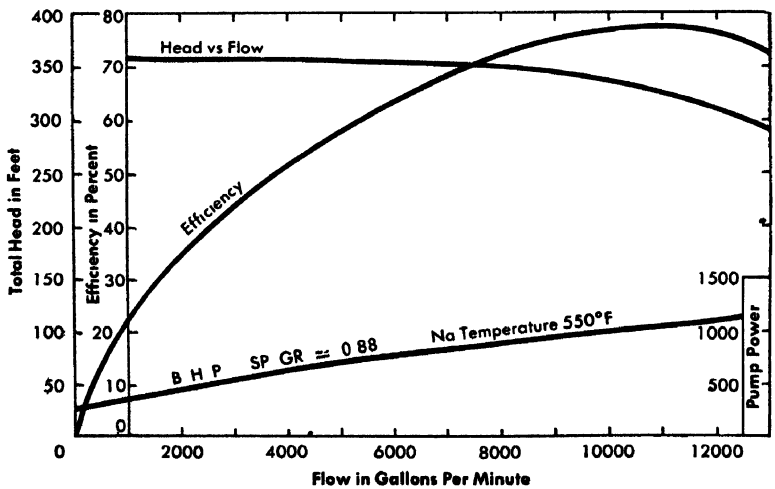

FIG. 4–67. Performance curves for primary sodium pump operating at full load.

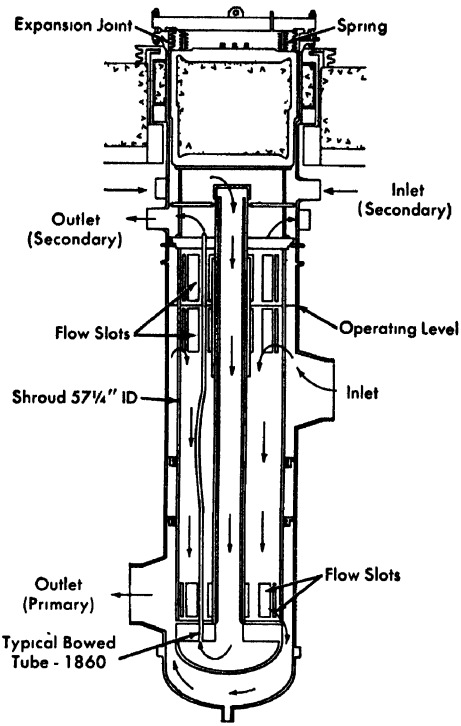

FIG 4–68 Intermediate heat exchanger.

Intermediate heat exchangers. The intermediate heat exchangers are shell-and-tube type units with primary sodium on the shell side and secondary sodium in the tubes (Fig 4–68). The tube bundles can be withdrawn without removing any sodium piping or draining the primary sodium. Secondary sodium enters the unit through the upper 12-inch nozzles, flows through the downcomer to the floating head, flows upward through the tubes and out through the lower 12-inch nozzles. The secondary sodium inlet and outlet nozzles are separated by a divider plate using piston rings as seals A slight leakage between the entering and leaving fluid is permitted. The downcomer is shielded, inside and outside, by stainless steel plates to remove some of the thermal stress from it. The tubes have a sinusoidal bend for about 1/3 their length, to allow for differential expansion. The tube-sheet-to-shell joint has a stainless steel O-ring gasket to prevent secondary sodium leakage into the primary sodium. The gasket is a tube filled with high-pressure nitrogen to increase its resilience. The ring is compressed by Inconel-X springs transmitting their force through the shield plug and load bars to the

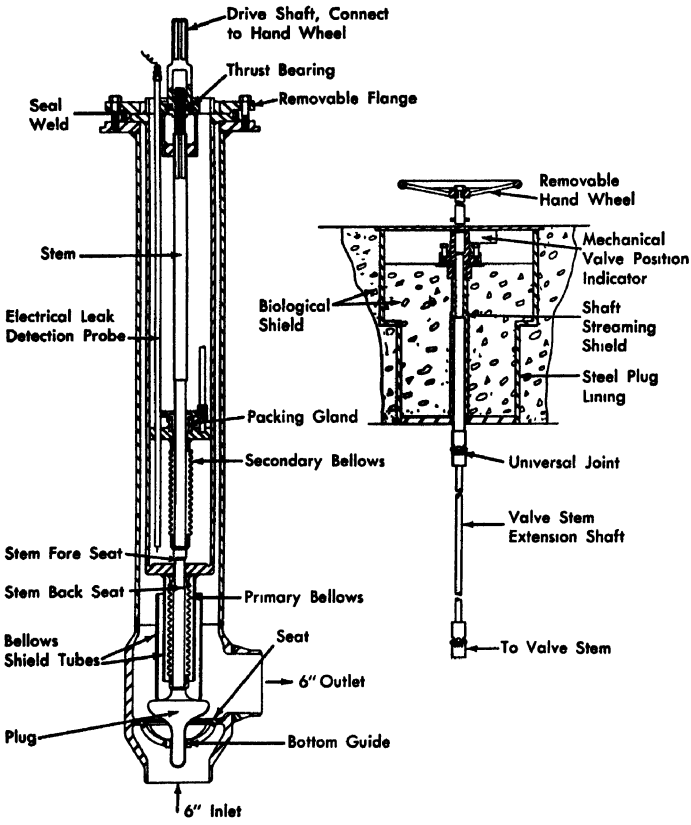

FIG. 4–69. Sodium throttle valve.

tube sheet. The shell extends through the operating floor to permit access to the top cover for removing the bundle The shell and shield plug of the unit are stepped to prevent radiation streaming through the floor The plug is filled with a serpentine (chemically the same as asbestos) rock aggregate and is grouted with cement to form the shield for the hole in the floor.

Blanket throttle valve This valve is an angle-type, double-bellows sealed valve, whose details are shown in Fig. 4–69 The entire valve assembly is contained within a pipe riser which is sealed above the level of the reactor sodium. With the system shut down, the valve's inner section can be withdrawn through a plug in the operating floor without draining the primary system. Used as a variable orifice, the valve controls coolant flow to the radial blanket over a range of 5 to 20% of the total flow, but the flow can never be inadvertently shut off, since the valve cannot be completely closed.

Secondary containment. A secondary containment pipe of chrome-molybdenum steel, 36 inches in diameter with walls 5/16-inch thick, surrounds the 30-inch sodium piping On the intermediate heat exchanger and pump tanks, carbon steel containment of 3/8-inch wall thickness is carried up to the reactor sodium level datum with clearance annuli of approximately 2½ inches. The system is open above the reactor sodium level datum On the pump discharge piping, carbon steel containment of 3/8-inch wall thickness is used with stainless steel bellows at the flowmeters The carbon steel walls will be applied in halves, then welded together with two longitudinal seam welds after the piping is erected.

Shielding. The 30-inch pipe inside the secondary shield wall is enclosed in a column of neutron shielding material varying in thickness from 9 to 20 inches. A streaming path is created between the pipe and the shielding column because of the air gaps required for free movement of the piping and containment. To break up this streaming path, shielding collars of calcium borate are inserted at two points on the riser inside the containment shell Two collars are also placed outside the containment shell to break up the streaming path.

Insulation and induction heating. In the areas where shielding covers the containment shell, insulation and induction heating coils will be applied over this shield material; where there is no shielding, the insulation and heating coils will be applied directly to the containment shell. In close quarters such as wall sleeves, molded aerogel will be used for insulation; at all other locations, diatomaceous silica insulation will be used The induction heating system uses the ferritic steel of the containment shell as a heating medium for the sodium pipe and tanks.

4–8.3 Secondary coolant system. The secondary coolant system is the intermediate link that transfers heat from the primary coolant system to the steam generator. It consists of the tube side of the intermediate heat exchanger, the shell side of the steam generator, and the secondary coolant pump. Secondary system coolant data are given in Table 4–12. Expansion space for the sodium is provided in the inert gas space above the sodium level in the pump and in the steam generator shell. A higher pressure will be maintained in the secondary coolant system to prevent radioactive primary coolant from leaking into unshielded areas. Since each secondary sodium loop is independent, a pump failure will not result in a flow reversal; therefore check valves are not required.

Emergency cooling system. The emergency cooling system provides a means of dissipating heat energy from the reactor following a scram due to failure of the primary electric power source After the scram, the quantity and duration of heat energy release depend upon the prior operating history, i.e., length of operating time and power level. The heat

TABLE 4–12

PERFORMANCE OF LIQUID METAL AND STEAM SYSTEMS AT 300-MW OPERATION; SECONDARY COOLANT SYSTEM

Secondary sodium coolant	*Sodium*
Flow rate per loop, lb/hr	4.4×10^6
Flow rate per loop, gpm at pump temp.	10,000
Total flow rate, lb/hr	13.2×10^6
Total flow rate, gpm at pump temp.	30,000
Temperature:	
Heat exchanger inlet, °F	500
Heat exchanger outlet, °F	750
Total sodium volume, ft^3	2,050
Total sodium weight, lb	111,000
Approximate sodium cycle time, sec	27
Piping system:	
Pipe size	16 in., $\frac{3}{8}$-in wall
Average fluid velocity in pipe, fps	18
Pipe material	$2\frac{1}{4}$% Cr-1% Mo
Design pressure, psig	300
Design temperature, °F	1000
Pressure drop, total psi	30
Pumping equipment:	
Number of pumps	3
Type	Mechanical Centrifugal Inert gas seal
Pump design	
Capacity (each), gpm	11,800
Temperature, °F	500
Total dynamic head, psi	22
Efficiency, %	80
Pumping power, kw	155
Total pumping power, kw	465

production of the reactor will decay rapidly immediately after scram has occurred, but the inertia of the sodium in the system and of the pumps is sufficient to maintain enough flow through the reactor to remove this heat without melting the fuel elements. Residual decay heat is removed by natural thermal circulation of the primary and secondary coolant fluids. Water is supplied to the steam generator by gravity from the deaerating heater. The steam produced will be vented to the atmosphere.

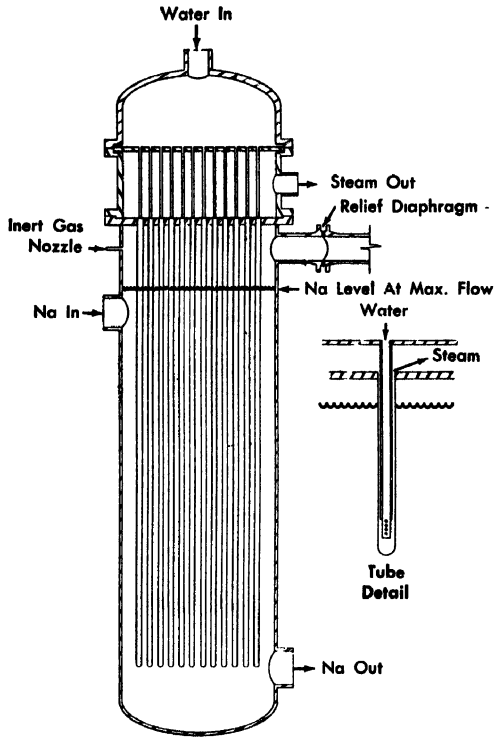

FIG 4–70 Sodium to steam-water heat exchanger.

Pumps. The construction of the secondary sodium pumps is basically the same as that of the primary pump shown in Fig. 4–65; however, there will be no shielding plug or check valve.

Steam generators. The steam generators are vertical, counterflow, shell-and-tube, once-through units with water and steam in the tubes and sodium on the shell side. The basic arrangement of this unit is shown in Fig 4–70 Steam power generating system data are given in Table 4–13.

4–8.4 Inert gas system. The purpose of the inert gas system is to maintain a positive inert atmosphere over the liquid sodium and thus prevent sodium oxidation. Argon is the reference gas used in the sodium systems. However, any one of the gases will work in the systems described below. Gas supply is maintained either by a gas trailer or one of two banks of gas cylinders. All these supply sources have pressure-indicator alarms to alert the operator to his gas supply conditions. Gas cylinders may be filled from a full gas trailer. The gas from the supply source is

TABLE 4–13

PERFORMANCE OF LIQUID METAL AND STEAM SYSTEMS AT 300-MW OPERATION; STEAM GENERATING SYSTEM

Steam generating equipment	
Number of units	3
Type	Once-through Bayonet tube Counterflow
Material:	
Tubes and headers	$2\frac{1}{4}$% Cr-1% Mo
Shell	$2\frac{1}{4}$% Cr-1% Mo
Fluid in tubes	Water and steam
Pressure loss, psi	15
Shellside fluid	Sodium
Pressure loss, ft	10
Design data, each unit	
Steam generating capacity, lb/hr	320,000
Steam conditions:	
Pressure, psia	600
Temperature, °F	740
Feedwater temperature, entering, °F	340
Secondary sodium data	
Flow, lb/hr	4.4×10^6
Temperature, °F:	
Entering	750
Leaving	500
Heat transferred, Btu/hr:	
Feed heating section	51.7×10^6
Evaporating section:	
First section	164.0×10^6
Second section	70.3×10^6
Superheating section	55.3×10^6
Total heat transfer	341.3×10^6
Heat-transfer area (based on tube OD)	
Feedwater section, ft^2	1350
Evaporating section, ft^2:	
First section	1410
Second section	440
Superheating section, ft^2	4900
Total area, ft^2	8100

(*continued*)

Heat flux	
Feed heating section, Btu/(hr)(ft²)	38,000
Evaporating section, Btu/(hr)(ft²)	
First section	116,300
Second section	160,000
Superheating section, Btu/(hr)(ft²)	11,300
Over-all heat transfer coefficient, Btu/(hr)(ft²)(°F):	
Feed heating section	405
Evaporation section:	
First section	1170
Second section	820
Superheating section	174
Logarithmic mean temperature difference	
Feed heating section	94.5
Evaporating section:	
First section, 70%	99.3
Second section, 30%	195.0
Superheating section	64.7

purified by bubbling it through NaK at 600 to 700°F to remove oxygen and water A vapor trap and an entrainment trap prevent carryover of NaK into the pure-gas stream. As a safety measure, a backflow trap is provided to protect the operators of the supply system from the backflow of NaK and the possibility of NaK burns. This trap is large enough to contain all the NaK in the system.

The flowsheet for the inert gas system for primary sodium is shown in Fig 4–71. Gas is circulated from the holdup and surge tank to the various seals and to the overflow tank. All the tanks containing sodium are equalized to the overflow tank pressure. Therefore, the system pressure is controlled by gas flow in and out of the overflow tank. From the overflow tank, the gas passes through the sodium vapor trap to remove radioactive sodium vapor and is then recompressed to 20 psi for reuse.

The pressure control valves on the inlet and outlet from the overflow tank keep the system nearly at atmospheric pressure (within a few inches of water). Gas enters or leaves the overflow tank to maintain the pressure. The effluent gas from the overflow tank is recompressed to conserve the high-purity inert gas.

Since the inert gas may possibly become contaminated with fission products, it may be necessary to purge the gas system before maintaining or removing equipment. A gas disposal system is included to handle contaminated gaseous wastes. All the effluent gases are stored for 30

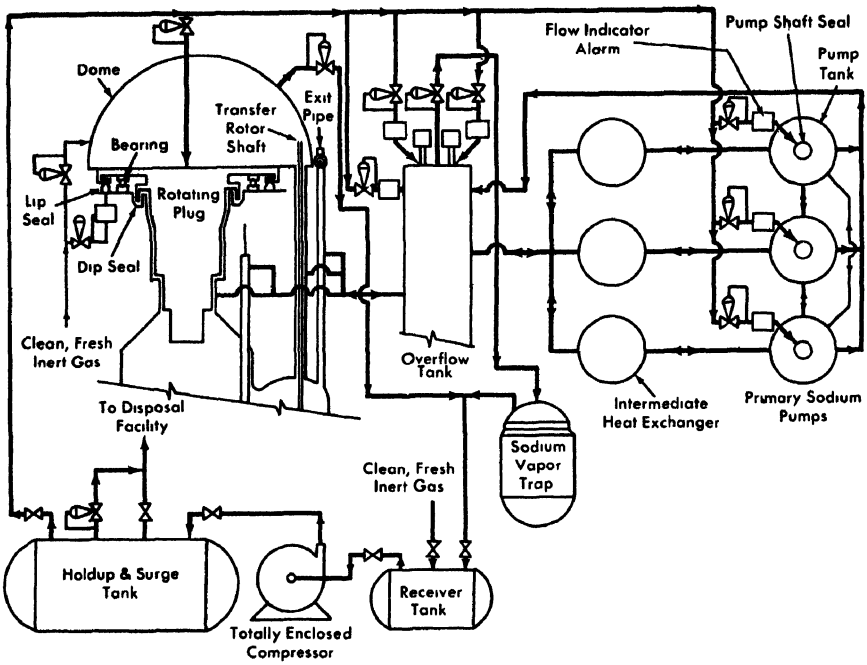

FIG. 4–71. Gas system layout for primary sodium loop.

days in a gas holder. The storage period allows time for the decay of most of the gaseous fission products except Kr^{85}, which has a 10.4-year half-life. After the decay period the gas in the gas holder is sampled and dispelled through a large air blower. The flow rate of the gas to the blower is adjusted so that the air-gas mixture from the blower is within offsite tolerance limits. Space is provided in the design for additional gas holders if they are required

4–8.5 Primary sodium service system. The sodium service system for the primary coolant loops is shown in Fig. 4–72 Pertinent data are given in Table 4–14. The primary sodium service system receives, stores, and repurifies the sodium received in railroad tank cars from the manufacturer. Solium is melted by heater coils on the cars and then transferred to storage tanks The sodium is filtered while being transferred. In the storage tanks, it is cold-trapped to remove sodium oxides. The purity of the sodium is checked by a plugging indicator, and an over-all chemical analysis is made before the reactor coolant loops are filled. The system is capable of purifying, and monitoring the purity, of the sodium from the primary system. Sodium can be recirculated from the primary system to the service system when desired. The system is designed to

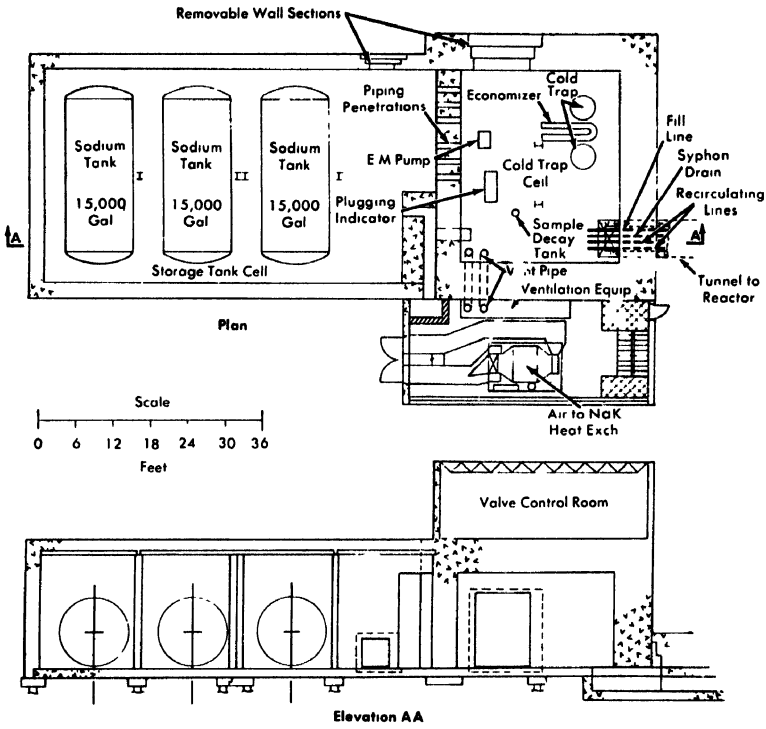

Fig. 4–72 Plan and elevation of sodium service building.

maintain an oxide content of 0.003% or less. Sodium of this high purity has a very low corrosion rate To assure that no hydrogen can enter the reactor with the sodium, the system will be free of moisture and hydrocarbons before it is filled. The system will monitor and remove hydrides as well as oxides It is also provided with a means of removing radioactive sodium for chemical analysis. After it has been allowed to decay in the cold-trap cell of the sample decay tank, the sodium will be transferred through piping to a sample container outside the cell. This container will then be removed for chemical analysis.

As indicated in Fig. 4–72, two separate shielded cells are provided, one for the storage tanks and the other for the purification equipment. The cell containing the purification equipment has concrete walls 6 ft thick because it will handle radioactive Na^{24}. The cell containing the storage tanks has walls 2½ ft thick; this shielding is for Na^{22} and anticipated dissolved fission products. Should it become necessary to dump radioactive sodium in the storage tanks, the sodium will be allowed to decay first in the reactor for a period of 10 days to 2 weeks, after which the only ra-

TABLE 4–14

PERFORMANCE OF LIQUID METAL AND STEAM SYSTEMS AT 300-MW OPERATION; PRIMARY SODIUM SERVICE SYSTEM

Cold trap collection vessel	
Rate of flow, gpm	100
Capacity, gal	500
Pressure drop, psi	11
Discharge temperature, °F	300
Design temperature drop, °F	50
Cooling load, Btu/hr	707,000
Cold trap economizer	
Type	U-shell and tube
Cold trap coolant	
Type	NaK
Flow rate, gpm	58
Temperature drop, °F	100
Plugging indicator	
Maximum flow rate, lb/hr	444
Pressure drop, psi	0.1
Storage tanks (3)	
Capacity, each, gal	15,000
Type of heaters	Resistance
Warmup time to 600°F (sodium), hr	300
Warmup time to 300°F (gas), hr	10
Maximum temperature, °F	700
Sodium service piping	
Type of heating	Induction
Warmup time, hr	72
Overflow pumps	
Type	Sump
Design flow, gpm	100
Discharge head, ft	75

dioactive sodium present will be Na^{22}. A third, unshielded cell contains the sodium building ventilation equipment and the heater-cooler system for the cold trap and plugging indicator.

System valves will be operated from a floor above the service cell, shielded to protect the operator against radiation.

4–8.6 Secondary sodium service system. The service system for the secondary coolant loops (not shown) will be similar to the primary system. However, no shielding will be required, since it will not handle radioactive sodium.

Cold trap. The cold trap will remove the oxides and hydrides from the sodium A schematic drawing of the cold trap as furnished by the Mine Safety Research Corporation is shown in Fig 4–73. The cold trap is kept cool by an external NaK cooling system. Oxide-laden sodium first passes through the shell side of an economizer, where it is cooled. It then passes into the cold trap, where the temperature is further reduced. As the sodium rises through the center portion of the cold trap, which is packed with a stainless steel woven wire mesh, its velocity is decreased. Oxides and hydrides precipitated out because of the decrease in temperature will collect in this area. Upon leaving the cold trap the sodium will

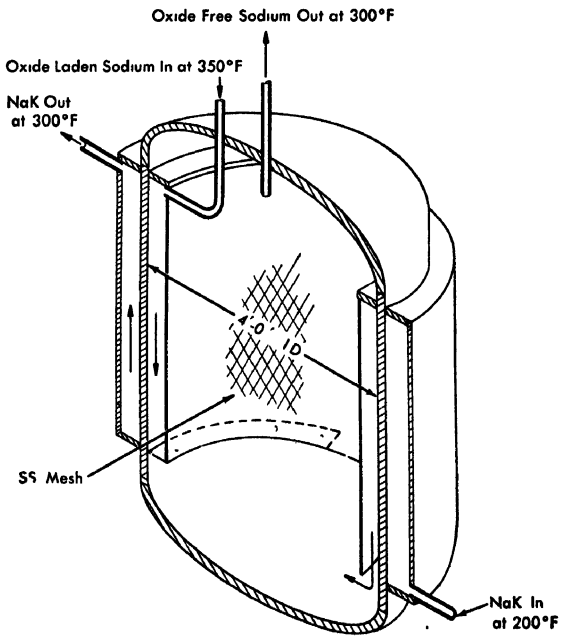

FIG. 4–73. Cutaway drawing of sodium cold trap.

pass through the tube side of the economizer to be warmed up by the entering oxide-laden sodium

Plugging indicator. The oxide or hydride content of the sodium will be checked by a plugging indicator. The sodium flows through a heat exchanger, where it is cooled by an external NaK cooling system. As the sodium is cooled, the temperature is recorded to determine the point at which the oxides or other materials begin to plug the indicator.

4–8.7 Overflow tanks. An overflow tank is located in the reactor building As the primary sodium expands with increasing temperature, it will flow through an overflow line from the reactor to the overflow tank. It can be pumped to the intermediate heat exchanger for return to the system. For cold-trapping, the sodium will be pumped from the overflow tank through the sodium service system (as previously described), and then back to the primary system.

Two sump-type pumps are located in the overflow tank, each with enough capacity to handle the required flow The pump shield plug, shaft, impeller, and casing are designed to be removed as a unit. This assembly can be disconnected from the overflow tank and removed by a direct vertical pull.

4–9. Reactor Building

4–9.1 General description. The reactor building is a steel pressure vessel designed to contain all radioactive fission products or radioactive sodium released by a mechanical or primary system failure or a reactor accident. The design is based on experimental and theoretical studies of postulated accidents that might cause a sodium-air reaction The vessel is designed for all normal loads, including wind loads, and for the additional loads calculated to result from pressure changes following a sodium fire in the building.

The containment vessel is a vertical cylinder with hemispherical top head and ellipsoidal bottom head. It is 72 ft in diameter and 120 ft high over-all. The design conditions are:

Steady-state positive internal pressure, 32 psig.
Steady-state negative internal pressure, 2 psig.
Steel design temperature, 650°F.

The vessel meets the requirements of the ASME Boiler and Pressure Vessel Code (Section VIII). It is constructed of ASTM A 201 Firebox Quality Grade B Steel (ASTM Designation A 300). Walls are $1\frac{1}{16}$ inches thick, double-butt welded, following Sections VIII and IX of the Code. These joints have been fully radiographed. The completed vessel

has been pressure-tested with air at 1.25 times the design pressure, in accordance with the ASME Code. A leakage rate test will be made to determine that the leakage is less than 500 ft^3 per 24 hr.

The weight of the containment vessel and its contents is transmitted uniformly through the bottom head to the underlying rock stratum by reinforced concrete foundations in which the bottom head is embedded. Personnel enter through an air lock with doors interlocked to prevent simultaneous opening. A smaller emergency air lock is also provided.

4–9.2 Building design criteria for an assumed sodium-air reaction. The potential hazard of a sodium fire and the problem of decay heat removal after permanent loss of coolant to the reactor core is a problem common to all sodium-cooled reactors. The temperature and pressure specifications for the vessel are based primarily on the consequences of a postulated sodium fire and on fission-product heating resulting from loss of coolant. A vacuum relief valve capable of handling 3600 ft^3/min of standard air will limit the negative internal pressure to 2 psi Calculations show that the design specifications are adequate

The following conditions were assumed for the maximum credible accident, as a basis for design calculations. On a windless day in summer with the air temperature 100°F and the building metal temperature 125°F, a major sodium leak develops below the operating floor. The reactor, which has been operating at 430 Mw to a maximum of 6 a/o burnup, loses most of its sodium. At the same time, the seals between the upper and lower compartments fail, and air from the upper compartment enters the lower, causing the leaking sodium to burn Three separate phases of the accident are considered: (1) sodium-burning phase, (2) fission-product heating phase, and (3) cooling phase

Sodium burning phase (Phase I) The sodium which floods the lower reactor compartment is assumed to burn, initially, at 5 lb/hr per square foot of burning surface. Experiments have shown this to be the maximum rate that can occur under the conditions. Once combustion begins, the burning rate is affected by two factors, the oxygen concentration and the resulting temperature. For the range of temperatures involved, the burning rate has been found to be almost independent of temperature. From this, it is concluded that the burning rate is controlled by a diffusion process rather than by the velocity of the chemical reaction. The burning rate should then be proportional to the product of the oxygen concentration and the square root of the absolute temperature. When the oxygen concentration falls below 5%, the reaction is assumed to stop; this assumption is based on experimental work reported by Knolls Atomic Power Laboratory.

The sodium continues to burn, governed by the above factors, releasing about 3900 Btu for each pound of sodium burned This heat is dissipated by (1) heating the air in the building, (2) heating the structural material in the building, and (3) heating the metal building shell

Comparing the rate of heat release by the burning sodium with the rate of heat transfer between the various components of the system, it is found that the temperature and pressure of the atmosphere in the building increase rapidly at first. Taking into account the dilution of the oxygen-containing atmosphere above the operating floor with the inert nitrogen atmosphere below this floor, gas temperature and pressure are calculated to reach 1240°F and 28 psig (their maximum values) about 7 min after the start of the accident.

During this period, relatively little heat has been transferred to the building, and at the time of maximum pressure the average building temperature is only 200°F. After the maximum temperature has been reached, the combination of reduced oxygen concentration and increased heat-transfer losses from the building atmosphere cause a reduction in temperature and pressure of the atmosphere at a rate nearly equal to the initial rate of rise. The results of the calculation are summarized in Fig. 4–74.

Fission products heating phase (Phase II) As the oxygen depletion in the building begins to limit the heat input from the burning sodium, the decay of the fission products in the reactor becomes the most important heat source. However, it is very difficult to predict the net effects of heat release from this source. Certainly, very high local temperatures exist, capable of melting both the reactor core and blanket as well as some of the steel structure within the building The heating is assumed to set up strong convection currents, causing a more or less general temperature rise throughout the building. For simplicity, the effects of the

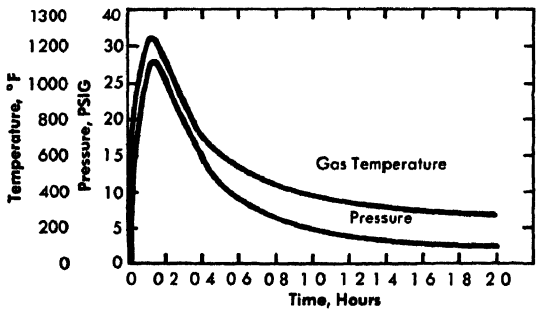

FIG. 4–74. Gas temperature and pressure for the assumed sodium-air accident, Phase I.

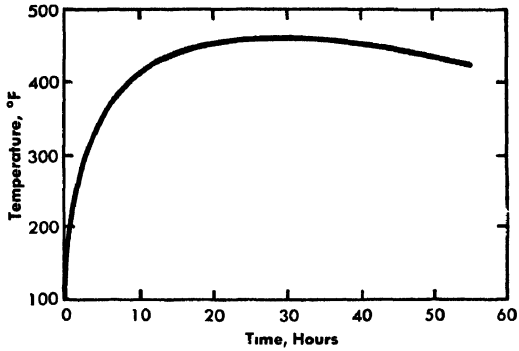

FIG. 4–75. Containment shell temperature for assumed accident, Phase II.

fission-product decay and of the heat capacity of the building and its internal components were calculated only for heat losses from conduction and convection through the uninsulated building to the air outside. The over-all heat-transfer coefficient was taken to be 1 Btu/(ft²) (hr) (°F).

The calculated time-dependent heat balances indicate that the building metal temperature increases rather slowly until, about one day after the beginning of the fire, the building metal reaches its maximum temperature, 460°F. The heat production from fission-product decay and the heat losses are then in equilibrium, and the temperature begins to drop very slowly A plot of the building shell temperature for this phase is given in Fig 4–75.

Cooling phase As the building cools, so does the building atmosphere. Because there is less oxygen in the building atmosphere, the pressure at normal temperatures will be about 3 psia less than before the accident. Since the building is designed for 2 psi, it might collapse if no equalizing relief valves were provided.

The sizing of these valves depends on the rate of pressure change possible Calculations indicate that the relief valves must be able to handle 3600 cfm of air at 60° F and one atmosphere with a differential pressure of 2 psi across the valve.

4–9.3 Building internals. A rotary crane, supported from the containment vessel wall, carries two separate trolleys and hooks (a 30-ton hook and a 150-ton sister hook). This crane will be used to remove equipment assemblies of the primary system, such as an intermediate heat exchanger tube bundle or a primary pump assembly, from their tanks to a decay tank, or from a decay tank to lay-down space on the operating floor. Equipment is removed from the building by unbolting the gasketed equipment door on the north side. This door rides on a trolley beam inside the building; the door opening is 11¼ ft wide and 13½ ft high.

The 5-ft-thick operating floor, supported on structural steel columns, is protected from gamma heating by a 3½-inch steel plate on the bottom. Steel plate on top of the floor will protect the concrete in the event of a sodium spill. A stepped radiation seal is placed around the periphery to allow differential expansion between the floor and the steel containment vessel. This seal is bridged with a rubber strip to prevent mixing of the atmosphere below and above the floor. The secondary shield wall consists of 30 inches of concrete, clad with 1/2-inch steel on both sides. In locations where gamma levels are high, a 2½-inch steel plate is suspended in front of the wall, leaving a 5-inch gap for convection cooling. Where this wall is penetrated by primary piping, there will be annular air gaps to allow free movement of the pipe and containment shells, and also layers of insulation. To keep neutrons from streaming through, a shielding collar is applied to the pipe where it leaves the wall.

4–9.4 Reactor building ventilation, heating, and cooling systems. In designing the system for ventilating, cooling, and heating the reactor building, the very different requirements of two areas were taken into account. One of these, above the operating floor, is accessible to personnel; the other area, below the operating floor, is not normally occupied. In the latter, a nitrogen atmosphere with not more than 5% oxygen is maintained.

Building ventilation system above floor. The system requirements for the upper (occupied) area are:

Pressure	Atmospheric
Design temperature, dry bulb, °F	75
Temperature range, °F	40 to 100
Relative humidity, %	30
Cooling load, max., Btu/hr	762,000
Heating load, max, Btu/hr	1,087,000
Outside range, °F	−10 to 100

This system employs electrical resistance heaters and expansion coils using Freon-12 for cooling. Two half-size coil and heater units are mounted 180 degrees apart above the main crane trolley with a combined fan capacity of approximately 8800 cfm. There is a refrigeration system in the vent building, which is next to the reactor building. Lake water is used as a cooling medium for the heat exchangers.

Air changes will be based on an hourly change of one inch of mercury difference in the pressure inside the building relative to that of the outside atmosphere. A silica-gel bed will be employed for dehumidification.

Building ventilation system below floor. The system for this area will be based on the following design data:

Nitrogen temperature, in, °F	125
Nitrogen temperature, out, °F	150
Pressure (gauge), in. Hg	−1/2
Nitrogen flow, cfm	25,000
Cooling load:	
Nuclear heat generation, Btu/hr	454,000
Equipment heat losses, Btu/hr	682,000
Total cooling load, Btu/hr	1,136,000

Since no heating requirements are to be met, this system is essentially a cooling system. There are provisions for removing oxygen and for maintaining a nitrogen pressure slightly below atmospheric. Two cooling systems are currently being considered.

In the first system, the nitrogen atmosphere would be circulated through water-to-nitrogen heat exchangers by centrifugal fans. This equipment would be housed in a vent building and would be designed for building pressure. Ducts would be needed for forced circulation of the nitrogen. Cooling would be controlled by dampers in the duct system and by thermostatic water-regulating valves at the heat exchangers.

The second system would employ a Freon-12 expansion coil and the related refrigeration equipment. This cooling coil could be located either in the vent building, with the nitrogen circulated through ducts, or inside the reactor building, in which case nitrogen would be recirculated within the reactor building.

4–10. Reactor Plant Shield System

4–10.1 Design criteria. The criteria for the design of the shield system are listed below.

Biological doses. All biological shields for the reactor building and for auxiliary buildings are being designed to ensure that plant personnel will receive no more than 1/3 of the total radiation dose presently allowed in Atomic Energy Commission installations during a 40-hr week. The resulting dose limit is 30 mr/wk, and corresponds to an hourly exposure rate of 0.75 mr/hr, which is taken in combined neutrons and gamma rays.

Activation of secondary coolant and equipment. Areas that are not occupied by people but which contain the secondary coolant, or equipment that must be maintained, will not be allowed to become radioactive. In these areas, the neutron fluxes will be no greater than 10^4 n/(cm^2) (sec), a

value low enough that induced activity in steel or sodium by neutron capture is insignificant.

Heating in the concrete. Concrete may be damaged and lose its effectiveness as a shield if it overheats or is subjected to intense radiation. Overheating can be caused by internal heat generation due to absorption of nuclear radiations or by too high an ambient temperature. If the temperature within the concrete rises above the boiling point of water, the hydrated water is lost and the value of the concrete as a shield is reduced. High internal heat generation within concrete due to radiation absorption causes not only loss of water but also internal stresses that lead to cracking, void formation, and a general loss of strength.

To prevent water loss from the concrete shields, the maximum internal temperature of the concrete will be kept below 200°F To avoid cracking and void formation the nuclear radiation energy fluxes reaching the concrete will be kept below 4×10^{10} Mev/(cm^2)(sec); maximum temperature differences within the concrete will not be allowed to exceed about 10°F.

4–10.2 Shield design. The general features of the shield system are shown in Fig. 4–76. The shield is in three parts: a primary shield in the primary shield tank, a secondary concrete shield surrounding the primary shield tank, and a biological shield that forms the operating floor and surrounds the containment vessel. This system divides the building into areas, each of which meets specific design criteria

Primary shield. The primary shield system, shown in Fig 4–76, consists of (1) the radial blanket that serves (in addition to its primary purpose of breeding plutonium) to attenuate the very high neutron fluxes from the core and to attenuate to a very low level the gamma radiation from the core, (2) a 12-inch thermal shield that protects the reactor vessel against radiation damage due to excessive neutron fluxes and attenuates to a very low level the secondary gamma radiation produced within the blanket, and (3) a graphite shield just outside the reactor vessel whose purpose is to moderate and capture neutrons escaping from the vessel. The graphite shield is divided into three layers: a 6-inch inner layer of 5% borated graphite, a 6-inch outer layer of 1% borated graphite, and a central portion of plain graphite or carbon. The nuclear heat generation in the shield is shown in Fig. 4–77. The inner layer of borated graphite is isolated from the remainder of the shield by 3 inches of insulation. More than 90% of the 60 kw of heat generation in the shield occurs in this layer. This arrangement allows the heat generated to return to the vessel, so that no internal cooling of the shield is necessary. The average temperature within the insulation is about 730°F and out-

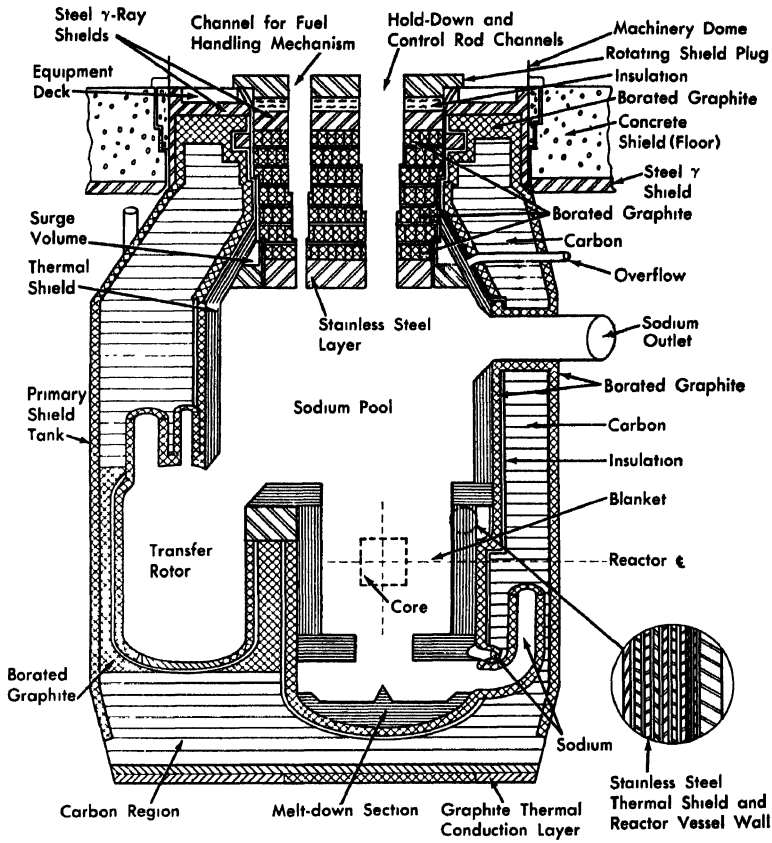

FIG 4–76 Primary shield system.

side the insulation about 350°F. The temperature distribution through the shield in the hottest region is shown in Fig. 4–78

The neutron leakage flux at the outside of this shield is limited to 2×10^8 n/(cm^2) (sec) This level is low enough that concrete is not damaged by heating due to neutron absorption. The neutron flux attenuation through the primary shield at the reactor centerline at full power is given in Fig. 4–79. The leakage gamma radiation from the shield will not be greater than 3000 r/hr at full power.

Secondary shield. This shield is a 30-inch concrete wall that completely surrounds the primary shield tank. Its purpose is to prevent the secondary sodium loops, the intermediate heat exchanger, and primary sodium pumps from becoming radioactive by neutron activation. As previously stated, this shield reduces the neutron flux to about 10^4 n/(cm^2) (sec). Both faces of the shield are clad with a 1/2-inch steel liner. In areas on

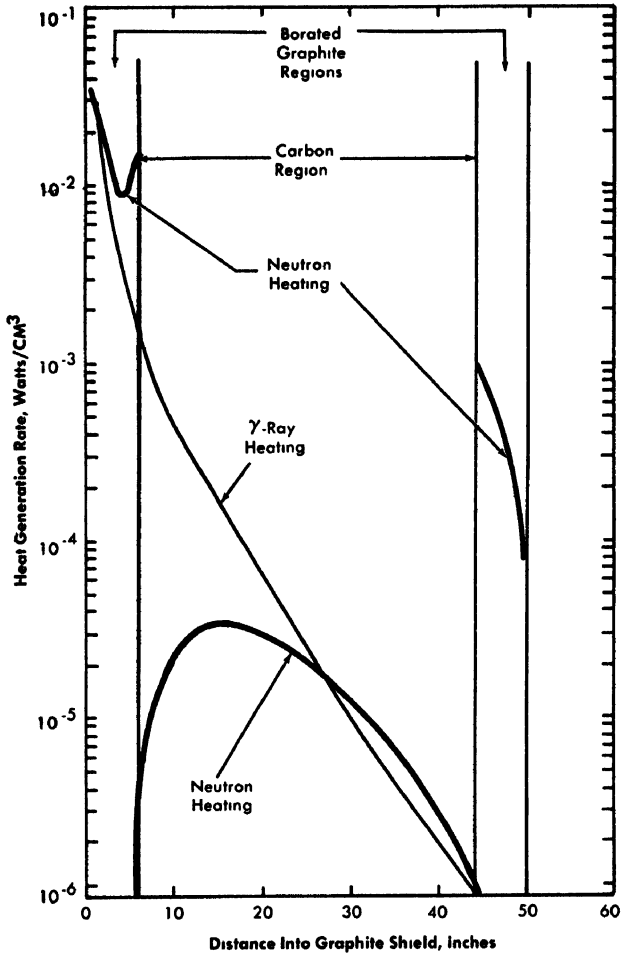

FIG. 4–77. Heat production in graphite shield.

the outer face close to the primary sodium loops, an extra steel thickness of 2 inches is necessary to protect against excessive heat generated within the concrete due to absorption of Na^{24} gamma rays from the primary coolant. This steel is added as a thermal shield in such a way as to form a 5-inch cooling gap between the wall and the added steel; this arrangement permits cooling by natural convection. The nuclear heat load due to heat generated in this wall and its protective steel is about 52 kw at full power. No extra steel shield is required on the inner face of the concrete because of the arrangement of primary loops and because the shielding around the 30-inch piping provides enough protection. The

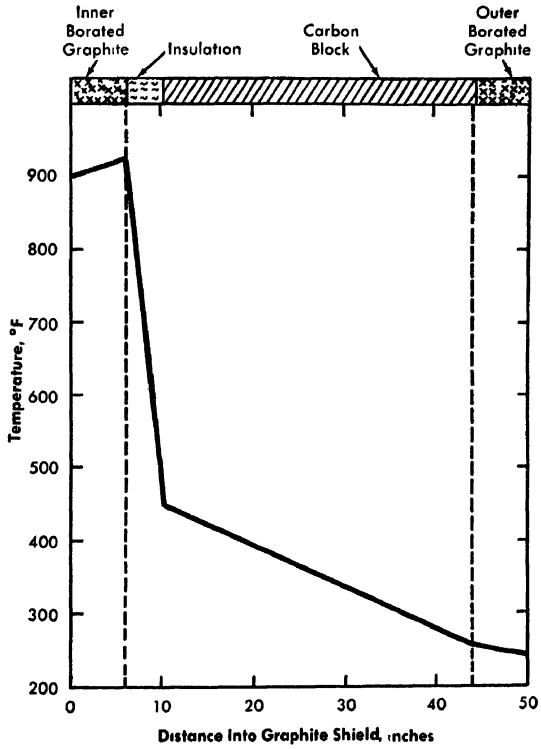

Fig. 4–78 Temperature distribution through graphite shield.

general gamma radiation level in the heat exchanger compartment at full power is of the order of 10^5 r/hr.

Biological shield. The biological shield comprises the 5-ft concrete and steel operating floor shield, plus a 7-ft concrete shield outside the containment building. The rotating shield plug on the reactor vessel is also an integral part of this shield. Ordinary concrete will be used, with a density of 150 lb/ft^3. Pouring will be controlled to give a uniform, voidless shield. The average amount of steel required on the bottom of the operating floor is 4 inches, varying from a minimum of 1½ inches to a maximum of more than 12 inches in small areas where the floor thickness is reduced below 5 ft.

Ordinary concrete was chosen instead of the equivalent thickness of heavy concrete because of the former's proven reliability, lower cost, and easier installation.

Sodium pipe shields. The leakage currents of neutrons from the reactor vessel out through the 30-inch primary sodium pipes and their associated annuli are so large at full power that special shielding is required

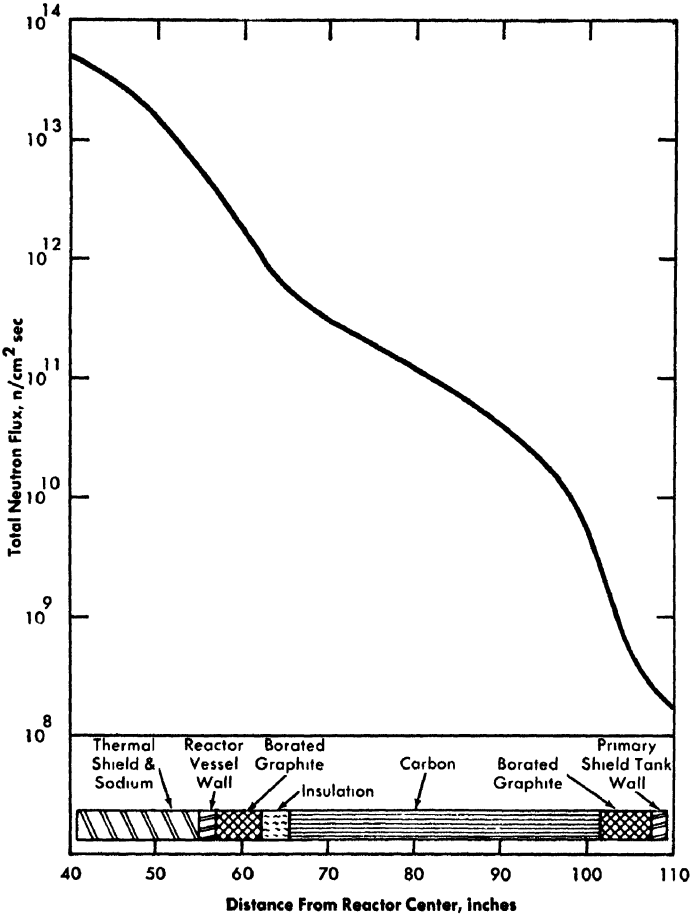

FIG. 4–79. Neutron flux attenuation through primary shield at reactor centerline.

around these lines for a considerable distance from the vessel. These shields must be able to withstand high temperatures and high thermal gradients. They are designed to prevent neutrons from reaching the heat-exchanger compartment, either by leakage through the secondary concrete wall or through the pipe annuli. Rings of shield material placed in the annuli prevent annular streaming.

Two materials now being considered for the pipe shield are a borated diatomaceous earth-aggregate concrete having 2 w/o boron and a calcium borate material having 10 w/o boron. The thicknesses in each case depend upon the location of the shield, but range from 11 to 20 inches for the borated concrete shield and from 9 to 17 inches for the calcium borate shield.

Shielding for streaming paths. The many penetrations through the shielding necessary to accommodate the various control and handling mechanisms, access plugs for the heat exchangers, sodium pumps, and other equipment, present potential voids and paths through which radiation can stream. Streaming in these areas is reduced to a minimum by filling all holes and voids with shield material where possible, using offsets or steps in the streaming paths, keeping clearances between moving parts to a minimum, and using patch shielding above or within the streaming paths if other methods cannot be used.

4–11. Materials

The basic factors governing the selection of structural and fuel materials for the Enrico Fermi Atomic Power Plant are (1) resistance to corrosion by liquid sodium, (2) physical and mechanical properties, (3) radiation stability, (4) nuclear properties, (5) fabricability, and (6) cost. The importance of each of these factors varies in degree with the location of the components in the plant, the most demanding requirements exist in the fuel, in the reactor vessel, and in components within the vessel.

4–11.1 Coolant and structural materials. *Corrosion resistance to the coolant* The coolant used in the primary and secondary system is sodium, with an average oxygen content of 10 to 30 ppm and a maximum of 50 ppm Ferrous alloys and nonferrous materials such as zirconium, cobalt-base alloys, and nickel-base alloys have been shown to have excellent resistance to liquid sodium attack for the range of temperatures and oxygen levels expected in the plant.

The corrosion resistance of type-304 stainless steel and 2¼% Cr-1% Mo carbon steel in sodium containing small amounts of NaOH was investigated to determine the effect of small leakages of water or steam from the steam generator into the secondary system. Specimens of the stainless and low-alloy steels exposed to molten sodium containing as much as 6% NaOH showed no significant attack. During the experiment in a thermally circulating loop, the extremities of the specimens were subjected to temperature differences of 950 and 750°F An additional test with 8% NaOH concentration and temperature differentials of 550 and 850°F confirmed results previously obtained.

Stainless steels. Stainless steel is used almost exclusively in the primary system. Type-304 stainless steel is used for the reactor vessel, its internal shielding, the handling mechanism and its auxiliary equipment, the intermediate heat exchanger, the pumps, and the primary piping system and its auxiliary equipment. Because of its greater strength,

type-347 stainless steel is used for the reactor support plates, hold-down plates and subassembly core. As alternates, types 316 and 321 have been substituted in some cases for reasons of availability or higher allowable design-stress values.

Low-alloy steels. Low-carbon ferritic 2¼% Cr-1% Mo steel is being used for the intermediate system, the steam generators, the auxiliary sodium systems, and the finned fuel-transfer pots. These uses of the 2¼% Cr-1% Mo steel are for service temperatures below 850°F. This steel is an economically attractive substitute for the more expensive high-alloy materials heretofore used almost exclusively in sodium systems for any temperature condition. The Cr-Mo ferritic steels can be substituted for the stainless steels in sodium service with satisfactory results, but temperature limitations are lower because of decarburization of the ferritic steels at temperatures of 900°F and above Decarburization is not the direct result of sodium metal attack, but is a carbon oxidation phenomenon occurring at elevated temperatures with the contained oxygen The loss of carbon has been shown to produce some loss of tensile strength, and the long-term effects on fatigue strength must be assumed to be appreciable, particularly for cyclic temperature service Nominally the 2¼% Cr-1% Mo ferritic steel is considered applicable for long-time sodium service at temperatures up to 850°F and the allowable stresses, as established in the ASME Pressure Vessel and Pressure Piping Codes, are considered adequate However, if the material is to be used for higher temperature service, a reduction of 20% in the stresses allowed by the Code is recommended

The primary shield tank is constructed of ASTMA285 Grade C carbon steel. The containment building is constructed of ASTMA201 Grade B firebox quality carbon steel.

Two-inch-thick boron steel castings of irregular shapes are used in the rotating plug. The cast boron steel is a plain-carbon steel conforming to ASTMA216 Grade WCB, with 1 to 1½% boron added. A major producer of alloy steel castings has prepared experimental heats of this alloy; the steel is readily machined by adaptations of standard techniques This material has negligible structural ductility, but its intended use as shielding material does not require much ductility. Additional fabricability tests are being conducted, and heat-treating is being investigated as a possible means of improving ductility.

Hard-surface materials. Stainless steels are susceptible to galling and self-welding, which can readily occur even at moderate unit loads. Seizure of moving parts due to self-welding has been known to occur. Since these phenomena are accelerated by higher temperature and higher degree of relative motion between the rubbing surfaces, reactor surfaces subjected to intermittent or continuing rubbing forces are protected by

surface hardening. Surface nitriding and sprayed or welded overlays of hard-facing materials, such as Colmonoy No 4, Colmonoy No. 6, and Stellite No. 6, are used extensively

Specifications for surface finish and cleaning. With few exceptions, the material specifications have been those of the American Society for Testing Materials. The surface finish requirements for material in the reactor vessel and its structures, except at points of discontinuity, is in the order of 500 rms; at points of discontinuity, the surface finish is in the order of 125 rms The reactor vessel will be cleaned by degreasing with a detergent and rinsing with water whose solids content is under 120 ppm and whose chloride-ion concentration is less than 10 ppm. This degree of cleanliness is adequate for sodium systems. The impurities, dissolved or suspended in the sodium, are cold-trapped and filtered from the system.

Radiation effects The reactor vessel has been designed to withstand an integrated neutron exposure which is within the range for which experimental information exists The flux exposure of the reactor vessel in a twenty-year lifetime and the experimental data now available are given in Table 4–15.

To keep a continual check on the mechanical and physical properties, surveillance tubes containing control specimens will be located in areas exposed to high radiation dosages. The specimens, cut and machined from the same sheet, plate, or bar as the section under scrutiny, will be

TABLE 4–15

RADIATION STABILITY CONSIDERATIONS
USED IN THE REACTOR VESSEL DESIGN

Parameter	Integrated flux, *nvt*	
	Exposure and spectrum	Fast, after 10-yr operation
Maximum exposure data available. No serious deleterious effects noted:		
3½ yr in MTR [6]	2.6×10^{22} (100 ev)	—
EBR-I core container and flow separator [7]	2.0×10^{21} (370 Kev)	—
Calculated exposure of vessel wall*	—	6×10^{21}
Calculated exposure of spot in blanket 12 in. from core (2.6×10^{14} *nv*)	—	7×10^{22}

*Based on ½-time at 300 Mw and ½-time at 430 Mw with 0.75 plant factor.

removed at periodic intervals, so that a complete and comparative service history will be available.

4–11.2 Shielding materials. *Serpentine rock.* Serpentine rock is the hydrous magnesium silicate $3MgO\text{-}2SiO_2\text{-}2H_2O$, a mineral associated with asbestos. It contains 13.48% of water of crystallization, and has good long-time water retention up to 800°F; therefore it is a good material for use as an intermediate temperature neutron shield. Its loose-stacked density is 100 to 110 lb/ft^3. As an aggregate, it can be mixed with cement, and pressed blocks can be made with 10 w/o cement. Casting can be done with 15 w/o cement, with a density range of 130 to 145 lb/ft^3. The resulting concrete aggregate has shielding properties similar to those of the serpentine rock.

Calcium borate. A commercial product sold as calcium borate is a mixture of ulexite, colemanite, calcium borate, and asbestos. Its low thermal conductivity (1.9 Btu/(hr)(ft^2)(°F)(in) at 600°F), boron content (10 w/o), and physical properties (density 65 to 70 lb/ft^3) make it a suitable thermal insulation where neutron shielding is of primary importance. It can be used at temperatures to 1000°F

4–11.3 Fuel and blanket materials. *Transformation kinetics and properties.* The fuel material for the Fermi Reactor is U-10 w/o Mo alloy, gamma stabilized by heat-treatment; the blanket material is U-2$\frac{3}{4}$ w/o Mo, homogenized and furnace-cooled. The U-Mo phase diagram, Fig 4–80, shows that the gamma transformation temperature is depressed by molybdenum additions and that a eutectoid point exists at about 11 w/o Mo. Transformation kinetics of the U-10 w/o Mo alloy, studied by Armour Research Foundation, indicate that gamma phase transformation is initiated after about 10 hr at 500°C, as shown in Fig. 4–81. The earliest time for start of the U-10 w/o Mo alloy gamma metastable transformation to alpha plus epsilon occurs after approximately 7 hr at 450°C Should the Mo composition vary from 9 w/o to 12 w/o, then the minimum time-temperature relationship for transformation to occur would range from 2$\frac{1}{2}$ hr at 500°C to 22 hr at 500°C. However, transformation is retarded by irradiation, as described in reference [4].

Additional work has shown a high dependency of the transformation kinetics on the homogeneity of the base alloy. The as-cast structure of the U-10 w/o Mo alloy shows essentially 100% gamma phase and a high degree of segregation. This segregation, or inhomogeneity, has been found to persist through the fabrication procedure, which involves hot extrusion at 1562 to 1796°F (850 to 980°C), followed by cold swaging. Spectroscopic examination has established that the molybdenum variation in extruded and swaged fuel pins is 3 to 12 w/o on a microinch basis,

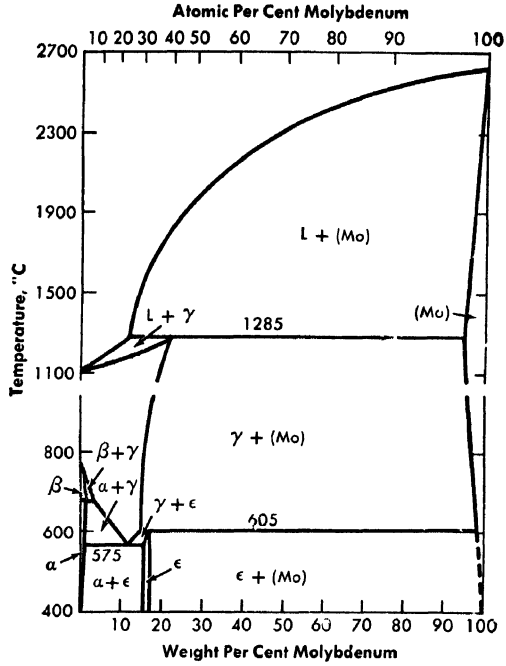

FIG 4–80 The uranium-molybdenum system.

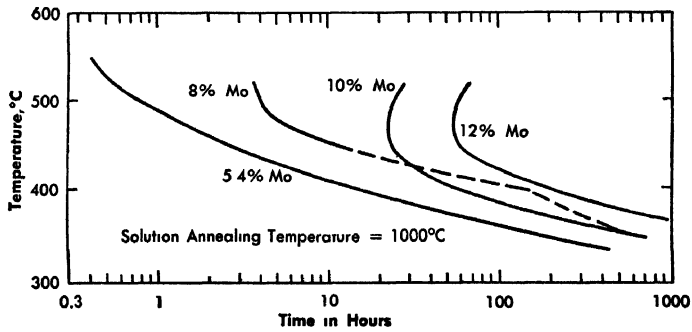

FIG 4–81 Time-temperature transition diagrams illustrating initial resistivity decrease for uranium-molybdenum alloys

and heat treatments are currently being investigated as a means for providing a homogeneous structure in the core pin.

Test results show that the strength properties and modulus of elasticity of the U-10 w/o Mo alloy decrease with increasing temperature from room temperature to 1250°F (675°C). Whereas the ductility of the alloy as indicated by the total elongation is quite low at 750°F (400°C), it increases at both higher and lower temperatures. Up to 500°F

TABLE 4–16

THERMAL EXPANSION OF GAMMA RETAINED URANIUM-10 W/O MOLYBDENUM ALLOY*

Temperature		Longitudinal direction		Transverse direction	
°C	°F	α/°C × 10^{-6}	α/°F × 10^{-6}	α/°C × 10^{-6}	α/°F × 10^{-6}
25	77	11.5	6.4	11.9	6.6
100	212	12.2	6.8	13.0	7.2
200	392	13.2	7.3	14 6	8.1
300	572	14.2	7.9	16.0	8.9
400	752	15.2	8.4	17.6	9.8
500	932	16.2	9.0	19.0	10.5
550	1022	16.6	9 2	19.8	11.0
600	1112†	16.6	9.2	19.8	11.0
700	1292	17.9	9.9	20.8	11.5
800	1472	19.2	10.6	21.8	12.1

*Heat-treated at 400°C and water-quenched.
†Transition temperature between 550°C and 600°C.

(260°C), the true stress values increased with increasing true strain from the start of loading until the specimens failed At higher temperature, however, the true stress reached a maximum at an intermediate strain value before rupture. This change in the characteristics of the true stress-true strain curves is believed to be associated with a change in metallurgical characteristics from low-temperature behavior to high-temperature behavior. The decrease in true stress at intermediate strain values at the higher test temperature probably results from a tendency of the metal to creep at a rate faster than applied strain rate.

In addition, the dimensional stability of this alloy, as fabricated into the reference fuel pins, has been evaluated under thermal cycling conditions. In cycling between 120 and 750°C, it was found that the U-10 w/o Mo alloy possesses high thermal stability, demonstrated by insignificant dimensional changes. Physical properties at various temperatures of the U-10 w/o Mo fuel alloy are given in Tables 4–16 and 4–17 and in Fig. 4–82. Mechanical properties at various temperatures are given in Table 4–18.

Radiation effects. A study of the radiation stability of the U-10 w/o Mo alloy is described in detail in references [4] and [5]. Postirradiation physical property measurements of density, dimensions, electrical resis-

TABLE 4–17

ADDITIONAL PERTINENT PHYSICAL PROPERTIES OF URANIUM-10 W/O MOLYBDENUM ALLOY

Electrical resistivity (measured at liquid nitrogen temperature):

Metallurgical state	Resistivity, μ ohm-cm^3
Retained gamma	73.1
Partially transformed	38.0
Transformed	3.4

Density (in retained gamma state):

Temperature		Density,
°C	°F	g cm^3
25	77	17.13
100	212	17.06
200	392	16.97
300	572	16.88
400	752	16 79
500	932	16.70
600	1112	16.62

Specific heat [between 300–400°C (572–752°F)]. 7.5 (±0.5) cal/mole °C

Melting point: 1130°C (2070°F)

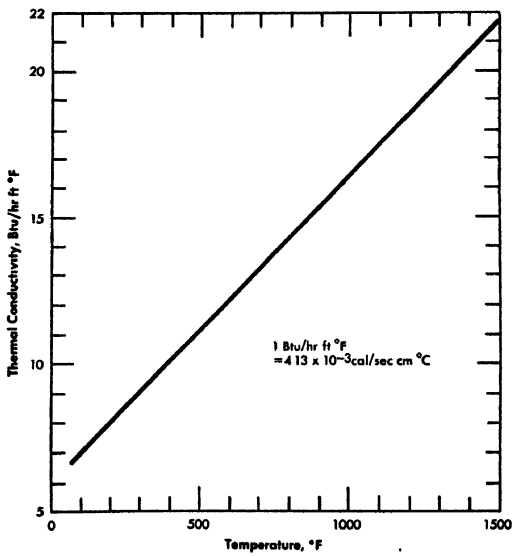

FIG. 4–82. Variation of thermal conductivity of U-10 w/o Mo alloy with temperature.

TABLE 4–18

TRUE STRESS-STRAIN DATA OF
URANIUM-10 W/O MOLYBDENUM ALLOY VERSUS TEMPERATURE*

Temperature		Ultimate tensile strength, psi	Yield strength, psi	True tensile strength, psi	Total elongation, %	Modulus of elasticity, 10^6 psi	Poisson's ratio
°C	°F						
24	75	140,000	140,000	168,000	8.5	13.10	0.358
121	250	105,000	101,000	155,000	11.75	11.80	0.311
260	500	92,000	85,000	137,000	10.75	10.96	0.508
399	750†	82,000	79,000	87,000	4 0	7.62	1.089
538	1000	52,000	44,000	54,000	38.0	5.06	1.166
676	1250	13,000	9,000	13,000	161.0	3.36	1.098

*Heat-treated one hour at 800°C, water-quenched, followed by heat-treating at 350°C one hour and water-quenched.
†Material probably transformed during test.

tivity, metallographic structure, fission gas, thermal conductivity, and thermal expansion have been conducted on specimens irradiated to beyond 2 total a/o burnup. The average decrease in density of test specimens with retained gamma, partially transformed, and transformed alpha-plus-epsilon structures was determined to be 2.4, 3.3, and 3.9% per a/o burnup, respectively.

Test data reported include those from specimens irradiated in the MTR and in CP-5. Specimens were bare, zirconium-clad with open ends, and zirconium-clad with ends capped. End caps were zirconium and stainless steel In general, it can be stated that (a) the radiation stability of the gamma-treated U-10 w/o Mo alloy is good to 2 a/o burnup below 1100°F and is good to 1/2 a/o burnup below 1350°F, (b) large physical changes such as swelling or ruptures have occurred at burnup less than 1½ a/o in material irradiated above 1100°F, and (c) ruptures have occurred in material that was fabricated improperly.

4–12. Control and Instrumentation

4–12.1 General description. The control and instrumentation systems for the Enrico Fermi Atomic Power Plant are designed to accommodate a maximum of 430 Mw reactor heat output even though the plant output will at first be limited to 30 Mw.

Systems design is similar to that for a conventional plant The control and instrumentation systems will provide for regulating, monitoring, and adjusting the main operating functions from a central control room. The number of controls will be the minimum required for adequate plant control. It takes one operator and an assistant in the main control room and one roving operator to run the plant. Essential control systems will be operable by either automatic or manual control within limits defined by the setpoints of the various modes of protection So far as possible, normal control will be automatic.

The general functions of the control systems include the following:

(1) Reactor plant operating control: automatic-manual control of primary and secondary coolant temperatures, manual control of primary and secondary sodium coolant flows, provision of signal for control of feedwater flow to the steam generators, and automatic-manual control of reactor power level.

(2) Reactor plant safety: provision of scram or fast-rundown trip signal from various reactor plant abnormal conditions.

(3) Primary and secondary inert gas blanket control: regulation of sodium gas blanket pressures and flow in primary system.

(4) Primary and secondary sodium servicing control: regulation of primary sodium purity.

Metering facilities will not be unnecessarily duplicated for normal control functions. If the instrument and detector devices for indication or readout instrumentation can also serve as metering elements for control, they will be so employed However, the safety system scram and fast rundown functions will be effectively isolated from both normal metering-indicating and normal control to minimize the number of reactor shutdowns due to instrument failure.

The control systems, with the exception of the safety system, are designed so that reactor plant shutdown resulting from instrument failure will be kept to a minimum. This will be fulfilled by providing for manual operation upon failure of a control component. The output of a defective control component or system will cause the control system to fail "as is," setting off an alarm so that the control operator can switch to manual operation.

In the reactor safety system, any failure will initiate channel trip signals (which will be indicated on an annunciator) and will shut down the plant only on coincidence of two or more trip signals Component failure causing malfunction of any of the various control systems will easily be determined by the operator. Failure of important functional devices will be annunciated Failures of less important devices will be indicated to the operator, to assure their detection

The safety system equipment will be repaired only by replacing components. In all other systems, the manual and automatic control circuits will be separated so that the automatic control system can be serviced at any time without interference with manual control. Control systems may be repaired in place or by substituting new components.

4–12.2 The operating control system. Ordinarily, this system will control the reactor plant from shutdown through the operating range to the maximum rated power output. It will include all equipment necessary for manual startup, monitoring the plant operation, manual and automatic control throughout the power range, and automatic power level setback. The last-named system will override the normal operating control system to reduce the power should it rise above a predetermined level. The following criteria apply to the operating control system:

(1) The reactor plant control system will be completely governed from a central panel in the main control room.

(2) The plant will be operated with full-rated sodium flow in all loops from no load to full load.

(3) The temperature program of the system for the 300-Mw core is shown in Fig. 4–83 and a corresponding temperature program for the 430-Mw core is shown in Fig. 4–84.

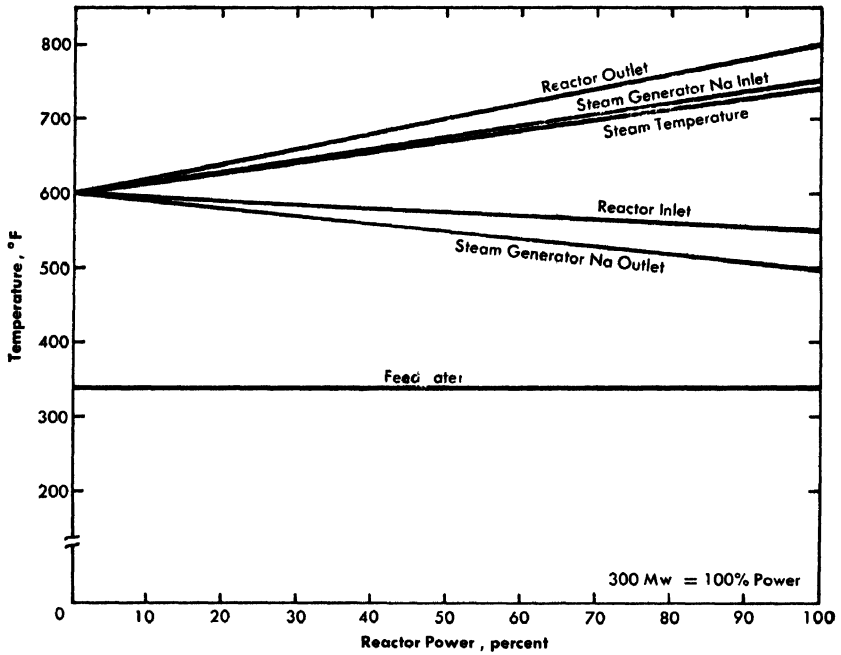

FIG. 4–83 Temperature schedule, 300-Mw full-power operation.

(4) The plant will be operated as a base load unit and the steam system will take whatever steam is generated by the reactor plant. Turbine power will be matched to reactor power by automatically controlling feedwater flow rate and the turbine throttle.

(5) Excess steam will be dumped automatically when pressure exceeds predetermined limits.

(6) Manual control of any component will always be possible upon failure of automatic control.

(7) Verification of control signals will be provided in order that transfer to manual control can be accomplished upon instrument failure.

(8) The velocity of the operating control rod is limited to give a maximum reactivity increase rate of 1¢/sec during startup and approximately 0.25¢/sec in the power range.

(9) The average rate of change of reactor power level will not be permitted to exceed 3 Mw/min. However, short-term transients of up to 30°F on reactor outlet coolant temperature will be considered tolerable.

(10) The neutron flux at the detectors will be a minimum of 3 n/(cm²)(sec) on initial startup before withdrawal of any of the safety rods. Neutron flux at full power will be approximately 1×10^{11}

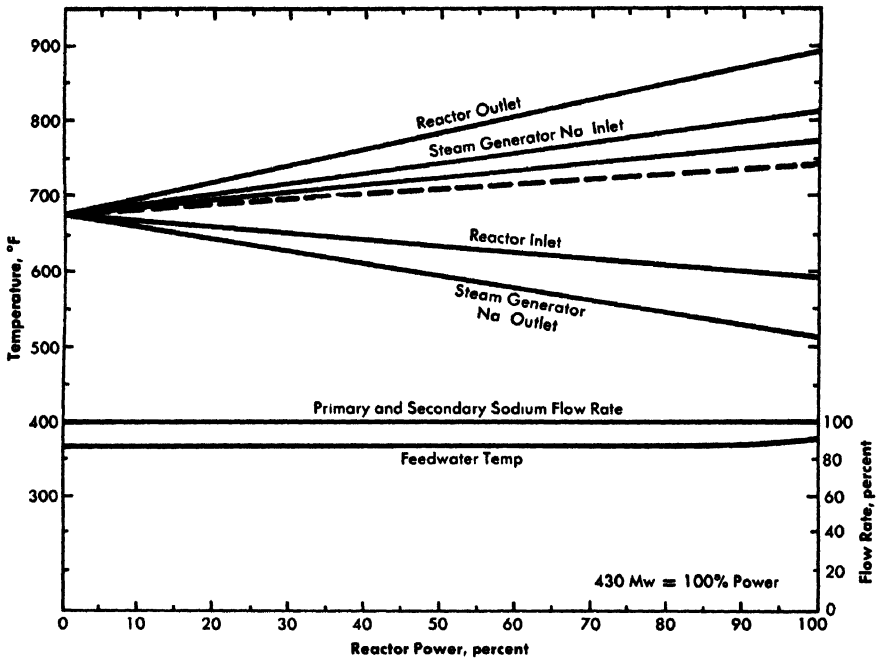

FIG. 4–84. Heat cycle system temperature and flow schedule, 430-Mw full-power operation Dashed curve indicates reactor sodium average temperature

n/(cm²)(sec) maximum Upon shutdown, the neutron flux would decay from approximately 3000 n/(cm²)(sec) immediately after shutdown to 30 n/(cm²)(sec) at the end of one day, and would diminish at a slow but reasonably constant rate thereafter.

(11) There will be safety system protection during all reactor operations No system disabling will be permitted.

(12) Reactor outlet and inlet temperatures will be maintained within ±10°F of the temperatures corresponding to a particular power level

(13) Primary and secondary coolant loop flows will be balanced (manually) at all times so that load will be shared equally (within ±3%).

(14) The following will be required during plant shutdown: (1) safety rods and operating control rods must be fully inserted, (2) reactor temperature must be maintained at approximately 600°F or above by manual adjustment of sodium flow, (3) reactor decay heat must be removed by the steam system (therefore, boiler feedwater control will be available), and (4) at least one channel of low-level neutron circuitry must be operating at all times for monitoring.

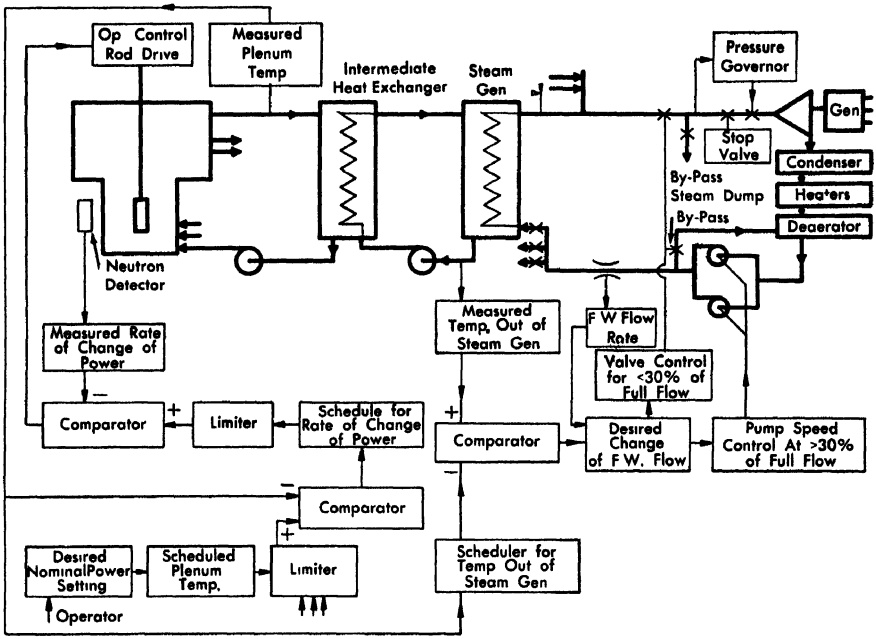

FIG. 4–85. Plant automatic control scheme for Enrico Fermi Atomic Power Plant.

Startup range. For reactor startup, monitoring equipment will indicate and record neutron flux level and reactor period A remote manual control station will enable the operator to withdraw or insert all eight safety rods simultaneously or independently Indicating lights will show for each safety rod that is not latched to its actuator Each of the eight safety rods will have position indicators Individual remote manual ON-OFF control stations will allow withdrawal or insertion of either of the two regulating control rods at a specified maximum rate. There will be a manual control station for starting the six sodium pumps and controlling their speeds These sodium pump speed-control devices will permit adjusting flow in any of the six loops independently, any corresponding primary and secondary loops simultaneously, or all six loops simultaneously. Signals will go to the power generating station for controlling the feedwater pumps. There will be manual control stations for operating each of the three flow balancing valves on the feedwater lines entering the steam generators. Steam generator isolation valves will require no operator supervision.

Power range. A schematic block diagram showing a concept of the power range operating control system is in Fig. 4–85. Reactor power is

automatically controlled to meet the demand set by the operator, but reactor power level changes will be at a safe, predetermined rate regardless of how the operator may manipulate the power set adjustment. All scheduled changes of power output will be initiated at the reactor, and the turbogenerator's share of the electrical system load will be automatically adjusted to accept the heat output of the reactor Otherwise, excess steam will be dumped when the pressure reaches a predetermined value.

The plant will operate as a base load unit. For each power level, there is a corresponding temperature at which the sodium must leave the reactor (see Fig. 4–83). To set the power at a particular level, it is necessary to adjust the reactor outlet temperature to the corresponding level. The temperature "error" (difference between the required or "demand" temperature and the actual reactor outlet temperature) will control the rate of change of power demand, with a positive upper limit of 3 Mw/min. This demand rate of change of power is compared with the actual rate of change, as sensed by a neutron flux derivative unit. The error (difference) between these two will cause the control servo system (at controlled velocity) to operate a selected control rod. The rod worth (reactivity change) per unit of rod movement varies over a range of about 3 to 1, depending upon the rod position. A feedback signal from a tachometer on the control rod drive motor is compared with the velocity demand signal, to control the servo-motor speed. As the required reactor outlet temperature is reached, the demanded rate of power change reduces to zero, and rod movement stops at, or very close to, the desired power level.

When primary sodium flow rate is adjusted and reactor sodium inlet and outlet temperatures are in accordance with power schedule, the power setting and actual power will agree.

The reactor inlet temperature must be controlled in order to obtain the correct temperature rise across the reactor and the correct reactor average temperature. This temperature is controlled by changing the rate of heat removal in the steam generator through variations of the boiler feedwater flow. Reference to Fig. 4–83 will show that for each power level there is a definite desired temperature for sodium leaving the reactor, and a corresponding reactor sodium inlet temperature. Temperature is measured at the sodium outlet of the steam generator (rather than at the reactor inlet), so that temperature changes will be sensed quickly. The steam generator sodium outlet temperature demand is set in relation to required load according to the temperature curve shown in Fig. 4–83 (thus, in effect, scheduling the reactor inlet temperature according to load). The actual temperature of the sodium at the steam generator outlet is compared with the demand value corresponding to the load, and a

signal is given which controls the speed of the boiler feed pumps through variable speed hydraulic couplings and controllers.

Below the minimum allowable flow rates for the boiler feed pumps, which corresponds to about 30% of full power, the feedwater recirculation valve and the valve in series with the steam generators will be operated to obtain desired feedwater flow rate. Above about 30% full power, the hydraulic couplings on the feedwater pump will be controlled to give desired flow rate.

The turbine throttle valve will be controlled by a pressure regulator to maintain a constant steam pressure at the turbine. Thus the turbine will accept the increased flow initiated by the feedwater pumps, so long as the electrical system will accept the increased energy output of the generator.

The bypass steam dump system will accept steam flow during plant startup and whenever steam pressure exceeds a preset value. In normal operation there will be no flow to the steam dump.

This method of operation has been checked by simulator studies made at the Holley Carburetor Company and has been provisionally demonstrated to be stable

Two boiler feed pumps will normally be used during full-power operation. A third pump will be used as a spare. A suitable signal for the feedwater control system will be furnished to the power-generating station.

Should the power or temperature rise to an abnormal level, the automatic power level setback system will override any automatic or manual functions of the operating control system and reduce reactor power to a predetermined level.

Sodium flow in all loops will be held constant, with only slight manual adjustments in speed to balance the heat output of the three loops.

4–12.3 The reactor safety system. This system initiates rapid plant shutdown upon predetermined abnormal conditions. Two ranges of operation may be arbitrarily established on the basis of thermal and nuclear considerations: (1) startup range and (2) power range. In the startup range, the system is essentially isothermal and the prime concern is to prevent nuclear transients. In the power range, thermal as well as nuclear transients must be prevented.

The reactor safety system provides the final stage of plant protection over the full range of reactor power from shutdown level to maximum power. The system initiates two types of shutdowns. Fast rundown will be designed to reduce reactor power level at a rate corresponding to that of flow decay in the reactor when the primary pumps are shut off. Scrams are designed for the fastest possible shutdown.

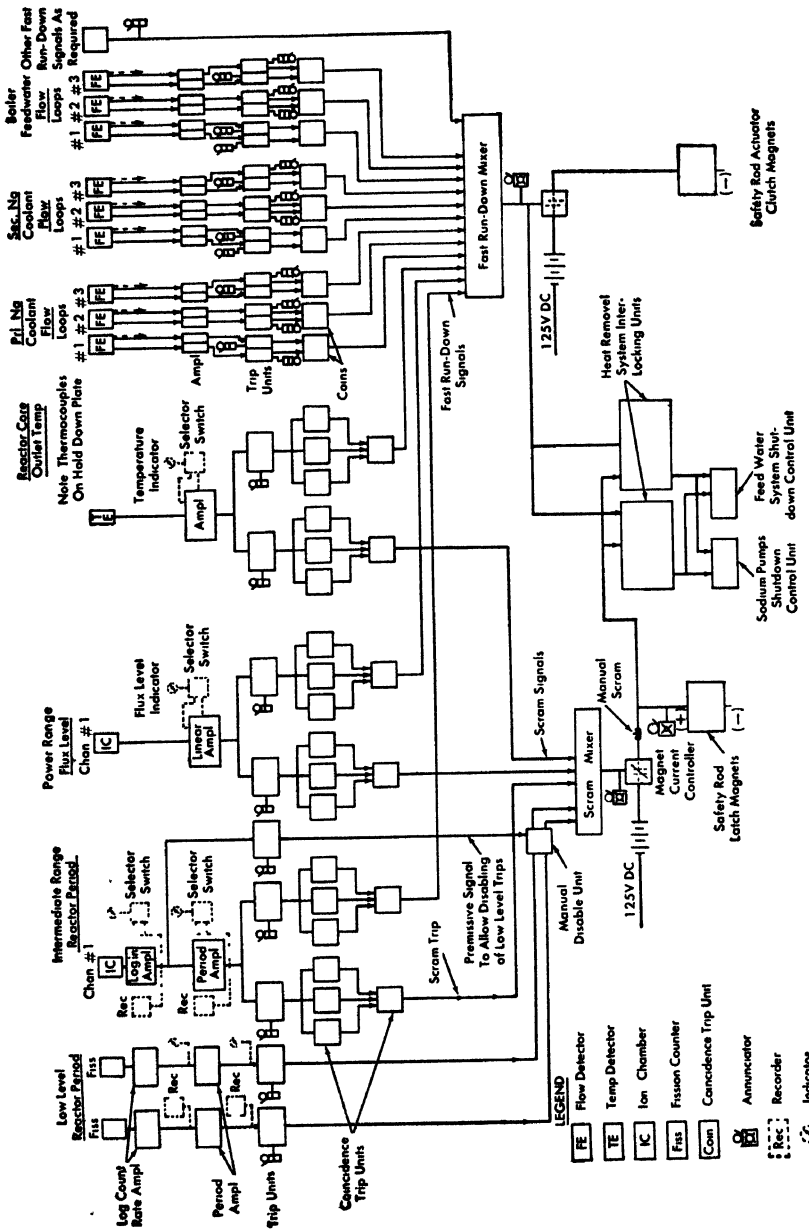

FIG 4-86. Functional block diagram of safety system.

The safety system initiates a fast rundown for unacceptable conditions of the following:

(1) Power level.
(2) Sodium flow.
(3) Boiler feedwater flow.
(4) Reactor temperature.
(5) Reactor period.
(6) Miscellaneous functions.

A scram is initiated for unacceptable conditions of:

(1) Reactor period.
(2) Power level.
(3) Reactor temperature.
(4) Miscellaneous conditions.

The following operation criteria and requirements apply to the reactor safety system:

(1) Operational monitoring of the safety system will be from a central panel in the main control room.

(2) The safety system will be completely automatic, with means for manual scramming at the control console.

(3) The safety system will accommodate 6 to 8 safety rods with latch magnets and clutches operating on a DC battery supply Release circuitry will provide for latch release times of 50 and 100 msec.

(4) Loss of AC power to the safety system will cause a fast rundown rather than a scram

(5) Fast rundown will reduce reactor power level at a rate corresponding roughly to the flow decay within the reactor when the primary pumps are shut off. This may be accomplished by releasing the drive clutches, by programming a sequential release of the latching magnets, or both.

(6) Scram will be accomplished by simultaneous release of all latching magnets.

(7) There will be protection against too-short reactor periods throughout the entire range of operation from initial startup to full power. Period trip points will be fixed at 20 sec for fast rundown and 10 sec for scram The trip points can be adjusted only by replacing components within the range from 100 to 5 sec.

(8) The neutron level trip point will be fixed at a predetermined value between 300 and 475 Mw, and can be changed only by replacing components.

(9) Temperature trip points will be fixed at a predetermined value between 900 and 1500°F, changeable only by replacing components.

(10) Both fast rundown and scram will be accompanied by transfer of the heat-removal system to emergency cooling as required.

A representative instrumentation system for the reactor plant safety system is shown in block diagram Fig. 4–86. For the low-level trip system, a period signal from the low-level count rate and period measuring

circuits is introduced into a unit which has a fixed trip point. An abnormal period signal fed into this trip unit will cause it to introduce a step-type signal into the final scram trip mixer of the safety system, and thereby produce a scram. Either of the two low-level trip channels will cause a scram on an "auctioneering" basis. As soon as the ion chamber channels begin to produce signals strong enough to be usable, a signal is given to the operator so that he can manually disable the low-level trip. Scrams are permitted on the low-level trip circuit to simplify equipment, since no undesirable thermal transients can result.

The power range trip system operates as follows. When any one of the various detectors indicates a condition that requires safety system action, the trip units in that particular channel feed signals into trip coincidence units. These units receive similar signals from all channels that sense an abnormal primary condition. Thus the output of the coincidence units provides a scram signal (or a fast rundown signal) to the final mixers in a particular shutdown chain. The output of this mixer initiates action to interrupt current to the scram magnet (to produce a scram), or initiates action to close the clutch solenoid circuit (to produce a fast rundown). Failure of any of the more vulnerable units within the safety system will be tolerated without causing a shutdown, but such failures are immediately annunciated, so that corrections can be made. The system shown provides period protection, neutron level protection, high-temperature protection, protection against loss of coolant flow or boiler feed flow, and an additional protection channel for future use for conditions as yet undetermined.

4–12.4 Primary and secondary inert gas control systems. Inert gas is used in the reactor systems to blanket the liquid metal surfaces so as to reduce the possibility of oxygen leaking into the coolant stream. Reliable automatic pressure control systems are required, along with the necessary backup devices, performance indicators, and manual override. The purpose of the primary gas system is to maintain atmospheric pressure in the vessel and tank gas plenums and to avoid pressure changes during transients. Sealing devices throughout prevent escape of radioactive materials. The secondary gas systems have no automatic pressure regulation.

4–12.5 Primary and secondary sodium service control systems. The sodium service systems maintain purity of the main sodium coolant. Plugging indicators give a measure of the oxygen combined with the sodium. This guides the operator to cold-trap the liquid when necessary.

4–12.6 Neutron source and nuclear detectors. A *neutron source* provides a measurable neutron flux at the detectors for initial startup and

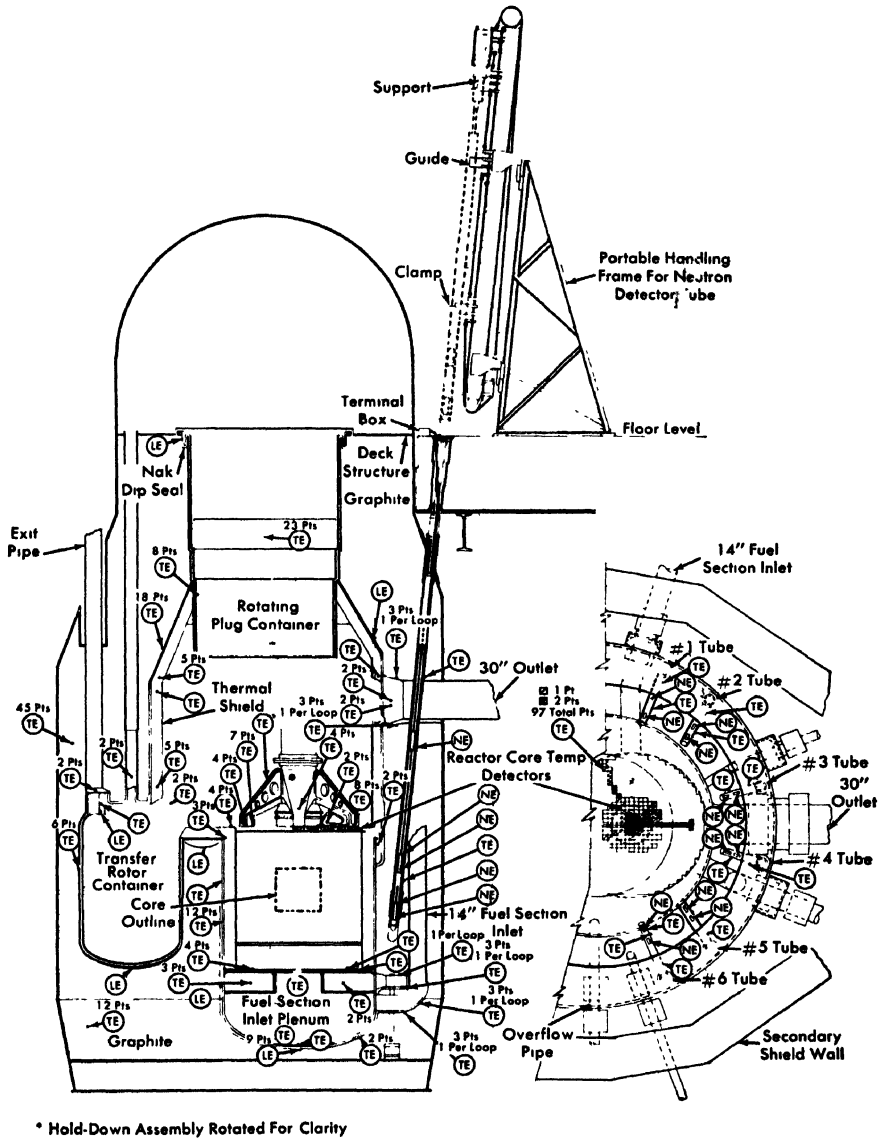

FIG. 4–87. Schematic drawing of reactor vessel instrumentation.

maintains a measurable flux when the reactor is shut down. This is a safety feature during startup and loading; it assures that the multiplication of the reaction can be determined by the instrumentation at all flux levels.

The photoneutron source will be made of antimony and beryllium. Antimony activation will be about 1200 curies at initial startup. The pres-

ent source design requires an antimony rod about 25 inches long and 1 inch in diameter. It is surrounded by a cylinder of beryllium about 25 inches long, with an outside diameter of 2 35 inches. The antimony rod has on its upper end a handling head identical to those on the fuel elements. The beryllium cylinder will be in a container with the same outside dimensions as those of a fuel subassembly can. The beryllium cylinder will be clad in stainless steel, the antimony in a material able to contain it at elevated temperatures.

Neutron detectors. The detectors measuring neutron flux will consist of proportional counters, fission counters, and gamma-compensated ion chambers. They will cover a range of about 10 decades from initial source level to full power, decreasing to about 9 decades for startup following full-power operation. The detectors should be capable of continuous operation for 10 years at 600°F in the flux range at the tube location. Figure 4–87 shows the location of the neutron detector tubes. Initial source level is the neutron flux existing at the instrument tubes under clean startup conditions with the neutron source installed in the reactor, all fuel and blanket elements loaded, and all safety and operating control rods fully inserted. In this case, the design minimum thermal flux at the counter locations will be 3 n/(cm²)(sec).

Proportional counters will be used to measure the lowest decades but will not be necessary for startup after power operation Fission counters will be used from operational startup level (after power operation) and will cover the next four or five decades Gamma-compensated ion chambers will cover the remaining decades to full power Neutron detector operating ranges and anticipated radiation levels are shown in Fig. 4–88.

Ion chambers will be required for power level measurement of neutron flux for all safety and control channels. These ion chambers will be used for flux measurements in the range of 10^4 to 10^{11} n/(cm²)(sec) with a corresponding range of gamma flux of 1500 r/hr to 10^6 r/hr Gamma compensation will be available on all current chambers, although compensation will be utilized only where required.

The number of detectors to be installed will be determined on the basis of the final reactor control and safety system design. However, the following quantities have been specified, with pertinent data:

	Operating range		*Must withstand*	
	Flux, n/(cm²)(sec)	*Gamma, r/hr*	*Flux, n/(cm²)(sec)*	*Gamma, r/hr*
Two proportional counters	3 to 10^5	1500		
Three fission counters	10 to 3×10^6	10^4	10^{11}	10^6
Ten compensated ion chambers	10^4 to 10^{11}	10^6	10^{11}	10^6

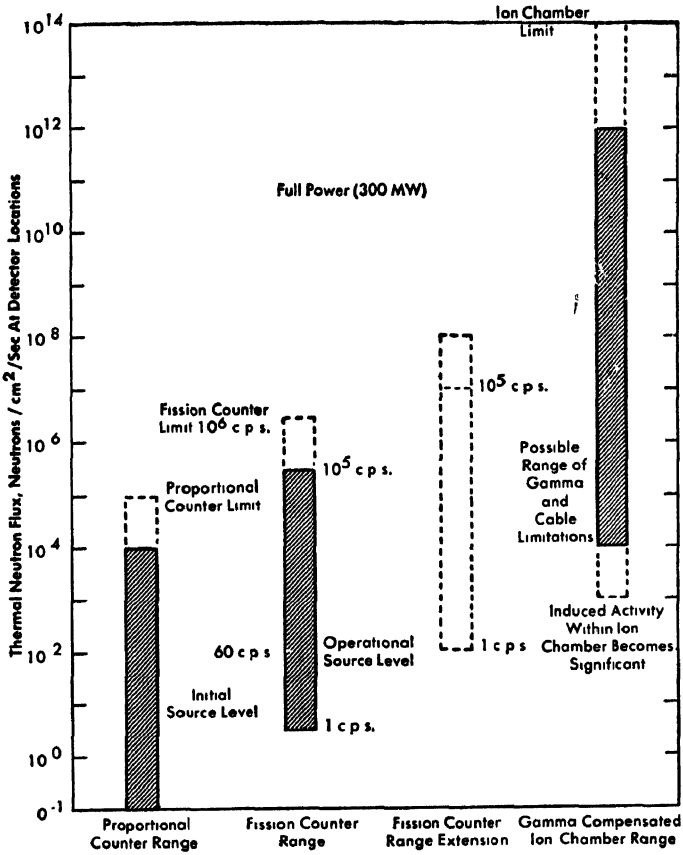

FIG. 4–88. Neutron detector operating ranges.

An ion chamber cooling system is being eliminated by using high-temperature detectors with mineral-insulated cables. Retracting the fission counters would extend their life during power operation and make it possible to extend the fission counting range. However, present plans are to avoid retracting the counters and to provide range extension, if necessary, by using extra counters in lower flux positions.

Cable connections to the detectors will be hermetically sealed and resistant to low frequency (5 to 75 cps) vibration, high temperature (600°F), and radiation damage. Detectors are to be electrically isolated from the equipment ground circuit within the guide tubes to reduce noise from potential gradients.

A cartridge unit suspended from a shielding plug in the operating floor will be placed in the instrument tube (Fig. 4–87). The cartridge assembly consists of a carrier rod having several detectors separately mounted,

with attached cables and a cartridge shielding plug long enough (about 5 ft) to reduce streaming of neutrons out of the tube to the surrounding level of the shield tank. Helical tubes to prevent streaming will guide the cable leads through the floor plug. After the best detector positions have been determined by flux mappings, the cables will be secured at the top of the plug by means of swagelock fittings (for gastightness). The entire assembly may be lifted out of the tube.

4–12.7 Non-nuclear detectors. *Temperature.* Temperature measurements are required to control and monitor the reactor, heat cycle loops, and auxiliary systems. Temperature data are needed also for stress analysis, heating checks, and component behavior information. Temperature measurements inside the reactor vessel, including the primary shield tank, will be made with iron-constantan thermocouples, in 1/8-inch OD stainless steel sheaths, insulated by MgO. Outside the vessel, where temperatures are lower and restrictions on space and response time are not so se-

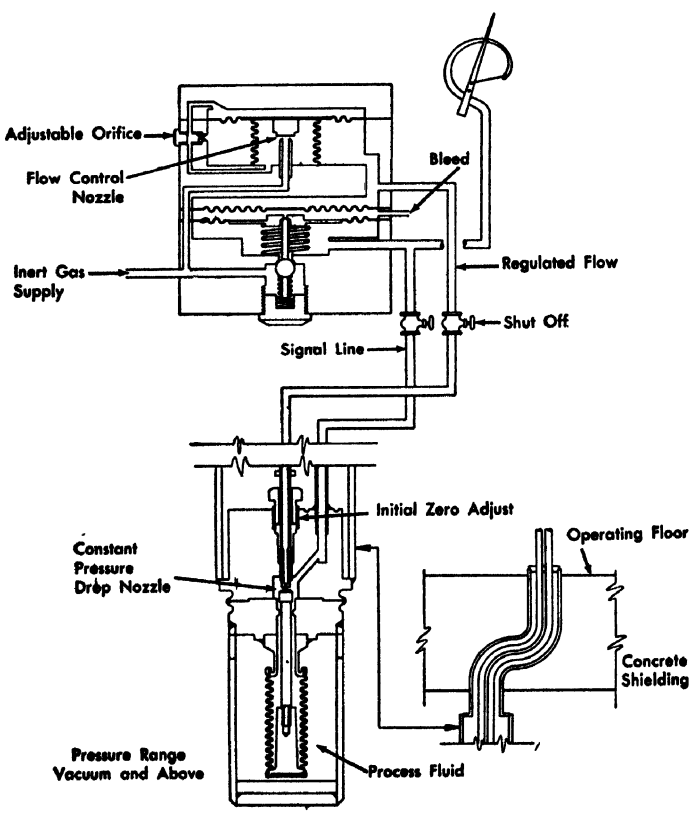

FIG. 4–89. High-temperature force balance pressure detector.

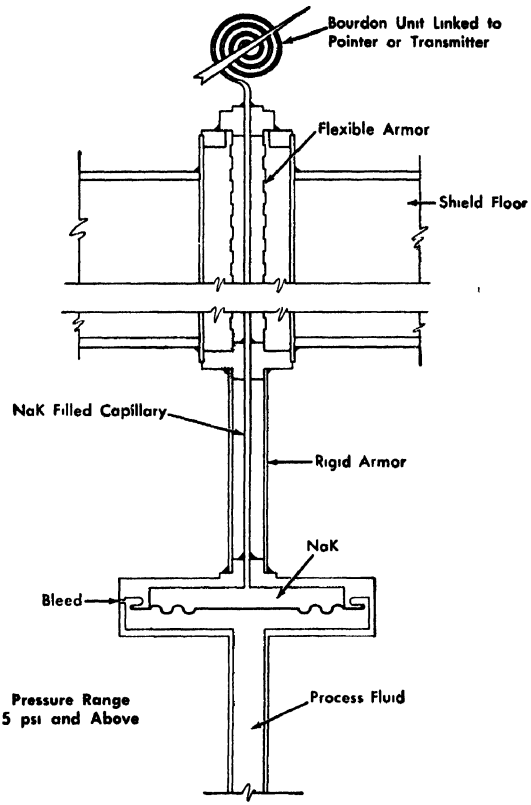

FIG. 4–90. High-temperature NaK-filled pressure detector.

vere, resistance or fluid-system elements will be used for high, sustained accuracy. Temperature measurements for heating and other information will be made by copper-nickel sheathed iron-constantan thermocouples. Sodium temperature measurements for control purposes will be made by resistance thermometers, with elements manufactured integral with the wall.

Pressure. Pressure measurements are required as operating information and to indicate the performance of various components in the systems. Where the process medium is radioactive and the fluid is sodium or its vapor, either a NaK-filled pressure system or a force-balance pneumatic system will be used to measure pressures. The force-balance, high-temperature pressure detector is shown in Fig. 4–89. Nitrogen will be used instead of control air to prevent a possible contamination of sodium in the event of a bellows rupture. The NaK-filled high-temperature pressure detector is shown in Fig. 4–90. This detector will be used

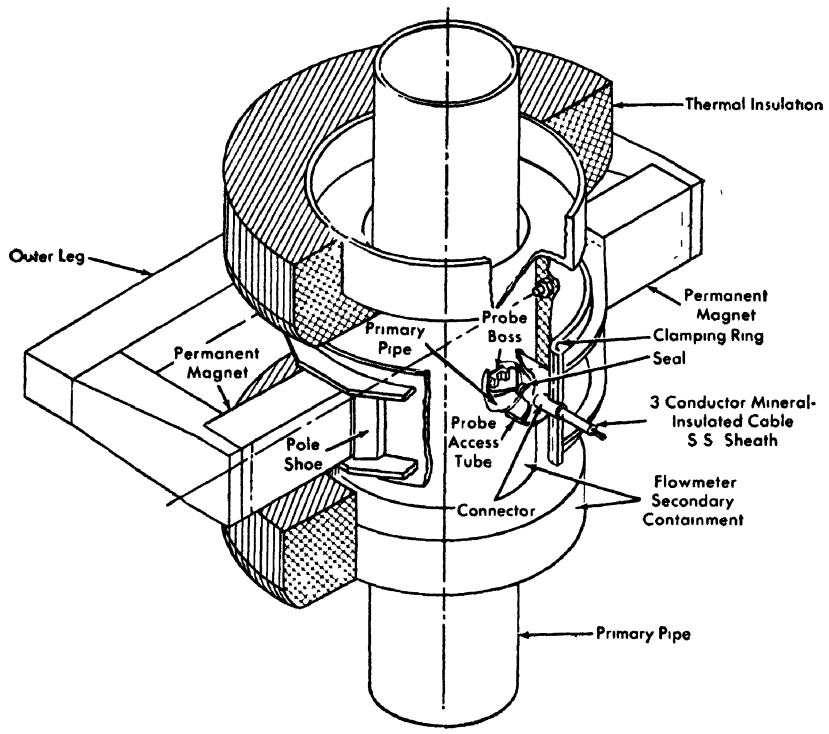

FIG. 4–91 Primary sodium system magnetic flowmeter

for ranges greater than 0 to 5 psi. For services other than those stated, conventional pressure transmitters will be utilized.

Flow. Flow measurements are needed to determine the heat output for control of the reactor, and to balance the flow in the coolant systems to obtain efficient plant operation. These measurements also provide a check on the operation and position of the throttle valves in the 6-inch sodium line supplying the coolant to the blanket. Flow in the liquid metal loops and sodium service systems will be measured by permanent magnet flowmeters, so that the piping integrity is not impaired. Steam, water, and inert gas flow will be measured by conventional means. Figure 4–91 shows a cross-sectional assembly of the permanent magnet flowmeters for installation in the primary loop Note the special design necessary to preserve the integrity of the secondary containment around this primary loop flowmeter.

Level. Coolant flows between the various components in the main operating loops, and the service systems require measurements to ensure that correct liquid levels are maintained. For continuous sodium level measurements, submerged pressure detectors will be used. Another pres-

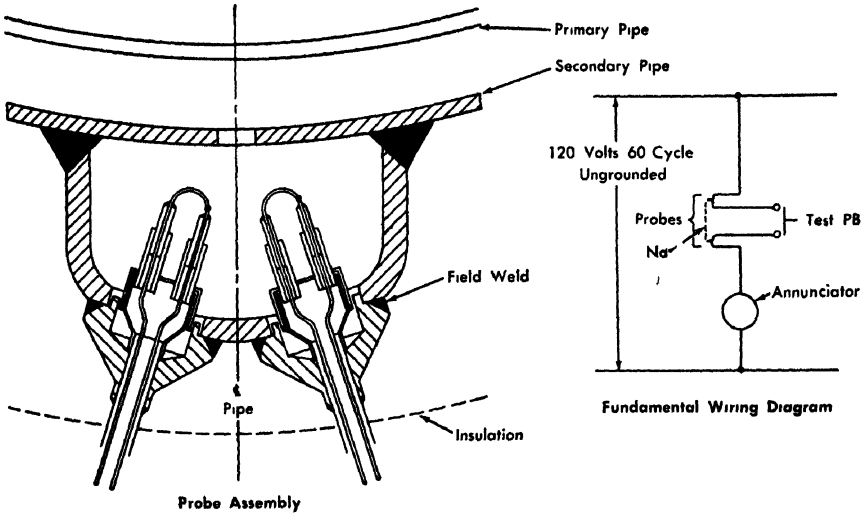

FIG. 4–92 Typical leak detector.

sure device will be installed in the gas space above the sodium to compensate for the gas head. These will be high-temperature, force-balance pressure detectors Conventional float level devices are being considered where replacement will be possible

It is also planned to use an auxiliary level device for the reactor vessel. This will be a small inductance probe, manually raised and lowered in a thimble to determine the level by observing the point at which a sudden change in inductance occurs.

Leak detection It is imperative that the operator be aware of any leakage of liquid sodium from the components of piping of the primary loop. The leak detector being used for this purpose is a double probe that utilizes the electrical conductivity of sodium in a circuit. The double-probe leak detector enables a remote continuity check to determine operability of the device. Figure 4–92 is a cross-sectional view of the leak detector and a typical schematic wiring diagram of the test and annunciator circuit.

4–12.8 Centralized control concept. Experience has shown that the more control of steam and process plants is centralized, the better and more reliable the performance, because communications are improved and operator responsibility can be coordinated with higher efficiency. This applies equally to conventional and nuclear power plants. Such centralized control is planned for the Enrico Fermi Atomic Power Plant.

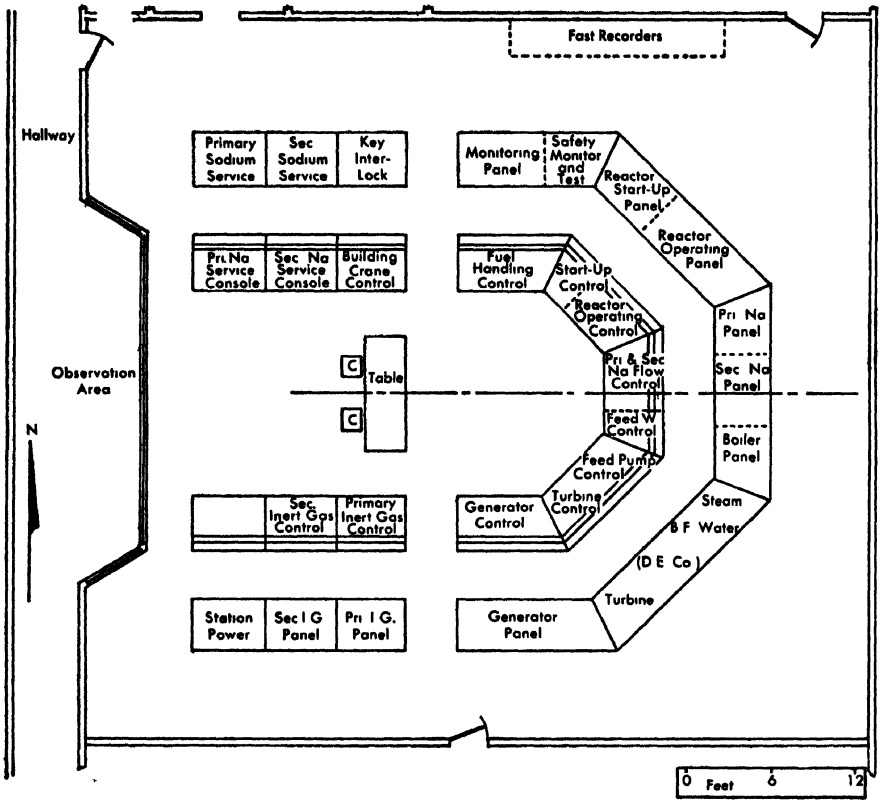

FIG. 4–93. Plan view of central control room.

It will provide all necessary facilities for controlling the reactor and plant auxiliaries that require frequent attention or affect reactor operation. Centralized control will also provide best facilities for coping with emergencies and will afford coordination during startup, load changes, and shutdown conditions.

The control room (Fig. 4–93) will be on the top floor of a three-story building adjacent to the turbogenerator building. Fuel handling will be controlled from this room. The material handling section of the control center will provide means for remote handling of radioactive plant components in the reactor building. It will be used in conjunction with remote television screens in direct view of the operator.

4–12.9 Cost of reactor construction. Table 4–19 presents some cost information pertaining to the Enrico Fermi Atomic Power Plant. The total costs shown for the reactor plant structures, the reactor plant equip-

ment, the primary sodium system, and the secondary sodium system include, in each case, the approximate purchase price of the components listed, the construction labor, and the estimated cost of other equipment not listed. Where possible, the actual purchase or contract price is indicated.

Atomic Power Development Associates, Inc., is composed of the following: Alabama Power Co., Atlantic City Electric Co, Baltimore Gas and Electric Co., Central Hudson Gas & Electric Corp., Cincinnati Gas & Electric Co., Cleveland Electric Illuminating Co., Connecticut Light & Power Co, Consolidated Edison Company of New York, Inc, Consumers Power Co., Detroit Edison Co, Delaware Power & Light Co, General Public Utilities Corp., Georgia Power Co., Gulf Power Co, Hartford Electric Light Co, Indianapolis Power & Light Co, Jersey Central Power & Light Co., Long Island Lighting Co., Metropolitan Edison Co., Mississippi Power Co., New Jersey Power & Light Co, New York State Electric & Gas Corp, Niagara Mohawk Power Corp., Pennsylvania Electric Corp, Philadelphia Electric Co, Potomac Electric Power Co, Public Service Electric and Gas Co., Rochester Gas and Electric Corp, Toledo Edison Co., Wisconsin Electric Power Co, Wisconsin Power and Light Co., Allis-Chalmers Manufacturing Co, Babcock & Wilcox Co, Bendix Aviation Corp., Commonwealth Associates, Inc, Ford Motor Co, General Motors Corp., Jackson & Moreland, Leeds & Northrup Co, Pittsburgh Consolidation Coal Co., Southern Services, Inc., United Engineers & Constructors Inc., Vitro Corporation of America.

References

1. B. Lubarsky and S. J. Kaufman, *Review of Experimental Investigations of Liquid-Metal Heat Transfer*, Report NACA-TN-3336, Lewis Flight Propulsion Laboratory, National Advisory Committee for Aeronautics, 1955

2 H A. Bethe, *Reactor Safety and Oscillator Tests*, Report APDA-117, Atomic Power Development Associates, Inc., 1956.

3 B C. Cerutti et al., ZPR-III, Argonne's Fast Critical Facility, *Nuclear Sci. and Eng.* 1(2), 126 (1956).

4 A. Del Grosso and D. O. Leeser, *The APDA Test Program on Selected Uranium Fuel Alloys*, Report APDA-122, Atomic Power Development Associates, Inc., June 1957.

5. J. E. Gates et al., *Stress-Strain of Irradiated Uranium 10 w/o Molybdenum*, Report APDA-BMI-638, Atomic Power Development Associates, Inc., Jan. 6, 1958.

6. M. H Bartz, Radiation Damage Observations at the MTR, in *Papers Prepared for Radiation Effects Review Meeting, Congress Hotel, Chicago, July 31–August 1, 1956*, USAEC Report TID-7515(Pt. 1), Phillips Petroleum Co., 1956.

7. R. E. Bailey and M E. Silliman, Fast Neutrons and the EBR-I Core Flow Separator, in *Symposium on Radiation Effects to Materials*, Vol. III, American Society for Testing Materials, June 1958. (To be published)

TABLE 4–19

FERMI PLANT CAPITAL COSTS IN THOUSANDS OF DOLLARS

	Approximate purchase price of components	Construction labor	Total	Equipment furnished by
A. *Reactor plant structures*	3,000	1,800	4,800	
1. Steel containment building complete, including all doors	750*			Chicago Bridge & Iron
B. *Reactor plant equipment*	6,000*	1,000	7,000	
1. Reactor vessel including internal shielding and supports	1,200			CE†
2. Rotating shield plug and drive	600			CE and GE‡
3. Control rods and actuators	500			Allis-Chalmers and GE
4. Hold-down mechanism	200			GE
5. Offset handling mechanism	300*			GE
6. Element transfer rotor assembly	150*			Snyder & Cross Eng.
7. Element transfer cask car	400			
8. Element transfer cleanup, storage, and disassembly equipment	1,000			
C. *Primary sodium system*	4,000	1,000	5,000	
1. Pumps	800*			Byron Jackson
2. Intermediate heat exchangers	2,000*			Alco

D. *Secondary sodium system*	3,000*	200	3,200	
1. Pumps	500			
2. Steam generators	1,500*			Griscom-Russell
E. *Fabrication of 100 fuel and 600 blanket subassemblies for initial loading, including reduction of UF^6 to metal, scrap recovery and losses, inspection*			2,800	
Estimated total cost of the reactor portion of the plant, including engineering, spare parts, interest and local taxes during construction, reactor portion of site development, and fabrication of fuel, but excluding the turbine generator and the turbine generator building			34,445	
Preoperational testing after construction, initial operation at low to full load, personnel training, and working capital			2,575	

*Actual purchase or contract price. †Combustion Engineering. ‡General Electric.

TABLE 4–19

TABLE 4–1

DESIGN AND PERFORMANCE DATA FOR THE ENRICO FERMI FAST BREEDER REACTOR

	Average radial blanket burnup (% of total atoms)	
	0.0%	0.2%
General characteristics; reactor core		
Core power, kw	281,000	265,000
Core volume, ft^3	11.65	11.65
Heat-transfer surface, ft^2	1,378	1,378
Average heat flux, Btu $(ft^2)(hr)$	696,000	656,000
Ratio, maximum to average heat flux	1.73	1.73
Power density, kw/ft^3	24,200	22,800
Specific power, kw/kg U^{235}	580	546
Core dimensions:		
Diameter, in.	30.5	30.5
Length, in.	31.0	31.0
Core coolant:		
Sodium flow rate, lb/hr	12,455,000	11,750,000
Flow area, ft^2	1.99	1.99
Velocity, fps	32.1	30.3
General characteristics, core blanket		
Blanket power, kw:		
Radial section		30,000
Axial section		5,000
Blanket volume, ft^3:		
Radial section		161
Axial section		13
Heat-transfer surface, ft^2:		
Radial section		9,250
Axial section		444
Average heat flux, $Btu/(ft^2)(hr)$:		
Radial section		11,100
Axial section		35,700
Maximum to average heat flux (radial)		40
General characteristics; heat transfer		
Maximum coolant temperature,* °F	1010	
Maximum cladding temperature,* °F	1055	

(*continued*)

	Average radial blanket burnup (% of total atoms)	
	0.0%	0.2%
Maximum fuel temperature,* °F	1316	
Maximum film temperature difference,* °F	60	
Maximum clad and oxide layer temperature difference,* °F	86	
Maximum uranium temperature difference (center to edge of fuel pin),* °F	266	

*Temperature with hot-channel factor based on a probability of the temperature occurring one time in a thousand.

Core design and performance

Core composition, vol. %:	
U^{235}	7.55
U^{238}	20.35
Zr, Mo, stainless steel	24.9
Sodium	47.2
Number of fuel subassemblies	91
Number of fuel pins per subassembly	144
Fuel alloy OD, in.	0.148
Cladding OD, in.	0.158
Cladding thickness, in.	0.005
Uranium alloy thermal conductivity (1100°F), Btu/(hr)(°F)(ft)	17.3
Average fuel alloy burnup, a/o	1.0

Blanket design and performance

Radial blanket dimensions, in.:	
Inside diameter	30.5
Outside diameter	78.5
Length	65
Axial blanket dimensions, in.:	
Diameter	30.5
Length	14
Number of radial blanket subassemblies	548
Number of rods per subassembly	25
Number of axial blanket subassemblies	182
Number of rods per subassembly	16

(continued)

Radial blanket element dimensions, in.:	
Clad outside diameter	0.443
Clad inside diameter	0.423
Uranium diameter	0.415
Sodium bond thickness	0.004
Axial blanket element dimensions, in.:	
Clad outside diameter	0.443
Clad inside diameter	0.423
Uranium diameter	0.415
Sodium bond thickness	0.004
Radial blanket composition, vol. %:	
Uranium	44.6
Sodium	34.7
SS, Mo	20.7
Maximum burnup in radial blanket, a/o	0.5
Axial blanket composition, vol. %:	
Uranium	28.3
Sodium	53.5
SS, Mo	18.2
Maximum plutonium buildup in radial blanket, a/o:	
First row of blanket subassemblies	1.7
Second row of blanket subassemblies	2.4
Outer row of blanket subassemblies	0.1

Reactor control

$\Delta k/k$ requirements, dollars*:	
Temperature override	0.20
Burnup, biweekly unloading	0.33
Growth, biweekly unloading	0.07
Fission product poisoning, biweekly unloading	0.02
Control margin	0.30
Total excess	0.92
Δk reactor hold-down, dollars	8.00
Total variable reactivity, dollars	8.92
Safety rods:	
Number	8
Reactivity per rod, dollars	1.00
Total stroke, in.	54
Length of poison material, in.	33
Reactivity per rod-inch, average, dollars	0.02
Eight-rod rate for 1$\dot{e}$ per sec, in/min	2
Time to remove eight rods, min	27
Area per rod, in^2	4
Weight per rod, lb	50
Scram rate of safety rods, dollars/sec	25

(*continued*)

Maximum fast rundown of safety rods, dollars/sec	0.75
Boron-10 required, per rod, kg	0.90
Operating control rods:	
Number	2
Total reactivity in both rods, dollars	0.92
Total stroke, in.	15
Reactivity per rod-inch, cents	6.1
Maximum reactivity insertion rate, dollars/sec	0.01
Area of rod, in^2	4.0
Weight of rod, lb	10
Boron-10 required, per rod, kg	0.47

*One dollar = reactivity change between delayed criticality and prompt criticality = 0.7% k_{eff}.

Reactor physics

Enrichment, w/o	28
Critical mass U^{235}, kg	485
Core conversion ratio	0 32
Blanket conversion ratio	0 80
Total conversion ratio	1.12
Radial/axial blanket Pu production	6
Median energy of core flux, Mev	0.25
Average core flux, n/(cm^2)(sec):	0.5×10^{16}
Ratio, maximum to average core power	1.73
Ratio, maximum to average core subassembly power	1.38
Ratio, maximum to average power in hottest subassembly	1.25
Average neutron generation time, sec	0.08
Effective delayed neutron fraction:	0.0069
Mean delay time of delayed neutrons, sec	12
Prompt neutron lifetime, sec	2.0×10^{-7}
Blanket fissions/total fissions	0.07
Isothermal core temperature coefficients of reactivity, $(\Delta k/k)/°C$:	
Axial fuel pin expansion	-2.8×10^{-6}
Ejection of compressed sodium	-0.5×10^{-6}
Reduced sodium density	-6.1×10^{-6}
Radial expansion of core	-3.0×10^{-6}
Doppler effect	-1.6×10^{-6}
Total core	-14.0×10^{-6}
Blanket:	
Uranium expansion	-0.8×10^{-6}
Reduced sodium density	-3.3×10^{-6}
Total blanket	-4.1×10^{-6}
Total reactor	-18.1×10^{-6}

(*continued*)

Reactor and containment vessels

Primary shield tank:	
Over-all height, over dome, ft	56.3
Height of primary shield tank, ft	40.2
Maximum diameter of primary shield tank, ft	24
Weight of primary shield tank, empty, lb	178,000
Primary shield tank material, carbon steel	ASTM A-285, GrC
Reactor vessel:	
Height of reactor vessel, ft	36.3
Maximum diameter of reactor vessel, ft	14.5
Maximum thickness of reactor vessel, in.	2
Weight of reactor vessel, without fuel, blanket and sodium, lb	760,000
Reactor vessel material, stainless steel	Type 304
Containment building:	
Over-all height of containment vessel, ft	120
Inside diameter of containment vessel, ft	72
Maximum thickness of containment vessel, in.	1.06
Containment vessel material, carbon steel	ASTM A-201, GrB Firebox; meets requirements A-300
Liquid metal and steam system:	
Gross electric capacity, Mw	104
Net electric power output, Mw	94
Net thermal efficiency, %	31.3
Sodium temperature, °F:	
Leaving reactor	800
Entering reactor	550
Sodium flow, lb/hr	13.2×10^6
System pressure drops:	
Design flow 300-Mw operation, lb/hr	13.2×10^6
Total pump head at design flow,* ft	330
Component head loss at design flow:	
Check valve and piping to tee, ft	6.8
16-in. and 14-in. piping (90%), ft	10.0
Reactor vessel inlet plenum, ft	13.5
Core, ft	~200.0
Hold-down mechanism, ft	27.7
30-in. piping, ft	1.1
Intermediate heat exchanger, ft	1.4
Total, ft	260.5
6-in. piping 10% flow throttle valve fully opened, ft	29.0
Inlet plenum to blanket, ft	13.5
Secondary sodium temperature, °F:	
Entering boiler	750
Leaving boiler	500

(*continued*)

Secondary sodium flow, lb/hr	13.2×10^6
Steam pressure, psia	600
Steam temperature, °F	740
Feedwater temperature, °F	340
Steam flow, lb/hr	9.6×10^5

*psi = (ft)(55/144).

CHAPTER 5

HEAVY-WATER POWER REACTORS*

5–1. Introduction

For neutron economy, heavy water is the best of all moderators. Practical reactors can be designed so that neutron absorption by heavy water is almost negligible. With so little absorption by the moderator, most D_2O reactors can tolerate reasonably large absorption by structural and fuel jacket materials and still have rather high neutron economy. Because of this, D_2O is a good moderator with any nuclear fuel cycle, and particularly with two specific fuel cycles: the natural uranium cycle, and the thorium-uranium cycle with very high conversion ratio. These two applications are emphasized in this chapter.

The moderating power ($\xi\Sigma_s$) of heavy water is not high, compared with that of H_2O for example. Hence, ratios of moderator volume to fuel volume in natural uranium, or slightly-enriched, D_2O reactors are generally large, and the D_2O volume needed for moderation is much larger than the required coolant volume. Thus, several coolants could possibly be used with D_2O moderation without losing too much in neutron economy. Often the structure and fuel jacketing characteristics imposed by the chosen coolant affect the neutron economy more than the neutron absorption of the coolant itself. Among the possible coolants are:

(1) *D_2O.* As a coolant, D_2O has the same advantage that it has as a moderator—a very low neutron absorption cross section. It also has the practical advantage of using the extensive technology developed for water-cooled reactors, but it has the disadvantage, common to aqueous coolants, of relatively low temperature limitations. Circulating high-pressure, hot D_2O to transport heat increases the D_2O investment and its rate of loss. D_2O-cooled reactors may employ either a large pressure vessel, or pressurized individual fuel-coolant tubes, a pressure-vessel reactor is described later in this chapter. A pressurized tube reactor similar to the plutonium recycle test reactor (Chapter 8) has been proposed to the AEC as a prototype power reactor [1]. The tube-type D_2O-cooled D_2O-moderated reactor is also being developed in Canada [2].

(2) *H_2O.* Ordinary water as coolant avoids circulating large volumes of D_2O. However, with D_2O and H_2O in the same reactor, D_2O loss and

*All figures in this chapter were furnished by the E. I. du Pont de Nemours and Company, except as noted.

contamination problems would be more serious. The higher neutron absorption by H_2O would increase the neutron losses. Severe design restrictions would be necessary to assure that a H_2O-cooled, D_2O-moderated reactor would not gain reactivity with loss of coolant. No reactors of this type are now being developed in the United States.

(3) *Gas.* With a gaseous coolant, a reactor can be designed to operate at high temperature Gases are available which, as coolants, have negligible neutron absorption; consequently, neutron economy does not suffer from their use. Some effort is necessary to attain high enough specific powers with gas-cooled D_2O reactors to keep the D_2O investment low. A reactor of this type is described in Chapter 6

(4) *Sodium* Liquid sodium has excellent thermal properties and reasonably low neutron absorption, but it is chemically incompatible with D_2O. A major problem is to ensure that the two liquids will always be kept separate, and to accomplish this without adding too much neutron-absorbing material to the reactor The AEC is supporting developmental work on this type of reactor by the Nuclear Development Corporation of America [3]. An early objective is to install a power plant of 10-Mw electrical output in Anchorage, Alaska, for the Chugach Electric Association, Inc

(5) *Organic liquids* With an organic liquid coolant, a D_2O-moderated reactor could be operated at higher temperature and lower pressure than with water cooling. Although an organic fluid could be used as both coolant and moderator, D_2O moderation gives better neutron economy and lower dissociation rate The D_2O-moderated reactor cooled by an organic, like that cooled by H_2O, may be troubled by a negative coolant-density coefficient of reactivity. It has seemed reasonable to defer this application of organic coolants until extensive results are available from the organic moderated reactor experiment (see Chapter 7)

(6) *Boiling D_2O* A special case of the D_2O-cooled and moderated reactor is the boiling D_2O reactor. This reactor type was described in 1955 [4]. The Experimental Boiling Water Reactor at Argonne National Laboratory is designed so it can be converted to use D_2O after the work with H_2O is completed [5] Design studies of uranium cores for this conversion are described in Reference 6. More recently, the attractive possibilities of employing the thorium-uranium fuel cycle in the D_2O boiler have been studied. This interest was stimulated by the good thermal performance of the Borax-IV reactor [7], which was fueled with a mixture of thorium and U^{235} dioxides jacketed with aluminum [8]. Nuclear properties of ThO_2-UO_2-D_2O systems are being studied experimentally [9]. The Laboratory now plans to use thoria-urania fuel elements when it converts the Experimental Boiling Water Reactor to D_2O operation.

The most extensive program in developing D_2O power reactors contemplates D_2O cooling and moderation with natural uranium fuel. An objective of the program is to develop design criteria for a large-scale (100-Mw electrical) plant. The program is being carried out for the AEC by the E. I. du Pont de Nemours Company. The project is expected to benefit on the one hand from high-temperature water technology developed for pressurized water reactors, and on the other hand from the specialized D_2O technology evolved in designing, constructing, and operating the production reactors at Savannah River

The first part of this chapter summarizes developmental work on the heavy-water power reactor. Since the main significance of D_2O as a reactor material is in the field of neutron physics, the latter part of the chapter briefly describes the reactor physics calculation methods adopted at the Savannah River Laboratory as a result of a large number of critical and exponential experiments on natural uranium lattices in D_2O. Finally, results of lattice measurements with thorium-uranium oxide in D_2O are summarized.

5–2. Design of a 100-Mw Electrical Power Plant Using Heavy Water as Reactor Moderator*

5–2.1 General considerations. Heavy water has special value because it can be used as a moderator for a natural uranium fueled reactor.

The chief advantages in using natural uranium are its availability and especially its lower cost. With natural uranium, not only is the cost low for the fuel burned, but also the value of the residual U^{235} in the spent fuel element is so low that its discard can be considered. On the other hand, a fuel element made from enriched uranium may still contain so much U^{235} that it cannot be discarded economically. Thus a power plant using partially or fully enriched uranium depends upon both a uranium enriching plant for new fuel elements, and a processing plant for recovering U^{235} from spent fuel. Shipping spent fuel elements to a recovery plant is usually expensive, especially where distances are great, and may have significant effect on over-all costs.

Natural uranium fuel, with a given fractional burnup of U^{235}, will generally produce more plutonium than will enriched fuel. A further advantage is that natural uranium can be fabricated and stored without criticality problems.

Before 1951 there was not in the world enough heavy water of high isotopic purity to moderate a large atomic power reactor. Since build-

*By Dale F. Babcock, E. I. du Pont de Nemours and Company.

ing and operation of the Savannah River Plant near Aiken, South Carolina, and the Dana Plant near Terre Haute, Indiana, heavy water has become readily available. The combined production capacity of these two plants is about 1000 tons/yr. Heavy water now can be purchased from the United States Atomic Energy Commission for $28 a pound. The D_2O content is approximately 99.85%; the remainder is H_2O.*

Whether or not to employ heavy water as the moderator of a power reactor will depend upon the cost of using it, in relation to benefits from its use. The investment charges for heavy water will, of course, depend on the annual fixed charge rate applied. For this calculation, the total charge against heavy water is taken as 15% per year, without attempting to break it down into components. If it is assumed that 130 tons of heavy water are required in operating a 100-Mw (electric) power plant, the annual charge against this investment will be

$$(130 \text{ tons})(2000 \text{ lb/ton})(\$28/\text{lb})(15\%/\text{yr}) = \$1.1 \times 10^6/\text{yr}.$$

If the electric plant operates at 75% of rated capacity, it will produce in one year 6.6×10^8 kwh; the charge against electric power because heavy water is used will be nearly 1.7 mills/kwh.

This cost may be offset by gains from heavy-water use. Here again a cost analysis is difficult because there are so many unknowns in the design and performance of nuclear power plants. However, a heavy-water moderated reactor fueled with natural uranium may be compared with a light-water moderated reactor using highly enriched uranium (90% U^{235}). The cost of the uranium burned in the enriched reactor is 3.1 mills/kwh, based upon $15/g of U^{235}, 1.25 g U^{235}/Mwd of fission energy, and 25% efficiency of converting fission energy to electricity. For the natural uranium reactor, the uranium burned costs 1.35 mills/kwh, at $18/lb of natural uranium, 4500 Mwd of fission energy from a ton of natural uranium, and 25% energy conversion. This cost calculation assumes that the spent fuel has no salvage value. The difference in cost of the two uranium fuels is 1.7 mills/kwh, which in this case exactly offsets the 15% charge against capital invested in heavy water.

There are other operating costs, equally difficult to estimate: for example, the cost of recovering uranium from spent fuel elements and reenriching it. This will probably cost at least 1 mill/kwh and possibly much more, depending upon the kind of fuel element used. For the natural uranium case, there would be costs of removing any light water that leaked into the heavy water and extra construction costs to prevent excessive loss of D_2O by leakage.

*This method of expressing the protium content of heavy water is used for convenience. Most of the protium in heavy water of this isotopic purity is in HDO and only a minor quantity is in H_2O.

This example is far from being a complete cost analysis, but it shows that heavy water can give benefits commensurate with the cost. Operating experience will be needed before costs can be estimated accurately enough for meaningful comparisons. Some of the unknowns are being evaluated for light-water reactors in the Pressurized Water Reactor at Shippingport, Pennsylvania, and in the Experimental Boiling Water Reactor at Argonne National Laboratory. Work is less advanced on heavy water reactors, but studies now under way may lead to building one or more heavy-water moderated, natural uranium fueled reactors.

5-2.2 Experience with D_2O at the Savannah River Plant. Using an expensive fluid such as heavy water in a power reactor raises many questions, such as the loss rate, hazards of handling, and dilution with light water. Fortunately, a partial answer to these questions can be obtained by reviewing the operation of the five large heavy-water reactors at the Savannah River Plant. These do not produce useful power, but they employ many of the same items (pumps, heat exchangers, and isotopic purification equipment) as a power reactor. Pressures and temperatures, however, are much lower; moderator pressure is approximately one atmosphere.

D_2O losses. Great care was taken in the design and construction at Savannah River to assure that losses of heavy water would not be great. Losses have averaged about 3% per year of the total inventory of heavy water in the reactor, heat exchangers, pumps, tanks, and other equipment. This rate has been surprisingly constant, differing little from one reactor to another. The smallest loss for a 6-month period for any reactor during 1956 and 1957 was at the rate of 2% per year. For a power reactor, loss rates may be higher because of the higher temperature and pressure, but the smaller number of valves, flanges, and stuffing boxes in a power reactor should be an offsetting factor.

The main heat exchangers at Savannah River were potential sources of leakage of large quantities of heavy water. All tubing was given a special pressure test before it was built into heat exchangers, and the heat exchangers were given many postfabrication tests. The exchangers were constructed with double tube sheets so that leakage of either D_2O or H_2O could be detected. So far, no leaks through the tube sheets have been found, but one or two tubes at the outside of tube bundles of several exchangers have vibrated and worn through at baffles, allowing major losses of heavy water. This example is not intended to prove that heat exchangers must leak; in fact, most of the heat exchangers at the Savannah River Plant have not leaked. It does show, however, that in spite of great care in design and fabrication, leaks may develop and instruments must be provided to detect them.

Mechanical seals are used on all pumps at Savannah River, and the small D_2O leakage through these seals is piped to a recovery system Operation of the mechanical seals and recovery system has been so successful that it should encourage their use on a power reactor, even though the higher temperatures and pressures might require further design and development Hermetically sealed pumps with canned rotors on the electric motor drives probably would not give benefits enough to justify the added cost.

Radiation-induced decomposition of D_2O. Decomposition of D_2O by radiation has not been a major problem at Savannah River, nor is it expected to be in a full-scale power plant. The heavy water in the Savannah River reactors is maintained at a high chemical purity by passing it through resin bed deionizers that increase its resistance to above 1 megohm/cm.

Tritium hazard. Enough tritium will be produced in the moderator to be hazardous to maintenance and operating personnel unless special precautions are taken With tritium content less than about 3×10^{-4} $\mu c/cm^3$ of air (as a result of a moderator leak or intentional opening of the D_2O system) the only special precaution at Savannah River has been to limit the time of exposure. For larger concentrations, air-supplied masks, rubber gloves, and rubber boots, or even air-supplied plastic suits have been required. Tritium concentrations greater than 10^{-1} $\mu c/cm^3$ have been found near a reactor just after discharge of fuel and after major spills. Similar concentrations could be expected near a power reactor, particularly after operation for a number of years, should a major leak occur.

Dilution of D_2O by H_2O. Maintaining heavy water at an isotopic purity of about 99.75 mol % requires vigilance, but it can be done and is being done at Savannah River. In a power reactor complex, light water will enter the D_2O system and provision must be made to remove it. The amount of H_2O entering the system will depend on the plant design and the carefulness of the operators. These generalities, however, are of little help to the designer, who must provide for reconcentration before he knows the rate at which H_2O must be removed. An entry rate of 2 lb/day of light water may reasonably be expected for a large power reactor. In some of the plutonium reactors, the rate is three or four times this, but portions of these reactor systems are often exposed to the air, at a higher pressure than the D_2O in the heat exchangers. These factors contribute to higher intake of light water. The cost of removing light water can be estimated from this relationship: 1000 lb/hr of steam in a well-designed vacuum distilling tower will remove 1 lb of H_2O per day from a 99.75 mol % D_2O liquid, as a 75 mol % D-25 mol % H mixture. It is not absolutely required that the moderator be maintained at this purity. If

only 99.5 mol % deuterium is maintained, the size of the purification equipment and the amount of steam can be halved (or the entry rate of light water can be doubled). The loss in nuclear reactivity from this extra light water content may, however, completely overbalance the savings in isotopic purification equipment. The loss in the nuclear reactivity is 1.5 to 3.0% for each mol % increase in H_2O.

Light water is separated from the heavy water of the Savannah River reactors by distilling at low pressure. This method requires several times as much energy for a given separation as does the dual-temperature process using hydrogen sulfide as the entraining agent [10]. On the other hand, ease of control, freedom from contamination, and ready availability of low pressure steam at an atomic power plant tend to make distillation more attractive. At Savannah River, two nearly identical distillation towers, each containing 90 actual plates, are used. Heavy water at about 99.75 mol % D_2O is fed onto the bottom plate of the first tower, and water at a slightly higher deuterium concentration is returned to the reactor from the calandria The vapor at the top of the first tower is condensed, pumped through a vaporizer, and fed into the base of the second tower. (A vapor compressor could be used for this service; then no steam would be required to vaporize the feed to the second tower, and total steam consumption would be halved.) Liquid from the base of the second tower is pumped into the top of the first. A reflux condenser and product drawoff complete the system. Pressure at the condenser of each tower is 80 mm of mercury, absolute. This unit rejects D_2O of about 75 to 80 mol % purity when the feed is 99.75 mol % D_2O.

At Savannah River, the slightly dilute heavy water is collected from the several purification systems and is further processed at a central plant. Whether this procedure would be followed at an atomic power plant or whether further processing would be done at the site would depend on relative convenience and costs. In either case, the steam required to further concentrate the light water enough so it could be discarded would be less than 100 lb/hr.

5–2.3 Design of the 100-Mw (electrical) reactor. The basic criteria guiding the present design study of heavy-water moderated power reactors are:

(1) The reactor should be capable of producing 100 Mw of electric power.

(2) The power reactor plant should be based on designs that require no more development work than could be accomplished on a schedule allowing completion of the plant by mid-1962.

(3) The fuel must be uranium containing not more than the natural abundance (0.71%) of U^{235}.

(4) The moderator and coolant must be heavy water.

The fuel element. Perhaps the most critical item in the design and operation of a power reactor is the fuel element. In selecting components of this element and its accessories, care must be taken that the excess nuclear reactivity will not be seriously impaired. The reactivity criteria do not allow use of stainless steel, molybdenum alloys, and other metals of moderate neutron cross section. Zircaloy-2 probably has the best properties, over-all, both for cladding the fuel and for housings to define the coolant passages. Zirconium is a close competitor but its lower strength and lower resistance to hot-water corrosion are objectionable. Aluminum and its alloys were not selected because it is difficult to use these materials for cladding uranium and because they do not resist corrosion as well as does Zircaloy-2.

Uranium metal was selected rather than uranium oxide for the initial development work largely because there was more experience in fabricating it. Metal is better for nuclear reactivity, but with some sacrifice in reactivity an operable oxide element could be designed. Experience at Savannah River shows that distortion of uranium metal by radiation damage might be acceptably small. Tests must be made with full-scale fuel elements under conditions approximating those expected in a power reactor before uranium metal can be accepted as a fuel material. Tests described below give only a partial answer.

A tube about 2 inches OD by 1½ inches ID by 15 ft long was selected as the preferred fuel-element shape (Fig. 5–1). This element would be clad outside and inside with Zircaloy-2 (or zirconium) by coextrusion, using a technique similar to that developed by Nuclear Metals, Inc. [11]. If Zircaloy-2 is chosen as the cladding material, the uranium core should be alloyed with about 2% zirconium to match the extrusion characteristics of the cladding. Addition of 2% zirconium to uranium reduces the corrosion rate in water at 275°C by two-thirds. A Zircaloy-2 housing tube, about 3 inches in diameter, would define the coolant passage.

A significant feature of this fuel element is the large mass of uranium that it contains (approximately 175 lb). The design was selected because it should be cheaper to manufacture a few massive elements than many small ones, and inspection and handling should be less troublesome. An objection to a large mass of uranium in a single element is that sheath failure could release so much uranium oxide and fission products that major decontamination would be required.

Experiments were made as a basis for judging how much uranium could be corroded from an element. Small holes bored through the cladding of test pieces of Zircaloy-2 clad uranium rod (about 0.3-inch OD) exposed the uranium to water at 225°C. Results are shown in the photographs of Fig. 5–2. Also shown are results of similar tests with rods of uranium-2 w/o zirconium clad with Zircaloy-2. These tests indicate that at 225°C, water attacks the 2% zirconium alloy more slowly than it at-

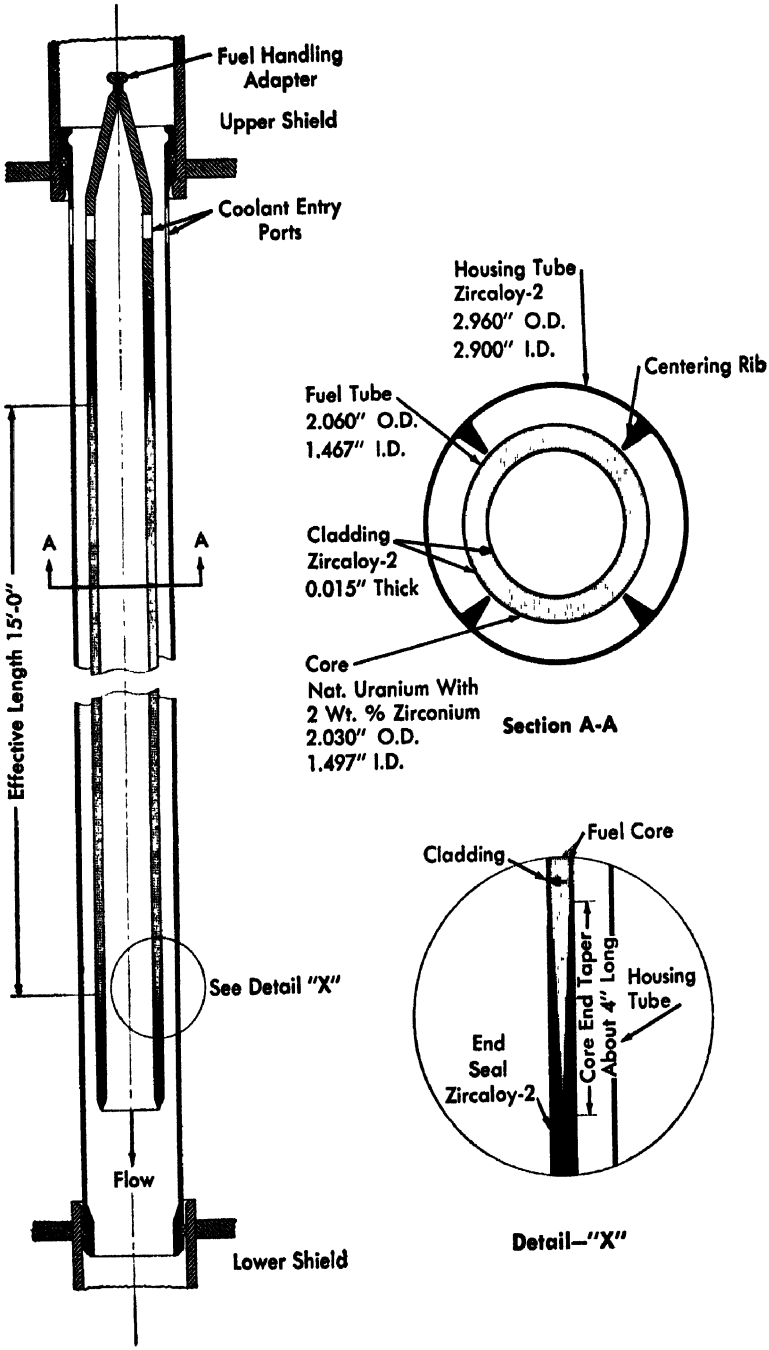

FIG 5–1. Fuel-element and housing tube.

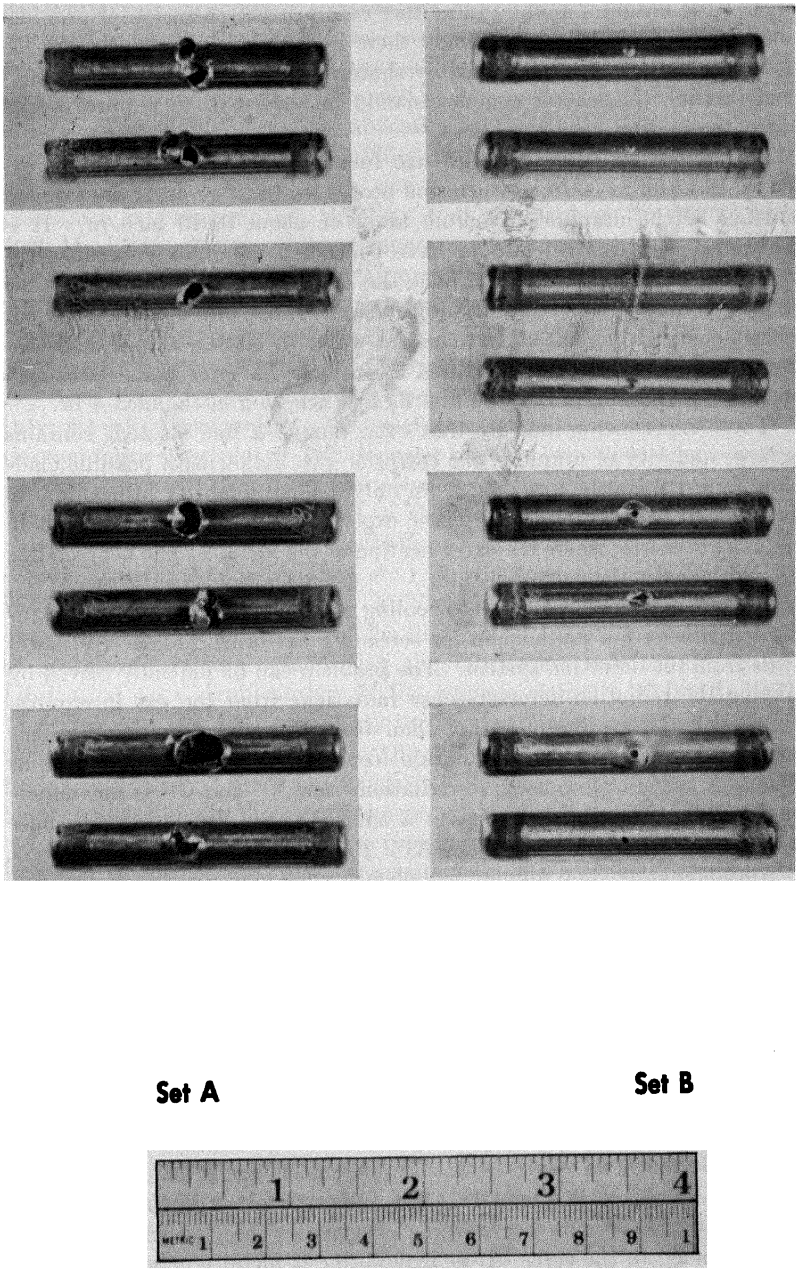

FIG. 5–2 Effect of water at 225°C on Zircaloy-2 clad fuel samples that were purposely defected.

tacks pure uranium metal. In neither case was the corrosion of uranium more than about 10 g/hr. Should there be a failure when the corrosion rate reaches this value, followed by shutdown, the spread of active material through the reactor complex should be too small to require special decontamination.

In another experiment, a full-size fuel tube was cut in two and exposed in water at 300°C. Corrosion proceeded back through the exposed surface of the uranium-zirconium alloy at about 0.040 inch/hr. It is presumed that this rate would have continued indefinitely because the corrosion products did not tear back the Zircolay cladding to increase the exposure area. However, uranium release rates are not constant for specimens with pinholes. In a test in water at 300°C, a fuel tube—intentionally made defective with a 0.040-inch diameter hole, 0.040-inch deep—released only 5 g in the first 3½ hr, then 25 g in the next 4 hr.

These experiments indicate that even though a fuel element contains a large quantity of uranium, the corrosion rate following a possible cladding failure might be low enough for only a small quantity of uranium to be released before detection. These experiments were not carried out in a nuclear reactor, where the extra heating of the metal by the neutron flux should increase the corrosion rate.

Escape of fission products into cooling water might be discovered readily if there were a mechanism for screening out other radioactive materials from the detection system. The problem can be partially solved by having the radiation detector sense radiations from the gas in equilibrium with the moderator rather than from the moderator itself. This method screens out intense radiation from such nonvolatile materials as Na^{24}. A time delay is used, so radiation from N^{16} and O^{19} is not important. This type of detector gives a spurious signal at startup because of the activation of air, producing A^{41}. Purging is a possible remedy.

Approximately fifty tubular fuel elements have been made of the general type described above, ranging in outside diameter from 2 inches up to about 3 inches Several were exposed in a high neutron flux (one to more than 5000 Mwd/tonU) with no apparent change in length and less than 0.4% increase in diameter. No bulges or other distortions were seen on the surface, nor was warping observed. The cladding remained tightly bonded to the core. After irradiation at metal temperatures and bulk water temperatures considerably below those desired for power reactors, this element was heated to 450°C. The only observable change was a further increase in the outside diameter of the tube to a total of 0 6%. This type of fuel element has not yet been irradiated in high-temperature water (above 200°C).

This fuel element is designed to operate in a power reactor with coolant flowing at 225 gpm through the assembly and maximum heat flux of

235 watts/cm². Maximum temperature at the center of the element is expected to be less than 550°C, and at the surface, about 300°C. In experiments at Savannah River, uranium withstood this maximum temperature for long periods with only moderate deformation (less than 0.5%) Above 700°C, cracks appeared in the metal. In some cases cracks were so large that the cladding broke and water reached the uranium, producing rapid corrosion and liberating fission products. The maximum exposure of test elements that operated up to 550°C was 2000 Mwd/ton. For the higher temperature test, the exposure was about one-third this Temperature of the uranium near the surface was below 200°C. The effect of raising surface temperature to 300°C is not known.

Only about 340 fuel assemblies of the type described would be required for a power reactor of 100-Mw (electric) capacity. The cost of producing these large fuel elements has been given much consideration, but there are still uncertainties. The chief question is the production rate of the fuel fabricating plant If five power reactors were operating, each of 100-Mw capacity, then 2500 fuel elements would be required per year At this production rate, the cost of the zirconium (or Zircaloy-2) plus the entire cost of fabrication, including the recycling of uranium and zirconium scrap (machine turnings, etc.), should be less than $7/lb of uranium contained in the element. At the AEC price of $18 a pound for uranium metal, the entire cost of the fuel element should be about $25/lb of contained uranium Increasing the fabrication rate should reduce fabrication costs significantly. If the average exposure of fuel is 3500 Mwd/ton and the efficiency of converting heat into electricity is 23%, then the cost of the fuel would be 2.6 mills/kwh, assuming that the spent fuel elements would have no salvage value Any value for the uranium and the plutonium in the spent element will reduce this cost.

Exposure of fuel elements of the type described almost certainly can be increased above the 3500 Mwd/ton assumed. If a few new fuel elements are charged into the reactor at frequent intervals and the elements that remain in the reactor are rearranged to best advantage, 5000 Mwd/ton might be achieved. W. B Lewis [12] has calculated that with highly efficient positioning of the fuel in a D_2O-moderated reactor of Canadian design, burnup might reach 10,000 Mwd/ton. With these higher burnups there would be proportionate reductions in fuel cost.

Control. The problem of controlling a heavy-water moderated reactor is almost as important as the fuel-element problem. A control system design for a natural uranium fueled, heavy-water moderated power reactor has been based on the following precepts:

(1) Control rods must be able to reduce the effective multiplication of the reactors (k_{eff}) to some value below unity (about 0.95). at any time in the reactor operating cycle.

(2) The number of control rod locations in the lattice and of rods in each location should be kept small to minimize the omission of fuel elements from the lattice and to minimize the number and complexity of drive linkages.

(3) If the reactor lattice is in a pressure vessel (rather than having a pressure tube around each fuel element) entry ports for the control rods should not be so large (nor crowd the surrounding fuel ports so much) that the cost of fabricating the pressure vessel head will be excessive. Thus the size of rod or rod cluster at each control location is limited.

(4) Each control element should be as simple as it can reasonably be, while serving its function.

(5) The rods must be designed and the control locations spaced to control axial and radial distributions of neutron flux, so that the maximum heat flux and uranium temperature will be as low as possible.

(6) The rods must have a long lifetime against burnout of neutron-absorbing atoms so that frequent replacement of rods will not be necessary.

In designing the control-rod system, control locations are distributed uniformly throughout a "controlled region" whose radius is taken equal to the maximum radius to which the radial flux distribution can be flattened. This is calculated from the extrapolated radius of the reactor and the maximum buckling that the lattice can achieve in its lifetime Enough control locations are placed in the controlled region to enable reduction of the effective multiplication (k_{eff}) from its highest possible value to about 0.95, by placing at each location a rod or cluster of rods no larger than required by precept (3) above.

The lattice buckling will decrease substantially when the reactor is taken to full power. Shortly after startup, therefore, control rods can be withdrawn from some of the outer control locations. These locations will always be vacant during xenon-equilibrium, full-power operation; therefore, rods in these outer locations should simply be large, single, and strongly absorbing (i.e., cadmium), in accordance with precept (4) above These will be called shim rods. The remaining control locations must afford sufficiently refined control to permit optimizing axial and radial flux distributions while compensating for the long-term reactivity change of the lattice. This function cannot be served adequately by a single rod in each control position. Instead, each position must contain a cluster of several rods, the number and features of which depend on several factors —buckling of the hot, poisoned lattice, useful lifetime desired for the rods, control strength required of the whole cluster, and allowable mechanical complexity of the drive linkages.

For best axial flux shaping, as much as possible of the control should be in partial-length vertical rods, nearly centered axially in the core. The size of the rods is determined by the range of buckling values that

the lattice assumes throughout its lifetime. In accordance with precept (6) above, the partial-length rods, and any other rods to be inserted in the reactor during much of its full-power operating time, should have a high concentration of neutron-absorbing atoms per unit length of rod ($\sim 10^{23}$/cm) to avoid frequent rod replacement. The cross section of the neutron-absorbing atoms must be large enough that rods within the limits imposed by precept (3) will produce the buckling changes required of them.

By way of illustration a control system is described for a natural uranium fueled, heavy-water moderated power reactor with a core 458 cm high and 153 cm in radius surrounded entirely by a heavy-water reflector 30 cm thick. The lattice is composed of tubular fuel elements in a 16 5-cm triangular array, contained in a pressure vessel. Moderator temperature is about 210°C at full power. Table 5–1 shows lattice bucklings at various stages of reactor operation (used as bases for designing the control system), dimensions of the radial and axial flattened regions that can be achieved, ideally, at two stages of full-power operation, and corresponding ideal values of the gross ratio of maximum-to-average flux in the reactor.

The control system occupies 19 lattice positions (taking the place of 19 fuel elements), spaced 49.5 cm in a triangular array, including the central lattice point in the reactor. In each of the outer 12 locations there is a cadmium-sheathed shim rod 8 9 cm in diameter. The seven central

TABLE 5–1

LATTICE BUCKLINGS AND FLUX SHAPE PARAMETERS

Power, Mw	Xenon	Exposure, Mwd/ton	Lattice buckling, $cm^{-2} \times 10^6$	Radial flat zone, maximum radius, cm	Axial flat zone, maximum height, cm	Maximum to average flux ratio in core
0	None	0	703	111		
460	None	0	369	74		
460	Equilibrium	0	250	27	119	1.7*
460	Equilibrium	1000	344	69	259	1.3*
0	None	1000	755	114		
460	None	1000	469	90		

*If the control rods were uniformly distributed throughout the reactor, rather than placed judiciously to shape the flux, the maximum to average flux ratio in the core would be about 2.4.

"control" locations each contain four rods: a full-length (3-cm diameter × 457 cm) cadmium rod, a full-length (3 cm diameter × 457 cm) stainless steel rod, and two partial-length stainless steel rods (180 cm × 2.2 cm diameter). The effectiveness of each rod and cluster of rods specified here has been established by measurements in the exponential facility at the Savannah River Laboratory.

Table 5–1 shows that lattice bucklings during normal full-power operation will vary from 250×10^{-6} cm^{-2} up to 344×10^{-6} cm^{-2}, permitting, ideally, maximum-to-average flux ratios of from 1.7 to 1.3 to be achieved. These ratios represent important reductions in maximum heat flux and uranium temperatures from those that would be obtained if no provisions were made for shaping the axial and radial flux distributions (Table 5–1). The control system described here will permit a close approach to these ideal values. The partial-length stainless steel rods in the reactor are expected to last at least four years; all other rods will have a much longer life.

Control systems for other types of natural uranium fueled, heavy-water moderated power reactors (i.e., D_2O-cooled with cold D_2O moderator, or gas-cooled with cold D_2O moderator) would not differ greatly from the one described here The number and spacing of the control locations and the diameter of the shim rods, dictated by engineering considerations and by cold, clean buckling, would be about the same. The number and sizes of the rods in the "control" clusters, determined by lattice buckling at full power, would probably be different

From the reactor physics standpoint, the safety rod system is simpler to design than the control rod system. The safety rod system is required to reduce the effective multiplication (k_{eff}) by about 2%. To avoid displacing fuel elements, the safety rods should be placed between fuel positions in the lattice. Safety rod locations should be distributed fairly uniformly throughout the lattice, although strict uniformity is not necessary.

The safety rod system for the reactor discussed above consists of 19 cadmium rods, 2.54 cm in diameter and about 58 cm apart in an approximately triangular array The safety rod system for other natural uranium fueled, heavy-water moderated power reactors would probably be similar.

Basic reactor arrangement. Engineering studies were made of four different reactor types. Each would be fueled with the tubular element described above. Important characteristics of these reactors are given below and in more detail in Table 5–2 (see pages 468–471). Figure 5–3 shows the basic design of a pressure shell or vessel reactor (reactor A) and Fig. 5–4 shows a pressure tube reactor (reactor D). These reactors are described in greater detail in Atomic Energy Commission Research and

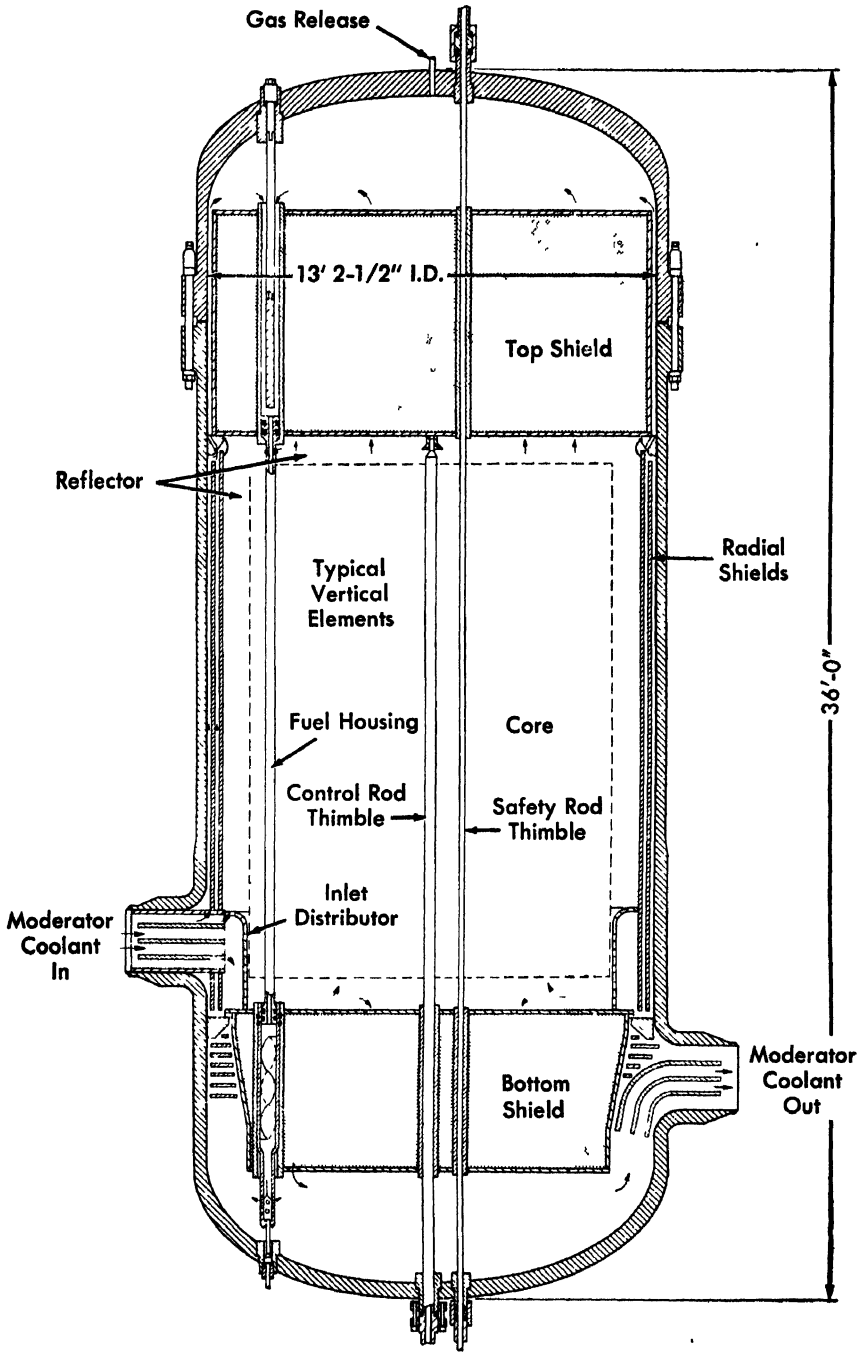

Fig. 5–3 Basic arrangement of pressure-vessel type reactor, case A.

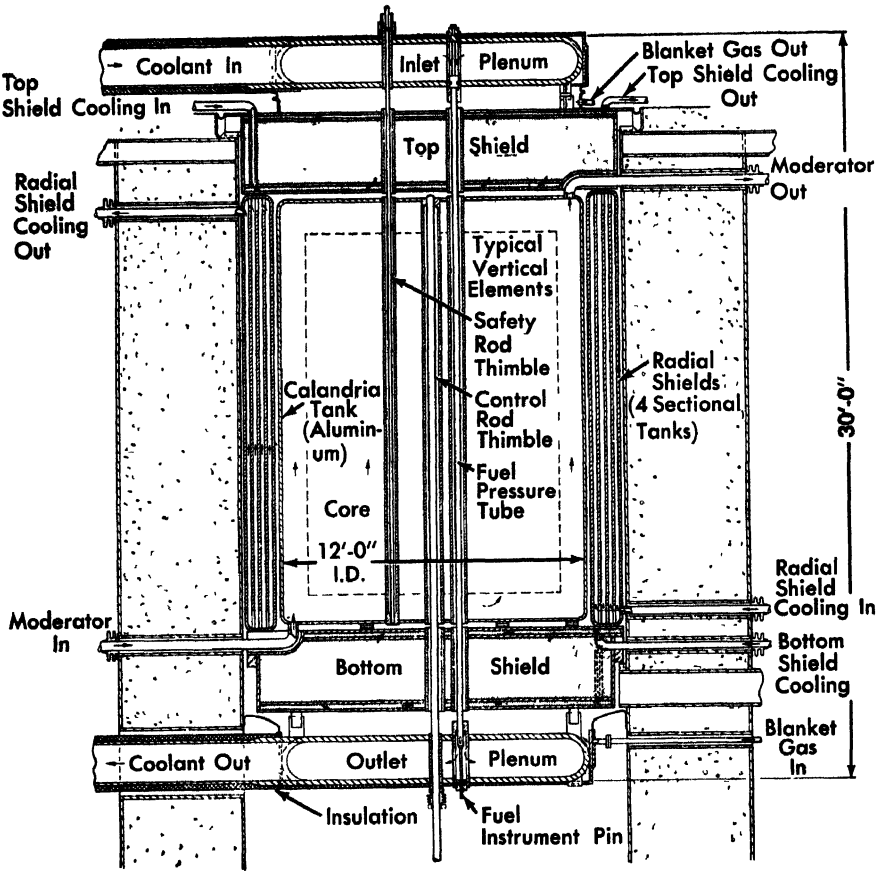

FIG. 5–4. Basic arrangement of pressure-tube type reactor, case D

Development Reports [13–16]. All would operate at a pressure of about 700 lb/in^2 and produce 100 Mw (net) of electric power. The core of each reactor would be a right cylinder about 10 ft in diameter and 15 ft long.

Reactor study case	*A*	*B*	*C*	*D*
Reactor type	Pressure vessel	Pressure vessel	Pressure vessel	Pressure tube
Type of housing tube around fuel element	Thin wall Zr	None	Thin wall Zr	Heavy wall Zr
Tube housing insulation	None	None	D_2O	MgO
Lattice spacing, inches	6 5	6 5	6.5	7 8
Number of fuel elements	340	310	310	225
Moderator temperature, °C	207	213	60	60

Reactor A has fewest uncertainties to be solved by further study or development Omission of housing tubes around the fuel elements in reactor B distinguishes it from reactor A. Elimination of the housing tube should allow much more distortion of fuel elements before it becomes difficult to remove them. On the other hand, detection of fuel-element failure would be more difficult, particularly if failure occurred only in the cladding on the outside of the tube Experiments with an electrically heated mockup of a fuel element without a housing tube showed that heat transfer from the outside surface of the tube to slowly flowing moderator should be adequate to prevent film burnout of the elements, even with power output 50% above the design value.

The design temperature for the moderator of both reactors A and B would be above 200°C. The chief disadvantage of this high temperature is its adverse effect on reactivity. Low moderator temperatures (about 60°C) should be attained in reactor C by separating the fuel coolant stream from the moderator. Insulation of the fuel housing tubes would be required to reduce heat loss to the moderator Gamma-ray heating of the moderator would not be avoided by insulation and would therefore result in degrading 7% of the total energy to temperatures not useful in power production.

A pressure shell (weighing approximately 150 tons) would be employed with reactors A, B, and C to withstand the 700-psi pressure required to keep the heavy water in the liquid state Reactor D would use a pressure-tube construction with only the fuel element and coolant at high pressure The moderator would be in a separate system at nearly atmospheric pressure. This would allow the moderator temperature to be low, but the gain in reactivity would be largely offset by the use of heavy-walled zirconium pressure tubes The chief advantage of reactor D lies in the fact that it can be constructed in pieces small enough for easier shipment to the construction site. Furthermore, new techniques would not need to be developed for fabricating larger pressure shells. Pressure tube reactor designs developed thus far have not been considered entirely adequate primarily because of shortcomings in methods for joining the zirconium pressure tubes to the header system. Major development and testing might be required before an acceptable pressure tube reactor could be constructed. On the other hand, techniques for building a pressure shell reactor are thought to require only minor development.

The operating temperature and pressure selected for the heavy water as coolant for the reactors described above are lower than for most nuclear power plants. In reactors A and B, a low operating temperature is required because reactivity is rapidly lost as moderator temperature is raised above 200°C. This is a consequence of the rapid reduction in

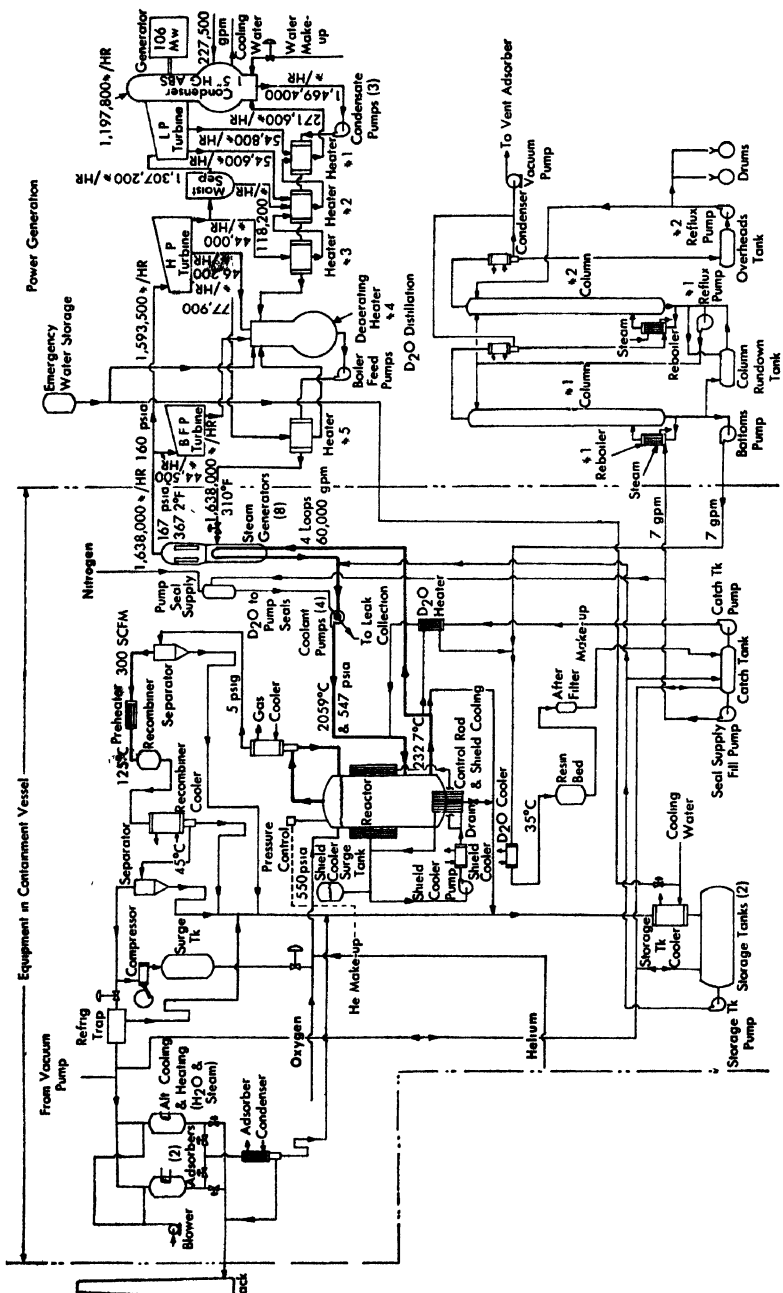

FIG 5-5 Flow diagram of reactor coolant and steam systems

moderator density. Reactors C and D do not have such high coolant temperature coefficients of reactivity because coolant temperature changes do not affect the moderator. If superheat were used, the optimum design temperature for the coolant of reactors C and D would be higher than for reactors A and B. Without superheat, there is less incentive to use a higher liquid temperature, because only small savings can be made in the cost of turbogenerating equipment as the pressure of the saturated steam is raised.

Mechanical design. In this section, some proposed mechanical aspects of reactor A and its auxiliary equipment are described (Figs. 5–3 and 5–5).

Reactor vessel. The reactor is shown schematically in Fig. 5-3. The cylindrical pressure vessel is of carbon steel, clad inside with type-304 stainless steel. The top and bottom of the vessel are closed by ellipsoidal dished heads. A bolted flange makes the top head removable. The modest design pressure requires vessel walls only 3 to 3½ inches thick, except in areas where reinforcement is needed. The heads must be 6 to 8 inches thick to compensate for the numerous penetrations.

Reactor shielding. Besides the radial thermal shields, the reactor has heavy shields above and below the core. These provide thermal protection for the vessel heads and, when the reactor is shut down, serve as biological shields for access to the top and bottom heads and to the equipment mounted on them. Each shield is approximately 3 ft deep, overall, and the bulk composition is one-half stainless steel and one-half water. Structural rigidity is provided by tubes welded at each end to a plate. Interstices are filled with Raschig rings or other particulate forms of stainless steel.

The shield tubes, arranged in an equilateral triangular pattern on a 6½-inch spacing, define the fuel positions in the reactor core. The top shield serves as the support grid for the fuel assemblies. These assemblies consist of fuel tubes centered inside Zircaloy housing tubes which define the coolant passages around the fuel. The tubes of the bottom shield engage with the lower end of the fuel housing tubes and conduct coolant into the plenum between the shield and the bottom head of the reactor vessel. Spiral muffs in the tubes of top and bottom shields permit water flow but prevent radiation leakage.

Shielding outside the reactor consists of concrete thick enough to prevent induction of radioactivity in surrounding facilities, and to permit human access to these facilities, at least during reactor shutdown.

Reactor hydraulics. Heavy water enters the reactor through four nozzles in the vessel wall immediately above the bottom shield. In passing upward through the core, the water surrounds the fuel housing tubes and functions as the moderator. Water enters the housing tubes through slots below the top shield and flows downward through the centers of the

fuel tube at 18 fps. The flow rate outside the tubes is 12 fps. Judicious sizing of the coolant entry slots at the top of the housing tubes provides a pressure gradient that drives a small fraction of the coolant through the top shield interstices to cool the shield. This detoured coolant rejoins the main coolant stream via the top shield tubes. The bottom shield is cooled by a small orificed flow, promoted by the difference in pressure between the coolant entering and leaving the reactor. This differential amounts to 10 to 15 psi.

Controls. The nuclear control system, as tentatively defined, consists of seven 4-rod clusters grouped near the center of the core and twelve shim rods forming a circle outside the clusters. The control clusters, each consisting of one full-length cadmium rod, one full-length stainless steel rod and two partial-length stainless rods, permit adjusting the axial and radial flux distributions and compensate for long-term reactivity changes of the lattice as discussed earlier in this section. The shim rods, as noted before, are principally to compensate for the large reactivity loss associated with startup and moderator heating

Safety shutdown is achieved by a set of 19 safety rods. These are physically and mechanically distinct from the control rods to minimize the chance of simultaneous inoperability.

Fuel handling. There are access openings in the top head, aligned with the fuel positions in the core. Removing a small plug from each fuel port in the vessel head is preferable to removing the entire head of a vessel more than 13 ft in diameter. The head will be removed only to repair or replace housing tubes or other internal parts too large to be removed through the fuel ports. Serious study is being given to the alternative of providing ports large enough to permit all foreseeable maintenance, so that the head need not be removable. However, reinforcing such large openings may require head thicknesses greater than are practical to fabricate.

A mobile cask suspended on an overhead crane transfers spent fuel from the reactor to a hatchway leading to the cooling basin. The same cask serves in charging fresh fuel. Fuel may be replaced once or twice a year, depending on experience.

Instrumentation. The reference plant, a prototype, is provided with more instrumentation than will probably be needed for later units of the same type. Facilities are provided for measuring temperature and flow, and activity level of the coolant leaving each fuel tube. Pins fixed in the bottom head engage orificed extension sleeves projecting downward from the tubes of the bottom shield. Coolant from each fuel tube passes through the shield tube, then through the extension sleeve and into the bottom head of the reactor through orifices in the lower wall of the extension sleeve. The upstream pressure at the orifices, indicative of the

flow, is conveyed to exterior instrumentation by a small tube in the fixed instrument pin. This tube provides a coolant sample for activity monitoring, and coolant temperature is measured by a thermocouple housed in the pin.

Nuclear instrumentation for the reactor is conventional, measuring neutron flux for startup and full-power operation Internal instruments are included for measuring axial and radial flux distribution in the core.

Primary cooling system. The primary cooling system consists of four parallel circuits, each containing two steam generators. a centrifugal pump, and the connecting piping and valves. Stainless or stainless-clad steel is used for all parts in contact with the coolant stream. In each circuit hot D_2O from the reactor flows first through the steam generators, then is pumped back to the reactor inlet. Valves in the 16-inch conduits allow the pump and steam generators to be isolated from the reactor.

On the basis of preliminary investigation, conventional centrifugal pumps are specified for the 15,000-gpm, 60-psi duty Leakage from the mechanical seals on the pump shafts will be collected and recovered. Should primary power fail, flywheels on the pump shafts assure gradual slowing down of the pump to standby speed while reactor power is falling Planning of the standby power system for the pumps has not been completed.

The two vertical-shell steam generators in each coolant circuit are in parallel. Primary D_2O flows through the U-tube bundle at the base of the unit. Steam generated in the water surrounding the bundle is dried as it passes through separating baffles above the water level and goes to the turbine

Reactor auxiliary systems Auxiliary systems include the reactor pressurizing system, the facilities for accommodating D_2O volume changes in the primary system, and the D_2O purification facilities Inert gas (helium) rather than vapor pressurization was chosen for the reference design. The need to recombine and recover dissociated D_2O gases is an important factor in this choice A gas blanket in the top of the reactor (not shown in Fig. 5–3) will displace an expensive volume of D_2O, an additional advantage of inert gas pressurizing. Equipment includes bulk helium storage, compressors, pressurized helium storage, and control valves. Recovery of deuterium gas from the helium blanket requires a cooler, moisture separator, preheater, catalytic recombiner, after-cooler, moisture separator, and a return pump and compressor. A purge stream from the recombining cycle is passed through absorbers to recover D_2O and is vented to a stack. Tritium in the purge stream is diluted safely for disposal by discharging ventilation fans into the same stack.

Ionic purity of the D_2O is maintained by withdrawing a stream from the primary cooling circuits and passing it through a cooler, a mixed-resin

deionizer, and a filter. Most of the purified stream is returned immediately to the reactor system by a catch tank, pump, and preheater. A small portion of cool deionized D_2O is pumped to a head tank as source of sealing fluid for the primary coolant pump seals. The remainder of the D_2O from the deionizer is fed to a distillation train which removes H_2O to keep the D_2O content of the system at 99.75 mol %. Bottoms from the carbon steel distillation train are returned to the deionizer feed line. The overhead product, approximately 80 mol % D_2O, is returned to a D_2O production facility for reprocessing

Power generating cycle A simplified diagram of the steam cycle is included in Fig. 5–5. Approximately 1,600,000 lb/hr of 150-psia saturated steam are required for a gross electrical output of 106 Mw. A single turbogenerator is assumed The turbine is tentatively specified as an 1800-rpm, tandem compound, double-flow unit with 43-inch final stage blades. Interstage moisture separation is required. Five stages of feedwater heating are indicated in Fig. 5–5, but this and other features in the cycle may be changed in the final design.

Equipment arrangement and buildings. A conceptual layout of plant facilities and equipment is shown in Figs. 5–6 through 5–10. The reactor vessel shown here differs somewhat from that described but arrangement considerations are similar.

A spherical rather than cylindrical container was selected for the reactor building because the spherical shape seemed best suited for the desired equipment arrangement. The size of the container is determined by layout considerations rather than by containment volume and pressure requirements Preliminary analysis shows that the 180-ft sphere walls should be at least 3/4-inch thick (in A201GrB Steel) for stability under outside loading. This appears adequate to contain the maximum credible accident of the reactor system

The sphere houses the reactor, the primary cooling system and the auxiliary systems except for the D_2O distillation train and drain tanks, which

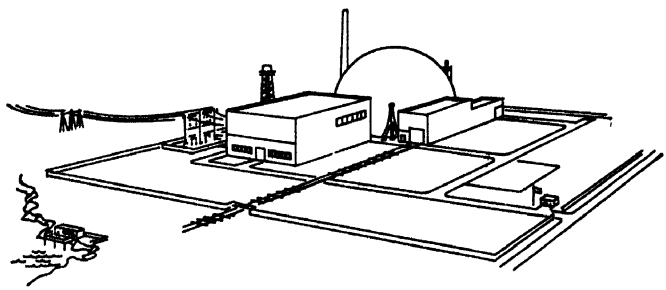

FIG. 5–6. Artist's conception of the heavy-water moderated power reactor.

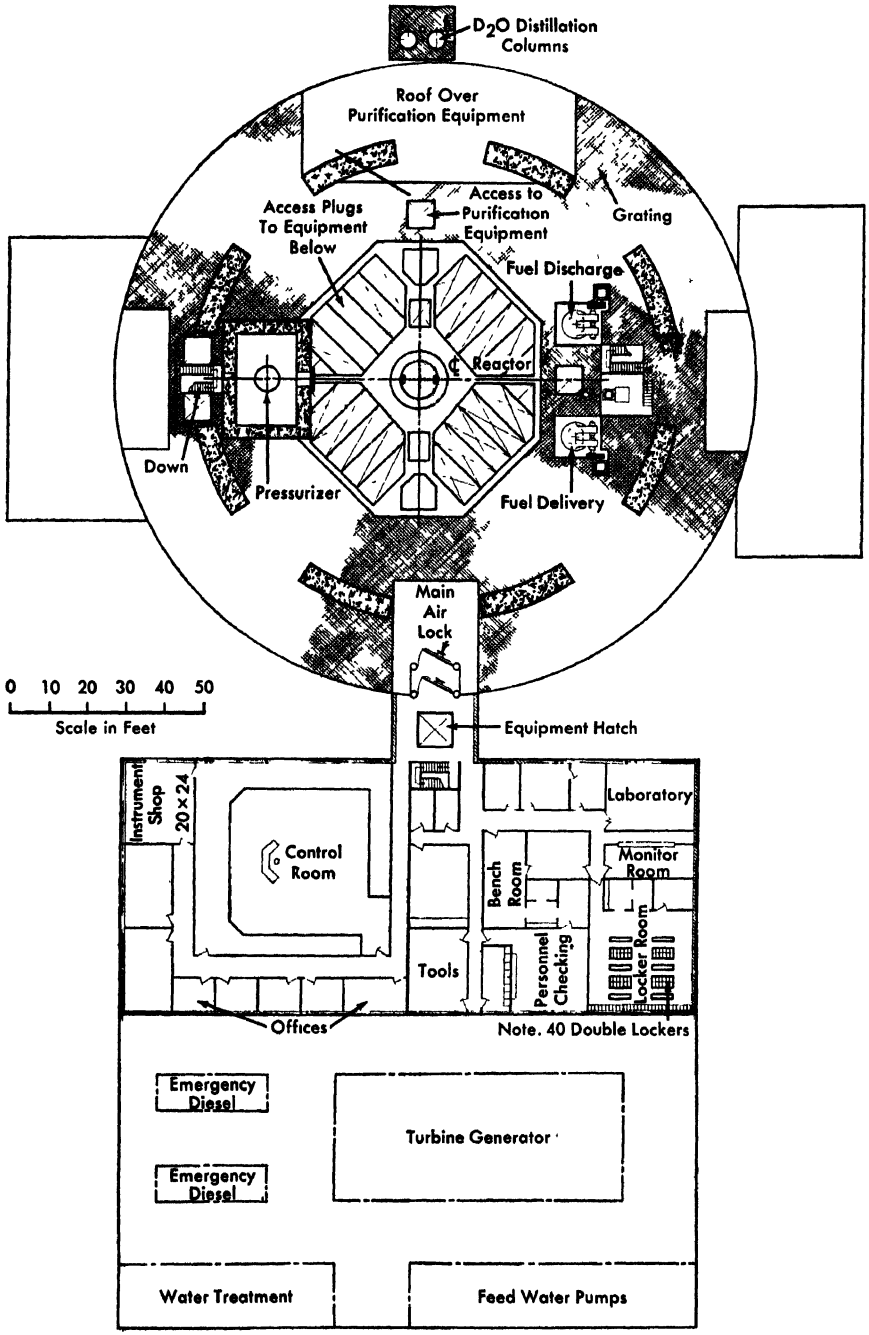

FIG. 5–7. Plan view of reactor and turbine-generator buildings at elevation +45 feet.

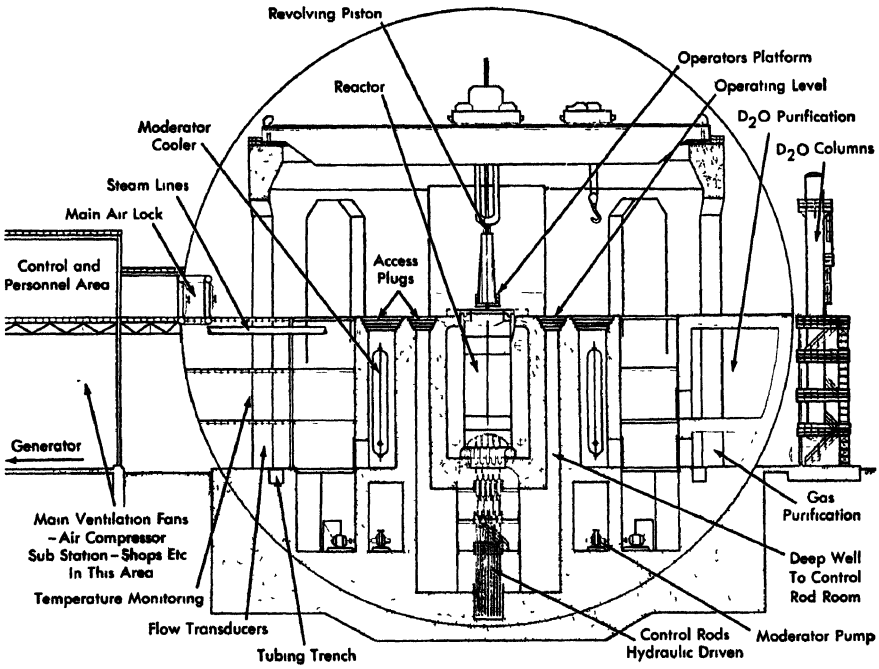

FIG. 5–8 Cross section of reactor building, looking north.

are outside adjacent to the sphere. The lowest point of the sphere is 45 ft below grade. The four coolant loops are segregated by shielding, in separate compartments. Thus, an idle loop can be inspected and maintained while the other three are in operation. The need for such segregation is being studied further. A revolving 120-ton bridge crane above the reactor has a maintenance trolley and a fuel cask trolley.

Personnel enter the sphere through an air lock at the principal operating level, 45 ft above grade. Small equipment, such as pumps, motors, and valves are taken through the personnel air lock with the reactor in operation. Larger equipment, such as steam generators, passes through a large bolted and seal-welded access door at the 45-ft level, with the reactor shut down. At least one air lock will provide emergency exit at a lower level.

The turbogenerator building, Fig. 5–7, is a steel-framed, transite-enclosed structure, 160 ft square and 70 ft high. The turbine bay is of full height, 90 ft wide and 160 ft long. It houses the turbogenerator, condenser, feedwater pumps and heaters, water treatment facilities, diesel engines for emergency power, and other auxiliaries. A crane services this equipment. The remaining bay of the turbine building, adjoining the

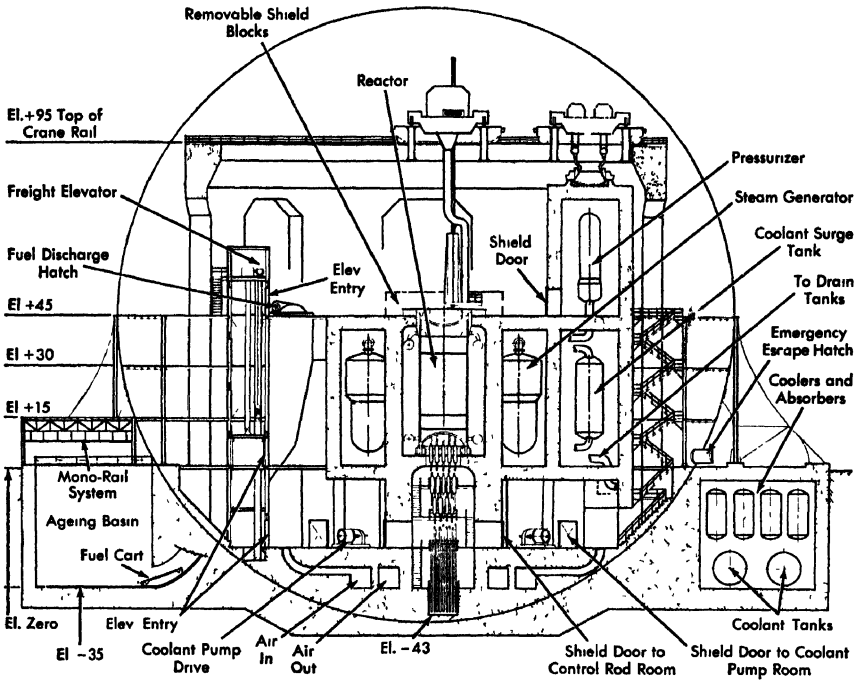

FIG. 5–9 Cross section of reactor building, looking west

containment sphere, is of two-story construction. The ground floor houses ventilating fans and electrical substation gear. The second story, connected to the personnel air lock of the sphere by an enclosed passageway, contains centralized controls for the reactor and turbogenerator, offices, laboratory, and personnel facilities.

The fuel-handling building, whose internal layout is not shown in the accompanying drawings, is 250 ft long and 75 ft wide. Lying outside but immediately adjacent to the sphere, it is arranged to provide access for both trucks and railway cars. The building houses areas for new fuel storage, cleaning and assembly, and includes a 30-ft deep aging and storage basin for spent fuel. This basin communicates with the sphere as shown in Fig. 5–9. Other facilities in this building include cranes, monorails, and casks for transporting spent fuel to a disposal area

5–2.4 Alternative design possibilities. As pointed out earlier, the reactor concept described is but one of several being considered While a variety of coolants might be used with the D_2O moderator and natural uranium fuel, emphasis has been on reactors using heavy water as both coolant and moderator. This combination was chosen because of neutron economy and because it uses Savannah River reactor experience.

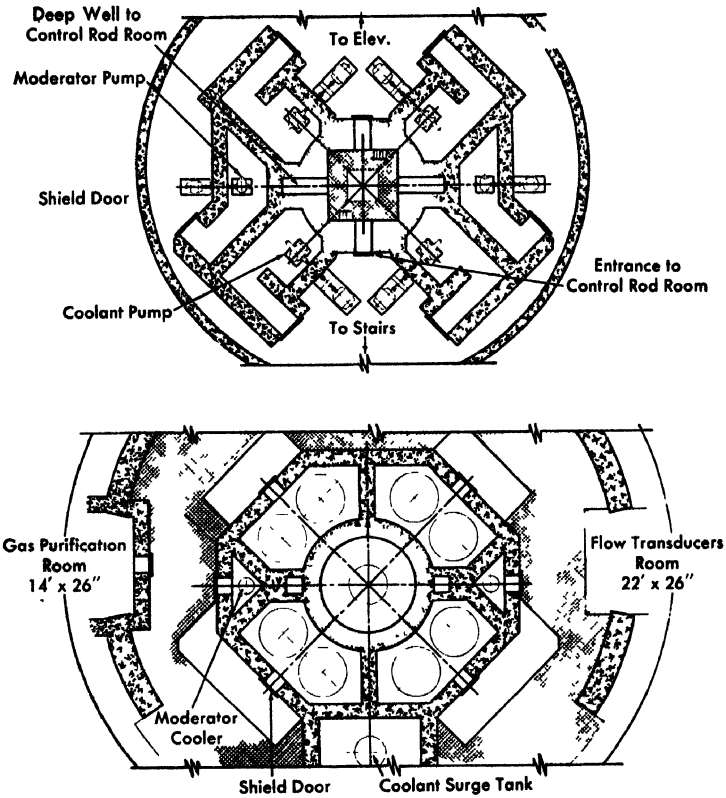

FIG. 5–10 Plan view of reactor building at elevations of −23 feet and +1 foot

Similarly, a pressure vessel instead of a pressure tube reactor was selected as the reference concept to benefit from industrial experience in fabricating pressurized water reactors. Utilization of existing experience in all fields was judged necessary to meet the short time schedule (5½ years for development and construction).

Although a pressure vessel was chosen for the reference design, this does not mean that it is the ultimate choice for long-range development. Conclusions cannot be drawn now, but certain attributes of the two designs affecting their relative merits are discussed.

As an example, a pressure tube reactor designed for a 100-Mw (electrical) power plant is shown in Fig. 5–4.

Major design problems of the pressure tube reactor discourage its immediate use in large power plants. Many of these are mechanical problems which probably can be solved by continued development effort. Advances are needed in basic metallurgy, metals fabrication, and mechanical

application to cope with problems of (1) providing structural safety without undue loss of neutron economy, (2) connecting pressure tubes to coolant distributors, and (3) containing D_2O.

In a D_2O-cooled reactor, the combined neutron captures of heavy-wall Zircaloy pressure tubes and the thinner tubes of a moderator-containing calandria imperil the reactivity of a natural uranium core. Connecting Zircaloy pressure tubes to stainless steel coolant distributors challenges the mechanical designer The close spacing of tubes, the nonweldability of the bimetallic coupling and the need for tube replaceability contribute to the difficulty. Typical of the development needs is a satisfactory method for bonding Zircaloy to stainless steel. Investigation of the alternatives of plenum chambers, pipe headers and individual pipes for distributing coolant to the pressure tubes has shown that these variants have considerable effect on other aspects of reactor design, but have only minor effect on the tube connection problem.

The D_2O moderator in a pressure tube reactor is kept at relatively low temperature to avoid pressure in the moderator container. The reactivity advantage of a cold moderator is appreciable, sometimes offsetting the parasitic loss caused by the pressure tubes. Other design problems accrue, however. Thermal insulation is needed between coolant and moderator. Even with perfect insulation, some 8% of the reactor heat is generated in the moderator by radiation effects. Part of this energy may be usable in feedwater heating, but it appears economically unattractive unless the moderator temperature is increased to a level where some pressurization is required.

Many problems of the pressure vessel reactor pertain to design details and construction of the massive vessel Development of pressurized H_2O reactors in this country has defined areas of greatest concern and established general feasibility limits on size, pressure rating, wall thickness, and related variables. The reactor under study is a member of the pressurized water reactor family, but its design is heavily influenced by factors which do not apply to H_2O reactors. Among these are:

(1) The lack of enrichment requires a large reactor core and severely limits the composition and quality of its structural materials.

(2) The cost of D_2O necessitates volumetric economy, ruling out its extensive use for shielding. Stringent measures must be applied throughout the system to avoid loss of D_2O.

Size is particularly important. A vessel can be built to operate at 2000 psi with the small enriched core of the typical pressurized H_2O reactor, but the larger vessel for a natural uranium core may be limited to 1000 to 1500 psi. Gradual advances in design and fabrication technology should improve pressure vessel potentialities.

The pressure tube reactor, now in a primitive development stage, appears capable of greater advancement, and with its inherent flexibility may contribute more to the ultimate attainment of economical power.

Pressure vessel reactors of two general types have been considered: (1) The hot-moderator reactor (reference design) using the flowing D_2O first as moderator, then as coolant, with the moderator and coolant temperature about equal, and (2) the cold-moderator design in which the moderator is isolated from the coolant and circulated through a separate external cooler, to keep the temperature between 60 and 80°C.

The reactivity advantage of a cold moderator is used to better advantage in the pressure vessel concept; with moderator and coolant pressurized equally, thin-walled housing tubes can be used around the fuel elements. The extra reactivity permits a reactor to be smaller for the same heat output. Longer fuel exposures can be attained, and higher coolant temperatures and pressures can be used with little loss of reactivity.

The cold moderator complicates reactor design. The divergent temperatures of coolant and moderator increase thermal stress problems. Reasonably efficient sealing is required to prevent gross intermixing of coolant and moderator As in the pressure tube reactor, thermal insulation of the housing tubes is necessary. The best insulation devised thus far is a thin layer of the inert gas used to pressurize the reactor and coolant circuits.

Final selection between the hot-moderator and cold-moderator concepts will require further experiments and analyses.

5-2.5 Cost considerations. The estimated cost of constructing the plant described in Article 5-2.3 is in the range of 65 to 85 million dollars, excluding costs of site acquisition, research, and development. This is almost twice as great as some current estimates for pressurized H_2O power reactor plants of comparable capacity Some of the difference (about $7 million) can be ascribed to the cost of D_2O. However, to make a meaningful cost comparison, one would have to know more about the design assumptions and the methods used in estimating the costs.

Assuming an annual plant factor of 80% and fixed charges on the investment at 15% per year, a 65 to 85 million dollar investment is equivalent to 14 to 18 mills/kwh of electricity. Other costs are assigned a probable range in the following table, producing a total cost of 18 to 26 mills/kwh for electricity produced in the subject plant.

The estimate below includes the cost of D_2O and the fuel inventory (1.5 reactor charges) as part of the plant investment to which annual charges of 15% are applied. If these materials are rented at lower rates, as is often assumed in cost evaluations, there will be commensurate savings. No credit is taken in this estimate for the value of plutonium produced in the reactor.

Item	*Estimated cost range, mills/kwh*
Fixed charges on investment	14 –18
Fuel consumption	2 – 4
D_2O loss	0.5– 1.5
Operation and maintenance	1.5– 2.5
Total	18 –26

This analysis is based on preliminary findings. The cost of individual items may fall outside the range indicated, but the range in total power cost is believed realistic for the first large-scale power plant using a reactor of this type.

Variations in reactor design within the latitudes discussed have small effect on power cost. The dominating component is the cost associated with plant investment, and only minor variations in investment are foreseen for the alternatives given

The greater initial reactivity of reactors with cold moderator should increase fuel exposure, perhaps by 50%, and thus reduce fuel cost by 1 or 2 mills/kwh. This saving, however, tends to be reduced by the loss of heat to a cold moderator. Design for higher pressure, an option not yet thoroughly explored, can improve plant thermal efficiency, although with saturated steam the improvement is somewhat limited.

Selection of a pressure tube rather than a pressure vessel design, now, would do little to promote economy in a D_2O cooled and moderated system. Fuel cost advantages from its cold moderator are largely nullified by parasitic neutron losses and by loss of heat to the moderator. Reduction in reactor cost, an objective of the pressure tube design, is prevented by the present high cost of fabricated Zircaloy products. Cost savings from higher operating pressures are prejudiced by increased neutron capture in thicker tubes and by limitations in the economy of power cycles using saturated steam.

The cost of electricity from the plant described here would have to be reduced by a factor of three to compete with coal-fired plants in this country. It is fair to ask whether there is potential for so great a reduction.

Re-examination of the cost items shows that if (1) fuel life were infinite, (2) D_2O losses were eliminated and (3) operating costs were negligible, it would still be necessary to halve the plant investment to compete successfully with conventional-fuel plants. With even a minimum allowance for fuel consumption and other operating costs the estimated investment would need to be divided by four. Accomplishment of either is hard to visualize now. However, the estimated costs are not excessive in comparison with those of other nuclear plants.

One of the most promising methods of cost reduction is to produce more power from a plant of given size. The reactor described was designed from the best available data, but in no case was the design pushed completely to the limit. Also, there is probably more conservatism in certain parts of the design than in others. Discovery and elimination of these restrictions by operating a prototype reactor might allow as much as a 50% increase in power output with only a modest increase in cost.

Through experience, design and construction methods should improve and plant component costs should decrease. Improvements that decrease fuel costs and increase exposure life, and improvements in reactor design, should lower costs. Further economy should come from building larger plants.

Major changes in the design concept, such as the following, might eventually prove economical:

(1) Use a direct cycle, eliminating the cost of the steam generator and the temperature drop which results from its use.

(2) Design the reactor to produce superheated steam.

Such design changes would require extensive development in fields of reactor physics, metallurgy, and mechanical design. They are not in the scope of this study.

5–2.6 Design of a test reactor (HWCTR). A major problem is to make natural uranium fuel elements inexpensively, to stand long irradiation at high temperatures and high heat dissipation There has been progress in developing metallic fuel tubes, but the fuel must be tested in a reactor. A small reactor, called the Heavy Water Components Test Reactor (HWCTR) has been proposed for this testing. It could also be used to test monitoring devices, control rod drives, safety rod mechanisms, seals, properties of irradiated construction materials, and service life of mild steel in hot D_2O. Experience in operating the smaller reactor should advance the design of a full-scale plant, and reduce costs of constructing and operating it.

The HWCTR would be D_2O cooled and moderated, capable of irradiating twelve natural uranium fuel assemblies, each 10 ft long, for long periods in a flux of 10^{14} n/(cm^2)(sec) (peak value). Each test fuel assembly would liberate about 2 Mw of heat. Fuel and coolant temperatures would be those of a large D_2O-cooled power reactor. Coolant flow to each test assembly would also be the same as for the large reactor.

To keep HWCTR small and limit its heat output, the central group of 12 natural uranium test assemblies is to be surrounded by a ring of 24 enriched uranium assemblies and this, in turn, by a thick reflector of heavy water. A cross section is shown in Fig. 5–11. Positions of the control rods, safety rods, and thermal shield are also shown. The flow and heat-

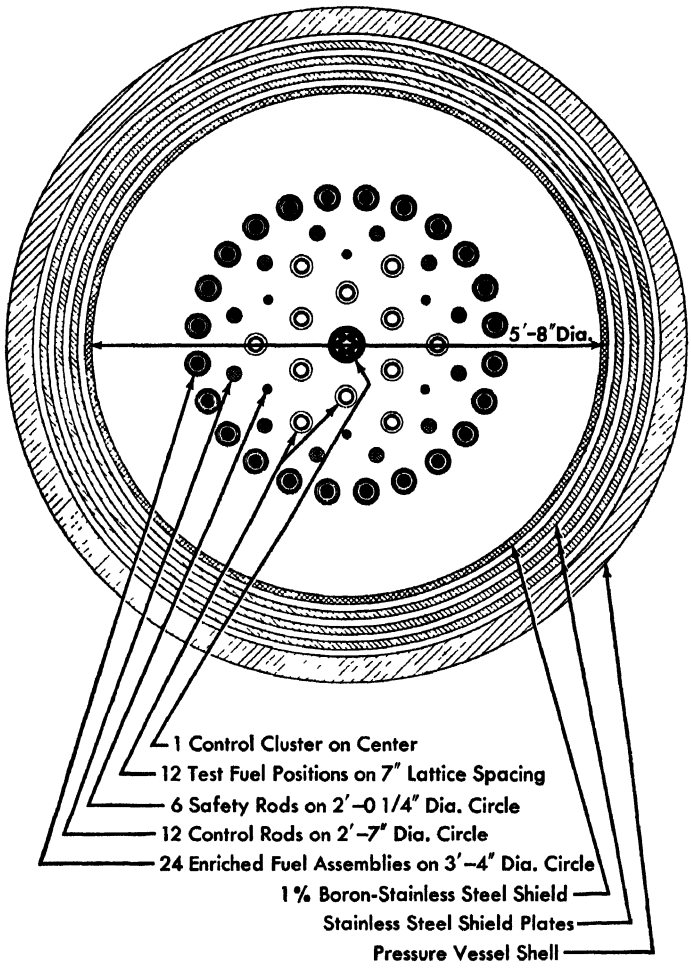

FIG. 5–11. Cross section of HWCTR.

transfer characteristics and dimensions of reactor components are summarized in Table 5–3 (see pages 472–474).

A preliminary pressure vessel design is shown in Fig. 5–12. The vessel, designed for 1500 psig at 285°C, is to be built of carbon steel lined with stainless steel. The center section of the vessel, 7 ft in diameter, contains the core, reflector, and thermal shield. The bottom biological shield is in the bottom section, 4½ ft in diameter. In the top section, 5 ft in diameter, are the top biological shield and the safety rods when they are raised (cocked). This upper section serves as inlet coolant plenum and heavy-water reservoir, providing space for expansion of heavy water and also

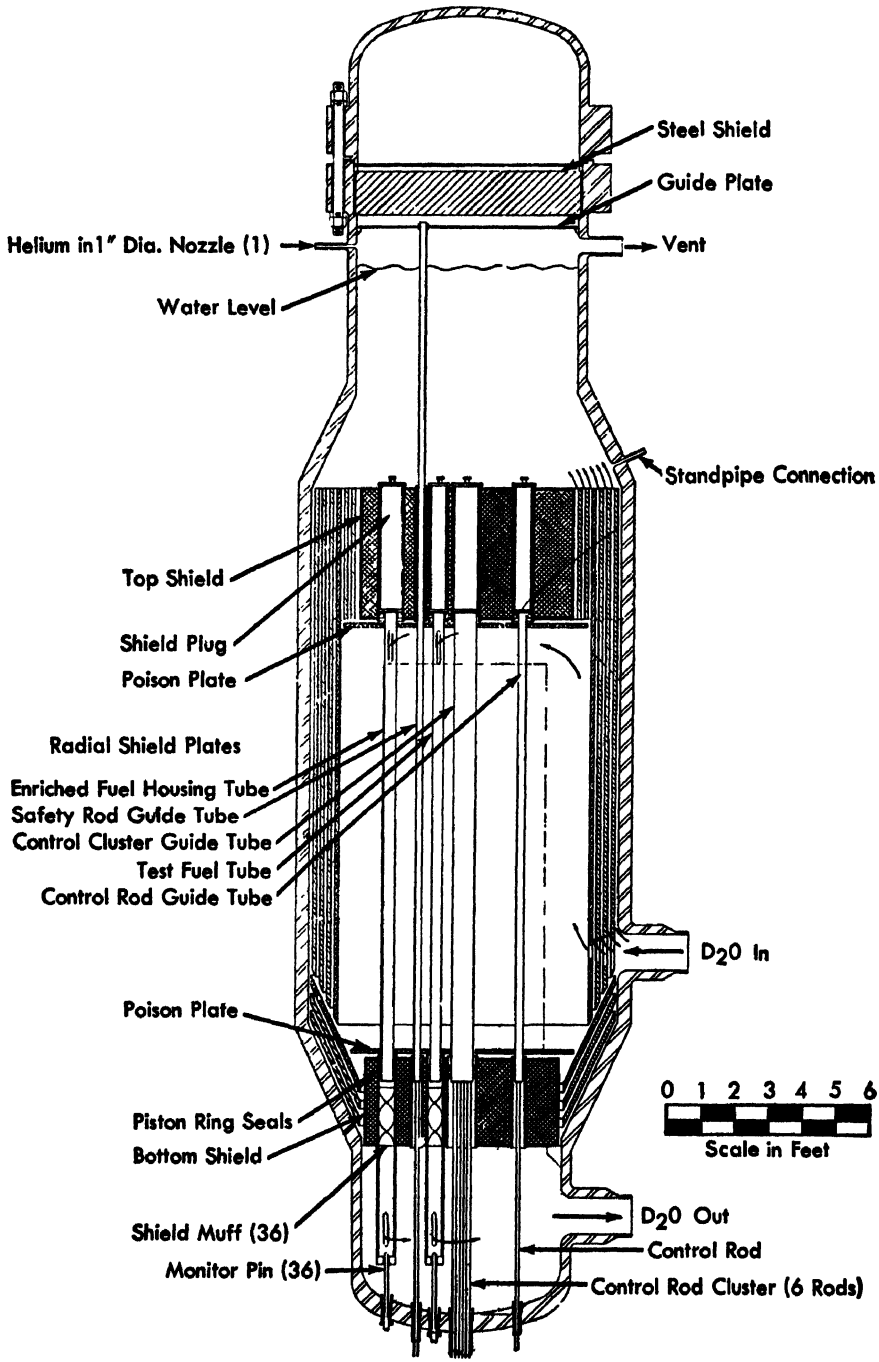

FIG. 5–12. Cross section of HWCTR pressure vessel.

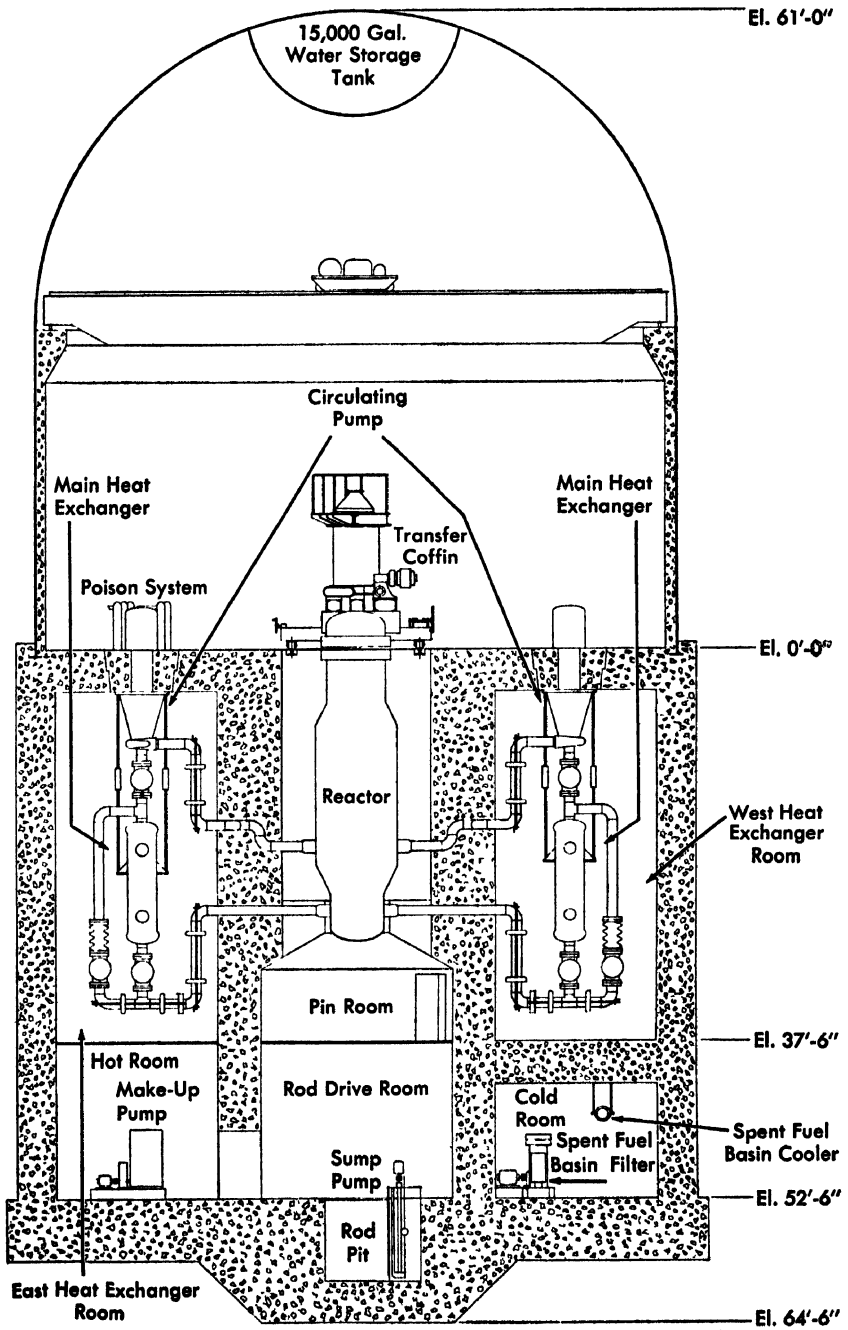

FIG 5–13. HWCTR containment building, showing arrangement of power components.

protecting against immediate loss of heavy water from the core in the event of a leak. The upper section also contains the pressurizing gas blanket of helium. The feasibility of installing one or two separate in-pile loops is being studied, but the design shown in Figs. 5–12 and 5–13 does not include such loops.

The present design is not intended to generate steam or electric power. The heat (62 Mw) is removed from the reactor by forced convection of heavy water, circulated through two loops to water-cooled heat exchangers. The cooling water is kept below the boiling temperature. Details of the cooling system are also summarized in Table 5–3.

5–3. The Physics of Natural Uranium, Heavy-water Reactors*

5–3.1 Introduction. In the course of the program to develop a natural uranium, heavy-water moderated reactor, the Savannah River Laboratory conducted an extensive experimental physics survey of natural uranium, heavy-water lattices. This survey included buckling measurements on more than two hundred cold, clean lattices, and measurements of the slowing-down area τ and the fast-fission factor ϵ. The effects of light water in the moderator and of changes in moderator temperature were also studied [17].

A self-consistent theoretical treatment was developed for calculating lattice bucklings. The calculated data were fitted to the experimental results by adjusting the parameters used in estimating resonance capture. After this adjustment, the calculated buckling values agreed with the measured values over wide ranges of lattice characteristics, with a standard deviation of about 0.20 m^{-2}. Although such accuracy is not sufficient to detail the parameters of a final design, these methods proved useful for surveying and evaluating effects of lattice design changes. Since the results of the experimental work are generally available [15–17], it has been judged most useful here to outline these calculation methods and some results of calculations that apply in a general way to reactor design.

The discussion is divided into two parts. The first treats methods of calculating lattice buckling and of estimating effects of temperature changes, fission products, and fuel exposure. Individual lattice parameters are considered in an order that facilitates calculation. The second part details the interaction between lattice parameters and objectives of reactor design. Generalized results are given wherever possible; illustrative examples are drawn from reactor designs considered in Section 5–2.

---

*By F. E. Driggers and D. S. St. John, E. I. du Pont de Nemours and Company.

5-3.2 Lattice parameters. *Density of D_2O.* In heavy-water reactors, reactivities and temperature coefficients depend strongly on the density, ρ_M, of the water. The density of pure D_2O in the range from 5 to 50°C is given by Kirshenbaum [18]. In the range from 30 to 250°C, ρ_M is given by Heiks et al. [19]. The latter set of data was normalized to the former at 40°C and all data were then fitted by polynomials in the moderator temperature, T_M. In the range from 5 to 50°C,

$$\rho_M = 1.10646 + 5.302 \times 10^{-5} T_M - 5\,333 \times 10^{-6} T_M^2 \text{ (g/cm}^3\text{)}.$$

The standard deviation of this fit is less than 0.002%. In the range from 5 to 250°C,

$$\rho_M = 1.10482 + 2.0374 \times 10^{-4} T_M - 9.8367 \times 10^{-6} T_M^2 + 5.1097 \times 10^{-8} T_M^3 - 1.6844 \times 10^{-10} T_M^4 + 2.0429 \times 10^{-13} T_M^5 \text{ (g/cm}^3\text{)}.$$

The standard deviation of this fit is about 0.01%.

Slowing-down area (τ). The slowing-down area for fission neutrons in pure D_2O is about 120 cm² at a temperature of 20°C [20]. To obtain the slowing-down area τ of a lattice at room temperature, this figure must be corrected for presence of: (1) light water, (2) cladding material (here assumed to be aluminum), and (3) uranium. A decrease in τ of 4 cm² is produced by adding 1% light water [21]. It is assumed that aluminum does not moderate neutrons at all and that the inelastic cross section of uranium makes it half as good a moderator as D_2O. Then, since τ is inversely proportional to the moderator density, the slowing-down area in the lattice is

$$\tau(20°\text{C}) = [120 - 4(\%\text{H}_2\text{O})]\left[\frac{V_T - V_{Al} - \frac{1}{2}V_U}{V_T}\right]^{-2}$$

$$\cong [120 - 4(\%\text{H}_2\text{O})]\left[1 + 2\,\frac{V_{Al}}{V_T} + \frac{V_U}{V_T}\right] \text{ (cm}^2\text{)},$$

where the volumes of aluminum, V_{Al}, and of uranium, V_U, are assumed to be small compared with the total volume, V_T.

For a temperature T_M other than 20°C,

$$\tau = \tau(20°\text{C})\left[\frac{\rho_M(20°\text{C})}{\rho_M(T_M)}\right]^2.$$

It is assumed that this density ratio is the same for pure D_2O and for a mixture of D_2O and H_2O containing 1 or 2% H_2O.

Thermal diffusion area (L^2). The thermal diffusion area L^2 is given by $L^2 = (3\bar{\Sigma}_a\bar{\Sigma}_{tr})^{-1}$, where $\bar{\Sigma}_a$ and $\bar{\Sigma}_{tr}$ are, respectively, the flux-weighted average absorption and transport cross sections of a "cell." The microscopic

cross sections of each component of the cell must be averaged over a Maxwellian distribution of neutron energies in equilibrium with the moderator at temperature T_M. Then the average thermal flux in each component must be calculated to obtain the flux-weighted cross-section averages in the cell.

Over the thermal range of energies, σ_{tr} may be taken as constant for each component. The value of σ_a for any one of the components is given by

$$\sigma_a = \sigma_{a0} \times \sqrt{\frac{\pi}{4}} \times \sqrt{\frac{293}{T_M(^\circ\mathrm{K})}} \times (\text{non-}1/v \text{ factor}),$$

where σ_{a0} is the cross section evaluated at 2200 m/sec. The non-$1/v$ factors are given in Reference 22.

The flux distribution in the cell is most easily calculated by approximating the cell with a model composed of concentric cylinders. The material between any two cylindrical boundaries is assumed to be homogeneous. The transport equation describing the thermal flux distribution can then be solved by the method of spherical harmonics. The method proposed by Amouyal [23] is about as accurate as the P-3 spherical harmonics approximation and is simpler to use, particularly for hand calculations.

Flux distributions have been calculated for a number of lattices containing tubular fuel assemblies. These results are useful in their own right and also show how L^2 varies with changes in characteristics of the cell.

Calculations were made for tubes of natural uranium of thickness t and inner radius R_i. The outer radius of the cell, R_o, was adjusted to give values of the volume ratio of moderator to fuel of 10, 20, 30, and 50.

Values of L^2 are plotted in Fig. 5–14 for

$$\Sigma_{a,F} = 0.32 \text{ cm}^{-1}, \quad \Sigma_{s,F} = 0.397 \text{ cm}^{-1},$$
$$\Sigma_{a,M} = 0.0001 \text{ cm}^{-1}, \quad \text{and} \quad \Sigma_{s,M} = 0.50 \text{ cm}^{-1}.$$

Changes in temperature alter the value of L^2 primarily by changing $\Sigma_{a,F}$ and $\Sigma_{s,M}$. For an assembly with a tube thickness t the L^2 at room temperature is obtained directly from Fig. 5–14. The change in L^2 produced by a change in temperature is given by

$$\Delta L^2 = \frac{V_M}{V_F}\left[(0.5 - \Sigma_{s,M})(5.7 + 2.8t) + \frac{4.4}{\Sigma_{a,M}}(0.32 - \Sigma_{a,F})\right].$$

This equation for ΔL^2 was obtained by fitting the results of a number of P-3 calculations made with values of $\Sigma_{a,F}$ and $\Sigma_{s,M}$ other than 0.32 and 0.50, respectively.

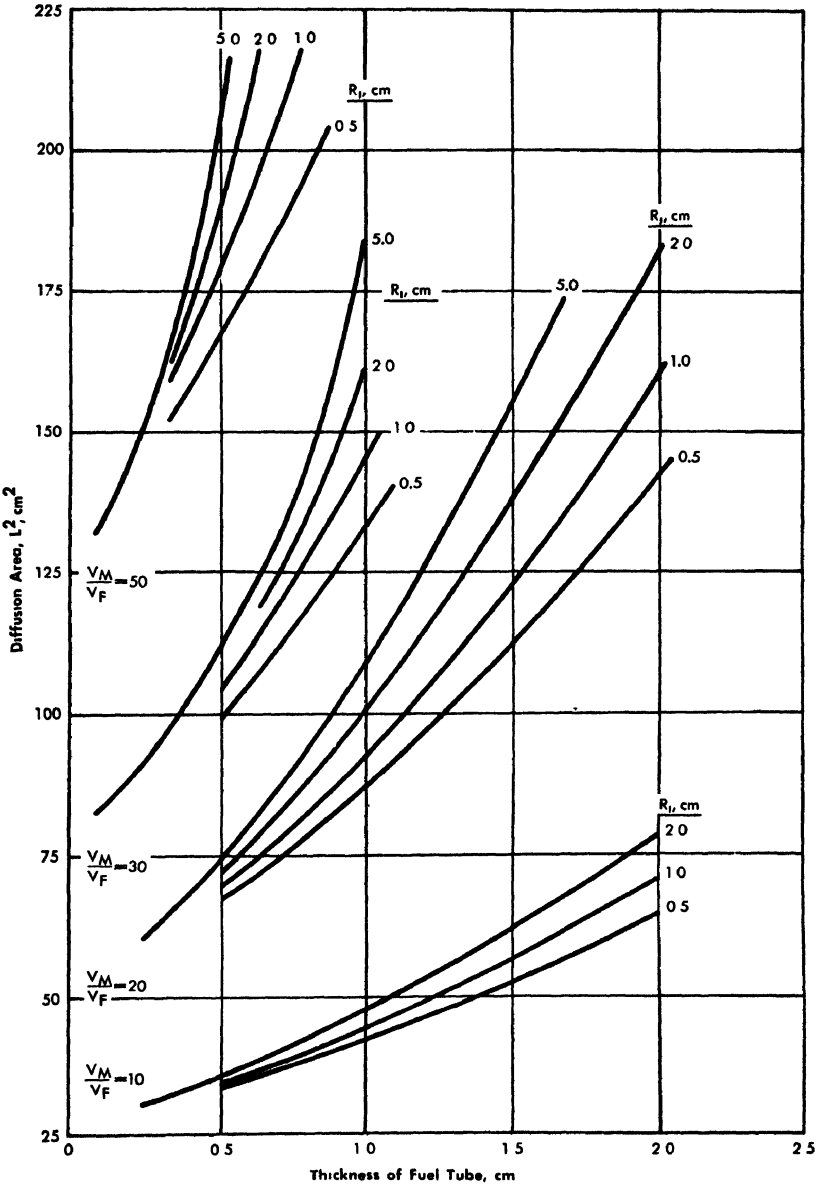

FIG. 5–14. Diffusion area L^2 in lattices of uranium tubes. R_1 = inner radius of tube; V_M/V_F = volume o

Thermal utilization (f). Thermal utilization f is defined as

$$f = \frac{(\Sigma_a V)_F}{\sum_i (\Sigma_a V d)_i},$$

where the denominator is summed over all the materials in the cell. Σ_{a_i} is the macroscopic absorption cross section of the ith cell component, V_i is the volume of the component, and d_i is the ratio of the average thermal flux in the component to the average thermal flux in the fuel.

The fractional absorption of thermal neutrons in the fuel is designated by f; the fractional absorption in all other components is $(1-f)$. The part of $(1-f)$ associated with moderator absorption is equal to the fractional absorption in the moderator, f_M, given by

$$f_M = \frac{(\Sigma_a V d)_M}{\sum_i (\Sigma_a V d)_i}.$$

The values of f_M are plotted in Fig. 5–15 for the lattices described above.

The correction to be added to f_M for other values of $\Sigma_{a,F}$ and $\Sigma_{s,M}$ was obtained in the same way as the L^2 correction:

$$\Delta f_M = 1.1 \times 10^{-3} \frac{V_M}{V_F} (0.32 - \Sigma_{a,F}) + 4.3 \times 10^{-5} (R_o - R_i - l)^{2.5} (\Sigma_{s,M} - 0.50).$$

To calculate the fractional absorption, f_C, in the cladding on the fuel tube, it is necessary to know the ratio, $d_C = \phi_C/\phi_F$, of the average thermal neutron flux in the cladding to the average flux in the fuel. This ratio is nearly independent of the cladding thickness and fuel-tube diameter over the range considered here. It is approximately equal to the ratio of average flux at the two fuel surfaces to the average flux inside the fuel tube. This ratio is shown in Fig. 5–16. Then,

$$f_C = \frac{(\Sigma_a V d)_C}{\sum_i (\Sigma_a V d)_i}.$$

Thermal reproduction factor (η). In calculating the reactivity of a lattice containing unexposed uranium at room temperature, a value of 1.327 is used for the thermal reproduction factor η (taken from Reference 22). However, η is a function of moderator temperature T_M, because the absorption cross sections of U^{235} and U^{238} do not have the same energy dependence; further, η is a function of exposure, since the cross section of Pu^{239} has still a different energy dependence. These variations were obtained from the equation

$$\eta = \frac{(\nu N \sigma_f)_{U^{235}} + (\nu N \sigma_f)_{Pu^{239}}}{(N\sigma_a)_{U^{238}} + (N\sigma_a)_{U^{235}} + (N\sigma_a)_{Pu^{239}} + (N\sigma_a)_{Pu^{240}}},$$

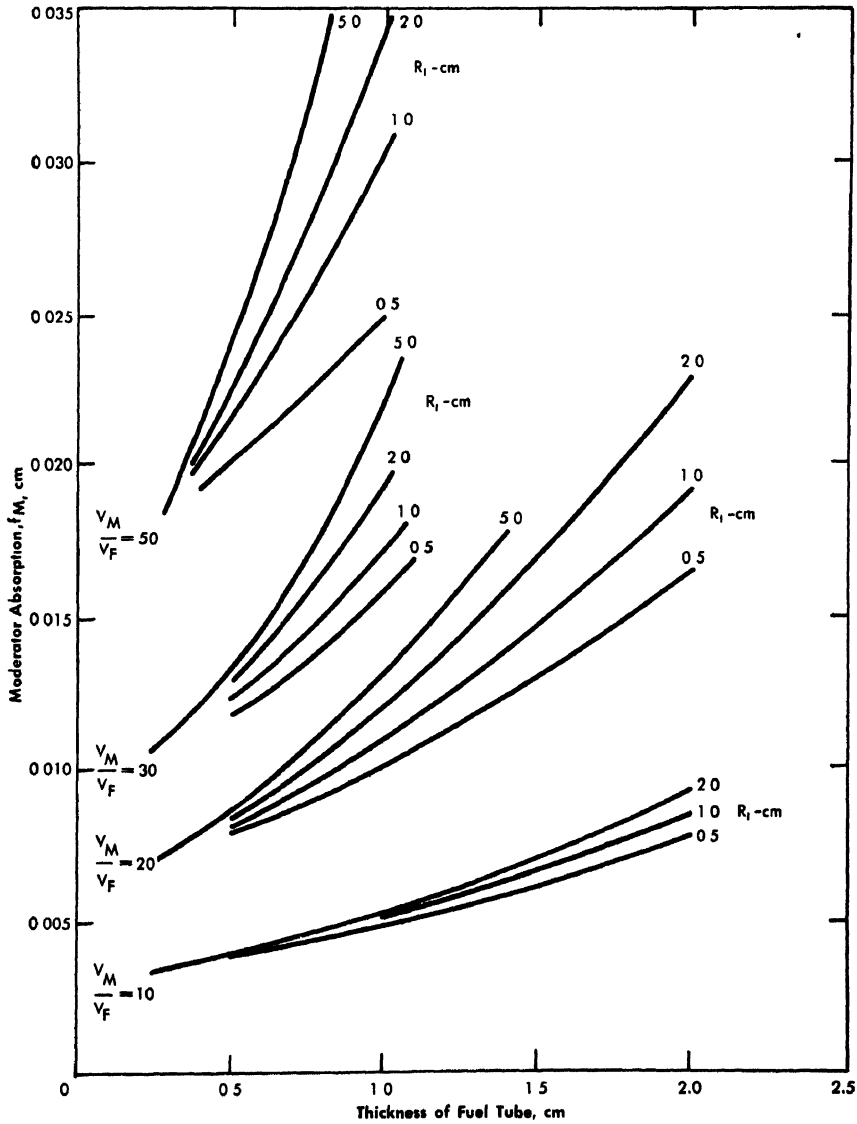

FIG. 5-15. Fractional absorption in moderator (f_M) in lattices of uranium tubes.

where ν is the number of fast neutrons produced per neutron absorbed in the fissionable isotope, and σ_f is the fission cross section. Values of $\Delta\eta/\eta = [\eta(25°C) - \eta(T_M)]/\eta(25°C)$ are plotted in Fig. 5-17 as a function of T_M for fuel exposures of 0, 1000, and 2000 Mwd/ton, for a natural uranium fueled reactor with $p = 0.91$

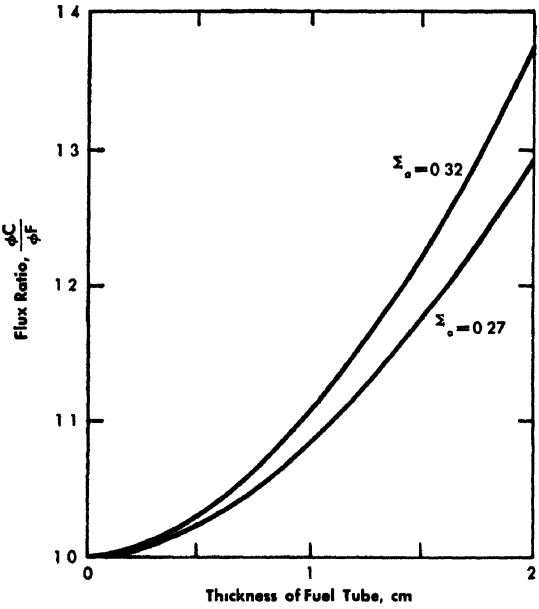

FIG. 5–16 Ratio of average flux in cladding to average flux in fuel (ϕ_C/ϕ_F)

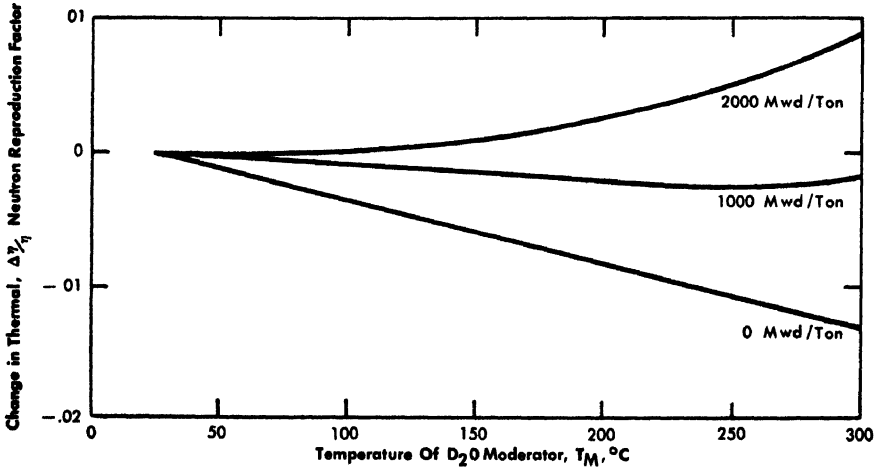

FIG. 5–17. Variation of η with temperature and exposure

Fast fission factor (ϵ). The line of demarcation between the fast fission factor ϵ and the resonance escape probability p is somewhat arbitrary, since fast absorptions may be counted either as resonance absorptions, or as decreases in the number of fast neutrons produced in the reactor per neutron produced in thermal fissions. The calculations have a simpler

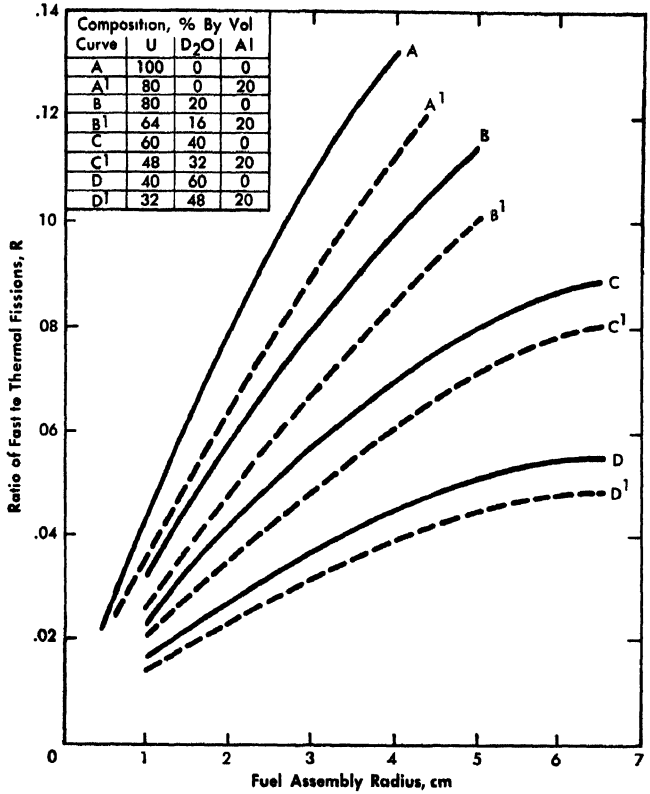

FIG. 5-18 Ratio (R) of fast fissions in U^{238} to thermal fissions in U^{235}.

form if all fast absorptions are included in p. In that case the fast fission factor is defined as

$$\epsilon = 1 + \frac{(\nu_f - 1)}{\nu_{th}} R,$$

where ν_f and ν_{th} are the average numbers of neutrons produced per fast fission in U^{238} and per thermal fission in U^{235}, respectively, and R is the ratio of fast fissions in U^{238} to thermal fissions in U^{235}

The method used to calculate R is an extension of one proposed by B. I. Spinrad [24]. In these calculations, the actual fuel assembly is replaced by a homogeneous cylinder having the same volume and composition. The calculated values of R are plotted in Fig. 5-18 as a function of the equivalent radius $\sqrt{A/\pi}$, where A is the cross-sectional area of the fuel assembly. The solid curves are plots of R for assemblies that contain no aluminum. The average compositions are given in the figure. The

reduction in R produced by replacing 20% of the U-D_2O volume in the fuel assembly by aluminum is indicated by the dashed line associated with each solid line. In calculating ϵ, values of $\nu_f = 2.51$ and $\nu_{th} = 2.46$ are used; then $\epsilon = 1 + 0.614R$.

Resonance escape probability (p). The method of calculating p was proposed by E. Critoph [20]. A fuel assembly is assumed to be a line source of fission neutrons at $r = 0$. These neutrons are assumed to slow down in a homogeneous mixture of the reactor components until they reach the energy E_{res}, at which energy they have a spatial distribution $q(r,E_{res})$. The number absorbed in resonances in the discrete fuel assemblies is then assumed to be

$$\frac{N_f V_f RI}{(\xi\Sigma_s)_M} \sum_i q(r_i,E_{res}),$$

where the summation is over all fuel assemblies. The number of neutrons slowing down into the resonance region is $\int_0^\infty q(r,E_{res})2\pi r dr$. The fraction absorbed is thus

$$(1-p) = \frac{\sum_i q(r_i,E_{res})}{2\pi\int_0^\infty r q(r,E_{res})dr}\left[\frac{N_f V_f RI}{(\xi\Sigma_s)_M}\right],$$

where $N_f V_f$ is the number of fuel atoms present, $(\xi\Sigma_s)_M$ is the moderating power of the moderator, and RI is the resonance integral, treated here as an adjustable parameter.

A value of E_{res} of 30 ev is recommended [17]. Then,

$$q(r,E_{res}) = \left[\frac{0.677}{4\pi\tau'}\right]e^{-r^2/4\tau'} + \left[\frac{0.323}{4\pi\tau''}\right]e^{-r^2/4\tau''},$$

where

$$\tau' = 99.2\left(\frac{\tau}{\tau_M}\right);\ \tau'' = (33.8)\left(\frac{\tau}{\tau_M}\right);\ \text{and}\ \left(\frac{\tau}{\tau_M}\right) = 1 + 2\left(\frac{V_{Al}}{V_T}\right) + \left(\frac{V_U}{V_T}\right).$$

This equation is obtained by correcting an analytical fit to the observed slowing-down distribution, at indium resonance energy, of fission source neutrons in D_2O [20].

Effective surface area. The resonance integral is a function of the ratio S_{eff}/M of the effective surface of the fuel assembly in cm² to the mass of the assembly in grams. The effective surface area is taken as

$$S_{eff} = S_P + \left(\frac{S_T - S_P}{G_0}\right)F,$$

where S_P is the area determined by the "tape measure" perimeter of the

uranium, S_T is the total uranium surface, and G_0 is the ratio of resonance flux at the surface of the assembly to the average flux in the interior:

$$G_0 = 0.1185\sqrt{A_U}I_0(0.237\sqrt{A_U})/I_1(0.237\sqrt{A_U}),$$

where A_U is the cross-sectional area of the uranium in the assembly, and I_0 and I_1 are Bessel functions. F is a measure of the extent to which the resonance flux is restored by the moderator inside the assembly.

If the fuel assembly consists of parallel plates separated by a distance D that is small compared with the plate dimensions, then

$$F_{pl}(\Sigma_s D) = \frac{\int_0^{\pi/2} \cos\theta\,(1 - e^{-\Sigma_s D \sec\theta})\,2\pi \sin\theta\, d\theta}{\int_0^{\pi/2} [\cos\theta\, 2\pi \sin\theta]\, d\theta},$$

where θ is the angle between the radius vector and the normal to the surface of the plates. This quantity is plotted in Fig. 5–19.

In the general case of a fuel assembly comprising a cluster of elements (plates, rods, etc.), the surfaces of which are parallel to the assembly axis, only one of the three integrations required can be carried out and plotted. For a point on an interior surface, the quantity $(1 - e^{-\Sigma_s r})\cos\alpha$ must be integrated over the solid angle out into the coolant. Here, Σ_s is the scattering cross section of the coolant, r is the distance along the radius vector to the nearest uranium surface, and α is the angle between the radius vector and the normal to the interior surface. If θ is the angle between the radius vector and a plane through the point perpendicular to the axis and ϕ is the angle between the projection of the radius vector onto this plane and the normal, then $r = D \sec\theta$ and $\cos\alpha = \cos\theta\cos\phi$. Here, D is the distance to the nearest uranium surface along the projection of the radius vector and is a function of ϕ but not of θ. The result of this integration is

$$F(\Sigma_s D) = 1 - \frac{4}{\pi}\int_0^{\pi/2} \cos^2\theta\, e^{-\Sigma_s D \sec\theta}\, d\theta.$$

This quantity is plotted also in Fig. 5-19.

For an arbitrary fuel assembly, the dependence of D on ϕ must be determined graphically and the integration over ϕ must be carried out numerically. Finally, the result must be integrated numerically over a set of points that represents the interior surface,

$$F_{cyl} = \left[\frac{1}{2(S_T - S_P)}\right]\int dS \int_{-\pi/2}^{\pi/2} [F(\Sigma_s D)\cos\phi]\, d\phi.$$

Often, the contribution of the effective interior surface is small and the

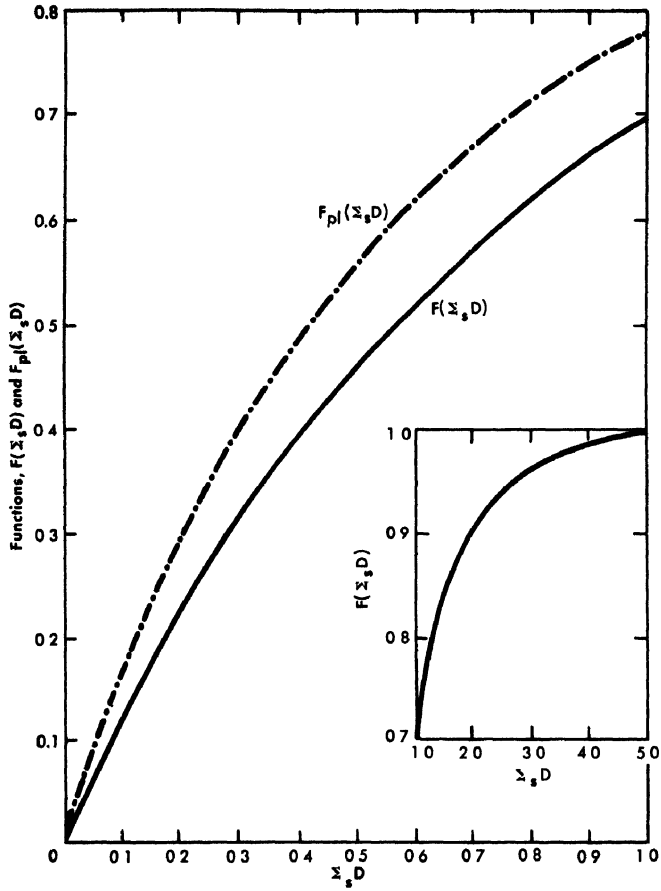

FIG. 5-19 The functions $F_{pl}(\Sigma_S D)$ and $F(\Sigma_S D)$

general process can be simplified by making a judicious guess of an equivalent plate spacing and then using the equation for F_{pl}.

Resonance integral. By comparing calculated and measured values of buckling, the following expressions for the resonance integral in barns were derived [17]. For uranium metal,

$$RI = \frac{6.2}{G_0} + 47\left(\frac{S_{eff}}{M}\right) - 70\left(\frac{S_{eff}}{M}\right)^2.$$

For uranium oxide,

$$RI = \frac{12.1}{G_0} + 16.4\left(\frac{S_{eff}}{M}\right).$$

The expression for $(1 - p)$ should be multiplied by a quantity $(1 - \beta)$, where β is the probability that a neutron that was counted as being absorbed in one assembly was actually absorbed in some other assembly. The correction, β, is given by Critoph [20]; its value is 0.01 for a lattice spacing of 5.5 inches and 0.001 for a lattice spacing of 6.8 inches.

These expressions for the resonance integral give values of p that include all high-energy and resonance-energy absorptions in U^{238} but do not include $1/v$ absorptions in U^{238} near thermal energies. These $1/v$ absorptions are included in the definition of f.

Buckling (B^2). The buckling of a lattice is defined by

$$\eta\epsilon pf = k = (1 + L^2B^2)(1 + \tau_1 B^2)e^{\tau_2 B^2},$$

where $\tau_1 = 0.378\tau$ and $\tau_2 = 0.622\tau$ [25]. Thus, if $M^2 = \tau_1 + \tau_2 + L^2$, then

$$B^2 \cong \left[\frac{k-1}{M^2}\right]\left[1 - \left(\frac{\tau(L^2 + 0.428\tau)}{M^2}\right)\left(\frac{k-1}{M^2}\right)\right].$$

Effects of light water. When H_2O is added to the moderator, the lattice parameters τ, L^2, p, and f are affected. These changes, in turn, depend on the effective absorption cross section of the cell, $\bar{\Sigma}_{a,\text{eff}}$, on B^2, and on p Calculated values of the change in buckling produced by the addition of 1 mol % of H_2O to the moderator are shown in Fig. 5–20 [17].

To obtain the change in buckling from these curves, the contributions obtained by interpolation in the B^2 family of curves and in the p family of curves are added algebraically and the sum is multiplied by the mol % change in H_2O.

Temperature coefficients As a reactor heats up, the buckling generally decreases because of changes in τ, L^2, η, p, and f. The change in τ is given in Glasstone [26] as

$$\frac{\tau}{\tau_0} = \left(\frac{\rho_0}{\rho}\right)^2 \left[1 - \left(\frac{1}{\tau_0}\right)\left(\frac{1}{3\bar{\xi}\bar{\Sigma}_s\bar{\Sigma}_T}\right) \ln\left(\frac{T}{T_0}\right)\right].$$

The effect of changes in temperature on L^2 and f_M can be estimated from the equations given in previous sections. Changes in temperature affect the values of $\Sigma_{a,F}$, which is proportional to $[T_M(°K)]^{-1/2}$, and of $\Sigma_{s,M}$, which is proportional to ρ_M, the density of the moderator. To a good approximation the value of f_C remains unchanged.

The major changes in p are due to the decrease in moderating power, $(\bar{\xi}\Sigma_s)_M$, and to the increase in the resonance integral because of Doppler broadening of the resonance peaks. Since $(\bar{\xi}\Sigma_s)_M \cong \rho$, where ρ is the

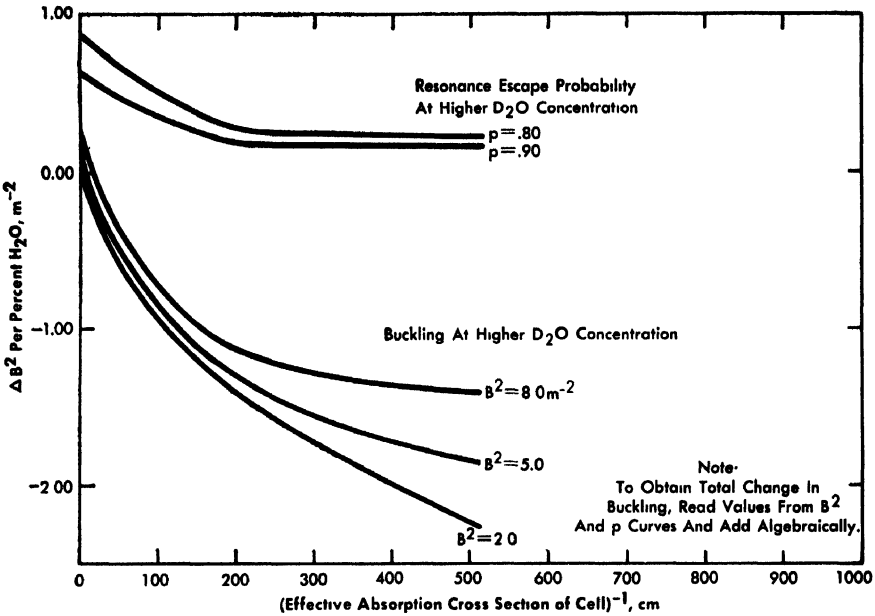

FIG. 5–20 Curves for determining change in buckling caused by small additions of H_2O

moderator density, the change in p associated with the moderator is

$$\frac{\Delta p}{p} = \left(\frac{1-p}{p}\right)\left(\frac{\Delta \rho}{\rho}\right)$$

The Doppler coefficient of the resonance integral is taken to be -1.2×10^{-4}/°C, which is the average of two published figures: -1.56×10^{-4}/°C [27] and -0.8×10^{-4}/°C [28]. The change in p associated with the fuel temperature is then

$$\frac{\Delta p}{p} = \frac{1-p}{p}\frac{\Delta(RI)}{(RI)} = +\left(1.2 \times 10^{-4}\,\frac{1-p}{p}\right) \text{ per °C.}$$

The total change, $\Delta p/p$, is the sum of these two effects.

All these changes are, to good approximation, independent of the fuel exposure. However, the change in η with temperature, which was discussed previously, does depend on exposure, as shown in Fig. 5–17.

Fission products. In calculating the operating reactivity of a reactor it is necessary to know the equilibrium concentrations of the fission products. For Xe^{135} and Sm^{149}, the reactivity effect can be estimated from the usual equations [26]. The number of Sm^{149} atoms produced per fission is

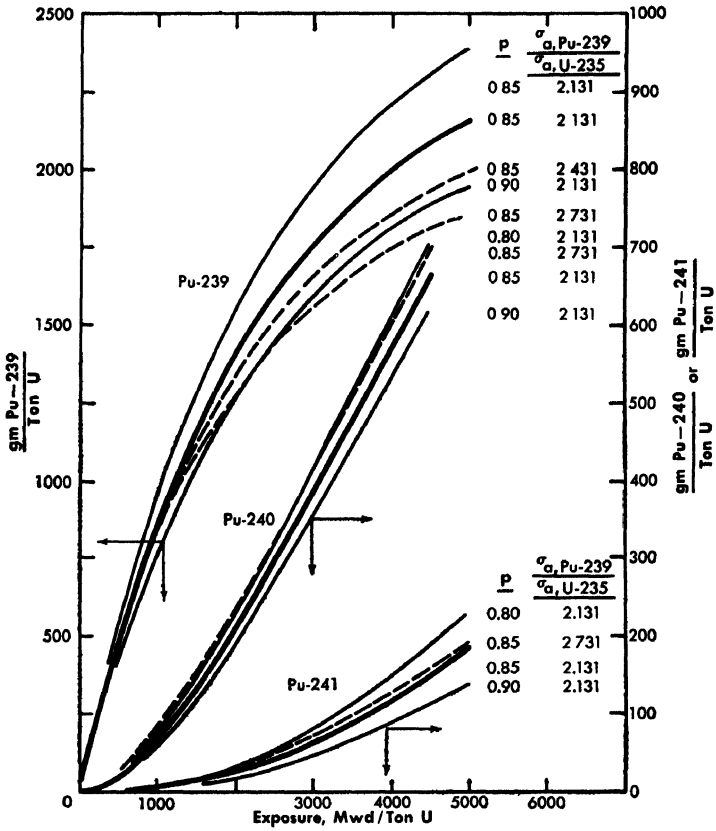

FIG. 5-21. Buildup of plutonium isotopes with fuel exposure.

0.012. The effect of other stable fission products with large cross sections is accounted for by increasing this number to 0.0152.

To a first approximation, poisoning due to all other fission products is proportional to the exposure; the relation used is

$$\frac{\Delta k_{fp}}{k} = -\frac{1}{f}(7.3 \times 10^{-6}) \qquad \text{(exposure in Mwd/ton)}.$$

Change of isotopic composition with exposure. The isotopic composition of the fuel as a function of exposure depends on all the isotopic cross sections, both thermal and resonance, and on the geometry of the fuel assembly as it affects self-shielding. However, the isotopic composition can be calculated rather accurately by assuming that all cross sections and parameters are constant with the exception of $\sigma_{a,Pu^{239}}$, which depends

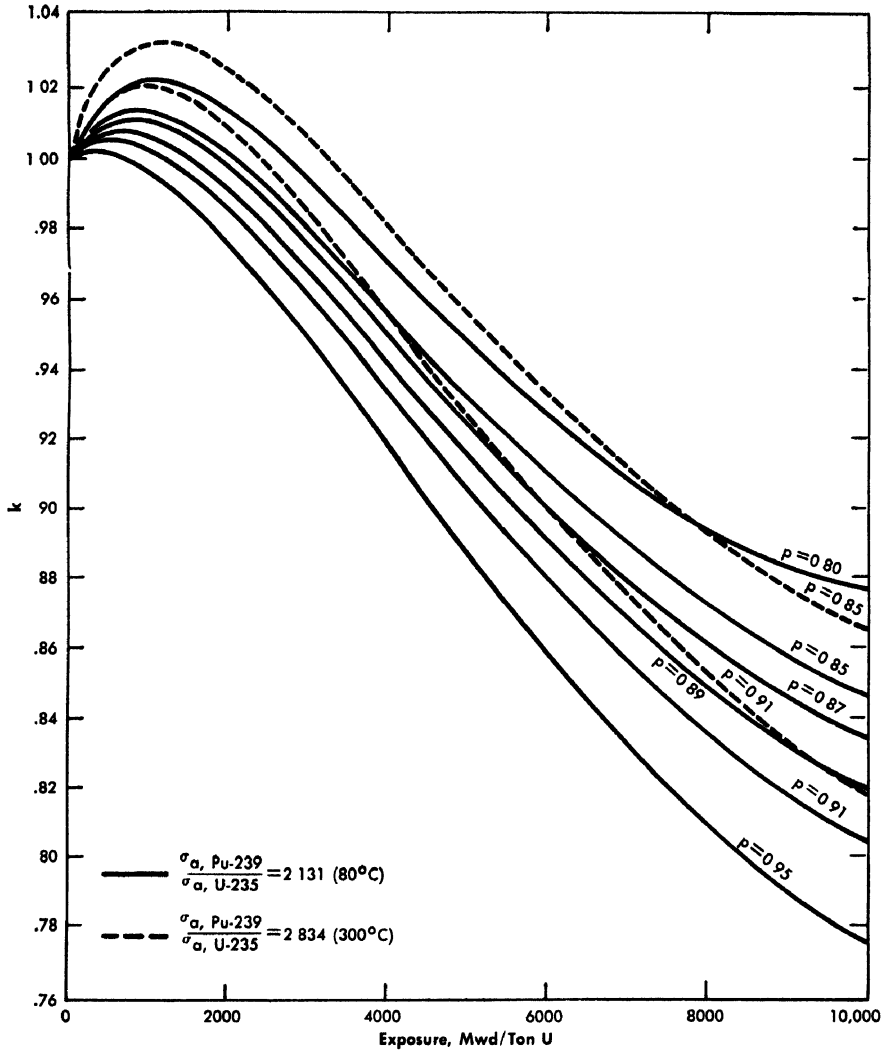

FIG. 5–22 Change of reactivity k with fuel exposure

strongly on temperature, and p, which depends on fuel geometry and on temperature.

Calculated values of the amounts of Pu^{239}, Pu^{240}, and Pu^{241} in grams per ton of fuel are shown in Fig. 5–21 as a function of the exposure in Mwd/ton. Several sets of curves are presented for several values of $\sigma_{a,Pu^{239}}/\sigma_{a,U^{235}}$, and of p. A uniform flux is assumed in the calculations. To calculate isotopic production in a whole reactor, the reactor can be divided into several regions over which the flux is approximately uniform and the curves in Fig. 5–21 can then be used for each region separately.

Variation of reactivity with exposure. Variations of k (the infinite multiplication constant) with exposure were calculated as part of the calculation of isotopic composition described in the previous section. In Fig. 5-22, k is shown as a function of exposure for two values of $\sigma_{a,Pu^{239}}/\sigma_{a,U^{235}}$ and for several values of p. For a specific lattice, the ordinate must be shifted to make the initial value of k greater than unity by the amount of excess reactivity held in the control system.

A thorough discussion of changes in isotopic composition and reactivity with exposure is given by Ioffe and Okenn [29].

Reflector savings. The increase in extrapolated dimensions of the reactor core due to the presence of a reflector depends on the radius and buckling of the core and on the reflector thickness and material. For a large, natural uranium, heavy-water reactor the variation due to the first two effects is small, and the reflector savings can be estimated from Table 5–4 for graphite and for heavy-water reflectors. The value quoted for zero reflector thickness applies to a core in a thin-walled tank surrounded by air.

Reactor kinetics parameters. The power transient in a reactor following a perturbation in the reactivity depends on the reactivity and on the delayed neutron and photoneutron groups. The characteristics of delayed neutron emission have been reported by Keepin [30]; those of photoneutron production have been reported by Bernstein [31].

The number of neutrons in each photoneutron group must be multiplied by the probability that the γ-rays producing them escape from the fuel assembly in which they were born. This probability varies from about 0.20 for heavy assemblies to about 0.50 for light assemblies. Even if all the γ-rays escape, the resulting photoneutrons are less than 10% as numerous as the delayed neutrons, and their effect on reactor oscillations and rapid transients is very small. It is only in calculations of heat generation in the reactor, more than two or three minutes after the reactor is shut down, that the photoneutrons make a significant contribution.

TABLE 5–4

REFLECTOR SAVINGS

Reflector thickness, cm	Heavy-water reflector, cm	Graphite reflector, cm
Zero	6	6
20	23	22
40	42	37
60	54	46
∞	73	55

The reactivity depends on the reactivity perturbation superimposed on the reactor and also on the resulting temperature changes of the various reactor components. These changes in turn depend on reactor hydraulics and power level [17].

5–3.3 Reactor design. *Lattice constants and reactor design.* The interplay between the physics constants of the reactor and the choice of design parameters for the reactor system can be summarized by noting that, at best, a natural uranium heavy-water lattice of infinite extent has a limited amount of excess reactivity. The design problem can then be viewed as one of determining the manner of "spending" this excess reactivity that is most successful in meeting design objectives. The excess reactivity can be "spent" on power distribution and leakage, on reactor control, on high power density, on corrosion resistance, and on long core life. The amount spent toward achieving any one of these objectives reduces the amounts available for the others.

Flux distribution and leakage. The amount of leakage of neutrons from the reactor depends on reactor size and flux distribution. Minimum leakage occurs when the power distribution is in the fundamental geometric mode of the reactor. The reactivity loss represented by this leakage is $M^2B_g^2$, in the one-group approximation, where M^2 is the migration area and B_g^2 is the geometrical buckling.

In a large reactor it may be desirable to flatten the power distribution to obtain a higher ratio of average-to-maximum power. For example, if enough neutron-absorbing material (poison) is inserted in a reactor to reduce the buckling in a central region to zero, and this "flattened" region is surrounded by a highly buckled region, the system will require more reactivity than a reactor of the same size in which the buckling is uniform throughout. The additional reactivity is required to provide the excess leakage neutrons and the neutrons that are absorbed in the poison In a reactor with a modest amount of flattening, the total reactivity associated with leakage from the reactor can be defined as

$$\Delta k_{\text{leak}} = \frac{\int M^2B^2\phi\, dV}{\int \phi\, dV} = M^2B_g^2b^2(1 - a),$$

where b^2 is the ratio of the buckling in the outer region to the geometrical buckling, and a is the fraction of the pile power generated in the flattened region. The total *additional* reactivity required for the flattened shape is $M^2B_g^2(b^2 - 1)$. The *additional* leakage reactivity is $M^2B_g^2[b^2(1 - a) - 1]$, and the reactivity associated with absorption in the poison is $M^2B_g^2b^2a$. The quantities $1/b^2$, a, and $\phi_{\text{avg}}/\phi_{\text{max}}$ are plotted in Fig. 5–23 for a cylindrical reactor with a height equal to its diameter. The central, flattened region has approximately the same shape as the reactor and extends over a

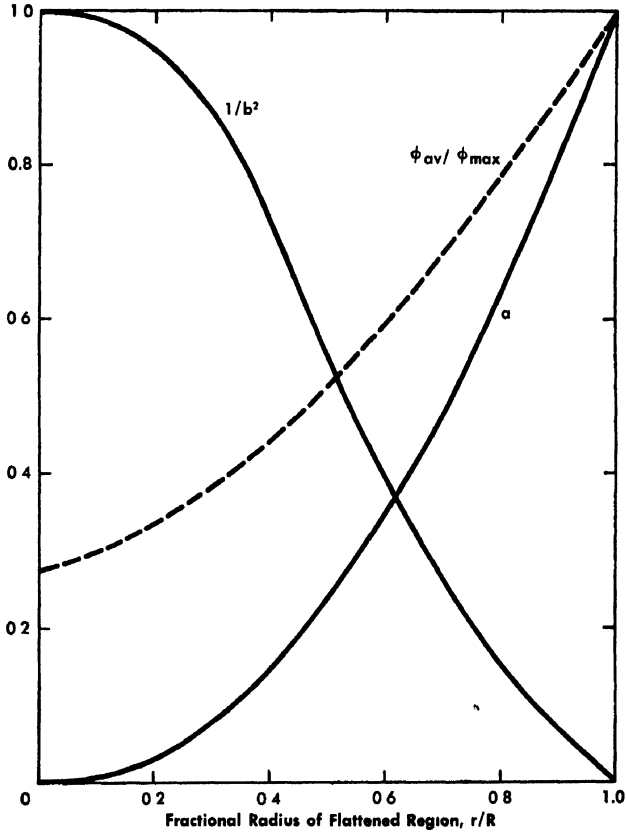

FIG. 5–23 Flux flattening characteristics of a cylindrical reactor. a = fraction of total power generated in flattened region. b^2 = buckling in outer region/geometrical buckling

fraction r/R of the pile radius and a slightly smaller fraction of the height. This flattened region is surrounded by a region of uniform buckling.

For example, if the power is flattened throughout half the radius of an unreflected reactor, the average-to-maximum power ratio is increased by 70%, from 0.30 to 0.51. The flattened region would contain 12% of the pile volume and produce 23% of the total power. The *additional* reactivity required is $0.82\ M^2B_g^2$, of which 49% is associated with leakage and 51% with absorption. This additional reactivity can amount to about 6.5% k for a 10-ft reactor and to about 2.9% k for a 15-ft reactor.

A useful approximate relation can be derived as follows. In the perturbation-theory approximation, the effect of a small absorber on k_{eff} is proportional to the square of the neutron flux, while the number of absorptions is proportional to the first power of the flux. In an unreflected

reactor of spherical or nearly spherical shape (such as a cube, or a cylinder with a height about equal to its diameter), $(\phi_0^2/\bar{\phi}^2) = 2(\phi_0/\bar{\phi})$, where ϕ_0 is the flux at the center of the pile. Thus, the total *additional* neutron loss to the pile by absorption plus leakage is approximately twice that by absorption alone. This implies the relation

$$ab^2 \cong b^2(1 - a) - 1 \qquad \text{or} \qquad a \cong \tfrac{1}{2}(1 - 1/b^2).$$

This relation holds fairly well for flattened regions extending up to half the pile radius and height.

Control During reactor operation, a minimum reserve of approximately 1% k must be held in the control rods to control the power level and power distribution and to override the xenon transients that accompany reductions in power.

The amount of reactivity that must be added to override the xenon transient after a reduction in power is shown in Fig. 5–24. It is generally not possible to maintain enough reserve reactivity in the control rods to override xenon in all circumstances; however, enough should be available to handle transients resulting from small, frequently encountered reductions in power. For example, as shown in the figure, 1% k in the control rods will allow xenon to be overridden after the power is reduced by about 40%. This relatively small amount of control used during operation should be dispersed throughout the reactor so that it can also be used for shaping the power distribution.

A larger amount of shim control must be provided to carry the reactor from the cold, clean condition to power operation. Reactivity is required

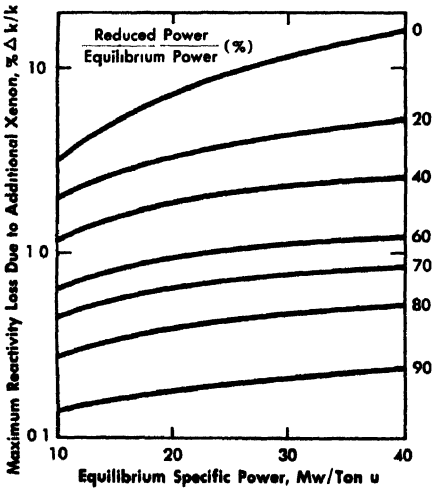

FIG. 5–24. Reactivity transients following a power reduction.

to compensate for fission-product poisoning and for the temperature coefficients. Equilibrium xenon and samarium poisoning require approximately 3.5% k. In a pressure tube reactor with a moderator temperature of 60°C, the loss of reactivity to the temperature coefficients is approximately 1.6% k For a pressure tank reactor with a 12-ft core and a moderator temperature of 200°C, the loss is about 7.8% k.

Power density It is desirable to operate the reactor at a high average specific power to minimize the investment and inventory per unit of power output. However, a high specific power generally results in higher fuel costs, more frequent shutdowns to change fuel, and a loss in reactivity because of high surface area, flattened flux shape, and high loss to xenon poison.

The reactor power can be limited by any one of several factors, and a reactor must not be grossly overdesigned with respect to any of these limits Commonly, there are limits on the fuel temperature to reduce the fuel failure rate, on the cladding temperature to minimize corrosion or softening of the cladding material, on the maximum heat flux to prevent burnout, and on the ability of the coolant system to remove heat from the reactor. For example, the tubular uranium element described in the first part of this chapter is designed for a maximum specific power of 40 Mw/ton, a metal temperature of 600°C, a zirconium cladding temperature of 320°C, and a maximum heat flux of 500,000 Btu/(ft²)(hr) [900,000 Btu/(ft²)(hr)].

If the power output is not limited by the temperature of the fuel and cladding, the amount of surface area required is determined from the maximum heat flux above which burnout will occur This burnout heat flux can be estimated from one of the formulas listed by Bonilla [32]

The reactor must be designed so that this burnout heat flux is not exceeded even during distortions of the power distribution, such as might occur from accidental misplacement of control rods or from an upset in the distribution of the xenon poison.

In order to operate at high specific powers, reactivity losses may be accepted that are associated with a higher surface-to-mass ratio of the fuel, with a flattened power distribution, and with a greater amount of xenon poisoning.

The reactivity loss associated with a higher surface-to-mass ratio of the fuel is made up of (1) a loss in thermal utilization produced by the higher cladding-to-uranium ratio, plus (2) a loss in resonance escape produced by the greater surface absorption. As an example, two fuel assembly designs that differ primarily in the surface-to-mass ratio will be compared. Let the first design consist of a single fuel tube about 3 inches in diameter and 0.4 inch thick, together with housing tubes and cladding, and let the second design consist of two concentric fuel tubes, each 0.25 inch

thick, that fit into the same outer housing tube and have the same total amount of uranium. The reactivity of each assembly can be calculated by the methods described in the previous sections. The reactivity of the double-tube assembly is found to be about 4% k lower than that of the single-tube assembly. The amount of reactivity required to maintain a flattened power distribution was discussed in a previous section.

The steady-state xenon poisoning depends on the specific power and upon ϵ and p [33]. For natural uranium heavy-water reactors, the maximum poisoning at high specific power is about 2.8% k At a specific power of 5 Mw/ton, the poisoning amounts to about 75% of the maximum and at 10 Mw/ton to about 87%.

Relation of reactor physics to corrosion resistance. A fuel-element failure can lead to the dispersal of radioactivity throughout the reactor system, inopportune shutdown, costly replacement of fuel elements, and even to damage of the reactor structure.

The frequency of fuel failures can be reduced by thicker fuel cladding and careful quality control. The hazards of a failure are much reduced when uranium oxide rather than metal is used as fuel. However, this course may result in a large reactivity loss.

If a small number of reactor shutdowns can be tolerated, it is sufficient to provide the kind of corrosion resistance that slows the rate of failure to allow time to detect and confirm the failure, schedule a reactor shutdown, and bring other units of the power network into operation Some combination of zirconium-uranium fuel alloy, proper heat-treatment of the fuel, and devices to detect fuel failure may result in a workable compromise.

If uranium oxide is used instead of uranium metal as the reactor fuel, the optimum (maximum buckling) lattice design will have about a 25% lower fuel-to-moderator ratio. The reactivity is decreased because of higher relative amounts of structural and cladding material, increased resonance absorption per uranium atom, and increased leakage associated with the higher migration area. On the other hand, p may be higher because of the smaller number of uranium atoms present. Figure 5–25 shows calculated bucklings as a function of lattice spacing for the metal assemblies described in the section below under *Application to reactor design*. The fuel in each of these assemblies is a tube 2 inches in diameter and 1/4-inch tick. Comparative bucklings are shown for oxide elements with tubes 0.4 inch thick that fit in the same housing tubes.

As shown in Fig. 5–25, the loss in cold, clean buckling in going from an optimum metal to an optimum oxide lattice is about 1.0 m^{-2}. This loss in buckling would represent only a small loss in k_{eff} for the pressure tank reactor, as the increased leakage would be compensated by the higher p. However, the buckling loss would correspond to a loss of about 3% k_{eff}

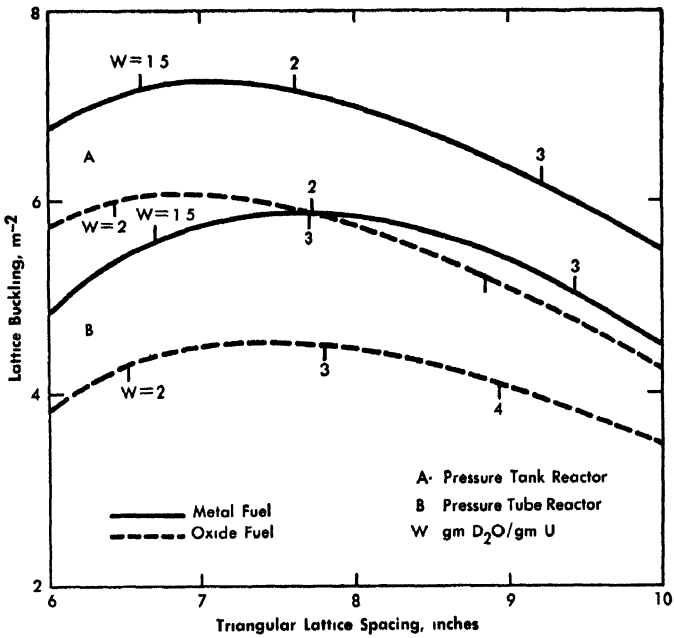

Fig. 5-25 Lattice bucklings with metal and oxide fuel elements.

in a pressure tube reactor, since it has a high relative absorption in the pressure tubes.

Because the oxide is only a little more than half as dense as uranium metal, using oxide instead of metal fuel will generally require more frequent fuel charging with the same exposure per ton of uranium.

The addition of relatively small amounts of zirconium to metallic uranium can reduce the rate of attack by water on the metal. The zirconium can be alloyed with the uranium or it can be in the form of very thin cladding on small uranium wires which are then pressed together.

An alloy of 2 w/o Zr in uranium reacts with hot water approximately one-fifth as rapidly as pure uranium. Adding this much zirconium results in a reactivity loss of only about 0.1% k. Corrosion tests on defective elements indicate that, with proper heat-treatment of the fuel alloy, it may be possible to operate several hours with a small hole in the cladding before the reactor must be shut down and the element discharged (see Section 5-2 and Reference 15).

Core life. Any excess reactivity above that required to control the hot, poisoned reactor can be used to extend the core life. The reactivity transient as a function of exposure was shown in Fig. 5-22 with p and moderator temperature as variable parameters. If radiation damage does not

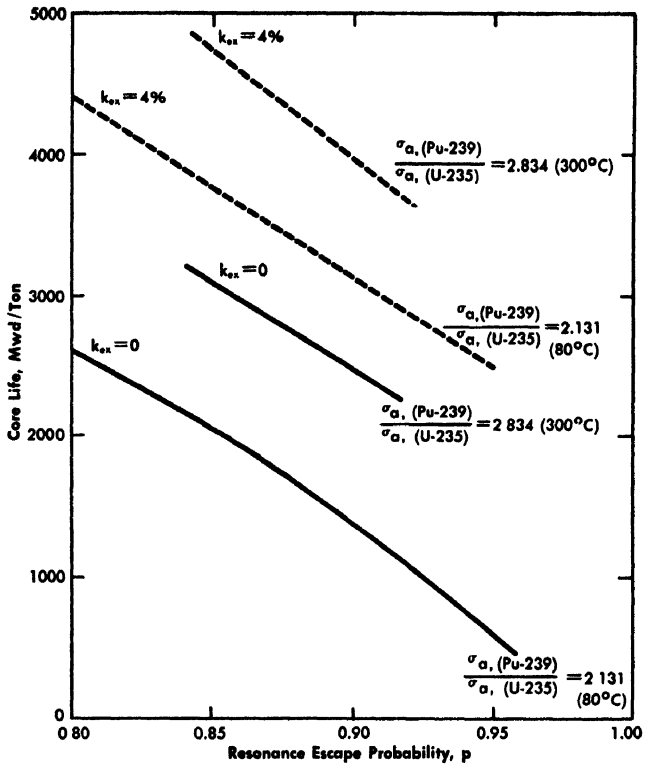

FIG 5–26. Reactivity life of reactor core.

limit fuel exposure, the core life may be defined as the exposure at which k falls below the minimum required to sustain operation. The core life is plotted in Fig. 5–26 as a function of p for moderator temperatures of 80 and 300°C and for initial values of the excess reactivity of 0 and 4%.

As may be seen from the figure, the core life is a more sensitive function of excess reactivity than of p. Consequently, increase in core life results, other things being equal, if p is increased to allow an equivalent increase in excess reactivity.

For a given value of excess reactivity, the life of the core is about 1000 Mwd/ton greater when the moderator temperature is 300°C than when it is 80°C, since the relatively higher Pu^{239} cross section increases the contribution of the plutonium to the reactivity. However, a higher moderator temperature ordinarily results in a lower excess reactivity. The net gain or loss in core life, as the moderator temperature is varied, depends on the other lattice parameters and on the size of the reactor, as well as on the fission cross section of Pu^{239} relative to that of U^{235}.

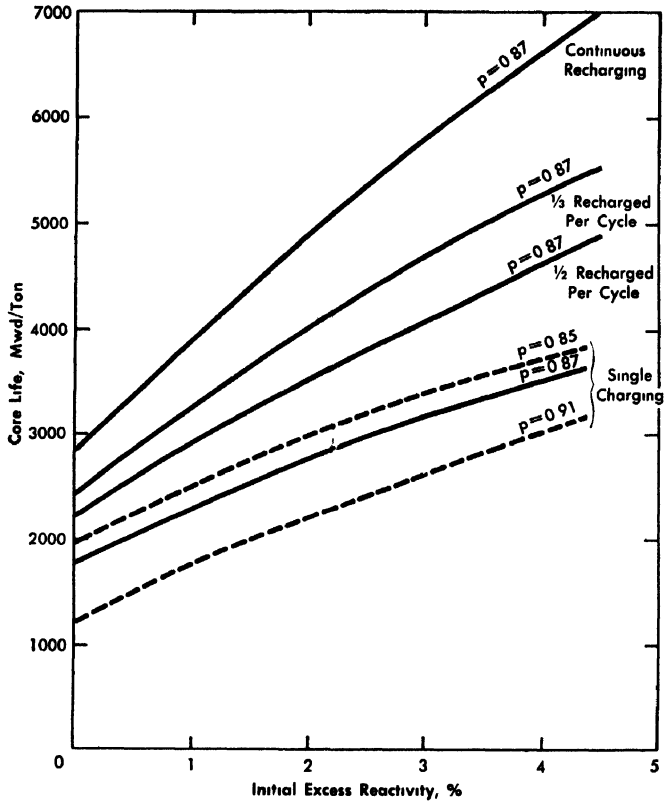

FIG. 5–27 Effect of multiple cycling on reactivity life of core

The maximum exposure of the fuel can be increased if a portion of the charge is periodically replaced by fresh fuel. In this manner spent fuel that by itself would provide a reactivity deficit can be balanced against fresh fuel of high reactivity. The advantage of multiple cycling in extending the average fuel exposure is shown in Fig. 5–27 The core life is shown as a function of initial excess reactivity for continuous recharging and for 1/3-, 1/2-, and full-load recharging. Continuous recharging approximately doubles the attainable fuel exposure. This fact places a premium on reactor designs that allow fuel assemblies to be recharged during operation [12].

Application to reactor design. By way of illustration, the methods discussed in the preceding sections will be applied to estimate lattice parameters of two representative reactor lattices: (1) a pressure tank reactor with the moderator at 207°C and with fuel elements in a 6.5-inch hexagonal lattice, and (2) a reactor with fuel assemblies in zirconium pressure tubes

TABLE 5–5

LATTICE PARAMETERS AND REACTIVITY BALANCES FOR REPRESENTATIVE REACTOR DESIGNS

	Pressure tank reactor	Pressure tube reactor
Core design		
Moderator temperature, °C	207	60
Lattice spacing, in.	6.5	7.8
Number of assemblies	340	225
Core radius, ft	5.2	5.1
Core height, ft	15.0	15.0
D_2O reflector thickness, ft	1.0	1.0
Fuel assembly design, in.		
Housing OD	2.96	3.36
Housing ID	2.90	3.16
Inner liner, OD	—	2.96
Inner liner, ID	—	2.90
Cladding, OD	2.06	2.06
Fuel, OD	2.00	2.00
Fuel, ID	1.49	1.49
Cladding, ID	1.43	1.43
Lattice parameters, cold		
η	1.327	1.327
ϵ	1.023	1.023
p	0.884	0.919
f	0.979	0.944
k_∞	1.175	1.178
L^2, m^2	0.0102	0.0152
τ, m^2	0.0129	0.0135
B^2, m^{-2}	7.15	5.89
Lattice parameters, hot		
η	1.307	1.323
p	0.859	0.918
f	0.946	0.912
k_∞	1.087	1.133
L^2, m^2	0.0153	0.0162
τ, m^2	0.0174	0.0138
B^2, m^{-2}	2.50	4.25

TABLE 5-5 (*Continued*)

	Pressure tank reactor	Pressure tube reactor
Reactivity balance, %		
Bare, cold, clean, $k_\infty - 1$	20.0	24.4
Loss to:		
Cladding and housings	1.6	4.8
H_2O in moderator (0.25%)	0.5	0.8
Leakage (cold, clean, $M^2B_0^2$)	4.9	6.1
Moderator temp., k_∞	5.5	1.3
Moderator temp., leakage	2.1	0.3
Xe + Sm	3.3	3.2
Excess k	1.1	7.1

in a 7.8-inch lattice with a moderator temperature of 60°C. These reactor designs were previously discussed in Section 5-2.

The fuel assemblies in the two examples are identical except for the heavy wall and insulation of the outer housing tube in the pressure tube design. The uranium fuel tube is 2.00 inches in outer diameter, 0.255 inch thick, and is clad with zirconium 0.030 inch thick. Table 5-5 lists comparative values of the lattice parameters and reactivity expenditures for these two designs.

Reactor stability. In designing control mechanisms and instrumentation of a power reactor, possible reactor instabilities must be taken into account. The control system, including the operator, must be capable of responding to any tendency toward spontaneous oscillations of the power level such as might result from an abrupt change in the power demand or in the control rod position, and the instruments and control devices must be distributed spatially in such a way that power distribution can be adjusted despite changes in xenon distribution.

Even though the temperature coefficients in a natural uranium heavy-water reactor are negative, the system may be unstable because of time lags between power changes and resulting changes in temperatures of the system. In general, a reactor will be stable if the coolant flows directly from the fuel channels into the moderator, so that a change in power level is followed quickly by an opposing reactivity change caused by the change in moderator temperature. Reactors in which the moderator is completely separate from the coolant are also stable, since a change in power demand does not affect the moderator temperature and therefore does not affect the reactivity.

However, if the coolant flows from the moderator into the fuel channels, the stability of the reactor system must be examined. In such a system, a change in power level results in an immediate change of coolant temperature, but the change in moderator temperature is delayed. The system is stable at low power levels so long as the negative temperature coefficients are small. Systems of this type, with large negative coefficients, may become unstable at high power levels.

The instability can be studied by solving the time-dependent equations relating the temperatures of the system to the reactor power and to the steam demand, together with the reactor kinetics equations. Even below the threshold for instability, small changes in power demand may lead to amplified oscillations that damp only slowly. The periods of the oscillations depend on the heat capacities and power levels. Typically, their length is of the order of one minute, or about twice the time required to pump all the coolant through the loop.

In a large reactor operating at sufficiently high flux levels, oscillations in power distribution can occur that are associated with a periodic redistribution of xenon poison [34]. These xenon oscillations will persist if the flux is greater than a threshold value which depends upon the size, flux distribution, and temperature coefficients of the reactor Even below this threshold, small perturbations in the xenon distribution, such as those due to control rod motion, may tend to be amplified into considerable power distortions.

Reactors may be subject to these oscillations if H^2/M^2 is of the order of 1000 or larger, where H is one linear dimension and M^2 is the migration area. For natural uranium heavy-water reactors, this size corresponds to a linear dimension of about 15 ft. Typical thermal neutron flux thresholds lie between 10^{13} and 10^{14} n/(cm^2)(sec) (2 5 to 25 Mw/ton), the range in which xenon burnup becomes important.

The oscillation periods are of the order of 30 hr; consequently there is time available to move control poisons to regulate the power distribution. Large reactors should be equipped with adequate devices to monitor and control power distributions. In a very large reactor, power monitors should be placed on a three-dimensional mesh with a pitch of approximately 10 migration lengths (about 5 ft in a natural uranium heavy-water reactor). Control poisons must be capable of regulating the power level in each region associated with such a monitor. The threshold is lower for a flat than for a sinusoidal power distribution, and is still lower if the flux dips in the center and divides the reactor into relatively isolated regions. Negative temperature coefficients increase the threshold for the xenon instability only if the temperature distribution changes in the same manner as does the power distribution.

5–4 Physics Data Relating to ThO_2-UO_2 Fueled Boiling Reactors*

5–4.1 Introduction. Since U^{233} has a high value of η in thermal fission, it may be possible to employ this fuel with D_2O moderator to achieve a very high conversion ratio, or possibly a net breeding gain. A heavy-water boiling reactor fueled with thorium and uranium oxides may be an attractive embodiment of this fuel-moderator system.

Evidence that oxide fuels resist attack by hot water and are capable of very high burnup has been supplemented by experience with the Borax IV reactor in the manufacture [7] and use [8] of urania-thoria fuel elements. It was originally anticipated that boiling reactors might be limited to power densities considerably lower than those of nonboiling pressurized water reactors. The excellent thermal performance of the Experimental Boiling Water Reactor (EBWR) and Borax IV alleviates concern over surface heat removal rates; it now appears that oxide fuels may place a different limitation on power density, arising from the poor thermal conductivity of the oxide Meanwhile, the first-recognized advantage of the boiling reactor—that it requires minimum operating pressure for a given steam temperature—remains This characteristic is more important for the heavy-water reactor, which must be large for good performance, than for reactors employing ordinary water for moderation

From the point of view of boiling-reactor design, thoria-urania has certain performance advantages, beyond those derived from the high value of η for U^{233}, over the use of urania alone In designing a boiling reactor there is a restriction not encountered in other reactor types—that of achieving a steam coefficient of reactivity which lies in a usable range. The value of this coefficient depends on the amount of resonance neutron absorption in the fertile material and, therefore, on the conversion ratio Because thorium has a higher ratio of thermal-to-resonance absorption than does U^{238}, the problems of reactor design are expected to be reduced

An experimental program has been started at Argonne National Laboratory to establish the nuclear properties of ThO_2-UO_2-D_2O systems. The initial results of this program and their application in planning modification of the EBWR to operate with urania-thoria and heavy water are summarized below.

5–4.2 Experimental results. Experiments have included both exponential and critical measurements; the fuel in both cases consisted of 0 234-inch diameter pellets of a fired mixture of ThO_2 and highly enriched

*This information was extracted from Reference 9 See also References 35 and 36.

UO_2 with a density of about 8.4 g/cm³. These pellets were 0.6 inch in height, and 100 were placed within a 0.241-inch ID, 0.309-inch OD aluminum tube to form a fuel rod 5 ft long. Pellets both with a 25:1 and a 50:1 atom ratio of thorium to U^{235} were available. The U^{235} content of the fuel rods averaged 12.04 and 6.025 g, respectively. For convenience in changing fuel, $3\frac{1}{8}$-inch square fuel rod holders were made, with end plates of perforated aluminum sheet having 5/16-inch diameter holes in a 3/8-inch triangular pattern, spaced by aluminum tubes at the corners. This permitted constructing a variety of lattices using a multiple of 3/8 inch for the lattice spacing. A fuel rod positioned in a holder is shown in Fig. 5–28. For the exponential measurement, the holders were always close packed (on 4-inch centers) in the exponential tank, and the desired fuel tube configuration was attained by suitable placement of fuel tubes in the holders. The measured diffusion area (L^2) of the system composed of D_2O and the close-packed array of empty fuel rod holders was 3110 ± 250 cm².

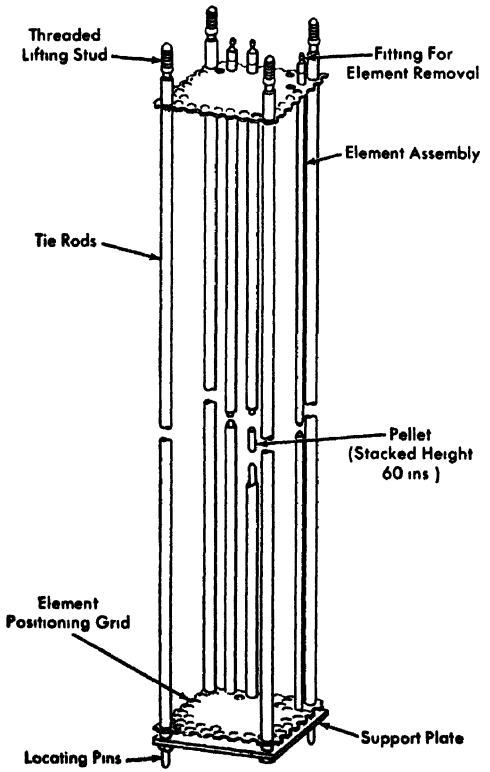

FIG. 5–28. Fuel rod holder. (Argonne National Laboratory)

TABLE 5–6

MATERIAL BUCKLINGS FOR SINGLE-ROD ThO_2-UO_2-D_2O LATTICES

Lattice spacing, a_0 (= $\frac{3}{8}$ in.)	$\frac{\text{Atoms Th}}{\text{Atom U}^{235}} = 25$, $B_m^2 \times 10^6$ cm^{-2}		$\frac{\text{Atoms Th}}{\text{Atom U}^{235}} = 50$, $B_m^2 \times 10^6$ cm^{-2}	
	Predicted	Observed	Predicted	Observed
$20a_0$	49	−26	−240	
17	159	77	−190	
14	331	158	−109	
12	502	343	−30	
10	745	558	86	
8	1095	849	262	65, 48*
7	1324	1060	385	
6	1594	1254*	535	202*
5	1903		713	
4	2227		905	643, 581*
3	2473	2012*	1030	812*
2	2250		734	555*

*Measured in 3-ft-diameter tank.

The measured bucklings from exponential experiments are given in Table 5–6. The lattices were all simple triangular ones with uniform rod spacing. In the table, center-to-center spacing is given in multiples of the minimum spacing (3/8 inch) provided by the rod holders. The measurements were made in tanks of 3- and 5-ft diameters. The estimated error of the measurements is $\pm 30 \times 10^{-6}$ cm^{-2} in the 5-ft tank, and about twice this amount in the 3-ft tank.

The table also gives values of buckling predicted by calculation with nuclear data available at the start of the experimental program. Values of the important quantities used were $\eta = 2.073$, $\tau = 125$ cm^2, and thorium resonance integral data reported [37] by Macklin and Pomerance.

A single lattice composed of clusters (3/8-inch spacing) of three 25:1 fuel pins with a 5¼-inch spacing between cluster points had a buckling of 709×10^{-6} cm^{-2}. Interpolation of experimental values for lattices of single fuel rods shows no major change in buckling due to self-shielding of the fuel rods. A temperature coefficient of

$$(1/B^2)(\Delta B^2/\Delta T) = -1.69 \times 10^{-3}/°\text{C}$$

TABLE 5–7

DATA FROM ThO_2-UO_2-D_2O CRITICAL EXPERIMENTS

Geometry of fuel:	Uniform	Uniform	Uniform	Slightly clustered	Fully clustered
Lattice spacing:	¾″ Triangular	1⅛″ Triangular	1½″ Triangular	¾″ Triangular, 4″ Pattern	⅜″ Triangular, 4″ Pattern
Volume fraction of constituents:					
D_2O	0.8462	0.9316	0.9615	0.8421	0.8379
Fuel	0.0882	0.0392	0.0221	0 0689	0.0667
Aluminum	0.0587	0.0261	0.0147	0.0836	0.0902
Void	0.0069	0.0031	0.0017	0.0054	0.0052
Area per fuel rod, in²	0.4875	1.0969	1.950	0.624	0.645
Range of $\frac{H, \text{ in.}}{R, \text{ in.}}$	$\frac{59.40}{10.158}$ to $\frac{40.668}{12.513}$	$\frac{58.355}{10.652}$ to $\frac{40.827}{12.687}$	$\frac{58.113}{12.849}$ to $\frac{50.925}{13.623}$	$\frac{60.00}{10.712}$ to $\frac{37.51}{14.381}$	$H_z = 42.475$ $H_x = H_y = 25.50$
B_g^2, $cm^{-2} \times 10^6$	1990	2090	1790	1890	
λ_H, axial reflector saving from flux plots	(9.0″)	(9.0″)	(9.0″)	9.0″	1780
λ_R from H, R, λ_H, and B_g^2	13.1″	12.0″	12.0″	13.2″	
τ by water worth, cm^2	172	175	176	178	
τ by fuel substitution, cm^2	147	151	155	155	
p, by fuel substitution	0.868	0.948	0.967	0.889	
p, by foil activation*	0.816				
center of fuel cluster				0.881	0.890
edge of control channel				0.940	
edge of fuel cluster					0.843
Effective resonance integral,† barns	20.5	20.1	21.9		
Thermal disadvantage factor	(1.10)	(1.20)	(1.30)		

*Corrected for 1, v contribution. †Using p from foil activation method.

TABLE 5–8

GENERAL CHARACTERISTICS OF A PROTOTYPE 60-MW BOILING REACTOR

Reactor type	Forced circulation, direct cycle, boiling D_2O moderated and cooled
Operating pressure, psig	600
Electrical power, kw	15,000
Core size:	
Height, ft	5
Diameter, ft	3.24
Fuel elements·	
Structural and clad material	Al-Ni
Thoria-urania rods, per cluster	28
Shroud diameter, in.	$2\frac{3}{8}$
Number of clusters required	66
Average power density, kw/liter of coolant	400
Average heat flux, Btu/(ft²)(hr)	271,000
Average steam voids in coolant, %	30

was observed over a range from 25 to 50°C for this system. For a lattice of single fuel rods in a $2\frac{3}{8}$-inch spacing, heating of water to 90°C yielded a temperature coefficient of -1.34×10^{-4}/°C.

Two types of critical experiments were made, employing (1) a uniform lattice spacing and (2) clusters of fuel tubes such as might be used in a core for the EBWR. Fuel rod holders were spaced on 4-inch centers and a group of 28 fuel rods, on 3/8-inch or 3/4-inch spacings, was placed at the center of each holder. The fuel in all cases contained the 25:1 ratio of thorium:U^{235}. Results are given in Table 5–7.

5–4.3 Characteristics of a 60-Mw (thermal) heavy-water thoria converter. One purpose of the experimental program on thoria-urania-heavy water lattices is to accumulate data for converting the EBWR to employ such lattices. The converted reactor (referred to as EBWR-II) is intended to be a small prototype reactor to demonstrate the direct-cycle boiling heavy-water concept. Considerations of heat transfer, hydrodynamics, and reactor safety interplay with those of reactor physics in the choice of design. The form of the EBWR-II oxide-fueled core will depend on the outcome of research in these fields and in mechanical and metallurgical engineering.

A fully clustered 28-rod fuel element (last column, Table 5–7), with a $2\frac{3}{8}$-inch diameter shroud, permits separating coolant and moderator.

TABLE 5–9

NUCLEAR CHARACTERISTICS OF A PROTOTYPE 60-MW BOILING REACTOR CALCULATED FROM CRITICAL EXPERIMENTS

	Prototype calculated value at 488°F	Experimental value at 68°F
Volume fractions		
Fuel	0.067	0.067
Al Structure	0.090	0.090
Void	0.005 (helium)	0.005 (air)
Coolant	0.128 (0.6216 g/cm³)	0.128 (1.11 g/cm³)
Stagnant Moderator	0.710 (0.888 g/cm³)	0.710 (1.11 g/cm³)
Enrichment		
Thorium atoms: U^{235} atoms	20:1	25:1
Core size		
Fuel height, in.	60	42 48
Diameter, in.	38.9	28 8
Reflector, in.:		
Top	12	0
Bottom	12	12
Radial	22.5	26.1
Lattice constants		
p	0.833	0.869
η, fuel	1.695	(1.641)
k_∞	1.361	(1.373)
L^2, cm²	45	(32)
τ, cm²	236	147
B^2, cm^{-2}	0.000961	0.001775
$\rho = 1 - \frac{(1 + L^2B^2)e^{\tau B^2}}{k_\infty}$ = reactivity available for fission products and burnup	0.038	0

This is necessary in forced-circulation, boiling heavy-water reactors because the volume of heavy water needed for moderation is more than is desired for cooling. The small diameter fuel rod favors heat transfer.

Heat-removal limitations in the EBWR facility require this prototype to be much smaller than the optimum heavy-water plant. However, a large plant can be expected to have coolant power densities, heat fluxes, and core heights comparable to those of the prototype. Fuel regeneration

performance data will be useful in designing a large thoria-heavy water system.

Tables 5–8 and 5–9 summarize the principal characteristics of this converter. The data in Table 5–9 were obtained in the critical experiments. Hence computation of lattice constants at 488°F involves mainly a calculation of changes in quantities rather than their absolute values.

An attractive feature of this design is the high coolant power density. In large plants which can employ a smaller separation of clusters it should be feasible to obtain high power with pressure vessels of reasonable size.

References

1 U S. Atomic Energy Commission, *AEC Authorizes Contract Negotiation with Carolinas Virginia Nuclear Power Associates on Proposed Reactor.* Press Release, Apr 25, 1958

2 J E Woolston, *The Canadian Study for a Full-Scale Nuclear Power Plant,* Report AECL-557, Atomic Energy of Canada, Ltd , January 1958

3 K Goldmann and C. K. Leeper, The Sodium-Cooled, D_2O-Moderated Reactor (SDR), 1958, paper presented at the Fourth Nuclear Engineering and Science Congress Held in Chicago, Ill , Mar. 17–21, 1958.

4 H P Iskenderian et al , Heavy Water Reactors for Industrial Power, Including Boiling Reactors, in *Proceedings of the International Conference on the Peaceful Uses of Atomic Energy,* Vol. 3 New York: United Nations, 1956 (P/495, p 157)

5 J M West et al , *The Experimental Boiling Water Reactor (EBWR),* USAEC Report ANL-5607, Argonne National Laboratory, May 1957.

6 H P Iskenderian, *20-Mw D_2O-Moderated Experimental Boiling Water Reactor Design Studies,* USAEC Report ANL-5685, Argonne National Laboratory, February 1957

7. J H. Handwerk and R. A Noland, Oxide Fuel Elements for BORAX-IV, in *Papers Presented at the Technical Briefing Session Held at Argonne National Laboratory, May 27–28, 1957,* USAEC Report TID-7535, Argonne National Laboratory, 1957.

8 B Maxon et al , Argonne National Laboratory, 1958. Unpublished

9. W C Redman et al., Properties of Exponential and Critical Systems of Thoria-Urania and Heavy Water and Their Application to Reactor Design, paper prepared for the Second International Conference on the Peaceful Uses of Atomic Energy, Geneva, 1958 (P/600)

10 P J. Selak and J. Finke, Heavy Water, A Review of Processes and Plants for Large-scale Production, *Chem. Eng. Progr.* **50,** 221–229 (1954).

11. A. R. Kaufman et al., Zirconium Cladding of Uranium and Uranium Alloys by Coextrusion, in *Fuel Elements Conference, Paris, November 18–23, 1957,* USAEC Report TID-7546, Nuclear Metals, Inc., 1958. (Book 1, p. 157)

12. W. B. LEWIS, *Low Cost Fueling Without Recycling*, Report DR-39, Atomic Energy of Canada, Ltd., 1956.

13. D. F. BABCOCK, *Power Reactor Studies, Quarterly Progress Report for February, March, and April, 1957*, USAEC Report DP-232, E. I. du Pont de Nemours & Company, 1957.

14. D. F. BABCOCK, *Power Reactor Studies, Quarterly Progress Report for May, June, and July, 1957*, USAEC Report DP-245, E. I. du Pont de Nemours & Company, 1957.

15. D. F. BABCOCK, *Power Reactor Studies, Quarterly Progress Report for August, September, and October, 1957*, USAEC Report DP-265, E. I du Pont de Nemours & Company, 1957

16. D. F. BABCOCK, *Power Reactor Studies, Quarterly Progress Report for November, December, and January, 1958*, USAEC Report DP-285, E. I du Pont de Nemours & Company, 1958

17 G. DESSAUER, Physics of Natural Uranium Lattices in Heavy Water, paper prepared for the Second International Conference on the Peaceful Uses of Atomic Energy, Geneva, 1958. (P/590)

18 I. KIRSHENBAUM, *Physical Properties and Analysis of Heavy Water*, National Nuclear Energy Series, Div III, Vol 4A New York: McGraw-Hill Book Company, Inc , 1951.

19 J. R HEIKS et al , *The Physical Properties of Heavy Water from Room Temperature to 250°C*, USAEC Report MLM-934, Mound Laboratory, Jan 12, 1954.

20 E CRITOPH, *Comparison of Theory and Experiment for Lattice Properties of D_2O-U Reactors*, Report CRRP-655, Atomic Energy of Canada, Ltd , July 26, 1956.

21. J. W. WADE, *Neutron Age in Mixtures of Light and Heavy Water*, USAEC Report DP-163, E I du Pont de Nemours & Company, June 1956

22. D. J. HUGHES and J A HARVEY, *Neutron Cross Sections*, USAEC Report BNL-325, Brookhaven National Laboratory, July 1, 1955; and supplements

23 A. AMOUYAL and P BENOIST, Nouvelle Méthode de Détermination du Facteur d'Utilisation Thermique d'une Cellule, *J. Nuclear Energy* **6**, 79 (1957).

24. B. I. SPINRAD, Fast Effect in Lattice Reactors, *Nuclear Sci and Eng.* **1**, 455 (1956).

25 F L. FRIEDMAN and A. WATTENBERG, *Age of Fission Neutrons in D_2O*, USAEC Report CP-3453, Argonne National Laboratory, 1946.

26 S. GLASSTONE and M C EDLUND (Eds), *The Elements of Nuclear Reactor Theory*. Princeton, N J.: D Van Nostrand Co., Inc , 1952.

27. M V. DAVIS, Resonance Absorption of Neutrons by Uranium Cylinders, *J. Appl. Phys.* **28**, 250 (1957).

28. G. W RODEBACK, *Temperature Coefficients of Uranium and Thorium Resonance Integrals*, USAEC Report NAA-SR-1641, North American Aviation, Inc., Sept. 1, 1956.

29. B. L. IOFFE and L. B OKENN, Long Term Reactivity Changes in Nuclear Reactors, *Atomnaya Energ* **1**, 80 (1956).

30. G. R. KEEPIN et al., Delayed Neutrons from Fissionable Isotopes of Uranium, Plutonium, and Thorium, *Phys. Rev.* **107**, 1044 (1957).

31. S. BERNSTEIN et al., *Yield of Photoneutrons from U-235 Fission Products in Heavy Water*, USAEC Report MonP-172, Oak Ridge National Laboratory, Sept 24, 1946

32 C. F BONILLA, *Nuclear Engineering*. New York: McGraw-Hill Book Company, Inc., 1957.

33. H. K CLARK and J. C ENGLISH, *Xenon Tables*, USAEC Report DP-200, E. I. du Pont de Nemours & Company, May 1957.

34. D RANDALL and D. S ST. JOHN, Xenon Spatial Oscillations, *Nucleonics* **16**(3), 32 (1958).

35. W. J. STURM et al, Exponential Studies of a Ceramic Mixture Thoria and Urania in Heavy Water Moderator, paper presented at the Second Winter Meeting of the American Nuclear Society, New York, Oct 28–30, 1957 (Session 2-2)

36. W. C REDMAN et al, Heterogeneous Critical Experiments with ThO_2, UO_2, and D_2O, paper presented at the Second Winter Meeting of the American Nuclear Society, New York, Oct 28–31, 1957 (Session 2-8)

37. R. L. MACKLIN and H. S POMERANCE, Resonance Capture Integrals, in *Proceedings of the International Conference on the Peaceful Uses of Atomic Energy*, Vol 5. New York: United Nations, 1956 (P/833, p. 96)

TABLE 5–2

CHARACTERISTICS OF NATURAL URANIUM-FUELED POWER REACTORS

General description

Reactor type: thermal neutron, D_2O moderated, heterogeneous
Fuel type: natural uranium metal
Moderator: heavy water (99.75 mol.% D_2O, 0.25 mol.% H_2O)
Coolant: heavy water (99.75 mol.% D_2O, 0.25 mol.% H_2O)
Cladding: zirconium or Zircaloy-2
Housing tubes: zirconium or Zircaloy-2
Radial reflector: 1-ft thick heavy water
Axial reflector: 1-ft thick heavy water
Active length of core: 15 ft
Steam system: saturated steam (H_2O) produced in boilers

	Reactor study cases			
	Case A	Case B	Case C	Case D
General plant performance				
Reactor type	Pressure vessel	Pressure vessel	Pressure vessel	Pressure tube
Reactor thermal power, Mw	435	439	479	433
Gross electrical power, Mw	106	107	106	106.3
Net electrical power, Mw	100	100	100	100.1
Over-all plant efficiency, %	23.0	22.8	20.9	23.1
Minimum operating power,† Mw	340	355	115	104
General reactor core characteristics				
Uranium inventory, tons	29.2	26.6	26.6	19.3
D_2O inventory, tons	131	123	133	117
Design exposure, Mwd/ton	3250	3200	4500	3500
Maximum heat flux, watts/cm^2	229	270	241	279
Average specific power, Mw/ton	14.9	16.5	18.0	22.4

(*continued*)

	Reactor study cases			
	Case A	Case B	Case C	Case D
Maximum specific power, Mw/ton	34.4	38.6	36.0	41.5
Maximum neutron flux, n/(cm²)(sec)	1.20×10^{14}	1.35×10^{14}	1.26×10^{14}	1.45×10^{14}
Fuel assembly				
Housing tube dimensions, in.:				
Outside diameter	2.960	—	3.060	3.360
Inside diameter	2.900	—	3.000	3.160
Inner liner outside diameter	—	—	2.960	2.960
Inner liner inside diameter	—	—	2.900	2.900
Insulation thickness, in.	None	None	0.02 D_2O	0.1 MgO
Housing tube design pressure, psig	—	100	100	1000
Fuel element dimensions, in.:				
Outside diameter	2.030	2.030	2.030	2.030
Inside diameter	1.497	1.497	1.497	1.497
Cladding outside diameter	2.060	2.060	2.060	2.060
Cladding inside diameter	1.467	1.467	1.467	1.467
Maximum surface temperature, °C	295	316*	317*	320
Maximum uranium temperature, °C	470	496	498	531
Lattice parameters				
Lattice spacing, in.	6.50	6.50	6.50	7.8
Number of fuel assemblies	340	310	310	225
Loaded radius, ft	5.23	5.0	5.0	5.12
Cold buckling, $cm^{-2} \times 10^{-6}$	692	726	657	575
Hot buckling, $cm^{-2} \times 10^{-6}$	243	254	442	403
Hot excess reactivity	0.0104	0.0096	0.0528	0.0568
Gross average-to-maximum flux	0.434	0.427	0.499	0.541

(*continued*)

TABLE 5–2 (*Continued*)

	Reactor study cases			
	Case A	Case B	Case C	Case D
Coolant system data				
Number of coolant loops	4	4	4	4
Coolant flow, gpm	60,000	60,000	60,000	60,000
Coolant supply pressure, psia	562	653	746	790
Coolant inlet temperature, °C	205.9	205.2	223.0	230.0
Average coolant outlet temperature, °C	232.7	232.2	248.1	254.6
Maximum coolant outlet temperature, °C	241.4	245.1	254.4	262.2
Inside coolant velocity, fps	17.8	48.3	17.0	24.6
Outside coolant velocity, fps	12.5	2.1	11.9	15.5
Total pressure drop, psi	34.0	78.7	33.1	37.9
Reactor vessel				
Design pressure, psig	711	829	951	Atmospheric
Internal diameter of shell, ft	13.2	12.7	12.7	12.9
Over-all length of shell, ft	41	41	41	30
Shell thickness, in.	3¼	3⅞	4	½
Approximate thickness of top head,‡ in.	7	8¼	8⅝	—
Approximate thickness of bottom head,‡ in.	8¼	9¾	10¼	—
Material of construction	Clad CS§	Clad CS§	Clad CS§	SS♦
Moderator system				
Average moderator temperature, °C	207	213	60	60
Moderator pressure, psia	547	660	693	Atmospheric
Saturation temperature, °C	247	258	261	101.6
Pile power lost to moderator, %	—	—	15	8

(*continued*)

	Reactor study cases			
	Case A	Case B	Case C	Case D
Heat exchange area for cooling moderator, ft²	—	—	7400	3870
Moderator flow, gpm	—	—	7750	4000
Pumps				
Water hp for pumping coolant	1130	2520	1100	1180
Water hp for pumping moderator	—	—	140	390
Water hp for pumping H_2O, miscellaneous	5000	5000	5000	5000
Pumps per coolant loop	1	1	1	1
Material of D_2O pumps	SS	SS	SS	SS
Steam generators				
Steam produced, lb/hr	1.46×10^6	1.47×10^6	1.60×10^6	1.33×10^6
Steam temperature, °C	186	186	203	210
Steam pressure, psia	167	167	240	277
Heat-transfer area in boiler, ft²	32,700	32,300	31,350	30,800
Material of tubes	SS	SS	SS	SS
Material of shell	CS▲	CS	CS	CS

†Level to which the design power can be reduced instantaneously without causing shutdown by xenon poisoning.
*Local boiling occurs on surface.
‡Does not include ¼-inch thickness of stainless steel cladding.
§Carbon steel clad with stainless steel.
♦Stainless steel
▲Carbon steel

TABLE 5–3

CHARACTERISTICS OF THE HEAVY-WATER COMPONENTS TEST REACTOR (HWCTR)

Reactor type	
Fuel: enriched uranium assemblies	93 w/o U^{235}
Fuel: test assemblies of natural uranium	Nat. U-2 w/o Zr
Moderator temperature, °C	239
Coolant	D_2O
Pressure resisting unit	Vessel or shell
Type of housing	Thin tube
Cladding and housing material	Zircaloy-2
Over-all characteristics	
Reactor power, Mw	61
Gross electric power, Mw	Zero
Natural uranium in reactor, kg	625
Enriched uranium in reactor, kg	26
Total D_2O inventory, tons	29.0
Coolant supply pressure, psia	1,000
Average coolant temperature, °C	226
D_2O coolant flow, gpm	9,600
Minimum operating power,* Mw	Zero
Design exposure, natural U, Mwd/ton	3,000
Design burnup, enriched U, %	50
Enriched fuel assembly	
Housing OD, in.	2.960
Housing ID, in.	2.900
Cladding OD, in.	2 300
Fuel OD, in.	2.240
Fuel ID, in.	2.060
Cladding ID, in.	2.000
Clad target OD, in.	1.080
Fuel cladding thickness, in.	0.030
Fuel length, ft	10
Weight of U^{235}, kg/ft	0.108
Housing design pressure, psig	100
Number of fuel assemblies	24
Coolant inlet temperature, °C	214
Coolant outlet temperature, °C	236
Moderator outlet temperature, °C	239
Inside coolant velocity, fps	17.0
Outside coolant velocity, fps	17.0
Maximum heat flux, watts/cm^2	211
Maximum sheath temperature, °C	286

Maximum fuel temperature, °C	433
Specific power, average,† Mw/ton	8.23
Specific power, maximum,† Mw/ton	13.10
Power per assembly, Mw	1.40
Coolant flow per assembly, gpm	232

Test assembly‡

Same dimensions as for fuel assembly of Case A, Table 5-2.	
Housing design pressure, psig	100
Number of fuel assemblies	12
Coolant inlet temperature, °C	214
Coolant outlet temperature, °C	236
Moderator outlet temperature, °C	239
Inside coolant velocity, fps	24.6
Outside coolant velocity, fps	17.3
Maximum heat flux, watts/cm^2	358
Maximum sheath temperature, °C	318
Maximum fuel temperature, °C	595
Specific power, average, Mw/ton	35
Specific power, maximum, Mw/ton	55
Power per assembly, Mw	1.80
Coolant flow per assembly, gpm	300

Physics parameters

Neutron balance and lattice design	pp. 25–28, DP-265 [6]

Reactor vessel

ID of shell, ft	7.0
IL of shell, ft	30
Shell thickness, in. §	4.0
Material of construction	Stainless steel clad carbon steel
Design pressure of shell, psi	1,500

Coolant system

Number of coolant loops	2
Total flow of coolant, gpm	9,600
Coolant supply pressure, psia	1,000
Reactor inlet temperature, °C	214
Reactor outlet temperature, °C	239
Total pressure drop, psi	42.1

Moderator system

Average temperature, °C	238
Saturation temperature, °C	285
Pile power generated in moderator, controls, and shields, %	10

(*continued*)

TABLE 5–3 (*Continued*)

Pumps	
Water hp for pumping coolant	235
Water hp for miscellaneous uses	50
Total water hp	285
Pumps per coolant loop	1
Material of coolant pump	Carbon steel
Heat exchangers, light-water cooled	
Total heat-transfer area, ft^2	2,000
Material of tubes	Stainless steel
Material of shell	Carbon steel
Flow to heat exchangers, gpm	4,400
Inlet water temperature, °C	20
Outlet water temperature, °C	74
Control and safety assemblies	
Number of control clusters	1
Number of rods in cluster	6
"Black" diameter of rods, cluster, in.	0.8
Number of rods in ring	12
"Black" diameter of rods, ring, in.	1.25
Number of safeties	6
"Black" diameter of safeties, in.	0.8
Total coolant flow for controls, gpm	255
Heat generation in side shield	
Neutron, Mw	0.67
Gamma, Mw	0.57
Heat generation in top shield	
Neutron, Mw	0.047
Gamma, Mw	0.024

*Level to which design power can be reduced instantaneously without causing shutdown by xenon poisoning.

†Expressed in the number of Mw that would be produced by a ton of natural uranium, if the natural uranium were placed in the same flux as the enriched uranium.

‡The hydraulic and thermal conditions are the most severe test conditions to which the natural uranium assemblies may ever be exposed. The temperature and heat fluxes are considerably higher than the corresponding design values listed in Table 5-2.

§Does not include a ¼-in. thickness of stainless steel cladding.

CHAPTER 6

GAS-COOLED REACTORS

6–1. Introduction

There are five classes of characteristics which are important in a heat-transfer medium as a reactor coolant: (a) compatibility with other reactor materials, (b) behavior under irradiation, (c) neutron absorption and moderating properties, (d) temperature limitations, and (e) heat-transfer and heat-transport characteristics, No known coolant can be rated as "excellent" in all categories Further, although these coolant characteristics determine to a large degree the design and performance of the reactor using a given coolant, it is obviously not possible to rate the importance of the different characteristics relative to one another, and it is therefore impossible to determine which are the "best" coolants on the basis of these characteristics alone. Rather, if one is to evaluate the usefulness of a given coolant at any given stage in the development of reactor technology, one must design the best possible reactor using the coolant and compare its cost and performance with those of the best reactors using other coolants.

All the gaseous reactor coolants presently under consideration are characterized by high temperature capability, negligible neutron moderating effect (at practical pressures), and relatively good resistance to radiation damage. Furthermore, although they differ from one another in thermal properties, they do not differ by orders of magnitude. These similarities are great enough to allow the discussion of gas-cooled reactors as a single class. This class of reactors is characterized by the use of a moderator in the solid or liquid form, and by temperature limits which are not inherent in the coolant itself, but are set by the limitations of other materials or by considerations of materials compatibility.

A further characteristic results from the heat-transfer and heat-transport properties of gaseous coolants. It is an oversimplification to say categorically that gaseous coolants are inferior in these properties, for many writers have pointed out that quite high rates of heat exchange per unit volume can be achieved with gaseous coolants if suitably designed heat-exchange surfaces can be used. It can be said, however, that the removal of large amounts of heat from large reactor volumes with gases requires either the penetration of the volume by rather large flow passages or the use of rather high gas pressure. Further, the attainment of high

heat fluxes at the heat-transfer surfaces requires either rather large temperature differences or rather high flow velocities and pressure gradients. At the present stage of reactor development, these characteristics do represent important limitations, and the specific power and power densities of gas-cooled reactors tend to be rather low.

The economic importance of achieving high heat-exchange performance will vary with other characteristics of the reactor. A low specific power with respect to the fuel (kilowatts per kilogram of fuel) may be economically acceptable if the fuel (including fabrication) is cheap enough that a large fuel inventory does not represent an unreasonably large capital investment per kilowatt of power capacity. Thus low specific power may be acceptable for a natural-uranium reactor, but unacceptable for a reactor which must employ fuel of higher enrichment. Similarly, if an expensive moderator is employed, the reactor power output per unit quantity of moderator must be sufficiently large that the moderator does not represent an unreasonably large capital investment per unit of power capacity. The economic significance of power density, as distinguished from specific power, is less easy to assess. It is certainly true that the capital cost of a nuclear plant of a given type will increase with its physical size, but it certainly cannot be said that the specific capital costs (dollars per kilowatt of capacity) of plants of differing types exhibit a simple relationship to the physical size of the plant per kilowatt of capacity It is sufficient here to say that the limitations on power density and specific power in gas-cooled reactors and their associated heat-exchange equipment are rather generally recognized as very important ones, and that improvement of these characteristics is effective in improving the economic performance of such reactors.

The earliest post-war work in the United States on gas-cooled power reactors was done in the period 1945–1947, during which time a substantial design and development program was carried out on a high-temperature helium-cooled power reactor [1]. This effort represented a frontal attack on the problem of efficient nuclear power generation, based on the reasoning that in the long run the best power reactors must prove to be those which combine excellent neutron economy with really high temperature capabilities. The concept utilized helium as the coolant, beryllium oxide as moderator (with graphite as an alternate), and fuel elements in which the fuel was diluted by moderator to increase the heat-transfer surface, to improve the thermal and mechanical properties of the fuel, and to "dilute" the effect of fission damage. Means of accomplishing the nuclear and thermal objectives without allowing fission products to escape from the fuel elements into the coolant stream were not, and still are not, known. The difficulties anticipated from the contamination of the coolant circuit, in addition to the uncertainties which existed in a number of areas

of the design at that early stage of power reactor technology, caused the project to be dropped after completion of the preliminary design, and the effort to be transferred to reactor types which gave promise of quicker development to a useful stage. The primary result of the latter effort has been the development of the water-cooled power reactors—boiling and nonboiling—which presently make up the majority of the power and propulsion reactors in the United States. Meanwhile the British development of the Calder Hall reactor type has demonstrated the type of performance that can be achieved if one pursues the concept of gas cooling with good neutron economy but lowers the objectives on thermal performance to the point where they can be met by fuel elements which are jacketed with "conventional" materials of low neutron absorption.

In the interim since 1947 some development of gas-cooled reactors for special purposes [2–4] has been carried out in the United States, and occasional conceptual designs for "nonmetallic" high-temperature reactors have been described (e.g., Reference 5), but work on large central-station plants of the gas-cooled type has been limited to general research and development. It has recently been decided that the gas-cooled concept should be re-examined in the light of the continuing development of reactor and nuclear fuel technology. The first step in such an examination should, of course, be an appraisal of existing gas-cooled types, and several evaluation studies [6,7,11,12] have been carried out under the sponsorship of the United States Atomic Energy Commission. Obviously, the production of a reliable evaluation of this sort is difficult and conclusions must be subject to some uncertainty; yet it does seem clear that the gas-cooled reactor of the Calder Hall type is not outstandingly attractive for the United States unless it has potentialities for improvement which are greater than those that might be expected from incremental design improvements The shortcoming of the reactor type is the high capital cost, both for the reactor proper and for the associated energy-conversion equipment This high cost may be attributed to the temperature limitations of the reactor materials and to the low power density, which, in turn, is itself related to the temperature limitations.

If we start with the presently operating type of gas-cooled reactor, characterized by graphite moderator, metallic uranium fuel, magnesium alloy jackets, and carbon dioxide coolant, and investigate possible changes of increasingly greater degree, the series of possibilities runs about as follows:

(1) Low-cross-section materials of higher temperature capability may be developed for fuel-element jackets. The possibilities appear to be beryllium and zirconium, or alloys in which these elements are major constituents. The technical feasibility of such jackets has not yet been established, and the economic attractiveness is, of course, unknown. The

temperature increases which may be utilized are relatively modest so long as uranium metal (or any of the known alloys of uranium metal with low-cross-section metals) is used as fuel, since the uranium metal temperature is not far below its permissible limit in present gas-cooled designs.

(2) If the higher temperature jackets discussed above are developed, their full temperature capabilities may be realized by changing from metallic uranium fuel to a nonmetallic compound of higher temperature performance. The most immediate possibility is UO_2. The lower uranium density in the oxide, relative to metallic uranium, causes a decrease in the maximum attainable reactivity. It is questionable whether an economically attractive gas-cooled reactor of the graphite-moderated type can be built utilizing natural uranium in the oxide form. The enrichment required for an attractive design would, however, be quite low, and it would be feasible, from the reactivity point of view, to operate such a reactor with natural uranium feed if plutonium were recycled

If substantial increases of coolant temperature above current values were obtained, the compatibility of CO_2 and graphite would be questionable, and protection of the graphite or change of coolant would be necessary. If the latter course were adopted, helium would probably be the preferred coolant.

(3) The goals of very high neutron economy and operation on natural uranium may be deferred, and "conventional" materials of high temperature capability and relatively high neutron absorption may be employed for fuel jackets, along with nonmetallic fuel slugs. The most obvious combination is a UO_2 element with a steel jacket. Again the attainment of the full temperature capability probably precludes the use of CO_2 with unprotected graphite. In addition to the improvement in coolant temperature which is achieved in this way, a very important increase in power density is possible: part of the increase results from the higher coolant outlet temperature itself, and part results from the higher fuel/moderator ratios which can be used with enriched fuel.

The enriched fuel approach results in a very substantial reduction of capital cost of the nuclear plant. The associated penalties are the use of more expensive fuel and a complex fuel cycle. To minimize the economic effects of these penalties it is necessary that the fuel lifetime be as long as possible Fortunately, UO_2 gives promise of quite long irradiation lifetime.

(4) Moderators other than graphite may be employed. Two possibilities are beryllium oxide and heavy water.

BeO has a much higher moderating power than graphite and, from the point of view of reactor physics, permits much higher power densities. Its mechanical properties are rather poor, and it cannot be considered a proven material for reactors of long lifetime requirements, although it has

been used as the moderator for a high-temperature reactor of relatively short life [8,9].

D_2O also has higher moderating power than graphite, and the lowest neutron-absorption cross section of all moderators. Hence both power densities and reactivity are inherently higher than with graphite moderation. All the schemes mentioned above for improving high-temperature performance of fuel elements apply to the D_2O-moderated reactor, but it may be said that, in general, a D_2O-moderated reactor can tolerate a lower nuclear performance of the fuel element at a given fuel enrichment than can the graphite-moderated reactor.

D_2O, a low-boiling-point liquid, must be insulated from the high-temperature gas coolant. Insulation and isolation barriers, of course, increase neutron absorption somewhat. The liquid state of the moderator may, however, be turned to advantage, for it makes possible the practical design of a pressure-tube reactor, with each fuel element and its coolant passage in a separate pressure tube, passing through the moderator and cooled by it. Among other advantages, this arrangement eliminates the reactor pressure vessel and its restrictions on reactor size and coolant pressure.

The present United States effort on gas-cooled central-station power reactors is focused on two major types, which between them encompass most of the approaches discussed above. Graphite-moderated reactors have been studied by the Oak Ridge National Laboratory and by Kaiser Engineers (with ACF Industries), under contract to the United States Atomic Energy Commission [10–14]. These studies indicate that the most promising immediate approach to a more economic reactor of the graphite-moderated type is through the use of enriched uranium oxide fuel elements with steel jackets. The second type is a heavy-water moderated, pressure-tube type currently under development by the General Nuclear Engineering Corporation for the East Central Nuclear Group,* which is the basis of a proposal by the East Central Nuclear Group and the Florida West Coast Nuclear Group† for a joint research and development effort with the United States Atomic Energy Commission for the construction of a 50-Mw (electrical) prototype.

---

*Member companies of the ECNG are: American Electric Power Service Corp (formerly American Gas & Electric Service Corp); the Cleveland Electric Illuminating Co.; Columbus & Southern Ohio Electric Co.; the Dayton Power & Light Co.; Indianapolis Power & Light Co.; Louisville Gas & Electric Co; Ohio Edison Co.; Pennsylvania Power Co.; Southern Indiana Gas & Electric Co; and the three principal operating companies of the West Penn Electric System: Monongahela Power Co., the Potomac Edison Co., and West Penn Power Co.

†Member companies of the FWCNG are Florida Power Corporation and Tampa Electric Company.

These approaches and their limitations will be discussed in some detail. In the two sections immediately following, the aspects of gas-cooled reactors that can be treated in a general way are discussed: heat transfer, coolant gases, and fuel elements. In following sections, characteristics of graphite-moderated reactors and D_2O-moderated reactors are discussed separately under the appropriate headings. Results of design and cost studies on graphite-moderated reactors are summarized, and general characteristics of the D_2O-moderated reactor are presented.

6–2. Heat Transfer and Choice of Coolant*

It is the purpose in this section to point out certain simple heat transfer and flow relationships that affect design of gas-cooled reactors, to present relationships relevant to heat-transfer performance of different gaseous coolants, and to consider the influence of heat transfer and other factors on choice of coolants. More detailed heat-transfer calculations, for a specific reactor design, are given in Reference 10.

6–2.1 Heat removal from a single channel. It is convenient to consider first the relationships for an individual fuel channel through which coolant gas flows in contact with the heat-transfer surfaces of one or more fuel elements of definable design. The heat output must satisfy the heat balance equation:†

$$H = \rho V A c_p (T_o - T_i). \tag{6–1}$$

It is evidently desirable to extract maximum heat from a coolant channel of given flow area, since greater flow area means greater neutron leakage. The heat output per channel is proportionate to the temperature rise $(T_o - T_i)$ across the whole channel. To realize high power density and keep pressure loss small, the coolant channels (and hence the reactor core) should be short. Again, the limitation is set by neutron leakage.

To fix the reactor inlet gas temperature T_i the over-all power-plant performance and the reactor heat-removal characteristics are considered together. Lowering T_i increases reactor heat output for a given mass flow of coolant and reduces the pumping power per unit of heat output. On the other hand, more heat-exchange surface is needed in steam generators and feedwater heaters, operating steam pressure is less, and steam cycle efficiency is lower. The design value of T_i is chosen to give lowest over-

*By M. F. Valerino, GNEC.

†Symbols used in the following equations are defined in Table 6–1.

TABLE 6–1

SYMBOLS USED IN HEAT-TRANSFER ANALYSIS

Symbol	Definition	Units
A	Flow area	ft^2
c_p	Constant-pressure specific heat of gas	Btu/(lb)(°F)
d	Equivalent diameter of flow passage	ft
F	Friction factor	dimensionless
g	Acceleration due to gravity	ft/sec^2
h	Heat-transfer coefficient	$Btu/(ft^2)(sec)(°F)$
H	Heat output	Btu/sec
k	Thermal conductivity of gas	Btu/(ft)(sec)(°F)
L	Length of uranium in channel	ft
p	Gas pressure	lb/ft^2
P	Ideal gas pump power	ft-lb/sec
q	Dynamic head, $\rho V^2/2g$	lb/ft^2
R	Gas constant	ft-lb/(lb)(°R)
S	Effective heat-transfer surface area	ft^2
S_T	Friction surface area	ft^2
T	Gas temperature	°R
$T_{w,max}$	Maximum temperature of heat-transfer surface	°R
V	Gas velocity	ft/sec
μ	Gas viscosity	lb/(ft)(sec)
ρ	Gas density	lb/ft^3
Δp	Over-all pressure drop	lb/ft^2
ΔT	Gas temperature rise across flow channel	°F
Nu	Nusselt number	hd/k
Pr	Prandtl number	$c_p\mu/k$
Re	Reynolds number	$\rho Vd/\mu$

Subscripts:

F	refers to friction loss accompanying heat transfer
M	refers to momentum loss due to gas acceleration
e	refers to extraneous friction losses
o	refers to gas conditions at reactor channel outlet
i	refers to gas conditions at reactor channel inlet
av	refers to average gas conditions in flow passage

Constants and exponents which characterize the form of the heat-transfer and flow equations [Eqs. (6–3) through (6–7)].

$a, b, C_1, m, n, r.$

all costs. Both reactor design conditions and the steam cycle are affected by the choice. Various studies by different design groups have given "optimum" values of T_i in the range 350 to 450°F.

The reactor outlet gas temperature T_o depends on the permissible operating temperature of the fuel element or jacket material, as governed by metallurgical and corrosion properties. The highest practical value of T_o is desirable not only for high power output (Eq. 6–1), but also for high steam temperature and high cycle efficiency. A high degree of steam superheat is also desired, to reduce moisture content at the exhaust of the steam turbines. For a specified jacket temperature, T_o can be increased only by increasing the effective heat-transfer surface area (for a given volume of fuel), and this increases the required pumping power. Beyond a certain point, the surface area and pumping power requirements increase very rapidly as T_o approaches the jacket temperature. Neutron physics requirements affect the fuel-element geometry and limit the amount of jacket material per unit volume of fuel. The quantity of jacket material will be nearly proportionate to the heat-transfer surface, whether the surface area is increased by further subdividing the fuel, or by adding fins to the jackets. As in the case of T_i, the value of T_o is chosen to give the lowest over-all costs, considering both the cost and performance of the reactor and power plant system and the fuel element costs. In several studies by different design groups T_o has been chosen 80 to 200°F lower than the fuel jacket design temperature.

The heat-removal rate H from a flow channel depends also on the gas weight flow, ρVA, pumped through the channel. In turn, the gas weight flow is limited by gas pumping power. The functional dependence is as follows:

$$\Delta p_F \simeq \tfrac{1}{2}\rho V^2 \frac{S}{A}.$$

The ideal pump power P_F is

$$P_F = \Delta p_F VA \simeq \tfrac{1}{2}\rho V^3 S.$$

Hence, utilizing Eq. (6–1):

$$\frac{\text{Pump power}}{\text{Heat output}} \simeq V^2 \frac{S}{A}.$$

Thus the pump power fraction (ratio of pump power to heat output) increases with the square of the gas velocity through the channel for a given ratio of surface to flow area. Hence, with coolant velocity at the point where the pump power fraction has reached its economic limit and the heat-transfer surface S has been approximately set by considerations

of outlet temperature, the power output can be increased only by increasing the coolant density ρ (Eq. 6–1). The pump power fraction relationship with Eq. (6–1) emphasizes the importance of operating at high gas pressure. For example, increasing gas pressure from 100 psia to, say, 300 psia permits a threefold increase in reactor power output without increasing the pump power fraction. Conversely, for this same increase in gas pressure, only one-third the coolant velocity is needed for the same reactor power output, and the pump power fraction (proportionate to V^2) is only one-ninth as large. Engineering and fabrication problems limit the gas pressure.

Although larger gas flow areas would increase reactor heat output and reduce pump power fraction such increases are limited by neutron leakage. Furthermore, the flow area A that can be utilized efficiently in transferring heat to the gas depends on the heat-transfer surface area of the fuel, among other factors. The restrictions on flow area A can be seen from the following functional relations:

$$H = hS(\overline{T_w - T}), \tag{6–2}$$

where $(\overline{T_w - T})$ is some average temperature difference between fuel jacket surface and gas, and h is the heat-transfer coefficient. In general, $h \simeq (\rho V)^n$, with n ranging from 0.7 to 1.0, depending on the type of heat-transfer surface and the turbulence of the gas stream.

From Eq. (6–1) and the heat-transfer expression,

$$\frac{A}{S} \simeq \frac{1}{(\rho V)^{1-n} c_p} \frac{(\overline{T_w - T})}{T_o - T_i}.$$

It is apparent that for a given type of heat-transfer surface with a given amount of turbulent mixing, the ratio A/S that can be used is determined principally by the design temperature conditions as characterized by the ratio $(\overline{T_w - T})/(T_o - T_i)$. Once these temperature differences have been specified, A/S is adjustable only within quite narrow limits.

Increasing turbulence can increase the heat-transfer coefficient h appreciably. Thus the required A/S ratio can be varied, and so can the channel heat output, without greatly changing the design temperatures. For example, using roughened (turbulence-promoting) rather than smooth-walled surfaces increases h and therefore A/S. If surface area is enlarged, the pump power fraction also increases; for some surface configurations the increase can be quite large. For economy of pumping power, smooth surfaces are usually chosen, but turbulence-producing surfaces (transverse-finned fuel elements) were used effectively in the British gas-cooled power reactors, after extensive experimentation.

If the heat-transfer surface area and flow area are both enlarged, the power output per channel can be increased without changing the pump power fraction S can be made larger by making the fuel pieces smaller, but other considerations may limit the practical degree of fuel subdivision: (a) the greater jacket volume (neutron-absorbing material), (b) the larger number of fuel pieces to be fabricated and handled, and (c) the possible need for (neutron-absorbing) structures to hold many small fuel pieces. Heat-transfer surface also can be enlarged by using extended or finned surfaces The fin material must conduct heat well, absorb few neutrons, and be strong and corrosion-resistant at the operating temperatures.

6–2.2 Relative performance of different gases. A quantitative approach is needed for comparing the coolant qualities of gases As a starting point, the heat-transfer and friction pressure loss relationships are represented by the usual equations:

$$\mathrm{Nu} = a\mathrm{Re}^n\mathrm{Pr}^m, \tag{6–3}$$

$$\Delta p_F = Fq_{\mathrm{av}}\frac{S}{A}, \tag{6–4}$$

$$F = \frac{b}{\mathrm{Re}^r}, \tag{6–5}$$

$$\Delta p_M = \frac{\rho V}{g}(V_o - V_i), \tag{6–6}$$

$$\Delta p_e = C_1 q_i, \tag{6–7}$$

where Nu, Re, and Pr are the Nusselt, Reynolds, and Prandtl numbers, respectively. The dynamic flow head, indicated by q_i, refers to reactor inlet conditions; the subscript "av" refers to average conditions in the flow channel. The pressure drop through the channel is Δp. Subscript F refers to the friction loss accompanying the heat-transfer process, subscript M to the momentum loss due to gas acceleration, and subscript e to extraneous losses from entrance-exit effects, fuel-element holders, etc. For convenience, Δp_e is expressed in terms of the inlet dynamic head; F is the usual friction factor used to measure friction losses accompanying heat transfer Equations (6–3) and (6–5) are in functional forms which have been found to correlate the heat-transfer and friction data for wide varieties of heat-transfer surfaces and flow-turbulence conditions. The constants and exponents, a, b, m, n, r are chosen on the basis of experimental data for the type of surface used. The perfect gas law, $p = \rho RT$, relates the gas state conditions.

For heat input variation having a cosine distribution along the flow channel, symmetrical about the channel midpoint, and of base length equal to the fuel length in the channel, the following equation can be derived:

$$\frac{T_{w,\max} - T_i}{T_o - T_i} = \tfrac{1}{2}[1 + \sqrt{1 + \gamma^2}], \tag{6–8}$$

where $\gamma = \pi\rho V A c_p/hS$, $T_{w,\max}$ is the maximum fuel element jacket temperature, and h is the heat-transfer coefficient (assumed constant at some average value) along the flow channel. To derive Eq. (6–8) the heat balance equation (6–1) and the heat convection equation (6–2) were employed, where $(T_w - T)$ is the local temperature difference between the heat-transfer surface and the gas, and varies along the channel length. For given temperature conditions, γ is uniquely determined by Eq. (6–8).

The ideal pumping power is $\Delta p\, VA \equiv P$.

The interdependence of the pertinent flow and heat-transfer variables can be calculated from Eqs. (6–1) through (6–8) For presentation of the final results, it is convenient to define certain "generalized pump power parameters," which are related to the actual pump power fraction by simple factors. These factors involve the arbitrarily chosen operating conditions (pressures and temperatures) but not the gas properties or the characteristics of the heat-transfer surfaces:

$$\left[\frac{P_F}{H}\right]^* = \left[\frac{p_i^2}{T_i}\right]\left[\frac{\Delta T}{T_i}\right]\left[\frac{1 - (\Delta p/2p_i)}{1 + (\Delta T/2T_i)}\right]\left[\frac{P_F}{H}\right], \tag{6–9}$$

$$\left[\frac{P_m}{H}\right]^* = \left[\frac{P_i^2}{T_i}\right]\left[\frac{\Delta T}{T_i}\right]\left[\frac{1}{\{[1 + (\Delta T/T_i)]/[1 - (\Delta p/p_i)]\} - 1}\right]\left[\frac{P_m}{H}\right], \tag{6–10}$$

$$\left[\frac{P_c}{H}\right]^* = \left[\frac{p_i^2}{T_i}\right]\left[\frac{\Delta T}{T_i}\right]\left[\frac{P_c}{H}\right]. \tag{6–11}$$

The ideal pump power has been separated into the contributions P_F, P_m, P_c, associated with the respective pressure drops Δp_F, Δp_m, Δp_c. The temperature rise and total pressure drop across the flow channel are indicated by the symbols ΔT and Δp. The ratio $\Delta p/p_i$ will generally be of the order of 0.02 to 0.05, so that its effect in the foregoing expressions is quite small.

The expressions for the pump power parameters, as derived from their definitions and Eqs. (6–3) through (6–7), are as follows:

$$\left[\frac{P_F}{H}\right]^* = \left[\frac{2b}{g}\right]\left[\frac{\pi}{4a}\right]^{(1+r)/(2-n)}\left[\frac{1}{\gamma}\right]^{(1+r)/(2-n)}[\rho V c_p]^t L^q \left\{\mu^s\left[\frac{R^2}{c_p^{(1+t)}}\right][Pr]^{(1-m)(1+r)/(2-n)}\right\}, \tag{6–12}$$

TABLE 6–2

PROPERTIES OF GASES SUITABLE FOR REACTOR COOLING

Property	Gas						
	H_2	He	N_2	Air	CO	CO_2	A
Molecular weight	2	4	28	29	28	44	40
Thermal conductivity, Btu/(ft)(°F)(hr):							
200°F	0 125	0 097	0 018	0 018	0 017	0 013	0 012
700°F	0 199	0 135	0 028	0 028	0 027	0 028	0 018
1300°F	—	0 172	0 037	0 039	—	0 042	0 025
Viscosity, centipoises:							
200°F	0 010	0 023	0 020	0 021	0 020	0 017	0.027
700°F	0 015	0 033	0 031	0 032	0 031	0 028	0 041
1300°F	0.020	0 044	0 041	0 042	0 044	0 041	0 054
Specific heat, Btu/(lb)(°F):							
200°F	3 47	1 24	0 249	0 241	0 250	0 217	0 124
700°F	3 51	1 24	0 259	0 254	0 262	0 262	0 124
1330°F	3 60	1 24	0 279	0 272	0 283	0 295	0 124
Density at STP, lb/ft^3	0 0052	0 0104	0 0727	0 0748	0 0727	0 114	0 104
Volumetric specific heat at STP, $Btu/(ft^3)(°F)$	0 0178	0 0129	0 0180	0 0179	0 0180	0 0238	0 0129

$$\left[\frac{P_m}{H}\right]^* = \left[\frac{2}{C_1}\right]\left[\frac{P_e}{H}\right]^* = \left[\frac{1}{g}\right][\rho V c_p]^2\left[\frac{R^2}{c_p^3}\right], \tag{6-13}$$

$$\left[\frac{H}{S\Delta T}\right] = \left[\frac{a}{\pi 4^{(1-n)}}\right]^{1/(2-n)}[\gamma]^{1/(2-n)}[\rho V c_p]^{1/(2-n)}$$
$$[L]^{(n-1)/(2-n)}\left\{\frac{c_p \mu^{(1-n)/(2-n)}}{Pr^{(1-m)/(2-n)}}\right\}, \tag{6-14}$$

$$\frac{A}{S} = \left[\frac{H}{S\Delta T}\right]\left[\frac{1}{\rho V c_p}\right], \tag{6-15}$$

where $t = (2 - r) + \dfrac{(1 - n)(1 + r)}{2 - n}$,

$$s = r - \frac{(1 - n)(1 + r)}{2 - n},$$

$$q = 1 - \frac{1 + r}{2 - n}.$$

These equations, by means of the parameter γ, take into account the effects of reactor temperature conditions. Fuel length L enters into Eqs. (6-12) and (6-14) in only a minor way since exponents on L have been found small for wide variations of heat-transfer surface types and turbulence conditions. The quantity $\rho V c_p$ is a measure of the heat transport out of the channel due to the gas flow. The gas property parameters affecting heat-removal rate and pump power fraction are lumped together in the bracketed quantity for each expression. Table 6-2 shows properties of various gases that might be considered as possible reactor coolants. A plot of the relationships expressed by Eqs (6-12), (6-14), and (6-15) is given in Fig. 6-1 for the various gas coolants, using the gas property values at 700°F from Table 6-2. In Fig. 6-1, $[P_F/H]^*$, $H/S\Delta T$, and A/S are plotted versus $\rho V c_p$ for the channel temperature condition

$$(T_{w,\max} - T_i)/(T_o - T_i) = 1.40.$$

The temperature condition is perhaps more meaningful if expressed as $(T_{w,\max} - T_o)/(T_o - T_i) = 0.40$. The flow and heat-transfer model assumed is for uninterrupted flow over smooth surfaces, in which case $a = 0.023$, $n = 0.8$, $m = 0.4$, $b = 0.046$, $r = 0.2$. Figure 6-1 gives the interdependence of the flow and heat-transfer variables. To illustrate the comparison of the different gases, Table 6-3 has been prepared from Fig. 6-1 and Table 6-2, giving the flow conditions, flow area requirements, and relative pump power fractions for the different gases to attain $H/S\Delta T = 0.07$ [for $(T_{w,\max} - T_i)/(T_o - T_i) = 1.40$].

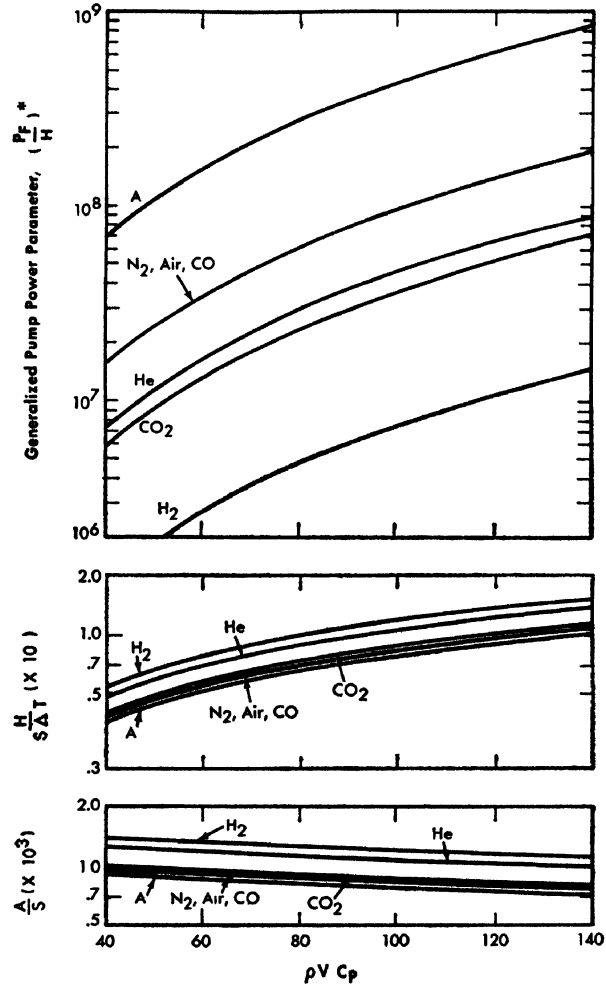

FIG. 6–1 Comparison of heat-transfer and pump power requirements for various gaseous coolants (GNEC) Flow over smooth-walled heat-transfer surfaces, $(T_{w,max} - T_i)/(T_o - T_i) = 1.4$.

For the same temperature conditions, heat-transfer surface area, and channel heat output, the channel flow area requirements are different for the different gases. The weight velocity ρV varies considerably from gas to gas because thermal conductivity and viscosity differ. Hydrogen is by far most economical of pumping power. On this basis, carbon dioxide is slightly inferior to helium, whereas nitrogen, air, and carbon monoxide require about 3.8 times as much pumping power as helium.

A criterion can be derived from Eqs. (6-12), (6-13), and (6-14) for evaluating gaseous coolants, assuming equal heat removal per unit of surface area, the same temperatures, and the same system pressure. Solving Eq. (6-14) for $\rho V c_p$ and substituting into Eqs. (6-12) and (6-13), we obtain the following as the criterion:

$$\left[\frac{P_F}{H}\right]^* \simeq \left[\frac{Pr^r}{\mu^{[(1-n)(t-n)]}}\right]\left[\frac{R^2}{c_p^{[1+t(2-n)]}}\right],$$

$$\left[\frac{P_m}{H}\right]^*, \quad \left[\frac{P_c}{H}\right]^* \simeq \left[\frac{Pr^{2(1-m)}}{\mu^{2(1-n)}}\right]\left[\frac{R^2}{c_p^{(5-2n)}}\right],$$

where $x = (1 - m)\{t + [(1 + r)/(2 - n)]\}$.

The relative values of $[P_F/H]^*$ thus obtained for the different gases are shown in Table 6-3, for a smooth-wall heat-transfer surface. The relative values of $[P_m/H]^*$ and $[P_c/H]^*$ are nearly the same as those for $[P_F/H]^*$. For example, for carbon dioxide the relative pump power due to momentum and extraneous losses is 1 46, compared with 1.00 for helium.

Because of the assumptions involved, the limitations to the use of Eqs. (6-12) through (6-15) require some discussion. The surface area S in Eq. (6-14) is the effective heat-transfer surface area; in determining $[P_F/M]^*$ by Eq (6-12), the friction surface area S_F was set equal to S. Multiplication of $[P_F/H]^*$, given by Eq. (6-12), by the factor $[S_F/S]^{1+r}$ will correct $[P_F/H]^*$ for any possible difference between friction surface and effective heat-transfer surface in a flow passage. For example, the channel wall surface contributes to friction loss but not to heat transfer. For finned heat-transfer surfaces, the effective fin surface for heat transfer is less than the actual friction surface by the ratio of fin effectiveness, η_f.

TABLE 6-3

RELATIVE HEAT-TRANSFER AND PUMPING POWER CHARACTERISTICS OF GASEOUS COOLANTS

Gas	$\rho V c_p$	ρV	A/S	$[P_F/H]^*$	Relative pump power for same heat output
H_2	54	15 5	1.3×10^{-3}	2.2×10^6	0.13
He	63	51	1.1×10^{-3}	17.0×10^6	1.00
CO_2	79	302	0.9×10^{-3}	23.0×10^6	1.35
N_2, air, CO	82	318	0.85×10^{-3}	65.0×10^6	3.80
A	91	735	0.78×10^{-3}	350.0×10^6	20.60

In turn, fin effectiveness depends on fin material, size, shape, and heat-transfer coefficient; thus S depends on the details of the specific design. It can be shown from Eqs. (6–1) and (6–8) that fin surface $H/\Delta T$ and $(T_{w,\max} - T_s)/(T_o - T_s)$ determine the heat-transfer coefficient for any given fin shape, size, and material. Hence η_f does not depend on which gaseous coolant is used; the ratio is the same for all. Thus the criterion established for comparing gas coolants should hold if flow area is adjusted for the particular heat-transfer and flow configurations. In any case, the important requirement is that the heat-transfer and friction relations be expressed in the form of Eqs. (6–3) and (6–5).

6–2.3 Heat removal from many channels. The discussion so far has been limited to single-channel characteristics. As the power density varies over the reactor in a definable manner (determined by nuclear considerations), the heat-removal rate of the channel with maximum power density determines the possible heat-removal rate from the other channels. The variation in power density along the flow channel was considered in the analysis of the single-channel characteristics. For high gas outlet bulk temperature, the limiting temperature of the fuel-element jacket must be approached in all flow channels irrespective of the heat-removal rate from the channel. This means adjusting the gas weight flow through each channel or group of channels in accordance with the heat output. Since the over-all pressure drop across the reactor is fixed, flow is controlled by varying flow resistance of the channels, either by changing channel diameters or using orifice plugs, or both. Reducing channel diameter reduces both flow area and gas velocity for a fixed over-all pressure drop. Orifice plugs have the very important advantage that they can be adjustable. Since the power density distribution over the reactor is not accurately known at first and may vary with fuel exposure, fuel repositioning, and control rod adjustments, adjustable orifices are desired.

Reference 10 compares calculated outlet gas temperatures for various combinations of flow control. Some results from Reference 10 illustrate flow-control effectiveness. Figure 6–2 shows radial power-density distribution and Fig. 6–3 shows how channel gas weight flow and outlet gas temperature vary across the reactor for a specified continuous variation of channel (or hole) diameter. The outlet gas temperature from the "hottest" channel (radius = 0) is 1050°F in this case, and the outlet gas bulk temperature is 1134°F. If no flow control were used, the bulk temperature would drop to 850°F. If the reactor face is divided into two regions (an inner circular and outer annular region), each with its own constant channel diameter, a bulk temperature of 968°F can be reached. If all channel sizes are held constant and a different orifice size

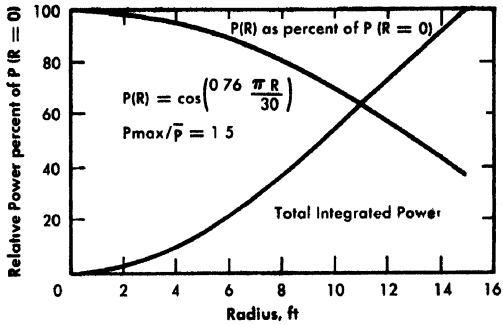

FIG. 6–2 Reactor radial power distribution (ORNL)

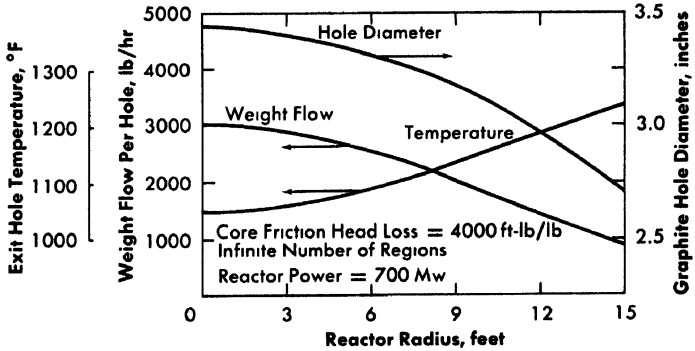

FIG 6–3 Effects of radial power distribution on reactor design (ORNL)

is used for each radial position of the flow channels, the outlet gas bulk temperature becomes 1070°F.

For the final design in the study of Reference 10 three different channel diameters and five orifice plug sizes were chosen (Fig. 6–4) (This case is not comparable with the one discussed in the preceding paragraph because temperature and flow conditions are different.) Figure 6–4 shows how the resulting outlet gas temperature varies across the reactor exit face. Outlet gas bulk temperature is 1007°F for the limiting jacket temperature of 1200°F. The outlet gas temperature from the "hottest" channel is 980°F.

In calculating heat removal performance, allowances must be made for the "hot-spot factor." The maximum permissible fuel-element jacket temperature is a most important limitation on heat removal. Hence it is convenient and logical to anticipate differences between predicted and actual reactor heat removal by applying a hot-spot factor to the fuel

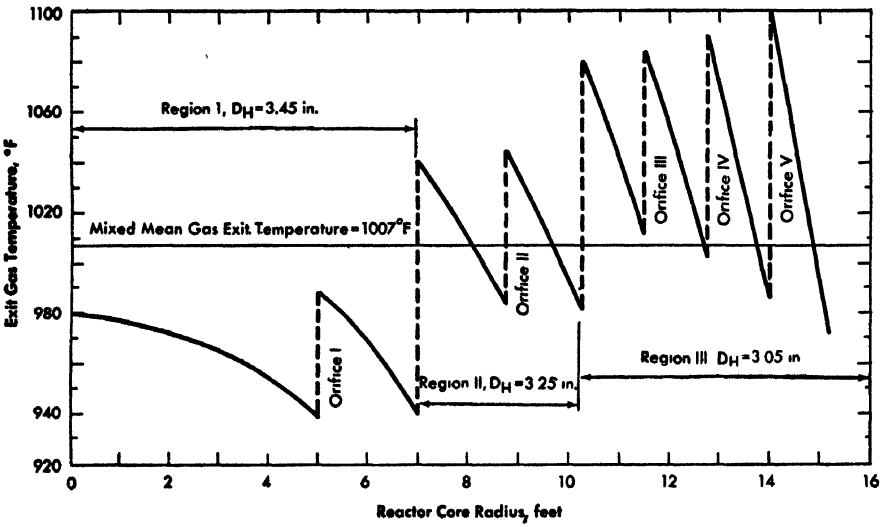

FIG. 6–4. Exit gas temperature profile for three fuel-channel diameters and five orifice sizes (ORNL)

jacket temperature. In practice, the maximum fuel jacket design temperature in the heat-transfer calculations is assumed somewhat lower than the maximum permissible temperature A realistic choice of this temperature margin requires a critical evaluation of effects of various factors not normally accounted for in design calculations These factors reflect lack of knowledge of the precise conditions prevailing in the reactor and lack of experimental information Examples of factors which may have to be accounted for by applying the hot-spot temperature margin are: (1) uncertainties in the local heat transfer coefficient as it varies along and around a fuel element (especially for clusters of fuel elements); (2) uncertainties in relative heat generation within the individual fuel elements of a cluster; (3) nonuniformity of gas temperature distribution across the flow cross section, due to the shape of the heat-transfer surface and to poor flow mixing; (4) flow irregularities due to fuel element holders; (5) differences between actual and calculated power density distribution; (6) normal tolerances in manufacture, assembly, and positioning of fuel elements in flow passages; and (7) possible bowing of fuel elements and resultant local restriction in flow area during operation.

6–2.4 Choice of coolant. The first consideration in choosing the coolant gas must be its chemical compatibility with reactor materials at operating temperatures. The most straightforward approach would be to use a

TABLE 6–4

COST AND AVAILABILITY OF GASES [15]

Gas	Cost, dollars per cubic foot (STP)	Availability
He	0.015 (FOB Amarillo, Texas)	U. S. (Italy and USSR)
A	0.074 (FOB Richland, Wash.)	0.93 vol. % of air*
Ne	42.50 (FOB Kennewick, Wash.)	0.0018 vol. % of air*
CO_2	0.003 (FOB Kennewick, Wash.)	World wide
CO	0.24 (FOB New Jersey)	World wide
H_2	0.10 (FOB Kennewick,, Wash.)	World wide
N_2	0.08 (FOB Kennewick, Wash.)	78.06 vol. % of air*

*Obtained by fractional distillation of liquid air.

chemically inert gas. Of these, only helium and argon are available at reasonably low cost (see Table 6–4). Argon gives relatively poor heat-removal performance (Fig. 6–1) and activates strongly under neutron bombardment Helium gives good performance, and in many respects is an attractive coolant. Its availability is restricted geographically* and its cost, although relatively low (Table 6–4) is yet high enough that sizable losses from the coolant system could not be tolerated economically. Aside from these considerations, the disadvantages of helium stem from its low molecular weight. The most important of these is the high rate of leakage of helium through small openings, and the consequent difficulty of achieving acceptably low leakage rates in a pressurized system.

Gases other than the chemically inert ones must be considered in relation to the temperatures at which they are to be used, the other materials in the system, and possible modification of the normal chemical behavior by radiation effects. Carbon dioxide is the only gas whose performance has been established by use in a reactor. It is compatible with the magnox alloys to about 450°C, with aluminum up to temperatures where

*The total supply of He is, however, reasonably large. Present U. S. production capacity is about 300 million cubic feet per year. The Bureau of Mines is reported to estimate 7 billion cubic feet of proven reserves in the four fields currently being utilized, and many other fields which are not being used [10]. A reactor for 200-Mw electrical output is expected to have an inventory of about 1 million cubic feet (STP).

the aluminum loses strength, and with stainless steel up to 800 or 900°C.* It begins to react appreciably with graphite, forming carbon monoxide, at temperatures in the neighborhood of 500°C.

Other conceivable possibilities for coolants among the chemically active gases are carbon monoxide, nitrogen, oxygen, and hydrogen. Oxygen might be used for reactors composed entirely of oxides, as for example a BeO moderated reactor fueled with unjacketed UO_2. The heat transfer properties of oxygen would be about the same as for nitrogen or air (Fig. 6–1). Hydrogen and carbon monoxide are both combustible in air, and carbon monoxide has the added disadvantage of toxicity. A combustible gas as coolant would add to the normal hazard of leaks in the coolant system and might greatly increase the hazards from a major break in the primary coolant system. The good heat-transfer properties of hydrogen are attractive, but its problems are severe and it is not being considered as a reactor coolant. Nitrogen is compatible with graphite up to high temperatures and with most fuel jacket materials up to reasonably high temperatures Its major disadvantages are its high absorption cross section (1.88 barns) and heat-transfer characteristics much poorer than those of carbon dioxide

In reactors designed to operate on natural uranium, a high neutron absorption cross section of the coolant gas can be a very severe disadvantage Nitrogen may be eliminated from consideration for such reactors; with it at high pressure operation with natural uranium would be impossible. The gaseous coolants usable with graphite moderated natural uranium reactors are carbon dioxide and helium. Carbon monoxide might be considered except for its combustibility problems Performance differs little between helium and carbon dioxide, although helium, at least on theoretical grounds, is slightly better. Leakage problems in high pressure helium systems are expected to be important, and there is little doubt that carbon dioxide is the more desirable coolant in the temperature ranges at which it can be used It is unfortunate that carbon dioxide begins to react significantly with graphite near, and perhaps slightly below, the temperatures desired for the exit gases of graphite-moderated reactors presently being considered. If graphite-CO_2 reaction rates prove to be low enough at the desired exit temperatures, or if a lasting protective layer can be found for the surface of the graphite coolant channel, carbon dioxide will no doubt be used for graphite moderated reactors Otherwise helium will be preferred, and the margin of this preference may well become greater as reactor operating temperatures are increased.

---

*For detailed discussions of compatibility of metals with gases see Section 6–3.

6–3. Fuels and Fuel-Element Materials*

As pointed out previously, the design and performance of a gas-cooled reactor are determined largely by its fuel element. Since we are discussing fuel elements which do not allow escape of fission products, both fuel and jacket materials must be considered. Two kinds of fuel materials are discussed: uranium metal (pure or alloyed) and uranium compounds such as the oxides.

The outstanding advantage of uranium metal is its high density, which favors high reactivity with a given enrichment. The outstanding disadvantage is the temperature limitation of the irradiated metal. Unless means are found for raising these limits, the temperature performance cannot greatly exceed that of present magnox-jacketed elements, even if a jacket of higher temperature capability is used Thus, there is a great incentive to use the oxide fuel

Because of poorer reactivity performance, a graphite-moderated power reactor with natural uranium oxide fuel does not appear feasible even with a jacket material of low cross section Thus, both uranium metal and uranium oxide leave something to be desired as fuel element materials; neither can now be eliminated as a prospective fuel for future gas-cooled reactors, even though recent studies (Sections 6–4.4, 6–4.5) emphasize superiority of the oxide.

Since neither class of fuel materials is entirely satisfactory, the characteristics of some present and prospective fuel and jacket materials are reviewed to indicate possibilities for improvements.

6–3.1 Uranium metal. The more important physical and chemical properties of uranium metal are given in Tables 6–5, 6–6, 6–7, and Figs. 6–5 through 6–11. References for the information—(16) through (33)—are at the end of this chapter.

Mechanical properties. Most of the data on mechanical properties are for alpha phase uranium. Because alpha uranium is anisotropic, test data are considerably affected by grain size, preferred orientation, and other texture factors, as well as by impurities, testing procedures, and testing temperatures. Effects of some of these factors on yield strength, tensile strength, and hardness are indicated in Figs. 6–12, 6–13, 6–14, and 6–15.

Irradiation effects. Operational life of uranium metal fuel has been severely limited by radiation damage which changes strength properties usually resulting in ductility decrease, growth (because of preferred orientation), and swelling.

---

*Compiled by F. Bevilacqua, GNEC.

TABLE 6–5

SOME PHYSICAL AND CHEMICAL PROPERTIES OF URANIUM [22]

Phase	Density [16–18]		Crystal structure [16,18]		
	g/cm³	°C	Lattice type	Atoms per unit cell	Lattice parameters
Alpha	18.7–19.0*	—	Orthorhombic	4	a_0 = 2.8541 ± 0.0003
	19.04†	25			b_0 = 5.8692 ± 0.0015
	19.05 ±0.02‡	25			c_0 = 4.9563 ± 0.0004
Beta	18.11	720	Tetragonal	30	a_0 = 10.759 ± 0.001
					c_0 = 5.656 ± 0.001
Gamma	18.06	805	Body-centered cubic	2	a_0 = 3.524 ± 0.002

Transformation point	*Transformation temperature*	
	Heating, °C	*Cooling, °C*
Alpha-beta	665.6	656.7
	671.9§	662.6§
Beta-gamma	771.1	766.5
Melting point	1129.8	1129.6
	1131.80 ± 0.4§	1133.0 ± 0.4§
Boiling point	3820	

Heat of fusion [21]: 4.7 kcal/mole

Heat of vaporization [21]: 106.7 ± 0.1 kcal/mole

Specific heat [22]: 6.649 cal/(mole)(°C) at 27°C
8.952 cal/(mole)(°C) at 427°C
11.107 cal/(mole)(°C) at 627°C

*Wrought material.
†Calculated from lattice parameters.
‡High-purity uranium, directionally solidified.
§Reference 19.

TABLE 6-6

MEAN THERMAL EXPANSION COEFFICIENTS OF ALPHA-URANIUM RODS FOR VARYING FABRICATION TREATMENTS AND PERCENT REDUCTION IN AREA [23]

(Parallel to rolling direction)

Treatment prior to final rolling	Nominal finish rolling temperature, °C	Mean thermal expansion coefficient, 10^{-6}/°C, at 25 to 100°C			
		0% reduction	10% reduction	45% reduction	70% reduction
600°C rolled 80%	300	13.42	10.16	8.62	8.94
600°C rolled 80% and beta-treated	300	15.98	12.8	10.02	9.17
600°C rolled 80% and beta-treated	600	15.86	14.9	13.39	12.71

TABLE 6-7

MEAN THERMAL EXPANSION COEFFICIENTS OF ALPHA-URANIUM RODS FOR VARYING TEMPERATURES OF ROLLING AND THERMAL TREATMENT, UNIFORM 75% REDUCTION IN AREA [24]

(Parallel to rolling direction)

Nominal rolling temperature, °C	Mean thermal expansion coefficient, 10^{-6}/°C, 25 to 100°C	
	As-rolled	Recrystallized at approximately 625°C
300	8.5	6.8
400	9.3	7.9
500	11.4	9.2
600	12.9	
640	14.1	

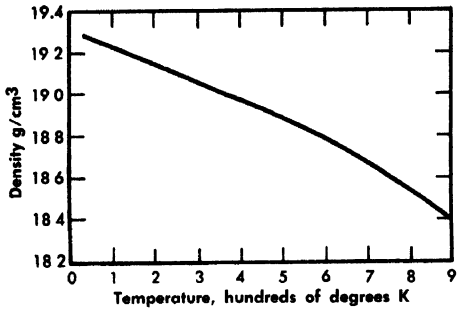

FIG. 6–5 Effect of temperature on density of alpha uranium [22]

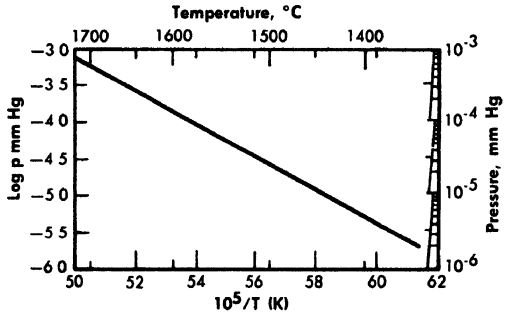

FIG. 6–6. Vapor pressure of uranium as a function of temperature [26]

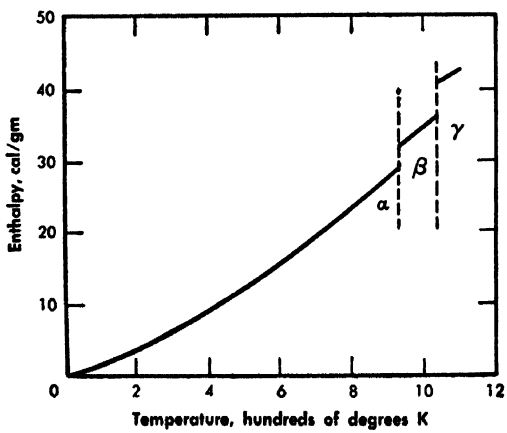

FIG. 6–7. Enthalpy of uranium. [22]

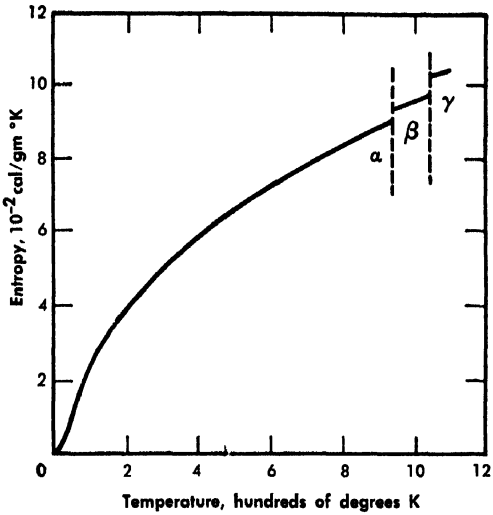

FIG 6–8 Entropy of uranium. [22]

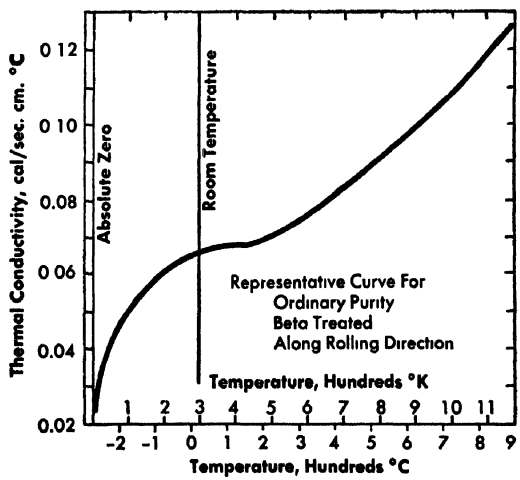

FIG. 6–9. Thermal conductivity of uranium [27]

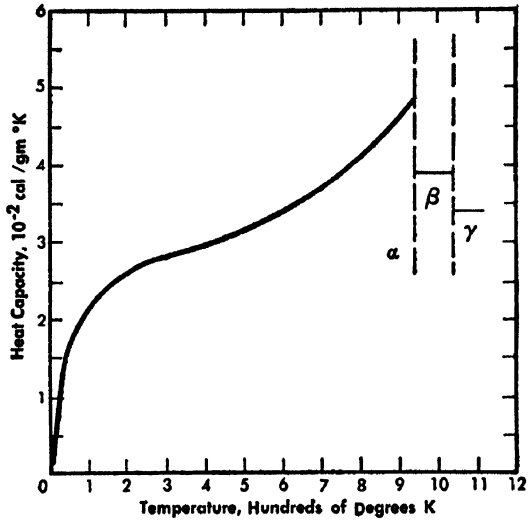

FIG. 6–10. Heat capacity of uranium. [22]

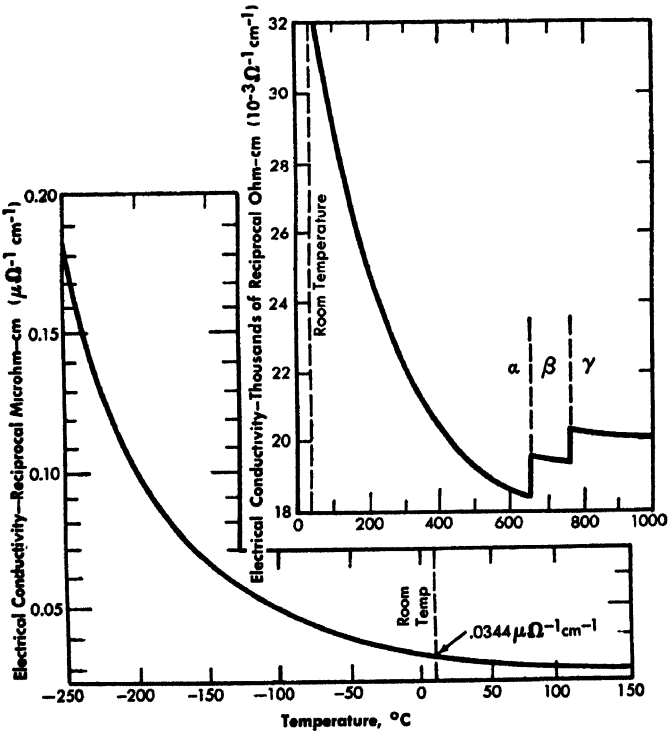

FIG. 6–11. Electrical conductivity of uranium. [28]

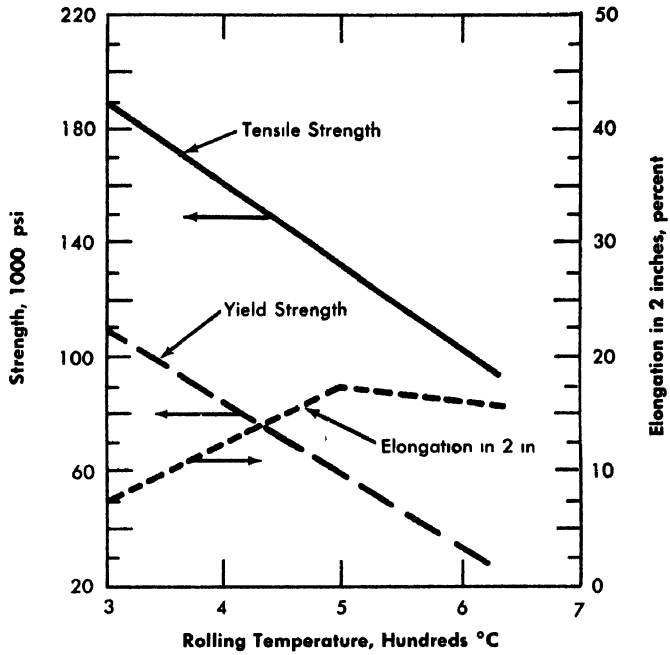

FIG. 6–12 Effect of final rolling temperature on tensile properties of as-rolled alpha uranium rod [24]

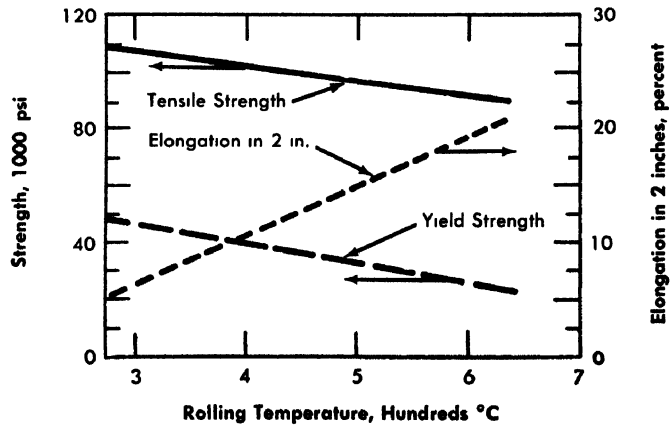

FIG. 6–13. Effect of final rolling temperature on tensile properties of as-recrystallized alpha uranium rod. [24]

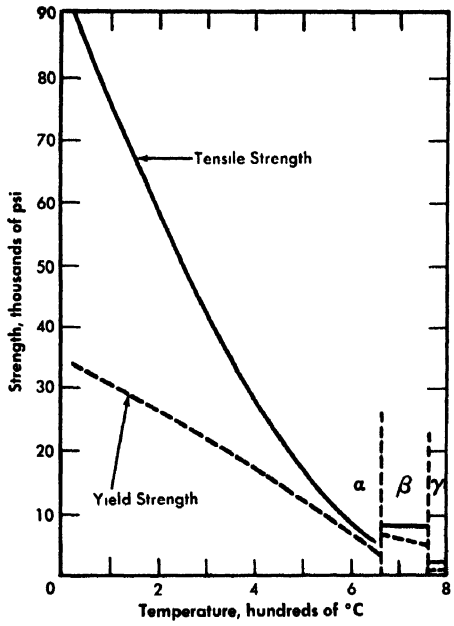

FIG. 6–14 Effect of temperature on yield strength and tensile strength of uranium. [33]

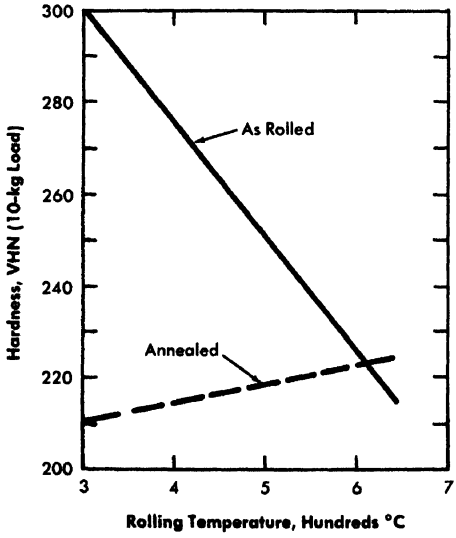

FIG. 6–15. Effect of final rolling temperature on the Vickers hardness of as-rolled and as-recrystallized alpha uranium rods [24]

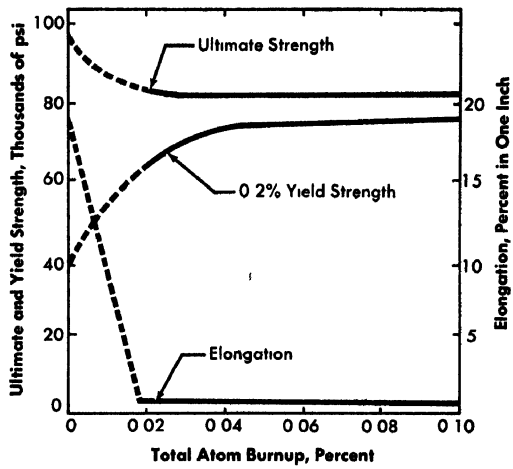

FIG 6–16 Effect of exposure on room-temperature properties of irradiated uranium [34]

The loss in ductility is illustrated in Fig. 6–16, which shows changes in ultimate strength, yield strength, and elongation Usually these changes are not important, as the fuel is not used as a structural material.

Of greater importance would be any effect of irradiation on thermal conductivity. Limited data [34–37] have shown a decrease in thermal conductivity of approximately 15 percent with irradiations up to 7.5×10^{19} nvt. Beyond this there appeared to be no further decrease. Although the accuracy of the tests was poor, the data were sufficient to indicate that little change is to be expected in thermal conductivity.

Growth-type radiation damage can cause severe dimensional changes in the uranium, often called dimensional instability. Such changes in a fuel element could cause it to plug the coolant channel, overheat, and fail; or could cause the jacket material to rupture, releasing fission products to the coolant.

Preferred crystal orientation affects the behavior of uranium under irradiation at low temperatures, as shown in Fig. 6–17. The effects of preferred orientation are discussed in References 38 and 39.

Figures 6–18, 6–19, 6–20, and 6–21 show effects of irradiation at low temperatures (less than 220°C) on uranium specimens with various fabrication histories [40]. A graphic summary of these changes is shown in Figs. 6–22, 6–23, and 6–24, which are plots of density, hardness, and elongation as functions of burnup.

The dimensional stability of uranium is affected also by the size of the individual grains in polycrystalline material [41]. Using powder metal-

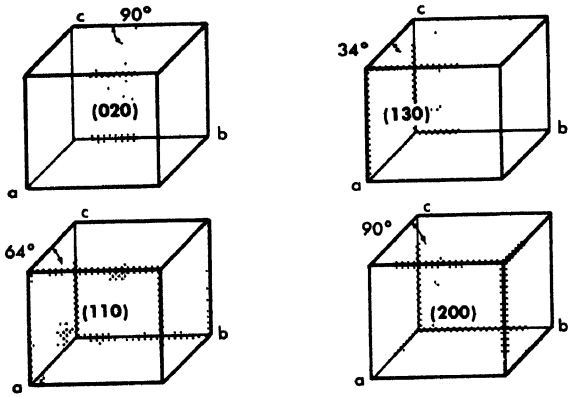

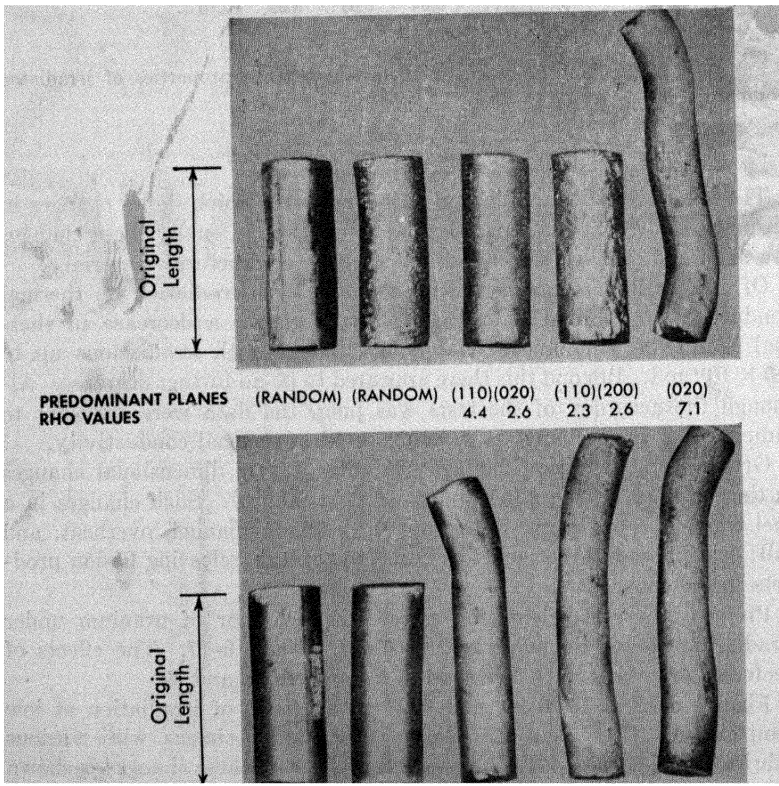

FIG. 6–17. Effects of preferred orientation on the dimensional stability of uranium during irradiation. Exposure, 10^{20} to 3×10^{20} nvt; temperature, 100 to 150°C. [34]

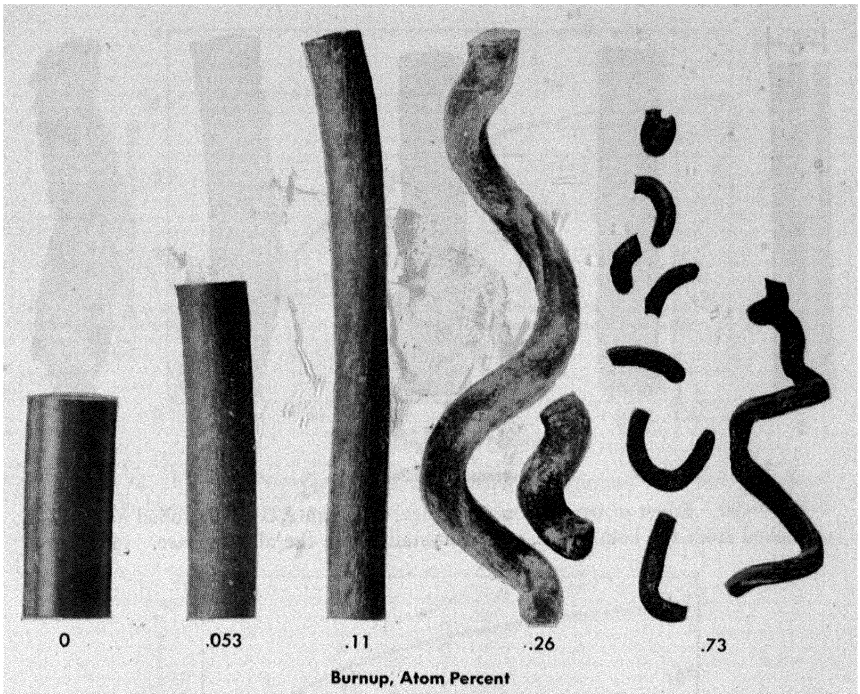

FIG. 6–18. Effect of irradiation on uranium specimens rolled at 300°C. [40]

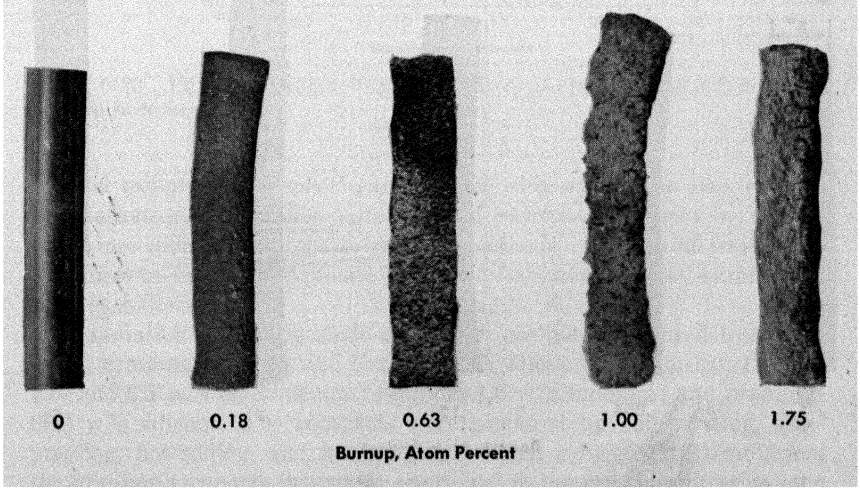

FIG 6–19. Effect of irradiation on typical uranium specimens rolled at 300°C and quenched from the beta phase. [40]

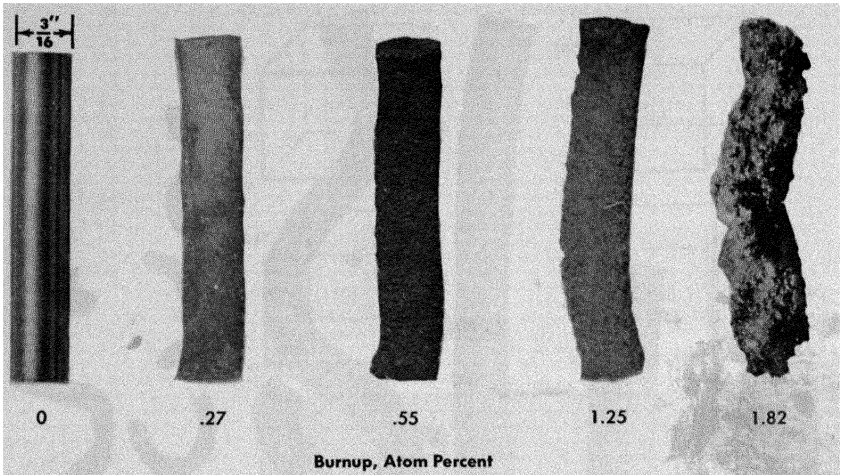

FIG. 6–20. Effect of irradiation on typical uranium specimens rolled at 300°C, quenched from the beta phase, and recrystallized in the alpha phase. [40]

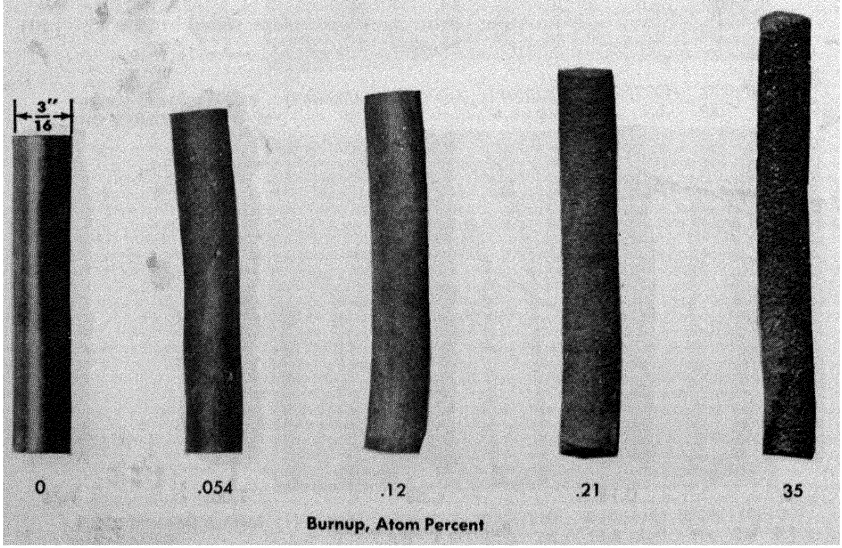

FIG. 6–21 Effect of irradiation on typical uranium specimens rolled at 600°C. [40]

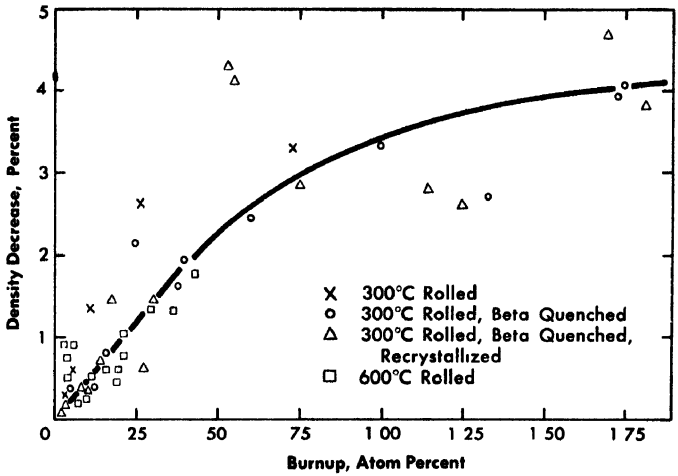

FIG. 6-22 Effect of irradiation on the density of uranium with four different fabrication histories [40]

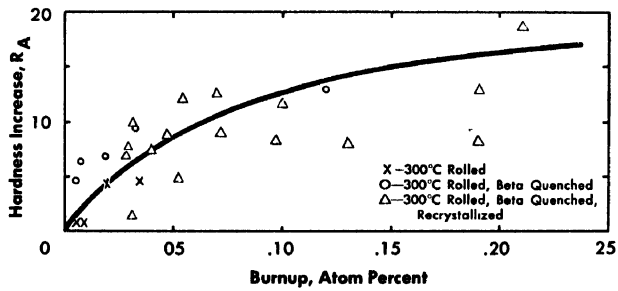

FIG. 6-23. Effect of irradiation on the hardness of uranium with different fabrication histories [40]

lurgical techniques, compacts can be made with small grain size, random orientation, and controlled porosity, and various alloys can be formed which are difficult to prepare by other methods. Results of irradiation experiments made by Argonne National Laboratory were summarized [42] as follows:

"Irradiation tests were made on powder compacts prepared from uranium, uranium hydride, and the following alloys: uranium-1.0, 1.4, 2.0, 2.5, and 3.5 w/o molybdenum; uranium-1.6 w/o niobium; and uranium-0.42 w/o silicon. The compacts were prepared by end-pressing, side-pressing, hot-rolling, and hot-swaging. When subjected to irradiation, the uranium compacts invariably shortened in the pressing direction; the compacts prepared from uranium hydride elongated in the pressing di-

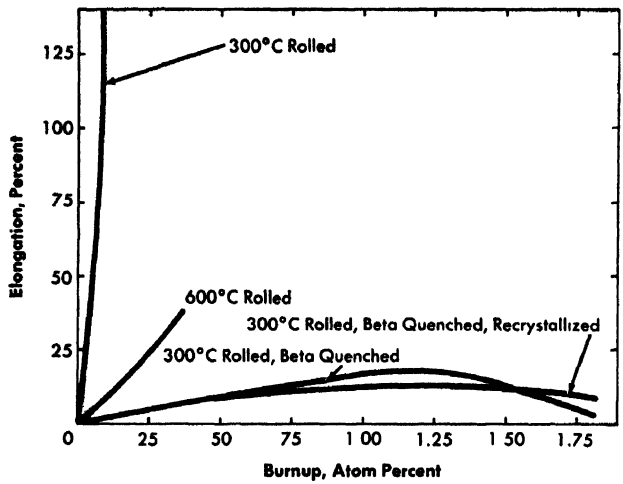

FIG. 6–24 Effect of fabrication history on the lengthwise growth of uranium under irradiation [40]

rection; the alloy compacts elongated in the direction of pressing, rolling, or swaging. The surface smoothness of the irradiated molybdenum alloy compacts improved with increasing molybdenum content, although dimensional stability tended to decrease The irradiated niobium alloy showed comparatively good surface smoothness and dimensional stability, but the silicon alloy specimens were badly roughened and elongated. Both the unalloyed and the alloyed compacts decreased in density under irradiation, and the rate of density decrease was found to depend strongly on the irradiation temperature "

Figures 6–25, 6–26, 6–27, and 6–28 show some results of these irradiations. Most of the specimens were irradiated while completely unrestrained. Since fuel elements will normally be clad or jacketed, changes may be inhibited to some extent by the cladding or jacketing material The effect of cladding thickness on the growth rate of a uranium alloy is shown in Fig. 6–29 [43].

Results of the above tests at temperatures higher than 400°C also show the third type of radiation damage, known as swelling. As differentiated from the grain growth effects, swelling means the expansion (probably caused by creep of the uranium at high temperatures under internal pressures) of accumulated fission-product gases. The effect of the irradiation temperature on swelling is shown in Fig. 6–30 [33,42,44]. This effect can sometimes be lessened by cladding the uranium and providing an axial hole in its center so that it can flow in the hottest region. Some

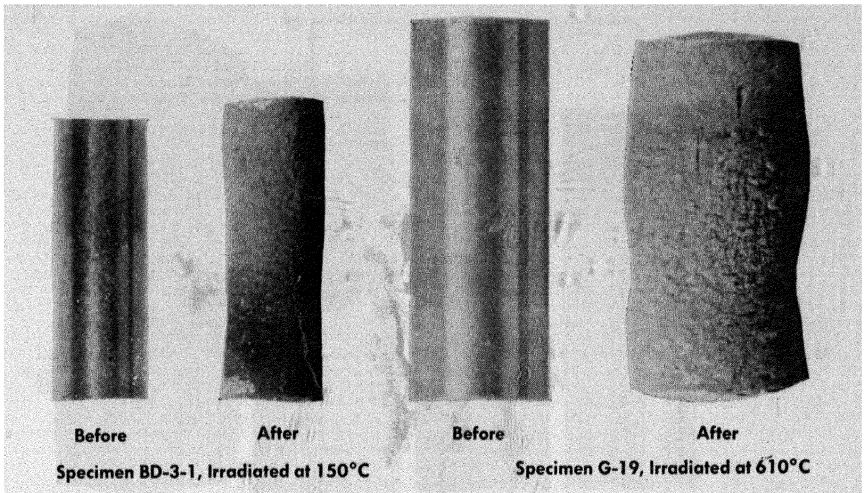

FIG. 6–25. Effect of 0.4 a/o burnup on uranium compacts end-pressed at 600°C, at differing irradiation temperatures. [42]

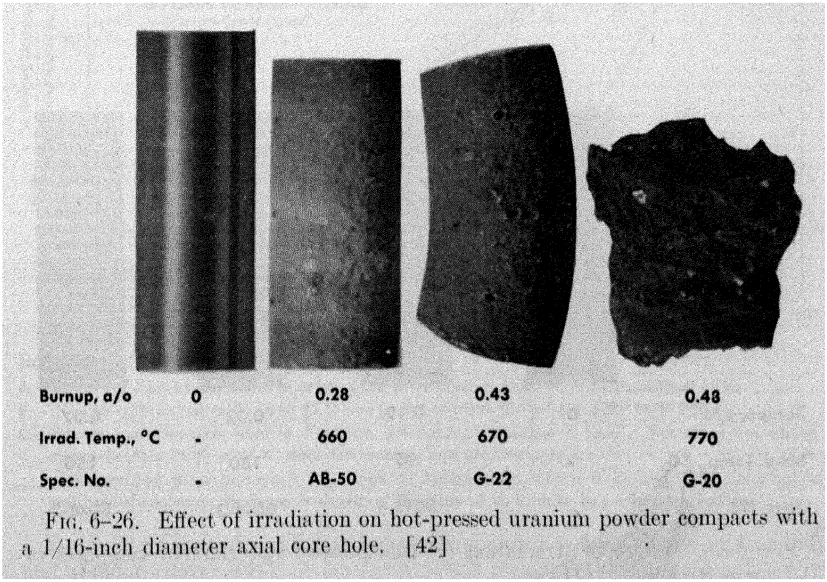

FIG. 6–26. Effect of irradiation on hot-pressed uranium powder compacts with a 1/16-inch diameter axial core hole. [42]

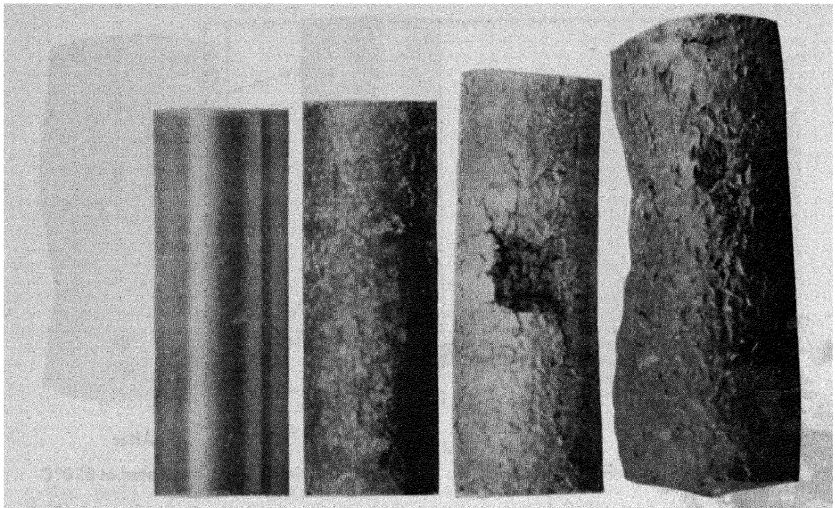

FIG. 6–27. Effect of irradiation on uranium compacts side pressed at 600°C to approximately 12.5% porosity. [42]

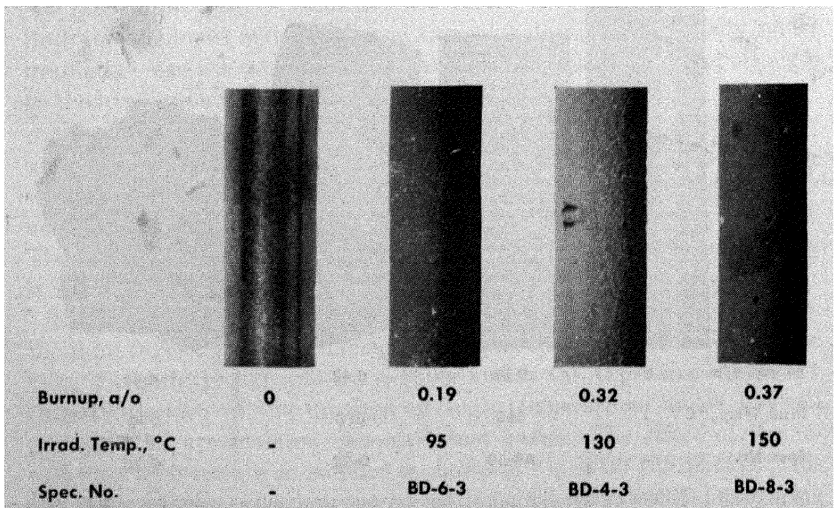

FIG. 6–28. Effect of irradiation on cold-pressed and sintered compacts of U-1.6 w/o Nb alloy. [42]

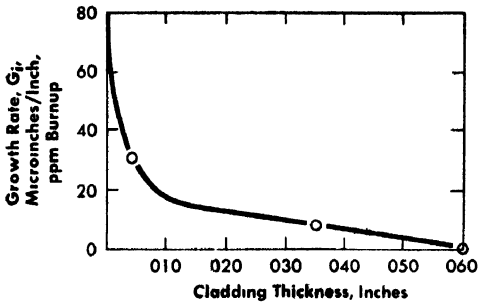

FIG. 6–29. Effect of Zircaloy-2 cladding thickness on the irradiation growth rate of specimens cut from a gamma quenched U-5 w/o Zr-1 5 w/o Nb EBWR plate The specimens were irradiated to 0 1% uranium atom burnup. [43]

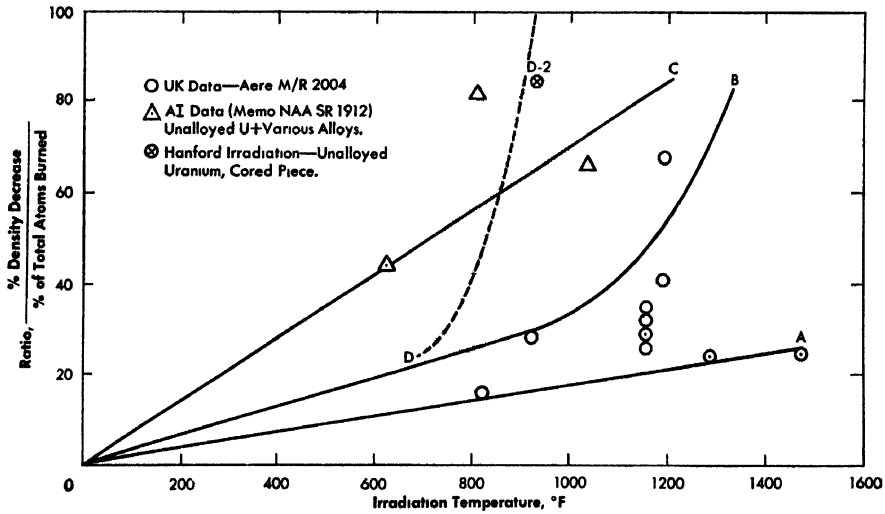

NOTES

A—The lower limit of unalloyed uranium data presented in AERE M/R 2004, August 1956.

B—This line approximates the best fit to unalloyed uranium data from AERE M/R 2004.

C—Private communication from M. Finniston, U.K.A.E.A., November 1, 1957. This curve lies above approximately 80% of U. K. data for uranium and uranium alloys.

The shaded area represents the range of temperature where U. S. and U. K. information indicates a nonlinear decrease in density. The bulk of U. S. data lies within this region.

FIG. 6–30. Effect of irradiation temperature on the volume change of uranium and uranium alloys. [44]

TABLE 6–8

DIMENSIONAL INSTABILITY IN URANIUM [34]

Factors where there is substantial agreement:

1. An (010) direction orientation results in maximum growth.
2. A (100) direction orientation results in maximum shrinkage.
3. An (001) direction orientation results in little or no change in dimension
4. Duplex orientations may promote or prevent growth or shrinkage, depending on type and degree of orientation.
5. Single crystals deform under irradiation, but not under thermal cycling.
6. A random orientation is stable when irradiated or thermally cycled.
7. High (400°C) or low (−100°C) temperature operation during irradiation minimizes dimensional instability.
8. There appears to be no limit on the degree of dimensional change under irradiation.
9. Growth appears to be a direct function of integrated flux.

Factors where there is inadequate information or lack of agreement:

1. Increased metal purity may increase the rate of irradiation growth
2. Growth rate appears greatest for oriented polycrystalline uranium, decreases as metal approaches or becomes a single crystal (definite disagreement on this).
3. Dimensional instability produced by irradiation and thermal cycling are qualitatively similar (definite disagreement).

---

verification of this possibility has been obtained by irradiation tests on two specimens of unalloyed uranium (1.3 inches in diameter and 4 inches long), with a 0.375-inch axial hole. The specimens were jacketed in 0.050-inch-thick aluminum and insulated from the jacket by 0.004 of an inch of aluminum oxide. They were irradiated under the following conditions: burnup, 0.091 to 0.108% of total atoms; surface temperature, 480°C to maximum 1000°C; operating power, 16.6 to 17.2 watts/g of U.

After irradiation there was no sign of warping and no external evidence of dimensional instability, but the axial hole in each specimen had closed uniformly over the length of the element. The average density of the metal changed from 18.9 to 17.7 g/cm^3 [45].

The dimensional instability of uranium, summarized by S. H Bush, is shown in Table 6–8.

Creep properties. Under neutron irradiation, the creep rate of uranium is greatly accelerated, and creep occurs at quite low stresses. This effect has been investigated in the United Kingdom [54,55].

Creep data for unirradiated uranium metal are contained in Reference

TABLE 6–9

RESULTS OF ALPHA-BETA THERMAL CYCLING OF UNALLOYED URANIUM [46]

Specimen* number	Preparation	Density, g/cm³		% change 500 cycles		Appearance after cycling
		Initial	Final	Length	Diameter	
U-2	Beta-treated, wrought	18.85	18.54	+31.6	+13.2	Growth in all directions
U-3	Beta-treated, wrought	18.82	17.95	+56 7	—	Spiny, cactuslike
U-4	Beta-treated, wrought	18.82	18.70	+ 9.09	+18.40	Completely distorted
U-5	Cold pressed and sintered	18.49	13.34	+12.98	+16.76	Mushroomed severely, one end, wrought

*$^3/_8$-inch diameter.

56. Values are given for as-cast uranium over wide ranges of stress and temperature and effects of alloy additions are shown for as-cast and grain-refined metal. The curves and other data give an indication of creep properties over short periods (50 to 100 days), but extrapolation to longer times is not straightforward. At 400°C and 6000 psi creep strains for differently fabricated specimens varied from 0.05% in 1200 hr to 0.35% in 1200 hr.

Temperature limitations. Temperature effects on unirradiated uranium (distinguished from swelling of irradiated fuel) are of two kinds: those for the uranium metal alone, and those concerned with the interaction of the uranium and the cladding.

For uranium metal alone, temperature limitations appear well defined. The alpha-beta transformation temperature, 665.6°C, represents a limit for alpha uranium. Heated beyond this point, uranium expands approximately one percent. As the whole specimen does not undergo this volume change at the same time, local stresses at boundaries lead to plastic deformation of the metal. As the phase change progresses throughout a fuel element, and especially as the cycle is repeated many times, the fuel element is progressively distorted. The effects of such cycling are tabu-

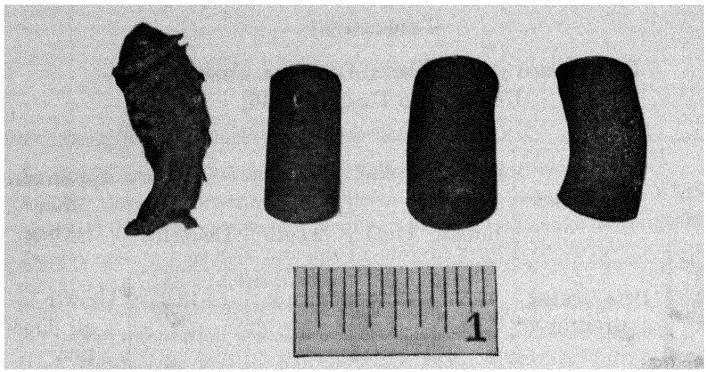

FIG. 6–31 Uranium alloys after cycling 500 times between the alpha-beta phases. [46]

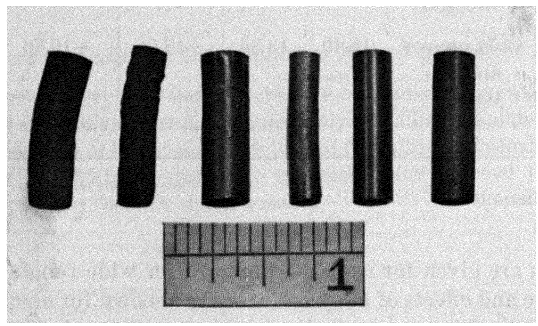

FIG. 6–32. Uranium-niobium alloys after cycling 500 times between the alpha-beta phases [46]

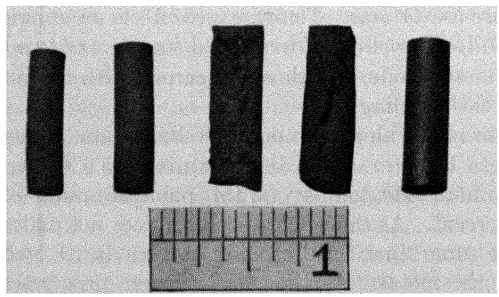

FIG. 6–33. Cold-pressed and sintered uranium alloys after cycling 500 times between the alpha-beta phases. [46]

lated in Table 6–9. Small additions of alloying materials decidedly affect the behavior. Figures 6–31, 6–32, and 6–33, showing results for various alloys, indicate the excellent potential of U-1.6 w/o Nb for high-temperature operation. A powder compact of U-1.6 w/o Nb showed good dimensional stability with low-temperature irradiation up to 0.37 a/o burnup (Fig. 6–28).

Growth rates from irradiation were compared with those from thermal cycling at Argonne National Laboratory [40] For unalloyed uranium, with various fabrication treatments, the kinds of dimensional changes were similar for the two processes, suggesting that thermal cycling experience can sometimes be used to predict irradiation changes. However, it has also been pointed out by Kittel and Paine [40] that no such similarity in behavior was found with uranium-base alloys. For example, a uranium-zirconium alloy elongated rapidly under thermal cycling, but shortened under irradiation. Thus, one should be cautious in using thermal cycling as an indication of irradiation behavior

Other temperature limitations of the uranium metal are associated with the growth and swelling under irradiation, discussed previously, and shown graphically in Figs 6–25 through 6–33. The second kind of temperature limitation has to do with the uranium-jacket interface temperature. The primary mechanism that determines this limitation is the solid-state diffusion of the uranium into the jacket material. Only limited data are available on the effects of irradiation on diffusion rates. Uranium-stainless steel diffusion has been investigated at fluxes of 4×10^{11} to 3×10^{12} nv and temperatures of 500 to 700°C for 16 days, with some diffusion occurring as low as 380°C [47]. Larger changes have been observed for uranium-zirconium and uranium-titanium [48–51]. However, no great effect of irradiation on diffusion has been noted which limits the use of uranium below 600°C.

Aluminum interacts with uranium to form brittle intermetallic compounds above ~350°C [52].

Iron, chromium, and manganese form low melting (~750° to 850°C) eutectics which would limit operation at these temperatures, even if the fuel element were not limited by the alpha-beta transformation temperature of 665°C. Some jacket deterioriation can occur by interdiffusion at temperatures below 600°C. Data on diffusion couples of Al-U, Fe-U, 347 S.S.-U, and Zn-U are shown in Table 6–10 [53]. The change in thickness for these couples can be correlated with time and temperature by the following equation, whose parameters are shown in Table 6–10:

$$d^n = At,$$

where n = an experimentally determined constant, d = thickness, t = time,

TABLE 6–10

DATA ON DIFFUSION COUPLES [53]

Couple	Temperature, °C	Time to penetrate 0.01 inch (0.025 cm)	n	E, kcal	Range applicable	A_0, cm²/sec
Al-U	300	90 days	2.0	12.0	250–450	1.12
Fe-U			2.6	20.4	600–700	
*347 SS-U	625	1 year	2.5	17.7	500–700	
Zn-U	740	45 days	2.0	44.3	600–	0.52

*A nominal 8–18 austenitic stainless steel stabilized with niobium.

$A = A_0 e^{-E/kT}$, A_0 = an experimentally determined constant, E = activation energy in cal/mol, k = gas constant, T = temperature in °K.

Compatibility with gases. Uranium metal fuel is jacketed to prevent corrosion by the coolant. Should a jacket fail, the uranium would be exposed to attack. Gaseous coolants, for the most part, are more compatible with uranium than is water, but for some of them the corrosion rate is extremely high.

(1) Air. The oxidation of uranium in air has been thoroughly covered in the literature [21]. Above 300°C the oxidation rate is very high [approximately 21 mg/(cm²)(hr)] [56,57]. Above 350°C, uranium burns in air.

(2) Nitrogen. The reaction with nitrogen is fairly slow below 500°C [56], but as the temperature is raised to 750°C the rate increases substantially; it has been measured as 12.1 mg/(cm²)(hr).

(3) Hydrogen. Uranium reacts very readily with hydrogen when the uranium surface is free of oxide. The corrosion increases rapidly with temperature reaching a maximum at 225°C. It then decreases because of the progressing rate of decomposition of UH_3. Above 430 to 440°C, hydrogen becomes increasingly soluble in uranium.

(4) Helium and argon. Corrosion by pure helium or argon would not be a problem, even at high temperature. However, commercial helium or argon may corrode uranium appreciably (sometimes faster than dry air) because of the impurity and moisture content.

(5) Carbon dioxide. Because it is abundant and cheap, and has good nuclear and thermal properties, carbon dioxide is now being used prevalently in gas-cooled reactors. For temperatures up to 500°C, the uranium corrosion rate in dry carbon dioxide is not serious [0.38 mg/(cm²)(hr)] [56,57].

(6) Other gases. Uranium metal is not attacked appreciably in carbon monoxide, methane, ethane, or natural gas up to 500°C, providing no impurities or moisture are present.

In general, dry gases such as helium, argon, carbon dioxide, carbon monoxide, and nitrogen, at least up to 500°C, are suitable as far as compatibility with uranium is concerned. The presence of any moisture in these gases can have a very severe effect on the corrosion rate, especially in the inert gases where the protective oxide film formed with air is not present.

6–3.2 Uranium metal jacket materials. To avoid corrosion from impurities and slight amounts of moisture in the coolant gases, uranium metal must be protected from the coolant. The jacket or can also helps to restrain the metal against swelling and prevents the escape of fission products to the coolant. The choice of a canning material depends on (1) its compatibility with the uranium and the coolant, (2) its strength at the operating temperature, (3) the effect of its nuclear characteristics, (especially its absorption cross section) on the reactor design, and (4) the fabricability of the material. Since all these factors affect the over-all fuel costs and other power costs in various ways, it is by no means easy to make an optimum selection.

Some of the important nuclear and engineering properties of various jacket materials are shown in Tables 6–11 and 6–12. The tensile strength values listed in the tables are for fully annealed material except where indicated, and are only representative values. Tensile properties can be improved by hardening (with sacrifice of ductility) and by alloying. Although the tensile strength properties at the various temperatures permit significant comparisons, another property, creep under stress (not shown in the table) must always be considered in selecting a material.

A rough figure of merit, in selecting a jacket or structural material for the least addition of parasitic neutron capture, is the ratio of the yield strength at a given temperature to the macroscopic thermal neutron absorption cross section. For a given stress the material thickness required is inversely proportionate to its strength, and the total neutron absorption increases directly with the thickness. Thus, a high ratio of yield strength to macroscopic absorption cross section means low parasitic absorption for a given strength requirement. Of course, other considerations besides strength often determine the thickness required. In Fig. 6–34 the ratio of yield strength to macroscopic absorption cross section is plotted against temperature for various jacket materials. It can be seen that throughout the temperature range from below 100°C to above 500°C beryllium stands out as being far superior to the rest of the materials. Below 300°C, magnesium, Magnox A-12, zirconium, and Zircaloy-2 are comparable, while above 300°C Zircaloy-2 and zirconium appear better. When hardened by

TABLE 6–11

SOME PROPERTIES OF MATERIALS WITH LOW THERMAL NEUTRON ABSORPTION [21, 58–62]

Material	Density, g/cm³	Melting point °C	Thermal conductivity		Thermal neutron cross sections (2200 m/sec)		Linear thermal expansion		Yield strength (0.2% offset), psi × 10^{-3}	Tensile properties§			
			k, cal/(cm)(°C)(sec)	t, °C	σ_a, barns	Σ_a, $cm^{-1} \times 10^3$	α in/(in)(°C) × 10^6	t, °C		Tensile strength, psi × 10^{-3}	Elongation, %	Test temp, °C	Modulus of elasticity, psi × 10^{-6}
Aluminum	2.7	660	0.503	100	0 230	13.9	28.7	0–600					
At. No. 13			0.530	200									
At. Wt. 26.98			0.546	400									
Type 1100-0	2.72	643–657	0.53	25	0.221	13.3	25.6	0–300	5 0	13	45	24	10
(annealed)									3.5	6	65	204	9
									1.0	2	85	371	4
Type 6061-T6	2.70	582–648	0.37	25	0.233	13.9	25.4	0–300	40	45	17	24	10
(hardened)									15	19	28	204	9
									2	3	95	371	4
Beryllium	1.848	1283	0.395†	20	0 010	1.23	11.54	25–100	30–45‡	35–95	1.5–7	20	42
At. No. 4	(1.79–1 86)*		0.38	200			13.46	25–200					
			0.37	600			17 23	25–700	17	30	19.8	530	38
Magnesium	1.74	650	0 376	20	0 063	2.72	29.9	0–500	14	27	16	20	6.5
At. No. 12													
At. Wt. 24.32													

Type Magnox A-12	1.74	650	0.276	0	0.064	2 5	27.9	20–400	16	20	8	20	6.5
			0.299	200					9.5–14	16	20	100	
			0.323	400					~.7	~1.5	~80	400	
Zirconium At. No. 40	6.44	1845	0.054	100	0 180	7.65	5.69–6.15	0–600	32	54.5	40	27	13.7
									17	36	50	150	
			0.045	300					7.8	18 8	55	345	10.7
			0 03	500					5 2	11.2	88	500	9.2
Zircaloy-2	6.45	1845	0.04	100	0.194	8.2	6.5	0–700	42	54.7	30	27	13.7
									17.5	23.5	40.4	345	10.7
			0.03	500					13.8	19.5	42.1	500	9.2

*Commercial grade beryllium. †Sintered powder specimen ‡Hot-pressed QMV.
§Values are for fully annealed specimens unless indicated.

TABLE 6–12

SOME PROPERTIES OF MATERIALS WITH MEDIUM THERMAL NEUTRON ABSORPTION [63–67]

Material	Density, g cm^{-3}	Melting point °C	Thermal conductivity		Thermal neutron cross sections (2200 m/sec)		Linear thermal expansion		Tensile properties§				
			k, cal/(cm)(°C)(sec)	t, °C	σ_a, barns	Σ_a cm$^{-1} \times 10^3$	in/(in)(°C) $\times 10^6$	t, °C	Yield strength (0.2% offset), psi $\times 10^{-3}$	Tensile strength, psi $\times 10^{-3}$	Elongation, %	Test temp., °C	Modulus of elasticity, psi $\times 10^{-6}$
Chromium	7.14	1850	0.16	20	2.9	240	6.2	20					
At. No. 24													
At. Wt. 52.01													
Iron	7.86	1539	0.175	20	2.53	214	11.7	20	26–32	42–48	22–28	~20	30
At. No. 26			0.105	500			16.2	500					
At. Wt. 55.85													
Stainless steel	7.92	1425–1510	0.035	100	2.99	219	18.7	0–650	30	80	50	25	28
Type 304			0.050	500					19	56	45	500	
Molybdenum	10.2*	2622	0.32	0	2.5	160	5.1	27	65	82	20	20	48
At. No. 42	(~9.3)†						5.1	500					
At. Wt. 95.95	(~6.0)‡		0.25	1000			5.5	1000		30.5	18.7	982	39
Nickel	8.9	1455	0.22	25	4.6	415	13.3	25–100					25
At. No. 28			0.152	300			14.4	25–300					
At. Wt. 58.69			0.148	500			15.5	25–600					
Type A-Nickel	8.89	1435–1445	0.145	0–100			13.3	25–100	21	63	51	25	~30
									19.5	61.5	54	315	~28
									10	21.5	76	649	~24
Niobium	8.4	2415	0.125	20	1.1	59.9	7.1	20	31.5	38	16	20	12.4
At. No. 41			0.140	300			7.3	300	25.5	36	~22	300	8
At. Wt. 92.91			0.156	600			7.55	600	20.5	28	40	600	4.7

*Drawn wire †Sintered ‡Pressed, unsintered §Values are for fully annealed specimens unless indicated

cold work, zirconium and Zircaloy-2 will appear better than magnesium and Magnox A-12 The rest of the materials, including stainless steel, are poorer.

The selection of the material must also take into consideration compatibility, creep strength, and costs. Many of the soft metals and alloys, such as aluminum and magnesium, will be limited by their creep properties at slightly elevated temperature.

Another selection factor is the effect of irradiation Effects of irradiation on metallic structural materials at doses greater than 10^{19} nvt are summarized [67] as follows:

(1) Hardness of metals usually increases, the greatest increase being for metal in the annealed condition

(2) Yield strength increases In stainless steel it may be tripled, and in annealed carbon steels it may be doubled Smaller increases are observed in stronger materials.

(3) Ultimate strength tends to increase only 10 to 30%; thus the yield strength approaches the ultimate strength.

(4) Elongation generally decreases, usually the greater the initial ductility, the greater the reduction in elongation.

(5) Creep tests are, so far, inconclusive

Aluminum. Aluminum has been widely used at low temperatures in reactors Detailed information on aluminum and most aluminum alloys is readily available. Since the date of publication [21], most of the work on aluminum has been to develop alloys that are corrosion resistant in water [68–73]. For gas-cooled reactors, aluminum's usefulness is limited by its poor mechanical properties at high temperatures (>400°C). It is compatible with all the gases except hydrogen up to ~600°C

Beryllium. It is well known that beryllium has outstanding characteristics for reactor applications Its characteristics have recently been described in detail in a USAEC-sponsored book, *The Metal Beryllium*, published by the American Society of Metals [62]. Its properties and uses have also been discussed in a paper by Beaver [135] In general, extensive use of beryllium has been prevented by its brittleness, high cost, and low availability. The high cost and limited availability are factors which will probably become less restrictive with increased use of the material. However, solving the brittleness problem is fundamental to the extensive use of beryllium for fuel element jackets and reactor structures. The general conclusions on the brittleness problem, by J. L. Klein et al. [62], follow:

"Study of the metallurgical factors which affect the room temperature ductility of beryllium has led to the development of methods for producing beryllium rod and sheet which have much more ductility than was

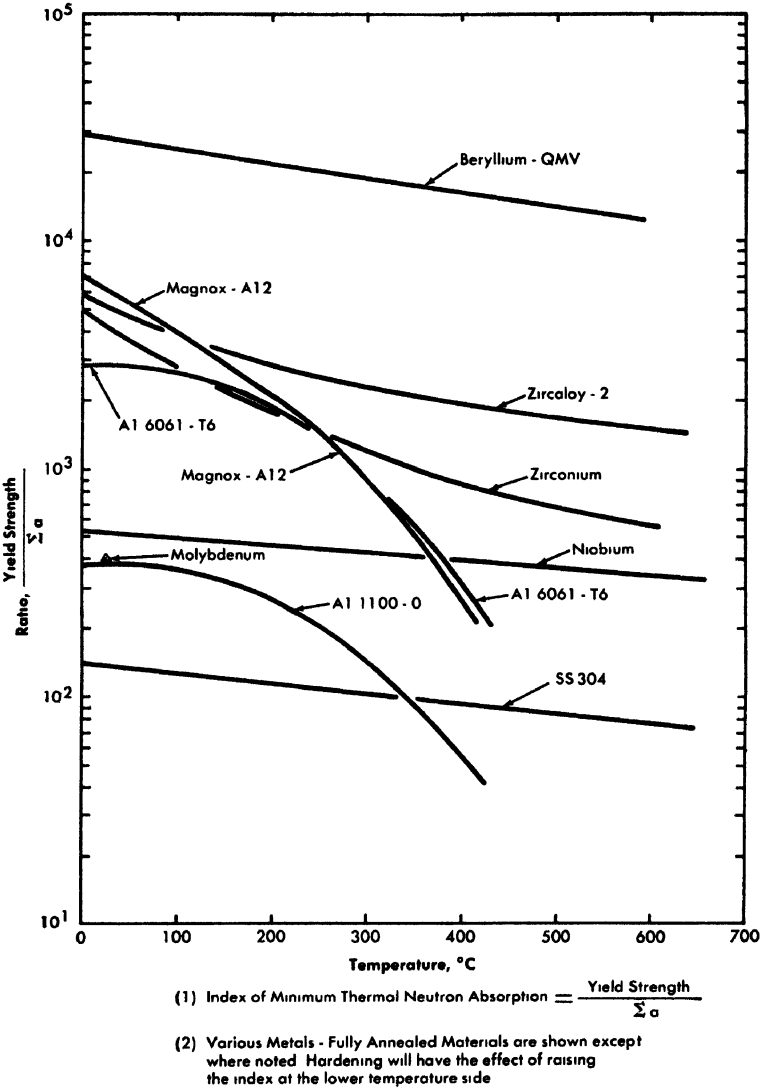

FIG. 6–34. Index of minimum thermal neutron absorption for various metals. (GNEC)

previously considered possible for this metal. Beryllium rods having undirectional ductility of the order of 20% elongation in tension can be produced by hot extruding cold-compacted powders. Beryllium sheet having ductilities of the order of 30 to 40% elongation in all directions in the plane of the sheet (two-dimensional ductility) can be produced by hot extruding flats from cold-compacted beryllium powder, followed by cross rolling at temperatures in the neighborhood of extrusion temperatures.

"Important factors in the consideration of room temperature ductility in beryllium are preferred orientation and microstructure. Results of studies of the behavior of beryllium single crystals permit an understanding of the behavior of polycrystalline beryllium when preferred orientation and microstructure are taken into account."

Beryllium is especially interesting for gas-cooled reactors because it has excellent nuclear properties combined with excellent strength at temperatures above 450°C. Studies of fabricating techniques and alloying are rapidly expanding the technology of beryllium [74–83].

Lengths of beryllium tubing, 4 inches OD, have been extruded experimentally in 5-ft lengths with walls 0.060 to 0.100 inch thick and in 6- to 8-ft lengths with walls 0.12 to 0.25 inch thick. The tensile strength of QMV beryllium has been increased to 50,000 psi at 600°C and 15,000 psi at 800°C by alloying it with iron in preliminary tests [77].

The compatibility of beryllium with these gases has been investigated:

(1) Air No severe corrosion occurs in air below 600°C [62] and corrosion is fairly slow up to 800°C [84]

(2) Oxygen [84] Sintered beryllium is reported to react slowly with oxygen between 350 and 950°C A modified form of the parabolic rate law was found to fit experimental data Below 600°C the corrosion is very small. Between 825 and 850°C the rate of attack doubles.

(3) Nitrogen [84] The reaction of sintered beryllium with nitrogen was investigated in the range from 650 to 925°C There was little corrosion below 650°C, but more reaction above 700°C.

(4) Hydrogen [84]. There was very little corrosion of beryllium in hydrogen between 300 and 780°C at a pressure of 2.3 cm of mercury.

(5) Carbon dioxide W. Munro and J Williams [85] investigated the corrosion of beryllium in dry and wet CO_2 at atmospheric pressure for the temperature range of 500 to 700°C The results indicate: corrosion is negligible up to 500°C in both dry and wet gas; in this range the weight gain follows the parabolic law $w^2 = kt$, where $k_{\text{dry gas}} \sim 5 \times 10^{-16}$ g^2/(cm^4)(sec) and $k_{\text{wet gas}} \sim 7 \times 10^{-16}$ g^2/(cm^4)(sec); at 600°C a film is formed which is protective in the dry gas only; above 650°C the film is no longer protective even to dry CO_2 gas.

Corrosion data on beryllium in water are reported as being very erratic because beryllium metal, consistently good and sound, has not been available [62]. With an adequate supply of uniform material, better and more consistent data can be expected. Such data should help to explain the poor corrosion behavior tendencies of beryllium in water as low as 270°C.

Studies by the United Kingdom on the compatibility of beryllium with metallic uranium showed excellent performance up to 600°C [86]. It was postulated that the good performance was due to the formation of a

beryllia diffusion barrier. Should this barrier break down, a rapid formation of UBe_{13} would be expected.

A problem in manufacturing beryllium is its toxicity. This has been covered by Eisenbud [62] in detail. The U. S. Atomic Energy Commission has recommended the following precautions in fabricating beryllium:

(1) The in-plant atmospheric concentration of beryllium should not exceed 2μ g/m^3 as an average throughout an 8-hour day.

(2) Even with the daily average within these limits, no one should be exposed to a concentration greater than 25μ g/m^3 for any period of time, however short.

(3) In the neighborhood of a plant handling beryllium compounds, the average monthly concentration should not exceed 0.01μ g/m^3.

Magnesium. The excellent nuclear properties of magnesium and its strength properties below 400°C have led to its use by the United Kingdom and France in several gas-cooled graphite-moderated reactors [87–93]. Properties of magnesium and some alloys developed by the British have been reported in detail by T. J Heal of the U.K.A E.A [61]. In general, the magnesium alloys developed appear to be compatible with uranium metal up to 450°C and can operate satisfactorily in carbon dioxide at this temperature. With Magnox A-12 alloy,* loss of the metal in dry carbon dioxide at 120 psi has reduced fuel jacket thickness by only 0.002 inch on the average, in 4 months. There was occasional pitting to depths not greater than 0.002 inch, but no increase after the first month [61].

Little is known of the behavior of molten magnesium or Magnox with carbon dioxide and the possible hazard of the Mg-CO_2 reaction at high temperatures. Ignition tests by the British [61] on Magnox alloys showed an ignition temperature of about 640°C in 160 psi CO_2 and no ignition up to 700°C in CO_2 flowing at 20 ft^3/hr at atmospheric pressure.

The strength properties of the magnesium alloys limit them to operation below 500°C; thus they are not usable in the higher temperature reactors for which gas cooling is so well suited

Zirconium. The physical and nuclear properties of zirconium and its alloys make it an excellent material for reactor use. Its thermal conductivity is too low, however, for it to be effective as a fin material for fuel elements. A detailed review of zirconium, "The Metallurgy of Zirconium" [59], sponsored by the AEC, has been published. Many of the data in this book, and further information from the U.K.A.E.A. have been condensed in an excellent review article "Zirconium and Its Alloys" by C. Tysack [94] and details will not be repeated here. Continued effort on development of zirconium alloys has improved fabricability and de-

*Pure magnesium with very small additions ($<1\%$) of aluminum and beryllium.

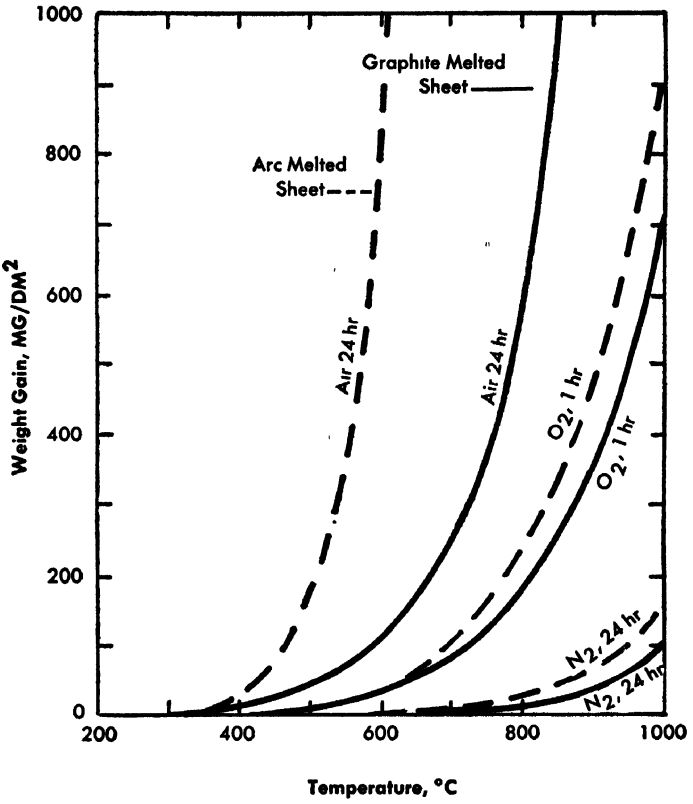

FIG. 6–35 Heat resistance of zirconium in air, oxygen, and nitrogen [96]

creased cost of the fabricated material. Cold working of the Zircaloy-2 alloys can increase the yield strength of the annealed material by approximately 30% while retaining good ductility Most recent work on zirconium alloys has been to improve their corrosion resistance in high temperature water; they have shown excellent performance for that purpose [95].

The reaction of zirconium in gases has been covered in detail by E. A. Gulbransen [59]. In general, zirconium is very unreactive with the several gases in air at room temperature. However, at slightly elevated temperatures, zirconium reacts readily with oxygen and hydrogen, and at higher temperatures with nitrogen [96]. It was found that after the initial rapid reaction, the weight gain data fit the parabolic rate law $w^2 = kt + c$, where w = weight gain, t is the time, k is the parabolic rate law constant, and c is the initial reaction constant. Figure 6–35 shows the weight gain as a function of temperature for reactions of zirconium with oxygen, air, and nitrogen. Hydrogen contamination with as little as 25

ppm can cause serious embrittlement under certain conditions, leading to failure.

Hayes and Robertson [97] have investigated the reaction of carbon monoxide, carbon dioxide, sulfur dioxide, propane, and steam with graphite-melted and arc-melted zirconium at temperatures above 500°C. These data, presented in Table 6–13, indicate that zirconium is not usable above 500°C except for a short time. Hayes and his associates [98] discovered the gas temperature limits for these reactions for the times shown in Table 6–14. The British data [94] in general substantiate the U. S. data and add substantially to the information on low temperature reaction of zirconium with carbon dioxide. Data taken with zirconium and Zircaloy-2 in dry carbon dioxide at 120 psia (see Table 6–15) show the iodide zirconium more resistant than Zircaloy or zirconium prepared by other methods.

Little systematic work has been done to develop a zirconium alloy resistant to gases at high temperature. An investigation of 23 alloy systems prepared by graphite-melting sponge zirconium, as shown in Table 6–16, indicated that only alloys containing iron, nickel, or silver, and certain copper-bearing ternary alloys, were better than pure zirconium in air at 650°C [59,99].

Further development of alloys resistant to carbon dioxide or to the impurities of helium may improve the prospect for zirconium as a material for gas-cooled reactors above 500°C

Niobium. Niobium is being investigated for application to nuclear reactors because it remains strong at high temperatures and has a thermal neutron absorption cross section much lower than that of stainless steel. Figure 6–34 shows that for low parasitic addition to the reactor, niobium ranks well above stainless steel; and at high temperature (>600°C) it is almost equal to zirconium and Zircaloy-2 which at present are not useful above 500 and 400°C, respectively, in carbon dioxide systems. Niobium forms well-behaved alloys with uranium. Also, a strong metallurgical bond can be produced between niobium cladding and uranium metal alloys [100].

Little is known of the behavior of niobium in gases other than nitrogen or oxygen. In nitrogen at 482°C, surface embrittlement occurs with a penetration of 0.001 inch in 1000 hr. An adherent nitride film limits the rate of attack. In oxidizing media above 500°C the metal forms a porous scale and oxidizes in direct proportion to the exposure time [100–102]; at 1371°C a runaway reaction has been observed between niobium and pure oxygen. Further studies [103–106] on the oxidation behavior of niobium alloys have shown that some improvement can be obtained but the rate is still too high for many applications. In addition to its poor oxidation resistance, the cost of high-purity ductile material is very high, approximately $200/lb.

TABLE 6–13

WEIGHT GAIN AND HARDNESS OF ARC-MELTED ZIRCONIUM IN VARIOUS GASES [59, 97]

	Temperature, °C	Weight gain, mg/dm²		Hardness, R_s	
		1 hr	24 hr	1 hr	24 hr
Carbon monoxide	500	12	43	85	81
	600	37	139	79	78
	700	78	208	77	78
	800	113	558	78	83
	900	107	441	75	93
	980	93		80	
Carbon dioxide	500	20	57	82	81
	600	52	127	78	78
	700	107	291	78	78
	800	205	558	78	81
	900	350	1030	73	95
	980	594		84	
Sulfur dioxide	500	7	19	86	85
	600	22	97	81	77
	700	5440			
Propane	500	13	17	85	85
	600	40	96	79	78
	700	48	204	77	84
	800	82	201	82	89
	900	80	317	83	97
Steam	400	0.4	4	89	88
	500	15	63	85	80
	600	40	174	79	78
	700	86	237	79	79
	800	182	502	80	82
	900	293	1064	78	96
	1000	519		84	

TABLE 6–14

HEATING LIMITS (SAFE TEMPERATURE, °C) FOR GRAPHITE- AND ARC-MELTED ZIRCONIUM [59, 97]

Medium	1 hr		24 hr	
	Graphite-melted	Arc-melted	Graphite-melted	Arc-melted
Air	700	800	500	700
O_2	700	800		800
N_2	800	900*	800	900*
H_2	600		500*	700*
CO	900	900	700	800
CO_2	900		650	700
SO_2	500	600	500	600
C_3H_8	900		900	
Steam	900	900	600	700

*May be 25 to 50°C lower.

TABLE 6-15

CORROSION PENETRATION OF ZIRCONIUM AND ZIRCALOY-2 IN DRY CARBON DIOXIDE AT 120 PSIA [72]

Temperature, °C	Material	Extrapolated penetration, inch × 10^3	
		After one year	After three years
400	Iodide Zr	0.05	0.085
400	C-melted Zr	0.06	0.097
400	Arc-melted Zr	0.087	0.17
400	C-melted Zircaloy-2	0.090	0.14
500	Iodide Zr	1.91	5.4
500	C-melted Zr	5.75	21.0
500	Arc-melted Zr	4.7	24.4
500	C-melted Zircaloy-2	22.6	78.0

TABLE 6-16

CORROSION OF ZIRCONIUM ALLOYS IN AIR AT 650°C [59]

Alloy element	Limit of addition, w/o	Corrosion rate, mg/cm² per day
Al	10	*
Be	5	*
B	5	*
Ce	5	*
Cr	10	600–1500
Co	46	600–1500
Co-Cr alloys:		
Co content	4	
Cr content	5	
Nb	12	
Cu	15	600–1500
Cu alloys with Fe, Co, or Ni		600
Cu content	5	
Fe, Co, or Ni content	5	
Fe	60	600
Mn	25	*
Mo	10	*
Ni	10	600
Si	5	*
Ag	10	600
Ta	30	*
Th	5	*
Sn	10	*
Ti	90	*
W	10	*
V	10	*
Zr		600–1500

*Alloy disintegrates in less than 24 hr.

Stainless steel. For application to gas-cooled reactors, the high nickel-chromium alloys [63] of iron have excellent physical properties but have large absorption cross sections. The stainless steels are resistant to corrosion by most of the gases up to 800° to 900°C and can be used as the jacket material for uranium or uranium dioxide. In the case of uranium metal, low-melting (~750° to 850°C) eutectics are formed with iron, chromium, and manganese which limit the operation of stainless-clad me-

tallic uranium fuel elements to below 750°C. Above approximately 600°C some kind of barrier may be required to limit the diffusion between uranium and stainless steel [47].

Chromium, nickel, and iron. These materials, having absorption cross sections similar to those of stainless steel, are now considered useful only as alloying elements.

Other jacket materials. Studies have also been made on the corrosion protection of uranium metal by various ceramic coatings and metallic diffusion layers. Ceramic glazes and methods of application have been developed which are suitable for the vitreous coating of uranium [107,108]. Coatings only one mil thick have been successfully applied to uranium and have retained good shock and abrasion resistance [109]. These coatings, although they dissolve rapidly in water at 130°C, show some possibility as a secondary barrier in the event of jacket failure in a water-cooled system, and as a primary or secondary barrier against gases or organic coolants.

Diffusion coatings of nickel, silicon, and copper-magnesium one mil thick have provided good corrosion protection to uranium in boiling water at 100°C [110]. Performance of these diffusion coatings under irradiation is not known.

6–3.3 Uranium dioxide. In general, uranium dioxide fuel elements have the advantages of being relatively inert chemically and relatively resistant to radiation damage. Their primary disadvantages are brittleness, relatively low fuel density, and low thermal conductivity. The latter disadvantage is somewhat compensated by the high permissible operating temperature; but, for a given heat flux, oxide fuel elements will probably have to be thinner than metal elements. This characteristic, combined with the low fuel density, usually causes a significant loss in neutron economy relative to that attainable with metal elements, and requires greater subdivision of the oxide fuel, which may increase fabrication costs. However, the attainment of high surface temperatures (>600°C) and good radiation stability at long burnups make UO_2 especially attractive in gas-cooled reactors where high temperatures are particularly useful. The general properties of uranium dioxide are given in Table 6-17.

The preparation of uranium dioxide and its sintering characteristics have been described in detail by Belle and Lustman [113]. Recent data on some of the properties which affect nuclear reactor design are presented below:

(1) Melting temperature. Various values have been given for the melting point of UO_2. However, the value 2878 ± 22°C (5212 ± 40°F) obtained by Lambertson and Mueller [114] has been generally used. More

TABLE 6–17

GENERAL PROPERTIES OF URANIUM DIOXIDE [111, 112]

Crystal structure	Face-centered cubic
Theoretical UO_2 density, g/cm³	10.97
Theoretical uranium density in UO_2, g/cm³	9.7
$\frac{\text{U atom/cm}^3 \text{ in } UO_2}{\text{U atom/cm}^3 \text{ in U metal}}$, ratio	0.515
Melting temperature (mean), °C	2760 (5000°F)
Linear coefficient of thermal expansion, in/(in)(°C)	11.2×10^{-6}
Specific heat (0 to 200°C), cal/(g)(°C)	0.056
Thermal conductivity, cal/(cm)(°C)(sec) (t = 1000°C, d = 10.97 gm/cm³)	0.008 [1 93 Btu/(ft)(°F)(sec)]
Tensile strength (approximate), psi	5000
Modulus of elasticity, psi	25×10^6
Index of refraction	2.35

recent data reported by Wisnyi and Pijanowski [112] indicated the melting point to be 2760 ± 30°C (5000 ± 44°F). The discrepancy may be accounted for by possible impurities in the UO_2. Small additions of impurities can vary the melting point radically, as shown by the binary systems diagrams prepared by the National Bureau of Standards [115].

(2) Thermal conductivity. The generally accepted values of thermal conductivity are those prepared by Kingery and Vasilos [116] The curve prepared from these values is generally higher than the curve prepared by the Armour Research Foundation (ARF) [117] One explanation of the lower values by ARF lies in the fact that their specimen was found to be badly cracked after the test was completed. These values may, however, be more representative of the thermal conductivity of the UO_2 specimens used in reactors which also crack radially under the operating thermal stresses. Table 6–18 shows the values corrected to 95% of theoretical UO_2 density, and Fig 6–36 is a plot of the data obtained [113].

(3) Modulus of elasticity. The modulus of elasticity of uranium dioxide as a function of temperature has been determined recently by the National Bureau of Standards (Fig. 6–37). Specimens were prepared from ammonia-precipitation diuranate and were fabricated to a density of 93% of theoretical [113].

(4) Summary. Other physical properties have been covered by Belle and Lustman [113]; a summary of the data, presented as conclusions to a paper at the Paris Fuel Element Conference [120], is reprinted below.

TABLE 6-18

THE VARIATION OF UO_2 THERMAL CONDUCTIVITY WITH TEMPERATURE [113]

Temperature		Thermal conductivity,* cal/(cm)(°C)(sec)	
°C	°F	Kingery & Vasilos	Armour Research Foundation
200	392	17.7×10^{-3}	12.3×10^{-3}
400	752	12.8×10^{-3}	9.4×10^{-3}
600	1112	9.9×10^{-3}	7.7×10^{-3}
800	1472	8.3×10^{-3}	6.2×10^{-3}
1000	1832	7.8×10^{-3}	5.7×10^{-3}
1200	2192		5.0×10^{-3}
1400	2552		4.6×10^{-3}
1600	2912		4.2×10^{-3}
—	—†‡	4.15×10^{-3}	

*Corrected to 95% of theoretical density.

†Data presented by Jakob [118] indicates that the thermal conductivity of powders is independent of density above 1000°C.

‡"Mr. W. D. Kingery has pointed out that in single-phase ceramics, lattice thermal conductivity may, under suitable conditions of elevated temperature or lattice disturbance by irradiation, be reduced to a minimum value, set by photon scattering, at mean free paths of the order of the lattice spacings; in the case of UO_2, such a minimum value would correspond to about 1 Btu/(ft)(°F)(hr)" [119].

Conclusions by Belle and Lustman [113]

"Characterization studies of various methods of UO_2 powder preparation showed that although powder properties such as particle size, surface area, and density of a UO_2 powder can vary over a wide range depending upon method of preparation, these properties can be controlled through judicious choice of variables in the preparation procedure. These variations in physical properties have a large effect on rates of sintering of compacted powder at elevated temperatures but a relatively minor effect on the structure of high-density UO_2.

"Some conclusions that can be made from the information obtained from sintering studies on UO_2 are the following:

"1. The characteristics for a powder to sinter rapidly to high density, to show little dependence of sintered density on green density, and to pro-

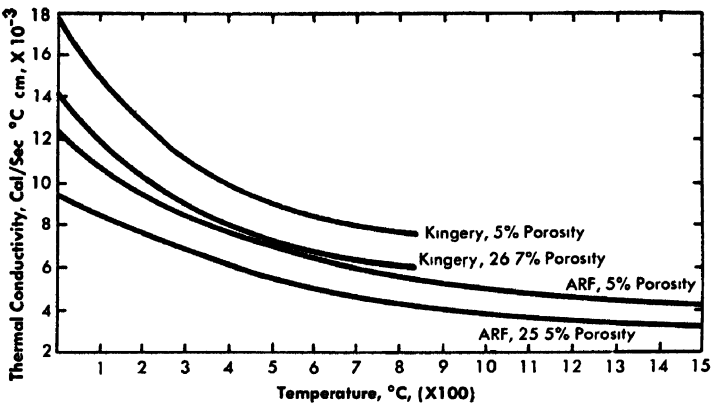

FIG. 6–36 Thermal conductivity of UO_2. [113]

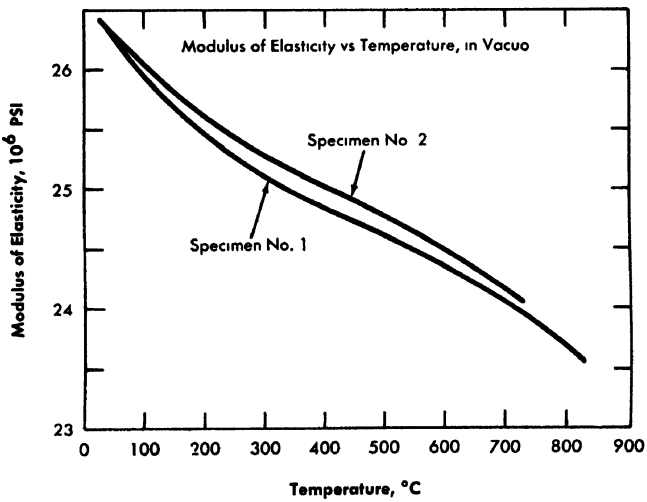

FIG 6–37 Modulus of elasticity of UO_2 *in vacuo*. [113]

duce a uniform grain structure in the sintered material are high surface area, high density, and either small particle size or a clustered particle size easily broken down uniformly to a small particle size.

"2. These properties can be achieved by a comminution process such as ball milling.

"3. Densification due to cold pressing occurs primarily through the progressive compression of the larger pores.

"4. Main mode of densification in the early stages of sintering is the decrease in the amount of open porosity, and the main difference among

various powder preparations is in the length of time required to reach the stage of nonconnected porosity.

"5. Sintering in hydrogen probably occurs through a plastic or viscous flow mechanism, whereas densification in steam sintering occurs by oxygen ion diffusion.

"6. Grain size is controlled by the density of UO_2.

"Results of studies on the physical properties of UO_2 can be summarized as follows:

"1. The melting point of UO_2 is 2760 ± 30°C.

"2. As expected, modulus of rupture of UO_2 increases with increase in temperature, whereas modulus of elasticity decreases with increase in temperature.

"3. UO_2 is an electronic conductor, an estimate from self-diffusion data shows that the ionic contribution is small.

"4. Magnetic susceptibility measurements indicate that, in high O/U ratio UO_2, the excess oxygen content is accommodated by interstitial occupancy.

"5. Neutron diffraction measurements indicate that excess oxygen enters the UO_2 lattice at definite positions and is not distributed at random.

"Extensions of phase equilibria studies for the UO_2-U_3O_8 system showed little changes from the recent phase diagram presented by Gronvold. These differences are in the location of the boundary of the UO_{2+x} phase and U_4O_{9+x} at temperatures of 1100 to 1350°F were obtained. It was found that the partial molar free energy of solution of oxygen in UO_{2+x} is a linear function of temperature.

"Oxidation of UO_2 in the temperature range 120 to 350°C proceeds by a diffusion mechanism whereby oxygen ions diffuse into interstitial positions in the UO_2 lattice These measurements are in agreement with diffusion data from CO_2-UO_2 exchange reactions. The reduction of U_4O_9 and U_3O_8 to UO_2 is a surface controlled reaction

"As revealed from self-diffusion kinetic measurements, the mobility of oxygen anions is much greater than that of uranium cations in UO_2; the activation energy for oxygen diffusion is 29.7 kcal/mole as compared with a value of 90 to 125 kcal/mole for uranium diffusion

"If properly fabricated, high-density UO_2 is stable to oxidation over long periods of time in degassed water and steam at neutral and high pH. In the presence of dissolved oxygen, however, UO_2 reacts to form a hydrated oxide $UO_3 \cdot 0.8H_2O$."

Irradiation performance of UO_2 Natural UO_2 fuel elements have been irradiated to burnups of four and five times that presently achievable with unalloyed natural uranium metal fuel. This higher burnup has the effect of reducing both the fabrication and reprocessing costs per

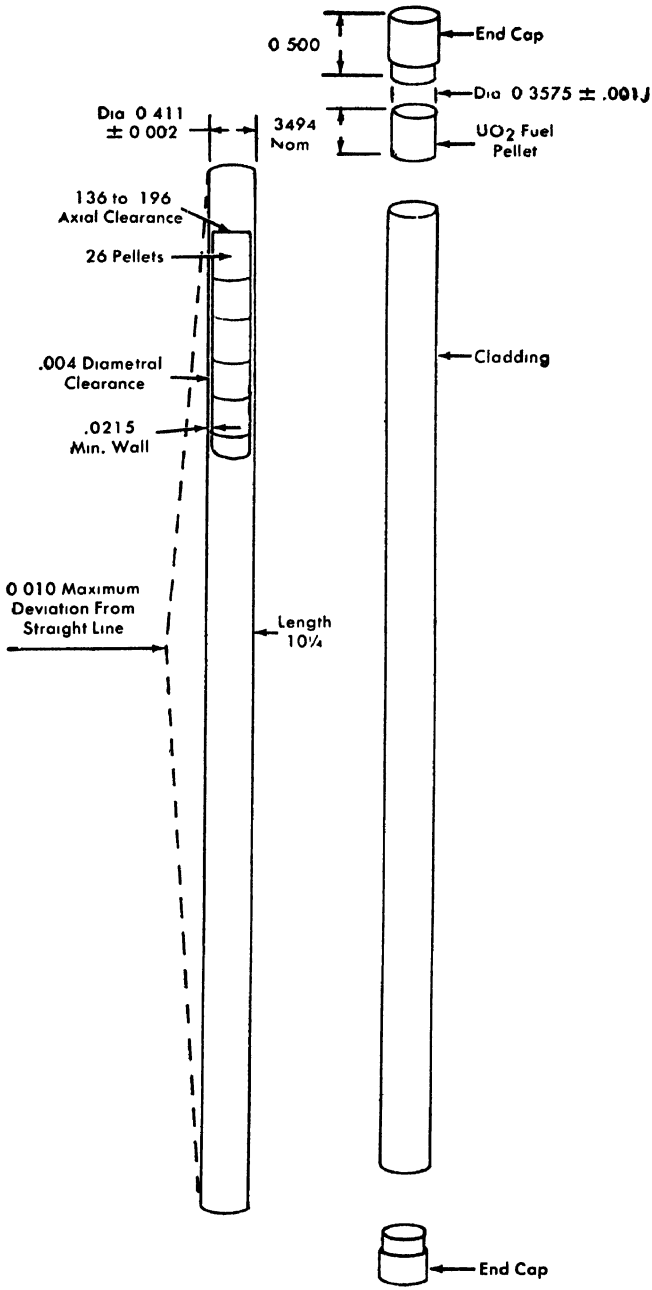

FIG. 6–38. Blanket fuel rod PWR Core I. [119]

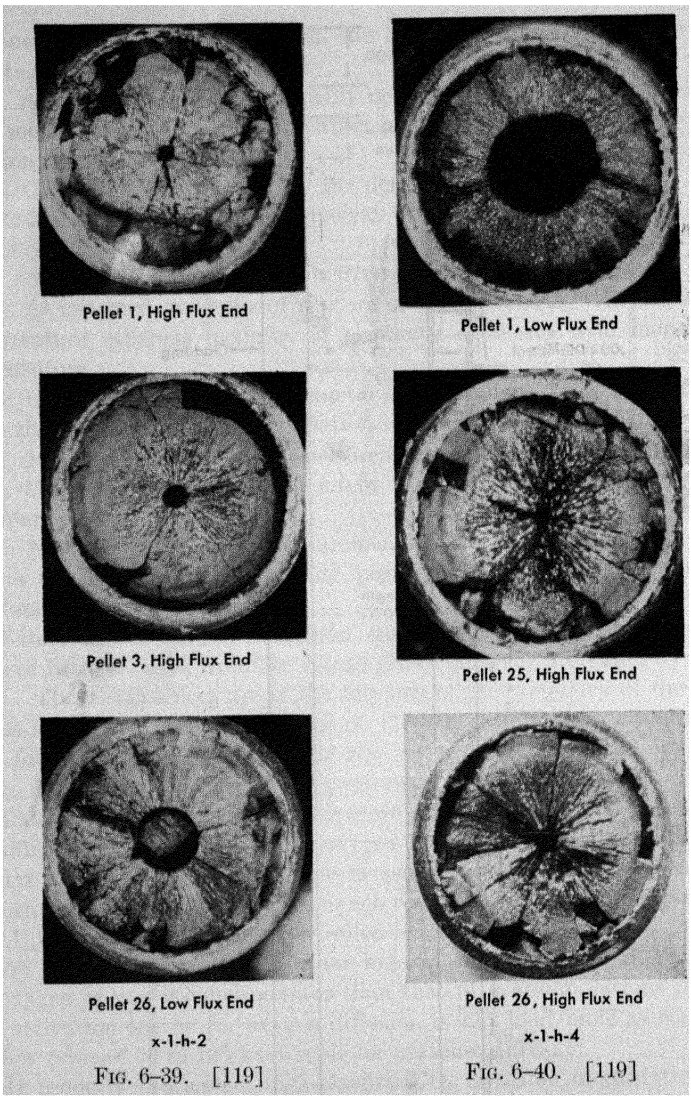

FIG. 6–39. [119]

FIG. 6–40. [119]

Figures 6–39 and 6–40 show molten zones and solidification craters in the UO_2 at various locations in specimens x-1-h-2 and x-1-h-4. After 48 days in reactor, specimens were removed; examination revealed center melting of the UO_2 in all specimens. Test conditions and performance were as given on the opposing page.

unit of heat produced. Since the behavior of these elements under irradiation and at high temperature is most important to the reactor designer, Bettis Plant* has conducted an extensive study on the effects of irradiation on UO_2 fuel elements (in the Pressurized Water Reactor development program). Detailed information on the results of these tests have recently been published [113,121,122].

The irradiation tests were mainly conducted with full-size PWR UO_2 fuel rods (Fig. 6–38). These rods consist of 10¼-inch-long Zircaloy-2 tubing (0.359 inch ID × 0.411 inch OD) in which 26 UO_2 fuel pellets (0.357 inch OD) of 93 to 95% of theoretical density are stacked. The heat-transfer bond is helium at atmospheric pressure Because of the number of rods and the large number of UO_2 fuel pellets per rod, these tests should be fairly representative of what will result from the use of similar fuel rods in a power reactor.

High-burnup data on the PWR blanket fuel rods tests is summarized in Tables 6–19 and 6–20. The experiments shown are those having the highest burnups achieved during the irradiation program. Many more tests have been conducted at various burnups and heat fluxes by Eichenberg et al. [119].

The general conclusions from these data by Eichenberg et al. are that no microstructural, dimensional, and property changes have been found

*A U. S. Government-owned laboratory facility operated by Westinghouse.

Specimen number	x-1-h-2	x-1-h-4
Heat flux,* Btu/(ft²)(hr)	473,000	487,000
Burnup,* Mwd/ton	2,820	2,910
UO_2 density, % theoretical	95	95
Enrichment, w/o U^{235} in total U	7.8	7.8
Diameter of defect hole, inches	0.005	None
Specimen dimensions, inches:		
UO_2 diameter	0.351	0.351
Clearance, diametral	0.008	0.008
Clearance, axial	0.190	0.190
Jacket-tube OD	0.413	0.413
Over-all length	10.25	10.25
Dimensional changes, inches·		
Diameter	0.001	0.000
Length	0.006	0.006
Melted center diameter	0.20–0.22	0.19–0.21
Crater diameter	0.04–0.17	0.025–0.100

* Heat flux values are based on calorimetric values obtained from the ΔT across test loop; burnup values were obtained from fission monitors.

TABLE 6–19

DESCRIPTION AND SUMMARY OF AVAILABLE DATA ON UNCYCLED ZIRCALOY-2 CLAD UO_2 FUEL ELEMENTS [119]

Spec. no.	Heat flux,* Btu/(ft²)(hr) × 10^{-3}	Burnup,* Mwd/t	Calculated central temperature, °C	Specimen dimensions, inches					Dimensional changes		Molten zone diameter	Fission gas release, % Kr^{85}
				UO_2 dia.	Clearance		Tubing OD	Over-all length	Dia.	Length		
					Dia.	Axial						
Experiments 14–12 *and* 13												
15H	370(f)	10900	2650	0.3445	0.0015	0	0.402	5.237	0	0	Not melted	5.0
18H	420(f)	13500	>2750	0.3445	0.0015	0	0.400	5 240	0	0	Not melted	8.1
19H	300(f)	6900	2200	0.3445	0.0015	0	0.402	5.238	0	0	Not melted	
Experiment 14–14												
82S	330(e)	14000	2400	0.3445	0.002	0.080	0.414	5.205	0	0	Not melted	
83S	540(e)	22000	>2750	0.3445	0.002	0.080	0.414	5.222	+0.012	0	0.200	
84S	600(e)	25000	>2750	0.3445	0.002	0.080	0.414	5.224	+0.015	0	0.230	
85S	300(e)	12000	2200	0.3445	0.002	0.080	0.414	5.206	0	0	Not melted	

Remarks: These two experiments were designed to study the effect of irradiation at high heat fluxes and to high burnups on hot-pressed natural UO_2. Sample 15H contained 95% dense hot-pressed UO_2 made from steam-oxidized material, while samples 18H and 19H contained 91% dense hot-pressed UO_2 made from MCW-UO_2. The steam-oxidized UO_2 is made by oxidizing uranium in an autoclave at 650°F and saturation pressure. MCW-UO_2 is made by reducing UO_3 with cracked ammonia. The results of these experiments indicate that hot-pressed UO_2 is quite stable when irradiated to high burnups and high heat fluxes.

Remarks: This experiment was designed to determine the effect of irradiation to extremely high burnups on PWR reference rods. The samples contained 93% dense cold-pressed and sintered natural UO_2 and were assembled to reference specifications. The Zircaloy-2 tubing for these rods, however, was machined from bar stock rather than extruded as is the case for the PWR reference rods, and this machined tubing was of somewhat dubious quality. The rods were irradiated in the MTR lattice for 1½ years and achieved an estimated burnup of 25,000 Mwd/t. Unfortunately, the cladding split on all the rods, permitting

the NaK to attack the UO_2, and also preventing any fission gas studies. In an attempt to determine if the cladding split because of a deterioration in the mechanical properties as a result of the high irradiation exposure, the hardness of the cladding of a high and low flux specimen was measured. Although no control hardness values are available, the hardness of the cladding on both of the samples was within the range of as-fabricated tubing.

Experiment 14–18

9B2	300(f)	6430	1400	0.3570	0.002	0	0.413	4.544	0	0	Not melted	0.25
9B3	900(f)	12400	>2750	0.3570	0.002	0	0.413	4.560	+0.009	+0.009	0.250	13.6
10B1	890(f)	12100	>2750	0.3570	0.002	0	0.413	4.506	+0.008	+0 015	0.275	15.3
10B2	300(f)	6100	2200	0.3570	0.002	0	0 413	4 518	0	0	Not melted	

Remarks: This experiment was designed to determine the effect of irradiation to very high burnups of 93% dense cold-pressed and sintered UO_2, enriched 6.24% U^{235} in total U. The Zircaloy-2 tubing was manufactured by the reference extrusion process. The UO_2 in the two higher exposure rods was molten over a considerable portion of the diameter, yet very little dimensional change occurred in the samples. The fission gas release values indicate that molten UO_2 retains considerably less of the fission gas than UO_2 irradiated below the melting point.

Experiment 14–19

24B1	340(f)	6700	2400	0.3510	0.008	0	0.413	—	0	—	Not melted	
24B2	670(f)	14400	>2750	0.3510	0.008	0	0.413	—	+0.002	—	0.290	
24B3	840(f)	15500	>2750	0.3510	0.008	0	0.413	—	+0.018	—	0.325	35.6
25B1	340(f)	7930	2400	0.3510	0.008	0	0.413	—	0	—	Not melted	1.2

Remarks: This experiment was designed to determine the effect of large diametral clearances (0.008 inch) on the behavior of reference PWR rods irradiated at high heat fluxes. Although a considerable portion of the UO_2 melted in the two higher exposure samples, the heat fluxes are not known to a sufficient degree of accuracy to ascertain the effect of the 0.008-inch diametral clearance as opposed to the reference 0.002-inch to 0.004-inch diametral clearance. Again, the effect of melting in the UO_2 can be noted in regard to the amount of fission gas released.

*Heat flux, burnup, and calculated center temperatures are based on estimates of nominal reactor fluxes when indicated by (e) and fission monitor results when indicated by (f). The estimates are good only to ±50%, while the fission monitor data are felt to be somewhat more accurate. The inconsistencies noted between the calculated center temperatures and the observed melting are presumably produced by these inaccuracies.

TABLE 6–20

DESCRIPTION AMD SUMMARY OF AVAILABLE DATA ON IRRADIATION-CYCLED ZIRCALOY-2 CLAD UO_2 FUEL ELEMENTS [119]

Spec. no.	Heat flux,* Btu/(ft²)(hr) × 10^{-3}	Burnup,* Mwd t	Specimen dimensions, inches					Number of cycles	Dimensional changes	
			UO_2 dia.	Clearance		Tubing OD	Over-all length			
				Dia.	Axial				Dia.	Length
Experiment 19–7										
N-5-9-C	450	18000	0.357	0.002	0.150	0.414	10.298	7000	0	0
N-5-7-C	450	18000	0.357	0.002	0.058	0.414	10.302	7000	0	0
N-5-9-B	450	9000	0.355	0.004	0.150	0.414	10 303	7000	0	0
N-5-10-B	450	9000	0.355	0.004	0.055	0 414	10.297	7000	0	0

Remarks: This test was designed to determine the effect of irradiation cycling to very high burnups on the possible dimensional instability of cycled rods. The rods contained 95% dense cold-pressed and sintered UO_2, enriched 6.2 w/o U^{235} in total U. No dimensional changes were produced as a result of the irradiation.

*Burnup and heat flux values are based on estimates of the thermal neutron flux in the various reactor locations and are considered to be accurate to only ±50%

except those associated with purely thermal effects. Grain growth in the UO_2 specimens occurred at the same temperatures, in-pile and out-of-pile. Gross radial cracking and some circumferential cracking were anticipated because of the large thermal gradients across the fuel, but the cracking appears to be independent of burnup, since further cracking at higher burnup was not observed. External dimensional changes were negligible even in fuel elements irradiated to burnups of 10,000 Mwd/t. It was also noted that temperatures above melting were achieved in the UO_2 irradiated to 25,000 Mwd/t without apparent damage or disintegration of the pellets. Figures 6–39 and 6–40 illustrate the type of cracking as well as the effect of center melting in UO_2 specimens.

A conclusion from the present irradiation data is that UO_2 fuel elements of this kind do not show an inherent tendency to fail during irradiation exposures up to 10,000 Mwd/t, and perhaps higher. Gross cracking of the oxide pellets does occur early in their life, the transfer of heat from the interior of the element to the jacket deteriorates slowly with exposure, and there is a release of some gaseous fission products from the oxide, which increases with oxide temperature. If the design of the fuel elements makes adequate allowance for these effects, the fractional rate of failure of such elements in a reactor, to maximum burnups of the order 10,000 Mwd/t, should be reasonably low.

Bonding material. The bonding material in the gap between the fuel pellet and the can will materially affect the heat transfer of the element. A list of bonding materials which may be used or which may contaminate the original material is shown in Table 6–21 along with the temperature drop through a one-mil bonding gap at a heat flux of 500,000 Btu/(ft²) (hr) [119]. Since the central temperature of the fuel will depend partly on the temperature drop in the heat-transfer bond, this temperature drop should

TABLE 6–21

URANIUM DIOXIDE BONDING MATERIALS [119]

Bonding material	Temperature drop in 0.001-inch bond gap,* °F
Helium	288
Xenon plus krypton	5400
Steam	1490
50% He + 50%(Xe + Kr)	900
Hydrogen	278
Lead	2.1

TABLE 6–22

MINIMUM HEAT FLUXES FOR MELTING AND GRAIN GROWTH [119]

Specimen description	Cold diametral clearance, inches	Observed heat flux, Btu/(ft²)(hr)		Grain growth temp., °C
		Melting	Grain growth	
Defected	0.005–0.008	370,000	340,000	2000
Defected	0.001–0.004	425,000	330,000	2050
Undefected	0.005–0.008	422,000	360,000	2250
Undefected	0.001–0.004	(530,000) est.	430,000	2300

be kept low. The mixing of fission-product xenon and krypton with the heat-transfer bond, or the mixing or substitution of reactor coolant for the bond material may substantially increase the central fuel temperature for the same surface heat flux.

Minimum heat fluxes for melting or grain growth The minimum heat fluxes at which melting or grain growth has been observed under various conditions are shown in Table 6–22 Although center melting has been observed in many specimens without apparent failure of the canned fuel element, more tests and performance data are required before center melting can reasonably be assumed as a safe operating condition for design purposes. Failures directly attributable to center melting have been observed; thus the center melting temperature of 2760°C may be a design temperature limit. One of the failures involving oxide melting occurred after two hours of operation with a 19.5% enriched UO_2 defected specimen in the hottest portion of a water-cooled test loop [119]. Figure 6–41 is a photograph showing a failed element. This failure was attributed to extensive melting of the fuel, and this conclusion was confirmed by metallographic evidence of high temperatures in the cladding near the failure It appears that the failure occured when a jet of molten UO_2, escaping through a crack in the outer ring of solid UO_2, impinged on the wall of the zirconium can. The cross-sectional structure of the UO_2, shown in Fig. 6–42, has a porous central crystalline area somewhat different from the molten zones observed in other tests, perhaps indicating that a superheated molten zone had developed.

Fission gas release. In general, the following conclusions by Lustman [122] summarize the information on fission gas release in UO_2:

(1) The release of fission gases from irradiated UO_2 is in all probability controlled by diffusion of the gases from the oxide matrix.

(2) The oxide density has a large effect on the gas release because the length of the diffusion path to the external surfaces varies with the density. There is experimental evidence that the fission gas release is much less for UO_2 specimens whose density is more than 90% of the theoretical. The gas released for 65% dense packed UO_2 is 40 to 50% [123]; for 91% dense pressed and sintered pellets it is only 3.1% [122,124]; for 95% dense pressed and sintered pellets the gas released is approximately 1% Figure 6–43 is a plot of the fractional fission gas release per hour as a function of irradiation temperature [125].

(3) Assuming the gas release is due to diffusion, the amounts released can be calculated with a correction for the density of the oxide specimen. Calculations agree, within a factor of three, with experimental data on irradiated PWR fuel rods

It should be noted that at high burnups the effects of the fission gas released within the jacket (even with dense 95% UO_2 pellets) must be taken into consideration [126]. Two major effects, here, are the pressure increase and the change in thermal conductivity of the helium bond Bettis plant [119] has reported that enough xenon and krypton are released in Core-I PWR reference fuel elements (1 w/o burnup and 1% gas release) to dilute the helium by 50%. See Table 6–20 for the effect on the gap temperature drop.

Fabrication of UO_2. Fuel pellets of UO_2 can be obtained commercially with bulk densities of 10.2 to 10.44 g/cm^3 (93 to 95% of theoretical density). Various sizes and shapes can be produced by powder metallurgy techniques [127–130]. Detailed information on the preparation, production, sintering, fabrication, and enclosure of UO_2 fuels is included in the above references.

Recently, Hanford [131] has been developing techniques for extruding UO_2 in the shape of rods of 1/4 to 3/4-inch diameter and up to 6 ft long for the Plutonium Recycle Program Reactor. Both "PWR Grade" and "Ceramic Grade" powders were used to achieve densities of 92% of theoretical or greater.

Canning materials Although UO_2 specimens are highly resistant to corrosion by various coolant gases, they still must be canned because of the severe thermal cracking and the release of fission product gases. There has been no evidence of any reaction between UO_2 and aluminum at less than 400°C [132]; between UO_2 and Zircaloy-2 at less than 600°C [133]; between UO_2 and niobium at less than 1000°C [134]; and between UO_2 and stainless steel at less than 1200°C. At temperatures above 600°C, there is evidence that zirconium will reduce UO_2 and become brittle [134].

A general review of fuel-element canning materials has been made in Article 6–3.2.

FIG. 6–41 Close-up of rod X-1-E-3, showing failure [119]

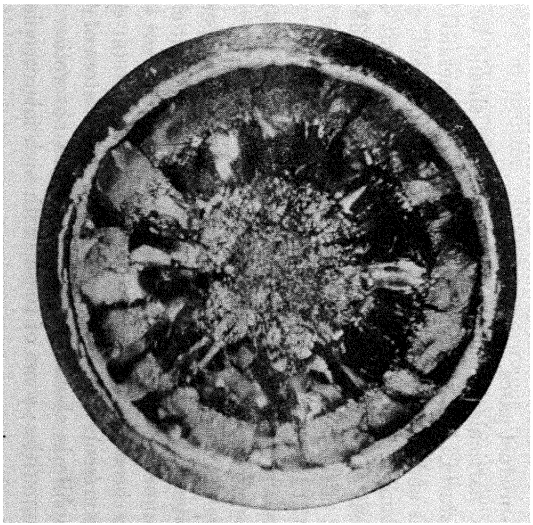

FIG. 6–42. Cross section from the lower end of rod x-1-e-3. [119]

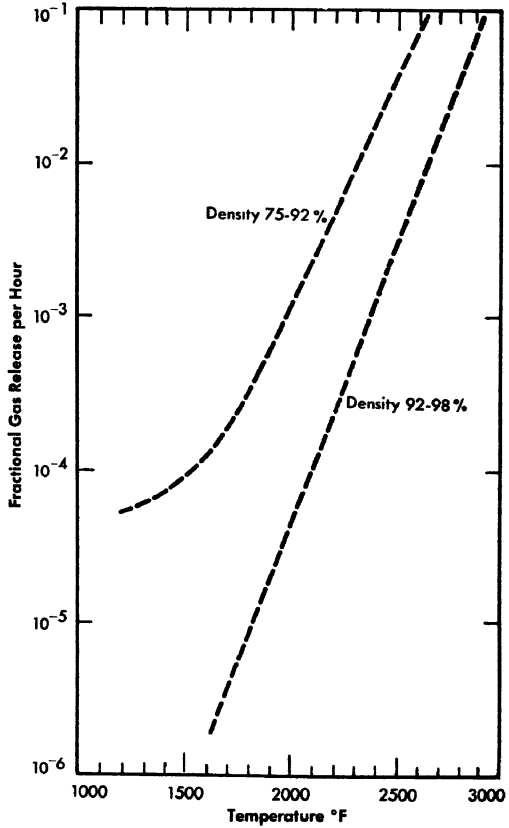

FIG 6–43. Fission gas release from natural UO_2. [125]

6–4. Graphite-Moderated Reactors*

6–4.1 General characteristics of gas-cooled, graphite-moderated reactors. Many characteristics of the reactors discussed here depend on the properties of graphite. There are numerous quantitative summaries of these properties [136,137] available. Mechanically, graphite has low tensile strength (*ca.* 1400 psi) and much higher crushing strength (*ca.* 6000 psi). It is brittle, but not perfectly elastic; some plastic flow occurs under stress even at room temperature. Graphite is a good material for high-temperature applications; its strength increases up to about 4500°F. It has high thermal conductivity (comparable to that of metals), and low elastic modulus (comparable to that of rolled lead). Consequently, it has high resistance to thermal stress or thermal shock damage. Both the mechanical and thermal properties of graphite are anisotropic.

The real density of graphite made from petroleum coke varies from 2.18 to 2.25 g/cm^3. The bulk density of graphite for reactor use lies in the range of about 1.6 to 1.7 g/cm^3, although higher bulk densities are possible. The pores that account for the difference between the real density and the bulk density render the graphite slightly permeable to gases

Graphite may be employed as a structural material as well as a moderator, although it has only limited strength in tension. Usually the reactor itself is largely built of graphite blocks which carry their own weight, and that of the fuel elements, as a compressive load. Graphite may also support fuel elements, but it has not been employed to clad them because it is permeable to fission-product gases.

Graphite reactors, particularly those cooled by gases, should be operated at high temperatures. This simplifies removing heat generated in the graphite by neutrons and gamma rays and, even more important, greatly reduces radiation damage caused by fast-neutron bombardment of the graphite. Discussions of radiation damage are in references [138–145] The most important effects are (1) growth in directions transverse to the extrusion axis, and (2) the accumulation of internal stored energy. Experience indicates that, at the temperatures contemplated in gas-cooled power reactors, these effects will be tolerable.

Nuclear properties of graphite strongly affect the design and performance of graphite-moderated reactors. Perhaps the most important characteristic is the thermal neutron absorption cross section. This cross section for pure carbon has been measured as 3.2 ± 0.2 millibarns (at a neutron velocity of 2200 m/sec). The cross section per carbon atom of AGOT "reactor grade" graphite is about 4.5 mb. The extra absorption in the graphite is due to impurities; some of these (with high microscopic cross

*Compiled by W. R. Baldwin and J. L Watkins, GNEC.

sections, such as B^{10}) will decrease significantly with time in the operating reactor if the thermal neutron flux is high enough. Graphites with lower neutron absorption cross section are on the market at prices somewhat higher than those for AGOT. Cross sections as low as 3.7 mb are quoted. In a reactor having a thermal utilization of 0.90, with most parasitic absorption in the graphite, a decrease of 0.1 mb in the graphite cross section corresponds to an increase in reactivity of about 0.25%. Using the better grades of graphite may well prove worth while. The neutron physics calculations presented here (Article 6–4.3) are based on a graphite cross section of 4.0 mb

Although the absorption cross section of the moderator determines the neutron economy that can be achieved with a given moderator, it is the moderating ratio, $\xi\Sigma_s/\Sigma_a$, that determines the amount of reactivity attainable with fuel of a given (low) enrichment In this ratio, ξ is the average logarithmic energy loss of a neutron per collision with a moderator atom, Σ_s is the scattering cross section in the neutron resonance energy region, and Σ_a is the thermal neutron absorption cross section. This ratio for graphite is large enough that practical power reactor operation can be attained with natural uranium fuel, provided the fuel is used in the dense metallic form and provided the absorption by fuel jackets and other parasitic materials is small compared with that of the graphite.

It is unlikely that enough reactivity for efficient power generation can be attained from natural uranium oxide fuel in a graphite lattice. This difference in neutron physics performance results from the fact that: (1) attainable reactivity is less with the oxide because its lower density decreases the absorption of uranium in ratio to that of parasitic materials, and increases the effective resonance integral of the U^{238}, and (2) high reactivity is necessary for power operation because of the greater loss of reactivity caused by the Doppler effect in the fuel elements at very high temperature.

Therefore, in natural uranium fueled, graphite-moderated reactors, coolant temperatures appear to be limited to those possible with high-density fuel elements. Oxide fuels might well be used in reactors of this type with natural uranium feed, should plutonium recycling prove feasible. The plutonium recycle calculations of Reference 146, although not directed toward this particular application, are useful in estimating potentialities of plutonium recycle in gas-cooled graphite-moderated reactors.

A second characteristic, determined by the moderating ratio, is the ratio of fuel volume to moderator volume at which reactivity reaches maximum For a given specific power (megawatts of power output per ton of fuel), this ratio then determines reactor power density. The power density tends to be rather low in natural-uranium-fueled graphite-moderated reactors.

Consequently, large reactors and large pressure vessels are required for high power output.

A further size consideration is that the reactor must be large enough that neutron leakage does not reduce neutron economy to unacceptable levels. The size necessary for a given fractional neutron leakage is determined (so far as the moderator is concerned) by the thermal neutron scattering cross section and by the slowing-down area τ. These quantities for graphite are of such magnitude that reactors approximately 20 ft in their smallest dimension are necessary to permit operation with natural uranium. For power output in the central station range, natural uranium reactors will generally have dimensions larger than this; consequently power density is a more important factor than neutron leakage in determining reactor size for central station application

The use of partially enriched fuel removes many restrictions placed on the graphite reactor by natural uranium fuel. Uranium oxide as fuel is quite feasible. In addition, moderately absorbing metals such as stainless steel can be considered for fuel jacketing, although low-absorption materials would be preferable. The ratio of fuel to moderator can be increased, with a consequent increase in power density and a substantial reduction in reactor size for a given power output. At the same time, the restrictions that neutron leakage places on reactor size are lessened because the greater absorption of the fuel reduces thermal neutron diffusion length, and because leakage is no longer so important.

For these reasons, investigation of gas-cooled, graphite moderated reactors has included an enriched type. Indeed, design studies indicate more economic promise for the enriched than for the natural uranium type. Results of these studies are described later in this chapter. The two sections immediately following summarize experiments on graphite lattices and give reactor physics calculations covering a wide range of possible lattices. These calculations were part of a gas-cooled reactor study at Oak Ridge National Laboratory, leading to the reactor design described later. Articles 6–4.4 and 6–4.5 describe, respectively, the natural uranium reactor design by the Kaiser Engineers-ACF group, and the enriched uranium designs by both the Kaiser-ACF group and Oak Ridge National Laboratory. In Article 6–4.6, various designs are compared and economic estimates based on them are tabulated.

6–4.2 Measured neutron physics characteristics of graphite-moderated lattices. The results of exponential measurements on natural-uranium graphite-moderated lattices are generally available [147–149]. For recent studies of graphite-moderated reactors, characteristics of lattices fueled with partially enriched uranium and uranium oxide are of interest. Although there are no measurements with oxide fuels, a number have been

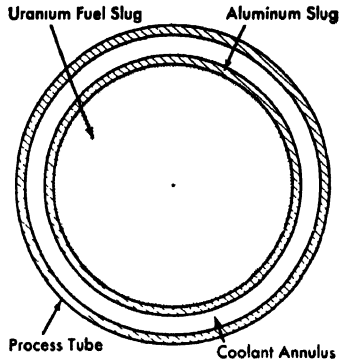

FIG. 6–44. Fuel arrangement for lattice measurements. (GNEC)

made with enriched uranium metal, as reported by Clayton [150,151]. The material in this section summarizes his papers.

Measurements reported were not aimed primarily at gas-cooled reactors. Therefore they included configurations that simulated water cooling channels, both filled and empty. Such "wet" lattice measurements are included here for whatever general information they add to the more directly applicable "dry" lattice results.

The exponential assemblies used were relatively small, about 48 inches wide. This size was usable (and necessary, in some cases, to avoid criticality) because of the high bucklings of the enriched lattices. Density of the graphite ranged between 1.65 and 1.66 g/cm^3. The diffusion length of the graphite, when corrected to a graphite density of 1.6 g/cm^3, was 54.2 ± 0.2 cm.

A square lattice configuration was used, with a range of lattice spacings. The fuel-element arrangement is illustrated in Fig. 6–44. The dimensions and materials for the fuel element-process tube assemblies are summarized in Table 6–23. Each channel through the graphite moderator was lined with an aluminum (2s) process tube, which fit the graphite hole with only a small clearance. The fuel slugs, jacketed with aluminum, were placed in a continuous row in the tube, centered to leave an annular coolant gap. Measurements were made with the gap filled with water ("wet" lattice) and empty ("dry" lattice). In some cases, annular fuel slugs were used; in these cases the central hole in the slug was lined with aluminum. The "wet" measurements with the hollow slugs were made with water in the hole in the slug (Configuration D, Table 6–24) and with water in both the hole and the outside coolant gap (Configuration E). The results of the buckling measurements are summarized in Tables 6–24 and 6–25. The absolute error in the buckling measurements is estimated

TABLE 6–23

DESCRIPTION OF MATERIALS USED FOR VARIOUS CONFIGURATIONS IN EXPONENTIAL EXPERIMENTS [150]

Material	Configuration									
	A	B-I	B-II	B-III	B-IV	C	D	E	F	G
Fuel enrichment, % U^{235}	0.94	1.007				1.007	1.007	1.44	90†	90†
Fuel slug length, cm	15.24	10.16				10.16		20.32	21.06	15.24
Fuel slug radius (outer), cm	1.70	1.17				2.11	2.11	1.74	1.705	1.705
Fuel slug radius (inner if hollow slug)							1.19	0.61		
Canned length, cm	16.19							21.92	23.01	16.94
Canned radius (outside), cm	1.83	1.27						1.87	1.81	1.81
Canned radius (inside), cm								0.48		
Slug density (solid), g/cm^3	18.9	18.9				18.9	18.9	18.9		
Slug density (equivalent, allowing for end caps), g/cm^3	17.8	18.1				18.7	18.9	17.5		
U^{235} per unit of canned length, g/cm									1.66	0.97
Outside radius of aluminum process tube, cm	2.20	1.55	1.59	1.91	2.20	2.20	2.20	2.20	2.20	2.20
Outside radius of aluminum tube in hole of hollow slug, cm							1.02			
Volume of process tube wall per unit length, cm^3/cm	2.31	1.36	0.87	1.75	2.31	0.97	0.97	0.97	2.31	2.31
Volume of aluminum in jacket per unit length, cm^3/cm	1.26	0.68	0.68	0.68	0.68			1.95		
Total volume of aluminum per unit length (including end caps), cm^3/cm	4.12	2.25	1.76	2.64	3.20	0.97	1.86	3.66		
Volume of water in coolant channel per unit length, cm^3/cm	2.41	1.03	1.93	4.61	7.84		2.38*	3.88	2.57	2.57
Radius of hole in graphite for process tube, cm	2.215	1 567	1.922	1.922	2.215	2.215	2.215	2.215	2.215	2.215

*The coolant channel is the hole in the uranium slug

†Remainder of fuel slug volume is 2s aluminum.

TABLE 6–24

MEASURED BUCKLINGS FOR ENRICHED-URANIUM GRAPHITE LATTICES [151]

Configuration (see Table 6–23)	Lattice spacing, inches	Atom (or molecular) ratios			Buckling (10^{-6} cm^{-2})
		H_2O/U	Al/U	C/U	
A	5 3/16	—	0.61	32.3	112
A	5 3/16	0.198	0.61	32.3	210
A	6 3/16	—	0.61	47.2	286
A	6 3/16	0.198	0.61	47.2	308
A	7 3/16	—	0.61	64.7	321
A	7 3/16		0.61	64.7	326
A	8 3/8	—	0.61	89.1	320
A	8 3/8	0.198	0.61	89.1	301
A	10 3/8	—	0.61	138.5	258
A	10 3/8	0.198	0.61	138.5	203
B-I	6 3/16	—	0 59	95.6	367
B-I	6 3/16	—	0.69	100.4	356
B-I	6 3/16	0.174	0.69	100.4	349
B-I	7	—	0.69	128.7	350
B-I	7	0.174	0.69	128.7	326
B-I	7 1/2	—	0.69	148.2	313
B-I	7 1/2	0.174	0.69	148.2	297
B-II	6 3/16	—	0.54	98.7	360
B-II	6 3/16	0.326	0.54	98.7	356
B-II	7	—	0.54	127.1	352
B-II	7	0.326	0.54	127.1	309
B-II	7 1/2	—	0.54	146.6	331
B-II	7 1/2	0.326	0.54	146.6	278
B-II	8 1/8	—	0.54	185.1	261
B-II	8 1/8	0.326	0.54	185.1	211
B-III	6 3/16	—	0.80	98.7	335
B-III	6 3/16	0.786	0.80	98.7	270
B-III	7	—	0.80	127.1	334
B-III	7	0.786	0.80	127.1	236
B-III	7 1/2	—	0.80	146.6	310
B-III	7 1/2	0.786	0.80	146.6	192
B-IV	6 3/16	—	0.97	97.1	307
B-IV	6 3/16	1.326	0.97	97.1	160
B-IV	7	—	0.97	125.5	320
B-IV	7	1.326	0.97	125.5	102
B-IV	7 1/2	—	0.97	145.0	292
B-IV	7 1/2	1.326	0.97	145.0	67

(continued)

TABLE 6–24 (*continued*)

Configuration (see Table 6-23)	Lattice spacing, inches	Atom (or molecular) ratios			Buckling (10^{-6} cm^{-2})
		H_2O/U	Al/U	C/U	
B-IV	8 3/8	—	0.97	183.5	245
B-IV	8 3/8	1.326	0.97	183.5	40
C	5 3/16		0.088	19.8	157
C	6 3/16		0.088	29.0	154
C	7		0.088	37.5	325
C	7 1/2		0.088	43.4	367
C	8 3/8		0 088	54.9	405
C	10 3/8		0.088	85.2	370
C	12 3/8		0.088	121.9	268
D	6 3/16	—	0.25	42.3	253
D	6 3/16	0.18	0.25	42.3	306
D	7 1/2	—	0.25	63.2	375
D	7 1/2	0.18	0.25	63.2	409
D	8 3/8	—	0.25	80.0	380
D	8 3/8	0.18	0.25	80.0	0
D	10 3/8	—	0.25	124 3	335
D	10 3/8	0.18	0.25	124 3	326
D	12 3/8	—	0.25	177.8	222
D	12 3/8	0.18	0.25	177.8	226
E	5 3/16	—	0.60	35.5	459
E	5 3/16	0.35	0.60	35 5	739
E	6 3/16	—	0.60	52.0	566
E	6 3/16	0.35	0.60	52 0	711
E	7 3/16	—	0.60	71.4	614
E	7 3/16	0.35	0.60	71.4	663
E	7 11/16	—	0.60	82.2	609
E	7 11/16	0.35	0.60	82.2	630
E	8 3/8	—	0.60	98.2	588
E	8 3/8	0.35	0.60	98.2	585
E	9 3/8	—	0.60	123.9	537
E	9 3/8	0.35	0.60	123.9	499
E	10 3/8	—	0.60	152.5	478
E	10 3/8	0.35	0.60	152.5	420

TABLE 6–25

BUCKLING FOR HIGHLY ENRICHED URANIUM

Lattice spacing, inches	Configuration F, 10^{-6} cm^{-2}		Configuration G, 10^{-6} cm^{-2}	
	Dry lattice	Wet lattice	Dry lattice	Wet lattice
4 3/16	1422	1855	1222	1572
5 3/16	1361	1612	1134	1323
6 3/16	1258	1368	1010	1078
7 3/16	1114	1163	877	897
8 3/8	972	965	736	709
10 3/8	719	678	519	470

to be $\pm 20 \times 10^{-6}$ cm^{-2}, and the relative values are expected to be consistent to within about $\pm 10 \times 10^{-6}$ cm^{-2}.

6–4.3 Neutron physics of gas-cooled, graphite-moderated reactors.* When gas-cooled designs were analyzed at Oak Ridge National Laboratory [10], reactor physics calculations were made covering a wide range of graphite-moderated lattices. The results, presented in this section, are useful in determining effects of various design variables on the neutron physics performance of such reactors. Results are summarized in Table 6–29 Calculation methods are described in enough detail to indicate the approximate accuracy that may be expected. For further discussion of the methods and results, the reader is referred to Reference 10.

Multiplication factor. The multiplication, or reproduction, factor of the fuel lattice is expressed by the classical four-factor formula $k = \eta\epsilon pf$, where η = direct yield of fission neutrons per neutron absorbed in fuel, ϵ = fast fission factor, p = resonance escape probability, and f = thermal utilization, the ratio of the number of thermal neutrons absorbed in fuel excluding those absorbed in U^{238} resonances, to the total number absorbed in the lattice, excluding those absorbed in the resonances of U^{238} and stainless steel.

The criticality constant is given by

$$k_{eff} = ke^{-B^2\tau}(1 + L^2B^2)^{-1}.$$

The neutron leakage factors are discussed in detail in a later paragraph.

*Prepared by A M. Perry, Oak Ridge National Laboratory.

TABLE 6–26

FAST FISSION FACTOR FOR CLUSTERS OF SEVEN UO_2 RODS

Rod diameter, inches	Fast fission factor, ϵ	
	For cluster	For equivalent single rod
0.5	1.016	1.018
0.75	1.024	1.026
1.00	1 028	1.034

Neutron yield. The yield of neutrons per neutron absorbed in fuel has been obtained directly from the measured neutron cross sections. There has been a traditional discrepancy between values of η obtained from the cross sections (referred to here as calculated values) and those inferred from exponential pile measurements, the latter values ranging from 1 26 to 1.35 for natural uranium at room temperatures. Figure 6–45 compares the calculated values of η as a function of enrichment with values based on exponential experiments. The process of obtaining η from the measured buckling values in the exponential experiments usually involves calculated values of the resonance escape probability p. Of the experimental values shown in the figure, only those reported by Kouts rest on measured values of p, and for these the disagreement with the calculated curve is comparatively small. In view of this fact, and also because there is no alternative for calculations involving enriched fuel at elevated temperatures, the decision has been made to employ calculated values of η in all cases.

Fast effect. Values of the fast fission factor ϵ for uranium-metal rods and for UO_2 rods are given in Fig. 6–46. For a cluster of rods, the value of ϵ is expected to be between that for a single rod of the cluster and that for a single rod of the same total cross sectional area as the cluster, and rather closer to the latter. An approximate calculation of the collision probability, P, for 7-rod clusters, yields values slightly smaller than those for the equivalent single rod (of some total cross-sectional area). Results for clusters of seven rods of various sizes are given in Table 6–26.

Resonance escape probability. The resonance escape probability p is written

$$p = \exp - \left\{ \frac{\sigma_{r,u} + [N_{cl}/N_u]\sigma_{r,cl}}{[N_m/N_u](\xi\sigma_s)_m + [N_{cl}/N_u](\xi\sigma_s)_{cl} + [N_o/N_u](\xi\sigma_s)_o + (\xi\sigma_s)_u} \right\},$$

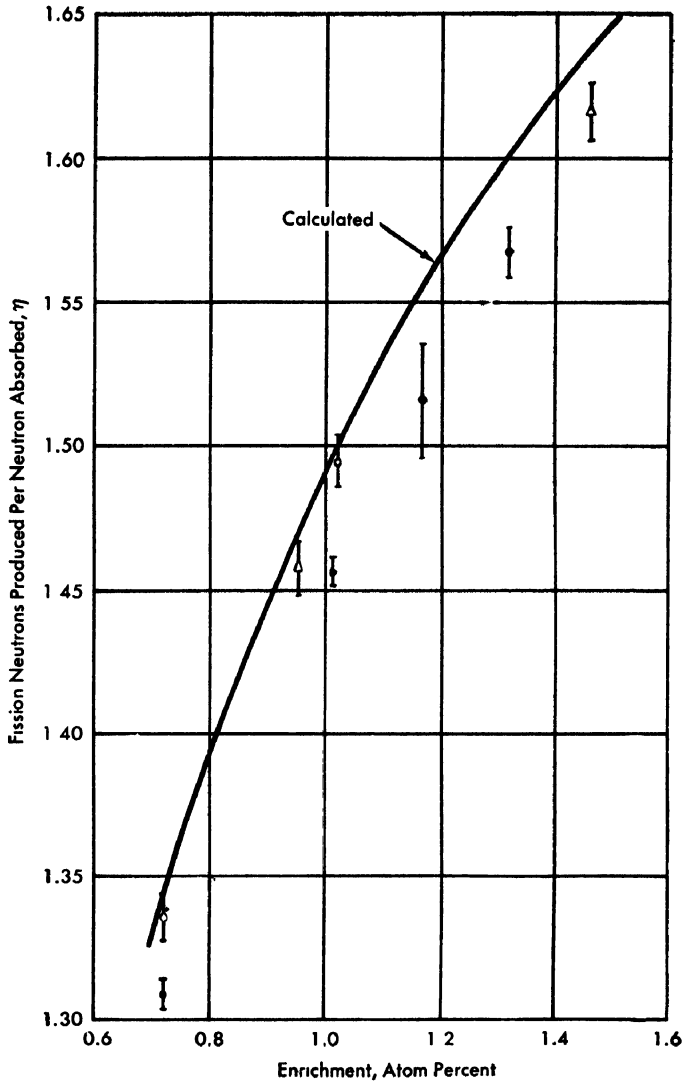

FIG 6–45. Fission neutrons produced per neutron absorbed in uranium [10]

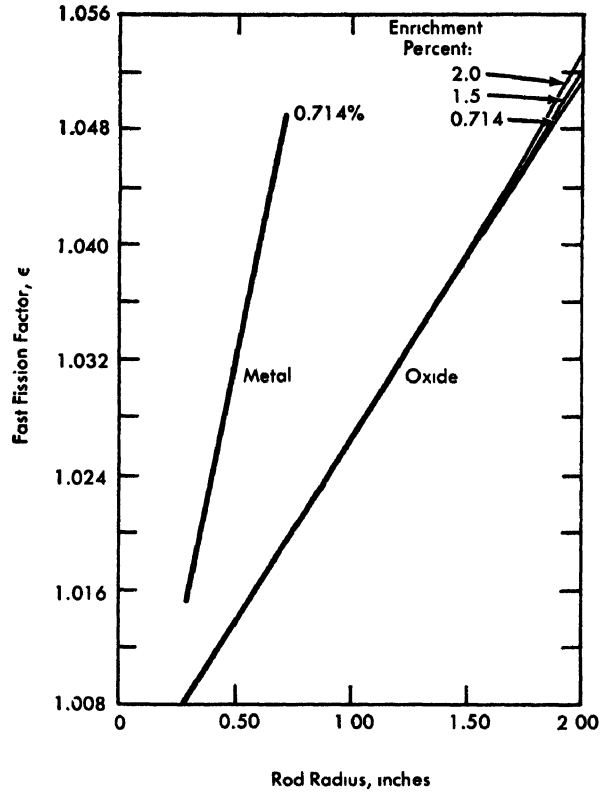

FIG. 6–46. Fast fission reaction for UO_2 and U metal rods. [10]

where σ_r = effective resonance integral, σ_s = elastic scattering cross section, ξ = average logarithmic energy loss of a neutron in elastic collisions, and N = number of atoms in a cell divided by the volume of the cell. The subscripts m, u, o, cl refer to moderator, uranium, oxygen, and cladding, respectively.

The problem of computing p reduces essentially to that of determining $\sigma_{r,u}$, the effective resonance integral of U^{238}. The theoretical treatment [152] of the subject is quite complex, and there are rather serious potential ambiguities associated both with the use of UO_2 instead of the metal, and with the cluster geometry. It is fortunate that the results of measurements made at Stockholm, by Hellstrand [153] on the resonance absorption of U^{238} in metallic and oxide rods, in various geometries including 7-rod clusters, have recently become available. With a $1/v$ contribution of 1.2 barns deducted from the volume absorption term, the resonance integral for UO_2 lumps is found by Hellstrand to be

$$\sigma_r = 4.05 + 26.6(S/M)^{\frac{1}{2}}; \; 0.08 \leq S/M \leq 0.7.$$

The experimental correlations of Hellstrand confirm a proposal by E. R. Cohen [153] that the surface to be used for a cluster of rods is the "rubber band" surface, that is, that of a membrane stretched tightly around the cluster.

It may be of interest to point out the relative importance of the terms in the exponent of the equation for p. For a typical lattice (3/4-inch diameter stainless steel clad rods, 8-inch lattice pitch, 2% enrichment), the UO_2 contributes about 2% of the denominator and the clad about 0.3%. In the numerator, the cladding contributes about 3%.

The temperature dependence of the resonance escape probability is quite important because it influences the change in reactivity of the reactor between room temperature and operating temperature, and because it contributes a significant negative component to the temperature coefficient of reactivity at operating temperature. The problem consists of two parts, that of determining the temperature dependence of the effective resonance integral, and that of determining the effective temperature of the fuel.

The temperature coefficient of the effective resonance integral has been reported for uranium metal by David and Rodeback [154,155], and for UO_2 by Creutz et al. [156]. Between 40 and 300°C, Davis finds

$$\left[\frac{1}{\sigma_r}\right]\left[\frac{d\sigma_r}{dT}\right] \simeq (1.56 \pm 0.12) \times 10^{-4} \text{ per °C};$$

the coefficient is constant over this range. Between 20 and 660°C, Rodeback reports

$$\left[\frac{1}{\sigma_r}\right]\left[\frac{d\sigma_r}{dT}\right] \simeq 0.9 \times 10^{-4} \text{ per °C}.$$

Between 20 and 1000°C, Creutz et al report

$$\left[\frac{1}{\sigma_r}\right]\left[\frac{d\sigma_r}{dT}\right] \simeq 2 \times 10^{-4} \text{ per °C}.$$

Davis' result was used in the calculations.

The mean temperature of the fuel has been determined rather approximately for an average heat flux. An average temperature was calculated for a single rod with a resonance absorption distribution, $b(r)$, taken from Hellstrand's measurements [153].

With

$$\bar{T} = \frac{\int_0^R T(r)b(r)r\,dr}{\int_0^R b(r)r\,dr}$$

(R = rod radius), it can be shown that

$$\sigma_r(T) = \sigma_r(20°\text{C}) \exp \{Z(\bar{T} - 20°\text{C})\},$$

where $Z = +1.56 \times 10^{-4}/°\text{C}$ is the temperature coefficient of the resonance integral. For $T(0) = 1274°\text{C}$ (2325°F) and $T(R) = 620°\text{C}$ (1150°F), it is found that $T = 760°\text{C}$ (1400°F).

For 8-inch lattice pitch, 3/4-inch diameter rods in a 7-rod cluster, a change in the uranium temperature from 20°C to 760°C will decrease p, and hence k, by about 3%.

Thermal utilization. The thermal utilization of a lattice cell is here defined as the ratio of the number of thermal neutrons absorbed in the fuel of the cell, including those attributable to the $1/v$ part of the U^{238} cross section to the total number of thermal neutrons absorbed in the cell In terms of the appropriate cross sections it is therefore written as

$$f = \frac{V_f \Sigma_a^f \bar{\phi}_f}{V_f \Sigma_a^f \bar{\phi}_f + V_m \Sigma_a^m \bar{\phi}_m + V_p \Sigma_a^p \bar{\phi}_p},$$

where Σ_a^f, Σ_a^m, and Σ_a^p are macroscopic effective absorption cross sections in the fuel, moderator, and poisons (cladding material, for example), respectively. The $\bar{\phi}_i$ are the average effective fluxes and the V_i are the volumes of the respective regions. The effective cross sections used in all room-temperature calculations were averaged over a Maxwellian flux spectrum with $T_n = 20°\text{C}$. High-temperature calculations were done with the cross sections derived as described in the immediately following section. The P_3 spherical harmonics approximation was used in computing the fluxes required to determine the thermal utilization. These calculations were done on the IBM 650 computer, using a program prepared at KAPL by J. W. Weil.

The only complication which arose with the use of the program came from the restriction that zero absorption was not allowed. In problems involving a single fuel rod in the cooling channel, the program was therefore made to compute the fluxes under the assumption that each component is continuous across the gap between the fuel and moderator regions. The procedure developed by Newmarch [157] was then used to take into account the depression of the flux across the cooling channel due to the probability that some neutrons will enter the cooling channel from the moderator and fail to strike the fuel rod.

In calculating flux patterns for more complicated cell geometries, like the 7-rod-cluster fuel elements, the problem was encountered of finding a one-dimensional model with which to approximate the fuel system for pur-

poses of flux calculations. Two approximations were studied. In the first approximation, all of the fuel was lumped into a single rod with all of the cladding material placed around the single rod. In the second approximation, the outer six rods of the cluster were replaced by an annulus of the same volume as the rods themselves. Half of the cladding of these six rods was placed on the inner surface of the annulus and half was placed on the outer surface. The annulus was located in the cooling channel in such a way that it was divided into two equal volumes by the circle which forms the locus of the centers of the original six rods The seventh rod of the cluster, the central rod, was represented by its actual radius and clad thickness

There is little difference between the values of k_∞ computed with the two models, the most important difference being a slightly higher k_∞ at the optimum lattice with the annulus model due to the greater homogenization of the highly absorbing clad. The balance between p and f is different, however, and because of this the calculations presented here were all done with the annulus model. The exact radius at which the outer rods are located has little effect on the calculations.

Cross sections Cross sections at operating temperature are needed for the calculation of initial reactivity and for the study of reactivity as a function of exposure For most purposes it was convenient to use effective one-group cross sections. Thus the resonance absorption effects of all materials other than U^{238} and stainless steel were included in effective cross sections $\hat{\sigma}$ as defined, for example, by Westcott [158]:

$$\hat{\sigma} = (\text{reaction rate per target nucleus})/Nv_{2200},$$
$$\hat{\sigma} = (g + rs)\sigma_{2200},$$

where N is the total neutron density, v_{2200} is the velocity 2.2×10^5 cm/sec, and σ_{2200} is the cross section for neutrons at that velocity. The flux spectrum is assumed to consist of a Maxwellian component at temperature T_n, plus a dE/E tail cut off at a lower limit of $5kT_n$. The factor g takes into account the averaging of the cross section over the Maxwellian part of the neutron distribution; r is $\sqrt{5\pi}/4$ times that fraction of neutrons which lies in the dE/E tail; and s depends on the resonance integral $\int_{5kT_n}^{\infty} \sigma\, dE/E$. For a $1/v$ absorber, $g = 1$ and $s = 0$.

The temperature T_n which best describes the thermal neutron distribution may be significantly different from the temperature T_m of the moderator atoms. For an infinite homogeneous medium with $1/v$ capture cross section, Coveyou et al. [159] find

$$T_n \simeq T_m(1 + 1.11AK),$$

where A is the mass number of the scatterer and

$$K = \left(\frac{2}{3}\right)^{\frac{1}{2}}\left(\frac{293}{T_m}\right)^{\frac{1}{2}} \frac{\Sigma_a(2.2 \times 10^5 \text{ cm/sec})}{\Sigma_s}.$$

Σ_a and Σ_s are the macroscopic cross sections of the absorbing and scattering species. The reliability of this recipe for computing T_n has been confirmed experimentally for homogeneous mixtures [160]. Although its usefulness for heterogeneous reactors is uncertain, it was considered the best guide available for the present study. The formula was applied to the heterogeneous reactor under consideration by replacing the lattice cell with one in which all materials are uniformly distributed over the cell; K is then computed with flux-weighted cross sections as suggested by disadvantage factors from the P_3 calculation. The results are given in Table 6–27.

An estimate of the factor r may be made by relating the fission-neutron production rate with the slowing-down density. The latter is in turn related to the magnitude of the dE/E tail in the neutron spectrum. When U^{235} and U^{238} are the only fissionable materials in the reactor, q_0 equals the number of neutrons produced in fission per unit time per unit volume of reactor, or

$$q_0 = \epsilon N_{25}\nu_{25}\left[gN_f^{\text{Maxwell}}v_{2200}\sigma_{f,2200}^{25} + \int_{5kT_n}^{\infty} \sigma_f^{25} \frac{q_0}{(\xi\Sigma_t)_{sd}} \frac{p(E)}{(1 + B^2\tau_E)} \frac{dE}{E}\right],$$

where q_0 is the slowing-down density at the upper energy limit of the slowing-down region; N_{25} is the number of U^{235} atoms per unit volume in the homogenized cell; N_f^{Maxwell} is the neutron density in the fuel, counting only those neutrons in the Maxwellian component; σ_f^{25} is the U^{235} fission

TABLE 6–27

NEUTRON TEMPERATURE FOR 8-INCH LATTICE PITCH, $7\frac{3}{4}$-INCH DIAMETER UO_2 RODS WITH $3\frac{1}{4}$-INCH COOLING CHANNEL (T_m–750°F)

U^{235}, a/o	T_n/T_m	T_m, °K
1.2	1.164	782
1.5	1.179	792
2.0	1.204	809
2.5	1.221	821

cross section; $(\xi\Sigma_t)_{sd}$ is the effective slowing-down power in the homogenized cell; and $q_0 p(E)/(\xi\Sigma_t)_{sd}(1 + B^2\tau_E)E$ is the non-Maxwellian part of the flux, where the effects of resonance absorption and leakage have been taken into account. The equation can be solved for q_0, to give

$$q_0 = \frac{N_{25}\nu_{25}gN_f^{\text{Maxwell}}v_{2200}\sigma_{f,2200}^{25}}{\frac{1}{\epsilon} - \frac{\nu_{25}N_{25}}{(\xi\Sigma_t)_{sd}}\frac{p'}{1 + B^2\tau'}\int_{5kT_n}^{\infty}\sigma_f^{25}\,dE/E}$$

where $p'/(1 + B^2\tau')$ is a mean value of this energy-dependent quantity.

Then r for neutrons in the fuel can be calculated in terms of q_0 from the relation

$$r = \frac{\sqrt{5\pi}}{4}\int_{5kT_n}^{\infty} -\frac{1}{v}\phi_{1/E}(E)\,dE/N_f$$

$$= \frac{\sqrt{5\pi}}{4}\frac{q_0}{(\xi\Sigma_t)_{sd}}\left(\frac{p'}{1 + B^2\tau'}\right)\int_{5kT_n}^{\infty}\frac{dE}{Ev}/N_f.$$

A calculation following the procedure just outlined was made for the 7-rod cluster of 0.75-inch diameter UO_2 rods of 2% enrichment, for 8.0-inch lattice pitch. The result was $r = 0.22$. With 1% enrichment the same lattice has $r = 0.11$. However, for the fuel lifetime calculations reported here, a value $r = 0.1$ was assumed for all cell configurations and all enrichments. Graphs of $\hat{\sigma}$ vs. neutron temperature and r for U^{235}, Pu^{239}, Pu^{240}, and Pu^{241} are given in Fig. 6–47. These are based on Westcott's results, with the cross sections from 400 to 600°C calculated from extrapolations of Westcott's g and s factors. In the case of Pu^{239}, where the extrapolations seem questionable, the point at 600°C was independently calculated by numerical integration of the cross section from BNL-325 over the Maxwell spectrum.

Verification of calculations. A check on the over-all accuracy of the methods used in the physics calculations was made by doing calculations for several lattices for which accurate data exist from exponential experiments. The results of the exponential experiments have been compared with the calculations by comparing the value of the thermal utilization implied by the experiment with that computed by the P_3 approximation. In the exponential experiment, B^2 is determined from the slope of the flux, and is related to the other constants of the reactor by the equation

$$1 = \frac{\eta\epsilon pfe^{-B^2\tau}}{1 + L^2B^2},$$

where $B^2 = B_\perp^2 + B_\parallel^2$, $L^2 = L_m^2(1 - f)T$, L_m is the diffusion length of the moderator, and T is the correction factor which takes into account the

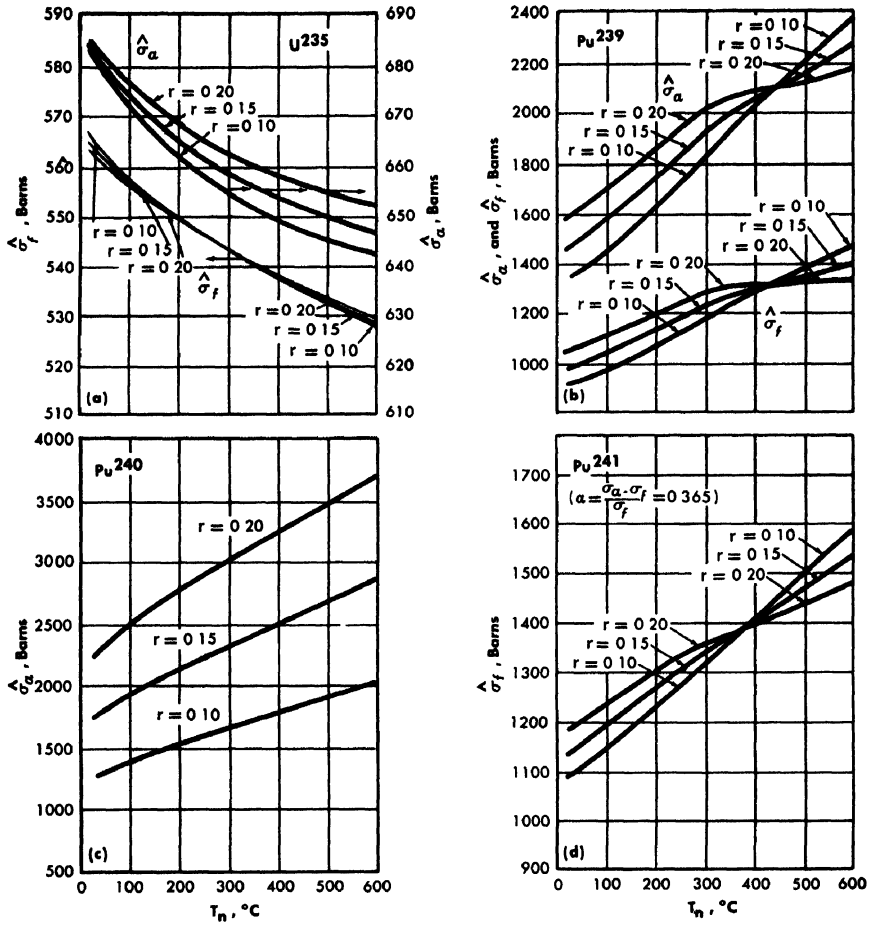

FIG. 6–47. Effective cross sections of uranium and plutonium as functions of neutron temperature. (a) U^{235}, (b) Pu^{239}, (c) Pu^{240}, (d) Pu^{241} [10]

voids of the cooling channels and the absorption in the clad. If the above equation is solved for the thermal utilization, the result is

$$f_{\text{exp}} = \frac{1 + L_m^2 T B^2}{\eta \epsilon p e^{-B^2\tau} + L_m^2 T B^2}.$$

Computed values for η, ϵ, p, τ, T, and L_m^2 are combined with the experimental value of B^2 to give f_{exp}. This is a rather stringent over-all check on the methods of calculation, since the term $L_m^2 T B^2$ is of order unity for most exponential experiments; thus the computed values of L^2, η, ϵ, and p all enter strongly in determining f_{exp}.

TABLE 6–28

SUMMARY OF CALCULATIONS ON EXPONENTIAL EXPERIMENTS

Rod diameter, cm	Void volume, cm^3/cm	Pitch, in.	B^2, μb	L^2, cm^2	τ, cm^2	η	ϵ	p	f_{exp}	f_{P_1}
3.41	0.00	4.19	1855	56.0	384	2.07	1.000	1.000	0.939	0.931
3.41	0.00	7.19	1163	194.7	348	2.07	1.000	1.000	0.888	0.882
3.41	0.00	10.38	678	451.3	340	2.07	1.000	1.000	0.794	0.806
3.41	2.57	7.19	1114	228.4	356	2.07	1.000	1.000	0.901	0.906
3.45	48.7	8.91	91.31	196.0	491	1.34	1.037	0.868	0.882	0.875

Comparisons of the above type were made for five exponential experiments Four of these were taken from the extensive measurements of E. D. Clayton* at Hanford and the fifth is a measurement by Booker, et al. [161] at Harwell. It was of interest to consider experiments with large cooling channel voids and the Harwell measurements, with a 3-inch-square cooling channel, were the best data found of this nature. The Hanford exponential experiments which were used contained highly enriched uranium-aluminum alloy fuel rods in both a "wet lattice" and a "dry lattice," that is, with and without water in the cooling channel. The absorption cross section in the alloy fuel element was about the same as that in a UO_2 element with 2% enrichment. A summary of these calculations is given in Table 6–28. The first three lines are the "wet lattice" calculations. Line four is the "dry lattice" calculation and line five is the Harwell measurement with the 3-inch-square cooling channel.

Results of lattice calculations. As mentioned before, the objective of these calculations was to determine the multiplication factor k of lattices

*Reference 150; see Section 6–4 2.

having fuel of various degrees of enrichment, various fuel-element geometries, and a wide range of lattice spacings. It should be kept in mind in examining the results of these calculations, that one of the major benefits expected to follow from the use of enriched fuel is a more compact lattice and consequently a higher power for a given core size. Another major benefit is the increase in average fuel exposure (and consequent reduction in power cost chargeable to fuel fabrication and reprocessing) that results from more reactive fuel.

Over 400 lattices have been studied, of which 337 are reported here. They fall into two main groups, lattices at room temperature, including uranium metal rods, UO_2 rods, and clusters of UO_2 rods, and lattices with a neutron temperature of 814°K (clusters only).

A description of the lattice and the values of η, ϵ, p, f, k, and the conversion ratio, R_c, are given for all cases in Table 6–29 which is divided into two sections:

(1) Moderator at room temperature (neutron temperature = 294°K):
   (a) Single UO_2 rod fuel element, stainless steel 430 clad.
   (b) Single uranium metal fuel rod, magnesium clad.
   (c) Seven-rod clusters of UO_2 fuel rods, stainless steel 430 clad.

(2) Moderator temperature = 750°F (neutron temperature = 814°K).
   (a) Seven-rod clusters of UO_2 fuel rods, stainless steel 430 clad.

A number of the relationships among the variables considered in Table 6–29 are plotted in Figs 6–48 through 6–53.

It will be noted that the steel specified for the calculations of Table 6–29 (and for all other calculations in this section) is type-430 stainless steel, whose thermal neutron absorption cross section is 0.2166 cm^{-1} (at 2200 m/sec). The corresponding cross section for type-304 stainless steel is 0.2465 cm^{-1}. Thus, for equal absorption, the thickness of 304 stainless steel is 0.88 that of 430 stainless steel; for example, 0.020-inch 430 stainless steel is equivalent to 0.0176-inch 304 stainless steel. Although 430 stainless steel was initially considered, the Oak Ridge gas-cooled reactor design is now predicated on the use of 304 stainless steel.

The absorption cross section for the TSF graphite in the calculations was taken as 4.0 mb for neutrons of 2200 m/sec velocity.

Loss of neutrons by leakage. In calculating the effect of neutron leakage on the multiplication factor the standard relation

$$k_{eff} = \frac{k_\infty e^{-B^2\tau}}{1 + L^2B^2}$$

has been used. The small size of the factors $B^2\tau$ and L^2B^2 for the reactors considered here allows this to be simplified into the form

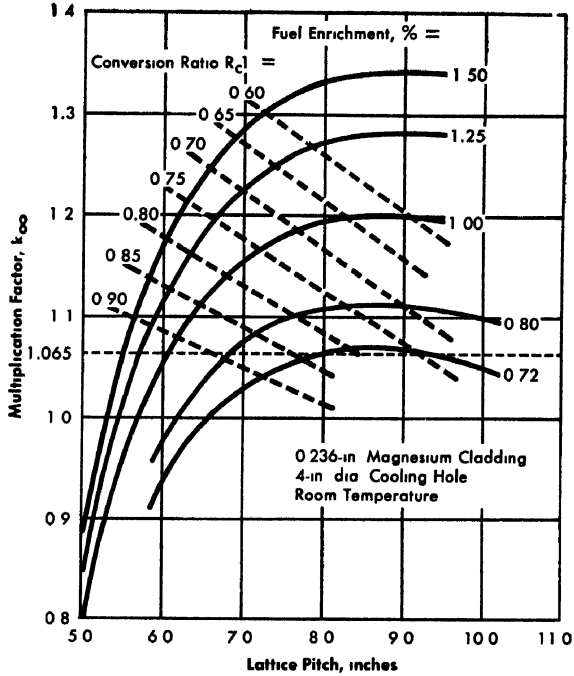

FIG. 6–48. The variation of multiplication factor with lattice pitch and enrichment 1 15-inch diameter uranium metal rods, $T_n = 20°C$. [10]

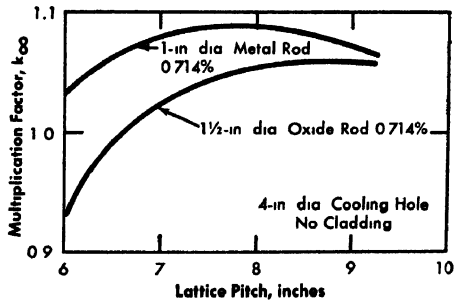

FIG. 6–49 U metal-UO_2 reactivity difference. [10]

$$k_{\text{eff}} \approx \frac{k_\infty}{1 + M^2B^2} = \frac{k_\infty}{1 + M_\parallel^2 B_\parallel^2 + M_\perp^2 B_\perp^2},$$

where $M_\parallel^2 = L_\parallel^2 + \tau_\parallel$ = axial migration area, $M_\perp^2 = L_\perp^2 + \tau_\perp$ = radial migration area, $B_\parallel^2 = \left(\frac{\pi}{H + 2\delta}\right)^2$ = axial buckling, $B_\perp^2 = \left(\frac{2.405}{R + \delta}\right)^2$ = radial buckling, and H and R are the core height and radius and δ is the reflector savings.

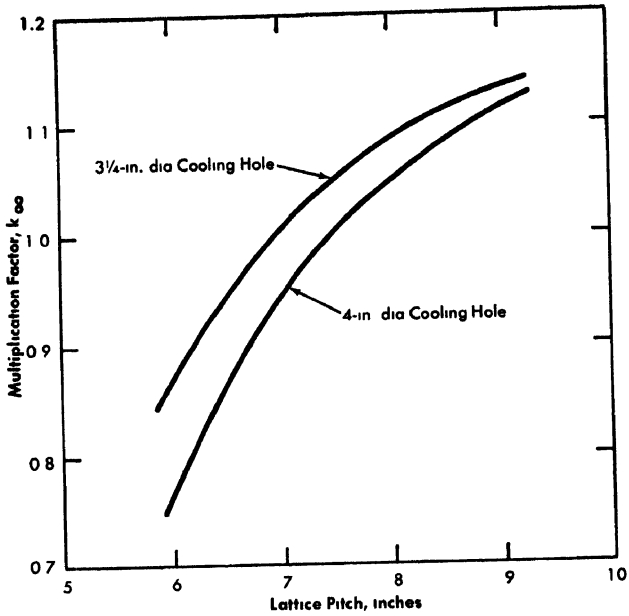

FIG. 6–50 Effect of cooling-channel diameter on multiplication factor. Seven UO_2 rods, 0 75 inch diameter, enrichment 1 25%, $T_n = 20°C$. [10]

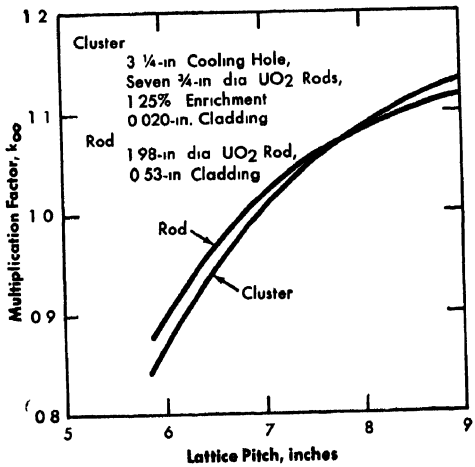

FIG 6–51. Comparison of cluster and single rod of equal volume. [10]

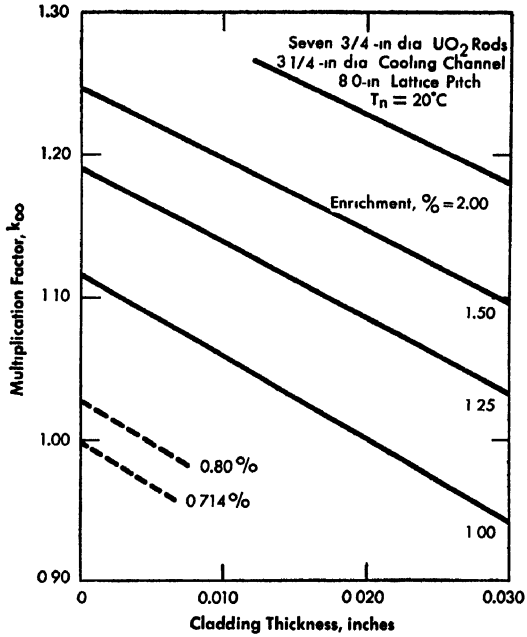

FIG 6–52 Effect of clad thickness on multiplication factor. [10]

The presence of the voids in the cooling channels increases both the age and the diffusion length for the lattice. The calculations of Behrens [162] have been used to determine this correction factor

For the reference reactor core design of the ORNL gas-cooled reactor study (seven 3/4-inch UO_2 fuel rods in a 3½-inch diameter cooling channel, 2% enrichment, 8-inch lattice pitch, 20-ft height, 30-ft core diameter, 2.5-ft reflector on all sides) the following quantities have been computed:

$$\tau_\perp = 409 \text{ cm}^2, \qquad \tau_\parallel = 419 \text{ cm}^2,$$
$$L_\perp^2 = 187 \text{ cm}^2, \qquad L_\parallel^2 = 194 \text{ cm}^2,$$
$$M_\perp^2 = 596 \text{ cm}^2, \qquad M_\parallel^2 = 613 \text{ cm}^2,$$
$$B_\perp^2 = 21.22 \times 10^{-6} \text{ cm}^{-2}, \qquad B_\parallel^2 = 18.05 \times 10^{-6} \text{ cm}^{-2},$$
$$M^2B^2 = 0.0237.$$

The sensitivity of the leakage in this core to such factors as lattice pitch, fuel enrichment, cooling-channel diameter, and core size is shown in Figs. 6–54 and 6–55.

Reactivity limitation on fuel exposure. The resistance of UO_2 fuel elements to unfavorable changes under irradiation makes possible very much longer fuel exposures than could be achieved with uranium metal fuel. Indeed, the relatively high fabrication cost expected for UO_2 fuel, as com-

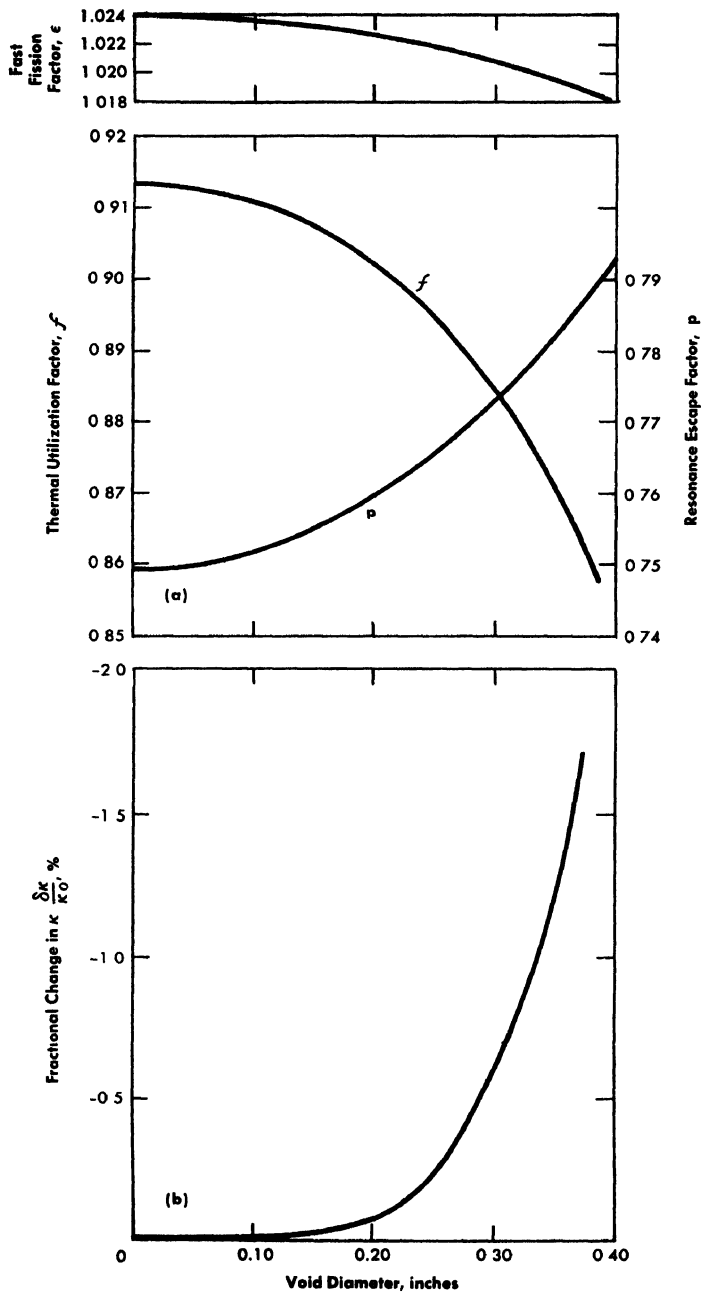

FIG. 6–53. Effect of central hole in fuel rods. (a) Effect on f, p, and ϵ. (b) Effect on multiplication factor. Seven UO_2 rods, 0.75-inch diameter, 3.25-inch cooling-channel diameter. [10]

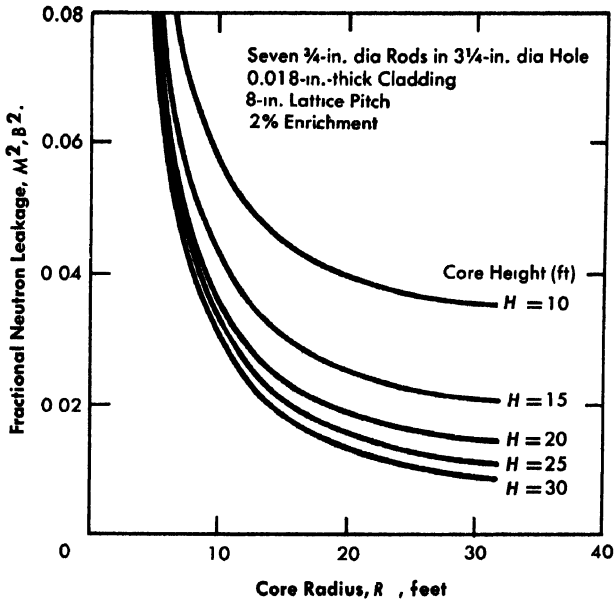

FIG. 6–54. The variation of neutron leakage with core height and diameter. [10]

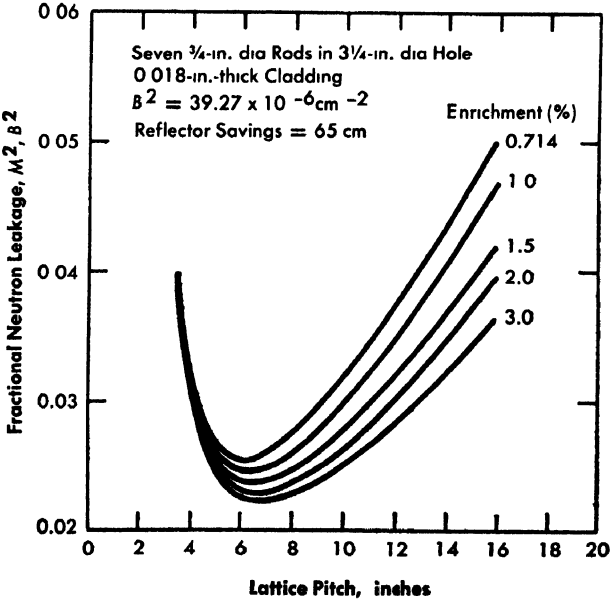

FIG. 6–55 Neutron leakage as a function of lattice pitch and enrichment. [10]

pared, for example, to the Magnox-clad uranium metal elements, makes long fuel irradiation a very urgent objective. One of the major problems in the nuclear analysis, therefore, is to obtain reasonably reliable estimates of the reactivity lifetime of the various possible fuel configurations and to determine the isotopic composition of the fuel as a function of exposure.

It will be helpful in discussing the problem of reactivity lifetime to recognize three distinct modes of fuel irradiation, which will yield different average fuel lifetimes. Case No. 1 is the "batch loading" case, in which all of the fuel is charged to the reactor at the same time and all discharged at the same time, when the reactivity of the fuel has fallen to the point where the chain reaction can no longer be maintained under the desired operating conditions. For this case the power density is assumed to be uniform throughout the pile. Case No. 2 is the same as Case No 1, except that the power distribution is not assumed to be uniform. In Case No. 3, the excess neutrons available with fresh fuel are used to extend the irradiation of old fuel that has a reactivity too low to sustain the pile by itself. Fresh fuel is added to the core and the most highly irradiated fuel is removed, more or less continuously, in such a way that a constant equilibrium composition of fuel is maintained at all times at all parts of the reactor. This is the case referred to by Spinrad [163] as the case of uniformly graded fuel irradiation

Many calculations have been made of the reactivity lifetime for various core configurations, and many workers have attempted to express these results in terms of sufficiently general parameters to permit application of the results to a variety of reactors There is enough difference, however, in the operating temperature, in the relative importance of epithermal absorptions, and in other aspects of the neutron balance to establish the need for independent calculations in the present case.

The immediate result of these calculations is the fuel lifetime corresponding to Case No. 1 (batch loading, uniform exposure). Values of the lifetime in megawatt days per metric ton of UO_2 are given in Fig. 6–56 as functions of lattice pitch and fuel enrichment for clusters of seven 0.75-inch diameter UO_2 rods, with 0.018-inch 430 stainless steel (equivalent) clad, and at an average neutron temperature of 814°K (~541°C).

The effective cross sections and values of ν used for the uranium and plutonium isotopes, reduced to 2200 m/sec values, were $\sigma_{a5} = 642$ b, $\sigma_{f5} = 525$ b, $\sigma_{a8} = 2.73$ b, $\sigma_{a9} = 2128$ b, $\sigma_{f9} = 1290$ b, $\sigma_{a0} = 1792$ b, $\sigma_{a1} = 2088$ b, $\sigma_{f1} = 1527$ b, $\nu_5 = 2.48$, $\nu_9 = 2.88$, $\nu_1 = 3.30$.

The lifetime indicated for the reference design (8-inch pitch, 2% enrichment) corresponds to a residence time of fuel in the reactor that is a large fraction of the design life of the reactor (20 years). The Case No. 1 lifetime (Fig. 6–56) is about 7350 Mwd/t. For continuous fueling, this should be increased to 14,000 to 15,000 Mwd/t. Since the specific power

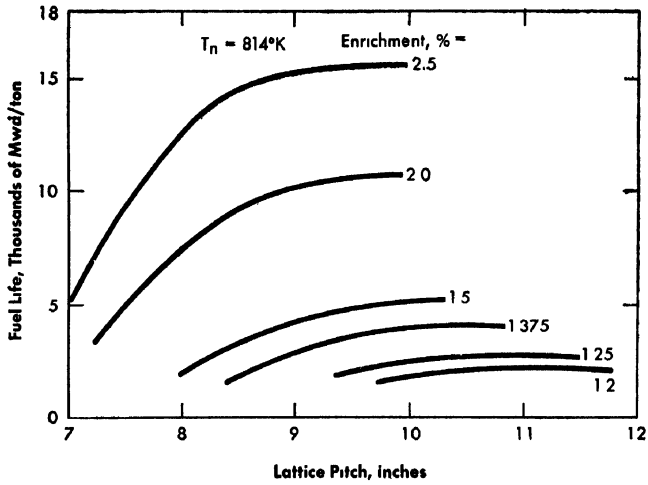

FIG 6–56. Fuel lifetime as a function of lattice pitch and enrichment Seven UO_2 rods, 0 75-inch diameter, $T_n = 814°K$. [10]

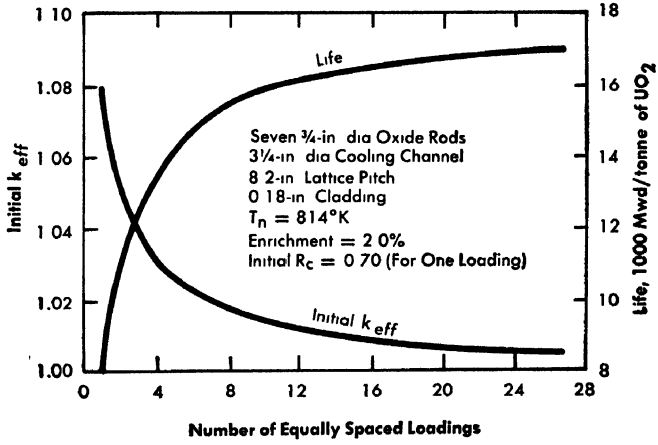

FIG. 6–57. Effect of staggered loading on fuel lifetime. [10]

level of the reference design is about 5 Mw/t, this would yield an average residence time of about 10½ years (load factor of 0.80). Since the devices that would permit continuous onstream loading of the reactor pose quite serious engineering problems, it is desirable to investigate the possibility of approximating the continuous loading cycle by reloading a rather substantial fraction of the total number of fuel channels at a time, at appropriate intervals. Figure 6–57 shows fuel lifetime (in Mwd/t) as a function of the number of intervals into which the loading cycle might be

divided. It is seen from Fig. 6–57 that ten steps will give nearly as long a fuel exposure as continuous loading. Also shown is the effective multiplication factor of the core after each refueling operation, which indicates the amount of reactivity the control rods must take care of with each fresh fuel charge.

It is recognized that with such long residence times as those mentioned above, an equilibrium fueling cycle might never be established in the lifetime of the reactor. The question of the best way to approach an equilibrium fueling cycle has not been resolved, though it is certain that there will be some sacrifice in average fuel exposure, averaged over all the fuel charged to the reactor throughout its life.

Temperature coefficient of reactivity. The effective multiplication constant can be written approximately as

$$k_{\text{eff}} = \frac{\eta\epsilon p f e^{-B^2\tau}}{(1 + L^2B^2)(1 + P)},$$

where P is the ratio of neutron absorptions in fission-product poison to those in fuel. If this expression is differentiated with respect to the moderator temperature, the moderator temperature coefficient of reactivity becomes

$$\frac{1}{k_{\text{eff}}}\frac{dk_{\text{eff}}}{dT} = \frac{1}{\epsilon}\frac{d\epsilon}{dT} + \frac{1}{f}\frac{df}{dT} + \frac{1}{\eta}\frac{d\eta}{dT} - \tau B^2\frac{1}{\tau}\frac{d\tau}{dT} - \frac{L^2B^2}{1 + L^2B^2}\frac{1}{L^2}\frac{dL^2}{dT} - M^2B^2\frac{1}{B^2}\frac{dB^2}{dT} - \frac{1}{1 + P}\frac{dP}{dT}.$$

(The resonance escape probability is assumed to be independent of the moderator temperature.) In this form it is convenient to calculate each part of the temperature coefficient separately and add them to obtain the over-all coefficient.

It was desired to compute the temperature coefficient as a function of both temperature and fuel exposure. This was done by using the temperature dependent cross sections previously discussed, together with the isotopic concentrations as functions of fuel exposure from the fuel lifetime calculations.

Values of the moderator temperature coefficient (not including contributions of xenon and samarium or the Doppler coefficient) are shown in Fig. 6–58. The coefficient is negative at all temperatures and fuel exposures. As Pu^{239} builds up in the fuel, the coefficient becomes less negative for temperatures below 600°K. A calculation for a natural uranium lattice, similar to that of the Calder Hall reactors, showed the moderator coefficient to become strongly positive, as expected, at exposures above about 1000 Mwd/t. In the present case, however, the coefficient levels out with

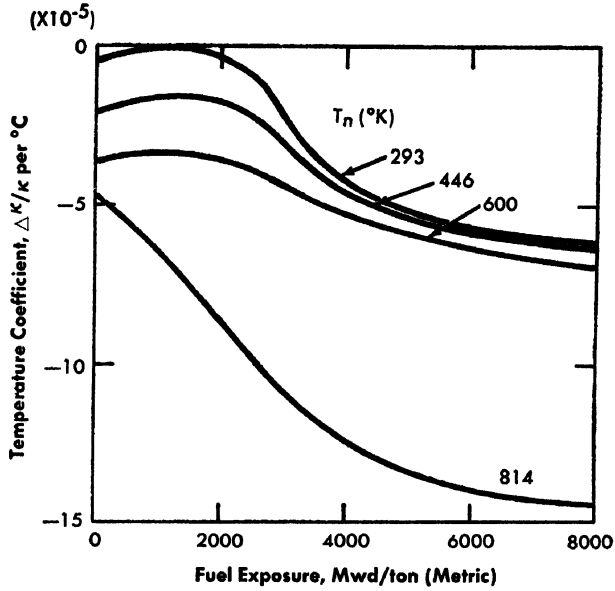

FIG. 6–58. Moderator temperature coefficient of reactivity as a function of neutron temperature and fuel exposure, excluding Xe^{135} and Sm^{149}. [10]

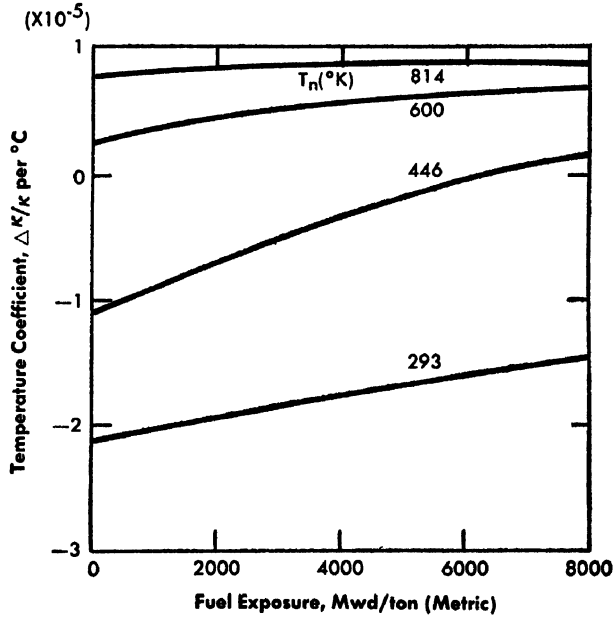

FIG. 6–59. Contribution of Xe^{135} and Sm^{149} to moderator temperature coefficient of reactivity. [10]

increasing exposure and then becomes more negative again. At a neutron temperature of 814°K, the trend of the temperature coefficient with increasing exposure is increasingly negative over the whole exposure range. The qualitative difference in behavior between the present case and the natural uranium-graphite reactors is probably due to the enrichment of the fuel and the much larger epithermal component of neutron energy spectrum. The latter factor emphasizes the relative importance of Pu^{240}, and may be responsible for the downward turn of the curves in Fig. 6–58 between 2000 and 4000 Mwd/t.

The curves of Fig. 6–59 show the contribution of the fission poisons Xe^{135} and Sm^{149} to the moderator temperature coefficient.

Calculation of the moderator temperature coefficient is a rather delicate matter, and further work on the cross sections will be required before these results can be established with certainty.

6–4.4 Natural uranium design studies.* Studies and cost estimates of gas-cooled graphite-moderated reactors have recently been made for the U. S. Atomic Energy Commission The objective was to develop designs incorporating the latest proven advances in reactor technology Prototype natural-uranium reactor and full-scale (optimum size) natural-uranium reactor designs by Kaiser Engineers are described here. The partially enriched designs are described in Article 6–4 5.

Natural uranium fueled prototype. The natural uranium prototype reactor is designed as a 55 Mw (net) electrical plant, presumably to be constructed at the National Reactor Testing Station in Idaho One multipurpose building houses the reactor plant, turbogenerator, warehouses, and offices; there are also a forced-draft cooling tower, a substation, and utilities. The reactor size is the smallest that can provide enough reactivity for 3000 Mwd/metric ton average fuel lifetime with natural uranium The total thermal power is 180 Mw (55 Mw net electrical). A perspective of the plant arrangement is shown in Fig. 6–60. Estimated design and construction cost of this prototype is $63.2 million. Major design features follow closely those of the 200-Mw optimized plant. (The rating of 220 Mw, corresponding to a reactor thermal power of 700 Mw, is calculated as the optimum for a reactor using a pressure vessel about as large as can possibly be cold-formed, field-assembled, and stress-relieved with present construction practices.) The design and performance characteristics of the natural uranium gas-cooled power reactor (GCPR) are listed in Table 6–30 (see pages 654–658).

*This material has been extracted from the Kaiser Engineers-ACF reports on the natural uranium reactor designs, References 11 and 12.

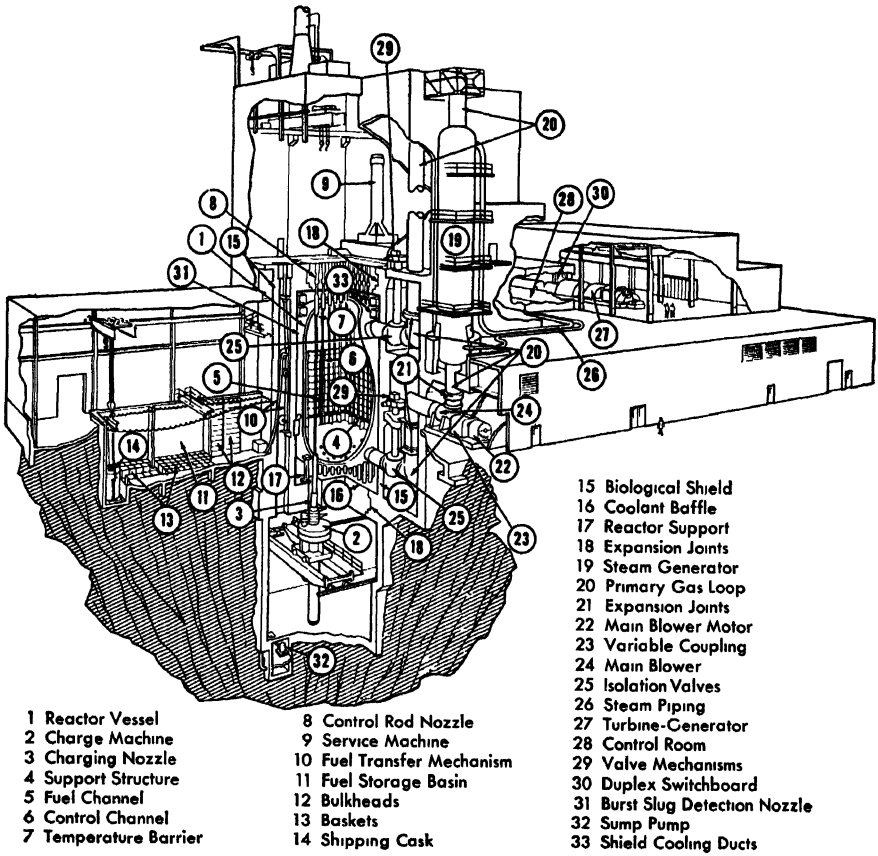

FIG. 6–60. Cutaway perspective of natural prototype GCPR. [11]

The prototype reactor core is in a cylindrical pressure vessel with hemispherical heads (Fig. 6–60). The vessel, 36 ft in diameter and 66 ft high, contains a temperature barrier surrounding the (35 × 25 ft) cylindrical graphite core. The natural uranium fuel is in vertical channels. With a lattice spacing of 8 inches, the fuel channels are approximately 4½ inches in diameter; each contains a stack of nine 2-ft-long fuel assemblies. Each assembly comprises a natural uranium fuel slug in a finned magnesium alloy can, assembled in a graphite sleeve. Cooling gas flows upward through the core; control rods enter from above; fuel is charged and discharged from beneath the reactor; and the reactor is serviced from above.

The cylindrical pressure vessel was found most economical for this reactor. It requires fabrication, erection, and stress-relieving techniques similar to those prospectively required for the 4-inch-wall spherical vessel of the optimum plant (Fig. 6–67).

The graphite stack, comprising both the moderator and reflector, is supported on a grid structure in the vessel. Rectangular blocks are keyed together to allow for expansion from temperature and radiation effects. The design allows for Wigner growth of the graphite, so that no damage can occur from Wigner energy release, even if the coolant system should fail.

As shown in Fig. 6–60, the prototype reactor is inside a concrete biological shield approximately 10 ft thick, with the reactor centerline nearly at grade. The fuel charge-discharge area is beneath the reactor vessel, its operating level 60 ft below grade. The CO_2 coolant gas enters the reactor vessel at 409°F and leaves at 800°F, then passes through two steam generators on opposite sides of the reactor vessel. Blowers circulate the CO_2 back to the reactor vessel in a closed system. The steam generators provide steam at dual pressures, with reheat, to the 55 Mw (net) turbogenerator.

Air, carbon dioxide, hydrogen, helium, nitrogen, and neon were compared in selecting the coolant gas. Based on costs and reliability, carbon dioxide was chosen.

The boron-steel control rods are positioned from the top of the reactor by cable drives. These rods can set off a scram by falling into the reactor. Reactor instrumentation is conventional. In addition, a burst slug detection system quickly identifies the channel in which a fuel element has failed.

The charge-discharge machine beneath the reactor can replace fuel elements or shuffle partly spent elements from one position to another while the reactor is in operation. A service machine above the top biological shield can replace spent control rods, and assist in removing jammed fuel elements and in flux plotting. This machine can operate without a reactor shutdown.

The steam power plant has two steam generator units that supply steam at dual pressures (regenerative-reheat) to a single turbogenerator (1450 psia and 750°F at the throttle). The turbine, nominally rated at 60,000 kw (64,000-kw gross capability), is directly connected to the hydrogen cooled generator (76,800 kva). Steam from the high-pressure turbine is reheated and mixed with the low pressure superheated steam. The combined flow at about 300 psia and 750°F then re-enters the turbine and finally passes to the condenser. The condenser is at ground floor level in the turbine building; the turbogenerator is on the operating floor, 27 ft above. Controls are centralized in one control room, convenient to both the reactor and steam plant facilities.

An induced-draft tower cools the condenser circulating water, maintaining a back pressure of $1\frac{3}{4}$ inches of mercury absolute. The estimated turbine heat rate is 9800 Btu/kwh. Equipment and control systems for the turbogenerator plant are conventional except for the steam generators.

It was necessary to go beyond preliminary design on some reactor components to ensure feasibility of concept and reasonably accurate plant performance and cost estimates. In this category are (1) charge-discharge machine, (2) fuel elements, (3) control rod drive mechanism, (4) service machine, and (5) steam generators.

Reactor core arrangement. The reactor core, a 24-sided right prism, is about 25 ft high and 35 ft across diametrically opposite corners. It is a graphite moderator structure surrounded by a graphite reflector, resting on a steel grid framework in the reactor vessel Moderator and reflector graphite are TSF and AGOT, respectively. Both grades have a density of 1.70 g/cm^3.

The core is pierced by vertical holes 4½ inches in diameter for fuel channels, and 3¼-inch vertical holes for control rods. Control rod holes are arranged with one at the center of each group of 16 fuel channels. All fuel channels and control rod holes extend through the graphite reflector at the top and bottom.

There are nine 26½-inch-long, vertically-stacked fuel assemblies in each channel, with a graphite dummy sleeve at top and bottom. The fuel assemblies occupy the moderator section of each fuel channel, and the dummy sleeves are in the reflector.

Fuel assemblies. The preferred fuel assembly is a cored cylinder of natural uranium metal two feet long encased in a helically finned magnesium alloy can, held at the center of a cylindrical graphite sleeve by graphite spiders at each end (Fig. 6–61). The sleeve supports the fuel elements in the coolant channel Nine such assemblies are stacked vertically in each of the 1532 fuel channels. Longitudinally finned cans were considered but

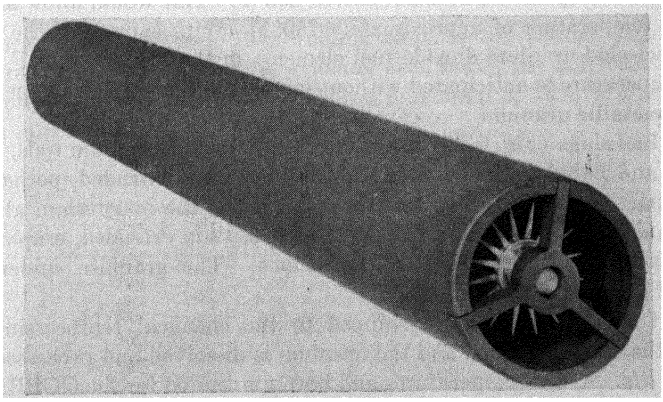

FIG. 6–61. General view of GCPR preferred fuel assembly, showing helically finned Magnox A-12 can positioned by graphite spider in graphite sleeve. (KE-ACF)

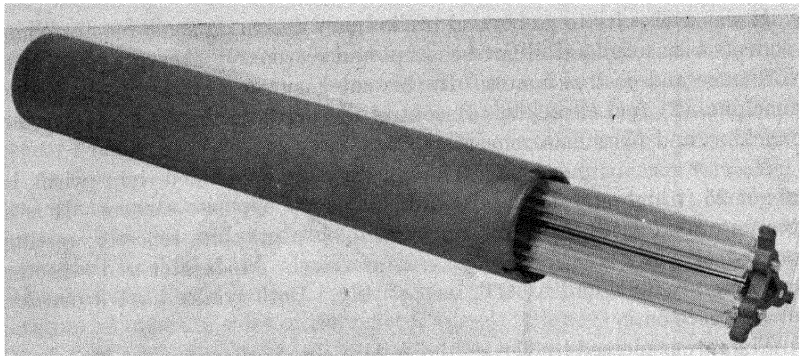

FIG. 6–62. General view of GCPR alternate fuel assembly showing a three fuel-element cluster in longitudinally finned cans, graphite spider, and graphite sleeve (KE-ACF)

analysis showed helical fins superior. Other fuel designs were considered:

(1) A cluster of three longitudinally finned fuel elements instead of a single helically finned fuel element (Fig. 6–62).

(2) A finned graphite support structure surrounding an unfinned can, instead of a finned magnesium alloy can.

(3) A uranium dioxide slug with unfinned stainless steel cladding

Fuel assemblies with uranium dioxide are used, but only in core arrangements in which metallic uranium fuel assemblies are also employed.

The anticipated life of the preferred fuel assembly is 3000 Mwd/metric ton of uranium, assuming that the prescribed loading is followed and that the surface temperature does not exceed 850°F. This would allow an outlet gas temperature of approximately 750°F. With enough of the stainless steel-clad uranium dioxide fuel elements in the core, an 800°F outlet gas temperature is anticipated without increasing the surface temperature of the metallic uranium.

The fuel slugs (Fig. 6–63) are made from wrought uranium rods, cut to length and bored. The magnesium alloy cans are extruded, perhaps by the impact process. Hydrostatic pressing bonds the magnesium alloy to the uranium. The graphite sleeves (Fig. 6–64) are extruded, graphitized, and machined to the required dimensions. The graphite spiders are molded or machined.

Spent fuel assemblies are shipped to the chemical reprocessing site where the can is removed and the uranium is dissolved and processed.

Fuel life. At the temperatures and burnups desired for the GCPR, radiation damage is limiting. The useful life of metallic uranium fuel has been found to depend upon its temperature during irradiation; the higher the temperature, the shorter the life. The following table shows the fuel

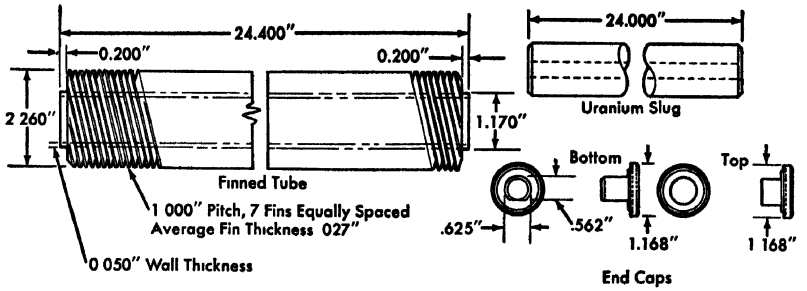

FIG 6-63. Details of GCPR preferred fuel element. [11]

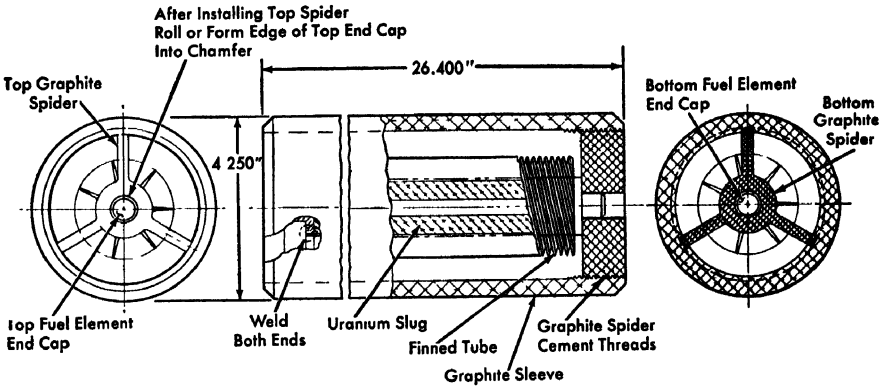

FIG. 6-64 GCPR preferred fuel assembly [11]

exposures that produce a 10% volume increase for various irradiation temperatures. Because there is evidence that fission gas is released when fuel volume increases more than 15%, a maximum of 10% is chosen for design purposes.

Irradiation temperature, °F	Exposure for 10% volume increase, Mwd/metric ton
752	4,000
797	3,000
842	2,000
887	1,500
932	1,000

Here, irradiation temperature means surface temperature (assumed to be 75° higher than gas outlet temperature). It is seen that fuel life de-

creases (and the operating fuel cost rises) as the maximum surface temperature increases.

The prototype reactor is designed so that the theoretical maximum fuel exposure is approached. A design study shows charging and discharging under load to be feasible and economical. The fuel is divided into the largest practical number of fuel assemblies in an individual channel. The benefits of positioning the assemblies to approach the theoretical maximum life can be balanced against the cost of the on-stream charge-discharge operation. For both the prototype and the optimum reactors a fuel life greater than 2500 Mwd/metric ton is found consistent with outlet gas temperatures of approximately 750°F for both fuel assembly designs ("preferred" and 3-rod cluster).

Channels fueled with oxide elements are not subject to the same surface temperature limitation; reactivity loss rather than radiation damage determines fuel life in this case. The oxide elements can be exposed to 4000 Mwd/metric ton. In the two-region core (using oxide and metal fuel in the respective regions) the outlet gas temperature of the metal-fueled channels can be dropped somewhat without lowering the 800°F average outlet temperature. Then the lifetime of the metal assemblies increases from 2500 to more than 3000 Mwd/metric ton.

To summarize, a simple loading scheme gives an average metallic-fuel life greater than that predictable from the maximum fuel surface temperature of each channel. For example, the life based on 850°F maximum surface temperature is about 1800 Mwd/metric ton. With the loading pattern described above, the average life is increased to 3000 Mwd/metric ton with the same maximum surface temperature. If both oxide and metallic fuel assemblies are used in a two-region core, their lives are expected to be 4000 and 3000 Mwd/metric ton respectively, for a gas outlet temperature of 800°F.

Graphite structure. The graphite structure (Fig. 6–65) consists of a keyed graphite moderator, a graphite reflector, steel base plates and top plates, peripheral restraints and base radial keys

The moderator and reflector form the 24-sided prism discussed above The design allows for Wigner growth, thermal expansion, and seismic forces. Finished machined graphite weight is approximately 2,000,000 lb

The moderator graphite (grade TSF) has the high purity necessary for the required reactivity. Moderator density was chosen in relation to cost. For the reflector graphite, the purity and density of the cheaper AGOT are acceptable. Two sizes of rectangular brick are used, of 117 and 222-lb finished weight. Bricks are stacked with their extrusion lines vertical, and the interconnecting graphite keys with their lines of extrusion horizontal (Fig. 6–65). This minimizes channel lattice changes from Wigner growth. Alternate levels of bricks are rotated 45 degrees about their ver-

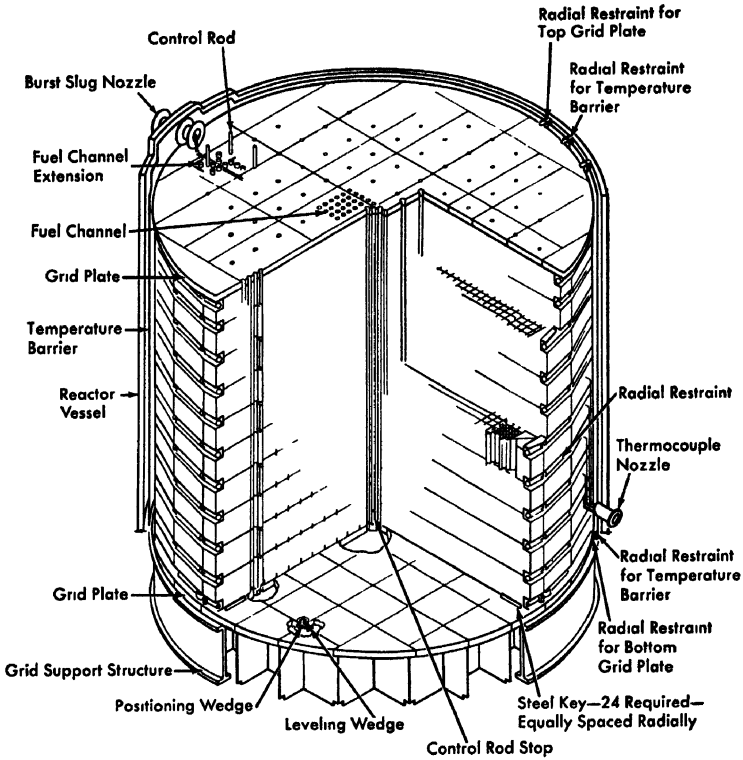

FIG 6–65 Graphite core configuration for natural prototype GCPR. [11]

tical axis to reduce vertical neutron streaming. Irradiation of the low temperature graphite in the GCPR results in storing about 30 cal/g per year. By annealing once a year at 900°F, 10 cal/g of this stored energy can be released. The remaining stored energy causes a transverse graphite growth of 0.02%/yr and a longitudinal growth of 0.01%/yr. The 1/8-inch gaps in the graphite provide for 1% total growth, more than adequate for the life of the reactor.

The graphite structure has 1532 vertical fuel channels ($4\frac{1}{2}$-inch diameter, 8-inch square spacing). There are also 97 vertical control rod channels of $3\frac{1}{4}$-inch ID on a 32-inch square spacing. The graphite reflector is $2\frac{1}{2}$ ft thick.

Steel restraint straps around the graphite at eleven levels limit radial movement, and 24 radial keys at the bottom level of the core interlock with the ring girder of the grid structure. The keys are designed to take a seismic loading for Zone 2.

Steel leveling base plates maintain vertical alignment and required

flatness of the graphite core. Each plate rests on twelve leveling pads which are welded flush to the top edges of the grid structure.

Steel top grid plates protect the graphite. The plate absorbs the impact load that would result if a control rod suspension wire failed. Then the control rod would fall safely into the graphite core, with its upper shock absorber striking the plate. The steel plates also support the burst slug detection piping matrix. The base and top plates have holes for access to the fuel and control channels, and for passage of coolant gas.

Reactor vessel. The reactor pressure vessel is in accordance with the ASME Pressure Vessel Code.

Studies indicate that a 4-inch wall and a 70-ft ID sphere are maximum vessel dimensions for the optimum reactor. A similar configuration for a prototype, scaled down from the 70-ft sphere, would not be economical; a 60-ft sphere would be needed to house nozzles and service operations. The 36-ft ID cylinder with hemispherical heads is entirely suitable for the prototype plant and is cheaper than the 60-ft sphere

The cylindrical prototype is believed to simulate satisfactorily the characteristics of the vessel for the optimum plant. Therefore, the prototype vessel is designed with 4-inch walls for the same pressure as that projected for the optimum plant. The vessel is 65 ft 10 inches high. An inner shell lines the cylinder and the top head, providing an annular space for flow of coolant gas.

The gas circulates upward through the core, except for a small amount channeled between the shells to keep the pressure vessel wall below 650°F. Two nozzles penetrate the bottom head for gas inlet and two the top head for gas outlet. Through the bottom head also pass sixty 12-inch nozzles, 52 for fuel charging and 8 for thermocouple wires The top head has 113 nozzles, 97 for access to control rod channels and 16 for burst slug detection tubes.

The core support structure rests on extensions of external support columns, with the load transferred through the vessel wall. Internal and external lugs and brackets are for seismic restraint. All supports are designed to permit only radial movement, horizontally, of the vessel and reactor core. The vessel is field-erected, stress-relieved, and pressure-tested. The exterior is insulated.

Control rod mechanisms Control rod mechanisms include drive and shock absorber assemblies. The drive assemblies, above the reactor, insert and withdraw control rods at the required speed. Shock absorbers at the top and bottom of each rod absorb the shock from a free-falling rod. Each assembly comprises a control rod, shield plug, drive mechanism, connecting linkage, spring shock absorber, and broach arrestor. All are alike; each can be operated as either shim or regulating rod; and all, being magnetically suspended, function as safety rods. The reactor

operator positions the shim rods either singly or in groups, while the neutron flux controller automatically positions the regulating rods.

The shim rods bring the reactor up to the approximate desired power level during startup and compensate for variations in reactivity caused by temperature changes, fuel depletion, and fission-product poisoning. The regulating rods counteract transient variations of reactivity.

The rods are steel tubes about 24½ ft long with 1½% by weight of boron added for 21 ft of the length. Each rod is suspended in its channel by a cable, passing through a shield plug to a winding drum. Shield plugs are steel cylinders filled with shielding material (equivalent to that of the biological shield); they fit into nozzles at the top of the reactor vessel. Winding drums and gears are in the upper end of the plugs. A drive assembly, above, drives each drum through a pressure seal. The drive assembly includes a synchronous motor, a gear train, a magnetic particle clutch, a centrifugal velocity damper, a position transmitter, limit switches, and a brake.

The entire unit can be removed for maintenance without disturbing the control rod. Limit switches stop the motor at the upper limit of rod travel and indicate when the rod has fallen free. The position transmitter always follows the rod position When power fails or a scram occurs, the clutch disengages in 10 msec and the rod falls, unwinding the cable At 4 fps, the velocity damper holds the speed constant; and during the last 2 ft of the stroke, the brake contacts, stopping the rod at its travel limit. Finally, the top shock absorber touches the grid plate on top of the reactor core. If a suspension cable breaks, and the rod falls free, the broach shock absorber at the bottom of the rod makes contact with a buffer stop during the last 11 inches of travel and brings the rod to rest. Fallen rods can be recovered and the entire control rod-shield plug assembly can be replaced during operation, by the service machine.

Fuel handling. Fuel handling includes storing new fuel components, preparing them for charging into the reactor core, charging and discharging the fuel, storing spent fuel during decay and finally shipping to the chemical processing plant. The fuel charging program is designed to obtain high burnup in a core whose neutron density is quite uneven. This means a daily routine of repositioning and replacing fuel elements.

New fuel assembly components (fuel elements, graphite sleeves, and end spiders) are stored in boxes in a special room. In the fuel preparation room, they are assembled for charging; then the charge-discharge machine inserts them in the reactor core. Spent fuel assemblies are transferred to the storage basin, dismantled, and stored under water for 100 days or more, then shipped in a shielded cask to the processing plant Graphite sleeves, after a short decay period in the basin, are dried in an oven and stored for reuse.

Burst slug detection system. Because flaws in the fuel container can release fission products to the coolant, its flow through a channel could be materially reduced by a burst slug, and the reactor damaged. A burst slug detection system detects a faulty slug and selects the channel containing it within a half-hour.

The system combines individual fuel channel sampling lines in a 10×10 matrix; samples from the 100 channels are drawn in 10 groups from 10 channels at a time in the x-direction and in 10 groups from 10 channels at a time in the y-direction. To monitor the 1532 channels, 312 lines are brought out of the reactor vessel, and these are manifolded to eight 40-port rotary selector valves and eight detection systems. Each system incorporates a cooler, a filter, and a detection unit. The gas samples are reintroduced into the main coolant system on the suction side of the main blowers by reciprocating compressors.

In the detection system, electrostatically deposited activity is read by a scintillation counter, amplified, and transmitted through read-out scalers, a decoder, and an electric typewriter. There are two spare detector units.

The precipitation chamber is a cylinder with a central wire maintained at a negative potential of several thousand volts with respect to the chamber wall. This chamber precipitates fission products from the gas sample onto the central wire. After a 40-sec "soaking" period, the wire is withdrawn from the chamber and a scintillation counter measures the activity. The signal from the detectors is sent to preamplifiers, amplifiers, and into analog digital read-out scalers with 10-channel information output, then to a decoder and an electric typewriter. A rotary switching mechanism on the selector valve transmits its position indication.

Fuel charge-discharge machine. The charge-discharge machine, a self-propelled, shielded pressure vessel beneath the reactor (Fig. 6–66), rides on a carriage and bridge, its mechanisms operated remotely from the control room. The operator can:

(1) Position the machine under any fuel charging nozzle.

(2) Purge, pressurize, and seal the machine to the nozzle.

(3) Remove the shield plug from the nozzle and stow it in the machine

(4) Insert in the reactor the extendable tube through which fuel elements are transferred from the magazine.

(5) Discharge, charge, or reposition fuel in any of the 36 channels serviced from a single nozzle.

(6) Withdraw the transfer tube, reinsert the shield plug, and seal the nozzle.

(7) Transport spent fuel to the unloading station.

(8) Return the machine to the loading station for a load of new fuel.

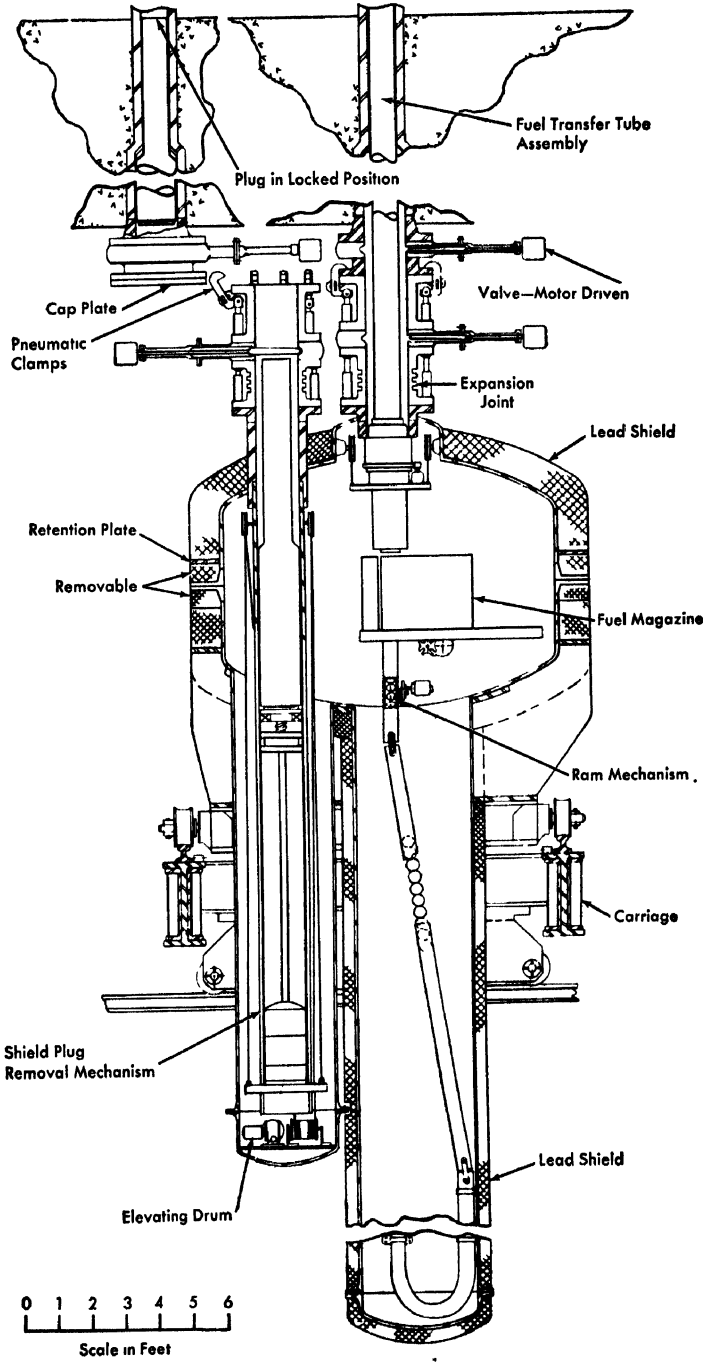

FIG. 6–66. GCPR charge-discharge machine [11]

Service machine. The service machine, a self-propelled, shielded pressure vessel above the reactor, contains mechanisms for servicing and performing certain maintenance functions with the reactor operating.

The reactor is serviced through control rod nozzles which extend through the shielding above the vessel Each nozzle services one control channel and 16 fuel channels. Riding on a carriage and bridge, the service machine can be positioned over the control rod nozzles, and the loading, unloading, storage, and rehearsal areas Mechanisms are operated from a control console on the carriage. The operator can:

(1) Position the machine over any nozzle.

(2) Purge, pressurize, and seal the machine to the nozzle.

(3) Remove, and stow in the machine, a control rod shield plug with the rod attached; an optical plug; or a shield plug (with or without instrumentation).

(4) Replace the stowed component with a preselected shield plug or plug assembly.

(5) Place or retrieve fuel elements containing thermocouples, dislodge fuel elements, and grapple for dropped rods or elements.

(6) Re-establish the seal at the control rod nozzle.

(7) Transport and unload spent fuel to the conveyor in the unloading area, or transport and unload control rods and shield plugs in the storage area.

(8) Reload the service machine for its next function

Heat transfer and pressure drop A critical factor in over-all performance is the rate at which heat can be removed economically from the reactor core. Good heat transfer is essential to high power output.

Extended surfaces (jacket fins) help promote good cooling of the fuel. Longitudinal, transverse, and helical fins were investigated Transverse and helical fins appeared about equal in heat transfer performance, and better than longitudinal ones, but for accurate prediction of their performance experiments would be necessary

The thermal output of the reactor is determined by the heat transfer performance and temperature limitations of the fuel material. Three temperature limits must be considered: the highest temperature anywhere in the uranium metal must be limited to 1200°F to prevent the α-β phase transition; the maximum uranium surface temperature determines fuel life; and the surface temperature of the magnesium alloy jacket must not exceed (approximately) 930°F. It is probably desirable to operate each channel so that one of the temperature limits is approached at some point in the channel. A variable orificing system does this. The flow through the unorificed channels limits the power level of the reactor and sets the core pressure drop.

Reactor coolant system. There are two gas coolant loops, each containing one steam generator and one motor-driven variable speed blower. An automatic gas filtering and drying system (continuous bypass) is provided.

The specifications for the carbon dioxide are:

Carbon dioxide	99.8% minimum, by weight
Upper limits for impurities:	
Hydrogen	0.1% by weight
Water	0.1% by weight
Nitrogen	100 ppm
Oxygen	100 ppm
Argon	1 ppm
Boron	0.1 ppm

Each coolant loop handles half the gas flow and, of course, half the reactor heat After leaving the reactor at 800°F the gas is cooled to 400°F in the steam generator, and returned to the reactor at 409°F (heated 9°F by the blower) The gas pressure at the reactor inlet is 285 psia (system pressure loss is 12 psi). The control system keeps the gas leaving the reactor at 800°F, and automatic controls at the steam generators hold the reactor gas inlet at 409°F

Two motor-driven variable-speed blowers, one in each coolant loop, are mounted directly beneath the steam generators. Each is designed to circulate half the total coolant flow against the system pressure differential. The pressure rise across the blowers is 12 psi, with gas entering at 400°F and 273 psia.

The main gas ducts have motor-operated isolating valves, so that either loop can be serviced without depressurizing the reactor. The steam generators and blowers are so arranged that the main gas piping for each circuit is in a single plane Stainless steel, bellows expansion joints are employed in the ducts Manually operated vent valves discharge gas through the vent system during maintenance shutdown. Safety valve and other gas system vents are discharged through high efficiency filters to remove radioactive particles

Steam generators Steam generators for a gas-cooled power reactor differ materially from standard boiler designs because the heat source is clean, high-pressure, radioactive gas at relatively low temperature; the gas flow is very large; and gas temperatures entering and leaving the steam generator are held constant. These factors coupled with the cleanliness and leak-tightness requirements, make equipment costs abnormally high. Basic features are that gas flows in the shell, water and steam flow

through the tubes, all tube sheets are accessible from outside the gas stream so that leaking tubes can be plugged, and the shell is assembled in large sections, with internal parts already in place and tested before shipment. Two steam generators, each of half the reactor capacity, operate on a dual-pressure reheat cycle. With the comparatively low gas temperature, this cycle proves most economical

The heat-exchange surface in the steam generators is divided into five main sections: (1) a low-pressure and a primary high-pressure economizer, in parallel, (2) a low-pressure evaporator, (3) a secondary high-pressure economizer, a primary low-pressure superheater and a primary reheater, all in parallel, (4) a high-pressure evaporator, and (5) a high-pressure superheater, secondary low-pressure superheater and a secondary reheater, all in parallel The steam pressures and temperatures are 1480 psia, 750°F at the high-pressure superheater outlet, and 315 psia, 750°F at the reheater and low-pressure superheater outlets. The feedwater temperature is 260°F to the high- and low-pressure economizers.

To reduce cost, the steam generators are installed outdoors. Each unit is supported at its base and thermal expansion is upward. The steam generators are higher than the reactor, providing gravity circulation of coolant to dispel the reactor decay heat during shutdown. The steam pressures in both high- and low-pressure circuits are normally greater than the gas pressure; hence, radioactive gas does not leak into the steam circuits from tube failure Instrumentation and alarms monitor excess moisture in the gas from steam or water leaks. During low-power operation, when the pressure in the reheaters drops below that of the gas, their steam flow is monitored.

Natural uranium fueled optimum plant. The optimum-size plant has the same basic design as the prototype; only differences in details will be described. Dimensions, temperatures, pressures, number of like components, and other numerical values are listed in Table 6–30.

The general plant arrangement is shown in Fig. 6–67. The estimated design and construction cost is $141,000,000 or $640 per gross electrical kilowatt (Table 6–30). The estimated cost of power is 16.2 mills/kwh, including fixed charges of 12.8 mills, based on a lifetime plant factor of 80% and an annual fixed charge rate of 14%

The optimum reactor would have one of these core arrangements:

(1) A single-region core of the prototype preferred elements, i.e., cored natural uranium metal slugs jacketed in helically-finned magnesium alloy. The bulk coolant outlet temperature would approach 750°F with a fuel life of 3000 Mwd/metric ton.

(2) A single-region core consisting of three-rod clusters of metal elements with longitudinally finned, magnesium alloy cladding. With 800°F coolant outlet, fuel life would be 3000 Mwd/metric ton.

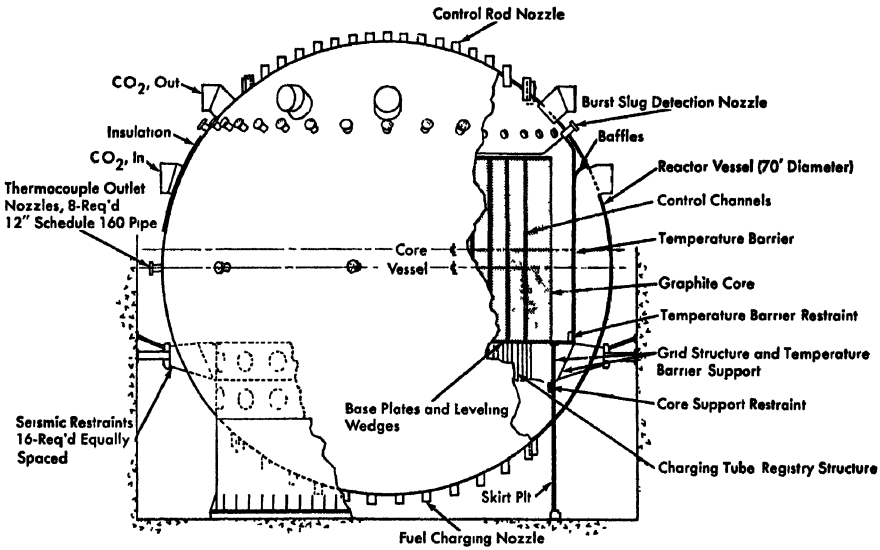

FIG 6–67 Optimum natural GCPR vessel assembly [12]

(3) A two-region core consisting of (a) a mixture in the central region of clustered natural uranium oxide stainless steel jacketed elements and prototype preferred elements, in separate channels, and (b) prototype preferred fuel elements in the outer region. The fuel channels with oxide elements may allow gas-cooled temperatures above 1000°F; with metal uranium elements, approximately 750°F. With a bulk coolant outlet temperature of 800°F, the average fuel life would be 3000 Mwd/metric ton.

In the steam power plant eight steam generators supply steam at dual pressures to a cross-compound turbogenerator unit. The turbine is directly connected to the hydrogen-cooled generators, which total 320,000 kva. Equipment and control systems are conventional except for the steam generators. The turbogenerator unit, as in the case of the prototype, operates on a dual-pressure regenerative reheat cycle.

Reactor core. The reactor core is similar to the prototype core, but larger. It is a 36-sided prism, 29 ft high and 50½ ft across opposite corners.

The total weight of finished machined graphite is approximately 4,900,000 lb; AGOT grade is used for both moderator and reflector. There are 3536 vertical fuel channels and 221 vertical channels.

Reactor vessel. The spherical reactor vessel comprises an outer pressure shell (70-ft diameter, 4-inch wall) and an inner temperature barrier. The outer shell, designed for a maximum pressure of 290 psig at

650°F, is of carbon steel plate. The inner temperature barrier is a 2¼-inch thick carbon steel cylinder whose inside diameter is 56 ft 8¾ inches with an upper hemispherical head. It is 46 ft high. Coolant gas from the steam generators flows down through the space between the pressure shell and the temperature barrier to keep the outer shell at a temperature not above 650°F. The gas then flows upward through the core.

Penetrations in the pressure shell include:

(1) Top penetrations: 48-inch CO_2 outlet and inlet nozzles, 12-inch vertical nozzles, 12-inch nozzles for the burst-slug detection system piping.

(2) Bottom penetrations: 12-inch thermocouple nozzles on the vessel centerline, and 12-inch nozzles for fuel charging and discharging.

The vessel support structure is fabricated from carbon steel plate. Steel rollers move horizontally to compensate for radial expansion of the vessel. The support grid for the reactor core rests on extensions of the external support columns which transfer the load through the vessel wall.

Burst slug detection system. The burst slug detection system is similar to that for the prototype.

Reactor coolant system. There are eight gas coolant loops, each with a steam generator and a motor-driven variable speed blower They are quite similar to those for the prototype.

Liquid carbon dioxide is stored at 450 psig and 20°F in three 50-ton insulated and refrigerated storage tanks The refrigeration system includes a compressor and submerged cooling coils in each tank.

Steam generators. The steam generators are like those for the prototype.

Steam power plant. In the dual-pressure, reheat steam cycle coolant gas temperatures are 800°F entering and 400°F leaving the eight steam generators. The improved performance of this system over comparable cycles is shown below:

	Turbine heat rate, Btu/kwh	*Gross power output, kw*
Dual-pressure reheat cycle	9,680	250,000
Dual-pressure nonreheat cycle	10,250	238,000
Single-pressure reheat cycle	10,640	229,000

The turbogenerator is a cross-compound, double-flow, condensing reheat turbine, rated at 250,000 kw, 3600/1800 rpm, directly connected to hydrogen-cooled generators of 320,000 kva, at 45 psig hydrogen pressure. The three 375-volt excitors are motor driven.

6–4.5 Enriched-uranium design studies. The application of partially enriched fuel to the graphite-moderated, gas-cooled concept has been investigated by Oak Ridge National Laboratory and also by the Kaiser Engineers-ACF group Both organizations chose as fuel elements cored cylinders of UO_2 jacketed in stainless steel. The Oak Ridge design used helium as coolant; the Kaiser-ACF group, carbon dioxide. In the latter case the choice is tentative because there are questions of feasibility of using CO_2 with graphite at temperatures in the 1000°F range. The design studies are summarized in the following sections.

Kaiser Engineers-ACF designs. Two designs have been studied by this group: that of a prototype plant of 44 Mw net electrical output, and that of an "optimum" size plant of 215 Mw. Their basic features are quite similar, and their structural designs, control systems, and fuel-handling machinery much like those of the natural uranium reactors (Article 6–4.4). Consequently, the designs are described only briefly, and their quantitative features summarized in Table 6–31 (see pages 659–662).

Partially enriched prototype. Four adjoining buildings house the reactor plant, turbogenerator, warehouses, and offices (Fig 6–68). Other facilities include the forced draft cooling tower, a substation, and utilities. Both prototype and optimum reactors are designed to operate at the same temperature, pressure, specific power, and fuel life. For the prototype reactor, the double-walled pressure vessel (Fig. 6–69) is an 18-ft ID carbon-steel cylinder with hemispherical heads, 40 ft high, its outer wall 3 inches thick The inner wall temperature barrier of stainless steel, 3/4 inch thick, keeps the outer carbon-steel wall at 650°F or less. The cylindrical graphite core is 16 ft in diameter and 18 ft high (Fig. 6–70). Vertical channels (4 inches in diameter with a spacing of 7 inches) contain six (stacked) 29-inch fuel assemblies Cooling gas passes up through the core. Control rods enter from above; fuel is charged and discharged from beneath, and the reactor is serviced from above.

The graphite structure is like that for the natural uranium designs.

The fuel assembly is a cluster of seven columns of enriched uranium dioxide pellets in stainless steel cans, supported in a graphite sleeve by top and bottom stainless steel spiders. The six outer fuel rods of the cluster are equally spaced, centered on a 2-inch circle. The fuel assembly is designed for 1000°F gas outlet temperature.

Each fuel rod, of 35 cored enriched uranium dioxide pellets, is 26.6 inches long. Each pellet is 0.7 inch long, 0.7 inch OD, and 0.32 inch ID. A magnesium oxide spacer pellet 0.19 inch long and 0.70 inch in diameter is placed at each end of each column of fuel pellets for thermal insulation of the end caps of the surrounding stainless steel can.

The pellets are in type-304 stainless steel cans 27½ inches long and 0.7 inch ID, with walls 20 mils thick. Top and bottom end caps, with

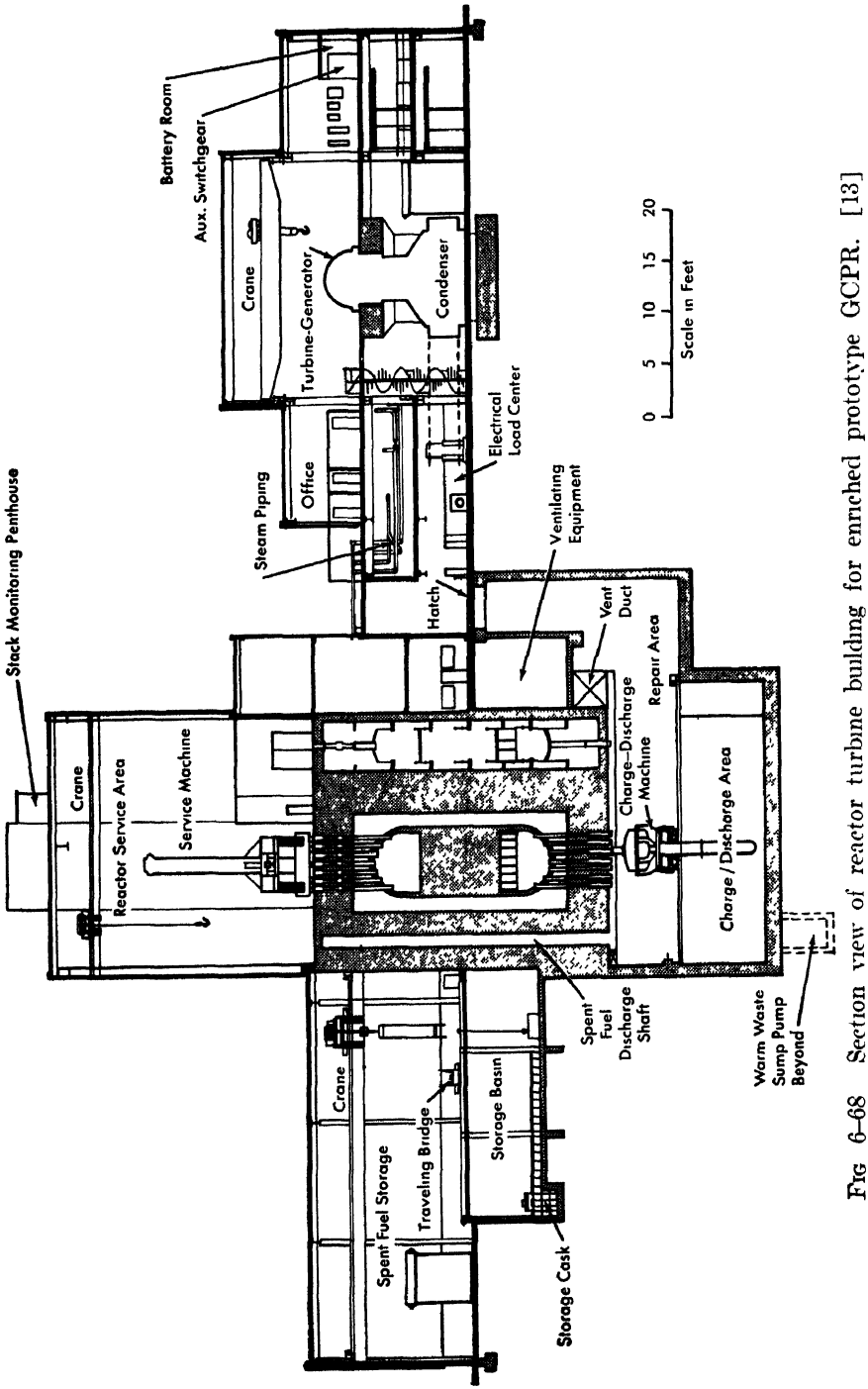

FIG 6-68 Section view of reactor turbine building for enriched prototype GCPR. [13]

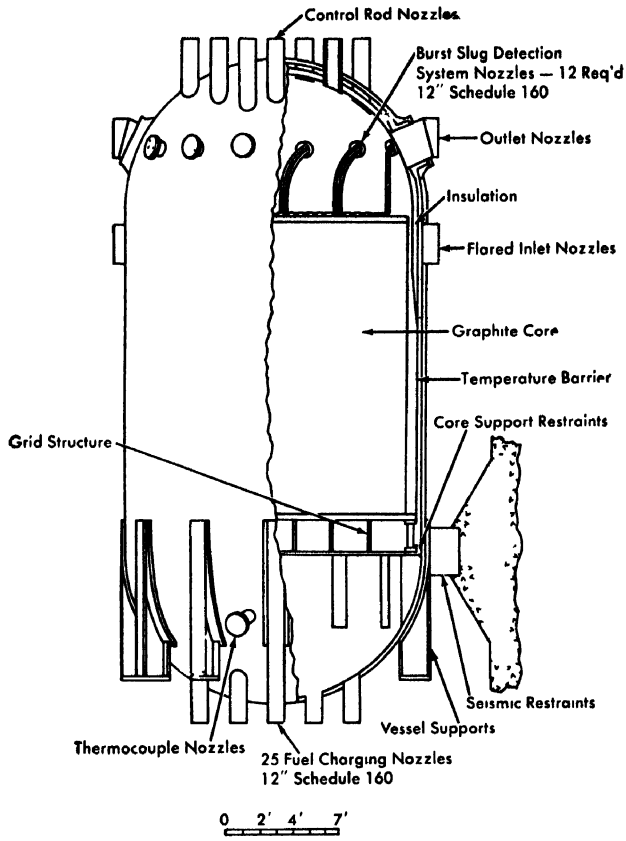

FIG. 6–69. Schematic diagram of reactor vessel assembly for enriched prototype of GCPR [13]

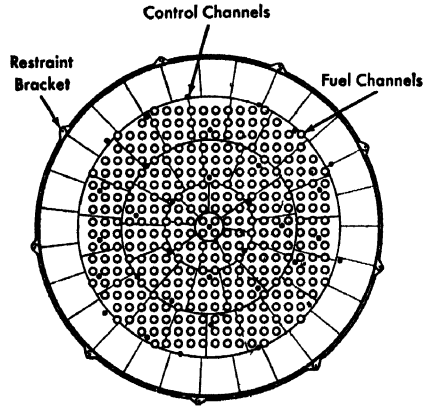

FIG. 6–70 Plan view of graphite core for enriched prototype GCPR. [13]

ends shaped and slotted to fit into the spiders, are welded to the ends of the can, gastight. The seven top end caps of the fuel rods in each cluster are welded to the top support spider, from which they and the bottom spider are suspended. After the subassembly of fuel rods and top spider has been inserted into the graphite sleeve, alternate bottom end caps of the peripheral rods are welded to the bottom spider, which laterally positions (but does not support) the lower ends of the rods. To minimize stresses developed by differential thermal expansion, only three of the rods are welded to the bottom spider.

The top spider, of 304 stainless steel, is a rim 3.28 inches OD, 0.09 inch thick, and 0.50 inch high, with a diametral bar crossed at right angles by two other bars 1 inch apart. All bars have the same height and thickness as the rim. The bottom spider is similar but only 3/8 inch high, and is notched to receive the lower rod end caps.

The fuel rods and spiders are surrounded by a graphite sleeve 29 inches long and 3.75 inches OD (which may have to be protected by silicon carbide or some other coating). The sleeve wall thickness is 0.375 inch. Internal shoulders machined at each end of the sleeve receive the top and bottom spiders.

The load of the internal subassembly is carried by the shoulder at the top of the sleeve. The sleeves also protect the moderator graphite and transmit the load of the fuel assemblies to the lower end of the fuel channels.

The control rods, of boron steel, are positioned from the top of the reactor by cable drives. Reactor instrumentation is conventional. There is also a burst slug detection system (see Article 6–4.4).

The charge-discharge machine is similar to that previously described.

Partially enriched optimum plant. The optimum plant, rated at 215 net electrical megawatts, is designed for location on the bank of a river in a section of the United States having an "average" winter and summer climate. One multipurpose building houses the reactor plant, turbogenerator, warehouses, and shop; other facilities include an office building, river pump house substation, and utilities.

The estimated design and construction cost of the optimum plant (253 Mw gross electrical) is $106,000,000 ($490/kw net). Switchyard and transmission lines are not included in this estimate, nor is cost of the development program. The estimated cost of power is 13.4 mills/kwh, of which fixed charges are 9.8 mills/kwh, based on a lifetime plant factor of 80% and 14% annual fixed charge rate.

The reactor is in a double-walled vessel consisting of a 26-ft-diameter carbon steel cylinder with hemispherical heads, 75 ft high. The vessel outer wall is 4 inches thick. The inner wall (temperature barrier), of stainless steel, is 1⅛ inches thick; the maximum temperature of the outer

wall is 650°F. The cylindrical graphite core is approximately 24 ft in diameter by 26 ft high. Each vertical fuel channel (4-inch diameter with a lattice spacing of 7 inches) contains a stack of nine 2-ft fuel assemblies. Cooling gas passes up through the core. Control rods enter from above; fuel is charged and discharged from beneath the reactor, and servicing is from above.

The single-region core contains fuel assemblies like those described for the prototype reactor, but enriched to 2.5% U^{235}. This enrichment is expected to provide an average fuel element lifetime of 10,000 Mwd/metric ton. Reactor design features are like those for the prototype.

*The Oak Ridge National Laboratory gas-cooled reactor design.** For the design study, a plant site was selected which is typical for United States power plants, meeting the practical requirements of rail and water transportation, a supporting power network, good construction conditions, and adequate labor. A cutaway perspective of the proposed plant is shown in Fig. 6–71, and a sectional view of the reactor building is shown in Fig. 6–72.

The plant is designed for base-load operation with ability to adjust automatically to load changes. The reactor will produce a gross thermal output of 687 Mw (250 electrical Mw gross at a heat rate of 9458 Btu/kwh). With a net efficiency of 32.8%, the electrical output is 225 Mw (net). The estimated cost of the entire facility is 94 million dollars or 420 dollars per net electrical kilowatt. The estimated total power cost (12.1 mills/kwh) includes fixed charges of 8.4 mills, fuel charges of 2.6 mills, and operation and maintenance costs of 1.1 mills. Fixed charges are based on 80% plant factor and 14% annual charge rate.

The reactor design has incorporated the following features:

(1) Stainless steel capsules for fuel cladding.

(2) Slightly enriched uranium dioxide for fuel material.

(3) Helium for reactor coolant.

Stainless steel was chosen as structural material because (1) its excellent high-temperature strength favors high exit-gas temperature and better heat-transfer and power-cycle performance, and (2) there is no catastrophic reaction between stainless steel and the important coolants which could initiate a graphite fire.

Using enriched fuel is not merely a matter of counteracting the nuclear poisoning of stainless steel. Rather, using enriched fuel has several other important consequences:

(1) It permits utilizing UO_2 which except for nuclear performance is greatly superior to uranium metal. UO_2 is not deformed by exposure

---

*This section is compiled from Reference 10: The ORNL Gas-Cooled Reactor, ORNL-2500, Oak Ridge National Laboratory, March 1958.

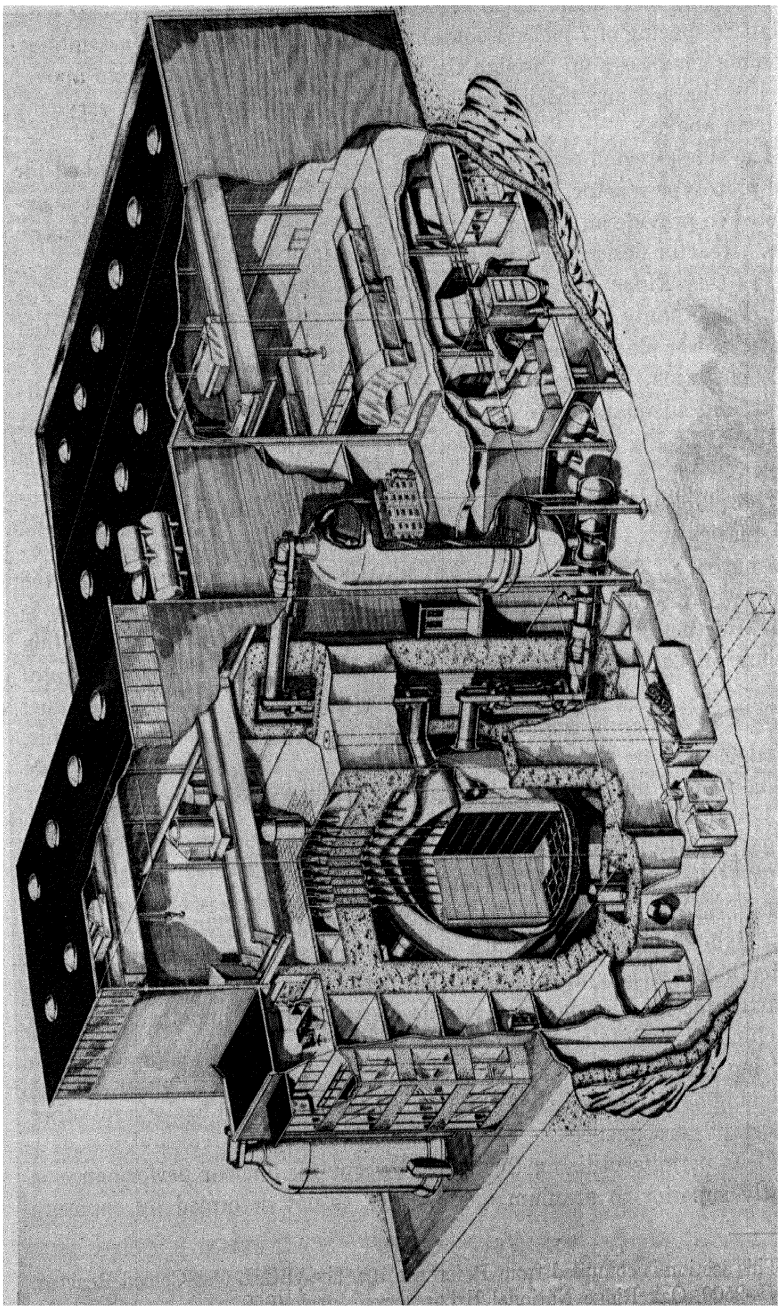

FIG. 6–71 Cutaway perspective of GCR-2 plant. [10]

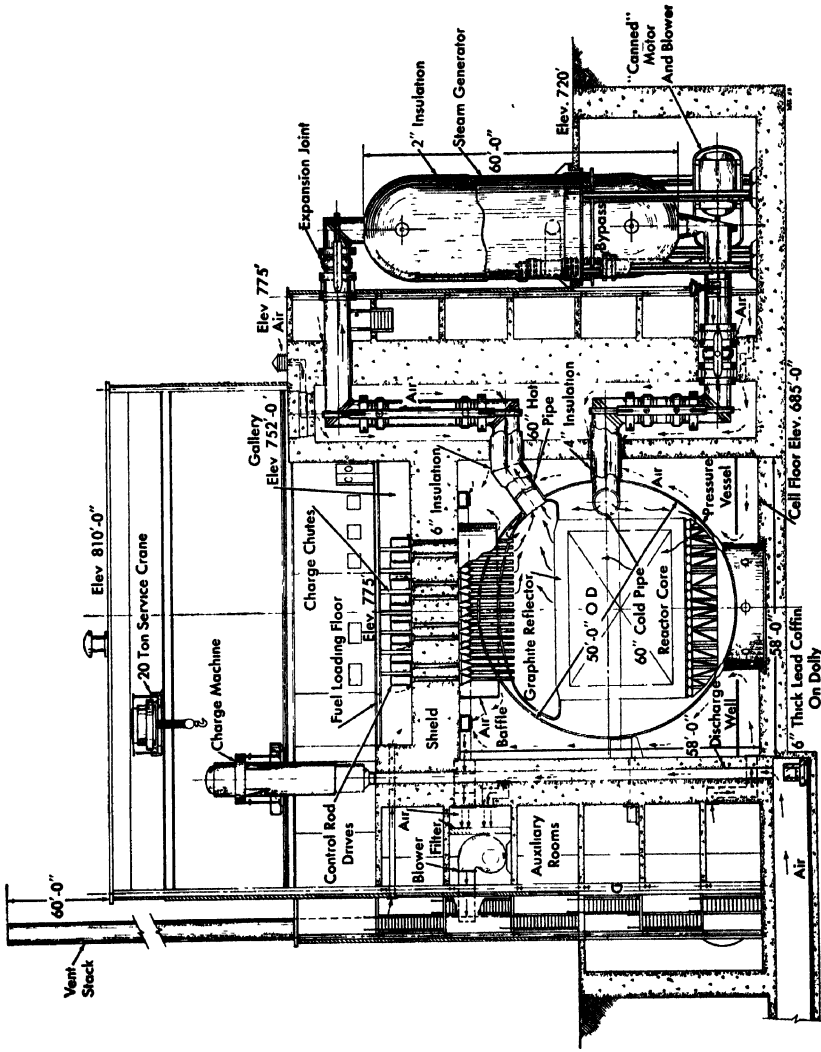

FIG. 6–72. Sectional view through reactor and reactor bay for GCR-2 [10]

(as is uranium metal) at low temperature. At higher temperatures UO_2 retains most of the fission product gases without severe distortion; the metal does not.

(2) Enriching beyond the minimum required for criticality provides enough excess reactivity so that the nuclear poisoning effect of the Pu^{240} can be overcome until Pu^{240} begins to serve as a fertile material (producing Pu^{241}). This overenrichment increases fuel life. At sufficiently long fuel life, the over-all fuel cost for partially enriched fuel becomes comparable to that for natural fuel. The partially enriched approach is based on the conviction that the necessary fuel life can be achieved with UO_2 elements, and that the benefits of enrichment in lowering capital cost can be enjoyed without an important increase in fuel cost.

(3) Enrichment reduces over-all capital cost through higher specific power. Costs/kw fall as power density is increased, since much of the total capital cost is independent of power level.

(4) Graphite-moderated, gas-cooled reactors with either natural uranium or only very slightly enriched uranium exhibit a positive moderator temperature coefficient of reactivity when fuel exposures exceed ~1000 Mwd/t. This is very important in the design of both the British and French power plants. Enriching the fuel shifts the absorption competition between plutonium and U^{235} so that a slightly negative moderator temperature coefficient is achievable over the entire range of reactivity lifetime.

Using stainless steel imposes a severe nuclear penalty that can be offset by raising the exit gas temperature. Once the design temperature substantially exceeds those at Calder Hall and Marcoule, the whole materials system based on CO_2 is in question, because of chemical reactions between CO_2 and graphite. To circumvent this problem, helium was selected for the GCR-2. Helium, of course, is not available on the world market; if it were available (at reasonable cost), it would perhaps become standard for such reactors. Its chemical inertness makes catastrophic oxidation almost impossible, since only its impurities can enter into such reactions.

Helium's high cost requires much better leaktightness than is required at Calder Hall, for example. No doubt, adequate leaktightness can be assured, at some expense, by careful design and construction. An over-all helium-leakage loss of 1% per day (more than ten times higher than is now achieved in large gas systems) would increase net power cost 0.05 mills/kwh.

Since the use of stainless steel allows system gas temperature to be high, carbon dioxide would probably be unsatisfactory as coolant, because of chemical reactions with graphite. Helium was therefore chosen despite its present limited commercial availability and its relatively high cost. A

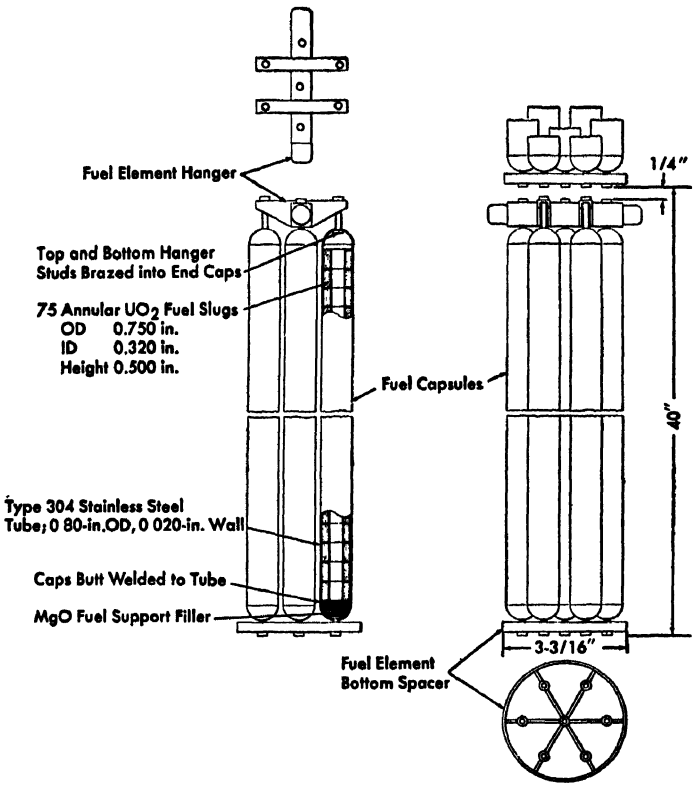

FIG. 6–73. GCR-2 fuel element assembly. [10]

more detailed discussion of considerations for choosing coolants was presented in Section 6–2.

The design and performance characteristics of the plant are summarized in Table 6–32 (see pages 663–666). A schematic diagram of the fuel element assembly is shown in Fig. 6–73.

Reactor core arrangement. The single-region core is a stack of keyed graphite blocks 30 ft in diameter by 20 ft high, surrounded by a 2½-foot-thick graphite block reflector (Figs. 6–71 and 6–72). The core is pierced vertically by 1597 fuel channels on an 8-inch square lattice. There are three fuel channel diameters: 345 channels have 3.45-inch diameters; 400 have 3.25-inch, and 852 have 3.05-inch diameters. These different channel sizes, aided by flow orifices, match the coolant flow to the varying power density across the reactor (see Section 6–2). Fuel element assemblies, stacked six to a channel, total 9582 in the core. The core has sixty-one 3-inch-square control rod penetrations spaced on a 40-inch-square lattice.

The neutron-absorbing sections of the control rods are hollow silver cylinders, each 18 ft long, 2 inches OD, and 1¼ inches ID. To provide adequate strength in the event of a large temperature overshoot, the silver is sheathed with type-304 stainless steel, 0.065 inch thick on the outside surface and 0.030 inch thick inside. The rods hang from stainless steel stranded cables, suspended from drums above the pressure vessel, just below the loading floor. Each cable supports 215 lb. A shock absorbing device is at the bottom of each rod.

Fuel-element assemblies. A fuel-element assembly (one top hanger, seven fuel capsules, and one bottom spacer) is shown in Figs. 6–73 and 6–74. The hanger is supported at two points, 180 degrees apart, in recesses in the graphite channel. In loading, the hanger is slid into vertical grooves in the channel and the assembly rotated until the hanger is engaged. The fuel capsule (Fig. 6–73), of 304 stainless steel, is 0.80 inch OD and 38.5 inches long with a 0.020-inch wall. It is filled with 75 UO_2 slugs and 2 MgO end spacers. Hemispherical end caps and a hanger attachment complete the capsule.

A fuel capsule assembly procedure is described as follows. The bottom cap is fusion-welded to one end of the tube using an automatic welder and helium backup atmosphere. The weld is inspected by x-ray, dye penetrant, and a helium mass spectrometer leak test. Welds defective at this stage can be repaired or cut out and replaced. After the bottom cap closure is complete, the assembly is cut to length, cleaned, and transferred to a controlled atmosphere chamber for placing the MgO end spacers and

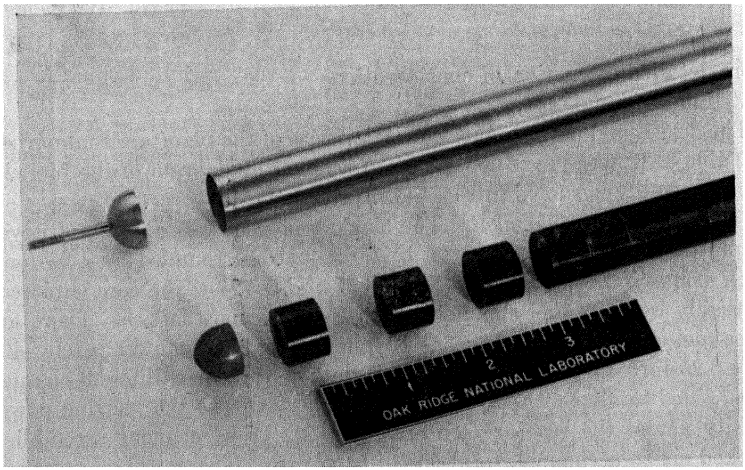

FIG. 6–74. Fuel capsule, showing GCR-2 fuel slugs and MgO spacer. [10]

loading the UO_2 slugs. To avoid contamination hazards, the top cap is welded in place in the controlled atmosphere chamber. After inspection of the weld by dye penetrant and x-ray, the element is evacuated, leak-tested, filled with helium, and the bottom cap filling hole welded shut. The final weld is examined by x-ray and dye penetrant.

The hanger design is based on a maximum stress of 2500 psi in the stainless steel; hangers will be nearly at the gas temperature (1000°F maximum). Besides keeping the metal volume and flow-obstructing areas of the fuel hanger small, it is desired also to limit the displacement of fuel in the channel by the hanger and spacer. For maximum strength over a long hanger life, casting appears favorable. One type of hanger is shown in Fig. 6–73, with the bottom spacer.

Fuel fabrication. Depending on how it is made, a particular uranium oxide product may be more or less suited for fabricating high-density fuel slugs. Vast differences in fabricability are illustrated in Fig. 6–75, showing two types of oxide (both derived from ammonium diuranate) as the granulated powder, the green compact, and the sintered pieces. The oxide at the top, fluffy and fine-grained, is well suited to the usual fabrication processes. It was cold-pressed at 20,000 psi in a steel die to a density of 40% and sintered to 93% of theoretical density. The oxide at the bottom of Fig. 6–75 was fabricated by the same procedure, but is completely unsuited to this process. Its green density is 58%, but the final sintered density is only 67%. For suitable pieces to be fabricated from this oxide, particle size would have to be reduced by milling and higher compacting pressures used.

The cost of fine-grained UO_2 could be much reduced by eliminating the fabrication step whereby UF_4 is reduced to uranium metal. In a process that has been proposed, UF_6 is dissolved in water to form UO_2F_2. Adding ammonium hydroxide forms insoluble ammonium diuranate which can be calcined to U_3O_8. The presence of the fluoride ion has been found to affect size and shape of the precipitate particle, further development work will be needed to obtain the desired characteristics.

Costs might further be reduced by eliminating the grinding usually required with sintered slugs to hold necessary tolerances. Three techniques are possible: (1) to relax tolerances, (2) to hold the length-to-diameter ratio less than one to minimize hour-glassing, and (3) to control process variables so that a highly reproducible product can be attained.

Graphite structure. The core graphite structure consists of blocks $8 \times 8 \times 40$ inches, with the fuel channel through the center parallel to the long axis. Upper and lower reflector blocks are $8 \times 8 \times 30$ inches. Each fuel channel comprises six core blocks stacked end to end, with reflector blocks beyond; the fuel length is 20 ft and the over-all length is 25 ft. A pilot in the bottom of each block fits into a hole in the block below to en-

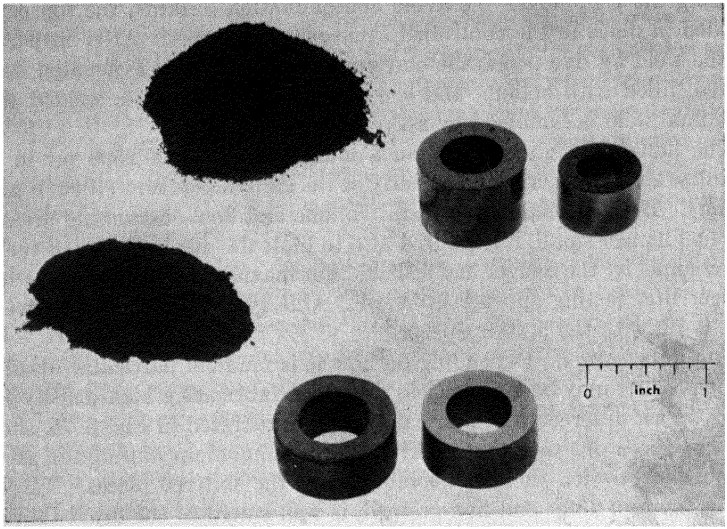

FIG. 6–75 Two types of UO_2 derived from ammonium diuranate and fabricated by same process. Above, fine-grained GCR-2 oxide; below, coarse-grained oxide. [10]

sure alignment of cooling holes. The pile as a whole is stable of its own weight, and there are lateral restraints. There is no provision for the bottom graphite course to move on the steel plate that supports it. Thermal expansion coefficients are about 6×10^{-6}/°F for the steel and about 3.6×10^{-6}/°F for the graphite. With the bottom of the pile normally at 450°F, and the diameter of the pile 420 inches, the relative expansion of the support plate is about 0.4 inch on the diameter, or about 0.008 inch per graphite block. Thus there will be a gap of 0.008 inch between adjacent blocks (at the bottom) when the reactor is hot.

The pile circumference increases 3 inches at the bottom and $4\frac{1}{2}$ inches at the top. Hoops (in tension) surround the reactor at the planes between courses of blocks.

No allowance is made for dimensional changes resulting from irradiation (Wigner growth). It is well known that the change in linear dimensions of graphite, for a given exposure level, depends on the graphite temperature during irradiation. Since the minimum graphite temperature in the reactor, during operation, will be greater than 450°F (230°C) a negligible change in graphite dimensions is expected to occur.

The entire pile will be prevented from moving very far, laterally (as during an earthquake), by a series of horizontal struts projecting outward towards the pressure vessel. These would not normally touch the pressure

vessel, but would limit any lateral displacement to about 1 inch. (Of course any occurrence that could produce such a displacement would require inspection of the whole system.)

Reactor vessel and shielding. The reactor vessel is a spherical pressure shell, 50 ft in diameter, with a 3½-inch wall of type SA 212-B carbon steel plate (Fig. 6–72). It will be designed for an operating pressure of 300 psig at a maximum shell temperature of 650°F. The gross vessel weight (including vessel and graphite supports, thermal barriers, nozzles, and insulation) will be 770 tons.

Since the entire inner surface is swept by the low-temperature gas returning to the reactor, the vessel wall temperature will stay close to a uniform value (450°F) at all power levels. This requires installing a baffle in the outlet gas region to keep the hot gas away from the vessel wall. Outside, the vessel is insulated to reduce heat losses and help equalize temperatures. Junctions between the pressure vessel and outlet pipes carrying hot helium are isolated thermally by means of sleeves and insulation to avoid severe thermal deformations from high-temperature gradients.

The support for the pressure vessel and the reactor is combined. A support skirt, 22 ft in diameter, transmits the reactor loads through the pressure vessel directly to the foundation. Thus, internal components do not produce additional stresses in the shell; the only shell stresses are those from its own weight and internal gas pressure.

Under full-power operating conditions, the temperature of the pressure vessel will be 450°F and that of the helium outlet pipe, 1000°F. This temperature difference can give rise to excessive thermal deformations around the main pipe junctions. The temperature gradients are attenuated by controlling the radial heat flow rate out of the pipe, through the addition of properly graded insulation inside and outside the pipe.

The weight of the reactor assembly (core and reflector) is carried on a platform 35 ft in diameter, supported by a system of radial trusses (Fig. 6–71). Directly under the reactor is a 2-inch-thick floor plate providing the bearing surface for the graphite. This plate has circular holes centered under the fuel channels so the helium coolant can pass up through the floor. The plate itself bears directly on a parallel array of 10-inch Junior beams placed on approximately 2-ft centers. The beams rest upon the radial trusses. The complete system of trusses is supported on the 22-ft circle that transmits the reactor weight to the pressure vessel support skirt.

A somewhat unconventional feature of the shield design is the use of a boron curtain around the outside of the graphite reflector. The curtain absorbs a high percentage of the thermal neutrons escaping from the graphite so that they will not be absorbed in the pressure vessel. This ar-

rangement reduces radiation damage and activation in the pressure vessel, and also reduces the heat generation in both the pressure vessel and the surrounding concrete shield. Further, it reduces the required thickness of concrete and simplifies the problems of shielding around the penetrations for gas ducts and for fuel loading and control rod drive equipment. The shield, of 1/2-inch borosilicate glass sheets, is supported by a wrought steel structure.

The biological shield of reinforced concrete (145 lb/ft^3) is octagonal, with flat slabs above and below the reactor (see Figs. 6–71 and 6–72). It is 9 ft thick, 67 ft high and 76 ft across the flats, the upper concrete slab is pierced by 69 fuel charge tubes, each tube to permit entrance for servicing 25 fuel channels. Four of the eight shield faces are double-walled to accommodate the coolant ducts, as illustrated in Fig 6–72; this arrangement reduces neutron streaming beyond the shield.

The concrete enclosures around the reactor and the pipes will be cooled and ventilated by air from 32,000-cfm exhaust blowers A filter bank before the blowers prevents venting any solid contaminating material to the atmosphere. The air inlet to each external duct is filtered and an inlet register balances the system air flow Air flow is directed into the reactor enclosure, which is held at a negative pressure. Air also flows into the reactor enclosure from the hot and cold helium pipe enclosures and through the annular spaces around the fuel loading channels and control rods in the upper shield

Gas system. Helium is chosen over carbon dioxide as the coolant gas because of its lower pumping power requirement for given power output and temperature conditions, and because it is possible that carbon dioxide and graphite may react at the coolant outlet temperature (Section 6–2).

For a given exit gas temperature, the mass flow of coolant required to remove a fixed quantity of heat is reduced as the inlet temperature is lowered. In addition, the mean gas density in the system is increased. Both effects decrease the flow velocity of the coolant and decrease the pumping power requirement. A value of 450°F for gas inlet temperature was chosen on the basis of steam generator costs and thermodynamic cycle efficiency. The pumping-power requirement also varies with the pressure of the gas in the system for a given set of gas temperatures. With system configuration, power level, and coolant temperatures fixed, the required mass flow of coolant is defined, but the volumetric flow, and consequently the pumping power, will be reduced if the system pressure is increased. For this design, with size, and hence cost, determined principally by nuclear requirements, the coolant pressure level should be as high as pressure vessel technology will permit, and the fuel capsule-surface temperature should be as high as the capsule material will allow.

The primary coolant is circulated through the four steam generator circuits by as many turbine blowers. The steady-state operating point for each blower, as determined by cooling requirements for the reactor core and pressure shell and the calculated system resistances, is 243 lb helium/sec at a head of 10,000 ft-lb/lb At a mean system pressure of 300 psia and blower inlet temperature of 450°F the suction volume of each blower will be approximately 122,000 cfm. Either a single centrifugal stage or two axial flow stages can meet these requirements with a design speed of 3600 rpm and ~6000 motor horsepower.

The gas piping system comprises four parallel circuits connecting the blowers, reactor vessel, and steam generators Each circuit has a bypass line from the blower to the steam generator, with a bypass control valve, and a valve in the line between the blower and the reactor. The system was laid out in one plane to minimize stress problems, with two right-angle bends in each pipe circuit, just inside the shield, to prevent streaming of radiation through the pipes.

Immediately inside the reactor pressure shell the inlet coolant stream is split into two parts (see Fig 6–72) The major part flows downward between the graphite and the pressure shell, cooling the latter regeneratively and finally entering the bottom of the core-cooling channels. It is not practical to provide regenerative cooling of the upper part of the pressure shell in the region of the penetrations for fuel loading and coolant outlet pipes, but it is desired to keep the material temperature below 650°F These parts are cooled by passing a stream of helium at inlet temperature between the pressure shell and the inner shell This secondary coolant stream (approximately 3% of the total coolant flow) removes heat generated in the pressure shell by radiation and provides a temperature buffer between the pressure shell and the reactor discharge temperature The secondary stream is finally mixed with the main stream through controlled leaks around the fuel loading tubes and the gas inlet pipes

The large pipe sizes required for the system result in fabrication problems more nearly akin to pressure vessel fabrication than to ordinary piping systems. It has been decided that piping fabrication required should adhere as closely as possible to the ASME Unfired Pressure Vessel Code where it is applicable. Piping subassemblies are small enough that they could be fabricated in off-site shops and shipped to the site for installation. These pieces could be stress relieved, pretested, and cleaned before shipment. All major subassemblies, as well as the final assembly, must be leak-tested. Pipe stresses will be relieved on site by electrical-resistance heater methods.

Gas flow is controlled by butterfly valves because, in the large size required, they can be designed for flow control without heavy body struc-

tures. To prevent stem leakage, a bellows-sealed stem actuates the butterfly through a linkage arrangement. Such a valve has been built in sizes up to 24 inches for gaseous-diffusion plants* and appears practical in larger sizes for this application. The valves for the helium system are in the 450°F piping and can, therefore, be fabricated from low-alloy steel.

Hinge-type expansion joints are most reliable in this application. In a system using such joints the bellows serve only as flexible sealing members at the pivot points; they are prevented from assuming system loads. Backup rings prevent bellows collapse under pressure, distribute the flexural deformation equally between corrugations, and serve as stops to limit hinge rotation.

Using helium as coolant emphasizes the problem of achieving an acceptably low leakage rate from the system. Pessimistically, it can be assumed that the losses might amount to 1% of the system volume per day; this would amount to an annual leakage loss of 3.65 times the helium inventory. As a practical matter, reducing the leakage rate even to 1% per day requires rigid control of fabrication. All joints should be welded, and all flanged connections sealed by metallic O-ring gaskets or by soft solder. Valves have bellows-sealed stems. To avoid losses at the blower shaft the blower and motor are placed inside the 300-psia gas system. Finally, the whole system must be leak-tested, using high-vacuum methods.

For those unfamiliar with high-vacuum fabrication and testing techniques, the AEC gaseous-diffusion plants give an example of the performance that can be expected. In these plants miles of pipe, thousands of tanks and heat exchangers, and tens of thousands of valves were installed and tested to leak rates of 2μ/hr, which, in a volume equivalent to that of the reactor system, represent a leak rate of only 0.03% per day. The additional cost of achieving such leaktightness is not a major factor in the total.

Fuel handling. Fuel is introduced into (and removed from) the reactor fuel channels by remotely operated equipment. This will be done from the top face of the core, so as not to interfere with the support structure for the pressure vessel. Since only about 10% of the fuel elements need to be replaced each year, fuel replacements will be made during annual shutdowns for inspection and maintenance of plant equipment.

The 1597 fuel channels must be loaded initially with fuel elements, and thereafter any element must be replaceable. Once the reactor has operated at power, it cannot be approached nearer than the fuel loading floor, which is separated from the pressure vessel by the 9-ft thick concrete biological shield. From this floor, the fuel must be handled by a remotely-operated mechanical system. There must be access openings through the

*USAEC gaseous-diffusion plants at Oak Ridge, Paducah, and Portsmouth.

concrete shield into the pressure vessel above the top face of the graphite, preferably (from the fuel handling point of view), a charge tube directly above each of the 1597 fuel channels. Since this is not feasible, the top face of the graphite is divided into square groups of 25 fuel channels, and a device called the "charging chute" gives access to each 25-channel group.

The charging chute, a long pipe, is inserted through the charge tube after the reactor has been shut down and brought to approximately atmospheric pressure (see Fig. 6–72). The bottom end of the chute registers in the central hole of any 25-hole group. Each of the 24 eccentric fuel channels lies on one of five circles around the central channel. Access to these eccentric channels is by means of an extension located at the bottom end of the chute, supported by a system of arms which position the chute extension radially.

Fuel elements are handled through the chutes by separate charging and discharging machines. These two machines are identical except that heavy lead shielding is used on the discharge machine only. Each machine, essentially a crane system, moves over the fuel loading floor. From a chamber containing a fuel assembly rack, a winch and cable system lowers a grab device through the charging chute and into the fuel channel. Solenoids control grabbing or releasing a fuel assembly, and rotate it to engage the hanger slot in the channel.

Since refueling operations include transferring fuel elements from one reactor location to another, the shielded discharge machine can transfer fuel elements between channels. In a power station, refueling must be carried out in a reasonable time. An annual refueling shutdown would require fuel loading in about 20% of the 1597 fuel channels. One charging and one discharging machine and five charging chutes, in 24-hr service could complete the operation in about two weeks.

6–4.6 Comparison of gas-cooled graphite-moderated reactor designs. Some characteristics of the designs that have been discussed are compared in Table 6–33. Estimated plant construction costs and power costs for the three large-scale reactors are compared in Table 6–34. These two tables illustrate some of the important differences between the natural uranium and enriched uranium reactors of the graphite-moderated, gas-cooled type. The natural uranium reactors are considerably larger for a given power capacity and their capital costs are consequently higher. With them, however, fuel costs can be low, even at rather modest fuel exposures. The enriched reactors, on the other hand, have lower capital costs but achieve low fuel cost only if the fuel exposure is quite long. It is fortunate that the uranium oxide fuel element (whose use requires enriched fuel in this reactor) appears capable of long life from the radiation-damage viewpoint.

TABLE 6–33

COMPARISON OF GAS-COOLED POWER REACTOR DESIGNS*

	Kaiser Engineers-ACF				ORNL
	Natural uranium		Partially enriched uranium		
	Prototype	Optimum	Prototype	Optimum	Optimum
Rated thermal output, Mw	180	700	125	600	700
Rated net electric output, Mw	55	220	44	215	225
Net thermal efficiency, %	30.6	31.4	35.3	35.8	32.1
Specific power, Mw metric ton	1.85	2.55	6.9	7.9	5.1
Enrichment, a/o	0.71	0.71	3.0	2.5	2.0
Uranium loading, metric tons	97.5	274	18.0	77	137
U^{235} inventory, kg	692	1,900	540	1,925	2,740
Fuel material	U-metal†	U-metal†	UO_2	UO_2	UO_2
Cladding material	Magnox A-12†	Magnox A-12†	SS 304	SS 304	SS 304
Average fuel exposure, Mwd metric ton	1500–3000†	1500–3000†	10,000	10,000	7350
Refueling scheme, during:	Operation	Operation	Operation	Operation	Shutdown
Core diameter × height, ft	35 × 25	50 × 29	12.2 × 18.5	20 × 26	20 × 30
Number of fuel channels	1532	3536	344	980	1597
Coolant gas	CO_2	CO_2	CO_2	CO_2	He
Coolant pressure, psia	280	275	387	370	300
Coolant outlet temperature, °F	700–800†	750–800†	1000	1000	1000
Coolant inlet temperature, °F	409	413	463	473	450
Number of coolant loops	2	8	2	6	4

Pressure vessel ID × height, ft (or sphere diameter, ft)	36 × 65	70	18 × 26	27 × 57	50
‡H.P. steam pressure, psia	1450	1450	2400	2400	950
H.P. steam temperature, °F	750	750	950	950	950
‡L.P. steam pressure, psia	300	300	750	750	(single pressure cycle)
L.P. steam temperature, °F	750	750	950	950	

*"Technical Aspects of the Report on the Gas-Cooled, Graphite-Moderated Reactor," Hearing before the Subcommittee on Legislation of the Joint Committee on Atomic Energy Congress of the United States, April 22, 1958 Government Printing Office, Washington, D C.

†Single-region U metal-Magnox rod cores limited to 1500 Mwd ton at 800°F or 750°F at 3000 Mwd ton. Alternate two-region core also proposed: natural U in UO_2 with stainless steel cladding for inner region and U metal with Magnox A-12 cladding for outer region to permit 3000 Mwd ton at 800°F.

‡H.P. = high pressure, L.P. = low pressure.

TABLE 6–34

RECONCILED GAS-COOLED POWER REACTOR COST ESTIMATES*

	Kaiser Engineers-ACF		ORNL
	Optimum, natural uranium	Optimum, enriched uranium	Optimum, enriched uranium
Plant characteristics			
Net electric power, Mw	220	215	225
Fuel exposure, Mwd/metric ton	3000	10,000	7400
Plant construction cost, millions of dollars			
Total direct costs	72	54	48
Ratio of total to direct costs†	1.75	1.75	1.75
Total design and construction costs	126	95	84
Other capital costs‡	15	11	10
Total capital costs	141	106	94
Unit plant cost, $/kw (elec), net	640	490	420
Power generation cost, mills/kwh			
Fixed charges, 14%/year, 80% plant factor	12.8	9.8	8.4
Operation and maintenance	1.2	1.1	1.1
Fuel	2.2	2.5	2.6
Total generation cost	16.2	13.4	12.1

*Reconciled to common basis by provision of equivalent auxiliary facilities and equivalent additive cost factors.

"Technical Aspects of the Report on the Gas-Cooled, Graphite-Moderated Reactor," Hearing before the Subcommittee on Legislation of the Joint Committee on Atomic Energy Congress of the United States, April 22, 1958. Government Printing Office, Washington, D. C.

†Total costs include 15 per cent indirect cost, 15 per cent escalation, 20 per cent contingencies, and 10 per cent engineering and design.

‡Includes interest during construction and working capital.

Reductions in plant size made possible by using enriched fuel are of two kinds. The first kind results from the greater freedom in selecting the fuel-to-moderator ratio, the degree of fuel subdivision, and the fraction of the reactor volume devoted to coolant passages. With this greater design latitude, higher power density is possible for the same material temperatures and pump-power fraction. The second source of higher specific performance results from using materials with higher temperature limits and thus, higher coolant temperatures. Not only efficiency, but also coolant heat transport capabilities are improved, and heat exchange and power generation equipment can be smaller. Future developments in fuel technology may possibly raise temperature limitations in natural uranium reactors. Other limitations on power density with natural uranium, related fundamentally to the nuclear properties of graphite, cannot be raised, although their limits may be approached more closely by refining reactor design. The enriched fuel reactor will probably always have a significant advantage with respect to specific power output, but this advantage must be weighed against the disadvantage of the more complex fuel cycle. The net advantage now seems to lie with the partially enriched reactor.

6–5. The D_2O-Moderated Gas-Cooled Reactor*

6–5.1 Fundamental characteristics of the concept. In the gas-cooled reactor, the basic neutron economy is determined by neutron physics characteristics of the moderator and whatever structural materials must be put into the moderator to contain the coolant and the fuel. The excellent neutron physics characteristics of D_2O make it attractive as a moderator for gas-cooled reactors. Design studies have indicated that good neutron economy can be attained with such reactors in practical designs and that natural uranium can probably be used as fuel without causing an unreasonable reduction of thermal performance.

The program on the D_2O-moderated, gas-cooled reactor type has been sponsored by two groups of utility companies, the East Central Nuclear Group and the Florida West Coast Nuclear Group. Design studies made by the General Nuclear Engineering Corporation under this sponsorship form the basis for a proposal to the United States Atomic Energy Commission for the construction of a 50-Mw electrical prototype of this reactor by the Florida West Coast Nuclear Group, with research and development to be financed by the East Central Nuclear Group and the AEC.

The physical characteristics of the moderator determine requirements of the reactor structure and thus define engineering problems in the design of a gas-cooled reactor, which in turn put further restrictions on neutron

*By J. R. Dietrich and M. F. Valerino, GNEC.

physics characteristics of the reactor. It is instructive to consider briefly the differences between D_2O- and graphite-moderated reactors that arise from the differences in physical properties, as distinguished from those which arise directly from nuclear properties and which give the D_2O moderator basic advantages with respect to reactivity, neutron economy, and power density.

The fundamental difference is that whereas graphite is a high-temperature moderator, D_2O is one whose temperature must be kept low. Although graphite conceivably could be operated at low temperature in a high-temperature gas-cooled reactor, the possibility is hardly a practical one, because of the difficulty of cooling the graphite at low temperatures and because of the greater susceptibility of graphite to radiation damage at low temperatures. Since D_2O is a liquid, the provision of adequate cooling at any desired practical temperature is a relatively simple and straightforward engineering task. A more difficult engineering problem is that of insulating the gas channels from the D_2O to minimize the flow of heat from the gas channels into the D_2O. The avoidance of such heat flow is necessary because the heat which leaks into the moderator cannot be utilized efficiently for the generation of mechanical energy at the low moderator temperature. To the extent that leakage heat is not utilized, or is utilized at low efficiency, the over-all efficiency of the nuclear power plant will suffer. Such a loss of efficiency would be reflected in fuel costs; however, it should not increase the capital cost of the steam generator and turbine equipment, as would a loss of efficiency due to low temperature of the main coolant stream.

The energy spectrum of thermal neutrons in the D_2O-moderated, gas-cooled reactor will be a lower-temperature spectrum than with graphite moderation. This difference has little effect when U^{235} alone is the fuel; it is more important when the fuel contains a significant fraction of plutonium. The fission cross section of Pu^{239} becomes relatively higher with respect to other cross sections as the neutron temperature increases, but the neutron regeneration factor η of Pu^{239} becomes poorer. Consequently, the low neutron temperature is advantageous when plutonium is recycled. However, this may not be so in cases where the short-term reactivity effect of Pu^{239} is the more important one, as in a once-through operation when the plutonium formed in the fuel serves only to extend the lifetime of the original fuel element. In general, for higher neutron temperatures the "plutonium peak" is higher, and so is the exposure at which a particular uranium fuel (at a given conversion ratio) loses a specific amount of reactivity. In comparing graphite and D_2O, the additional reactivity available with the D_2O moderator will usually more than compensate for the effect of neutron temperature on reactivity variation, and longer fuel life is to be expected with D_2O.

Possible types of gas-cooled D_2O reactors. As indicated above, the D_2O-moderated, gas-cooled reactor will consist of a tank of D_2O penetrated by channels which contain fuel elements, and through which the gas coolant flows. The channels are insulated from the surrounding moderator. The gas coolant must be at high pressure for reasonable power densities to be attained. A pressure vessel can enclose the whole reactor, or the fuel coolant tubes can be made strong enough to contain the pressurized gas, with the moderator left unpressurized. The pressurized-tube concept does not seem readily applicable to a high-temperature, graphite-moderated reactor.

With the D_2O moderator, both the pressure vessel and the pressure tube systems have advantages. Using the pressure vessel minimizes parasitic absorption of neutrons by structural material, and can probably be designed to give maximum specific power for a given fuel enrichment. However, the pressure vessel size must be quite large, for both neutron economy and high power output. With gas cooling, the diameter of the D_2O vessel must be about 15 ft or more so neutron leakage will be low, and a still larger vessel would be needed for a reactor of high power output.

The pressure-tube reactor has a number of advantages, chief of which is that it has no size limit. A related advantage is that once the design for a relatively large reactor has been established, a change to some other size requires minimum engineering effort, and probably no research or development. Other advantages are flexibility of fuel repositioning and reloading, ease of detecting and isolating failed fuel elements, and absence of a large reservoir of stored mechanical energy in a single container of pressurized gas. This reactor type is now being studied in the United States.

Effect of pressure tube on reactor physics. Pressure tubes in the D_2O moderator absorb additional neutrons. The combination (D_2O plus pressure tube) can be regarded as a composite moderator whose macroscopic cross section includes the absorption of both D_2O and pressure tubes.

If the pressure tube has a wall thickness t, a radius R (assumed large with respect to t, so that we need not specify inner and outer radius), a length L, and is composed of a material having a macroscopic cross section Σ_a cm^{-1}, then the total absorption cross section, Σ_p cm^2, of the tube is given by:

$$\Sigma_p = 2\pi RLt\,\Sigma_a.$$

If the gas coolant, in flowing through the tube, experiences a temperature rise ΔT and leaves the tube at a velocity V and a density ρ, the total power P removed by the gas per pressure tube is given by

$$P = A\rho V c_p \Delta T,$$

where c_p is the heat capacity of the gas at constant pressure over the tem-

perature range of ΔT and A is the cross-sectional area for gas flow per pressure tube.

The pressure tube will contain thermal insulation, whose neutron absorption is here assumed small compared with that of the pressure tube, and the fuel elements plus their jackets, fins, end fittings, and perhaps other fuel structures. The neutron absorption of the fuel element materials is assigned here to the fuel element rather than to the moderator. The volume occupied by the fuel, the thermal insulation, and the fuel-element materials does represent a loss of flow area for the gaseous coolant. If it is assumed that, after these losses have been subtracted, a fraction α of the internal cross-sectional area of the tube remains for gas flow, then the flow area A is given by

$$A = \alpha \pi R^2.$$

Furthermore, for a given gas at a given temperature, the density is very nearly proportionate to the pressure p : $\rho = \beta p$, where β is a characteristic constant of the gas at a given temperature. The required thickness t of the pressure tube is related to the gas pressure, the tube radius, and the design stress s of the tube wall by the equation

$$t = \frac{Rp}{s}.$$

Applying these relations and taking the ratio of total absorption cross section (cm^{-1}) per tube to total power output per tube, we find

$$\frac{\Sigma_p}{P} = \frac{2L\Sigma_a}{\alpha\beta V s c_p \Delta T}.$$

If $\Sigma_{a,\mathrm{mod}}$ is used to designate the macroscopic absorption cross section of the "moderator," where the "moderator" is considered to be a mixture of D_2O and pressure tubes, this cross section can be expressed by

$$\Sigma_{a,\mathrm{mod}} = \Sigma_{a,D_2O} + D\left[\frac{2L\Sigma_a}{\alpha\beta V s c_p \Delta T}\right],$$

where D is the power density per cubic centimeter of D_2O or, more precisely, the total power output of the reactor divided by the total volume of D_2O in the reactor core. A similar equation can be written in terms of the specific power S_{D_2O}, with respect to the moderator: i.e., the number of megawatts of heat power generated per ton (2000 lb) of D_2O in the core:

$$\Sigma_{a,\mathrm{mod}} = \Sigma_{a,D_2O} + CS_{D_2O}\left[\frac{2L\Sigma_a}{\alpha\beta V s c_p \Delta T}\right],$$

where C is an appropriate constant.

In designing the reactor, the designer will (1) choose for the pressure tubes the material having the lowest ratio of absorption cross section to permissible design stress, (2) choose ΔT as high as possible, with the gas inlet temperature the lowest economically useful for power generation and the outlet temperature limited by the materials used, and (3) probably accept whatever gas is compatible with the materials at the desired temperatures, thus fixing c_p. The maximum usable velocity will be determined by pressure drop considerations, and will be fixed within fairly narrow limits by the choice of coolant gas. Clearly, from the standpoint of neutron absorption, pressure loss, and specific power, the shortest possible tube is desirable. Therefore, it may be worth while to shorten the reactor until axial leakage of neutrons begins to be quite important, to reduce the loss of neutrons by absorption in the pressure tube for a given specific power.

If carbon dioxide is the coolant gas, an exit velocity of approximately 100 fps is about maximum because of pressure drop. For reasonable gas pressures α is in the range about 0.5. (Note that in the expression for moderator absorption the gas pressure enters only insofar as it influences α.) As pressure is increased, the ratio of fuel volume per tube to flow area per tube will also increase, and for this reason α will tend to decrease. Further, the thickness of insulation required is independent of the tube diameter; therefore, a decrease in tube diameter (increase in pressure) will again tend to decrease α. However, if there is appreciable neutron absorption by the thermal insulation, higher pressures will tend to decrease the ratio of absorption to power output. Furthermore, if the pressure used is too low, the neutron loss by leakage becomes important. The net effect is that there will be an optimum value for the coolant pressure, but it is not sharply defined, particularly if the problem of providing adequate heat-transfer surface is ignored. After taking this and other practical considerations into account, it appears that the desirable coolant pressure may be about 500 psi, but the value is not critical so long as the amount of heat-transfer surface per unit volume of coolant passage can be varied.

With carbon dioxide as the chosen coolant, an exit velocity of 100 fps is assumed. If L is taken as 18 ft, α as 0.5, the inlet temperature as 400°F, and the exit temperature as 1000°F, and if the pressure tube is assumed to be Zircaloy-2 with a design stress of 10,000 psi, then the expression for the moderator absorption cross section becomes

$$\bar{\Sigma}_{a,\text{mod}} = \bar{\Sigma}_{a,D_2O} + (1.49 \times 10^{-5}) S_{D_2O},$$

where the notation $\bar{\Sigma}$ signifies that the cross section has been averaged over a Maxwellian neutron energy distribution (at 100°C). The specific power in the equation approximates that which would be characteristic of the pressure tube of highest power output in the reactor; it is therefore higher

by perhaps 20 to 50% than the average specific power in the core. Also, the procedure of "homogenizing" the D_2O and the pressure tubes gives a somewhat pessimistic value for the effective cross section of the "moderator," since the disadvantage factor for the actual tubes will be lower than that for a uniform mixture. On the other hand, no allowance has been made in $\Sigma_{a,\text{mod}}$ for any absorption by thermal insulation or structures associated with the insulation.

A reasonable target value for the specific power in the above equation is probably about 15 Mw (thermal) per ton of D_2O. This would correspond to an average specific power in the core of at least 10 Mw/t, and a specific power relative to the entire D_2O inventory of well over 5 Mw/t. For this case, $\Sigma_{a,\text{mod}}$ would amount to 3.1×10^{-4} cm^{-1}. The moderating ratio $\xi\Sigma_s/\bar{\Sigma}_a$ for this mixture of D_2O and pressure tubes, at 100°C, would be 1760, as compared with 238 for graphite.* Therefore the nuclear properties of a pressure tube D_2O-moderated reactor should be significantly better than those of a pressure vessel graphite-moderated reactor.

Possible fuel elements. As in the case of the graphite-moderated gas-cooled reactor, the possible performance of a D_2O-moderated, gas-cooled reactor depends very strongly on the fuel elements available The somewhat better nuclear performance of the D_2O reactor, however, affects the relative importance of the prospective fuel element types. Some types of fuel elements that appear to have good prospects are discussed below.

(1) Uranium metal with magnesium or aluminum jackets. The D_2O-moderated reactor has a comfortable margin of reactivity when fueled with metal elements with low cross-section jackets. This extra reactivity can be used to attain high power density through flux flattening, undermoderating the reactor, or shortening it to improve conditions for gas heat transport. Or it can be used to give quite long fuel life with natural uranium, if metal uranium elements can be developed to withstand the radiation damage. The limitation of these fuel elements is the maximum gas temperature. which is probably between 700 and 800°F, considerably lower than that desired for an efficient power cycle.

(2) Uranium oxide with beryllium jacket. This element has not yet been developed, but it is probable that the incentive for its development as a fuel element for D_2O reactors is considerably greater than that for its development as an element in graphite-moderated reactors. The indications are that with such an element the D_2O reactor would achieve quite attractive performance and that, if plutonium recycle were used with such elements, the equivalent enrichments attainable by the addition of the re-

*σ_a (2200 m/sec) is taken as 4.0 mb.

cycled plutonium to natural uranium would be sufficiently high to approach optimum thermal performance.

(3) Uranium oxide with steel jacket. There is little probability that operation with natural uranium can be achieved in a pressure tube D_2O reactor fueled with steel-jacketed fuel elements. However, natural uranium feed with plutonium recycled would probably be feasible in such a system. Steel-jacketed enriched UO_2 elements are now considered as an interim possibility whose technical feasibility is in little doubt, and as a possible economically attractive method of utilizing plutonium recycle.

6–5.2 Design concept. One advantage of the pressure tube reactor is that the design of the reactor structure and that of the fuel element are relatively independent, except insofar as the performance of the fuel element determines the temperature conditions for parts of the reactor structure. Consequently, a reactor structure can be designed that will in principle, and probably in practice, accommodate a variety of possible fuel element types. This lack of restriction on the fuel-element design makes it feasible to take advantage of any advances in fuel-element design that may be achieved during the life of the reactor

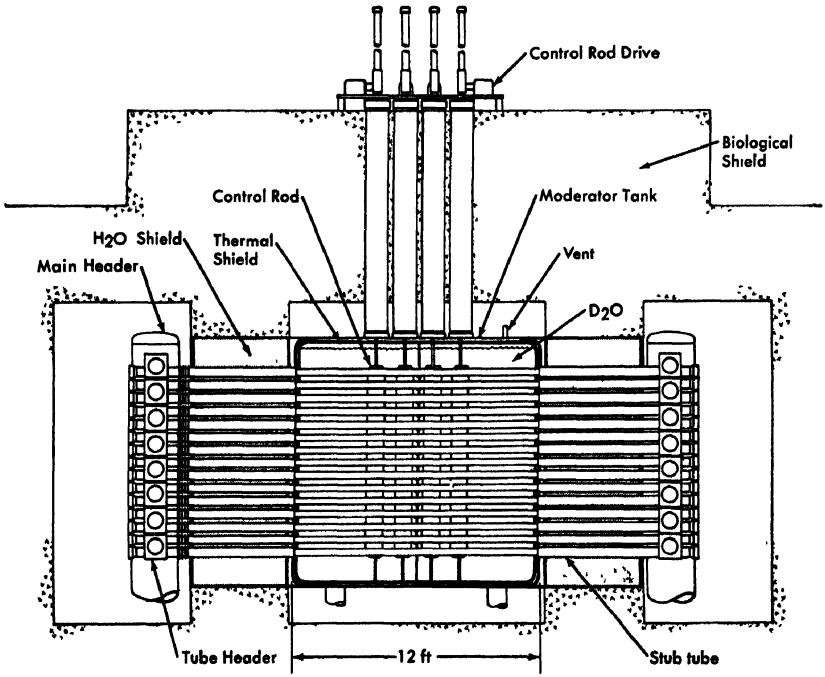

FIG. 6–76. Schematic longitudinal cross section of D_2O-moderated, gas-cooled reactor prototype (GNEC)

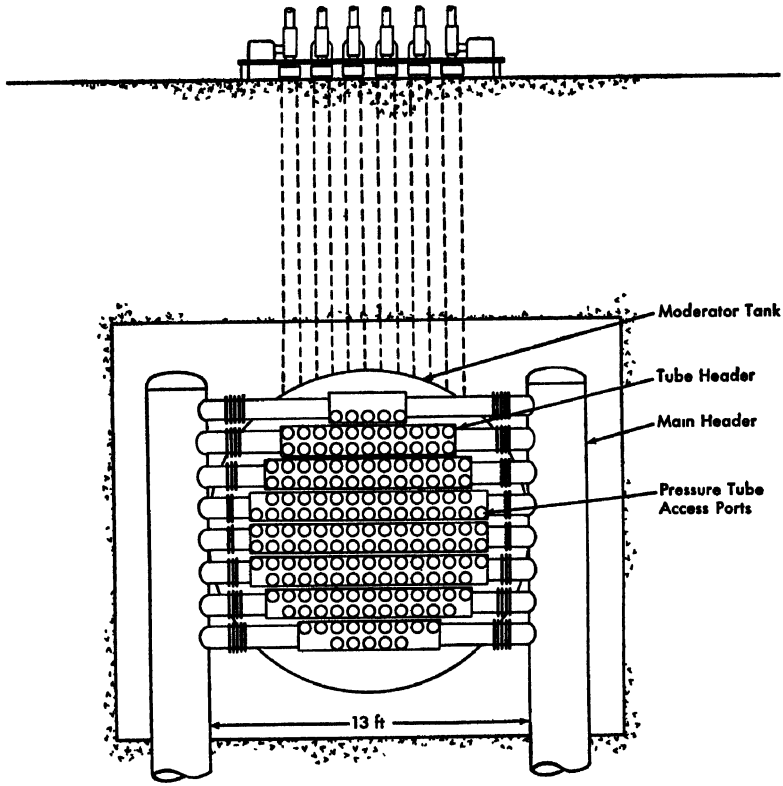

FIG. 6–77. End view of D_2O-moderated, gas-cooled reactor prototype. (GNEC)

The reactor design being developed by General Nuclear Engineering Corporation for the ECNG-FWCNG is shown schematically in Figs. 6–76 and 6–77. The prototype reactor of 50 Mw (electrical) output is shown, but the same design principles would apply for a larger reactor. It is the objective in this design to make pressure tube replacement a practical operation, and avoid any construction that would subject any nonreplaceable parts of the structure to possible damage by a pressure tube failure. Calandria-type construction is therefore avoided. A further objective is to include the thermal insulation inside the pressure tube so the pressure tube wall can operate at low temperature in contact with the D_2O.

Figure 6–76 is a longitudinal cross section in a vertical plane. The moderator is in a steel tank that has a stub tube at each end for each of the zirconium pressure tubes Each pressure tube extends completely through its two stub tubes and makes a watertight, gastight seal with the coolant header tube at each end, as shown in Fig. 6–78. Each stub tube, in turn, is joined at its outer end to a header tube, with a bellows at one

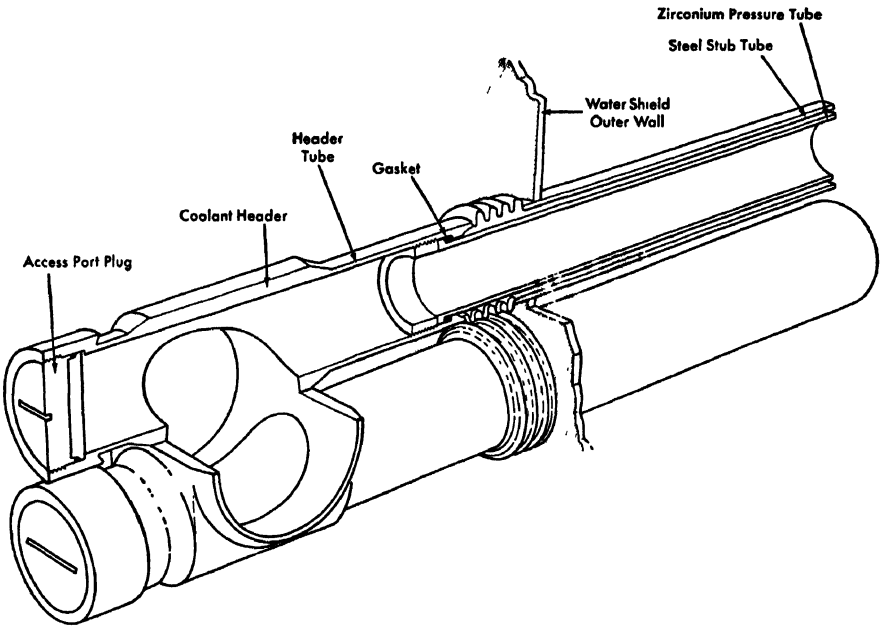

FIG. 6–78. Detail of pressure tube end connection and header (GNEC)

end to accommodate thermal expansion. The stub tubes thus form sleeves around the ends of the pressure tubes; the annulus between the stub tube and the pressure tube contains D_2O. From the end view of the reactor (Fig. 6–77) it is evident that the horizontal rows of pressure tubes feed in pairs into horizontal headers, which, in turn, are connected to the two vertical main headers. The control rods, flat absorbing slabs, operate vertically in the spaces between vertical rows of pressure tubes.

There is an iron-water shield at each end of the reactor tank, thick enough to permit access to the headers when the reactor is shut down. Then, the headers, fuel-handling equipment, and associated items in the space between the iron-water shield and the biological shield can be maintained by direct methods. The iron-water shield is penetrated by the stub tubes and the coaxial pressure tubes (see Fig. 6–78). The connections between the pressure tubes and the header tubes are made outside this shield wall. Therefore, a pressure tube can be replaced by direct maintenance procedures during shutdown.

Fuel is loaded and unloaded through access ports (Fig. 6–78) in the space between the biological shield and the iron-water shield. A loading-unloading machine connects onto the access port by means of a gripper, and seals the port against loss of coolant gas after the plug has been removed. Loading-unloading machines at each end of the reactor provide

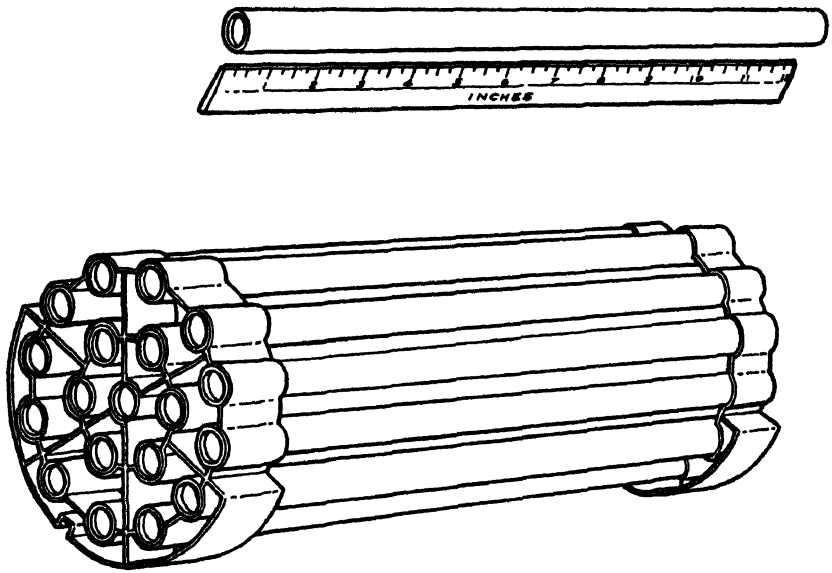

FIG 6–79 Fuel-element bundle steel-jacketed prototype (GNEC)

maximum versatility in the scheduling of fuel loading and reloading The machines are controlled remotely from outside the biological shield during reactor operation

The pressure tubes, made of zirconium or Zircaloy, have high-temperature insulating liners. Research and development on the pressure tubes and insulation are now under way Although there is no doubt as to the technical feasibility of zirconium or Zircaloy pressure tubes, experiments are needed to design tubes with minimum wall thickness for a given pressure, to study tube failures, to evaluate radiation effects, and to develop and test seals and gaskets. Developing the insulating liner involves minimizing neutron absorption as well as providing an adequate barrier to heat flow.

The fuel element to receive the major development effort for this reactor will be enriched uranium oxide jacketed with beryllium. Since the feasibility of this element has not been proven, design of the prototype reactor is proceeding on the assumption that steel-jacketed UO_2 elements will be used for initial loading if necessary. A fuel element bundle of the latter type is shown in Fig. 6–79. The 19 cylindrical elements are assembled into the bundle by brazing to an end structure made of thin sheet steel. Twelve bundles would be contained in each pressure tube. The bundle is supported by its end structure, which rides on the insulating

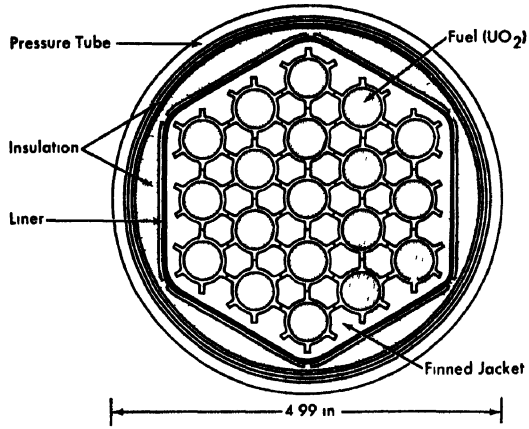

FIG. 6–80. Pressure tube and fuel arrangements for UO_2 fuel elements. (GNEC)

liner of the tube. For this design, the insulating liner has a continuous full-length key that engages the slot at the bottom of each fuel element end structure for alignment. Carbon dioxide has been chosen as coolant, at a pressure of 520 psia, for the reference design. This choice may be reconsidered with respect to compatibility as research and development proceeds.

6–5.3 Performance of prototype. The prototype reactor, because of its small size and high neutron leakage, cannot operate with natural uranium fuel However, as it is to be the forerunner of large reactors that can be designed to operate on natural uranium, high neutron economy is an important design objective The preferred fuel element for the prototype is therefore a uranium oxide fuel element with a finned beryllium jacket. The pressure tube will contain clusters of 19 such elements (Fig 6–80). For purposes of performance calculations, the Zircaloy pressure tube is assumed to have a wall thickness of 0.125 inch. The insulation is assumed to be low-density magnesium oxide, with an inner liner of beryllium metal, 0.031 inch thick. The fuel elements, made up of cylindrical pellets of UO_2, 1/2 inch in diameter, are jacketed in 0.040-inch-thick beryllium, with longitudinal beryllium fins of the same thickness

The estimated performance of the prototype reactor with the beryllium jacketed fuel elements is summarized in Table 6–35. The enrichment for a fuel life of 10,000 Mwd/t with segmental fuel reloading is calculated to be 1.2% U^{235}. Also shown in Table 6–35 is the calculated performance of the same reactor with steel-jacketed UO_2 fuel elements. The jackets are of type-304 stainless steel, 0.015 inch thick. They are not finned, and

TABLE 6-35

PERFORMANCE OF BERYLLIUM-JACKETED AND STEEL-JACKETED FUEL ELEMENTS IN PROTOTYPE REACTOR

	Be-jacketed	Steel-jacketed
Moderator tank diameter, ft	13	13
Moderator tank length, ft	12	12
Effective diameter of core, ft	10	10
Core length, ft	12	12
Lattice type	Square	Square
Lattice spacing, in.	8	8
Number of pressure tubes	177	177
Number of fuel tubes per bundle	19	19
Diameter of fuel pellets, in.	0.50	0.50
Fuel material	UO_2	UO_2
Enrichment, % U^{235}	1.2	1.8
Conversion ratio	0.69	0.55
Coolant	CO_2	CO_2
Coolant pressure, psia	520	520
Coolant entrance temperature, °F	350	350
Coolant exit temperature, °F	1070	1020
Maximum jacket surface temperature, °F	1200	1400
Average coolant velocity in un-orificed pressure tube, fps	120	160
Total heat output rate, Mw	173	229
Fuel loading, tons UO_2	17.3	17.3
D_2O in tank, tons	46.2	46.2
Specific power, thermal Mw/ton UO_2	10.0	13.2
Specific power, thermal Mw/ton D_2O	3.75	4.96
Electrical power for circulating blowers, Mw	4.3	5.7
Net electric output, Mw	53	70
Net efficiency, %	30.5	30.5

therefore must operate with higher surface temperatures. However, eliminating the fins increases the available coolant flow area and reduces the friction pressure loss, so that coolant flow rate and total power output are higher. The design power of the reactor is 50 Mw electrical, but the higher power attainable with the steel jacketed elements is presented in the table to illustrate the characteristics of such elements. For a fuel life of 10,000 Mwd/t the required fuel enrichment with the steel jacketed elements is 1.8% U^{235}.

6–5.4 Performance of large reactor. It is quite important to determine whether reasonably good thermal performance and fuel lifetime can be attained with a large D_2O-moderated, gas-cooled reactor using natural UO_2 as fuel. Successful results depend strongly on developing fuel jackets, pressure tubes, and insulating liners of low neutron absorption cross section. As an interim estimate, a set of performance calculations was made, using what appeared (on the basis of present knowledge) to be reasonable constructions for the pressure tube, insulating liner, and fuel elements. The reactor physics calculation methods were checked against the best available experimental data on UO_2 lattices. The assumptions and reactor physics calculations are discussed here briefly.

The pressure tube and fuel element arrangement was consistent with the following heat-removal specifications. The carbon dioxide pressure is 520 psia, the inlet gas temperature 350°F, and the outlet temperature 1050°F. The maximum temperature of the beryllium jacket surface is set at 1200°F, and the heat-removal rate per average pressure tube in the reactor at 1 2 Mw. The reactor core is assumed to be 18 ft long and 20 ft in diameter. No reflector is used in the axial direction but a 1-ft circumferential D_2O reflector (or equivalent graphite reflector) is assumed The over-all ratio of maximum to average power density in the core is assumed to be 2.5, and the axial power density is assumed to vary as a cosine function. For an estimated over-all cycle efficiency of 30% the pumping power, including the effect of estimated pressure losses in the circuits outside the reactor, is approximately 9% of the net electric output.

The fuel and pressure tube arrangement calculated to satisfy the above requirements is as follows:

(1) Pressure tube. Zircaloy-2, 5.3-inch outside diameter, and 0.120-inch wall thickness based on a design stress of 12,500 psi at an assumed tube wall operation temperature of 140°C

(2) Fuel. 0.50-inch diameter, UO_2 rods of 10.4 g/cm^3 density, arranged as a 19-rod cluster in a pressure tube, with a center-to-center spacing of 0.83 inch in the cluster.

(3) Fuel cladding. 0.04-inch-thick beryllium

(4) Fins. Longitudinal beryllium fins on each fuel rod in the cluster; six fins per rod; fin dimensions: 0.04 inch thick, 0.12 inch high.

(5) Liner. 0.025-inch-thick beryllium placed between gas flow space and insulation layers.

(6) Insulation layers. 0.10-inch-thick annulus of ZrO_2 (50% porosity), 0.10-inch-thick annulus of MgO, plus stagnant gas gaps.

Reactivity calculations were made for several lattice pitches of the pressure tubes in D_2O moderator. The moderator purity was taken as 99.75% D_2O. The calculation methods used for determining cold-clean k_∞ for the clumped UO_2 rod lattices were compared with existing experimental data.

Two sources of experimental data were available. Reference 164 presents material buckling measurements based on critical D_2O height data, and Reference 165 presents k_∞ measurements obtained by a null reactivity coefficient method. The cold-clean values of k_∞ as calculated and as given in Reference 1 were compared for the 19-rod cluster assemblies; agreement within $\pm 0.2\%$ was obtained. Comparison with the data of Reference 2 for both the dry and wet lattices (space within rod cluster either was void or contained D_2O) was not nearly as good. The calculated cold-clean k_∞ values for the four assemblies compared were from 0.3 to 1.1% higher than those indicated by the measurements. The discrepancies in the comparative results for the two different sets of data have not been explained. To give equal weight to the two sets of data obtained by different experimental approaches, the values of cold-clean k_∞ presented here are those given by the calculation method, arbitrarily reduced by 0.5%. Thus the cold-clean k_∞ values presented herein do not vary more than $\pm 0.7\%$ from the experimental data of either Reference 164 or 165.

The initial hot-operating k_∞ value is obtained by accounting for (1) the increased temperature (and reduced density) of the D_2O moderator during operation (taken as 100°C), (2) the equilibrium Xe^{135} and Sm^{149} poisoning, and (3) the Doppler broadening of the U^{238} resonances. The equilibrium Xe^{135} and Sm^{149} poisoning are based on the average specific power of 9 Mw per ton of uranium in the UO_2, which was indicated by the heat-transfer calculations. The total effective fractional yield for Xe^{135} was taken as 0.064 and for Sm^{149} as 0.016; the reactivity required for equilibrium Xe^{135} and Sm^{149} poisoning is 3.4%. The Doppler coefficient of the U^{238} resonance integral was taken to be 1.6×10^{-4}/°C assigned to the volume absorption term of the resonance integral, which was taken as 10.5 barns for UO_2. Large uncertainties exist in the value of the Doppler coefficient. Because the Doppler effect is important at the high fuel temperatures employed with UO_2 fuel, calculations were also made with the Doppler coefficient taken as 1.2×10^{-4}/°C. This latter value is more representative of the average of experimental values. The mean fuel temperature corresponding to a given power density is calculated as a volume-weighted average over the fuel rod cross section. The Doppler effect was based on the mean fuel temperatures at the average power density of the reactor; a correction was applied, using perturbation theory, for the variation in mean fuel temperature over the reactor core volume. The reactivity loss due to change in resonance escape probability from the cold-clean to hot-operating condition amounts to 3.6% for an 8-inch lattice pitch and 1.9% for a 10-inch pitch (Doppler $\simeq 1.6 \times 10^{-4}$/°C). The bulk of the effect is from the Doppler broadening associated with the high effective temperature of the fuel ($\sim$1300°C). There is a small contribution due to the decrease in moderating power of the D_2O associated with the slightly-

lowered D_2O density. The decrease in η of the fuel with increase in moderator temperature results in a 0.5% reduction in k.

The slowing-down area of the lattice is calculated by applying corrections to the slowing-down area in the D_2O to account for (1) the presence of the pressure tube and materials in the pressure tube, and (2) the effect of voids represented by the gas flow and stagnant gas insulating spaces. The void correction is made by using Behren's results [162]. The thermal diffusion area is obtained from the flux- and volume-weighted absorption and transport cross sections of the materials in a lattice cell and is corrected for voids by use of Behren's results.

The physics calculation results are presented in Table 6–36 for the 8-inch, 9-inch, and 10-inch lattice pitches. Even for the large reactor size chosen, neutron leakage is significant, contributing about 6% loss in reactivity. The large migration area of the lattice is due principally to the large effect of voids at the close lattice spacing and to the large thermal diffusion area characteristic of dilute lattices at wide spacing. For the 9-inch lattice spacing, the total loss in reactivity in going from the cold-clean to the hot-operating condition includes 3.4% for equilibrium Xe^{135} and Sm^{149} poisoning, 2.5% for Doppler effect and change in D_2O slowing-down power, and approximately 0.7% due to change in η of the fuel. The possible precision assigned to the k_{eff} values is $\pm 1.2\%$, estimated as follows: (1) $\pm 0.7\%$ for prediction of k_∞ (cold-clean) as previously discussed, (2) a possible overestimation of the reactivity loss due to the Doppler effect by approximately 0.4% (roughly equivalent to the difference in Doppler coefficient between 1.6×10^{-4} and 1.2×10^{-4}/°C), and (3) a possible underestimation of the migration area by approximately 10% due to unaccounted-for neutron-streaming corrections and corresponding to approximately 0.4% reactivity. Actually, in the migration area calculations some conservatism was used in applying Behren's results to allow for possible additional streaming effects.

For the 9-inch lattice, the calculations give $k_{eff} = 1.00$, with the possibility that it may be as high as 1 012 or as low as 0.988. For the 10-inch lattice the calculations give $k_{eff} = 1.025$, with possible limits of 1.037 and 1.013. These margins of uncertainty are large in terms of attainable fuel exposures; however they can only be reduced by experimental measurements.

The specific power and estimated attainable fuel exposure for the given size reactor are presented in Table 6–37 for the different lattice pitches. As previously mentioned, heat-transfer calculations indicate a heat output of 1.2 Mw for the average pressure tube (based on a maximum to average power density of 2.5) and an average specific power of 9 Mw/t U. For constant reactor size, the power output varies with lattice pitch, as shown in Table 6–37. The specific power in Mw/t D_2O decreases rapidly with

TABLE 6-36

RESULTS OF LATTICE CALCULATIONS FOR NATURAL UO_2-FUELED, GAS-COOLED, D_2O-MODERATED POWER REACTOR

Core: 18 feet length × 20 feet diameter
Reflector: one-foot D_2O or equivalent graphite radial reflector; no axial reflector

Lattice pitch, in.	8	9	10
Volume D_2O/equivalent U volume	22.9	32.2	42.6
Lattice constants, cold-clean:			
η	1.330	1.330	1.330
ϵ	1.015	1.015	1.015
p	0.856	0.895	0.919
f	0.939	0.934	0.929
U^*	0.995	0.995	0.995
k_∞	1.079	1.122	1.146
Lattice constants, hot-operating:			
η	1.321	1.321	1.321
ϵ	1.015	1.015	1.015
p	0.828	0.873	0.903
f	0.910	0.906	0.901
U^*	0.995	0.995	0.995
k_∞	1.004	1.055	1.086
$M_\parallel^2$	661	684	742
$M_\perp^2$	587	627	695
$1 + M_\parallel^2 B_\parallel^2 + M_\perp^2 B_\perp^2$	1.052	1.055	1.060
k_{eff}	0.954	1.000	1.0245
Initial conversion ratio	0.934	0.838	0.777
Estimated precision of quoted k_{eff} (hot-operating) value	±0.012	±0.012	±0.012

Note: U^* is factor used to adjust calculated k_∞ to obtain best over-all agreement (within ±0.7%) with results of two separate sets of lattice measurements, i.e., $k_\infty = \eta\epsilon p f U^*$.

increase in lattice spacing; at the 9-inch lattice pitch, the specific power is 4.5 Mw/t D_2O and decreases to 3.4 Mw/t D_2O for the 10-inch lattice pitch, assuming the use of a graphite reflector.

Estimated attainable fuel exposures corresponding to the k_{eff} and initial conversion ratio values given in Table 6–36 are presented in Table 6–37. Several fuel burnup conditions are considered which can be approached in practice by different fuel reloading or shuffling procedures. The case of

TABLE 6–37

ESTIMATED PERFORMANCE OF LARGE GAS-COOLED, D_2O-MODERATED REACTOR WITH VARIOUS FUELS

Fuel material	UO_2	UO_2	UO_2	UO_2	U metal
Enrichment	Natural	Natural	Natural	1.0% enriched	Natural
Lattice type	Square	Square	Square	Square	Triangular
Lattice pitch, in.	8	9	10	8	10
Total thermal power, Mw	820	640	520	820	470
Specific power, Mw/ton U	9.0	9.0	9.0	9.0	3.82
Specific power, Mw/ton D_2O:					
With graphite reflector	6.4	4.5	3.4	6.4	
With D_2O reflector	4.8	3.5	2.7	4.8	2.4
Inlet coolant temperature, °F	350	350	350	350	300
Exit coolant temperature, °F	1050	1050	1050	1050	670
k_∞, cold-clean	1.079	1.122	1.145		1.124
k_∞, hot-operating	1.003	1.055	1.084	1.126	1.085
k_{eff}, hot-operating	0.953	1.000	1.025	1.073	1.050
Initial conversion ratio	0.934	0.838	0.777	0.773	0.81
Estimated fuel burnup, Mwd/ton U:					
Uniform fuel burnup		1800	2600	4600	
Uniformly graded fuel irradiation		2900	4500	8000	
Push-fuel-through equilibrium cycle		2500	3800	6800	

uniform fuel burnup of a single fuel charge is approached by proper shifting of the fuel during its irradiation exposure. The push-fuel-through equilibrium cycle is a practical approach to the idealized case of uniformly graded fuel irradiation. For the push-fuel-through cycle, Table 6–37 indicates an exposure of 2500 Mwd/t for the 9-inch lattice and of 3800 Mwd/t for the 10-inch lattice. If the initial reactivity were 1.2%

higher than given in the table (equal to the estimated uncertainty in the k_{eff} value tabulated in Table 6–36), the fuel exposure would increase to 4500 Mwd/t for the 10-inch lattice utilizing the push-fuel-through cycle.

Also included in Table 6–37, in the last two columns, are the results of calculations for reactors fueled with 1.0% enriched uranium oxide and natural uranium metal. The conditions for the slightly-enriched oxide case and the calculation methods are identical with those for the natural uranium oxide cases considered. The benefits resulting from the enrichment are apparent in the specific power and in the increased fuel life.

The calculations for the uranium metal fuel, made at an earlier stage in the reactor design program, have not been checked against experimental results as carefully as the oxide calculations. However, they suffice to show some of the characteristics of a metal-fueled reactor. A different fuel and pressure tube arrangement was used with the metal fuel and, of course, the limiting coolant temperatures were different also. The pressure tube-fuel element arrangement assumed in the calculations is shown in Fig. 6–81. The insulation is low-density magnesium oxide and each of the seven fuel slugs rests in a separate hexagonal flow channel having walls of magnesium alloy. The finned fuel jackets are of magnesium alloy and the maximum surface temperature is limited to 750°F. There is little doubt that a reactor of this type would operate with natural uranium fuel with a comfortable reactivity margin. Fuel life estimates have not been included in the table for this arrangement because the available excess reactivity is quite evidently more than enough to provide a radiation life longer than that of present uranium metal fuel elements. It has been as-

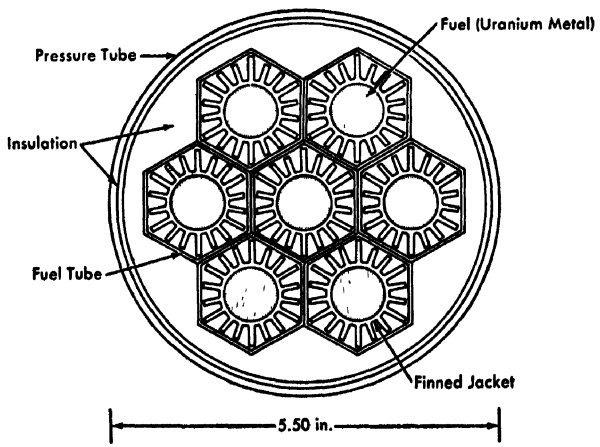

FIG. 6–81. Pressure tube and fuel arrangements for uranium metal fuel elements. (GNEC)

sumed in the heat-removal calculations that some of the excess reactivity would be used for radial flux flattening, to achieve a maximum/average power density ratio, radially, of 1.30. The uranium metal case was calculated to illustrate the characteristics of the reactor with metal fuel, with no attempt to optimize the lattice for specific power. It seems possible that a reactor fueled partly with uranium metal and partly with uranium oxide might perform well. The pressure tube reactor is particularly adaptable to such composite schemes, as separate external circuits can be used for the coolant fractions from the different types of fuel channels.

REFERENCES

1. C ROGERS MCCULLOUGH, *Summary Report on Design and Development of High Temperature Gas-Cooled Power Pile*, USAEC Report MonN-383, Oak Ridge National Laboratory, 1947

2 T SZEKELY, *Direct Cycle Reactors for Aircraft Nuclear Propulsion*, paper presented at the Fourth Nuclear Engineering and Science Conference Held in Chicago, Ill, March 17–21, 1958. (Preprint 93, Session XI, American Institute of Chemical Engineers)

3 D S SELENGUT, *The Nuclear Design of Aircraft Reactors*, paper presented at the Fourth Engineering and Science Conference Held in Chicago, Ill., March 17–21, 1958. (Preprint 97, Session XIII, American Institute of Chemical Engineers)

4 *Congressional Record, Proceedings and Debates of the 85th Congress, Second Session* **104**(6), 391 (Jan. 15, 1958)

5 FARRINGTON DANIELS, Small Gas-Cycle Reactor Offers Economic Promise, *Nucleonics* **14**(3), 34–41 (March 1956).

6 A PUISHES et al, *Comparison of Calder Hall and PWR Reactor Types*, USAEC Report AECU-3398, Atomic Energy Division, American Standard, Mar. 1, 1957.

7. W. F. BANKS, *A Further Evaluation of the Calder Hall Type of Nuclear Power Plant*, USAEC Report NAA-SR-1955, Atomics International, North American Aviation, Inc, June 1957

8 E S BETTIS et al., The Aircraft Reactor Experiment—Design and Construction, *Nuclear Sci. and Eng* **2**(6), 804–825 (November 1957)

9. E. S. BETTIS et al., The Aircraft Reactor Experiment—Operation, *Nuclear Sci and Eng.* **2**(6), 841–853 (November 1957).

10 OAK RIDGE NATIONAL LABORATORY, *The ORNL Gas-Cooled Reactor*, USAEC Report ORNL-2500, 1958.

11 KAISER ENGINEERS and ACF INDUSTRIES, *Gas Cooled Power Reactor, Preliminary Design, 55,000 Kw Prototype, Natural Uranium Nuclear Power Plant*, USAEC Report IDO-2021(Rev 1), March 1958

12. KAISER ENGINEERS and ACF INDUSTRIES, *Gas Cooled Power Reactor, Feasibility Study, Optimum Natural Uranium Nuclear Power Plant*, USAEC Report IDO-2022(Rev 1), March 1958.

13. KAISER ENGINEERS and ACF INDUSTRIES, *Gas Cooled Power Reactor, Feasibility Study, 44,000 Kw Prototype, Partially Enriched, Uranium Nuclear Power Plant,* USAEC Report IDO-2023(Rev. 1), March 1958.

14. KAISER ENGINEERS and ACF INDUSTRIES, *Gas Cooled Power Reactor, Feasibility Study, Optimum Partially Enriched Uranium Nuclear Power Plant,* USAEC Report IDO-2024(Rev. 1), March 1958.

15. E. R. RUDOCK, *Coolant Gas Selection for a Gas Cooled Reactor, Section V, A Parametric Study of the Gas Cooled Reactor Concept, Addendum,* USAEC Report HW-54727, Hanford Atomic Products Operation, Mar. 1, 1958.

16 M. H. MUELLER, Lattice Parameters of Alpha-Uranium, Appendix I, in *Deformation Mechanisms of Alpha-Uranium Single Crystals,* by L. T. Lloyd and H. H. Chiswick, USAEC Report ANL-5367, Argonne National Laboratory, 1955.

17. B. BLUMENTHAL, *The Melting of High Purity Uranium,* USAEC Report ANL-5019, Argonne National Laboratory, 1953

18. J. THEWLIS, Structure of Uranium, *Nature* **168,** 198–199 (1951).

19. ARGONNE NATIONAL LABORATORY, *Metallurgy Division Quarterly Report, January, February, and March 1957,* USAEC Report ANL-5717, Mar. 31, 1957.

20. E G RAUH and K J. THORN, Vapor Pressure of Uranium, *J. Chem. Phys* **22,** 1414–1420 (1954)

21. *The Reactor Handbook,* Vol. 3, General Properties of Materials, USAEC Report AECD-3647, 1955

22. L. C. LOWELL and T L LLOYD, Argonne National Laboratory, 1958. Unpublished.

23. M. H. MUELLER et al., *Effect of Varying Reduction on the Preferred Orientation in Rolled Uranium Rods,* USAEC Report ANL-5194, Argonne National Laboratory, May 3, 1954.

24 R M MAYFIELD et al , *Mechanical Properties of Rolled Uranium Rods,* USAEC Report ANL-5296, Argonne National Laboratory, July 1, 1956.

25 J. R BRIDGE et al , X-Ray Diffraction Determination of the Coefficients of Expansion of Alpha-Uranium. To be published by American Institute of Mining and Metallurgical Engineers.

26. E. G RAUH and K. J. THORN, Vapor Pressure of Uranium, *J. Chem. Phys.* **22,** 1414–1420 (1954).

27. K F SMITH, *The Thermal Conductivity of Uranium,* USAEC Report ANL-5700(Pt A), Argonne National Laboratory, April 1957.

28. K. F. SMITH, *The Electrical Conductivity of Uranium,* USAEC Report ANL-5700(Pt B), Argonne National Laboratory, April 1957.

29 E. A. LONG et al., The Heat Capacities of Uranium, UO_3 and UO_2 from 15°K to 300°K, *J. Chem. Phys.* **20,** 695–699 (1952).

30. G E MOORE and K. H. KELLEY, High Temperature Heat Contents of Uranium, Uranium Dioxide and Uranium Trioxide, *J. Am. Chem. Soc.* **69,** 2105–2107 (1947).

31. D. C. GINNINGS and R. J. CORRUCCINI, Heat Capacities at High Temperatures of Uranium, Uranium Trichloride and Uranium Tetrachloride, *J. Research Natl. Bur. Standards* **39,** 309–316 (1947).

32. J. M. NORTH, *A High Temperature Adiabatic Calorimeter; The Specific*

Heat of Uranium Between 100° and 800°C, Report AERE M/R 1016, Great Britain, Atomic Energy Research Establishment, 1952.

33. R. E. HUESCHEM and H J SANDERSON, Hanford Atomic Products Operation, 1953. Unpublished.

34. S H. BUSH, Irradiation Effects in Uranium, in *Fuel Elements Conference, Paris, November 18–23, 1957*, USAEC Report TID-7546, Hanford Atomic Products Operation, 1958. (pp 591–615)

35. W. K. WOODS and S. S JONES, *Measurements of Slug Temperatures—Final Report*, USAEC Report HW-10558, Hanford Atomic Products Operation, July 27, 1948.

36. D. S. BILLINGTON, Radiation Damage in Reactor Materials, in *Proceedings of the International Conference on the Peaceful Uses of Atomic Energy*, Vol. 7. New York: United Nations, 1956. (P/744, pp. 421–432)

37. S. S JONES, Hanford Atomic Products Operation, 1955. Unpublished.

38. O. K. SHUPE et al., *Effects of Various Preferred Orientations on the Dimensional Stability of Uranium*, USAEC Report HW-54605, Hanford Atomic Products Operation, Jan. 20, 1958.

39 H. H. CHISWIK, *Effects of Preferred Orientation and Grain Size on Dimensional Stability of Uranium on Thermal Cycling and Irradiation*, USAEC Report ANL-4955, Argonne National Laboratory, March 1956.

40. J. H. KITTEL and S. H. PAINE, *Effects of High Burnup on Natural Uranium*, USAEC Report ANL-5539, Argonne National Laboratory, May 1, 1957.

41 S H. PAINE and J. H KITTEL, Irradiation Effects in Uranium and Its Alloys, in *Proceedings of the International Conference on the Peaceful Uses of Atomic Energy*, Vol 7. New York: United Nations, 1956. (P/745, pp. 445–454)

42. J. H. KITTEL and S. H. PAINE, *Effects of Irradiation on Powder Compacts of Uranium and Some Uranium-Base Alloys*, USAEC Report ANL-5664, Argonne National Laboratory, June 1957.

43. ARGONNE NATIONAL LABORATORY, *Metallurgy Division Quarterly Report, October, November, and December, 1955*, USAEC Report ANL-5541, June 1956

44. KAISER ENGINEERS and ACF INDUSTRIES, *Gas-Cooled Power Reactor, Preliminary Design, 55,000 Kw Prototype Natural Uranium Nuclear Power Plant*, USAEC Report IDO-2021(Rev. 1), March 1958

45 J. E. MINOR, Hanford Atomic Products Operation, 1956. Unpublished.

46. A. L. EISS and H. S. KALISH, Sylvania-Corning Nuclear Corp , 1957. Unpublished

47. R. WEIL and S H. PAINE, *Effect of Irradiation Upon Interdiffusion of Stainless Steel and Uranium*, USAEC Report ANL-5346, Argonne National Laboratory, July 15, 1953.

48. KNOLLS ATOMIC POWER LABORATORY, Diffusion Studies of Uranium, in *Reactor Materials, Section III, Progress Report No. 49, August 1950*, USAEC Report KAPL-395, Sept. 20, 1950. (p. 23)

49. KNOLLS ATOMIC POWER LABORATORY, *Reactor Materials, Section III, Progress Report No. 50, September 1950*, USAEC Report KAPL-415, Oct. 27, 1950

50 J B. LAMBERT, *Behavior of SIR Fuels Irradiated in Sodium (Final Report,*

PT-105-108-P) (*Special Request KAPL-79, The Beta Experiment*), USAEC Report HW-25330(Del.), Hanford Atomic Products Operation, August 1952.

51. D. R MASH and B. F. DISSELHORST, *Uranium-Zirconium Diffusion Studies*, USAEC Report LRL-143, Livermore Research Laboratory, California Research and Development Co., June 1954.

52. R KIESSLING, The Solid State Reaction between Uranium and Aluminum, in *Proceedings of the International Conference on the Peaceful Uses of Atomic Energy*, Vol. 9. New York: United Nations, 1956. (P/786, pp. 69–73)

53. H. M. FINNISTON and J. P. HOWE (Eds.), *Progress in Nuclear Energy, Series V, Metallurgy and Fuels*, Vol. I New York: McGraw-Hill Book Company, Inc., 1956. (p 506)

54. A. H. COTTRELL, The Physics of Nuclear Reactors: The Effects of Irradiation on the Physical Properties of Solids, *Brit. J. Appl. Phys.* Suppl. No. *5*, S43-S53 (July 1956).

55. A C. ROBERTS and A. H. COTTRELL, Creep of Alpha-Uranium During Irradiation with Neutrons, *Phil. Mag.* [8]1, 711–717 (August 1956).

56 R W NICHOLS, Uranium and Its Alloys, *Nuclear Engineering* **2**(18), 355–365 (September 1957).

57. J. J KATZ and E RABINOWITCH, *The Chemistry of Uranium*, National Nuclear Energy Series, Div VIII, Vol 5 New York: McGraw-Hill Book Company, Inc., 1951

58. FREDERICK R. SHOBER et al., *The Mechanical Properties of Zirconium and Zircaloy-2*, USAEC Report BMI-1168, Battelle Memorial Institute, Feb. 18, 1957.

59. B. LUSTMAN and F KERZE, Jr (Eds.), *The Metallurgy of Zirconium*, National Nuclear Energy Series, Div VIII, Vol. 4 New York: McGraw-Hill Book Company, Inc., 1955

60. *Alcoa Aluminum Handbook* Pittsburgh, Pa: Aluminum Company of America, 1956

61. T J. HEAL, Magnesium and Its Alloys; Applications in Nuclear Engineering, *Nuclear Engineering* **3**(23), 52–61 (February 1958).

62. D. W WHITE, Jr, and J. E BURKE, (Eds.), *The Metal Beryllium*, Cleveland: American Society for Metals, 1955.

63 *Metals Handbook*, Cleveland: American Society for Metals, 1948.

64 C R TOTTLE, The Physical and Mechanical Properties of Niobium, *J Inst Metals* **85**, 375–378 (1957).

65 D. S OLIVER, *The Elements of Groups IVA, VA, VIA and Beryllium—Physical and Mechanical Properties*, Report FRDC/P-33, Great Britain, Culcheth Laboratories, May 29, 1953.

66. WESTINGHOUSE ELECTRIC CORP., AVIATION GAS TURBINE DIVISION, *Development of Niobium Base Alloys, First Quarterly Progress Report*, Report A-2173(WEC), April 1956.

67. MEMBERS OF SOLID STATE DIVISION, OAK RIDGE NATIONAL LABORATORY, A Brief Summary of Research on Radiation Effects in Solids, in *Papers Prepared for Radiation Effects Review Meeting, Congress Hotel, Chicago, July 31–August 1, 1956*, USAEC Report 7515[Pt. 2(Del.)], August 1956. (pp. 5–100)

68. R M. HAAG and F. C ZYZES, *Corrosion of Aluminum in High-Tempera-*

ture Water. III. Inhibition of Corrosion by Sodium Silicate, USAEC Report KAPL-1741, Knolls Atomic Power Laboratory, Feb. 28, 1957.

69. J. E. Draley and W. E. Ruther, *Experiments in Corrosion Mechanism: Aluminum at High Temperatures,* USAEC Report ANL-5658, Argonne National Laboratory, April 1957

70. Argonne National Laboratory, *Metallurgy Division Quarterly Report, January, February, and March, 1956,* USAEC Report ANL-5563, June 1956.

71. E. L. Martinec, *Corrosion of an Aluminum-Nickel Alloy in a Reactor Test Loop,* USAEC Report ANL-5783, Argonne National Laboratory, September 1957

72 J. A Ayres, Hanford Atomic Products Operation, 1957 Unpublished

73 V. H. Troutner, *High Temperature Aqueous Corrosion Product Films on Aluminum,* USAEC Report HW-53389, Hanford Atomic Products Operation, Nov. 15, 1957.

74 Brush Beryllium Co, *Research and Development Progress Report for April, May and June 1955,* USAEC Report COO-306, July 29, 1955

75. Brush Beryllium Co., *Research and Development Progress Report for July, August and September 1955,* USAEC Report COO-307, Nov. 1, 1955.

76. Brush Beryllium Co., *Research and Development Progress Report for October, November and December 1955,* USAEC Report COO-308, March 1956

77 Brush Beryllium Co., *Research and Development Progress Report for January, February, and March 1956,* USAEC Report COO-309, August 1956

78 K. G Wikle and R. Magalski, *Brazing Beryllium Tubing to High-Temperature Alloy Collars,* USAEC Report COO-310, Brush Beryllium Co., June 1956

79. N Maropis and J. B Jones, *Investigation of Ultrasonic Grain Refinement in Beryllium,* USAEC Report NYO-7788, Aeroprojects, Inc, February 1957.

80 J Greenspan, *A Preliminary Investigation of the Tensile Properties of Beryllium Couplings,* USAEC Report NMI-1196, Nuclear Metals, Inc, Dec. 11, 1957

81 J Greenspan, *Ductility in Beryllium Related to Grain Orientation and Grain Size,* USAEC Report NMI-1174, Nuclear Metals, Inc, Aug. 9, 1957.

82 Nuclear Metals, Inc, *Quarterly Progress Report for the period January 1, 1957 through March 31, 1957,* USAEC Report NMI-1176, May 20, 1957

83 D S. Kneppel, *Corrosion of Beryllium in 600°F Water,* USAEC Report NMI-1190, Nuclear Metals, Inc, Sept 10, 1957.

84. E A Gulbransen and K. F Andrew, The Kinetics of the Reactions of Beryllium with Oxygen and Nitrogen and the Effect of Oxide and Nitride Films on Its Vapor Pressure, *J Electrochem Soc.* 97, 383–395 (1950).

85. W. Munro and J. Williams, *The Reaction of Beryllium with Carbon Dioxide in the Temperature Range 500–700°C,* Report AERE-M/M-108, Great Britain, Atomic Energy Research Establishment, 1956.

86. L. R. Williams and P. B. Eyre, The Metallurgy of Beryllium; Its Nuclear Applications, *Nuclear Eng* 3(22) 9–18 (January 1958).

87. L Grainger and A. B. McIntosh, Metallurgical Developments, paper presented at British Nuclear Energy Conference-Symposium on Calder Hall Works Nuclear Power Plant, 1956.

88. How the Stations Compare, *Nuclear Power* **2**(10), 54–56 (February 1957).

89. Hinkley Point; Anticipated 500Mw Output, *Nuclear Eng.* **2**(19), 423–426 (October 1957)

90. Hinkley Contract Awarded, *Nuclear Power* **2**(18), 397 (October 1957).

91. Bradwell, *Nuclear Power* **2**(18), 401–436 (October 1957).

92. S. E. LEWIS, Nuclear Physics at Bradwell, *Nuclear Power* **2**(18), 414–415 (October 1957)

93. Hinkley Point; The World's Biggest Nuclear Power Station, *Nuclear Power* **2**(19), 450–454 (November 1957).

94. C TYZACK, Zirconium and Its Alloys, *Nuclear Eng.* **3**(24), 102–114 (March 1958).

95. W. H. ZINN (Comp), Zirconium and Zirconium Alloys, in *Technical Progress Review—Power Reactor Technology* **1**(2), 35–38 (February 1958).

96. E A. GULBRANSEN and K. F. ANDREW, Kinetics of the Reactions of Zirconium with Oxygen, Nitrogen, and Hydrogen, *J. Metals* **1**(8), Trans. 515–526 (1949)

97. E T. HAYES and A. H. ROBERTSON, Effects of Heating Zirconium in Air, Oxygen, and Nitrogen, *J. Electrochem Soc.* **96**, 142–151 (1949)

98. E T. HAYES and Co-WORKERS, U. S. Bureau of Mines Technical Progress Report 9, Dec. 21, 1951

99. C T ANDERSON et al , *A Preliminary Survey of Zirconium Alloys*, Report BM-RI-4658, U. S. Bureau of Mines, 1950.

100. BATTELLE MEMORIAL INSTITUTE. Part I. Niobium Technology, Nuclear Technology Briefs, Reactor Materials, AEC Press Release No TI-3, Mar. 19, 1958

101. E. A. GULBRANSEN and K. F. ANDREW, Kinetics of the Reactions of Columbium and Tantalum with Oxygen, Nitrogen, and Hydrogen, *J. Metals* **188**(3), Trans. 586–599 (March 1950).

102. E. A GULBRANSEN and K. F. ANDREW, Oxidation of Niobium Between 375°C and 700°C, *J. Electrochem. Soc.* **105**, 4–9 (January 1958).

103. S J. PAPROCKI and J T STACY, *Investigation of Some Niobium-Base Alloys*, USAEC Report BMI-1143, Battelle Memorial Institute, Oct. 31, 1956.

104. C. T SIMS et al , *Studies of the Oxidation and Contamination Resistance of Binary Niobium Alloys*, USAEC Report BMI-1169, Battelle Memorial Institute, Feb. 19, 1957.

105. H J. CLEARY, Nuclear Metals Inc., 1956. Unpublished.

106. C. A. BARRETT and F. I CLAUS, Oxidation of Niobium-Chromium Alloys at Elevated Temperatures, paper presented at the Washington Meeting of the Electrochemical Society, May 1957.

107. C. W. KRYSTYNIAK and D. D. CROOKS, *Pretreatment of Uranium for the Application of Ceramic Castings*, USAEC Report KAPL-1340, Knolls Atomic Power Laboratory, May 4, 1955.

108. G. L. PLOETZ and H. G. SOWMAN, Knolls Atomic Power Laboratory, 1956. Unpublished.

109. D. W. SHANNON, Hanford Atomic Products Operation, 1958. Unpublished.

110. P. CHIOTTI et al., Ames Laboratory, 1955. Unpublished.

111. J. R. JOHNSON et al., *The Technology of Uranium Oxide, A Reactor Material,* USAEC Report ORNL-2011, Oak Ridge National Laboratory, Feb. 21, 1956.

112. L. G. WISNYI and S. PIJANOWSKI, Knolls Atomic Power Laboratory, 1956. Unpublished.

113 J BELLE and B LUSTMAN, Properties of UO_2, in *Fuel Elements Conference, Paris, November 18–23, 1957,* USAEC Report TID-7546, Westinghouse Atomic Power Division, 1958 (Book 2, pp. 442–515)

114 W. A LAMBERTSON and M H. MUELLER, Uranium Oxide Phase Equilibrium Systems. II. UO_2-MgO, *J. Am. Ceram, Soc.* **36**, 332–334 (1953).

115 S. M. LANG et al, High-Temperature Reactions of Uranium Dioxide with Various Metal Oxides, *Natl. Bur Standards (U. S.), Circ 568* (Feb 20, 1956).

116 W D. KINGERY et al, Thermal Conductivity X. Data for Several Pure Oxide Materials Corrected to Zero Porosity, *J Am Ceram. Soc* **37**, 107–110 (February 1954)

117. J. C HEDGE and I B FIELDHOUSE, *Thermal Conductivity of* UO_2, USAEC Report AECU-3381, Armour Research Foundation, Sept 22, 1956.

118 M JAKOB and G. A. HAWKINS, *Elements of Heat Transfer and Insulation,* 2nd ed New York John Wiley & Sons, Inc., 1950.

119 J. D. EICHENBERG et al., *Effects of Irradiation on Bulk* UO_2, USAEC Report WAPD-183, Westinghouse Atomic Power Division, October 1957

120 J. BELLE and B LUSTMAN, Properties of Uranium Dioxide, in *Fuel Elements Conference, Paris, November 18–23, 1957,* USAEC Report TID-7546, Westinghouse Atomic Power Division, 1958 (Book 2, pp. 442–515)

121. J M MARKOWITZ et al, *Release of Fission Gases from Irradiated Uranium Dioxide. Part I Apparatus for the Measurement of Fission Gas Release from Fuel Materials During Pile Irradiation,* USAEC Report WAPD-180, Westinghouse Atomic Power Division, July 1957.

122 B. LUSTMAN, *Release of Fission Gases from* UO_2, USAEC Report WAPD-173, Westinghouse Atomic Power Division, March 1957.

123 J. F ECKEL et al, Knolls Atomic Power Laboratory, 1956. Unpublished

124. J BELLE and L J JONES, *Résumé of Uranium Oxide Data, IX,* USAEC Report WAPD-TM-44, Westinghouse Atomic Power Division, Mar. 15, 1957

125. W H WILSON and T O. ZIEBOLD, Naval Reactors Branch, Division of Reactor Development, AEC, 1957 Unpublished

126. J. D. EICHENBERG et al., Effects of Irradiation on Bulk Uranium Dioxide, in *Fuel Elements Conference, Paris, November 18–23, 1957,* USAEC Report TID-7546, Westinghouse Atomic Power Division, 1958. (Book 2, pp. 616–716)

127 C D HARRINGTON, Preparation and Properties of Uranium Dioxide Powder, in *Fuel Elements Conference, Paris, November 18–23, 1957,* USAEC Report TID-7546, Mallinckrodt Chemical Works, 1958. (Book 2, pp. 369–383)

128. L. C WATSON, Production of Uranium Dioxide for Ceramic Fuels, in *Fuel Elements Conference, Paris, November 18–23, 1957,* USAEC Report TID-7546, Atomic Energy of Canada, Ltd., 1958. (Book 2, pp. 384–401)

129. R. KIESSLING and U RUNFORS, Sintering of Uranium Dioxide, in *Fuel Elements Conference, Paris, November 18–23, 1957,* USAEC Report TID-7546, Aktiebolaget Atomenergi (Sweden), 1958. (Book 2, pp. 402–413)

130. E. A. EVANS et al., Fabrication and Enclosure of Uranium Dioxide, in *Fuel Elements Conference, Paris, November 18–23, 1957*, USAEC Report TID-7546, Hanford Atomic Products Operation, 1958 (Book 2, pp. 414–431)

131. D. R. STENQUIST and R. J. ANICETTI, *Extrusion of Uranium Dioxide Fuel Cores*, USAEC Report HW-51747, Hanford Atomic Products Operation, Dec. 1, 1957.

132. W. W. WEST, E. I. du Pont de Nemours & Company, Savannah River Laboratory, 1954. Unpublished.

133. M. W. MALLETT et al., *The Kinetics of the Zirconium-Uranium Dioxide Reaction*, USAEC Report BMI-1028, Battelle Memorial Institute, Aug. 15, 1955.

134. J. F. WHITE (ed.), *Minutes of UO_2 Conference at Chalk River, Ontario, January 5 and 6, 1956*, USAEC Report TID-7514, General Electric Company, Aircraft Nuclear Propulsion Department.

135. W. W. BEAVER, *Beryllium Materials and Components for High Temperatures Application*, paper presented at a meeting of the American Nuclear Society.

136. L. M. CURRIE et al., The Production and Properties of Graphite for Reactors, in *Proceedings of the International Conference on the Peaceful Uses of Atomic Energy*, Vol. 8 New York: United Nations, 1956 (P/534, pp. 451–473)

137. T. J. NEUBERT et al., *The Structure and Properties of Artificial and Natural Graphite*, USAEC Report ANL-5524, Argonne National Laboratory, February 1956.

138. G. R. HENNIG and J. E. HOVE, Interpretation of Radiation Damage to Graphite, in *Proceedings of the International Conference on the Peaceful Uses of Atomic Energy*, Vol. 7. New York: United Nations, 1956. (P/751, pp. 666–675)

139. R. E. NIGHTINGALE and J. F. FLETCHER, *Radiation Damage to Graphite from 30°C to 185°C*, USAEC Report HW-47776(Rev.), Hanford Atomic Products Operation, Sept. 26, 1957.

140. R. E. NIGHTINGALE and W. A. SNYDER, *Distribution of Radiation Damage in Graphite*, USAEC Report HW-49626(Rev.), Hanford Atomic Products Operation, June 18, 1957.

141. S. B AUSTERMAN, *Stored Energy Release in Graphite Irradiated at Low Temperatures*, USAEC Report NAA-SR-1564, Atomics International, North American Aviation, Inc., Oct. 1, 1956.

142. R. E. DURAND and D. J. KLEIN, *The Effect of Reactor Irradiation at Temperatures between 400°C and 700°C on the Thermal Conductivity of Graphite*, USAEC Report NAA-SR-1520, Atomics International, North American Aviation, Inc., July 15, 1956.

143. K E. HORTON and R. L. CARTER, Radiation-Induced Hardness Changes in Graphite, *Nuclear Sci. and Eng* 2(4), 513–515 (July 1957)

144. T. J NEUBERT and R. B. LEES, Stored Energy in Neutron-Bombarded Graphite, *Nuclear Sci. and Eng.* 2(6), 748–767 (November 1957)

145. G. R. HENNIG, A Chemical Model of Radiation Damage in Graphite, *Nuclear Sci. and Eng.* 3(5), 514–528 (May 1958).

146. L. J. BARBIERI et al., *Plutonium Recycle in the Calder Hall Type Reactor,*

USAEC Report ASAE-S-8, Atomic Energy Division, American Standard, Jan. 1, 1958.

147. D. E. DAVENPORT, Exponential Experiments in Graphite Systems, in *Proceedings of the International Conference on the Peaceful Uses of Atomic Energy*, Vol. 5. New York: United Nations, 1956. (P/599, pp. 309–316)

148 E. D. CLAYTON, *Exponential Pile Measurements in Graphite-Uranium Lattices*, USAEC Report AECD-3677, Hanford Atomic Products Operation, 1954.

149 I KAPLAN and J. CHERNICK, Uranium Graphite Lattices—The Brookhaven Reactor, in *Proceedings of the International Conference on the Peaceful Uses of Atomic Energy*, Vol. 5. New York: United Nations, 1956. (P/606, pp. 293–308)

150 E. D CLAYTON, Buckling Measurements with Enriched Uranium in Graphite Systems, paper presented at French-American Meeting on Graphite Reactors at Brookhaven National Laboratory, Nov. 12–15, 1957

151. E. D. CLAYTON, Exponential Measurements with Enriched Uranium in Graphite Lattices, paper presented at the Third Annual Meeting of the American Nuclear Society, June 10–12, 1957.

152 E. P WIGNER et al, *Resonance Absorption of Neutrons by Spheres*, *J. Appl. Phys* **26**, 260–270 (1955)

153 E HELLSTRAND, *Measurements of the Effective Resonance Integral in Uranium Metal and Oxide in Different Geometries*, Report AEF-84, Aktiebolaget Atomenergi, Stockholm, June 1957.

154 M V. DAVIS, Resonance Absorption of Neutrons by Uranium Cylinders, *J Appl. Phys.* **2**, 250–255 (1957)

155 G. W. RODEBACK, *Temperature Coefficients of Uranium and Thorium Resonance Integrals*, USAEC Report NAA-SR-1641, Atomics International, North American Aviation, Inc., 1956.

156 E. CREUTZ et al, Effect of Temperature on Total Resonance Absorption of Neutrons by Spheres of Uranium Oxide, *J Appl Phys* **26**, 276–279 (1955)

157. D A NEWMARCH, A Modification to the Diffusion Theory of the Thermal Fine Structure in a Reactor to Account for the Effect of Air Channels, *J. Nuclear Energy* **2**, 52–58 (1955)

158 C H WESTCOTT, *The Specification of Neutron Flux and Effective Cross Sections in Reactor Calculations*, Report CRRP-662, Atomic Energy of Canada, Ltd, Aug 15, 1956

159. R R COVEYOU et al., Effect of Moderator Temperature upon Neutron Flux in Infinite Capturing Medium, *J Nuclear Energy* **2**, 153–167 (1956).

160. M. J POOLE, *A Measurement of the Neutron Spectra in Aqueous Moderators and Reactor Lattices by Time-of-Flight Methods Using a Pulsed Linear Accelerator*, Report NRDC-95, Great Britain, Atomic Energy Research Establishment, 1956

161. D. V. BOOKER et al., *The Measurements of the Laplacian in a Lattice of Uranium Metal Rods and Graphite*, Report AERE-N/R-134, Great Britain, Atomic Energy Research Establishment, 1956.

162. D. J. BEHRENS, The Effect of Holes in a Reacting Material on the Passage of Neutrons, *Proc. Phys Soc. (London)* **62A**, 607–616 (1949).

163. B. I. SPINRAD et al., Reactivity Changes and Reactivity Lifetimes of Fixed-Fuel Elements in Thermal Reactors, in *Proceedings of the International Conference on the Peaceful Uses of Atomic Energy*, Vol. 5. New York: United Nations, 1956. (P/835, pp. 125–140)

164. L. ISAKOFF (Comp.), *Power Reactor Studies, Quarterly Progress Report, August, September, and October 1957*, USAEC Report DP-265, E. I. du Pont de Nemours & Company, February 1958.

165. THE STAFF OF NUCLEAR PHYSICS RESEARCH, *Nuclear Physics Research Quarterly Report, April, May, June 1957*, USAEC Report HW-51983, Aug. 14, 1957.

TABLES

6–29, 6–30, 6–31, and 6–32

TABLE 6–29

CALCULATED NEUTRON PHYSICS CHARACTERISTICS OF VARIOUS GAS-COOLED, GRAPHITE-MODERATED REACTORS

I. Moderator at room temperature (neutron temperature = 294°K)

(a) Single UO_2 rod fuel element, type-430 stainless steel jacket.

Case number	Rod diameter, inches	Clad thickness, inches	Enrichment, a/o	Cooling hole diameter, inches	Lattice pitch, inches	η	ϵ	p	f	k_∞	R_c
1	1.50	0.040	0.714	3.00	6.27	1.339	1.020	0.7761	0.8149	0.864	1.009
2	1.50	0.040	0.714	3.00	6.97	1.339	1.020	0.8209	0.8009	0.898	0.918
3	1.50	0.040	0.714	3.00	7.67	1.339	1.020	0.8534	0.7854	0.915	0.852
4	1.50	0.040	0.714	3.00	8.36	1.339	1.020	0.8777	0.7685	0.921	0.803
5	1.50	0.040	0.714	3.00	9.06	1.339	1.020	0.8965	0.7505	0.919	0.765
6	1.50	0.040	0.80	3.00	6.27	1.392	1.020	0.7761	0.8231	0.907	0.949
7	1.50	0.040	0.80	3.00	6.97	1.392	1.020	0.8209	0.8093	0.943	0.858
8	1.50	0.040	0.80	3.00	7.67	1.392	1.020	0.8534	0.7941	0.962	0.792
9	1.50	0.040	0.80	3.00	8.36	1.392	1.020	0.8777	0.7773	0.969	0.743
10	1.50	0.040	0.80	3.00	9.06	1.392	1.020	0.8965	0.7597	0.967	0.705
11	1.50	0.040	1.00	3.00	5.58	1.491	1.020	0.7117	0.8502	0.920	0.981
12	1.50	0.040	1 00	3.00	6.27	1.491	1.020	0.7761	0.8382	0.989	0.849
13	1.50	0.040	1.00	3.00	6.97	1.491	1.020	0.8209	0.8255	1.031	0.758
14	1.50	0.040	1.00	3.00	7.67	1.491	1.020	0.8534	0.8107	1.052	0.692
15	1.50	0.040	1.00	3.00	8.36	1.491	1.020	0.8777	0.7946	1.061	0.643
16	1.50	0.040	1.25	3.00	4.88	1.580	1.020	0.6142	0.8733	0.864	1.101
17	1.50	0.040	1.25	3 00	5.58	1.580	1.020	0.7117	0.8643	0.991	0.901

18	1.50	0.040	1.25	3.00	6.27	1.580	1.020	0.7761	0.8533	1.067	0.769
19	1.50	0.040	1.25	3.00	6.97	1.580	1.020	0.8209	0.8406	1.112	0.678
20	1.50	0.040	1.25	3.00	7.67	1.580	1.020	0.8534	0.8263	1.136	0.612
21	1.50	0.000	0.714	3.00	6.27	1.339	1.020	0.7822	0.9396	1.004	1.009
22	1.50	0.000	0.714	3.00	6.97	1.339	1.020	0 8261	0.9217	1.040	0.918
23	1.50	0.000	0.714	3.00	7.67	1.339	1.020	0.8578	0.9023	1.057	0.852
24	1.50	0.000	0.714	3.00	8.36	1.339	1.020	0 8815	0.8812	1.061	0.803
25	1.50	0.000	0.714	3.00	9.06	1.339	1.020	0.8997	0.8592	1.056	0.765
26	1.50	0.000	0 80	3.00	5.58	1.392	1.020	0.7190	0.9574	0.977	1.081
27	1.50	0.000	0.80	3.00	6.27	1.392	1.020	0.7822	0.9415	1.046	0.949
28	1.50	0.000	0.80	3.00	6.97	1.392	1.020	0.8261	0.9242	1.084	0.858
29	1.50	0.000	0.80	3.00	7.67	1.392	1 020	0.8578	0.9055	1.103	0.792
30	1.50	0 000	0.80	3.00	8.36	1.392	1 020	0.8815	0.8857	1.108	0.743
31	1.50	0.000	1.00	3.00	4.88	1.491	1.020	0 6228	0.9731	0.922	1.181
32	1.50	0.000	1.00	3.00	5.58	1.491	1.020	0.7190	0.9585	1.048	0.981
33	1.50	0.000	1.00	3.00	6.27	1.491	1.020	0.7822	0.9440	1.123	0.849
34	1.50	0.000	1.00	3.00	6.97	1.491	1.020	0.8261	0.9285	1.167	0.758
35	1.50	0.000	1.00	3.00	7.67	1 491	1 020	0.8578	0.9128	1.191	0.692
36	1.50	0.060	1.00	3.00	6.27	1.491	1.020	0.7728	0.7903	0.929	0.849
37	1 50	0.060	1.00	3.00	6.97	1.491	1.020	0.8182	0.7730	0.968	0.758
38	1.50	0.060	1.00	3.00	7.67	1.491	1.020	0.8512	0 7648	0.990	0.692
39	1.50	0.060	1.00	3.00	8 36	1.491	1.020	0.8758	0 7500	0.999	0.643
40	1.50	0.060	1.00	3.00	9.06	1.491	1.020	0 8948	0.7342	0.999	0.605
41	1.50	0.060	1.25	3.00	5.58	1 580	1.020	0.7079	0.8185	0.934	0.901
42	1.50	0.060	1.25	3.00	6.27	1.580	1.020	0.7728	0.8085	1.007	0.769
43	1.50	0.060	1.25	3.00	6.97	1.580	1.020	0.8182	0.7968	1.051	0.678
44	1.50	0.060	1.25	3.00	7.67	1.580	1.020	0.8512	0.7837	1.075	0.612
45	1.50	0.060	1.25	3.00	8.36	1.580	1.020	0.8758	0.7692	1.086	0.563
46	1.50	0.060	1.50	3.00	4.88	1.646	1.020	0.6099	0 8399	0.860	1.047

(continued)

TABLE 6–29 (*Continued*)

Case number	Rod diameter, inches	Clad thickness, inches	Enrichment, a/o	Cooling hole diameter, inches	Lattice pitch, inches	η	ϵ	p	f	k_∞	R_c
47	1.50	0.060	1.50	3.00	5.58	1.646	1.020	0.7079	0.8317	0.988	0.847
48	1.50	0.060	1.50	3.00	6.27	1.646	1.020	0.7728	0.8223	1.067	0.715
49	1.50	0.060	1.50	3.00	6.97	1.646	1.020	0.8182	0.8107	1.114	0.624
50	1.50	0.060	1.50	3.00	7.67	1.646	1.020	0.8512	0.7981	1.141	0.558
51	1.50	0.060	2.00	3.00	4.88	1.737	1.020	0.6099	0.8586	0.928	0.981
52	1.50	0.060	2.00	3.00	5.58	1.737	1.020	0.7079	0.8510	1.067	0.781
53	1.50	0.060	2.00	3.00	6.27	1.737	1.020	0.7728	0.8419	1.153	0.649
54	1.50	0.060	2.00	3.00	6.97	1.737	1.020	0.8182	0.8309	1.204	0.558
55	1.50	0.060	2.00	3.00	7.67	1.737	1.020	0.8512	0.8185	1.234	0.492
56	1.50	0.080	1.00	3.00	6.27	1.491	1.020	0.7697	0.7451	0.872	0.849
57	1.50	0.080	1.00	3.00	6.97	1.491	1.020	0.8155	0.7342	0.911	0.758
58	1.50	0.080	1.00	3.00	7.67	1.491	1.020	0.8488	0.7219	0.932	0.692
59	1.50	0.080	1.00	3.00	8.36	1.491	1.020	0.8738	0.7084	0.941	0.643
60	1.50	0.080	1.00	3.00	9.06	1.491	1.020	0.8931	0.6938	0.942	0.605
61	1.50	0.080	1.25	3.00	5.58	1.580	1.020	0.7041	0.7753	0.880	0.901
62	1.50	0.080	1.25	3.00	6.27	1.580	1.020	0.7697	0.7657	0.950	0.769
63	1.50	0.080	1.25	3.00	6.97	1.580	1.020	0.8155	0.7555	0.993	0.678
64	1.50	0.080	1.25	3.00	7.67	1.580	1.020	0.8488	0.7433	1.017	0.612
65	1.50	0.080	1.25	3.00	8.36	1.580	1.020	0.8738	0.7299	1.028	0.563
66	1.50	0.080	1.50	3.00	4.88	1.646	1.020	0.6056	0.7983	0.812	1.047
67	1.50	0.080	1.50	3.00	5.58	1.646	1.020	0.7041	0.7913	0.935	0.847
68	1.50	0.080	1.50	3.00	6.27	1.646	1.020	0.7697	0.7823	1.011	0.715

69	1.50	0.080	1.50	3.00	6.97	1.646	1.020	0.8155	0.7718	1.057	0.624
70	1.50	0.080	1.50	3.00	7.67	1.646	1.020	0.8488	0.7599	1.083	0.558
71	1.00	0.000	0.714	3.00	4.88	1.339	1.014	0.7843	0.9401	1.001	1.003
72	1.00	0.000	0.714	3.00	5.58	1.339	1.014	0.8442	0.9150	1.049	0.879
73	1.00	0.000	0.714	3.00	6.27	1.339	1.014	0.8815	0.8887	1.064	0.801
74	1.00	0.000	0.714	3.00	6.97	1.339	1.014	0.9066	0.8583	1.056	0.749
75	1.00	0.000	0.714	3.00	7.67	1.339	1.014	0.9243	0.8249	1.035	0.713
76	1.00	0.000	0.80	3.00	4.88	1.392	1.014	0.7843	0.9430	1.044	0.943
77	1.00	0.000	0.80	3.00	5.58	1.392	1.014	0.8442	0.9220	1.099	0.819
78	1.00	0.000	0.80	3.00	6.27	1.392	1.014	0.8815	0.8955	1.114	0.741
79	1.00	0.000	0.80	3.00	6.97	1.392	1.014	0.9066	0.8655	1.108	0.689
80	1.00	0.000	0.80	3.00	7.67	1.392	1.014	0.9243	0.8317	1.085	0.653
81	1.00	0.040	1.00	3.00	4.88	1.491	1.014	0.7843	0.8044	0.944	0.843
82	1.00	0.040	1.00	3.00	5.58	1.491	1.014	0 8442	0.7878	0.998	0.719
83	1.00	0.040	1.00	3.00	6.27	1.491	1.014	0.8815	0.7691	1.019	0.641
84	1.00	0.040	1.00	3.00	6.97	1.491	1.014	0.9066	0.7484	1.021	0.589
85	1.00	0.040	1.00	3.00	7.67	1.491	1.014	0.9243	0.7257	1.010	0.553
86	1.00	0.040	1.25	3.00	4.88	1.580	1.014	0.7843	0.8241	1.025	0.763
87	1.00	0.040	1.25	3.00	5.58	1.580	1.014	0.8442	0.8070	1.083	0.639
88	1.00	0.040	1.25	3.00	6.27	1.580	1.014	0.8515	0.7887	1.108	0.561
89	1.00	0.040	1.25	3.00	6.97	1.580	1.014	0.9066	0.7692	1.112	0.509
90	1.00	0.040	1.25	3.00	7.67	1.580	1.014	0.9243	0.7484	1.104	0.473
91	1.00	0.040	1.50	3.00	4.88	1.646	1.014	0.7762	0.8391	1.087	0.709
92	1.00	0.040	1.50	3.00	5.58	1.646	1.014	0.8379	0.8237	1.152	0.585
93	1.00	0.040	1.50	3.00	6.27	1.646	1.014	0.8766	0.8067	1.180	0.507
94	1.00	0.040	1.50	3.00	6.97	1.646	1.014	0.9026	0.7873	1.186	0.455
95	1.00	0.040	1.50	3.00	7.67	1.646	1.014	0.9210	0.7659	1.177	0.419
96	1.00	0.060	1.00	3.00	4.88	1.491	1.014	0.7721	0.7431	0.867	0.843
97	1.00	0.060	1.00	3.00	5.58	1.491	1.014	0.8347	0.7277	0.918	0.719

(*continued*)

TABLE 6-29 (*Continued*)

Case number	Rod diameter, inches	Clad thickness, inches	Enrichment, a/o	Cooling hole diameter, inches	Lattice pitch, inches	η	ϵ	p	f	k_∞	R_c
98	1.00	0.060	1.00	3.00	6.27	1.491	1.014	0.8741	0.7112	0.940	0 641
99	1.00	0.060	1.00	3.00	6.97	1.491	1.014	0.9005	0.6933	0.944	0.589
100	1.00	0.060	1.00	3.00	7.67	1.491	1.014	0.9192	0.6742	0.937	0.553
101	1.00	0.060	1.25	3.00	4.88	1.580	1.014	0.7721	0.7673	0.949	0.763
102	1.00	0.060	1.25	3.00	5.58	1.580	1.014	0.8347	0 7530	1.007	0.639
103	1.00	0.060	1.25	3.00	6.27	1.580	1.014	0.8741	0.7376	1.033	0.561
104	1.00	0.060	1.25	3.00	6.97	1.580	1.014	0.9005	0.7193	1.038	0.509
105	1.00	0 060	1.25	3.00	7.67	1.580	1.014	0.9192	0.7000	1.031	0.473
106	1.50	0.000	0.714	4.00	6.27	1.339	1.020	0 7439	0.9498	0.965	1.086
107	1.50	0.000	0.714	4.00	6.97	1.339	1.020	0.8024	0.9320	1.021	0.965
108	1.50	0.000	0.714	4.00	7.67	1.339	1.020	0.8423	0.9123	1.049	0.882
109	1.50	0.000	0.714	4.00	8.36	1.339	1.020	0.8709	0.8911	1.060	0.823
110	1.50	0.000	0.714	4.00	9.06	1.339	1.020	0.8923	0.8679	1.058	0.779
111	1.50	0.040	0.80	4.00	6.27	1.392	1.020	0.7370	0.8306	0.869	1.026
112	1.50	0.040	0.80	4.00	6.97	1.392	1.020	0.7967	0.8177	0.925	0.905
113	1.50	0.040	0.80	4.00	7.67	1.392	1.020	0.8375	0.8030	0.956	0.822
114	1.50	0.040	0.80	4.00	8.36	1.392	1.020	0.8669	0.7865	0.968	0.763
115	1.50	0.040	0.80	4.00	9.06	1.392	1.020	0.8888	0.7667	0.967	0.719
116	1.50	0.060	1.00	4.00	6.27	1.491	1.020	0.7334	0.7965	0.888	0.926
117	1.50	0.060	1 00	4 00	6.97	1.491	1.020	0.7937	0.7846	0.947	0.805
118	1.50	0.060	1.00	4.00	7.67	1.491	1.020	0.8351	0.7715	0.980	0.722
119	1.50	0.060	1.00	4.00	8.36	1.491	1.020	0.8648	0.7570	0.996	0.663

120	1.50	0.060	1.00	4.00	9.06	1.491	1.020	0.8870	0.7404	0.999	0.619
121	1.50	0.060	1.50	4.00	6.27	1.646	1.020	0.7334	0.8281	1.020	0.792
122	1.50	0.060	1.50	4.00	6.97	1.646	1.020	0.7937	0.8167	1.088	0.671
123	1.50	0.060	1.50	4.00	7.67	1.646	1.020	0.8351	0.8044	1.128	0.588
124	1.50	0.060	1.50	4 00	8.36	1 646	1.020	0.8648	0.7902	1.147	0.529
125	1.50	0.060	1.50	4.00	9.06	1.646	1.020	0.8870	0.7744	1.153	0.485

(b) Single uranium metal fuel rod, magnesium jacket.

136	1.00	0.00	0.714	4.00	6.27	1.339	1.030	0.8103	0.9382	1.048	0.951
137	1.00	0.00	0.714	4.00	6.97	1.339	1.030	0.8552	0.9160	1 080	0.857
138	1.00	0.00	0.714	4.00	7.67	1.339	1.030	0.8851	0.8926	1.089	0.795
139	1.00	0.00	0.714	4.00	8.36	1.339	1.030	0.9065	0.8679	1.085	0.750
140	1.00	0.00	0.714	4.00	9.06	1.339	1.030	0 9221	0.8406	1.069	0.718
141	1.00	0.32	0.714	4.00	6.27	1.339	1.030	0.8021	0.9336	1.033	0.951
142	1.00	0.32	0.714	4.00	6.97	1.339	1.030	0.8487	0.9128	1.068	0.857
143	1.00	0.32	0.714	4.00	7.67	1.339	1.030	0.8799	0.8900	1.080	0.795
144	1.00	0.32	0.714	4.00	8.36	1.339	1.030	0.9021	0.8646	1.076	0.750
145	1.00	0.32	0.714	4.00	9.06	1.339	1.030	0.9185	0 8370	1.060	0.718
146	1.00	0.32	0.80	4.00	5.58	1 392	1.030	0.7272	0.9517	0.996	0.891
147	1.00	0.32	0.80	4.00	6.27	1.392	1.030	0.8021	0.9365	1.077	0.797
148	1.00	0.32	0.80	4.00	6.97	1.392	1.030	0.8487	0.9165	1.115	0.735
149	1.00	0.32	0.80	4.00	7.67	1.392	1 030	0.8799	0.8945	1.129	0.690
150	1.00	0.32	0.80	4.00	8.36	1.392	1.030	0.9021	0.8702	1.126	0.658
1001	1.15	0.60	0.72	4.00	6.0	1.342	1.032	0.7141	0.9482	0.937	1.103
1002	1.15	0.60	0.72	4.00	7.0	1.342	1.032	0.8046	0.9245	1.030	0.927
1003	1.15	0.60	0.72	4.00	8.0	1.342	1.032	0.8570	0.8971	1.065	0.825
1004	1.15	0.60	0.72	4.00	9.0	1.342	1.032	0.8904	0.8666	1.068	0.761
1005	1.15	0.60	0.72	4.00	10.0	1.342	1.032	0.9130	0.8329	1.053	0.717

(continued)

TABLE 6–29 (*Continued*)

Case number	Rod diameter, inches	Clad thickness, inches	Enrichment, a/o	Cooling hole diameter, inches	Lattice pitch, inches	η	ϵ	p	f	k_∞	R_c
1006	1.15	0.60	0.80	4.00	6.0	1.392	1.032	0.7141	0.9499	0.975	1.048
1007	1.15	0.60	0.80	4.00	7.0	1.392	1.032	0.8046	0.9262	1.071	0.872
1008	1.15	0.60	0.80	4.00	8.0	1.392	1.032	0.8570	0.8990	1.107	0.770
1009	1.15	0.60	0.80	4.00	9.0	1.392	1.032	0.8904	0.8690	1.112	0.706
1010	1.15	0.60	0.80	4.00	10.0	1.392	1.032	0.9130	0.8369	1.098	0.662
1011	1.15	0.60	1.00	4.00	5.0	1.491	1.032	0.5334	0.9710	0.797	1.305
1012	1.15	0.60	1.00	4.00	6.0	1.491	1.032	0.7141	0.9535	1.048	0.948
1013	1.15	0.60	1.00	4.00	7.0	1.491	1.032	0.8046	0.9313	1.153	0.772
1014	1.15	0.60	1.00	4.00	8.0	1.491	1.032	0.8570	0.9065	1.195	0.670
1015	1.15	0.60	1.00	4.00	9.0	1.491	1.032	0.8904	0.8766	1.201	0.606
1016	1.15	0.60	1.25	4.00	5.0	1.580	1.032	0.5334	0.9730	0.846	1.225
1017	1.15	0.60	1.25	4.00	6.0	1.580	1.032	0.7141	0.9530	1.110	0.868
1018	1.15	0.60	1.25	4.00	7.0	1.580	1.032	0.8046	0.9310	1.222	0.692
1019	1.15	0.60	1.25	4.00	8.0	1.580	1.032	0.8570	0.9078	1.269	0.590
1020	1.15	0.60	1.25	4.00	9.0	1.580	1.032	0.8904	0.8828	1.282	0.526
1021	1.15	0.60	1.50	4 00	5.0	1.646	1.032	0.5334	0.9744	0.883	1.171
1022	1.15	0.60	1.50	4.00	6.0	1.646	1.032	0.7141	0.9571	1.162	0.814
1023	1.15	0.60	1.50	4.00	7.0	1.646	1.032	0.8046	0.9372	1.281	0.638
1024	1.15	0.60	1.50	4.00	8.0	1.646	1.032	0.8578	0.9135	1.330	0.536
1025	1.15	0.60	1.50	4.00	9.0	1.646	1.032	0.8904	0.8872	1.342	0.472

(c) Seven-rod clusters of UO_2 fuel rods, type-430 stainless steel jacket.

181	0.50	0.000	0.714	3.25	5.0	1.339	1.016	0.6126	0.9692	0.808	1.358
182	0.50	0.000	0.714	3.25	6.0	1.339	1.016	0.7413	0.9442	0.952	1.092
183	0.50	0.000	0.714	3.25	7.0	1.339	1.016	0.8147	0.9195	1.019	0.940
184	0.50	0.000	0.714	3.25	8.0	1.339	1.016	0.8605	0.8945	1.047	0.845
185	0.50	0.000	0.80	3.25	5.0	1.392	1.016	0.6126	0.9709	0.841	1.298
186	0.50	0.000	0.80	3.25	6.0	1.392	1.016	0.7413	0.9470	0.993	1.032
187	0.50	0.000	0.80	3.25	7.0	1.392	1 016	0.8147	0.9232	1.064	0.880
188	0.50	0.000	0.80	3.25	8.0	1.392	1.016	0.8605	0.8994	1.095	0.785
189	0.50	0.020	1.25	3.25	5.0	1.580	1.016	0.6046	0.8603	0.835	1.118
190	0.50	0.020	1.25	3.25	6.0	1.580	1.016	0.7349	0.8453	0.997	0.852
191	0.50	0.020	1.25	3.25	7.0	1.580	1.016	0.8096	0.8294	1.078	0.700
192	0.50	0.020	1.25	3.25	8.0	1.580	1.016	0.8565	0 8120	1.116	0.605
276	0.50	0.020	1.25	2.50	5.0	1.580	1.016	0.6749	0.8509	0.922	0.970
277	0.50	0.020	1.25	2.50	6.0	1.580	1.016	0.7734	0 8342	1.035	0.771
278	0.50	0.020	1.25	2.50	7.0	1.580	1.016	0.8334	0.8160	1.091	0.650
279	0.50	0.020	1.25	2.50	8.0	1.580	1.016	0.8724	0.7960	1.114	0.572
280	0.50	0.020	1.25	2.50	9.0	1.580	1.016	0.8992	0.7754	1.119	0.518
281	0.50	0.020	1.25	2.50	10.0	1.580	1.016	0.9183	0.7532	1.110	0.480
282	0.50	0.020	1.50	2.50	5.0	1.646	1.016	0.6749	0.8665	0.978	0.916
283	0.50	0.020	1.50	2.50	6.0	1.646	1 016	0.7734	0.8500	1.099	0.717
284	0.50	0.020	1.50	2.50	7.0	1.646	1.016	0.8334	0.8323	1.160	0.596
285	0.50	0.020	1.50	2.50	8.0	1.646	1.016	0.8724	0.8135	1.187	0.518
286	0.50	0.020	1.50	2.50	9.0	1.646	1.016	0.8992	0.7932	1.192	0.464
287	0.50	0.020	1.50	2.50	10.0	1.646	1.016	0.9183	0.7723	1.186	0.426
288	0.50	0.020	2.00	2.50	5.0	1.737	1.016	0.6749	0.8891	1.059	0.850
289	0.50	0.020	2.00	2.50	6.0	1.737	1.016	0.7734	0.8740	1.193	0.651
290	0.50	0.020	2.00	2.50	7.0	1.737	1.016	0.8334	0.8573	1.261	0.530

(*continued*)

TABLE 6–29 (*Continued*)

Case number	Rod diameter, inches	Clad thickness, inches	Enrichment, a/o	Cooling hole diameter, inches	Lattice pitch, inches	η	ϵ	p	f	k_∞	R_c
291	0.50	0.020	2 00	2.50	8.0	1.737	1.016	0.8724	0.8395	1.293	0.452
292	0.50	0.020	2.00	2.50	9.0	1.737	1.016	0.8992	0.8202	1.302	0.398
293	0.50	0.020	2.00	2.50	10.0	1.737	1.016	0.9183	0.8003	1.297	0.360
153	0.75	0.000	0.714	3.25	6.0	1.339	1 024	0.6064	0.9716	0.808	1.371
154	0.75	0.000	0 714	3.25	7.0	1.339	1.024	0.7077	0.9540	0.926	1.161
155	0.75	0.000	0.714	3.25	8.0	1.339	1.024	0 7755	0.9360	0.995	1.021
156	0.75	0.000	0.714	3.25	9.0	1.339	1.024	0.8222	0.9186	1.036	0.924
157	0.75	0.000	0.80	3.25	6.0	1.392	1.024	0.6064	0.9728	0.841	1.311
158	0.75	0.000	0.80	3.25	7.0	1.392	1.024	0.7077	0.9556	0.964	1.101
159	0.75	0.000	0.80	3.25	8.0	1 392	1.024	0.7555	0.9386	1 038	0.961
160	0.75	0.000	0 80	3.25	9.0	1.392	1.024	0.8222	0.9216	1.080	0.864
161	0.75	0.000	1.25	3.25	6.0	1.580	1 024	0.6064	0.9774	0.959	1.131
162	0.75	0.000	1.25	3.25	7.0	1.580	1.024	0.7077	0.9642	1.104	0.921
163	0.75	0.000	1.25	3.25	8.0	1.580	1.024	0.7755	0.9500	1.192	0.781
164	0.75	0.000	1.25	3.25	9.0	1.580	1.024	0.8222	0.9325	1.241	0.684
165	0.75	0.000	1.50	3 25	6.0	1.646	1.024	0.6064	0.9790	1.001	1.077
166	0.75	0 000	1 50	3.25	7.0	1.646	1.024	0.7077	0.9675	1.154	0.867
167	0.75	0.000	1 50	3.25	8.0	1.646	1.024	0.7755	0.9550	1.248	0.727
168	0.75	0.000	1.50	3 25	9.0	1.646	1.024	0 8222	0.9385	1.301	0.630
211	0.75	0.020	1.00	3.25	6.0	1.491	1.024	0.5995	0.8780	0.804	1.211
212	0.75	0.020	1.00	3.25	7.0	1.491	1.024	0.7021	0.8650	0.927	1.001
213	0.75	0.020	1.00	3.25	8.0	1.491	1.024	0.7704	0.8517	1.002	0.861

214	0.75	0.020	1.00	3.25	9.0	1 491	1.024	0.8179	0.8372	1.046	0.764
215	0.75	0.020	1.00	3.25	10.0	1.491	1.024	0.8522	0.8206	1.068	0.693
216	0.75	0.020	1.00	3.25	11.0	1.491	1.024	0.8777	0.8000	1.072	0.648
169	0.75	0.020	1.25	3.25	6.0	1.580	1.024	0.5995	0.8947	0.868	1.131
170	0.75	0.020	1.25	3.25	7.0	1.580	1.024	0.7021	0.8836	1.004	0.921
171	0.75	0 020	1 25	3.25	8.0	1.580	1 024	0.7704	0.8705	1 085	0.781
172	0.75	0.020	1.25	3 25	9.0	1.580	1.024	0.8179	0.8551	1.132	0.684
209(a)	0.75	0.020	1.25	3.25	10.0	1.580	1.024	0 8522	0.8370	1.154	0.613
209	0.75	0.020	1 25	3.25	11.0	1.580	1.024	0.8777	0.8175	1.161	0.568
173	0.75	0.020	1.50	3.25	6.0	1.646	1 024	0.5995	0.9053	0.915	1.077
174	0.75	0.020	1.50	3.25	7.0	1.646	1.024	0.7021	0 8942	1 058	0.867
175	0.75	0.020	1.50	3.25	8.0	1.646	1.024	0.7704	0.8820	1.145	0.727
176	0.75	0.020	1.50	3.25	9.0	1.646	1.024	0.8179	0.8675	1.196	0.630
210(a)	0.75	0.020	1.50	3 25	10.0	1.646	1.024	0.8522	0.8500	1 221	0.559
210	0.75	0.020	1.50	3.25	11.0	1.646	1.024	0.8777	0.8308	1.229	0.514
270	0.75	0.020	2.00	3.25	6.0	1.737	1.024	0.5995	0.9203	0.981	1.011
271	0.75	0.020	2.00	3.25	7.0	1.737	1.024	0.7021	0.9091	1 135	0.801
272	0.75	0.020	2.00	3.25	8.0	1.737	1.024	0.7704	0.8960	1.228	0.661
273	0.75	0.020	2.00	3.25	9.0	1.737	1.024	0.8179	0.8817	1.283	0.564
274	0.75	0.020	2.00	3.25	10.0	1.737	1 024	0.8522	0.8662	1.313	0.493
275	0.75	0.020	2.00	3.25	11.0	1.737	1.024	0.8777	0.8497	1.326	0.448
294	1.00	0.020	1.25	4.00	8.0	1.580	1.028	0.6428	0 9039	0.944	1.055
295	1.00	0.020	1.25	4.00	9.0	1.580	1.028	0.7147	0.8915	1.035	0.907
296	1.00	0.020	1.25	4.00	10.0	1.580	1.028	0.7674	0.8776	1.094	0.797
297	1.00	0.020	1.25	4.00	11.0	1.580	1.028	0.8068	0.8625	1.130	0.716
298	1.00	0.020	1.25	4.00	12.0	1.580	1.028	0.8371	0.8465	1.151	0.653
299	1.00	0.020	1.25	4.00	13.0	1.580	1.028	0.8609	0.8300	1.160	0.604
300	1.00	0.020	1.50	4.00	8.0	1.646	1.028	0.6428	0.9125	0.992	1.001
301	1.00	0.020	1.50	4.00	9.0	1.646	1.028	0.7147	0.9012	1.090	0.853

(*continued*)

TABLE 6–29 (*Continued*)

Case number	Rod diameter, inches	Clad thickness, inches	Enrichment, a/o	Cooling hole diameter, inches	Lattice pitch, inches	η	ϵ	p	f	k_∞	R_c
302	1.00	0.020	1.50	4.00	10.0	1.646	1.028	0.7674	0.8882	1.153	0.743
303	1.00	0.020	1.50	4.00	11.0	1.646	1.028	0.8068	0.8737	1.192	0.662
304	1.00	0.020	1.50	4.00	12.0	1.646	1.028	0.8371	0.8577	1.215	0.599
305	1.00	0.020	1.50	4.00	13.0	1.646	1.028	0.8609	0.8404	1.224	0.550
306	1.00	0.020	2.00	4.00	8.0	1.737	1.028	0.6428	0.9252	1.062	0.935
307	1.00	0.020	2.00	4.00	9.0	1.737	1.028	0.7147	0.9142	1.167	0.787
308	1.00	0.020	2.00	4.00	10.0	1.737	1.028	0.7674	0.9020	1.236	0.677
309	1.00	0.020	2.00	4.00	11.0	1.737	1.028	0.8068	0.8885	1.280	0.596
310	1.00	0.020	2.00	4.00	12.0	1.737	1.028	0.8371	0.8732	1.306	0.533
311	1.00	0.020	2.00	4.00	13.0	1.737	1.028	0.8609	0.8570	1.318	0.484
II. Moderator temperature = 750°F (neutron temperature = 814°K)											
(a) Seven-rod clusters of UO_2 fuel rods, type-430 stainless steel jacket.											
342	0.50	0.018	1.25	2.50	5.0	1.539	1.016	0.6531	0.8639	0.882	1.064
343	0.50	0.018	1.25	2.50	6.0	1.539	1.016	0.7570	0.8502	1.006	0.849
344	0.50	0.018	1.25	2.50	7.0	1.539	1.016	0.8208	0.8356	1.072	0.717
345	0.50	0.018	1.25	2.50	8.0	1.539	1.016	0.8625	0.8200	1.106	0.630
346	0.50	0.018	1.25	2.50	9.0	1.539	1.016	0.8912	0.8028	1.119	0.571
347	0.50	0.018	1.25	2.50	10.0	1.539	1.016	0.9118	0.7847	1.119	0.529
348	0.50	0.018	1.50	2.50	5.0	1.609	1.016	0.6531	0.8783	0.938	1.006

349	0.50	0.018	1.50	2.50	6.0	1.609	1.016	0.7570	0.8655	1.071	0.791
350	0.50	0.018	1.50	2.50	7.0	1.609	1.016	0.8208	0.8518	1.143	0.659
351	0.50	0.018	1.50	2.50	8.0	1.609	1.016	0.8625	0.8370	1.180	0.572
352	0.50	0.018	1.50	2.50	9.0	1.609	1.016	0.8912	0.8204	1.195	0.513
353	0.50	0.018	1.50	2.50	10.0	1.609	1.016	0.9118	0.8025	1.196	0.471
354	0.50	0.018	2.00	2.50	5.0	1.706	1.016	0.6531	0.8994	1.018	0.933
355	0.50	0.018	2.00	2.50	6.0	1.706	1.016	0.7570	0.8875	1.165	0.718
356	0.50	0.018	2.00	2.50	7.0	1.706	1.016	0.8208	0.8746	1.244	0.586
357	0.50	0.018	2.00	2.50	8.0	1.706	1.016	0.8625	0.8610	1.287	0.499
358	0.50	0.018	2.00	2.50	9.0	1.706	1.016	0.8912	0.8456	1.306	0.440
359	0.50	0.018	2.00	2.50	10.0	1.706	1.016	0.9118	0.8289	1.310	0.398
384	0.50	0.018	2.50	2.50	5.0	1.770	1.016	0.6531	0.9140	1.074	0.889
385	0.50	0.018	2.50	2.50	6.0	1.770	1.016	0.7570	0.9033	1.230	0.674
386	0.50	0.018	2.50	2.50	7.0	1.770	1.016	0.8208	0.8914	1.316	0.542
387	0.50	0.018	2.50	2.50	8.0	1.770	1.016	0.8625	0.8780	1.362	0.455
388	0.50	0.018	2.50	2.50	9.0	1.770	1.016	0.8912	0.8635	1.384	0.396
389	0.50	0.018	2.50	2.50	10.0	1.770	1.016	0.9118	0.8478	1.390	0.354
248	0.75	0.018	1.20	3.25	6.0	1.522	1.024	0.5657	0.9037	0.797	1.260
249	0.75	0.018	1.20	3.25	7.0	1.522	1.024	0.6744	0.8936	0.940	1.035
250	0.75	0.018	1.20	3.25	8.0	1.522	1.024	0.7486	0.8837	1.031	0.881
251	0.75	0.018	1.20	3.25	9.0	1.522	1.024	0.8001	0.8723	1.088	0.775
252	0.75	0.018	1.20	3.25	10.0	1.522	1.024	0.8377	0.8591	1.122	0.697
253	0.75	0.018	1.20	3.25	11.0	1.522	1.024	0.8655	0.8438	1.138	0.639
230	0.75	0.018	1.25	3.25	6.0	1.539	1.024	0.5657	0.9059	0.808	1.245
231	0.75	0.018	1.25	3.25	7.0	1.539	1.024	0.6744	0.8961	0.953	1.020
232	0.75	0.018	1.25	3.25	8.0	1.539	1.024	0.7486	0.8858	1.045	0.866
233	0.75	0.018	1.25	3.25	9.0	1.539	1.024	0.8001	0.8748	1.103	0.760
234	0.75	0.018	1.25	3.25	10.0	1.539	1.024	0.8377	0.8622	1.138	0.682
235	0.75	0.018	1.25	3.25	11.0	1.539	1.024	0.8655	0.8466	1.155	0.624

(*continued*)

TABLE 6–29 (*Continued*)

Case number	Rod diameter, inches	Clad thickness, inches	Enrichment, a /o	Cooling hole diameter, inches	Lattice pitch, inches	η	ϵ	p	f	k_∞	R_c
236	0.75	0.018	1.375	3.25	6.0	1.576	1.024	0.5657	0.9109	0.832	1.214
237	0.75	0.018	1.375	3.25	7.0	1.576	1.024	0.6744	0.9016	0.982	0.989
238	0.75	0.018	1.375	3.25	8.0	1.576	1.024	0 7486	0.8913	1.077	0.835
239	0.75	0.018	1.375	3.25	9.0	1.576	1.024	0.8001	0.8797	1.135	0.729
240	0.75	0.018	1.375	3.25	10.0	1.576	1.024	0.8377	0.8667	1.172	0.651
241	0.75	0.018	1.375	3.25	11.0	1.576	1.024	0.8655	0.8530	1.192	0.593
242	0.75	0.018	1.50	3.25	6 0	1.609	1.024	0.5657	0.9160	0.854	1.187
243	0.75	0.018	1.50	3.25	7.0	1.609	1.024	0.6744	0.9067	1.008	0.962
244	0.75	0.018	1.50	3.25	8.0	1.609	1.024	0.7486	0.8972	1.107	0.808
245	0.75	0.018	1.50	3.25	9.0	1.609	1.024	0.8001	0.8866	1.169	0.702
246	0.75	0.018	1.50	3.25	10.0	1.609	1.024	0.8377	0.8744	1.207	0.624
247	0.75	0.018	1.50	3.25	11.0	1.609	1 024	0.8655	0.8595	1.226	0.566
336	0.75	0.018	2.00	3.25	6.0	1.706	1.024	0.5657	0.9290	0.918	1.114
337	0.75	0.018	2.00	3.25	7.0	1.706	1 024	0.6744	0.9205	1.084	0.889
338	0.75	0.018	2.00	3.25	8.0	1.706	1.024	0.7486	0.9115	1.192	0.735
339	0.75	0.018	2.00	3.25	9.0	1.706	1.024	0.8001	0.9015	1.261	0.629
340	0.75	0.018	2.00	3.25	10.0	1.706	1.024	0.8377	0.8900	1.302	0.551
341	0.75	0.018	2.00	3.25	11.0	1.706	1.024	0.8655	0.8771	1.326	0.493
378	0.75	0.018	2.50	3.25	6.0	1.770	1.024	0.5657	0.9391	0.963	1.070
379	0.75	0.018	2.50	3.25	7.0	1.770	1.024	0.6744	0.9312	1.138	0.845
380	0.75	0.018	2.50	3.25	8.0	1.770	1.024	0.7486	0.9226	1.251	0.691
381	0.75	0.018	2.50	3.25	9.0	1.770	1.024	0.8001	0.9133	1.325	0.585

382	0.75	0.018	2.50	3.25	10.0	1.770	1.024	0 8377	0.9025	1.370	0.507
383	0.75	0.018	2.50	3.25	11 0	1.770	1 024	0 8655	0.8901	1.396	0.449
360	1.00	0.018	1.25	4.00	8.0	1.539	1.028	0.6091	0.9174	0.884	1.155
361	1.00	0.018	1.25	4.00	9 0	1.539	1.028	0.6861	0.9087	0.986	0 996
362	1.00	0.018	1.25	4.00	10.0	1.539	1 028	0.7430	0.8993	1.057	0.878
363	1.00	0.018	1.25	4.00	11.0	1.539	1.028	0.7860	0.8890	1.106	0.789
364	1.00	0.018	1.25	4.00	12.0	1.539	1.028	0.8192	0.8770	1.137	0.720
365	1.00	0.018	1.25	4.00	13.0	1.539	1 028	0.8454	0.8634	1.155	0.666
366	1.00	0.018	1.50	4.00	8.0	1.609	1 028	0.6091	0.9255	0.932	1.097
367	1.00	0.018	1.50	4.00	9.0	1.609	1 028	0.6861	0 9170	1.041	0.938
368	1.00	0.018	1.50	4.00	10 0	1 609	1.028	0.7430	0.9082	1.116	0.820
369	1.00	0.018	1.50	4.00	11 0	1.609	1.028	0.7860	0.8980	1.168	0.731
370	1.00	0.018	1.50	4 00	12.0	1.609	1.028	0.8192	0.8866	1.201	0.662
371	1.00	0.018	1.50	4.00	13 0	1.609	1.028	0.8454	0.8731	1.221	0.608
372	1.00	0.018	2.00	4.00	8.0	1.706	1.028	0.6091	0.9369	1.001	1.024
373	1 00	0.018	2.00	4.00	9 0	1.706	1.028	0.6861	0.9288	1.118	0.865
374	1.00	0.018	2.00	4.00	10.0	1 706	1.028	0.7430	0.9200	1.199	0.747
375	1.00	0.018	2.00	4.00	11.0	1.706	1.028	0.7860	0.9100	1.254	0.658
376	1.00	0.018	2.00	4.00	12.0	1 706	1.028	0.8192	0.8991	1.292	0.589
377	1.00	0.018	2.00	4.00	13.0	1.706	1.028	0.8454	0.8867	1.315	0.535
390	1.00	0.018	2.50	4.00	8.0	1 770	1.028	0.6091	0.9439	1.046	0.980
391	1.00	0.018	2.50	4.00	9.0	1.770	1.028	0.6861	0.9361	1 169	0.821
392	1.00	0.018	2.50	4.00	10.0	1.770	1.028	0.7430	0.9275	1.254	0.703
393	1.00	0.018	2.50	4.00	11.0	1.770	1.028	0.7860	0.9178	1.313	0.614
394	1.00	0.018	2.50	4.00	12.0	1.770	1.028	0.8192	0.9066	1.351	0.545
395	1.00	0.018	2.50	4.00	13.0	1.770	1.028	0.8454	0.8930	1.374	0.491

(concluded)

TABLE 6-30

DESIGN AND PERFORMANCE CHARACTERISTICS OF THE NATURAL URANIUM GAS-COOLED POWER REACTOR (GCPR)

	Prototype	Optimum
General characteristics		
Reactor thermal output, Mw	180	700
Gross electrical output, Mw	64	253
Net electrical output, Mw	55	220
Net thermal efficiency, %	30.6	31.4
Reactor core		
Coolant material	CO_2	CO_2
Moderating material	Graphite, grade TSF	Graphite, grade AGOT
Nominal core diameter, ft	35	50
Nominal core height, ft	25	29
Machined weight of graphite, tons	1000	2440
Graphite density, g/cm^3	1.70	1.70
Number of fuel channels	1532	3536
Channel spacing	Square	Square
Channel pitch, in.	8	8
Diameter of fuel channels, in.	4.50	4.50
Fuel		
Composition	U metal*	U metal*
U^{235} enrichment, a/o	0.71	0.71
Total weight of uranium, metric tons	97.5	274
Average burnup, Mwd/metric ton	1500–3000*	1500–3000*
Fuel element assembly (preferred)		
Fuel slug:		
Geometry	Cored metal rod	Cored metal rod
Outside diameter, in.	1.160	1.160
Inside diameter, in.	0.375	0.375
Length, in.	24.00	24.00
Fuel slugs per element cluster	1	1
Fuel jacket:		
Geometry	Helically finned tube	Helically finned tube
Material	Magnox A-12	Magnox A-12
Outside diameter, in.	1.27	1.27
Wall thickness, in.	0.05	0.05
Length (excluding end caps), in.	24.40	24.40
Fin tip diameter, in.	2.25	2.25

	Prototype	Optimum
Assembly container:		
Geometry	Open-ended sleeve	Open-ended sleeve
Material	Graphite	Graphite
Inside diameter, in.	2.50	2.50
Outside diameter, in.	4.25	4.25
Length, in.	26.4	26.4
Assemblies per channel	9 with dummy sleeves each end	11 with dummy sleeves, each end
Channel diameter, in.	4.50	4.50
Biological shield		
Material	Reinforced concrete	Reinforced concrete
Vertical side thickness, ft	9.5	9.5
Top and bottom slab thickness, ft	10.5	10.5
Density, lb/ft^3	~145	~145
Shape	Octagonal	Octagonal
Shield cooling	Forced air	
Control mechanisms		
Control rods:		
Geometry	Tubes	Tubes
Material	Borated steel	Borated steel
Composition, w/o B	1.5	1.5
Shim rods:		
Number	77	97
Total worth, % $\Delta k/k$	9.0	
Regulating rods:		
Number	3	3
Total worth, % $\Delta k/k$	<0.5	
Control channels:		
Diameter	3.25	3.25
Number	97	221
Lattice type	Square	Square
Lattice spacing, in.	32	32
Rod drives:		
Rod suspension	SS cable	SS cable
Drive, operating	AC motor, winch	AC motor, winch
Drive, scram	Gravity	Gravity
Reactor vessel		
Shape	Cylindrical, hemispherical heads	Spherical

(*continued*)

	Prototype	Optimum
Material	Carbon steel SA 212-B	Carbon steel SA 212-B
Dimensions:		
Inside diameter, ft	36	70
Wall thickness, in.	4	4
Height, over-all, ft	65	70
Maximum design pressure	300	300
Maximum design temperature, °F	650	650
Reactor coolant		
Coolant material	CO_2	CO_2
Outlet pressure	285	275
Total flow, lb/hr	6.04×10^6	24×10^6
Inlet temperature, °F	409	413
Outlet temperature, °F	700–800*	750–800*
Number of inlet pipes	2	8
Number of outlet pipes	2	8
Pipe inside diameter, ft	4	4
Circuit pressure drop, psi	12	17
Coolant blowers:		
Type	Motor driven, axial flow	Motor driven, axial flow
Number	2	8
Total electrical pumping power, Mw	4.4	24.6
Steam generator		
Type	Dual-pressure, reheat	Dual-pressure, reheat
Number	2	8
Steam conditions at high pressure outlet:		
Temperature, °F	750	750
Pressure, psia	1480	1480
Steam conditions at reheater outlet:		
Temperature, °F	750	750
Pressure, psia	315	315
Steam conditions at low pressure outlet.		
Temperature, °F	750	750
Pressure, psia	315	315
Gas inlet conditions:		
Temperature, °F	800	800
Pressure, psia	280	275

(*continued*)

	Prototype	Optimum
Gas outlet conditions:		
Temperature, °F	400	400
Pressure, psia	275	270
Feedwater temperature, °F	260	260
Thermal performance		
Steam cycle heat rate, Btu/kwh	9800	9680
Reactor thermal power, Mw	180	700
Average reactor specific power, Mw/metric ton	1.85	255
Maximum uranium, center temperature, °F	1200	1200
Maximum uranium surface, temperature, °F	929	900
Reactor coolant flow, lb/hr	6×10^6	24×10^6

Physics†

Temperature	Room	Operating	Room	Operating
Thermal utilization, f	0.9126	0.9218 (clean) 0.8997 (poisoned)	0.8973	0.9082 (clean) 0.8830 (poisoned)
Resonance escape probability, p	0.8807	0.8740	0.8807	0.8735
Fast fission factor, ϵ	1.0283	1.0283	1.0283	1.0283
Thermal regeneration factor, η	1.3359	1.3049	1.3359	1.3049
Infinite multiplication factor, k	1.1041	1.0810 (clean) 1 0551 (poisoned)	1.0856	1.0645 (clean) 1.0345 (poisoned)
Perpendicular diffusion area, $L_\perp^2$, cm^2	435.2	532.4	428.0	524.4
Parallel diffusion area, $L_\parallel^2$, cm^2	510.2	624.1	501.7	614.7
Perpendicular slowing-down area, $\tau_\perp$, cm^2	496.5	496.5	496.5	496.5
Parallel slowing-down area, $\tau_\parallel$, cm^2	568.6	568.6	568.6	568.6
Perpendicular geometric buckling, $B_\perp^2$, cm$^{-2} \times 10^4$	0.2213	0.2213	0.1035	0.1035
Parallel geometric buckling, $B_\parallel^2$, cm$^{-2} \times 10^4$	0.1917	0.1917	0.1400	0.1400
Initial effective multiplication factor, k_{eff}	1.0596	1.0330 (clean) 1.0083 (poisoned)	1.0594	1.0362 (clean) 1.0074 (poisoned)

(continued)

	Prototype	Optimum
Equilibrium xenon poisoning, % Δk	−1.77	−2.18
Equilibrium samarium poisoning, % Δk	−0.70	−0.70
Total temperature effect, % Δk	−2.66	−2.32
Thermal flux, n/(cm^2)(sec):		
Average in total core	1.1×10^{13}	1.4×10^{13}
Maximum	2.4×10^{13}	3.1×10^{13}

*Single-region U metal-Magnox rod cores limited to 1500 Mwd/ton at 800°F or 750°F at 3000 Mwd/ton. Alternate two-region core also proposed; natural U in UO_2 with stainless steel cladding for inner region and U metal with Magnox A-12 cladding for outer region to permit 3000 Mwd/ton at 800°F.

†Based on longitudinally finned fuel-element loading for optimum reactor and helically finned fuel-element loading for prototype reactor. Substitution of helical finns in optimum case does not yield a significant difference in results.

TABLE 6–31

DESIGN AND PERFORMANCE CHARACTERISTICS OF THE ENRICHED URANIUM, GAS-COOLED POWER REACTOR (GCPR)

	Prototype	Optimum
General characteristics		
Reactor thermal output, Mw	125	600
Gross electrical output, Mw	51	253
Net electrical output, Mw	44	215
Net thermal efficiency, %	35.3	35.8
Reactor core		
Coolant material	CO_2	CO_2
Moderating material	Graphite, grade AGOT	Graphite, grade AGOT
Nominal core diameter, ft	16	24
Nominal core height, ft	18.5	26
Machined weight of graphite, tons	170	500
Graphite density, g/cm^3	1.70	1.70
Number of fuel channels	344	980
Channel spacing	Square	Square
Channel pitch, in.	7	7
Diameter of fuel channels, in.	4.00	4.00
Fuel		
Composition	UO_2	UO_2
U^{235} enrichment, a/o	3.0	2.5
Total weight of uranium, metric tons	18.0	77
Average burnup, Mwd/metric ton	10,000	10,000
Fuel assembly (preferred)		
Fuel pellet:		
Geometry	Cored and sintered UO_2 pellets	Cored and sintered UO_2 pellets
Number per fuel rod	35	35
Length, in.	0.70	0.70
Outside diameter, in.	0.75	0.75
Inside diameter, in.	0.32	0.32
Fuel rod end-spacers:		
Function	Thermal insulation	Thermal insulation
Geometry	Sintered MgO pellets, one each end	Sintered MgO pellets, one each end
Length, in.	0.19	0.19
Diameter, in.	0.75	0.75

(*continued*)

	Prototype	Optimum
Fuel rods per element-cluster	7	7
Fuel jacket or can:		
Geometry	Finless tubes, end-capped	Finless tubes, end-capped
Material	Stainless steel, type 304	Stainless steel, type 304
Inside diameter, in.	0.75	0.75
Wall thickness, in.	0.020	0.020
Length (excluding end caps), in.	27.5	27.5
Assembly support spider (upper and lower):		
Function	Positioning of fuel rods in cluster	Positioning of fuel rods in cluster
Material	Stainless steel, type 304	Stainless steel, type 304
Graphite support sleeve:		
Function	Cluster container	Cluster container
Geometry	Hollow cylinder	Hollow cylinder
Length, in.	29.0	29.0
Outside diameter, in.	3.75	3.75
Wall thickness, in.	0.375	0.375
Assemblies per fuel channel	6	9
Biological shield		
Material	Reinforced concrete	Reinforced concrete
Vertical side thickness, ft	10 (minimum)	10 (minimum)
Top and bottom slab thickness, ft	10 (minimum)	10 (minimum)
Density, lb/ft^3	~145	~145
Shape	Octagonal	Octagonal
Control mechanisms		
Control rods:		
Geometry	Tubes	Tubes
Material	Borated steel	Borated steel
Composition, w/o B	1.5	1.5
Number of shim rods	21	37
Number of regulating rods	3	3
Rod drives:		
Rod suspension	SS cable	SS cable
Drive, operating	AC motor, winch	AC motor, winch
Drive, scram	Gravity	Gravity

(*continued*)

	Prototype	Optimum
Reactor vessel		
Shape	Cylindrical, hemispherical heads	Cylindrical, hemispherical heads
Material	Carbon steel SA 212-B	Carbon steel SA 212-B
Dimensions.		
Inside diameter, ft	18	27
Wall thickness, in.	3	4
Height, over-all, ft	26	57
Maximum design pressure, psi	418	400
Maximum design temperature, °F	650	650
Reactor coolant		
Coolant material	CO_2	CO_2
Outlet pressure	387	370
Total flow, lb/hr	2.9×10^6	14×10^6
Inlet temperature, °F	463	473
Outlet temperature, °F	1000	1000
Number of inlet pipes	2	6
Number of outlet pipes	2	6
Pipe inside diameter, ft	2.5	3
Circuit pressure drop, psi	23	40
Coolant blowers:		
Type	Motor-driven, axial flow	Motor-driven, axial flow
Number	2	6
Total electrical pumping power, Mw	3.2	28
Steam generator		
Type	Dual-pressure, reheat	Dual-pressure, reheat
Number	2	6
Steam conditions:	°F psia	°F psia
At high-pressure outlet	950 2430	950 2430
At reheater outlet	950 780	950 780
At low-pressure outlet	950 780	950 780
Gas inlet	1000 385	1000 368
Gas outlet	450 380	450 363
Feedwater temperature	307	307

(*continued*)

	Prototype	Optimum
Thermal performance		
Steam cycle heat rate, Btu/kwh	8500	8420
Reactor thermal power, Mw	125	600
Average reactor specific power, Mw/metric ton	6.9	7.9
Maximum fuel cladding temperature, °F	1300	1300
Reactor coolant flow, lb/hr	2.9×10^6	14×10^6
Physics		
Temperature	Operating	Operating
Infinite multiplication factor, k_∞	1.2345 (clean)	1.1728 (clean)
	1.2011 (poisoned)	1.1370 (poisoned)
Initial conversion ratio, I.C.R.	0.635	0.68
Effective multiplication factor, k_{eff}	1.1365 (clean)	1.1216 (clean)
	1.1057 (poisoned)	1.0922 (poisoned)
Thermal flux:		
Average in total core, n/(cm^2)(sec)	0.9×10^{13}	1.7×10^{13}
Maximum, n/(cm^2)(sec)	1.7×10^{13}	4.3×10^{13}
Estimated fuel lifetime, Mwd/metric ton	10,000	10,000

TABLE 6–32

DESIGN AND PERFORMANCE CHARACTERISTICS OF THE OAK RIDGE NATIONAL LABORATORY GAS-COOLED REACTOR

General characteristics	
Reactor thermal output, Mw	700
Gross electrical output, Mw	252
Net electrical output, Mw	225
Net over-all efficiency, %	32.1
Reactor core	
Moderating material	Graphite, grade TSF
Nominal core diameter, ft	30
Nominal core height, ft	20
Height of graphite, ft	25
Distance across corners of graphite, ft	35
Machined weight of graphite, tons	1122
Graphite density, g/cm^3	1.65
Graphite block dimensions:	
Length, in.	40
Width, in.	8
Depth, in.	8
Total graphite volume, ft^3	21,784
Number of fuel channels	1,597
Number of fuel charge tubes	69
Channel lattice	Square
Channel pitch, in.	8
Diameter of fuel channels, in.	345 at 3.45; 400 at 3.25; 852 at 3.05
Fuel	
Composition	UO_2
U^{235} enrichment, a/o	2.0
Total weight of uranium, metric tons	137
Average burnup, Mwd/metric ton	7350
Average UO^2 density, g/cm^3	10.4

	Fuel slug	*Fuel capsule*	*Fuel Assembly*
Material	UO_2	Stainless steel, 304	—
Outside diameter, in.	0.75 ± 0.005	0.80	—
Inside diameter, in.	0.32 ± 0.010	0.78	—
Length, in.	0.50 ± 0.003	3.85	40 (nominal)
Comments	75 slugs stacked in one capsule.	7 capsules in radial array in assembly; 67,074 total	9,582 total

(*continued*)

Control rods

Number	61
Material	Silver
Dimensions:	
Outside diameter, in.	2.00
Inside diameter, in.	1.25
Length, ft	18
Sheath material (inside and out)	Stainless steel
Rod suspension	SS cable
Drive, operating	AC motor, winch
Speed, in./min	8.48
Drive, scram	Pneumatic
Speed, in./min	8.48
Physics (reactivity)	
Average reactivity per rod, % $\Delta k/k$	0.24
Normal in-speed, average ($\Delta k/k$) sec	10^{-4}
Fast in-speed, average ($\Delta k/k$) sec	10^{-3}
Normal out-speed, average ($\Delta k/k$) sec	10^{-4}

Shielding

Thermal neutron shield material	Borosilicate glass
Thickness, in.	0.5
Biological shield	
Material	Concrete
Thickness, ft	9
Density, lb/ft^3	145
Shape	Octagonal
Distance across flats, ft	76
Height, ft	67
Total weight on foundation, tons	23,400
Cooling	Forced
Coolant	Air

Pressure vessel

Shape	Spherical
Material	Carbon steel, SA 212-B
Dimensions:	
Outside diameter, ft	50
Wall thickness, in.	3.25
Volume, ft^3	63,333
Operational pressure, psig	300
Maximum temperature, °F	650
Design stress, psi	15,000
Gross vessel weight, lb	1,541,000

(*continued*)

Reactor coolant

Coolant material	Helium gas
Working pressure, psia	300
Total flow (normal), lb/sec	972
Inlet temperature, °F	450
Outlet temperature, °F	1000
Number of inlet pipes	4
Number of outlet pipes	4
Diameter of pipe, ID, ft	5
Mean coolant velocity	
Cool pipe, fps	100
Hot pipe, fps	161
Total helium volume (at working pressure), ft^3	107,000
Circuit pressure drop, psi	6.61
Coolant blowers·	
Type	Axial
Number per reactor	4
Number per steam generator	1
Power for four blowers, Mw	18.3
Adiabatic efficiency, %	80

Steam generator

Type	Single-pass helium to water-steam
Number	4
Dimensions:	
Shell height between heads, ft	40
Shell height including heads, ft	60
Inside diameter, ft	20
Wall thickness, in.	2.75
Gas nozzles:	
Inlet, ID, ft	5.0
Outlet, ID, ft	5.0
Bypass, ID, ft	2.5
Steam outlet drums:	
Length, ft	21.5
Outside diameter, in.	28.0
Wall thickness, in.	1.875
Feedwater inlet drums:	
Length, ft	19.5
Outside diameter, in.	28.0
Wall thickness, in.	1.0
Feedwater pressure, psia	1020
Steam outlet pressure, psia	950

(*continued*)

Thermal performance

Reactor thermal output, Btu/hr	2.39×10^9
Fuel capsule:	
Total external surface, ft^2	45,050
Total internal surface, ft^2	42,760
Maximum internal surface heat flux, Btu/(ft^2)(hr)	96,000
Average internal surface heat flux, Btu/(ft^2)(hr)	56,000
Approximate average surface temperature, °F	1000
Maximum design surface temperature in hot zone, °F	1200
Maximum allowable surface temperature, °F	1500
Steam generator (each):	
Gas inlet temperature, °F	1000
Gas outlet temperature, °F	450
Feedwater inlet temperature, °F	325
Steam outlet temperature, °F	950
Steam superheat, °F	412
Gas flow rate, lb/sec	243
Steam flow rate, lb/sec	505,000
Feedwater flow plus losses, lb/sec	510,000

Physics

Graphite absorption cross section, mb:	
Core	4.0
Reflector	4.0
Temperature coefficient, per °C:	
Fuel, $\Delta k/k$	-4.7×10^{-5}
Moderator ($t_m = 400°C$), maximum, $\Delta k/k$	-14×10^{-5}
Moderator ($t_m = 400°C$), minimum, $\Delta k/k$	-4×10^{-5}
Total excess reactivity, % $\Delta k/k$	10
Thermal flux (2200 m/sec), n/(cm^2)(sec)	5×10^{12}
Reactivity invested in control rods, % $\Delta k/k$	14.5
Average reactivity per rod, % $\Delta k/k$	0.24

CHAPTER 7

ORGANIC COOLED AND MODERATED REACTORS*

7–1 INTRODUCTION†

Since the days of the Manhattan Project reactor engineers have considered using a hydrocarbon fluid as moderator, coolant, or combination moderator-coolant in nuclear reactors. Hydrocarbons have several obvious advantages over light or heavy water; these are discussed in the next section. However, interest in these materials for reactor use was for a long time somewhat inhibited, for two reasons:

(1) Natural uranium, hydrogen-moderated assemblies were known to be incapable of sustaining a nuclear chain reaction;

(2) Hydrocarbon materials were known to be unstable in a high-intensity radiation field; but the degree of instability, its relation to temperature, and the changes in physical properties resulting from radiation damage were completely unknown.

Interest in the hydrocarbons as reactor materials was revived when enriched uranium became available in the early 1950's. Work commenced independently in several laboratories in the United States to determine the stability of organics under the influence of radiation and heat. Different devices were used as radiation sources: test holes in various reactors, spent fuel elements, Co^{60} sources, and Van de Graaff-type electrostatic generators. Many different classes of organic materials were studied under temperature conditions ranging from room temperature to about 1000°F.

The first general meeting of workers in the organic field was held in August, 1953, at Downey, California. It was found that there was considerable qualitative agreement concerning the relative stability of organic compounds. The aromatic materials were reported to have exhibited the greatest amount of stability under irradiation. The 1953 meeting marked the transition from the general exploratory phase to a better-organized and more systematic study of the aromatic hydrocarbons. Since that time, most of the experimental and analytical effort has been devoted to the polyphenyls.

---

*All figures in this chapter were furnished by the Atomics International Division of North American Aviation, Inc.

†By E. F. Weisner, Atomics International.

There are several advantages derived from using an organic material as reactor moderator and as coolant. First, it permits low-pressure operation; fluid temperatures in the 500 to 700°F range may be used without accompanying high pressures. Diphenyl boils at 492°F at atmospheric pressure, and its vapor pressure at 700°F is only 7.5 atmospheres (112 psia). The terphenyls boil at approximately 700°F at atmospheric pressure. Practical operating pressures for organic reactors appear to be in the range below 300 psia, whereas pressurized water reactors require pressures in the 2000-psi range.

Second, the corrosion rate of most common materials in organics is so low as to be almost negligible. This permits using such standard engineering materials as low-carbon steels and aluminum throughout the primary coolant system In addition, no exothermic chemical reactions occur between the organic and uranium or between the organic and water. The corrosion rate of uranium in organic is low, and consequently few fission products would get into the coolant stream even if a fuel jacket should fail. The distillation purification system used to remove the higher polymers that form under irradiation will also remove the radioactive impurities from the organic. This tends to maintain the activity of the organic system at a low level, so that little, if any, shielding is required for the primary coolant system, except for the reactor vessel itself (The OMRE* primary coolant system is completely unshielded.)

Because radiation levels are low, maintenance may be performed on and around the primary coolant system while the reactor is operating. This has proved to be entirely feasible at the OMRE. No special equipment is required; the pumps, process equipment, valves, and instrumentation are similar to those used in the petroleum industry. The system need not be completely leaktight, small leaks through seals and packings present no unusual difficulties.

The principal problem associated with using organic materials in nuclear reactors results from the fact that they decompose under radiation. Decomposition manifests itself in many ways: gases are produced and released; the physical properties of the fluid, such as density, viscosity, specific heat, thermal conductivity, and carbon-to-hydrogen ratio, are altered; and materials of higher molecular weight (polymers) with unknown properties and mutual solubilities are produced. (These effects are further described in Section 7–2.) The decomposition rate increases as the temperature rises, which is to be expected, since organic materials usually undergo thermal decomposition at elevated temperatures There is also some concern that one or more of the decomposition products formed may tend to deposit on (foul) heat-transfer surfaces.

---

*The Organic Moderated Reactor Experiment. See Section 7–4.

In a working reactor, the decomposed materials will have to be more or less continuously removed and new undamaged organic added as makeup. Whether all the polymers should be removed is still unknown; there is some evidence that they are either more stable than the original material or that they tend to inhibit decomposition. In some experiments (discussed in Section 7-3) decomposition rate has been seen to decrease as polymer content increased. In a particular reactor plant, however, an excessively high equilibrium polymer content cannot be allowed, because the higher viscosity leads to lower heat-transfer coefficients and higher pumping power.

Like most organic materials, the polyphenyls are flammable, but because they have rather high spontaneous ignition temperatures (about 1000°F) they are not particularly hard to handle. Flammable mixtures of polyphenyl cannot be obtained in air by vaporization at normal ambient temperatures. (The ambient temperature needs to be at least 230°F for diphenyl and 415°F for paraterphenyl before there will be enough vapor for ignition by a spark or flame. Ordinary refinery practice and precautions are effective to prevent fires.)

Handling polyphenyls at normal ambient temperatures presents no health hazard, since the concentrations that can be inhaled are very low. Some precautions are required at higher temperatures, especially with irradiated organic materials. No particular problems have been encountered in handling these materials at the OMRE.

There is a basic limitation on the upper temperatures at which organic materials may be used. This limit is in the 900 to 1000°F range, where thermal decomposition becomes excessive even without nuclear radiation. It appears that organic fluids will find their greatest use in nuclear reactors in the temperature range from 300 to about 800°F

Since the August 1953 meeting, knowledge of organic materials for reactor use, and of the polyphenyls in particular, has expanded manifold. Several test loops have operated both in-pile and out-of-pile, and one reactor (the OMRE) is in use There is no longer any doubt about the technical feasibility of the organic reactor concept, whether the organic is used as moderator, coolant, or both. The decomposition rate at temperatures in the 600 to 700°F range is not excessive when the organic is used for both moderation and cooling. The makeup would be much less, of course, if the organic were used as a coolant only. The variation in decomposition rate with temperature and with polymer content has not been explored over a wide range; however, it appears to increase with higher temperature and decrease with increasing polymer content. These aspects are being more fully explored by the OMRE.

The physical property changes resulting from radiation damage and polymer buildup have been measured for the more important proper-

ties. These are reported in Section 7–2. Within the range studied, the decomposition products have always been completely soluble in the original material. There has been no evidence of film formation or fouling on any heat-transfer surface where the surface temperature was below 800°F and the organic velocity exceeded a few feet per second. The heat-transfer characteristics of irradiated polyphenyls are completely predictable within the ranges studied and have not been observed to change with time for constant temperature and constant polymer conditions.

The operation of the OMRE has proved that conventional equipment, such as valves, pumps, and seals, works very satisfactorily. The irradiated organic can be purified by distillation with a high degree of success. The impurities are also removed with the damaged material, leaving nonradioactive and purified organic for return to the main system. The venting of gaseous decomposition products is handled routinely and without complication.

In summary: as of April 1958, there remains only one major unknown regarding the use of organic materials in nuclear reactors, the decomposition rate as a function of temperature and polymer content. This information is now being generated at the OMRE, as described in Section 7–4. Meanwhile, design of reactors of the type described in Section 7–5 is proceeding, so that final engineering and construction of Organic Moderated Reactor power plants may begin in the near future.

7–2. Effects of Radiation on Organic Liquids*

Broadly speaking, radiation particles (such as gamma photons, beta particles, neutrons, and alpha particles) transfer energy to materials by interacting with either the electrons or the nuclei of atoms. Organic liquids are damaged by all particles or energy-transfer processes that are more energetic than the dissociation bond energy (4 to 6 ev). Thus, in mixed in-pile radiation, only the thermal neutrons do not contribute directly to organic liquid damage. Since radiation damage to organic compounds results from ionization [1,2], it is expected that all types of ionizing radiation will cause similar damage, and the extent of damage will be nearly proportional to the amount of energy absorbed [3].

7–2.1 Causes of radiation damage. Gamma radiation interacts mainly by Compton scattering to produce electrons which are ionizing particles. Fast neutrons are slowed by scattering and, for hydrocarbons, the energy released is transferred primarily to the hydrogen nuclei. Resulting pro-

*By R. H. J. Gercke, AI.

tons then cause ionization in much the same manner as do the electrons from gamma radiation [1–4]. In organic materials damaged by ionizing radiation, damage from the displaced atoms is masked by damage from ionization [1].

For neutron energies above a few Mev, inelastic scattering may occur, increasing in importance as the neutron energy rises However, below 10 Mev, inelastic scattering should not be of major consequence since (1) it is absent when scattering with hydrogen and collisions with hydrogen predominate, and (2) even for such collisions the energy released by the corresponding gamma ray is, on the average, a small fraction of the energy carried by the recoil atom. Inelastic scattering is therefore considered an unimportant contributor to energy transfer.

Elastic collision is the principal process by which neutrons lose their energy. As a result of an elastic scattering, the struck atom acquires kinetic energy which is dissipated by ionization, excitation, and elastic collisions with other atoms. More rarely, a nuclear reaction takes place in which a gamma ray, a proton, or an alpha particle is emitted. The recoil atoms, protons, and alpha particles lose their energy within a small fraction of a centimeter of the point of collision. The energy carried by the capture gamma rays may be absorbed at large distances from the point where the neutron was absorbed, but since the cross section for fast neutron absorption is very small, gamma rays do not contribute substantially to the energy transferred [4] during neutron moderation. Consequently, on the macroscopic scale, the energy imparted by a neutron may be considered as absorbed at the collision site, resulting in high ionization density.

It appears that the mechanisms by which the various radiation particles transmit their energy to organic liquids differ mainly in ionization density. Cyclotron beams provide a powerful tool for studying these variations. Schuler and Allen [5], using the Brookhaven 60-inch cyclotron, have irradiated both aqueous solutions and pure cyclohexane with 40-Mev helium ions (energy loss 1.88 ev per angstrom), with 20-Mev deuterons (0.46 ev/A), and with 2-Mev electrons (0.02 ev/A). For the organic liquid studied (cyclohexane), the yield of hydrogen obtained was quantitatively identical over this wide range of ionization density. Large differences were observed for aqueous solutions.

Bopp and Sisman [1] studied the effects of high-energy radiation on hydrocarbon plastics and elastomers. They report equivalent effects for electron and mixed in-pile radiation when change in several properties is used as an index of damage. In their work, a wide range of ratios of neutron to gamma-photon absorbed energies was used. In some cases, two-thirds of the total energy transferred to the hydrocarbon was deposited by neutrons, the rest by gamma photons.

Collins and Calkins [2] have irradiated a number of plastics and elastomers using both pure gamma exposures and mixed in-pile radiation. They found no definite pattern in their data to indicate greater damage by either mixed pile or gamma irradiation. In their capsule irradiation of the alkyl benzenes (355°F) and diphenyl, methyl diphenyl, and orthoterphenyl (280 to 700°F), two-thirds to one-half of the total energy absorbed was from neutrons.

Zebroski and Kinderman [6] have compared the radiation effects due to 1-Mev electrons and Co^{60} gamma photons on a number of organic liquids. Careful irradiation of normal propyl, isopropyl, and benzyl acetate by both electrons and gamma rays gave results quantitatively identical both for total gas yield per unit of energy absorbed and for gas composition. These experiments throw some light on the possible effect of variations in intensity, since the electron radiation had a higher radiation intensity than the gamma radiation by a factor of 720.

High-temperature capsule irradiations in the Brookhaven reactor have been compared with fast-electron bombardment results. Putting the mixed in-pile radiation on an energy absorption basis, the value of G* thus obtained for orthoterphenyl is in excellent agreement with electron results. In another series of capsule experiments on the terphenyls by Colichman and Gercke [7] carried out at the Materials Testing Reactor (MTR), the G-values calculated on an energy absorption basis give excellent agreement between the electron and mixed in-pile irradiations

Using the same technique of calculation, Nakazato and Gercke [8] have calculated a G-value for irradiation damage obtained in a circulating loop experiment with mixed in-pile radiation. In yet another experiment with a mixed in-pile loop in the MTR at elevated temperatures (approximately 650°F), G-values obtained for the several polyphenyls are in good agreement with those obtained by electron bombardment.

In the several mixed in-pile irradiations carried out on the polyphenyls (see Table 7–1), the energy deposited by fast neutrons varies from 5 to 30% of the total energy absorbed by the organic liquid. No effect on the decomposition rate, G, is indicated.

One method of detecting differences in break-down mechanism is to compare decomposition products. The decomposition polymer for the terphenyls (Santowax R) caused by fast electron bombardment seems to be similar, if not identical, with that caused by mixed in-pile irradiation. When density and viscosity of irradiated Santowax R are compared over a range of polymer content, results show agreement within the limits of ex-

---

*The G-value is a measure of radiation damage and is usually given in terms of molecules produced (of either polymer or gas) per 100 ev of energy absorbed. G_p and G_{gas} are symbols used for the G-value for polymer and gas, respectively.

TABLE 7-1

SUMMARY OF THE DECOMPOSITION RATES FOR THE POLYPHENYLS

Type of radiation	Energy deposited by neutrons, % of total	G_p*	Composition
Electrons, 1 Mev [7]	0	0.06-0.08	Ortho-, meta-, para-terphenyl at 660°F
Electrons, 1 Mev [9]	0	0.08	Ortho-terphenyl at 750°F
		0.09	Meta-terphenyl at 750°F
		0.02	Para-terphenyl at 750°F
Electrons, 1 Mev [10]	0	0.06	Para-terphenyl at 660°F
		0.08	Santowax R at 660°F
Mixed in-pile circulating loop, MTR, A-14 [8]	5	0.05	Ortho-terphenyl at 200°F
Mixed in-pile Capsule, BNL-E25 [11]	30	0.07	Ortho-terphenyl at 700°F
Mixed in-pile circulating loop, MTR, A-13 [12]	18	0.12	Santowax O-M at 630°F
			Santowax R at 645°F
			Diphenyl at 684°F

*The number of molecules of polymer produced per 100 ev of radiation energy absorbed. G_p values quoted are averages between the high initial and low final values.

perimental error, indicating that the nature of the polymer is at least similar. The radiolytic decomposition gases are also very similar; the main constituents for both the electron and the in-pile experiments are hydrogen, methane, and ethane. Similarity of breakdown mechanism is indicated.

Various investigators have concluded that a one-to-one relationship exists between energy deposition and bond cleavage for organic liquids and solids when the damage is caused by ionizing radiation. Efforts to date to evaluate the mechanism of energy transfer between various radiation particles present in mixed in-pile radiation fields lead to the conclusion that

The important end result for each particle is that of ionizing radiation. A careful analysis of the transfer mechanism by which fast neutrons impart their energy to organic liquids indicates that whatever difference may exist between the effects of fast-neutron and electron or gamma photon energy deposition should be attributed to differences of ionization density. Experiments carried out to study the effect of ionization density on the decomposition rate of organic liquids (cyclohexane) have shown no variation. In other studies of radiation intensity as a variable of radiation damage, no effect has been observed, for the organic liquids, over a wide range of radiation intensities.

G-polymer has been found independent of the percent of total energy deposited by neutron energy transfer over the range studied (up to 30% deposited by neutron energy loss). Decomposition rates for hydrocarbon plastics and elastomers have also been studied as a variable of energy deposited by neutrons. No effect was observed. The range covered was from 0 to 67% of total energy deposition by neutrons.

7–2.2 Effects of radiation damage to polyphenyls. Available experimental data on radiolysis of organic compounds shows the polyphenyls, as a class, most promising for application as organic coolant-moderators (see Table 7–2).

Within the past several years, radiation studies have been conducted on a variety of organic materials at elevated temperatures [7–9,14,15]. The three terphenyl isomers were extensively tested using 1-Mev electrons from a Van de Graaff generator, capsule experiments at ~80°F in mixed in-pile reactor irradiation, and elevated temperature capsule irradiation by fast gamma photons (see Tables 7–3 and 7–4 and Figs. 7–1 through 7–4). Two in-pile loop tests were made at elevated temperatures with mixtures of terphenyls as well as with diphenyl and isopropyl diphenyl [8,12]. Also evaluated, but less extensively, were compounds such as diphenyl, isopropyl diphenyl, naphthalene, and phenanthrene [14,15].

7–2.3 Effects of radiation damage on the properties of organic coolant materials. A number of properties discussed below are important in considering organic materials for use as coolant-moderators [16].

(1) The materials should be commercially available and economical to use. Relatively costly materials may be considered if their decomposition rates are low enough. Since technical grade terphenyls now cost six to nine times more than the commercially available isomeric terphenyl mixtures, it would not be economical to use one of these unless its decomposition rate were substantially less than that of the mixtures of isomeric terphenyls; the latter have an estimated replenishment cost of less than one mill per electrical kilowatt-hour.

TABLE 7-2

SUMMATION OF RADIATION CHANGES IN ORGANIC COMPOUNDS

	Major G values determined
Saturated hydrocarbons	−M,* 4–9; H_2, 2–6; CH_4, 0.06–1
Unsaturated aliphatic and alicyclic hydrocarbons	Polymer, 10–2000; crosslink, 6–14; H_2, ∼1, CH_4, 0.1–0 4
Aromatic hydrocarbons	Polymer, ∼1; H_2, 0.04-0.1; CH_4, 0.001–0.08
Halides	½I_2, 2–4, HI, 0; ½Br_2, 0–0.5; HBr, 0–15; ½Cl_2, 0; HCl, ∼4
Alcohols	−M, 3–12; H_2, 1–3.5; hydrocarbons, 0.5–1.5; carbonyl, 1–2; vic-glycol, 0.5–1.5
Carboxylic acids	−M, >0.3; CO_2, 0.5–4, CO, <0.5; H_2, 0.5–2
α-Amino acids	−M, 3–10; NH_3, ∼1; CO_2, ∼1; amine, ∼1
Quaternary ammonium salts	−M, 1–1000; amine, 1–1000

*The symbol "−M" represents the starting material that is permanently altered; *i.e.*, G_M = number of molecules of starting material permanently altered per 100 ev of energy absorbed.

TABLE 7-3

IN-PILE DECOMPOSITION OF TERPHENYLS*

Material	Polymer produced, wt. %	Gas evolution, cm^3/gm
Ortho-terphenyl	38.3	2.04
Meta-terphenyl	32.6	1.35
Para-terphenyl	25.4	0.38
4 per cent para- + 96 per cent meta-terphenyl	33.9	0.66

*Exposed in VH-3 hole, Materials Testing Reactor. Integrated fluxes were: thermal neutrons (based on foil measurements) = 1.0×10^{19} n/cm²; (>1 Mev) neutrons (based on foil measurements) = 1.53×10^{17} n/cm²; gamma-rays (based on graphite heating) = 30 w-hr/g.

TABLE 7–4

COMPARISON OF TERPHENYL *G* VALUES

Terphenyl	Gas produced, 10^{-24} cm^3/ev		
	Electron*	Reactor	Electron to reactor ratio
Ortho-	2.1	2.0	1.05
Meta-	2.1	1.4	1.50
Para-	0.52	0.38	1.37

*Electron-irradiation *G* values are at a dosage of 44.1 w-hr/g, equivalent to energy absorbed by terphenyl during reactor irradiations to 10^{19} *nvt*.

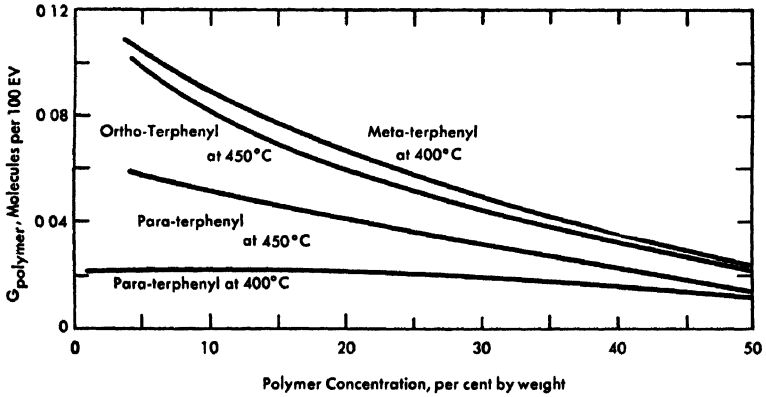

FIG 7–1. Values of $G_{polymer}$ from Van de Graaff irradiations

(2) A low coolant vapor pressure is desirable for both mechanical and safety reasons. Gas solubility in the organic coolant (from both pressurization and evolved gases) increases with increased total pressure above the coolant. Lower vapor pressure reduces risk of loss-of-pressure accidents and their aftermaths. The effect of boiling of the coolant near the heat-transfer surface is as yet unknown.

(3) Viscosity must be reasonably low to avoid uneconomically high pumping power requirements. However, if necessary, viscosity increases can be compensated to some extent by changes in the reactor design.

(4) The organic material must transfer heat without fouling heat-transfer surfaces. Heat-transfer and fouling characteristics are discussed

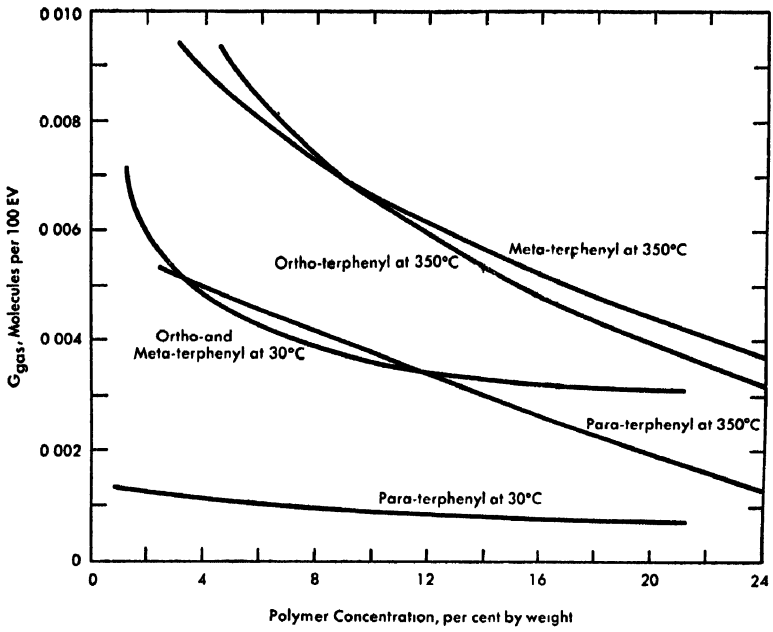

FIG. 7–2 Values of G_{gas} from Van de Graaff irradiations.

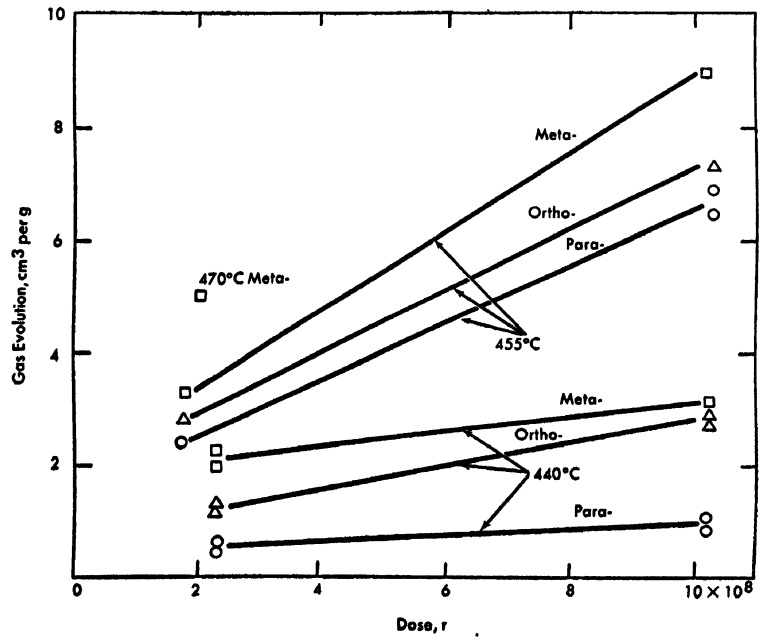

FIG. 7–3. Gas evolution after high-temperature gamma-ray irradiation.

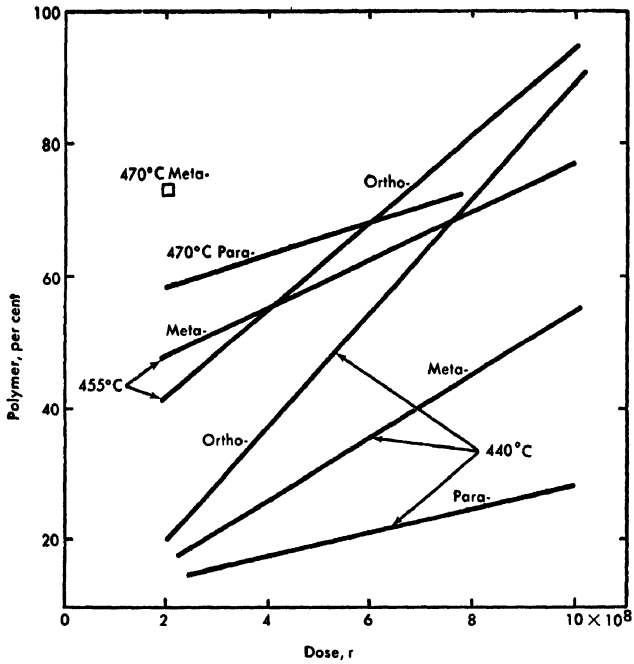

FIG. 7–4. Polymer formation after high-temperature gamma-ray irradiation.

in Section 7–3. The properties affecting heat-transfer performance are density, heat capacity, viscosity, and thermal conductivity.

(5) The threshold temperature, at which the rate of radiation decomposition increases greatly, should be safely above the maximum expected at the heat-transfer surface. The heat-transfer surface is more likely to foul when its temperature exceeds the threshold temperature, which has been shown to vary from 750 to 850°F for the polyphenyl organic compounds of interest.

(6) The radiation decomposition products should be soluble over the range of compositions and temperatures to be used. The polyphenyls extensively studied to date are satisfactory in this regard. Organic liquids whose decomposition products are sparingly soluble could probably not be used in reactor applications.

(7) The melting point must be below the operating temperature required in reactor operation. Also important are the precautions necessary to prevent freezing at points which must normally be kept cool. This is not a serious problem; it can be resolved by installing preheating and intermediate cooling systems with close temperature control at critical points (seals, condensers, traps, and control rod drives).

TABLE 7-5

COMPARATIVE PROPERTIES OF ORGANIC COOLANTS

	Diphenyl	Santowax R*	Santowax O-M*	Isopropyl diphenyl
Melting range, °F	156	140–293	100	−40 to + 28
Boiling point, °F	491	700	650	552
Vapor pressure at 800°F, psia	220	38	57	190
Hydrogen density at 620°F, atoms/cm^3	3.04×10^{22}	3.18×10^{22}	3.18×10^{22}	3.74×10^{22}
Typical cost, $/lb	0.15	0.17	(0.75)	1.25
Viscosity, centipoise (600°F)	0.24	0.32	0.32	0.19
Specific heat (600°F), Btu/(lb)(°F)	0.61	0.60	0.60	0.60
Thermal conductivity (600°F), Btu/(hr)(°F)(ft)	0.66	0.66	0.66	0.66

*Commercial organics manufactured by Monsanto Chemical Company.

(8) Hydrogen atom density (moderating ability) is important, but differences in this property among the suggested coolants appear relatively minor (Table 7–5). Calculations of moderating properties (moderating ratios and neutron age to thermal energy) for polyphenyls, substituted polyphenyls, and fused-ring hydrocarbons show them suitable for use in organic-moderated reactors. Moderating ratios for all these various organic compounds are about the same as for water; this would be expected, since hydrogen has the major effect on both slowing down and absorption. There are only relatively small differences in the neutron age to thermal energy among the various polyphenyls and naphthalene, these differences being inversely proportional to the square of the hydrogen density. All these organics exhibit higher age values than does water, but the difference decreases as the temperature of the fluid increases. Differences in moderating properties among these various hydrocarbons are less important than are other properties discussed (for example, vapor pressure, melting points, etc.).

The organic coolant properties of greatest interest [17] are those bearing directly on heat transfer, moderating ability, and safety aspects. These properties are affected by the buildup of radiation decomposition products. A number of important physical properties were determined

for the four organic coolant liquids studied in the organic in-pile loop (isopropyl diphenyl, diphenyl, Santowax R, and Santowax O-M). Density and viscosity were measured for each of the four fluids over the temperature range 300 to 850°F as a function of radiation decomposition. Enthalpy and specific heat were obtained for several organic coolants, including some in-pile-irradiated materials. Melting point and hydrogen density were determined also as functions of radiation decomposition for the four fluids. The coolant samples used were withdrawn from the loop during operation of the in-pile loop experiments

Density. For the four coolants studied in the in-pile loop experiment, liquid densities have been determined over the temperature range 300 to 850°F and as a function of radiolytic decomposition. A modified Lipkin pipet, pressurized with nitrogen, was used to permit measurements above the normal boiling point. The pipet containing the sample was placed in a constant-temperature air bath, the temperature was raised in steps, and the increase in volume was observed with a cathetometer. The volume as a function of height was established by calibrating with mercury. Density was measured every 75°F between 300 and 850°F. The over-all maximum error is estimated to be less than 0.3%.

In each case, density increases with increasing high-boiler residue content (Fig. 7–5) At 600°F, the density increases due to 35% high-boiler residue are 7.2% for isopropyl diphenyl, 8.16% for diphenyl, 6.16% for Santowax O-M, and 4.2% for Santowax R (Fig. 7–6).

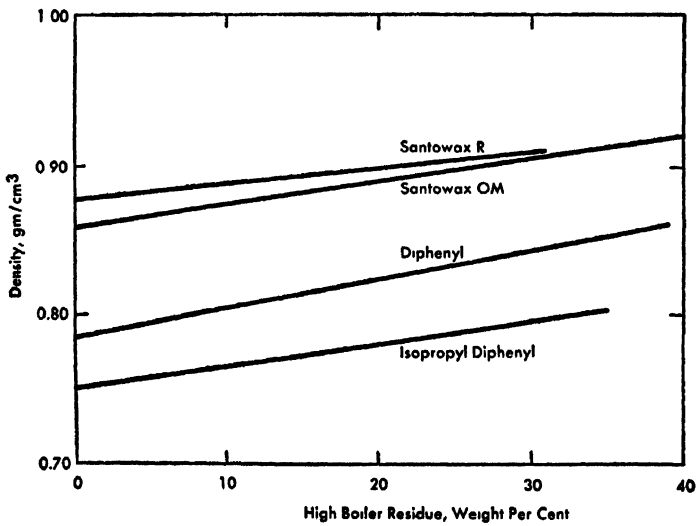

FIG. 7–5. Density of irradiated coolants at 600°F.

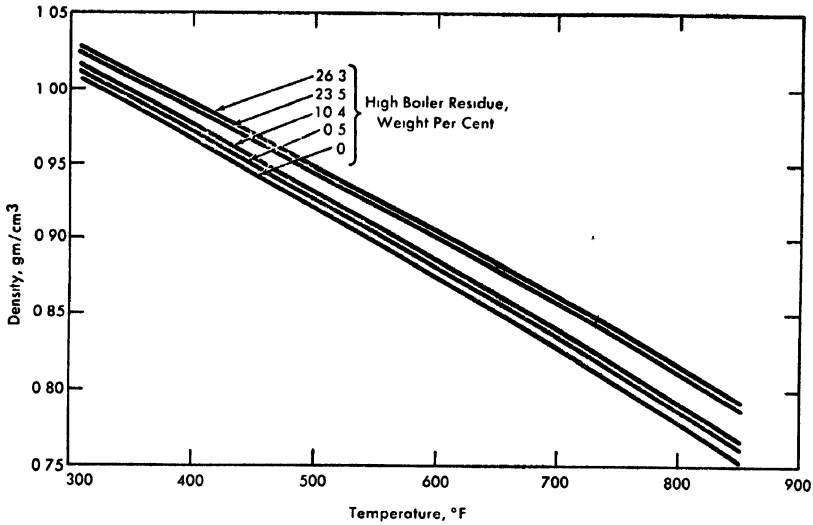

FIG. 7–6. Density of irradiated Santowax R

Viscosity. Viscosity, also, has been studied as a function of temperature and radiation decomposition for the four coolants, over the temperature range 300 to 850°F. An Ostwald capillary pipet, immersed in a constant-temperature air bath, was pressurized with nitrogen to permit measurements above the normal boiling point. The over-all errors in the relative viscosities are estimated to be ±0.7%, and in the absolute values, ±2%.

All four coolants showed similar increases in viscosity with increasing high-boiler residue content; they are compared at 600°F in Fig. 7–7. As a typical example, the viscosity-temperature relationship is shown for Santowax R at several stages of decomposition in Fig. 7–8. Note that at operating temperatures the viscosity of the partly decomposed coolants is reasonably low for purposes of heat transfer and pumping power. The viscosities of the four coolants containing 35% high-boiler residue at 600°F are as follows: 0.47 centipoise for isopropyl diphenyl; 0.54 cp for diphenyl; 0.75 cp for Santowax R; and 0 73 cp for Santowax O-M.

Specific heat and enthalpy. Enthalpy and specific heat were determined experimentally in the temperature range 350 to 850°F for the following polyphenyl liquids: (1) an unirradiated ortho-, meta-terphenyl mixture containing 89% ortho-, and 11% meta-terphenyl; (2) radiation-decomposed 2/3 ortho-, 1/3 meta-terphenyl by weight containing 32% high-boiler residue; (3) unirradiated OMRE coolant containing 16% diphenyl, 46% ortho-, 32% meta-, and 6% para-terphenyl.

Enthalpy as a function of temperature was determined with a modified Southard [18] "drop" calorimeter using (1) a furnace to heat a capsule

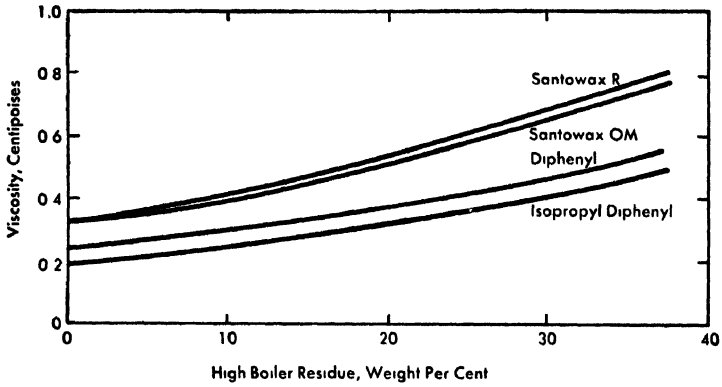

FIG. 7–7. Viscosity of irradiated coolants at 600°F.

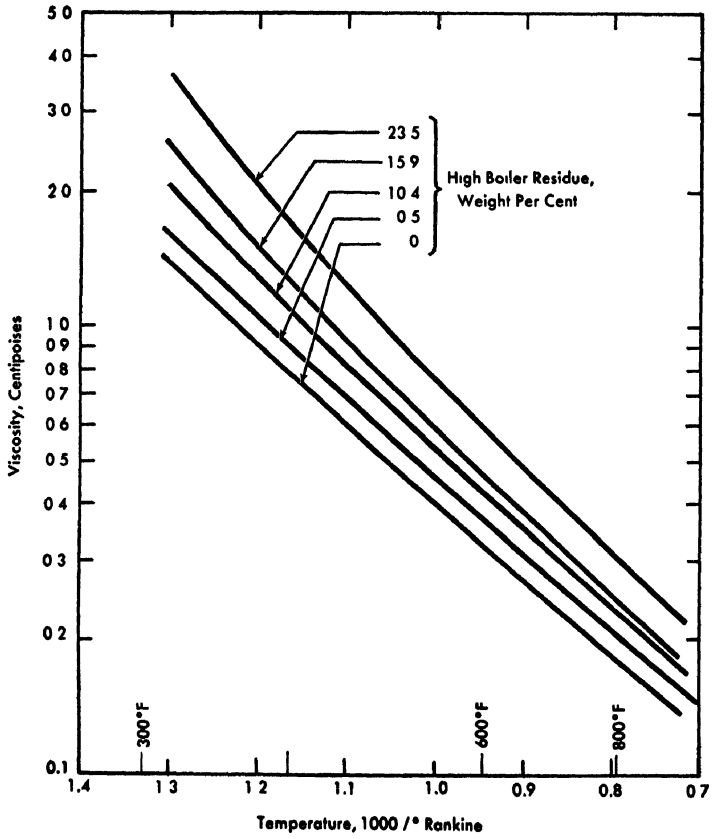

FIG. 7–8. Viscosity of irradiated Santowax R.

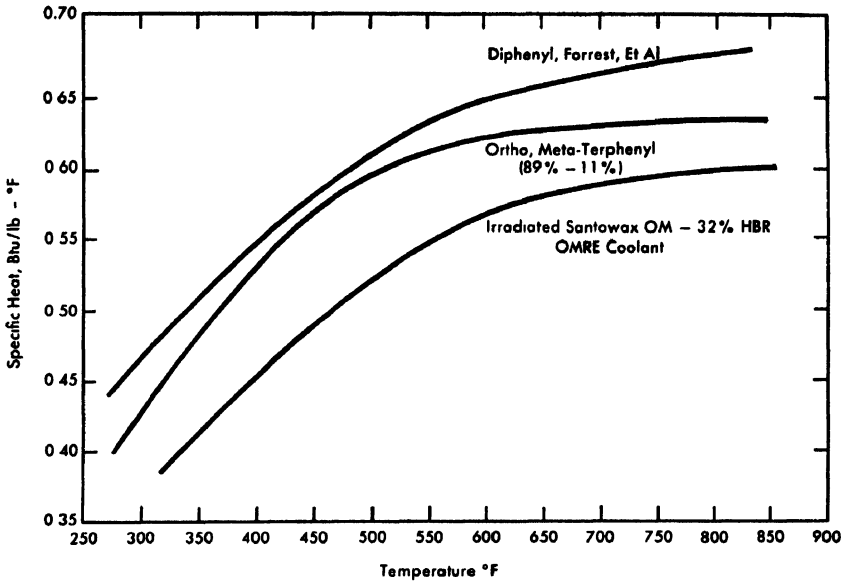

FIG. 7-9. Specific heat of organic coolants.

containing the sample to the desired temperature, and (2) a massive copper block calorimeter, essentially adiabatic, to measure the heat evolved in cooling the sample (and capsule) to the known base temperature. The temperature rise when the sample capsule is dropped from the furnace into the adiabatic copper block calorimeter is measured very accurately with a resistance thermometer (a copper wire 300 ft long spiraled around the exterior of the copper block).

The average deviation for the experimental enthalpy values is about 3%. However, duplicate runs at the same temperature show a precision within about 1.5%. Maximum error for the specific heat is less than 9%. Specific heats based on the experimental enthalpies are shown in Fig. 7-9. The diphenyl data of Forrest et al. [19] are shown for comparison. Specific heat does not seem to vary significantly with radiolytic decomposition.

Melting point. The final melting point (or liquidus temperature) was determined as a function of radiation decomposition for the four coolants. Each sample was frozen completely and then slowly heated until all the coolant was liquefied, as determined by direct observation. The data are presented in Fig. 7-10. For all four materials, the melting point decreases with increasing radiation decomposition. In the case of ortho-, meta-terphenyl, the melting point increases slightly after reaching a minimum

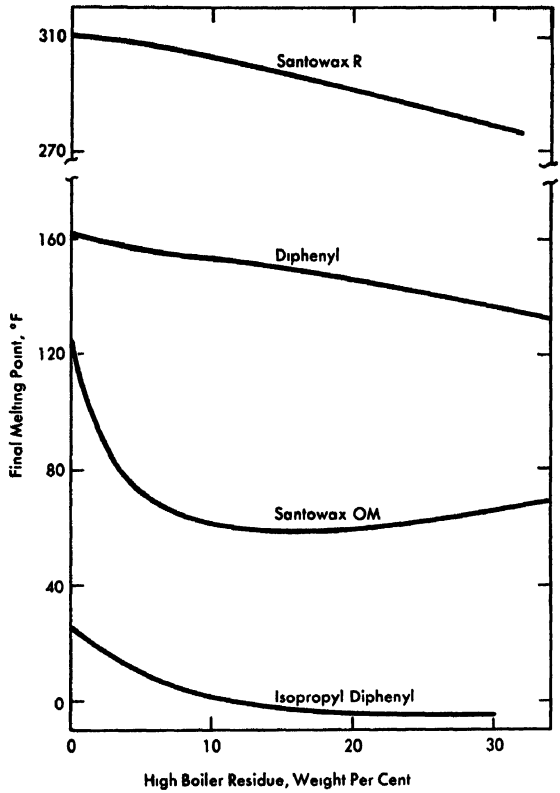

FIG. 7–10. Melting point of irradiated coolants.

at 15% high-boiler residue. The average lowering due to an increase to 35% high-boiler residue for all four fluids is approximately 35°F.

Carbon-to-hydrogen ratio. The carbon and hydrogen content of irradiated coolants was measured, to find out how coolant decomposition affects moderating ability. Samples of these irradiated coolants were analyzed: diphenyl, isopropyl diphenyl, Santowax O-M, and Santowax R. The carbon-to-hydrogen ratio increases with increasing high-boiler residue concentration for all four. The increase when high-boiler residue increases from zero to 35% is as follows (see Fig. 7–11):

	Carbon-to-hydrogen ratio, % increase
Isopropyl diphenyl	4.8
Diphenyl	3.1
Santowax O-M	1.8
Santowax R	1.6

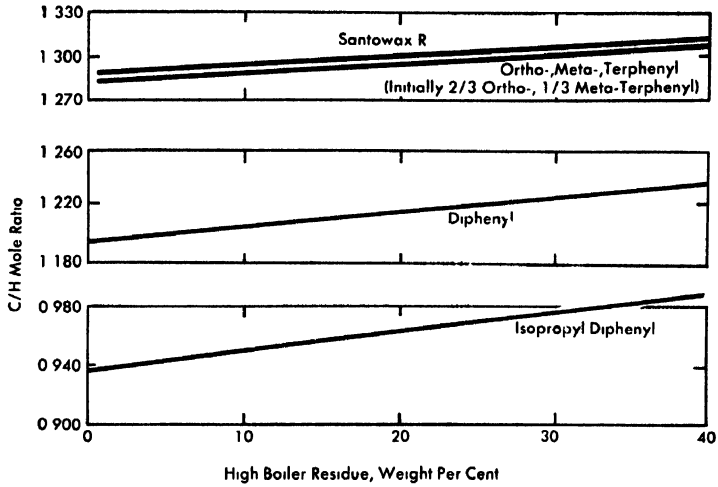

FIG. 7–11 Carbon-to-hydrogen ratio of irradiated coolants

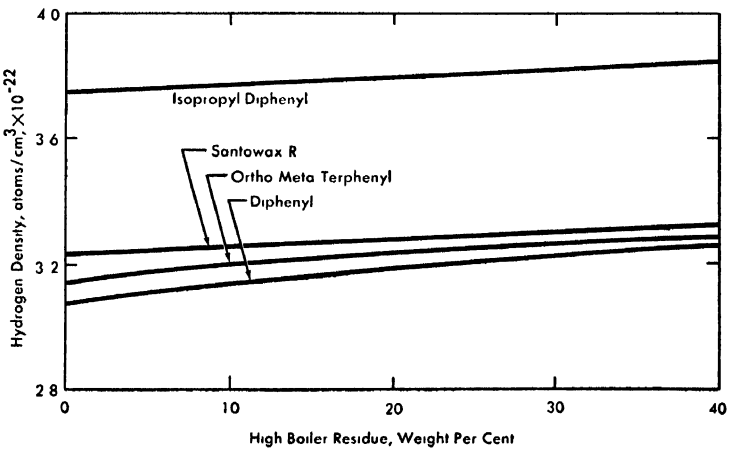

FIG. 7–12 Hydrogen density of irradiated coolants at 600°F.

The carbon-to-hydrogen ratio rises with increasing decomposition. At the same time, the hydrogen density also increases, so that the loss of hydrogen with decomposition is more than overcome by its increase in density. Hydrogen density (at 600°F) is shown in Fig. 7–12 for the four irradiated coolants. For Santowax R, the hydrogen density is shown as a function of temperature in Fig. 7–13.

Summary of physical properties studies. Table 7–5 shows some properties of the four coolants studied; the only significant differences are in

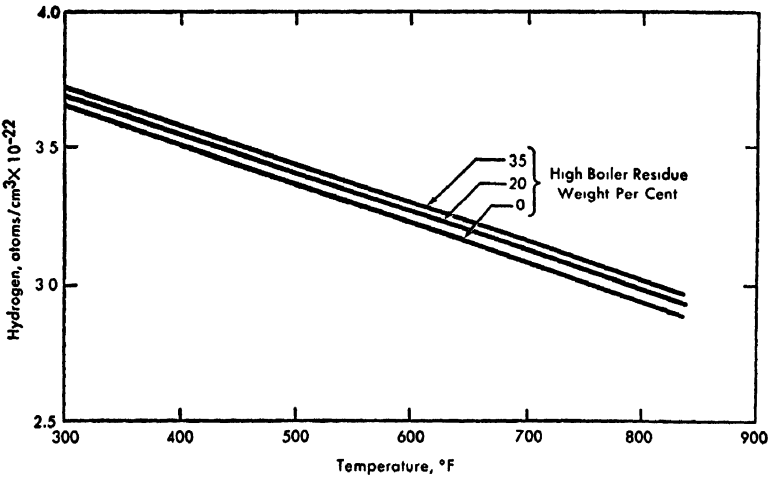

FIG 7–13 Hydrogen density of irradiated Santowax R.

TABLE 7–6

ESTIMATED PROPERTIES OF ORGANIC COOLANT
(ORTHO-, META-TERPHENYL)
AS A FUNCTION OF RADIATION DECOMPOSITION AT 600°F

	High-boiler residue, w/o				Change due to 30% HBr, %
	0	10	20	30	
Viscosity, centipoise	0.32	0.41	0.51	0.65	+103.
Density, g/cm³	0.859	0.874	0.890	0.906	+ 5.4
Specific heat, Btu/(lb)(°F)	0.60	0.60	0.60	0.60	0
Thermal conductivity, Btu/(hr)(°F)(ft) [20]	0.066	0.066	0.066	0.066	0
N_H, hydrogen atoms/cm³ × 10^{-22}	3.15	3.19	3.22	3.26	+ 3.6
Melting point, °F	125	59	57	66	—

vapor pressure, melting point, and cost. None of the four has a clear-cut advantage over the others. Santowax R, for example, has both low vapor pressure and low cost, but a high melting point. This disadvantage, however, can be overcome by reactor plant design.

The effect of radiation decomposition on these properties has been found quite similar for all four coolants studied. The changes in the properties studied are shown in Table 7-6 as a function of increasing high-boiler residue content, using Santowax O-M as a typical example (at 600°F).

7-3. Heat Transfer and Fouling Characteristics of the Polyphenyls*

At the beginning of the OMRE program, a most important question was: what are the operating limitations in using polyphenyls as heat-transfer fluids in nuclear reactors? To answer the question, a series of experiments was planned, including heat-transfer studies with out-of-pile and in-pile circulating loops.

7-3.1 Out-of-pile study. The out-of-pile study was undertaken to find the limiting conditions for heat-transfer-surface fouling, i.e., deposition of fluid decomposition products that decrease the over-all heat-transfer coefficient [21]. Decomposition products are formed by the action of either high temperature or radiation To detect fouling, it was necessary first to understand the heat-transfer properties of the fluids under investigation. Therefore, the out-of-pile study consisted of two parts: first, to measure and correlate the heat-transfer properties of the fluids; second, to purposely foul a heat-transfer surface to determine the effect of operating parameters on fouling rates.

A laboratory heat-transfer loop was used for the out-of-pile study (Fig. 7-14). System pressure was controlled by compressed nitrogen in the upper part of the surge tank. The organic fluid was circulated by a canned-rotor centrifugal pump having a capacity of 5 gpm at 60 psi. Particulate matter was removed by a 200-mesh screen installed upstream of the turbine flowmeter. The test heater was fabricated from a thin-walled, type-304 stainless steel tube. A center-tapped, electrical resistance heating circuit was used.

The fluids studied were diphenyl, Santowax R,† and a mixture of Santowax O† and Santowax M† (Santowax O-M), the latter being commercial terphenyl mixtures. Compositions are given in Table 7-7. These fluids were chosen because earlier laboratory investigations had demonstrated their high thermal and radiation stability.

The various operating parameters were investigated over the following ranges:

*By D. W. Bareis, AI
†See footnote of Table 7-7.

Fluid temperatures	480 to 770°F
Heater surface temperatures	565 to 875°F
Fluid velocities	5 to 25 fps
Heat fluxes	40,000 to 290,000 Btu/(hr) (ft^2)
Reynolds numbers	20,000 to 300,000

The ranges selected gave a reasonable variation in the parameters and covered the conditions expected in the fuel elements of the OMRE core. All heat-transfer runs were made with the loop at 300 psig.

A heat-transfer coefficient was calculated for each run from data obtained at a point on the test section away from the terminal connections, to avoid end effects. The first attempt to correlate the heat-transfer coefficients was made by using the Sieder-Tate equation [22] developed for viscous organic fluids. The values of specific heat and thermal conductivity required for this correlation were estimated [23,24]. Figure 7–15 shows that the experimental data deviated consistently from the Sieder-Tate equation at the lower Reynolds numbers.

Consequently, an equation was sought that would give the least standard deviation for the data, by varying the coefficients and exponents of the dimensionless groups used for heat-transfer correlations. An IBM-704 digital computer was used The viscosity ratio, μ/μ_w, as found in the

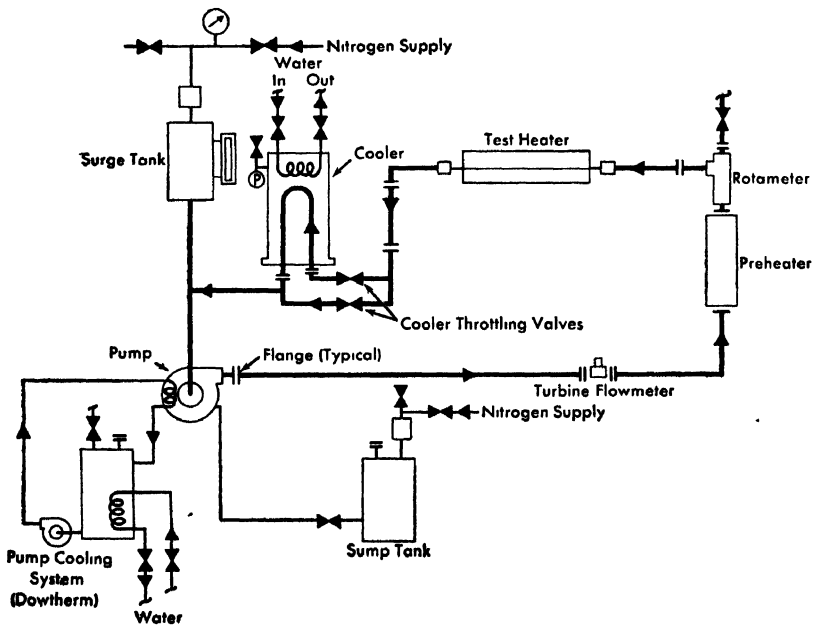

FIG. 7–14. Flow diagram of heat-transfer loop.

TABLE 7-7

COMPOSITIONS OF SANTOWAX R AND SANTOWAX O-M

Constituent	Santowax R, w/o	Santowax O-M, w/o
Ortho-terphenyl	12	65
Meta-terphenyl	60	32
Para-terphenyl	28	3

Sieder-Tate equation, was eliminated because it was found to vary only slightly during the runs investigated. The equation best fitting all the data is

$$Nu = 0.015Re^{0.85}Pr^{0.3}.$$

The comparison between the experimental data and the polyphenyl equation is shown in Fig. 7-16. The standard deviation for the data is ±9%. It should be noted that the polyphenyl heat-transfer equation is based on estimated specific heats and thermal conductivities. Therefore, the equation coefficient and Prandtl number exponent may change when the specific heats and thermal conductivities are determined experimentally.

Experimental data obtained for diphenyl heat transfer by Ewing [25] were correlated by the above equation with a deviation of ±5% (see Fig. 7-16). Thus the polyphenyl heat-transfer equation developed in this study appears to be accurate enough to predict heat-transfer coefficients for polyphenyl reactor coolants.

After the studies mentioned above were completed, a series of high-temperature runs were made under conditions expected to foul heat-transfer surfaces. These runs were made at steady-state conditions for periods ranging from 25 to 90 hr for each run.

The first three runs were made with Santowax R at heat-transfer surface temperatures up to 985°F. The loop was not operated above 1000°F because of the pressure limitation of 300 psi on the loop components. A velocity of 15 fps and fluid temperature of 750°F were chosen for these runs to simulate design conditions of the OMRE fuel elements. The conditions at the reference point on the test heater are shown in Fig. 7-17. The dotted lines represent the standard deviation for heat-transfer coefficients as predicted by the polyphenyl equation. Note that the deviation of the data points is less than that predicted by the polyphenyl equation. If fouling had occurred, the measured heat-transfer coefficients would have dropped below the predicted values because of greater temperature drop across the fouled film on the heat-transfer surface.

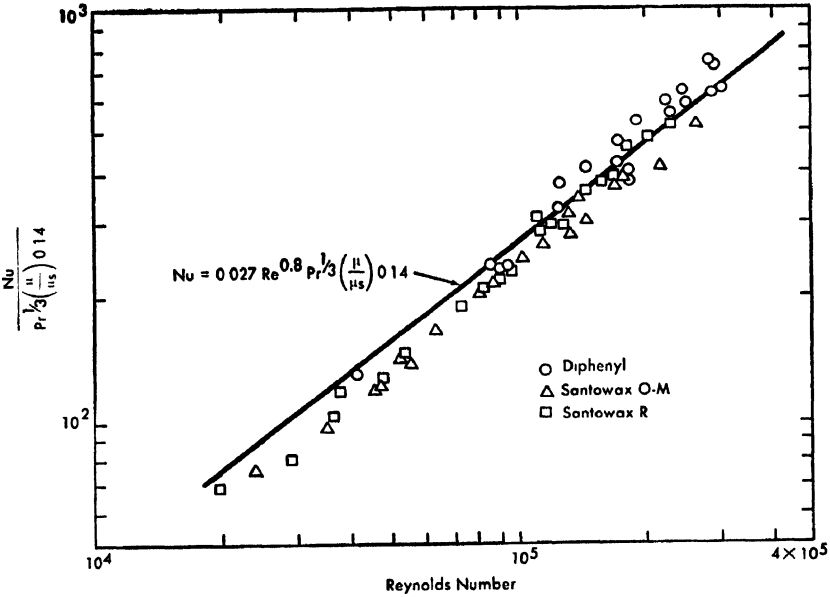

FIG. 7–15 Correlation of polyphenyl heat-transfer data with Sieder-Tate equation

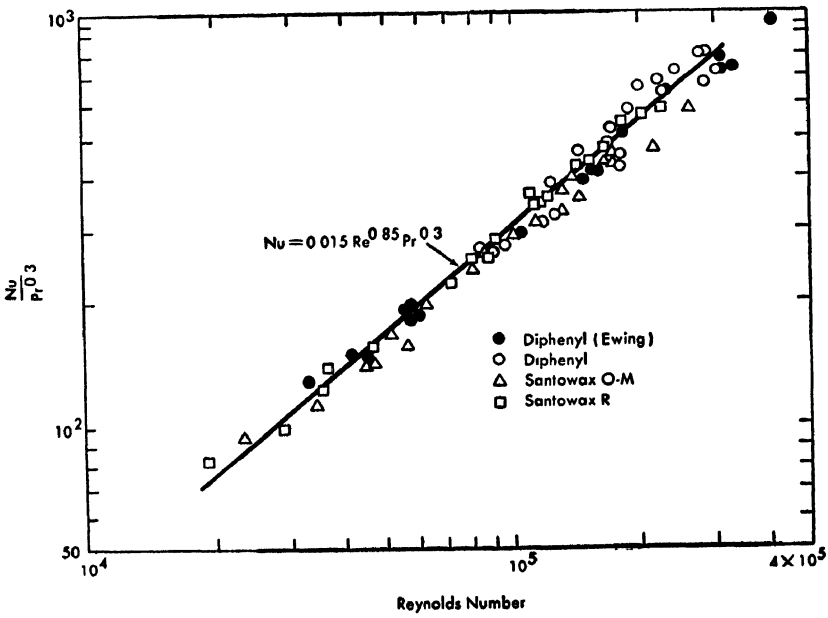

FIG. 7–16. Proposed correlation of polyphenyl heat-transfer data.

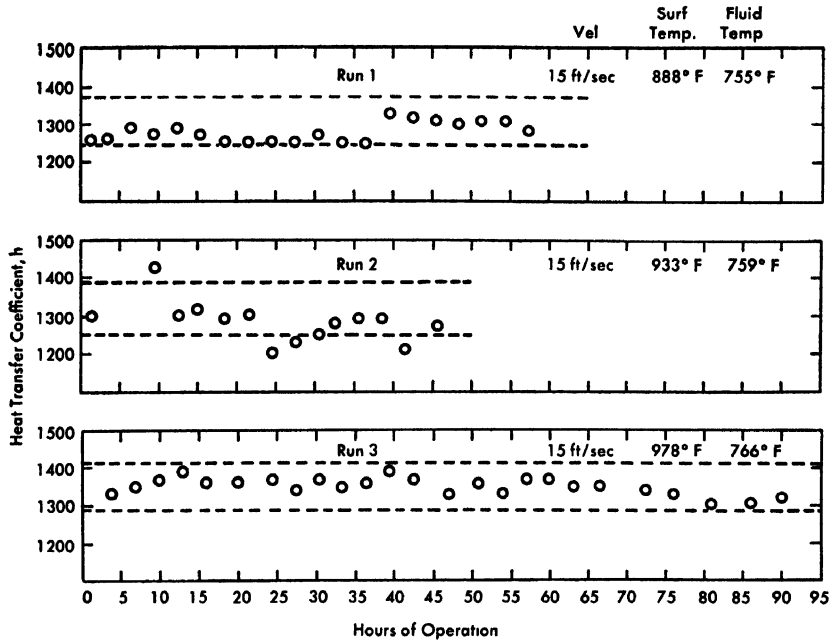

FIG. 7–17 High-temperature Santowax R tests.

After these runs were completed, the test heater was examined Except for surface darkening, no buildup of organic decomposition products was observed. This examination confirmed that heat-transfer surfaces had not fouled during the high-temperature Santowax R runs.

Next, a series of runs was made with Santowax O-M, which more closely resembled the fluid chosen for the OMRE coolant. The operating conditions at the reference point on the test heater are shown in Figs. 7–18 and 7–19. Note that the operating conditions for Run 3 and Run 4 were similar. After completion of Run 4, it was decided that lower fluid velocities might produce fouling at lower surface temperatures. Consequently, the test-heater surface temperature was lowered to approximately 900°F for runs at fluid velocities of 10 and 5 fps. The experimental data points in Fig. 7–18 indicate that no fouling occurred during Runs 5 and 6. Then the heater surface temperature was raised to approximately 960°F for runs at fluid velocities of 10 and 5 fps. Again the experimental data points, as shown in Fig. 7–19, indicate that no fouling occurred during Runs 7 and 8. An examination of the heat-transfer surface after the Santowax O-M runs were completed confirmed that no fouling had occurred.

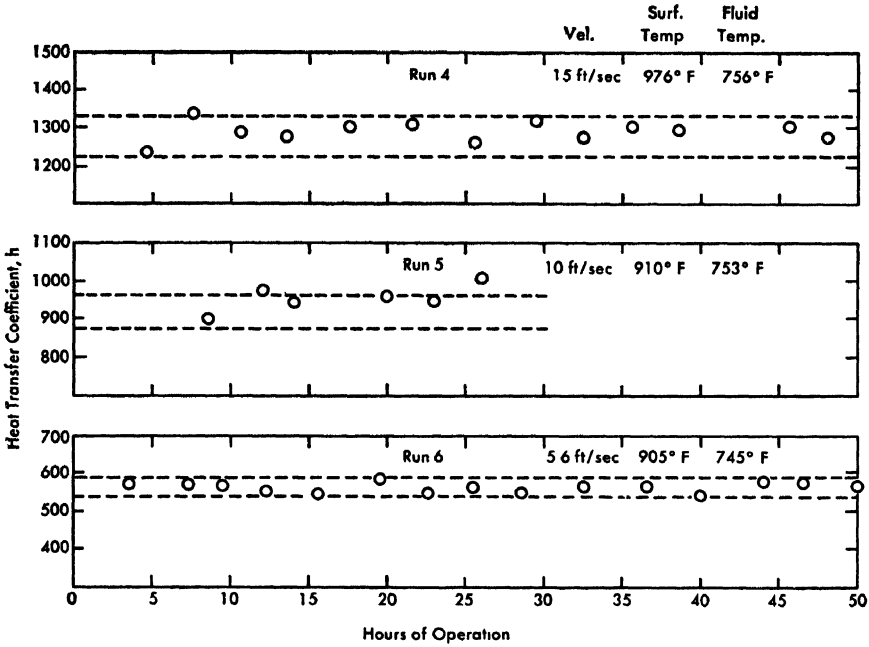

FIG. 7–18. High-temperature Santowax O-M tests

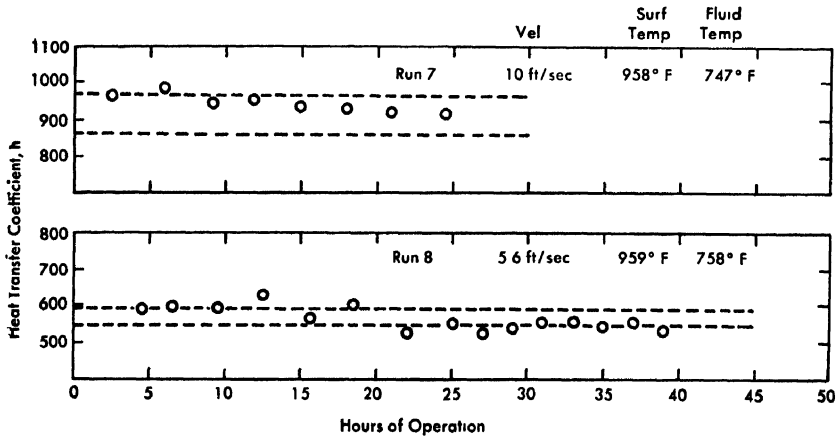

FIG. 7–19. High-temperature Santowax O-M tests.

The results presented above indicate that the polyphenyls may be used under operating conditions much more severe than had been anticipated. However, the effect of higher concentrations of decomposition products on the fouling tendency of polyphenyls is yet to be determined.

7–3.2 In-pile study. The in-pile study was undertaken to determine the rate of radiation decomposition of typical organic coolants and the effects of decomposition products on their heat-transfer properties [26]. It was decided to irradiate the fluids and to determine their heat-transfer properties under conditions similar to those expected in the OMRE core.

The irradiation facility chosen was the Materials Testing Reactor (MTR) at the National Reactor Testing Station in Idaho. A circulation loop was designed having an in-pile section with a uranium heater element for insertion into the A-13 reflector position of the MTR. The flow diagram of the loop is shown in Fig. 7–20. The out-of-pile section had a resistance test heater, similar in design to the one used for the laboratory heat-transfer loop, which provided the same operating conditions as the uranium heater with the exception of the radiation field. At full power, the maximum fluxes in the in-pile section at the reactor midplane were: 2×10^{13} thermal neutrons/(cm^2) (sec), 1×10^{12} fast neutrons/(cm^2) (sec), and 0.6 watt/g of gamma heating.

The four fluids chosen for this study were isopropyl-diphenyl, diphenyl, Santowax R, and Santowax O-M. The isopropyl-diphenyl consisted of 55 w/o meta-isomer and 45 w/o para-isomer. These fluids were irradiated at bulk fluid temperatures between 500 and 700°F The maximum heat-transfer surface temperatures were 800°F, with heat fluxes as high as 200,000 Btu/(ft^2) (hr) Each fluid was irradiated for one MTR cycle; then diphenyl was irradiated for a three-cycle test New in-pile sections were used with each fluid tested so that the uranium heater surface could be examined in the hot cell after each irradiation test.

The irradiation of the test fluids produced gas and higher-molecular-weight materials referred to here as high-boiler residue. A distillation method was used to analyze for the amount of high-boiler residue formed, since the decomposition products were found to be much less volatile than the starting materials. The radiation dosage was measured with gamma calorimeters and neutron-flux monitor wires. The observed decomposition rates are presented in Fig. 7–21 In calculating G_p, a high-boiler residue molecular weight of 460 was used. Radiation damage was assumed to be a function of energy absorption, regardless of the type of radiation. For this test facility, the energy absorbed from gamma photons was 82% of the total; the other 18% was from the slowing down of neutrons. The maximum error in the decomposition rates presented is probably about ±25%, largely due to unavoidable inaccuracy in measuring the incident radiations.

Decomposition rates were similar, decreasing as high-boiler-residue concentration increased for all four fluids. There appears to be less scatter in the data at higher concentrations of high-boiler residue. These results are slightly higher than those previously reported [27–29].

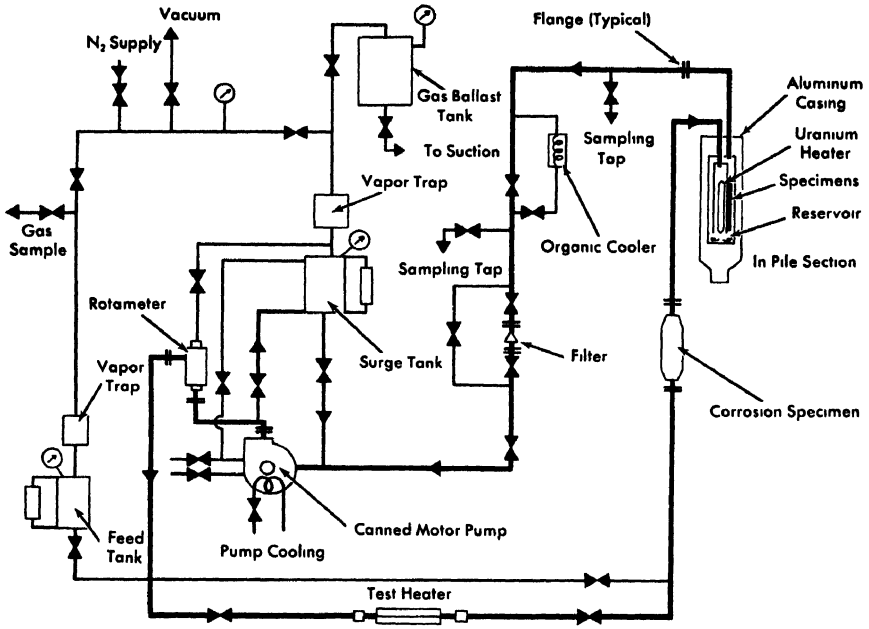

FIG. 7–20 Schematic flow diagram of organic in-pile loop.

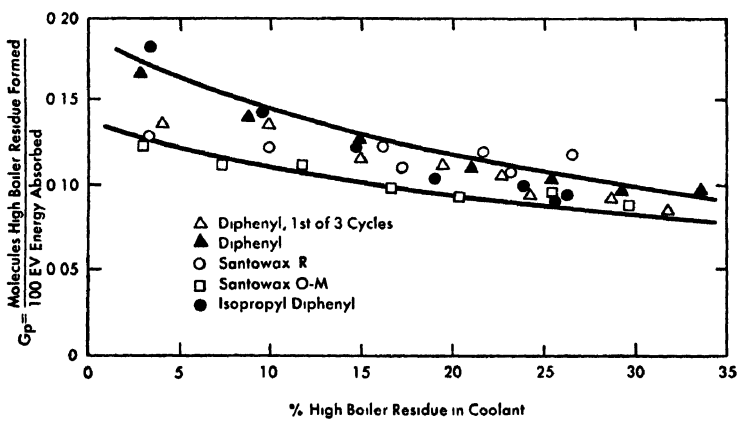

FIG 7–21. In-pile decomposition rates of polyphenyls.

The heat-transfer coefficients, measured at the external resistance heater, remained constant during the irradiations. There was no apparent change in the heat-transfer properties of the fluids tested as the high-boiler residue concentrations increased to the final values. The average

deviation of the heat-transfer data was the same as that observed during the out-of-pile heat-transfer studies.

Analysis of the in-pile heat-transfer data indicated no gradual increase in the film temperature drop which could be attributed to surface fouling. Except for a surface darkening of the uranium heaters, revealed by hot-cell examinations, there was no visual evidence of fouling. However, in some cases heat-transfer coefficients measured in the in-pile uranium heater were approximately 10% lower than would have been predicted from the coefficients observed at the external heater. Considering the accuracy ($\pm 15\%$) of the in-pile measurements, a hot-side scale factor of 10% is tentatively recommended for in-pile heat-transfer design.

Corrosion samples were inserted in both out-of-pile and in-pile locations in the MTR loop [30]. Mild steel, aluminum, stainless steel, magnesium, and zirconium samples were exposed to the irradiated organic fluids. The magnesium and zirconium samples showed weight gains from oxide and hydride formation, respectively. Because the hydrocarbon contained oxygen and water in the parts-per-million range, it is probable that the magnesium oxide was formed by reaction of the magnesium with oxygen or water. The zirconium hydride was probably formed due to reaction with nascent hydrogen, the most prevalent gaseous radiolytic product.

The stainless-steel and aluminum samples exhibited good corrosion resistance with insignificant weight changes and only slight surface discolorations. The mild steel samples displayed insignificant weight changes, but the surfaces were blackened by the hydrocarbon.

Even though these specimens were exposed for short times, they served to show that radiation has little effect on corrosion and that conventional structural materials have good corrosion resistance. The low radioactivity level showed that corrosion products were absent from the circulating irradiated fluids.

At the end of the in-pile loop studies, the out-of-pile equipment, pump, valves, external heater, and stagnant and cool sections of piping showed no fouling or deposition of insoluble materials or residues.

In summary, the in-pile study has shown that (1) the four polyphenyls tested behaved similarly, (2) decomposition rates depended on total energy absorption and were predictable from capsule irradiations, (3) the heat-transfer properties were predictable from changes in physical properties and fouling appeared unlikely under the conditions expected in the OMRE core, and (4) corrosion of conventional structural materials and activation of the polyphenyls were negligible. It is concluded that polyphenyls are well suited for removing heat from nuclear reactor cores at temperatures appropriate for generating electrical power. Further research is required to determine the maximum permissible operating temperatures for these fluids.

7–4. The Organic Moderated Reactor Experiment (OMRE)*

7–4.1 Objectives. The Organic Moderated Reactor Experiment represents the final test in a research and development program designed to demonstrate the feasibility of the concept of an organic moderated and cooled power reactor. The reasons for the interest in this concept and its advantages have been described. All out-of-pile and in-pile capsule and loop tests have indicated that some types of organic compounds are stable enough to make their use in nuclear power reactors feasible, both technically and economically. A full-scale reactor experiment is now essential to establish the feasibility of the concept. This experiment is the OMRE (Organic Moderated Reactor Experiment). It is not a prototype of a nuclear power plant, but rather a full-scale irradiation facility designed to study the behavior of the most promising organic compounds under conditions similar to those encountered in power reactor applications.

It is the purpose of the OMRE to provide a conclusive test of:

(1) The technical feasibility of the concept of an organic moderated and cooled power reactor. The OMRE will show whether or not this type of reactor can be operated continuously and reliably without serious problems from decomposition of the moderator-coolant or fouling of heat-transfer surfaces

(2) The economic feasibility of this concept. From the cost viewpoint, it is essential to know what the hydrocarbon decomposition rates will be in a power reactor, so that makeup costs can be estimated. The OMRE will provide this information.

7–4.2 Engineering bases. The OMRE was designed to meet the following basic criteria:

Maximum fuel-element surface temperature	800°F
Bulk coolant temperature	500 to 700°F
Maximum coolant velocity through core	15 fps

The fuel surface temperature was limited to 800°F because even without radiation damage, hydrocarbons may break down excessively at temperatures higher than this. A temperature of 500°F is considered to be about the lowest temperature desirable for power reactor applications, and the 700°F upper limit on the bulk temperature is essential to provide enough temperature driving force for heat transfer from the fuel elements to the coolant. The velocity of 15 fps was chosen to limit the amount of erosion in the piping system and keep the total flow rate of hydrocarbon in the OMRE within reasonable limits (9200 gpm).

Selection of moderator-coolant. The original design of the OMRE was based on the use of diphenyl as moderator, reflector and coolant. Di-

*By C. A. Trilling, AI.

TABLE 7–8

COMPOSITION AND PHYSICAL PROPERTIES OF THE INITIAL OMRE COOLANT

Composition	*w/o*
Diphenyl	16.0
Ortho-terphenyl	46.1
Meta-terphenyl	31.8
Para-terphenyl	6.1

Physical properties	*Temperature range* 500°F	700°F	800°F
Specific gravity	0.91	0.81	0.77
Specific heat, Btu/(lb)(°F)	0.52	0.59	0.60
Viscosity, centipoises	0.46	0.23	0.17
Thermal conductivity, Btu/(hr)(°F)(ft)	0.069	0.063	0.061
Vapor pressure, lb/in^2 abs	5.3	42.9	94.5
Melting point range	The mixture is a thick slurry, practically solid at 70°F, and becomes completely liquid at 200°F.		

phenyl was chosen because there was reliable information on its physical properties, and because it was commercially available at low cost Its relatively low melting point made preheating easy, and its relatively high vapor pressure set design requirements high enough to allow for later use of other similar hydrocarbons (with lower vapor pressures).

Much information had been obtained on the physical properties and behavior of the terphenyls by the time construction of the OMRE was completed. It was decided then to use a commercial mixture of polyphenyls having a much lower vapor pressure than diphenyl. This mixture consists mainly of ortho- and meta-terphenyl, with smaller amounts of diphenyl and para-terphenyl. It is commonly known by its trade name of Santowax O-M. The composition and physical properties of the OMRE coolant are shown in Table 7–8.* The data presented in this table apply

*The composition of the initial OMRE Coolant differs from that of the Santowax O-M previously described in Table 7–7. The composition of this material differs from batch to batch because of changes in process conditions but, generally speaking, any material consisting mainly of ortho- and meta-terphenyl is known as Santowax O-M.

TABLE 7–9

ESTIMATED PERFORMANCE DATA FOR THE ORGANIC MODERATED REACTOR EXPERIMENT USING SANTOWAX O-M

Bulk coolant inlet temperature, °F	500	500	700	700
Bulk coolant outlet temperature, °F	525	518	710	708
Reactor power, Mw	14.8	10.9	6.2	4.8
Peak-to-average flux ratio	3.16	3.16	2.80	2.80
High-boiler residue, w/o	0	35	0	35
Viscosity ratio, μ/μ_o	1.00	2.43	1.00	2.20
Average heat flux, Btu/(ft²)(hr)	74,000	55,000	31,000	24,000
Maximum heat flux, Btu/(ft²)(hr)	230,000	174,000	87,000	68,000
Average specific power, kw/kg	580	430	240	190
Maximum specific power, kw/kg	1830	1360	670	530
Average thermal neutron flux in fuel, n/(cm²)(sec)	2.0×10^{13}	1.5×10^{13}	9.5×10^{12}	7.4×10^{12}
Maximum thermal neutron flux in fuel, n/(cm²)(sec)	6.5×10^{13}	4.8×10^{13}	2.7×10^{13}	2.1×10^{13}

only to the initial unirradiated charge of coolant. Irradiation of the coolant during operation of the reactor will obviously change both its composition and its physical properties.

Reactor performance. The estimated performance data for the OMRE are shown in Table 7–9. These are based on the specified design objectives of maximum fuel-element surface temperature of 800°F, bulk coolant temperatures of 500 to 700°F, and a maximum coolant velocity through the core of 15 fps. The physical property data used are those of Santowax O-M; any changes in characteristics of the coolant during operation will necessarily change some of the values in the table.

The values presented were estimated for four operating conditions: inlet coolant temperatures of 500 and 700°F, high-boiler residue concentrations of zero and 35% (initial loading and maximum expected normal steady state concentration). The presence of 35% high-boiler residue was assumed to increase the hydrocarbon viscosity by a factor of 2.43 at 500°F,

TABLE 7-10

PHYSICS PARAMETERS
FOR THE ORGANIC MODERATED REACTOR EXPERIMENT

	Moderator temperature	
	500°F	700°F
Fast diffusion coefficient, D_f, cm	1.275	1.442
Fermi age, τ, cm^2	83.0	107.9
Thermal neutron energy, ev	0.046	0.056
Thermal diffusion coefficient, D_{th}, cm	0.317	0.382
Square of thermal diffusion length, L^2, cm^2	5.00	7.24
Buckling, B_g^2, cm^{-2}	39.7×10^{-4}	37.1×10^{-4}
Thermal utilization, f	0.729	0.755
Infinite multiplication factor, k_∞	1.517	1.570

and by a factor of 2.20 at 700°F. Under these various conditions the average temperature rise of the coolant varies from 8 to 25°F, the reactor power from 4.8 to 14.8 Mw, the maximum heat flux from 68,000 to 230,000 Btu/(ft^2) (hr), and the average thermal neutron flux in the fuel from 0.74×10^{13} to 2.0×10^{13} n/(cm^2) (sec) At a power of 14 8 Mw, the average thermal and fast neutron fluxes in the core are approximately 4.9×10^{13} and 2.2×10^{14} n/(cm^2) (sec), respectively. Table 7-10 presents a summary of the basic physics parameters used in the design of the OMRE.

7-4.3 Description of the OMRE. The OMRE is located at the National Reactor Testing Station (NRTS) near Idaho Falls, Idaho. The site is in the south-central area of the NRTS about three miles east of the Central Facilities Area and two miles south and west of the SPERT site. The facilities and location were selected for economy of shielding, containment, venting of exhaust gases, and waste disposal.

Reactor. The reactor vessel (Fig. 7-22) is a mild alloy steel (1/2% Mo-1%Cr) pressure tank, 4½ ft in internal diameter, 28 ft tall, with a wall thickness of 1 inch. Designed to the ASME Unfired Pressure Vessel Code for a maximum allowable operating pressure of 400 psia, it was completely stress relieved, and welds were 100% x-rayed. Its normal operating pressure is 200 psig.

The core of the reactor, located in the lower part of the vessel, uses plate-type, stainless steel-UO_2 fuel elements. A cutaway perspective of the fuel element is shown in Fig. 7-23 and a photograph in Fig. 7-24.

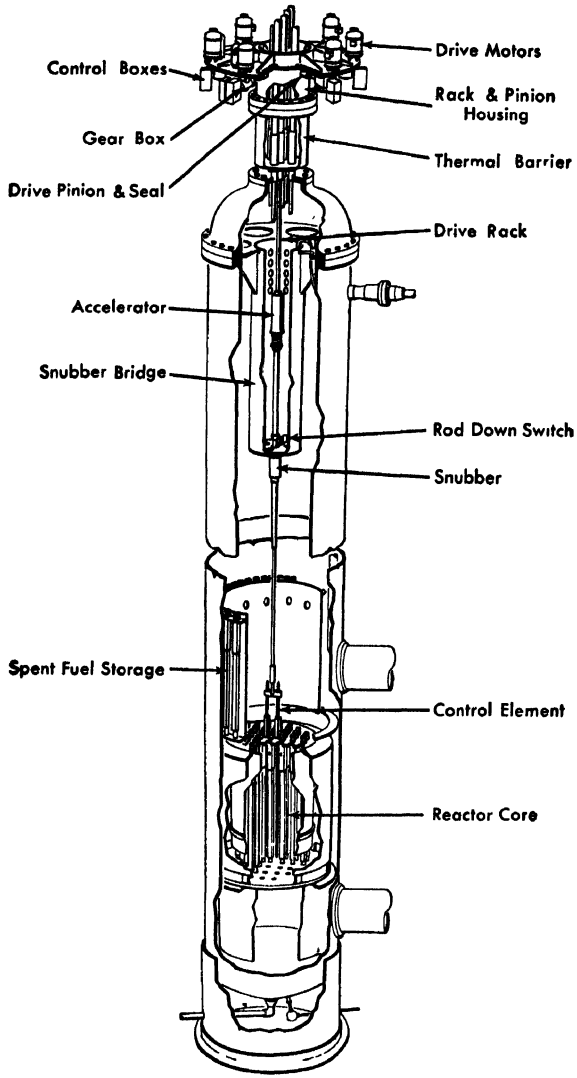

FIG. 7–22. Cutaway drawing of OMRE reactor vessel.

This type of element was selected because of its large surface-to-volume ratio and the advanced stage of development of its manufacturing technology. Each fuel plate consists of a 20-mil-thick central matrix of 25 w/o highly enriched UO_2 and 75 w/o stainless steel, clad on each side with 5 mils of stainless steel. Each element is assembled from 16 fuel plates separated by a 134-mil coolant gap, two inactive end plates, and two side closure plates. The side and end plates are seam-welded at the corners

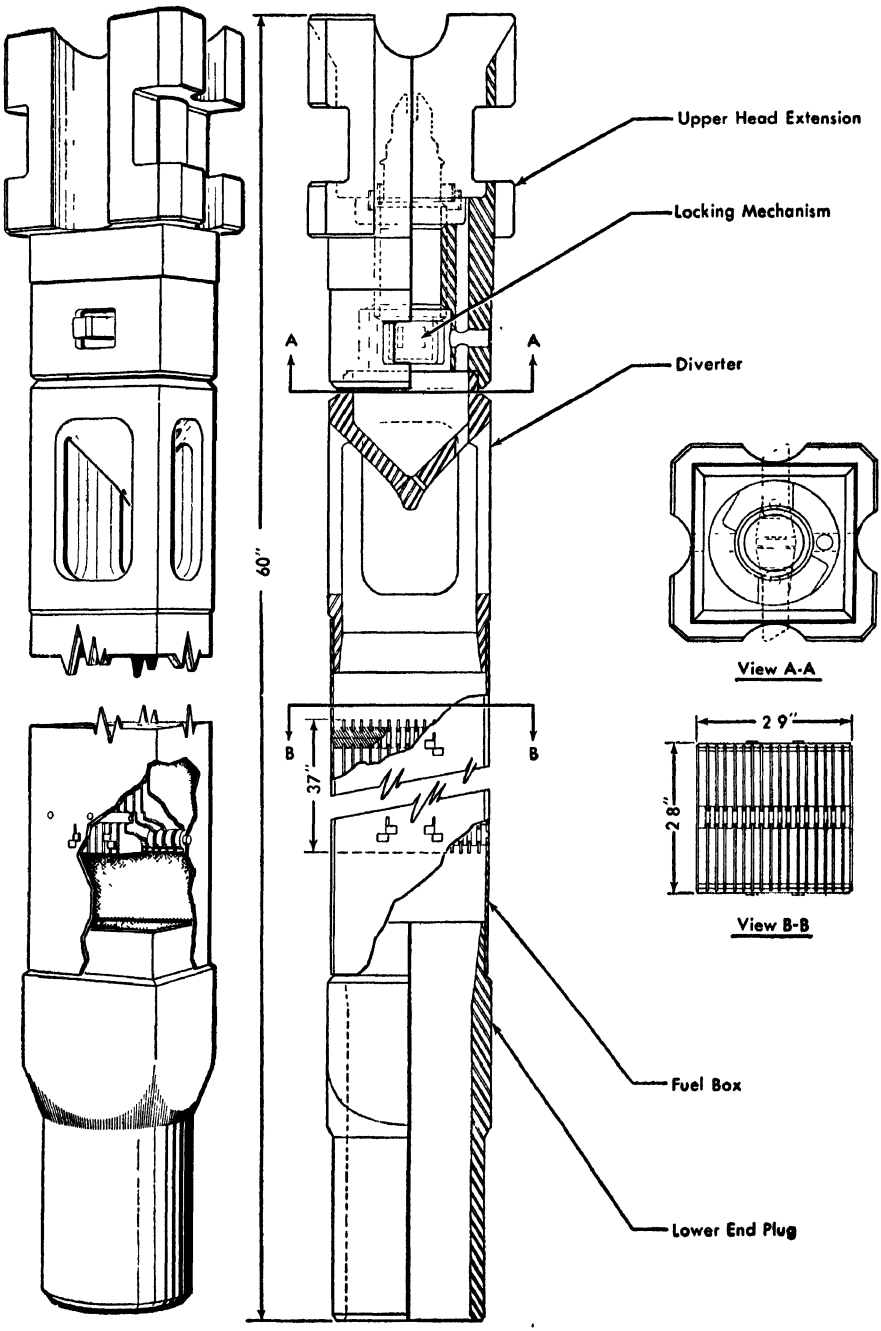

FIG. 7–23. Details of OMRE fuel element.

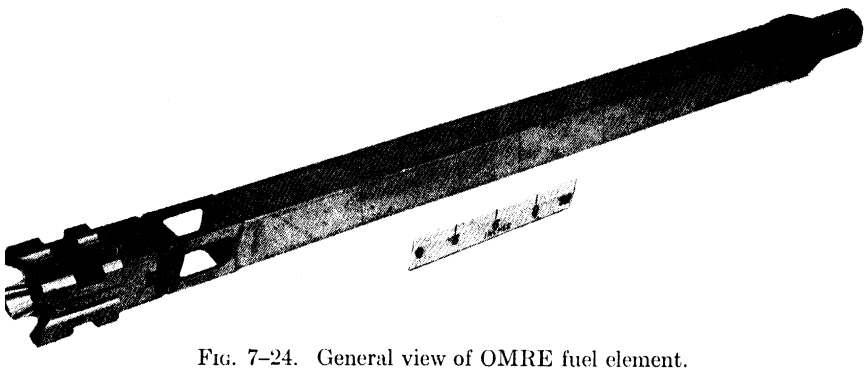

FIG. 7–24. General view of OMRE fuel element.

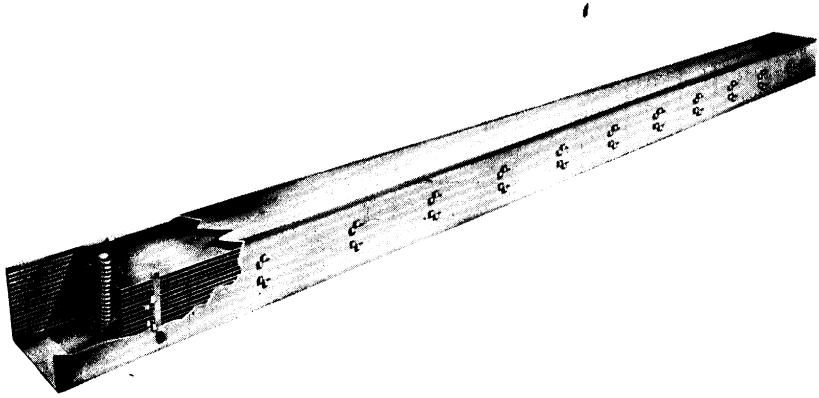

FIG. 7–25. Perspective of OMRE fuel box assembly.

to form a rectangular box 2.8 by 2.9 inches in cross section (Fig. 7–25). The dimensions of the active fuel plates are 36 by 2.5 inches.

The 50-mil-thick side plates of the box are longitudinally grooved to a depth of 30 mils to receive and space the fuel plates. The plates, free to move in the longitudinal grooves, are held stationary near the inlet end of the box by a retaining bar, welded to the side plates, which engages notches in the fuel plates. The other end of the fuel plate is free, to allow for differences in thermal expansion. Spacer pins near each end of the fuel box engage slots in each end of the fuel plates. The side plate grooves are deep enough for the plate to expand transversely. Two fuel plates are equipped with split tabs which protrude through slots in the side plates and are bent over, to prevent the side plates from bowing under internal pressure. The fuel boxes are supported by end boxes, held in a $4\frac{1}{2}$-inch square lattice by upper and lower grid plates.

Thirty-one fuel elements with 25.5 kg of U^{235} in all were loaded into the core, providing enough excess reactivity to compensate for temperature effects, xenon poisoning, and fuel burnup. One space in the lattice holds an antimony-beryllium neutron source; five additional spaces were provided to allow for uncertainty in the nuclear calculations.

A thermal shield 2 inches thick is inside the vessel, separated from it by a 2-inch annular passage. The shield rests on the lower grid-plate support, which is welded to the inner wall of the vessel. The upper grid plate is, in turn, supported by the thermal shield.

Coolant from the bottom plenum enters the lower end boxes of the fuel elements, flows upward between the fuel plates into the upper end boxes, and discharges into the spaces between the fuel elements. Flowing downward around the outside of the fuel elements, it cools the control rods and thermal shield A final pass between the thermal shield and reactor tank discharges the coolant to the 14-ft-deep pool that forms the biological shielding above the reactor core

The OMRE is regulated by twelve control rods symmetrically located between the fuel elements. The rods are 1¼-inch steel tubes loaded over a 36-inch length with compacted boron carbide powder The twelve rods, hung in pairs from six hanger rods, are driven through rack-and-pinion drives, to perform double functions of control and safety. One pair of rods, driven through a differential gear by a fast regulating motor and a low shim motor, continuously regulates reactor operation. Shimming is done by all six pairs of rods. For scram, a solenoid-operated ball-type latch releases the rods; a kick-off spring ensures downward acceleration at least equal to that of gravity.

Fuel elements will be removed only to examine (in a "hot cell") the surface of the fuel plates for evidence of fouling. Normally, a spent fuel element removed from the core will be transferred to a spent fuel storage rack along the wall of the vessel above the upper grid plate.

Process system. The OMRE flow diagram is shown in Fig. 7–26. The reactor core, located near the bottom of the vessel, is shielded by a pool of hydrocarbon 14 ft deep. Nitrogen provides an inert atmosphere above the pool and maintains a 200 psig pressure on the system, corresponding to a saturation temperature of 920°F for the OMRE coolant. Nitrogen continuously purges the surface of the coolant, prevents buildup of hydrogen and light hydrocarbon decomposition gases, and sweeps these gases to the exhaust stack. An expansion tank takes care of the large change in volume of the hydrocarbon during temperature transients (34% between 200 and 700°F).

The cooling system circulates 9200 gpm of coolant from the reactor to an airblast heat exchanger, where the heat is dissipated to the atmosphere. (Using an airblast heat exchanger rather than a steam generator

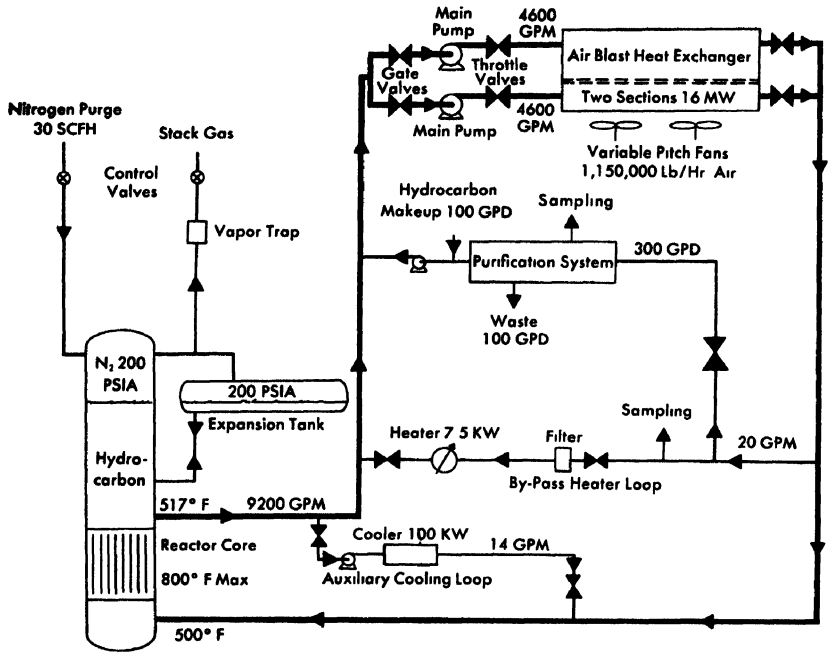

FIG. 7–26 Schematic flow diagram

simplifies temperature control over the wide experimental range.) Two 4600-gpm centrifugal hot-oil pumps, operating in parallel, circulate the coolant. The mechanical seals on these pumps are cooled by recirculating a small stream of the cooled hydrocarbon discharged from the pumps; the small leakage is collected in drums for disposal. An auxiliary coolant system, rated at 100 kw, removes after-glow heat during reactor shutdown, when the main coolant loop is inoperative. A spray cooler removes heat from this loop.

The test section of the bypass heater loop provides continuous information on the change in heat-transfer properties of the hydrocarbon during reactor operation It consists of an electric heater, and temperature and flow instrumentation for determining heat transfer coefficients as functions of irradiation time of the coolant in the reactor. It also provides a convenient record of how radiation damage affects heat-transfer behavior of the coolant outside the reactor.

The purification system removes a small batch of damaged hydrocarbon from the main coolant stream every day, purifies it by low-pressure distillation (20 mm Hg), returns the purified material (with additional fresh makeup) to the reactor system, and rejects to waste storage the high-boiler residue resulting from radiation damage. A batch system is used

because it allows the flexibility required for an experimental system. However, a continuous system would be used in a full-scale power plant.

Except for the reactor vessel, the whole system is made of carbon steel. All components have equipment to preheat the system above the melting point of the hydrocarbon and keep the coolant molten during extended shutdowns. Induction heating is used on the vessels and piping, the pumps and valves are traced with heating cable, and the airblast heat exchanger has an oil burner.

Instrumentation and control. Operation of the OMRE is controlled by regulating.

(1) Maximum fuel-plate surface temperature.
(2) Reactor inlet temperature.
(3) Coolant flow rate

The coolant flow rate is controlled by two 10-inch globe valves downstream of the main pumps. These valves, normally fully open, are used for throttling only during low-velocity tests. An orifice plate in the inlet line to the reactor measures flow.

The inlet temperature to the reactor is determined by the outlet temperature from the airblast heat exchanger. A controller continuously regulates the flow of air across the bundles of finned tubes by adjusting louvres above them. Additional temperature control is provided by manual, but remote, adjustment of the pitch of the fans on the airblast heat exchanger.

Controlling the maximum fuel-plate surface temperature presents a problem: on which fuel element, on which fuel plate, and at what location on the plate will a hot point occur? Obviously only a limited number of temperature measurements can be taken. Seven fuel elements are instrumented in the core of the OMRE: the central element, the three elements estimated to operate in the highest flux in one quadrant, and one element in each of the other three quadrants to check the flux symmetry (Fig. 7–27). Each of these elements has three appropriately located surface thermocouples on its hottest plate (the active plate closest to the moderator gap and farthest from any control rods), and its adjacent coolant channel is equipped with two coolant outlet thermocouples. The signal for controlling the maximum fuel-element surface temperature is derived from the hottest of these thermocouples. As conditions change, connections can be altered to derive control always from the hottest-reading thermocouple. Allowance is made for the possibility of a hot spot at an unmonitored location. As shown in Fig. 7–27, the temperature-error signal derived from the control thermocouple energizes a drive motor that changes the set point on the flux level controller, thus leading to corrective action by the regulating rod.

Reactor safety is assured by means of interlocks, alarms, and scrams. The reactor shuts down automatically whenever any of the following conditions exists:

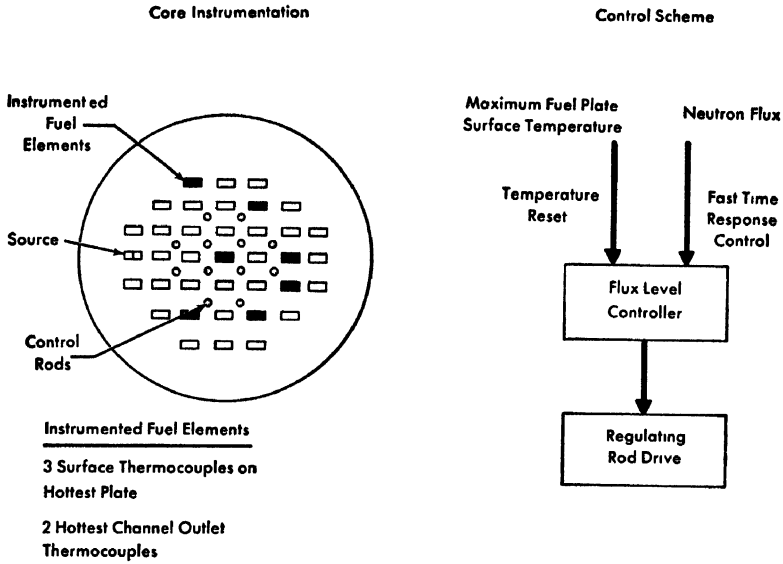

FIG 7–27. Maximum fuel plate surface temperature control.

(1) Reactor period less than 5 sec.
(2) Reactor power level greater than a predetermined safe limit.
(3) Fuel-element surface or coolant-channel outlet temperature more than 10°F above preset temperature.
(4) Main coolant flow rate less than 90% of normal operating rate.
(5) Reactor vessel pressure less than 175 psig.
(6) Reactor vessel pressure greater than 225 psig.
(7) Low liquid level in the reactor.
(8) Power loss to the main coolant pumps.
(9) Power loss to the airblast heat exchanger.

In addition to the instrumentation required for control and safety, the OMRE has temperature, pressure, flow, and radiation instrumentation designed to provide maximum information on the operation of the reactor and the behavior of the hydrocarbon. There are also sampling taps for obtaining coolant and gas samples for laboratory evaluation.

General arrangement of plant. The over-all arrangement of the OMRE facility is shown in perspective in Fig. 7–28, and in plan in Fig. 7–29. The reactor is located outside the operations building under a corrugated sheet-steel shed to protect the control element drives from the weather and to shelter maintenance personnel. The reactor vessel is for the most part buried underground. The core lies well below ground level. Inlet and outlet coolant pipes are attached to the tank just below and above the re-

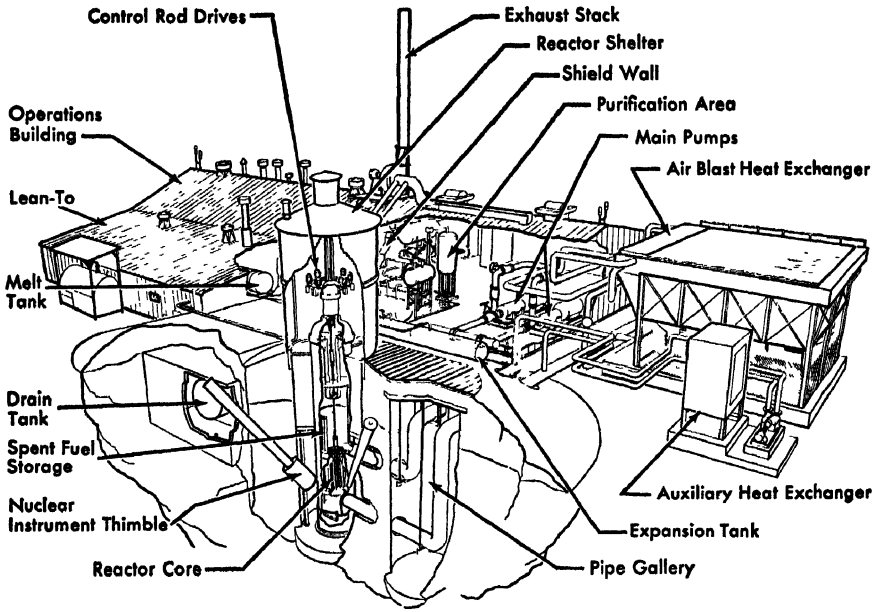

FIG 7–28 Perspective view of OMRE facility.

actor core. They pass horizontally through separate tunnels to a pipe well, where they rise to ground level. The hot outlet pipe then goes to the pumps in the operations building, then out-of-doors to the airblast heat exchanger. The inlet pipe, connected to the cold end of the heat exchanger, completes the coolant loop.

The operations building, a one-story, steel-frame structure with floor area 32 by 84 ft, is divided into two areas by a concrete slab shielding wall 2 ft thick. The process area, adjacent to the reactor and airblast heat exchanger, contains the main coolant pumps and valves, the purification system, the air compressor (for pneumatically operated valves and instruments), and various related equipment. The radiation level in this area may be high enough to limit accessibility. In the area on the other side of the wall are the control room, the chemical laboratory, the mechanical room, and the lavatory. The control room houses the switch gear, control console for the reactor, instruments for the heat-transfer and purification systems, and the handles of valve-stem gear drives which pass through the concrete wall to valves in the radioactive process area. The laboratory has a fume hood and sampling and testing equipment for chemical analysis of the coolant and its decomposition products. A 20- by 40-ft lean-to, attached to the operations building, is shielded from the reactor and process area by an extension of the concrete slab wall. Of steel frame con-

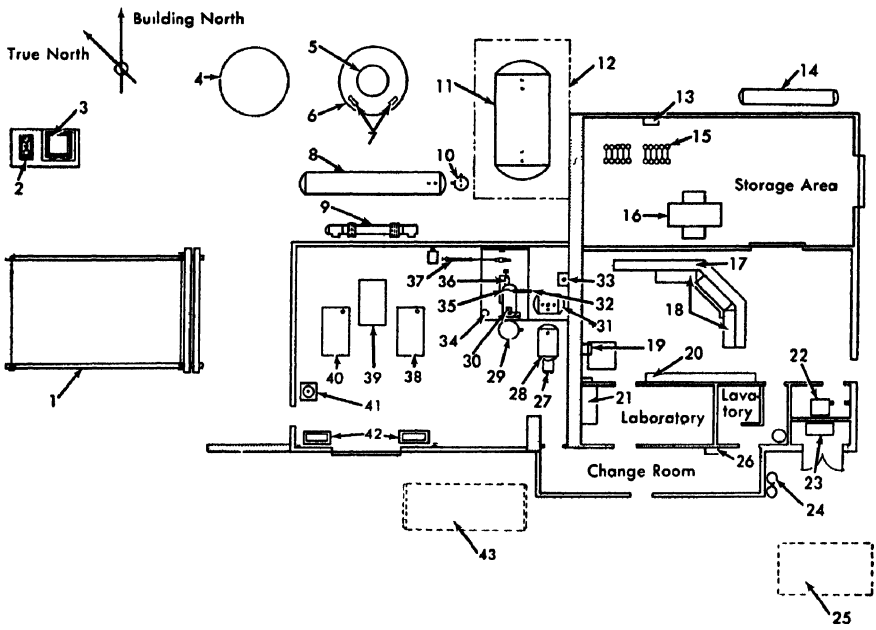

1 Air Blast Heat Exchanger
2 Auxiliary Pump
3 Evaporative Cooler
4 Pipe Gallery
5 Reactor Tank
6 Reactor Gallery
7 Electrical Terminal Box
8 Expansion Tank
9 Expansion Header
10 Reactor Vapor Trap
11 Drain Tank
12 Drain Tank Pit
13 Water Booster Pump
14 CO_2 Tank
15 Nitrogen Manifold
16 Melt Station
17 Console Wiring Access Pit
18 Console
19 Transformer
20 Switch Gear
21 Fume Hood
22 Furnace
23 Emergency Generator
24 Laboratory Gas Manifold
25 Oil Tank
26 Stack Monitor
27 Waste Hold Tank
28 Still Supply Tank
29 Vacuum Still
30 Distillate Condenser
31 Feed Tank
32 Vapor Trap
33 Vacuum Pump
34 Still Cooler
35 Distillate Hold Tank
36 Feed Pump
37 By Pass Heater
38 Main Pump A
39 Pump Pit
40 Main Pump B
41 Air Compressor Tank
42 Air Compressor
43 Waste Storage Tank

FIG. 7–29. OMRE equipment layout plan.

struction, it forms the workshop area and houses nonradioactive process equipment, such as the melt station, the nitrogen supply and manifolds, and the water supply and treatment system.

The three principal areas described have separate ventilation systems to minimize hazards of spreading radioactivity or fire. A carbon dioxide flooding system protects the process area and the reactor shelter against fire.

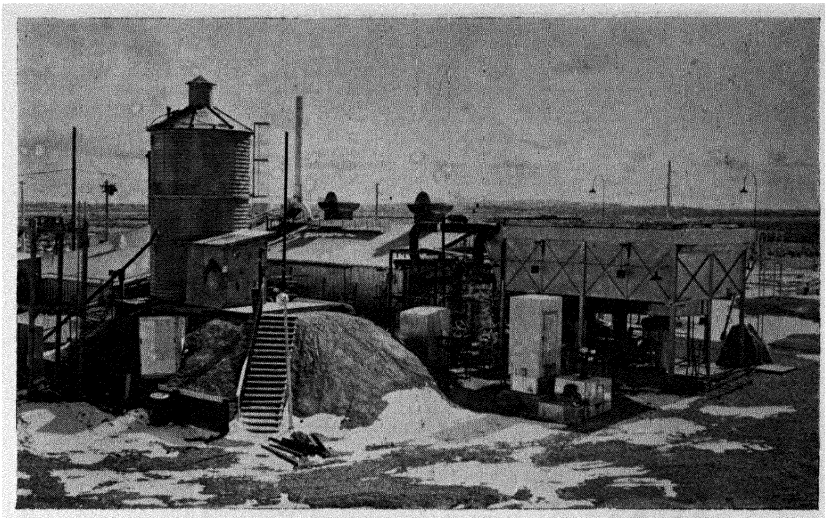

FIG. 7–30. OMRE facility from the northwest.

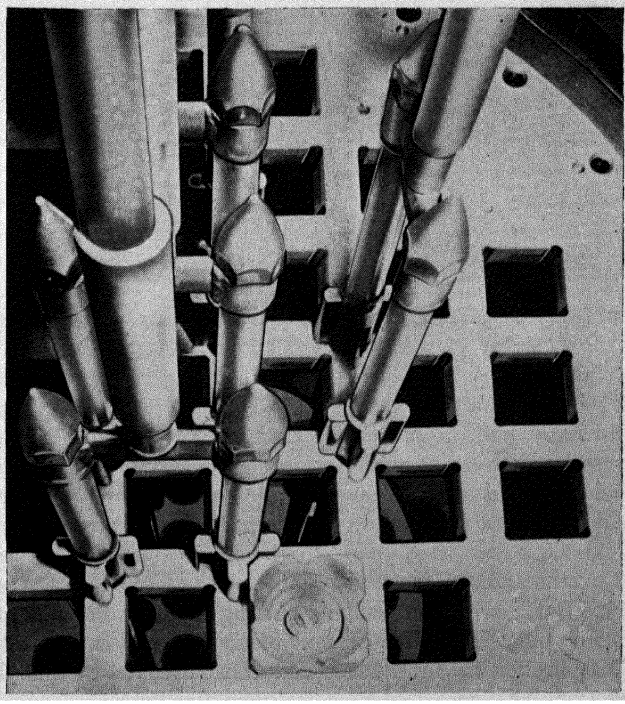

FIG. 7–31. View of upper grid plate, control rods, and fuel elements.

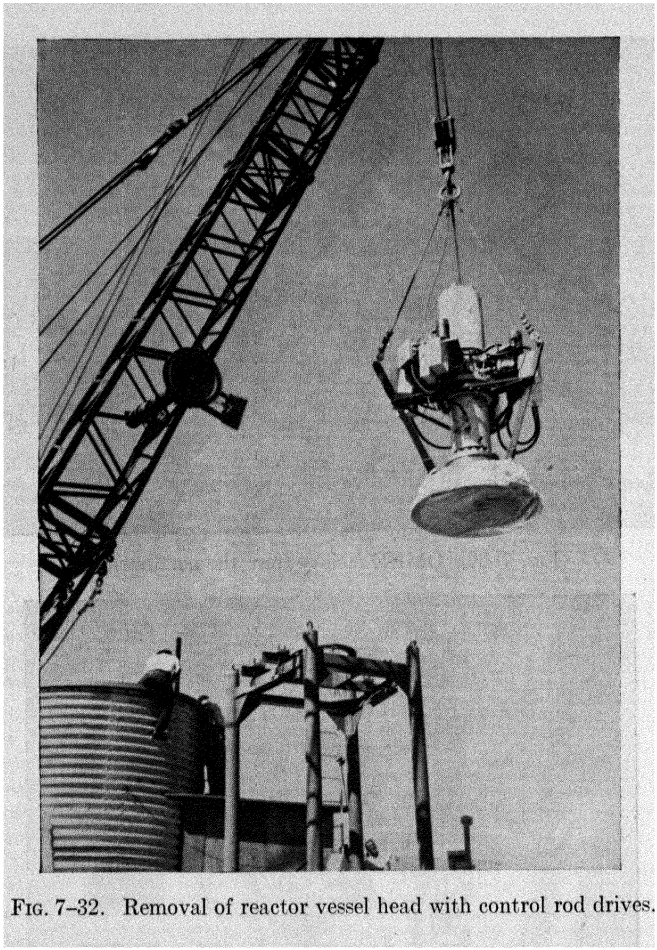

FIG. 7–32. Removal of reactor vessel head with control rod drives.

Figure 7–30 shows a typical view of the outside of the OMRE facility, the control room, and the process area. Figure 7–31 is the inside of the reactor vessel before filling with coolant; it shows the upper grid plate, the control rods, and a fuel element in position. Figure 7–32 illustrates the normal procedure for opening the reactor vessel.

7–4.4 Construction. Conceptual plans for the OMRE were started in July 1955. Detailed design and engineering analysis began in October 1955. In February 1956, procurement of major components was begun. Ground was broken in June 1956, and construction was completed in May 1957.

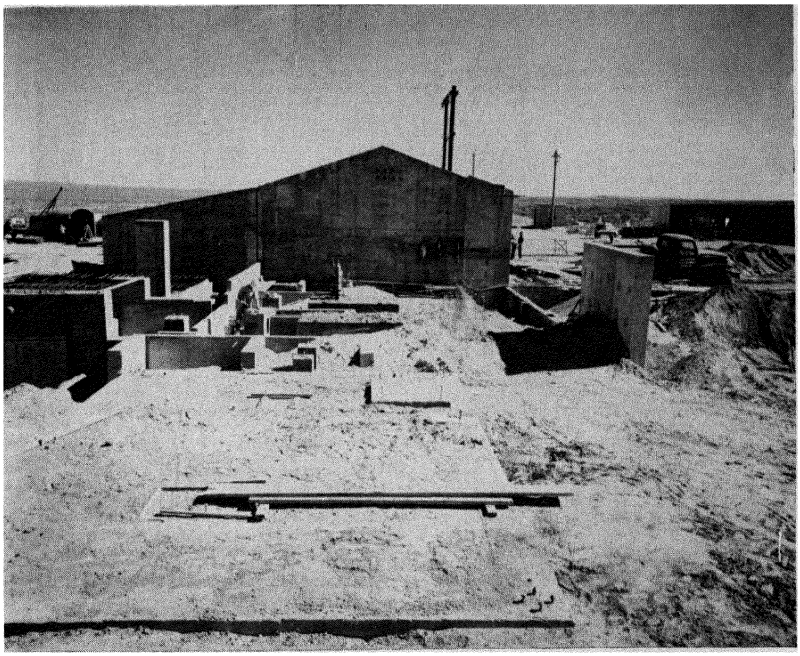

FIG. 7–33. Concrete shielding wall between the control room and the power area.

Various stages of construction are illustrated by the photographs. Figure 7–33 shows the concrete shielding wall between the control room and the process area in the operations building, as well as the drain tank vault and the foundations for the airblast heat exchanger. Figure 7–34 illustrates the installation of the reactor vessel into its corrugated cavity liner. Figure 7–35 is a view of the inside of the reactor vessel, the upper grid plate, the fuel-element storage rack, and the control rods. Figure 7–36 is an over-all view of the OMRE facility at completion of construction.

The cost of constructing the OMRE was $2,372,000, and the cost of fabricating the first core was $262,000.

7–4.5 Preoperational Testing. Preoperational testing lasted from May 1957 through the end of August 1957. All the individual components and instruments were checked and the performance of the whole system was tested under simulated operating conditions. The testing period was in two main phases: kerosene circulation (May and June), and polyphenyl circulation (July and August). Other testing (done concurrently with either kerosene or polyphenyl circulation, or both) included individual com-

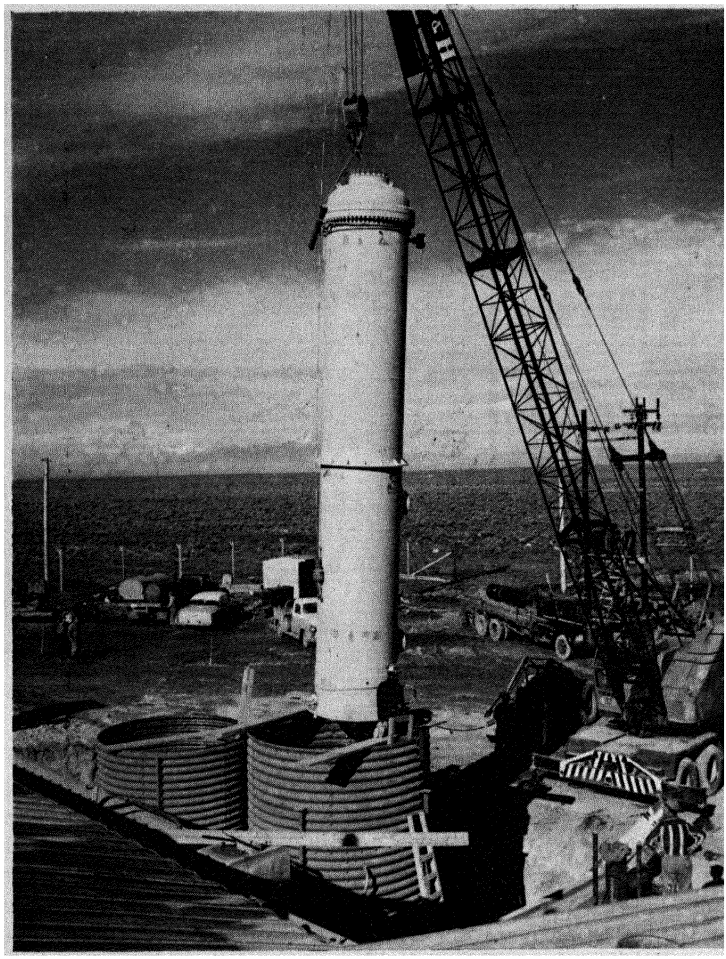

ponent and instrument checkouts, and tests of the induction heating, control rods and drives, fuel-element handling procedures, and purification of the polyphenyls.

Kerosene circulation tests. To keep water out of the system so as to avoid the possibility of corrosion (or of introducing impurities by corrosion inhibitors), kerosene was used for all hydrostatic tests. Kerosene proved excellent for the initial preoperational tests of the OMRE. Its hydrodynamic properties are fairly similar to those of hot polyphenyls (at

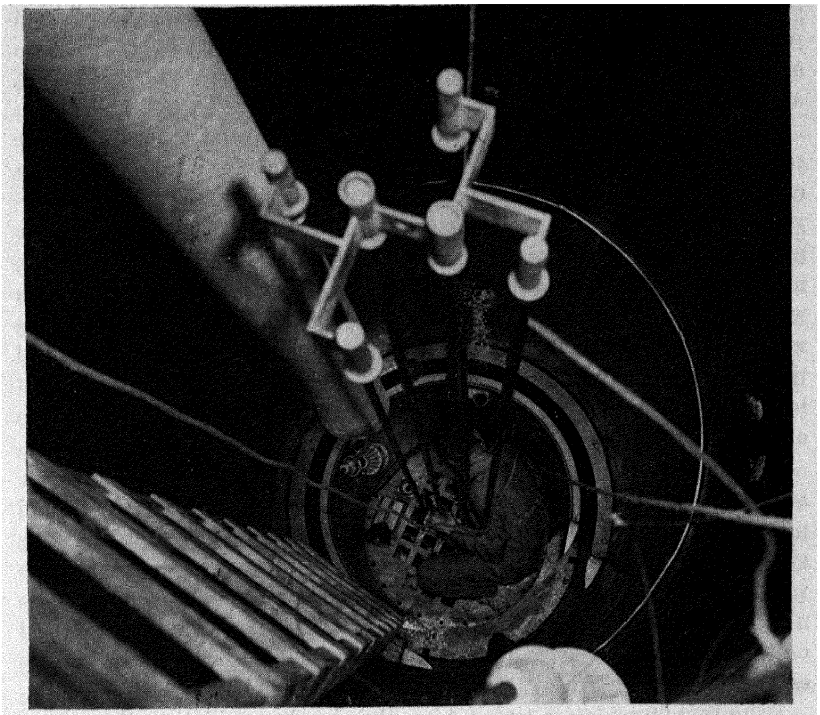

FIG. 7–35. Interior view of reactor vessel.

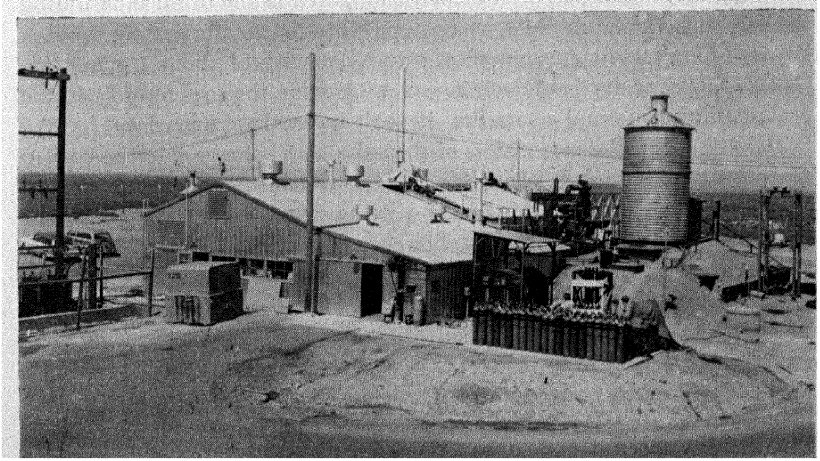

FIG. 7–36. OMRE facility at completion of construction.

operating temperatures) and, being liquid at room temperature, it did not present the freezing problems associated with cold polyphenyls. The kerosene was circulated at temperatures up to 350°F, pressures up to 300 psig, and flow rates up to 9000 gpm. There were no difficulties and no leaks.

Control rod and drive tests, instrumentation tests, and calibrations were satisfactory. An attempt was made to use kerosene for cleaning the various vessels and piping. As mentioned above, the whole OMRE system beyond the pressure vessel was constructed of carbon steel, since the organic moderator-coolant causes negligible corrosion of standard construction materials. This choice of materials made it necessary to clean the system with the circulating fluid after construction was completed. The kerosene was circulated continuously through the normal operational filter, and through a special absorbent filter installed for the purpose. Much particulate matter, mainly metal filings, rust, and welding slag, was collected; the amounts increased with increasing temperature.

After the kerosene circulation tests, the kerosene was drained from the system, and its last traces were removed by evaporation from the heated pipes and vessels. When further drying removed no more kerosene, the system was opened and allowed to cool. All moving components were visually examined for wear and tear. There was no evidence of any significant damage. Large quantities of dirt and rust, however, still remained on the walls of the vessels and piping. Final cleaning was done later by circulating polyphenyl.

Polyphenyl circulation tests. After the visual examination, the system was closed once more, preheated, pressurized, and filled with the polyphenyl coolant-moderator mixture to be used in operating the OMRE. This mixture, which had been melted and stored in the drain tank during the kerosene circulation tests, was pumped into the reactor system through the feed pump, a diaphragm pump with a capacity of about 1 gpm. Although this capacity is quite sufficient to provide the makeup of organic coolant during normal operation, it took more than four days for the initial filling. All later transfers of the polyphenyl charge into the system after drainage were done pneumatically to save time.

The polyphenyl circulation test conditions were similar to those for the kerosene tests. The temperature, however, was raised to 500°F by use of the preheating furnace on the airblast heat exchanger. Operation was quite satisfactory, but leaks developed at some flanged joints. Spirally wound metal-asbestos gaskets had originally been installed during construction, and a spare set of soft iron gaskets had been provided in case the original gaskets proved unsatisfactory. The system was drained and the leaky gaskets were replaced with the soft iron gaskets; they have performed satisfactorily since their installation. A failure of the mechanical seals on one of the main coolant pumps and on the auxiliary pump necessi-

tated draining the system once more to allow replacing the seals. Testing of the performance of the control rods and drives, and of various components and instruments, continued throughout the polyphenyl circulation tests. System cleanup was carried out by filtering and distilling the coolant in the purification system, whose performance proved highly satisfactory.

Induction heating tests. Since the polyphenyls are practically solid at room temperature, it was necessary to preheat the whole OMRE system before filling it, and to keep it hot during preoperational and low power tests. Sixty-cycle electrical induction heating was installed to preheat the vessels and piping. This system was chosen because of its extreme simplicity, ease of maintenance, and expected reliability. In addition to induction heating, an oil furnace and a blower were provided to preheat the banks of finned tubes on the airblast heat exchanger by blowing hot air across them.

The main problem in designing the heating system was lack of adequate information on the performance of such induction heating circuits. The design was based on empirical equations whose application had not been verified for this type of system It was, therefore, essential that the OMRE preheating system be tested as early as possible. Tests with and without kerosene in the system disclosed design strong points and weaknesses. There was no problem in bringing the vessels, large piping, valves and fittings (10 and 16 inches) to temperatures of 250 to 300°F at a uniform, controlled rate Practically no changes were required on the induction heating circuits installed for these components

However, there were difficulties with the small piping, valves, and fittings (2 inches and under), and associated components. On the large vessels and pipes, a single circuit covered a single component, or only part of a component; but on the smaller pipes (to keep the number of circuits small) single circuits were used to preheat great lengths of pipe and many valves and fittings. Unfortunately, the heating requirements of the various parts of the piping were found to vary so much that changes were required in the heating circuits thus installed. Some circuits were rearranged and resistance heaters were installed on the small valves. After the changes were made, the entire system could be preheated to 300°F without resorting to the oil furnace and blower on the airblast heat exchanger.

Control rod and drive tests Control rods and drives for the OMRE had been tested as prototypes before they were installed in the reactor. Additional tests were carried out in the kerosene and the polyphenyls. Main problems included: (1) aligning the drive racks supported from the pinions on top of the vessel with the hanger rods holding the poison elements, (2) achieving satisfactory operation of the control rod downseated

microswitches in the polyphenyls, (3) installing bulky drive and position indicator gear transmissions, and (4) manufacturing satisfactory release latch cams. From this work was developed a highly satisfactory and reliable control and safety system for the OMRE, with safety rod drop times of 500 to 600 msec from scram signal.

Fuel-element handling tests. Polyphenyls several feet thick are opaque. Therefore, it was essential to know that loading and unloading fuel elements from the core could be done without visual aid. For this purpose a rotating platform was installed on the top flange of the reactor vessel, indexed radially and peripherally for all lattice positions in the upper grid plate. The platform could position a guide tool directly above any upper grid plate lattice position. A fuel-element handling tool 20 ft long was lowered through the guide to install a fuel element in a chosen position. The indexed platform, guide tool, and fuel-element handling tool were first tested blind, with the reactor vessel dry. Later operation was checked after filling the reactor vessel, first with kerosene, then with polyphenyl. The system has proved highly reliable.

Purification system tests. Performance of the purification system, a single-stage low pressure distillation unit, was first tested with a eutectic mixture of diphenyl and ortho-terphenyl which is liquid at about 80°F The sole problem was behavior of the vapor trap upstream from the vacuum pump, which tended to plug quickly because it was too small. Employing the vapor trap as a reflux condenser and installing a large receiving tank between it and the vacuum pump eliminated the problem.

After the diphenyl-ortho-terphenyl eutectic tests were completed, others were carried out with the operational polyphenyl mixture These proved highly satisfactory. In the absence of high-boiling decomposition tars, the purification unit performed an excellent separation of the dirt, filings, rust, and slag from the coolant. Since then the unit has been on practically continuous duty, cleaning the main coolant system. Since its capacity is only about 400 gal/day (ample for ordinary operational requirements), it would have required a 15- to 20-day shutdown for this unit to clean up the system initially. Since this did not appear feasible, the coolant was not passed through the purification system in a once-through operation; instead, every purified batch was returned to the bulk of the coolant in the system during the main preoperational tests.

Sidestream purification brought about only a slow exponential decrease in concentration of impurities instead of the linear decrease that otherwise could have been achieved After critical assembly, however, an unrelated mechanical problem necessitated draining the system and caused a two-week shutdown. During and after the shutdown, most of the coolant underwent once-through purification. Success of this operation leads to the conclusion that for an organic moderated and cooled reactor which

has a purification plant, special cleaning during construction can be kept to a minimum, the purification unit can complete required cleanup of the reactor coolant, vessels, and piping.

7–4.6 Fuel-loading and low-power tests. *Critical assembly.* Preoperational testing of the OMRE was completed on September 2, 1957. The reactor vessel was then opened, and the criticality structure was installed above it. This structure is designed to support the control rod drives when the reactor vessel is open. Critical loading can then proceed without removing and reinstalling the reactor vessel head for every fuel-element addition. The source capsule was installed, containing antimony oxide previously irradiated at the Materials Testing Reactor. The reactor was loaded and brought to criticality on September 17, 1957. Twenty fuel elements, containing 16.4 kg of U^{235}, were required at 250°F.

Three weeks later, mechanical failure of a flow deflector skirt between the two grid plates in the reactor vessel made it necessary to unload the reactor, drain the system, and remove the fuel-element storage rack and upper grid plate An improved deflector skirt was manufactured and installed. The OMRE again went critical, eleven days after the failure was discovered.

Loading of excess reactivity. Three major criteria determined the additional fuel loading required for normal OMRE operation:

(1) Enough reactivity was to be provided to allow up to 1800 Mwd at temperatures as high as 700°F, with equilibrium xenon and samarium poisoning at power levels up to 16 Mw.

(2) Reactivity was to be low enough for complete reactor shutdown at any temperature in case the two control rod pairs of highest worth failed to scram.

(3) With maximum coolant delivery from the pumps fixed, it was essential that the fewest possible fuel elements be added, so that coolant flow through each element would remain as large as possible.

Approximately 3 9% reactivity was required to provide the fuel burnup necessary for reactor operation. Another 3.9% was needed for equilibrium xenon and samarium poisoning. Calculations showed no need for additional reactivity for high-temperature operation because OMRE core reactivity would be approximately the same at 700°F as at 250°F. This prediction was verified in practice. A total core loading of 7.8% reactivity was indicated.

Loading successive fuel elements showed the worth of each to be approximately 0.7%. Altogether, 11 elements were added, completing a 31-element core with a total U^{235} content of 25.5 kg.

Preliminary control rod calibrations and measurements of the temperature coefficient of reactivity during loading showed that the reactor could

TABLE 7–11

CORE CHARACTERISTICS
OF THE ORGANIC MODERATED REACTOR EXPERIMENT

Critical mass at 250°F	20 fuel elements (16.4 kg U^{235})
Complete loading	31 fuel elements (25.5 kg U^{235})
Reactivity at 250°F	7.87% $\Delta k/k$
Reactivity at 450°–480°F	8.76% $\Delta k/k$
Reactivity at 700°F	7.82% $\Delta k/k$
Shutdown reactivity at 250°F:	
All 6 control rod pairs inserted	−8.20% $\Delta k/k$
4 outer control rod pairs inserted 2 inner control rod pairs withdrawn	−2.62% $\Delta k/k$
Equilibrium xenon and samarium	−3.88% $\Delta k/k$
Fuel burnup	−3.94% $\Delta k/k$

be shut down from maximum reactivity with the two control rod pairs of highest worth completely withdrawn from the core Measurement of flow through the core after the reactor was loaded and the dummy plugs had been inserted in the core yielded a maximum coolant velocity of 14.5 fps. These findings satisfied the original OMRE design objectives.

Basic information on OMRE core loading is presented in Table 7–11. Figure 7–37 shows a cross section of the core. It consists of 31 fuel elements, seven of which have five thermocouples each, three at the surface of the hottest plate and two at the outlet from the hottest coolant channel. In addition, it includes an antimony oxide-beryllium neutron source and five dummy plugs, two loaded with corrosion coupons.

Control rod calibrations. Immediately after the critical loading, preliminary control rod calibrations were started and continued throughout loading of excess reactivity. Final calibrations were made after loading had been completed. Differential worths of rods and groups of rods were obtained by the period method. As the degree of insertion of the rod under calibration was varied, other rods were adjusted to maintain criticality The differential calibration was made for the entire operating range of each rod. A typical control rod calibration is shown in Fig. 7–38, which presents both the differential worth (reactivity per inch) and the integrated worth of control rod pair No. 1. The data were obtained with minimum interaction from other rods, since the rods nearest No. 1 were almost out of the core during calibration, and control rod pair No. 6 (on the opposite side of the core) was used to maintain criticality.

Each of the outer control rod pairs, calibrated with a minimum of interaction, was found to be worth 2.5 to 3.0% k_{eff} with a full core loading.

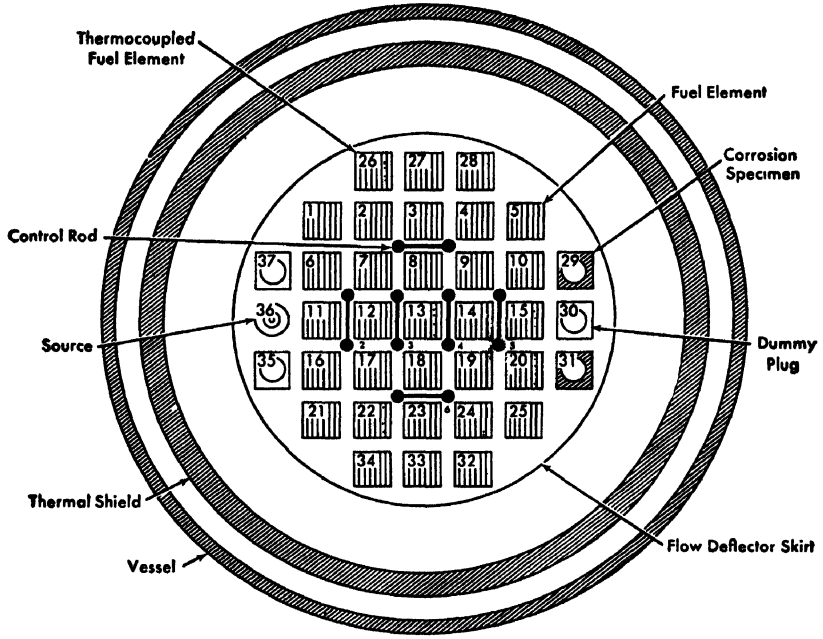

FIG. 7–37. OMRE core layout.

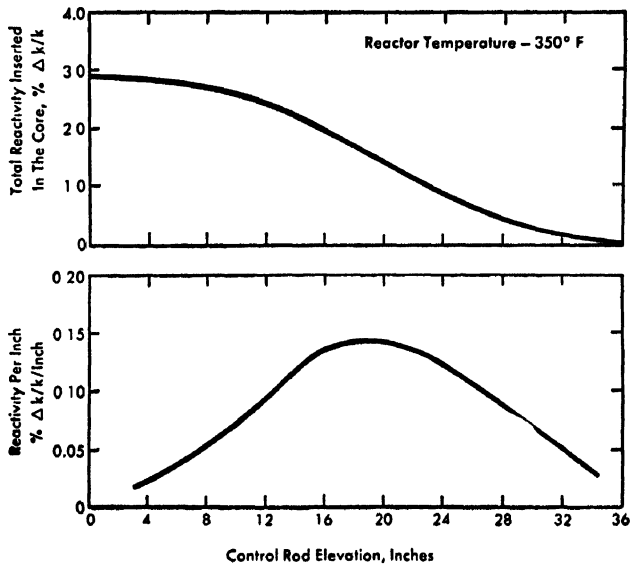

FIG. 7–38 Typical control rod calibration.

The inner rod pairs could be calibrated only with a major amount of interaction from the outer pairs; under those conditions their worth was 3.2 to 3.3% each.

Additional calibrations were made on ganged rod operation, including the outer and the inner groups of rods. Shutdown reactivity data were estimated from inverse multiplication measurements made with all six rod pairs fully inserted, as well as with the four outer pairs fully inserted and the two inner pairs withdrawn completely. Values obtained are in Table 7–11.

Flux distribution measurements. Flux mapping in the OMRE core was limited to determining the thermal flux distribution in a single fuel element in core lattice position No. 23 (Fig. 7–37). This was a special element from which the bottom end box could be detached and the individual fuel plates removed. Gold foils were attached in various locations on five of the 16 active fuel plates. Axial and transverse flux distributions were obtained on individual plates; a transverse flux distribution was taken from plate to plate across the element Both transverse distributions clearly showed the anticipated effect of flux peaking in the hydrocarbon gap between adjacent fuel elements; the flux was appreciably depressed at the center of each plate as well as at the central plates of the element. The axial distribution showed the normal effect of flux peaking a few inches below the bottom of the nearest pair of control rods.

Mass and void coefficient measurements. To obtain the mass coefficient of reactivity, a fuel element was removed from the core and the associated change in reactivity was measured by the change in critical elevation of the control rods Measurements were made in lattice positions 18, 23, and 33 (Fig. 7–37) at a core temperature of 250°F. Results are in Table 7–12

These data plainly indicate that the worth of each element decreases as it is located farther from the center of the core. Values presented include some error, since they are based on control rod calibrations with the core fully loaded and make no allowance for change resulting when the given element is removed from the core.

In like manner, the void coefficient of reactivity was measured by replacing a standard OMRE fuel element with a special element sealed to prevent moderator-coolant entering the fuel box, and measuring the associated reactivity change by the change in critical elevation of the control rods. This yielded information on the reactivity effect that could be anticipated from hydrocarbon vapor bubbles forming if boiling occurred in the core. Measurements were made in lattice positions 18, 23, and 33 (Fig. 7–45) at core temperatures of 250, 300, and 350°F. Results are in Table 7–12.

TABLE 7–12

MASS AND VOID COEFFICIENTS OF REACTIVITY

	Fuel element location		
	18	23	33
Mass coefficient:			
% $(\Delta k/k)$/fuel element	3.50	2.45	1.10
Void coefficient:			
% $(\Delta k/k)$/void element at 250°F	−0.427	−0.367	−0.240
% $(\Delta k/k)$/void element at 300°F	−0.497	−0.452	−0.327
% $(\Delta k/k)$/void element at 350°F	−0.575	−0.565	−0 435
Void coefficient:			
% $(\Delta k/k)$/cm^3 of void at 250°F	-1.18×10^{-4}	-1.01×10^{-4}	-0.66×10^{-4}
% $(\Delta k/k)$/cm^3 of void at 300°F	-1.37×10^{-4}	-1.25×10^{-4}	-0.90×10^{-4}
% $(\Delta k/k)$/cm^3 of void at 350°F	-1.58×10^{-4}	-1.56×10^{-4}	-1.20×10^{-4}

The void had a strongly negative effect under all conditions tested. It increases with higher temperature and drops with greater distance from the center of the core. Again, the values are subject to some error because it is uncertain what effect the void had on calibration of the control rods measured.

Flow and pressure coefficient measurements. Changes in reactivity associated with changes in coolant flow or nitrogen pressure above the coolant were measured by observing how these changes affected the critical elevations of the control rods. Results are in Table 7–13.

The magnitude of these changes in reactivity is very small, practically within limits of experimental error, since minor core temperature changes could easily invalidate most reactivity effects attributed to flow or pressure.

Temperature coefficient measurements. The temperature coefficient of the OMRE was measured by raising the temperature of the coolant gradually from 200 to 700°F and observing the corresponding changes in critical elevations of the control rods. The preheating system raised the temperature from 200 to 435°F; nuclear heat from the reactor brought it to 700°F.

TABLE 7–13

FLOW AND PRESSURE COEFFICIENTS OF REACTIVITY
(Change in reactivity from no-flow to full-flow at 250°F, 240 psig: $-0.045\%\ \Delta k/k$)

Pressure step, psig	Change in reactivity per pressure step ($\%\ \Delta k/k$)	
	Increasing pressure (250°F)	Decreasing pressure (400°F)
0–25	+0.0325	−0.005
25–50	+0.0135	−0.020
50–100	−0.0180	−0.050
100–150	−0.0203	−0.070
150–200	−0.0225	−0.070
200–240	−0.0180	−0.050

There was no difficulty with measurements in the low-temperature range. However, as soon as nuclear heat was applied, the effects of xenon poisoning became evident. This caused results to vary from test to test. Several times the tests had to be repeated. The most reliable data were obtained by maintaining reactor power level at 2 Mw, establishing equilibrium xenon concentration, and controlling the temperature by the heat-rejection system. Even then, the xenon equilibrium was disturbed by two spurious reactor scrams, introducing xenon transients that were quite small in absolute magnitude, but sufficient to overshadow some temperature effects in the region where these effects were weakest.

Results are shown in Figs. 7–39 and 7–40. In the first figure, the two curves were matched at a temperature of 425°F, since xenon poisoning at a power level of 2 Mw did not permit a continuous measurement through this point. Over-all results: the temperature coefficient in the OMRE is strongly positive at temperatures below 400°F, strongly negative above 500°F, and changes from positive to negative in the range 435 to 485°F. The total positive reactivity effect associated with temperature above 400°F does not exceed 0.10%, and is probably somewhat smaller. It does not affect OMRE operational safety.

7–4.7 Power operation. *Reactor control tests.* A series of tests was carried out to study OMRE behavior under various transient conditions during power operation. Manual and automatic control of both the reactor and the airblast heat exchanger, tested at power levels up to 12 Mw,

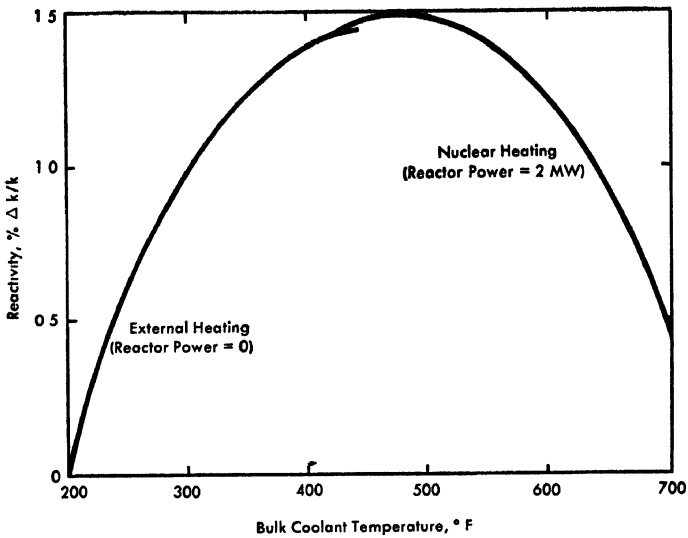

FIG 7–39. Effect of temperature on reactivity of OMRE core.

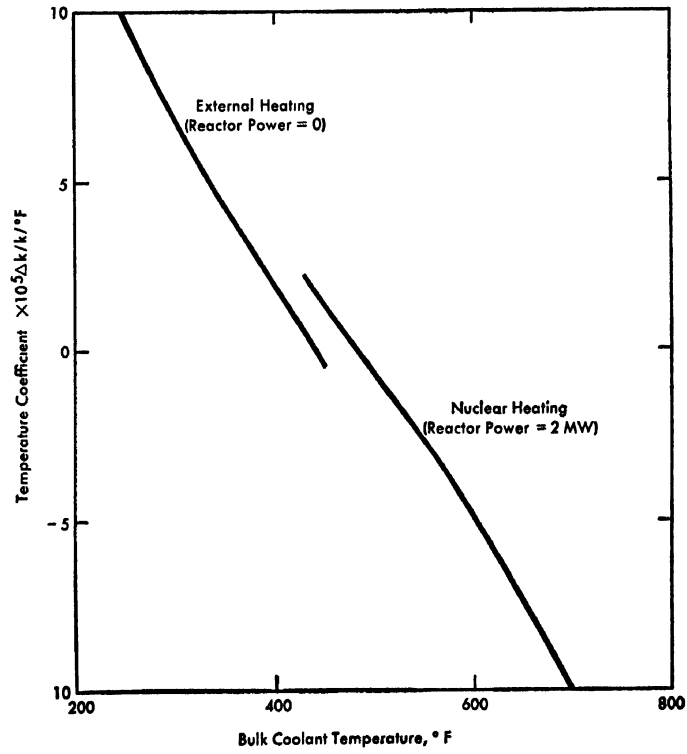

FIG. 7–40. Temperature coefficient of reactivity.

proved highly satisfactory. Steady-state operation went smoothly and the control system responded well to transient disturbances.

Better understanding of OMRE core characteristics resulted when the reactor was exposed to reactivity transients without attempt at either manual or automatic control. Low frequency oscillations became evident, with periods in excess of ten minutes. These proved to be divergent at temperatures below 600°F and convergent above 600°F. However, they did not present control problems.

This behavior can be understood if the core is regarded as composed of two types of regions: (1) those within the boundaries of the fuel elements, and (2) those outside these boundaries.

The temperature coefficient of reactivity in Type 1 regions is strongly negative over the range of interest. In Type 2 regions the temperature coefficient is strongly positive over the same range. Coefficient values for both regions were confirmed experimentally. In the OMRE, all the coolant flows from regions 1 to regions 2, and the temperature in regions 2 is always higher than that in regions 1 by an amount directly proportional to the power level of the reactor and inversely proportional to the flow rate through the core. The net result is a power coefficient which, because of the relative magnitudes of the temperature coefficients in the two regions, is positive below and negative above approximately 600°F. Its magnitude is small, about 3×10^{-5} $\Delta k/k$ per Mw at full flow at 550°F, and it is felt that it presents no problem in the operation of the OMRE, or any hazard to its safety.

Buildup of high-boiling decomposition products. Although the steady-state operating program of the OMRE had barely started, the reactor through January 1958 had accumulated 80 Mwd of power operation at bulk coolant temperatures ranging from 500 to 700°F and fuel plate surface temperatures up to 750°F. Coolant samples from the main loop have been taken routinely and analyzed for high-boiler residue content (defined as any material less volatile than para-terphenyl). Figure 7–41 shows weight of high-boiler residue formed as a function of the number of megawatt-days of reactor operation. The data, obtained under widely varying conditions of temperatures, were all in the range of interest for power reactor operation. They yield a preliminary value of 3.8 pounds of high-boiler residue formed per megawatt-hour of operation. Because it uses highly enriched fuel and has a large volume of hydrocarbon in core and reflector, the OMRE is estimated to generate a very high fraction, approximately 8.4%, of its power by direct interaction of neutron and gamma radiation with the organic moderator-coolant. (For the full-scale power plants discussed in Section 7–5, this fraction is between 3.7 and 4.2%.) On this basis, the OMRE data yield an initial G_p value of 0.12 molecule formed per 100 ev of energy absorbed, well within the range

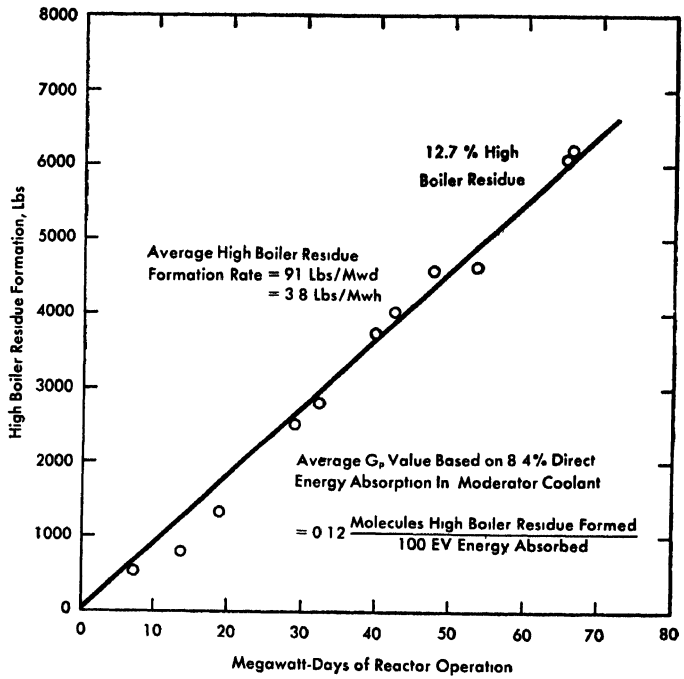

FIG 7–41. High boiler residue formation in the OMRE preliminary data.

of data obtained from electron and in-pile irradiation for similar conditions Although these decomposition figures are preliminary, they inspire confidence in the reliability of the electron and in-pile data, and in their applicability to larger scale reactors.

Induced radioactivity in coolant. A promising feature of the organic moderated and cooled reactor concept is the fact that radioactivity induced in the coolant-moderator during its passage through the core is low, with consequent low radiation levels for primary coolant system components and piping. Thus even while the reactor is operating, components of the primary system are accessible for maintenance.

Most coolant radioactivity is induced in the inorganic impurities present in the hydrocarbon. Before each batch of coolant was accepted for OMRE, a sample of it was analyzed by activation in the Materials Testing Reactor. The chief inorganic impurities found in the samples were sodium, magnesium, chlorine, and copper. In most cases, amounts were small enough to be accepted. As mentioned previously, the coolant removed quantities of rust, metal filings, welding slag, and other impurities from the walls of the vessels and piping during preoperational testing. Most of such impurities were separated by distilling the coolant. Table

TABLE 7–14

SHORT-LIVED ACTIVITIES IN OMRE COOLANT

Activity	Half-life	Impurity	Concentration, ppm
Na^{24}	15.0 hr	Sodium	0.10
Mn^{56}	2.58 hr	Manganese	0.03
Cl^{38}	37.3 min	Chlorine	2.0
Cu^{64}	12.8 hr	Copper	0.2
Cu^{66}	5.1 min		

7–14 shows sources of main short-lived activities present in OMRE coolant (as determined by activation analysis).

Radiation levels as measured at various points of OMRE primary piping and components during power operation have been very low Figure 7–42 shows radiation levels measured at 10 Mw. The highest level in the process area was 80 mr/hr at the surfaces of the 10-inch pipes and of the system filter In the center of the area, the radiation level was 13 mr/hr, less than twice tolerance Airborne activity was always well below breathing tolerance. Thus, the area is accessible for ordinary maintenance even during full-power operation.

The reactor shelter area was not designed for access during operation Radiation measured there was actually lower than anticipated and, since much of this comes from fast and thermal neutrons streaming from the reactor cavity and pipe gallery, it could be greatly reduced by refinements in design.

The low radioactivity of gases purged to the stack should also be mentioned. Gas activities are much diluted with air from the building ventilation system, and have so far not exceeded the level of breathing tolerance.

7–4.8 Evaluation of results. Now in operation, the OMRE is thoroughly testing the organic moderator-coolant concept. Satisfactory operation with no evidence of fouling on heat-transfer surfaces has shown the technical feasibility of the concept at high-boiler residue concentrations up to 12%.

Preliminary measurements of coolant decomposition rates have confirmed data from electron and in-pile irradiation experiments, indicating that decomposition rates in organic moderated and cooled power reactors can be predicted reliably from small-scale capsule and loop experiments.

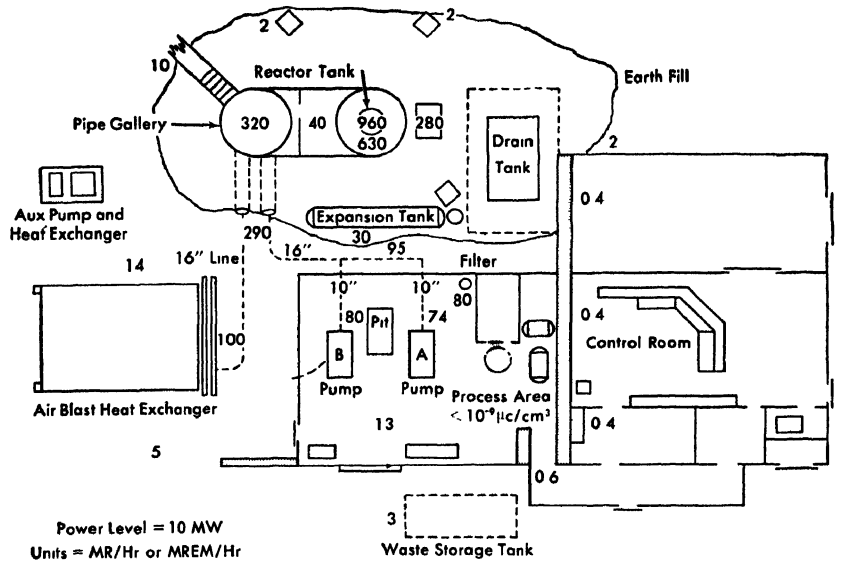

FIG 7–42 Radiation survey of OMRE area Early operation at 10 Mw.

It is expected that the present operations will more conclusively confirm that hydrocarbon makeup rates will be low, an important factor in achieving economic feasibility.

7–4.9 Future program. By the fall of 1958 OMRE operation should have demonstrated conclusively the feasibility of the reactor concept. Bulk coolant and fuel plate surface temperatures will then be raised progressively to determine operational temperature limits.

The OMRE will also test the performance and burnup characteristics of low-enrichment fuel elements especially designed and developed for large organic moderated and cooled power reactors It will test components to improve performance and reduce maintenance in large plants. It will also be possible to use the OMRE for large-scale testing of promising hydrocarbon moderator-coolants other than diphenyl and terphenyls.

7–5. POWER REACTORS EMPLOYING ORGANIC LIQUIDS*

7–5.1 Introduction. As moderators and coolants for power reactors, the organic fluids selected have the following advantages:

(1) Their corrosion of most common materials is negligibly small.

(2) They do not react with water.

*By C. W. Wheelock, AI.

(3) They do not damage fuel and cladding materials by reacting chemically with them.

(4) Coolant temperatures as high as 600°F can be used without high pressure.

(5) The coolant does not become strongly radioactive; hence the shielding needed for primary loop equipment is relatively light.

(6) Standard engineering materials and mechanical components can be used in the reactor system. Mild steel and aluminum suffice for most of the equipment, and pumps, process equipment, and instruments are similar to those used in the petroleum industry.

(7) The plant as a whole and single components are not too heavy to be considered for ship propulsion or other applications where low weight is an advantage.

The basic question, to which answers are being sought in the OMRE program is: will the technical problems and costs of controlling the effects of coolant damage (from radiation and heat) prove too burdensome?

Thus far, the answers from OMRE experience have been favorable. Some power plant cost studies based on this experience have shown that prospective future over-all costs for various organic-moderated reactor applications by 1965 might be as low as

Electricity generation	8.6 mills/kwh
Process steam	$0.47 per million Btu
Oil tanker operation, from the Persian Gulf to Philadelphia, Pa.	$10.50 per long ton

These cost estimates are based on a credit of $30/g for plutonium produced.

OMR safety. Because the consequences of an accident that would expose the public to radiation or radioactive contamination are so serious, safety is a prime requisite in selecting and designing a nuclear power plant. Organic-moderated reactors have these valuable safety features: (1) They operate at low pressure, and can operate at a temperature below the atmospheric boiling point of the coolant. (2) They can be designed to have a negative temperature coefficient of reactivity. (3) All reactor materials, including the coolant, are chemically compatible. (4) The coolant does not become radioactive.

Operating pressure. Rapid loss of coolant from a reactor system not only can disperse contaminants but can also endanger the reactor by permitting temperatures to rise abnormally. A low operating pressure contributes to safety because vessels, piping and seals are less likely to break, coolant leaks out slowly if a break occurs, and less energy is immediately available to expel the coolant from a broken system. At the low operat-

ing pressure of the OMR (about 120 psia), many high-pressure problems are avoided. Since the primary loop pressure is lower than that of the steam system, radioactive materials are less likely to leak into the steam turbine, condenser, and feed pumps.

Boiling point of the coolant. Because the reactor operates below 700°F (the atmospheric boiling point of the OMR coolant terphenyl), loss of primary loop pressure would not cause the coolant to vaporize and be lost from the system.

Temperature coefficient of reactivity. The OMR has a negative temperature coefficient of reactivity large enough to ensure that the reactor is stable to fluctuations in load, and to counteract accidental reactivity additions. The negative coefficient results principally from the geometry of the reactor core, which is designed to be slightly undermoderated at operating temperature. Because the organic moderator expands more than the other core materials with an increase in temperature, the neutron leakage becomes more pronounced as the temperature is increased. Similarly, the reactivity change is negative if a void is introduced in the core, as by surface boiling.

Radioactivity of coolant. The organic coolant used in the OMR is terphenyl, a hydrocarbon which consists entirely of carbon and hydrogen atoms, neither of which becomes appreciably radioactive in a reactor. The only sources of radiation in the primary coolant loops are impurities in the organic. The concentration of impurities is kept very low by the processing system; therefore the normal radiation intensity from the primary loop is very low.

OMR applications. Organic-moderated reactors have been considered for power production in three major types of plant installation: electric power generation, process heating, and ship propulsion. In all these applications, the basic reactor and primary system are similar; the reactor size, auxiliary systems, and mode of operation are varied to meet specific requirements.

Three types of OMR plant installations are described in the following sections: a small and a large electric power generating station, a small and a large plant for producing process steam, and a 38,000 dead-weight-ton oil tanker. The characteristics of these systems are listed in Tables 7–15 and 7–16.

7–5.2 Electric power generating plants. The electric power generating plants described have rated net electrical outputs of 11,400 and 150,000 kw, respectively. The larger of these plants does not necessarily employ the largest organic-moderated reactor that would be economical, but for plant capacities larger than this there might well be advantages

TABLE 7–15

GENERAL CHARACTERISTICS OF OMR APPLICATIONS
(Costs projected to 1965)

Application	Electric power generation		Process heating		38,000 DWT* oil tanker
Reactor power, thermal Mw	45.5	575	75	1,100	70
Rated power, net electrical kw	11,400	150,000			
Rated power, shaft hp					20,000
Steam pressure, psig	415	415	150	150	450
Steam pressure, atm	28 2	28.2	10.2	10.2	30.6
Steam temperature, °F	550	550	358	358	580
Steam temperature, °C	288	288	181	181	304
Steam rate, total lb hr	162,000	7.17×10^6	224,000	$3\ 29 \times 10^7$	230,000
Steam rate, total kg, hr	73,700	3.25×10^6	102,000	1.54×10^7	104,000
Sea speed (loaded), knots					18
Cargo capacity, bbls					330,000
Cargo capacity, Persian Gulf to Philadelphia, long tons/yr					284,000
Plant cost, $, net kw (estimated)	560	180			
Plant cost, $ 'rated hp (estimated)					200
Plant cost, $/$10^6$ Btu/hr capacity (estimated)			2.90	0.77	
Power cost†, mills/kwh (estimated)	20.4	8 6			
Power cost, cents/10^6 Btu (estimated)			98	47	
Cargo transportation cost,† (estimated) $/long ton (Persian Gulf to Philadelphia)					10.5

*Deadweight-ton or tons "dead weight." †Net cost with $30 g credit for plutonium produced.

TABLE 7–16

REACTOR CHARACTERISTICS

Application	Electric power generation		Process heating		38,000 DWT oil tanker
Thermal power, Mw	45.5	575	75	1,100	70
Core height, ft	4 5	10	4.5	10	6
Core height, meters	1.38	3.05	1.38	3.05	1.84
Core diameter, ft	4.5	11.3	4.5	11.3	6
Core tank diameter, ft	6.0	14.5	6.0	14.5	8.5
Core tank diameter, meters	1.84	4.42	1.84	4 42	2.60
Moderator and coolant	Polyphenyl (values given pertain to commercial terphenyl)				
Number of coolant loops	2	6	2	6	2
Coolant flow rate, 10^6 lb/hr	5.1	43	5.1	43	10.3
Coolant flow rate, gpm	11,000	93,000	11,000	93,000	22,260
Coolant flow rate, liters sec	700	5,800	700	5,800	1,400
Coolant outlet temperature, °F	600	622	500	500	622
Coolant outlet temperature, °C	316	328	260	260	328
Number of fuel elements	63	325	63	325	110
Number of control rods	6	16	6	16	10
Fuel element type	Flat plate with extended surface cladding				
Fuel material	Uranium metal with stabilizing alloys				
Fuel cladding material	Aluminum				
Fuel enrichment, w/o U^{235}	1.8	1.5	1.8	1.5	1.6
Fuel loading, kg U^{235}	120	1,280	120	1,280	245
Fuel loading, kg U	6,650	86,500	6,650	86,500	15,700

(*Continued*)

TABLE 7-16 (*continued*)

Application	Electric power generation		Process heating		38,000 DWT oil tanker
Fuel surface temperature, maximum, °F	750	750	750	750	750
Fuel surface temperature, maximum, °C	399	399	399	399	399
Fuel burnup, average Mwd/short ton	3,000	3,000	3,000	3,000	1,440
Fuel burnup, average w/o U^{235}	20	24	20	24	11.8
Refueling frequency, months (80% plant factor)	4	4	2.5	2.1	15
Fuel elements replaced per refueling	12	48	12	48	110
Polyphenyl makeup rate, lb/thermal Mw-hr	1.5	1.5	1.4	1.4	1.5
Polyphenyl makeup rate, kg/thermal Mw-hr	0.68	0.68	0.64	0.64	0.68
Thermal neutron flux (average with clean core), $n/(cm^2)(sec)$	2×10^{13}	1.5×10^{13}	4×10^{13}	3×10^{13}	10^{13}
Conversion ratio, initial (atoms Pu/atom U^{235} destroyed)	0.60	0.73	0.60	0.73	0.63
Temperature coefficient, Δk °C	-10^{-4}	-7×10^{-5}	-10^{-4}	-7×10^{-5}	-10^{-4}

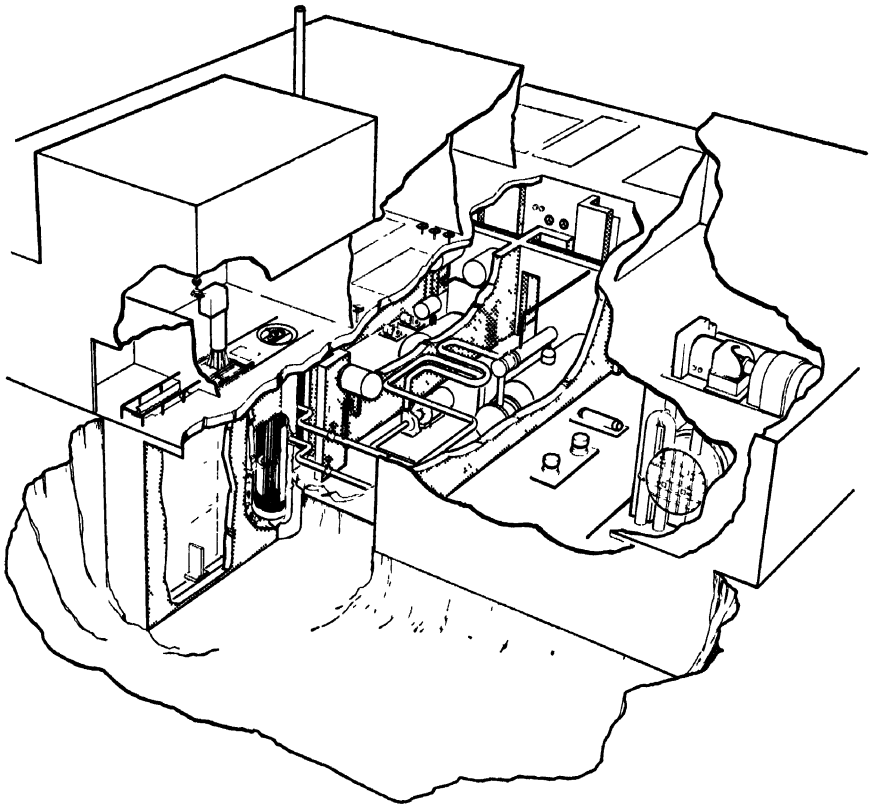

Fig. 7–43. Conceptual view of power plant

in using more than one reactor with a single set of servicing facilities. The arrangement of a small OMR plant is shown in Fig. 7–43.

In an OMR power plant, fission heat is transferred by the organic coolant, which circulates in parallel primary loops from the reactor core to the steam generators. The number of loops may vary from two to six or more, depending on the size of the plant. Steam from the steam generators is utilized in a turbogenerator to produce electricity. A degassing and pressurizing system, continuously handling a sidestream of the coolant, removes gas from the organic fluid and controls the pressure of the primary loop systems. Purity of the organic is maintained by a system which extracts residue and impurities. Auxiliary systems provide pressure relief, emergency cooling, and heating for the piping, valves, and vessels.

The building which houses an OMR power plant must provide working areas and equipment cells, functionally arranged in relation to each

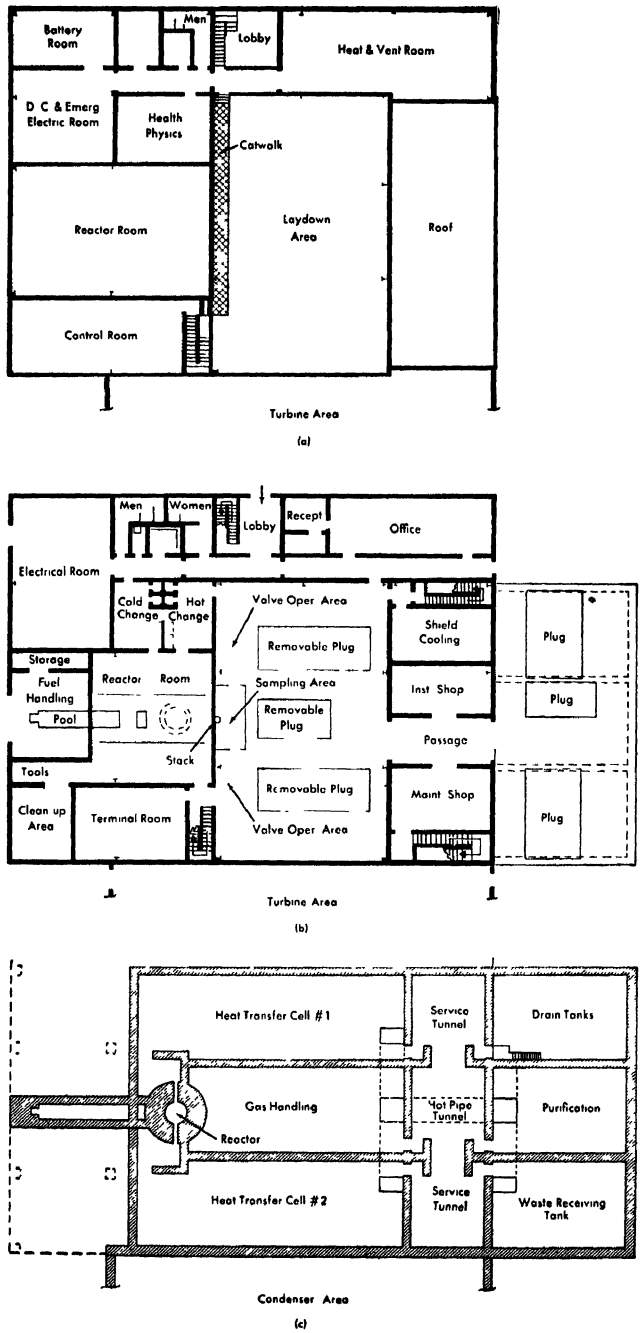

FIG 7–44. Power plant building plan: (a) mezzanine, (b) ground floor, (c) basement

other. These include the reactor room, the irradiated fuel canal, and the organic handling areas. Other areas, such as the control room, turbine, and condenser areas, should be located to provide convenient access for operation. Because the OMR plant has a low accident potential and there is no chance of dangerous exothermic chemical reactions, there is no need for a gastight closure. However, the building is designed for containment, with all the organic handling equipment in sealed cells and with the ventilating system maintaining continuous airflow to all areas subject to contamination.

The building plans for the smaller plant (Fig. 7–44) represent a typical OMR layout.

Reactor. The reactor consists of the core assembly, control-safety rods, shielding, and foundations. The assembly of uranium-bearing fuel elements is positioned near the bottom of a vertical cylindrical tank filled with a liquid hydrocarbon that serves as moderator, coolant, and reflector, and provides shielding above the fuel elements Control rods are arranged among the fuel elements in the core The core is encircled by a steel inner thermal shield that supports grid plates above and below.

The coolant is pumped into the region above the core (upper plenum). Thence it flows downward through the fuel elements into a plenum beneath the lower grid plate, then upward through the annulus between the core tank and the inner thermal shield, and, finally, out of the core tank to the primary coolant loop.

The core tank is suspended from the core cavity liner, supported by a surrounding concrete and steel foundation The reactor and equipment for the 11,400-kw plant are shown in Figs. 7–45 and 7–46. Sizes given in the following discussion are for the 11,400-kw design Some of the more important dimensions for the larger plant are listed in Table 7–16

Core tank and accessories The reactor vessel, of low carbon steel, is 6 ft in diameter and 25 ft high, with walls 1 inch thick. It is designed for an operating pressure of 300 psig at 650°F. A guide pin, welded to the bottom head, centers the vessel during installation and provides lateral support. Coolant inlet and outlet nozzles penetrate the vessel above the core. Other nozzles are for the control rod cables and the leads from thermocouples that measure the coolant outlet temperature of each fuel channel. A reinforced head is bolted and sealed by a soft metal gasket to the top flange of the reactor vessel. Internal hot gas circulation heats the vessel, as is necessary before introducing the hydrocarbon coolant; after shutdown, coolant temperature in the reactor is controlled by circulating the coolant through an external heater.

Foundations and shielding. The reactor core is below the ground. It is encircled by an inner thermal shield, a steel reactor tank, an outer thermal shield, thermal insulation, a steel cavity liner, and about 3 ft of con-

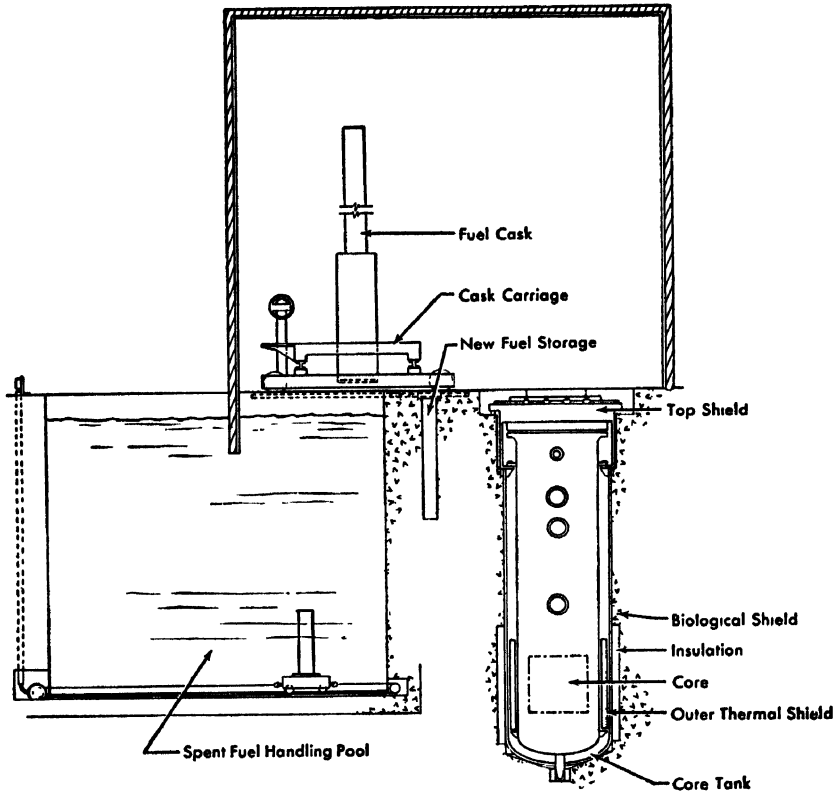

FIG. 7–45. Vertical section of reactor assembly.

crete below ground level. Shielding above the core consists of the steel upper grid plate, about 15 ft of hydrocarbon coolant, and a steel top head 6 inches thick. The reactor, the main heat-transfer loops, and organic process systems are shielded with ordinary concrete.

Pipe galleries for the primary heat-transfer loops are shielded by 2 ft of concrete. So are the vaults for the degasifier and gas-handling systems, organic purification system, organic waste holdup and disposal system, and reactor drain system. Access to the vaults and galleries is through offset entrance ways or removable stepped plugs or hatches. Heat generated outside the reactor thermal shield and that escaping through the insulation is removed by circulating water coils on the core cavity liner.

Fuel handling. The fuel-handling system (Fig. 7–53) removes spent fuel elements from the reactor core and replaces them with new elements. The handling system also inserts and removes control rods and the neutron source. The system consists of the fuel-handling and indexing shield,

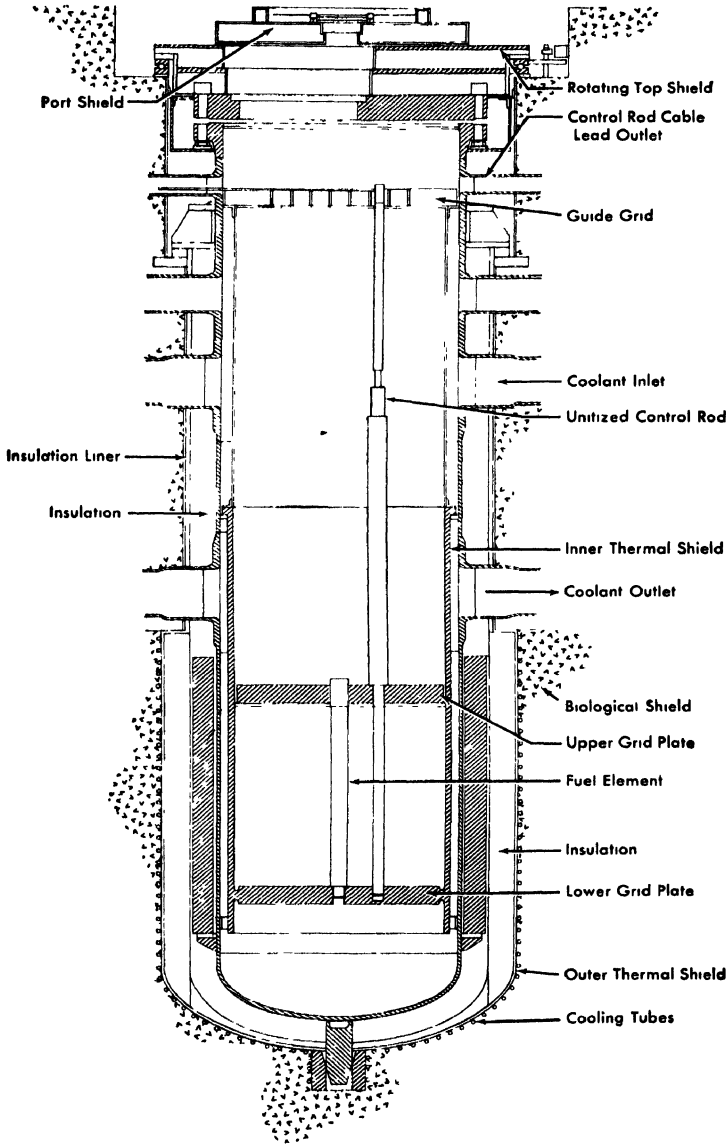

FIG 7–46. Reactor core tank assembly.

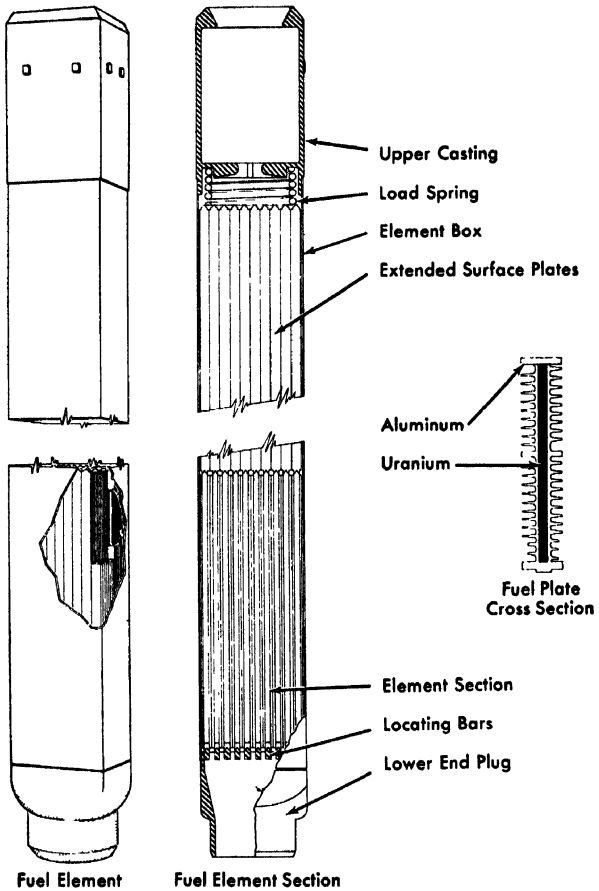

FIG 7–47. Diagram of fuel element

the fuel-element guide tube, the fuel-transfer cask, the fuel-storage pool, and the new fuel-transfer cells.

Fuel elements. The fuel elements are spaced 6 inches, center to center, in a square array. They are built up of finned plates of slightly enriched metallic uranium with stabilizing alloys, jacketed in an extended-surface aluminum extrusion (Fig. 7–47). The assembled fuel elements have a handling device at the top and a locating fitting at the bottom. They are supported from the lower grid plate, and are restrained from lateral movement by an upper grid plate. The fuel elements, control rods, and neutron source form a right cylindrical core about 4.5 ft in diameter and 4.5 ft high.

Control-safety rods. Six control rods regulate the reactor and provide emergency shutdown. Each rod unit, consisting of the poison element,

rod drive, and position indicator, is a compact assembly that can be inserted into a standard fuel position in the core. To operate the rods a series of magnets are alternately energized to hold, lower, or raise the poison element in small steps. Electrical leads for the rod drives and position indicators enter the reactor tank through a nozzle. All moving parts of the control rod are in a sealed tube. An upper guide grid supports the top of the control rods and a framework along which control rod cables are led to the periphery of the core tank.

Whenever the power to the drive is interrupted, the poison rod falls by gravity into the reactor core

Nuclear aspects. The U^{235} fraction in the fuel is about 0.018. With a full core loading of new fuel elements (63) of this enrichment, an infinite multiplication factor (k_∞) of 1.17 and an effective multiplication factor (k_{eff}) of 1.08 are expected at the moderator operating temperature (575°F average). At 45.5 Mw (thermal) with the above fuel loading, the average and maximum thermal neutron fluxes are about 2×10^{13} and 3×10^{13} n/(cm^2) (sec), respectively The initial conversion ratio is approximately 0.60. The temperature coefficient of reactivity is negative, about $-5.9 \times 10^{-5} (\Delta k/k)/°F$ at 575°F.

The excess reactivity ($\Delta k/k$) is about 7.4% for a full loading of new fuel elements. The excess is required for control, and to compensate for fuel depletion and poisoning. The five shim-safety rods control about 15% reactivity and the regulating rod has a total worth of about 0.6%.

Primary cooling. The primary heat-transfer system is divided into parallel loops, two for the small and six for the large plant. In each loop, the hydrocarbon coolant is pumped from the reactor vessel to one steam generator and back to the reactor. Each coolant loop can be isolated from the reactor by blocking valves. Pressure and flow surges are absorbed in a surge tank partially filled with nitrogen gas. The heat-transfer diagram is shown in Fig. 7–48.

The main heat-transfer lines are of carbon steel, 14 and 24 inches in diameter for the small and large plants, respectively The piping and all associated equipment are insulated, and are heated by steam tracing The main coolant pumps are carbon steel centrifugal pumps with mechanical, water-cooled shaft seals. Pumps are rated at 5,500 and 16,000 gpm in the respective plant sizes.

Pressurizing and degassing. Loop operating pressure is maintained at about 120 psia by a pressure-controlled valve which regulates the flow of organic into the degassing tank. Pressurizing pumps force organic continuously from the degassing tank back into the primary loops. The system comprises a pressure letdown valve, a degassing tank, pressurizing pumps, and associated condenser equipment. Coolant taken from the

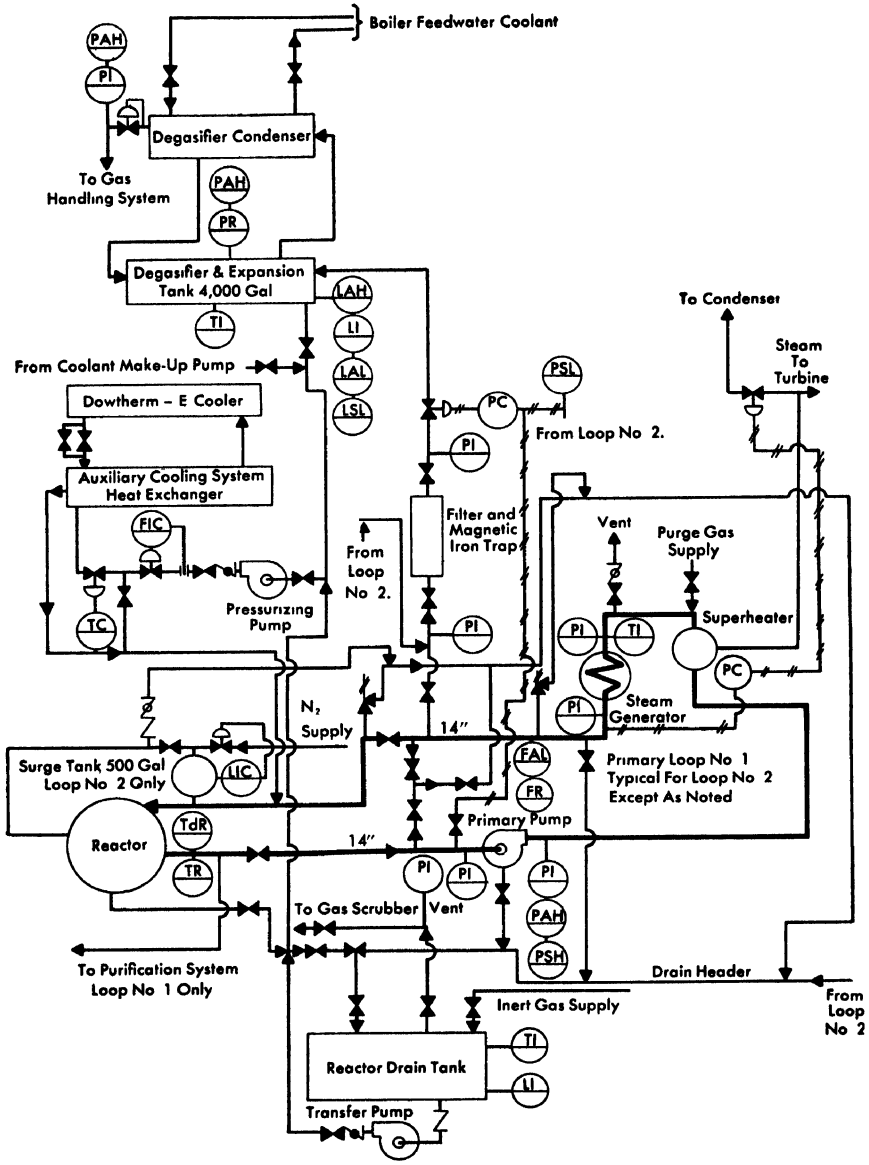

FIG. 7–48. Heat-transfer and degassing system.

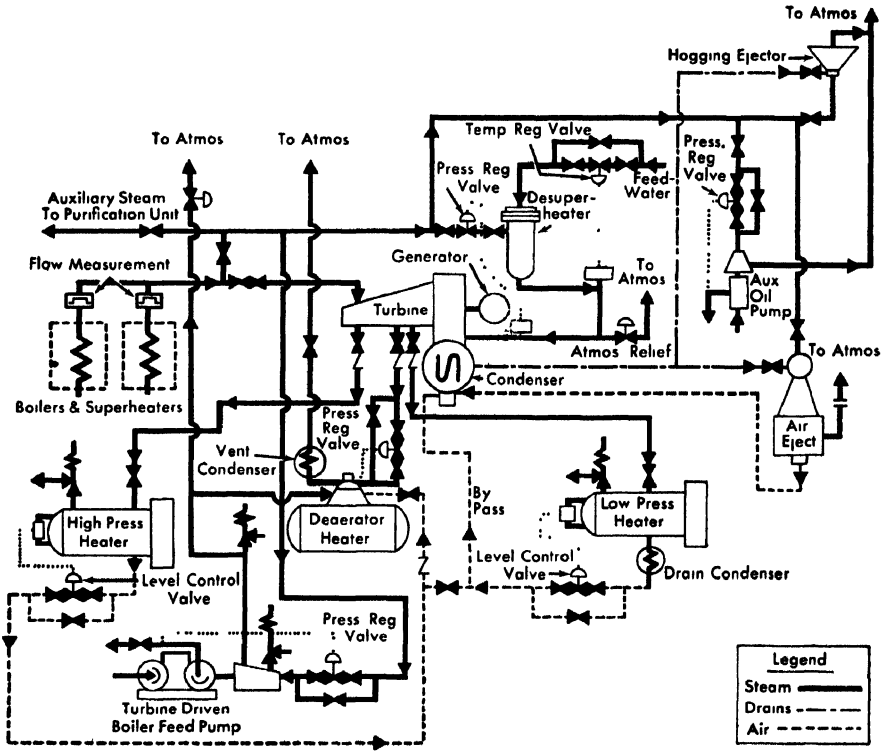

FIG. 7–49. Power plant steam system.

primary loops downstream from the heat exchangers is passed through filters to remove particulate matter.

The degasifier system continuously removes gas and vapor from decomposition of the coolant, gases introduced with the coolant makeup, water vapor from small water or steam leaks, and gases diffusing from the surge tank into the coolant. The degassing tank also serves as an expansion tank for the primary system.

Organic purification. Damage to the organic coolant by radiation and high temperature makes a purification system necessary. Steady-state concentration of polymer in the coolant is maintained between 15 and 30% by weight by continuously passing a small sidestream of coolant through a vacuum flash still. Impurities and organic materials less volatile than para-terphenyl are removed by this system Radioactive gases are removed by the degassing system.

Steam generation. There is one steam generator in each primary coolant loop. The two steam generators in the small plant and six in the large plant deliver 162,000 and 7,170,000 lb of steam per hour, respectively, to

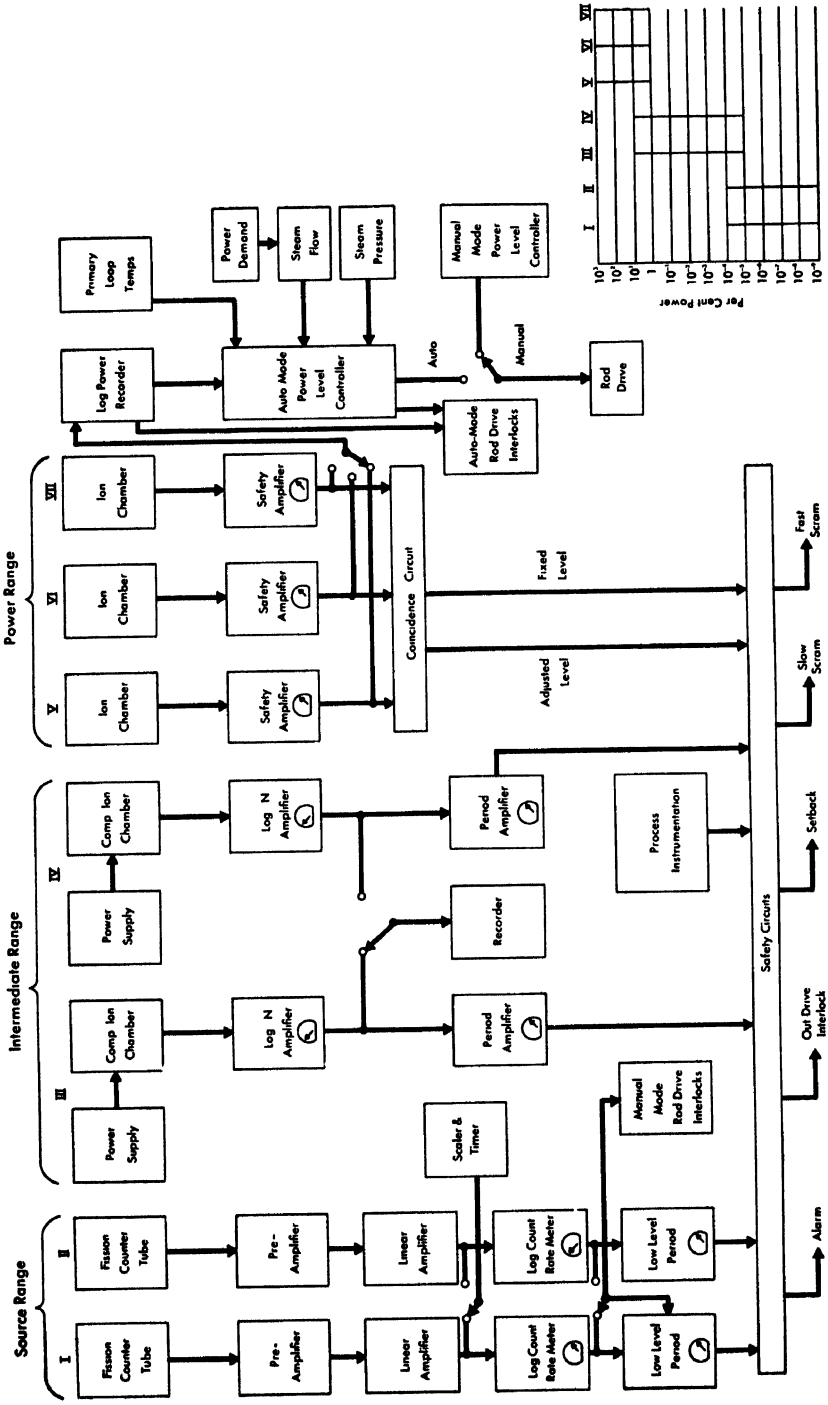

FIG 7-50 Power level control system.

the turbine at 415 psia and 550°F. Shell-and-tube steam evaporators with integral steam separators have water in the shell and hydrocarbon coolant in the tubes. At rated load, water from the feedwater heaters enters an economizer section in the steam evaporator at 337°F, and dry steam leaves the steam separator at 448°F. The steam superheater is a shell-and-tube unit with steam in the tubes and hydrocarbon coolant in the shell. At rated load, dry saturated steam from the steam separator enters the superheater at 448°F and 415 psia, and superheated steam leaves the unit at 550°F.

Power generation. Steam from the organic-heated steam generators is piped to a turbine in the turbogenerator area of the plant A regenerative steam cycle employs three stages of steam extraction for feedwater heating A deaerator is used in the 40-psia extraction system. The plant steam system is diagrammed in Fig 7–49 A conventional turbogenerator produces 12,500 and 160,000 kw of gross electric power for the small and large plants, respectively, with net efficiencies of 25 and 26%.

Control. The reactor is controlled and its power level and operation are monitored by a combination of nuclear and non-nuclear instrumentation. At operating power levels, the reactor will be controlled to produce the heat required for delivering a demanded amount of steam or electricity. With reactor power varying over a prescribed range, control will be automatic so long as set ranges of pressures, temperature, flow rates, fluid levels, radiation levels, etc., are maintained When one of these deviates from the set range, an alarm sounds and a signal indicates the condition. If the condition endangers the system, power level is reduced Because the temperature and power coefficients of reactivity are negative, a fast-acting reactivity control system is not essential for normal operation.

The control system adjusts reactor power output to turbogenerator requirements, holding steam pressure constant at the turbine throttle. A signal proportional to steam flow rate goes from a steam flow recorder on the main steam header directly into the neutron flux controller. This is the primary control signal for reactor power level. The same signal goes from the steam flow recorder to a power computer. The power computer determines the reactor coolant outlet temperature required to keep the steam pressure constant, and sends a corresponding signal to the temperature recorder-controller.

Control is automatic over the power generation range from 15 to 110% of rated power. For startup, the operator manipulates the controls, using nuclear startup instrumentation. Fission chambers and compensated ion chambers measure neutron flux. The operator receives period information from derivative circuits, and the rate of power increase is limited to safe values by period interlocks. The power level control system is diagrammed in Fig. 7–50 and the reactor control system in Fig. 7–51.

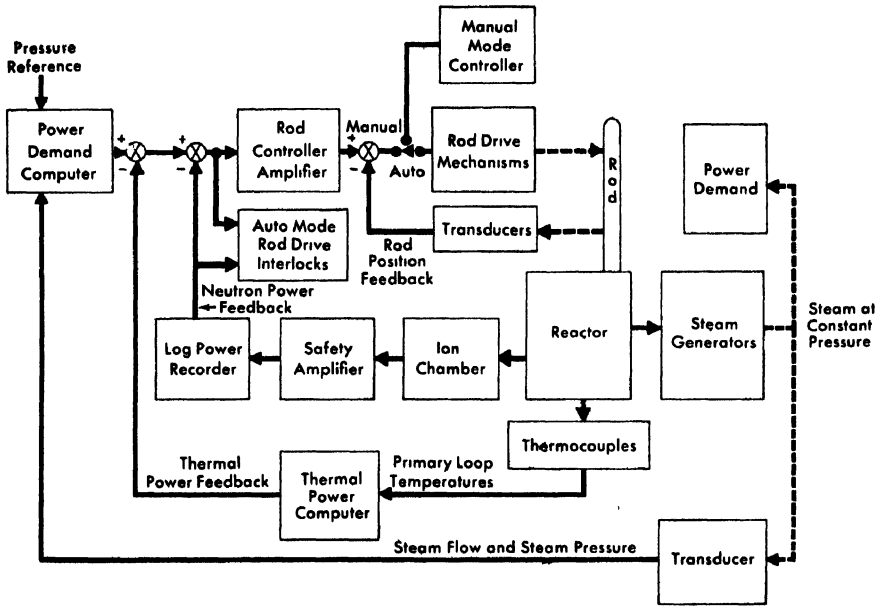

FIG. 7–51 Reactor instrumentation and control

Operational and economic aspects. The relatively simple operation of the Organic Moderated Reactor Experiment (OMRE) is favorable to adoption of organic-moderated reactors for commercial use. The cost of producing electric power from an OMR-powered plant has yet to be demonstrated, but construction and operation costs can be estimated. It appears that for larger plants a net power cost of about 8.4 mills/kwh (with $30/g credit for plutonium) can probably be achieved by the time a second or third large plant is built.

Estimates of plant costs are given as a function of plant size in Fig. 7–52. Power generation cost estimates are given in Fig. 7–53, and fuel cost components in Table 7–17. Costs are in 1957 U. S. dollars for a plant located in this country. Current AEC prices are applied in calculating chemical processing, inventory charge, and burnup costs of fuel A plant utilization factor of 0.80 was assumed.

Plant costs. Plant costs have been estimated for two plant sizes, 11,400 and 150,000 kw. The building estimates include site improvements but not the site. Turbogenerator system estimates do not include switchyard facilities. The plant costs given include only 30% of the analytical and design engineering costs involved in the first plant of the OMR type. The lower value is felt to be representative of the effort required for the second or third plant built. Annual fixed charges are assumed to be 15% of the total plant costs.

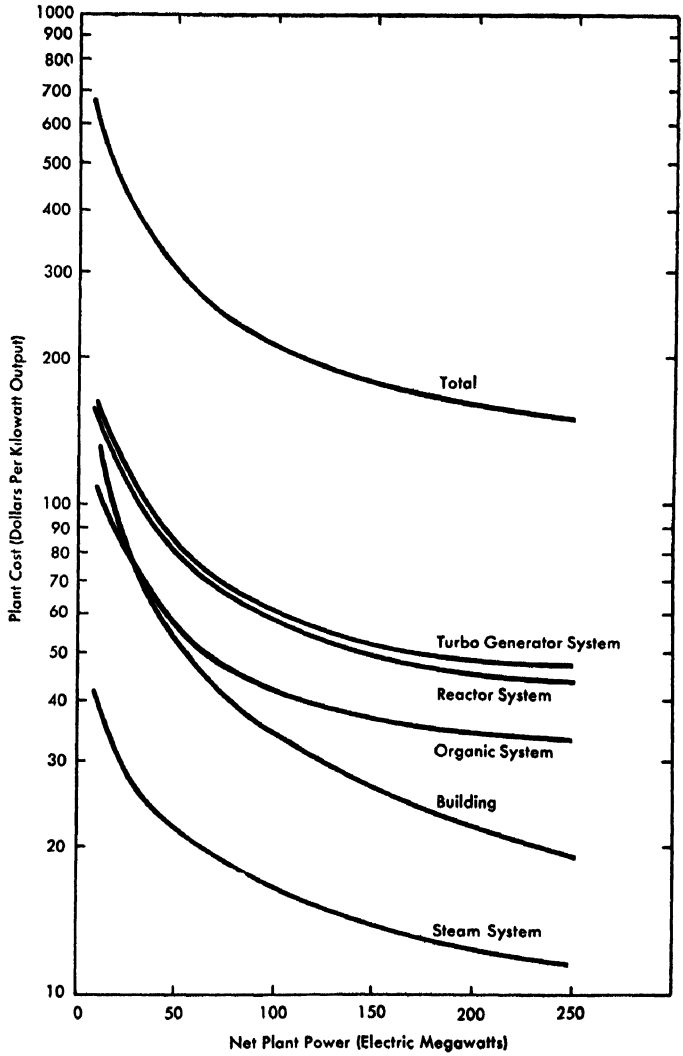

FIG 7–52 Plant costs for OMR power plant.

Fuel costs. Estimated fuel costs for a 150-Mw plant are given in Table 7–17, and fuel costs as a function of plant size in Fig. 7–53. Average fuel-element irradiation was assumed to be 3000 Mwd per ton (2000 lb). From Fig. 7–53, it is apparent that fuel costs are a major factor in the cost of power from a commercial organic-moderated plant and that they vary little with plant size. However, if plutonium credits are applied to reduce fuel costs, net cost of fuel will decrease with larger plant size because the conversion ratio is larger.

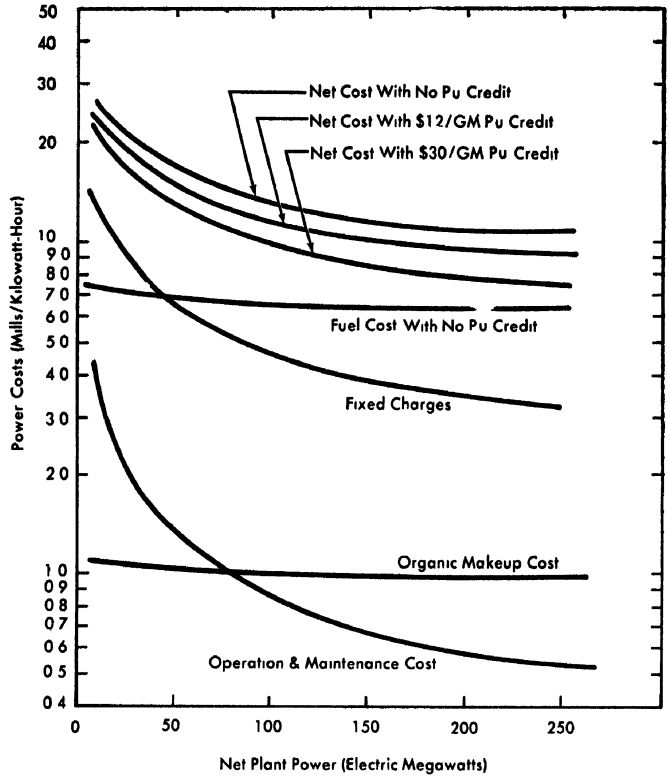

FIG. 7–53. Electric power costs from OMR power plants

In computing inventory charges on fuel, 4% of its initial value was used for a complete reactor loading plus a one-year supply

Operation and maintenance The principal component of operation and maintenance costs for a small OMR plant is operating labor; for a large plant, it is organic makeup.

Organic makeup cost is nearly constant at about 1 mill/kwh, but is slightly less for larger plants because the thermal efficiency is slightly greater.

The larger the plant, the larger the crew, of course, but even the smallest plant requires a sizable staff. Although it appears feasible to operate an OMR plant as part of a station system, reducing operating manpower requirements considerably, the costs are estimated for a complete operating crew in Table 7–18. Salary costs, including employer costs, were estimated at $12,000 per year for supervisors, $7500 per year for specialists and special trades, $6000 per year for operators, and $5000 per year for secretarial employees.

TABLE 7–17

FUEL COSTS FOR 150-MW OMR POWER PLANT

	Annual cost*	
	dollars/year	mills/kwh
Inventory (4% of value of fuel held)	898,000	0.85
Prefabrication conversion (UF_6 to metal)†	314,000	0.30
Fabrication‡	542,000	0.51
Burnup (cost of U^{235} destroyed)†	2,530,000	2.40
Recovery of uranium† (chemical separation and conversion of uranium to UF_6)	2,234,000	2.12
Recovery of plutonium† (chemical recovery and conversion to metal)	182,000	0.17
Shipping costs	151,200	0.14
Total costs	6,851,200	6.49
Pu value at \$12/g	1,431,000	1.36
Net fuel cost with \$12/g Pu credit	5,420,200	5.13
Pu value at \$30/g	3,577,000	3.40
Net fuel cost with \$30/g Pu credit	3,274,200	3.09

*Plant factor, 0.80 of rated annual capacity. Fuel life, 3000 Mwd/ton average (2000 lb/ton)

†Current AEC cost quotations

‡Five-inch-square by 10-ft-long uranium-metal, plate-type elements with extended surface aluminum cladding.

7–5.3 Process and space heating. Although generation of electricity is the most commonly discussed use for nuclear power, large and steadily rising needs for industrial process heating and for heating homes and commercial buildings will also place a large demand upon the industry in the future In areas where natural gas is cheap, little consideration will be given to nuclear power, but where this convenient fuel is not cheap or is being depleted rapidly, nuclear power will come into use. The advantages of organic-moderated reactors, discussed earlier, are believed to be particularly applicable. Adapting these reactors to heat production is discussed below. Depending on the application, the required temperature may vary over a wide range; here, 150 psia saturated steam has been arbitrarily assumed

At 150 psia, steam has a saturation temperature of 358°F, and the optimum organic coolant temperature will probably be lower than for the

TABLE 7-18

OMR POWER PLANT STAFF

	Number required	
	11,400-kw plant	150,000-kw plant
Plant superintendent	1	1
Assistant plant superintendent	1	1
Technical and administrative staff	2	5
Secretary	1	1
Total staff	5	8
Operating shifts (4 each):		
Shift supervisor (engineer)	1 (4)	1 (4)
Chief plant operator	1 (4)	1 (4)
Plant operator	1 (4)	2 (8)
Operator helper	1 (4)	2 (8)
Instrument technician	1 (4)	1 (4)
Total operating crew	20	28
Maintenance:		
Electronic technician	1	2
Instrument repairman	1	2
Electrician	1	3
Steam fitter-welder	1	1
Mechanic	1	2
Yardman		1
Total maintenance crew	5	11
Total plant staff	30	47

higher-temperature steam cycles previously described. The organic temperature at the reactor outlet has been arbitrarily set at 500°F for the following discussion. At this lower coolant temperature, the reactors previously described (with minor changes), will produce from 75 to 1100 Mw of thermal power.

Reactor. Reactor core designs for process heat applications are the same as for electric power generating OMR's. Maximum fuel-element surface temperature, coolant flow rate, reactor foundations and structure, and fuel-handling systems are also the same. Because of the higher power level, the thermal shield is increased in thickness and the power range of

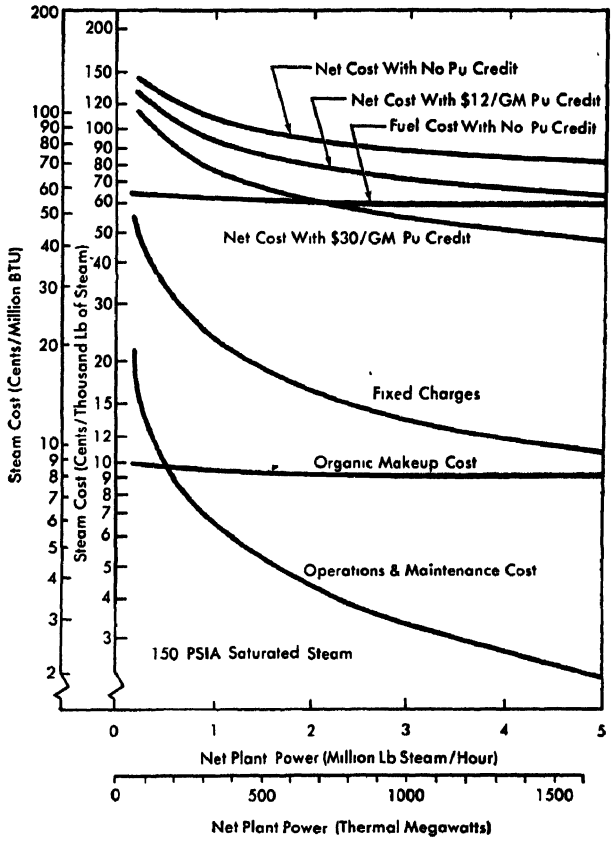

Fig. 7–54 Process heat costs from OMR steam plants.

the reactor instrumentation is extended. None of these changes requires significant design modifications.

Systems. Because the flow rate is the same, the primary cooling system is unchanged, as are the pressurization and degassing system and the organic purification system.

The steam generator does not include a superheater, but with the higher steam output and the slightly lower average temperature difference between the organic and the boiling water, the evaporator surface requirement is about twice as great. Further, because the specific volume of steam is considerably greater, the evaporator drums, the moisture separators, the steam lines, valves, etc., must be larger.

Either electric motor or steam turbine drives can be used for plant equipment and auxiliaries. Some of the equipment will require electric drives or an outside supply of steam to start up the plant.

The plant control system is basically unchanged, but specific process requirements must be known to establish its characteristics. In general, control should be less complex than for an electric power generating station.

Operational and economic aspects Operations are further simplified when the plant is used to produce process heat. Although a reactor and organic system of a specific size operate at a higher thermal power, temperatures are lower and control requirements are usually simpler. Eliminating the turbogenerator also simplifies operation. The higher thermal power makes more frequent fuel reloading necessary, but this does not increase the number of operators required. The total manpower estimate for the small process heat plant is 25, as compared with 30 for the power plant. For the large plant, the respective requirements are 38 and 47.

The estimated (future) total and incremental costs of producing 150 psia saturated steam from 80°F water are given in Fig. 7–54. Again the estimates apply to the second or third large plant built. Net process steam costs from the larger plant are about $0 47 per million Btu ($0.56 per thousand pounds of steam) if plutonium is credited at $30 a gram For process heat, fuel costs are a higher fraction of the total than for producing electricity

7–5.4 Marine propulsion. As nuclear power becomes competitive in industry, it is expected also to compete with traditional propulsion for merchant vessels. Nuclear power can provide ships long operating periods, with practically no change in cargo capacity Today a supertanker operating between the Persian Gulf and the United States east coast consumes bunker fuel equivalent to about 7% of its cargo capacity. The same ship, making the voyage around the Cape of Good Hope rather than through the Suez Canal, would consume bunker oil equivalent to 10% of its cargo capacity. In contrast, a nuclear-powered tankship would have the same cargo capacity throughout the voyage.

The OMR concept is especially attractive for marine propulsion because the hydrogen-moderated reactor core is small for a specified power output and thus the amount of reactor shielding is minimized. The low radioactivity level of the primary coolant system also favors low shielding weight. The accessibility of the equipment for operation and the expected feasibility of making the reactor safe without gastight containment are further OMR advantages.

In a study conducted for the U. S. Maritime Administration, Atomics International has established the criteria for an OMR power plant to provide the 20,000 shaft horsepower for driving a tankship of 38,000 deadweight tons.

Tankship description The tanker described for this application is similar to the ships built for Grand Bassa Tankers, Inc., by the Newport News Shipbuilding and Drydock Company in 1952–54. This supertanker has a deadweight tonnage of 38,000. Power requirements are supplied by the reactor plant for which data are given in Tables 7–15 and 7–16. The reactor supplies power for propulsion, crew and passenger facilities, auxiliary power, and Butterworth heating (tank cleaning). Figure 7–55 shows the aft section of the single-screw tanker with forecastle, amidships house, and poop house. The vessel is subdivided by watertight and oiltight transverse and longitudinal bulkheads to form cargo tanks for petroleum products of different grades. Fuel-oil tanks carry only a small supply of diesel oil for emergency power.

Machinery spaces are aft; the reactor compartment is forward in the machinery space The moderately shielded reactor compartment contains the reactor, the primary coolant system, the steam generators, and superheaters. The whole structure and equipment are supported on a system of floors and girders forming the double bottom.

Around the sides and ends of the reactor compartment, a cofferdam space is used to store diesel oil (or salt-water ballast), which serves as a final shield between the reactor room and inhabited spaces Spaces outboard of the reactor room and above it are subdivided and assigned to services primarily associated with the reactor They include the primary coolant system pump motors, the purification and gas-handling room, and the control room The propulsion turbines are aft of the reactor compartment and the cargo pump room is forward. The cargo pumps are driven by vertical turbines that exhaust to the auxiliary condenser in the engine compartment.

Two casings are provided above the engine compartment. The forward casing is arranged for a crane that will handle the refueling casks aboard ship A hatch at the forward end of this casing on the boat deck permits a shoreside crane to lift fuel-transfer casks off and on the vessel. The after casing is for access to the main turbines and gears, and as space for lube oil gravity tanks and the deaerating feedwater heater.

Reactor. The reactor core design is similar to that described for the OMR power plants. Basic characteristics of both types of power plant are given in Table 7–16. The reactor core produces 70,000 Mw of thermal power in a volume 6 ft high by about 6 ft in diameter. The core tank and accessories, the organic moderator coolant, the fuel elements, and the control rods are similar to those of the land-based OMR plants. The nuclear aspects of the core are similar except for the effects of the greater fuel loading required for more than a year's operation between refuelings.

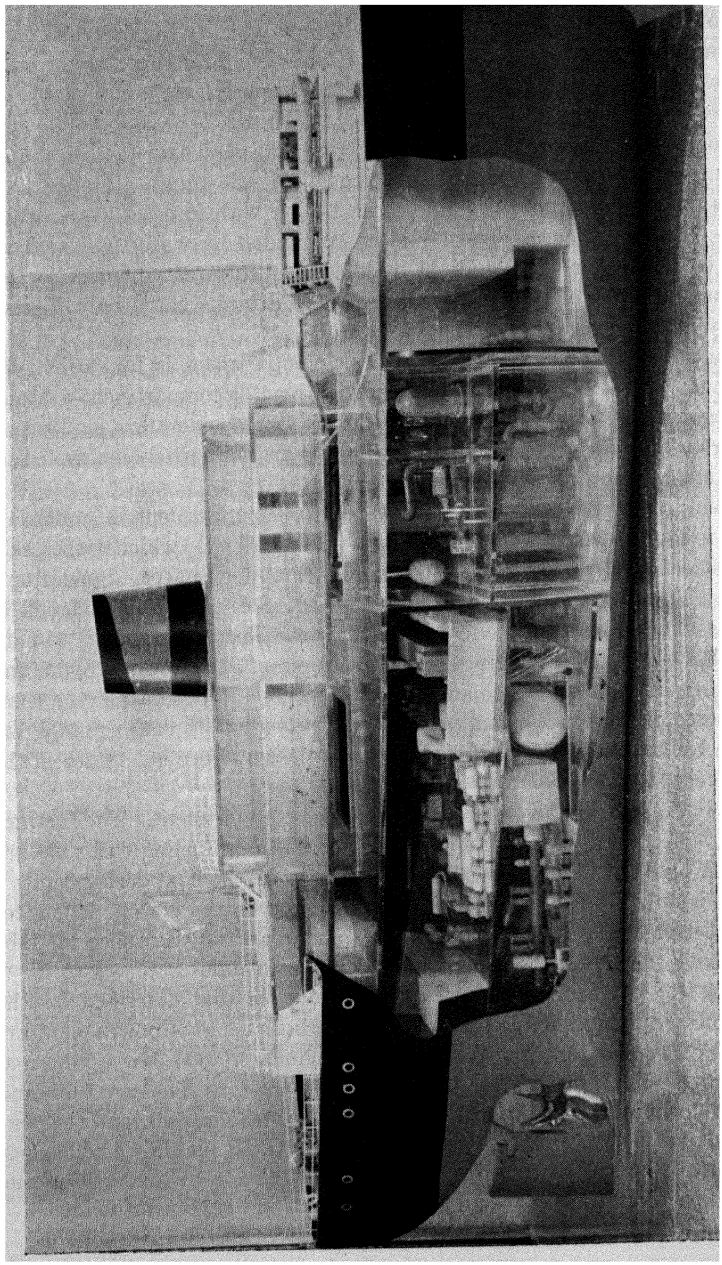

FIG. 7–55. Conceptual view of tanker

Shielding. Although concrete shielding is most economical for land-based plants, it is relatively poor for applications requiring small weight and volume.

The reactor radiation shield is composed of three regions: a neutron-moderating and absorbing region surrounding the reactor, a gamma-ray absorbing region surrounding the reactor, and a gamma-ray absorbing region surrounding the reactor compartment and purification room.

To reduce corrosion in the shield tanks, a hydrocarbon rather than water is used as the neutron moderator surrounding the reactor. Consequently the tanks can be made of carbon steel, with minimum induced radioactivity levels at the shield surface after shutdown. The hydrocarbon liquid is estimated to be capable of withstanding operation for a period of four years before replacement will be necessary. Boral sheet is employed for absorbing thermal neutrons, and steel for absorbing gamma rays.

The purification room contains the coolant distillation and waste polymer disposal equipment. Because most of the activated corrosion products and impurities are extracted with the waste polymer, the purification room requires some shielding. For most areas the steel bulkheads and walls around the purification room provide adequate shielding protection.

Fuel handling. One core loading of fuel will operate the tanker for about 15 months. During this time, the ship can make more than nine round trips between the Persian Gulf and Philadelphia, delivering more than 2.5 million barrels of oil. With refueling needed so infrequently, it is most feasible to employ shoreside facilities for refueling. These facilities include the fuel cask, storage for a complete core loading of both new and spent fuel, a 30-ton crane capable of servicing both the ship and the dockside fuel storage facilities, organic storage tanks, and miscellaneous spare parts and tools. The top shield of the reactor rotates, and fuel handling is carried out much as with the land-based designs.

Organic handling systems. The heat-removal system, primary loop pressurization and degassing system, and coolant purification system are similar to those in previously described plants. About 11,000 gpm of organic coolant is circulated through each of the two primary loops. Steam is generated at 450 psia and 580°F in two steam generators at a total rate of 230,000 lb/hr. Usually the organic residues would be burned in a land-based plant. At sea they could be burned, stored, or dumped.

Propulsion equipment and auxiliaries. The ship propulsion unit is a cross-compound, double-reduction set, with one high-pressure turbine, one low-pressure turbine, and one double-reduction gear connected to the turbines by flexible couplings. Three feedwater heating stages are utilized. The exhaust end of the low-pressure turbine contains impulse wheels to

drive the ship astern. The turbines are so designed and fitted that either one can be operated separately, in case of accident, to the other.

If the steam propelling system is damaged, the steam supply lost, or equipment fails, "take-home" power is provided by two 400-hp electric motors connected in tandem to the first reduction pinion of the main reduction gear. The motors are driven by one of two 1000-kva diesel generators in the aft end of the engine room. The second diesel generator is a source of emergency power for the reactor cooling equipment, controls, and instruments. The two "take-home" motors are connected to the pinion by a bolted coupling that can be readily closed when required.

The ship's electrical generating system consists of one 3-phase turbogenerator rated at 1875 kva and the two diesel generators. The remainder of the ship's engine room equipment is conventional, including main and auxiliary steam systems, auxiliary exhaust system, feed and condensate system, circulating water system, lube oil system, distilling plant, fire system, bilge and ballast system, Butterworth system, diesel oil service and transfer system, control air system, cargo oil system, and refrigeration, dehumidification, and air conditioning systems.

Operational and economic aspects. The ultimate consideration for any commercial vessel is economy To appraise the OMR-powered tanker, its total operating costs are compared with those of a conventional vessel of the same hull design and an equivalent power plant. To eliminate some of the many variables, it was assumed that both vessels would ply continually between Kuwait, in the Persian Gulf, and Philadelphia, via the Suez Canal This is a round trip of 17,000 nautical miles with payload carried in one direction only.

The number of possible round trips per year is calculated as follows. Average sea speed for both the conventional and the nuclear ship is 18 knots, equivalent to 39.4 days at sea per round trip. Allowing two days for canal transit and a total of 4.3 days in port, the total round trip time is 45.7 days It is estimated that both ships, conventional and nuclear tanker, will have 345 operating days per year. Refueling of the OMR power plant, estimated to require six days every fifteen months, can be accomplished during the ship's annual overhaul. Accordingly, both ships will make 7.55 round trips per year Table 7–19 summarizes the annual operating costs for the two vessels, assuming both vessels load to the same displacement.

Most important of all operating costs are the capital charges. A conventional 38,000 DWT tanker is estimated to cost $10,570,000, or $300 per deadweight ton, for American construction. Of this, $370,000 is estimated to be the installed cost for boilers, fuel-oil equipment, fans, uptake, and other items which will be replaced by the nuclear plant. The cost of the nuclear-powered ship is the difference between the above two figures

TABLE 7–19

ANNUAL OPERATING COSTS FOR 38,000 DWT TANKSHIPS

Item	Conventional	OMR
	(Thousands of dollars)	
Depreciation and interest	847.0	1,138.3
Insurance	131.7	175.3
Repairs	148.5	163.4
Crew	389.0	427.9
Subsistence	36.6	40.2
Stores	23.5	25.9
Canal tolls	221.6	217.1
Port charges	36.6	36.0
Overhead	45.1	45.1
Total, excluding fuel	1,879.6	2,269.2
Fuel cost	738.3	690.0*
Total	2,617.9	2,959.2
Annual cargo capacity, tons	268,500	284,500
Cost per ton cargo	$9.75	$10.46

*Includes credit for plutonium.

plus the estimated cost for the nuclear system and its auxiliaries, or $4,000,000. Thus the original cost for the OMR tankship is estimated at $14,200,000. Capital charges for both conventional and nuclear ships are calculated on the same basis. Depreciation is taken at a uniform rate over a 20-year period, without allowance for salvage. Interest is computed at 5%. Average interest on the declining balance over the 20-year period is taken as 3% of the initial cost.

Insurance, a direct function of value, is taken at $5000 plus 1.2% of the shipyard cost for each vessel. Maintenance and repairs for the OMR-powered vessel are arbitrarily increased 10% to allow for the increased complexity of the heat source.

Crew costs are based on U. S. flag operation. The complement of the nuclear ship is 53, compared with 46 for the oil-fired tanker. Extra hands include those on board for routine reactor control and maintenance. The costs of stores and supplies are considered proportional to displacement and shaft horsepower. Subsistence is assumed to be proportional to the crew's wages.

Invariant expenses are port charges of $36,600 and overhead at $45,100 per year. Canal tolls, based on deadweight tonnage, amount to $221,600 for the oil-fired ship, and slightly less for the OMR. The final expense item is that of fuel. For the conventional ship, fuel-oil consumption is estimated at 0.536 lb per shaft horsepower hour. At 18 knots, 117 tons per day or 36,000 tons per year are required.

Fuel cost is estimated at $3.10 per barrel or $20 50 per long ton. Thus, the annual fuel cost for the conventional vessel amounts to $738,300. In estimating fuel costs for the OMR tanker, the approach was the same as discussed in preceding sections of this chapter. Plutonium was credited at $30/g.

References

1. C D. Bopp and O. Sisman, *Radiation Stability of Plastics and Elastomers*, USAEC Report ORNL-1373, Oak Ridge National Laboratory, July 23, 1953; C D. Bopp and O Sisman, *Physical Properties of Irradiated Plastics*, USAEC Report ORNL-928, Oak Ridge National Laboratory, June 29, 1951

2. C. G. Collins and V. P Calkins, *Radiation Damage to Elastomers, Plastics, and Organic Liquids*, USAEC Report APEX-261, General Electric Company, Aircraft Nuclear Propulsion Department, September 1956.

3 A O Allen, Effects of Radiation on Materials, in *The Science and Engineering of Nuclear Power*, Vol. 2. Cambridge, Mass : Addison-Wesley Press, Inc , 1948. (Chap 13)

4. W S Snyder and J Neufeld, *Calculated Depth Dose Curves in Tissue for Broad Beams of Fast Neutrons*, USAEC Report ORNL-1872, Oak Ridge National Laboratory, May 5, 1955

5 R. H. Schuler and A O Allen, Radiation-Chemical Studies with Cyclotron Beams (communication to the editor), *J Am Chem Soc* 77, 507 (1955).

6. E. L. Zebroski and E M Kinderman, *A Comparison of High-Energy Electron and Gamma Irradiation Effects on Organic Liquids*, Report WADC-TR-57-141, Stanford Research Institute, Feb 21, 1957

7. E L Colichman and R H J Gercke, Radiation Stability of Polyphenyls, *Nucleonics* **14**(7), 50–54 (1956)

8. S Nakazato and R. H. J. Gercke, *Organic In-Pile Loop NAA-18*, USAEC Report NAA-SR-1592, Atomics International, North American Aviation, Inc , July 1, 1956.

9. E L. Colichman and R Fish, Resistance of Terphenyls to Heat and Radiation, *Nucleonics* **15**(2), 72 (1957).

10. T. H. Bates et al , *The Radiation and Thermal Stability of Some Potential Organic Moderator-Coolants Part I Electron Irradiation of Para-Terphenyl and Santowax R*, Report AERE-C/R-2121, Great Britain, Atomic Energy Research Establishment, May 8, 1957.

11. R. Balent and J. Wetch, Atomics International, North American Aviation, Inc., 1954. Unpublished.

12. W. N. Bley, *Radiation Effects on Engineering Properties of Polyphenyl Reactor Coolants: An In-Pile Loop Experiment*, USAEC Report NAA-SR-2470, Atomics International, North American Aviation, Inc., 1958 (To be published)

13. B. M. Tolbert and R. M. Lemmon, Radiation Decomposition of Pure Organic Compounds, *Radiation Research* **3**, 52–67 (1955)

14. R. O. Bolt et al., Organics as Reactor Moderator-Coolants: Some Aspects of Their Thermal and Radiation Stabilities, in *Proceedings of the International Conference on the Peaceful Uses of Atomic Energy*, Vol. 7. New York: United Nations, 1956 (P/742, pp 546–555)

15. M McEwen, *Preliminary Engineering Study of Organic Nuclear Reactor Coolant-Moderators*, Report RE-CR-964, Monsanto Chemical Co., Mar. 31, 1956

16 E L. Colichman and R H J Gercke, Selection of Organic Materials as Reactor Coolant-Moderators, in Symposium on Radiation Effects on Materials, Vol. 2, *Am Soc Testing Materials Spec Tech. Publ No. 220*, 1958.

17. R H. J Gercke, OMRE Research and Development Program, in *Proceedings of the SRE-OMRE Forum Held at Los Angeles, California, February 12 and 13, 1958*, USAEC Report TID-7553, Atomics International, North American Aviation, Inc., 1958

18. J. C. Southard, A Modified Calorimeter for High Temperatures. The Heat Content of Silicone, Wollastonite, and Thorian Dioxide Above 25°, *J Am. Chem Soc* **63**, 3142–3146 (1941)

19 H. O. Forrest et al, The Specific Heat of Biphenyl, *Ind Eng. Chem* **23**, 37–39 (1931)

20 J F D Smith, The Thermal Conductivity of Liquids, *Trans. Am Soc. Mech. Engrs* **58**, 719–725 (1936).

21. M Silberberg and D. A Huber, Heat Transfer Characteristics of Polyphenyl Reactor Coolants, paper presented at the Fourth Nuclear Engineering and Science Conference Held in Chicago, Ill, March 17–21, 1958 (P/145) (To be published by the American Institute of Chemical Engineers)

22. E N Sieder and G E Tate, Heat Transfer and Pressure Drop of Liquids in Tubes, *Ind Eng Chem* **28**, 1429–1435 (1936)

23. C S. Cragoe, Thermal Properties of Petroleum Products, *Natl. Bur. Standards (U. S) Misc Publ., No 97*, 1929

24 J F D Smith, The Thermal Conductivity of Liquids, *Trans. Am. Soc. Mech Engrs.*, **58**, 719–725 (1936)

25. C T. Ewing et al, *Heat Transfer Studies on a Forced Convection Loop with Biphenyl and Biphenyl Polymers*, Report NRL-4990, Naval Research Laboratory, July 16, 1957.

26 W N. Bley, *Radiation Effects on Engineering Properties of Polyphenyl Reactor Coolants: An In-Pile Loop Experiment*, USAEC Report NAA-SR-2470, Atomics International, North American Aviation, Inc., 1958 (To be published)

27 E. L. Colichman and R H. J Gercke, Radiation Stability of Polyphenyls, *Nucleonics* **14**(7), 50–54 (1956).

28. E. L. Colichman and R. Fish, Resistance of Terphenyls to Heat and Radiation, *Nucleonics* **15**(2), 72 (1957).

29. T. H. Bates et al., *The Radiation and Thermal Stability of Some Potential Organic Moderator-Coolants. Part I. Electron Irradiation of Para-Terphenyl and Santowax R,* Report AERE-C/R-2121, Great Britain, Atomic Energy Research Establishment, 1957.

30 H. E Kline et al , Dynamic Corrosion Tests of Materials in Irradiated Organics, paper presented at the Fourth Nuclear Engineering and Science Conference Held in Chicago, Ill , March 17–21, 1958. (To be published by the American Institute of Chemical Engineers)

CHAPTER 8

PLUTONIUM RECYCLING IN THERMAL REACTORS*

8–1. Introduction and Objectives

Reactors which use natural or slightly enriched uranium fuel produce plutonium, some of which is fissioned in place, and some remains in the fuel elements when they are finally removed from the reactor. The residual plutonium can be recovered from the spent fuel elements and put back in the reactor with a fresh fuel charge, an operation called "recycling."

Power reactors can be designed to operate with natural uranium, but there are advantages in enriching it. Enrichment can extend the useful life of a fuel loading by increasing its initial reactivity; thus it can increase the amount of energy produced from the fuel. When the recycled plutonium is fissioned, it increases the production of new plutonium in the reactor, and leads to further fissions and further buildup of plutonium for the next recycle operation. Plutonium recycling can thus provide a limited amount of fuel enrichment for power reactors in a self-sustaining operation with natural uranium feed, independent of uranium isotope separation.

The U. S. Atomic Energy Commission, through its Hanford Laboratories, is developing technology for recycling plutonium economically in thermal heterogeneous power reactors This effort, the plutonium recycle program, will include studies of reactor design parameters in relation to over-all fuel costs, and experiments to develop economical fuel fabrication and recovery processes. An experimental reactor, the Plutonium Recycle Test Reactor (PRTR), is being built.

It is in these areas—(1) reactor physics, (2) plutonium utilization analyses, (3) fuel element development, and (4) chemical processing—that most of the work is being done. The objectives are:

(1) To obtain the physics data necessary for efficient use of plutonium as fuel material. As a fissile material, plutonium differs in fundamental

---

*Compiled by S. Goldsmith, Hanford Atomic Power Operations. Material for this chapter was supplied by R W. Benoliel, E A. Evans, M. D. Freshley, J C Fox, H. Harty, R. E. Heineman, B. R Leonard, W. L. Lyons, P. R. McMurray, M. Lewis, C A. Rohrmann, and J. R Triplett. J B Work and L. H. McEwen reviewed the manuscript. All figures in this chapter were furnished by the Hanford Laboratories.

The Hanford Laboratories are operated for the Atomic Energy Commission under contract by the General Electric Company.

nuclear properties from the better understood U^{235}. On continued exposure, Pu^{239} is converted to a mixture of higher isotopes, whose composition depends on the conditions of irradiation. Mixtures of plutonium isotopes can be used for enrichment in many ways and irradiation behavior can vary materially with the method of enrichment used. These considerations, as they affect the technical and economic relationships of plutonium recycling, are the basic subjects of the program of theoretical physics analysis and experimentation.

(2) By applying the results of the studies, to evaluate a wide range of system designs for power reactors in various economic situations The objective of this continuing effort is to integrate the experimental, theoretical, and developmental results, as they become available, into a rational and up-to-date evaluation of prospective plutonium recycling applications, and to establish promising paths for further developmental work.

(3) To develop methods of fabricating inexpensive, stable fuel elements for plutonium recycling. For plutonium recycling to be economical, cheap and reliable fuel elements must be developed for a variety of reactors Although work is being done at many locations to develop uranium-bearing fuel elements for industrial power reactors, far less has been done about plutonium-bearing elements. Uranium and plutonium are somewhat similar metallurgically and chemically, but there are important differences which require special techniques for making plutonium-bearing elements. These differences include the highly toxic nature of plutonium and the necessity for devising fuel elements with relatively low plutonium content. By contrast, natural and slightly enriched uranium, as fuel materials, already have low U^{235} content.

Power reactor fuels can be enriched with plutonium in a number of ways. Spike enrichment, utilizing low concentrations of plutonium in inert carriers, leads to a high throughput of enriched fuel pieces. With uniform enrichment, all fuel elements contain plutonium, and must be given special handling during fabrication. Zone-uniform enrichment, which comprises the suspension of plutonium in fuel elements containing uranium and the use of this material in selected regions of the reactor, may also be used.

The development of good uranium fuels does not contribute uniquely to plutonium recycling. However, such a development does establish fuel design and fabrication capabilities which are useful and necessary for certain types of recycle operation such as the two-region, uranium-spike plutonium loading. Furthermore, uranium fuel developments often serve as initial "stand-ins" for the later use of plutonium in similar fuel designs. Uranium fuel development for the plutonium recycle program thus far has been on ceramic fuel types. Extensive work on metallic uranium fuels is being done at Hanford and elsewhere under other programs, and the re-

sults will of course be used when they are appropriate.

(4) To develop efficient and economic chemical processing methods and equipment for the recovery of plutonium from irradiated fuel, in a form suitable for preparation of recycle elements.

This phase of the program is concerned with the development of process methods of two classes: those that can be used in the experimental program for processing irradiated test fuels, and those that can be applied commercially.

Aqueous chemical processing methods used in plutonium production plants can be applied to uranium fuel elements for the experimental program. Only the dissolution steps need be modified to accommodate contemplated variations in uranium elements.

Aqueous methods can be used for processing plutonium-containing fuel elements but it is considered probable that other methods, such as pyrochemical methods, can be developed which will be preferable both for the test program and for prospective commercial application.

In the development of processes for commercial application it is necessary to consider the relation of the chemical processing plants to the reactors and fuel preparation plants. These considerations will help determine the optimum capacity of the typical commercial plant, and may determine the choice between continuous and batch operations. They may also indicate the economic degree of decontamination from fission products, in relation to the choice of direct, remote, or semiremote processes for subsequent fuel preparation.

The work completed to date on the plutonium recycle program is described later in this chapter under the above headings. Since the recycle program is relatively new, benefiting in many areas from established developments in reactor technology, a large part of this early work has been concerned with establishing the foundations for later efforts. Part of this work has been analytical. Another important phase of the work has been concerned with planning, designing, and beginning construction of two new facilities which will be the major tools of the program The purposes of these facilities (a fuel fabrication facility and an experimental plutonium reactor) are discussed in the following paragraphs, and the designs of the facilities themselves are described in the final sections of this chapter

The fuel fabrication facility will greatly extend the capabilities for fabricating plutonium-bearing fuel elements. Present facilities, although adequate for fabricating cast aluminum-plutonium fuel elements in developmental quantities, are being modified to develop fabrication methods for several other plutonium-bearing element concepts and to fabricate the first loadings of plutonium-bearing fuel elements for the experimental reactor. The new facility will be a pilot plant for fabricating a variety of plutonium fuel elements by various methods, in sufficient quantity for

experimental reactor loadings and for estimating costs of fabricating plutonium fuels commercially. This plutonium fabrication pilot plant will cost four million dollars. Preliminary construction started in March 1958. Occupancy is scheduled to start in late 1959 and construction is to be completed in 1960.

The experimental reactor is being built to (1) permit direct investigation of reactivity and long exposure plutonium isotope effects which cannot be adequately predicted at present, (2) provide for irradiation testing of plutonium-bearing fuel elements, (3) provide pilot-plant quantities of prototype irradiated fuels for use in the fuels reprocessing and fuels fabrication development programs, and (4) provide for pilot-plant scale demonstrations of factors involved in the economics of various fuel cycles. The reactor will be useful for other work, such as investigating the control characteristics of plutonium-fuel reactors, related directly or indirectly to plutonium recycling. The reactor is to be constructed with a minimum diversion of research and development effort; still, a prudent regard for the capital investment involved and the need for reliability have required substantial design verification testing, and materials and engineering development. Construction of the Plutonium Recycle Test Reactor (PRTR) which will cost about $15 million, was started in March, 1958. Initial use is scheduled for 1960.

8–2. Progress and Results

8–2.1 Physics. The objective of the physics studies is to develop methods for predicting, analyzing, and evaluating plutonium fuel cycle performance in thermal heterogeneous reactors Extensions of the same methods to other fuel cycles and reactor types are also desired, particularly for purposes of comparative evaluation Both theoretical and experimental studies have been directed toward this objective. The types of investigations are varied. Up to the present time they have included: (1) nuclear characteristics of plutonium fuels, (2) determination of effective cross sections, (3) single-pass fuel burnup analysis, (4) steady-state recycle analysis, (5) plutonium cross-section measurements, and (6) determination of constants for lattices containing plutonium enrichment

Nuclear characteristics of plutonium fuels. Either plutonium or U^{235}, when used for thermal reactor enrichment, may be employed in three ways: (1) as "spike" enrichment distributed through a reactor in special fuel elements, diluted only with inert materials; (2) as "uniform" enrichment, distributed in all the fuel elements, mixed with U^{238}; (3) as "zone" enrichment in which one or more zones of a reactor are uniformly enriched and the others unenriched or spike-enriched.

The two fissionable materials are not completely interchangeable. For example, the yield of neutrons per thermal neutron absorbed is initially

TABLE 8–1

EFFECT OF MODERATOR TEMPERATURE ON NUCLEAR PROPERTIES OF U^{235} AND Pu^{239}

Average moderator temp., °C	Average neutron energy (kT) ev	Fast neutrons produced per thermal neutron absorbed in:		$\bar{\sigma}$, Effective cross section, barns*			
				Fission		Absorption	
		U^{235}	Pu^{239}	U^{235}	Pu^{239}	U^{235}	Pu^{239}
75	0.030	2.083	2.006	456	652	538	936
200	0.041	2.094	1.936	378	631	444	939
350	0.054	2.102	1.875	326	693	381	1060
600	0.075	2.103	1.871	267	834	312	1280

* $\bar{\sigma} = (\frac{1}{2})\sqrt{\pi} f\sigma(kT)$, where $\sigma(kT)$ is the monoenergetic cross section at the temperature T, associated with the most probable energy of a Maxwell distribution, and f is a correction factor for departure from the "$1/v$" law

4 or 5% less for Pu^{239} at 75°C moderator temperature. Moreover, as Pu^{239} is irradiated and higher isotopes are formed, the yield of neutrons in plutonium drops more rapidly than in the case of U^{235}. Pu^{239}, however, competes more successfully than U^{235} for neutrons Therefore, nonproductive absorption of neutrons in coolant, jackets, structural materials, and fission products will be decreased when U^{235} atoms are replaced by an equal number of Pu^{239} atoms. As shown in Table 8–1, some Pu^{239} nuclear properties are markedly affected by neutron energy in the thermal region while the same properties of U^{235} are almost unaffected. Thus the behavior of plutonium may be quite different in reactors with high moderator temperatures than in reactors with relatively low moderator temperatures.

Not all neutrons absorbed by U^{235} or Pu^{239} cause fission. Significant amounts of these isotopes are converted by neutron capture into thermally nonfissionable U^{236} and Pu^{240}. The fraction of the atoms that fission is given by the ratio of the fission cross section to the absorption cross section for the specific isotope. This quantity is a function of the neutron energy, and therefore of moderator temperature. Over the range 75°C to 600°C, the fraction of U^{235} atoms fissioned is essentially constant, while for Pu^{239} it varies as shown in Table 8–2. Because a smaller proportion of the Pu^{239} atoms are fissioned, more of them must be destroyed to produce the same amount of heat as that produced by the same number of U^{235}

TABLE 8–2

EFFECT OF MODERATOR TEMPERATURE ON THE AVAILABLE HEAT ENERGY FROM FISSION

Average moderator temp., °C	Average neutron energy (kT), ev	Fraction of atoms fissioned		Available fission energy per gram destroyed, cal × 10^9	
		U^{235}	Pu^{239}	U^{235}	Pu^{239}
75	0.030	0.85	0.70	4.4	3.6
200	0.041	0.85	0.67	4.4	3.5
350	0.054	0.85	0.65	4.4	3.4
600	0.075	0.85	0.65	4.4	3.4

atoms. Thus, with a 75°C moderator a reactor must consume about 0.85/0.70, or 1.21 Pu^{239} atoms to produce the same amount of heat as is produced in the destruction of one U^{235} atom.

When a fuel element reaches some minimum heat generation rate or neutron production rate it must be removed from the reactor. The maximum practical residence time of a fuel element in a reactor is a function of the concentration of fissionable material per cycle in the reactor. Once the burnup per cycle has been established it is possible to calculate the number of cycles theoretically necessary to recover the energy in any specified fraction of the fissionable material in the fuel element. Table 8–3 shows the number of cycles necessary to recover 95, 98, or 99% of the energy in the original U^{235} or Pu^{239} for various degrees of burnup per cycle. To minimize processing and fabrication costs for a given total burnup, a minimum number of cycles should be employed. It is apparent from Table 8–3 that burnups of about 50% per cycle are essential if fewer than seven cycles are to achieve at least 95% total burnup. The limiting burnup per cycle depends on many factors and may be different for U^{235} and plutonium. Thus nuclear properties as well as fuel-element stability may set the exposure limits.

Under comparable conditions of neutron flux and atom density, Pu^{239} generates heat at a greater rate than U^{235} because of its higher fission cross section. For a plutonium fuel element to replace a single U^{235} element at the same surface heat-transfer rate, the Pu^{239} must be less concentrated than the U^{235} it replaces. As a result of the lower concentration of fissionable isotope and higher fission cross section, plutonium fuel elements with the same initial and final heat production rates as U^{235} fuel elements are

TABLE 8–3

NUMBER OF CYCLES TO ACHIEVE PRESCRIBED TOTAL BURNUPS

Burnup per cycle, % fissionable atoms	Total burnup, % fissionable atoms		
	95%	98%	99%
	Number of cycles		
15	18.4	24.0	28.0
25	10.4	13.6	16.0
50	4.34	5.65	6.65
75	2.16	2.83	3.32
90	1.30	1.70	2.00
98	—	1.00	1.18

depleted faster and must be replaced more frequently. The relative throughput rate is approximately the ratio of the absorption cross sections. Because the absorption cross section of Pu^{239} increases with increasing energy of the incident neutrons, while that of U^{235} decreases, plutonium fuel elements must be replaced even more frequently in reactors with high moderator temperatures. The variation in the relative throughput of spike fuel elements for Pu^{239} and U^{235} with moderator temperature is shown by the solid curve in Fig. 8–1. Roughly 1.7 times as many Pu^{239} as U^{235} fuel elements are required at 75°C, while four times as many are required at 600°C.

Plutonium which has accumulated high exposure, whether through single or repeated irradiations, contains appreciable amounts of Pu^{240} and Pu^{241}. The thermally fissionable Pu^{241} is formed from the fertile Pu^{240} which is formed from Pu^{239}. The formation of Pu^{241} helps to maintain the reactivity of the fuel elements, and lower their throughput rate. In Fig. 8–1 the throughput, represented by the dotted line, is calculated from a detailed reactor example in which about 40% of the plutonium was assumed to consist of the isotopes Pu^{239} and Pu^{241}, the remainder being nonfissionable Pu^{240} and Pu^{242}. Only 1.1 (at 75°C) to 1.7 (at 600°C) times as many plutonium as U^{235} fuel elements would be required in this example.

The relationships are more complicated in the case of U^{238} bearing fuel elements enriched with plutonium because fresh Pu^{239} is generated from the U^{238}. Extensive analyses have not yet been made of throughput rates

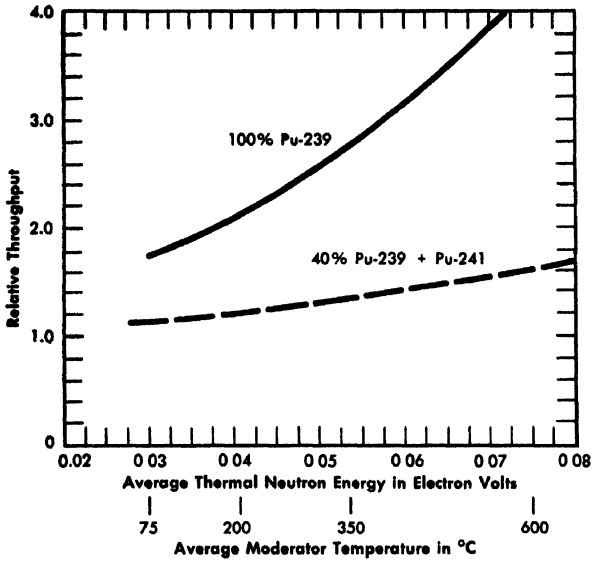

FIG. 8–1. Throughput of spike plutonium fuel elements relative to U^{235}. Basis: (1) Pu and U^{235} calculated as "spike" enrichment (2) Both cases are assumed to have the same initial and the same final heat transfer rates.

for mixtures of plutonium and U^{238} relative to those for mixtures of U^{235} and U^{238}.

Determination of effective cross sections. Most problems to be solved in the development of simple methods for analyzing fuel cycle performance may be grouped under the single heading, determination of effective cross sections. Other problems, such as those relating to reactor kinetics, control, and criticality, are only indirectly related to the main objective of fuel cycle evaluation.

The effective cross section may be regarded as a proportionality constant which relates the rate of the particular nuclear process to the specific heat generation in the fuel. As such, it represents the combined effects of neutrons at all energies and at all positions within a fuel element. Its determination from basic nuclear data is very complicated, even when all the necessary data are available. There arises a need, therefore, to define and study quantities intermediate in generality between the basic information and the ultimate effective cross section. Such quantities as fast fission factor, effective resonance integral, neutron temperature, and cadmium ratio are more or less directly measurable, and when properly specified can provide an approximate value of the effective cross section.

The notation for effective cross sections introduced by C. H. Westcott [1] reflects this fact. The form used for effective cross sections is

$$\hat{\sigma} = \sigma_0(g + rs),$$

where σ_0 is the 2200 m/sec, or 20°C, cross section and g is a function of the neutron temperature such that when the spectrum is purely Maxwellian, i.e, in thermal equilibrium with a scattering medium, the reaction rate per atom is given by $nv_0g\sigma_0$, where n is the true neutron density and v_0 is 2.2×10^5 cm/sec. In practice the spectrum contains a non-Maxwellian portion, and if the cross section above thermal energies departs from the "normal" variation with energy of $E^{-\frac{1}{2}}$, an additional contribution to the effective cross section is required This contribution is proportional both to the relative intensity of the non-Maxwellian portion of the spectrum, and to the amount by which the cross section exceeds the $E^{-\frac{1}{2}}$ variation over the epithermal range The term rs accounts for these epithermal effects. The factor r, the spectral index, is inversely proportional to the cadmium ratio, while the factor s is proportional to the effective resonance integral

The limitations of this simple notation are obvious. No account at all is taken of the cross sections in the fission spectrum region. (This is not, however, particularly difficult to incorporate in the computer codes.) The transitional region of the spectrum, between the Maxwellian and slowing down or E^{-1} regions, is largely neglected; this neglect is serious when the temperature is such that the lowest resonances of Pu^{239} and Pu^{241} fall in this region. The transitional and Maxwellian regions of the spectrum are further distorted in close-packed H_2O lattices to the extent that the simple Westcott notation is of doubtful usefulness except as a temporary expedient for general survey purposes. Finally, the effective resonance integral itself is strongly dependent upon the fuel geometry and composition, and is both inconvenient to measure and as yet impossible to compute accurately from basic data

These limitations are the reasons for the physics objectives of the recycle program. The effective cross sections themselves are directly measurable by observing the relative reaction rates of the different nuclear processes in the fuel. Such measurements alone would have little predictive value for fuel cycles and reactor types other than those directly studied in the experimental irradiation program. A broader experimental and theoretical approach is therefore necessary. Its objectives are the clarification of the poorly known factors making up the effective cross sections, and the reduction of the remaining uncertainties to empirically manageable proportions.

Single-pass fuel burnup calculations. In planning and interpreting experimental studies, in evaluating plutonium recycle applicability under nonsteady-state conditions, and in operating and programming the experimental reactor, it is necessary to determine the isotopic composition and reactivity of the reactor fuel elements as these change under the irradiation process. This "fuel burnup" problem, long familiar in reactor analysis, is here further described as "single-pass" to distinguish it from the steady-state recycle analysis to be described later.

Two very different types of calculation are performed in analyzing fuel burnup. The first is a simple calculation using the effective cross sections described in the previous section in fully linearized burnup equations. The following assumptions are inherent in this method:

(1) The variations of flux, composition, and neutron energy spectrum with respect to position in the reactor are neglected.

(2) The variations of flux and spectrum with time are neglected.

(3) The variations of all reactor parameters except concentrations of uranium and plutonium isotopes with time and position in the reactor are neglected.

(4) The time variation of the shielding factors resulting from the variations of flux and spectrum within a fuel element is neglected; the shielding factors themselves are cursorily treated.

Such a calculation, although invaluable for surveys and general planning, is not accurate enough for analyzing and interpreting data from an operating reactor. A second and far more elaborate method is being developed for machine computation.

The method will be described briefly to illustrate the types of processes that enter the problem. It utilizes Monte Carlo and multigroup diffusion techniques in combination with the burnup equations to follow the isotopic changes of the fuel and the accompanying spectral changes as functions of time and of position in the reactor.

The computer code involves the multigroup diffusion method applied to the entire reactor, which is divided into about ten regions of space and a similar number of neutron energy groups. The burnup equations are applied to these diffusion regions separately, and the Monte Carlo method is applied to systems consisting of individual cells, control rods, etc., within the regions. The program proceeds in a series of time steps, as follows:

(1) The macroscopic flux distribution is calculated for the entire reactor by multigroup diffusion theory, using group constants determined by the cross section library from the most recent Monte Carlo and burnup results.

(2) Changes of isotopic concentration are calculated in certain regions

of the reactor; the number of time steps between burnup calculations may differ in the different regions.

(3) The microscopic distribution of flux is calculated for certain of the systems within the regions by the Monte Carlo method; the number of time steps between Monte Carlo calculations for a given system is in general greater than the number of time steps between burnup calculations; the boundary conditions and normalizing factors for each system are provided by the multigroup diffusion computation.

(4) The group constants for the diffusion calculation are recomputed by the library section whenever the Monte Carlo or burnup calculations require these to change.

The cross-section library lists for each isotope the name, atomic weight, incident velocity below which elastic scattering is isotropic in the center-of-mass system, and a specification of the type of inelastic scattering spectrum to be used. The latter may be the name of one of three tabulated spectra or else a constant to be used in the calculation of the spectrum by the evaporation model For each diffusion and Monte Carlo energy group, the library also lists the elastic, inelastic, and absorption cross sections, the neutron yields associated with inelastic and absorption events, and the coefficients of the first three terms in the spherical harmonic expansion of the differential elastic cross section. These tables are prepared when necessary by a cross section preparation code from a basic library of cross-section data and resonance parameters, and from the fluxes obtained from previous Monte Carlo results. Special provision is made for functionally defined cross sections, such as $1/v$ absorption constant scattering, and Breit-Wigner one-level scattering and absorption with Doppler broadening. The code also generates, for the Monte Carlo calculation, complete sets of Doppler-broadened Breit-Wigner resonances distributed with constant spacing and radiation widths, and with the neutron and fission widths randomly drawn from Porter-Thomas distributions These are used wherever detailed information on actual cross sections is lacking.

The Monte Carlo calculation itself will not be described in detail, except to remark that full use is made of acceleration techniques, sequential sampling, and importance weighting to reduce running time. The calculation also utilizes analytic expectation values in addition to the basic statistical tallies The conditions at the boundaries of the Monte Carlo system are determined by diffusion theory albedo values, which in turn depend upon diffusion coefficients determined by the Monte Carlo boundary tallies

The diffusion calculation is of a straightforward multigroup type, with isotopic concentrations, slowing-down matrix elements, cross sections and other group constants obtained from the other portions of the program as described above. The burnup calculations are also straightforward, since

the necessary information is completely developed in the other portions of the code.* Portions of the code may, of course, be used independently for special purposes. The burnup equations, the Monte Carlo and the diffusion portions of the code may be isolated and used separately, at great savings in running time, when the full capabilities are not required

Steady-state recycle analysis. The economics analysis surveys of fuel cycles in thermal reactors require investigation of an extremely large number of cases, since the number of independent parameters is very high. Detailed calculation of lattice physics, fuel exposure and throughput of fuel for each of these cases is prohibitively time-consuming and costly. A group of computational methods has therefore been developed which are based upon the simplified model of the effective cross section described above, but are sufficiently accurate and flexible for the requirements of the economics surveys. These methods are incorporated in the Generalized Plutonium Recycle (GPR) code for the IBM-650 computer.

The basis of analysis is the steady-state system, in which material is flowing at a constant rate through a reactor or group of reactors, separation plants, and fuel reprocessing facilities. The composition of material at each stage of the cycle remains constant in time. This leads to a "material balance" condition, which means that the amount of plutonium produced in one exposure cycle in the reactor, less losses in processing, is just sufficient to provide the recycled fuel for the next cycle If more than one reactor is involved in the system, the processing loss factors may be adjusted to allow for the export of fuel from individual reactors, or the import of fuel in arbitrary amounts, but always on a steady-state basis. A second condition is imposed to satisfy the requirements of reactor criticality. The composition of the fuel must satisfy a "reactivity balance" condition which is dependent upon the neutron economy of the reactor.

These two constraints are already sufficient to provide a highly coupled system, but in some cases a third constraint is necessary. If the recycled fuel is not blended with the external feed (uniform fuel enrichment), a specific power balance condition must be imposed. Practical reactor operation requires limits to be set on the relative heat generations in the two types of fuel. These limits determine the relative concentrations of fissionable isotopes when the flux distribution is specified, and these concentrations in turn are reflected in the values given to the r and s factors in the effective cross sections.

---

*The entire code, known as RBU (reactor burnup) is being developed by personnel of the American-Standard Atomic Energy Division, American Radiator and Standard Sanitary Corporation, for the Hanford Laboratories Operation. Although planned for use in the Plutonium Recycle Program it is entirely general in applicability. It is being initially coded for the IBM-704 computer.

The concentrations of plutonium isotopes are determined in terms of their steady-state values, namely the values at which the rates of destruction by burnup and processing loss are equal to the rates of formation from other materials, starting with U^{238}. They are essentially independent of the cycle exposure. The fission products are not assumed to burn out, but are assigned (at present) a single absorption cross section for reactivity purposes. The U^{235} (and U^{238}) cross sections are averaged over a single exposure cycle, so that in effect the reactivity balance condition is met by determining first the U^{235} concentration required for criticality, then the cycle exposure such that this concentration is the average over the cycle. In a reactor which is being charged and discharged continuously, with each fuel element receiving the same exposure, there will be a uniform distribution of exposures through the reactor at any given time; the operations of averaging over an exposure cycle at one point, and averaging over the reactor at a given instant of time, are equivalent.

The balance conditions for the uniformly enriched, one-region case are expressed in the requirement that the following relationship be satisfied between the exposure T, the effective cross sections $\hat{\sigma}$, and loss rates F. Newton-Raphson iteration is employed.

$$\frac{k_\infty}{\epsilon} = \frac{\bar{N}_{25}(T)\hat{\sigma}_{f25}\nu_{25} + \bar{N}_{28}(T)\hat{\sigma}_{a28}Y_{\mathrm{Pu}}}{\bar{N}_{25}(T)\hat{\sigma}_{a25} + \bar{N}_{28}(T)\hat{\sigma}_{a28}(1 + A_{\mathrm{Pu}}) + \bar{A}_P(T) + A_{NF}} = \text{constant},$$

where T = flux-time for one exposure cycle, $\int_{\text{cycle}} \phi(t)dt$,

$$\bar{N}_{25}(T) = \bar{N}_{25}(0)\,\frac{1 - e^{-\hat{\sigma}_{a25}T}}{\hat{\sigma}_{a25}T},$$

and

$$\bar{N}_{28}(T) = \bar{N}_{28}(0)\,\frac{1 - e^{-\hat{\sigma}_{a28}T}}{\hat{\sigma}_{a28}T}$$

are isotopic concentrations for U^{235} and U^{238} respectively, averaged over one exposure cycle (or over the reactor at one time),

$$Y_{\mathrm{Pu}} = \frac{\hat{\sigma}_{f49}\nu_{49}}{\hat{\sigma}_{a49} + F_{49}} + \frac{\hat{\sigma}_{c49}\hat{\sigma}_{a40}\hat{\sigma}_{f41}\nu_{41}}{(\hat{\sigma}_{a49} + F_{49})(\hat{\sigma}_{a40} + F_{40})(\hat{\sigma}_{a41} + F_{41})}$$

and

$$A_{\mathrm{Pu}} = \frac{\hat{\sigma}_{a49}}{\hat{\sigma}_{a49} + F_{49}} + \frac{\hat{\sigma}_{c49}\hat{\sigma}_{a40}}{(\hat{\sigma}_{a49} + F_{49})(\hat{\sigma}_{a40} + F_{40})} + \frac{\hat{\sigma}_{c49}\hat{\sigma}_{a40}\hat{\sigma}_{a41}}{(\hat{\sigma}_{a49} + F_{49})(\hat{\sigma}_{a40} + F_{40})(\hat{\sigma}_{a41} + F_{41})}$$

are respectively the neutron yield from plutonium and the neutron absorption in plutonium per absorption in U^{238},

$$\bar{A}_P(T) = \left[\frac{\bar{N}_{25}(0) - \bar{N}_{25}(T)}{1 + \alpha_{25}}\left(1 + \frac{(\epsilon - 1)\nu_{25}}{\nu_{28} - 1 - \alpha_{28}}\right)\right.$$

$$+ \frac{T}{2}\bar{N}_{28}(T)\hat{\sigma}_{a28}\left(\frac{\hat{\sigma}_{f49}}{\hat{\sigma}_{a49} + F_{49}} + \frac{\hat{\sigma}_{c49}\hat{\sigma}_{a40}\hat{\sigma}_{f41}}{(\hat{\sigma}_{a49} + F_{49})(\sigma_{a40} + F_{40})(\hat{\sigma}_{a41} + F_{41})}\right.$$

$$\left.\left. + Y_{Pu}\frac{\epsilon - 1}{\nu_{28} - 1 - \alpha_{28}}\right)\right]\hat{\sigma}_{aFP} + \bar{N}_{26}(T)\hat{\sigma}_{a26}$$

$$+ \left[\frac{\bar{N}_{25}(0) - \bar{N}_{25}(T)}{\hat{\sigma}_{a25} - \hat{\sigma}_{a26}}\right]\hat{\sigma}_{a26}\hat{\sigma}_{c25}$$

$$+ \frac{\bar{N}_{28}(T)\hat{\sigma}_{a28}\hat{\sigma}_{c49}\hat{\sigma}_{a40}\hat{\sigma}_{c41}\hat{\sigma}_{a42}}{(\hat{\sigma}_{a49} + F_{49})(\hat{\sigma}_{a40} + F_{40})(\hat{\sigma}_{a41} + F_{41})(\hat{\sigma}_{a42} + F_{42})}$$

represents the sum of parasitic absorptions in fission products, U^{236} and Pu^{242}, and

$$A_{NF} = \frac{1 - f_0}{f_0}\sum_{\text{a fuel}}(0)$$

represents the nonfuel absorptions corresponding to an initial thermal utilization f_0.

In the two-region or spike-enriched type of analysis, the starting point is the one-region analysis described above. The reactor average uranium concentrations are then expressed in terms of those in the feed region alone. For all materials, the reactor-average concentrations obtained from the uniform case are divided between the two regions according to the ratio of flux-volume in the spike region to that in the feed region, denoted by Q. This latter quantity is determined from the requirement that the ratio of specific power generation in the feed region to that in the spike region be a given constant H. Since the exposures given the two types of fuel need not be the same, the formulas of the preceding paragraph become considerably more elaborate. The effective cross sections must be recalculated once Q is known, since Q determines the r factor in the effective cross sections. Average concentrations and cycle exposure are recalculated with the new cross sections, and the resulting new value of Q is compared with the old. Iteration continues until satisfactory agreement is reached.

The input information required consists of the values of k_∞, ϵ, r, g, s, A_{NF}, and $N_{25}(0)$ appropriate to the feed and loss rates for the fuel materials. Effective cross sections are then generated, followed by the calculation of exposure for the uniform case which requires usually three or four iterations. Steady-state and discharge concentrations of fuel isotopes are calculated, and exposure in megawatt-days per ton is computed. The physics parameters η, f, and p may also be generated. The program may optionally go on to re-evaluate the reactor as a two-region case as described above, in which the above results are determined for each region.

Results of this type of calculation are, of course, directly applicable only to the ideal situation of continuous uniform irradiation of fuel and fully steady-state isotopic composition. Application of these methods to poorly thermalized reactors or to cases involving high rates of extraction or supply of plutonium from external sources, requires more careful specification of the effective cross section than is provided by the Westcott notation discussed above.

Experimental program. During the period preceding the completion of the PRTR, experimental physics work has been directed toward improving knowledge of the microscopic cross sections of the plutonium isotopes as functions of neutron energy, and toward determining the neutron physics parameters of lattice and fuel arrangements to be used.

Neutron cross sections. The low-energy neutron cross sections of the plutonium and transplutonium nuclides are of special importance in the analysis of plutonium recycle processes. The knowledge of the more important cross sections has improved significantly over the past few years although several major gaps still exist Cross-section studies of these nuclides have been carried out at the Hanford Laboratories using a neutron crystal spectrometer [2]. Other important information has been obtained with the fast chopper spectrometers at the Argonne National Laboratory and at the Materials Testing Reactor [2]. Pile neutron cross sections have been measured at the Chalk River Laboratory [3] and the Knolls Atomic Power Laboratory [4]. The more recent advances in the knowledge of neutron cross sections important to this program will be briefly outlined.

Previous investigations on Pu^{239} had indicated a large discrepancy between the directly measured variation with neutron energy of η, the average number of fission neutrons produced per absorption, and the variation deduced from total and fission cross-section measurements. Data have now been obtained on the energy variations of η and total and fission cross sections which form a consistent set over the energy interval of 0.02 ev to 0.4 ev. Results from both Hanford Laboratories and ANL agree to a precision which approaches one percent for the energy variation of these parameters. The best value for the absolute fission cross section is ob-

tained for pile neutrons. The Chalk River results are analyzed to give a 2200 m/sec fission cross section of 750 barns. These results form a consistent set of values for the fission cross sections of the four primary fissionable isotopes.

The large resonance in Pu^{240} at 1 ev has been studied with good resolution using the crystal spectrometer. A detailed fit to the experimental data has been obtained for a Doppler broadened Breit-Wigner single level formula. A resonance width, Γ, equal to 32.3 ± 1.5 mv and an E_0 of 1.056 ± 0.003 ev was obtained from the fit. Measurements at Argonne National Laboratory (ANL) and at the Materials Testing Reactor (MTR) give values of the width of 34.5 mv and a peak total cross section of 174,000 barns, in reasonable agreement with the presumably more precise value obtained with the crystal spectrometer The MTR measurements have included the resonance structure to 119 ev The thermal absorption cross section calculated from the resonance parameters is 280 barns at 2200 m/sec. No direct monoenergetic measurements are complete to compare with this value The calculated infinite dilution resonance integral is about 8400 barns, in good agreement with a measured value at Chalk River of 8700 ± 800 barns.

The shape of the fission cross section curve of Pu^{241} has been determined from 0.003 ev to 1 0 ev with the crystal spectrometer to a precision of about one percent below 0 3 ev As the curve is not easily fitted by single level non-interfering resonance formulae, effective cross-section values have been obtained by numerical computation The Chalk River pile neutron fission cross-section value reduces to a 2200 m/sec value of 1020 barns using the shape of the fission curve Preliminary measurements of the energy variation of the total cross section have been obtained with the Brookhaven (BNL) fast chopper [5]. Pile neutron values of absorption cross section, η, and ν are available from other experiments at Knolls Atomic Power Laboratory (KAPL).

For Pu^{242} two total cross-section resonances have been observed by Argonne at 2.65 and 53.6 ev The resonance integral of 570 barns calculated from the resonance parameters does not agree with the value of 1275 barns obtained at Chalk River from pile neutron irradiations.

Measurements of lattice parameters. The Physical Constants Testing Reactor (PCTR) has been used to determine the cold-clean lattice parameters of possible PRTR loadings and the uranium-oxide temperature coefficient of reactivity. The results outlined here were obtained using standard techniques developed over the past two years and described elsewhere [6,7].

The measured values of k_∞ and f for D_2O moderated lattices having 19-rod clusters of 0.504-inch OD uranium-oxide (UO_2) fuel or mixed clusters of 16 uranium-oxide rods and three plutonium-aluminum alloy rods

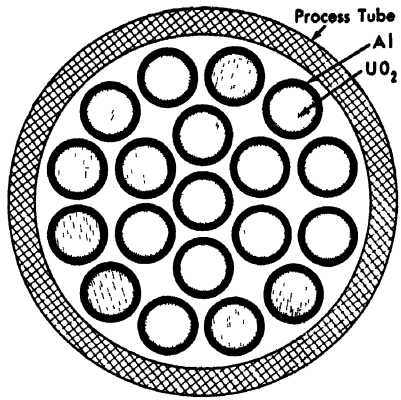

UO_2 rod diameter	0.504 inch
Al cladding thickness	0.030 inch
Clearance between rods	0.070 inch
Process tube ID	3.25 ± 0.010 inches
UO_2 density	92 ± 1% of theoretical

FIG. 8–2. Nineteen-rod cluster fuel element.

in the inner ring (Fig. 8–2) are given in Table 8–4 for two triangular lattice spacings. Measurements of the resonance escape probability p and fast fission factor are also given in Table 8–4 for the 8-inch lattice spacing with 19 UO_2 rods cooled with D_2O. The use of this p and ϵ together with the measured values of k_∞ and f in the four-factor formula $k_\infty = \eta f \epsilon p$ yields a value of η for natural uranium oxide of 1.334 ± 0.014 In contrast, a treatment of the data for the two lattice spacings by the method of Mummery [8] yields an η of 1.31 and a p for the 8-inch lattice of 0.881

Measurements on a three-component tubular UO_2 fuel element assembly of the type shown in Fig. 8–3 are given in Table 8–5. The errors in f are of the order of 0.3%. The errors in k_∞ vary from 3 mk* for those lattices with k_∞ near unity, to about 5% of $(k_\infty - 1)$ for high k_∞ lattices. The error in k_∞ is therefore almost 6 mk for the plutonium-enriched, 8-inch lattices.

The measurement of $(1/p)(\Delta p/\Delta T)_{\text{fuel}}$ for the 19-rod cluster of UO_2 rods in the 8-inch lattice with air coolant gives $-(2.4 \pm 0.2) \times 10^{-5}/°C$ over the temperature range from 20 to 365°C. The variation in the

*(1.0) $mk = (1.0 \times 10^{-3})\, k$.

TABLE 8–4

PHYSICS CHARACTERISTICS OF 19-ROD CLUSTER FUEL ELEMENT

Lattice spacing, in.	Coolant	$\frac{V_{mod}}{V_{UO_2}}$	$\frac{V_{coolant}}{V_{mod}}$	$\frac{V_{Al}}{V_{UO_2}}$	$\frac{V_{Pu\ Al}}{V_{UO_2}}$	f	k_∞
7	Air	8.264	—	1.004	—	0.904	1.013
7	D_2O	8.264	0.133	1.004	—	0.897	1.005
8	Air	11.809	—	1.004	-	0.898	1.060
8	D_2O	11.809	0.093	1.004	--	0.892	1.048
8	D_2O	$p = 0.865 \pm 0.009$,		$\epsilon = 1.0178 \pm 0.0017$			
7	Air	9.814	--	1.192	0.1875	0.9044	1.073
7	D_2O	9.814	0.133	1.192	0.1875	0 9051	1.062
8	Air	14.023	—	1.192	0.1875	0.9039	1.117
8	D_2O	14.023	0.093	1.192	0.1875	0.8982	1.112

Fuel diameter, 0.504 in.
UO_2 density, 10.1 g/cm^3 (average)
Aluminum clad thickness, 0.030 in.
Moderator (and coolant), 99.75% D_2O (molecular %)
Aluminum process tube { ID 3.25 in. / OD 3.50 in.
Aluminum shroud tube { ID 3.75 in. / OD 4.00 in.
Pu concentration, 1.78 w/o in aluminum
Pu composition: 239, 93.6%; 240, 5.9%; 241, 0.46% (by weight)
Zr-2 clad thickness, 0.030 in.
Rod spacings, 0.648 in. (center to center)
V = volume

effective resonance integral Σ for this fuel cluster with temperature is then found to be

$$\frac{1}{\Sigma_0}\frac{\Delta\Sigma}{\Delta T} = (2.0 \pm 0.2) \times 10^{-4}/°C,$$

where Σ_0 is the effective resonance integral at 20°C.

8–2.2 Plutonium utilization analyses. The extent to which plutonium will be recovered from spent fuel elements and used in thermal power reactors will undoubtedly be controlled by considerations of cost. Cost will be the major factor in the choice of processes at each step in the fuel cycle. The factors that make up the cost of recycling plutonium may be divided into (1) reactor costs, which include capital, operating, and main-

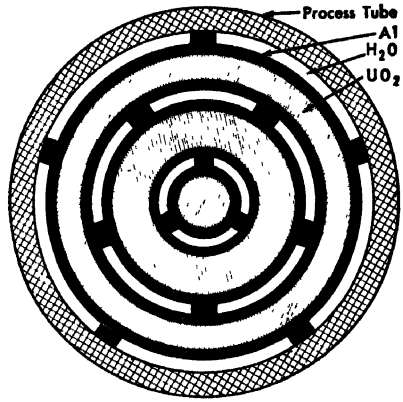

UO_2 rod diameter	0.600 inch	Coolant annuli thickness:	
UO_2 inner tube ID × OD	1.000 × 1.804 inches	Inner	0.140 inch
UO_2 outer tube ID × OD	2.214 × 3.000 inches	Middle	0.145 inch
Al cladding thickness	0.030 inch	Outer	0.095
		Process tube ID	3.25 ± 0.010 inches
		UO_2 density	92 ± 1% of theoretical

FIG. 8–3. Nested tubular fuel element.

TABLE 8–5

PHYSICS CHARACTERISTICS OF TUBULAR UO_2 FUEL ELEMENT

Lattice	Coolant	$\frac{V_{mod}}{V_{UO2}}$	$\frac{V_{coolant}}{V_{mod}}$	$\frac{V_{Al}}{V_{UO2}}$	f	k_∞
8	Air	8.2653	—	0.7146	0.9246	1.0549
8	D_2O	8.2653	0.0478	0.7146	0.9208	1.0493

UO_2 density, 10.121 g/cm³ (average)
Aluminum clad thickness, 0.030 in.
Moderator (and coolant), 99.75% D_2O (molecular %)
Aluminum process tube, 3.25 in. ID × 0.125 in. wall
Aluminum shroud tube, 3.75 in. ID × 0.125 in. wall
Fuel dimensions, in.:
Central rod: 0.592 OD
Inner ring: 1.006 ID, 1.800 OD
Outer ring: 2.220 ID, 2.993 OD

tenance costs, and (2) total fuel costs, which include raw materials, separations, fabrication and inventory costs as well as credits for uranium or plutonium in the spent fuel. Because power reactor capital and operating cost experience are lacking, studies have been focused on fuel costs only.

Because of the health hazards associated with handling plutonium, special precautions must be taken to protect those who work with it. As a result, fabrication costs will be greater than for similar uranium fuel elements.

Per unit of energy produced, the sum of all the fuel cost factors except the cost of plutonium must be less for plutonium fuel than the total cost of uranium fuel, if plutonium is to have any dollar value as reactor fuel. Depending on the relative values of plutonium and uranium, and therefore, their relative prices on the open market, an operator may choose to fuel his reactor with uranium or plutonium or both; he may choose to recover or not to recover uranium and plutonium from spent fuel; and he may choose to sell the recovered materials or recycle them in his own reactor. Although analysis cannot at the present stage of development prove the future method of utilization, or the worth of plutonium, it is still instructive to apply some analytical techniques and to draw whatever conclusions are presently justified. Simplified analytical methods are presented first to acquaint the reader with some general aspects of the plutonium recycle concept. Following that, a detailed analysis now in progress is described.

First a method is described for estimating the maximum value of plutonium as a heat source in a specific reactor. Second, a method is explained and described for estimating the relative values of plutonium and uranium as contributors to the neutron production in specific reactors. Finally, an illustrative example is presented of a detailed fuel cycle analysis for a specified set of conditions. This analysis when performed in complete detail uses a minimum number of arbitrary assumptions and entails a large number of time-consuming and tedious calculations. It has therefore been programmed for automatic computers. At the time of this writing, data are still being calculated and interpreted for some systems. With the completion of the program a sufficient number of systems will have been analyzed to cover the logical ranges of all the variables.

The value of plutonium as a heat source. The value of plutonium enrichment relative to U^{235} enrichment will be influenced by fuel processing and fabrication costs, reactor characteristics, and the isotopic composition of the plutonium used for enrichment, but the value of plutonium as a source of heat in any given reactor will be no greater than the maximum amount one could afford to pay for nuclear fuel.

It appears that a total fuel cost as low as perhaps 2 mills/kwh must be

TABLE 8-6

VALUE OF U^{235} AND Pu^{239} AS RECOVERABLE ELECTRICAL POWER

Average moderator temperature, °C	Available electrical energy,* Mwd/g		Value of material, $/g for each mill/kwh of fuel cost	
	U^{235}	Pu^{239}	U^{235}	Pu^{239}
75	0.21	0.17	5.04	4.08
200	0.21	0.17	5.04	4.08
350	0.21	0.16	5.04	3.84
600	0.21	0.16	5.04	3.84

*Assuming 25% conversion of heat to electricity.

achieved before nuclear power will be widely used—at least in the United States [10] This conclusion is based on the relatively high capital costs of nuclear reactors and the high investment charges for nuclear fuels Assuming that fuel processing and fabricating costs account for about half of the total fuel costs there remains an allowable cost for the fuel material itself of about 1 mill/kwh. This number will depend somewhat upon the ratio of labor costs to material costs in each case If 25% of the reactor heat is converted to electricity, each gram of U^{235} or Pu^{239} fissioned will produce about 6,000 kwh of electricity and should thus have a fuel value of about six dollars Taking into account the neutron absorptions that do not lead to fission, Table 8-6 shows the values of the two materials as reactor fuels on this basis.

A caution should be expressed regarding the use of the data in Table 8-6, since they are based upon the use of the effective cross sections shown in Table 8-1 Results of future physics studies in the recycle program will show how these data must be modified for various reactor designs.

In most power reactors fission leads to the formation of other fissionable atoms, as well as heat. For example, in uranium-fueled power reactors high fuel element exposures are always associated with the fissioning *in situ* of significant amounts of plutonium. By recycling the unfissioned plutonium discharged from such reactors, even further plutonium fission will be attributable to the initial U^{235} enrichment.

The magnitude of this effect is a function of the conversion ratio in the reactor. If, for example, 0.8 g of fissionable plutonium is formed for each gram of U^{235} or Pu^{239} destroyed, the net consumption of fissionable material is only 0.2 g. With infinite fuel element exposure, or with an infinite

number of recycle operations, the value of plutonium would approach \$4.08/0.2 or \$20.40 per gram.

Although this value is based on an assumed value of 1 mill/kwh for fuel material and an 0.8 conversion ratio, it is significant only if the costs of recovery and fabrication can be kept low enough to make recycling worth-while.

This method of analysis emphasizes the importance of capital costs in the total cost of nuclear power. If capital costs can be reduced, a greater proportion of the total will be available for fuel material, and it may be considered that the value of plutonium is increased; the incentive for developing recycle technology should then become still greater.

The value of plutonium as a neutron source. In addition to providing heat in a reactor, the fuel material provides neutrons, and the fundamental role of an enrichment material is that of a neutron source. The analytical method described in this section is an attempt to characterize the value of plutonium relative to uranium as a neutron source.

We shall take as a measure of a fuel material's neutron contribution, the neutron production factor η, defined as the number of fast neutrons produced per thermal neutron absorbed in the fuel. Mathematical formulations of η differ according to the ultimate use for which its calculation is intended. The most common formulation is simply the ratio of the total number of neutrons produced by all the fissionable atoms in the fuel to the total number of thermal neutrons absorbed by *all* the atoms in the fuel. Absorptions by matrix and jacketing materials are included in this formulation of η, which is used to calculate the infinite multiplication factor k_∞ by the four-factor formula:

$$k_\infty = \eta \epsilon p f,$$

where ϵ is the fast fission factor, p is the resonance escape probability, and f is the thermal utilization factor. The numerical value of η must satisfy the requirement $k_\infty > 1.00$ for the reactor to be operable In fact, unless this condition is fulfilled, other formulations of η lose significance. If fulfillment of this condition is arbitrarily assumed, a modified formulation of η, related to fuel exposure, may be used to assess the neutron value of a fuel element. This modified neutron production factor, called η', is the number of neutrons produced, minus the number of neutrons absorbed in nonfertile and nonfissionable uranium and plutonium isotopes, per thermal neutron asborbed in the fissionable uranium and plutonium isotopes in the fuel material. Through the expression $r_0 = \eta' - 1 - L$, the factor η' is related to r_0, the initial conversion or regeneration ratio of a reactor, and to L, the number of neutrons lost by leakage and parasitic capture per thermal neutron absorbed in the fissionable isotopes. Because higher ini-

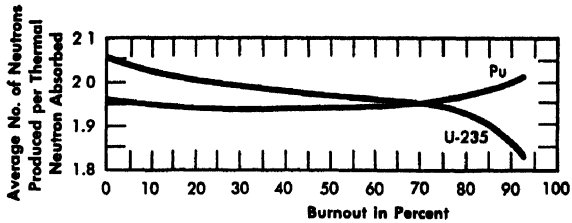

Basis: Moderator temperature = 80°C. Fission products removed after every 50% burnout. 0% burnout refers to 100% U^{235} or Pu^{239}. Neutron Absorptions in Pu^{240} and U^{238} not included.

FIG. 8–4 Fast neutrons produced per thermal neutron absorbed, as a function of burnout

tial regeneration ratios generally permit higher fuel exposures, and because higher exposure usually results in less cost per unit of energy removed, it is evident that η' may be used as a measure of fuel element value. For a given set of fuel fabrication and processing costs, η' may also be used as a measure of fuel material value.

It should be emphasized that η' differs from η because it does not take into consideration neutron absorption in matrix and jacketing materials or in fertile isotopes. Numerical values of η' for U^{235} and plutonium in a typical power reactor are shown in Fig. 8–4 in which the abscissae, identified as "Burnout in Percent," represent (100% minus % U^{235}) and (100% minus % Pu^{239}) respectively. The relative concentrations of the plutonium isotopes are functions of the percent burnout of Pu^{239}. The curve for U^{235} shows a high initial value for η' which decreases slightly with irradiation because of the increasing concentration of U^{236}. The curve for plutonium starts at a numerically lower η' and rises slightly after the concentration of Pu^{241} becomes large enough to make a significant contribution. Since the values of η' for both Pu and U^{235} change only slightly over a wide range of burnups, it appears that the relative values of the two materials as fuel elements may be almost independent of their degree of burnup.

The initial conversion ratio r_0 that a reactor with a given fast effect ϵ and neutron loss factor L can achieve with a fuel material may be calculated by substituting the corresponding value of η' for that material from Fig. 8–4 into the expression for r_0. If the program of fuel reloading is specified, a relation may be derived between r_0 and the number of fissions attainable in the fuel material per original fissionable atom in the material, as limited by reactivity loss.* Such a relationship, for uniformly graded fuel irradiation, was used to determine the maximum attainable exposures (expressed as fissions per initial fissionable atom) for the fuels

*E.g., see Section 3.5 of Reference 26.

specified by Fig. 8–4. These maximum exposures may be regarded as measures of the relative values of fuel elements containing the fuel mixtures in question.

Such comparisons have been made for several values of L (Fig. 8–5). The attainable exposures ("fuel element values") have been normalized to unity for the case of 100% U^{235} in a reactor having a loss fraction, $L = 0.10$. The situation represented in these curves is the following. A fuel element is considered which is made of a mixture of U^{238} and other isotopes, either of the uranium or of the plutonium family. In either case the isotopic composition of the material added to the U^{238} is that which would result from the irradiation of U^{235} (or Pu^{239}, as the case might be) to a degree of burnup specified along the abscissas of the graph. The ordinate, called the relative fuel element value, is a number proportional to the exposure attainable with the fuel element if it is used in a reactor having a neutron loss fraction, L, of the specified amount. The relative value is arbitrarily normalized to unity for a fuel element composed of pure U^{235} and pure U^{238} in a reactor having $L = 0.1$.

It is evident from the figure that the value of L might be looked upon as a measure of the neutron "efficiency" of the reactor, the "efficiency" being higher for a lower value of L. It may be seen that the values, as defined here, of fissionable plutonium and U^{235} depend upon this "efficiency" of the reactor in which they are used. For example, a U^{235} fuel element placed in a reactor that loses 0.25 neutron per neutron absorbed has a value of about 60% of the value that the same element would have if it were burned in a reactor that loses 0 1 neutron per neutron absorbed

The value of Pu^{239} from Fig. 8–5 is roughly 75% of the value of U^{235} in reactors of comparable "efficiency." However, it should be realized that when plutonium is substituted for U^{235} in a reactor, the "efficiency" is improved by the higher neutron cross section values of plutonium. In effect, the thermal utilization is improved and the diffusion length is reduced, both of which reduce the L term in the expression for r_0.

Finally, the value of fissionable plutonium appears to stay nearly constant regardless of its isotopic concentration. It appears that the value of plutonium may even surpass that of uranium for highly exposed material. Moreover, more rigorous calculations, made for selected specific reactors, indicate that the results expressed in Fig. 8–5 may even be pessimistic as to the value of plutonium relative to U^{235}. These more rigorous analyses employed a computer code to calculate the changes in reactivity with exposure for various mixtures of plutonium isotopes or U^{235} with U^{238} to form uniformly enriched fuel elements.

Characterization of fuel value by means of the η' concept is subject to the very important limitation that the infinite multiplication factor k_∞ must be greater than 1.00 by some determinable amount. Since k_∞ is de-

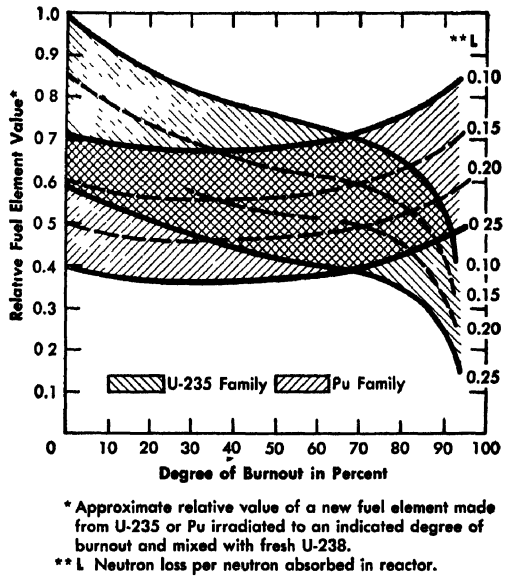

FIG. 8-5. Approximate relative values of U^{235} and Pu^{239} as fuel elements in various reactors.

pendent upon η (not η'), it is necessary to consider η as well as η' when determining a value for a fuel material. When plutonium containing significant percentages of Pu^{240} replaces U^{235} in a fuel element, the value of η appropriate to the four-factor formula is decreased. Unless compensating adjustments are made, the value of k_∞ may thus be reduced until the reactor will not operate. A possible adjustment is to increase the resonance escape probability, p. This can be done by reducing the U^{238}-to-moderator ratio, and to a lesser extent by altering fuel geometry. The resonance escape probability cannot always be raised sufficiently, however, since its maximum value is 1.0 and a usual value in reactors is 0.8 to 0.9. In this event, it might be economical to increase k_∞ by adding U^{235} to the system, thereby raising both η and f. In some cases examined in greater detail, this method has improved the cost situation.

Very loosely then, the successful adjustment of these reactor parameters allows a consideration of Pu^{240} as a fertile material analogous to U^{238} rather than as a poison analogous to U^{236} or Pu^{242}. With satisfaction of this design constraint, the value of plutonium appears to be dominated by the concentration of fissionable isotopes Pu^{239} and Pu^{241} and not by the concentration of the fertile isotope Pu^{240} or the parasitic isotope Pu^{242}. Furthermore, the foregoing discussion implies that a reactor designed for optimum performance using plutonium fuels (i.e., higher values of p, or

greater amounts of enrichment to increase η and f) may not be of optimum design for the use of a U^{235} fuel. Thus it appears that plutonium and uranium may not be interchanged in a given reactor, unless compensating changes are made to its lattice parameters, without incurring a cost penalty for burning a fuel in a reactor not optimized for that fuel.

Detailed fuel cycle analysis. The methods described so far provide means for analyzing the potential utilization of plutonium fuels without detailed cost estimates for the various process steps. As stated originally, such methods are useful for educational purposes or for rough approximations. They usually result in comparisons with uranium fuels rather than independent analyses of plutonium recycle.

A thorough evaluation of the recycle concept requires detailed analysis of each step in the process for a large variety of reasonable engineering and economic parameters. A computer program has been developed that uses the physics data generated by the Generalized Plutonium Recycle computer program, previously described, along with ranges in basic engineering and economic variables. An illustrative example is presented here as an aid in describing the program, and to help the reader understand its capabilities. The example is divided into two parts: in the first the fuel costs for a plutonium-fueled system are discussed without comparing them to a uranium system, and in the second a comparison is made with a uranium system to bring out relative values of plutonium and uranium as before.

In the first part of the example the reactor recycles and reuses all self-produced plutonium (self-sustaining recycle operation) Economic optimums are sought as a function of uranium feed enrichment, cost of fuel jacketing, and the reactor parameter k_∞/ϵ. Other cost factors are estimated but are not varied. Fuel costs rather than total power costs are calculated.

The second part of the example describes a comparison of the self-sustaining plutonium recycle system with a similarly optimized U^{235} system. As a result of the comparison it is possible to assign a value to plutonium that would allow the two systems to produce power at the same fuel cost. This result is discussed further after the example is described.

(1) Illustrative example—Part I. For illustrative purposes only, a reactor lattice is chosen with a thermal utilization factor f of 0.87 and k_∞/ϵ of 1.10 when operated in a self-sustaining manner on equilibrium plutonium and natural uranium feed. The fast fission factor, ϵ, is included with k_∞ from the four-factor formula, to simplify the fuel exposure calculations. The quantity k_∞/ϵ is a convenient parameter because its required numerical value is an inverse function of reactor physical size, i.e., smaller reactors of a given type have a greater percentage neutron leakage and require a higher value of k_∞/ϵ to be operable. Other parameters

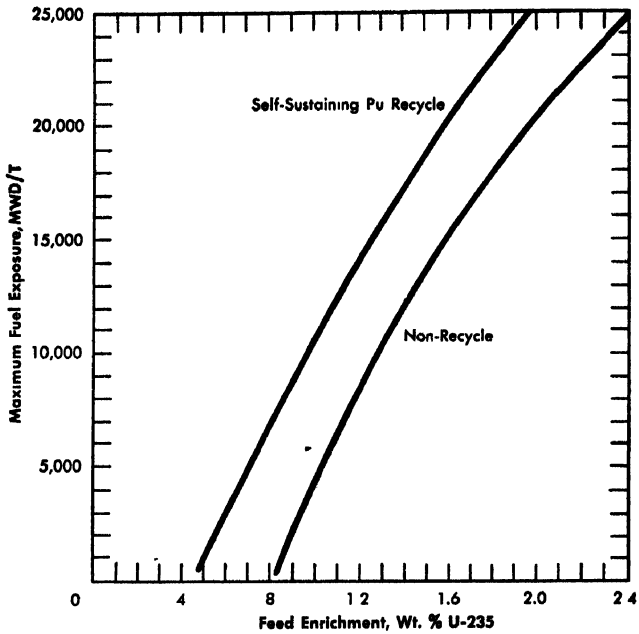

FIG. 8–6. Maximum fuel exposure as a function of feed enrichment for the uniformly enriched example reactor.

used in this example are shown in Table 8–7 The plutonium generated during any cycle is considered to be chemically isolated, mixed with fresh U^{238} and a stated amount of U^{235}, and fed back in reactor fuel elements for another irradiation cycle. Fuel exposures to satisfy the reactivity requirements of the example reactor are calculated for each of the various feed enrichments. The so-called "graded" charge-discharge system is used in which fuel rods are discharged in sequence when each rod's time-averaged reactivity equals the average reactivity for the reactor. The results of these calculations are shown in Fig. 8–6.

Based on these exposures, fuel costs were calculated for assumed fuel element fabrication costs ranging from \$22.00/lb U to \$38.00/lb U. These fabrication costs are based on estimated jacket tubing costs ranging from \$2.00/lb U to \$14.00/lb U as indicated in Table 8–7. In Fig. 8–7 fuel cost at a fuel element fabrication cost of \$22.00/lb U is shown as a function of the U^{235} concentration in the feed. It is evident that larger reactors (small values of k_∞/ϵ) achieve the lowest fuel costs. The general shape of the curves in Fig. 8–7 is due to the fact that the maximum attainable fuel exposure is nearly a direct function of feed enrichment. Therefore, fuel costs decrease rapidly to a minimum as the enrichment is increased, since

TABLE 8–7

CONDITIONS FOR ILLUSTRATIVE EXAMPLE

Variables	Values
In-reactor parameters	
k_∞/ϵ	1.10
Resonance escape probability, cold clean value, natural enrichment	0.89
Thermal utilization factor, cold clean value, natural enrichment	0.87
Feed enrichment, w/o U^{235}	0.4 to 3.0
Average moderator temperature, °C	80
Out-of-reactor parameters	
Time to reprocess fuel, days	365
Reprocessing yield, %	97
Economic variables	
Chemical reprocessing cost, $/lb U	2.50
Thermal to electrical power conversion, %	25
Load factor, operating days/day	0.9
Level factor, % of rated capacity	90
Use rate for depreciating assets	Not applicable
Use rate for nondepreciating assets, %/yr	6.0
Base price of natural uranium, $/kg U	40 00
Unit cost of separating U^{235} from U^{238}, $/unit of separative work	40.00
Fuel element description	
Cluster of 19 round rods, jacket OD, in.	0.530
Fuel core, OD, in.	0.500
Fuel core material	Sintered and ground UO_2
Jacketing material	Zirconium or aluminum tubing

fuel cost is inversely proportional to exposure. The costs gradually increase past the minimum point because the cost of U^{235} contained in the fuel element is not a direct function of enrichment, and because the rate of exposure increase drops off with increased feed enrichment. The minima shown in Fig. 8–7 are broad; for example, for a k_∞/ϵ of 1.03, the uranium feed enrichment can vary between 0.7 and 1.9% U^{235} without exceeding the minimum fuel cost by 10%. The minima should be more pronounced if inventory charges of the order of 15%/year are assessed.

Repeating these calculations for other values of fuel fabrication cost, one is able to identify minimum fuel costs as a function of uranium feed

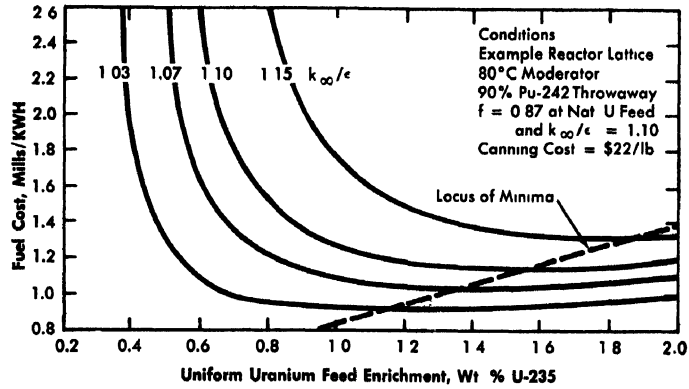

FIG. 8–7 Fuel costs as a function of uranium feed enrichment for equilibrium plutonium recycle.

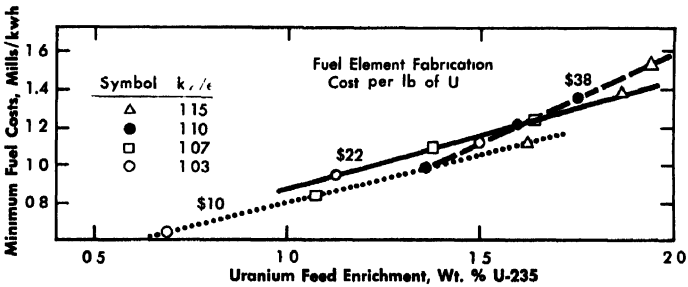

FIG. 8–8 Loci of minimum fuel costs for various uranium feed enrichment.

enrichment and fuel fabrication cost. This is illustrated in Fig. 8–8. Note that as the fuel element fabrication cost increases, the minimum fuel cost increases and also that the minima occur at higher feed enrichments. This emphasizes the fact that more expensive fuel elements must achieve higher exposures in order to minimize their cost.

It also appears that the use of natural uranium feed will result in fuel costs within 10% of the minimum if both k_∞/ϵ and fuel fabrication costs are low enough. Moreover, it can be shown that for the cases shown in Fig. 8–8, lower fuel costs will result from recycling the plutonium discharged in spent fuel elements, rather than discarding it and providing extra U^{235} to make up for resultant loss of reactivity.

Fuel costs are, of course, only a part of the over-all cost picture. A total cost analysis must also consider the capital cost of the reactor, its

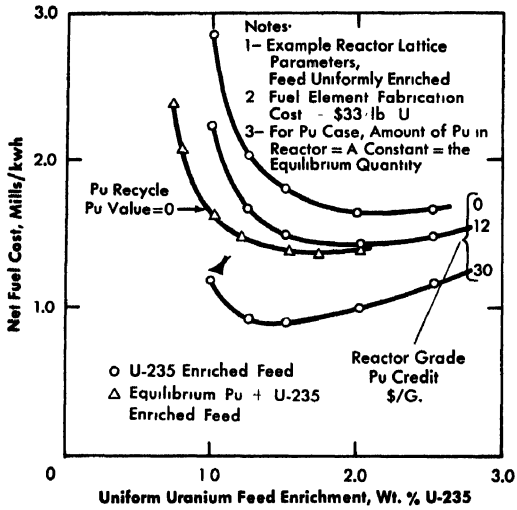

FIG. 8–9. Effect of initial U^{235} concentration on example reactor fuel costs.

operating costs, and limitations such as those imposed by heat-transfer limits and safety considerations. Furthermore, eliminating questions as to the value of plutonium by specifying self-sustaining operation would appear to restrict the results of such calculations to what may be special situations. To complete the analysis, then, a comparison with a similarly optimized U^{235} system is necessary.

(2) Illustrative example—Part II Preparatory to making the comparison between plutonium and uranium fuels, net fuel costs for uranium-only operation were calculated for each enrichment and the corresponding fuel exposure. From these calculations, the fuel costs for each assumed jacket tubing cost and plutonium credit value were determined. Sample results are illustrated in Fig. 8–9. The minimum fuel costs, as read from such graphs, are listed with their corresponding feed compositions in Table 8–8. Note that as the credit value for plutonium varies from zero to \$30/g, the minimum fuel costs occur at different feed compositions varying from 2.2 to 1.0% U^{235}. These minimum costs are then compared with the corresponding costs for the plutonium-enriched case. Differences in the fuel costs for comparable examples are calculated and are shown in Fig. 8–10 as a function of the value of plutonium.

As shown by Fig. 8–10, the fuel costs of the example reactor would be equal for the two methods of operation at a plutonium value of about thirteen dollars per gram of contained fissionable isotopes. This number is not a measure of the intrinsic market value of plutonium of this composition. This value is for a specific plutonium composition employed in a

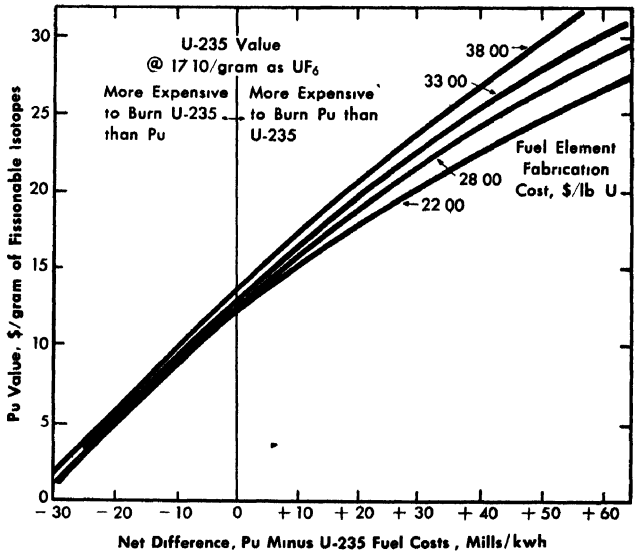

FIG. 8–10 Difference in costs for uniformly enriched example reactor as a function of plutonium value.

specific reactor with a specific mixture of U^{235} and U^{238}. Even then, it depends on the cost of making power with uranium-only fuel in the same reactor

The value of plutonium thus determined by its use in a particular reactor system might represent ultimate market worth only if such a reactor should prove so attractive that many future power reactors would duplicate it. Actually, the value of plutonium or U^{235} in reactors is not a unique quantity but is dependent upon many things, including the "efficiency" of the reactor. As discussed previously, if a U^{235} fuel element is given a value of 1.0 when burned in a reactor that loses 0.1 neutron/neutron absorbed in the fissionable fuel its comparative value drops to about 0.6 when it is placed in a reactor that loses 0.25 neutron/neutron absorbed in the fissionable fuel. This shift in value is often neglected in the U^{235} case, since the price of U^{235} (and therefore presumably its value) is based on the cost of obtaining it from the natural state rather than upon its value as a reactor fuel.

Measurement of plutonium value by the methods employed in these analyses requires a knowledge of relative fuel preparation costs. With the limited data available, the best possible estimates of the fuel prepara-

TABLE 8–8

EXAMPLE REACTOR FUEL COSTS FOR ECONOMICALLY OPTIMUM FUEL COMPOSITIONS

Fuel element fabrication cost, $/lb U	Jacket tubing cost, $/lb U	Pu value, $/g	Uniform U^{235} enrichment		Uniform Pu enrichment*	
			Wt. fraction U^{235} in fuel material	Fuel cost, mills kwh	Wt. fraction U^{235} in feed material	Fuel cost, mills/kwh
38.00	14.00	0	0.022	1.71	0.017	1.45
		5	0.021	1.66	0.017	1.48
		7	0.021	1.62	0.017	1.49
		10	0.020	1.55	0.017	1.52
		12	0.020	1.51	0.017	1.54
		15	0.019	1.44	0.017	1.57
		30	0.015	1.02	0.017	1.70
33.00	10.00	0	0.021	1.66	0.016	1.40
		5	0.021	1.61	0.016	1.43
		7	0.020	1.56	0.016	1.44
		10	0.019	1.49	0.016	1.47
		12	0.019	1.44	0.016	1.49
		15	0.018	1.38	0.016	1.52
		30	0.0145	0.91	0.016	1.66

28.00	6.00	0	0 020	1.58	0.015	1.33
		5	0 020	1.53	0.015	1.36
		7	0.0195	1.48	0.015	1.37
		10	0 019	1.41	0.015	1.40
		12	0.0175	1.35	0 015	1.42
		15	0.0175	1.27	0.015	1.45
		30	0.0136	0.78	0.015	1.59
22.00	2.00	0	0.020	1.50	0.014	1.26
		5	0.0195	1.45	0.014	1.28
		7	0 019	1.40	0.014	1.29
		10	0.018	1.32	0.014	1.32
		12	0.017	1.26	0.014	1.34
		15	0.0155	1.17	0.014	1.37
		30	0 010	0 56†	0.014	1.51

*All plutonium recycled; therefore, only inventory charges are affected by changing plutonium value.
†Lowest value calculated, not a minimum.

TABLE 8–9

VARIABLES AND RANGES UNDER STUDY

Variables	Range of values	
	Minimum	Maximum
In-reactor parameters		
k_∞ / ϵ	1.03	1.30
Resonance escape probability (approximate)	0.60	0.95
Thermal utilization factor (approximate)	0.7	0.95
Uranium feed enrichment for U^{238} bearing fuel, w/o U^{235}	0.28	3.0
Uranium enrichment for localized or "spike" enrichment, w/o U^{235}	20	100
Average moderator temperature, °C	80	600
Average specific power, Mw/ton	0 1	20
Plutonium compositions	Determined from above parameters	
Out-of-reactor parameters		
Time to reprocess fuel, days	90	730
Reprocessing yields, %	80	99
Economic variables		
Use rate for depreciating assets,* %/yr	1½	20
Use rate for nondepreciating assets,* %/yr	zero	18½
Chemical reprocessing costs, $/lb U	zero	20
Uranium-only fuel preparation costs, $/lb U (for fuel containing a mixture of U^{235} and U^{238})	zero	40
Uranium-only fuel preparation costs, $/lb U (for fuel containing U^{235} only)	zero	20
Ratio of plutonium-bearing fuel preparation costs to uranium-only costs	1.0	4.0
Base price of natural uranium, $/kg U	10	80
Unit cost of separating U^{235} from U^{238}, $/separative unit	20	320

*Increments between rates for depreciating and nondepreciating assets of 0, 1½, 3, and 5% are planned.

tion costs were made for both cases. To obtain meaningful cost relationships, the same materials, accounting procedure, degree of automation, etc., were stipulated. The major cost differences stem from the extra costs of handling the extremely toxic plutonium during fabrication. Since data were lacking, this was arbitrarily assumed to cost 50% extra in labor and overhead charges and 100% extra in capital equipment charges.

(3) Computer program. To extend the type of analysis described in this example to enough cases to characterize plutonium fuels more adequately, the previously mentioned computer program is being used. Since it is not feasible to investigate the effect of each variable in detail, the program has been limited to appropriate combinations of the variables indicated in Table 8–9.

The computer codes provide for solution of regionally enriched operation, such as with seed core and blanket arrangements, or spike-enriched operation as well as uniformly enriched operation The economic analysis provides for depreciation of all capital expenditures for fuel, except for the salvage value. The program thus evaluates changes in fuel element salvage value as U^{235} and plutonium composition varies with burnout The cost of enriched uranium is varied by postulating a hypothetical diffusion plant cascade with various assumed unit values for separative work and natural uranium costs.

Even with the limitations expressed in Table 8–9 the application of the program is only partially complete at this time No general conclusions about the potential value of plutonium have been formulated. From preliminary data, however, it appears that plutonium will have a positive value, probably large enough for the plutonium recycle concept to be widely applied in the future.

8–2.3 Fuel element
done to develop fuel
and to develop econon
has been focused on fi
component nested tub
initial loading for the

The 19-rod cluster c
clad with Zircaloy-2
lars to form the cluste

The three-componer
sists of two concentric
with 0.030-inch wall th
the fuel components, and between the outer component and the process tube.

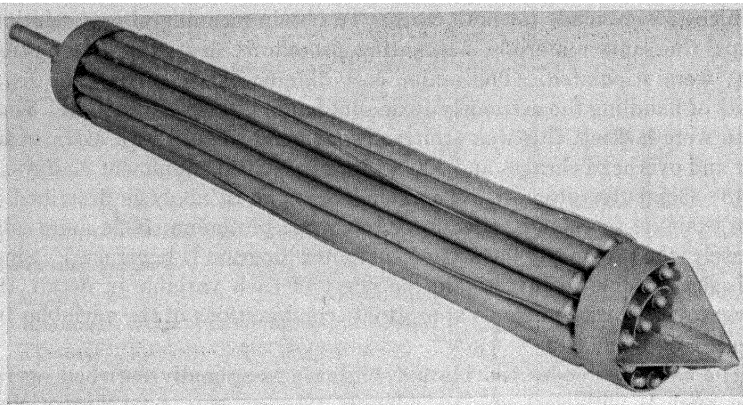

FIG. 8–11. PRTR-type 19-rod cluster fuel assembly.

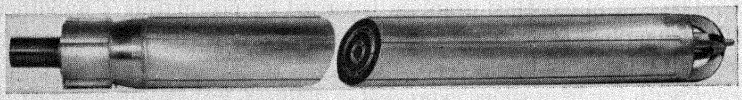

FIG. 8–12. PRTR tubular fuel element.

Health hazards and special handling problems associated with plutonium fuel fabrication Plutonium is both fissionable and radioactive. Thus, health and safety hazards are involved in the manufacture of plutonium fuel elements. The relatively low critical mass of plutonium necessitates precautions against accumulating large amounts in one place. Moreover, since the critical mass depends upon environmental conditions, every accumulation of plutonium must be considered in terms of its form and environment. The small amounts of material involved in research and development work do not usually create criticality problems, but in the fabrication of plutonium-bearing fuel elements critical mass considerations are of real concern.

The health hazard, which is relatively independent of quantity, arises primarily from 5.15-Mev alpha particles. In body tissue, these have an average range of about 45 microns and severely damage any area on which plutonium happens to deposit. Every precaution must be taken to prevent plutonium from entering the body since it is deposited in the bones and excreted very slowly. The maximum permissible body burden of

plutonium fixed in bone matter is currently 0.04 μc or about 0.5 μg [11]. At Hanford, no one is permitted to work with plutonium or a biologically similar isotope, if his body burden is judged to exceed one-fifth of the permissible limit as determined by periodic monitoring of urine.

Plutonium is sometimes thought of as being an alpha emitter only. However, mixtures of plutonium isotopes give off significant amounts of low energy gamma and x-radiation. Even with low-exposure plutonium, close-contact handling must be limited to prevent excessive hand exposures. For work with high-exposure plutonium, shielded or remote manipulation may be required. The radiations associated with the higher isotopes of plutonium and uranium are discussed in Reference 25.

Plutonium handling equipment is commonly housed in sealed glove boxes or hoods maintained slightly below atmospheric pressure so that contaminated air cannot leak into laboratory areas. Operations are performed through long gauntlet gloves sealed to the box. Materials containing plutonium must be encased while being handled outside the hooded enclosures. Air exhausted from boxes and hoods must be filtered to reduce the plutonium concentration to less than 2×10^{-12} mc/cm^3.

The necessary special handling techniques increase the costs of fabricating plutonium fuel elements. However, cleaning methods have been developed by which aluminum-plutonium alloys have been decontaminated to the point where no smearable or loose contamination is detectable on their surfaces. Simpler and more economical handling and fabrication techniques may be suitable for such materials.

Metallic core fuel elements. (1) Aluminum-plutonium core material. There is more fuel fabrication information for aluminum-plutonium alloys than for any other plutonium-containing fuel material. Because the Al-U and Al-Pu alloy systems are similar, irradiation data on Al-U systems are considered to be generally applicable to Al-Pu systems. Aluminum-plutonium alloys reduce plutonium contamination problems and are easy to fabricate. There are several simplified reprocessing and fuel element fabrication schemes that could make these elements very economical for spike enrichment.

Work on aluminum-plutonium alloys usually centers on the two phase structures between aluminum and $PuAl_4$ compound, mostly near the eutectic composition, which is about 14 w/o Pu in aluminum. Since the solubility of elemental plutonium in aluminum is extremely low, the plutonium will exist as the compound $PuAl_4$ dispersed in a matrix of primary crystals of pure aluminum or in the eutectic mixture [12]. This is an ideal dispersion-type fuel material since the hard and brittle fissionable phase, $PuAl_4$, is dispersed in a continuous matrix of low cross section structural material. Such dispersion concentrates structural damage caused by fission in highly localized regions surrounding the dispersed fis-

sionable particles. Hence, around the region of radiation damage this type of fuel material provides a structurally sound region free of fission products [13].

Al-Pu alloys have been successfully cast by adding metallic plutonium to molten aluminum in open-hearth furnaces Submerged in the molten aluminum, the plutonium is protected from air oxidation. Any surface oxide on the plutonium is reduced by the aluminum.

The effects of gravity and inverse segregation of the more dense $PuAl_4$ phase can be minimized by such techniques as casting into water-cooled copper molds and by carefully adjusting the pouring rates and temperatures. Rods 12 inches long and 1/2 inch in diameter containing as much as 20 w/o Pu in Al, have been cast in thick-walled graphite molds with a minimum of segregation and shrinkage cavities [14]. The segregation problem becomes more acute as the plutonium concentration is increased, and carefully controlled directional solidification is necessary to eliminate piping and other shrinkage cavities.

Reactor fuel core materials should resist corrosion by the coolant in order to limit damage to the reactor in the event of a fuel element failure. Adding silicon may improve the aqueous corrosion resistance of Al-Pu alloy core materials at high temperatures.

If metallic plutonium is needed for preparation of cast aluminum-plutonium alloys, prior steps of hydrofluorination and bomb reduction are required. These operations substantially raise preparation costs for Al-Pu alloys. Manufacturing processes that combine the reduction step with the alloy formation may lower costs The "cryolite process" involves heating mixtures of PuO_2, aluminum, and cryolite to form aluminum-plutonium alloys [15,16]. Work has been done to evaluate this process as a means of preparing aluminum-plutonium fuel material for plutonium recycle application [17]. Plutonium losses encountered with the cryolite process are low (about 0.2%), and overall costs should compare quite favorably with methods requiring metallic plutonium for formation of Al-Pu alloys. The recommended procedure is to prepare a master alloy, which is diluted with aluminum during remelting and fabrication of the fuel element. This process has been successfully demonstrated on a semi-continuous basis in which additions of aluminum and plutonium oxide and withdrawals of alloy product and waste cryolite are made with the reaction crucible held at 1050 to 1080°C. A semi-continuous cell, in which the by-product aluminum oxide is reduced electrolytically, has been investigated. It appears to offer a means to avoid the disposal or recovery of plutonium from spent cryolite and crucibles.

(2) Other plutonium alloy core materials. Plutonium alloys other than Al-Pu hold promise as core materials for fuel elements. However, the technology of these alloys is not well developed and much remains to be

done before they will become usable. Uranium-plutonium-fissium* and zirconium-plutonium alloys hold promise. Other possible diluent materials for plutonium are beryllium, magnesium, silicon, and thorium.

Much work has been done at the Argonne National Laboratory on the uranium-plutonium-fissium alloy [18] Irradiation tests on pin-type specimens indicate that the alloy is dimensionally stable.

Zirconium-plutonium alloys are also under consideration, but high fabricating and processing costs may preclude their use as fuel element materials. Metallic dispersion-type fuel materials containing plutonium in various combinations are further possibilities.

The "self-shielded" plutonium fuel element utilizes concentrated plutonium and takes advantage of the high thermal absorption cross section of plutonium to limit its fissioning to the fuel core surface. This self-shielding effect increases the fuel element lifetime for a given change in reactivity, and thereby reduces the throughput of plutonium fuel elements. Such a fuel element may consist of a plutonium or high density PuO_2 core of small diameter in a thick-walled jacket Major disadvantages are the very high heat transfer rates required to obtain reasonably high specific powers and the high inventory costs arising from the high concentrations of plutonium in the fuel elements Problems associated with high core temperatures of self-shielded fuel elements may be avoided by substituting high density PuO_2 for metallic plutonium as the core material.

Fuel element fabrication Cheap, reliable fuel element fabrication techniques can contribute significantly to development of economic plutonium fuel elements Because Al-Pu alloy core material appears to offer the greatest potential for the immediate future, much effort has been concentrated on fabrication techniques for fuel elements containing this alloy.

Methods of casting aluminum-plutonium alloy core material directly into cladding by air or mechanical pressure injection are being investigated. For convenience in these experiments, pure aluminum is used in lieu of the Al-Pu alloy. The differences in casting properties are small enough to permit such a substitution

To date, the most satisfactory method has been to force molten aluminum by air pressure into heated, evacuated cladding tubes made of stainless steel or Zircaloy. Satisfactory aluminum castings as long as 8 feet with densities up to 96% of theoretical have been obtained in cladding tubes 1/2 inch in diameter. Radiographs show the aluminum to be relatively sound although it contains some micro-shrinkage voids and a

*Fissium is a term used here to describe qualitatively a material which contains those fission product elements not removed by pyrometallurgical reprocessing of reactor fuels (see Chapter 3).

few gas voids. The pattern of the micro-shrinkage shows that the aluminum feeds into the cladding through a tube of solidified metal adjacent to the inside cladding surface. X-rays also show that the core material is in intimate contact with the cladding. Bonding has been observed between the aluminum core and the stainless steel or Zircaloy cladding. Since the aluminum conforms to the exact shape of the cladding tube, the dimensional tolerances of the cladding tube can possibly be relaxed, and fabrication costs reduced. Several techniques for reducing air pressure injection cast Al-Pu fuel elements with contamination-free external surfaces are being developed.

The use of mechanical pressure instead of air pressure injection is a more conventional die-casting technique. The molten alloy is mechanically forced directly into the Zircaloy or stainless steel cladding tube and allowed to solidify while the pressure is maintained. This method has all the advantages of air pressure injection and, in addition, may reduce the number of micro-shrinkage voids because the alloy can be injected more rapidly and at higher pressure. Four-foot lengths of 1/2-inch diameter cladding tubes have been successfully filled with aluminum by this method. Radiographs reveal the castings to be relatively free of voids. Bonding has been observed between the core and the cladding.

Extrusion as a method of producing aluminum-plutonium fuel elements has certain advantages from the standpoint of reducing required handling and costs. Extrusion methods lend themselves readily to the fabrication of plutonium-bearing fuel elements, and can be used for a variety of fuel element geometries Extrusion equipment is compact and well suited for operation in a protective enclosure. Experiments on aluminum and alloys of aluminum have used uranium as a stand-in for plutonium. Results have been satisfactory and will be applied to aluminum-plutonium alloys. Rods have been extruded from cast billets. Coextrusions of cast billets in aluminum sheathing have also been made. Coextrusions have the advantage of extruding fuel and cladding, as a bonded integral unit. A further possible advantage is the reduction of the contamination problem associated with plutonium.

Alloy segregation difficulties may be reduced by using powder metallurgy techniques to fabricate fuel element cores. Aluminum or aluminum alloy powder is mixed with a powdered plutonium intermetallic compound such as $PuAl_4$, or plutonium-containing oxides such as PuO_2 or PuO_2-UO_2 mixed crystal oxides. It is then hot- or cold-compacted to a suitable green density. The green compacts are hot-extruded into rods, or coextruded in aluminum sheathing. If PuO_2 is used as the fissionable material, the aluminum reduction steps for preparing metallic plutonium are eliminated. Blended mixtures of aluminum powder and UO_2, as a stand-in for PuO_2, have been cold compacted and hot extruded or coextruded in aluminum

sheathing. The oxide content varied from 2 to 20 w/o UO_2 and the compacted billets were hot-extruded through shear dies with an extrusion ratio of 9 to 1. The oxide particles must be outgassed to prevent swelling of the extrusions upon heating Extrudability of aluminum powder-UO_2 compacts is about the same as that of cast aluminum and the same techniques can be used.

Swaging is a fabrication method that has the advantage of reducing handling in fuel element fabrication. Metallic as well as ceramic fuel elements can be swaged. Swaging cast rods reduces porosity. Long rods can be swaged from cast billets. Swaging can also be used to size fuel element cladding onto core materials Powdered oxides and mixtures of oxides and powdered metals have been successfully compacted to high densities by swaging directly in the cladding

There is no extensive information available on the irradiation performance of plutonium fuel elements. At Chalk River, Canada, Al-Pu alloys have been irradiated with satisfactory results [19]. At Hanford, one-half inch diameter capsules of Al-1.6 w/o Pu clad in Zircaloy have been successfully irradiated at 60% burnout of the Pu atoms with no observable deleterious effects. Elsewhere in the United States, Pu-Al alloys have been irradiated to relatively high burnups of the plutonium atoms, and no difficulties were attributed to malfunction of the alloy due to irradiation [20–22].

Ceramic fuel elements. In ceramic fuels, the core material may contain PuO_2, UO_2, mixed crystals of PuO_2-UO_2, or plutonium oxide dispersed uniformly either in an inert material or in uranium dioxide.

Ceramic cores, easily prepared with a variety of physical properties and shapes, can be incorporated in many different fuel element designs. For example, ceramic core materials have been used in fuel elements in the form of (1) unsintered powders, (2) sintered, small diameter cylinders, (3) inert carriers, such as graphite, impregnated with PuO_2, and (4) massive, large diameter, sintered oxide tubes.

Because PuO_2 and UO_2 are chemically similar and experiments with PuO_2 are hazardous, UO_2 has been used whenever possible to develop processes under study. It should be relatively easy to adapt the processes to special techniques for handling PuO_2 or mixtures of PuO_2 and UO_2, but fabrication costs may be significantly higher.

(1) Core materials. It has been observed that commercially available fissionable raw materials, such as natural uranium dioxide, frequently vary in fabrication behavior from one batch to the next. With fissionable materials obtained from plutonium recycle reactors, this variation may be even greater. Reliable methods, therefore, are necessary for characterizing these raw materials so that powder preparation and activation methods can be developed which promote the fabrication of ceramic fuel cores

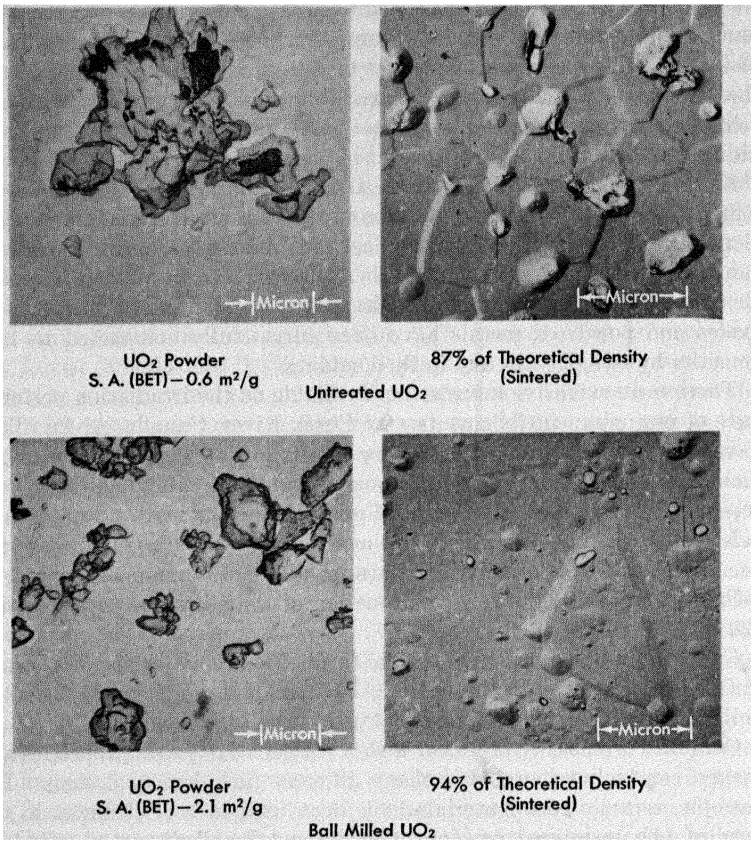

FIG. 8–13. Effect of particle surface area on behavior of "PWR grade" uranium dioxide sintered at 1750°C for 8 hours.

of reproducibly high quality. Electron microscopy, surface area measurements, and air permeability techniques have been employed to characterize uranium dioxide powders, and the same techniques, in general, are expected to be applicable to plutonium oxides. In Fig. 8–13 are illustrated electron micrographs which reveal a typical correlation between the particle size and surface characteristics and the sinterability of UO_2 powders The sintered densities obtained with the smaller particles are relatively high. Normally, the higher density product is desirable in reactor fuel elements, because of the increased nuclear reactivity, fission product retention, thermal conductivity, and stability in high temperature coolants.

Particle size reduction of commercially available UO_2 powders by ball

milling markedly increases the density obtained by sintering. The effectiveness of the ball milling operation is increased by using a combination ball mill-air classifier unit. Uranium dioxide powder has also been produced from UO_3 or untreated UO_2, using an oxidation-reduction cycle in a fluidized bed. The temperatures employed in the fluidized bed are 450 to 500°C and 525°C for the oxidation and reduction steps, respectively. This process greatly increases the surface area of the treated powders and thus improves sintering characteristics. Uranium dioxide powder activated by such methods has been compacted and sintered to densities as great as 98% of the theoretical, crystallographic density.

For fuel elements containing loose, unsintered powder, as described below, it is necessary only to grade the powder so that a relatively high packed density is obtained. When compacted, a powder having a very low surface area generally yields the highest density unsintered fuel element cores.

Ceramic cores made up of physical mixtures of PuO_2 and UO_2 powders introduce a problem in the post-irradiation chemical processing. It has been found difficult to dissolve the PuO_2 in such cores. However, the mixed crystal oxide PuO_2-UO_2 tends to alleviate this difficulty. This mixed oxide is prepared by the coprecipitation of ammonium diuranate and plutonium hydroxide from nitric acid solutions by the addition of ammonium hydroxide or ammonia gas The precipitate is filtered, dried, and transformed to the mixed oxide by hydrogen reduction at temperatures above 700°C.

Impregnating porous, inert carrier materials with plutonium oxide may offer a relatively simple method of obtaining plutonium-bearing fuel cores. Several types of carrier materials, such as sintered magnesium oxide, sintered beryllium oxide, and graphite, are available. Graphite cylinders have been impregnated with PuO_2 by first boiling the graphite pieces in plutonium (IV) nitrate solution, drying the graphite pieces at about 100°C, heating them to the calcination temperature, and finally firing at 1000°C. Better distribution of the plutonium is achieved if the pieces are rotated during the drying and calcination steps. Concentrations of 100 mg of oxide per cubic centimeter have been readily obtained in a single impregnation cycle In multiple cycles, concentrations as high as 600 mg/cm^3 have been achieved. The ultimate concentration is apparently limited by the available pore space of the graphite. The precision of impregnation is determined by the uniformity of the graphite, its density, and the concentration of the impregnating solution. It has been possible to predict the plutonium concentration of the impregnated graphite within 5 to 10%.

(2) Core compaction, sintering, and finishing. Uranium dioxide can be formed into cylinders, tubes, and other shapes by conventional ceramic

processes, such as warm or cold pressing, isostatic pressing, extrusion, and slip casting. Compacts thus formed from powder prepared as described in the previous section are sintered in 1600°C hydrogen to densities up to 98% of the theoretical. Sintered uranium dioxide fuel cores for the initial Plutonium Recycle Test Reactor fuel cycle studies will have a minimum density of 94%. The sintered UO_2 cores of the tubular fuel element illustrated in Fig. 8–12 consist of short sections of tubing approximately 2 inches long, with a wall thickness of approximately 3/8 inch.

Sintered uranium dioxide rods and the outer surfaces of sintered tubes can be finished by belt centerless grinding. Conventional hard-wheel centerless grinders cause chipping and cracking of large tubular pieces. Rejects caused by chipping or cracking are virtually eliminated by the use of belt-type grinders, if the edges of the pieces are chamfered very slightly (approximately 0.03 inch). Internal surfaces of the tubular pieces can be finished with conventional internal grinding equipment. It has been found possible to control tolerances of the internal and external diameters of UO_2 pieces to within ± 0.001 inch by grinding.

(3) Jacketing and assembly of sintered cores. Zircaloy tubing, a jacketing material of great interest in the plutonium fuel study, is commercially available. Tubing of small diameters can be formed by extrusion; tubing of relatively large diameters can be fabricated by roll-forming and welding Zircaloy strip.

Spacing members are required for accurate positioning of fuel element components in relation to each other and to the reactor coolant channel. Spirally wound wire attached to and stretched between the ends of each of the rod elements has been used for hydraulic studies and, to a limited extent, for in-reactor tests to obtain required spacing. Spacing may also be obtained by attaching ribs to the cladding along the entire length of the fuel element. Two methods of fabricating cladding materials with attached ribs show promise. The first involves extrusion of tubing having integral ribs; the second employs a high frequency resistance welding technique to attach ribs to the cladding. The high frequency welding process may minimize the area of the heat affected zone and thus help prevent dimensional changes or loss of corrosion resistance of the zirconium alloy.

Small-diameter fuel rods are closed by fusion-welding a cap into each end of the jacketing tube. To obtain a reliable closure of the two-component nested tubular elements, techniques are being developed for resistance seam welding a hemitoroidal piece into the space between two coaxial jacketing tubes, and fusion welding a tubular end fitting in place. The double closure reduces the possibility that defective welds will cause reactor shutdowns. The initial resistance seam weld is expected to alleviate the outgassing problem which is frequently encountered in making a

fusion-welded closure in a fuel element which is partially filled with helium.

(4) Simultaneous compaction and jacketing techniques. Fabrication methods which combine manufacturing operations required in fuel element manufacture offer the possibility of significantly reducing fuel element costs. Methods have been developed by which unsintered powders are simultaneously compacted and jacketed In one of these methods unsintered powder is vibrated or mechanically tamped into the jacket tube Assembly of the fuel element is completed by welding end caps to the tube. Core densities approximately 60 to 70% of the theoretical have been obtained with UO_2 powder. A modification of this method employs an extruded aluminum jacket consisting of two coaxial tubes having six integral radial spacers, the cross section being represented by six truncated sectors having common radii After the ceramic fuel material, such as UO_2 powder, has been poured into it, the aluminum can is closed, placed over a mandrel and subjected to pressures up to 50,000 psi in an isostatic press. The uranium dioxide can be thus compacted to 65 to 70% of the theoretical crystallographic density, while at the same time the outer aluminum tube is deformed to create uniform longitudinal coolant channels

Simultaneous compaction and jacketing can also be accomplished by swaging a metal tube containing the ceramic fuel material. Specially prepared uranium dioxide in zirconium or stainless steel jackets has been compacted to about 85 to 90% of the theoretical density by cold swaging; densities greater than 90% of the theoretical can be obtained by swaging at temperatures of 600 to 850°C Uranium dioxide powders have also been swaged in aluminum alloy tubes, with resulting densities about 5% less than those achieved in zirconium or stainless steel jackets. The density of the uranium dioxide core is reproducible within plus or minus one percent for any given batch of UO_2 powder and a particular jacket material.

(5) Irradiation performance Irradiation tests on ceramic core materials fabricated by several different methods have been performed under a variety of test conditions. Uranium dioxide in the form of sintered and unsintered fuel element cores clad in aluminum, stainless steel, or Zircaloy have been tested

Fuel elements containing unsintered UO_2 powder enriched to 3% U^{235} were irradiation tested at power levels high enough to cause extensive sintering, relocation, and fusion of the core material. The powder in these elements originally had a packed density of 35 to 40% of the theoretical; after irradiation, the average density was approximately 90% of the theoretical. A cross section of one test element after irradiation is illustrated in Fig. 8–14. The power generation in this element was about 40 watts per gram of core material. The core material after irradiation contained

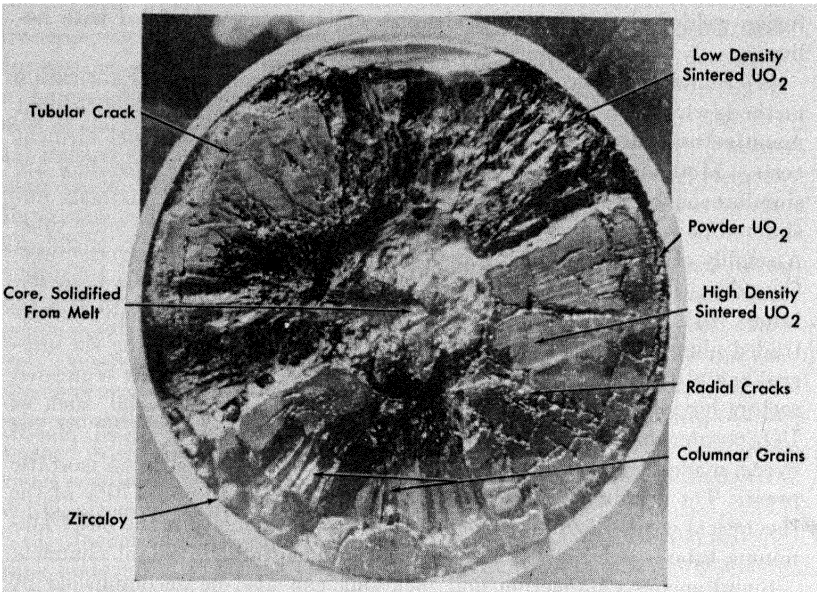

FIG. 8–14. Irradiated UO_2 powder.

large columnar grains of UO_2 extending from a central core to a circumferential crack approximately 1/16 inch from the cladding wall (Fig. 8–14). This grain pattern would indicate that fuel elements of this type can be operated with a surprisingly large fraction of the core in a molten condition—if one accepts the usual assumption that such a grain pattern is formed only during solidification of molten uranium dioxide. However, temperature calculations indicate that melting did not occur in that portion of the fuel element containing the columnar grains. Additional fuel elements of this type are therefore being irradiated to investigate the apparent anomaly.

An aluminum jacketed, tubular fuel element containing enriched uranium dioxide powder compacted by isostatic pressing, as described above, has been irradiation tested. The calculated maximum heat flux was 295,000 Btu/(hr)(ft^2)(°F), with a bulk coolant temperature of approximately 100°F. The power generation was 52 watts/g UO_2. There was no evidence of mechanical instability of the assembly during irradiation.

Capsules containing untreated uranium dioxide compacted to about 90% of the theoretical density by hot swaging in Zircaloy tubing at 600°C have been irradiated to relatively low exposures. Sectioning of these cap-

sules revealed that some sintering and cracking of the UO_2 had occurred during the irradiation.

A three-rod assembly of UO_2 cold swaged to about 85% of the theoretical density was irradiated to 100 Mwd/t in coolant at 100°F. The UO_2 was contained in stainless steel tubes 12 inches long with a wall thickness of 0.030 inch. This test was performed principally to determine the dimensional stability of such a fuel assembly. The test indicated that unsintered UO_2 cores of relatively high densities can be heated as high as 2200°C without causing permanent deformation of the relatively cold cladding by expansion Sintering of the powder during irradiation presumably decreases the volume of the core material, providing space for the differential thermal expansion of the core and jacket.

Tubular test fuel elements with cores of sintered uranium dioxide have been irradiated. Zircaloy-jacketed tubular elements, having dimensions of 1.44-inch OD × 0.4 inch ID × 9 inch length, were irradiated to relatively short exposures at heat fluxes of 500,000 Btu/(hr) (ft^2) (°F). There was no evidence of nonuniform heat transfer, ratcheting, or dimensional changes other than the usual cracking caused by thermal gradients in the sintered oxide core.

A tubular fuel element 1.44 inch OD × 0.4 inch ID × 4 inch in length was deliberately defected with a 0.014-inch diameter hole through the cladding, and the void space in the fuel element was filled with water. This element was subjected to the greatest rate of power increase safely obtainable in the Materials Testing Reactor. There was no evidence of jacket deformation or other problems as a result of the waterlogging

8–2.4 Chemical processing of fuel elements from plutonium recycle reactors. The selection of chemical processes for recovery of plutonium from spent fuel will depend on such factors as the number of reactors to be serviced, the types of fuel elements, the degree of decontamination required, the extent of recovery needed, and the quantities of materials to be processed. Conversely, the design of the reactor may well be influenced by the economics of the chemical processing methods. At Hanford, fuels from the Plutonium Recycle Test Reactor will be processed in existing facilities which are being modified inexpensively to accommodate a variety of power reactor fuels. Research and development on alternative processes are continuing in order to develop the design requirements for a preferred, completely integrated plutonium recycle system. Various types of processing plants and methods that have been considered are described below.

Types of processing plants. One concept is to use one central plant for processing the fuel from several reactors. This consideration has merit, particularly if the separation plant is already in existence, or if several

similar reactors can be located so as to favor construction of a central processing plant. There is also incentive for developing chemical processing techniques for a small processing plant closely coupled to the reactor. Among the factors which may combine to make this type of plant attractive are: (1) shipping costs can be minimized in this way, (2) some reactor fuel materials are uniquely amenable to specialized, low cost processes, and (3) it may prove feasible to develop small plants utilizing simple, compact aqueous or pyrochemical schemes.

Special problems may be encountered in chemical processing to support the Plutonium Recycle Test Reactor For example, different types of fuel loadings will be processed; small batches must be segregated, and varying requirements will be imposed on the chemical processing in order to evaluate the feasibility and optimum conditions of recycle. While service processing is being performed for the test reactor, development must proceed on processes which will contribute to achieving lowest over-all costs of irradiation, reprocessing, and refabrication combined.

Types of processes For a central processing plant, continuous solvent extraction processes can be used, with the additional processes required to remove cladding and to dissolve fuel materials For the close-coupled plant, where only a single fuel is to be processed, a small, low-investment batch, aqueous, or pyrochemical plant may be found most satisfactory.

The problem of jacket removal has been studied more extensively in connection with aqueous processing than for pyroprocessing For pyroprocesses, removal of both aluminum and zirconium cladding by halide volatilization has been considered Aluminum claddings are also compatible with certain pyrochemical processes which have been proposed for plutonium-aluminum alloy fuels. Although it is considered feasible to remove stainless steel claddings by chemical methods, mechanical removal may be preferred for either aqueous or pyrochemical processing.

Dissolution of zirconium cladding. For dissolving zirconium alloy jackets, it is desirable to use a process that is compatible with existing stainless steel equipment. This will avoid the need for providing additional, more complex processes or parallel dissolution facilities constructed of different materials. A process would be preferred which could be applied also to processing Plutonium Recycle Test Reactor fuel elements in existing facilities. For these reasons, the Zirflex process has been emphasized—it employs aqueous ammonium fluoride solutions that have been found satisfactory for use in existing stainless steel equipment [23].

The Zirflex process selectively dissolves zirconium or Zircaloy cladding of reactor fuels. Either of two solutions, ammonium fluoride or ammonium nitrate-ammonium fluoride, may be employed as the reagent. With ammonium fluoride solutions, zirconium is dissolved according to the equation

$$Zr(s) + 6NH_4^+ + 6F^- \rightarrow ZrF_6^= + 2NH_4^+ + 4NH_3(g) + 2H_2(g).$$

With mixtures of ammonium nitrate and ammonium fluoride in which nitrate is present in a ration of 0.5 mole nitrate per mole zirconium or higher, the dissolution reaction proceeds according to the equation

$$Zr(s) + 6.5NH_4^+ + 6F^- + 0.5NO_3^- \rightarrow ZrF_6^= + 2NH_4^+ + 5NH_3(g) + H_2O.$$

With this mixture there is minimum evolution of hydrogen and the tin in Zircaloy-2 may be dissolved simultaneously with the zirconium and discarded with the cladding waste Either of these solutions can be used safely in stainless steel equipment. Dissolution rates for Zircaloy-2 in boiling 6-molar ammonium fluoride are of the order of 100 mils/hr, whereas corrosion rates for stainless steel are only of the order of 0.5 mil/month

The dissolution rate of Zircaloy-2 increases with increasing ammonium fluoride concentration up to six molar, but decreases beyond six molar, as shown in Fig 8–15. The decreased rate of attack with high ammonium fluoride concentrations is probably due to the formation of insoluble ammonium fluozirconate on the reacting surface.

The fuel core materials are attacked by ammonium fluoride solutions at a much slower rate than is Zircaloy-2. The rate of attack of uranium metal and of sintered uranium dioxide in boiling six molar ammonium fluoride is about 30 times slower than for Zircaloy-2 Aluminum-plutonium alloy reacts initially quite rapidly, but the reaction rate decreases markedly as a protective deposit, presumably aluminum fluoride, forms. Fluorides of either uranium or plutonium formed by reaction with ammonium fluoride solution are quite insoluble, especially when the cladding solution is cooled. Thus, losses of fissionable material on the order of 0.1% or less are expected to result when the cladding solution is discarded after being centrifuged.

Core dissolution. After cladding has been removed by the Zirflex process, portions of the uranium and plutonium in the fuel core material are present as solid fluorides It is necessary to dissolve these materials as well as the bulk of the fuel core; at the same time, it is desirable that fluoride ion be either removed or complexed, to avoid severe corrosion of stainless steel process equipment. The fluorides can be converted to hydrous oxides, which can be washed to remove fluoride before dissolution in nitric acid. Alternatively, the fluorides can be dissolved directly in aluminum nitrate, or aluminum nitrate-nitric acid mixtures may be employed to complex the fluoride ion with aluminum.

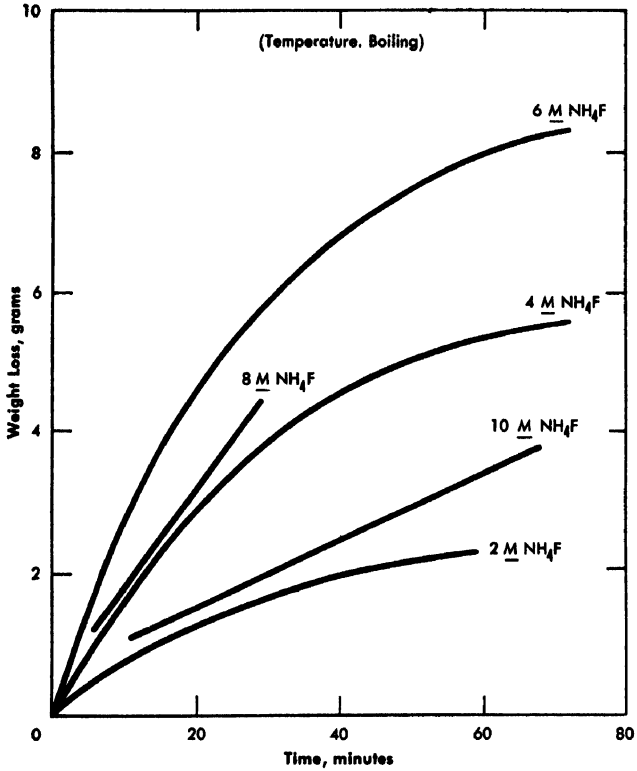

FIG. 8–15. Dissolution of Zircaloy-2 in NH_4F solutions.

Uranium metal or uranium dioxide core materials dissolve readily in boiling nitric acid. Mixtures of uranium and plutonium oxides may require the presence of some hydrofluoric acid in the nitric acid for complete plutonium dioxide dissolution. On the other hand, uranium dioxide containing the mixed crystal oxide, UO_2PuO_2, is dissolved completely in boiling concentrated nitric acid.

Aluminum-plutonium alloy dissolves readily in boiling six- to eight-molar nitric acid if 0.005-molar mercuric nitrate is present as a catalyst.

A possible flowsheet for decladding and dissolving Zircaloy-2-clad uranium dioxide fuel elements from the Plutonium Recycle Test Reactor is shown in Fig. 8–16. Feed solution prepared in this manner could be processed by solvent extraction, by anion exchange, or by a suitable combination of these methods.

Aqueous processing methods applicable to fuels from plutonium recycle reactors. Aqueous processes can be depended upon to process plutonium-

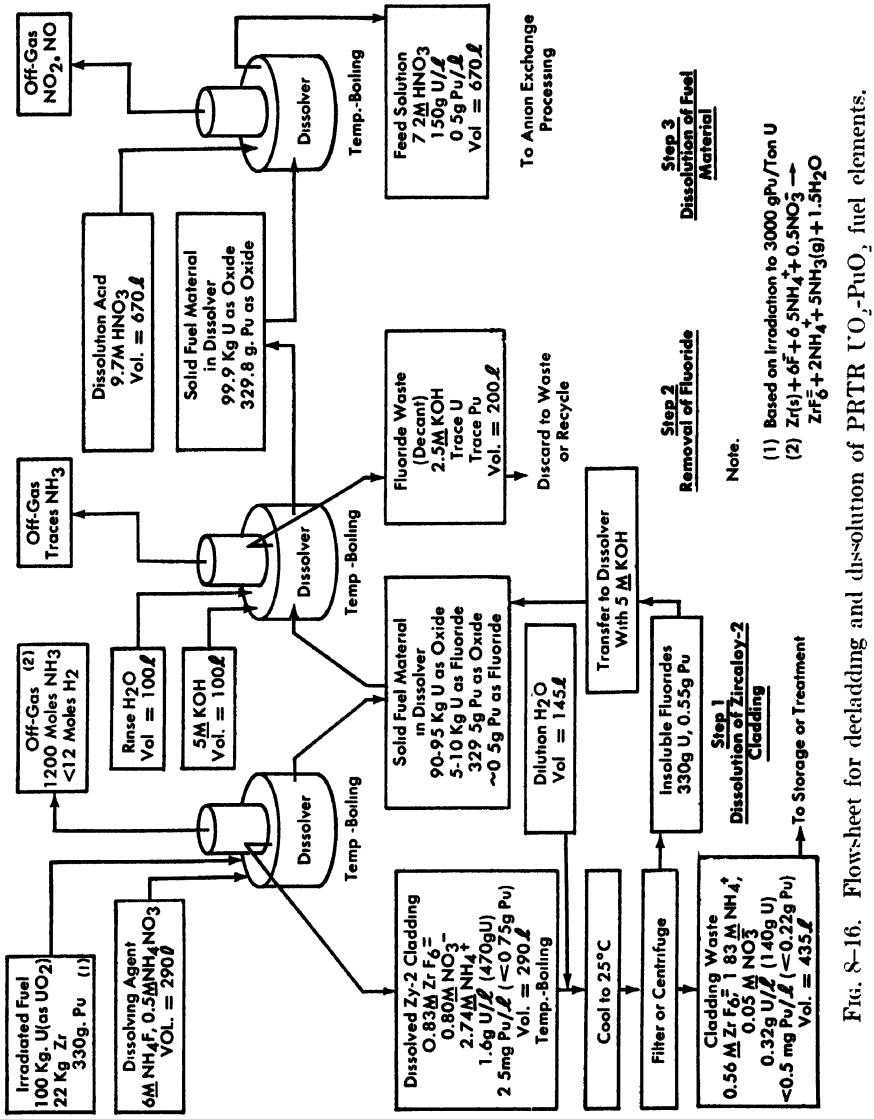

FIG. 8–16. Flowsheet for decladding and dissolution of PRTR UO_2-PuO_2 fuel elements.

bearing reactor fuels in the near future. As now conceived, the prime functions of a typical aqueous process for the Plutonium Recycle Test Reactor are: to remove fuel cladding; to dissolve fuel cores; to separate the plutonium from the mixture of uranium, plutonium, and fission products; and to purify the product plutonium. These functions can be conducted in the existing Hanford separation processes, but differences in starting materials, product specifications, and volume throughput for power reactor fuels may permit or require processes different from those now being used. Conventional aqueous solvent extraction processes may, however, continue to be the preferred technique for large-scale central processing plants.

Anion exchange decontamination and purification of plutonium. Low-cost recovery of plutonium alone from a reactor fuel is potentially achievable by using simple anion exchange resin columns rather than more complex liquid-liquid extraction equipment. This method has been investigated at Hanford, and it appears attractive for aqueous processing of typical power reactor fuels [24] It also seems well suited to the scale of operation required for plutonium processing.

Several commercially available anion exchange resins have been found to absorb readily the plutonium nitrate anionic complex from solutions containing seven molar nitric acid The absorption process is highly selective, separating plutonium from all of the common impurities, including uranium and fission products. Elution is readily accomplished with dilute (0.35 to 0.75 molar) nitric acid solutions.

Resin capacities (at 50% breakthrough) of 60 to 120 g Pu/liter of resin bed are attainable when the columns are operated at temperatures of 50 to 60°C. Mass flow rates of 80 mg Pu/cm^2 minimum can be achieved under these conditions Absorption and elution rates will vary somewhat with the particle size and the degree of cross-linkage of the particular resin chosen. A smaller particle size gives increased rates; the higher the degree of cross-linkage in the resin, the lower the rates. Temperature has a marked effect upon absorption and elution rates. Increasing the temperature from 25 to 60°C increases the absorption rate by a factor of 12 and the elution rate by a factor of about three Data comparing the plutonium elution rate among several resins of practical interest are given in Table 8–10.

A plutonium concentration in the product effluent stream of 50 to 60 g/liter may be obtained at 40 to 60°C with Dowex-1 (50 to 100 mesh) or Permutit SK (20 to 50 mesh) ; these resins permit a more rapid elution rate than others tested.

Purification of the plutonium from impurities is enhanced by a washing cycle wherein the plutonium-laden resin bed is washed at 60°C with seven molar nitric acid. A plutonium feed solution purposely contaminated

TABLE 8-10

RATES FOR ELUTION OF PLUTONIUM FROM VARIOUS COMMERCIAL RESINS WITH 1.0-MOLAR HNO_3 AT 60°C

Anion resin	Time for 90% elution, min	Time for 99% elution, min
Dowex 1, X-1 (50–100 mesh)	2.5	5.0
Permutit SK (20–50 mesh)	10	21
Dowex 1, X-4 (50–100 mesh)	25	52
Permutit S-1 (50–100 mesh)	80	225
Duolite A-42LC (20–50 mesh)	105	315
Amberlite IRA-401 (20–50 mesh)	120	360
Dowex 1, X-4 (20-50 mesh)	120	360
Amberlite IRA-400 (20–50 mesh)	250	600
Duolite A-101 (16-50 mesh)	425	1,100
Dowex 1, X-8 (50-100 mesh)	425	1,100

with common cation impurities to a level of *ca.* 3×10^6 ppm plutonium was shown to yield a product containing less than 138 parts of total metallic impurities per million parts of plutonium after washing with a volume of nitric acid equal to 15 times the bed volume

Uranium can be effectively separated from plutonium in a similar manner Decontamination factors exceeding 10^6 for uranium have been obtained under operating conditions of practical interest Resin capacities for plutonium are somewhat reduced in the presence of large excesses of uranium However, plutonium product solutions containing 50 g Pu/liter are readily achieved, provided the uranium concentration in the feed does not exceed 200 g/liter, and the ratio of uranium to plutonium in the feed does not exceed 300. Acceptable recovery and purification can be obtained with feeds exceeding these limits, but product solutions containing less than 50 g Pu/liter result.

Anion exchange purification results in excellent decontamination of plutonium from fission products Decontamination factors in excess of 10^4 for a single cycle and greater than 10^7 for two cycles of anion exchange have been demonstrated

An important factor in considering anion exchange processing for reactor fuels is the useful life of the resin. Damage to the anion exchange resins suffered through chemical attack by seven molar nitric acid at temperatures up to 60°C is relatively insignificant. However, degradation of the resin through irradiation or a combination of damage due to radiation

and chemical attack is a much more severe problem than chemical damage alone in many potential applications. Studies of the stability of certain resins exposed to Co^{60} gamma irradiation have shown that doses in excess of 3.5×10^8 r for Amberlite IRA-401 and 4×10^8 r for Permutit SK are required before these resins are damaged so much that they are useless On this basis, a usable lifetime of two weeks for continuous exposure to hot feed solution, or about one month actual operating lifetime, may be conservatively predicted.

For relatively small scale and particularly nonroutine operations, the loss of resin and the method of replacement does not present severe operating or cost problems.* However, for prolonged, routine, large scale applications, there may be strong economic incentives to provide alternative processes avoiding the problems associated with radiolytic degradation of the resin. A combination of solvent extraction for gross decontamination with anion exchange for concentrated product recovery may be selected.

A schematic flowsheet illustrating possible conditions for the anion exchange processing of fuels from the Plutonium Recycle Test Reactor is presented in Fig. 8–17.

Pyrochemical processing methods applicable to fuels from plutonium recycle reactors. The technology of pyrochemical processing methods is at present insufficiently developed to have immediate application in processing plutonium-bearing fuel materials for thermal reactors. Certain pyrochemical methods, however, are being investigated on a development scale for possible application to fuels from the Plutonium Recycle Test Reactor and to plutonium fuels in general.

The method of preparing aluminum-plutonium alloy fuel materials by reducing plutonium compounds with aluminum using a molten cryolite flux has already been described. Conceivably this process could be used to enrich or reconstitute aluminum-plutonium fuels which have undergone partial depletion. This would probably be the simplest way to introduce plutonium into spent fuel to maintain reactivity. At the same time certain decontaminations from fission-product elements, particularly those of the alkali and alkaline earth groups, are inherently possible by extraction into cryolite. However, no significantly large over-all gamma decontamination factor can be realized. A remote, shielded facility for the subsequent refabrication would therefore be necessary.

Alternative schemes have been studied for reconstituting aluminum-plutonium fuel alloy by removing aluminum, thus maintaining the required weight fraction of plutonium in the alloy. The processes that have been demonstrated on a laboratory scale [17] are: (1) removal of alumi-

*One pound of resin at a cost of $2 to $3/lb is sufficient for the recovery of over 20 g of plutonium in a single loading.

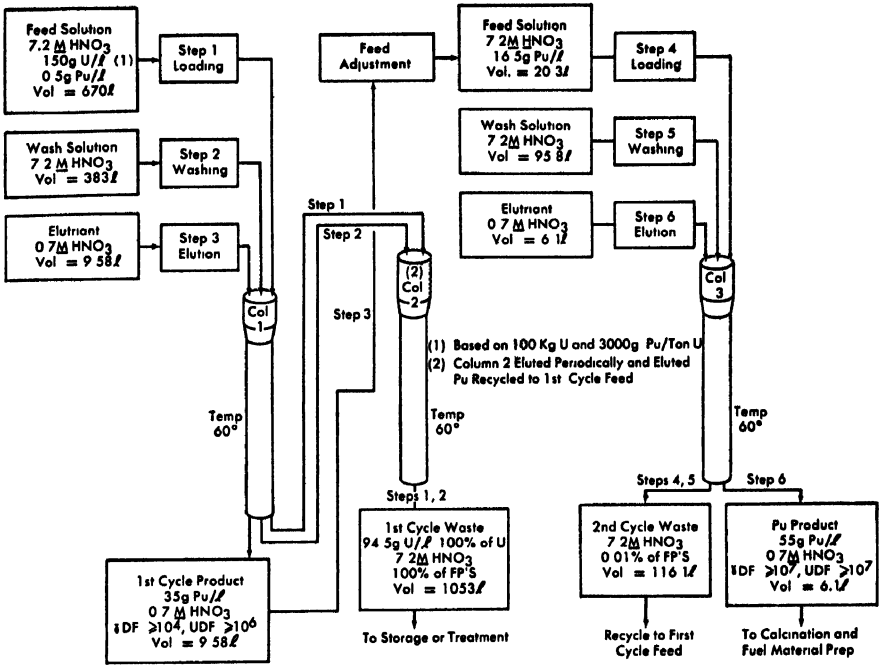

FIG. 8–17. Flowsheet for anion exchange processing of PRTR fuel solution.

num as a volatile chloride by reaction with chlorine or zinc chloride, (2) removal of aluminum as the volatile subfluoride by reaction with aluminum trifluoride, and (3) removal of aluminum by anodic oxidation in a cell employing cryolite as the electrolyte.

Other experimental work has pertained to the pyrochemical treatment of sintered uranium oxide fuel material. It has been shown, for example, that UO_2 can be reduced in a system containing aluminum metal and a molten chloride salt mixure, with the plutonium present being extracted into the salt phase. While the pyrochemical processing methods show attractive possibilities, much research and development work will be required before they can be economically utilized.

8–3. MAJOR EXPERIMENTAL FACILITIES

8–3.1 The plutonium fabrication pilot plant. Since the central problem in the economic recycling of plutonium is the development of processing and fabrication methods which will produce reliable fuel elements cheaply, the design and equipment of the pilot plant for fuel element fabrication are of interest. The equipment is specifically related to the proc-

esses which are to be investigated on an experimental and pilot plant scale. Design features of the building, although influenced by considerations of versatility and experimental flexibility, indicate some of the basic necessary features of a full-scale fabrication plant.

Chief among these are features which minimize health and safety hazards in handling plutonium and plutonium-bearing materials. The pilot plant for example will contain full-scale fuel element fabrication equipment enclosed in inert atmosphere and vacuum type containers.

Building. The Plutonium Fabrication Pilot Plant will consist of a one-story office and service area of about 7,000 square feet and a two-story process area with 20,000 square feet on each floor (Fig 8–18). In general, large process fabrication equipment, ceramic fuel element fabrication equipment, and fuel element assembly and testing equipment will be on the first floor About 60% of the second floor will be available for shops and for future plutonium fuel element fabrication equipment and development laboratories.

The building will be of airtight design for proper ventilation and contamination control. A combination of concrete, masonry, and structural steel will be used for its construction. Wherever practical, individual pieces of equipment or unit processes will be compartmented to confine the potential spread of contamination to as small an area as possible.

The second floor process area will include the building supply and exhaust ventilation equipment The ventilation system is designed to provide air conditioning for occupant comfort and process control and to establish pressure differentials so that air flow will be from zones having the least to the zones having the highest contamination probability.

Equipment. The Pilot Plant will contain a variety of equipment for fuel-element fabrication, including a 30-kw tilt pour induction furnace capable of melting and casting in a high vacuum. Facilities will be provided for the aluminum reduction of PuO_2 under a cryolite flux, for induction melting and casting in an inert atmosphere, and for the injection or die casting of fuel elements directly into their jacketing materials. A hooded lathe will permit the machining of plutonium-containing materials.

One of the larger pieces of fabricating equipment will be a 1250-ton extrusion press enclosed in a vacuum chamber which can be evacuated and then backfilled with a purified inert atmosphere to slightly less than atmospheric pressure. This type of container is used where operations are performed that require extreme atmospheric purity or where quality control is of prime importance. A 14-inch × 14-inch, two high-four high rolling mill will be enclosed in a similar container. A similar, though unhooded, rolling mill will be used for rolling clad fuel materials. A stationary die swaging machine enclosed in an inert atmosphere glove box will be used for swaging plutonium containing fuel rods to final dimen-

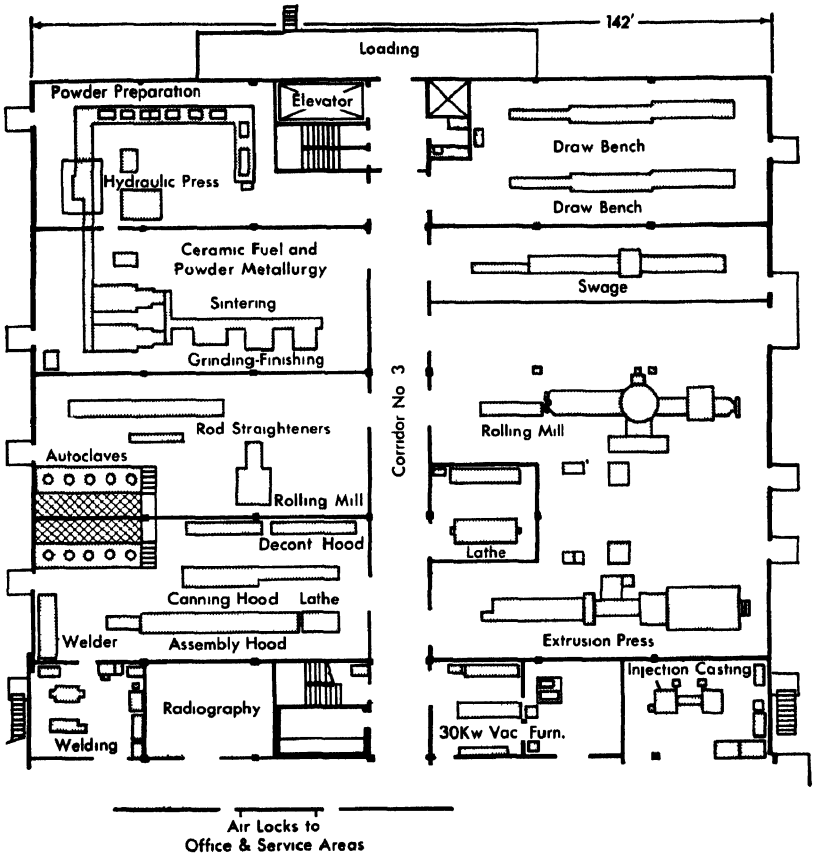

FIG. 8–18 Plutonium fabrication pilot plant, first floor plan.

sions. A vacuum furnace will be attached to the swage hood for annealing material between passes or swaging at elevated temperatures. Two 25,000-lb pull draw benches will be provided. One will be used for draw-sizing and stretch-straightening plutonium-containing fuel cores, the other for final draw sizing of clad fuel elements.

The ceramic fuel-element fabrication equipment, capable of producing reactor loadings of ceramic fuel materials, will be enclosed in glove boxes. This equipment will include a 300-ton pelleting press, two hydrogen sintering furnaces, and equipment needed for grinding, mixing, classifying, and finishing.

In addition to the major process equipment mentioned above, equipment required for fuel element assembly, radiographic examination, decontamination, testing, and inspection will be provided.

8–3.2 The plutonium recycle test reactor. In support of the Plutonium Recycle Program, an experimental reactor, the Plutonium Recycle Test Reactor (PRTR), has been designed and is now under construction. The PRTR will have the experimental flexibility necessary to investigate a wide range of physics variables and fuel element designs associated with plutonium recycle. Operating conditions of the PRTR such as specific power, coolant temperature, and pressure are fairly typical of power reactors in general. No prejudgment of the best type of reactor for plutonium recycle application is intended by the design chosen for the PRTR. The PRTR design was selected by establishing criteria for a suitable experimental reactor and then examining various reactor types to determine which type best met the criteria.

The reactor is intended to provide information on fuel burnup with and without plutonium enrichment, and data for steady-state cycle analyses. It is to provide a facility for testing a wide range of fuel element designs and to make possible the investigation of various coolants, moderators, reflectors, fuel enrichments, and flux patterns applicable to plutonium recycle. The reactor core can be replaced so that changes may be made in lattice spacing, core diameter, reflector material and perhaps even moderators, should such modifications appear attractive.

Criteria for selection of reactor type. Testing the reliability of proposed fuel elements requires that they be exposed under service conditions comparable to those encountered in typical power reactors now under design. Thermal neutron fluxes of about 5×10^{14} n/cm^2 sec and ambient coolant temperatures near 500°F are typical. Many power reactors now under design utilize light water or heavy water as a coolant To enhance the direct applicability of experimental results the reactor type chosen should utilize an aqueous coolant. A maximum operating pressure of about 1200 psi is considered reasonable for achieving the desired operating temperatures without incurring excessive costs for pressure piping. The utilization of the test reactor as a means to pilot the use of plutonium in many power reactor types requires that the test reactor design have maximum flexibility for the use of special coolants or unusual ambient conditions. Since fuel elements being evaluated will occasionally fail, the easy accommodation of such failures is also a desirable feature.

Inasmuch as certain practical types of power reactors may be capable of forming plutonium in sufficient quantity to maintain self-sustaining operation [i.e., using natural (or perhaps depleted) uranium feed material and self-produced plutonium], it was decided that the experimental reactor should have this capability. The neutron energy spectrum is quite important in determining the performance with plutonium recycle; it appears that in general a low energy spectrum may be desirable. It was therefore decided that a reactor with a low temperature moderator should

be used for the test reactor. To facilitate the interpretation of reactivity and other physics measurements, reactor control systems which do not create serious perturbations in neutron flux were also judged to be advantageous.

Comparison of reactor types. The characteristics of reactor designs likely to meet all or most of the above criteria were compared. Suitable candidates were considered to be (1) a light-water moderated pressure tank-type reactor, (2) a graphite moderated reactor comprising a highly-enriched U^{235} fringe region and a small removable central core, (3) a light-water cooled graphite-moderated pressure tube reactor, and (4) a heavy-water moderated pressure-tube reactor cooled by light or heavy water. Preliminary design studies were performed on each of the reactor types to determine operating characteristics, and construction and operating costs These studies are summarized in the following paragraphs.

A light-water moderated, pressure tank type reactor is smaller in size and possibly lower in cost than the other types considered, but has less experimental flexibility, particularly for fuel-element testing. With this type of reactor, monitoring the performance of individual fuel channels may be difficult; installing special cooling loops may present serious design problems associated with the pressure vessel; and using mechanical control may result in core flux perturbations which, in turn, make it difficult to interpret reactivity measurements. This type of reactor is not best suited for frequent removal and recharging of individual fuel columns and does not permit tests using a moderator of one material and a coolant of another. Furthermore, it is a type of reactor which appears to require an undermoderated neutron spectrum to achieve good neutron economy. Such a spectrum is probably not optimum for plutonium recycle application.

A fringe region graphite moderated reactor would be (1) expensive to operate owing to high U^{235} usage and (2) of relatively little practical utility as a fuel testing facility because of the small size of the central test core. A reactor of this type would be primarily an experimental physics facility designed to make possible the accurate measurement of fuel reactivity at intervals during the exposure cycle The same objectives can be attained in other ways, such as by the use of the Physical Constants Testing Reactor* and other test reactors. Therefore, this reactor type does not fulfill the criteria established for the experimental reactor.

A graphite moderated, light-water cooled reactor would (1) allow some degree of experimental flexibility, (2) operate on an equilibrium fuel cycle in a reasonably small reactor size, and (3) not be more costly than

*An existing reactivity measurement facility at Hanford.

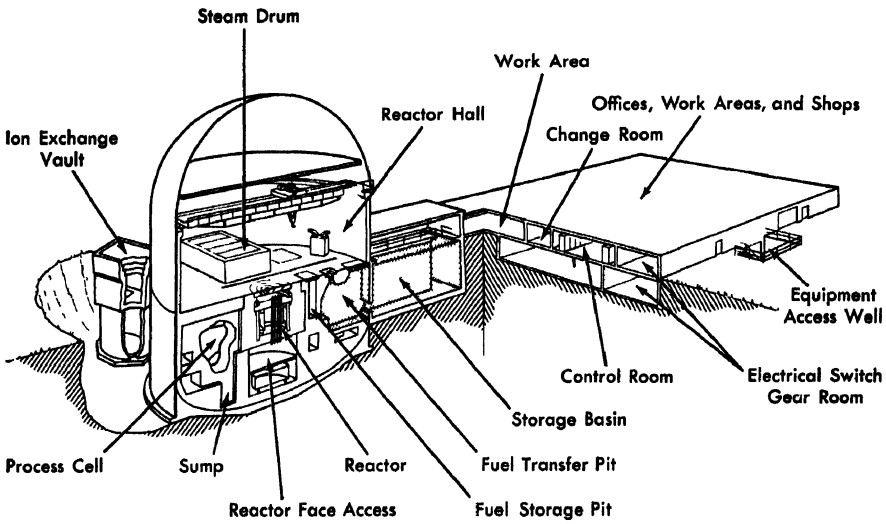

FIG. 8–19. Plutonium Recycle Test Reactor.

the other types (except the first). Its prime disadvantages are the need for developing a practical means of regulating moderator temperature and the difficulty of changing lattice spacing to enable study of this variable. This reactor type nearly met the criteria for the experimental reactor and was eliminated mainly because the heavy water type discussed below was found to be even more suitable.

A heavy-water moderated and cooled pressure-tube reactor appeared to offer the greatest experimental flexibility of the types considered. With this reactor it is possible to modify and monitor individual tubes. The control systems specified do not result in neutron flux perturbations. The moderator temperature is lower and the degree of attainable moderation is higher than in other types. Thus, it can achieve a high uranium exposure. Moderator and coolant are separate, so that light water, heavy water, or other coolant can be used at appropriate times. Its estimated capital costs were found to be only slightly greater than for the graphite moderated reactor. Operating costs were estimated to be lower.

For these reasons the heavy-water moderated reactor was considered best suited to experimental needs. As has been noted previously this determination was based on experimental utility and has no necessary relationship to the type of reactor that might be most beneficial for a commercial power plant.

Description of the Plutonium Recycle Test Reactor. The PRTR, a heavy-water cooled and moderated reactor utilizing 85 vertical pressure

tubes, has a heat dissipation capacity of 70 Mw. The reactor and appurtenances are estimated to cost $15,000,000. Construction is currently under way and will require about 30 months; startup is scheduled in 1960 The PRTR will be located adjacent to the Hanford Laboratories at the AEC's Hanford Plant A detailed description of the PRTR is given in the sections that follow.

(1) General arrangement. The PRTR building, illustrated in Fig. 8–19, consists of two parts: (a) the containment vessel housing the reactor and process equipment, and (b) the service building housing the control room, offices, auxiliary equipment and the storage basin. The reactor is located axially, below the main floor level, in the containment vessel, and comprises a moderator-reflector tank pierced by vertical pressure tubes containing the fuel elements. It is surrounded by shielding which permits access to all sides of the reactor. Coolant piping is connected to the pressure tubes outside the top and bottom shields Process equipment is housed in a cell adjacent to one side of the reactor. Other cells house instrumentation and shops, and provide space for future installation of experimental facilities and special coolant loops.

(2) Core and reflector. The heavy-water moderator, which is unpressurized, is contained within an aluminum tank called the calandria. This cylindrical calandria, as shown in Fig. 8–20, is approximately ten feet in height and seven feet in diameter. It is designed for proper circulation of heavy water to avoid "hot spots" and control problems, to permit primary control of the reactor by regulating moderator level with a gas balance control system, and to shut down or scram the reactor by dumping the moderator from the calandria to a storage tank below. Passing vertically through the calandria are 85 fuel channels, 18 shim control

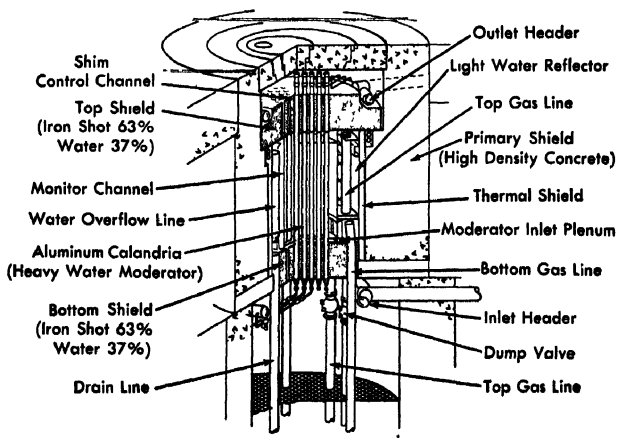

FIG. 8–20. PRTR core and shielding.

channels, and 13 flux monitor channels. The 85 fuel channels are arranged in an equilateral triangular 8-inch lattice.

To provide insulation between the hot primary coolant and the relatively cool moderator, a double tube fuel channel is used. The outer tubes are aluminum and are an integral part of the calandria; the inner (process) tubes contain the pressurized primary coolant and fuel elements.

Attached to the lower side of the calandria is an annular dump chamber which is connected to the calandria by a water trap weir. The dump chamber serves two purposes: (a) It acts as a collecting header for a part of the moderator effluent. About one-third of the moderator effluent continually flows over the weir and is returned to the moderator storage tank located beneath the reactor, by an 8-inch drain line. (b) It acts as a temporary storage volume for a significant fraction of the moderator during a reactor scram. This storage space being adjacent to the calandria considerably increases the shutdown rate. The dump chamber is also connected to the moderator storage tank by three 8-inch gas lines.

Attached to the side of the calandria at the top is an annular gas header, which is also connected to the moderator storage tank by four 8-inch lines normally closed by the dump valves. In case the water level should accidentally rise high enough to flow into the gas header a drain system to the moderator storage tank is provided. Also attached to the side of the calandria near the top is an annular drain header which carries away about 70% of the moderator effluent when the moderator level is at its normal operating height When the moderator height is below this drain system, as it will be during the reactor startup, the entire moderator effluent passes over the weir and out the dump chamber drain.

The moderator cooling inlet flow is fed into the calandria by nozzles in the top plate of a flat plenum chamber at the bottom of the calandria. Initially the design called for the moderator to be pressurized to about 50 psi Thus, moderator temperature could be varied sufficiently to give required "shim" reactivity control. However, the poor neutron economy at high moderator temperatures, the increased cost of the calandria tank when compared with an unpressurized moderator, and the fact that the mechanical shim controls will fulfill the reactivity control function satisfactorily, made it desirable not to pressurize the moderator. The temperature of the moderator leaving the reactor was fixed at the highest value consistent with reasonable assurance that local boiling would not occur in the calandria. The temperature of the moderator entering the calandria was a compromise between high temperature and high flow. While high flow tends to give uniformity of moderator temperature, it also tends to increase the cost of the components in the system. The compromise re-

sulted in the specification of moderator inlet temperature of 137°F and an outlet of 160°F at a flow of about 1100 gpm.

Three types of side reflectors were considered for incorporation in the PRTR design: graphite, heavy water, light water. A water reflector was selected in preference to graphite because of greater flexibility, lower cost, easier removal for core replacement, greater ease in cooling and a less difficult structural support problem Light water was chosen in preference to heavy water principally for cost considerations. However, if it appears desirable at a later date, heavy water can be substituted for the light water reflector. This ability to change fits well with the flexibility concept for this reactor.

The reflector container is an annular tank surrounding the calandria between the dump chamber and the top gas header. The inner, top, and bottom walls of the reflector tank are common to various walls of the calandria and as a result the reflector and moderator vessels form a single assembly. All connections in these vessels are parallel to the vertical axis to make possible the disassembly and replacement of the reactor core.

(3) Process tubes The 85 vertical process tube assemblies in the PRTR provide water-cooled channels through the reactor in which uranium and plutonium fuel elements or experimental assemblies can be irradiated. Heavy water as coolant will flow upward in each tube at a maximum rate of about 120 gpm. Process tubes are individually piped to a single circular water header at each face of the reactor This allows the reactor to be used with maximum flexibility since tubes can be monitored individually or piped to separate cooling systems.

Fuel elements will be suspended by hangers from the outlet nozzle at the top of the process tube assemblies, as illustrated in Fig 8–21. Process tubes will be formed from Zircaloy-2, with an inside diameter of 3.25 inches and a nominal wall thickness of 0.154 inch The allowable design stress of 14,400 psi is 80% of the stress required to produce a secondary creep rate of 10^{-7} in/(in)(hr) at 500°F in vacuum annealed Zircaloy-2. A clearance of 1/4 inch between the process tube and calandria shroud tube acts as a heat barrier between the hot coolant and cool moderator water. Process tubes are tapered to a reduced diameter at the lower end to simplify the design of fittings and the replacement of tubes in the event of damage of fuel-element failure.

(4) Fuel elements. The fuel elements for the PRTR initial loadings will have thin walled Zircaloy-2 jackets filled with either sintered uranium oxide or plutonium-aluminum alloy. These will be assembled either into clusters of 19 small rods approximately 9 ft long or into a nested group of two coaxial tubes with a center rod, approximately 7 ft long, as shown in Figs. 8–10 and 8–12.

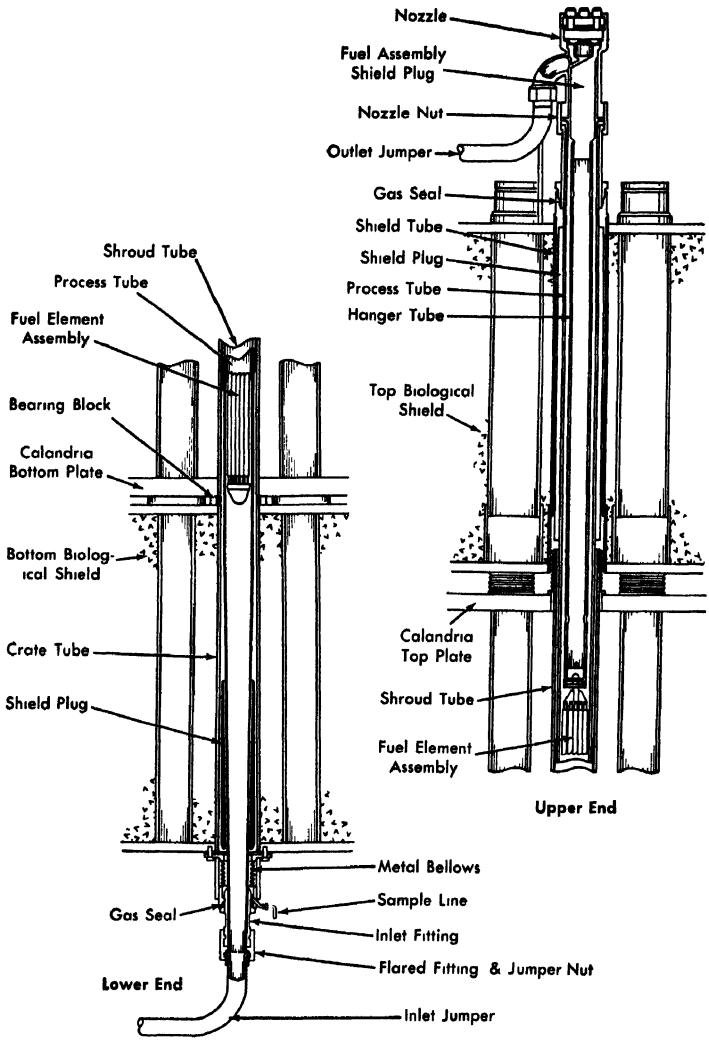

FIG 8–21. PRTR process tube assembly.

Considerations governing the choice of fuel element type and size were:

(a) Satisfactory fuel elements must be available for reactor startup by early 1960.

(b) Fuel elements must be suitable for the reactor operating conditions (for uranium elements, approximately 1200 kw/tube, 5000 Mwd/t exposure, 550°F coolant).

UO_2 and Pu-Al alloy were chosen as core materials for the PRTR fuel elements. The UO_2 was selected because of its compatibility with high temperature water in the event of cladding failure. As an initial approach in developing plutonium fuel elements, the Pu-Al alloy was chosen because of satisfactory experience with U-Al fuel elements. It also seemed likely that, with experience, fabrication costs of Pu-Al alloy fuels can be significantly reduced Zircaloy was specified as cladding material because it has a low cross section and is compatible with the PRTR cooling system. A nested tubular UO_2 fuel element was chosen as the most promising, versatile configuration which could meet uranium content and pressure drop requirements. The 19-rod cluster type Pu-Al alloy fuel element was selected because fabrication techniques and procedures for it are already well developed.

(5) Shielding The shield of the Plutonium Recycle Test Reactor consists of top and bottom primary shields, a top secondary shield, and circumferential thermal and biological shields. The top and bottom primary shields attenuate neutrons to prevent excessive activation of the reactor piping. Because the Zircaloy process tubes filled with heavy water must pass through these shields it is economically desirable to make them as thin as possible. They consist of 40-inch deep cylindrical containers filled with iron shot and water. The mixture has a density of 285 lb/ft^3. The calandria and core assembly of the reactor are supported on the bottom primary shield, while the top primary shield supports the process piping and fuel assemblies Both of the primary shields are cooled by circulating the water of the water-shot mixture. The top secondary shield consists of a series of removable concrete slabs, 27 inches thick, with a density of 320 lb/ft^3 Its top surface is level with the reactor hall floor.

Circumferentially, the reactor core is surrounded by more-conventional thermal and biological shields The biological shield consists of a cylindrical wall of high density concrete, 71 inches thick and 21 ft in height The side of the shield adjacent to the operations area is filled with iron-limonite concrete with a density of 270 lb/ft^3, while the opposite half is filled with magnetite-limonite concrete with a density of 215 lb/ft^3. The 6-inch thick iron thermal shield is next to the inside face of the biological shield. The inside faces of the concrete biological shield, as well as the thermal shield, are cooled by circulating water from the sanitary water supply.

The top primary and secondary shields are designed to give dose rates in the reactor hall of 5 mrem/hr or less during reactor operation. The radial shields are designed to give a maximum dose rate in the operation cell and in the process cell of 1 mrem/hr and 10 mrem/hr, respectively.

(6) Coolant systems. The reactor heat is removed by circulating heavy water through a boiler-type heat exchanger. Steam generated in the exchanger is dissipated in the Columbia River.

The primary coolant circuit comprises:

(a) Three recirculating mechanical shaft-seal pumps (one standby) which circulate 8400 gpm of heavy water at 1150 psi through the reactor, a drum heat exchanger, and flash tank. The differential head across these pumps is 80 psi.

(b) A pressurizer, 3 ft in diameter and 13 ft 6 inches tall, located near the pump inlet, accommodates expansion and contraction of the coolant.

(c) A heat exchanger at a high elevation near the reactor outlet header.

(d) Auxiliary piping, valves, and instruments.

The primary coolant is circulated by operating two of the three recirculating pumps Shaft seal pumps were chosen because they cost less and are cheaper to operate than canned motor pumps.

Under maximum power conditions of 70-Mw output, the reactor heat will increase the temperature of the primary coolant from 480°F to 530°F. The coolant is passed through the primary tube and shell heat exchanger, where it is cooled to 480°F. Heat is removed in the secondary coolant system by boiling 191,000 lb of water per hour at 200°F into 425 psia steam. The steam is throttled to maintain 425 psia in the exchanger. It is then piped to the river, where it is dissipated.

(7) Helium gas system. Gas pressurization of the PRTR primary coolant was chosen in preference to steam pressurization primarily because of its greater speed of pressurization and depressurization One advantage of the PRTR pressure tube design over a pressure vessel design is the ability to heat and cool the primary coolant rapidly without creating excessive thermal stresses in the reactor components. To take full advantage of this ability, fast pressurization and depressurization are desired Helium was chosen as the working gas because of its availability, lack of induced radioactivity, and chemical inertness

The major functions of the reactor helium system are:

(a) To provide pressurization for the primary coolant. The pressurization system is composed of a high-pressure storage tank, an intermediate-pressure storage tank, a high-pressure booster compressor, an intermediate-pressure compressor, and appropriate valves, coolers, water traps, etc.

(b) To provide a helium blanket for the moderator and a working fluid for the gas balance system. This system is described in more detail in the following section on Control and Safety Systems.

(c) To provide an inert and unactivated gas blanket around the reactor core, and a working fluid for the water leak-detection system.

(d) To provide a high-pressure fluid for standardizing of the pressure and flow instrumentation.

(8) Control and safety systems. The control and safety systems of the PRTR consist of the primary control system, which provides for automatic operation of the reactor; a manually adjustable shim control system; and the emergency safety system A feature of the PRTR is the use of moderator level regulation for reactivity control as well as for emergency shutdown.

Primary control of reactivity is obtained by adjusting the level of the heavy-water moderator within the calandria. As shown in Fig. 8–22, the desired moderator level is maintained by applying a differential pressure between the helium gas volume within the calandria and that at the surface of the outflow weir. The moderator will seek a level where its liquid head exactly balances the applied pressure differential.

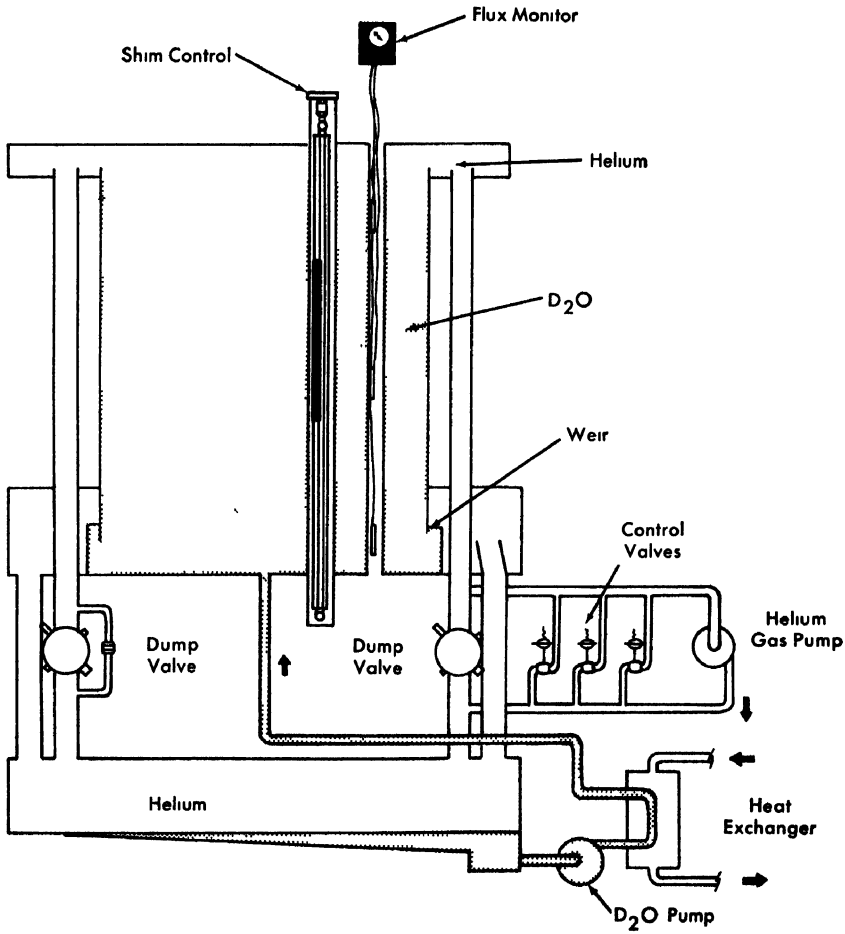

Fig. 8–22. PRTR control system

The pressure differential is maintained by a positive displacement gas compressor shunted by a series of control valves, so arranged that the positions of the valves determine the pressure differential. By changing the control valve setting, the pressure differential, and thus the moderator level, may be varied. The control valves are operated by an automatic controller which responds to changes in the power level and period of the reactor. A programming unit in the controller provides for automatic startup, operation, and shutdown of the reactor according to preset schedules. The controller maintains a constant reactor power level during normal operation and will shut the reactor down by opening the control valves if any operating component fails. Moderator level is controllable over a 6-ft range. The normal operating range is within 6 inches of the maximum level. In this range the precision of reactivity control is ± 0.03 *mk* and the maximum rates of reactivity change by control adjustment are ± 0.10 and -0.20 *mk*/sec. Criticality in the "cold clean" condition is expected to be attained with a moderator level of about 78 inches. At this point the corresponding expected precision of control is ± 0.10 *mk*, and the maximum control rates are ± 0.40 *mk*/sec

The shim control system provides a method for supplemental reactivity adjustments It can make gross adjustments to maintain the moderator level within the normal operating range, to compensate for fuel burnout, and to provide for partial xenon override It can make fine adjustments to flatten neutron flux or, if desired for experimental purposes, to depress the flux in portions of the reactor. The shim controls consist of 36 neutron absorbing rods, each three feet in length, spaced in pairs through the reactor core. The rods run vertically through the calandria, and are exposed directly to the moderator. In the "withdrawn" position they are concealed within the bottom shield. A central structural "backbone" of aluminum in each shim assembly guides vertical motion of the pair of rods.

Each rod is moved individually by a loop of miniature stainless steel stud chain, driven through a reduction gear train by a high-speed electric motor. Small synchro-generators are provided for remote indication of rod position. The motors and position transmitters are concealed within the top shield of the reactor above a shielding plug. Connections to the rod drive gear trains are made by flexible shafts. Rod motion is controlled through a series of switches in the control room. Maximum speed of rod travel is 60 in/min and rod positions are indicated on dials in the control room. Each shim assembly, with rods, drive motors, and position transmitters, is completely contained between the top and bottom faces of the reactor. Assemblies can be removed from the reactor and replaced by using the fuel element charge-discharge equipment. Total reactivity of the shim control system is 36 *mk* with each rod having a strength of about 1 *mk*.

Reactor scram (emergency shutdown) is accomplished quickly by a rapid drainage of the moderator from the calandria. Scram is automatic whenever a condition develops which may damage the reactor or its auxiliary facilities. Scrams can also be initiated by the operator.

For a scram, the calandria is drained rapidly by equalizing the gas pressures in the calandria and the dump chamber. The high and low pressure gas volumes of the gas pressure balance system are connected by four 8-inch lines. During operation these lines are closed by four extremely quick-opening dump valves of special design These dump valves are held closed by solenoids. When there is a scram signal, current to the solenoids is interrupted and the valves open fully within 0.1 sec. Gas pressures then equalize within milliseconds. At the same time the compressor in the pressure balance system stops and the control valves open.

Upon equalization of gas pressures, the moderator within the calandria immediately begins to spill over the outflow weir into the dump chamber at the base of the calandria. A small portion of the discharged moderator is returned to the storage tank beneath the reactor by an 8-inch drain line; the bulk of the flow is initially retained in the dump chamber. Helium displaced from the dump chamber is carried to the storage tank by three additional 8-inch lines whose entrances are elevated within the dump chamber. When the moderator level in the calandria has fallen 2 ft the dump chamber is filled to capacity. Drainage of the calandria then continues at a reduced rate with the flow limited by the capacity of the four lines connecting the dump chamber to the storage tank, until the moderator has fallen to the level of the outflow weir. Within 0.7 sec of a scram signal the moderator level will fall 2 ft, reducing reactivity by 18 *mk*. Within 6 sec the moderator surface will be at the level of the outflow weir. The corresponding decrease in reactivity is approximately 960 *mk*. The moderator dump system is so sized that failure of any two of the four dump valves to open will not appreciably affect the safety of the system.

(9) Instrumentation. The major instrumentation and safety circuits may be divided into nine functional systems Additional instrumentation of standard types will monitor flow, temperature, pressure, and other characteristics of the gas system, coolant purification systems, and building services such as ventilation. The nine major systems are:

Flux monitors. Seven channels of reactor flux instrumentation are used. The startup channel consists of a fission chamber with a remotely controlled positioning device, linear amplifier, logarithmic count rate meter, recorder and period amplifier. The period amplifier will "scram" the reactor on too short a period. Two logarithmic channels consist of compensated ion chambers, logarithmic amplifiers, period amplifiers and recorders. The period amplifiers will be connected in the reactor safety circuit. Three high-level channels consisting of three compensated ion

chambers, linear amplifiers and recorders, will be connected in the reactor safety circuit. An interconnection circuit with the logarithmic channels will cause a scram if less than two of the three high level channels do not indicate "on-scale" signals. The galvanometer channel is made up of two neutron-sensitive ion chambers, a differential galvanometer and a level galvanometer. Ion current from the two chambers will be summed.

Flow monitors. The inlet flow rate to each of the 85 process tubes will be monitored by a venturi. Connected to the venturi will be a differential pressure cell equipped to permit print-out and read-out of the flow rate in each process tube. The flow monitor system is provided with high and low flow trips which are connected into the reactor scram circuit.

Temperature monitors. The temperature monitor will measure the temperature of the coolant leaving each process tube and actuate alarms if an over-temperature exists. The temperature sensing element will be a resistance temperature detector located on the outlet of each process tube Bridge and read-out circuitry, a recorder, and a print-out system will be in the control room

Water activity monitor. The water activity monitor consists of two main systems: the primary coolant activity monitor, and the secondary coolant activity monitor. The primary coolant activity monitor will monitor small samples of coolant from each process tube by means of cation and anion columns and a gamma scintillation detector Traces of fission products from the rupture of fuel elements will be detected. The secondary coolant activity monitor will monitor the secondary coolant for gamma radiation to detect traces of primary coolant that may have leaked from the heat exchangers.

Power calculation system The power calculator system will monitor the power level of the reactor by measuring the heat removed by the primary and secondary coolants. The system will consist of two channels, one measuring primary loop power and the second measuring secondary loop power. Each channel will consist of a temperature difference bridge and flow measuring instrumentation. The output signal will be used to calibrate the power signal from the neutron flux channels.

Reactor thermocouple system. Temperature of the moderator, the reflector, the thermal shield, the top and bottom shields, and the main side shields will be measured by metallic sheathed, magnesium oxide insulated thermocouples.

Steam generation system. Standard power plant instrumentation will be used to control the steam generation system. The reactor shutdown circuit will be actuated by low feedwater pressure, low steam drum level or high steam drum pressure.

Building radiation monitor system. Beta- and gamma-sensitive ion chambers will be positioned in various locations inside the reactor shell.

Air samples from enclosures containing primary coolant and moderator piping will be monitored with beta-sensitive detectors for traces of tritium.

Reactor safety circuit. The reactor safety circuit will cause a reactor shutdown by opening the dump valves to lower the moderator level. This shutdown will occur when certain conditions exist that would result in marginal reactor safety. Circuits will be designed "failsafe"; i e., failure of safety circuits components which would disarm subsequent trip signals will cause a reactor shutdown.

(10) General architecture. The containment vessel, illustrated in Fig. 8–19, is an all-welded steel right cylinder, 80 ft in diameter by 61 ft high, with a hemispherical dome and a hemiellipsoidal bottom The vessel is 121 ft high and extends about 75 ft above grade The above-grade portion of the vessel has three inch insulation protected by a waterproof membrane In general, the vessel is designed in accordance with Section VIII of the ASME Pressure Vessel Code for a 15 psig pressure.

The reactor hall floor, which is slightly above grade, is constructed of ordinary concrete 5 ft thick for radiation shielding. The reactor hall houses the steam drum, decontamination equipment, fuel handling cask, fuel storage transfer and handling facilities, and a circular 30-ton overhead crane with a five ton auxiliary hoist. One personnel air lock, 10 ft in diameter by 15 ft long, gives normal access into the containment vessel reactor hall from the service area via the storage basin area. An emergency personnel air lock is provided for egress under emergency conditions or failure of the main air lock doors. There is also an equipment access door, opening from the reactor hall directly to the outside.

The space below grade is divided into a process equipment cell, an experimental equipment cell, and a three-level instrument and hot shop cell. These cells are separated by ordinary concrete radial shielding walls 5 ft thick The reactor and all components associated with radioactive materials, except the ion exchangers, are located below the reactor hall floor and below grade for containment and radiation shielding. A reinforced concrete vault directly outside the containment vessel houses the ion exchangers and provides for ultimate disposal of the spent ion-exchange units.

The lower reactor face access room, housing the inlet piping, dump valves and moderator storage tank, is directly below the reactor. Personnel access to this room is from the process cell

An underwater fuel-element storage basin, approximately 12 ft wide × 40 ft long × 26 ft deep, is located next to the containment vessel. The fuel element discharge pit, in the reactor hall floor, is connected to the storage basin by a 24-inch valve which is kept closed during reactor operation to maintain the integrity of the containment vessel

The single story service building, 100 ft long × 80 feet wide, is attached

to the process area via the storage basin. On the ground floor of the service building are the control room, offices, locker rooms, lunch room, rest rooms, ventilation equipment room, maintenance and instrument shops, electrical switch-gear rooms, and storage rooms. The building has a partial basement and a 40-foot wide utility tunnel which extends to the containment vessel. The basement and utility tunnel house the plant air compressors, light-water process pumps, process water reservoir, process area ventilation supply unit, water treatment equipment, 480 volt switchgear room, and battery room. One exterior stairway and an equipment access well to the basement are provided.

(11) Ventilation system. The ventilation system: (a) assists in the control of contamination by providing directional control of air flow within the building, (b) maintains temperature, humidity and air cleanliness conditions, and (c) provides safe discharge of contaminated air.

Two independent ventilation systems are provided so as to prevent the spread of potentially contaminated air from the process area to the service area. The buildings are heated and cooled by the ventilation units. Reactor steam will be supplied to the heating coils during normal operation. Steam will be supplied from an external source during reactor shutdown.

Air flow in the containment vessel will be from areas least likely to become contaminated to those more likely to become contaminated The air will then be exhausted to the atmosphere by an air exhaust fan at a normal rate of 5000 cfm. Air will be exhausted down through the crack opening around the removable top shield of the reactor vessel to prevent spread of potentially contaminated air from the top face of the reactor to the reactor hall.

Quick-closing containment valves will be installed in the supply and exhaust ductwork to seal the containment vessel completely should an accident occur. This will prevent gross contamination of the surrounding area

Recirculating air systems with chilled water condensers will be in the containment vessel to recover heavy water which may escape as steam from leaks in the primary coolant system. These systems will direct air through spaces having the highest leak potential.

(12) Fuel-handling system. Fuel elements will be removed from and loaded into the individual process tubes while the reactor is shut down, through a hole in the concrete secondary shield. This is normally closed with a shielding plug, placed eccentrically in a disk which is in turn in a larger disk. Both disks can be rotated. In this way a port of minimum size can service all process tubes. The shielding floor is not disturbed during discharging operations. A large self-propelled fueling vehicle, Fig. 8–23, is used for the charge-discharge operation. This vehicle carries an

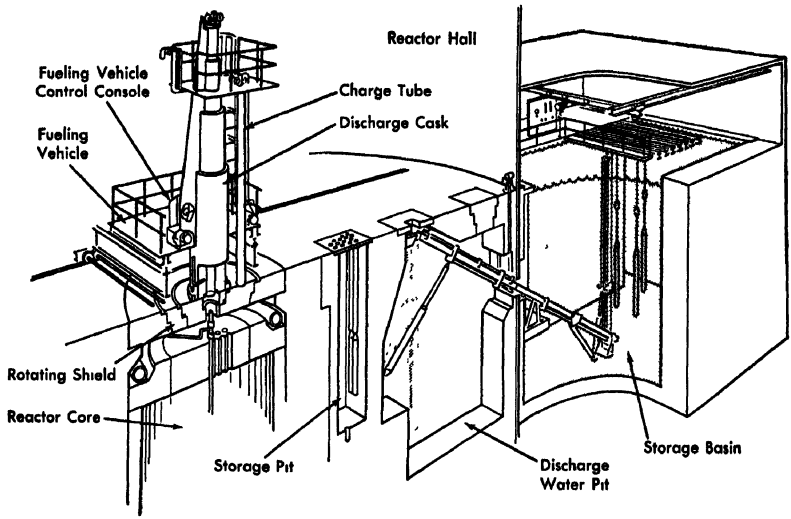

FIG. 8–23. PRTR fuel-handling system.

unshielded tube for the charging of unirradiated fuel elements and a heavily shielded cask for handling irradiated fuel elements The vehicle is about 25 ft high and weighs about 50 tons. Twelve and a half inches of lead shielding protect personnel during discharging operations The operator will control all operations while riding the vehicle. Although shields and structure keep the operator from seeing the various operations directly, the equipment is not "remotely controlled" in the ordinary sense.

New fuel elements are removed from their shipping casks and stored in a pit under the floor of the reactor hall. The fueling vehicle can withdraw any element from the storage pit, carry it to the reactor and insert it into an opened process tube. When discharging, the vehicle and discharge cask are positioned over the proper process tube, and the irradiated element is withdrawn into the cask, and transported by the vehicle to an underwater transfer conveyor system. A carrier in the transfer conveyor system receives the element from the cask, tips it up to an inclined position and transports it through the containment vessel wall endwise into a similar conveyor system in the storage basin where the whole assembly is again set upright.

The basin is equipped with a bridge crane for moving the fuel elements from the carrier to the storage position The conveyor system can operate in reverse order to return an irradiated fuel element to the reactor for further exposure. The system can handle the various fuel elements or the process tubes, with or without nozzles attached, with equal facility.

Consideration was given to discharging irradiated fuel elements from both the top and bottom of the reactor. Top discharge was chosen because it simplified the design of the process tube, the fuel elements, and the general building arrangement. With top discharge, the process tube can be reduced in size at the lower tip and designed for easy replacement. Tubes do not have to be drained for fuel discharge; thus the shutdown cooling provisions are simplified. Moreover, fuel elements do not require removable or collapsible supports if the top-discharge arrangement is used.

References

1 C. H. Westcott, *Effective Cross Section Values for Well-Moderated Thermal Reactor Spectra*, Report CRRP-680, Atomic Energy of Canada, Ltd, Jan. 25, 1957

2 W. W Havens, Jr (Ed), *Proceedings of the International Conference on Neutron Interactions with the Nucleus, Held at Columbia University, September 9–13, 1957*, USAEC Report TID-7547, 1958

3 J P Butler et al., The Neutron Capture Cross Section of Pu-238, Pu-242, and Am-243 in the Thermal Epicadmium Regions, *Can J Phys.* **35**, 147–155 (1957)

4. D E. McMillan et al, *A Measurement of Eta and Other Fission Parameters for U-233, Pu-239, and Pu-241, Relative to U-235, at Sub-Cadmium Neutron Energies*, USAEC Report KAPL-1464, Knolls Atomic Power Laboratory, 1955

5 R B. Schwartz, Total Cross Sections of Pu-241, *Bull Am. Phys Soc* (To be published)

6 D D Lanning and D J Donahue, in *Physics Research Quarterly Report, January, February, March, 1956*, USAEC Report HW-43441, Hanford Atomic Products Operation, 1956. (pp 7–21)

7 R E. Heineman et al, in *Nuclear Physics Research Quarterly Report, April, May, June, 1957*, USAEC Report HW-51983, Hanford Atomic Products Operation, 1957 (pp 55–66)

8 P W Mummery, The Experimental Basis of Lattice Calculations, in *Proceedings of the International Conference on the Peaceful Uses of Atomic Energy*, Vol 5 New York United Nations, 1956 (P/429, pp 282–287)

9 E A Eschbach et al, A Rule-of-Thumb for Estimating the Applicability of Plutonium Recycle in Thermal Power Reactors, *Nucleonics* (To be published)

10 L Roddis, Division of Reactor Development, AEC, 1956 Unpublished

11 Recommendations of the International Commission on Radiological Protection, *Brit J Radiol., Suppl 6* London British Institute of Radiology, 1955

12 R D Moeller and F W Schonfeld, *Alloys of Plutonium with Aluminum*, USAEC Report LA-1000, Los Alamos Scientific Laboratory, Feb 13, 1950

13 M D Freshley, *Plutonium-Aluminum Fuel Element Development*, USAEC Report HW-52457, Hanford Atomic Products Operation, Sept 18, 1957

14. W. J Bailey et al., *Fabrication of Plutonium-Aluminum Fuel Elements for Lattice Tests in Support of PRTR*, USAEC Report HW-51855, Hanford Atomic Products Operation, 1958.

15. H A. Saller, Preparation and Properties of the Aluminum-Uranium Alloys, in *Nuclear Sci Technol.*, USAEC Report TID-2501 (Del), July 1948 (pp. 1–12)

16 O. J. C. Runnalls, Atomic Energy of Canada, Ltd, 1953 Unpublished

17 W. L. Lyon, Preparation and Reprocessing of Plutonium-Aluminum Alloy, a Power Reactor Fuel Material, paper prepared for the Second International Conference on the Peaceful Uses of Atomic Energy, Geneva, 1958. (P/546)

18. J. H. KITTEL and L. R. KELMAN, *Effects of Irradiation on Some Uranium-Plutonium Alloys*, USAEC Report ANL-5706, Argonne National Laboratory, 1958.

19. O J C RUNNALLS, Atomic Energy of Canada, Ltd, 1955 Unpublished.

20. A. B SHUCK, *The Manufacture of Aluminum Clad Aluminum-Plutonium Alloy Irradiation Specimens*, USAEC Report ANL-5043, Argonne National Laboratory, Apr. 17, 1952

21 R. J. BEAVER, *Pertinent Specifications for Fabrication of Plutonium Fuel Elements*, USAEC Report CF-55-7-76, Oak Ridge National Laboratory, July 20, 1955.

22. R E TATE, Los Alamos Scientific Laboratory, 1956. Unpublished.

23. J. L SWANSON, Removal of Zircaloy Cladding by Dissolution in Ammonium Fluoride Solution, paper presented at the 1958 Annual Meeting of the American Chemical Society, San Francisco, April 1958

24. J. L RYAN and E. J WHEELWRIGHT, Application of Anion Exchange to the Reprocessing of Plutonium Fuels, paper prepared for the Second International Conference on the Peaceful Uses of Atomic Energy, Geneva, 1958. (P/915)

25 J. W. ULLMAN, Heavy Element Isotopic Buildup, in *Symposium on the Reprocessing of Irradiated Fuels, Held at Brussels, Belgium, May 20–25, 1957*. USAEC Report TID-7534, Oak Ridge National Laboratory, 1957 (Book 3, p 1080)

26 B. I SPINRAD et al., Reactivity Changes in Fixed Fuel Thermal Reactors, in *Proceedings of the International Conference on the Peaceful Uses of Atomic Energy*, Vol 5. New York· United Nations, 1956 (P/835, Table III, p 131)

INDEX